NDOT Research Report

Report No: RDT06-002

Development of a Seismic Design Method for Reinforced Concrete Two-Way Bridge Column Hinges

February 2006

Prepared by Research Division
Nevada Department of Transportation
1263 South Stewart Street
Carson City, Nevada 89712

This work was sponsored by the Nevada Department of Transportation. The contents of this report reflect the views of the authors, who are responsible for the facts and the accuracy of the data presented herein. The contents do not necessarily reflect the official views or policies of the State of Nevada at the time of publication. This report does not constitute a standard, specification, or regulation.

TECHNICAL REPORT DOCUMENTATION PAGE

Report No. **RDT06-002**	2. Government Accession No.	3. Recipient's Catalog No.
4. Title and Subtitle **Development of a Seismic Design Method for Reinforced Concrete Two-Way Bridge Column Hinges**	5. Report Date **February 2006**	
	6. Performing Organization Code	
7. Author(s) **Cheng, Zhiyuan; Saiidi, M. "Saiid"; Sanders, David H.**	8. Performing Organization Report No. **CCEER-06-01**	
9. Performing Organization Name and Address **Center of Civil Engineering Earthquake Research** **Department of Civil & Environmental Engineering / 258** **University of Nevada Reno** **Reno Nevada 89557**	10. Work Unit No.	
	11. Contract or Grant No. 723-02-803	
12. Sponsoring Agency Name and Address **Nevada Department of Transportation** **1263 South Stewart** **Carson City, Nevada 89712**	13. Type or Report and Period Covered	
	14. Sponsoring Agency Code **NDOT**	

15. Supplementary Notes

16. Abstract

Two-way hinges are commonly used in bridge columns to eliminate moment transfer to adjoining members. In the absence of a specific method to analyze and design two-way hinges, the shear capacity of two-way hinges is determined using the shear friction method (SFM). However, under lateral forces, hinges are under a combination of axial load, shear, and moment, and the shear transfer mechanism is different from that assumed in SFM. The main objective of this study was to develop a method for seismic design of two-way hinges. The study consisted of five parts: (1) development of a primary design method, (2) investigation of the shake table response of large-scale hinged models, (3) refinement of the initial design method, (4) analytical modeling including the development of a method to determine hinge shear spring properties, and (5) development of methods to address different aspects of the hinge design including an illustrative example. The preliminary design method was developed based on the expected mechanism of the two-way hinge force and moment transfer. The experimental studies consisted of shake table testing of five 1/3-scale reinforced concrete bridge column specimens with two-way hinge details under simulated earthquake record obtained during the 1994 Northridge earthquake. The effects of several important parameters were included in tests. It was found that shear forces are transferred through friction with a coefficient that is less than 0.5 due the cyclic load effects. The final proposed method included provisions to account for hinge confinement and check for gap closure. The proposed method led to results with close correlation with the experimental data obtained in this and previous studies.

17. Key Words **two-way hinge, bridge columns, design method, shake table, large-scale hinged models, modeling, illustrative example, axial load, shear, and moment.**		18. Distribution Statement **Unrestricted. This document is available through the National Technical Information Service, Springfield, VA 21161**	
19. Security Classif. (of this report) **Unclassified**	20. Security Classif. (of this page) **Unclassified**	21. No. Of Pages **571**	22. Price

ABSTRACT

Two-way hinges are commonly used in bridge columns to eliminate moment transfer to adjoining members. In the absence of a specific method to analyze and design two-way hinges, the shear capacity of two-way hinges is determined using the shear friction method (SFM). However, under lateral forces, hinges are under a combination of axial load, shear, and moment, and the shear transfer mechanism is different from that assumed in SFM. The main objective of this study was to develop a method for seismic design of two-way hinges. The study consisted of five parts: (1) development of a preliminary design method, (2) investigation of the shake table response of large-scale hinged models, (3) refinement of the initial design method, (4) analytical modeling including the development of a method to determine hinge shear spring properties, and (5) development of methods to address different aspects of the hinge design including an illustrative example.

The preliminary design method was developed based on the expected mechanism of two-way hinge force and moment transfer. The experimental studies consisted of shake table testing of five 1/3-scale reinforced concrete bridge column specimens with two-way hinge details under simulated earthquake record obtained during the 1994 Northridge earthquake. The effects of several important parameters were included in tests. It was found that shear forces are transferred through friction with a coefficient that is less than 0.5 due the cyclic load effects. The final proposed method included provisions to account for hinge confinement and check for gap closure. The proposed method led to results with close correlation with the experimental data obtained in this and previous studies.

ACKNOWLEDGMENTS

The authors wish to express their gratitude to the Nevada Department of Transportation for sponsoring this project. Specifically, the contributions of Troy Martin are gratefully acknowledged. However, opinions, findings, and conclusions expressed in this report are those of the authors and do not necessarily reflect the views of NDOT.

Thanks are due to Dr. Patrick N. Laplace, Mr. Paul Lucas, Mr. Hoon Choi, Mr. Vu Phan and Mr. Robert Nelson, who helped at various stages of the experimental program.

This report is based on a Ph.D. dissertation by the first author supervised by the other authors.

TABLE of CONTENTS

LIST of TABLES

CHAPTER 2

CHAPTER 3

CHAPTER 4

CHAPTER 5

LIST of FIGURES

CHAPTER 1

CHAPTER 2

CHAPTER 3

CHAPTER 4

CHAPTER 5

CHAPTER 6

CHAPTER ONE

INTRODUCTION

1.1 Introduction

Reinforced concrete hinges of various types have been used since the early age of last century. The first example, known as saddle bearings, was concrete imitations of conventional steel roller pivots. About 1910, a French engineer Augustin Mesnager developed a type of concrete hinge, which consisted of reinforcement bars crossing each other in a gap between the members. With the realization that the strength of the concrete in the throat of a Mesnager hinge was considerable, Eugene Freyssinet, another engineer from France, designed concrete hinge with little or no reinforcement passing through the hinge throat. In 1923, Freyssinet hinge was first used in Candelier Bridge project (Fig. 1-1). Since then, reinforced concrete hinges have been extensively used in reinforced concrete structures.

In many reinforced concrete highway bridges, hinges exist at the column-to-foundation or column-to-superstructure interface (Figs. 1-2 and 1-3). According to the current design approach, the foundation must be designed to be at least as strong as the columns that it supports. Because the cost of the bridge foundation can represent a significant portion of the total cost of a bridge, engineers have used hinges at column bases to reduce the column moment transferred to the foundation, thus reducing the size and cost of the foundation. The hinge must still resist shear and carry the axial compressive load of the column.

To accomplish hinge type behavior, the hinge is usually built by stopping all column longitudinal reinforcement at the column base and providing certain amount vertical reinforcement at hinge section. In addition a layer of compressible material is placed around the perimeter of hinge. The detail results in a smaller effective cross-section at the column base and, thus, a reduced hinge capacity in the column. To a great extent, hinge detailing has been based on engineering judgment. The behavior and safety of concrete hinges have been studied only on a limited basis.

There are two types of concrete hinges: one-way and two-way hinges. A one-way hinge transmits moment in the strong direction but it prevents moment transfer in the weak direction. The hinge is nearly free to rotate in the weak direction and it works much like a door hinge. An ideal two-way hinge does not transfer moment in any direction of rotation, and it works like a ball joint. One-way hinges are typically found in pier walls and single column bents, while two-way hinges are used in multi-column bents. Three types of reinforcement may be used in two-way hinges: (1) distributed bars, (2) clustered bars, and (3) steel pipes. The focus of this research was on two-way hinges with distributed bars.

In recent years, moderate and large earthquakes have caused significant damage to bridges around the world. The 1989 Loma Prieta and 1994 Northridge

earthquake in California are but two examples. These earthquakes subjected a large number of bridges of various types to intense ground shaking. Damage resulting from these earthquakes ranged from none to moderate, with older bridges completely collapsing. Even though modern bridges generally performed well, these earthquakes prompted worldwide re-evaluation of many of the design procedures, analysis methods and construction details used in bridges located in the regions of high seismic hazard.

Severe earthquakes subject a bridge to many cycles of large-amplitude load reversals. Therefore, connections such as two-way hinges must be capable of undergoing large deformations. Another desirable feature for hinges is the ability to dissipate energy during the inelastic deformation cycles. While most of the experimental studies to date have subjected structural members and simple bents to prescribed histories of cyclic displacement reversals, little experimental or field data exist to validate the performance of two-way hinges under the intense and complex three-dimensional dynamic loading condition expected during major earthquakes.

Two-way hinges are currently designed using the compressive axial capacity of the section and the lateral load capacity based on the shear friction theory. Past tests at University of Nevada, Reno, and other studies have shown that one-way and two-way hinges experience large rotations under lateral loads and that the conventional shear friction mechanism does not exist in two-way hinges. A reliable procedure for design of two-way hinges including a rational method to determine the shear capacity of the hinge is needed.

1.2 Past Research

Little is known about the behavior of bridge column hinges, although the concept of using a hinge at a column end to release moment transfer has been employed for almost a century. Research was conducted in England in the late 1950s and 1960s; however, there is no research data available between that time and the time of the pilot one-way hinge study conducted by Saiidi et al. (Ref. 38 and 39) in the late 1980s. Less information is available regarding two-way hinges, except for the studies of Lim et al. (1991) and Haroun et. al. (1993). A summary of reinforced concrete hinge research is provided in this section.

1.2.1 Two-Way Hinges

Lim et al. (Ref. 25) conducted a study in 1989 to investigate the behavior of two-way hinges. Small (1/20) and large (1/5) scale column specimens with two-way hinge detail at the base were tested by applying lateral cyclic loading at the top of the column. The 1/20-scale specimens were tested first in order to provide insight into the general behavior before selecting the parameters for the 1/5-scale testing program. The specimens were tested with two different details: a hinge detail providing horizontal gap only, and another incorporating a detail providing both vertical and horizontal gaps. Flexure dominated the failure mechanism in all specimens and high levels of displacement ductility were reached. Load carrying capacity of the specimens that incorporated a vertical gap

in the hinge was approximately 10 percent lower than that of those with horizontal gap only. The authors concluded that two-way hinges with both details exhibited stable moment-deflection hysteresis curves and continued to absorb energy even at a high displacement ductility. More severe strength degradation was observed in specimens with higher column aspect ratios. A two-way hinge design procedure was proposed. The failure mechanism of the column with two-way hinges was considered to be either flexural failure or shear friction failure of the hinge.

Haroun, et al. (Ref. 17) conducted six 0.4 – scale two-way hinge column tests under reverse cyclic lateral load applied at top of the column. The columns were based on a scaled version of the standard details employed by the California Department of Transportation (Caltrans). The variables examined included hinge details with or without shear keys, levels of ductility, and the axial load level. Flexure dominated the failure mechanism and high levels of ductility were reached for all columns. Following these tests, the load was moved to the bottom of the columns in order to fail the hinges in shear. Based on test results, it was concluded that the presence or absence of a depressed key has very little effect on the lateral resistance. The authors concluded that (1) the ultimate strength of the hinged column was governed by the strength of the column, (2) the shear failure mechanism is diagonal tension failure of the whole column section, and (3) the strength of the section can be predicted by code specifications (Ref. 3) for reinforced concrete beam shear design.

1.2 .2 One-Way Hinges

Several studies were conducted at the University of Nevada, Reno. Among the four investigations, three studies were focused on one-way hinge behavior in the strong direction, and the fourth was to study the performance of one-way hinges in the weak direction.

Saiidi et al. (Ref. 38) tested four 1/8-scale one-way reinforced concrete hinge specimens in 1988, the hinge details were scaled models of the Rose Creek Bridge in Northern Nevada. Three of the four specimens were loaded monotonically and had aspect ratio of 1, 2 and 3. The fourth specimen was tested cyclically with aspect ratio of 3. To simplify testing, the effect of axial force was not included. The objectives of this project were to study the uniaxial moment transfer in the strong direction of the one-way column hinges, to evaluate the effect of varying aspect ratio on the shear and flexural capacity of the specimens, and to determine if the shear friction theory was a valid method for hinge shear capacity estimation. It was concluded that flexural failure occurred in all four specimens. The failure mode was very different from that assumed in the shear friction method. The shear friction method overestimated the shear capacity of the hinge in the strong direction. The mechanism that resisted shear before dowel action took place was the aggregate interlock within the compression zone of the hinge.

As a continuation of early work, Saiidi et al. (Ref. 39) tested four 1/6 – scale hinge specimens in the strong direction. Two test variables were considered in the study, loading type (cyclic vs. monotonic) and shear span-to-depth aspect ratio. The effect of axial load was introduced to simulated the weight of the

superstructure. Based on test results, the authors concluded that (1) the shear friction method does not give reasonable estimate of lateral hinge strength, and that the primary shear resistance developed only in the compression zone of the hinge interface, (2) as the aspect ratio was decreased, the energy dissipation capacity of the hinge also decreased, (3) dowel action of the hinge did not occur until large displacements were achieved, and (4) the load-displacement curves showed pinching and indicated that the energy absorption capacity in the hinge was relatively small.

A follow up study, conducted by Saiidi et al. (Ref. 19) in 1993, was the third project in the one-way hinge series that looked at the behavior of one-way hinge in the strong direction. Many variables were considered in the testing, including aspect ratio, type of loading (monotonic or cyclic), arrangement of steel in the hinge region, and hinge throat thickness relative to hinge width, to study their effects on the hinge flexural and lateral strength, energy absorption capacity, shear slip and compressive strength of concrete in the hinge. Five 1/6-scale column specimens were tested; three shear specimens and three compression specimens. It was concluded that the current method of analysis for determining shear capacity of the hinge, based on shear friction theory, can lead to unconservative results. A preliminary method was proposed for lateral load design of one-way hinges. A repair method was presented which can be used to restore the strength and ductility capacity of a damaged hinge with inadequate reinforcement development length.

As the fourth part of the UNR studies on one-way hinges, Sanders et al. (Ref. 40) investigated the behavior and shear capacity in the weak direction of one-way hinges. Three identical 5/16-scale specimens that represented the Rose Creek Bridge hinges were constructed and tested. The only test variable was the number of loading cycles applied to specimens. The first test specimen was tested monotonically. The same specimen was tested again by subjecting the hinge to pure shear. The second specimen was tested by applying a limited number of cycles in pure shear, while the last specimen was tested by applying many cycles in pure shear. Based on the investigation, it was concluded that (1) One-way hinges in the weak direction have very little energy absorption capacity due to the heavy pinching effects in the hysteresis curves, (2) the failure mechanism for one-way hinges in the weak direction did not resemble the shear friction mechanism, and (3) the concrete that covers the ends of the longitudinal reinforcement in the column greatly influences the behavior of the one-way hinge in weak direction. An analysis method based on the wedge model was proposed to estimate the one-way hinge shear capacity. By calculating both shear capacities by the wedge model and dowel/friction model and choosing the lesser of the two, the method can determine the mode of failure and the shear capacity of the hinge in weak direction.

1.3 Current Practice

Codified guidelines for the design of two-way hinge details do not currently exist. As a result, there is considerable variation in the design and detailing of

two-way hinges. Traditionally, it has been believed that the failure mechanism of two-way hinges is either in compression or shear. In addition, one study has suggested that the shear failure mechanism of the two-way hinge is diagonal tension failure involving the entire column section and that the shear strength can be predicted by code equations for reinforced concrete beam-column elements.

Currently, the most common approach to the two-way hinge design is to determine the hinge section size based on axial compressive capacity, and to design for the shear by providing the amount of longitudinal steel required based on the conventional shear friction theory. A horizontal joint with 6.35 mm (¼ inch) to 12.7 mm (½ inch) thick expansion joint material is provided at the throat region around the hinge perimeter to create partial discontinuity between the column and the footing or superstructure. A typical design for a two-way hinge is shown in Fig. 1-4.

Several questions can be raised about the behavior of the two-way hinge under seismic loading. Lateral forces are introduced to bridge columns through loads acting primarily at the deck level; therefore, a substantial flexure moment is expected at the column base where the hinge is located. Shear friction theory was developed under the condition of pure shear and the effect of flexure moment was not initially included. Also, even though the hinge is assumed to be a pin connection, moment is developed at the hinge section, this will result in a noticeable increase in the shear and axial load in the column. Gap closure, due to contact of the edges of the outer column with the top of the footing, will lead to higher moments and increased degradation in the hinge. Finally, due to the sudden shape changes at the hinge range, the horizontal discontinuity can increase the distress in the hinge.

1.4 Objectives and Scope

The primary objectives of this study were to evaluate the current practice for design of two-way hinge details in reinforced-concrete bridge columns, to investigate the performance of two-way hinges subjected to combined vertical and lateral loads including seismic forces, to experimentally investigate the seismic performance of columns incorporating such details, and finally to develop a comprehensive and reliable design method for practical application.

Five one-third-scale specimens (THD-1, THD-2, THD-3, THD-4 and THD-5) were constructed and tested on one of the shake tables at University of Nevada, Reno structures lab using the 1994 Northridge earthquake record obtained at the Sylmar County Hospital ground floor. Many variables that might affect the hinge and column performance were considered in the specimen design, such as level of axial load, column aspect ratio, hinge steel ratio, and the diameter of the hinge. These parameters were chosen such that a wide range of realistic conditions for two-way hinges could be studied.

The test results provided useful information based on dynamic large scale testing, which allowed the design method to be evaluated and modified. A procedure for two-way hinge design including a rational method to determine the shear capacity of the hinge, a shear model for two-way hinge column deflection

calculation and also a practical method to predict the two-way hinge confined concrete properties were developed.

CHAPTER TWO

SPECIMENS DESIGN AND PRELIMINARY ANALYSIS

2.1 Introduction

Five large-scale specimens were tested at the UNR large-scale structural lab. The specimens were designed such that the effects of potentially critical parameters could be simulated and studied. Several parameters that may affect the hinge and column performance are described in Section 2.2. Section 2.3 explains the two-way hinge shear failure mechanism and its preliminary design method. The design procedure for the specimens including detailing is discussed in Section 2.4. Materials properties are documented in Section 2.5 and Section 2.7. The preliminary analysis, including moment-curvature analysis, force-deflection calculation and nonlinear time history analysis are reported in Section 2.6.

2.2 Test Variable

The influence of several variables on the behavior of bridge columns with two-way hinge details was investigated through five test specimens. A summary of the details of the five specimens is given in Table 2-1. The parameters evaluated in this study included:

- Column aspect ratio;
- Magnitude of axial load;
- Amount of column longitudinal reinforcement;
- Amount of hinge longitudinal reinforcement;
- Ratio of hinge diameter to column diameter;
- Confinement in two-way hinge.

Two column height-to-width ratios were investigated in the study: 3 and 4. The two aspect ratios were achieved by varying the height of specimen while keeping the column cross-sectional dimension constant.

Four levels of axial load index (ALI) were studied: $P / (f'_c A_h) = 0$, 0.13, 0.21 and 0.33, where A_h is the gross cross-section area of the hinge. The nominal ALIs are based on concrete design strength of 34.5MPa (5000 psi). The actual values of ALIs varied depending on the actual concrete strength and were 0.19, 0.12, 0.23, 0, and 0.35 for THD1 to THD5, respectively.

While the columns were of the same diameter, their longitudinal reinforcement was different. The longitudinal bars were 14-#7, 13-#7, 14-#4, 10-#5, and 10-#7 corresponding to column steel ratio of 4.2%, 3.9%, 1.4%, 1.5% and 3% for THD1 to THD5, respectively. Two hinge longitudinal reinforcing ratios of 1% and 1.3%, consisting of 7 -# 3 for hinge diameter of 254 mm (10 in.) and 6 -#3 for hinge diameter of 200 mm (8 in.) were used.

Two hinge to column diameter ratios were investigated in the test, 0.625 and 0.5. While keeping the column cross section dimensions constant, different diameter ratios were achieved by changing the diameter of two-way hinges.

Two hinge spiral reinforcing volume ratios of 0.9% and 1.2% were studied. The transverse reinforcement for all the hinges was the same and consisted of a spiral made from 8 gauge smooth welded wire with a pitch of 2.54cm (1 in.) for all specimens. However, because the hinge diameters varied, the spiral steel ratio also changes.

2.3 Two-way Hinge Preliminary Design Method

2.3.1 Failure Mechanism

As mentioned in Chapter 1, the shear-friction method is currently used by bridge designers to determine the ultimate shear capacity of the hinge section. However, because lateral forces are introduced into bridge columns through loads acting primarily at the deck level; there can be significant flexural cracking and rotation at the column base hinge throat making the conventional shear friction assumption questionable.

The shear friction method is described in the ACI building code and AASHTO bridge specifications. This method assumes that as concrete segments slide relative to each other, the aggregate at the interface move up and over each other causing a gap that puts the steel crossing the shear plane in tension. This clamping action of the reinforcement can be supplemented by externally applied compression forces across shear plane. Therefore, the total clamping force is the tensile yielding force plus the applied compressive force. The shear friction mechanism is shown in Fig. 2-1.

The mechanical behavior of two-way hinge, shown in Fig. 2-2, is considerably different than that discussed in the shear friction method. Usually, a large flexural crack forms in the concrete, limiting the contact area for aggregate interlock to the compression zone of the section. The net compressive force is the summation of the reinforcing steel force and the concrete force crossing this contact region. Thus, the resultant compressive force may be very different from that obtained using the shear friction assumption that all the bars are in tension. The hinge shear strength can be evaluated as a function of the normal force on the contact surface. The normal force results from flexure and the applied forces normal to the crack surface. To make a realistic prediction of shear strength, the effective compression force, as the result of flexure at hinge, must be considered. In addition, under dynamic cyclic type loading such as earthquakes, the hinge will build up residual tensile strain in the reinforcing steel which prevents the crack along the shear plane from closing immediately after the load has reversed. After the initial cycle is completed, the shear stiffness of the hinge is lower than before and the hinge experiences slip until the flexural cracks closes and the shear strength and stiffness is increased. Further reversed cyclic motion results in similar behavior. The sliding at the hinge interfaces reduces the roughness at the interface, thus reducing the portion of shear resistance provide by aggregate interlock.

Hinge shear strength can also be developed by dowel action across the shear plan once significant slippage has occurred. Figure 2-3 illustrates the three mechanisms for development of shear strength due to dowel action: flexure of the

reinforcing steel, shear across the dowels, and "kinking" of the dowels (Ref. 32). Due to the possible large slip at the hinge, the hinge bar would deform, and most likely, kinking mechanism will dominate the dowel action.

2.3.2 Preliminary Design Method

On the basis of preliminary investigation and a survey of the literature, the following preliminary design recommendations were proposed and applied in design of five two-way hinge specimens. The recommendations are given in a step-by-step manner along with explanations.

1) Determine the hinge section and the required longitudinal steel:

- Hinge section diameter:

$$f_{hinge} \approx (1/2 \leftrightarrow 2/3) f_{col} \quad (2\text{-}1)$$

Where:

ϕ_{hinge} = diameter of hinge section, and

ϕ_{col} = diameter (or side dimension) of column section.

- In the hinge, use minimum longitudinal reinforcement permitted by AASHTO:

$$A_s \geq 0.01 A_g \quad (2\text{-}2)$$

Where:

A_s = hinge longitudinal reinforcement steel area.

2) Design hinge transverse reinforcement using Mortensen and Saiidi's performance based design method (Ref. 37), for a target curvature ductility of 10.

3) Find hinge confined concrete properties. Hinges experience "double confinement" provided by the hinge spiral and the confinement provide by column above and the footing below. The hinge confined concrete properties are found by incorporating the following modified confined lateral pressure and spiral steel ratio into Mander's method for f'_{cc}, ε_{cc} and ε_{cu}.

$$f_l = \left[(2 f_y A_{sh} / D' s_h)_{hinge} + (2 f_y A_{sh} / D' s_h)_{column} \right] \quad (2\text{-}3)$$

$$r_s = \left[\left(4 A_{sh} / D' s_h\right)_{hinge} + \left(4 A_{sh} / D' s_h\right)_{column} \right] \quad (2\text{-}4)$$

Where:

f_l = effective hinge confined lateral pressure,

? ρ_s = hinge effective volumetric ratio of confining steel,

f_y = yield strength of the reinforcement,

A_{sh} = spiral bar area,

D' = diameter of the confined core, and

s_h = spiral pitch.

4) Determine hinge shear capacity based on two-way hinge mechanism described in the previous section:

- Run moment curvature analysis, locate the neutral axial of the section, and find areas under compression for concrete and steel: A_{cc} and A_{cs}.

- $V_n = \mu\,(0.85 f'_c A_{cc} + f_y A_{cs})$, $\mu=1$ (tentative) (2-5)

  Where:

  A_{cc} = hinge concrete area under compression,
  A_{sc} = hinge steel area under compression,
  f_y = yield strength of the hinge longitudinal reinforcement, and
  f'_c = hinge concrete compressive strength.

5) Calculate hinge ultimate shear demand:

$$V_u=(M_c+M_h)/L \quad (2\text{-}6)$$

Where:

M_c = column section ultimate moment capacity,
M_h = hinge section ultimate moment capacity, and
L = column height.

6) Check to see if $\phi V_n > V_u$, if not adjust either the hinge longitudinal bars, the size of hinge section, or both and repeat steps 1 to 6 until the shear capacity is sufficient. Note that no strength reduction factor is specified at this preliminary stage.

2.4 Specimen Design

Due to the limitations of testing equipment and cost considerations, tests are not usually carried out at full scale. This is especially true for shaking table tests, where limitations arise from the physical size of the table, as well as from limits on the displacements, accelerations and velocities that can be imposed by the table. Thus, most test specimens need to be constructed at a reduced scale.

As a result of these considerations, the diameter of the model column was set at 40.6cm (16 in.) which corresponds to a model to typical prototype length scale factor of 1/3. This scale factor was used to compute specimen dynamic properties as well as the shake table input earthquake motion.

2.4.1 Model Scaling

The scale factor needs to be applied in a way that stresses would not be scaled and real concrete and steel could be used. Scaling rules are relatively straight-forward for statically loaded specimens. For dynamic tests, time and time-dependant parameters (such as acceleration, velocity and strain rate) must also be considered. Table 2-2 summarizes dimensional similitude requirements for dynamic tests. In this case, strains developed in the test specimen and prototypes are identical, and by using the same materials in the model and prototype, the same stresses would be anticipated in both. A more complete treatment of similitude requirements is presented by Krawinkler and Moncarz (Ref. 4).

It should be noted that it is not always practical or physically possible to scale all quantities properly. For instance, if a very small-scale model is used, scaling concrete and steel will become a problem, the usage of micro-concrete and wire fabric will affect specimen cracking, bond and other aspects of the behavior. Therefore it is desirable that specimens be designed and constructed as near to full-scale as possible.

In this project, the mass-rig system, shown in Fig. 2-4, was used to provide the inertial mass for the testing. The axial load was applied to the specimen through two prestressed high strength threaded rods. Therefore, the applied axial load and inertial mass usually did not perfectly match. To account for this difference, the time compression factor of the input earthquake record was multiplied by the square root of w_i / p, where w_i is the weight of the inertia mass, and p is the applied axial load.

In this project, nearly all of the properties of the test specimen were able to be modelled in accordance to the relations contained in Table 2-2. The only exception was the mass density of the concrete, which was not changed. The required density to preserve similitude needs to be higher, in order to maintain the same level of rotational inertial. However, the error in using regular concrete for the specimen is considered negligible because the mass of the column itself is small in comparison to the total inertial mass being considered for the testing.

2.4.2 Description of the Specimens

The specimens used in this study were referred to as THD-1 to THD-5. In this notation, "T" stands for test specimen, "H" for hinge, "D" for detail, and "1" to "5" for specimen number. Hence, five, one-third scale specimens were constructed and tested on a shake-table at the UNR Large-Scale Structures Lab.

The specimens primarily consisted of two concrete segments as shown in Fig. 2-5 to Fig. 2-9. The column segment measured 407 mm (16 in.) diameter, and a reduced circular section that formed a two-way hinge located on top of the column. Along with these two main elements, a footing and a loading head were also designed and constructed as shown in the drawings.

Major parameters that might affect the hinge and column performance were included in the models. These parameters included the axial load, column aspect ratio, hinge steel ratio, and the diameter of the hinge. Figures 2-5 to 2-9 show the dimensions and reinforcing details of the specimens. Table 2-1 lists the main parameters for the five specimens. All specimens except for THD-3 were designed to fail in shear at the hinge after plastic hinging of the base. Model THD-3 was designed with a larger hinge shear capacity so that it would fail in column flexure, as would be done in bridge design. Columns THD-1 and 2 had different aspect ratios to change the moment shear ratio in the hinge. In THD-4, the axial load was reduced to near zero to determine the performance of hinges in which the overturning moments have cancelled the dead load axial compression. The hinge diameter in THD-5 was reduced to 200 mm (8 in.) to determine the effect of higher axial stress and smaller hinges on the shear capacity. In all specimens, the hinge gap was 2.5 cm (1 in.) This would correspond to 76 mm (3 in.) in a full-scale hinge, which is considerably larger than the hinge gaps in bridge construction. The gap was intentionally made large to avoid gap closure and build-up of large moments at hinges.

2.4.3 Hinge Reinforcement

2.4.3.1 Longitudinal Reinforcement

The longitudinal reinforcement of the hinges consisted of 7-#3 for all the specimens except THD-5. This resulted in a reinforcement ratio of 1.3% for THD-5 and 1% for the other four specimens as listed at Table 2-1. Several factors led to the selection of hinge longitudinal steel. First, the amount of steel reinforcement needs to satisfy the minimum steel requirement permitted by AASHTO provision for axially loaded members which is 1%. Secondly, the hinge reinforcement needs to provide certain amount of hinge shear capacity so that the anticipated failure mode described previously at Section 2.4.2 can be achieved. The preliminary design method was used for design, an iterative approach was applied, and design adjustments were made to satisfy the requirements.

The development length of the #3 bar into the column was checked for both tension and compression using the requirements of the AASHTO Bridge Design Specifications (Ref. 2). The development length was over designed in order to avoid damage due to bar pull out. The bars were anchored in the loading head using 90-degree hooks that were bend outwards as shown in Figs. 2-5 to 2-9.

2.4.3.2 Spiral Reinforcement

The spiral reinforcement consisted of W2.1 smooth wire, which has a cross section area of 13.54 mm^2 (0.021 $in.^2$) and a diameter of 4.1mm (0.162 in.). A continuous spiral with a pitch of 2.5 cm (1 in.) was provided along the entire height of the hinge longitudinal bar. The resulting volumetric ratio of the spiral reinforcement was 0.9% for THD-1 to THD-4, and 1.2% for THD-5, respectively. The transverse reinforcement was designed using the Mortensen-Saiidi method; a non-iterative performance-based design (PBD) method which was developed for confinement reinforcement in concrete columns. The flexibility of this method allows the engineer to design columns for specified performance levels, utilizing a target curvature ductility and moment curvature analysis (Ref. 37). In order to achieve the ductile performance for the hinge specimen, a target calculated curvature ductility of 10 was used in the calculations. Using curvature ductility of 10 as design target is based on the recommendation of the original PBD method study (Ref. 37).

2.4.4 Column Reinforcement

2.4.4.1 Longitudinal Reinforcement

The primarily consideration needed in the design of the column longitudinal reinforcement was to make sure the desirable failure mode can be achieved. As mentioned in previous sections, all specimens except for THD-3 were designed to fail in shear at the hinge and not in the columns. The preliminary design method which was described in section 2.3.2 was applied to specimen design and an iterative approach was used to obtain the target failure mode during the tests. As a result, the longitudinal reinforcement ratio of the columns varied from 1.4% to 4.2% as listed in Table 2-1. The column longitudinal bars were developed into the footing using 90 hooks, bent outwards with a bend diameter of $6d_b$ as shown in

Figs. 2-5 to 2-9. At the hinge end, the bars were stopped at the end of the column with no hook.

2.4.4.2 Spiral Reinforcement

The spiral reinforcement consisted of #3 deformed rebar, which has a cross section area of 71 mm^2 (0.11 $in.^2$) and a diameter of 9.52 mm (0.375 in.) A continuous spiral with a pitch of 38 mm (1.5 in.) was applied along the entire height of the column longitudinal bar. The resulting volumetric ratio of the spiral reinforcement was 1.96%. The transverse reinforcement was designed using Caltrans Bridge Design Specification (Equations 8-62 and 8-62a) to ensure the sufficient confinement for the column core, such that the specimen plastic shear can be reached. There was at least a 20% margin against the column shear failure to ensure column flexural failure for THD-3 and hinge shear failure for rest of the four specimens could be achieved during the testing. Tests and experience show that columns containing the amount of spirals required by the Caltrans method exhibit considerable toughness and ductility.

2.4.5 Footing and Top Loading Head

Each column was connected to a square footing at the base and a loading head at the top (Figs. 2-10 and 2-11). The footing was designed to rigidly attach the column to the shake table deck and provide uplift restraint for the specimen. The footing plan dimensions were chosen to be 1.83 m x 1.83 m (6 ft x 6 ft). The dimensions were based on the tie down grid spacing of the shake table deck and the calculated bearing stress between the footing and table deck during the test. Fourteen PVC 7.6 cm (3 in.) ducts were placed through the height of the footing in order to provide tie-down holes that allow the passage of the tie down rods. The clamping load used in each rod was approximately 111 KN (25 kips). The height of the footing was selected in such a way that the height of the columns (hinge included) plus the height of the footing and the thickness of the grout 3.8 cm (1.5 in.) matched the distance between the shake table deck and the sets of holes of the mass rig plate. Overturning moment, bearing, punching shear as well as one way shear checks were made in the design of the footing. The design forces on the footing were based on the full development of the specimen capacity. The footing was designed to remain elastic during the tests.

The loading head was designed to provide rigid attachment between the specimens and connecting plate which was post-tensioned to the head using Dywidag bars. Therefore, the specimens were loaded in double curvature, to develop the necessary shear and moment in the two-way hinges. The plane dimensions of the head were 1 m x 1m (40 in. x 40 in.) and were controlled by the connecting plate dimensions between the specimen and dual link assembly. The head width was required to be less than the width of the two post tensioning rods passing along the side of the head for the axial load system. Six PVC pipes 5 cm (2 in.) diameter were cast in the column head to provide holes for the bolts in order to attach the head to the link assembly. The head was designed to remain elastic

during the tests. It was checked for bending and shear caused by the full development of the plastic moment and shear capacity of the hinge at the top.

The footing was cast first with a cold joint at the column-footing interface, while the head was cast monolithically with the two-way hinge at top of the column. The specimen was symmetric in the vertical direction. Both column longitudinal bars and hinge longitudinal bars were anchored into the footing and head as described in Sections 2.4.3.1 and 2.4.4.1. The development length was checked against AASHTO specifications (Ref. 2), and found to be sufficient for full development.

2.5 Materials Properties

All material used for the construction were available locally. The concrete was designed and supplied by Reno-Sparks Ready Mix. Longitudinal and footing steel was supplied by Northern Nevada Rebar. W2.1 smooth wire spiral was provide by Western Steel Wire Inc. and fabricated at Camblin Steel Service. Steel and concrete cylinder tests were performed at the University of Nevada, Reno, Civil and Environment Engineering lab.

The concrete mix design was based on modeled properties of the typical bridge columns. To maintain approximate similitude between the specimen and real bridge column, 9.5 mm (3/8 in) maximum aggregate was used in the mix design. The required 28 day strength of 34.5 MPa (5000 psi) was specified for the design of the all specimens. In addition, specified minimum yield strength of 414 MPa (60 ksi) was selected for all the reinforcement used in the design. The mix design used for this project is shown in Table 2-3.

2.6 Preliminary Analysis

Computer analysis was used to predict the behavior of each specimen before testing. Computer analysis was also needed to make sure that each specimen could reach failure before exceeding the shake table capacity. The analysis was also helpful in planning an effective instrumentation scheme. The shake table specifications are given in Table 2-4. Two computer programs were used in the preliminary analysis. First, the RCMC program was used to determine the moment and curvature capacities for column and hinge cross-sections (Ref. 44). Second, the RC-Shake program was used to analyze specimens dynamically by subjecting them to earthquake motion records (Ref. 21).

2.6.1 Moment-Curvature Analysis

A moment-curvature relationship can be used to estimate the effective sectional stiffness for an elastic model, and provides the basis for computing the lateral force-displacement relationship of the column specimens. By integrating the moment-curvature over the length of the member, flexural deformation of the specimen under complex loading condition can be predicted.

The moment-curvature relationship of any section can be calculated using well-known mechanics principles. Typically, the section is discretized into a number of fibers, each of which is assigned a uniaxial constitutive model

corresponding to the material it represents. Consistent with Bernoulli-Navier beam theory, sections are assumed to remain plane during deformation. The moment-curvature curve is obtained by calculating the section moment corresponding to a certain imposed curvature and axial load. Typically, this is accomplished by iteratively solving for a neutral axis depth that satisfies axial load equilibrium. For reinforced concrete members, especially column members, confined concrete should be modeled differently than unconfined concrete to account for enhancements in strength and strain capacities.

For this study, moment-curvature analysis was carried out using a computer program called RCMC (Reinforced Concrete Moment Curvature) which was developed by Webhe and Saiidi (Ref. 44) at the University of Nevada, Reno. The program computes the moment and curvature for a concrete section at different values of concrete strains while incorporating the effect of axial load. It assumes that the axial load is applied to the center of the cross section.

To perform the RCMC analysis, the properties of the reinforcement and the confined and unconfined concrete materials were needed. Basic properties of the concrete and steel were taken according to the recommendations in Caltrans SDC, Section 3.2.

The Hognestad model (Ref. 32) was used for the unconfined concrete stress-strain relationship, whereas Mander's model (Ref. 26) was used to model the confined concrete for the column section. For the two-way hinge sections, the confinement characteristics are subject to judgment because the section is highly confined by the rigid head and the column core section as well as the additional confinement provide by the spiral of the hinge itself (Ref. 19 and 39) There was no codified method available that could be referred to in order to calculate the confinement criteria for such situation. A rational method to define the hinge confinement properties was assumed in the study, details of which are described in Section 5.3.3. Table 2-5 summarizes the material property for the steel and concrete.

The parabolic strain hardening model was used to model the stress-strain relationship of the steel. The curve is shown in Fig. 2-12. The model consists of three segments. The first segment represents the elastic range of the steel with a constant modulus of elasticity of steel, E. The second segment (segment 1-2) corresponds to the yield plateau. The third segment (segment 2-3) represents the strain hardening curve recommended by Priestley et al. (Ref. 33) defined by the following equation:

$$f_s = f_y\left(1.5 - 0.5\left(\frac{0.12 - e_s}{e_{su} - e_{sh}}\right)^2\right) \qquad (2\text{-}7)$$

Where

f_s = steel stress,

f_y = steel yield stress,

? ε_{sh} = strain at beginning of strain hardening, and

? ε_{su} = ultimate tensile strain.

The M-ϕ curves were idealized as bilinear models for each specimens column and hinge sections (Fig. 2-13 through Fig. 2-21). The elastic portion of idealized curve passes through the M-ϕ point that corresponds to the first reinforcement bar yield. The ultimate points in the actual and idealized curves coincide. In addition, the idealized post-yielding segment is obtained by balancing the areas between actual and the idealized M-ϕ curves while forcing the branch to pass through the ultimate point. The coordinates of the idealized curves are shown in Table 2-6 for all the specimens.

2.6.2 Lateral Force-Displacement Analysis

To characterize the dynamic hysteresis force-displacement response, a backbone curve based on the monotonic force-displacement response is needed. Therefore, the moment curvature relationships need to be converted to force-displacement curves. Simple methods using the moment area theorem and an assumed plastic hinge length are often applied.

Components that contribute to the top displacement of the reinforced concrete column are assumed to be due to bending along the column height, shear, and fixed end rotation resulting from slip of the longitudinal reinforcement out of the joint (yield penetration) at the fixed end. Figure 2-22 shows a cantilever column subjected to a lateral load. Approximate shapes of the slip (Δ_s), shear (Δ_v) and bending (Δ_b) deformations along the column length are shown. Using a flexibility-based approach, the top displacement is the sum of the three components, as indicated by Equation 2-8.

$$\Delta = \Delta_b + \Delta_s + \Delta_v \tag{2-8}$$

Normally, the force-deflection analysis is carried out for a cantilever case where one end of the member is fixed, without any degree of freedom, and the other end is completely free. Since the direction of the applied lateral force or displacement remains in one plane, the free end has three degrees of freedom: lateral displacement, vertical displacement, and rotation around the axis normal to the force plane. In case of a member bent in double-curvature where the two ends are fixed, to obtain the top deflection, the column may be divided into two single-curvature cantilever columns (top column and bottom column). The boundary between the two cantilevers is where the column moment inflection point is located. At this specific location the two column deflection slope match each other when they come together. The column inflection point can be located using the yield moment capacity of the “top column” and “bottom column” assuming that both cantilevers reach their yield moment under the same load. Figure 2-23 illustrate the above discussion. As a result, the top displacement of a double curvature column is the sum of the six components from the “top column” and the “bottom column”, as indicated by the following equation.

$$\begin{aligned} \Delta &= \Delta_{top-column1} + \Delta_{bottom-column2} \\ \Delta &= \Delta_{top-b} + \Delta_{top-s} + \Delta_{top-v} + \Delta_{bottom-b} + \Delta_{bottom-s} + \Delta_{bottom-v} \end{aligned} \tag{2-9}$$

For an ideal cantilever column with zero moment at the top, the deformation at yield is calculated as follows:

$$\Delta_y = \Delta_{b(y)} + \Delta_{s(y)} + \Delta_{v(y)} \tag{2-10}$$

Where

$\Delta_{b(y)}$ = flexural deformation at yield

$\Delta_{s(y)}$ = bond slip deformation at yield

$\Delta_{v(y)}$ = shear deformation at yield

The yield deflection Δ_b due to flexure for cantilever columns can be calculated by the following equations:

$$\Delta_{b(y)} = \int_0^l fx\,dx = \frac{1}{3} f_y l^2 \tag{2-11}$$

Where

l = cantilever column height,

ϕ, ϕ_y = curvature, and curvature at effective yield, and

x = section location along column height.

The yield deflection Δ_s due to bond slip can be calculated using the modified Wehbe and Saiidi method (Ref. 44). The modification was applied to the formulation of the bond slip yield rotation. As a result, the yield rotation is directly calculated from the effective yield curvature instead of using the yield points of the calculated moment-curvature relationship. The modified equations are listed as follows:

$$\Delta_{s(y)} = q_{s(y)} l \tag{2-12a}$$

$$q_{s(y)} = f_y f_y d_b \Big/ 8u \tag{2-12b}$$

$$u = 20\sqrt{f_c'} \Big/ d_b \le 5.5(MPa) \qquad u = 9.5\sqrt{f_c'} \Big/ d_b \le 800(psi) \tag{2-12c}$$

Where

l = cantilever column height,

d_b = longitudinal bar diameter,

$\theta_{s(y)}$ = rotation at fix end due to bond slip at yield,

f_y = longitudinal bar yield stress,

f'_c = concrete compressive strength, and

u = average bond strength.

Park and Paulay (Ref. 32) developed expressions for the shear stiffness of beam elements with diagonal cracks accordance with truss action. This expression was adopted to calculate the cantilever column deflection due to shear. The equations are shown as following:

$$\Delta_{v(y)} = V_y l \Big/ K_{v,45} \tag{2-13a}$$

$$K_{v,45} = E_s b_w d r_v \Big/ 1 + 4n r_v \tag{2-13b}$$

Where

l = cantilever column height,
V_y = applied shear force at yield,
$K_{v,45}$ = shear stiffness for cracked members of a unit length,
ρ_v = shear reinforcement ratio = A_v / sb_w,
A_v = area of shear reinforcement,
b_w = section width,
s = spacing of shear reinforcement,
n = modular ratio = E_s / E_c,
E_s = elastic modulus of shear reinforcement,
E_c = Young's modulus of normal weight concrete, and
d = effective section depth.

The equivalent lateral force capacity V can be calculated from the moment curvature analysis results:

$$V_{(yield,ultimate)} = \frac{M_{(yield,ultimate)}}{l} \tag{2-14}$$

Where

l = cantilever column height,
$M_{(yield, ultimate)}$ = the effective yield and ultimate moment for M-ϕ analysis,
$V_{(yield, ultimate)}$ = lateral force at yield and ultimate.

The post-yield bending response of a reinforced concrete member is highly nonlinear. In addition to bending, the force-displacement model must also include contribution of the other components. In some cases, a more approximate method may be desirable to expedite the assessment of the force-displacement response. A widely used simplified model is to use an estimated plastic hinge to determine plastic deformations. As a result, the ultimate deformation can be calculated as the summation of the deformation at yield and plastic deformation as follows:

$$\Delta_u = \Delta_{b(y)} + \Delta_{v(u)} + \Delta_p \tag{2-15}$$

Where

$\Delta_{b(y)}$ = flexural deformation at yield
$\Delta_{v(u)}$ = shear deformation at ultimate

$$= \Delta_{v(u)} = V_u l \Big/ K_{v,45} \tag{2-16}$$

Δ_p = plastic deformation
V_u = applied shear force at ultimate

The plastic deformation of the cantilever column, with plastic rotation assumed to be concentrated at mid-height of the plastic hinge, is calculated as follows:

$$\Delta_p = q_p \left(l - \frac{l_p}{2} \right) \tag{2-17}$$

Where

l = cantilever column height,

l_p = plastic hinge length,
θ_p = plastic rotation = $(\phi_u - \phi_y)l_p$,
ϕ_u = ultimate curvature from moment-curvature relation, and
ϕ_y = effective yield curvature from moment-curvature relation.

Many empirical plastic hinge length models have been proposed in the past. In this study, the method by Priestley et al. (Ref. 33) was used as the baseline for analysis. The Priestley method was derived using experimental results of reinforcement bridge piers. The equations form the basis of method used in ATC32 report (Ref. 5). It has two components in the expression, the 1st term mainly accounts for column bending after yield, and the 2nd term accounts for the bond slip before and after yield.

For regular columns, the plastic hinge length l_p is defined as following:

$$l_p = 0.08l + 0.15 f_y d_b (ksi)$$
$$l_p = 0.08l + 0.022 f_y d_b (MPa) \quad (2\text{-}18)$$

Where

l = cantilever column height,
d_b = longitudinal bar diameter, and
f_y = longitudinal bar yield stress.

For the column with a reduced section detail at fixed end, the plastic hinge length l_p is defined as following:

$$l_p = g + 0.3 f_y d_b (ksi)$$
$$l_p = g + 0.044 f_y d_b (MPa) \quad (2\text{-}19)$$

Where

g = gap thickness between the column and support.

Despite the advantage, the pure Priestley method has limitations. The column shear deformation was not included. The method was originally intended for use in the failure analysis of bridge columns and in some cases the ultimate deflection is under estimated.

The calculated force deflection curves for the five specimens are plotted in Fig. 2-24, and the detail calculated values are listed in Table 2-6.

2.6.3 Dynamic Analysis

Although the static force-displacement analysis can predict the maximum response (maximum lateral force and displacement), it can not predict the structure response due to increasing dynamic excitations. To predict these effects and select the input ground motion as well as the testing protocol, a dynamic analysis by RC-Shake was performed for all five specimens.

Dynamic analysis program RC-Shake was developed by Laplace et al. (Ref. 21). It is a nonlinear single-degree-of-freedom analysis program. RC-Shake incorporates the equation of motion for the mass rig system used at the UNR Large Scale Structural lab including earthquake amplitude scaling and many shaking table parameters. The equation of motion is solved using the Newmark Beta time-step method.

In this study, a hysteresis models for reinforced concrete called the QHyst develop by Saiidi and Sozen (Ref. 36) was applied. The QHyst model is a stiffness degrading model that includes pseudo-bond slip effects. The primary curve of the model is a bilinear curve with an ascending post-yielding branch, and the stiffness degradation is accounted for at unloading and load reversal. In order to run the program with QHyst model, the column elastic stiffness, post yield stiffness and the yield force were required. These parameters were obtained from the bilinear lateral force-displacement curves described previously. A damping factor of 5% along with an unloading Beta factor of 0.25 was used in the analyses. The yield and ultimate lateral force were calculated using Equation 2-14.

Figure 2-25 and Figure 2-26 show the earthquake records (El Centro record and Northridge Sylmar record) used as input motion in the dynamic analysis of the five specimens. The time scale factor was applied to these motions in order to take into account the scale effect and the difference between the inertial mass and the mass associated with the axial load (see Section 2.4.1). The selection of the earthquake motion for the test was based on two specimens (THD-1 and THD-2), these two were scheduled to be tested first. A comparison of the dynamic analysis results for the two specimens is listed in the Table 2-7. The Sylmar record was selected based on the maximum displacement ductility demand. RC-Shake force-displacement hysteresis curves for specimens THD-1 and THD-2, subject to the Northridge Sylmar record, are shown in Figs. 2-27 and 2-28. In order to allow for comparison of response among all specimens, the Sylmar record was also selected as the input motion of the remaining three specimens.

The testing protocols for each specimen were developed based on the dynamic response obtained from RC-Shake with the estimated properties of the specimen. Small increments of Sylmar record were applied to the specimens to determine the elastic response and to find the effective yield point. Once the effective yield point was identified, the amplitude of the input motion was increased until failure. More discussion can be found in sections 3.5 and 3.6, regarding the input ground motion and testing sequence.

2.7 Measured Materials Properties

2.7.1 Steel Reinforcement Properties

All the reinforcement except the smooth welded wire of hinge spiral were specified as grade 60 ASTM 706 steel. Three samples of different size reinforcement were tested monotonically with strain rate of approximately of 10^{-4} per second using an MTS testing machine at the UNR Large Scale Structures lab. The resulting stress-strain relationships are shown in Fig. 2-29 through Fig. 2-34. Figure 2-29 and 2-30 show a typical stress-strain relationship for the W2.1 smooth wire and #3 column spiral reinforcement. No clear yield point could be found from these curves. The 0.2% offset method described in ASTM A370 Section 13.2.1 was used to determine the effective yield strength. Table 2-8 presents the average values of the yield strength, the ultimate strength, strain at the beginning of strain hardening and ultimate tensile strain of the sample reinforcement for all the specimens.

2.7.2 Concrete Properties

The specified concrete compressive strength was 34.5 MPa (5000 psi) with 9.52 mm (3/8 in.) maximum aggregate size. Compressive strength tests were performed for each batch of concrete at 7, 14 and 28 days after casting, and additional cylinders were tested on the day of testing. In each case, three 150 mm by 300 mm (6 in. by 12 in.) cylinders were tested monotonically, and the average results are listed in Table 2-9 for footing, column and hinge, respectively.

CHAPTER THREE

EXPERIMENTAL PROGRAM

3.1 Introduction

This chapter discusses the specimen construction procedure, the test setup of the shake table experiments, the details of the instrumentation used to collect data as well as the shake table input motions and the testing protocols. Sections 3.2 and 3.3 describe the construction procedure for the specimens and the test setup. The purpose and location of various instruments used to collect the data are discussed in Section 3.4. The ground motions used in the tests are presented in Section 3.5, while Section 3.6 describes the testing sequence for all five specimens tested in this study.

3.2 Construction

All five specimens were constructed at James E. Rogers & Louis Wiener Large-Scale Structures Laboratory at the University of Nevada, Reno. The columns were built in two groups. Specimens THD-1 and THD-2 were designed and constructed first (Group 1). Approximately six months after testing of the first two models, the remaining three models (Group 2) THD-3, THD-4 and THD-5 were designed and constructed. The design of these three was affected by the experimental results from the first two specimens.

The construction procedure and sequence for all five specimens was identical. The construction site was prepared by cleaning and leveling the casting slab, and setting up the wooden platform for the footing bottom as well as the footing form. Meanwhile, column rebar cage and hinge rebar cage were fabricated in the reinforcement shop, and shipped to the UNR site. The strain gauges were then installed at critical locations on the longitudinal and lateral reinforcement. Heat shrink plastic tubing of different diameters was used to protect the strain gauge wires against damage during concrete casting.

The lower layer of the footing reinforcement was first laid in the bottom forms, the column cages were then installed in the middle of the footings, and were tied down to the bottom reinforcement layer (Fig. 3-1). PVC pipes were installed vertically to provide holes extending through the footing. These holes were needed for attaching the specimen to the shake table simulator platform and letting the two axial force rods pass through the footing. Four vertical hooks were installed in the footing for each specimen to allow lifting of the specimens. The top layers of reinforcement were then placed and tied in the footing along with the vertical stirrups (Fig. 3-2). The footing in each group of specimens was cast from the same ready mix concrete batch. Test cylinders, 152 mm (6 in.) in diameter and 305 mm (12 in.) in height, were taken from all the concrete batches. The footings were then covered and cured for several days.

The construction of the column form was started at least three days after footing concrete was poured. The joint area at the column-footing interface was

cleaned in preparation for casting the columns. The hinge rebar cages and column forms were then put in place (Fig. 3-3), followed by the installation of 8 mm (5/16 in.) and 4.76 mm (3/16 in.) diameter threaded rods that were inserted transversely into the column to a depth of approximately 76.2 mm (3 in.) in order to attach displacement transducers for measuring the curvature distribution along the column plastic hinge zone as well measuring the shear slippage at hinges. The columns in each group were cast from a single concrete batch. The columns were then cured for at least 7 days before the formwork for hinge and loading head started.

The interfaces between the hinge and column was cleaned in preparation for casting of the two-way hinge and loading head (Fig. 3-4). Hinge and head forms were then installed and put in place. The bottom layer reinforcement in the loading head was first laid in the forms, and then PVC pipes were installed horizontally to provide holes extending through the head. The holes were needed for attaching the link from the mass rig to the specimens. Finally, the top layers of head reinforcement were placed and tied along with the vertical stirrups (Fig. 3-5). The hinges and the head were then cast monolithically. Hinges and heads in the same specimen group were cast from the same concrete batch. The specimens were then covered and cured for 14 days before their formwork was removed. Figure 3-6 shows the specimens just after the forms were removed.

3.3 Test Setup

The typical system used for single column shake table test at the UNR Large-scale Structural Laboratory consisted of a MTS shake table, a separate inertia mass system (Mass Rig) and the axial load system (Fig. 2-4). The mass rig is an eight pin space frame with concrete blocks placed on its deck. These concrete blocks combined with the effective inertial force of the mass rig frame provide the inertia mass applied to each specimen. Different number of concrete blocks can be assembled in order to meet the inertial mass requirement for each test. The mass rig was connected to the specimen through a horizontal link (Fig. 2-4), thus the inertia lateral force could be transferred to the specimen. The axial load system consisted of a steel spreader beam placed at top of the specimen, two Enerpac 60 kip (30 ton) hole rams, a Reddick accumulator, two load cells and two high strength steel threaded rods that extended from the rams through the footing and anchored to the base of the footing (Fig. 2-4). The axial load generated by two rams was transferred to the specimen through the spreader beam which was mounted on top of the head. The axial load was kept constant by the Reddick accumulator connected to the ram. The load was monitored through the two load cells between the ram and spreader beam.

In order to test specimens in double curvature, increasing the shear demand while reducing the flexural demand, a double swiveled link was used at the top of the column to transmit the lateral load from the mass rig and to restrict rotation of the loading head. The specimens were set with two-way hinges on the top of the column. Since the specimen was loaded in double curvature, the moment and shear demand for the column and hinge were the same as in the

prototype column where the hinge was at the base of the column. The footing was rigidly attached to the deck of the shake table using prestressing rods to achieve a fixed support. The specimen footing had 14 holes matching the location of the tie-down holes in the shake table deck, which form a 10 x 10 square grid with a spacing of 305 mm (12 in.), A 38 mm (1.5 in.) layer of non-shrink grout was placed between the footing and the shake table deck to provide a smooth contact surface in order to ensure a uniform distribution of bearing stresses. The footing was then attached to the shake table with 14 steel threaded rods. Figure 3-7 shows the side view of the setup.

Identical test setups were used for specimens THD-1, THD-3 and THD-5. The actual test setup is shown in Fig. 3-8. Four concrete blocks were placed on the mass rig. The total inertia mass was 445 KN (100 kips) that come from the weight of four concrete blocks (89 KN/ 20 kips each) plus the effective mass of the mass rig frame and other attachments and hardware. The axial load 445 KN (100 kips) was applied through the rams to match the inertia mass. Figure 3-9 shows the test setup for specimen THD-2. Two concrete blocks were used in this case. The total inertia mass was 267 KN (60 kips) instead of the 445 KN (100 kips) for the previously described three specimens. In THD-4 no axial loads were applied to simulate the case in which the overturning moment in a two-column bent has cancelled the gravity axial load, but the inertial mass was kept the same as that in THD-1, THD-3, and THD-5. Four concrete blocks were used for this test.

3.4 Instrumentation

An extensive instrumentation scheme was used to monitor the global response of the specimen, as well as the local deformations and strains at selected locations. More than 100 data channels were used in each of the shake table tests. Several types of instruments were used, including displacement transducers, accelerometers, load cells and strain gauges. The data were recorded at a rate of 100 sample per second. More detailed information on the instrumentation is presented below. A complete listing of all the instruments used and the distribution of the channels is provided in Table 3-1.

3.4.1 Shake Table Instrumentation

A shake table at the University of Nevada, Reno James E. Rogers and Louis Wiener Large-Scale Structures Laboratory was used to conduct the column tests. The table measures 4.3 m x 4.5 m (14 ft x 14.6 ft) in dimensions, and is equipped with a 2-degrees of freedom control system. The accelerations are monitored through four accelerometers placed at the four sides of the table, and four displacement transducers acting along the outer horizontal actuators (two in each direction). Those measurements allow the computation of acceleration, velocity and displacement components in 2 horizontal degrees of freedom.

3.4.2 Accelerometers

Accelerations were directly read by accelerometers mounted at critical locations on the specimen. A Kinematics FBA-11g accelerometer was used to

measure the horizontal acceleration at the top of the specimen. It was located at the end of the horizontal link next to the specimen head. The total lateral load applied on the column consisted of the link force plus and inertial force due to the mass of the link connection, the tributary specimen mass, and the axial loading system hardware. The measured acceleration at the top of the specimen was applied to calculate the inertial force due to these additional masses.

3.4.3 Lateral and Axial Loads

The lateral load was measured by two 667 KN (150 kip) Lebow load cells that were attached to the double swiveled links. These load cells capture the lateral force due to the mass rig inertial force and the mass rig P-Δ force due to the overturning effect, but does not capture the additional inertial force from the swiveled link system, the axial load system hardware, and the tributary mass of the specimen itself. The accelerometer placed at the top of the specimen and the additional mass were used to calculate the lateral inertial force not captured by the load cells.

The vertical axial load in the specimen was monitored by two load cells, Sensotec Model 41 (445 KN / 100 kips) and Model 43 (889 KN / 200 kips). The load cells were located in line with the threaded rods that were pre-stressed to provide the axial load.

3.4.4 Lateral Displacement Transducer

Global displacement were directly measured by linear potentiometers, Temposonic LA-Series 91 cm (36 in), that were installed on stiff instrumentation frames located off the shake table. Multiple potentiometers measured displacements at the top and bottom on the loading head. Other potentiometers monitored the lateral displacements at several locations along the column height. Some of the locations corresponded to the rods used for curvature measurements. These measurements were used to compute the relative displacements and the deflected shape of the column. Shear deformation could also be estimated by subtracting deformations obtained through curvature reading using the curvature instruments on the face of the columns.

The deflection of the hinge was measured by two additional displacement transducers (Novotecknik TR-100). They were horizontally mounted between the top of the column and bottom of the head; therefore, the relative displacement between these two was captured. This displacement provided data on the hinge horizontal deformation (Figs. 3-11 to 3-15).

The displacement of the shake table was measured using displacement transducers located along the table actuators as discussed in Section 3.4.1. The displacement of the footing was monitored by additional displacement transducers in the event of slip of the specimen relative to the table. The location and labels for various displacement transducers are shown in Fig. 3-11 through Fig. 3-15.

3.4.5 Strain Gauges

Strain gauge series YFLA-2-5 (rated to measure large post yield strains) distributed by Texas Measurements were installed on the longitudinal and transverse reinforcement to monitor strain histories during the testing. The potential critical zones, such as the column and hinge plastic hinge region as well as reinforcement development length range, were selected as the locations for strain gauges. Figures 3-16 through 3-20 show the locations and designations of the strain gauges.

3.4.6 Curvature Transducers

A series of Novotechnik TR-50 (50 mm (2 in)) displacement transducers were used to measure relative displacements between different sections along the height of the column. The transducers measured the displacement between 5/16th (8 mm (5/16 in)) diameter rods crossing the section in the plastic hinge region. The rods were installed during construction. Table 3-2 and Figs. 3-11 through 3-15 show the coordinates and configuration of the curvature transducers for each specimen. Those measurements were used to estimate the average curvatures and axial deformation along the specimen height.

The average strain at each location was calculated from the measured deflection divided by the gauge length. Once the average strains from both side of the specimen at same section level were calculated, then the average curvature over the gauge length was calculated as follows:

$$f_i = \frac{e_{iL} - e_{iR}}{D + X_{iL} + X_{iR}} \qquad (3\text{-}1)$$

Where:

ε_{iL} = average strain in level i at left side of the specimen,
ε_{iR} = average strain in level i at right side of the specimen,
X_{iL} = distance from instrument to column surface at level i on the left side of the specimen,
X_{iR} = distance from instrument to column surface at level i on the right side of the specimen, and
D = diameter of the specimen section.

The curvature instruments can be used to calculate the specimen deflection due to the flexure and bond slip by integrating the curvature using the moment-area theorem. The results capture the total deflection less the shear deformation.

3.4.7 Panel Instruments

The panel zone instruments were used in addition to the Temposonic (LA-Series) displacement transducers for measuring the lateral deflection of the specimen. The panel zone instrument plans are shown in Figs. 3-11 through 3-15. Each panel consisted of 5 Novotecknik displacement transducers that allow measurement of total displacement at the corner of each panel. Although shear deformation of the specimen can not be directly computed from these instruments due to the influence of flexure and bond slip rotation, shear deformation can be

estimated by subtracting the deformations obtained from curvatures from the nodal deflections calculated based on panel instruments.

To calculate panel deflection, a kinematic matrix [A] was formulated using the panel zone instrument dimensions (Table 3-3). Since the relative instrument deflections {γ} were recorded for each time step, the relationship between the kinematic matrix, instrument vector, and the panel displacements can be listed as:

$$\{g\} = [A]\{\Delta\} \tag{3-2}$$

Where

[A] = Kinematic matrix formulated using the panel zone coordinates,

{γ} = relative deflection measured by panel zone instruments, and

{Δ} = absolute displacement at the panel zone node.

The absolute displacement at each panel zone node can be solved as the following:

$$\{\Delta\} = [g]\{A\}^{-1} \tag{3-3}$$

3.5 Input Motions

As mentioned, all five specimens were subjected to the horizontal component from a scaled ground motion recorded at the Sylmar County Hospital parking ground floor during the 1994 Northridge Earthquake (Fig. 2-26). This motion was selected because it could be amplified to fail the column specimens without exceeding the shake table limits (Table 2-3).

Earthquake motions considered for this study included the 1940 Imperial Valley Earthquake (El Centro) and the 1994 Northridge Earthquake (Sylmar). Both earthquake motions were analyzed on THD-1 and THD-2 using RC-Shake. The earthquake records were amplified in successive runs until the shake table limit was reached. The duration of the earthquake was scaled by $\sqrt{l_r}$ as dictated by the modeling rules (Table 2-2). The length scale l_r of 1/3 for this study produced a time scaling of 0.58. Hence, the time step between the recorded accelerations for the original ground motion was multiplied by 0.58.

Dynamic analysis under scaled ground motions were previously discussed in Section 2.6.3. Based on the analysis, the Sylmar record produced the higher amplitude specimen displacement compare with El Centro motion (Table 2-6); it reached a maximum displacement ductility of 7.2 and 8.7 for THD-1 and THD-2, respectively. The corresponding values under the El Centro record were only 4.4 and 6.7. As a result, the Sylmar motion was selected for this study.

The Northridge Earthquake had a moment magnitude of 6.7. The Sylmar record was recorded at Sylmar, at 9.9 km (6.2 miles) from fault rupture on firm alluvium soil condition with a peak acceleration of 592.6 cm/s^2 (0.6 g). The typical time scaled Sylmar acceleration history used for testing is shown in Fig. 3-21, and the time scaled elastic response spectrum is shown in Fig. 3-22.

3.6 Testing Protocols

The testing protocols for each specimen are shown in Table 3-4. For each of the runs, the desired peak acceleration is also included in the table. The testing

sequence was developed based on the dynamic response obtained from the program RC-Shake with the estimated properties of the each specimen. The shake table was tuned before testing each specimen to minimize the difference between the target and the achieved table accelerations. A series of low level tests were then performed that consisted of a small fraction of the record as input to the shake table to determine the elastic response and to find the effective yield point. Once the effective yield point was identified, the amplitude of the input record was increased until failure. Testing was stopped when the lateral resistance of the column degraded significantly or laboratory safety became a concern. Notice that in order to allow for comparison among specimens, the testing protocols for all specimens were kept approximately the same. Intermittent free vibrations tests were conducted to detect changes in the effective period of the specimen after the runs. The Fourier amplitude spectra from these tests were computed to identify the frequency and damping of the specimens.

CHAPTER FOUR

EXPERIMENTAL RESULTS

4.1 Introduction

This chapter describes the results obtained from the tests of the five two-way hinge specimens. For each specimen, the response and damage occurring during each run are described in Section 4.2. Global response measures such as table acceleration performance, specimen dynamic properties, lateral force- displacement relationships, and curvature profile are discussed in Section 4.3. Section 4.4 presents local response measures such as hinge shear slippage and rotation, hinge and column moment demands as well as rebar strains.

4.2 Observed Specimens Responses

Specimen THD-1

Under 0.5 x Sylmar (Peak-Ground-Acceleration, PGA=0.3g) motion, visible flexural cracks were formed at the base of the column (Fig. 4-1). At 1.25 x Sylmar (PGA=0.75g), the first shear crack appeared at the hinge and concrete started to spall at the base of the column (Fig. 4-2). Hinge concrete started to spall during 1.5 x Sylmar (PGA=0.9g) together with exposure of the column spirals at the base (Fig.4-3). Right after the motion of 2.25 x Sylmar (PGA=1.35g), a crack was formed at the bottom of loading head and extended to where the hinge and loading head meet. The hinge region deteriorated extensively, with spalling and permanent sliding and rotation. The deterioration increased as the input motion increased (Fig. 4-4). THD-1 failed at 2.875 x Sylmar (PGA=1.725g). The hinge and a small part of the column edge shear off from the top of the column (Fig. 4-5). Table 4-1 summarizes the observed performance of THD-1.

Specimen THD-2

Visible flexural cracks were seen at the base of the column after 0.25 x Sylmar (PGA=0.15g) event. At 0.75 x Sylmar (PGA=0.45g), first hinge crack was formed together with yielding of the longitudinal rebar at the column base (Fig 4-6). Under 1.5 x Sylmar (PGA=0.75g), spalling took place at both the hinge and column base (Fig. 4-7). After the motion of 2.0 x Sylmar (PGA=1.2g), a wide crack was formed at the bottom of the loading head and extended to the intersection of the hinge and head, along with extensive spalling at the two-way hinge (Fig. 4-8). At 2.25 x Sylmar (PGA=1.35g), hinge gap closed due to the significant hinge rotation. The head hit the edge of the column top and caused minor damage (Fig. 4-9). At 2.5 x Sylmar (PGA=1.5g), combined with the exposure of the hinge spiral, hinge gap closed again. Figure 4-10 shows the hinge after this run. Based on the observation and supplemental studies after the test, it was believed that after this event; the hinge strength was provided mainly by the dowel action. The deterioration substantially increased at the event of 2.625 x Sylmar (PGA=1.575g) as the hinge gap was reduced due to the crushing of the hinge concrete (Fig. 4-11). The test was stopped after 3.0 x Sylmar (PGA=1.8g) when the specimen

experienced large permanent offset between the loading head and the column. Table 4-2 summarizes the observed performance of specimen THD-2 during the testing.

Specimen THD-3

This specimen was designed to fail in flexure and not hinge shear. At 0.25 x Sylmar (PGA=0.15g), visible flexural cracks appeared at the base of the column. First hinge crack was seen at motion of 0.75 x Sylmar with PGA=0.45g (Fig. 4-12). Under 1.25 x Sylmar (PGS=0.75g), spalling was seen at both the hinge region and column base; while cracks were found at the bottom of the loading head close to the hinge-head joint (Fig. 4-13). At 1.75 x Sylmar (PGA=1.05g), due to the severe spalling of the clear cover at the column base, the longitudinal reinforcement of column was exposed (Fig. 4-14). Hinge gap closed at 2.0 x Sylmar (PGA=1.2g) due to significant rotation at the hinge. At 2.25 x Sylmar (PGA=1.35g), the hinge gap was reduced due to crushing of concrete by the vertical load (Fig. 4-15). THD-3 failed at motion of 2.5 x Sylmar (PGA=1.5g) in flexure at both ends of the specimen. Four longitudinal rebar ruptured at the base (Fig. 4-16), and at least one longitudinal hinge bar ruptured (because the hinge gap is set back not all the longitudinal hinge bars could be observed). Table 4-3 summarizes the observed response of specimen THD-3 after each run.

Specimen THD-4

This specimen had no axial load applied to the specimen to simulate the effect of uplift due to overturning moments. The first crack was seen at 0.1 x Sylmar (PGA=0.06g). At 0.5 x Sylmar (PGA=0.3g), a diagonal shear crack appeared at the hinge (Fig. 4-17). Concrete spalling was seen in the hinge under 0.75 x Sylmar with PGA=0.45g (Fig. 4-18). At the next motion of 1.0 x Sylmar (PGA=0.6g), the hinge spalled extensively, together with exposure of the hinge spirals. THD-4 failed at 1.25 x Sylmar (PGA=0.75g). The hinge longitudinal reinforcement fractured and the loading head was sheared off at the hinge and separated from the column (Fig. 4-19). Table 4-4 summarizes the observed performance of specimen THD-4 during the testing.

Specimen THD-5

In this specimen, the hinge diameter was relatively small (50% of the column diameter as opposed to 62.5% in the others). Flexural cracks were visible at the base of the column at 0.25 x Sylmar (PGA=0.15g). At 0.5 x Sylmar (PGA=0.3g), first hinge spalling was seen while a crack was developed at the base of the column (Fig. 4-20). Spalling took place at the base of the column at 1.5 x Sylmar with PGA=0.9g (Fig. 4-21). Under motion of 1.75 x Sylmar (PGA=1.05g), the hinge gap closed due to the large rotation at the hinge, together with the exposure of the spirals at hinge (Fig. 4-22). The loading head showed some twisting. At 2.0 x Sylmar (PGA=1.2g), more significant movement was seen due to the concrete in the smaller hinge gap crushing (Fig. 4-23). Based on the observation and follow up analysis, it is believed that after this event, dowel action took place at the shear plane of the hinge. The deterioration under 2.75 x Sylmar (PGA=1.65g) was quite substantial (Fig. 4-24). The permanent deformation was large, and the only connection between the head and column was the hinge

longitudinal rebar. The test was stopped after 3.0 x Sylmar (PGA=1.8g) because the specimen experienced large permanent deformation and at least one of the longitudinal bars ruptured at the column base (Fig. 4-25). Table 4-5 summarizes the observed performance of specimen THD-5.

4.3 Global Response Measures

4.3.1 Target and Measured Ground Acceleration

The shake table was tuned to reproduce the target earthquake acceleration history of a low-amplitude version of the Sylmar record. The tuning amplitude was kept sufficiently small to prevent any yielding in the columns. Because of the interaction between the table and the specimen, as the model enters the nonlinear range the tuning parameters change, and it is not always possible for the control system to retune the table. As a result differences are seen between the achieved and target motions.

A comparison of the achieved and target signals can be made using peak acceleration as well as elastic response spectra. The spectral ratios are better indicators for determining shake table performance than the PGAs. The PGA does not capture the frequency content of the motion and thus performance of the table in duplicating the response of interest. Nonetheless both parameters were calculated and evaluated. Tables 4-6 through 4-10 show the achieved and target value of peak acceleration and spectral acceleration for each shaking table motion. Target and achieved elastic response spectra are shown in Figs. 4-26 through 4-86. The program RC-Shake (Ref. 21) was used to calculate the elastic response using Newmark's Beta method and a damping ratio of 5%. The recorded table acceleration history for each motion was used to calculate the achieved spectra. Included in each response spectra comparison plots are the specimen effective periods. These periods were calculated using the chord stiffness (effective stiffness) of the specimens. The chord stiffness was found from the experimental results by dividing the force over the displacement at the point with the maximum lateral displacement.

Tables 4-6 through 4-10 also show the ratios of the achieved and target peak acceleration and spectral acceleration at the specimen effective period for all five specimens. The average ratios for PGA were 0.92, 0.96, 1.01, 1.18 and 0.98 for specimen THD-1 through THD-5, respectively. Over all, the correlation between the target and achieved peak accelerations was close. However, there were variations between the target and achieved response spectra. This was due to changes in shaking table parameters in the feedback loop of the table drive system. These discrepancies are generally more pronounced in the low period range of the spectra (T<0.3 sec.). The discrepancies have little impact on the potential specimen response because the effective period of the specimens for the runs of primary interest generally exceeds 0.4 sec.

Tables 4-6 through 4-10 list the ratios of achieved and target spectral accelerations. The average ratios were 0.82, 0.88, 0.96, 0.85 and 0.8 for specimen THD-1 through THD-5, respectively. The shake table performance was considered to be acceptable.

4.3.2 Specimen Dynamic Properties

Prior to testing each column and intermittently between successive shake table runs, a series of free vibration tests were performed to obtain the dynamic characteristics of the specimen. Square displacement waves were applied to the shake table that put the columns in vibration. These vibrations were of low amplitude to ensure that they do not cause additional damage in the specimens.

The response and decay in the amplitudes of the column response were used to estimate the period of vibration and damping properties at low deformations. By obtaining the Fouries spectrum of the free vibration, it was possible to approximate the fundamental period of the specimen. The recorded results from the accelerometer attached at the end of the swiveled link close to the specimen head were used for this purpose.

With fundamental period known, the following equation was used in order to calculate the stiffness of the specimen at the corresponding motion. Table 4-11 through 4-15 show the calculated periods and stiffness.

$$K = 4p^2 m / T^2 \qquad (4\text{-}1)$$

Where

m = specimen inertia mass

T = specimen fundamental period

Based on free vibration data, the equivalent viscous damping ratio was calculated using the decrement logarithmic method. The damping ratio can be calculated using Equation 4-2 (Ref. 10):

$$x \cong \frac{1}{2pj} In \frac{a_n}{a_{n+j}} \qquad (4\text{-}2)$$

Where

ξ = equivalent viscous-damping ratio

a_n = n^{th} specimen top peak acceleration values in the response history.

a_{n+j} = $(n+j)^{th}$ specimen top peak acceleration values in the response history.

j = number of the cycles

Tables 4-11 through 4-15 show the dynamic properties for all five specimens, including the period, frequent, stiffness and damping ratio based on the free vibration tests.

In general, the specimen fundamental periods and damping ratios increase with increasing damage. The increasing in the measured damping is as a result opening and closing of cracked section. The longer period reflect the reduction in stiffness as the specimen experiences larger degree of nonlinearity.

4.3.3 Axial Load Variations

The axial load system was discussed in Section 3.4.3. The variation of the axial load was controlled by an accumulator connected to the hydraulic jacks. The

target axial loads were 267 KN (60 kips) for specimen THD-2, 445 KN (100 kips) for specimens THD-1, THD-3 and THD-5. Due to the zero axial load requirements for specimen THD-4, the axial load system was not included in its test setup; therefore, specimen THD-4 is excluded from this discussion. The axial load system was connected to an accumulator to minimize the fluctuation of the axial load. Nonetheless some deviation from the target axial load occurred. To determine if the deviations were significant, the axial loads were monitored during each test. The measured axial load histories are shown in Figs. 4-87 through 4-90. The variation of the axial load is summarized in Table 4-16 for all specimens. The performance of the axial load system was satisfactory with a ratio of 97%, 98%, 95% and 100% between the averaged achieved and target loads for THD-1, THD-2, THD-3 and THD-5, respectively. The average applied load was determined by averaging the axial load data recorded during the complete loading history.

4.3.4 Column Top Acceleration Histories

The absolute acceleration history data measured by an accelerometer attached to the rigid link between the mass rig and loading head are shown in Figs. 4-91 through 4-95. These acceleration data were used to calculate the additional inertia force that was not captured by the load cell which was in line with the link system.

Peak absolute specimen acceleration, shown in Table 4-17, steadily increased for the motions up through the motions that caused significant yielding (1.25 x Sylmar, 1.5 x Sylmar, 0.75 x Sylmar, 0375 x Sylmar and 1.25 x Sylmar for THD-1 through THD-5, respectively). Subsequently, the peaks for each run fluctuated between a narrow range (0.87g to 1.02g, 0.75g to .94g, 0.45g to 0.69g, 0.33g to 0.42g and 0.72g to 0.98g for THD-1 thorough THD-5). The maximum acceleration of 1.02g occurred during 2.0 x Sylmar for specimen THD-1.

4.3.5 Lateral Force-Displacement Hysteresis Relationships

Figures 4-96 to 4-100 show the cumulative lateral load-displacement hysteresis loops for all five specimens. The horizontal deflection consists of the components due to 1) flexure deformation of the column, 2) bond slip rotation at both column ends, 3) horizontal slippage at the hinge and 4) shear deformation along the column height. The lateral effective force is the summation of the link load cell reading plus the calculated inertial force from the additional mass, such as the link, axial loading system and up part of the specimen, using the acceleration recorded at top of the specimen.

The hysteresis loops for all five specimens are very stable even at displacement ductility level of μ=6 which exceeds the Caltrans bridge column design target displacement ductility demand of μ=5. The lateral displacement ductility capacities were 7.1, 8, 8.6, 5.5 and 10.4 from THD-1 to THD-5 respectively. In calculating the ductilities, the yield displacement was established by using the equal energy (area) method. Detail discussions relating to idealize force-displacement curve are presented in Section 4.3.7.

The peak lateral force in THD-3 was controlled by the column and the hinge flexure capacity, as intended. The lateral load capacity of the other four specimens was limited by hinge shear resistance. All five specimens showed gradual loss of stiffness as the displacement amplitude increased.

Strength degradation was not observed in the response of THD-1 and THD-4 until sudden shear failure of hinge during the last run. However, strength degradation did occur in THD-2, THD-3 and THD-5 starting at moderate amplitudes. The strength performance of these three specimens was quite different. For THD-3, due to the flexure failure in both the column and the hinge, the capacity dropped by 49% at the end of the testing and as a result, the failure point was re-defined at where the lateral load decreased by 20% of the peak lateral force. Specimens THD-2 and THD-5 were damaged at the hinge by shear at first and the lateral strength dropped by 11% and 12%, respectively. Then the dowel action mechanism appeared to take over the response and the lateral capacity increased. Typically, the failure point and maximum load was defined at the point when the force drop and before dowel action occurred. All specimens except THD-3 showed considerable residual displacements.

Specimen THD-1

Figures 4-101 through 4-105 show an essentially elastic response for each motion with no noticeable loss in stiffness. Figure 4-106 shows the response for 1.25 x Sylmar. This response shows slight inelastic deformation and yielding of the column. Minor strength loss likely due to the hinge shear damage was seen during 1.5 x Sylmar (Fig. 4-107). A gain in strength was seen during 2 x Sylmar (Fig. 4-109) possibly due the hinge dowel action mechanism starting to control the response. The maximum lateral force was recorded during this motion. The final response for 2.875 x Sylmar is shown in Fig. 4-114. This motion caused a large drop in lateral load capacity and large permanent deformation due to the hinge shearing off the column. Overall, the THD-1 force-displacement hysteresis curves show that the stiffness degraded and the permanent deformation increased while the specimen went through the events. The lateral strength of THD-1 followed a classic “back-bone” shape with generally positive slope until failure occurred.

Specimen THD-2

Figures 4-115 to 4-117 show that the response during the first three runs was elastic. Figure 4-118 shows the response for 0.75 x Sylmar. This response began to show yielding and included some plastic deformation. Figure 4-124 shows strength loss likely due to the hinge shear damage. During the subsequent run (Fig. 4-126) the hinge dowel action mechanism led to an increase in the lateral capacity. This response also shows increased energy dissipation and a significant residual displacement. The final motion was 3.0 x Sylmar. The motion caused a large head slippage due to the hinge collapse. Overall, the THD-2 hysteresis curves showed stiffness degradation, as well as the significant shifting of the hysteresis loops, which indicates the large permanent displacement of the specimen.

Specimen THD-3

This specimen was designed to fail in flexure and not hinge shear. Figures 4-130 to 4-132 show the elastic response with stable stiffness. Figure 4-133 shows the response with inelastic deformation due to yielding. The response under 2.0 x Sylmar (Fig. 4-138) shows sudden strength increase attributed to gap closure. The maximum lateral force was recorded during this motion. Significant strength loss occurred in the final 2.5 x Sylmar motion due to the longitudinal bar rapture at the column and hinge (Fig. 4-140). Overall, the THD-3 hysteresis curves showed that the stiffness and strength degraded as the input acceleration amplitude increased. Also, the shifting of the hysteresis loops indicated permanent displacement at top of the specimen.

Specimen THD-4

Elastic response with stable stiffness can be seen in Fig. 4-141 and 4-142. Figure 4-143 shows the response with inelastic deformation and some pinching. Figures 4-144 to 4-147 show large energy dissipation with a gradual increase in the lateral load capacity. The maximum lateral force was recorded during 1.25 x Sylmar (Fig. 4-147). Significant strength loss occurred in the same motion due to the shear failure of the hinge. The THD-4 hysteresis curves show that the stiffness and strength degraded as the input acceleration amplitudes increased. Some permanent displacement is also evident. Compared with other specimens, the shear and displacement capacities are significantly lower due to the zero axial load.

Specimen THD-5

Figures 4-148 through 4-151 show a general elastic response for each motion with insignificant loss in stiffness. The response for 1.0 x Sylmar (Fig. 4-152) shows limited yielding. Figure 4-155 shows a sudden strength increase most likely due to the gap closure. After 1.75 x Sylmar, Fig. 4-156 shows some strength loss due to the hinge shear failure. Large energy dissipation along with residual displacement increasing was noticeable. Figure 4-157 shows the hinge dowel action mechanism started to control the response and the lateral capacity constantly increased. The final motion was 3.0 x Sylmar. This motion caused a large head slippage due to the hinge collapse along and large permanent deformation (Fig. 4-160). More extensive permanent deformation was observed under second repeated 3.0 Sylmar motion, the maximum lateral force was also recorded during this motion (Fig. 4-161). The THD-5 hysteresis curves show stiffness degradation and significant shifting of the hysteresis loops, which indicate the large permanent displacement of the specimen.

4.3.6 Force-Displacement Envelopes

An envelope of the cumulative force-displacement hysteresis curves was developed for each specimen based on the peak lateral forces with the corresponding displacements at all the runs. To determine the ductility capacity, it is necessary to define consistently a failure point. The data from the last test run does not necessarily constitute the failure point. Generally, the failure point for the envelope curve was assumed either by the peak displacement with corresponding force or at the displacement where the load was at 80% of the maximum force.

The measured peak forces with the corresponding displacements and the peak displacement with the corresponding forces at each motion are listed in Tables 4-18 through 4-22 for all the specimens. Figures 4-162 through 4-166 show the envelopes of the accumulated force displacement hysteresis curves for THD-1 to THD-5, respectively.

4.3.7 Idealized Force-Displacement Curves

To quantify the ductility capacity of the specimens, the measured envelopes (Figs. 4-167 to 4-171) were idealized by elasto-plastic curves. Because of the variation of the force-displacement curves, the approach to establish the elastic slope is on "trial and error" basis to find the best fitting curve. There are three basic ways to find the "1st yield point" of the column: a) taking the force-displacement point that corresponds to the first reinforcement bar yield, b) In some cases, the 1st yield point is not on the envelope, then taking the force corresponding to the first reinforcement yield and finding the corresponding displacement on the envelope using linear interpolation, and c) Taking ½ of the maximum force and finding the corresponding displacement on the envelope. The last method is useful especially when no strain data are available. Once the elastic slope is found, the effective yield point is established by using the equal energy (area) method, equalizing the area between the measured and the idealized curves to the point of defined failure. For the specimen THD-3, this was when the load dropped to 80% of the maximum load. The post-yielding slope is zero for this idealization.

Figure 4-167 through 4-171 show the envelopes and idealized elasto-plastic curves of force-displacement relationships for all five specimens.

Table 4-23 shows the measured values of peak displacement, displacement ductility and drift. The ductility was calculated based on the idealized elasto-plastic curves. The peak drift ratio achieved was 10%, 12%, 10%, 6% and 18% for THD-1 to THD-5, respectively.

4.3.8 Deflection Profiles

Horizontal displacements were monitored along the column height and the free end (Figs. 3-13, 3-14 and 3-15) in specimens THD-3, THD-4 and THD-5 using displacement transducers. The measured peak displacements for the three specimens are shown in Figs. 4-172 to 4-174 for all motions. Actual displacement measurements are indicated by markers. Some initial displacement cycles are not shown to avoid congestion. The upper two data points show the displacements immediately above and below the hinge. The large relative displacements between these two indicate the hinge horizontal deformation. It can be seen that the column (the segment below the hinge) profiles were nearly linear.

4.3.9 Panel Deformations

The displacements at the panel nodes were calculated using the measured relative deformations obtained from the Novotecknik transducers. The node deflection calculation procedure was described in Section 3.4.7. They were solved

at every time step. A Matlab subroutine developed for this study was used to solve the nodal displacements using the corresponding kinematic matrix.

Tables 4-24 to 4-28 present a comparison between the deflections at the top panel nodes and the column top deflection measured with the displacement transducer for the predominant direction of the motions. A relative narrow range from 82% to 118% was found between the panel zone deflections and the displacement recorded from transducer located at column top immediately below the hinge (hinge shear slippage was subtracted from the column head displacement).

4.3.10 Curvature Profiles

Novotecknik displacement transducers were used to measure curvature in the potential plastic hinge regions at the top and bottom of the specimen. The strain on each side of specimen was calculated by dividing the vertical displacement measured by each Novotecknik transducer and the gauge length. The curvature calculation procedure was presented in Section 3.4.6, the procedure assumes that the sections remained plane.

The curvature profiles for all five specimens are plotted in Figs. 4-175 to 4-179. The curvature points represent the average curvature over different gauge lengths for the dominant direction of the motion. Curvature measurements are plotted over the entire height. The initial motion responses show essentially a linear curvature distribution along the entire specimen height. Discrepancies in distribution at these small displacement levels may be due to instrument error. As expected, large motions reveal a nonlinear curvature distribution for all specimens. The top hinge shows much higher curvatures than the base of the column due to the small flexural capacity of the hinge section.

4.3.11 Flexural and Bond Slip Deformation

The curvature profiles were used to calculate the flexural deformation by integrating the curvature using the moment-area method. The curvatures were assumed to be constant over the corresponding gauge lengths. A linear distribution was assumed for the specimen middle range where no instruments were placed. The curvature profiles at the peak force at each run are shown at Figs. 4-175 to 4-179 for all five specimens. The flexural deformation was calculated only for the peak values of lateral force that correspond to the predominant direction of motion. Figure 4-180 through 4-184 show the force-flexural deformation for all the specimens. Additional rotation due to the bond slip at the both ends was included in the first set of the curvature instruments. Therefore, the flexural deformation calculated by these instruments includes a component from the bond slip effect that can not be uncoupled.

4.4 Local Response Measures

4.4.1 Hinge Shear Slippage

Two displacement transducers (NV-35 and NV-47 for THD-1 (Fig. 3-11), NV-36 and NV-47 for THD-2 (Fig. 3-12), TR100-4 and THD100-2 for THD-3 (Fig.

3-13), THD-4 (Fig. 3-14) and THD-5 (Fig. 3-15)) were installed to monitor sliding of the hinge. Figures 4-185 to 4-189 show the cumulative lateral load-slippage hysteresis loops for all five specimens, respectively. The data shown are the average of the measured data on the two sides of the hinge. The hinge horizontal deformation consists of components due to 1) horizontal slippage in the hinge, and 2) flexure deformation of the hinge. However, due to the extra small aspect ratio, the flexure deformations are negligible. The lateral effective force is the summation of the link load cell reading plus the calculated inertial force from the additional mass, such as link, axial loading system and top part of the specimen, using the acceleration recorded at top of the specimen. Notice Figures 4-186 and 4-189 for THD-2 and THD-5 are limited to certain runs due to data lose at end of the tests.

The hysteresis loops for all five specimens show a reasonable level of energy dissipation. The responses generally show strength degradation at larger amplitudes. In all specimens but THD-3 the degradation of strength is due to the deterioration of the shear strength of the hinge. In THD-3, however, flexural failure of the hinge and the column initiated the loss of strength. The curves in THD-4 show severe pinching effect due to the very low axial load. The clamping force in this specimen was small and hence, as the load cycled, large displacements occurred before the reinforcement was re-engaged and provided shear capacity.

Figures 4-190 through 4-194 show the hinge force-slippage envelopes. Due to different failure modes of the individual specimens, the peak lateral force for THD-3 was controlled by the column and the hinge flexural capacity. The lateral load capacity of the other four specimens was limited by hinge shear resistance. All other four specimens showed gradual loss of stiffness as the displacement amplitude increased.

Strength degradation was not observed in the response for specimens THD-1 and THD-4 until sudden shear failure at the end at the tests. Strength degraded in specimens THD-2, THD-3 and THD-5. The strength performance of these three specimens was similar. At the peak lateral force of 382 KN (85.8 Kips), 236 KN (53 Kips) and 277 KN (62.2 kips) with corresponding slippage of 1.04 mm (0.04 in), 1.24 mm (0.049 in) and 1.24 mm (0.049 in) for THD-1, THD-2 and THD-5, the hinge started to yield and lateral stiffness dropped significantly. In the next motion, the lateral strength dropped by 2%, 11% and 12%, respectively. Then the dowel action controlled the response, and the lateral capacity increased until the end of the tests. The maximum measured slippages for these three specimens are 33 mm (1.3 in), 39.4 mm (1.55 in) and 60 mm (2.36 in), respectively.

4.4.2 Hinge and Column Moment Demands

The moment demands at the column section at the column base and the hinge section at the top were calculated using the force recorded in the load cell attached to each link and the geometry, as well as lateral force due to additional mass. Figure 4-195 illustrates the locations of the links and the moment arms used to calculate the moments. The P-Δ effect due to the axial load and the weight of the head were included in the calculation of the moment demands for both locations. The moment demands were calculated at the same time as the values

of the forces used in the developing the envelopes in the predominant direction of motion. Figures 4-196 through 4-200 show the moments at the top and bottom of the specimens.

The inflection point for each specimen was found based on the moment diagram. Table 4-29 summarizes the distance of the inflection point from the bottom of the specimens. As expected, the inflection point was close to the top of the specimens because the moment capacity of the hinge was considerably lower than that of the column. The figures and table show the shifting of the inflection pint at each motion of every specimen. In general, the variation of the inflection points is relatively small.

4.4.3 Hinge Rotation

The hinge rotation was recorded by two displacement transducers placed at opposite sides of the hinge. The vertical instruments measuring the extension and compression, Δ_L and Δ_R of the hinge segment were placed at a distance of w. The rotation of the hinge segment is assessed using Equation 4-3:

$$q = (\Delta_L - \Delta_R) / w \qquad (4\text{-}3)$$

Figures 4-201 through 4-205 show the history of hinge rotations for generally all the motions. Under high amplitudes in specimens THD-2 and THD-5 the transducers were either removed or their limits were exceeded.

Figures 4-206 through 4-210 show the envelopes of the measured force-hinge rotation hysteresis curves for all five specimens. Under similar level of Sylmar motion, relatively high rotations were recorded in specimen THD-2 and THD-5 compared with the rest of the specimen due to the different level of applied axial load and smaller hinge section size.

4.4.4 Strains

A large number of strain gauges were mounted on longitudinal and spiral steel bars to provide data that can be used to trace the strain history at various locations in the specimen, and to correlate internal strains to observed damage and bar bucking or fracture. The numbers and positions of strain gauges on longitudinal and transverse reinforcement for the five specimens are shown in Figs. 3-16 to 3-20. At each run, the strain history of each gauge was recorded with the maximum reading limit of 0.2. The maximum measured strains generated at each motion were tabulated and classified into four groups according to the position of the strain gages. The 1st and 2nd groups were for the gauge on the column longitudinal and transverse reinforcement, respectively. The 3rd and 4th groups were for the gauges on hinge longitudinal and transverse reinforcement, respectively. All of these groups are shown in Tables 4-30 to 4-72 for all five specimens. From these tables, the maximum response of each run could also be shown.

Another way to examine the strain gauge data response was to study the strain histories. For each gauge in each specimen, the strain history was plotted. The strain histories plots of all gauges are shown in the appendices. Using these

figures, the behavior of each gage with loading could be examined. However, because strain gauges on reinforcement in the plastic hinge are likely to fail after few cycles before reaching the maximum level run at the end of the tests, their usefulness in tracing strain demands due to repeated excitations may be lost and inconsistent data will be recorded. As a result, the data, which was recorded after the strain gauge was broken, are removed for the strain history plots along with the maximum responses of these runs which are listed in Table 4-30 through 4-72. In the tables, the damaged data was shown as "NA" which means the data is not available.

Column Longitudinal Reinforcement

The maximum and minimum values of strains are summarized in Table 4-30 to 4-31, 4-37 to 4-38, 4-45 to 46, 4-55 to 56, and 4-64 to 65. Where strains passed yield, the strains are written in bold font. Column longitudinal reinforcement started to yield as early as 0.5 x Sylmar for THD-1, THD-2, THD-3, 0.25 x Sylmar for THD-4, and 0.5 x Sylmar for THD-5. The first yielding occurred at column bases. Yielding started to spread in the column reinforcement as the runs continue.

Column Spirals

The maximum and minimum values of strains are summarized in Tables 4-32 to 33, 4-39 to 40, 4-47 to 48, 4-57 to 58 and 4-66 to 67. Where strains passed yield, the strains are written in bold font. The spiral strains show relatively consistent strains along the column height. Yielding did not occur until the high level runs near the end of the tests. Recorded strains in the spirals were generally low.

Hinge Longitudinal Reinforcement

The maximum and minimum values of strains are summarized in Table 4-34 to 35, 4-41 to 42, 4-49 to 51, 4-59 to 61 and 4-68 to 70. Where strains passed yield, the strains are written in bold font. The longitudinal bars had strains below yield up to 0.5 x Sylmar for THD-1, 0.25 x Sylmar for THD-2, 0.25 x Sylmar for THD-3, 0.1 x Sylmar for THD-4 and 0.25 x Sylmar for THD-5. The strains at the hinge gaps exceeded yield in subsequent runs. Very large strains occurred after hinge shear damage was observed.

Hinge Spirals

The maximum and minimum values of strains are summarized in Tables 4-36, 4-43 to 44, 4-52 to 54, 4-62 to 63 and 4-71 to 72. Where strains passed yield, the strains are written in bold font. Yielding strain was recorded at 1.25 x Sylmar for THD-1, 2.25 x Sylmar for THD-2, 1.5 x Sylmar for THD-3 and THD-5. The spiral strains show relatively consistent strains during the series of increasing motion. The peak spiral strains in the hinges were relatively large. Most of the gauges located near the hinge throat were damaged during the late stage of the tests.

CHAPTER FIVE

ANALYTICAL STUDIES

5.1 Introduction

One of the overall objectives of this study was to evaluate procedures currently used for predicting the seismic performance of reinforced concrete bridge column two-way hinges. To this end, some of the experimental results presented in Chapter 4 are compared in this chapter with the results predicted using several analysis methods and modeling approaches. Linear elastic as well as inelastic analyses were included. The ability of these methods to predict various global and local engineering response parameters of interest was assessed. Once calibrated with the experimental data, the best-fit analytical model was used to simulate the effect on the seismic response of the test specimens of various loading conditions not considered in the shaking table tests.

Section 5.2 describes the strain rate effect on the material properties of the specimens. Section 5.3 discuses the two-way hinge section confinement, along with a proposed two-way hinge confinement model. Two-way hinge shear strength and shear-slippage models are discussed in detail in Sections 5.4 and 5.6, respectively. The validity of the proposed shear strength model in analysis of test data obtained by other researchers is evaluated in Section 5.5. Section 5.7 presents methods for determining two-way hinge rotation and plastic hinge length. Moment-Curvature analysis and load deflection calculations are presented in Sections 5.8 and 5.10. Section 5.9 explains the bond-slip at ends of reinforced concrete members and the average bond stress determined based on experimental data from this study. Parametric analysis is discussed in Section 5.11 to address the effect of the axial load level, column longitudinal steel ratio, and hinge cross section size on the specimen and two-way hinge behavior.

5.2 Strain Rate Effect

Stress-strain properties of the concrete and steel are determined by slow monotonic tests. High rate of loadings such as earthquake ground motions can affect the properties of the materials. High strain rate increases the yield strength and ultimate strength of steel. Sadrossadat and Saiidi (Ref. 35) studied the effect of the high strain rate based on tests of ASTM A615 standard reinforcing bars. According to this study the yield strength and ultimate strength increase as a function of strain rate as follows:

$$R_{sy} = \frac{f_y^{'}}{f_y} = \left(\frac{SRI}{10^{-4}} \right)^a \qquad (5\text{-}1)$$

$$R_{su} = \frac{f_u^{'}}{f_u} = \left(\frac{\dot{e}_{uave}}{10^{-4}} \right)^{\frac{2}{3}a} \tag{5-2}$$

$$a = 0.022\left(\frac{f}{f_8} \right)^{0.15} - 0.006\left(\frac{f_y}{60} \right) \tag{5-3}$$

$$SRI = K\dot{e}_{yave} \tag{5-4}$$

$$K = \left(\frac{\dot{e}_y}{\dot{e}_{0.5y}} \right)^{0.5} \tag{5-5}$$

Where:

R_{sy}, R_{su} = strain rate factors for steel yield and ultimate strength;
SRI = strain rate index;
f_y, f'_y = static and dynamic yield strength of steel (ksi);
f_u, f'_u = static and dynamic ultimate strength of steel (ksi);
f = diameter of the rebar;
f_8 = diameter of bar #8, ϕ=25.4 mm (1 in);
$\dot{e}_y$, $\dot{e}_{0.5y}$ = strain rate at yield and strain rate at half yield;
$\dot{e}_{yave}$ = average strain rate between half yield and yield;
$\dot{e}_{uave}$ = average strain rate between zero strain to ultimate strain.

High strain rate also increases the compressive capacity of concrete. Kulkarni and Shah (Ref. 20) studied the effect of high strain rate based on monotonic tests of reinforced beams conducted at high loading rates and recommended the following factor for increase in concrete strength due to the effect of strain rate

$$R_c = 0.022Ln\left(\frac{\dot{e}}{10^{-4}} \right) + 0.9973 \tag{5-6}$$

Where:

R_c = strain rate factors for concrete compressive strength,
$\dot{e}$ = strain rate.

Equations 5-1, 5-2 and 5-6 were used to calculate the effect of the strain rate on yield strength of steel and concrete compression strength as well as the ultimate strength of steel. The measured strain rate in the specimens was determined as follows

$$\dot{e} = \frac{e_{i+1} - e_i}{\Delta t} \tag{5-7}$$

Where:

$\dot{e}_i$ = measured strain rate at time ith;

$\dot{e}_{i+1}$ = measured strain rate at time i+1th;

Δt = time step.

Since strain rate increase the yield and ultimate strength of the steel, the motion at which the extreme longitudinal bars half-yielded and yielded was used to study the strain rate effect. The typical strain rate history and strain rate versus strain are plotted in Fig. 5-1 and Fig. 5-2. Figures 5-1 and 5-2 are based on the data recorded from strain gauge SG2B6 on THD-2 during the 0.5 x Sylmar motion. The strain rates used to calculate the stain rate effect were taken as the rate corresponding to the strain immediately after the 1st steel yielding strain and the strain after half steel yielding strain was reached. Strain rates were calculated for strain gauges placed on the extreme longitudinal bars located at base on the column and hinge throat.

Table 5-1 shows the amplification factors for the strength of steel for all five specimens. The measured yield strength and the bar diameters are also included. The relative increase in the yield strength and ultimate strength were found using Equations 5-1 and 5-2. The average increases in the strength of the column and hinge longitudinal steel yield strength were 9.4% and 7.6%, respectively. The increases in the ultimate strength for the column and hinge bars were 6.3% and 5%, respectively.

The data for extreme longitudinal bars that yielded in compression were used to study the strain rate effect in the concrete. Implied in this approach is that perfect bond exists between concrete and steel in compression and hence, they undergo the same strain. This approach also recognizes the fact that the unconfined concrete strength and steel yield stress occur at approximately the same strain of 0.002. The same procedure used to find the strain rate in tensile steel was used. Table 5-2 shows the strain rate and the amplification factor in concrete compression strength for all specimens. Equation 5-6 was applied in the strain rate effect calculation. The average increases in the concrete compression strength were 9% and 8% for the concrete of columns and hinges, respectively.

5.3 Confined Concrete Model

5.3.1 Mander, Priestley and Park's Model

Mander, Priestley, and Park (Ref. 26) and others have developed a general model for concrete confined by various types of transverse reinforcements. The Mander model has been widely used in analyzing columns with both circular and rectangular cross sections. In this study only the stress-strain relationship for circular columns confined with spiral under monotonically applied load is considered. To develop the model, Mander conducted tests on full-scale confined RC columns, with a concrete strength of 30 MPa (4.35 ksi) and steel yield strength of about 300 MPa (43.5 Ksi). Mander related the confined concrete strength, f'_{cc}, to the confining pressure, f'_l, provided by the lateral reinforcement. For circular

sections, the confined concrete properties are described by the following equations:

$$f'_{cc} = f'_c\left(2.254\sqrt{1+\frac{7.94f'_l}{f'_c}}-\frac{2f'_l}{f'_c}-1.254\right) \quad (5\text{-}8)$$

$$e_{cc} = 0.002\left[1+5\left(\frac{f'_{cc}}{f'_c}-1\right)\right] \quad (5\text{-}9)$$

$$e_{cu} = 0.004+\frac{1.4r_s f_{yh}e_{su}}{f'_{cc}} \quad (5\text{-}10)$$

$$f_l = \frac{2f_{yh}A_{sp}}{D's} \quad (5\text{-}11)$$

Where:

f'_{cc} = confined concrete compressive strength;
ε'_{cc} = confined concrete strain at confined strength;
ε'_{cu} = lower (conservative) ultimate concrete compression strain;
f'_l = maximum effective lateral pressure;
f'_c = unconfined concrete compressive strength;
$\rho_s = {}^{4A_{sp}}\!/_{D's}$ = volumetric ratio of confining steel;
f_{yh} = confining steel tension yield strength;
ε_{su} = confining steel strain at maximum tensile stress;
A_{sp} = confining steel bar area;
D' = diameter of the confining steel;
s = the longitudinal spacing of the hoop or spiral.

5.3.2 Previous Hinge Confined Model

A column hinge is typically formed by reducing the column cross-section over a very small portion of its height. It has been demonstrated that the concrete in the hinge region of a column-footing connection has a higher effective strength and a higher strain at the peak stress ("peak" strain) than unconfined concrete (Ref. 19 and 39). This improved response is due to the confinement provided by the larger concrete sections above and below the hinge.

Some researchers have investigated the increased bearing strength due to the confinement provided by the unloaded area or concrete surrounding a bearing area. Hawkins (Ref. 16) summarized the results of 230 experimental tests performed to evaluate the bearing capacity of concrete loaded with rigid steel plates. He proposed the following relationship as a conservative estimate of the ultimate bearing capacity:

$$\frac{f'_{cc}}{f'_c} = 1+50\sqrt{f'_c}\left(\sqrt{A_2/A_1}-1\right) \quad (5\text{-}12)$$

Where:

A_1 = area of the column section;

A_2 = area of the hinge section;
f'_{cc} = hinge concrete compressive strength, in psi;
f'_c = compressive strength from a cylinder test, in psi.

In using this relationship it is assumed that the ratio of the supporting surface to the loaded area is less than 4.

A series of uniaxial compression tests were carried out on plain concrete specimens containing hinges by Griezic et. al. (Ref. 16) to study the complete stress-strain response of the hinge confined concrete. The parameters evaluated in the tests included one-way hinge action, two-way hinge action, and the dimensions of hinge cross section. Based on the experimental results of eighteen tests and analytical studies, expressions were presented for the confined concrete strengths and the corresponding strains of the hinge concrete.

$$f'_{cc} = a_1 f'_c \tag{5-13}$$

$$e'_{cc} = a_2 e'_c \tag{5-14}$$

$$a_1 = \left[1 - 0.5k_1\left(1 - \frac{b_1}{b_2}\right)\right]^{-1} \tag{5-15}$$

$$a_2 = 1 + 2.5a_1\left(1 - \frac{b_1}{b_2}\right) \tag{5-16}$$

Where:

f'_{cc} = hinge concrete compressive strength;
ε'_{cc} = hinge concrete strain corresponding to f'_{cc};
α_1 = hinge confinement factor for strength, $a_1 \le 3.5$ for two-way hinge, $a_1 \le 1.7$ for one-way hinge;
α_2 = hinge confinement factor for peak strain, $a_2 \le 7.5$ for two-way hinge, $a_2 \le 4.0$ for one-way hinge;
f'_c = concrete compressive strength from the cylinder test;
ε'_c = concrete strain corresponding to the peak compressive stress;
b_1 = hinge cross section dimension;
b_2 = column cross section dimension;
k_1 = hinge confinement coefficient, $k_1 = 1.9$ for two-way hinge, $k_1 = 1.1$ for one-way hinge.

5.3.3 Proposed Concrete Confined Model for Two-Way Hinge

For the two-way hinges with distributed longitudinal reinforcement, the hinge core concrete is confined by the spiral and the concrete of the adjacent members (usually the column and the footing). The passive lateral confining pressure exerted by the transverse reinforcement and by the concrete of the adjacent members would subject the hinge core concrete to a state of triaxial compression, enhancing both the axial compression strength and ductility of hinge concrete. Figure 5-3 illustrates the flow of force through a two-way hinge. The flow of compressive stresses through the hinge causes both vertical compressive

stresses and horizontal compressive stress. The horizontal confining stresses provided by the column and the footing were assumed to be equivalent to the lateral confining pressure from the column spirals. As a result, the concrete of the hinge clear cover is confined by the lateral pressures provided by the column spiral. The hinge core concrete is confined by the lateral pressure which is the summation of lateral pressure from the column spiral and spiral of the hinge itself.

Through this study, a comprehensive approach was developed to determine the two-way hinge concrete properties. In this proposed method, the effective confining pressure of the hinge section is related to the hinge concrete confined strength, strain and ultimate strain. The circular section two-way hinge confined concrete properties can be determined by incorporating the following modified lateral pressure and confining steel ratio into Mander's method for f'_{cc}, ε_{cc} and ε_{cu} (Equation 5-8,5-9,5-10).

$$f_l = \left(\frac{2 f_{yh} A_{sp}}{D' s}\right)_{hinge} + \left(\frac{2 f_{yh} A_{sp}}{D' s}\right)_{column} \quad (5\text{-}17)$$

$$r_s = \left(\frac{4 A_{sh}}{D' s}\right)_{hinge} + \left(\frac{4 A_{sh}}{D' s}\right)_{column} \quad (5\text{-}18)$$

Where:

f'_l = effective hinge core confined lateral pressure;
ρ_s = hinge core effective volumetric ratio of confining steel;
f_{yh} = yield strength of the confining steel;
A_{sp} = confining steel bar area;
D' = diameter of the confining steel;
s = the longitudinal spacing of the hoop or spiral.

Figures 5-4 through 5-8 show the two-way hinge confined concrete stress-strain relationship which were calculated using above method for all five specimens respectively. A comparison between the proposed hinge confinement model and previous models such as Hawkins's model (Ref. 16) and Griezic (Ref. 16) model was done in order to see the correlations among these methods. Table 5-3 summarizes the results which include f'_{cc} and ε_{cc}. The maximum difference of 11% was found among the hinge confined compressive strength (f'_{cc}) by applying these three methods. The differences in the hinge concrete strain (ε_{cc}) ranging from 17% to 54% were found between the calculated results of the proposed method and Griezic's method. However, it should be noted that Griezic's method was developed based on the tests of plain concrete column hinges. As a result, the Griezic's method does not take into account the increase in hinge ductility due to the confining steel; therefore the lower values of the concrete strain are understandable.

The hinge confined concrete ultimate strains (ε_{cu}) based on the proposed method are also included in the table. Note that the other existing methods do not provide equations for estimating the ultimate concrete strains and hence no comparisons can be made.

5.4 Hinge Shear Strength

5.4.1 Shear Friction Method

The shear friction method (SFM) has been widely used in the design of two-way reinforced concrete bridge column hinges in order to calculate the hinge capacity. The method is described in the ACI 318 building code (Ref. 3) and the AASHTO bridge specifications (Ref. 1 and 2). The SFM assumes that as concrete segments slide relative to each other they cause a gap. The tendency for forming the gap causes tension in the steel crossing the crack. Figure 2 -1 shows the shear friction mechanism. The reaction from the tension in the steel is a compressive force perpendicular to the crack. The shear friction is this reaction force multiplied by a friction factor. If an axial load is present, it is added to the reaction force. The following equation defines the shear friction capacity V_n:

$$V_n = m\left(A_s f_y + N\right) \quad (5\text{-}19)$$

$$V_n = m\left(A_s f_y + N\right) + cA_c \quad (5\text{-}20)$$

Equation 5-19 is presented in ACI 318 building code (Ref. 3) and the AASHTO Standard Specifications (Ref. 2), and Equation 5-20 is recommended by the AASHTO LRFD Code (Ref. 1).

Where:

V_n = nominal shear resistance, (Kips) or (N);

μ = shear friction factor;

A_s = cross sectional area of all reinforcement acting normal to the shear plane, (in^2) or (mm^2);

f_y = yield stress of the reinforcement, (ksi) or (MPa);

N = compression force acting normal to the plane, (Kips) or (N);

A_c = area of concrete engaged in shear transfer (in^2) or (mm^2);

c = concrete cohesion factor, (ksi) or (MPa).

Both codes place the following limits on V_n used in Equation 5-21 and 5-22.

$$V_n \le 0.2 f'_c A_c \quad (5\text{-}21)$$

$$V_n \le 800 A_c \quad \text{(lb)} \quad (5\text{-}22a)$$

$$V_n \le 5.5 A_c \quad \text{(N)} \quad (5\text{-}22b)$$

The above limits are in part because the majority of the test data that formed the basis of SFM were for concrete with compressive strength of 28 MPa (4 ksi). The ACI 318 code also limits the reinforcement yield strength f_y to be 413.7 MPa (60 ksi). According to the ACI 318 and AASHTO codes, a friction coefficient of 0.6 is used for concrete cast on not intentionally roughened hardened concrete surface. In addition, a concrete cohesion factor of 0.7 MPa (101.5 psi) is specified by AASHTO LRFD.

Table 5-4 shows the measured shear and calculated shear friction capacities for the specimens which experienced hinge shear failure (THD-1, 2, 4 and 5). In these four specimens, the SFM significantly overestimated the hinge shear capacity (from 10% to 49%) if the code limits (Eq. 5-21 and Eq. 5-22) were not applied. These limits do not define the shear friction mechanism. However,

Equations 5-21 and 5-22 (The equations for the upper limit, which control in the case of the test specimens) yield results with scatter over a wide range in term of the ratio of the calculated and measured capacities. The SFM (with the limits applied) underestimated the capacity by 41% in THD-5 and overestimated the capacity by 19% in THD-2 (Table 5-4). From the test data, it was concluded that the shear friction method was not a valid method in predicting the shear capacity of two-way concrete bridge column hinges.

Table 5-5 compares the measured two-way hinge shear capacities with calculated values applying AASHTO standard specifications method (Ref. 2) and the AASHTO LRFD design specifications (Ref. 1). The calculated shear strength based on the AASHTO standard specifications underestimated the capacity by 41% in THD-5 and overestimated the capacity by 19% in THD-2 (Table 5-5). By applying AASHTO LRFD (Ref. 1), the calculated versus measured ratio were varied from 59% to 126%. Since the ratios of the calculated (both AASHTO codes) and measured capacities scatter over a wide range, it can be concluded that neither AASHTO standard specifications nor AASHTO LRFD was valid in two-way hinge shear capacity prediction.

5.4.2 Conventional Diagonal Shear Method

The diagonal tension shear mechanism is commonly used to estimate the reinforced concrete member shear capacity. The beam shear mechanism is considered to be one possible mode of failure in the study by McLean (Ref. 25). In a reinforced concrete member, flexure and shear combine to create a biaxial state of stress. Cracks are formed when the principal tensile stress exceed the tensile strength of concrete (Fig. 5-9). In a region of high shear force, significant principal tensile stresses, also referred to as diagonal tension, are generated at approximately 45^o to the axis of the member. These will result in inclined (diagonal tension) cracks. With few exceptions these inclined cracks are extensions of flexural cracks. In testing of the hinge specimens diagonal shear failure was not observed in any of the specimens. However, during THD-4 test, a diagonal crack did form in the hinge throat area but did not extend into the column.

The ACI 318 (Ref. 3) approach to determine the nominal shear strength of the diagonal tension mechanism is to consider the total nominal shear contribution from concrete and shear reinforcement, thus,

$$V_n = V_c + V_s \tag{5-23}$$

Where:

V_n = nominal shear strength;
V_c = concrete shear strength;
V_s = shear strength of the shear reinforcement.

For reinforcement concrete members subjected to axial load simultaneously with shear on the cross section, the influence of axial load is specified in following Equation:

$$V_c = 2\left(1 + \frac{N_u}{2000A_g}\right)\sqrt{f'_c}\,b_w d \tag{5-24}$$

Where:

N_u = axial load, lb;
A_g = cross section, in^2;
b_w = width of web, in;
d = effective depth of section, in;
f'_c = 28-day compressive strength of concrete, psi.

The ACI expression for V_s is stated as:

$$V_s = \frac{A_v f_y}{s} \tag{5-25}$$

Where:

A_v = the area of shear reinforcement within a distance s;
f_y = shear reinforcement yield tension strength;
s = shear reinforcement spacing.

The ACI318 code also places limit on V_c used in Equation 5-24 and V_s in Equation 5-25.

$$V_c \le 3.5\sqrt{f'_c} \tag{5-26}$$

$$V_s \le 8\sqrt{f'_c} b_w d \tag{5-27}$$

Table 5-5 shows the measured shear and calculated diagonal shear capacities for the specimens which had hinge shear failure (THD-1, 2, 4 and 5). In all this four specimens, the diagonal shear method underestimated the hinge shear capacity.

The equations yield results which scatter over a wide range in term of the ratio of calculated capacity vs. tested shear capacity, varied from 47% 89% (Table 5-5). From the test data and the hinges observed performance, it was concluded that the diagonal shear method was not a valid method in predicting the shear capacity of two-way concrete bridge column hinges. It was quite obvious that the unique geometric condition of the two-way hinge, especial the extremely small hinge aspect ratio, prevents the formation of the 45^o diagonal tension crack across the hinge section.

5.4.3 Proposed Two-Way Hinge Shear Strength Method

As mentioned in Chapter 2, the mechanical behavior of two-way hinges, as shown in Fig. 2-2 is different than that conventional shear friction and diagonal tension shear mechanisms. In reality, lateral forces are introduced to bridge columns through loads acting primarily at the deck level. Therefore, a substantial flexural moment is introduced to the hinge section. In order to estimate the hinge shear strength, those effects due to flexure and axial load must be taken into consideration. Usually, as a result of moment on the hinge section, the flexural crack initiate from one side of the hinge surface and propagate across the section. This flexural crack limits the hinge contact area for aggregate interlock from a full hinge section to the compression zone of the section. The net compressive force is the summation of the reinforcing steel force and the concrete force crossing this contact region. Therefore, the resultant compressive force may be very different from that obtained using the conventional shear friction assumption that all the

bars are in tension. Knowing that hinge shear strength can be evaluated as a function of the normal force on the contact surface, the preliminary hinge shear design method (Section 2.3.2) was proposed as:

$$V_n = m(0.85 f'_c A_{cc} + f_y A_{cs}) \quad (5\text{-}28)$$

Where:

A_{cc} = area of the concrete under compression;
A_{cs} = area of hinge reinforcement under compression;
f'_c = 28-day compressive strength of hinge concrete;
f_y = yield strength of hinge reinforcement;
μ = friction factor (Initially used as 1 per ACI recommendation).

The concrete and reinforcement strains vary across the section due to the variation in the distance to neutral axial. The constant steel yield strength f_y and concrete compression strength f'_c used in the preliminary equation (Equation 5-28) were only to simplify the process. In order to make the prediction of hinge shear strength more accurate, the effective compression force was used in the final version of proposed two-way hinge shear strength method:

$$V_n = m(C_c + C_s) \quad (5\text{-}29)$$

$$C_c + C_s = P + T_s \quad (5\text{-}30)$$

Where:

C_c = compression force at concrete;
C_s = compression force in hinge rebar;
T_s = tension force in rebar;
P = applied axial load;
μ = 0.45, shear friction factor.

Table 5-6 shows the calculation for the two-way hinge shear friction factor based on the test data. Specimen THD-3 failed in flexure, not hinge shear failure, thus it was excluded in this calculation. With a standard deviation value 0.05 and and average value of μ= 0.48, a rounded μ value of 0.45 was recommended in this study for design practice. Comparing with the corresponding friction factor (μ=0.6 for concrete cast against hardened concrete that is not intentionally roughened) suggested in ACI 318, the relatively low shear friction factor of μ=0.45 is mainly due to the cyclic loading effect. The cyclic sliding at the hinge reduces the aggregate roughness at the interface, thus reducing the portion of shear resistance provide by aggregate interlock.

Table 5-5 shows the results of the proposed final hinge shear method (Eq. 5-29) and the measured shear capacities of specimens THD-1, THD-2, THD-4 and THD-5. The equation yields results which scatter over a relatively narrow range in term of the ratio of calculated versus the measured shear capacities, varied from 82% to 107%, with a standard deviation of 0.11. THD-3 was excluded from these comparisons because it failed in flexure at the column and the top hinge. not in shear.

Figures 5-10 through 5-14 illustrate the measured ultimate strengths and compare with the calculated strengths. Also shown are shear and flexural

capacities for different column aspect ratios based on the section properties of each hinge specimen.

Included in the graphs are the results from the ACI SFM with and without the upper limit. The calculated shear corresponding to flexural failure was obtained by dividing the calculated ultimate moment capacities at the two ends of the columns by the specimen clear height. It can be seen that in all the cases the calculated hinge shear strength based on proposed method show much better correlations to the test data, including specimen THD-3 which is clearly showing that it would fail in flexure.

The post failure strength for two-way hinges is important because it provides insight into the strength and stiffness degradation trend that are needed for proper modeling of the hinge behavior. There was evidence that hinge post shear failure strength was provided by the hinge steel dowel action. The detail discussion of hinge post failure of dowel action mechanism will be presented in Section 5.6.2.

5.5 Evaluation of the Proposed Method Using Other Research Data

It is critical for the development of an accurate, objective and generally applicable method to evaluate the procedure utilizing research data obtained by other researchers. In this section, the results of previous research on reinforced concrete bridge column bents with hinge details are used to validate the proposed two-way hinge shear strength model discussed in Section 5.4.

Since the late 90s, a series of large-scale two-column bridge bent shake table studies have been conducted at University of Nevada, Reno. Among these specimens, many of the columns were detailed with two-way hinges at the base. The test data from Pulido et al. (Ref. 34), Nada et al. (Ref. 31), Moustafa et al. (Ref. 30), Chandane et al. (Ref. 8) and Sureshkumar et al. (Ref. 42) were collected and utilized in this calibration. There were wide parameter variations among these specimens. The parameters included: a) Column aspect ratio, b) Magnitude of axial load, c) Amount of hinge longitudinal reinforcement, d) Two-way hinge size, and e) Hinge bar configuration. A summary of the key parameters for specimens is given in Table 5-7.

In order to apply the proposed two-way hinge shear strength model, moment-curvature analysis needs to be performed for both columns in the bent. Due to the overturning effects, the two columns are subject to different axial loads when the bent is subject to lateral loading. The column axial loads were calculated under the combined action of the vertical load and the maximum applied lateral load. These axial loads were used in the moment curvature analysis of the hinge. The summation of the net compressive forces from both columns section was substituted as C_s+C_c into Equation 5-29. The hinge shear resistance for the bent was determined by following the proposed equation.

In Table 5-8, the proposed hinge shear strength model is used to calculate the two-column bent hinge shear strength of ten two-column bents that were tested on a shake table in five different studies, for which the key parameters varied widely as reported in Table 5-7. By comparing the calculated and measured

hinge shear strengths, four specimens which were reported to experience hinge failure during the tests had ultimate shear strength greater or close to the calculated values. The average value of the ratio of the calculated strength to test strength is 0.89, and standard deviation is 0.089. The rest of the six specimens which reported no hinge failure during the test observation had ultimate applied shear forces far below the calculated hinge shear capacity with a n average ratio of 1.43 in terms of calculated hinge shear strength versus the maximum applied lateral load.

Based on the data reported in Table 5-8 as well as the previously reported results from the current study, it can be seen that the proposed hinge shear strength method reflect the trends in the experimental data very closely, and it is hence appropriate to be used for two-way hinge design.

5.6 Hinge Shear Force-Displacement Model

5.6.1 Existing Models

Little is known about the analytical modeling of the hinge shear sliding. Recently, a study was conducted by Moustafa, et al. (Ref. 30). Based on experimental results from tests of two-column bridge piers with two-way hinges at column bases, a hinge shear-slippage model was developed. Fig. 5-15 shows that the shear-slippage model can be represented by three major segments. Segment 1 represents the peak shear-sliding capacity. Segment 1 is only valid from zero slippage to a sliding displacement of δ, where δ is equal to the roughed depth at the shear plane surface, about 6 mm (1/4 in) in this case. After reaching this displacement, strength degradation was began shown in the figure. This is modeled by segment 2. The degradation in strength is due to the destruction of the aggregate interlock. Based on best experimental data fitting curve, the slope of segment 2, K2 is taken as -6.25 KN/mm (-35 kip/in). The last segment slope K3 is based on a survey which was done on related experimental work to complete the shear-slippage envelope. In a related study by Silva, et al (Ref. 41), the shear-friction behavior of the sacrificial interior shear keys was investigated. The shear keys were tested untill failure under different types of loading. Based on the data from that study, the slope of the last segment of the envelope, K3 is taken as -7 KN/mm (-40 kip/in), as shown in Fig. 5-15.

For the hinge peak shear capacity which controls the segment 1 of the hinge shear-slippage mode, the governing equation was presented as following:

$$Q = m \times C \tag{5-31}$$

Where:

Q = hinge peak shear capacity;

C = the compression force acting at the friction interface surface;

μ = shear friction coefficient, 0.7.

Note that the recommendation by Moustafa was based on indirect measures of the hinge behavior. The hinges were part of a pier in which the exact force in each pier could not be measured. The proposed model provided a preliminary analytical tool that led to reasonable estimates of the lateral load-displacement response of the piers.

5.6.2 Proposed Hinge Shear-displacement Model

As described in Section 4.4.1, experimental results have shown that the shear failure of two-way hinges can be separated into two stages including the friction force provided by the hinge compression zone aggregate interlock at relatively small displacements followed by dowel action at larger displacements. Accordingly, a shear-slippage relationship similar to that described at Section 5.6.1 can be adopted with some modifications.

Under large shear-slippage, the hinge bars deform under dowel action. Larger slippage would occur when the friction, due to the resultant compressive load, is overcome. Dowel strength across shear plane can be developed by three mechanisms: the flexure of reinforcing bars, the shear strength across the bars, and the kinking of the reinforcement (Ref. 32). The kinking mechanism is illustrated in Fig. 5-16, where the associated shear force V is also expressed in terms of the yield strength of the bar. Based on past test results (Ref. 32), the kinking of the reinforcement is likely to be the major source of dowel action, particularly when small size bars are used.

Figure 5-17 shows the proposed two-way hinge shear model. The model consists of four segments. Segments 1 to 3 represent the hinge shear-slippage relationship when the hinge shear is controlled by compression zone aggregate interlock mechanism. Segment 4 represents the hinge shear-slip curve when the hinge shear is controlled by the kinking mechanism. The first three break points correspond to the shear yielding, peak shear-sliding capacity, and the transition point where kinking mechanism start controlling the hinge performance. The ultimate point is the kinking capacity of the hinge longitudinal reinforcement.

Point 1 is defined by the hinge shear capacity and shear deformation in the cracked hinge section. The hinge shear capacity can be calculated by applying proposed hinge shear strength Equation 5-29 (Section 5.4.3). The hinge shear yield deformation can be found from the expressions described by Park and Paulay (Ref. 32) that are based on the truss mechanism. The shear deformation of cracked reinforced concrete members can be found as follows:

$$\Delta_{v,45} = q_v l \tag{5-32}$$

$$q_v = V_n \Big/ K_{v,45} \tag{5-33}$$

$$K_{v,45} = \frac{r_v}{1 + 4nr_v} E_s b_w d \tag{5-34}$$

Where:

$D_{v,45}$ = deflection due to shear force on the cracked section;
q_v = rotation due to shear force;
l = member length;
V_n = hinge shear capacity;
$K_{v,45}$ = shear stiffness for cracked member of a unit length;

r_v = shear reinforcement ratio = $\frac{A_v}{sb_w}$;

E_s = elastic modulus of the steel reinforcement;

E_c = elastic modulus of concrete = $4733\sqrt{f'_c}$ (MPa), $57000\sqrt{f'_c}$ (psi);

n = modular ratio = $\frac{E_s}{E_c}$;

b_w = section width perpendicular to the applied shear;

d = effective section depth parallel to applied shear.

s = spacing of shear reinforcement.

Point 2 is defined by the hinge shear capacity (Eq. 5-29) and a sliding displacement of δ. Referring to experimental results as well as the previous study (Ref. 30), the displacement δ was about 6 mm (0.25 in), which was equal to the roughed depth at the shear plane.

The hinge shear strength is reduced in Segment 3 due to the loss of the aggregate interlock. Based on the test data of this study as listed in Table 5-9, an average shear capacity drop of 30% between the points of slippage δ (Point 2) and slippage 2δ was observed. Therefore, the slope of Segment 3 envelope can be calculated by using Equation 5-35. By knowing the slope of the envelope, the shear capacity in this segment can be expressed by Equation 5-36:

$$k = {0.3V_n}/{d} \tag{5-35}$$

$$V = V_n - k(x - d) \tag{5-36}$$

Where:

x = shear slippage;

d = shear plane roughed depth = 6.35 mm (0.25 in);

k = slope of the envelope of segment No. 3.

As was mentioned before, when the shear slippage becomes large, the kinking dowel action dominates the hinge shear performance. The shear capacity for the kinking model can be expressed by the following equation (Ref. 32), an effective friction factor between concrete and gravel which equal to 0.4 was adopted for this calculation (Ref. 45):

$$V = m_a N + V_d \tag{5-37}$$

$$V_d = A_s f_u \cos a \tag{5-38}$$

Where:

N = applied axial force;

V_d = kinking shear strength of the bars ;

m_a = effective friction factor =0.4 (Ref. 45);

A_s = reinforcement area normal to the shear plane;

f_u = ultimate stress of hinge reinforcement;

a = kinking angle (use 60^o for ultimate point);

$\cos\alpha = x \Big/ \sqrt{x^2 + (g + 2d_b)^2}$;

g = hinge gap height;

d_b = diameter of hinge reinforcement.

In order to locate point No. 3, Equations 5-36 and 5-37 needs to be solved for the slippage x and hinge shear force, which would define the transition point from the aggregate interlock mechanism to the kinking dowel action.

The ultimate point can be defined by the hinge shear force and slippage using Equation 5-37. Based on observations during the tests as well as the subsequent analyses, kinking angle of 60^o is recommended to calculate the ultimate shear capacity. Since the kinking angle is a function of slippage x (Equation 5-38), ultimate slippage can be back calculated by knowing ultimate kinking angle 60^o.

Figures 5-18 through 5-21 show comparison of the proposed hinge shear force-slippage model along with the shear-slippage envelope recorded during the test for specimens THD-1, THD-2, THD-4 and THD-5. THD-3 was excluded from these comparisons because it failed in flexure. As shown in the figures, the proposed hinge shear model fit experimental results reasonably well for THD-1, THD-2, and THD-5. The exception for THD-4 is due to the early termination of the test. THD-4 test was ended at 1.25 x Sylmar motion after observing a significant drop in the capacity and concern for safety.

5.7 Hinge Rotation

5.7.1 Existing Hinge Rotation Calculation Method

Calculated rotation consisted of rotation due to elastic and plastic flexural deformation of the hinge section plus rotation due to bar slippage. The flexural rotation for hinge (excluding bond slip rotation) at yield and ultimate is calculated as follows:

$$q = f \times g \qquad (5\text{-}39)$$

Where:

f = curvature for hinge section;

g = hinge gap;

θ = hinge rotation due to flexure.

Bond-slip in an ordinary reinforced concrete connection exists primarily in the joint anchorage system, as shown in Fig. 5-22. Bar slippage in a typical reinforced concrete column and beam section is due to the elongation of longitudinal bar in the anchorage zones that are significantly stiffer and stronger than the member. Adjacent to a hinge there are two such anchorage zones that are rotating relative to each other: the full column segment and the loading head, as shown in Fig. 5-23. Bond-slip due to rotation can, therefore, be twice that of what would be anticipated in a normal reinforced concrete member. This assumption is examined in Section 5.9 using the measured data from this study. Therefore, the hinge rotation due to bond-slip at yield can be calculated by Equation 2-12b and applying a factor of 2 to Account for the “double bond-slip” in

the hinge. The hinge rotation due to bond-slip at ultimate is calculated using Wehbe method (Ref. 44) as follows:

$$\Delta l_u = \frac{(e_s + e_y)(f_s + f_y)d_b}{8u} + \frac{e_y f_y d_b}{8u} \quad (5\text{-}40)$$

$$q_u = \frac{\Delta l_u}{N.A.} \quad (5\text{-}41)$$

Where:

Dl_u = bar extension due to bond-slip at ultimate stage;
ε_s = bar strain at hinge ultimate stage;
ε_y = hinge bar yield strain;
f_s = bar strain at hinge ultimate stage;
f_y = hinge bar yield strain;
d_b = hinge bar diameter;
u = average bond strength (Equation 2-12c);
θ_u = rotation due to bond-slip at ultimate stage;
N.A. = section neutral axis distance to the extreme bar in tension.

The calculated rotation based on the method described above is presented in Table 5-10. A maximum ratio of calculated and measured at hinge yield is 11% among all five specimens, with a standard deviation of 0.07. However, at the ultimate stage, a wider range of calculated and measured ratios was obtained, with a maximum ratio of 151% and a standard deviation of 0.42. Figures 5-24 through 5-28 show the comparison curves of hinge load-rotation envelopes based on experimental and analytical results. The calculated points based on the above method are superimposed on the experimental plots.

The large ratio of the calculated and measured rotations should be viewed in light of the fact that rotation measurement had to be terminated prior to the ultimate earthquake runs due to movement of transducer attachments (Section 4.4.3). The "measured" ultimate rotations were based on the last set of reliable data obtained; typically, one or two runs prior to failure.

5.7.2 Proposed Two-Way Hinge Rotation Calculation Method

Two-way hinges are assumed to be pin connections, but moment actually does develop at the hinge section. In addition, the bearing of the edge of the outer column with the top of the footing (gap closure) will result in an increase in the plastic shear transferred to the footing. Therefore, gap closure needs to be taken into consideration and be avoided in the two-way hinge design procedure. In order to prevent two-way hinge gap closure, two-way hinge rotational capacity and gap closure demand needs to be realistically determined.

An empirical formula was developed in this study to determine a more reliable estimate of the rotation in two-way hinges. The proposed formula attempts to improve the correlation between the calculated and measured data and reduce the standard deviation by using a plastic hinge length that accounts for spread of plasticity into the members that adjoin the hinge.

Based on analyses and test results from this study, by adopting an equation for the gap area in the jacketed columns (Ref. 33), a reasonable estimate for the plastic hinge length when the plastic hinge forms in the two-way hinge region is proposed as:

$$L_p = g + 0.022 f_y d_b \quad (f_y \text{ in MPa}) \tag{5-42}$$

$$L_p = g + 0.15 f_y d_b \quad (f_y \text{ in ksi}) \tag{5-43}$$

Where:

g = hinge gap;
L_p = hinge plastic length;
f_y = yield strength of hinge bar;
d_b = hinge bar diameter.

The above equations include the concentrated plasticity at the hinge, as well as the yield strain penetration of the longitudinal reinforcement into the adjoining elements, such at below footing and above column. The second term in Equations 5-42 and 5-43 makes allowance for additional rotation at the critical section resulting from strain penetration of the longitudinal reinforcement.

Table 5-11 shows the development for the two-way hinge plastic hinge length based on the test data from this study. With a standard deviation value 0.04 and an average factor of 0.13 for second term in Equation 5-43. Comparing with the corresponding factor 0.3 suggested by Priestley (Ref. 33) for jacketed column, the rounded factor of 0.15 was recommended in this study for two-way hinge design.

The two-way hinge total rotation is the sum of elastic and plastic rotations. Therefore, the hinge rotation can be calculated as follows:

$$q_n = q_e + q_p \tag{5-44}$$

$$q_e = g\ f_y \tag{5-45}$$

$$q_p = L_p(f_u - f_y) \tag{5-46}$$

Where:

ϕ_y = hinge section effective yield curvature;
ϕ_u = hinge section ultimate curvature;
θ_n = hinge ultimate rotation;
θ_e = hinge elastic rotation;
θ_p = hinge plastic rotation;
g = two-way hinge gap thickness;
L_p = plastic hinge length.

Table 5-12 shows the results of the proposed hinge plastic rotation calculation results (Equations 5-43 through 5-46) and the measured hinge rotations for all five specimens during their last recorded motion. The results, ratio of calculated vs. tested hinge ultimate rotation, varying from 82% to 161%, with a standard deviation value of 0.31.

As illustrated in Fig. 5-29, the rotation demand for gap closure can be calculated based on the column and hinge geometric condition with assumption that the hinge cross section rotation axis passes through the centroid of the hinge

section. Therefore, hinge rotation corresponding to gap closure can be calculated as follows:

$$q_{close} = \sin^{-1}\left(\frac{g}{0.5D}\right) \quad (5\text{-}47)$$

Where:

g = two-way hinge gap height;
D = Column diameter.

Table 5-13 shows the results from applying Equation 5-47 and the measured hinge rotation of all five specimens at their last recorded motion. The results, ratio of calculated vs. test hinge ultimate rotation, varied from 0.88 to 1.36, with a standard deviation of 0.19 and an average ratio of 1.22.

By comparing results from Equation 5-44 and 5-47, hinge gap heights which prevent gap closure can be solved. The detail example of two-way hinge gap closure calculation is presented in Chapter 6.

5.8 Moment-Curvature Analysis

The moment curvature analysis was performed using programs RCMC (Ref. 21) and XTRACT (Ref. 18). The resulting M-ϕ relationships were used to determine plastic hinge parameters that were used to perform a pushover analysis using program SAP2000. RCMC input and parameters were discussed in Section 2.6.1. The idealization of the material properties in XTRACT was done with Mander's model for concrete and bilinear steel with parabolic strain hardening for steel. In using both programs, the input of hinge concrete properties were calculated based on the discussion in Section 5.3.3.

The measured yield and ultimate stress of reinforcement and the measured concrete compression strength described in Section 2.7 were increased due to the strain rate effect (Section 5.2). These properties with the effect of strain rate were used as input for the M-ϕ analysis (Tables 5-14 and 5-15). The average values of the measured axial load discussed in Section 4.3.3 were applied in the analysis. Bilinear idealizations of the M-ϕ curves were done based on the principle of equalizing the areas under each curve. The procedure was described in Section 2.6.1.

Column Sections

The analysis results of RCMC with and without strain rate effect are shown in Figs. 5-30 through 5-34 for the column section in the five specimens. The S.R.E. in figures stands for the strain rate effect and indicates that the RCMC analysis that included the effect of the material properties. As listed in Table 5-14, the difference in the idealized moments due to strain rate effect ranged from 4.6% to 10.9% for yield moments and 3.9% to 7.8% for ultimate moments. Similarly, the difference in idealized yield curvatures ranged between 8.1% and 11% while the ultimate curvature differences varies from 8.2% to 5.1%.

A comparison between RCMC and XTRACT was done to ensure the accuracy and reliability of M-ϕ analysis results. The same material properties with strain rate effect used in RCMC were used in XTRACT. Figures 5-30 to 5-34 present the calculated M-ϕ curves using RCMC and XTRACT. Differences

ranging 1.9% and 5.7% were found between the plastic moments calculated from these two programs. The ultimate curvature varied from 2.2% to 12% for all the five specimens. The difference in the concrete and steel model, as well as the failure criteria, and strength reduction factor used in RCMC and XTRACT can produce some differences in the final results. However, in general, these differences are acceptable considering the level of approximation in other steps of the structural analysis.

Hinge Sections

The analysis results for hinge sections using RCMC with and without strain rate effects (SRE) are shown in Figs. 5-35 through 5-39 for the all five specimens. As listed in Table 5-17, the difference in the idealized moments due to strain rate effect ranged from 3.1% to 7.5% for yield moments and 4% to 5.2% for ultimate moments. The difference in the idealized yield curvature ranged between 2% and 11.7% while the difference in the ultimate curvature varies from 1.6% to 12.2%.

Figures 5-35 to 5-39 present the calculated M-ϕ curves using RCMC and XTRACT. Differences between 2.5% and 8.1% were found between the plastic moments calculated from this two program. The ultimate curvature varied from 4.1% to 11.6% using different programs. The difference was due to similar reasons that were described in the previous section. However, in general, these differences are small and acceptable.

5.9 Bond Slip

Reinforced concrete members with moment connections require that the main reinforcement be developed into adjoining joints or adjacent members such as footing or head in the two-way hinge specimen, to attain the flexural capacity at the connection interface. The development of main reinforcement is provided through bond stresses between the steel bar and the surrounding concrete. The strains associated with stresses along the tensile bar development length create additional elongation of the tensile bar at the connection interface. This effect is referred to as bond slip. When a reinforced concrete column is subjected to lateral loads, the bond slip at the column joints produces relative rotation between the column and the connecting member. Bond slip deflection is defined as the column lateral deflection resulting from bond slip rotation.

As shown in Table 5-10, a major part of the rotation at two-way hinge is due to bond slip at hinge ends. Therefore, a study of the two-way hinge bond slip behavior and dynamic loading effect on the average bond stress along the reinforcement was carried out. The peak average bond stress developed along the hinge longitudinal bar was determined from the measured data and compared with values typically used in the design. The average bond stress (u) between reinforcement bars and the surrounding concrete was determine using the longitudinal steel strains over the bar length. For uniform bond stress along the anchorage length, l, the force equilibrium of the bar between two strain gauges leads to:

$$u = \frac{f_s d_b}{4l} \tag{5-48}$$

Where:

u = bar average bond stress;
l = distance between the two strain gauges;
f_s = axial stress on the rebar;
d_b = nominal bar diameter.

Six strain gauges were placed on the hinge longitudinal bars with a spacing of 76mm (3 in.) and 102 mm (4 in.) (Fig. 3-16 to 3-20). The average bond stresses were found between each pair of adjacent gauges using Equation 5-48. Using the longitudinal bar strains recorded at strain gauges, the steel stresses were evaluated using the measured reinforcement properties. Typical calculated average bond stress (u) plots for different hinge longitudinal bars in specimen THD-2 are given in Figure 5-40. Similar plots form the rest of the specimens were excluded because the strain gauges were damaged and the data were not complete.

In Fig. 5-40, the average bond strengths are normalized with respect to $\sqrt{f'_c}$, and the peak average bond strengths for each runs are plotted against input motion history. Each curve indicates the average bond strengths at a specific location on the hinge reinforcement. The legend in the figure refers to this specific point location, for example, (+6") indicates the point which was located at 152 mm (6 inch) above middle section of the two-way hinge.

As indicated in Fig. 5-40, a similar pattern was evident in the data points locations at 152 mm (6 inch) above and 127 mm (5 inch) below the hinge for different bars (A and B). The bond stresses increased by a constant rate until the maximum bond stress was reached. After reaching the peak stress, as a result of bond deterioration and stress redistribution as well as the plasticity of the reinforcement, the bond stress deteriorated at a relatively slow rate. For instance, a maximum average bond stress about $20\sqrt{f'_c}$ was reached between the motion of 0.5 x Sylmar and 0.75 x Sylmar while the bond stress was about $7\sqrt{f'_c}$ during the run of 2.625 x Sylmar. As generally expected, the bond strength at free end is less than the bond near the point of maximum tension. Therefore, as shown in Fig. 5-40, from 0.1 x Sylmar until 2 x Sylmar, the bond stress at 241 mm (9.5 inch) below the hinge was less than the corresponding value at 127 mm (5 inch) below the hinge. However, due to the post yielding redistribution of the bond, a gradual shifting in the bond resistance from the point of maximum tension toward the free end was also observed in the figure after 2 x Sylmar motion. In addition to above discussion, it should be noted that the peak average bond strength value show little variation for different bars and locations.

The average bond stress for useable data from all five specimens was calculated based on the hinge longitudinal bar strain readings in the column and the loading head. Table 5-18 shows the results. As seen in the plots and table, there is no significant difference between the average bond strength developed

from either end of the two-way hinge. Therefore, the two-way hinge "double bond-slip" assumption which was described in Section 5.7.1 shown to be valid.

Table 5-19 shows the maximum average bond strengths obtained from this study. The average bond strengths obtained from 20 longitudinal bars in the five specimens is calculated as a function of $\sqrt{f'_c}$ before and after the first yield of the bars. The average bond stress showed a relatively good correction with the results from the average bond strength empirical expression proposed by Leet (Ref. 23):

$$u = \frac{20\sqrt{f'_c}}{d_b} \le 5.5 \qquad \text{(MPa)} \qquad (5\text{-}49)$$

$$u = \frac{9.5\sqrt{f'_c}}{d_b} \le 800 \qquad \text{(psi)} \qquad (5\text{-}50)$$

Where:

u = bar average bond stress;
f'_c = concrete compressive strength;
d_b = nominal bar diameter using consistent units.

The calculated results from Leet 's equation are also presented in Table 5-19 for comparison.

Although the average bond stress obtained from this study was based on the results of dynamic loading tests, the specimen reached similar normalized peak bond stresses as did the monotonic beam test which the Leet's equation was based on. Therefore, the results indicate cyclic loading may not influence the peak bond stress significantly. However, cyclic loading may still impact the post-peak strength deterioration. Although some studies such as Lehman's (Ref. 24) recommend that the average bond stress before the first steel yielding is approximately twice the bond stress after the yielding, the present study showed that there is only approximately 20% difference between the average bond stress before and after steel yielding.

The data in Table 5-19 also show that Leet's equation used in Section 5.6.1 provides a reasonable estimate of the bond strengths.

5.10 Load Deflection Analysis

The total deflection including flexural, bond slip, and shear deformations were determined using hand calculations. A comparison between the push over analysis performed using SAP2000 (Ref. 11) was done based on the section properties from RCMC and including the effect of the bond slip and shear deformations. A comparison of the experimental and the analytical force-displacement curves are presented in this section.

5.10.1 Deflection Calculation Based on Flexure Failure

The method for calculating the ultimate deflections for the specimens was presented in Section 2.6.2. In the proposed approach, the additional plastic flexural deflection past the yield point is based on the assumption that plastic

rotations occur at mid-depth of the plastic hinge length. The plastic length for the column was calculated according to the expressions given by Priestley et. al (Ref. 33). The plastic length for the two-way hinge was determined by the equation that was proposed in Section 5.7.2 from this study. The calculated two-way hinge plastic hinge lengths for all five specimens are summarized in Table 5-12.

Yield flexural deflections were based on the idealized yield curvatures. The idealized effective yield curvatures are listed in Tables 5-16 and 5-17. The flexural deflections at the effective yield point were obtained using Equation 2.11. In order to obtain the total yield lateral deflections, the calculated displacement due to shear and bond slip were added to the calculated flexural deflections. Table 5-20 lists the calculated total lateral deflections at yield as well as the components from flexural, shear, and bond slip. The ultimate deflections which consist of yield flexural, shear deflection under ultimate load and plastic deflection based on the plastic hinge length are listed in Table 5-21 for all five specimens.

Figures 5-41 through 5-45 show the comparison between the analytical and measured top deflection for all five specimens. Differences of 29.4%, 30.6%, 59.5%, 30.7% and 60.6% were found between the analytical and the experimental ultimate deformation for THD-1 to THD-5, respectively. The difference between the calculated and measured peak lateral force were 2%, 11.6%, 9.7%, 18% and 14.4% for THD-1 to THD-5, respectively. The analytical results slightly overestimated the specimens lateral load capacity but underestimated the ultimate deflections by a large amount. The difference between the measured and calculated deflections is attributed to two factors: (1) the specimens had significant shear deformation particularly at the hinges, and (2) the Mander's confinement model used in estimating the ultimate curvature is conservative and leads to underestimation of the failure deflection. In the push-over analyses described in the next section the shear deformations were included.

5.10.2 Push-Over Analysis

The push-over analysis is a nonlinear static analysis in which the specimen is pushed laterally by incremental lateral forces until the specimen fails. This analysis can predict the peak seismic demands (peak seismic forces and displacements), and it can potentially show the type of failure and the locations where failure starts. This helps to identify the critical elements and joints in each specimen, which in turn helps to determine the cause of failure and how to control it. SAP2000 (Ref. 11) program was used for the push-over analysis. The analytical model used in this program was the lumped plasticity model (Fig. 5-46). In SAP2000, the inelastic behavior is modeled by plastic hinges at critical section. The M-θ relationship for column base rotational spring included the effect of bond slip and plastic hinging at the base and shear deformation of the column. However, the M-θ relationship for the two-way hinge at top only included the effect of hinge flexure and bond slip deformations. The shear deformation at the two-way hinge was accounted for by a shear spring (V-Δ hinge) at the two-way hinge. The proposed shear model (Section 5.6.2) was applied to determine the

input properties for the hinge shear. The cross section properties from RCMC analysis were used in the analysis.

As shown in Fig. 5-47, two frame elements were connected together to simulate the column with a two-way hinge at top. Rotational springs were assigned to the column base and middle height of two-way hinge. In addition, a shear spring was also assigned at middle height of two-way hinge to model the two-way hinge shear behavior. The footing and top head were modeled by horizontal frame elements with large section properties to prevent rotation at the boundaries.

The column and hinge moment of inertia about the bending axis for the frame were modified to take into account the effect of cracking, bond slip deformation, and shear deformation at the effective yield as follows:

$$I_e = \frac{M_y}{f_y E_c} \times \frac{\Delta_{b(y)}}{\Delta_y} \tag{5-51}$$

Where:

I_e = effective moment inertia;
M_y = idealized yield moment capacity from M-ϕ analysis;
f_y = idealized yield curvature from M-ϕ analysis;
E_c =elastic modulus of concrete = $4733\sqrt{f'_c}$ (MPa), $57000\sqrt{f'_c}$ (psi);
D_y = calculated total yield deflection, Section 2.6.2 and 5.10.1;
$D_{b(y)}$ = calculated yield flexural deflection, Section 2.6.2 and 5.10.1.

The moment of inertia about the bending axis used in the model of each specimen for column and two-way hinge was calculated using Eq. 5-51.

The rotational spring properties used in SAP2000 are presented in Table 5-22. The idealized yield and ultimate moment were found using RCMC program and included the strain rate effect. The yield and ultimate rotations were calculated as flowing:

$$q_y = \frac{\Delta_y}{L} \tag{5-52}$$

$$q_u = \frac{\Delta_u}{L} \tag{5-53}$$

Where:

q_y = effective yield rotation;
q_u = effective ultimate rotation;
D_y = calculated yield deflection;
D_u = calculated ultimate deflection;
L = length between the ends and inflection point (Section 2.6.2).

The input properties for the shear spring at the two-way hinge for SAP 2000 are listed in Table 5-23. The two-way hinge shear model that was described in Section 5.6.2 was used to determine all the parameters.

Figures 5-48 through 5-52 show a comparison of the measured force displacement curves and the results of the program SAP2000 analyses for all specimens. Compared with the calculated results discussed in Section 5.10.1, an

improved correlation between the analytical and experimental results was achieved. The coordinates of the elasto-plastic idealization of the experimental and SAP2000 results are listed in Table 5-24. The difference between the equivalent lateral loads of the experimental and SAP2000 results were 3.7%, 16.5%, 4.3%, 14.7% and 6.2% for THD-1 to THD-5, respectively. Differences between the ultimate displacement of the experimental and SAP2000 push-over results were 6.6%, 5%, 10.1%, 46.5% and 18.6% for THD-1 to THD-5, respectively.

5.11 Parametric Analyses Based on Test Specimens

5.11.1 Effect of Axial Load Level

To examine the effects of axial load level on the specimen as well as the two-way hinge as listed in Table 2-1, specimens THD-4 and THD-2 were tested with axial load levels of 0 and $0.06f'_cA_{col}$, while THD-1, THD-3 and THD-5 had an axial load level of $0.1f'_cA_{col}$. The force-displacement hysteresis curves for the five specimens are shown in Figures 4-96 to 4-100, respectively. Comparing the force-displacement hysteresis curves for THD-1 (10% of f'_cA_{col}), THD-2 (6% of f'_cA_{col}) and THD-4 (0 axial load), it can be seen that there is little difference in the overall behavior of the these three specimens. The hysteresis curves for the specimens subjected to lower axial load level were slightly more pinched than those with the higher axial load level.

In addition, the effect of axial load level on the specimen energy dissipation effectiveness can be observed from the figures (Fig. 4-96, 4-97, and 4-99). By observing the larger hysteresis loop area for higher axial load specimen, the increase in the energy dissipation effectiveness due to higher axial load was clearly pronounced through the figures..

Figures 4-185 through 4-189 show the two-way hinge shear-slippage hysteresis curves for THD-1 to THD-5, respectively. The figures show the importance axial load has on the two-way hinge shear-slippage relationship. From Fig. 4-185 for THD-1, Fig. 4-186 for THD-2 and Fig. 4-188 for THD-4, the higher axial load resulted in a greater drop in hinge shear strength during the ultimate stage of the tests. However, the increase rate of hinge slippage subjected to the lower axial load is greater compared to that of higher axial load specimen, such as THD-1.

Table 5-6 shows the two-way hinge shear friction factor μ calculation based on experimental data. Due to different level of applied axial load, the hinge axial load ratios varied from near 0% for THD-4, 15.3% for THD-2, 25.5% for THD-1 to 39.8% for THD5. As a result, a wide variation of effective compressive force (Cc+Cs) was seen in Table 5-6. However, regardless of the wide variation in (Cc+Cs), the shear friction factor μ remained consistent.

5.11.2 Effect of Column Longitudinal Steel Ratio

To evaluate the effects of column longitudinal steel ratio on the behavior of the specimens as well as the two-way hinges, test results for specimens with different column steel ratio of 4.2% (THD-1) and 1.4% (THD-3) are compared. As

listed in Table 2-1, aside from the column steel ratios, THD-1 and THD-3 were identical in terms of column aspect, hinge detail and applied axial load. The difference in performance was due to the effect of the column steel ratio as well as the difference in the column lateral stiffness.

The force-displacement hysteresis curves for THD-1 and THD-3 are shown in Figs. 4-96 and 4-98, respectively. As described in Chapter 4, THD-1 failed by hinge shear while THD-3 failed in column flexure. Specimen THD-3 reached a larger displacement ductility than THD-1(Table 4-23), indicating that the ductility effectiveness decreased as the two-way hinge specimen column steel ratio as well as the specimen lateral stiffness increased.

The hinge shear-slippage hysteresis curves for THD-1 and THD-3 are shown in Fig. 4-185 and 4-187, respectively. It can be seen in these two figures that greater degradation in strength occurred as the column steel ratio and stiffness decreased. It can also be seen that the lateral force drop was more drastic in THD-1 than THD-3. The chance of a hinge brittle shear failure increases with a stiffer column.

Figure 5-53 compares hinge rotation for similar input ground accelerations. A substantial difference between the hinge rotation curves for specimens THD-1 and THD-3 was found. As the motions increased from 0.25 x Sylmar to 2 x Sylmar, an average of 60.4% more rotation was observed for the specimen THD-3. Therefore, the observation from Fig. 5-53 indicates that the two-way hinge rotation significantly increased when the column longitudinal steel ratio and the specimen lateral stiffness were reduced.

5.11.3 Effect of Hinge Size

To evaluate the effects of two-way hinge size on the behavior of the specimens as well as the two-way hinge itself, test results for specimens with different hinge dimension of 254 mm (10 in) diameter (THD-1) and 203.2 mm (8 in) diameter (THD-5) are compared. As listed in Table 2-1, aside from the hinge dimension, THD-1 and THD-5 were similar in terms of column steel ratio, column aspect ratio, and applied axial load. Therefore, any difference in the response was mainly due to effect of hinge size.

The force-displacement hysteresis for THD-1 and THD-5 are shown in Fig. 4-96 and 4-100, respectively. The hysteresis curves for the specimen with smaller size hinge (THD-5) had greater residual displacement than those from the large size hinge (THD-1) due to the early spalling of two-way hinge of THD-5. In addition, the effect of two-way hinge size on the energy dissipation effectiveness is also can be observed from the figures. However, the increase in the energy dissipation of the smaller size hinge was mainly due to dowel action mechanism of the hinge steel that occurred after a drop in the capacity.

The hinge shear-slippage hysteresis curves for THD-1 and THD-5 are shown in Fig. 4-185 and 4-189, respectively. It can be seen in these two figures that a greater degradation in strength occurred in THD-5, indicating that hinge shear degrade quicker as the hinge cross section decreased.

Figure 5-53 shows the comparison of specimens hinge rotation subject to similar input ground accelerations. The motions increased from 0.1 x Sylmar to 2.5 x Sylmar, an average of 46% more rotation was observed in THD-5 than THD-1. Therefore, hinge rotation will likely be larger in smaller hinges as expected.

CHAPTER SIX

PROPOSED TWO-WAY HINGE DESIGN METHOD

AND NUMERICAL EXAMPLE

6.1 Introduction

Based on the results of this study, design recommendations for two-way hinges are presented in this chapter. The design recommendations are given in a step-by-step manner. Comments are also included in each step to assist in interpretation of the recommendations.

A numerical example is also presented in this chapter to illustrate the two-way hinge design recommendations.

6.2 Step-by-Step Design Recommendations

Recommendations for the design of two-way hinge are as follows:

1) Determine the hinge section and the required longitudinal steel:

- Hinge area:

$$A_g \geq P_u \Big/ 0.2 f_c^{'}$$

Where:

A_g: gross area of hinge section;
P_u: design axial load;
f'_c: concrete compressive strength.

- Use minimum longitudinal reinforcement permitted by AASHTO provision for columns:

$$A_s \geq 0.01 A_g$$

Where:

A_s: hinge longitudinal reinforcement steel area.

2) Hinge transverse reinforcement design, using Mortensen and Saiidi's performance based design method (Ref. 37), for a target curvature ductility of 10.

3) Find hinge confined concrete properties. Hinges experience a "double confinement" from the hinge spiral and the confinement provide by surrounding column above and the footing below. Determine the effective confined lateral pressure and spiral steel ratio for use in Mander's method for f'_{cc}, ε_{cc} and ε_{cu}.

$$f_l = \left[(2 f_y A_{sh} / D^{'} s_h)_{hinge} + (2 f_y A_{sh} / D^{'} s_h)_{column} \right]$$

$$r_s = \left[\left(4A_{sh} \Big/ D^{'} s_h\right)_{hinge} + \left(4A_{sh} \Big/ D^{'} s_h\right)_{column} \right]$$

Where:

f_l: effective hinge confined lateral pressure;
? ρ_s: hinge effective volumetric ratio of confining steel;
f_y: yield strength of the reinforcement;

A_{sh}: spiral bar area;
D': diameter of the confined core;
s_h: spiral pitch.

4) Determine the flexural capacity of the hinge using the confined concrete properties. Make sure the hinge moment can be resisted by the footing. Adjust the hinge size, the longitudinal bar ratio, or both as necessary.

5) Calculate hinge shear capacity:

- Run moment curvature analysis; find section compression force (axial load change due to overturning moment needs to be included in the analysis):

  $C = C_c + C_s = P + T_s$

  Where:

  C: result compression force;
  C_c: compression force in concrete;
  C_s: compression force in reinforcement;
  P_u: design axial load;
  T_s: tension force in rebar.

- $\phi V_n = \phi\mu\, C = \phi\mu\, (C_c + C_s)$, use $\mu = 0.45$.

  Where:

  ϕ: strength reduction factor, 0.85.

6) Calculate hinge plastic shear demand:

$V_u = (M_c + M_h) / L$

Where:

M_c: column section plastic moment;
M_h: hinge section plastic moment;
L: column height.

7) Check to see if $\phi V_n > V_u$, if not adjust the hinge longitudinal bars, the size of the hinge section, or both, and repeat steps 1 to 7 until the shear capacity is sufficient.

8) Check for hinge gap closure. Determine if $\theta_n < \theta_{close}$, determine hinge gap thickness.

- Assume a hinge gap g = 100 mm (4 in).
- Nominal two-way hinge ultimate rotation:

  $L_p = g + 0.022 f_y d_b$ (f_y in MPa) (5-42)

  $L_p = g + 0.15 f_y d_b$ (f_y in ksi) (5-43)

  $q_n = q_e + q_p$ (5-44)

  $q_e = g\, f_y$ (5-45)

  $q_p = L_p (f_u - f_y)$ (5-46)

- Two-way hinge rotation for hinge closure:

  $q_{close} = \sin^{-1}\left(g \big/ 0.5D \right)$ (5-47)

  Where:

  D: column diameter.

- Check to see if $\theta_n < \theta_{closure}$, if not then increase hinge gap thickness until sufficient gap is provided to prevent gap closure.

9) Detailing of the two-way hinge section:

- Distribute the hinge longitudinal reinforcement around the section.
- Provide spiral for the hinge section, and extend into column and footing at least a distance of 1.25Ld (L_d = longitudinal bar tension development length).

6.3 Design Example

6.3.1 Design Example in US Customary Units

A circular bridge column has a clear height of 20 ft and diameter of 60 inch, 3% of longitudinal steel ratio, with column spiral of #7@4". Column design axial load and plastic moment are $P_u = 8\%A_g f'_c = 1131$ kips and $M_u = 11875$ kip-ft. The unconfined concrete compressive strength is 5000 psi; concrete strain at peak strength, ε_c, is 0.0021; the concrete ultimate strain, ε_u, is 0.0035; the steel yield strength, f_y, is 60 ksi; steel ultimate strength, f_u, is 80 ksi; steel strain at beginning of strain hardening, ε_{sh}, is 0.015; and steel strain at ultimate strength, ε_{su}, is 0.15.

1) Determine the hinge area and hinge longitudinal steel:

$A_g = P_u / 0.2f'_c = 1131 / (0.2 \times 5) = 1131$ in^2

Based on the required area, hinge diameter is:

$D_h = 38$ inch, with $A_g = 1134$ in^2.

$A_{s\ min} = 0.01 \times 1134 = 11.34$ in^2

Use 20-#7, $A_s = 12$ in^2 >11.34 in^2 O.K.

1st trial will be the section with $D_h = 38$ inch and 20-#7 longitudinal steel.

2) Using Mortensen and Saiidi method (Ref. 37), design the hinge spiral:

- Run M-ϕ analysis of the section which was defined at step 1, using unconfined concrete properties for the section. Find c and ϕ_y and calculate ϕ_u and ε_{cu} with target curvature ductility of $\mu \geq 10$:

  c = 13.54 inch

  $\phi_y = 0.0001094$ rad/in

  $\phi_u = \mu\phi_y = 10 \times 0.0001094 = 0.001094$ rad/in

  $\varepsilon_{cu} = c\phi_u = 13.54 \times 0.001094 = 0.0148$

- Calculate spiral steel ratio:

  $\rho_{sp} = (\varepsilon_{cu} - 0.004)(f'_c / f_y \varepsilon_{su}) = (0.0148-0.004)(5/60/0.15) = 0.006$

  Use #3 @ 2" spiral, $\rho_{sp} = 4A_s / D's = 4 \times 0.11 / (33 \times 2)$

  $= 0.0067 > 0.006$ O.K!

3) Determine hinge concrete confinement properties using Mander's equation with modified confined lateral pressure and spiral steel ratio for the hinge core concrete:

$$f_l = \left[(2 f_y A_{sh} / D's_h)_{hinge} + (2 f_y A_{sh} / D's_h)_{column} \right]$$

$= 2 \times 60 \times 0.11 / (33 \times 2) + 2 \times 60 \times 0.6 / (55.1 \times 4)$

$= 0.5265$ ksi

$$r_s = \left[\left(4A_s / D's\right)_{column} + \left(4A_s / D's\right)_{hinge}\right]$$

= 4 x 0.6 / (55.1 x 4) + 4 x 0.11 / (33 x 2)

= 0.0176

$$f'_{cc} = \left(-1.254 + 2.254\sqrt{1 + 7.94 f'_l / f'_c} - 2 f'_l / f'_c\right) f'_c$$

= (-1.254 + 2.254 x (1+7.94 x 0.5265 / 5)$^{1/2}$-2 x 0.5265 / 5) x 5

= 7.948 ksi

$$e_{cc} = 0.002\left[1 + 5\left(f'_{cc} / f'_c - 1\right)\right]$$

= 0.002 x (1+5 (7.948 / 5-1))

= 0.0079

$$e_{cu} = 0.004 + 1.4 r_s f_{yh} e_{su} / f'_{cc}$$

= 0.004 + 1.4 x 0.0176 x 60 x 0.15 / 7.948

= 0.0319

For the concrete outside the hinge core, use column confined core properties which are based on Mander's model, f'_{cc} = 6.965 ksi, ε'_{cc} =0.0059, ε'_{cu} = 0.0237.

4) Check if the footing is sufficiently strong to resist the hinge moment. From M-ϕ analysis of the hinge using confined concrete properties:

M_{hu} = 2208 kip-ft = 18.6% of column plastic moment.

Assume OK!

5) Find hinge shear capacity, based on results of hinge M-ϕ analysis:

M_{hu} = 2208 kip-ft.

T_s = 561.3 kips

$C = C_c + C_s = T_s + P$ =561.3 + 1131 =1692.3 kips

$\phi V_n = \phi\mu C$ = 0.85 x 0.45 x 1692.3 = 647.3 kips

6) Calculate column plastic shear demand based on column and hinge section plastic moments.

$V_u = (M_u + M_{hu}) / L$ = (11875 + 2208) / 20 = 704.2 kips

7) Check.

V_n = 647.3 kips < V_u = 704.2 kips No Good!

Design needs to be revised by increasing either the hinge section area or hinge steel ratio. In this case the difference between the shear demand and capacity is small. Therefore the hinge steel ratio will be increased. Repeat steps 4 to 7 until the design converges.

Repeat step 4: Use 22-#8 as hinge longitudinal steel, re-run M-ϕ analysis.

M_{hu} = 2562.5 kip-ft = 21.5% of column plastic moment

Assume OK!

Repeat step 5: From the latest M-ϕ analysis, T_s = 826.1 kips.

C = 826.1 + 1131 = 1957 kips

ϕV_n = 0.85 x 0.45 x 1957 = 748.6 kips

Repeat step 6: New column plastic shear.

V_u = (11875 + 2562.5) / 20 = 721.9 kips

Repeat step 7: V_n = 748.6 kips > V_u = 721.9 kips

Design O.K..

8) Check two-way hinge gap closure, and determine hinge gap thickness:

Assume g = 4 inch first.

$L_p = g + 0.15 f_y d_b$

= 4 + 0.15 x 60 x 1 =13 in

ϕ_y = 0.00015 rad/in

ϕ_u = 0.00396 rad/in

$q_e = g\ f_y$

= 4 x 0.00015 = 0.0006 rad

$q_p = L_p(f_u - f_y)$

= 13 x (0.00396 – 0.00015) = 0.0496 rad

$q_n = q_e + q_p$

= 0.0006 + 0.0496 = 0.0502 rad

$q_{close} = \sin^{-1}\left(g / 0.5D\right)$

= $\sin^{-1}$ [4 / (0.5 x 60)] =0.1337 rad

θ_n = 0.0502 rad < $\theta_{closure}$ = 0.1337 rad

Design O.K..

9) Horizontal gap is selected as 4 inch.

Figure 6-1shows the details of the final two-way hinge.

6.3.2 Design Example in SI Units

A circular bridge column has a clear height of 6.1 m and diameter of 1520 mm, 3% of longitudinal steel ratio, with column spiral of #7@102mm. Column design axial load and plastic moment are $P_u = 8\%A_g f'_c$ = 5033 KN and M_u =16103 KN-m. The unconfined concrete compressive strength is 34.5 MPa; concrete strain at peak strength, ε_c , is 0.0021; the concrete ultimate strain, ε_u , is 0.0035; the steel yield strength, f_y , is 414 MPa; steel ultimate strength, f_u , is 552 MPa; steel strain at beginning of strain hardening, ε_{sh} , is 0.015; and steel strain at ultimate strength, ε_{su} , is 0.15.

1) Determine the hinge area and hinge longitudinal steel:

$A_g = P_u / 0.2f'_c$ = 5033 / (0.2 x 34.5) = 7295 cm^2

Based on the required area, hinge diameter is:

D_h = 965 mm, with A_g = 7314 cm^2.

$A_{s\ min}$ = 0.01 x 7314 =73.14 cm^2

Use 20-#7, A_s = 77.4 cm^2 >73.14 cm^2 O.K.

1st trial will be the section with D_h = 965 mm and 20-#7 longitudinal steel.

2) Using Mortensen and Saiidi method (Ref. 37), design the hinge spiral:

- Run M-ϕ analysis of the section which was defined at step 1, using unconfined concrete properties for the section. Find c and ϕ_y and calculate ϕ_u and ε_{cu} with target curvature ductility of $\mu \geq 10$:

  c = 341.6 mm

  ϕ_y = 0.0043 rad/m

  $\phi_u = \mu\phi_y$ = 10 x 0.0043 =0.043 rad/m

$\varepsilon_{cu} = c\phi_u = 341.6 \times 0.043 \times 10^{-3} = 0.0148$

- Calculate spiral steel ratio:

$\rho_{sp} = (\varepsilon_{cu} - 0.004)(f'_c / f_y \varepsilon_{su})$

$= (0.0148-0.004)(34.5/414/0.15) = 0.006$

Use #3 @ 51 mm spiral, $\rho_{sp} = 4A_s / D's = 4 \times 71 / (838 \times 50.8)$

$= 0.0067 > 0.006$ O.K!

3) Determine hinge concrete confinement properties using Mander's equation with modified confined lateral pressure and spiral steel ratio for the hinge core concrete:

$$f_l = \left[(2 f_y A_{sh} / D' s_h)_{hinge} + (2 f_y A_{sh} / D' s_h)_{column}\right]$$

$= 2 \times 414 \times 71 / (838 \times 50.8) + 2 \times 414 \times 387 / (1400 \times 101.6)$

$= 3.63$ MPa

$$r_s = \left[\left(4A_s / D' s\right)_{column} + \left(4A_s / D' s\right)_{hinge}\right]$$

$= 4 \times 387 / (1400 \times 101.6) + 4 \times 71 / (838 \times 50.8)$

$= 0.0176$

$$f'_{cc} = \left(-1.254 + 2.254\sqrt{1 + 7.94 f'_l / f'_c} - 2 f'_l / f'_c\right) f'_c$$

$= (-1.254 + 2.254 \times (1+7.94 \times 3.63 / 34.5)^{1/2} - 2 \times 3.63 / 34.5) \times 34.5$

$= 54.8$ MPa

$$e_{cc} = 0.002\left[1 + 5\left(f'_{cc} / f'_c - 1\right)\right]$$

$= 0.002 \times (1+5 (54.8 / 34.5-1))$

$= 0.0079$

$$e_{cu} = 0.004 + 1.4 r_s f_{yh} e_{su} / f'_{cc}$$

$= 0.004 + 1.4 \times 0.0176 \times 414 \times 0.15 / 54.8$

$= 0.0319$

For the concrete outside the hinge core, use column confined core properties which are based on Mander's model, $f'_{cc} = 48$ MPa, $\varepsilon'_{cc} = 0.0059$, $\varepsilon'_{cu} = 0.0237$.

4) Check if the footing is sufficiently strong to resist the hinge moment. From M-ϕ? analysis of the hinge using confined concrete properties:

$M_{hu} = 2994$ KN-m = 18.6% of column plastic moment.

Assume OK!

5) Find hinge shear capacity, based on results of hinge M-ϕ analysis:

$M_{hu} = 2994$ KN-m

$T_s = 2498$ KN

$C = C_c + C_s = T_s + P = 2498 + 5033 = 7531$ KN

$\phi V_n = \phi \mu C = 0.85 \times 0.45 \times 7531 = 2880.5$ KN

6) Calculate column plastic shear demand based on column and hinge section plastic moments.

$V_u = (M_u + M_{hu}) / L = (16103 + 2994) / 6.1 = 3131$ KN

7) Check.

$V_n = 2880.5$ KN $< V_u = 3131$ KN No Good!

Design needs to be revised by increasing either the hinge section area or hinge steel ratio. In this case the difference between the shear demand and capacity is

small. Therefore the hinge steel ratio will be increased. Repeat steps 4 to 7 until the design converges.

Repeat step 4: Use 22-#8 as hinge longitudinal steel, re-run M-ϕ analysis.

M_{hu} = 3475 KN-m = 21.5% of column plastic moment

Assume OK!

Repeat step 5: From the latest M-ϕ analysis, T_s = 3676 KN.

C = 3676 + 5033 = 8709 KN

ϕV_n = 0.85 x 0.45 x 8709 = 3331 KN

Repeat step 6: New column plastic shear.

V_u = (16103 + 3475) / 6.1 = 3209.5 KN

Repeat step 7: V_n = 3331 KN > V_u = 3209.5 KN

Design O.K..

8) Check two-way hinge gap closure, and determine hinge gap thickness:

Assume g = 100 mm first.

$$L_p = g + 0.022 f_y d_b$$

= 100 + 0.022 x 414 x 25.4 = 331.3 mm

ϕ_y = 0.00592 rad/m

ϕ_u = 0.156 rad/m

$$q_e = g\ f_y$$

= (100/1000) x 0.00592 = 0.0006 rad

$$q_p = L_p(f_u - f_y)$$

= 331.3 x (0.156 – 0.00592) / 1000 = 0.0496 rad

$$q_n = q_e + q_p$$

= 0.0006 + 0.0496 = 0.0502 rad

$$q_{close} = \sin^{-1}\left(g \big/ 0.5D\right)$$

= $\sin^{-1}$ [100 / (0.5 x 1524)] =0.1316 rad

θ_n = 0.0502 rad < $\theta_{closure}$ = 0.1316 rad

Design O.K.

9) Horizontal gap is selected as 100 mm.

Figure 6-2 shows the details of the final two-way hinge.

CHAPTER SEVEN

SUMMARY AND CONCLUSIONS

7.1 Summary

Two-way hinges are commonly used in bridge columns to reduce column moment transfer to foundation. Codified guidelines for the design of two-way hinge details do not exist. Currently, the most common approach for two-way hinge design is to determine the hinge section size based on pure axial compressive load capacity, and to design for the hinge lateral load capacity by providing the amount of longitudinal steel required based on the shear friction method. Several issues can be raised about the behavior of the two-way hinge under seismic loading. First, flexural moment can occur at the column base where the hinge is located. Since the shear friction theory was developed under the condition of pure shear; the combination of the flexure moment was not included. Second, the flexural moment at the hinge will result in an increase in the plastic shear in the column over the assumed value. The added flexural moment and shear might exceed the capacity of the foundation.

A research program was undertaken in this study to evaluate the performance of reinforced concrete bridge columns with two-way hinges. Only two-way hinges with distributed steel bars were included in the study. The research objectives were to investigate the performance of two-way hinges subjected to combine vertical and lateral loads including seismic forces and to develop a comprehensive and reliable design method for practical application. The research program consisted of an experimental investigation and an analytical study. The experimental phase involved testing of five 1/3 scale bridge column specimens on the shake table under unidirectional shaking using a real earthquake motion. The ground motion used was the Northridge earthquake motion recorded at the Sylmar county hospital station. The analytical phase of the investigation consisted of the evaluation and verification of existing models and a new proposed method from this study by comparing the measured experimental results to those obtained from the analysis.

The test specimens consisted of circular reinforced concrete columns with two-way hinge details at the top. The specimens were designed such that the effects of potentially critical parameters could be isolated and studied. The parameters evaluated in this study included the column aspect ratio, magnitude of the axial load, column steel ratio, hinge steel ratio, and the two-way hinge diameter. These parameters were examined to study their effects on hinge strength, energy dissipation and hinge shear slippage. The specimens were tested in double curvature under increasing amplitudes of the Sylmar record using a shake table at the University of Nevada, Reno. The specimens were instrumented extensively to monitor the global response as well as the local deformation and strains. Several types of instruments were used including displacement transducers, accelerometers, load cells, and strain gauges. In the report the results of the

experimental study were presented; differences in behavior were observed; and the effects of the parameters investigated in the testing program were discussed.

Analytical studies were conducted on all five specimens. Existing methods and models to assess two-way hinge shear strengths, force-displacement response relationship, confinement at the hinge region and the dynamic strain rate effects on steel and concrete were evaluated. Using the experimental results, modifications and improvement to the existing methods were proposed as appropriate. In particular, the shear capacity of the two-way hinge and the rotation of hinge were studied in detail. A new approach was developed for estimating the lateral strength of two-way hinges as well as the rotation of the hinge. In addition, for a more accurate estimation of the moment-curvature relationship for two-way hinges, a new approach was recommended for determining the confined concrete properties of the hinge. A simple shear-slippage model was also developed for two-way hinges based on the experimental results and literature review. The model was implemented in the pushover analysis for all five specimens.

As an outcome of this research, a comprehensive design methodology for two-way hinge design was proposed. A design example was also developed to illustrate the application of the recommendations.

7.2 Conclusions

Based on the experimental and analytical studies performed in this research, the following observations and conclusions were drawn on various aspects of the performance and design of two-way hinges with distributed bars:

1) When subjected to dynamic lateral load under constant axial load, column with two-way hinge details of this study exhibited stable hinging and ductile behavior.
2) The dynamic testing of the specimens showed that when cracks are developed over the entire hinge section significant shear slippage could take place between the column and footing thus reducing the energy absorption capacity of the member.
3) The current method for determining the shear capacity of the hinge, based on the shear friction theory, can lead to erroneous results. The classical shear friction type behavior in which the two segments of the concrete slide parallel to each other was not observed in any of the specimens.
4) Initially shear forces in two-way hinges are resisted by friction only in the compression zone. Under large deformations, dowel action of the hinge longitudinal bars provides shear resistance. This failure phenomenal was implemented in the new proposed two-way hinge shear-slippage model.
5) The average effective friction coefficient at shear failure of the test specimens was approximately 0.45. This coefficient is lower than the value specified in design codes because of the cyclic effects and grinding of the hinge aggregate.
6) The proposed two-way hinge design method produced a close and conservative estimation of the lateral-load strength of two-way hinges.
7) Concrete in the hinge region is capable of sustaining large strains because it is well confined by both the hinge spirals and the adjacent column and footing.

The use of the method recommended in this study to predict the complete stress-strain response of concrete in two-way hinges resulted in a reasonably accurate prediction of the response.

8) The dowel action of the hinge reinforcement prevented total failure of the hinge. However, because the dowel action is realized only after large slippage of the hinge, it should not be used as the mechanism to determine the hinge shear capacity of the hinge.
9) To prevent hinge gap closure, the thickness of the hinge gap should be sufficient to allow for anticipated rotation at the two-way hinge. Insufficient joint thickness will result in unexpected additional moments and shear that will be transferred to the adjacent elements and potentially cause damage
10) A procedure for checking hinge closure was developed in this study. The proposed method produced a conservative estimate of the hinge rotation.
11) The measured average bond strength along the hinge longitudinal bars was in close agreement with the empirical expression of Leet's (Ref. 23).
12) Test data from the hinged specimens showed limited cracking on either side of the hinge. Therefore concentrated strains occur at the hinge location and bond slip analysis needs to account for bar slippage in the column and the footing.

REFERENCES

1. **AASHTO**, *LRFD Bridge Design Specification, second edition,* American Association of State Highway and Transportation officials, Washington, DC, 1998.

2. **AASHTO**, *Standard Specification for Highway Bridge, 17th edition,* American Association of State Highway and Transportation officials, Washington, DC, 2002.

3. **American Concrete Institute Committee 318**, "Building Code Requirements for Structural Concrete (ACI 318-02)", American Concrete Institute, Farmington Hills, Michigan, 2002.

4. **American Concrete Institute Committee 444**, "Dynamic Modeling of Concrete Structures", Publication SP-73, American Concrete Institute, Farmington Hills, Michigan, 1982.

5. **Applied Technology Council**, "Improved Seismic Design Criteria for California Bridge: Provisional Recommendations", Report No. ATC-32, Redwood City, CA, 1996.

6. **Base, G. D**., "Test on Four Prototypes Reinforced Concrete Hinges", *Cement and Concrete Association,* No. 17, London, May 1965.

7. **CALTRANS**, *Seismic Design Criteria version 1.3*, Engineering Service Center, Earthquake Engineering Branch, California Department of Transportation, Sacramento, CA, 2004.

8. **Chandane S. S., Sanders, H. D. and Saiidi, M. S.,** "Static and Dynamic Performance of RC Bridge Bents with Architectural-Flared Columns", Report No. CCEER-03-08, University of Nevada, Reno, 2003.

9. **Cheng, Z, Saiidi, M. and Sanders, D.** "Development of Seismic Design Method for Reinforced Concrete Two-Way Bridge Column Hinges", SEAOC 75th Annual Convention Conference Proceedings, San Diego, CA, 2005.

10. **Chopra, A.,** "Dynamics of Structures", Prentice Hall, USA, 1995.

11. **Computer and Structures INC.,** "Structural Analysis Program SAP-2000", Version 8, Berkeley, California, USA, June 2002.

12. **Correal, F. J., Saiidi, S., and Sanders, D.,** "Seismic Performance of RC Bridge Columns Reinforced with Two Interlocking Spirals", Report No. CCEER-04-06, University of Nevada, Reno, 2004.

13. **Eligehausen, R., Popov, P. E. and Bertero, V. V.,** "Local Bond Stress-Slip Relationships of Deformed Bars under Generalized Excitations", Earthquake Engineering Research Center, 83-23. Berkeley, CA, 1983.

14. **Elwood J. K. and Moehle P. J.,** "Shake Table Tests and Analytical Studies on the Gravity Load Collapse of Reinforced Concrete Frames", Pacific Earthquake Engineering Research Center, Report No. 2003/01, Richmond, CA, 2003.

15. **Gere, M. J. and Timoshenko, P. S.,** "Mechanics of Materials", Fourth Editon, PWS Publishing Company, Boston, MA, USA, 1997.

16. **Griezic, A., Cook, D. W. and Mitchell, D.,** "Stress-Strain Characteristics of Confined Concrete in Column "Hinges"", ACI Materials Journal, Vol. 95(4), pp. 419-428, ACI, Farmington Hills, Michigan, 1995.

17. **Haroun, M.A., Pardeon, G.C., and Shepard, R.** "Shear strength of pinned columns", *Proc., 2nd Annual Seismic Research Workshop*, CALTRANS, Sacramento, CA, 1993.

18. **Imbsen and Associates INC. and Chadwell, C.,** "Cross Section Analysis Program XTRACT", Version 3.0.3, Sacramento, CA, 2004.

19. **Jiang, Y., and Saiidi, M.** "Response and design of R/C one-way pier hinges in strong direction", *ASCE Journal of Structural Engineering*, Vol. 121, No. 8, ASCE, Reston, VA, 1995.

20. **Kulkarni, S.M., and S. P. Shah,** "Response of Reinforced Concrete Beams at High Strain Rates", ACI Structural Journal, Vol. 95, No. 6, November-December 1998.

21. **Laplace, P., Sanders, D., and Saiidi, M.,** "Experimental Study and Analysis of Retrofit Flexure and Shear Dominated Circular Reinforced Concrete Bridge Columns Subjected to Shake Table Excitation", Report No. CCEER-01-6, University of Nevada, Reno, 2001.

22. **Laplace, P., Sanders, D., Douglas, B., and Saiidi, M.,** "Shake Table Testing of Flexure Dominated Reinforced Concrete Bridge Columns", Report No. CCEER-99-13, University of Nevada, Reno, 1999.

23. **Leet K.,** "Reinforced Concrete Design", Second Edition, McGraw-Hill, INC., Hightstown, NJ, USA, 1991.

24. **Lehman E. D. and Moehle P. J.,** "Seismic Performance of Well-Confined Concrete Bridge Columns", Pacific Earthquake Engineering Research Center, Report No. 1998/01, Richmond, CA, 2000.

25. **Lim, K.Y., McLean, D.I., and Henley, E.H.,** "Moment-Reducing Hinge Details for the Bases of Bridge Columns", *Transportation Research Record,* No. 1275, Bridge research, pp. 1-11. TRB, Washington, DC, 1990.

26. **Mander, J. Priestley, M.J.N and Park, R.,** "Theoretical Stress-Strain Model for Confined Concrete Columns", ASCE Journal of Structural Engineering, Vol. 114, No 8, August 1988.

27. **Mattock, A. H., Johal, L. and Chow, H. C.,** "Shear Transfer in Reinforced Concrete with Moment of Tension Acting Across the Shear Plane", Journal of Prestressed Concrete Institute, Vol. 20(4) pp. 76-93, Chicago, IL , 1975.

28. **Melek, M., Wallace, W. J. and Conte, P., J.,** "Experimental Assessment of Columns with Short Lap Splices Subjected to Cyclic Loads", Pacific Earthquake Engineering Research Center, Report No. 2003/04, Richmond, CA, 2003.

29. **McGuire W., Gallagher R., Ziemian D.,** "Matrix Structural Analysis", First Edition, John Wiley & Sons, New York, 1979.

30. **Moustafa, K., Sanders, H. D. and Saiidi, M. S.,** "Impact of Aspect Ratio on Two-Column Bent Seismic Performance", Report No. CCEER-04-03, University of Nevada, Reno, 2004,

31. **Nada, M. H., Sanders, H. D. and Saiidi, M. S.,** "Seismic Performance of RC Bridge Frames with Architectural-Flared Columns", Report No. CCEER-03-03, University of Nevada, Reno , 2003.

32. **Park, R. and Paulay, T.,** "Reinforced Concrete Structures", John Wiley & Sons, USA, 1975.

33. **Priestley, N., Seible, F., Calvi, G.,** "Seismic Design and Retrofit of Bridges", John Wiley & Sons, New York, 1996.

34. **Pulido, P. C., Saiidi, S., and Sanders, D.,** "Seismic Performance and Retrofitting of Reinforced Concrete Bridge Bents", Report No. CCEER-02-01, University of Nevada, Reno , 2002.

35. **Sadrossadat, M. S. and Saiidi, M. S.,** "Effect of Constant and Variable Strain Rates on Stress-Strain Properties and Yield Propagation in Steel Reinforcing Bars", (accepted for publication), ACI Material Journal, ACI, Farmington Hills, Michigan, 2006.

36. **Saiidi, M.,** "Hysteresis Model for Reinforced Concrete", ASCE Journal of Structural Engineering, Vol. 108 No. ST5, pp 1077-1087, 1982.

37. **Saiidi, M., Mortensen, J.,** "A new performance-based Design for spirals in bridge columns," *Proceedings of the 7th US Conference* on Earthquake Engineering, Paper No.214, Session 62, DC-5c, 100pp. Boston, Massachusetts, July 2002.

38. **Saiidi, M., Orie, J. L. and Douglas, B.** "Lateral load response of reinforced concrete bridge columns with a one-way pinned end", *ACI Structural Journal*, Vol. 85(6), pp. 609-616, ACI, Farmington Hills, Michigan, 1988.

39. **Saiidi, M., and Straw, D.** "Monotonic and cyclic response of one-way R/C Bridge pier hinges in the strong direction", *ACI Structural Journal,* Vol. 90(5), pp. 568-573, ACI, Farmington Hills, Michigan, 1993.

40. **Sgambelluri, M., Sanders, H. D. and Saiidi, M. S.,** "Behavior of One-Way Reinforced Concrete Bridge Column Hinges in the Weak Direction", Report No. CCEER-99-12, University of Nevada, Reno, 1999.

41. **Silva, P. F., Megallly, S. and Seible, F.,** "Seismic Performance of Sacrificial Interior Shear Keys", ACI Structural Journal, ACI, Farmington Hills, Michigan, March-April 2003.

42. **Sureshkumar, K., Saiidi, S., Itani M. A. and Ladkany, S.,** "Seismic Retrofit of Two-Column Bents with Diamond Shape Columns", Report No. CCEER-04-09, University of Nevada, Reno, 2004.

43. **Viwathanatepa, S., Popov, P. E. and Bertero, V. V.,** "Effects of Generalized Loadings on Bond of Reinforcing Bars Embedded in Confined Concrete Blocks", Earthquake Engineering Research Center, 79-22, Berkeley, CA, 1979.

44. **Wehbe, N., Saiidi, S., and Sanders, D.,** "Effects of Confinement and Flare on the Seismic Performance of Reinforced Concrete Bridges Columns", Report No. CCEER-97-2, University of Nevada, Reno, 1997.

45. **Yusuf A. A.'s** WWW Super Civil Cd, Retrieved February, 2005, from http://www.supercivilcd.com/FRICTION.htm.

Table 2-1 Summary of Specimens

Specimen	THD-1	THD-2	THD-3	THD-4	THD-5
Column Height (mm)	1219 (48")	1626 (64")	1219 (48")	1219 (48")	1219 (48")
Column Diameter (mm)	406 (16")	406 (16")	406 (16")	406 (16")	406 (16")
Hinge Diameter (mm)	254 (10")	254 (10")	254 (10")	254 (10")	203 (8")
Column Aspect Ratio (L / D)	3	4	3	3	3
Area Ratio (A_{hinge}/A_{column})	0.39	0.39	0.39	0.39	0.28
Column Longitudinal Rebar	14 - # 7	13 - # 7	14 - # 4	10 - # 5	10 - # 7
Column Longitudinal Steel Ratio	4.20%	3.88%	1.40%	1.50%	3.0%
Column Spiral	#3 @ 38mm (1.5")				
Column Spiral Volume Ratio	1.96%				
Hinge Longitudinal Rebar	7 - # 3				6 - # 3
Hinge Longitudinal Steel Ratio	1.0%	1.0%	1.0%	1.0%	1.31%
Hinge Spiral	W2.1 @ 25mm (1")				
Hinge Spiral Volume Ratio	0.9%				1.20%
Axial Load (KN)	445 (100 Kips)	267 (60 Kips)	445 (100 Kips)	0	445 (100 Kips)
Column Axial Load Ratio ($P/A_{col}f'c$)	9.9%	6.0%	9.9%	0.0%	9.9%
Hinge Axial Load Ratio ($P/A_{hinge}f'c$)	25.5%	15.3%	25.5%	0.0%	39.8%

Table 2-2 Model Scale Factors for Different Parameters

Quantity	Target Scale Factor	Scale Factor Value Used
Model Scale	l_r	1/3
Length	l_r	1/3
Time (F_{axial}/ M_{mass} = 1)	$l_r^{1/2}$	0.577
Time (F_{axial}/ M_{mass} ? 1)	$(M_{mass}/F_{axial})^{1/2} l_r^{1/2}$	
Period	$l_r^{1/2}$	0.577
Frequency	$l_r^{-1/2}$	1.732
Displacement	l_r	1/3
Velocity	$l_r^{1/2}$	0.577
Acceleration	1.0	1
Mass Density	l_r^{-1}	3
Strain	1.0	1
Stress	1.0	1
Strain Rate	$l_r^{-1/2}$	1.732
Modulus of Elasticity	1.0	1
Force	l_r^2	0.111
Moment	l_r^3	0.037
Energy	l_r^3	0.037

Table 2-3 Concrete Mix Design

Criteria	Quantity	
	SI unit	US Customary
28-Day Compressive Strength	34.78 MPa	5000 psi
Design Air Content	2.1%	2.1%
Water/Cement Ratio	0.42	0.42
Cement-Nevada Type II	3.137 KN ($0.102\ m^3$)	705 lbs ($3.589\ ft^3$)
Water	1.312 KN ($0.134\ m^3$)	295 lbs ($4.729\ ft^3$)
No. 8 Stone-Paiute Pit	5.21 KN ($0.205\ m^3$)	1170 lbs ($7.242\ ft^3$)
Sand-Paiute Pit	7.81 KN ($0.306\ m^3$)	1755 lbs ($10.82\ ft^3$)
Master Builders 344N	0.0136 KN ($0.015\ m^3$)	49 oz ($0.052\ ft^3$)
Masters Builders Micro Air	0 KN ($0.016\ m^3$)	0 oz ($0.567\ ft^3$)
Supplier: Reno-Sparks Ready Mix	Prodect ID# 501500	Prodect ID# 501500

Table 2-4 Shaking Table Specifications

Items	Table Capacity
Table Size (m)	4.3 x 4.3 (14ft x 14ft)
Table Self-weight (KN)	150 (33 Kips)
Max. Payload (KN)	445 (100 Kips)
Max. Acceleration (g)	1g at 445 KN (100 Kips), 2.4g at 0 KN
Max. Velocity (cm/sec)	100 (40 in/sec)
Max. Static Displacement (cm)	±35.6 (14 in)
Max. Dynamic Displacement (cm)	±30.5 (12 in)
Roll Capacity (KN-m)	542 (400 Kips-in)
Pitch Capacity (KN-m)	1356 (1000 Kip-ft)
Yaw Capacity (KN-m)	542 (400 Kips-in)
Max. Actuator Force (KN)	734 (165 Kip)
Operation Frequency (Hz)	1 to 30

Table 2-5 Input Material Properties for Preliminary Moment-Curvature Analysis

Specimen		THD-1 to THD-4			THD-5		
		Column Core	Hinge Cover	Hinge Core	Column Core	Hinge Cover	Hinge Core
Confined Concrete	f'_{cc} (MPa)	57.1 (8.29 Ksi)	57.1 (8.29 Ksi)	64.8 (9.39 Ksi)	57.1 (8.29 Ksi)	57.1 (8.29 Ksi)	66.8 (9.69 Ksi)
	e_{cc}	0.0086	0.0086	0.0108	0.0086	0.0086	0.0114
	e_{cu}	0.0284	0.0284	0.0352	0.0284	0.0284	0.037
Unconfined Concrete	f'_c (MPa)	34.5 (5 Ksi)			34.5 (5 Ksi)		
	e_{co}	0.002			0.002		
	e_{sp}	0.005			0.005		
Reinforcement	f_y (MPa)	414 (60 Ksi)			414 (60 Ksi)		
	e_{sh}	0.015			0.015		
	f_u (MPa)	552 (80 psi)			552 (80 psi)		
	e_{su}	0.12			0.12		

Table 2-6 Preliminary Analysis Results

	Units	THD-1		THD-2		THD-3		THD-4		THD-5	
		Column	Hinge	Column	Hinge	Column	Hinge	Column	Hinge	Column	Hinge
M_{1st}	Kip-in	1957	415.7	1913	327.4	1356	415.7	1039	159.5	1921	329.3
	KN-m	221.1	47.0	216.2	37.0	153.2	47.0	117.4	18.0	217.1	37.2
f_{1st}	rad/in	0.000207	0.000484	0.000223	0.000425	0.000249	0.000484	0.00024	0.000332	0.000234	0.000962
	rad/m	0.008	0.019	0.009	0.017	0.010	0.019	0.009	0.013	0.009	0.038
M_y	Kip-in	3138	522.3	2830	417	1575	522.3	1225	229.8	2476	349.4
	KN-m	354.6	59.0	319.8	47.1	178.0	59.0	138.4	26.0	279.8	39.5
f_y	rad/in	0.00033	0.00061	0.00033	0.00054	0.00029	0.00061	0.00028	0.00048	0.00030	0.00102
	rad/m	0.013	0.024	0.013	0.021	0.011	0.024	0.011	0.019	0.012	0.040
M_{ult}	Kip-in	3467	532.5	3247	450.6	1744	532.5	1477	272.9	2720	342.4
	KN-m	391.8	60.2	366.9	50.9	197.1	60.2	166.9	30.8	307.4	38.7
f_{ult}	rad/in	0.0060	0.0101	0.0070	0.0129	0.0087	0.0101	0.0102	0.0161	0.0061	0.0104
	rad/m	0.235	0.397	0.277	0.506	0.342	0.397	0.402	0.632	0.241	0.409
V_y	Kips	76.3		50.7		43.7		30.3		58.9	
	KN	339.3		225.8		194.4		134.9		261.9	
D_y	in	0.369		0.549		0.234		0.240		0.338	
	cm	0.936		1.395		0.595		0.610		0.858	
$K_{elastic}$	kip/in	206.9		92.4		186.6		126.3		174.3	
	KN/m	36209.1		16163.2		32650.4		22096.9		30509.5	
V_{ult}	Kips	77.7		54.8		44.5		36.0		57.7	
	KN	346.0		244.0		198.2		160.2		256.7	
D_{ult}	in	2.629		4.790		2.475		3.728		2.704	
	cm	6.68		12.17		6.29		9.47		6.87	
$K_{plastic}$	kip/in	0.659		0.964		0.381		1.630		-0.498	
	KN/m	115.3		168.7		66.6		285.2		-87.2	

Table 2-7 Comparison of RC-Shake Dynamic Analysis for THD-1 and THD-2 under El Centro and Sylmar Motion

Specimen	THD-1		THD-2	
Earthquake Motion	El Centro	Sylmar	El Centro	Sylmar
Unscaled EQ Acceleration (g)	0.317	0.606	0.317	0.606
Scaled EQ Acceleration Factor	3.584	1.875	5.735	3
Scaled EQ Acceleration (g)	1.14	1.14	1.82	1.82
Unscaled Duration (s)	54	30	54	30
Scale Time Factor	0.577	0.577	0.577	0.577
Scaled Duration (s)	31.2	17.3	31.2	17.3
Specimen Max. Tip Deflection (mm)	41 (1.61 in.)	67 (2.65 in.)	93 (3.65 in.)	121 (4.78 in)
Specimen Max. Lateral Force (KN)	391 (87.9 Kips)	401 (90.2 Kips)	274 (61.7 Kips)	279 (62.8 Kips)
Max. Ductility Ratio	4.37	7.17	6.64	8.70

Table 2-8 Reinforcement Test Material Properties

Specimen	Reinforcement	Size	f_y		e_{sh}	f_u		e_{su}
			MPa	Ksi		MPa	Ksi	
THD-1	Col. Longitudinal	#7	426	61.8	0.01	690	100	0.15
	Col. Spiral	#3	421	61	N.A.	646	93.7	0.14
	Hinge Longitudinal	#3	510	74	0.003	752	109	0.15
	Hinge Spiral	W2.1.	365	53	N.A.	467	67.7	0.09
THD-2	Col. Longitudinal	#7	426	61.8	0.01	690	100	0.15
	Col. Spiral	#3	421	61	N.A.	646	93.7	0.14
	Hinge Longitudinal	#3	558	81	0.0064	789	114.5	0.1
	Hinge Spiral	W2.1.	400	58	N.A.	467	67.7	0.11
THD-3	Col. Longitudinal	#4	432	62.6	0.009	683	99	0.16
	Col. Spiral	#3	421	61	N.A.	646	93.7	0.14
	Hinge Longitudinal	#3	565	82	0.012	772	112	0.12
	Hinge Spiral	W2.1.	386	56	N.A.	467	67.7	0.14
THD-4	Col. Longitudinal	#5	454	65.9	0.01	696	101	0.14
	Col. Spiral	#3	421	61	N.A.	646	93.7	0.14
	Hinge Longitudinal	#3	565	82	0.012	772	112	0.12
	Hinge Spiral	W2.1.	386	56	N.A.	467	67.7	0.14
THD-5	Col. Longitudinal	#7	432	62.7	0.008	718	104.2	0.14
	Col. Spiral	#3	421	61	N.A.	646	93.7	0.14
	Hinge Longitudinal	#3	565	82	0.012	772	112	0.12
	Hinge Spiral	W2.1.	386	56	N.A.	467	67.7	0.14

Table 2-9 Concrete Compressive Strength

	Day	Units	THD-1	THD-2	THD-3	THD-4	THD-5
Hinge	7	psi	3730	5030	3540	3540	3540
		MPa	25.7	34.7	24.4	24.4	24.4
	14	psi	5823	5450	4720	4720	4720
		MPa	40.1	37.6	32.5	32.5	32.5
	28	psi	7310	5870	5540	5540	5540
		MPa	50.4	40.5	38.2	38.2	38.2
	Test	psi	7720	5910	5660	5640	5310
		MPa	53.2	40.7	39.0	38.9	36.6
Column	7	psi	3510	3510	4760	4760	4760
		MPa	24.2	24.2	32.8	32.8	32.8
	14	psi	4430	4430	5660	5660	5660
		MPa	30.5	30.5	39.0	39.0	39.0
	28	psi	5040	5040	7190	7190	7190
		MPa	34.8	34.8	49.6	49.6	49.6
	Test	psi	5160	5100	7490	7320	7420
		MPa	35.6	35.2	51.6	50.5	51.2
Footing	7	psi	3790	3790	4090	4090	4090
		MPa	26.1	26.1	28.2	28.2	28.2
	14	psi	4280	4280	4870	4870	4870
		MPa	29.5	29.5	33.6	33.6	33.6
	28	psi	5000	5000	5630	5630	5630
		MPa	34.5	34.5	38.8	38.8	38.8
	Test	psi	5820	5710	6170	5810	5960
		MPa	40.1	39.4	42.5	40.1	41.1

Table 3-1 Summary of Instrument Channel

		THD-1	THD-2	THD-3	THD-4	THD-5
Shake Table	**Displacement**	1	1	1	1	1
	Acceleration	1	1	1	1	1
Specimen Acceleration		1	1	1	1	1
Load Cells	**Lateral load**	2	2	2	2	2
	Axial load	2	2	2	2	2
Lateral Deflection Transducer		5	3	14	14	14
Transducer	**Curvature**	16	16	16	16	16
	Panel	12	12	12	12	12
	Hinge Slippage	2	2	2	2	2
	Footing Slippage	0	0	3	3	3
Strain Gauge	**Column Longi.**	19	16	19	20	20
	Column Spiral	19	21	14	14	14
	Hinge Longi.	13	20	23	23	22
	Hinge Spiral	4	20	19	20	20
Sum of Channel Number:		97	117	129	131	130

Table 3-2 Curvature Transducer Coordinates

Specimen	Transducer	Gauge Length		Distance from Column Face		Transducer	Gauge Length		Distance from Column Face	
		(mm)	(in)	(mm)	(in)		(mm)	(in)	(mm)	(in)
THD-1	NV-27	32	1.25	76	3	NV-48	32	1.25	51	2
	NV-54	133	5.25	64	2.5	NV-49	133	5.25	51	2
	NV-88	127	5	38	1.5	NV-56	127	5	89	3.5
	NV-85	140	5.5	38	1.5	NV-38	127	5	102	4
	NV-84	140	5.5	51	2	NV-18	121	4.75	51	2
	NV-11	114	4.5	38	1.5	NV-51	114	4.5	38	1.5
	NV-25	127	5	64	2.5	NV-44	121	4.75	51	2
	NV-36	114	4.5	64	2.5	NV-05	133	5.25	51	2
THD-2	NV-72	25	1	89	3.5	NV-30	25	1	89	3.5
	NV-48	130	5.125	146	5.75	NV-02	140	5.5	152	6
	NV-45	127	5	102	4	NV-19	133	5.25	102	4
	NV-90	133	5.25	76	3	NV-18	140	5.5	89	3.5
	NV-50	117	4.625	114	4.5	NV-84	140	5.5	140	5.5
	NV-70	127	5	73	2.875	NV-60	137	5.375	89	3.5
	NV-69	133	5.25	67	2.625	NV-05	140	5.5	108	4.25
THD-3	NV-42	25	1	127	5	NV-47	25	1	127	5
	NV-36	140	5.5	108	4.25	NV-08	146	5.75	127	5
	NV-35	102	4	76	3	NV-40	108	4.25	76	3
	NV-46	108	4.25	57	2.25	NV-44	108	4.25	70	2.75
	NV-43	95	3.75	133	5.25	NV-45	102	4	108	4.25
	NV-37	108	4.25	114	4.5	NV-34	114	4.5	105	4.125
	NV-38	102	4	76	3	NV-33	102	4	64	2.5
	NV-41	124	4.875	51	2	NV-48	127	5	64	2.5
THD-4	NV-42	25	1	121	4.75	NV-47	25	1	127	5
	NV-34	121	4.75	114	4.5	NV-08	140	5.5	127	5
	NV-33	108	4.25	70	2.75	NV-40	102	4	76	3
	NV-46	114	4.5	64	2.5	NV-43	114	4.5	70	2.75
	NV-44	102	4	76	3	NV-45	102	4	89	3.5
	NV-37	102	4	83	3.25	NV-36	102	4	89	3.5
	NV-38	108	4.25	133	5.25	NV-35	108	4.25	146	5.75
	NV-41	127	5	140	5.5	NV-48	127	5	152	6
THD-5	NV-47	25	1	146	5.75	NV-42	25	1	133	5.25
	NV-35	114	4.5	140	5.5	NV-08	114	4.5	127	5
	NV-36	102	4	89	3.5	NV-40	102	4	83	3.25
	NV-45	102	4	76	3	NV-46	102	4	89	3.5
	NV-44	102	4	146	5.75	NV-43	102	4	140	5.5
	NV-37	108	4.25	140	5.5	NV-34	108	4.25	135	5.33
	NV-38	108	4.25	102	4	NV-33	108	4.25	102	4
	NV-41	102	4	95	3.75	NV-48	108	4.25	102	4

Table 3-3 Panel Instrument Dimension

THD-1			THD-2			THD-3			THD-4			THD-5		
Panel	Length		Panel	Length		Panel	Length		Panel	Length		Panel	Length	
Instrument	(mm)	(in)	Instrument	(mm)	(in)	Instrument	(mm)	(in)	Instrument	(mm)	(in)	Instrument	(mm)	(in)
NV-87	368	14.5	**NV-85**	365	14.4	**TR50-29**	343	13.5	**TR50-20**	368	14.5	**TR50-29**	349	13.8
NV-68	419	16.5	**NV-15**	419	16.5	**TR100-6**	397	15.6	**TR50-6**	387	15.3	**TR100-6**	438	17.3
NV-45	375	14.8	**NV-62**	429	16.9	**TR50-7**	397	15.6	**TR50-30**	375	14.8	**TR50-19**	343	13.5
NV-20	419	16.5	**NV-41**	391	15.4	**TR50-19**	422	16.6	**TR50-19**	406	16.0	**TR50-30**	425	16.8
NV-61	413	16.3	**NV-24**	448	17.6	**TR50-30**	416	16.4	**TR50-31**	413	16.3	**TR50-27**	432	17.0
NV-66	419	16.5	**NV-86**	429	16.9	**TR50-27**	425	16.8	**TR50-7**	413	16.3	**TR50-7**	425	16.8
NV-19	362	14.3	**NV-55**	425	16.8	**TR50-20**	346	13.6	**TR50-29**	375	14.8	**TR50-20**	362	14.3
NV-4	425	16.8	**NV-25**	435	17.1	**TR100-1**	403	15.9	**TR50-26**	381	15.0	**TR100-1**	438	17.3
NV-64	375	14.8	**NV-9**	362	14.3	**TR50-31**	400	15.8	**TR50-27**	375	14.8	**TR50-31**	349	13.8
			NV-38	429	16.9									
			NV-39	422	16.6									
			NV-66	391	15.4									

Table 3-4 Test Loading Protocol

	THD-1		THD-2		THD-3		THD-4		THD-5	
Run No.	**x Sylmar**	**Peak acc. (g)**	**x Sylmar**	**Peak acc. (g)**	**x Sylmar**	**Peak acc. (g)**	**x Sylmar**	**Peak acc. (g)**	**x Sylmar**	**Peak acc. (g)**
1	0.1	0.06	0.1	0.06	0.1	0.06	0.1	0.06	0.1	0.06
2	0.25	0.15	0.25	0.15	0.25	0.15	0.25	0.15	0.25	0.15
3	0.5	0.30	0.5	0.30	0.5	0.30	0.375	0.23	0.5	0.30
	FREE VIBRATION									
4	0.75	0.45	0.75	0.45	0.75	0.45	0.5	0.30	0.75	0.45
5	1	0.61	1	0.61	1	0.61	0.75	0.45	1	0.61
	FREE VIBRATION									
6	1.25	0.76	1.25	0.76	1.25	0.76	1	0.61	1.25	0.76
7	1.5	0.91	1.5	0.91	1.5	0.91	1.25	0.76	1.5	0.91
8	1.75	1.06	1.75	1.06	1.75	1.06			1.75	1.06
9	2	1.21	2	1.21	2	1.21			2	1.21
	FREE VIBRATION								FREE VIBRATION	
10	2.25	1.36	2.25	1.36	2.25	1.36			2.25	1.36
11	2.5	1.52	2.5	1.52	2.5	1.52			2.5	1.52
12	2.625	1.59	2.625	1.59					2.75	1.67
13	2.75	1.67	2.75	1.67					3	1.82
14	2.875	1.74	2.875	1.74					3	1.82
15			3	1.82						

Table 4-1 Performance of Specimen THD-1

Run	Motion (x Sylmar)	PGA (g)	Observed Performance		
			Two-Way Hinge	Column	Others
1	0.1	0.06	No visible damage		
2	0.25	0.15	No visible damage		
3	0.5	0.3	No visible damage	Flexural crack at column base	
4	0.75	0.45		More flexural crack at column base	
5	1	0.6			
6	1.25	0.75	Visible shear crack at hinge	Spalling at column base	
7	1.5	0.9	Minor spalling at hinge	Column base spiral visible	
8	1.75	1.05	Spalling at hinge	Column base spalling	
9	2	1.2	More spalling at hinge	Column base longitudinal rebar visible	
10	2.25	1.35			Crack at bottom of head
11	2.5	1.5	Significant hinge spalling	Spalling at other side of column base	More crack at bottom of head
12	2.625	1.575	Hinge spiral visible	Significant spalling at both side of column	
13	2.75	1.65	Hinge permanent rotation	Column permanent deformation	
14	2.875	1.725	Hinge sheared off, separated from column		Column top cover sheared off

Table 4-2 Performance of Specimen THD-2

Runs	Motion (x Sylmar)	PGA (g)	Observed Performance		
			Two-Way Hinge	Column	Others
1	0.1	0.06	No visible damage		
2	0.25	0.15	No visible damage		
3	0.5	0.3	No visible damage	Column base visible crack	
4	0.75	0.45	Hinge shear crack	Flexural crack at column base	
5	1	0.6	Hinge shear crack		
6	1.25	0.75	Hinge spalling	Spalling at column base.	
7	1.5	0.9	More hinge spalling	Column base spalling	
8	1.75	1.05	Spalling at both side of hinge	More spalling at column base.	
9	2	1.2		Spalling at column base, spiral visible	Big crack at bottom of header
10	2.25	1.35	Hinge gap closed, hit column top edge		Column top cover damage
11	2.5	1.5	Hinge gap closed again, longitudinal rebar visible		
12	2.625	1.575	Hinge crush down, gap narrowed	More spalling at column base.	Loading head permanently offset from column center line.
13	2.75	1.65			
14	2.875	1.725	Hinge collapse		
15	3	1.8			Large permanent offset between head and column

Table 4-3 Performance of Specimen THD-3

Run	Motion (x Sylmar)	PGA (g)	Observed Performance		
			Two-Way Hinge	Column	Others
1	0.1	0.06	No visible damage		
2	0.25	0.15	No visible damage		
3	0.5	0.3	No visible damage	Column base crack	
4	0.75	0.45	Hinge visible crack	More cracking in the column base	
5	1	0.6	Hinge spalling at one side		
6	1.25	0.75	Hinge spalling at both side		Crack in head bottom.
7	1.5	0.9	Hinge spalling	Spalling at column base, column spiral visible	Crack in head
8	1.75	1.05	Significant hinge spalling	Longitudinal rebar visible at column base	
9	2	1.2	Gap Closed, hinge spiral visible	More spalling at column base	
10	2.25	1.35	Hinge crush down, permanent rotation		
11	2.5	1.5	One hinge rebar ruptured	Four longitudinal rebar ruptured at column base	

Table 4-4 Performance of Specimen THD-4

Run	Motion (x Sylmar)	PGA (g)	Observed Performance		
			Two-Way Hinge	Column	Others
1	0.1	0.06	No visible damage	Crack at column base	
2	0.25	0.15			
3	0.375	0.225		Significant crack at column base,	
4	0.5	0.3	Shear crack at both side of the hinge	More crack at column base	
5	0.75	0.45	Hinge spalling at both side		
6	1	0.6	Hinge significant spalling, spiral visible	Crack at column base, no visible spalling	
7	1.25	0.75	Hinge shear off, hinge rebar fractured		

Table 4-5 Performance of SpecimenTHD-5

Run	Motion (x Sylmar)	PGA (g)	Observed Performance		
			Two-Way Hinge	Column	Others
1	0.1	0.06	No visible damage		
2	0.25	0.15	Hinge crack	Crack at oneside of the column base	
3	0.5	0.3	Hinge spalling	More cracks at column base	
4	0.75	0.45	More spalling at hinge		
5	1	0.6			
6	1.25	0.75		Column base crack increase	
7	1.5	0.9	Spalling at both side of the hinge	Spalling at one side of the column base	
8	1.75	1.05	Gap closed, hinge spiral visible		
9	2	1.2	Hing crush down	More spalling at column base	
10	2.25	1.35			
11	2.5	1.5	Hinge core damage, gap narrowed		Column top cover sheared off
12	2.75	1.65		Column permanent deformation	
13	3	1.8	One hinge longitudinal rebar fracture		
14	3	1.8	Large permant slippage between hinge and column		

Table 4-6 Target and Achieved Table Peak Accelerations & Spectral Acceleration for Specimen THD-1

Input Motion	PGA (g)		PGA Ratio	Specimen	SA (g)		SA Ratio
(xSylmar)	Target	Achieved	(Achieved/Target)	Period	Target	Achieved	(Achieved/Target)
0.1	0.06	0.08	1.27	0.270	0.13	0.14	1.08
0.25	0.15	0.15	1.00	0.270	0.34	0.35	1.03
0.5	0.30	0.30	0.98	0.287	0.68	0.63	0.93
0.75	0.45	0.39	0.86	0.293	0.99	0.74	0.75
1	0.61	0.55	0.91	0.315	1.31	0.89	0.68
1.25	0.76	0.69	0.92	0.343	1.38	1.1	0.80
1.5	0.91	0.81	0.90	0.417	1.45	1.26	0.87
1.75	1.06	0.94	0.88	0.440	1.94	1.3	0.67
2	1.21	1.05	0.87	0.470	2.26	1.4	0.62
2.25	1.36	1.12	0.82	0.506	1.99	1.25	0.63
2.5	1.52	1.20	0.80	0.543	1.5	1.14	0.76
2.625	1.59	1.27	0.80	0.569	1.33	1.18	0.89
2.75	1.67	1.41	0.84	0.596	1.16	1.16	1.00
2.875	1.74	1.79	1.03	0.641	1.26	0.96	0.76

Table 4-7 Target and Achieved Table Peak Accelerations & Spectral Acceleration for Specimen THD-2

Input Motion	PGA (g)		PGA Ratio	Specimen	SA (g)		SA Ratio
(xSylmar)	Target	Achieved	(Achieved/Target)	Period	Target	Achieved	(Achieved/Target)
0.1	0.06	0.04	0.63	0.303	0.14	0.11	0.79
0.25	0.15	0.16	1.06	0.303	0.34	0.33	0.97
0.5	0.30	0.30	0.98	0.303	0.68	0.63	0.93
0.75	0.45	0.44	0.97	0.328	0.98	0.87	0.89
1	0.61	0.61	1.00	0.368	1.08	1.03	0.95
1.25	0.76	0.64	0.85	0.425	1	1.1	1.10
1.5	0.91	0.82	0.90	0.457	1.65	1.46	0.88
1.75	1.06	1.15	1.09	0.540	1.6	1.32	0.83
2	1.21	1.38	1.14	0.607	0.93	0.7	0.75
2.25	1.36	1.45	1.06	0.670	1	0.8	0.80
2.5	1.52	1.44	0.95	0.704	1.27	1.04	0.82
2.625	1.59	1.52	0.96	0.753	1.4	1.21	0.86
2.75	1.67	1.56	0.93	0.817	1.42	1.23	0.87
2.875	1.74	1.64	0.94	0.860	1.31	1.11	0.85
3	1.82	1.69	0.93	0.885	1.26	1.08	0.86

Table 4-8 Target and Achieved Table Peak Accelerations & Spectral Acceleration for Specimen THD-3

Input Motion	PGA (g)		PGA Ratio	Specimen	SA (g)		SA Ratio
(xSylmar)	Target	Achieved	(Achieved/Target)	Period	Target	Achieved	(Achieved/Target)
0.1	0.06	0.07	1.14	0.227	0.12	0.13	1.08
0.25	0.15	0.15	0.97	0.227	0.29	0.56	1.93
0.5	0.30	0.30	1.00	0.262	0.62	0.76	1.23
0.75	0.45	0.45	0.98	0.331	0.89	0.76	0.85
1	0.61	0.42	0.69	0.452	1.18	1	0.85
1.25	0.76	0.54	0.72	0.483	1.35	0.81	0.60
1.5	0.91	0.73	0.81	0.573	0.7	0.47	0.67
1.75	1.06	1.10	1.04	0.663	0.83	0.69	0.83
2	1.21	1.50	1.24	0.787	0.98	0.78	0.80
2.25	1.36	1.82	1.33	0.925	0.83	0.77	0.93
2.5	1.52	1.87	1.23	1.042	1.1	0.84	0.76

Table 4-9 Target and Achieved Table Peak Accelerations & Spectral Acceleration for Specimen THD-4

Input Motion	PGA (g)		PGA Ratio	Specimen	SA (g)		SA Ratio
(xSylmar)	Target	Achieved	(Achieved/Target)	Period	Target	Achieved	(Achieved/Target)
0.1	0.06	0.05	0.89	0.361	0.1	0.09	0.90
0.25	0.15	0.17	1.12	0.361	0.25	0.27	1.08
0.375	0.23	0.28	1.22	0.403	0.31	0.3	0.97
0.5	0.30	0.36	1.19	0.476	0.54	0.34	0.63
0.75	0.45	0.57	1.25	0.528	0.51	0.32	0.63
1	0.61	0.79	1.31	0.604	0.41	0.38	0.93
1.25	0.76	0.97	1.28	0.739	0.67	0.55	0.82

Table 4-10 Target and Achieved Table Peak Accelerations & Spectral Acceleration for Specimen THD-5

Input Motion	PGA (g)		PGA Ratio	Specimen	SA (g)		SA Ratio
(xSylmar)	Target	Achieved	(Achieved/Target)	Period	Target	Achieved	(Achieved/Target)
0.1	0.06	0.05	0.81	0.261	0.12	0.11	0.92
0.25	0.15	0.17	1.09	0.261	0.31	0.3	0.97
0.5	0.30	0.29	0.95	0.303	0.66	0.59	0.89
0.75	0.45	0.41	0.91	0.348	0.8	0.55	0.69
1	0.61	0.55	0.92	0.362	1	0.79	0.79
1.25	0.76	0.71	0.94	0.419	1.2	0.9	0.75
1.5	0.91	0.83	0.92	0.491	1.55	0.91	0.59
1.75	1.06	0.90	0.84	0.555	0.9	0.61	0.68
2	1.21	1.23	1.02	0.596	0.8	0.6	0.75
2.25	1.36	1.45	1.06	0.786	1.1	0.82	0.75
2.5	1.52	1.65	1.09	0.829	1.04	0.825	0.79
2.75	1.67	1.75	1.05	0.885	1	0.86	0.86
3	1.82	1.95	1.07	0.920	1.1	0.97	0.88
3	1.82	1.99	1.10	0.980	1.2	1.02	0.85

Table 4-11 Dynamic Properties from Free Vibration for THD-1

Previous Motion (xSylmar)	Frequency (Hz)	Period (sec.)	Stiffness (Kip/in)	Stiffness (KN/mm)	Damping Ratio
0.1	3.955	0.253	160.0	28.0	3.1%
0.75	3.54	0.282	128.2	22.4	4.1%
1.0	3.76	0.266	144.6	25.3	7.3%
2.0	2.74	0.365	76.8	13.4	8.7%

Table 4-12 Dynamic Properties from Free Vibration for THD-2

Previous Motion (xSylmar)	Frequency (Hz)	Period (sec.)	Stiffness (Kip/in)	Stiffness (KN/mm)	Damping Ratio
0.1	3.565	0.281	130.0	22.7	3.3%
0.75	3.02	0.331	93.3	16.3	4.3%
2.0	2.148	0.466	47.2	8.3	5.0%

Table 4-13 Dynamic Properties from Free Vibration for THD-3

Previous Motion (xSylmar)	Frequency (Hz)	Period (sec.)	Stiffness (Kip/in)	Stiffness (KN/mm)	Damping Ratio
0.1	3.66	0.273	137.0	24.0	6.1%
0.75	3.03	0.330	93.9	16.4	7.0%
2.0	2.88	0.347	84.8	14.8	10.2%

Table 4-14 Dynamic Properties from Free Vibration for THD-4

Previous Motion (xSylmar)	Frequency (Hz)	Period (sec.)	Stiffness (Kip/in)	Stiffness (KN/mm)	Damping Ratio
0.1	2.73	0.366	76.2	13.3	3.4%
0.5	1.758	0.569	31.6	5.5	4.5%
0.75	1.66	0.602	28.2	4.9	5.9%

Table 4-15 Dynamic Properties from Free Vibration for THD-5

Previous Motion (xSylmar)	Frequency (Hz)	Period (sec.)	Stiffness (Kip/in)	Stiffness (KN/mm)	Damping Ratio
0.1	3.46	0.289	122.4	21.4	4.2%
1.0	2.73	0.366	76.2	13.3	5.3%
1.25	2.93	0.341	87.8	15.4	5.0%
2.0	2.24	0.446	51.3	9.0	6.7%

Table 4-16 Axial Load Variation

	Units	THD-1	THD-2	THD-3	THD-4	THD-5
Target Axial Load	**(KN)**	445	267	445	N/A	445
	(Kips)	100	60	100	N/A	100
Max. Axial Load	**(KN)**	466	287.6	484	N/A	484
	(Kips)	104.7	64.6	108.8	N/A	108.8
Min. Axial Load	**(KN)**	394	233	362	N/A	404
	(Kips)	88.5	52.4	81.3	N/A	90.8
Average Axial Load	**(KN)**	430	260.3	423	N/A	444
	(Kips)	96.6	58.5	95.1	N/A	99.8

Table 4-17 Peak Accelerations at Top of the Specimens

Motion		THD-1	THD-2	THD-3	THD-4	THD-5
0.1 x Sylmar	**Max (g)**	0.21	0.11	0.18	0.09	0.14
	Min (g)	-0.27	-0.14	-0.17	-0.11	-0.11
0.25 x Sylmar	**Max (g)**	0.32	0.32	0.39	0.34	0.32
	Min (g)	-0.34	-0.34	-0.31	-0.24	-0.33
0.375 x Sylmar	**Max (g)**	N/A	N/A	N/A	0.32	N/A
	Min (g)	N/A	N/A	N/A	-0.31	N/A
0.5 x Sylmar	**Max (g)**	0.51	0.61	0.46	0.28	0.46
	Min (g)	-0.54	-0.55	-0.49	-0.33	-0.53
0.75 x Sylmar	**Max (g)**	0.73	0.79	0.49	0.34	0.46
	Min (g)	-0.73	-0.61	-0.67	-0.37	-0.62
1.0 x Sylmar	**Max (g)**	0.77	0.88	0.46	0.28	0.63
	Min (g)	-0.74	-0.78	-0.56	-0.39	-0.71
1.25 x Sylmar	**Max (g)**	1.01	0.84	0.60	0.33	0.67
	Min (g)	-0.87	-0.71	-0.69	-0.42	-0.80
1.5 x Sylmar	**Max (g)**	0.92	0.89	0.58		0.64
	Min (g)	-0.76	-0.84	-0.66		-0.85
1.75 x Sylmar	**Max (g)**	0.99	0.92	0.52		0.58
	Min (g)	-0.83	-0.81	-0.63		-0.96
2.0 x Sylmar	**Max (g)**	1.02	0.92	0.56		0.54
	Min (g)	-0.80	-0.83	-0.56		-0.75
2.25 x Sylmar	**Max (g)**	0.97	0.94	0.44		0.58
	Min (g)	-0.81	-0.85	-0.47		-0.72
2.5 x Sylmar	**Max (g)**	1.01	0.81	0.44		0.58
	Min (g)	-0.76	-0.77	-0.45		-0.79
2.625 x Sylmar	**Max (g)**	0.92	0.75		N/A	N/A
	Min (g)	-0.78	-0.77			N/A
2.75 x Sylmar	**Max (g)**	0.93	0.84			0.57
	Min (g)	-0.83	-0.61			-0.79
2.875 x Sylmar	**Max (g)**	0.88	0.87	N/A		N/A
	Min (g)	-0.80	-0.73			N/A
3.0 x Sylmar (1)	**Max (g)**	N/A	0.93			0.64
	Min (g)		-0.67			-0.99
3.0 x Sylmar (2)	**Max (g)**		N/A			0.55
	Min (g)					-0.88

Table 4-18 Measured Peak Lateral Force and Displacement for THD-1

Motion	Peak Force								Peak Displacement							
	Maximum				Minimum				Maximum				Minimum			
	Force		Displacement		Force		Displacement		Displacement		Force		Displacement		Force	
xSylmar	(KN)	(Kips)	(mm)	(inch)	(KN)	(Kips)	(mm)	(inch)	(mm)	(inch)	(KN)	(Kips)	(mm)	(inch)	(KN)	(Kips)
0.1	67.8	15.2	2.60	0.10	-69.7	-15.7	-1.85	-0.07	2.68	0.11	65.9	14.8	-2.22	-0.09	-66.2	-14.9
0.25	129.0	29.0	4.78	0.19	-128.6	-28.9	-4.90	-0.19	5.06	0.20	110.2	24.8	-4.90	-0.19	-128.6	-28.9
0.5	209.5	47.1	9.65	0.38	-215.7	-48.5	-9.84	-0.39	9.90	0.39	206.1	46.3	-9.84	-0.39	-215.7	-48.5
0.75	292.7	65.8	15.72	0.62	-252.9	-56.8	-12.47	-0.49	15.98	0.63	288.2	64.8	-12.79	-0.50	-251.8	-56.6
1.0	328.2	73.8	19.83	0.78	-269.3	-60.5	-14.92	-0.59	20.76	0.82	317.0	71.2	-15.19	-0.60	-267.1	-60.0
1.25	368.4	82.8	32.07	1.26	-312.6	-70.3	-19.64	-0.77	33.94	1.34	349.0	78.4	-19.84	-0.78	-312.0	-70.1
1.5	362.1	81.4	37.73	1.49	-285.7	-64.2	-17.71	-0.70	37.98	1.50	351.1	78.9	-18.20	-0.72	-282.4	-63.5
1.75	375.2	84.3	44.90	1.77	-300.5	-67.5	-20.63	-0.81	45.39	1.79	368.9	82.9	-20.63	-0.81	-300.5	-67.5
2.0	380.9	85.6	52.36	2.06	-306.3	-68.8	-21.75	-0.86	54.11	2.13	379.1	85.2	-21.75	-0.86	-306.3	-68.8
2.25	376.6	84.6	60.58	2.39	-302.2	-67.9	-23.91	-0.94	61.59	2.42	374.3	84.1	-23.91	-0.94	-302.2	-67.9
2.5	375.3	84.3	66.39	2.61	-306.7	-68.9	-26.42	-1.04	67.82	2.67	375.2	84.3	-27.05	-1.07	-300.2	-67.5
2.625	374.1	84.1	73.00	2.87	-301.3	-67.7	-25.41	-1.00	73.32	2.89	370.5	83.3	-26.99	-1.06	-293.5	-65.9
2.75	381.3	85.7	84.51	3.33	-318.5	-71.6	-31.63	-1.25	85.74	3.38	374.3	84.1	-33.29	-1.31	-311.8	-70.1
2.875	378.3	85.0	120.51	4.74	-324.9	-73.0	-37.74	-1.49	120.68	4.75	299.5	67.3	-38.74	-1.53	-323.7	-72.7

98

Table 4-19 Measured Peak Lateral Force and Displacement for THD-2

Motion	Peak Force								Peak Displacement							
	Maximum				Minimum				Maximum				Minimum			
	Force		Displacement		Force		Displacement		Displacement		Force		Displacement		Force	
xSylmar	(KN)	(Kips)	(mm)	(inch)	(KN)	(Kips)	(mm)	(inch)	(mm)	(inch)	(KN)	(Kips)	(mm)	(inch)	(KN)	(Kips)
0.1	32.3	7.3	2.18	0.09	-35.1	-7.9	-2.50	-0.10	2.52	0.10	29.5	6.6	-3.15	-0.12	-33.7	-7.6
0.25	81.4	18.3	5.93	0.23	-86.8	-19.5	-7.46	-0.29	6.53	0.26	76.5	17.2	-7.85	-0.31	-84.0	-18.9
0.5	152.5	34.3	15.28	0.60	-137.6	-30.9	-14.30	-0.56	15.28	0.60	152.5	34.3	-14.50	-0.57	-132.0	-29.7
0.75	195.1	43.8	24.60	0.97	-161.7	-36.3	-18.18	-0.72	24.60	0.97	195.1	43.8	-18.18	-0.72	-161.7	-36.3
1.0	221.6	49.8	36.65	1.44	-211.1	-47.4	-27.77	-1.09	37.19	1.46	221.1	49.7	-27.98	-1.10	-204.3	-45.9
1.25	223.1	50.1	41.12	1.62	-189.6	-42.6	-26.37	-1.04	41.52	1.63	213.5	48.0	-26.37	-1.04	-189.6	-42.6
1.5	235.9	53.0	57.40	2.26	-217.4	-48.9	-31.18	-1.23	62.71	2.47	231.0	51.9	-31.18	-1.23	-217.4	-48.9
1.75	243.8	54.8	78.90	3.11	-211.2	-47.5	-32.73	-1.29	82.31	3.24	240.3	54.0	-34.73	-1.37	-207.8	-46.7
2.0	242.2	54.4	92.53	3.64	-218.9	-49.2	-40.97	-1.61	98.58	3.88	236.4	53.1	-42.63	-1.68	-216.5	-48.6
2.25	239.1	53.7	110.30	4.34	-224.1	-50.4	-49.58	-1.95	110.30	4.34	239.1	53.7	-50.05	-1.97	-220.7	-49.6
2.5	218.9	49.2	111.87	4.40	-221.9	-49.9	-54.29	-2.14	112.71	4.44	213.9	48.1	-55.00	-2.17	-175.5	-39.4
2.625	212.3	47.7	127.38	5.02	-214.0	-48.1	-44.14	-1.74	128.96	5.08	207.6	46.7	-57.28	-2.26	-198.9	-44.7
2.75	236.5	53.1	134.67	5.30	-170.7	-38.4	-30.17	-1.19	142.47	5.61	206.9	46.5	-39.15	-1.54	-165.4	-37.2
2.875	243.0	54.6	159.19	6.27	-210.6	-47.3	-17.48	-0.69	164.30	6.47	225.5	50.7	-25.48	-1.00	-193.4	-43.5
3	249.9	56.2	186.51	7.34	-195.8	-44.0	-10.81	-0.43	187.59	7.39	247.3	55.6	-12.90	-0.51	-153.6	-34.5

Table 4-20 Measured Peak Lateral Force and Displacement for THD-3

Motion	Peak Force								Peak Displacement							
	Maximum				Minimum				Maximum				Minimum			
	Force		Displacement		Force		Displacement		Displacement		Force		Displacement		Force	
xSylmar	(KN)	(Kips)	(mm)	(inch)	(KN)	(Kips)	(mm)	(inch)	(mm)	(inch)	(KN)	(Kips)	(mm)	(inch)	(KN)	(Kips)
0.1	53.8	12.1	1.54	0.06	-53.0	-11.9	-1.56	-0.06	1.54	0.06	53.8	12.1	-1.80	-0.07	-47.4	-10.7
0.25	112.1	25.2	4.28	0.17	-104.1	-23.4	-4.61	-0.18	4.28	0.17	112.1	25.2	-4.61	-0.18	-104.1	-23.4
0.5	182.4	41.0	11.14	0.44	-160.8	-36.1	-9.41	-0.37	11.14	0.44	182.4	41.0	-9.43	-0.37	-158.8	-35.7
0.75	215.5	48.4	23.56	0.93	-174.6	-39.2	-11.21	-0.44	24.07	0.95	211.5	47.5	-12.00	-0.47	-170.2	-38.3
1.0	217.6	48.9	27.05	1.06	-176.8	-39.7	-16.58	-0.65	27.53	1.08	211.5	47.5	-16.58	-0.65	-176.8	-39.7
1.25	228.5	51.3	38.93	1.53	-193.2	-43.4	-21.41	-0.84	41.23	1.62	225.0	50.6	-23.36	-0.92	-183.0	-41.1
1.5	233.8	52.5	51.51	2.03	-198.6	-44.6	-27.64	-1.09	55.67	2.19	226.6	50.9	-27.74	-1.09	-189.5	-42.6
1.75	231.2	51.9	64.22	2.53	-197.9	-44.5	-32.14	-1.27	76.30	3.00	220.9	49.6	-38.58	-1.52	-189.6	-42.6
2.0	253.2	56.9	85.98	3.39	-181.0	-40.7	-32.52	-1.28	95.67	3.77	200.2	45.0	-37.33	-1.47	-174.9	-39.3
2.25	207.8	46.7	112.37	4.42	-157.6	-35.4	-23.86	-0.94	122.87	4.84	202.9	45.6	-31.36	-1.23	-147.6	-33.2
2.5	161.0	36.2	161.11	6.34	-134.5	-30.2	-30.13	-1.19	171.51	6.75	133.9	30.1	-30.24	-1.19	-131.2	-29.5

Table 4-21 Measured Peak Lateral Force and Displacement for THD-4

Motion	Peak Force								Peak Displacement							
	Maximum				Minimum				Maximum				Minimum			
	Force		Displacement		Force		Displacement		Displacement		Force		Displacement		Force	
xSylmar	(KN)	(Kips)	(mm)	(inch)	(KN)	(Kips)	(mm)	(inch)	(mm)	(inch)	(KN)	(Kips)	(mm)	(inch)	(KN)	(Kips)
0.1	37.4	8.4	2.53	0.10	-38.4	-8.6	-2.30	-0.09	2.59	0.10	35.5	8.0	-2.30	-0.09	-38.4	-8.6
0.25	89.3	20.1	7.83	0.31	-100.5	-22.6	-7.86	-0.31	7.88	0.31	86.9	19.5	-7.86	-0.31	-100.5	-22.6
0.375	121.8	27.4	14.15	0.56	-109.7	-24.6	-9.73	-0.38	15.02	0.59	118.6	26.7	-10.12	-0.40	-105.3	-23.7
0.5	126.4	28.4	19.18	0.76	-93.4	-21.0	-8.89	-0.35	19.31	0.76	124.0	27.9	-9.18	-0.36	-92.3	-20.8
0.75	141.6	31.8	26.35	1.04	-101.6	-22.8	-10.28	-0.40	27.96	1.10	137.2	30.8	-10.28	-0.40	-101.6	-22.8
1.0	153.8	34.6	45.34	1.79	-98.7	-22.2	-9.90	-0.39	46.17	1.82	151.6	34.1	-10.16	-0.40	-94.4	-21.2
1.25	169.7	38.1	65.42	2.58	-92.4	-20.8	-8.81	-0.35	74.73	2.94	114.7	25.8	-9.43	-0.37	-90.4	-20.3

Table 4-22 Measured Peak Lateral Force and Displacement for THD-5

Motion	Peak Force								Peak Displacement							
	Maximum				Minimum				Maximum				Minimum			
	Force		Displacement		Force		Displacement		Displacement		Force		Displacement		Force	
xSylmar	(KN)	(Kips)	(mm)	(inch)	(KN)	(Kips)	(mm)	(inch)	(mm)	(inch)	(KN)	(Kips)	(mm)	(inch)	(KN)	(Kips)
0.1	49.8	11.2	1.88	0.07	-48.9	-11.0	-2.18	-0.09	1.88	0.07	49.8	11.2	-2.18	-0.09	-48.9	-11.0
0.25	123.7	27.8	6.34	0.25	-110.9	-24.9	-5.49	-0.22	6.34	0.25	123.7	27.8	-5.49	-0.22	-110.9	-24.9
0.5	220.3	49.5	14.26	0.56	-174.6	-39.2	-9.18	-0.36	14.28	0.56	211.6	47.6	-9.64	-0.38	-171.9	-38.6
0.75	243.7	54.8	17.86	0.70	-191.7	-43.1	-11.33	-0.45	17.86	0.70	243.7	54.8	-11.33	-0.45	-191.7	-43.1
1.0	276.9	62.2	25.51	1.00	-233.5	-52.5	-16.23	-0.64	26.07	1.03	265.6	59.7	-16.23	-0.64	-233.5	-52.5
1.25	297.7	66.9	37.39	1.47	-248.3	-55.8	-19.01	-0.75	39.15	1.54	291.3	65.5	-20.59	-0.81	-240.0	-53.9
1.5	309.5	69.5	51.72	2.04	-240.0	-53.9	-21.50	-0.85	51.82	2.04	301.4	67.7	-21.59	-0.85	-232.8	-52.3
1.75	330.9	74.4	55.36	2.18	-222.3	-50.0	-20.70	-0.82	102.02	4.02	-21.0	-4.7	-20.70	-0.82	-222.3	-50.0
2.0	292.1	65.6	93.11	3.67	-217.0	-48.8	8.19	0.32	97.61	3.84	283.0	63.6	7.52	0.30	-213.5	-48.0
2.25	301.3	67.7	111.47	4.39	-219.8	-49.4	10.27	0.40	113.80	4.48	296.9	66.7	9.68	0.38	-214.3	-48.1
2.5	315.7	70.9	129.54	5.10	-215.1	-48.3	19.89	0.78	136.71	5.38	312.6	70.2	16.63	0.65	-208.1	-46.8
2.75	342.6	77.0	161.13	6.34	-206.7	-46.4	31.78	1.25	161.64	6.36	342.4	76.9	28.38	1.12	-202.9	-45.6
3.0	369.1	82.9	192.28	7.57	-215.1	-48.3	54.52	2.15	193.17	7.61	360.5	81.0	44.98	1.77	-191.7	-43.1
3.0	365.9	82.2	213.04	8.39	-219.8	-49.4	62.32	2.45	218.34	8.60	359.5	80.8	62.11	2.45	-217.4	-48.9

Table 4-23 Measured Peak Displacement, Displacement Ductility and Drift

Motion	THD-1				THD-2				THD-3				THD-4				THD-5			
	Displacement		Deflection Ductility	Drift	Displacement		Deflection Ductility	Drift	Displacement		Deflection Ductility	Drift	Displacement		Deflection Ductility	Drift	Displacement		Deflection Ductility	Drift
xSylmar	(mm)	(inch)		(%)	(mm)	(inch)		(%)	(mm)	(inch)		(%)	(mm)	(inch)		(%)	(mm)	(inch)		(%)
0.1	2.60	0.10	0.15	0.2%	2.18	0.09	0.09	0.1%	1.54	0.06	0.1	0.1%	2.53	0.10	0.2	0.2%	1.88	0.07	0.1	0.2%
0.25	4.78	0.19	0.28	0.4%	5.93	0.23	0.25	0.4%	4.28	0.17	0.3	0.4%	7.83	0.31	0.6	0.6%	6.34	0.25	0.3	0.5%
0.375	N/A				N/A				N/A				14.15	0.56	1.1	1.2%	N/A			
0.5	9.65	0.38	0.56	0.8%	15.28	0.60	0.65	0.9%	11.14	0.44	0.8	0.9%	19.18	0.76	1.5	1.6%	14.26	0.56	0.7	1.2%
0.75	15.72	0.62	0.92	1.3%	24.60	0.97	1.05	1.5%	23.56	0.93	1.7	1.9%	26.35	1.04	2.0	2.2%	17.86	0.70	0.9	1.5%
1.0	19.83	0.78	1.16	1.6%	36.65	1.44	1.56	2.3%	27.05	1.06	1.9	2.2%	45.34	1.79	3.5	3.7%	25.51	1.00	1.2	2.1%
1.25	32.07	1.26	1.88	2.6%	41.12	1.62	1.75	2.5%	38.93	1.53	2.8	3.2%	71.00	2.80	5.5	5.8%	37.39	1.47	1.8	3.1%
1.5	37.73	1.49	2.21	3.1%	57.40	2.26	2.45	3.5%	51.51	2.03	3.7	4.2%	N/A				51.72	2.04	2.5	4.2%
1.75	44.90	1.77	2.63	3.7%	78.90	3.11	3.36	4.9%	64.22	2.53	4.6	5.3%					55.36	2.18	2.6	4.5%
2.0	52.36	2.06	3.07	4.3%	92.53	3.64	3.95	5.7%	85.98	3.39	6.1	7.1%					93.11	3.67	4.4	7.6%
2.25	60.58	2.39	3.55	5.0%	110.30	4.34	4.70	6.8%	120.00	4.72	8.6	9.8%					111.47	4.39	5.3	9.1%
2.5	66.39	2.61	3.89	5.4%	111.87	4.40	4.77	6.9%	N/A								129.54	5.10	6.2	10.6%
2.625	73.00	2.87	4.27	6.0%	127.38	5.02	5.43	7.8%									N/A			
2.75	84.51	3.33	4.95	6.9%	134.67	5.30	5.74	8.3%									161.13	6.34	7.7	13.2%
2.875	120.68	4.75	7.07	9.9%	159.19	6.27	6.79	9.8%									N/A			
3	N/A				187.59	7.39	8.00	11.5%									192.28	7.57	9.2	15.8%
3					N/A												218.34	8.60	10.4	17.9%

Notice: Last data point of Specimen THD-3 is based on displacement corresponding to 80% force of peak loading.

Table 4-24 Measured Top Panel Nodes Deflection & Specimen Top Deflection for THD-1

Motion (xSylmar)	Top Node Deflection		Top Column Deflection		D_{col} / D_{Node}	Force	
	(mm)	(inch)	(mm)	(inch)		(KN)	(Kips)
0.1	2.07	0.08	2.26	0.09	109%	32.3	7.3
0.25	4.94	0.19	5.74	0.23	116%	81.4	18.3
0.5	13.35	0.53	14.95	0.59	112%	152.5	34.3
0.75	20.46	0.81	24.17	0.95	118%	195.1	43.8
1.0	31.95	1.26	35.90	1.41	112%	221.6	49.8
1.25	36.64	1.44	40.35	1.59	110%	223.1	50.1
1.5	54.96	2.16	56.16	2.21	102%	235.9	53.0
1.75	77.55	3.05	76.90	3.03	99%	243.8	54.8
2.0	90.26	3.55	89.69	3.53	99%	242.2	54.4
2.25	90.30	3.56	105.96	4.17	117%	239.1	53.7
2.5	91.97	3.62	102.96	4.05	112%	218.9	49.2
2.625	93.13	3.67	103.63	4.08	111%	212.3	47.7
2.75	98.76	3.89	105.41	4.15	107%	236.5	53.1
2.875	106.02	4.17	N/A			243.0	54.6
3	121.14	4.77	N/A			249.9	56.2

Table 4-25 Measured Top Panel Nodes Deflection & Specimen Top Deflection for THD-2

Motion (xSylmar)	Top Node Deflection		Top Column Deflection		D_{col} / D_{Node}	Force	
	(mm)	(inch)	(mm)	(inch)		(KN)	(Kips)
0.1	2.07	0.08	2.26	0.09	109%	32.3	7.3
0.25	4.94	0.19	5.74	0.23	116%	81.4	18.3
0.5	11.35	0.45	14.95	0.59	132%	152.5	34.3
0.75	19.46	0.77	24.17	0.95	124%	195.1	43.8
1.0	31.95	1.26	35.90	1.41	112%	221.6	49.8
1.25	36.64	1.44	40.35	1.59	110%	223.1	50.1
1.5	54.96	2.16	56.16	2.21	102%	235.9	53.0
1.75	77.55	3.05	76.90	3.03	99%	243.8	54.8
2.0	90.26	3.55	89.69	3.53	99%	242.2	54.4
2.25	90.30	3.56	105.96	4.17	117%	239.1	53.7
2.5	91.97	3.62	102.96	4.05	112%	218.9	49.2
2.625	93.13	3.67	103.63	4.08	111%	212.3	47.7
2.75	98.76	3.89	105.41	4.15	107%	236.5	53.1
2.875	106.02	4.17	N/A			243.0	54.6
3	121.14	4.77	N/A			249.9	56.2

Table 4-26 Measured Top Panel Nodes Deflection & Specimen Top Deflection for THD-3

Motion (xSylmar)	Top Node Deflection		Top Column Deflection		D_{col} / D_{Node}	Force	
	(mm)	(inch)	(mm)	(inch)		(KN)	(Kips)
0.1	1.43	0.06	1.45	0.06	102%	53.8	12.1
0.25	4.20	0.17	4.15	0.16	99%	112.1	25.2
0.5	10.15	0.40	10.69	0.42	105%	182.4	41.0
0.75	22.86	0.90	22.31	0.88	98%	215.5	48.4
1.0	21.61	0.85	25.46	1.00	118%	217.6	48.9
1.25	32.40	1.28	36.74	1.45	113%	228.5	51.3
1.5	43.79	1.72	48.69	1.92	111%	233.8	52.5
1.75	55.08	2.17	60.43	2.38	110%	231.2	51.9
2.0	70.99	2.79	77.70	3.06	109%	253.2	56.9
2.25	109.27	4.30	98.84	3.89	90%	207.8	46.7
2.5	128.57	5.06	142.50	5.61	111%	161.0	36.2

Table 4-27 Measured Top Panel Nodes Deflection & Specimen Top Deflection for THD-4

Motion (xSylmar)	Top Node Deflection		Top Column Deflection		D_{col} / D_{Node}	Force	
	(mm)	(inch)	(mm)	(inch)		(KN)	(Kips)
0.1	2.48	0.10	2.44	0.10	98%	37.4	8.4
0.25	7.39	0.29	7.43	0.29	101%	89.3	20.1
0.375	13.74	0.54	13.21	0.52	96%	121.8	27.4
0.5	18.18	0.72	17.27	0.68	95%	126.4	28.4
0.75	25.24	0.99	22.70	0.89	90%	141.6	31.8
1.0	41.83	1.65	37.54	1.48	90%	153.8	34.6
1.25	63.51	2.50	51.92	2.04	82%	169.7	38.1

Table 4-28 Measured Top Panel Nodes Deflection & Specimen Top Deflection for THD-5

Motion (xSylmar)	Top Node Deflection		Top Column Deflection		D_{col} / D_{Node}	Force	
	(mm)	(inch)	(mm)	(inch)		(KN)	(Kips)
0.1	1.73	0.07	1.67	0.07	96%	49.8	11.2
0.25	5.68	0.22	6.09	0.24	107%	123.7	27.8
0.5	12.62	0.50	13.68	0.54	108%	220.3	49.5
0.75	16.03	0.63	17.05	0.67	106%	243.7	54.8
1.0	24.34	0.96	24.16	0.95	99%	276.9	62.2
1.25	36.23	1.43	35.10	1.38	97%	297.7	66.9
1.5	48.44	1.91	48.65	1.92	100%	309.5	69.5
1.75	50.33	1.98	47.46	1.87	94%	330.9	74.4
2.0	58.88	2.32	59.95	2.36	102%	292.1	65.6
2.25	68.28	2.69	73.28	2.89	107%	301.3	67.7
2.5	77.01	3.03	87.61	3.45	114%	315.7	70.9
2.75	95.74	3.77	N/A			342.6	77.0
3.0	112.10	4.41	N/A			369.1	82.9
3.0	118.06	4.65	N/A			365.9	82.2

Table 4-29 Distance of the Inflection Point from Bottom of the Specimens

Motion	THD-1		THD-2		THD-3		THD-4		THD-5	
xSylmar	(in)	(mm)	(in)	(mm)	(in)	(mm)	(in)	(mm)	(in)	(mm)
0.1	37.6	955	53.8	1366	42.0	1066	41.7	1058	46.4	1179
0.25	37.4	950	50.6	1285	41.8	1061	40.2	1022	44.0	1118
0.375	N/A		N/A		N/A		41.0	1043	N/A	
0.5	38.4	976	50.5	1281	41.1	1044	42.1	1070	42.0	1066
0.75	39.9	1013	50.9	1293	42.1	1069	43.1	1094	41.3	1050
1.0	40.0	1015	52.1	1323	42.3	1074	43.3	1099	40.9	1039
1.25	40.8	1036	51.8	1315	42.9	1089	46.5	1180	41.5	1055
1.5	39.8	1012	52.5	1334	43.3	1101	N/A		42.7	1083
1.75	40.1	1018	52.0	1320	43.2	1096			46.8	1190
2.0	40.7	1034	52.3	1328	48.5	1233			44.7	1134
2.25	40.9	1038	58.4	1484	47.3	1202			44.9	1141
2.5	41.3	1050	56.5	1434	41.7	1060			45.3	1150
2.625	42.2	1071	58.5	1486	N/A				N/A	
2.75	42.3	1075	57.5	1460					41.1	1044
2.875	47.6	1210	54.2	1376					N/A	
3	N/A		52.8	1341					38.6	979
3			N/A						38.2	970

Table 4-30 Measured Strain (Micro Strain) in Column Longitudinal Bars for THD-1

Strain Gauge No.		Motion (x Sylmar)													
		0.10	0.25	0.50	0.75	1.00	1.25	1.50	1.75	2.00	2.25	2.50	2.63	2.75	2.875
SG2B1	Max.	28	31	38	52	28	28	28	35	54	82	84	103	206	268
	Min.	12	10	10	-14	-21	-7	-2	-4	-9	-14	-26	-23	0	0
SG2B4	Max.	7	11	56	76	76	56	58	71	58	73	73	71	213	277
	Min.	-2	-2	-2	-20	-73	-62	-47	-47	-58	-65	-73	-189	-227	-295
SG4B4	Max.	-88	-72	-69	-69	-69	-69	-69	-69	-69	-72	-72	-72	4	6
	Min.	-168	-196	-196	-168	-269	-237	-223	-223	-237	-288	-297	-313	-290	-377
SG5B4	Max.	-6	-6	-6	1	-1	-1	-6	-6	-6	-6	-6	-6	-6	-8
	Min.	-60	-87	-89	-77	-160	-136	-155	-179	-182	-241	-260	-260	-253	-329
SG6B1	Max.	-28	0	47	191	296	284	328	349	387	389	373	415	421	548
	Min.	-74	-100	-107	-60	-42	-23	-14	-69	-132	-174	-228	-344	-926	-1203
SG4B1	Max.	-61	-35	23	233	479	423	463	472	496	496	477	519	507	659
	Min.	-110	-124	-135	-72	-65	-72	-82	-105	-173	-238	-298	-475	-1199	-1559
SG3B4	Max.	-145	-139	-89	271	435	428	486	504	513	556	553	560	724	941
	Min.	-215	-233	-228	-188	-378	-405	-430	-450	-450	-450	-470	-450	-448	-582
SG7B4	Max.	-70	-65	-65	244	362	411	426	437	500	504	500	504	571	742
	Min.	-159	-188	-206	-157	-328	-355	-372	-372	-375	-357	-412	-417	-372	-484
SG4B3	Max.	376	1049	**2225**	**3413**	**5714**	**5573**	**6740**	**7478**	**9164**	**11041**	**11909**	**15301**	**18932**	**24612**
	Min.	-671	-1060	-1652	**-2958**	**-4868**	**-5065**	**-5538**	**-5942**	**-6107**	**-6035**	**-6030**	**-6406**	**-5708**	**-7420**
SG3B5	Max.	176	712	1585	**2601**	**10417**	**11682**	**13984**	**16583**	**18996**	**20971**	**22199**	**25209**	**24051**	**31266**
	Min.	-699	-1040	-1558	-1882	**-2108**	-917	-648	-116	693	1485	**2418**	**2977**	**4242**	**5514**

104

Table 4-31 Measured Strain (Micro Strain) in Column Longitudinal Bars for THD-1 (Continued)

Strain Gauge No.		Motion (x Sylmar)													
		0.10	0.25	0.50	0.75	1.00	1.25	1.50	1.75	2.00	2.25	2.50	2.63	2.75	2.875
SG7B3	Max.	352	1039	2115	4614	6873	5085	6232	7106	8762	10611	11278	15033	18508	24061
	Min.	-670	-1124	-1902	-5945	-8405	-9000	-10477	-12245	-13357	-14113	-14642	-16369	-15992	-20790
SG5B3	Max.	446	1069	2157	5431	8035	5747	7021	7986	10139	12671	13839	18549	23009	29911
	Min.	-693	-1163	-1918	-7766	-9282	-9898	-11365	-13149	-14267	-15032	-15457	-17187	-17022	-22129
SG6B5	Max.	224	914	1916	9633	15081	17242	20963	24311	19117	11815	5898	5716	5325	6922
	Min.	-695	-1119	-1865	-2772	-4238	-1804	-1464	-473	1329	2714	2977	2313	2026	2634
SG8B5	Max.	254	915	1864	6134	13423	15230	18913	23341	27471	30950	33879	40390	42878	55742
	Min.	-692	-1088	-1793	-2765	-3818	-1851	-1543	-794	424	1648	3130	3534	4689	6096
SG8B2	Max.	457	1163	2267	5328	10199	7648	9342	10644	13000	15542	16114	20328	23261	30239
	Min.	-594	-981	-1722	-6444	-9111	-10211	-12367	-14881	-17275	-19833	-21859	-26984	-29802	-38742
SG2B3	Max.	444	1041	2018	3323	8995	6645	7791	8749	10417	12516	13244	16789	19187	24944
	Min.	-477	-816	-1374	-3271	-6228	-7205	-9168	-11545	-13572	-15244	-16891	-81484	-81484	N/A
SG1B6	Max.	845	1461	2366	11417	16222	18248	22280	26166	32143	7208	7152	6908	6035	7846
	Min.	12	-313	-936	-1266	-588	1044	1309	-81350	-81350	-2605	-2344	-5093	-9505	-12356
SG5B5	Max.	292	900	1777	8701	13971	15814	19505	23907	27946	32190	N/A	N/A	71096	92425
	Min.	-473	-748	-1357	-1727	-1830	-229	160	1053	2619	4031	5977	6859	10314	13408
SG7B2	Max.	194	570	1512	2251	2622	2919	3478	4754	7398	8903	9740	12159	15368	19979
	Min.	-283	-515	-877	-1609	-2025	-2307	-2747	-3247	-3189	-2681	-2413	-2314	-1845	-2398

105

Table 4-32 Measured Strain (Micro Strain) in Column Spiral for THD-1

Strain Gauge No.		Motion (x Sylmar)													
		0.10	**0.25**	**0.50**	**0.75**	**1.00**	**1.25**	**1.50**	**1.75**	**2.00**	**2.25**	**2.50**	**2.63**	**2.75**	**2.875**
SG1B1	**Max.**	12	12	16	67	186	209	272	381	535	667	800	1168	**5296**	**6885**
	Min.	-2	-2	-5	5	5	39	49	70	112	170	207	240	323	420
SG3B2	**Max.**	-15	-20	-22	-29	85	73	92	108	126	161	177	221	1474	1916
	Min.	-31	-36	-50	-103	-117	-119	-124	-117	-103	-73	-43	-10	-1	-2
SG5B2	**Max.**	-17	-19	-40	-119	-131	-175	-187	-201	-226	-238	-247	-198	-103	-134
	Min.	-33	-52	-91	-170	-236	-271	-292	-331	-385	-434	-473	-494	-517	-673
SG7B5	**Max.**	100	110	128	184	415	475	536	583	660	797	914	1105	1575	2048
	Min.	86	86	86	79	89	170	203	235	287	380	457	522	606	788
SG3B1	**Max.**	32	35	41	65	60	46	65	86	111	134	144	155	144	187
	Min.	18	18	21	11	-68	-82	-86	-86	-89	-96	-96	-105	-107	-139
SG1B2	**Max.**	-8	-8	-15	-76	-103	-73	-25	10	43	80	96	110	124	161
	Min.	-22	-27	-43	-159	-286	-330	-346	-365	-374	-386	-390	-404	-409	-532
SG6B4	**Max.**	48	48	48	181	260	274	279	277	260	202	202	181	130	169
	Min.	22	22	22	51	70	41	41	0	-55	-113	-161	-209	-252	-328
SG8B1	**Max.**	6	8	6	-18	-82	-177	-171	-166	-166	-159	-159	-150	-157	-204
	Min.	-8	-11	-18	-133	-205	-222	-233	-238	-245	-252	-261	-268	-286	-372

Table 4-33 Measured Strain (Micro Strain) in Column Spiral for THD-1 (Continued)

Strain Gauge No.		Motion (x Sylmar)													
		0.10	0.25	0.50	0.75	1.00	1.25	1.50	1.75	2.00	2.25	2.50	2.63	2.75	2.875
SG5B1	Max.	5	14	72	162	234	269	343	427	492	543	589	668	654	850
	Min.	-14	-14	-7	56	28	12	0	-5	-7	-5	7	7	18	24
SG6B2	Max.	6	11	20	92	295	463	616	712	738	761	761	828	936	1216
	Min.	-8	-8	-171	-283	-287	-285	-283	-273	-297	-304	-320	-299	-297	-386
SG1B5	Max.	5	5	84	296	551	660	809	1004	1182	1296	1366	1505	1524	1981
	Min.	-13	-20	-13	-46	-50	-50	-53	-64	-55	-36	-13	1	43	55
SG1B4	Max.	6	6	6	-89	-142	-216	-218	-135	-15	77	149	301	375	487
	Min.	-43	-47	-165	-343	-491	-518	-583	-611	-592	-611	-636	-606	-606	-788
SG2B6	Max.	-36	-36	-17	-10	-22	41	148	231	282	347	415	603	645	838
	Min.	-62	-80	-85	-222	-289	-287	-280	-285	-273	-268	-266	-254	-252	-328
SG6B3	Max.	21	21	21	21	26	144	362	602	829	1270	1462	2066	1952	**2537**
	Min.	-77	-176	-343	-787	-1025	-297	-59	-25	19	69	163	261	508	661
SG3B3	Max.	7	56	53	5	5	-14	-14	-2	5	5	2	5	5	6
	Min.	-21	-21	-21	-67	-95	-95	-116	-123	-137	-165	-151	-167	-151	-196
SG3B6	Max.	21	23	33	56	121	130	162	167	169	199	223	299	491	638
	Min.	-7	-34	-48	-4	21	21	14	21	51	63	49	42	47	61

Table 4-34 Measured Strain (Micro Strain) in Hinge Longitudinal Bars for THD-1

Strain Gauge No.		Motion (x Sylmar)													
		0.10	0.25	0.50	0.75	1.00	1.25	1.50	1.75	2.00	2.25	2.50	2.63	2.75	2.875
SG5B9	Max.	-87	-26	347	1546	**2251**	**2438**	**2673**	**2915**	**3112**	**3281**	**3438**	**3795**	**3788**	**4924**
	Min.	-176	-230	-366	-587	-1204	-1415	-1563	-1714	-1857	-1944	-1974	-2033	**-2138**	**-2780**
SG8B9	Max.	-49	30	341	1318	2040	**2225**	**2241**	**2564**	**4221**	**5560**	**6329**	**7780**	**71811**	**93355**
	Min.	-162	-232	-414	-692	-1431	-1674	-1957	**-2204**	**-2648**	**-2901**	**-3041**	**-3417**	**-11817**	**-15363**
SG3B9	Max.	-34	54	361	1452	1930	2056	**2237**	**2422**	**2571**	**2708**	**2826**	**3045**	**3066**	**3985**
	Min.	-166	-233	-308	-389	-675	-851	-1020	-1227	-1387	-1506	-1587	-1666	-1684	**-2190**
SG7B8	Max.	-169	-85	540	1128	1384	1375	1552	1685	1941	**2186**	**2274**	**2622**	**3006**	**3908**
	Min.	-287	-350	-453	-705	-1129	-1266	-1411	-1556	-1740	-1929	-2075	**-2313**	**-2455**	**-3192**
SG1B8	Max.	-74	35	508	954	1112	1140	1235	1321	1526	1630	1704	1900	**2136**	**2777**
	Min.	-225	-307	-425	-620	-869	-975	-1117	-1289	-1463	-1635	-1751	-1923	-2025	**-2633**
SG1B11	Max.	-58	234	1128	**3014**	**14520**	**18565**	**26331**	**71717**	**N/A**	**N/A**	**N/A**	**N/A**	**N/A**	**N/A**
	Min.	-402	-623	-1085	-1415	-1508	-1292	**-4815**	**-4168**	**N/A**	**N/A**	**N/A**	**N/A**	**N/A**	**N/A**

107

Table 4-35 Measured Strain (Micro Strain) in Hinge Longitudinal Bars for THD-1 (Continued)

Strain Gauge No.		Motion (x Sylmar)													
		0.10	0.25	0.50	0.75	1.00	1.25	1.50	1.75	2.00	2.25	2.50	2.63	2.75	2.875
SG6B9	Max.	-137	54	418	1864	2329	2136	2332	2946	4418	5847	5835	74803	74803	97244
	Min.	-406	-572	-914	-1687	-2053	-2173	-2263	-2305	-2268	-2131	-2119	-20044	-80012	-104015
SG2B9	Max.	-579	-293	974	2083	2766	2590	3431	71802	N/A	N/A	N/A	N/A	N/A	N/A
	Min.	-870	-1039	-1332	-1834	-2611	-2764	-3308	-10083	-18740	-15532	-16620	-13911	-11417	-14842
SG3B8	Max.	-475	-144	1441	8013	15329	13178	17283	20888	38613	65525	51451	17404	20804	27045
	Min.	-752	-906	-1129	-1041	605	850	889	719	-1099	261	4520	-8451	-81108	-105440
SG7B9	Max.	-149	-23	201	1772	2675	2727	2918	3217	4004	4646	4464	73158	73158	95106
	Min.	-375	-508	-793	-1129	-1353	-1545	-1699	-1904	-1925	-2154	-2427	-2938	-12479	-16222
SG6B8	Max.	-705	-486	470	1422	1854	1660	1966	2113	2421	2808	3100	4320	71550	93016
	Min.	-999	-1158	-1431	-2159	-2728	-2933	-3197	-3505	-3878	-4254	-4489	-4835	-4734	-6154
SG4B8	Max.	-728	-514	829	1710	2057	1978	2238	2424	2891	3709	4583	7205	72306	93998
	Min.	-986	-1137	-1312	-1974	-2551	-2660	-2781	-2934	-3341	-4155	-4692	-5670	-80032	-104041

Table 4-36 Measured Strain (Micro Strain) in Hinge Spiral for THD-1

Strain Gauge No.		Motion (x Sylmar)													
		0.10	0.25	0.50	0.75	1.00	1.25	1.50	1.75	2.00	2.25	2.50	2.63	2.75	2.875
SG5B8	Max.	29	41	59	75	92	89	92	96	115	134	117	96	110	143
	Min.	1	-8	-11	3	8	6	8	10	13	15	15	-11	15	19
SG2B8	Max.	7	14	19	46	70	79	95	128	162	158	153	176	181	235
	Min.	-7	-7	-93	-58	-62	-65	-74	-83	-104	-102	-95	-104	-97	-126
SG2B2	Max.	43	54	59	75	82	63	66	70	97	145	148	138	118	153
	Min.	18	4	6	6	4	6	6	13	25	15	6	0	43	56
SG8B7	Max.	-10	-10	-13	178	320	429	529	640	815	922	789	685	808	1050
	Min.	-34	-45	-66	-22	6	20	-15	-206	280	266	287	178	-5774	-7507

Table 4-37 Measured Strain (Micro Strain) in Column Longitudinal Bars for THD-2

Strain Gauge No.		Motion (x Sylmar)														
		0.1	0.25	0.5	0.75	1	1.25	1.5	1.75	2	2.25	2.5	2.625	2.75	2.875	3
SG4B5	Max.	17	19	26	31	38	45	61	68	29	26	8	-4	-4	43	108
	Min.	5	5	-4	-4	3	17	10	-22	-25	-97	-115	-132	-199	-208	-308
SG8B5	Max.	20	22	27	32	53	62	81	104	120	118	53	41	18	62	71
	Min.	6	-3	-12	-12	-1	9	6	-22	-33	-63	-119	-98	-170	-175	-303
SG3B2	Max.	96	106	127	147	159	136	140	115	90	69	-1	27	64	34	11
	Min.	76	73	62	4	-26	-35	-61	-91	-167	-253	-209	-126	-105	-102	-91
SG7B6	Max.	1	3	12	15	19	22	26	152	173	335	319	398	321	273	252
	Min.	-13	-36	-99	-122	-95	-69	-136	-157	-190	-150	-320	-280	-480	-427	-329
SG6B5	Max.	-3	-5	0	0	4	4	7	79	139	379	362	446	332	281	244
	Min.	-19	-51	-133	-158	-140	-96	-200	-258	-319	-237	-395	-319	-547	-479	-326
SG5B2	Max.	36	46	71	97	181	225	265	270	223	286	265	270	326	422	433
	Min.	-8	-13	6	50	74	74	41	-15	-106	-160	-190	-190	-199	-214	-256
SG4B1	Max.	-18	42	79	84	119	135	191	212	200	191	273	277	287	284	273
	Min.	-114	-170	-197	-197	-170	-46	-14	19	-7	-132	-69	-76	12	79	112
SG4B7	Max.	262	895	2042	**2665**	**2852**	**6571**	**13027**	**17035**	**20131**	**21772**	**21527**	**22530**	**23895**	**27079**	**30367**
	Min.	-277	-683	-1149	-1376	-1880	-1894	-2248	-643	-109	309	1205	1415	**3064**	**3519**	**4266**
SG8B1	Max.	124	766	1684	**2102**	**3006**	**2894**	**3499**	**5806**	**9392**	**11317**	**11582**	**12878**	**9976**	**10429**	**10764**
	Min.	-394	-810	-1338	-1703	-2088	**-2139**	**-2932**	**-4382**	**-4196**	**-3787**	**-3450**	**-3334**	**-3415**	**-3697**	**-4106**

109

Table 4-38 Measured Strain (Micro Strain) in Column Longitudinal Bars for THD-2 (Continued)

Strain Gauge No.		Motion (x Sylmar)														
		0.1	0.25	0.5	0.75	1	1.25	1.5	1.75	2	2.25	2.5	2.625	2.75	2.875	3
SG3B6	Max.	385	1117	2232	9168	11518	12341	18327	23959	28536	30765	30513	31794	34272	39593	45576
	Min.	-322	-776	-1295	-1383	-1363	-697	-1302	-429	118	795	2243	2739	5541	6549	8237
SG5B6	Max.	490	1373	2734	10375	14045	15040	22311	29264	35081	38600	38903	40981	44899	52805	70709
	Min.	-363	-911	-1510	-1608	-1766	-913	-1556	-410	657	1883	4130	5202	9461	11151	13959
SG2B2	Max.	167	987	1828	2328	6127	5536	7834	8580	11000	13555	13638	15038	11475	12166	12674
	Min.	-401	-788	-1368	-1836	-2446	-3730	-7111	-8208	-8937	-8374	-7316	-6974	-7265	-8164	-9292
SG1B7	Max.	367	1131	2374	7111	12860	13608	20317	27094	32712	35743	35881	37412	40679	48129	70290
	Min.	-397	-918	-1542	-1825	-2795	-1661	-2933	-1841	-1019	309	3370	4085	8815	9953	12014
SG2B6	Max.	430	1260	2566	6067	13420	14709	22798	31347	38382	42499	42898	45015	49190	57650	67112
	Min.	-381	-922	-1584	-2157	-3052	-1567	-2777	-1388	-518	876	3927	4617	10124	11797	14986
SG7B1	Max.	229	1099	2115	2537	11672	8918	11626	12765	15265	13892	15342	11813	5550	5413	19199
	Min.	-391	-769	-1393	-2123	-4967	-4703	-8969	-14088	-19472	-14995	-6870	-4197	-3135	-8222	-6392
SG7B7	Max.	304	1013	2357	2799	9068	10505	16013	23257	28870	31458	30267	31204	33269	38229	43459
	Min.	-261	-601	-1019	-1489	-1710	-999	-1266	-750	490	1483	2103	2124	3833	4296	4908
SG7B2	Max.	225	985	1873	2268	6138	5397	7302	8726	11249	13470	12981	14307	71818	N/A	N/A
	Min.	-280	-589	-1112	-1774	-2805	-4018	-7804	-11502	-14165	-13978	-12335	-11949	-23919	-18787	-22944

110

Table 4-39 Measured Strain (Micro Strain) in Column Spiral for THD-2

Strain Gauge No.		Motion (x Sylmar)														
		0.1	0.25	0.5	0.75	1	1.25	1.5	1.75	2	2.25	2.5	2.625	2.75	2.875	3
SG5B5	Max.	22	29	50	59	80	87	122	159	131	115	154	108	291	229	122
	Min.	8	10	13	17	22	31	34	31	22	13	-3	-27	-80	-55	-89
SG7B5	Max.	15	18	34	76	97	85	62	36	97	176	360	511	279	272	313
	Min.	4	4	4	11	22	32	6	-50	-80	-94	-113	-131	-120	-85	-68
SG3B1	Max.	49	61	70	80	117	126	168	199	204	318	292	393	304	295	243
	Min.	33	33	38	45	70	84	91	103	96	94	91	94	138	126	101
SG2B5	Max.	9	9	12	12	2	2	33	81	58	65	44	40	40	42	40
	Min.	-5	-2	-2	-2	-16	-16	-14	-19	-23	-23	-28	-21	-26	-12	-30
SG8B8	Max.	-4	1	1	3	-4	-4	1	1	-4	-6	-4	-1	10	15	15
	Min.	-15	-15	-13	-13	-22	-22	-27	-45	-59	-64	-62	-64	-64	-64	-50
SG2B1	Max.	16	18	21	25	25	32	39	47	56	75	70	75	82	89	91
	Min.	2	2	2	2	-3	0	2	11	23	28	37	44	49	42	32
SG6B6	Max.	13	13	13	17	10	10	13	78	94	117	113	122	115	115	124
	Min.	-1	-1	1	3	-8	-6	-11	-11	1	3	13	20	22	24	27
SG3B5	Max.	-5	-3	-3	-1	-8	-8	-5	6	-17	-28	-35	-35	-38	-38	-47
	Min.	-19	-17	-17	-15	-21	-19	-19	-31	-54	-66	-77	-91	-96	-103	-114
SG4B2	Max.	19	21	26	33	35	42	68	133	140	154	147	166	154	177	203
	Min.	3	5	5	10	-2	7	7	19	28	42	45	42	42	45	49
SG8B6	Max.	5	7	10	14	10	14	24	31	35	45	54	61	63	70	73
	Min.	-7	-7	-7	-2	-11	-2	0	3	-4	-9	-9	-9	-4	-11	-21

111

Table 4-40 Measured Strain (Micro Strain) in Column Spiral for THD-2 (Continued)

Strain Gauge No.		Motion (x Sylmar)														
		0.1	0.25	0.5	0.75	1	1.25	1.5	1.75	2	2.25	2.5	2.625	2.75	2.875	3
SG4B6	Max.	9	11	16	18	16	20	32	202	230	239	251	262	251	267	295
	Min.	-3	-3	-1	2	-10	-5	-3	2	76	74	74	79	85	83	85
SG6B1	Max.	34	34	36	34	50	61	82	192	201	215	215	215	215	215	219
	Min.	20	17	20	17	24	27	31	38	64	68	73	78	82	87	92
SG3B7	Max.	-3	8	31	56	83	81	124	174	269	348	428	459	425	518	582
	Min.	-19	-19	-12	-3	-5	-26	-46	-60	-26	-3	2	15	2	-12	-23
SG6B7	Max.	7	11	32	127	248	332	753	1120	1378	1455	1392	1374	1478	1718	2013
	Min.	-14	-28	-26	14	11	0	-3	37	79	195	197	206	202	206	276
SG1B1	Max.	14	42	153	179	195	211	244	452	480	498	450	464	487	545	556
	Min.	0	-4	-2	10	19	51	51	86	79	51	40	37	28	26	19
SG5B7	Max.	43	59	59	71	191	228	337	432	534	592	534	613	576	664	710
	Min.	-6	-22	-31	-20	-17	-3	-6	-8	-8	-8	-20	-10	-15	-8	1
SG1B6	Max.	-4	43	56	19	59	82	196	319	467	537	527	516	553	676	829
	Min.	-20	-25	-20	-48	-111	-118	-141	-159	-164	-180	-206	-199	-187	-178	-164
SG6B2	Max.	20	27	74	109	148	160	169	118	141	139	90	69	13	13	6
	Min.	-3	-3	8	27	64	69	-17	-105	-224	-326	-378	-415	-438	-503	-601
SG8B7	Max.	28	56	107	135	228	258	325	332	421	504	502	576	469	528	590
	Min.	5	2	0	5	-5	53	72	93	109	130	153	163	165	179	191
SG2B7	Max.	-8	-1	-1	23	87	74	136	169	62	16	25	39	55	69	78
	Min.	-26	-38	-61	-61	-61	-38	-63	-98	-128	-165	-209	-232	-295	-399	-487

112

Table 4-41 Measured Strain (Micro Strain) in Hinge Longitudinal Bars for THD-2

Strain Gauge No.		Motion (x Sylmar)														
		0.1	0.25	0.5	0.75	1	1.25	1.5	1.75	2	2.25	2.5	2.625	2.75	2.875	3
SG5B11	Max.	-83	73	634	864	1102	1202	1330	1532	1702	1877	1974	1856	1006	12	15
	Min.	-239	-406	-714	-1042	-1317	-1456	-1610	-1733	-1831	-1919	-1805	-1701	-1635	-919	-569
SG1B4	Max.	-152	22	607	1296	1601	1846	**2440**	**2984**	**3524**	**4259**	**4264**	**2866**	868	861	866
	Min.	-347	-535	-806	-958	-1200	-1219	-1469	-1723	-2023	-2189	-2113	-1274	-230	566	-225
SG1B11	Max.	-252	565	1696	2098	**7260**	**8395**	**12528**	**16450**	**21189**	**26911**	**24250**	**23660**	**7332**	**3969**	**3876**
	Min.	-912	-1304	-1998	**-2779**	**-3835**	**-5031**	**-6132**	**-6169**	**-6399**	**-6145**	**-2841**	**-82489**	**-5686**	1633	**2585**
SG6B9	Max.	-358	718	**2697**	**11077**	**18948**	**17369**	**21190**	**25082**	**30734**	**69834**	**N/A**	**N/A**	**N/A**	**N/A**	**N/A**
	Min.	-1147	-1551	-2206	-1640	-1317	-1315	-1678	**-2419**	**-4157**	**-6139**	**-5114**	**-4812**	**-6106**	**-2211**	-1069
SG2B4	Max.	-32	671	**2597**	**4605**	**11135**	**20194**	**51205**	**76132**	**79268**	**N/A**	**N/A**	**N/A**	**N/A**	**N/A**	**N/A**
	Min.	-697	-1234	-1882	**-2364**	**-6160**	**-5643**	**-6379**	**-1814**	**930**	**274**	**44647**	**54817**	**54263**	**79268**	**79268**
SG5B3	Max.	-495	-75	1235	**2874**	**4118**	**5768**	**28645**	**42961**	**35070**	**10004**	**8343**	**8324**	**7128**	**5592**	**5038**
	Min.	-714	-792	-853	-883	**-2106**	**-2545**	**-2417**	464	**2933**	**2995**	**2842**	**2477**	-269	**4335**	**4686**
SG2B9	Max.	-548	651	**3897**	**11355**	**20704**	**25251**	**24137**	**30149**	**34766**	**36899**	**68310**	**N/A**	**N/A**	**N/A**	**N/A**
	Min.	-1396	-1727	**-2150**	-488	1762	**-83111**	**N/A**	**N/A**	**N/A**	**N/A**	**N/A**	**N/A**	**N/A**	**N/A**	**N/A**
SG5B9	Max.	-527	337	1384	1618	**8087**	**7239**	**9568**	**6174**	**636**	**67781**	**N/A**	**N/A**	**N/A**	**N/A**	**N/A**
	Min.	-1293	-1634	**-2117**	**-2596**	**-3222**	**-3322**	**-4841**	**-4618**	**-3466**	**-3424**	**67781**	**N/A**	**N/A**	**N/A**	**N/A**
SG8B3	Max.	63	492	**2496**	**5702**	**23033**	**26066**	**43028**	**65151**	**76884**	**N/A**	**N/A**	**N/A**	**N/A**	**N/A**	**N/A**
	Min.	-494	-796	-992	-1044	-1178	**2357**	**2417**	**4510**	**6381**	**-30745**	**-85470**	**N/A**	**N/A**	**N/A**	**N/A**
SG4B3	Max.	-419	-153	1195	**3449**	**11742**	**15323**	**31285**	**35555**	**10974**	**7108**	**2014**	**72596**	**N/A**	**N/A**	**N/A**
	Min.	-580	-629	-655	-653	-508	967	1583	**3587**	**3974**	**-4465**	-1700	**-80316**	**N/A**	**N/A**	**N/A**

113

Table 4-42 Measured Strain (Micro Strain) in Hinge Longitudinal Bars for THD-2 (Continued)

Strain Gauge No.		Motion (x Sylmar)														
		0.1	0.25	0.5	0.75	1	1.25	1.5	1.75	2	2.25	2.5	2.625	2.75	2.875	3
SG7B8	Max.	-599	524	1858	**2285**	**10214**	**9344**	**11756**	**13835**	**17788**	**22418**	**29004**	**68956**	**N/A**	**N/A**	**N/A**
	Min.	-1406	-1736	**-2116**	**-2599**	**-3329**	**-2650**	**-3466**	**-4357**	**-6266**	**-6345**	**-2299**	1865	**4737**	**68956**	**N/A**
SG7B11	Max.	-448	265	1365	1638	1988	1984	**2242**	**2768**	**4092**	**8362**	**8039**	**3908**	**67650**	**N/A**	**N/A**
	Min.	-1115	-1366	-1747	-2010	**-2663**	**-2900**	**-3221**	**-3415**	**-4517**	**-6492**	**-5731**	**-3189**	**-2335**	**67650**	**N/A**
SG7B4	Max.	-62	296	1374	**2764**	**3295**	**3927**	**14618**	**21815**	**28090**	**30082**	**26583**	**70901**	**N/A**	**N/A**	**N/A**
	Min.	-518	-741	-912	-1085	**-2343**	**-2567**	**-6211**	**-6772**	**-7360**	**-8159**	**2443**	**19096**	**70901**	**N/A**	**N/A**
SG2B3	Max.	-299	-208	298	1599	**2154**	**2457**	**3157**	**7967**	**16938**	**19119**	**12300**	**72055**	**N/A**	**N/A**	**N/A**
	Min.	-386	-433	-454	-530	-1375	-1582	**-2134**	**-4063**	**-4016**	**-3864**	**-2287**	**-11409**	**72055**	**N/A**	**N/A**
SG1B8	Max.	-166	29	593	788	923	990	1152	1382	1739	2043	**2208**	**71157**	**N/A**	**N/A**	**N/A**
	Min.	-388	-507	-871	-1305	-1560	-1690	-1973	**-2291**	**-2532**	**-2616**	**-2474**	**-2154**	**71157**	**N/A**	**N/A**
SG6B8	Max.	-136	-94	262	593	776	888	1058	1309	1586	1767	1821	1670	**70177**	**N/A**	**N/A**
	Min.	-194	-236	-354	-720	-1187	-1366	-1625	-1962	**-2146**	-2074	-1988	-1687	**-1459**	**70177**	**N/A**
SG6B3	Max.	-224	-210	-13	498	653	797	1042	1336	1688	2000	2077	**71174**	**N/A**	**N/A**	**N/A**
	Min.	-293	-520	-687	-835	-1349	-1353	-1455	-1557	-1649	-1724	-1724	-1256	**71174**	**N/A**	**N/A**
SG4B4	Max.	-150	-131	-81	16	91	226	393	556	752	849	832	773	**70634**	**N/A**	**N/A**
	Min.	-204	-204	-209	-209	-638	-784	-1167	-1311	-1391	-1436	-1495	-1417	-1332	**70634**	**N/A**
SG8B11	Max.	-80	-78	-45	108	141	192	252	326	396	482	552	**71580**	**N/A**	**N/A**	**N/A**
	Min.	-103	-122	-122	-431	-635	-716	-900	-1039	-1136	-1090	-1062	**-2221**	**-7297**	**71580**	**N/A**
SG1B3	Max.	-129	-129	-129	-56	160	235	314	505	580	603	680	**69721**	**N/A**	**N/A**	**N/A**
	Min.	-181	-181	-372	-643	-977	-907	-1073	-954	-998	-1068	-1020	-852	-1027	**69721**	**N/A**

Table 4-43 Measured Strain (Micro Strain) in Hinge Spiral for THD-2

Strain Gauge No.		Motion (x Sylmar)														
		0.1	0.25	0.5	0.75	1	1.25	1.5	1.75	2	2.25	2.5	2.625	2.75	2.875	3
SG4B9	Max.	-4	10	31	37	33	33	33	8	-22	-27	-54	-175	-223	-287	-265
	Min.	-20	-24	-50	-45	-77	-88	-258	-441	-438	-329	-512	-528	-528	-578	-569
SG3B4	Max.	21	21	69	74	71	74	165	238	165	90	14	-52	-52	-199	-144
	Min.	-4	-4	-4	0	-4	-4	-4	-4	-133	-151	-176	-224	-279	-297	-252
SG3B9	Max.	49	136	143	147	117	129	126	268	361	**2752**	2079	**70219**	**N/A**	**N/A**	**N/A**
	Min.	-235	-290	-281	-235	-216	-239	-458	-684	-1459	-956	126	-67	**70219**	**N/A**	**N/A**
SG7B3	Max.	39	44	46	48	120	130	175	199	427	**20326**	**26680**	**10487**	**73440**	**N/A**	**N/A**
	Min.	15	17	-38	-131	-265	-344	-593	-799	-742	-419	**10611**	939	-134	**73440**	**N/A**
SG6B11	Max.	41	48	46	6	-17	-27	-50	-110	-50	-36	**70524**	**N/A**	**N/A**	**N/A**	**N/A**
	Min.	22	15	-22	-308	-431	-431	-554	-643	-780	-1645	**-8070**	-1466	**-17971**	**-14573**	**70524**
SG2B11	Max.	17	34	85	139	192	211	295	381	416	430	575	549	**69019**	**N/A**	**N/A**
	Min.	-4	1	8	41	52	78	85	106	111	134	169	199	-456	**69019**	**N/A**
SG5B4	Max.	-63	-63	-56	-11	7	9	76	150	492	718	436	**65697**	**N/A**	**N/A**	**N/A**
	Min.	-132	-137	-157	-157	-152	-114	-130	-114	-137	-206	-354	-253	**65697**	**N/A**	**N/A**
SG7B9	Max.	15	17	24	20	27	-45	-73	-119	-388	-597	-729	**69300**	**N/A**	**N/A**	**N/A**
	Min.	1	4	-1	-17	-68	-124	-281	-678	**-2457**	**-3270**	**-3134**	**-14125**	**-2647**	**69300**	**N/A**
SG4B8	Max.	-7	2	20	30	20	32	41	190	180	187	180	**70250**	**N/A**	**N/A**	**N/A**
	Min.	-21	-17	-12	-10	-33	-21	-21	-17	23	20	25	**-7821**	**-7497**	**70250**	**N/A**
SG1B5	Max.	28	28	35	70	79	86	112	123	130	142	151	**69146**	**N/A**	**N/A**	**N/A**
	Min.	14	8	3	8	19	19	3	12	8	-9	-34	-16	**69146**	**N/A**	**N/A**

115

Table 4-44 Measured Strain (Micro Strain) in Hinge Spiral for THD-2 (Continued)

Strain Gauge No.		Motion (x Sylmar)														
		0.1	0.25	0.5	0.75	1	1.25	1.5	1.75	2	2.25	2.5	2.625	2.75	2.875	3
SG3B11	Max.	0	0	0	9	74	81	118	197	186	188	251	**69374**	**N/A**	**N/A**	**N/A**
	Min.	-14	-14	-16	-21	0	-4	-60	-111	-155	-188	-222	**-3413**	**-20033**	**69374**	**N/A**
SG3B8	Max.	14	14	16	21	28	28	53	396	463	561	593	**69449**	**N/A**	**N/A**	**N/A**
	Min.	-2	0	2	0	-5	-2	0	7	35	32	39	**-12958**	**-15284**	**69449**	**N/A**
SG6B4	Max.	22	22	22	3	20	22	27	29	32	76	76	**69289**	**N/A**	**N/A**	**N/A**
	Min.	-4	-4	-4	-4	-4	-1	-4	-1	-4	-4	-4	-4	**69289**	**N/A**	**N/A**
SG8B9	Max.	6	4	8	6	11	69	264	176	176	148	299	**68774**	**N/A**	**N/A**	**N/A**
	Min.	-8	-8	-8	-10	-10	-50	-229	-159	-175	-166	-329	**-2920**	**-2530**	**68774**	**N/A**
SG5B8	Max.	1	4	10	15	10	10	15	34	68	96	87	**69058**	**N/A**	**N/A**	**N/A**
	Min.	-13	-10	-6	1	-6	-6	-3	-1	-3	-1	-8	-453	-1307	**69058**	**N/A**
SG3B3	Max.	14	14	14	17	21	92	218	216	236	220	314	**69016**	**N/A**	**N/A**	**N/A**
	Min.	-4	-4	-4	-4	-27	-29	-77	-31	-24	-4	-125	-130	**69016**	**N/A**	**N/A**
SG4B11	Max.	4	2	2	4	7	39	82	77	79	68	161	**73107**	**N/A**	**N/A**	**N/A**
	Min.	-12	-12	-12	-14	-12	-33	-61	-47	-56	-45	-127	-106	**73107**	**N/A**	**N/A**
SG2B8	Max.	8	10	17	26	24	28	33	49	63	72	84	**67537**	**N/A**	**N/A**	**N/A**
	Min.	-6	-6	1	3	-8	-2	1	1	3	10	19	31	**67537**	**N/A**	**N/A**
SG8B4	Max.	4	-14	-2	-2	4	150	590	230	274	205	719	**70331**	**N/A**	**N/A**	**N/A**
	Min.	-21	-21	-21	-21	-19	-166	-512	-168	-238	-194	-731	-558	**-3312**	**70331**	**N/A**
SG1B9	Max.	2	4	7	11	-3	55	342	195	153	46	88	**68955**	**N/A**	**N/A**	**N/A**
	Min.	-12	-10	-12	-12	-26	-59	-261	-175	-287	-268	-371	-2550	-194	**68955**	**N/A**

116

Table 4-45 Measured Strain (Micro Strain) in Column Longitudinal Bars for THD-3

Strain Gauge No.		Motion (x Sylmar)										
		0.1	0.25	0.5	0.75	1	1.25	1.5	1.75	2	2.25	2.5
44	Max.	-32	-14	15	20	26	20	9	20	26	38	44
	Min.	-90	-113	-131	-125	-102	-102	-78	-84	-61	-61	-1585
45	Max.	-10	7	7	7	7	7	7	7	7	7	7
	Min.	-54	-54	-121	-121	-54	-54	-54	-54	-54	-54	-54
46	Max.	-130	-84	-49	-31	-37	-31	-31	-14	15	33	115
	Min.	-177	-200	-223	-235	-218	-212	-194	-177	-148	-37	-753
47	Max.	-4	-4	-4	-4	-4	-4	-4	-4	-4	-57	-4
	Min.	-137	-290	-442	-495	-495	-502	-502	-489	-369	-369	-290
48	Max.	13	509	**2355**	**3173**	**3301**	**9019**	**10771**	**13685**	**16302**	**19351**	**N/A**
	Min.	-448	-670	-939	-1015	-1173	-1313	-1243	-1885	-1827	-1476	-688
49	Max.	8	152	812	963	1073	1137	1183	**2109**	**2613**	**2572**	**2619**
	Min.	-189	-305	-502	-646	-641	-710	-780	-843	-907	-837	-432
50	Max.	32	1029	**2960**	**9533**	**10784**	**17827**	**23444**	**31906**	**37917**	**47260**	**N/A**
	Min.	-518	-843	-1283	-1608	-1457	-1393	-1446	-1475	-1840	-820	**-28340**
51	Max.	215	1423	**2800**	**3781**	**9944**	**13446**	**32525**	**22072**	**23181**	**23665**	**25311**
	Min.	-381	-795	-1449	**-2201**	**-2487**	-1052	-608	-801	-637	-264	1376
52	Max.	106	1239	**2801**	**15004**	**16214**	**24071**	**32956**	**46827**	**58284**	**77328**	**N/A**
	Min.	-470	-834	-1439	-1656	-464	-769	-411	799	3424	-1116	**-42451**
53	Max.	-140	597	1874	**8984**	**7767**	**11067**	**17113**	**15045**	**13932**	**13655**	**N/A**
	Min.	-541	-743	-936	-1105	-580	-407	1082	790	1062	**-166821**	**N/A**

117

Table 4-46 Measured Strain (Micro Strain) in Column Longitudinal Bars for THD-3 (Continued)

Strain Gauge No.		Motion (x Sylmar)										
		0.1	0.25	0.5	0.75	1	1.25	1.5	1.75	2	2.25	2.5
54	Max.	249	1516	3108	7954	14095	21770	26703	39142	41536	40147	40141
	Min.	-413	-901	-1720	-4056	-2749	-2342	-3632	-7507	-11638	-22049	-68553
55	Max.	235	1420	2495	3523	12510	18848	22915	35062	38531	40343	41941
	Min.	-334	-747	-1438	-2606	-2054	-1740	-2420	-3605	-4842	-10710	-16130
56	Max.	325	1512	8310	17227	19259	29625	42093	59391	72557	183933	N/A
	Min.	-752	-1317	-2772	-4460	-3930	-6957	-7935	-7591	-82175	2903	36086
57	Max.	212	1321	5963	14916	16775	26154	37129	179165	N/A	N/A	N/A
	Min.	-841	-1418	-2711	-3685	-3232	-4676	-5130	-27421	-13249	179165	N/A
58	Max.	625	1541	11039	12672	15389	22727	28122	39952	42959	49506	9102
	Min.	-760	-1305	-2542	-7171	-6768	-9423	-12325	-16421	-18209	N/A	N/A
59	Max.	201	884	8090	6452	4131	3724	401	-1313	9215	39965	-1814
	Min.	-642	-954	-2109	-3729	-3199	-2992	-3959	-5255	-14293	-8442	N/A
60	Max.	50	440	1834	2473	2787	6924	6523	21327	31523	24400	1149
	Min.	-472	-751	-1315	-1739	-2047	-3412	-195787	N/A	N/A	N/A	N/A
61	Max.	115	701	1758	1868	2356	4254	7615	10866	12102	13211	14853
	Min.	-483	-959	-1748	-2363	-2543	-3646	-5365	-4691	-3867	-3606	-3066
77	Max.	20	20	343	499	660	821	846	987	1103	1144	1149
	Min.	-186	-297	-771	-1003	-1003	-1063	-1118	-1164	-1164	-1224	-1164

Table 4-47 Measured Strain (Micro Strain) in Column Spiral for THD-3

Strain Gauge No.		Motion (x Sylmar)										
		0.1	0.25	0.5	0.75	1	1.25	1.5	1.75	2	2.25	2.5
62	Max.	-2	15	33	50	44	68	56	74	62	74	**N/A**
	Min.	-37	-43	-37	-25	-37	-37	-31	-20	-8	-2	**-35874**
63	Max.	-220	-220	-220	-214	-196	-185	-185	-185	-173	-173	-167
	Min.	-249	-255	-255	-255	-231	-237	-243	-237	-231	-226	-220
64	Max.	-266	-266	-254	-237	-243	-237	-237	-231	-237	-231	-103
	Min.	-307	-318	-313	-313	-313	-313	-307	-301	-289	-284	-266
65	Max.	-68	-80	-80	-80	-63	-68	-74	-80	-68	-51	-45
	Min.	-109	-115	-115	-115	-98	-109	-115	-115	-115	-109	-98
66	Max.	44	50	50	50	44	44	62	85	85	102	137
	Min.	9	9	15	15	9	9	15	21	33	39	56
67	Max.	5	5	5	114	132	132	126	132	132	132	162
	Min.	-32	-32	-32	-32	-32	-32	-32	-32	-26	-14	11
68	Max.	2	2	7	7	13	13	19	37	48	60	130
	Min.	-33	-33	-28	-33	-22	-22	-22	-10	2	7	25

Table 4-48 Measured Strain (Micro Strain) in Column Spiral for THD-3 (Continued)

Strain Gauge No.		Motion (x Sylmar)										
		0.1	0.25	0.5	0.75	1	1.25	1.5	1.75	2	2.25	2.5
69	Max.	-188	-188	-188	-188	-147	-158	-158	-164	-164	-164	-158
	Min.	-223	-223	-223	-223	-188	-188	-199	-205	-199	-205	-199
70	Max.	43	78	159	223	200	264	497	677	770	840	509
	Min.	-15	-21	14	78	54	-27	-50	-33	-33	-44	31
71	Max.	-10	25	262	361	355	471	720	1154	**36262**	**52678**	**184034**
	Min.	-50	-68	-62	54	77	48	42	54	**N/A**	**N/A**	**N/A**
72	Max.	52	92	144	376	462	641	699	849	919	1000	**N/A**
	Min.	-35	-41	-23	-18	46	104	237	271	295	139	202
73	Max.	-143	-27	234	757	1175	1013	1454	1965	**2442**	**N/A**	**N/A**
	Min.	-196	-190	-161	-161	-85	-10	124	257	542	**-40431**	**-27697**
74	Max.	48	83	48	**11346**	**15677**	**24568**	**27853**	**42843**	**34703**	123	280
	Min.	-40	-103	-260	**N/A**	**N/A**	**N/A**	**N/A**	**N/A**	**N/A**	**N/A**	**N/A**
75	Max.	-35	17	86	254	266	312	358	492	584	781	1551
	Min.	-76	-116	-64	17	69	86	86	17	-47	-145	-111

120

Table 4-49 Measured Strain (Micro Strain) in Hinge Longitudinal Bars for THD-3

Strain Gauge No.		Motion (x Sylmar)										
		0.1	0.25	0.5	0.75	1	1.25	1.5	1.75	2	2.25	2.5
1	Max.	6	18	353	537	710	894	1251	1614	1972	**2106**	1787
	Min.	-172	-234	-351	-479	-541	-697	-870	-1060	-1417	-1440	-1306
2	Max.	-70	75	434	1029	1284	1798	**2527**	**13608**	**16436**	**18130**	**18327**
	Min.	-203	-364	-550	-792	-1001	-1336	-2042	**-2678**	**-2204**	451	**N/A**
3	Max.	-77	214	1436	1756	1915	**2463**	**8076**	**7756**	**3211**	**24559**	**44719**
	Min.	-340	-585	-1059	-1305	-1253	-1430	**-3080**	**-2275**	-1602	**N/A**	**N/A**
4	Max.	-302	-115	1281	1862	**2316**	**2682**	**3020**	**3939**	**5434**	**5218**	-57
	Min.	-517	-691	-912	-1081	-1116	-1424	-1709	**-2116**	**-2494**	**-2884**	**-2134**
5	Max.	-1155	451	**4437**	**8534**	**12805**	**23320**	**3832**	**2348**	**51602**	**2371**	2016
	Min.	-1691	**-2302**	**-3692**	**-4862**	**-3122**	-1790	1068	1597	**-198024**	-1499	**N/A**
6	Max.	-411	-78	1064	2031	**2189**	**11811**	**15524**	**22838**	**22428**	**15254**	**22200**
	Min.	-575	-681	-757	-1220	-1548	-1583	-1559	-1606	-1325	2037	**3290**
7	Max.	-50	674	**2955**	**12484**	**16353**	**24767**	**29948**	**34371**	**46182**	**N/A**	**N/A**
	Min.	-587	-989	-1695	**-7110**	**-5050**	**-4391**	**-5850**	**-2786**	**-134006**	**N/A**	**N/A**
8	Max.	-100	614	**3119**	**11537**	**18731**	**28823**	**35818**	**51541**	**N/A**	**N/A**	**N/A**
	Min.	-545	-867	-1236	-937	714	**2382**	**3459**	**4940**	**-7084**	**N/A**	**N/A**

121

Table 4-50 Measured Strain (Micro Strain) in Hinge Longitudinal Bars for THD-3 (Continued)

Strain Gauge No.		Motion (x Sylmar)										
		0.1	0.25	0.5	0.75	1	1.25	1.5	1.75	2	2.25	2.5
9	Max.	-576	-330	995	11302	12058	16030	18122	20361	N/A	N/A	N/A
	Min.	-693	-728	-711	-687	2377	2940	3450	4118	-31333	-21829	N/A
10	Max.	-619	188	10726	22457	23194	23165	17127	14982	N/A	N/A	N/A
	Min.	-1092	-1419	-1571	2882	6109	6869	3251	-143950	N/A	N/A	N/A
11	Max.	-561	123	3265	21457	23288	26798	10471	2732	8629	N/A	N/A
	Min.	-1023	-1374	-1690	-1877	2884	1931	-3427	-2099	-2948	-1427	N/A
12	Max.	-817	-364	1614	17054	18110	24815	11921	6492	12106	40249	N/A
	Min.	-1089	-1205	-1176	-1170	3052	3058	1927	N/A	N/A	N/A	N/A
13	Max.	-430	-45	1284	1972	3687	13687	14987	17122	N/A	N/A	N/A
	Min.	-663	-757	-827	-885	-1025	-984	2567	-13072	N/A	N/A	N/A
14	Max.	-89	177	902	2509	1894	1738	1442	1627	2045	6279	4887
	Min.	-252	-368	-751	-2694	137	154	-675	-1110	-1087	-594	2202
15	Max.	-184	-324	493	1407	1761	2390	3937	8096	29282	28342	N/A
	Min.	-436	-1060	-3289	-1511	-3225	-1404	-2263	-2774	-3048	-2532	1348
16	Max.	-253	-114	118	2188	2287	3069	22003	36489	N/A	N/A	N/A
	Min.	-433	-584	-1686	-4197	-6916	-8001	N/A	N/A	N/A	N/A	N/A

Table 4-51 Measured Strain (Micro Strain) in Hinge Longitudinal Bars for THD-3 (Continued)

Strain Gauge No.		Motion (x Sylmar)										
		0.1	0.25	0.5	0.75	1	1.25	1.5	1.75	2	2.25	2.5
17	Max.	-679	-323	442	991	1254	1499	1663	1815	1961	N/A	N/A
	Min.	-807	-883	-971	-1783	-1578	-1748	-1794	-1899	-2022	-32237	-21620
18	Max.	-174	-127	-34	142	434	680	797	943	1025	1014	N/A
	Min.	-221	-233	-268	-408	-449	-584	-713	-800	-835	-724	-555
19	Max.	-55	-5	-5	128	147	198	350	400	603	622	337
	Min.	-188	-194	-207	-226	-220	-258	-340	-416	-467	-467	-479
20	Max.	-255	-92	240	124	299	1080	3510	6104	N/A	N/A	N/A
	Min.	-378	-471	-657	-1077	-2208	-3076	-4714	-11417	-11720	N/A	N/A
21	Max.	-172	-154	-119	-3	55	213	346	457	521	N/A	N/A
	Min.	-213	-230	-247	-451	-626	-783	-923	-1034	-1092	-36229	-754
22	Max.	-105	-111	-111	-76	105	227	238	157	192	2870	N/A
	Min.	-163	-198	-221	-338	-623	-798	-798	-798	-1287	-6737	-2970
23	Max.	-221	-198	-180	-163	-122	-92	-69	31	207	230	N/A
	Min.	-257	-257	-251	-251	-221	-227	-221	-180	-87	-22	-16

Table 4-52 Measured Strain (Micro Strain) in Hinge Spiral for THD-3

Strain Gauge No.		Motion (x Sylmar)										
		0.1	**0.25**	**0.5**	**0.75**	**1**	**1.25**	**1.5**	**1.75**	**2**	**2.25**	**2.5**
24	**Max.**	62	73	97	120	103	109	120	120	132	161	161
	Min.	21	27	-9	-55	-61	-55	-20	21	44	21	50
26	**Max.**	-18	5	279	343	639	1344	**5347**	1192	**2327**	**11463**	**33501**
	Min.	-59	-70	-76	-47	34	63	**N/A**	**N/A**	**N/A**	**N/A**	**N/A**
27	**Max.**	-41	92	307	249	272	441	493	540	644	540	388
	Min.	-111	-111	-128	-99	-82	-76	-36	34	40	57	86
28	**Max.**	-97	-74	108	143	172	283	383	406	289	283	295
	Min.	-132	-144	-156	-109	-115	-121	-62	-203	-156	-9	37
29	**Max.**	167	179	357	570	694	937	1114	1499	1872	**2446**	1268
	Min.	-4	-28	-16	43	7	43	43	114	315	570	505
30	**Max.**	-30	11	324	865	764	966	**10640**	**3204**	**N/A**	**N/A**	**N/A**
	Min.	-166	-201	-257	-353	-156	-45	-1070	6	56	**N/A**	**N/A**
31	**Max.**	194	194	200	349	430	713	741	419	**N/A**	**N/A**	**N/A**
	Min.	165	102	107	113	251	119	-665	-1098	**-8251**	**-41651**	**N/A**
32	**Max.**	3	120	167	173	173	190	307	307	313	301	348
	Min.	-32	-61	-32	-26	-26	-32	-32	-26	-26	-26	38

124

Table 4-53 Measured Strain (Micro Strain) in Hinge Spiral for THD-3 (Continued)

Strain Gauge No.		Motion (x Sylmar)										
		0.1	0.25	0.5	0.75	1	1.25	1.5	1.75	2	2.25	2.5
33	Max.	11	23	34	46	58	81	110	140	146	175	187
	Min.	-36	-42	-53	-48	-24	-18	-1	11	40	70	81
34	Max.	-38	-32	-21	-3	-27	-15	26	61	96	131	**N/A**
	Min.	-67	-85	-102	-97	-120	-114	-108	-91	-91	-79	-21
35	Max.	60	60	60	66	66	72	78	189	195	201	**N/A**
	Min.	43	43	43	43	43	43	43	43	43	43	-321
36	Max.	44	44	50	44	44	50	61	67	73	90	96
	Min.	3	3	9	3	9	9	15	21	26	38	50
37	Max.	139	144	150	150	127	150	208	225	**N/A**	**N/A**	**N/A**
	Min.	104	110	115	115	87	75	92	104	**-43653**	**-5756**	**N/A**
38	Max.	18	23	23	23	29	29	35	41	41	46	**N/A**
	Min.	-23	-23	-17	-11	-11	-11	-11	-6	-6	0	**-21892**
39	Max.	14	20	26	37	26	37	37	55	72	84	**N/A**
	Min.	-21	-21	-21	-26	-32	-32	-32	-26	-15	3	20
40	Max.	-48	-48	-48	-42	-48	-48	-42	-31	-25	-19	**N/A**
	Min.	-82	-82	-77	-82	-88	-82	-77	-77	-59	-59	-48

Table 4-54 Measured Strain (Micro Strain) in Hinge Spiral for THD-3 (Continued)

Strain Gauge No.		Motion (x Sylmar)										
		0.1	0.25	0.5	0.75	1	1.25	1.5	1.75	2	2.25	2.5
41	Max.	244	250	255	267	284	290	342	354	331	389	412
	Min.	215	221	221	221	209	215	232	238	215	250	267
42	Max.	57	57	57	57	57	57	57	57	57	57	**N/A**
	Min.	-60	-60	-60	-60	-60	-66	-66	-60	-66	-101	**N/A**
43	Max.	-221	-221	-215	-215	-192	-198	-180	-180	-198	-174	-157
	Min.	-256	-256	-256	-256	-238	-238	-244	-244	-250	-250	-233

125

Table 4-55 Measured Strain (Micro Strain) in Column Longitudinal Bars for THD-4

Strain Gauge No.		Motion (x Sylmar)						
		0.1	0.25	0.375	0.5	0.75	1	1.25
44	Max.	38	49	43	32	-3	-61	-102
	Min.	3	3	3	-3	-119	-212	-328
45	Max.	33	38	50	73	114	172	271
	Min.	-2	-2	3	9	15	-2	-43
46	Max.	32	49	61	55	90	125	136
	Min.	2	2	-3	-21	-15	-32	-126
47	Max.	56	56	100	233	454	614	813
	Min.	-60	-93	-93	-93	-93	-93	-137
48	Max.	710	2074	**2213**	1946	**2248**	**2178**	**2138**
	Min.	-405	-869	-974	-1026	-1107	-1392	-1769
49	Max.	674	**2132**	**3912**	**6872**	**12782**	**16818**	**21830**
	Min.	-290	-811	-651	-357	1068	**3934**	**4505**
50	Max.	1054	**3096**	**3782**	**3288**	**3934**	**4137**	**4474**
	Min.	-534	-1208	-1697	-1848	**-2273**	**-3337**	**-4762**
51	Max.	752	1958	**2646**	**4534**	**9225**	**14645**	**22950**
	Min.	-256	-711	-897	-804	-221	367	**2675**
52	Max.	991	**2691**	**3318**	**2993**	**4009**	**5182**	**8380**
	Min.	-327	-768	-1262	-1447	**-2208**	**-3705**	**-6173**
53	Max.	752	**2278**	**2730**	**2394**	**2905**	**3288**	**9787**
	Min.	-241	-612	-867	-995	-1140	-1349	-1262

126

Table 4-56 Measured Strain (Micro Strain) in Column Longitudinal Bars for THD-4 (Continued)

Strain Gauge No.		Motion (x Sylmar)						
		0.1	0.25	0.375	0.5	0.75	1	1.25
54	Max.	983	**2292**	**10432**	**12678**	**15447**	**23155**	**33903**
	Min.	-351	-804	-646	1431	1869	**2897**	**6645**
55	Max.	802	1705	**6247**	**7223**	**8325**	**13603**	**22042**
	Min.	-187	-486	-426	789	789	1001	**3133**
56	Max.	-8413	-1134	830	-886	**3735**	**-16456**	**-16258**
	Min.	**-10212**	**-18223**	**-20473**	**-20099**	**-20550**	**-20902**	**-20797**
57	Max.	298	994	**4128**	**3050**	**3896**	**4476**	**4615**
	Min.	-177	-362	-553	293	125	-327	-988
58	Max.	1067	**5542**	**15713**	**19479**	**23804**	**34823**	**49528**
	Min.	-602	-842	827	**3425**	**4961**	**7174**	**13110**
59	Max.	625	**3259**	**12775**	**16008**	**20156**	**31790**	**47983**
	Min.	-267	-449	44	**3183**	**4133**	**5753**	**12394**
60	Max.	479	1594	**2283**	2097	**2721**	**3253**	**4169**
	Min.	-665	-1535	**-2586**	**-3182**	**-5979**	**-7812**	**-8046**
61	Max.	703	1689	**2942**	**6747**	**8366**	**11904**	**14665**
	Min.	-370	-875	-1316	-1188	-527	-51	610
76	Max.	113	598	805	776	1036	1088	1192
	Min.	-130	-649	-1042	-1180	-1209	-1295	-1319

Table 4-57 Measured Strain (Micro Strain) in Column Spiral for THD-4

Strain Gauge No.		Motion (x Sylmar)						
		0.1	0.25	0.375	0.5	0.75	1	1.25
62	Max.	34	51	74	92	144	237	335
	Min.	-7	-7	17	28	28	57	86
63	Max.	44	44	55	61	96	154	200
	Min.	3	3	3	15	26	44	73
64	Max.	19	19	19	13	25	19	19
	Min.	-16	-16	-16	-22	-10	-16	-22
65	Max.	-4	24	29	29	40	51	155
	Min.	-20	-20	-20	-20	-53	24	24
66	Max.	40	40	35	35	29	29	29
	Min.	0	0	0	0	-6	-18	-18
67	Max.	38	32	26	26	20	26	78
	Min.	-3	3	-3	-3	-9	-9	-3
68	Max.	35	29	-11	-29	64	53	53
	Min.	6	0	-40	-64	29	18	12

Table 4-58 Measured Strain (Micro Strain) in Column Spiral for THD-4 (Continued)

Strain Gauge No.		Motion (x Sylmar)						
		0.1	0.25	0.375	0.5	0.75	1	1.25
69	Max.	36	42	7	42	65	234	240
	Min.	-11	-11	-11	-11	-5	7	42
70	Max.	85	125	178	207	271	405	574
	Min.	50	44	67	90	96	143	178
71	Max.	14	293	328	323	328	168	128
	Min.	-41	-41	-41	-41	-156	-305	-460
72	Max.	119	248	289	295	342	529	658
	Min.	20	32	73	108	114	190	143
73	Max.	59	245	437	618	618	990	1496
	Min.	-5	-5	-5	1	-5	12	117
74	Max.	98	220	249	244	249	220	203
	Min.	-77	-135	-205	-228	-280	-391	-548
75	Max.	54	60	60	60	60	60	60
	Min.	-5	-5	-147	-188	-194	-194	-194

Table 4-59 Measured Strain (Micro Strain) in Hinge Longitudinal Bars for THD-4

Strain Gauge No.		Motion (x Sylmar)						
		0.1	0.25	0.375	0.5	0.75	1	1.25
1	Max.	83	298	508	560	630	665	723
	Min.	-39	-120	-126	-161	-219	-219	-236
2	Max.	25	187	222	262	720	419	454
	Min.	-33	-56	-56	-114	-254	-143	-97
3	Max.	546	**2774**	**12947**	**12231**	**12387**	**16013**	**25632**
	Min.	-43	-32	61	**9206**	**8871**	**9044**	**N/A**
4	Max.	501	1452	1815	1971	**2253**	**12030**	**3078**
	Min.	-202	-260	-698	-831	-981	-1027	**2409**
5	Max.	319	1706	**2240**	**2147**	**2624**	**2467**	**2322**
	Min.	-169	-564	-715	-906	-1028	-1075	-1011
6	Max.	54	890	1067	940	1128	1134	1987
	Min.	-129	-123	-73	-112	-140	-173	-539
7	Max.	182	1179	3135	-1370	**-2258**	-1935	**N/A**
	Min.	-424	-1722	**-4664**	**-9100**	**-11107**	**-60916**	**N/A**
8	Max.	999	**10874**	**22391**	**24789**	**24887**	**31833**	**N/A**
	Min.	-423	-544	**5367**	**10753**	**11701**	**11088**	**14376**
9	Max.	722	1898	**2605**	**2889**	**3874**	**4876**	**5919**
	Min.	-211	-500	-686	-825	-975	-1132	-935

Table 4-60 Measured Strain (Micro Strain) in Hinge Longitudinal Bars for THD-4 (Continued)

Strain Gauge No.		Motion (x Sylmar)						
		0.1	0.25	0.375	0.5	0.75	1	1.25
10	Max.	1229	6195	8643	16261	N/A	N/A	N/A
	Min.	-333	-939	-408	2325	2949	N/A	N/A
11	Max.	1158	12657	14506	12423	N/A	N/A	N/A
	Min.	-334	-697	4786	5682	-27497	-23278	N/A
12	Max.	464	4112	11054	12214	15764	35969	N/A
	Min.	-127	-115	1671	8190	8549	9953	12168
13	Max.	1197	6309	40300	89817	N/A	N/A	N/A
	Min.	-706	-809	N/A	-201759	-201759	76120	-201759
14	Max.	406	1211	1576	1906	12442	16849	N/A
	Min.	-578	-879	-984	-1198	-2154	-642	511
15	Max.	276	764	2611	3459	4551	N/A	N/A
	Min.	-682	-1060	-1426	-1763	-4010	-27289	-39306
16	Max.	551	1042	1711	1319	892	903	N/A
	Min.	-199	-285	-1151	-389	-66	-106	90

Table 4-61 Measured Strain (Micro Strain) in Hinge Longitudinal Bars for THD-4 (Continued)

Strain Gauge No.		Motion (x Sylmar)						
		0.1	0.25	0.375	0.5	0.75	1	1.25
17	Max.	98	754	1026	1015	1200	1160	N/A
	Min.	-6	-6	93	58	35	-47	-139
18	Max.	137	588	905	1040	1116	1216	N/A
	Min.	-104	-315	-638	-802	-931	-1013	N/A
19	Max.	66	229	305	346	358	428	N/A
	Min.	-28	-45	-151	-180	-268	-291	N/A
20	Max.	87	419	414	361	612	804	N/A
	Min.	-35	-187	-309	-326	-525	-909	-6561
21	Max.	19	89	183	207	219	248	N/A
	Min.	-16	-10	31	84	66	60	-21079
22	Max.	34	69	69	81	115	202	N/A
	Min.	-6	-18	-18	-12	-64	-151	-180
23	Max.	24	47	168	353	324	364	1242
	Min.	-23	-40	-23	18	-52	-138	-231

Table 4-62 Measured Strain (Micro Strain) in Hinge Spiral for THD-4

Strain Gauge No.		Motion (x Sylmar)						
		0.1	**0.25**	**0.375**	**0.5**	**0.75**	**1**	**1.25**
24	**Max.**	36	42	54	54	89	83	89
	Min.	-10	2	7	7	36	36	31
25	**Max.**	38	79	125	119	177	177	189
	Min.	3	9	26	32	73	73	79
26	**Max.**	29	29	40	58	58	69	75
	Min.	-41	-76	-129	-141	-193	-234	-228
27	**Max.**	99	257	415	321	309	303	391
	Min.	-12	-6	64	134	128	99	105
28	**Max.**	24	187	181	158	187	176	158
	Min.	-17	-17	-11	-17	-11	-17	-17
29	**Max.**	38	114	337	530	583	654	**52160**
	Min.	-149	-319	-683	-864	-1040	**-4744**	**N/A**
30	**Max.**	13	18	-28	70	134	464	643
	Min.	-40	-867	-693	-213	-254	-265	1
31	**Max.**	42	118	281	217	264	895	**N/A**
	Min.	6	-17	-64	-128	-99	-99	47
32	**Max.**	23	57	57	57	249	127	**N/A**
	Min.	-12	-12	5	17	5	-70	-70
33	**Max.**	13	144	144	151	144	144	**N/A**
	Min.	-21	-21	-21	-15	-21	-21	**-48181**

133

Table 4-63 Measured Strain (Micro Strain) in Hinge Spiral for THD-4 (Continued)

Strain Gauge No.		Motion (x Sylmar)						
		0.1	0.25	0.375	0.5	0.75	1	1.25
34	Max.	37	43	61	49	37	14	N/A
	Min.	-3	-3	8	2	-21	-56	-18197
35	Max.	14	19	37	43	19	25	N/A
	Min.	-16	-10	2	2	-27	-21	-42968
36	Max.	70	70	107	107	101	107	N/A
	Min.	-22	-22	-22	-22	-22	-22	-46523
37	Max.	26	32	43	66	95	72	N/A
	Min.	-9	-3	8	14	-9	-3	-1035
38	Max.	23	29	35	41	35	35	N/A
	Min.	-12	-6	0	6	6	0	12
39	Max.	N/A	N/A	N/A	N/A	N/A	N/A	N/A
	Min.	N/A	N/A	N/A	N/A	N/A	N/A	N/A
40	Max.	16	28	34	45	16	16	N/A
	Min.	-19	-7	-1	10	-19	-13	-7
41	Max.	32	38	44	50	38	N/A	N/A
	Min.	-2	3	3	3	3	-34718	-36242
42	Max.	-6	46	64	157	630	373	N/A
	Min.	-41	-65	-82	-105	41	-35	-40708
43	Max.	25	31	43	48	37	43	N/A
	Min.	-15	-4	2	8	2	8	-39726

134

Table 4-64 Measured Strain (Micro Strain) in Column Longitudinal Bars for THD-5

Strain Gauge No.		Motion (x Sylmar)													
		0.10	0.25	0.50	0.75	1.00	1.25	1.50	1.75	2.00	2.25	2.50	2.75	3.00	3.00
44	Max.	125	125	125	125	131	137	258	265	265	258	258	131	137	125
	Min.	-2	-8	-8	-8	58	-39	-51	-57	-87	-87	-87	-385	-591	-718
45	Max.	3	14	32	26	43	101	72	136	136	90	67	-96	-44	-67
	Min.	-38	-44	-55	-84	-90	-49	-67	-55	-55	-96	-310	-478	-258	-194
46	Max.	33	33	43	157	198	353	353	358	363	379	482	363	353	203
	Min.	-76	-86	-117	-122	-86	-76	-143	-117	-122	-127	-86	-24	-137	-406
47	Max.	-107	-78	-2	39	254	400	423	417	376	225	-43	-206	-136	-95
	Min.	-165	-200	-200	-165	-183	-148	-90	-305	-323	-532	-655	-602	-567	-416
48	Max.	315	1326	**2536**	**2675**	**2850**	**3320**	**10250**	**10889**	**12912**	**14674**	**17511**	**19476**	**20708**	**20830**
	Min.	-237	-592	-970	-1104	-1365	-1464	-1563	-406	100	286	937	2071	**3367**	**3628**
49	Max.	-97	494	1296	1425	1970	**2175**	**2192**	**2175**	**2315**	**2573**	**2725**	**2807**	**3165**	**3317**
	Min.	-595	-999	-1421	-1579	-1802	-1995	**-2141**	**-2282**	**-2586**	**-3008**	**-3617**	**-4050**	**-4320**	**-4536**
50	Max.	318	1144	2011	2086	**3470**	**8251**	**11333**	**11467**	**14224**	**16789**	**17743**	**15951**	**12532**	**10926**
	Min.	-333	-735	-1206	-1415	-1950	**-2247**	-1927	-1200	-857	-426	539	**2999**	**4599**	**3959**
51	Max.	-26	595	1419	1601	**2186**	**3046**	**3736**	**3958**	**4227**	**4666**	**4754**	**4572**	**5994**	**7105**
	Min.	-552	-973	-1465	-1599	-1722	**-2319**	**-3003**	**-3219**	**-3886**	**-4495**	**-5162**	**-5466**	**-5770**	**-6431**
52	Max.	636	1852	**4312**	**10138**	**14159**	**19161**	**25256**	**25788**	**31965**	**38691**	**48380**	**58267**	**68453**	**75383**
	Min.	-433	-982	-1579	-1894	-1859	-1339	-480	1413	**2670**	**4347**	**8105**	**14766**	**23316**	**30615**
53	Max.	386	1143	2017	**4657**	**7874**	**10945**	**14511**	**14802**	**18293**	**22366**	**28793**	**34644**	**40681**	**44987**
	Min.	-302	-640	-1048	-1164	-1077	-558	-185	596	1085	1895	**4010**	**7885**	**12337**	**16113**

135

Table 4-65 Measured Strain (Micro Strain) in Column Longitudinal Bars for THD-5 (Continued)

Strain Gauge No.		Motion (x Sylmar)													
		0.10	0.25	0.50	0.75	1.00	1.25	1.50	1.75	2.00	2.25	2.50	2.75	3.00	3.00
54	Max.	18	245	571	664	822	717	717	717	758	804	839	903	N/A	N/A
	Min.	-197	-360	-581	-698	-477	-552	-686	-721	-762	-832	-843	-710	-30011	-155542
55	Max.	55	900	2083	2491	6070	9590	10371	9852	10173	10936	9981	7498	N/A	N/A
	Min.	-616	-1070	-1688	-1886	-3081	-4783	-6689	-6654	-7586	-9160	-13170	-17221	-57805	-42004
56	Max.	247	1045	8639	9983	12284	14144	18217	18247	27267	N/A	N/A	N/A	N/A	N/A
	Min.	-340	-487	-651	1414	N/A	N/A	N/A	N/A	N/A	N/A	N/A	N/A	N/A	N/A
57	Max.	401	1447	6497	8323	11854	16691	22498	36945	42429	N/A	N/A	N/A	N/A	N/A
	Min.	-541	-952	-1304	-171	-749	-928	N/A	N/A	N/A	N/A	N/A	N/A	N/A	N/A
58	Max.	-1115	-640	1147	1535	3206	3809	3554	2985	3026	3426	3554	10270	3357	38094
	Min.	-1539	-1666	-1394	-1463	-2565	-3290	-4218	-3963	-5448	-4810	-5042	-5970	-10866	-194152
59	Max.	112	1000	2051	2337	5567	8826	8546	7827	8365	9726	18130	12529	13393	13621
	Min.	-565	-1126	-2066	-2463	-7235	-9116	-11072	-11580	-13145	-15400	-19984	-25667	-31957	-37739
60	Max.	261	459	383	138	91	63001	57045	50961	58311	68029	50326	56100	80704	105401
	Min.	-399	-1186	-2423	-2143	-1874	N/A	N/A	N/A	N/A	N/A	N/A	N/A	N/A	N/A
61	Max.	19	536	1192	1389	1894	1993	4001	1494	1006	873	530	257	228	159
	Min.	-486	-909	-1629	-1937	-2146	-2413	-2448	-2564	-2976	-3719	-3382	-3545	-3945	-3469
76	Max.	130	748	1645	1709	1901	2280	2530	2664	4027	2641	1569	1587	1505	1388
	Min.	-231	-446	-685	-738	-947	-843	-895	-971	-1157	-1017	-10	-773	-1227	-1058
77	Max.	-7	150	360	458	813	1046	1261	1296	1319	1400	1418	1551	1772	2354
	Min.	-222	-414	-710	-844	-978	-1286	-1245	-1187	-1082	-931	-954	-972	-966	-1024

Table 4-66 Measured Strain (Micro Strain) in Column Spiral for THD-5

Strain Gauge No.		Motion (x Sylmar)													
		0.10	0.25	0.50	0.75	1.00	1.25	1.50	1.75	2.00	2.25	2.50	2.75	3.00	3.00
62	Max.	31	37	48	66	204	568	707	805	932	1065	1117	1169	1343	1637
	Min.	-4	-4	2	8	37	152	291	407	499	696	828	863	805	811
63	Max.	39	39	44	39	73	514	711	838	1470	**2582**	**2414**	**2286**	**2182**	**2252**
	Min.	4	4	10	4	10	68	259	346	479	1047	2055	2043	1823	1806
64	Max.	36	36	77	88	158	345	386	467	572	648	677	742	841	899
	Min.	1	1	1	7	30	123	193	217	257	327	397	421	368	374
65	Max.	76	76	99	99	185	642	856	931	1024	1162	1203	1151	1220	1290
	Min.	35	35	47	53	58	197	365	434	480	573	648	654	544	492
66	Max.	22	22	45	97	190	417	522	615	662	708	743	819	923	981
	Min.	-13	-19	-13	-2	22	97	173	249	324	400	435	446	452	464
67	Max.	30	36	47	47	152	461	496	519	548	630	682	682	699	758
	Min.	-5	-5	1	7	24	100	263	321	309	315	333	344	356	362
68	Max.	14	66	305	410	486	754	888	999	1104	1186	1256	1337	1489	1559
	Min.	-27	-56	-80	-51	-27	54	142	194	235	288	317	346	375	434

Table 4-67 Measured Strain (Micro Strain) in Column Spiral for THD-5 (Continued)

Strain Gauge No.		Motion (x Sylmar)													
		0.10	0.25	0.50	0.75	1.00	1.25	1.50	1.75	2.00	2.25	2.50	2.75	3.00	3.00
69	Max.	49	49	72	90	252	837	1156	1266	1260	1324	1451	1434	1370	1306
	Min.	14	14	20	14	20	101	310	432	489	455	420	455	443	501
70	Max.	23	40	115	173	324	555	752	763	1012	1249	1504	1811	2082	**2453**
	Min.	-18	-41	-70	-81	-29	87	156	179	173	220	301	416	532	682
71	Max.	18	53	175	228	443	938	1578	1549	1916	**2673**	**4018**	**5258**	**6842**	**7913**
	Min.	-29	-29	6	47	82	134	204	408	455	676	1159	**2155**	**3244**	**4647**
72	Max.	30	59	105	128	326	593	738	744	918	1058	1185	1435	1720	2091
	Min.	-11	-23	-17	-23	6	70	128	151	157	181	233	297	221	-476
73	Max.	17	23	256	384	605	907	1210	1402	1524	1856	**2263**	**2688**	**3741**	**3997**
	Min.	-35	-41	-12	64	93	209	267	442	430	477	605	680	948	1571
74	Max.	80	254	329	323	329	358	352	277	265	237	213	208	242	532
	Min.	-59	-100	-140	-169	-198	-181	-204	-163	-111	-181	-239	-279	-129	86
75	Max.	-25	33	61	-25	61	314	240	337	251	165	837	590	50	-226
	Min.	-65	-151	-134	-174	-226	-186	-94	-278	-473	-450	-519	-898	-1318	-1473

Table 4-68 Measured Strain (Micro Strain) in Hinge Longitudinal Bars for THD-5

Strain Gauge No.		Motion (x Sylmar)													
		0.10	**0.25**	**0.50**	**0.75**	**1.00**	**1.25**	**1.50**	**1.75**	**2.00**	**2.25**	**2.50**	**2.75**	**3.00**	**3.00**
1	**Max.**	-8	44	50	56	236	363	421	427	421	601	543	601	555	369
	Min.	-153	-199	-442	-512	-570	-692	-709	-744	-674	-709	-674	-756	-703	-385
2	**Max.**	-162	-97	26	50	155	249	414	461	502	560	637	695	654	302
	Min.	-215	-238	-261	-279	-285	-308	-297	-314	-291	-285	-303	-279	-238	-15
3	**Max.**	-658	-90	293	334	462	578	583	578	467	409	375	311	3	-844
	Min.	-1023	-1319	-1841	**-2143**	**-2503**	**-2688**	**-2746**	**-2694**	**-2305**	**-2294**	**-2416**	**-2340**	**-2149**	-1470
4	**Max.**	-370	-67	334	409	619	584	595	770	1165	1427	1078	1258	**2136**	**6257**
	Min.	-695	-1021	-1276	-1398	-1555	-1712	-1660	-1590	-1334	-1090	-1509	-1358	-1055	194
5	**Max.**	-483	-231	425	706	1485	1907	**2235**	**2200**	**2212**	**2323**	**2487**	**2540**	**2218**	859
	Min.	-694	-870	-1045	-1081	-1174	-1315	-1245	-1245	-1163	-1092	-1127	-688	-430	431
6	**Max.**	-764	-688	-257	92	1197	**2152**	**2466**	**2204**	1000	-426	-4388	1151	**7988**	**12555**
	Min.	-816	-874	-979	-1060	-1188	-1340	-1310	-1444	-1863	**-10358**	**-11278**	**-9649**	**-5273**	-7
7	**Max.**	-1977	-662	**3661**	**4847**	**8197**	**7402**	**4148**	**N/A**	**N/A**	**N/A**	**N/A**	**N/A**	**N/A**	**N/A**
	Min.	**-3087**	**-5266**	**-7527**	**-7465**	**-8747**	**-13666**	**-23834**	**-76968**	**N/A**	**N/A**	**N/A**	**N/A**	**N/A**	**N/A**
8	**Max.**	-910	-220	**3549**	**5506**	**7583**	**7716**	**7636**	**7139**	**8857**	**11027**	**9355**	**9574**	**N/A**	**N/A**
	Min.	-1567	**-2190**	-2051	138	988	1618	1678	-1348	1193	**5075**	1837	**2481**	**4252**	**N/A**

139

Table 4-69 Measured Strain (Micro Strain) in Hinge Longitudinal Bars for THD-5 (Continued)

Strain Gauge No.		Motion (x Sylmar)													
		0.10	0.25	0.50	0.75	1.00	1.25	1.50	1.75	2.00	2.25	2.50	2.75	3.00	3.00
9	Max.	-702	-535	275	1189	**16235**	**19450**	**25915**	**24782**	**60859**	**49207**	-1304	**N/A**	**N/A**	**N/A**
	Min.	-835	-910	-986	-997	**-111023**	**-89529**	**-166564**	**N/A**	**N/A**	**N/A**	**N/A**	**N/A**	**N/A**	**N/A**
10	Max.	-479	-5	1131	**2683**	**11735**	**23650**	**44628**	**58610**	**47298**	**N/A**	**N/A**	**N/A**	**N/A**	**N/A**
	Min.	-994	-1685	**-2247**	**-2311**	**-2534**	**-2944**	**-2224**	**-194033**	**7525**	**N/A**	**N/A**	**N/A**	**N/A**	**N/A**
11	Max.	-1757	-1509	-715	-298	970	**6840**	**9399**	**N/A**	**N/A**	**N/A**	**N/A**	**N/A**	**N/A**	**N/A**
	Min.	-1914	-1995	-2099	**-2192**	**-2724**	**-6106**	**-7582**	**-8804**	**N/A**	**N/A**	**N/A**	**N/A**	**N/A**	**N/A**
12	Max.	**N/A**	**N/A**	**N/A**	**N/A**	**N/A**	**N/A**	**N/A**	**N/A**	**N/A**	**N/A**	**N/A**	**N/A**	**N/A**	**N/A**
	Min.	**N/A**	**N/A**	**N/A**	**N/A**	**N/A**	**N/A**	**N/A**	**N/A**	**N/A**	**N/A**	**N/A**	**N/A**	**N/A**	**N/A**
14	Max.	-237	-150	24	-80	-376	-428	-909	-1060	-1037	**N/A**	**N/A**	**N/A**	**N/A**	**N/A**
	Min.	-793	-1617	-2099	**-2853**	**-3270**	**-4546**	**-4593**	**-5555**	**-5793**	**-6304**	**-19290**	**N/A**	**N/A**	**N/A**
15	Max.	-654	-75	431	-648	-1531	-1868	-1787	-1787	-850	**N/A**	**N/A**	**N/A**	**N/A**	**N/A**
	Min.	-1153	-1517	-1726	**-5757**	**-2609**	**-3519**	**-3944**	**-4105**	**-3600**	**-3303**	**N/A**	**N/A**	**N/A**	**N/A**
16	Max.	-501	-216	466	1031	1445	1235	**4802**	**3374**	**N/A**	**N/A**	**N/A**	**N/A**	**N/A**	**N/A**
	Min.	-711	-810	-874	-909	-1055	-991	**-4185**	**-6219**	-1550	**N/A**	**N/A**	**N/A**	**N/A**	**N/A**

140

Table 4-70 Measured Strain (Micro Strain) in Hinge Longitudinal Bars for THD-5 (Continued)

Strain Gauge No.		Motion (x Sylmar)													
		0.10	0.25	0.50	0.75	1.00	1.25	1.50	1.75	2.00	2.25	2.50	2.75	3.00	3.00
17	Max.	-1010	-912	-360	-17	337	75	-29	-75	-81	N/A	N/A	N/A	N/A	N/A
	Min.	-1057	-1098	-1179	-1185	-1249	-889	-767	-1028	-1405	-1283	N/A	N/A	N/A	N/A
18	Max.	37	135	176	158	100	-131	-525	-577	-531	-548	N/A	N/A	N/A	N/A
	Min.	-386	-779	-1017	-1063	-1179	-1659	-1578	-1549	-1457	-1399	-1254	N/A	N/A	N/A
19	Max.	-140	-140	-2	-140	-146	38	181	348	767	1140	1129	N/A	N/A	N/A
	Min.	-272	-376	-525	-525	-738	-755	-990	-1220	-749	-686	-893	-939	N/A	N/A
20	Max.	-502	-455	32	238	913	1647	1988	2000	**2111**	N/A	N/A	N/A	N/A	N/A
	Min.	-549	-614	-702	-760	-907	-1101	-1166	-1201	-1342	-1166	N/A	N/A	N/A	N/A
21	Max.	-510	-516	-434	-347	56	913	1158	1047	N/A	N/A	N/A	N/A	N/A	N/A
	Min.	-545	-586	-673	-755	-1064	-1338	-1443	-1495	-1495	N/A	N/A	N/A	N/A	N/A
22	Max.	311	416	509	550	667	830	737	754	743	743	783	N/A	N/A	N/A
	Min.	-80	-191	-360	-471	-641	-1300	-1557	-1814	-2006	**-2158**	**-2537**	**-2642**	N/A	N/A
23	Max.	-424	-424	-261	-174	187	2842	1416	1381	N/A	N/A	N/A	N/A	N/A	N/A
	Min.	-471	-517	-569	-593	-703	-721	670	636	566	N/A	N/A	N/A	N/A	N/A

Table 4-71 Measured Strain (Micro Strain) in Hinge Spiral for THD-5

Strain Gauge No.		Motion (x Sylmar)													
		0.10	0.25	0.50	0.75	1.00	1.25	1.50	1.75	2.00	2.25	2.50	2.75	3.00	3.00
24	Max.	56	56	56	56	56	56	68	68	178	184	189	189	184	184
	Min.	-8	-8	-8	-8	-8	39	39	39	39	39	44	44	44	39
25	Max.	10	10	10	10	54	176	187	214	214	214	225	231	225	225
	Min.	-7	-7	-7	-7	-7	37	37	43	48	48	48	37	54	70
26	Max.	98	116	122	248	308	494	686	680	452	482	518	644	524	494
	Min.	50	50	50	62	68	170	170	128	98	50	-22	-88	-58	50
27	Max.	18	47	244	267	302	319	342	336	319	331	331	325	348	365
	Min.	-34	-28	-17	-11	1	58	116	134	163	151	180	180	192	209
28	Max.	60	83	124	130	153	211	240	269	298	292	269	246	252	275
	Min.	19	25	31	37	13	-33	-16	13	165	130	112	106	83	147
29	Max.	10	51	63	228	375	834	**6393**	**N/A**	**N/A**	**N/A**	**N/A**	**N/A**	**N/A**	**N/A**
	Min.	-125	-125	-178	-196	-266	-7	181	**-20696**	**N/A**	**N/A**	**N/A**	**N/A**	**N/A**	**N/A**
30	Max.	1	89	77	-144	19	-202	-237	**5623**	**15798**	**17354**	**19816**	**21628**	**23156**	**N/A**
	Min.	-103	-196	-527	-695	-742	-1148	-1480	-1689	**2992**	**12795**	**14032**	**17482**	**18539**	**17360**
31	Max.	178	311	433	467	827	792	722	**N/A**	**N/A**	**N/A**	**N/A**	**N/A**	**N/A**	**N/A**
	Min.	33	-42	-100	-152	-54	16	-66	**-40361**	-1734	**N/A**	**N/A**	**N/A**	**N/A**	**N/A**
32	Max.	33	33	51	57	196	841	1108	1131	1160	980	1207	**N/A**	**N/A**	**N/A**
	Min.	-2	-2	10	10	22	103	225	318	254	271	295	-1599	**N/A**	**N/A**
33	Max.	81	81	112	81	112	124	-72	-114	**N/A**	**N/A**	**N/A**	**N/A**	**N/A**	**N/A**
	Min.	-10	-59	-72	-84	-194	-267	-475	-389	-328	**N/A**	**N/A**	**N/A**	**N/A**	**N/A**
34	Max.	17	35	29	23	87	23	-64	613	2316	**N/A**	**N/A**	**N/A**	**N/A**	**N/A**
	Min.	-41	-53	-59	-82	-59	-298	-519	-578	-502	280	**N/A**	**N/A**	**N/A**	**N/A**

Table 4-72 Measured Strain (Micro Strain) in Hinge Spiral for THD-5 (Continued)

Strain Gauge No.		Motion (x Sylmar)													
		0.10	0.25	0.50	0.75	1.00	1.25	1.50	1.75	2.00	2.25	2.50	2.75	3.00	3.00
35	Max.	113	113	113	113	113	306	724	911	N/A	N/A	N/A	N/A	N/A	N/A
	Min.	-24	-24	-30	-74	-143	-136	63	294	-6212	-45565	N/A	N/A	N/A	N/A
36	Max.	106	106	112	112	118	258	112	-58	-76	N/A	N/A	N/A	N/A	N/A
	Min.	-22	-22	-22	-22	-10	-143	-338	-399	-283	-5328	-39085	-95499	N/A	N/A
37	Max.	57	63	74	74	150	666	932	793	526	N/A	N/A	N/A	N/A	N/A
	Min.	22	22	28	22	39	39	22	161	132	-210	N/A	N/A	N/A	N/A
38	Max.	161	161	161	161	211	211	211	211	224	355	405	548	N/A	N/A
	Min.	30	30	37	30	68	74	86	143	143	143	143	68	-37180	N/A
39	Max.	49	55	55	55	61	190	190	196	196	237	N/A	N/A	N/A	N/A
	Min.	-4	-10	-10	-10	-10	37	37	37	37	43	67	N/A	N/A	N/A
40	Max.	51	51	74	74	127	494	802	N/A	N/A	N/A	N/A	N/A	N/A	N/A
	Min.	16	16	28	5	-65	-269	-368	-6089	-240	N/A	N/A	N/A	N/A	N/A
41	Max.	38	44	55	49	67	131	125	142	136	177	206	N/A	N/A	N/A
	Min.	3	9	15	15	15	49	61	73	73	67	73	38	N/A	N/A
42	Max.	13	13	13	7	25	89	94	106	94	164	N/A	N/A	N/A	N/A
	Min.	-22	-22	-22	-28	-22	25	36	42	48	48	-34319	-41412	N/A	N/A
43	Max.	17	17	28	28	40	75	93	104	N/A	N/A	N/A	N/A	N/A	N/A
	Min.	-19	-13	-7	-13	-7	28	40	46	57	N/A	N/A	N/A	N/A	N/A

143

Table 4-1 Performance of Specimen THD-1

Run	Motion (x Sylmar)	PGA (g)	Observed Performance		
			Two-Way Hinge	Column	Others
1	0.1	0.06	No visible damage		
2	0.25	0.15	No visible damage		
3	0.5	0.3	No visible damage	Flexural crack at column base	
4	0.75	0.45		More flexural crack at column base	
5	1	0.6			
6	1.25	0.75	Visible shear crack at hinge	Spalling at column base	
7	1.5	0.9	Minor spalling at hinge	Column base spiral visible	
8	1.75	1.05	Spalling at hinge	Column base spalling	
9	2	1.2	More spalling at hinge	Column base longitudinal rebar visible	
10	2.25	1.35			Crack at bottom of head
11	2.5	1.5	Significant hinge spalling	Spalling at other side of column base	More crack at bottom of head
12	2.625	1.575	Hinge spiral visible	Significant spalling at both side of column	
13	2.75	1.65	Hinge permanent rotation	Column permanent deformation	
14	2.875	1.725	Hinge sheared off, separated from column		Column top cover sheared off

Table 4-2 Performance of Specimen THD-2

Runs	Motion (x Sylmar)	PGA (g)	Observed Performance		
			Two-Way Hinge	Column	Others
1	0.1	0.06	No visible damage		
2	0.25	0.15	No visible damage		
3	0.5	0.3	No visible damage	Column base visible crack	
4	0.75	0.45	Hinge shear crack	Flexural crack at column base	
5	1	0.6	Hinge shear crack		
6	1.25	0.75	Hinge spalling	Spalling at column base.	
7	1.5	0.9	More hinge spalling	Column base spalling	
8	1.75	1.05	Spalling at both side of hinge	More spalling at column base.	
9	2	1.2		Spalling at column base, spiral visible	Big crack at bottom of header
10	2.25	1.35	Hinge gap closed, hit column top edge		Column top cover damage
11	2.5	1.5	Hinge gap closed again, longitudinal rebar visible		
12	2.625	1.575	Hinge crush down, gap narrowed	More spalling at column base.	Loading head permanently offset from column center line.
13	2.75	1.65			
14	2.875	1.725	Hinge collapse		
15	3	1.8			Large permanent offset between head and column

Table 4-3 Performance of Specimen THD-3

Run	Motion (x Sylmar)	PGA (g)	Observed Performance		
			Two-Way Hinge	Column	Others
1	0.1	0.06	No visible damage		
2	0.25	0.15	No visible damage		
3	0.5	0.3	No visible damage	Column base crack	
4	0.75	0.45	Hinge visible crack	More cracking in the column base	
5	1	0.6	Hinge spalling at one side		
6	1.25	0.75	Hinge spalling at both side		Crack in head bottom.
7	1.5	0.9	Hinge spalling	Spalling at column base, column spiral visible	Crack in head
8	1.75	1.05	Significant hinge spalling	Longitudinal rebar visible at column base	
9	2	1.2	Gap Closed, hinge spiral visible	More spalling at column base	
10	2.25	1.35	Hinge crush down, permanent rotation		
11	2.5	1.5	One hinge rebar ruptured	Four longitudinal rebar ruptured at column base	

Table 4-4 Performance of Specimen THD-4

Run	Motion (x Sylmar)	PGA (g)	Observed Performance		
			Two-Way Hinge	Column	Others
1	0.1	0.06	No visible damage	Crack at column base	
2	0.25	0.15			
3	0.375	0.225		Significant crack at column base,	
4	0.5	0.3	Shear crack at both side of the hinge	More crack at column base	
5	0.75	0.45	Hinge spalling at both side		
6	1	0.6	Hinge significant spalling, spiral visible	Crack at column base, no visible spalling	
7	1.25	0.75	Hinge shear off, hinge rebar fractured		

Table 4-5 Performance of SpecimenTHD-5

Run	Motion (x Sylmar)	PGA (g)	Observed Performance		
			Two-Way Hinge	Column	Others
1	0.1	0.06	No visible damage		
2	0.25	0.15	Hinge crack	Crack at oneside of the column base	
3	0.5	0.3	Hinge spalling	More cracks at column base	
4	0.75	0.45	More spalling at hinge		
5	1	0.6			
6	1.25	0.75		Column base crack increase	
7	1.5	0.9	Spalling at both side of the hinge	Spalling at one side of the column base	
8	1.75	1.05	Gap closed, hinge spiral visible		
9	2	1.2	Hing crush down	More spalling at column base	
10	2.25	1.35			
11	2.5	1.5	Hinge core damage, gap narrowed		Column top cover sheared off
12	2.75	1.65		Column permanent deformation	
13	3	1.8	One hinge longitudinal rebar fracture		
14	3	1.8	Large permant slippage between hinge and column		

Table 4-6 Target and Achieved Table Peak Accelerations & Spectral Acceleration for Specimen THD-1

Input Motion	PGA (g)		PGA Ratio	Specimen	SA (g)		SA Ratio
(xSylmar)	Target	Achieved	(Achieved/Target)	Period	Target	Achieved	(Achieved/Target)
0.1	0.06	0.08	1.27	0.270	0.13	0.14	1.08
0.25	0.15	0.15	1.00	0.270	0.34	0.35	1.03
0.5	0.30	0.30	0.98	0.287	0.68	0.63	0.93
0.75	0.45	0.39	0.86	0.293	0.99	0.74	0.75
1	0.61	0.55	0.91	0.315	1.31	0.89	0.68
1.25	0.76	0.69	0.92	0.343	1.38	1.1	0.80
1.5	0.91	0.81	0.90	0.417	1.45	1.26	0.87
1.75	1.06	0.94	0.88	0.440	1.94	1.3	0.67
2	1.21	1.05	0.87	0.470	2.26	1.4	0.62
2.25	1.36	1.12	0.82	0.506	1.99	1.25	0.63
2.5	1.52	1.20	0.80	0.543	1.5	1.14	0.76
2.625	1.59	1.27	0.80	0.569	1.33	1.18	0.89
2.75	1.67	1.41	0.84	0.596	1.16	1.16	1.00
2.875	1.74	1.79	1.03	0.641	1.26	0.96	0.76

Table 4-7 Target and Achieved Table Peak Accelerations & Spectral Acceleration for Specimen THD-2

Input Motion	PGA (g)		PGA Ratio	Specimen	SA (g)		SA Ratio
(xSylmar)	Target	Achieved	(Achieved/Target)	Period	Target	Achieved	(Achieved/Target)
0.1	0.06	0.04	0.63	0.303	0.14	0.11	0.79
0.25	0.15	0.16	1.06	0.303	0.34	0.33	0.97
0.5	0.30	0.30	0.98	0.303	0.68	0.63	0.93
0.75	0.45	0.44	0.97	0.328	0.98	0.87	0.89
1	0.61	0.61	1.00	0.368	1.08	1.03	0.95
1.25	0.76	0.64	0.85	0.425	1	1.1	1.10
1.5	0.91	0.82	0.90	0.457	1.65	1.46	0.88
1.75	1.06	1.15	1.09	0.540	1.6	1.32	0.83
2	1.21	1.38	1.14	0.607	0.93	0.7	0.75
2.25	1.36	1.45	1.06	0.670	1	0.8	0.80
2.5	1.52	1.44	0.95	0.704	1.27	1.04	0.82
2.625	1.59	1.52	0.96	0.753	1.4	1.21	0.86
2.75	1.67	1.56	0.93	0.817	1.42	1.23	0.87
2.875	1.74	1.64	0.94	0.860	1.31	1.11	0.85
3	1.82	1.69	0.93	0.885	1.26	1.08	0.86

Table 4-8 Target and Achieved Table Peak Accelerations & Spectral Acceleration for Specimen THD-3

Input Motion	PGA (g)		PGA Ratio	Specimen	SA (g)		SA Ratio
(xSylmar)	Target	Achieved	(Achieved/Target)	Period	Target	Achieved	(Achieved/Target)
0.1	0.06	0.07	1.14	0.227	0.12	0.13	1.08
0.25	0.15	0.15	0.97	0.227	0.29	0.56	1.93
0.5	0.30	0.30	1.00	0.262	0.62	0.76	1.23
0.75	0.45	0.45	0.98	0.331	0.89	0.76	0.85
1	0.61	0.42	0.69	0.452	1.18	1	0.85
1.25	0.76	0.54	0.72	0.483	1.35	0.81	0.60
1.5	0.91	0.73	0.81	0.573	0.7	0.47	0.67
1.75	1.06	1.10	1.04	0.663	0.83	0.69	0.83
2	1.21	1.50	1.24	0.787	0.98	0.78	0.80
2.25	1.36	1.82	1.33	0.925	0.83	0.77	0.93
2.5	1.52	1.87	1.23	1.042	1.1	0.84	0.76

Table 4-9 Target and Achieved Table Peak Accelerations & Spectral Acceleration for Specimen THD-4

Input Motion	PGA (g)		PGA Ratio	Specimen	SA (g)		SA Ratio
(xSylmar)	Target	Achieved	(Achieved/Target)	Period	Target	Achieved	(Achieved/Target)
0.1	0.06	0.05	0.89	0.361	0.1	0.09	0.90
0.25	0.15	0.17	1.12	0.361	0.25	0.27	1.08
0.375	0.23	0.28	1.22	0.403	0.31	0.3	0.97
0.5	0.30	0.36	1.19	0.476	0.54	0.34	0.63
0.75	0.45	0.57	1.25	0.528	0.51	0.32	0.63
1	0.61	0.79	1.31	0.604	0.41	0.38	0.93
1.25	0.76	0.97	1.28	0.739	0.67	0.55	0.82

Table 4-10 Target and Achieved Table Peak Accelerations & Spectral Acceleration for Specimen THD-5

Input Motion	PGA (g)		PGA Ratio	Specimen	SA (g)		SA Ratio
(xSylmar)	Target	Achieved	(Achieved/Target)	Period	Target	Achieved	(Achieved/Target)
0.1	0.06	0.05	0.81	0.261	0.12	0.11	0.92
0.25	0.15	0.17	1.09	0.261	0.31	0.3	0.97
0.5	0.30	0.29	0.95	0.303	0.66	0.59	0.89
0.75	0.45	0.41	0.91	0.348	0.8	0.55	0.69
1	0.61	0.55	0.92	0.362	1	0.79	0.79
1.25	0.76	0.71	0.94	0.419	1.2	0.9	0.75
1.5	0.91	0.83	0.92	0.491	1.55	0.91	0.59
1.75	1.06	0.90	0.84	0.555	0.9	0.61	0.68
2	1.21	1.23	1.02	0.596	0.8	0.6	0.75
2.25	1.36	1.45	1.06	0.786	1.1	0.82	0.75
2.5	1.52	1.65	1.09	0.829	1.04	0.825	0.79
2.75	1.67	1.75	1.05	0.885	1	0.86	0.86
3	1.82	1.95	1.07	0.920	1.1	0.97	0.88
3	1.82	1.99	1.10	0.980	1.2	1.02	0.85

Table 4-11 Dynamic Properties from Free Vibration for THD-1

Previous Motion (xSylmar)	Frequency (Hz)	Period (sec.)	Stiffness (Kip/in)	Stiffness (KN/mm)	Damping Ratio
0.1	3.955	0.253	160.0	28.0	3.1%
0.75	3.54	0.282	128.2	22.4	4.1%
1.0	3.76	0.266	144.6	25.3	7.3%
2.0	2.74	0.365	76.8	13.4	8.7%

Table 4-12 Dynamic Properties from Free Vibration for THD-2

Previous Motion (xSylmar)	Frequency (Hz)	Period (sec.)	Stiffness (Kip/in)	Stiffness (KN/mm)	Damping Ratio
0.1	3.565	0.281	130.0	22.7	3.3%
0.75	3.02	0.331	93.3	16.3	4.3%
2.0	2.148	0.466	47.2	8.3	5.0%

Table 4-13 Dynamic Properties from Free Vibration for THD-3

Previous Motion (xSylmar)	Frequency (Hz)	Period (sec.)	Stiffness (Kip/in)	Stiffness (KN/mm)	Damping Ratio
0.1	3.66	0.273	137.0	24.0	6.1%
0.75	3.03	0.330	93.9	16.4	7.0%
2.0	2.88	0.347	84.8	14.8	10.2%

Table 4-14 Dynamic Properties from Free Vibration for THD-4

Previous Motion (xSylmar)	Frequency (Hz)	Period (sec.)	Stiffness (Kip/in)	Stiffness (KN/mm)	Damping Ratio
0.1	2.73	0.366	76.2	13.3	3.4%
0.5	1.758	0.569	31.6	5.5	4.5%
0.75	1.66	0.602	28.2	4.9	5.9%

Table 4-15 Dynamic Properties from Free Vibration for THD-5

Previous Motion (xSylmar)	Frequency (Hz)	Period (sec.)	Stiffness (Kip/in)	Stiffness (KN/mm)	Damping Ratio
0.1	3.46	0.289	122.4	21.4	4.2%
1.0	2.73	0.366	76.2	13.3	5.3%
1.25	2.93	0.341	87.8	15.4	5.0%
2.0	2.24	0.446	51.3	9.0	6.7%

Table 4-16 Axial Load Variation

	Units	THD-1	THD-2	THD-3	THD-4	THD-5
Target Axial Load	**(KN)**	445	267	445	N/A	445
	(Kips)	100	60	100	N/A	100
Max. Axial Load	**(KN)**	466	287.6	484	N/A	484
	(Kips)	104.7	64.6	108.8	N/A	108.8
Min. Axial Load	**(KN)**	394	233	362	N/A	404
	(Kips)	88.5	52.4	81.3	N/A	90.8
Average Axial Load	**(KN)**	430	260.3	423	N/A	444
	(Kips)	96.6	58.5	95.1	N/A	99.8

Table 4-17 Peak Accelerations at Top of the Specimens

Motion		THD-1	THD-2	THD-3	THD-4	THD-5
0.1 x Sylmar	**Max (g)**	0.21	0.11	0.18	0.09	0.14
	Min (g)	-0.27	-0.14	-0.17	-0.11	-0.11
0.25 x Sylmar	**Max (g)**	0.32	0.32	0.39	0.34	0.32
	Min (g)	-0.34	-0.34	-0.31	-0.24	-0.33
0.375 x Sylmar	**Max (g)**	N/A	N/A	N/A	0.32	N/A
	Min (g)	N/A	N/A	N/A	-0.31	N/A
0.5 x Sylmar	**Max (g)**	0.51	0.61	0.46	0.28	0.46
	Min (g)	-0.54	-0.55	-0.49	-0.33	-0.53
0.75 x Sylmar	**Max (g)**	0.73	0.79	0.49	0.34	0.46
	Min (g)	-0.73	-0.61	-0.67	-0.37	-0.62
1.0 x Sylmar	**Max (g)**	0.77	0.88	0.46	0.28	0.63
	Min (g)	-0.74	-0.78	-0.56	-0.39	-0.71
1.25 x Sylmar	**Max (g)**	1.01	0.84	0.60	0.33	0.67
	Min (g)	-0.87	-0.71	-0.69	-0.42	-0.80
1.5 x Sylmar	**Max (g)**	0.92	0.89	0.58		0.64
	Min (g)	-0.76	-0.84	-0.66		-0.85
1.75 x Sylmar	**Max (g)**	0.99	0.92	0.52		0.58
	Min (g)	-0.83	-0.81	-0.63		-0.96
2.0 x Sylmar	**Max (g)**	1.02	0.92	0.56		0.54
	Min (g)	-0.80	-0.83	-0.56		-0.75
2.25 x Sylmar	**Max (g)**	0.97	0.94	0.44		0.58
	Min (g)	-0.81	-0.85	-0.47		-0.72
2.5 x Sylmar	**Max (g)**	1.01	0.81	0.44		0.58
	Min (g)	-0.76	-0.77	-0.45		-0.79
2.625 x Sylmar	**Max (g)**	0.92	0.75		N/A	N/A
	Min (g)	-0.78	-0.77			N/A
2.75 x Sylmar	**Max (g)**	0.93	0.84			0.57
	Min (g)	-0.83	-0.61			-0.79
2.875 x Sylmar	**Max (g)**	0.88	0.87	N/A		N/A
	Min (g)	-0.80	-0.73			N/A
3.0 x Sylmar (1)	**Max (g)**	N/A	0.93			0.64
	Min (g)		-0.67			-0.99
3.0 x Sylmar (2)	**Max (g)**		N/A			0.55
	Min (g)					-0.88

Table 4-18 Measured Peak Lateral Force and Displacement for THD-1

Motion	Peak Force								Peak Displacement							
	Maximum				Minimum				Maximum				Minimum			
	Force		Displacement		Force		Displacement		Displacement		Force		Displacement		Force	
xSylmar	(KN)	(Kips)	(mm)	(inch)	(KN)	(Kips)	(mm)	(inch)	(mm)	(inch)	(KN)	(Kips)	(mm)	(inch)	(KN)	(Kips)
0.1	67.8	15.2	2.60	0.10	-69.7	-15.7	-1.85	-0.07	2.68	0.11	65.9	14.8	-2.22	-0.09	-66.2	-14.9
0.25	129.0	29.0	4.78	0.19	-128.6	-28.9	-4.90	-0.19	5.06	0.20	110.2	24.8	-4.90	-0.19	-128.6	-28.9
0.5	209.5	47.1	9.65	0.38	-215.7	-48.5	-9.84	-0.39	9.90	0.39	206.1	46.3	-9.84	-0.39	-215.7	-48.5
0.75	292.7	65.8	15.72	0.62	-252.9	-56.8	-12.47	-0.49	15.98	0.63	288.2	64.8	-12.79	-0.50	-251.8	-56.6
1.0	328.2	73.8	19.83	0.78	-269.3	-60.5	-14.92	-0.59	20.76	0.82	317.0	71.2	-15.19	-0.60	-267.1	-60.0
1.25	368.4	82.8	32.07	1.26	-312.6	-70.3	-19.64	-0.77	33.94	1.34	349.0	78.4	-19.84	-0.78	-312.0	-70.1
1.5	362.1	81.4	37.73	1.49	-285.7	-64.2	-17.71	-0.70	37.98	1.50	351.1	78.9	-18.20	-0.72	-282.4	-63.5
1.75	375.2	84.3	44.90	1.77	-300.5	-67.5	-20.63	-0.81	45.39	1.79	368.9	82.9	-20.63	-0.81	-300.5	-67.5
2.0	380.9	85.6	52.36	2.06	-306.3	-68.8	-21.75	-0.86	54.11	2.13	379.1	85.2	-21.75	-0.86	-306.3	-68.8
2.25	376.6	84.6	60.58	2.39	-302.2	-67.9	-23.91	-0.94	61.59	2.42	374.3	84.1	-23.91	-0.94	-302.2	-67.9
2.5	375.3	84.3	66.39	2.61	-306.7	-68.9	-26.42	-1.04	67.82	2.67	375.2	84.3	-27.05	-1.07	-300.2	-67.5
2.625	374.1	84.1	73.00	2.87	-301.3	-67.7	-25.41	-1.00	73.32	2.89	370.5	83.3	-26.99	-1.06	-293.5	-65.9
2.75	381.3	85.7	84.51	3.33	-318.5	-71.6	-31.63	-1.25	85.74	3.38	374.3	84.1	-33.29	-1.31	-311.8	-70.1
2.875	378.3	85.0	120.51	4.74	-324.9	-73.0	-37.74	-1.49	120.68	4.75	299.5	67.3	-38.74	-1.53	-323.7	-72.7

98

Table 4-19 Measured Peak Lateral Force and Displacement for THD-2

Motion	Peak Force								Peak Displacement							
	Maximum				Minimum				Maximum				Minimum			
	Force		Displacement		Force		Displacement		Displacement		Force		Displacement		Force	
xSylmar	(KN)	(Kips)	(mm)	(inch)	(KN)	(Kips)	(mm)	(inch)	(mm)	(inch)	(KN)	(Kips)	(mm)	(inch)	(KN)	(Kips)
0.1	32.3	7.3	2.18	0.09	-35.1	-7.9	-2.50	-0.10	2.52	0.10	29.5	6.6	-3.15	-0.12	-33.7	-7.6
0.25	81.4	18.3	5.93	0.23	-86.8	-19.5	-7.46	-0.29	6.53	0.26	76.5	17.2	-7.85	-0.31	-84.0	-18.9
0.5	152.5	34.3	15.28	0.60	-137.6	-30.9	-14.30	-0.56	15.28	0.60	152.5	34.3	-14.50	-0.57	-132.0	-29.7
0.75	195.1	43.8	24.60	0.97	-161.7	-36.3	-18.18	-0.72	24.60	0.97	195.1	43.8	-18.18	-0.72	-161.7	-36.3
1.0	221.6	49.8	36.65	1.44	-211.1	-47.4	-27.77	-1.09	37.19	1.46	221.1	49.7	-27.98	-1.10	-204.3	-45.9
1.25	223.1	50.1	41.12	1.62	-189.6	-42.6	-26.37	-1.04	41.52	1.63	213.5	48.0	-26.37	-1.04	-189.6	-42.6
1.5	235.9	53.0	57.40	2.26	-217.4	-48.9	-31.18	-1.23	62.71	2.47	231.0	51.9	-31.18	-1.23	-217.4	-48.9
1.75	243.8	54.8	78.90	3.11	-211.2	-47.5	-32.73	-1.29	82.31	3.24	240.3	54.0	-34.73	-1.37	-207.8	-46.7
2.0	242.2	54.4	92.53	3.64	-218.9	-49.2	-40.97	-1.61	98.58	3.88	236.4	53.1	-42.63	-1.68	-216.5	-48.6
2.25	239.1	53.7	110.30	4.34	-224.1	-50.4	-49.58	-1.95	110.30	4.34	239.1	53.7	-50.05	-1.97	-220.7	-49.6
2.5	218.9	49.2	111.87	4.40	-221.9	-49.9	-54.29	-2.14	112.71	4.44	213.9	48.1	-55.00	-2.17	-175.5	-39.4
2.625	212.3	47.7	127.38	5.02	-214.0	-48.1	-44.14	-1.74	128.96	5.08	207.6	46.7	-57.28	-2.26	-198.9	-44.7
2.75	236.5	53.1	134.67	5.30	-170.7	-38.4	-30.17	-1.19	142.47	5.61	206.9	46.5	-39.15	-1.54	-165.4	-37.2
2.875	243.0	54.6	159.19	6.27	-210.6	-47.3	-17.48	-0.69	164.30	6.47	225.5	50.7	-25.48	-1.00	-193.4	-43.5
3	249.9	56.2	186.51	7.34	-195.8	-44.0	-10.81	-0.43	187.59	7.39	247.3	55.6	-12.90	-0.51	-153.6	-34.5

Table 4-20 Measured Peak Lateral Force and Displacement for THD-3

Motion	Peak Force								Peak Displacement							
	Maximum				Minimum				Maximum				Minimum			
	Force		Displacement		Force		Displacement		Displacement		Force		Displacement		Force	
xSylmar	(KN)	(Kips)	(mm)	(inch)	(KN)	(Kips)	(mm)	(inch)	(mm)	(inch)	(KN)	(Kips)	(mm)	(inch)	(KN)	(Kips)
0.1	53.8	12.1	1.54	0.06	-53.0	-11.9	-1.56	-0.06	1.54	0.06	53.8	12.1	-1.80	-0.07	-47.4	-10.7
0.25	112.1	25.2	4.28	0.17	-104.1	-23.4	-4.61	-0.18	4.28	0.17	112.1	25.2	-4.61	-0.18	-104.1	-23.4
0.5	182.4	41.0	11.14	0.44	-160.8	-36.1	-9.41	-0.37	11.14	0.44	182.4	41.0	-9.43	-0.37	-158.8	-35.7
0.75	215.5	48.4	23.56	0.93	-174.6	-39.2	-11.21	-0.44	24.07	0.95	211.5	47.5	-12.00	-0.47	-170.2	-38.3
1.0	217.6	48.9	27.05	1.06	-176.8	-39.7	-16.58	-0.65	27.53	1.08	211.5	47.5	-16.58	-0.65	-176.8	-39.7
1.25	228.5	51.3	38.93	1.53	-193.2	-43.4	-21.41	-0.84	41.23	1.62	225.0	50.6	-23.36	-0.92	-183.0	-41.1
1.5	233.8	52.5	51.51	2.03	-198.6	-44.6	-27.64	-1.09	55.67	2.19	226.6	50.9	-27.74	-1.09	-189.5	-42.6
1.75	231.2	51.9	64.22	2.53	-197.9	-44.5	-32.14	-1.27	76.30	3.00	220.9	49.6	-38.58	-1.52	-189.6	-42.6
2.0	253.2	56.9	85.98	3.39	-181.0	-40.7	-32.52	-1.28	95.67	3.77	200.2	45.0	-37.33	-1.47	-174.9	-39.3
2.25	207.8	46.7	112.37	4.42	-157.6	-35.4	-23.86	-0.94	122.87	4.84	202.9	45.6	-31.36	-1.23	-147.6	-33.2
2.5	161.0	36.2	161.11	6.34	-134.5	-30.2	-30.13	-1.19	171.51	6.75	133.9	30.1	-30.24	-1.19	-131.2	-29.5

Table 4-21 Measured Peak Lateral Force and Displacement for THD-4

Motion	Peak Force								Peak Displacement							
	Maximum				Minimum				Maximum				Minimum			
	Force		Displacement		Force		Displacement		Displacement		Force		Displacement		Force	
xSylmar	(KN)	(Kips)	(mm)	(inch)	(KN)	(Kips)	(mm)	(inch)	(mm)	(inch)	(KN)	(Kips)	(mm)	(inch)	(KN)	(Kips)
0.1	37.4	8.4	2.53	0.10	-38.4	-8.6	-2.30	-0.09	2.59	0.10	35.5	8.0	-2.30	-0.09	-38.4	-8.6
0.25	89.3	20.1	7.83	0.31	-100.5	-22.6	-7.86	-0.31	7.88	0.31	86.9	19.5	-7.86	-0.31	-100.5	-22.6
0.375	121.8	27.4	14.15	0.56	-109.7	-24.6	-9.73	-0.38	15.02	0.59	118.6	26.7	-10.12	-0.40	-105.3	-23.7
0.5	126.4	28.4	19.18	0.76	-93.4	-21.0	-8.89	-0.35	19.31	0.76	124.0	27.9	-9.18	-0.36	-92.3	-20.8
0.75	141.6	31.8	26.35	1.04	-101.6	-22.8	-10.28	-0.40	27.96	1.10	137.2	30.8	-10.28	-0.40	-101.6	-22.8
1.0	153.8	34.6	45.34	1.79	-98.7	-22.2	-9.90	-0.39	46.17	1.82	151.6	34.1	-10.16	-0.40	-94.4	-21.2
1.25	169.7	38.1	65.42	2.58	-92.4	-20.8	-8.81	-0.35	74.73	2.94	114.7	25.8	-9.43	-0.37	-90.4	-20.3

Table 4-22 Measured Peak Lateral Force and Displacement for THD-5

Motion	Peak Force								Peak Displacement							
	Maximum				Minimum				Maximum				Minimum			
	Force		Displacement		Force		Displacement		Displacement		Force		Displacement		Force	
xSylmar	(KN)	(Kips)	(mm)	(inch)	(KN)	(Kips)	(mm)	(inch)	(mm)	(inch)	(KN)	(Kips)	(mm)	(inch)	(KN)	(Kips)
0.1	49.8	11.2	1.88	0.07	-48.9	-11.0	-2.18	-0.09	1.88	0.07	49.8	11.2	-2.18	-0.09	-48.9	-11.0
0.25	123.7	27.8	6.34	0.25	-110.9	-24.9	-5.49	-0.22	6.34	0.25	123.7	27.8	-5.49	-0.22	-110.9	-24.9
0.5	220.3	49.5	14.26	0.56	-174.6	-39.2	-9.18	-0.36	14.28	0.56	211.6	47.6	-9.64	-0.38	-171.9	-38.6
0.75	243.7	54.8	17.86	0.70	-191.7	-43.1	-11.33	-0.45	17.86	0.70	243.7	54.8	-11.33	-0.45	-191.7	-43.1
1.0	276.9	62.2	25.51	1.00	-233.5	-52.5	-16.23	-0.64	26.07	1.03	265.6	59.7	-16.23	-0.64	-233.5	-52.5
1.25	297.7	66.9	37.39	1.47	-248.3	-55.8	-19.01	-0.75	39.15	1.54	291.3	65.5	-20.59	-0.81	-240.0	-53.9
1.5	309.5	69.5	51.72	2.04	-240.0	-53.9	-21.50	-0.85	51.82	2.04	301.4	67.7	-21.59	-0.85	-232.8	-52.3
1.75	330.9	74.4	55.36	2.18	-222.3	-50.0	-20.70	-0.82	102.02	4.02	-21.0	-4.7	-20.70	-0.82	-222.3	-50.0
2.0	292.1	65.6	93.11	3.67	-217.0	-48.8	8.19	0.32	97.61	3.84	283.0	63.6	7.52	0.30	-213.5	-48.0
2.25	301.3	67.7	111.47	4.39	-219.8	-49.4	10.27	0.40	113.80	4.48	296.9	66.7	9.68	0.38	-214.3	-48.1
2.5	315.7	70.9	129.54	5.10	-215.1	-48.3	19.89	0.78	136.71	5.38	312.6	70.2	16.63	0.65	-208.1	-46.8
2.75	342.6	77.0	161.13	6.34	-206.7	-46.4	31.78	1.25	161.64	6.36	342.4	76.9	28.38	1.12	-202.9	-45.6
3.0	369.1	82.9	192.28	7.57	-215.1	-48.3	54.52	2.15	193.17	7.61	360.5	81.0	44.98	1.77	-191.7	-43.1
3.0	365.9	82.2	213.04	8.39	-219.8	-49.4	62.32	2.45	218.34	8.60	359.5	80.8	62.11	2.45	-217.4	-48.9

Table 4-23 Measured Peak Displacement, Displacement Ductility and Drift

Motion	THD-1				THD-2				THD-3				THD-4				THD-5			
	Displacement		Deflection Ductility	Drift	Displacement		Deflection Ductility	Drift	Displacement		Deflection Ductility	Drift	Displacement		Deflection Ductility	Drift	Displacement		Deflection Ductility	Drift
xSylmar	(mm)	(inch)		(%)	(mm)	(inch)		(%)	(mm)	(inch)		(%)	(mm)	(inch)		(%)	(mm)	(inch)		(%)
0.1	2.60	0.10	0.15	0.2%	2.18	0.09	0.09	0.1%	1.54	0.06	0.1	0.1%	2.53	0.10	0.2	0.2%	1.88	0.07	0.1	0.2%
0.25	4.78	0.19	0.28	0.4%	5.93	0.23	0.25	0.4%	4.28	0.17	0.3	0.4%	7.83	0.31	0.6	0.6%	6.34	0.25	0.3	0.5%
0.375	N/A				N/A				N/A				14.15	0.56	1.1	1.2%	N/A			
0.5	9.65	0.38	0.56	0.8%	15.28	0.60	0.65	0.9%	11.14	0.44	0.8	0.9%	19.18	0.76	1.5	1.6%	14.26	0.56	0.7	1.2%
0.75	15.72	0.62	0.92	1.3%	24.60	0.97	1.05	1.5%	23.56	0.93	1.7	1.9%	26.35	1.04	2.0	2.2%	17.86	0.70	0.9	1.5%
1.0	19.83	0.78	1.16	1.6%	36.65	1.44	1.56	2.3%	27.05	1.06	1.9	2.2%	45.34	1.79	3.5	3.7%	25.51	1.00	1.2	2.1%
1.25	32.07	1.26	1.88	2.6%	41.12	1.62	1.75	2.5%	38.93	1.53	2.8	3.2%	71.00	2.80	5.5	5.8%	37.39	1.47	1.8	3.1%
1.5	37.73	1.49	2.21	3.1%	57.40	2.26	2.45	3.5%	51.51	2.03	3.7	4.2%	N/A				51.72	2.04	2.5	4.2%
1.75	44.90	1.77	2.63	3.7%	78.90	3.11	3.36	4.9%	64.22	2.53	4.6	5.3%					55.36	2.18	2.6	4.5%
2.0	52.36	2.06	3.07	4.3%	92.53	3.64	3.95	5.7%	85.98	3.39	6.1	7.1%					93.11	3.67	4.4	7.6%
2.25	60.58	2.39	3.55	5.0%	110.30	4.34	4.70	6.8%	120.00	4.72	8.6	9.8%					111.47	4.39	5.3	9.1%
2.5	66.39	2.61	3.89	5.4%	111.87	4.40	4.77	6.9%	N/A								129.54	5.10	6.2	10.6%
2.625	73.00	2.87	4.27	6.0%	127.38	5.02	5.43	7.8%									N/A			
2.75	84.51	3.33	4.95	6.9%	134.67	5.30	5.74	8.3%									161.13	6.34	7.7	13.2%
2.875	120.68	4.75	7.07	9.9%	159.19	6.27	6.79	9.8%									N/A			
3	N/A				187.59	7.39	8.00	11.5%									192.28	7.57	9.2	15.8%
3					N/A												218.34	8.60	10.4	17.9%

Notice: Last data point of Specimen THD-3 is based on displacement corresponding to 80% force of peak loading.

Table 4-24 Measured Top Panel Nodes Deflection & Specimen Top Deflection for THD-1

Motion (xSylmar)	Top Node Deflection		Top Column Deflection		D_{col} / D_{Node}	Force	
	(mm)	(inch)	(mm)	(inch)		(KN)	(Kips)
0.1	2.07	0.08	2.26	0.09	109%	32.3	7.3
0.25	4.94	0.19	5.74	0.23	116%	81.4	18.3
0.5	13.35	0.53	14.95	0.59	112%	152.5	34.3
0.75	20.46	0.81	24.17	0.95	118%	195.1	43.8
1.0	31.95	1.26	35.90	1.41	112%	221.6	49.8
1.25	36.64	1.44	40.35	1.59	110%	223.1	50.1
1.5	54.96	2.16	56.16	2.21	102%	235.9	53.0
1.75	77.55	3.05	76.90	3.03	99%	243.8	54.8
2.0	90.26	3.55	89.69	3.53	99%	242.2	54.4
2.25	90.30	3.56	105.96	4.17	117%	239.1	53.7
2.5	91.97	3.62	102.96	4.05	112%	218.9	49.2
2.625	93.13	3.67	103.63	4.08	111%	212.3	47.7
2.75	98.76	3.89	105.41	4.15	107%	236.5	53.1
2.875	106.02	4.17	N/A			243.0	54.6
3	121.14	4.77	N/A			249.9	56.2

Table 4-25 Measured Top Panel Nodes Deflection & Specimen Top Deflection for THD-2

Motion (xSylmar)	Top Node Deflection		Top Column Deflection		D_{col} / D_{Node}	Force	
	(mm)	(inch)	(mm)	(inch)		(KN)	(Kips)
0.1	2.07	0.08	2.26	0.09	109%	32.3	7.3
0.25	4.94	0.19	5.74	0.23	116%	81.4	18.3
0.5	11.35	0.45	14.95	0.59	132%	152.5	34.3
0.75	19.46	0.77	24.17	0.95	124%	195.1	43.8
1.0	31.95	1.26	35.90	1.41	112%	221.6	49.8
1.25	36.64	1.44	40.35	1.59	110%	223.1	50.1
1.5	54.96	2.16	56.16	2.21	102%	235.9	53.0
1.75	77.55	3.05	76.90	3.03	99%	243.8	54.8
2.0	90.26	3.55	89.69	3.53	99%	242.2	54.4
2.25	90.30	3.56	105.96	4.17	117%	239.1	53.7
2.5	91.97	3.62	102.96	4.05	112%	218.9	49.2
2.625	93.13	3.67	103.63	4.08	111%	212.3	47.7
2.75	98.76	3.89	105.41	4.15	107%	236.5	53.1
2.875	106.02	4.17	N/A			243.0	54.6
3	121.14	4.77	N/A			249.9	56.2

Table 4-26 Measured Top Panel Nodes Deflection & Specimen Top Deflection for THD-3

Motion (xSylmar)	Top Node Deflection		Top Column Deflection		D_{col} / D_{Node}	Force	
	(mm)	(inch)	(mm)	(inch)		(KN)	(Kips)
0.1	1.43	0.06	1.45	0.06	102%	53.8	12.1
0.25	4.20	0.17	4.15	0.16	99%	112.1	25.2
0.5	10.15	0.40	10.69	0.42	105%	182.4	41.0
0.75	22.86	0.90	22.31	0.88	98%	215.5	48.4
1.0	21.61	0.85	25.46	1.00	118%	217.6	48.9
1.25	32.40	1.28	36.74	1.45	113%	228.5	51.3
1.5	43.79	1.72	48.69	1.92	111%	233.8	52.5
1.75	55.08	2.17	60.43	2.38	110%	231.2	51.9
2.0	70.99	2.79	77.70	3.06	109%	253.2	56.9
2.25	109.27	4.30	98.84	3.89	90%	207.8	46.7
2.5	128.57	5.06	142.50	5.61	111%	161.0	36.2

Table 4-27 Measured Top Panel Nodes Deflection & Specimen Top Deflection for THD-4

Motion (xSylmar)	Top Node Deflection		Top Column Deflection		D_{col} / D_{Node}	Force	
	(mm)	(inch)	(mm)	(inch)		(KN)	(Kips)
0.1	2.48	0.10	2.44	0.10	98%	37.4	8.4
0.25	7.39	0.29	7.43	0.29	101%	89.3	20.1
0.375	13.74	0.54	13.21	0.52	96%	121.8	27.4
0.5	18.18	0.72	17.27	0.68	95%	126.4	28.4
0.75	25.24	0.99	22.70	0.89	90%	141.6	31.8
1.0	41.83	1.65	37.54	1.48	90%	153.8	34.6
1.25	63.51	2.50	51.92	2.04	82%	169.7	38.1

Table 4-28 Measured Top Panel Nodes Deflection & Specimen Top Deflection for THD-5

Motion (xSylmar)	Top Node Deflection		Top Column Deflection		D_{col} / D_{Node}	Force	
	(mm)	(inch)	(mm)	(inch)		(KN)	(Kips)
0.1	1.73	0.07	1.67	0.07	96%	49.8	11.2
0.25	5.68	0.22	6.09	0.24	107%	123.7	27.8
0.5	12.62	0.50	13.68	0.54	108%	220.3	49.5
0.75	16.03	0.63	17.05	0.67	106%	243.7	54.8
1.0	24.34	0.96	24.16	0.95	99%	276.9	62.2
1.25	36.23	1.43	35.10	1.38	97%	297.7	66.9
1.5	48.44	1.91	48.65	1.92	100%	309.5	69.5
1.75	50.33	1.98	47.46	1.87	94%	330.9	74.4
2.0	58.88	2.32	59.95	2.36	102%	292.1	65.6
2.25	68.28	2.69	73.28	2.89	107%	301.3	67.7
2.5	77.01	3.03	87.61	3.45	114%	315.7	70.9
2.75	95.74	3.77	N/A			342.6	77.0
3.0	112.10	4.41	N/A			369.1	82.9
3.0	118.06	4.65	N/A			365.9	82.2

Table 4-29 Distance of the Inflection Point from Bottom of the Specimens

Motion	THD-1		THD-2		THD-3		THD-4		THD-5	
xSylmar	(in)	(mm)	(in)	(mm)	(in)	(mm)	(in)	(mm)	(in)	(mm)
0.1	37.6	955	53.8	1366	42.0	1066	41.7	1058	46.4	1179
0.25	37.4	950	50.6	1285	41.8	1061	40.2	1022	44.0	1118
0.375	N/A		N/A		N/A		41.0	1043	N/A	
0.5	38.4	976	50.5	1281	41.1	1044	42.1	1070	42.0	1066
0.75	39.9	1013	50.9	1293	42.1	1069	43.1	1094	41.3	1050
1.0	40.0	1015	52.1	1323	42.3	1074	43.3	1099	40.9	1039
1.25	40.8	1036	51.8	1315	42.9	1089	46.5	1180	41.5	1055
1.5	39.8	1012	52.5	1334	43.3	1101	N/A		42.7	1083
1.75	40.1	1018	52.0	1320	43.2	1096			46.8	1190
2.0	40.7	1034	52.3	1328	48.5	1233			44.7	1134
2.25	40.9	1038	58.4	1484	47.3	1202			44.9	1141
2.5	41.3	1050	56.5	1434	41.7	1060			45.3	1150
2.625	42.2	1071	58.5	1486	N/A				N/A	
2.75	42.3	1075	57.5	1460					41.1	1044
2.875	47.6	1210	54.2	1376					N/A	
3	N/A		52.8	1341					38.6	979
3			N/A						38.2	970

Table 4-30 Measured Strain (Micro Strain) in Column Longitudinal Bars for THD-1

Strain Gauge No.		Motion (x Sylmar)													
		0.10	0.25	0.50	0.75	1.00	1.25	1.50	1.75	2.00	2.25	2.50	2.63	2.75	2.875
SG2B1	Max.	28	31	38	52	28	28	28	35	54	82	84	103	206	268
	Min.	12	10	10	-14	-21	-7	-2	-4	-9	-14	-26	-23	0	0
SG2B4	Max.	7	11	56	76	76	56	58	71	58	73	73	71	213	277
	Min.	-2	-2	-2	-20	-73	-62	-47	-47	-58	-65	-73	-189	-227	-295
SG4B4	Max.	-88	-72	-69	-69	-69	-69	-69	-69	-69	-72	-72	-72	4	6
	Min.	-168	-196	-196	-168	-269	-237	-223	-223	-237	-288	-297	-313	-290	-377
SG5B4	Max.	-6	-6	-6	1	-1	-1	-6	-6	-6	-6	-6	-6	-6	-8
	Min.	-60	-87	-89	-77	-160	-136	-155	-179	-182	-241	-260	-260	-253	-329
SG6B1	Max.	-28	0	47	191	296	284	328	349	387	389	373	415	421	548
	Min.	-74	-100	-107	-60	-42	-23	-14	-69	-132	-174	-228	-344	-926	-1203
SG4B1	Max.	-61	-35	23	233	479	423	463	472	496	496	477	519	507	659
	Min.	-110	-124	-135	-72	-65	-72	-82	-105	-173	-238	-298	-475	-1199	-1559
SG3B4	Max.	-145	-139	-89	271	435	428	486	504	513	556	553	560	724	941
	Min.	-215	-233	-228	-188	-378	-405	-430	-450	-450	-450	-470	-450	-448	-582
SG7B4	Max.	-70	-65	-65	244	362	411	426	437	500	504	500	504	571	742
	Min.	-159	-188	-206	-157	-328	-355	-372	-372	-375	-357	-412	-417	-372	-484
SG4B3	Max.	376	1049	**2225**	**3413**	**5714**	**5573**	**6740**	**7478**	**9164**	**11041**	**11909**	**15301**	**18932**	**24612**
	Min.	-671	-1060	-1652	**-2958**	**-4868**	**-5065**	**-5538**	**-5942**	**-6107**	**-6035**	**-6030**	**-6406**	**-5708**	**-7420**
SG3B5	Max.	176	712	1585	**2601**	**10417**	**11682**	**13984**	**16583**	**18996**	**20971**	**22199**	**25209**	**24051**	**31266**
	Min.	-699	-1040	-1558	-1882	**-2108**	-917	-648	-116	693	1485	**2418**	**2977**	**4242**	**5514**

104

Table 4-31 Measured Strain (Micro Strain) in Column Longitudinal Bars for THD-1 (Continued)

Strain Gauge No.		Motion (x Sylmar)													
		0.10	0.25	0.50	0.75	1.00	1.25	1.50	1.75	2.00	2.25	2.50	2.63	2.75	2.875
SG7B3	Max.	352	1039	2115	4614	6873	5085	6232	7106	8762	10611	11278	15033	18508	24061
	Min.	-670	-1124	-1902	-5945	-8405	-9000	-10477	-12245	-13357	-14113	-14642	-16369	-15992	-20790
SG5B3	Max.	446	1069	2157	5431	8035	5747	7021	7986	10139	12671	13839	18549	23009	29911
	Min.	-693	-1163	-1918	-7766	-9282	-9898	-11365	-13149	-14267	-15032	-15457	-17187	-17022	-22129
SG6B5	Max.	224	914	1916	9633	15081	17242	20963	24311	19117	11815	5898	5716	5325	6922
	Min.	-695	-1119	-1865	-2772	-4238	-1804	-1464	-473	1329	2714	2977	2313	2026	2634
SG8B5	Max.	254	915	1864	6134	13423	15230	18913	23341	27471	30950	33879	40390	42878	55742
	Min.	-692	-1088	-1793	-2765	-3818	-1851	-1543	-794	424	1648	3130	3534	4689	6096
SG8B2	Max.	457	1163	2267	5328	10199	7648	9342	10644	13000	15542	16114	20328	23261	30239
	Min.	-594	-981	-1722	-6444	-9111	-10211	-12367	-14881	-17275	-19833	-21859	-26984	-29802	-38742
SG2B3	Max.	444	1041	2018	3323	8995	6645	7791	8749	10417	12516	13244	16789	19187	24944
	Min.	-477	-816	-1374	-3271	-6228	-7205	-9168	-11545	-13572	-15244	-16891	-81484	-81484	N/A
SG1B6	Max.	845	1461	2366	11417	16222	18248	22280	26166	32143	7208	7152	6908	6035	7846
	Min.	12	-313	-936	-1266	-588	1044	1309	-81350	-81350	-2605	-2344	-5093	-9505	-12356
SG5B5	Max.	292	900	1777	8701	13971	15814	19505	23907	27946	32190	N/A	N/A	71096	92425
	Min.	-473	-748	-1357	-1727	-1830	-229	160	1053	2619	4031	5977	6859	10314	13408
SG7B2	Max.	194	570	1512	2251	2622	2919	3478	4754	7398	8903	9740	12159	15368	19979
	Min.	-283	-515	-877	-1609	-2025	-2307	-2747	-3247	-3189	-2681	-2413	-2314	-1845	-2398

105

Table 4-32 Measured Strain (Micro Strain) in Column Spiral for THD-1

Strain Gauge No.		Motion (x Sylmar)													
		0.10	**0.25**	**0.50**	**0.75**	**1.00**	**1.25**	**1.50**	**1.75**	**2.00**	**2.25**	**2.50**	**2.63**	**2.75**	**2.875**
SG1B1	**Max.**	12	12	16	67	186	209	272	381	535	667	800	1168	**5296**	**6885**
	Min.	-2	-2	-5	5	5	39	49	70	112	170	207	240	323	420
SG3B2	**Max.**	-15	-20	-22	-29	85	73	92	108	126	161	177	221	1474	1916
	Min.	-31	-36	-50	-103	-117	-119	-124	-117	-103	-73	-43	-10	-1	-2
SG5B2	**Max.**	-17	-19	-40	-119	-131	-175	-187	-201	-226	-238	-247	-198	-103	-134
	Min.	-33	-52	-91	-170	-236	-271	-292	-331	-385	-434	-473	-494	-517	-673
SG7B5	**Max.**	100	110	128	184	415	475	536	583	660	797	914	1105	1575	2048
	Min.	86	86	86	79	89	170	203	235	287	380	457	522	606	788
SG3B1	**Max.**	32	35	41	65	60	46	65	86	111	134	144	155	144	187
	Min.	18	18	21	11	-68	-82	-86	-86	-89	-96	-96	-105	-107	-139
SG1B2	**Max.**	-8	-8	-15	-76	-103	-73	-25	10	43	80	96	110	124	161
	Min.	-22	-27	-43	-159	-286	-330	-346	-365	-374	-386	-390	-404	-409	-532
SG6B4	**Max.**	48	48	48	181	260	274	279	277	260	202	202	181	130	169
	Min.	22	22	22	51	70	41	41	0	-55	-113	-161	-209	-252	-328
SG8B1	**Max.**	6	8	6	-18	-82	-177	-171	-166	-166	-159	-159	-150	-157	-204
	Min.	-8	-11	-18	-133	-205	-222	-233	-238	-245	-252	-261	-268	-286	-372

Table 4-33 Measured Strain (Micro Strain) in Column Spiral for THD-1 (Continued)

Strain Gauge No.		Motion (x Sylmar)													
		0.10	0.25	0.50	0.75	1.00	1.25	1.50	1.75	2.00	2.25	2.50	2.63	2.75	2.875
SG5B1	Max.	5	14	72	162	234	269	343	427	492	543	589	668	654	850
	Min.	-14	-14	-7	56	28	12	0	-5	-7	-5	7	7	18	24
SG6B2	Max.	6	11	20	92	295	463	616	712	738	761	761	828	936	1216
	Min.	-8	-8	-171	-283	-287	-285	-283	-273	-297	-304	-320	-299	-297	-386
SG1B5	Max.	5	5	84	296	551	660	809	1004	1182	1296	1366	1505	1524	1981
	Min.	-13	-20	-13	-46	-50	-50	-53	-64	-55	-36	-13	1	43	55
SG1B4	Max.	6	6	6	-89	-142	-216	-218	-135	-15	77	149	301	375	487
	Min.	-43	-47	-165	-343	-491	-518	-583	-611	-592	-611	-636	-606	-606	-788
SG2B6	Max.	-36	-36	-17	-10	-22	41	148	231	282	347	415	603	645	838
	Min.	-62	-80	-85	-222	-289	-287	-280	-285	-273	-268	-266	-254	-252	-328
SG6B3	Max.	21	21	21	21	26	144	362	602	829	1270	1462	2066	1952	**2537**
	Min.	-77	-176	-343	-787	-1025	-297	-59	-25	19	69	163	261	508	661
SG3B3	Max.	7	56	53	5	5	-14	-14	-2	5	5	2	5	5	6
	Min.	-21	-21	-21	-67	-95	-95	-116	-123	-137	-165	-151	-167	-151	-196
SG3B6	Max.	21	23	33	56	121	130	162	167	169	199	223	299	491	638
	Min.	-7	-34	-48	-4	21	21	14	21	51	63	49	42	47	61

Table 4-34 Measured Strain (Micro Strain) in Hinge Longitudinal Bars for THD-1

Strain Gauge No.		Motion (x Sylmar)													
		0.10	0.25	0.50	0.75	1.00	1.25	1.50	1.75	2.00	2.25	2.50	2.63	2.75	2.875
SG5B9	Max.	-87	-26	347	1546	**2251**	**2438**	**2673**	**2915**	**3112**	**3281**	**3438**	**3795**	**3788**	**4924**
	Min.	-176	-230	-366	-587	-1204	-1415	-1563	-1714	-1857	-1944	-1974	-2033	**-2138**	**-2780**
SG8B9	Max.	-49	30	341	1318	2040	**2225**	**2241**	**2564**	**4221**	**5560**	**6329**	**7780**	**71811**	**93355**
	Min.	-162	-232	-414	-692	-1431	-1674	-1957	**-2204**	**-2648**	**-2901**	**-3041**	**-3417**	**-11817**	**-15363**
SG3B9	Max.	-34	54	361	1452	1930	2056	**2237**	**2422**	**2571**	**2708**	**2826**	**3045**	**3066**	**3985**
	Min.	-166	-233	-308	-389	-675	-851	-1020	-1227	-1387	-1506	-1587	-1666	-1684	**-2190**
SG7B8	Max.	-169	-85	540	1128	1384	1375	1552	1685	1941	**2186**	**2274**	**2622**	**3006**	**3908**
	Min.	-287	-350	-453	-705	-1129	-1266	-1411	-1556	-1740	-1929	-2075	**-2313**	**-2455**	**-3192**
SG1B8	Max.	-74	35	508	954	1112	1140	1235	1321	1526	1630	1704	1900	**2136**	**2777**
	Min.	-225	-307	-425	-620	-869	-975	-1117	-1289	-1463	-1635	-1751	-1923	-2025	**-2633**
SG1B11	Max.	-58	234	1128	**3014**	**14520**	**18565**	**26331**	**71717**	**N/A**	**N/A**	**N/A**	**N/A**	**N/A**	**N/A**
	Min.	-402	-623	-1085	-1415	-1508	-1292	**-4815**	**-4168**	**N/A**	**N/A**	**N/A**	**N/A**	**N/A**	**N/A**

107

Table 4-35 Measured Strain (Micro Strain) in Hinge Longitudinal Bars for THD-1 (Continued)

Strain Gauge No.		Motion (x Sylmar)													
		0.10	0.25	0.50	0.75	1.00	1.25	1.50	1.75	2.00	2.25	2.50	2.63	2.75	2.875
SG6B9	Max.	-137	54	418	1864	2329	2136	2332	2946	4418	5847	5835	74803	74803	97244
	Min.	-406	-572	-914	-1687	-2053	-2173	-2263	-2305	-2268	-2131	-2119	-20044	-80012	-104015
SG2B9	Max.	-579	-293	974	2083	2766	2590	3431	71802	N/A	N/A	N/A	N/A	N/A	N/A
	Min.	-870	-1039	-1332	-1834	-2611	-2764	-3308	-10083	-18740	-15532	-16620	-13911	-11417	-14842
SG3B8	Max.	-475	-144	1441	8013	15329	13178	17283	20888	38613	65525	51451	17404	20804	27045
	Min.	-752	-906	-1129	-1041	605	850	889	719	-1099	261	4520	-8451	-81108	-105440
SG7B9	Max.	-149	-23	201	1772	2675	2727	2918	3217	4004	4646	4464	73158	73158	95106
	Min.	-375	-508	-793	-1129	-1353	-1545	-1699	-1904	-1925	-2154	-2427	-2938	-12479	-16222
SG6B8	Max.	-705	-486	470	1422	1854	1660	1966	2113	2421	2808	3100	4320	71550	93016
	Min.	-999	-1158	-1431	-2159	-2728	-2933	-3197	-3505	-3878	-4254	-4489	-4835	-4734	-6154
SG4B8	Max.	-728	-514	829	1710	2057	1978	2238	2424	2891	3709	4583	7205	72306	93998
	Min.	-986	-1137	-1312	-1974	-2551	-2660	-2781	-2934	-3341	-4155	-4692	-5670	-80032	-104041

Table 4-36 Measured Strain (Micro Strain) in Hinge Spiral for THD-1

Strain Gauge No.		Motion (x Sylmar)													
		0.10	0.25	0.50	0.75	1.00	1.25	1.50	1.75	2.00	2.25	2.50	2.63	2.75	2.875
SG5B8	Max.	29	41	59	75	92	89	92	96	115	134	117	96	110	143
	Min.	1	-8	-11	3	8	6	8	10	13	15	15	-11	15	19
SG2B8	Max.	7	14	19	46	70	79	95	128	162	158	153	176	181	235
	Min.	-7	-7	-93	-58	-62	-65	-74	-83	-104	-102	-95	-104	-97	-126
SG2B2	Max.	43	54	59	75	82	63	66	70	97	145	148	138	118	153
	Min.	18	4	6	6	4	6	6	13	25	15	6	0	43	56
SG8B7	Max.	-10	-10	-13	178	320	429	529	640	815	922	789	685	808	1050
	Min.	-34	-45	-66	-22	6	20	-15	-206	280	266	287	178	-5774	-7507

Table 4-37 Measured Strain (Micro Strain) in Column Longitudinal Bars for THD-2

Strain Gauge No.		Motion (x Sylmar)														
		0.1	0.25	0.5	0.75	1	1.25	1.5	1.75	2	2.25	2.5	2.625	2.75	2.875	3
SG4B5	Max.	17	19	26	31	38	45	61	68	29	26	8	-4	-4	43	108
	Min.	5	5	-4	-4	3	17	10	-22	-25	-97	-115	-132	-199	-208	-308
SG8B5	Max.	20	22	27	32	53	62	81	104	120	118	53	41	18	62	71
	Min.	6	-3	-12	-12	-1	9	6	-22	-33	-63	-119	-98	-170	-175	-303
SG3B2	Max.	96	106	127	147	159	136	140	115	90	69	-1	27	64	34	11
	Min.	76	73	62	4	-26	-35	-61	-91	-167	-253	-209	-126	-105	-102	-91
SG7B6	Max.	1	3	12	15	19	22	26	152	173	335	319	398	321	273	252
	Min.	-13	-36	-99	-122	-95	-69	-136	-157	-190	-150	-320	-280	-480	-427	-329
SG6B5	Max.	-3	-5	0	0	4	4	7	79	139	379	362	446	332	281	244
	Min.	-19	-51	-133	-158	-140	-96	-200	-258	-319	-237	-395	-319	-547	-479	-326
SG5B2	Max.	36	46	71	97	181	225	265	270	223	286	265	270	326	422	433
	Min.	-8	-13	6	50	74	74	41	-15	-106	-160	-190	-190	-199	-214	-256
SG4B1	Max.	-18	42	79	84	119	135	191	212	200	191	273	277	287	284	273
	Min.	-114	-170	-197	-197	-170	-46	-14	19	-7	-132	-69	-76	12	79	112
SG4B7	Max.	262	895	2042	**2665**	**2852**	**6571**	**13027**	**17035**	**20131**	**21772**	**21527**	**22530**	**23895**	**27079**	**30367**
	Min.	-277	-683	-1149	-1376	-1880	-1894	-2248	-643	-109	309	1205	1415	**3064**	**3519**	**4266**
SG8B1	Max.	124	766	1684	**2102**	**3006**	**2894**	**3499**	**5806**	**9392**	**11317**	**11582**	**12878**	**9976**	**10429**	**10764**
	Min.	-394	-810	-1338	-1703	-2088	**-2139**	**-2932**	**-4382**	**-4196**	**-3787**	**-3450**	**-3334**	**-3415**	**-3697**	**-4106**

109

Table 4-38 Measured Strain (Micro Strain) in Column Longitudinal Bars for THD-2 (Continued)

Strain Gauge No.		Motion (x Sylmar)														
		0.1	0.25	0.5	0.75	1	1.25	1.5	1.75	2	2.25	2.5	2.625	2.75	2.875	3
SG3B6	Max.	385	1117	2232	9168	11518	12341	18327	23959	28536	30765	30513	31794	34272	39593	45576
	Min.	-322	-776	-1295	-1383	-1363	-697	-1302	-429	118	795	2243	2739	5541	6549	8237
SG5B6	Max.	490	1373	2734	10375	14045	15040	22311	29264	35081	38600	38903	40981	44899	52805	70709
	Min.	-363	-911	-1510	-1608	-1766	-913	-1556	-410	657	1883	4130	5202	9461	11151	13959
SG2B2	Max.	167	987	1828	2328	6127	5536	7834	8580	11000	13555	13638	15038	11475	12166	12674
	Min.	-401	-788	-1368	-1836	-2446	-3730	-7111	-8208	-8937	-8374	-7316	-6974	-7265	-8164	-9292
SG1B7	Max.	367	1131	2374	7111	12860	13608	20317	27094	32712	35743	35881	37412	40679	48129	70290
	Min.	-397	-918	-1542	-1825	-2795	-1661	-2933	-1841	-1019	309	3370	4085	8815	9953	12014
SG2B6	Max.	430	1260	2566	6067	13420	14709	22798	31347	38382	42499	42898	45015	49190	57650	67112
	Min.	-381	-922	-1584	-2157	-3052	-1567	-2777	-1388	-518	876	3927	4617	10124	11797	14986
SG7B1	Max.	229	1099	2115	2537	11672	8918	11626	12765	15265	13892	15342	11813	5550	5413	19199
	Min.	-391	-769	-1393	-2123	-4967	-4703	-8969	-14088	-19472	-14995	-6870	-4197	-3135	-8222	-6392
SG7B7	Max.	304	1013	2357	2799	9068	10505	16013	23257	28870	31458	30267	31204	33269	38229	43459
	Min.	-261	-601	-1019	-1489	-1710	-999	-1266	-750	490	1483	2103	2124	3833	4296	4908
SG7B2	Max.	225	985	1873	2268	6138	5397	7302	8726	11249	13470	12981	14307	71818	N/A	N/A
	Min.	-280	-589	-1112	-1774	-2805	-4018	-7804	-11502	-14165	-13978	-12335	-11949	-23919	-18787	-22944

110

Table 4-39 Measured Strain (Micro Strain) in Column Spiral for THD-2

Strain Gauge No.		Motion (x Sylmar)														
		0.1	0.25	0.5	0.75	1	1.25	1.5	1.75	2	2.25	2.5	2.625	2.75	2.875	3
SG5B5	Max.	22	29	50	59	80	87	122	159	131	115	154	108	291	229	122
	Min.	8	10	13	17	22	31	34	31	22	13	-3	-27	-80	-55	-89
SG7B5	Max.	15	18	34	76	97	85	62	36	97	176	360	511	279	272	313
	Min.	4	4	4	11	22	32	6	-50	-80	-94	-113	-131	-120	-85	-68
SG3B1	Max.	49	61	70	80	117	126	168	199	204	318	292	393	304	295	243
	Min.	33	33	38	45	70	84	91	103	96	94	91	94	138	126	101
SG2B5	Max.	9	9	12	12	2	2	33	81	58	65	44	40	40	42	40
	Min.	-5	-2	-2	-2	-16	-16	-14	-19	-23	-23	-28	-21	-26	-12	-30
SG8B8	Max.	-4	1	1	3	-4	-4	1	1	-4	-6	-4	-1	10	15	15
	Min.	-15	-15	-13	-13	-22	-22	-27	-45	-59	-64	-62	-64	-64	-64	-50
SG2B1	Max.	16	18	21	25	25	32	39	47	56	75	70	75	82	89	91
	Min.	2	2	2	2	-3	0	2	11	23	28	37	44	49	42	32
SG6B6	Max.	13	13	13	17	10	10	13	78	94	117	113	122	115	115	124
	Min.	-1	-1	1	3	-8	-6	-11	-11	1	3	13	20	22	24	27
SG3B5	Max.	-5	-3	-3	-1	-8	-8	-5	6	-17	-28	-35	-35	-38	-38	-47
	Min.	-19	-17	-17	-15	-21	-19	-19	-31	-54	-66	-77	-91	-96	-103	-114
SG4B2	Max.	19	21	26	33	35	42	68	133	140	154	147	166	154	177	203
	Min.	3	5	5	10	-2	7	7	19	28	42	45	42	42	45	49
SG8B6	Max.	5	7	10	14	10	14	24	31	35	45	54	61	63	70	73
	Min.	-7	-7	-7	-2	-11	-2	0	3	-4	-9	-9	-9	-4	-11	-21

111

Table 4-40 Measured Strain (Micro Strain) in Column Spiral for THD-2 (Continued)

Strain Gauge No.		Motion (x Sylmar)														
		0.1	0.25	0.5	0.75	1	1.25	1.5	1.75	2	2.25	2.5	2.625	2.75	2.875	3
SG4B6	Max.	9	11	16	18	16	20	32	202	230	239	251	262	251	267	295
	Min.	-3	-3	-1	2	-10	-5	-3	2	76	74	74	79	85	83	85
SG6B1	Max.	34	34	36	34	50	61	82	192	201	215	215	215	215	215	219
	Min.	20	17	20	17	24	27	31	38	64	68	73	78	82	87	92
SG3B7	Max.	-3	8	31	56	83	81	124	174	269	348	428	459	425	518	582
	Min.	-19	-19	-12	-3	-5	-26	-46	-60	-26	-3	2	15	2	-12	-23
SG6B7	Max.	7	11	32	127	248	332	753	1120	1378	1455	1392	1374	1478	1718	2013
	Min.	-14	-28	-26	14	11	0	-3	37	79	195	197	206	202	206	276
SG1B1	Max.	14	42	153	179	195	211	244	452	480	498	450	464	487	545	556
	Min.	0	-4	-2	10	19	51	51	86	79	51	40	37	28	26	19
SG5B7	Max.	43	59	59	71	191	228	337	432	534	592	534	613	576	664	710
	Min.	-6	-22	-31	-20	-17	-3	-6	-8	-8	-8	-20	-10	-15	-8	1
SG1B6	Max.	-4	43	56	19	59	82	196	319	467	537	527	516	553	676	829
	Min.	-20	-25	-20	-48	-111	-118	-141	-159	-164	-180	-206	-199	-187	-178	-164
SG6B2	Max.	20	27	74	109	148	160	169	118	141	139	90	69	13	13	6
	Min.	-3	-3	8	27	64	69	-17	-105	-224	-326	-378	-415	-438	-503	-601
SG8B7	Max.	28	56	107	135	228	258	325	332	421	504	502	576	469	528	590
	Min.	5	2	0	5	-5	53	72	93	109	130	153	163	165	179	191
SG2B7	Max.	-8	-1	-1	23	87	74	136	169	62	16	25	39	55	69	78
	Min.	-26	-38	-61	-61	-61	-38	-63	-98	-128	-165	-209	-232	-295	-399	-487

112

Table 4-41 Measured Strain (Micro Strain) in Hinge Longitudinal Bars for THD-2

Strain Gauge No.		Motion (x Sylmar)														
		0.1	0.25	0.5	0.75	1	1.25	1.5	1.75	2	2.25	2.5	2.625	2.75	2.875	3
SG5B11	Max.	-83	73	634	864	1102	1202	1330	1532	1702	1877	1974	1856	1006	12	15
	Min.	-239	-406	-714	-1042	-1317	-1456	-1610	-1733	-1831	-1919	-1805	-1701	-1635	-919	-569
SG1B4	Max.	-152	22	607	1296	1601	1846	**2440**	**2984**	**3524**	**4259**	**4264**	**2866**	868	861	866
	Min.	-347	-535	-806	-958	-1200	-1219	-1469	-1723	-2023	-2189	-2113	-1274	-230	566	-225
SG1B11	Max.	-252	565	1696	2098	**7260**	**8395**	**12528**	**16450**	**21189**	**26911**	**24250**	**23660**	**7332**	**3969**	**3876**
	Min.	-912	-1304	-1998	**-2779**	**-3835**	**-5031**	**-6132**	**-6169**	**-6399**	**-6145**	**-2841**	**-82489**	**-5686**	1633	**2585**
SG6B9	Max.	-358	718	**2697**	**11077**	**18948**	**17369**	**21190**	**25082**	**30734**	**69834**	**N/A**	**N/A**	**N/A**	**N/A**	**N/A**
	Min.	-1147	-1551	-2206	-1640	-1317	-1315	-1678	**-2419**	**-4157**	**-6139**	**-5114**	**-4812**	**-6106**	**-2211**	-1069
SG2B4	Max.	-32	671	**2597**	**4605**	**11135**	**20194**	**51205**	**76132**	**79268**	**N/A**	**N/A**	**N/A**	**N/A**	**N/A**	**N/A**
	Min.	-697	-1234	-1882	**-2364**	**-6160**	**-5643**	**-6379**	**-1814**	**930**	**274**	**44647**	**54817**	**54263**	**79268**	**79268**
SG5B3	Max.	-495	-75	1235	**2874**	**4118**	**5768**	**28645**	**42961**	**35070**	**10004**	**8343**	**8324**	**7128**	**5592**	**5038**
	Min.	-714	-792	-853	-883	**-2106**	**-2545**	**-2417**	464	**2933**	**2995**	**2842**	**2477**	-269	**4335**	**4686**
SG2B9	Max.	-548	651	**3897**	**11355**	**20704**	**25251**	**24137**	**30149**	**34766**	**36899**	**68310**	**N/A**	**N/A**	**N/A**	**N/A**
	Min.	-1396	-1727	**-2150**	-488	1762	**-83111**	**N/A**	**N/A**	**N/A**	**N/A**	**N/A**	**N/A**	**N/A**	**N/A**	**N/A**
SG5B9	Max.	-527	337	1384	1618	**8087**	**7239**	**9568**	**6174**	**636**	**67781**	**N/A**	**N/A**	**N/A**	**N/A**	**N/A**
	Min.	-1293	-1634	**-2117**	**-2596**	**-3222**	**-3322**	**-4841**	**-4618**	**-3466**	**-3424**	**67781**	**N/A**	**N/A**	**N/A**	**N/A**
SG8B3	Max.	63	492	**2496**	**5702**	**23033**	**26066**	**43028**	**65151**	**76884**	**N/A**	**N/A**	**N/A**	**N/A**	**N/A**	**N/A**
	Min.	-494	-796	-992	-1044	-1178	**2357**	**2417**	**4510**	**6381**	**-30745**	**-85470**	**N/A**	**N/A**	**N/A**	**N/A**
SG4B3	Max.	-419	-153	1195	**3449**	**11742**	**15323**	**31285**	**35555**	**10974**	**7108**	**2014**	**72596**	**N/A**	**N/A**	**N/A**
	Min.	-580	-629	-655	-653	-508	967	1583	**3587**	**3974**	**-4465**	-1700	**-80316**	**N/A**	**N/A**	**N/A**

113

Table 4-42 Measured Strain (Micro Strain) in Hinge Longitudinal Bars for THD-2 (Continued)

Strain Gauge No.		Motion (x Sylmar)														
		0.1	0.25	0.5	0.75	1	1.25	1.5	1.75	2	2.25	2.5	2.625	2.75	2.875	3
SG7B8	Max.	-599	524	1858	**2285**	**10214**	**9344**	**11756**	**13835**	**17788**	**22418**	**29004**	**68956**	**N/A**	**N/A**	**N/A**
	Min.	-1406	-1736	**-2116**	**-2599**	**-3329**	**-2650**	**-3466**	**-4357**	**-6266**	**-6345**	**-2299**	1865	**4737**	**68956**	**N/A**
SG7B11	Max.	-448	265	1365	1638	1988	1984	**2242**	**2768**	**4092**	**8362**	**8039**	**3908**	**67650**	**N/A**	**N/A**
	Min.	-1115	-1366	-1747	-2010	**-2663**	**-2900**	**-3221**	**-3415**	**-4517**	**-6492**	**-5731**	**-3189**	**-2335**	**67650**	**N/A**
SG7B4	Max.	-62	296	1374	**2764**	**3295**	**3927**	**14618**	**21815**	**28090**	**30082**	**26583**	**70901**	**N/A**	**N/A**	**N/A**
	Min.	-518	-741	-912	-1085	**-2343**	**-2567**	**-6211**	**-6772**	**-7360**	**-8159**	**2443**	**19096**	**70901**	**N/A**	**N/A**
SG2B3	Max.	-299	-208	298	1599	**2154**	**2457**	**3157**	**7967**	**16938**	**19119**	**12300**	**72055**	**N/A**	**N/A**	**N/A**
	Min.	-386	-433	-454	-530	-1375	-1582	**-2134**	**-4063**	**-4016**	**-3864**	**-2287**	**-11409**	**72055**	**N/A**	**N/A**
SG1B8	Max.	-166	29	593	788	923	990	1152	1382	1739	2043	**2208**	**71157**	**N/A**	**N/A**	**N/A**
	Min.	-388	-507	-871	-1305	-1560	-1690	-1973	**-2291**	**-2532**	**-2616**	**-2474**	**-2154**	**71157**	**N/A**	**N/A**
SG6B8	Max.	-136	-94	262	593	776	888	1058	1309	1586	1767	1821	1670	**70177**	**N/A**	**N/A**
	Min.	-194	-236	-354	-720	-1187	-1366	-1625	-1962	**-2146**	-2074	-1988	-1687	**-1459**	**70177**	**N/A**
SG6B3	Max.	-224	-210	-13	498	653	797	1042	1336	1688	2000	2077	**71174**	**N/A**	**N/A**	**N/A**
	Min.	-293	-520	-687	-835	-1349	-1353	-1455	-1557	-1649	-1724	-1724	-1256	**71174**	**N/A**	**N/A**
SG4B4	Max.	-150	-131	-81	16	91	226	393	556	752	849	832	773	**70634**	**N/A**	**N/A**
	Min.	-204	-204	-209	-209	-638	-784	-1167	-1311	-1391	-1436	-1495	-1417	-1332	**70634**	**N/A**
SG8B11	Max.	-80	-78	-45	108	141	192	252	326	396	482	552	**71580**	**N/A**	**N/A**	**N/A**
	Min.	-103	-122	-122	-431	-635	-716	-900	-1039	-1136	-1090	-1062	**-2221**	**-7297**	**71580**	**N/A**
SG1B3	Max.	-129	-129	-129	-56	160	235	314	505	580	603	680	**69721**	**N/A**	**N/A**	**N/A**
	Min.	-181	-181	-372	-643	-977	-907	-1073	-954	-998	-1068	-1020	-852	-1027	**69721**	**N/A**

Table 4-43 Measured Strain (Micro Strain) in Hinge Spiral for THD-2

Strain Gauge No.		Motion (x Sylmar)														
		0.1	0.25	0.5	0.75	1	1.25	1.5	1.75	2	2.25	2.5	2.625	2.75	2.875	3
SG4B9	Max.	-4	10	31	37	33	33	33	8	-22	-27	-54	-175	-223	-287	-265
	Min.	-20	-24	-50	-45	-77	-88	-258	-441	-438	-329	-512	-528	-528	-578	-569
SG3B4	Max.	21	21	69	74	71	74	165	238	165	90	14	-52	-52	-199	-144
	Min.	-4	-4	-4	0	-4	-4	-4	-4	-133	-151	-176	-224	-279	-297	-252
SG3B9	Max.	49	136	143	147	117	129	126	268	361	**2752**	2079	**70219**	**N/A**	**N/A**	**N/A**
	Min.	-235	-290	-281	-235	-216	-239	-458	-684	-1459	-956	126	-67	**70219**	**N/A**	**N/A**
SG7B3	Max.	39	44	46	48	120	130	175	199	427	**20326**	**26680**	**10487**	**73440**	**N/A**	**N/A**
	Min.	15	17	-38	-131	-265	-344	-593	-799	-742	-419	**10611**	939	-134	**73440**	**N/A**
SG6B11	Max.	41	48	46	6	-17	-27	-50	-110	-50	-36	**70524**	**N/A**	**N/A**	**N/A**	**N/A**
	Min.	22	15	-22	-308	-431	-431	-554	-643	-780	-1645	**-8070**	-1466	**-17971**	**-14573**	**70524**
SG2B11	Max.	17	34	85	139	192	211	295	381	416	430	575	549	**69019**	**N/A**	**N/A**
	Min.	-4	1	8	41	52	78	85	106	111	134	169	199	-456	**69019**	**N/A**
SG5B4	Max.	-63	-63	-56	-11	7	9	76	150	492	718	436	**65697**	**N/A**	**N/A**	**N/A**
	Min.	-132	-137	-157	-157	-152	-114	-130	-114	-137	-206	-354	-253	**65697**	**N/A**	**N/A**
SG7B9	Max.	15	17	24	20	27	-45	-73	-119	-388	-597	-729	**69300**	**N/A**	**N/A**	**N/A**
	Min.	1	4	-1	-17	-68	-124	-281	-678	**-2457**	**-3270**	**-3134**	**-14125**	**-2647**	**69300**	**N/A**
SG4B8	Max.	-7	2	20	30	20	32	41	190	180	187	180	**70250**	**N/A**	**N/A**	**N/A**
	Min.	-21	-17	-12	-10	-33	-21	-21	-17	23	20	25	**-7821**	**-7497**	**70250**	**N/A**
SG1B5	Max.	28	28	35	70	79	86	112	123	130	142	151	**69146**	**N/A**	**N/A**	**N/A**
	Min.	14	8	3	8	19	19	3	12	8	-9	-34	-16	**69146**	**N/A**	**N/A**

115

Table 4-44 Measured Strain (Micro Strain) in Hinge Spiral for THD-2 (Continued)

Strain Gauge No.		Motion (x Sylmar)														
		0.1	0.25	0.5	0.75	1	1.25	1.5	1.75	2	2.25	2.5	2.625	2.75	2.875	3
SG3B11	Max.	0	0	0	9	74	81	118	197	186	188	251	**69374**	**N/A**	**N/A**	**N/A**
	Min.	-14	-14	-16	-21	0	-4	-60	-111	-155	-188	-222	**-3413**	**-20033**	**69374**	**N/A**
SG3B8	Max.	14	14	16	21	28	28	53	396	463	561	593	**69449**	**N/A**	**N/A**	**N/A**
	Min.	-2	0	2	0	-5	-2	0	7	35	32	39	**-12958**	**-15284**	**69449**	**N/A**
SG6B4	Max.	22	22	22	3	20	22	27	29	32	76	76	**69289**	**N/A**	**N/A**	**N/A**
	Min.	-4	-4	-4	-4	-4	-1	-4	-1	-4	-4	-4	-4	**69289**	**N/A**	**N/A**
SG8B9	Max.	6	4	8	6	11	69	264	176	176	148	299	**68774**	**N/A**	**N/A**	**N/A**
	Min.	-8	-8	-8	-10	-10	-50	-229	-159	-175	-166	-329	**-2920**	**-2530**	**68774**	**N/A**
SG5B8	Max.	1	4	10	15	10	10	15	34	68	96	87	**69058**	**N/A**	**N/A**	**N/A**
	Min.	-13	-10	-6	1	-6	-6	-3	-1	-3	-1	-8	-453	-1307	**69058**	**N/A**
SG3B3	Max.	14	14	14	17	21	92	218	216	236	220	314	**69016**	**N/A**	**N/A**	**N/A**
	Min.	-4	-4	-4	-4	-27	-29	-77	-31	-24	-4	-125	-130	**69016**	**N/A**	**N/A**
SG4B11	Max.	4	2	2	4	7	39	82	77	79	68	161	**73107**	**N/A**	**N/A**	**N/A**
	Min.	-12	-12	-12	-14	-12	-33	-61	-47	-56	-45	-127	-106	**73107**	**N/A**	**N/A**
SG2B8	Max.	8	10	17	26	24	28	33	49	63	72	84	**67537**	**N/A**	**N/A**	**N/A**
	Min.	-6	-6	1	3	-8	-2	1	1	3	10	19	31	**67537**	**N/A**	**N/A**
SG8B4	Max.	4	-14	-2	-2	4	150	590	230	274	205	719	**70331**	**N/A**	**N/A**	**N/A**
	Min.	-21	-21	-21	-21	-19	-166	-512	-168	-238	-194	-731	-558	**-3312**	**70331**	**N/A**
SG1B9	Max.	2	4	7	11	-3	55	342	195	153	46	88	**68955**	**N/A**	**N/A**	**N/A**
	Min.	-12	-10	-12	-12	-26	-59	-261	-175	-287	-268	-371	-2550	-194	**68955**	**N/A**

116

Table 4-45 Measured Strain (Micro Strain) in Column Longitudinal Bars for THD-3

Strain Gauge No.		Motion (x Sylmar)										
		0.1	0.25	0.5	0.75	1	1.25	1.5	1.75	2	2.25	2.5
44	Max.	-32	-14	15	20	26	20	9	20	26	38	44
	Min.	-90	-113	-131	-125	-102	-102	-78	-84	-61	-61	-1585
45	Max.	-10	7	7	7	7	7	7	7	7	7	7
	Min.	-54	-54	-121	-121	-54	-54	-54	-54	-54	-54	-54
46	Max.	-130	-84	-49	-31	-37	-31	-31	-14	15	33	115
	Min.	-177	-200	-223	-235	-218	-212	-194	-177	-148	-37	-753
47	Max.	-4	-4	-4	-4	-4	-4	-4	-4	-4	-57	-4
	Min.	-137	-290	-442	-495	-495	-502	-502	-489	-369	-369	-290
48	Max.	13	509	**2355**	**3173**	**3301**	**9019**	**10771**	**13685**	**16302**	**19351**	**N/A**
	Min.	-448	-670	-939	-1015	-1173	-1313	-1243	-1885	-1827	-1476	-688
49	Max.	8	152	812	963	1073	1137	1183	**2109**	**2613**	**2572**	**2619**
	Min.	-189	-305	-502	-646	-641	-710	-780	-843	-907	-837	-432
50	Max.	32	1029	**2960**	**9533**	**10784**	**17827**	**23444**	**31906**	**37917**	**47260**	**N/A**
	Min.	-518	-843	-1283	-1608	-1457	-1393	-1446	-1475	-1840	-820	**-28340**
51	Max.	215	1423	**2800**	**3781**	**9944**	**13446**	**32525**	**22072**	**23181**	**23665**	**25311**
	Min.	-381	-795	-1449	**-2201**	**-2487**	-1052	-608	-801	-637	-264	1376
52	Max.	106	1239	**2801**	**15004**	**16214**	**24071**	**32956**	**46827**	**58284**	**77328**	**N/A**
	Min.	-470	-834	-1439	-1656	-464	-769	-411	799	3424	-1116	**-42451**
53	Max.	-140	597	1874	**8984**	**7767**	**11067**	**17113**	**15045**	**13932**	**13655**	**N/A**
	Min.	-541	-743	-936	-1105	-580	-407	1082	790	1062	**-166821**	**N/A**

117

Table 4-46 Measured Strain (Micro Strain) in Column Longitudinal Bars for THD-3 (Continued)

Strain Gauge No.		Motion (x Sylmar)										
		0.1	0.25	0.5	0.75	1	1.25	1.5	1.75	2	2.25	2.5
54	Max.	249	1516	3108	7954	14095	21770	26703	39142	41536	40147	40141
	Min.	-413	-901	-1720	-4056	-2749	-2342	-3632	-7507	-11638	-22049	-68553
55	Max.	235	1420	2495	3523	12510	18848	22915	35062	38531	40343	41941
	Min.	-334	-747	-1438	-2606	-2054	-1740	-2420	-3605	-4842	-10710	-16130
56	Max.	325	1512	8310	17227	19259	29625	42093	59391	72557	183933	N/A
	Min.	-752	-1317	-2772	-4460	-3930	-6957	-7935	-7591	-82175	2903	36086
57	Max.	212	1321	5963	14916	16775	26154	37129	179165	N/A	N/A	N/A
	Min.	-841	-1418	-2711	-3685	-3232	-4676	-5130	-27421	-13249	179165	N/A
58	Max.	625	1541	11039	12672	15389	22727	28122	39952	42959	49506	9102
	Min.	-760	-1305	-2542	-7171	-6768	-9423	-12325	-16421	-18209	N/A	N/A
59	Max.	201	884	8090	6452	4131	3724	401	-1313	9215	39965	-1814
	Min.	-642	-954	-2109	-3729	-3199	-2992	-3959	-5255	-14293	-8442	N/A
60	Max.	50	440	1834	2473	2787	6924	6523	21327	31523	24400	1149
	Min.	-472	-751	-1315	-1739	-2047	-3412	-195787	N/A	N/A	N/A	N/A
61	Max.	115	701	1758	1868	2356	4254	7615	10866	12102	13211	14853
	Min.	-483	-959	-1748	-2363	-2543	-3646	-5365	-4691	-3867	-3606	-3066
77	Max.	20	20	343	499	660	821	846	987	1103	1144	1149
	Min.	-186	-297	-771	-1003	-1003	-1063	-1118	-1164	-1164	-1224	-1164

Table 4-47 Measured Strain (Micro Strain) in Column Spiral for THD-3

Strain Gauge No.		Motion (x Sylmar)										
		0.1	0.25	0.5	0.75	1	1.25	1.5	1.75	2	2.25	2.5
62	Max.	-2	15	33	50	44	68	56	74	62	74	**N/A**
	Min.	-37	-43	-37	-25	-37	-37	-31	-20	-8	-2	**-35874**
63	Max.	-220	-220	-220	-214	-196	-185	-185	-185	-173	-173	-167
	Min.	-249	-255	-255	-255	-231	-237	-243	-237	-231	-226	-220
64	Max.	-266	-266	-254	-237	-243	-237	-237	-231	-237	-231	-103
	Min.	-307	-318	-313	-313	-313	-313	-307	-301	-289	-284	-266
65	Max.	-68	-80	-80	-80	-63	-68	-74	-80	-68	-51	-45
	Min.	-109	-115	-115	-115	-98	-109	-115	-115	-115	-109	-98
66	Max.	44	50	50	50	44	44	62	85	85	102	137
	Min.	9	9	15	15	9	9	15	21	33	39	56
67	Max.	5	5	5	114	132	132	126	132	132	132	162
	Min.	-32	-32	-32	-32	-32	-32	-32	-32	-26	-14	11
68	Max.	2	2	7	7	13	13	19	37	48	60	130
	Min.	-33	-33	-28	-33	-22	-22	-22	-10	2	7	25

Table 4-48 Measured Strain (Micro Strain) in Column Spiral for THD-3 (Continued)

Strain Gauge No.		Motion (x Sylmar)										
		0.1	0.25	0.5	0.75	1	1.25	1.5	1.75	2	2.25	2.5
69	Max.	-188	-188	-188	-188	-147	-158	-158	-164	-164	-164	-158
	Min.	-223	-223	-223	-223	-188	-188	-199	-205	-199	-205	-199
70	Max.	43	78	159	223	200	264	497	677	770	840	509
	Min.	-15	-21	14	78	54	-27	-50	-33	-33	-44	31
71	Max.	-10	25	262	361	355	471	720	1154	**36262**	**52678**	**184034**
	Min.	-50	-68	-62	54	77	48	42	54	**N/A**	**N/A**	**N/A**
72	Max.	52	92	144	376	462	641	699	849	919	1000	**N/A**
	Min.	-35	-41	-23	-18	46	104	237	271	295	139	202
73	Max.	-143	-27	234	757	1175	1013	1454	1965	**2442**	**N/A**	**N/A**
	Min.	-196	-190	-161	-161	-85	-10	124	257	542	**-40431**	**-27697**
74	Max.	48	83	48	**11346**	**15677**	**24568**	**27853**	**42843**	**34703**	123	280
	Min.	-40	-103	-260	**N/A**	**N/A**	**N/A**	**N/A**	**N/A**	**N/A**	**N/A**	**N/A**
75	Max.	-35	17	86	254	266	312	358	492	584	781	1551
	Min.	-76	-116	-64	17	69	86	86	17	-47	-145	-111

120

Table 4-49 Measured Strain (Micro Strain) in Hinge Longitudinal Bars for THD-3

Strain Gauge No.		Motion (x Sylmar)										
		0.1	0.25	0.5	0.75	1	1.25	1.5	1.75	2	2.25	2.5
1	Max.	6	18	353	537	710	894	1251	1614	1972	**2106**	1787
	Min.	-172	-234	-351	-479	-541	-697	-870	-1060	-1417	-1440	-1306
2	Max.	-70	75	434	1029	1284	1798	**2527**	**13608**	**16436**	**18130**	**18327**
	Min.	-203	-364	-550	-792	-1001	-1336	-2042	**-2678**	**-2204**	451	**N/A**
3	Max.	-77	214	1436	1756	1915	**2463**	**8076**	**7756**	**3211**	**24559**	**44719**
	Min.	-340	-585	-1059	-1305	-1253	-1430	**-3080**	**-2275**	-1602	**N/A**	**N/A**
4	Max.	-302	-115	1281	1862	**2316**	**2682**	**3020**	**3939**	**5434**	**5218**	-57
	Min.	-517	-691	-912	-1081	-1116	-1424	-1709	**-2116**	**-2494**	**-2884**	**-2134**
5	Max.	-1155	451	**4437**	**8534**	**12805**	**23320**	**3832**	**2348**	**51602**	**2371**	2016
	Min.	-1691	**-2302**	**-3692**	**-4862**	**-3122**	-1790	1068	1597	**-198024**	-1499	**N/A**
6	Max.	-411	-78	1064	2031	**2189**	**11811**	**15524**	**22838**	**22428**	**15254**	**22200**
	Min.	-575	-681	-757	-1220	-1548	-1583	-1559	-1606	-1325	2037	**3290**
7	Max.	-50	674	**2955**	**12484**	**16353**	**24767**	**29948**	**34371**	**46182**	**N/A**	**N/A**
	Min.	-587	-989	-1695	**-7110**	**-5050**	**-4391**	**-5850**	**-2786**	**-134006**	**N/A**	**N/A**
8	Max.	-100	614	**3119**	**11537**	**18731**	**28823**	**35818**	**51541**	**N/A**	**N/A**	**N/A**
	Min.	-545	-867	-1236	-937	714	**2382**	**3459**	**4940**	**-7084**	**N/A**	**N/A**

121

Table 4-50 Measured Strain (Micro Strain) in Hinge Longitudinal Bars for THD-3 (Continued)

Strain Gauge No.		Motion (x Sylmar)										
		0.1	0.25	0.5	0.75	1	1.25	1.5	1.75	2	2.25	2.5
9	Max.	-576	-330	995	11302	12058	16030	18122	20361	N/A	N/A	N/A
	Min.	-693	-728	-711	-687	2377	2940	3450	4118	-31333	-21829	N/A
10	Max.	-619	188	10726	22457	23194	23165	17127	14982	N/A	N/A	N/A
	Min.	-1092	-1419	-1571	2882	6109	6869	3251	-143950	N/A	N/A	N/A
11	Max.	-561	123	3265	21457	23288	26798	10471	2732	8629	N/A	N/A
	Min.	-1023	-1374	-1690	-1877	2884	1931	-3427	-2099	-2948	-1427	N/A
12	Max.	-817	-364	1614	17054	18110	24815	11921	6492	12106	40249	N/A
	Min.	-1089	-1205	-1176	-1170	3052	3058	1927	N/A	N/A	N/A	N/A
13	Max.	-430	-45	1284	1972	3687	13687	14987	17122	N/A	N/A	N/A
	Min.	-663	-757	-827	-885	-1025	-984	2567	-13072	N/A	N/A	N/A
14	Max.	-89	177	902	2509	1894	1738	1442	1627	2045	6279	4887
	Min.	-252	-368	-751	-2694	137	154	-675	-1110	-1087	-594	2202
15	Max.	-184	-324	493	1407	1761	2390	3937	8096	29282	28342	N/A
	Min.	-436	-1060	-3289	-1511	-3225	-1404	-2263	-2774	-3048	-2532	1348
16	Max.	-253	-114	118	2188	2287	3069	22003	36489	N/A	N/A	N/A
	Min.	-433	-584	-1686	-4197	-6916	-8001	N/A	N/A	N/A	N/A	N/A

Table 4-51 Measured Strain (Micro Strain) in Hinge Longitudinal Bars for THD-3 (Continued)

Strain Gauge No.		Motion (x Sylmar)										
		0.1	0.25	0.5	0.75	1	1.25	1.5	1.75	2	2.25	2.5
17	Max.	-679	-323	442	991	1254	1499	1663	1815	1961	N/A	N/A
	Min.	-807	-883	-971	-1783	-1578	-1748	-1794	-1899	-2022	-32237	-21620
18	Max.	-174	-127	-34	142	434	680	797	943	1025	1014	N/A
	Min.	-221	-233	-268	-408	-449	-584	-713	-800	-835	-724	-555
19	Max.	-55	-5	-5	128	147	198	350	400	603	622	337
	Min.	-188	-194	-207	-226	-220	-258	-340	-416	-467	-467	-479
20	Max.	-255	-92	240	124	299	1080	3510	6104	N/A	N/A	N/A
	Min.	-378	-471	-657	-1077	-2208	-3076	-4714	-11417	-11720	N/A	N/A
21	Max.	-172	-154	-119	-3	55	213	346	457	521	N/A	N/A
	Min.	-213	-230	-247	-451	-626	-783	-923	-1034	-1092	-36229	-754
22	Max.	-105	-111	-111	-76	105	227	238	157	192	2870	N/A
	Min.	-163	-198	-221	-338	-623	-798	-798	-798	-1287	-6737	-2970
23	Max.	-221	-198	-180	-163	-122	-92	-69	31	207	230	N/A
	Min.	-257	-257	-251	-251	-221	-227	-221	-180	-87	-22	-16

Table 4-52 Measured Strain (Micro Strain) in Hinge Spiral for THD-3

Strain Gauge No.		Motion (x Sylmar)										
		0.1	**0.25**	**0.5**	**0.75**	**1**	**1.25**	**1.5**	**1.75**	**2**	**2.25**	**2.5**
24	**Max.**	62	73	97	120	103	109	120	120	132	161	161
	Min.	21	27	-9	-55	-61	-55	-20	21	44	21	50
26	**Max.**	-18	5	279	343	639	1344	**5347**	1192	**2327**	**11463**	**33501**
	Min.	-59	-70	-76	-47	34	63	**N/A**	**N/A**	**N/A**	**N/A**	**N/A**
27	**Max.**	-41	92	307	249	272	441	493	540	644	540	388
	Min.	-111	-111	-128	-99	-82	-76	-36	34	40	57	86
28	**Max.**	-97	-74	108	143	172	283	383	406	289	283	295
	Min.	-132	-144	-156	-109	-115	-121	-62	-203	-156	-9	37
29	**Max.**	167	179	357	570	694	937	1114	1499	1872	**2446**	1268
	Min.	-4	-28	-16	43	7	43	43	114	315	570	505
30	**Max.**	-30	11	324	865	764	966	**10640**	**3204**	**N/A**	**N/A**	**N/A**
	Min.	-166	-201	-257	-353	-156	-45	-1070	6	56	**N/A**	**N/A**
31	**Max.**	194	194	200	349	430	713	741	419	**N/A**	**N/A**	**N/A**
	Min.	165	102	107	113	251	119	-665	-1098	**-8251**	**-41651**	**N/A**
32	**Max.**	3	120	167	173	173	190	307	307	313	301	348
	Min.	-32	-61	-32	-26	-26	-32	-32	-26	-26	-26	38

124

Table 4-53 Measured Strain (Micro Strain) in Hinge Spiral for THD-3 (Continued)

Strain Gauge No.		Motion (x Sylmar)										
		0.1	0.25	0.5	0.75	1	1.25	1.5	1.75	2	2.25	2.5
33	Max.	11	23	34	46	58	81	110	140	146	175	187
	Min.	-36	-42	-53	-48	-24	-18	-1	11	40	70	81
34	Max.	-38	-32	-21	-3	-27	-15	26	61	96	131	**N/A**
	Min.	-67	-85	-102	-97	-120	-114	-108	-91	-91	-79	-21
35	Max.	60	60	60	66	66	72	78	189	195	201	**N/A**
	Min.	43	43	43	43	43	43	43	43	43	43	-321
36	Max.	44	44	50	44	44	50	61	67	73	90	96
	Min.	3	3	9	3	9	9	15	21	26	38	50
37	Max.	139	144	150	150	127	150	208	225	**N/A**	**N/A**	**N/A**
	Min.	104	110	115	115	87	75	92	104	**-43653**	**-5756**	**N/A**
38	Max.	18	23	23	23	29	29	35	41	41	46	**N/A**
	Min.	-23	-23	-17	-11	-11	-11	-11	-6	-6	0	**-21892**
39	Max.	14	20	26	37	26	37	37	55	72	84	**N/A**
	Min.	-21	-21	-21	-26	-32	-32	-32	-26	-15	3	20
40	Max.	-48	-48	-48	-42	-48	-48	-42	-31	-25	-19	**N/A**
	Min.	-82	-82	-77	-82	-88	-82	-77	-77	-59	-59	-48

Table 4-54 Measured Strain (Micro Strain) in Hinge Spiral for THD-3 (Continued)

Strain Gauge No.		Motion (x Sylmar)										
		0.1	0.25	0.5	0.75	1	1.25	1.5	1.75	2	2.25	2.5
41	Max.	244	250	255	267	284	290	342	354	331	389	412
	Min.	215	221	221	221	209	215	232	238	215	250	267
42	Max.	57	57	57	57	57	57	57	57	57	57	**N/A**
	Min.	-60	-60	-60	-60	-60	-66	-66	-60	-66	-101	**N/A**
43	Max.	-221	-221	-215	-215	-192	-198	-180	-180	-198	-174	-157
	Min.	-256	-256	-256	-256	-238	-238	-244	-244	-250	-250	-233

125

Table 4-55 Measured Strain (Micro Strain) in Column Longitudinal Bars for THD-4

Strain Gauge No.		Motion (x Sylmar)						
		0.1	0.25	0.375	0.5	0.75	1	1.25
44	Max.	38	49	43	32	-3	-61	-102
	Min.	3	3	3	-3	-119	-212	-328
45	Max.	33	38	50	73	114	172	271
	Min.	-2	-2	3	9	15	-2	-43
46	Max.	32	49	61	55	90	125	136
	Min.	2	2	-3	-21	-15	-32	-126
47	Max.	56	56	100	233	454	614	813
	Min.	-60	-93	-93	-93	-93	-93	-137
48	Max.	710	2074	**2213**	1946	**2248**	**2178**	**2138**
	Min.	-405	-869	-974	-1026	-1107	-1392	-1769
49	Max.	674	**2132**	**3912**	**6872**	**12782**	**16818**	**21830**
	Min.	-290	-811	-651	-357	1068	**3934**	**4505**
50	Max.	1054	**3096**	**3782**	**3288**	**3934**	**4137**	**4474**
	Min.	-534	-1208	-1697	-1848	**-2273**	**-3337**	**-4762**
51	Max.	752	1958	**2646**	**4534**	**9225**	**14645**	**22950**
	Min.	-256	-711	-897	-804	-221	367	**2675**
52	Max.	991	**2691**	**3318**	**2993**	**4009**	**5182**	**8380**
	Min.	-327	-768	-1262	-1447	**-2208**	**-3705**	**-6173**
53	Max.	752	**2278**	**2730**	**2394**	**2905**	**3288**	**9787**
	Min.	-241	-612	-867	-995	-1140	-1349	-1262

126

Table 4-56 Measured Strain (Micro Strain) in Column Longitudinal Bars for THD-4 (Continued)

Strain Gauge No.		Motion (x Sylmar)						
		0.1	0.25	0.375	0.5	0.75	1	1.25
54	Max.	983	**2292**	**10432**	**12678**	**15447**	**23155**	**33903**
	Min.	-351	-804	-646	1431	1869	**2897**	**6645**
55	Max.	802	1705	**6247**	**7223**	**8325**	**13603**	**22042**
	Min.	-187	-486	-426	789	789	1001	**3133**
56	Max.	-8413	-1134	830	-886	**3735**	**-16456**	**-16258**
	Min.	**-10212**	**-18223**	**-20473**	**-20099**	**-20550**	**-20902**	**-20797**
57	Max.	298	994	**4128**	**3050**	**3896**	**4476**	**4615**
	Min.	-177	-362	-553	293	125	-327	-988
58	Max.	1067	**5542**	**15713**	**19479**	**23804**	**34823**	**49528**
	Min.	-602	-842	827	**3425**	**4961**	**7174**	**13110**
59	Max.	625	**3259**	**12775**	**16008**	**20156**	**31790**	**47983**
	Min.	-267	-449	44	**3183**	**4133**	**5753**	**12394**
60	Max.	479	1594	**2283**	2097	**2721**	**3253**	**4169**
	Min.	-665	-1535	**-2586**	**-3182**	**-5979**	**-7812**	**-8046**
61	Max.	703	1689	**2942**	**6747**	**8366**	**11904**	**14665**
	Min.	-370	-875	-1316	-1188	-527	-51	610
76	Max.	113	598	805	776	1036	1088	1192
	Min.	-130	-649	-1042	-1180	-1209	-1295	-1319

Table 4-57 Measured Strain (Micro Strain) in Column Spiral for THD-4

Strain Gauge No.		Motion (x Sylmar)						
		0.1	0.25	0.375	0.5	0.75	1	1.25
62	Max.	34	51	74	92	144	237	335
	Min.	-7	-7	17	28	28	57	86
63	Max.	44	44	55	61	96	154	200
	Min.	3	3	3	15	26	44	73
64	Max.	19	19	19	13	25	19	19
	Min.	-16	-16	-16	-22	-10	-16	-22
65	Max.	-4	24	29	29	40	51	155
	Min.	-20	-20	-20	-20	-53	24	24
66	Max.	40	40	35	35	29	29	29
	Min.	0	0	0	0	-6	-18	-18
67	Max.	38	32	26	26	20	26	78
	Min.	-3	3	-3	-3	-9	-9	-3
68	Max.	35	29	-11	-29	64	53	53
	Min.	6	0	-40	-64	29	18	12

Table 4-58 Measured Strain (Micro Strain) in Column Spiral for THD-4 (Continued)

Strain Gauge No.		Motion (x Sylmar)						
		0.1	0.25	0.375	0.5	0.75	1	1.25
69	Max.	36	42	7	42	65	234	240
	Min.	-11	-11	-11	-11	-5	7	42
70	Max.	85	125	178	207	271	405	574
	Min.	50	44	67	90	96	143	178
71	Max.	14	293	328	323	328	168	128
	Min.	-41	-41	-41	-41	-156	-305	-460
72	Max.	119	248	289	295	342	529	658
	Min.	20	32	73	108	114	190	143
73	Max.	59	245	437	618	618	990	1496
	Min.	-5	-5	-5	1	-5	12	117
74	Max.	98	220	249	244	249	220	203
	Min.	-77	-135	-205	-228	-280	-391	-548
75	Max.	54	60	60	60	60	60	60
	Min.	-5	-5	-147	-188	-194	-194	-194

Table 4-59 Measured Strain (Micro Strain) in Hinge Longitudinal Bars for THD-4

Strain Gauge No.		Motion (x Sylmar)						
		0.1	0.25	0.375	0.5	0.75	1	1.25
1	Max.	83	298	508	560	630	665	723
	Min.	-39	-120	-126	-161	-219	-219	-236
2	Max.	25	187	222	262	720	419	454
	Min.	-33	-56	-56	-114	-254	-143	-97
3	Max.	546	**2774**	**12947**	**12231**	**12387**	**16013**	**25632**
	Min.	-43	-32	61	**9206**	**8871**	**9044**	**N/A**
4	Max.	501	1452	1815	1971	**2253**	**12030**	**3078**
	Min.	-202	-260	-698	-831	-981	-1027	**2409**
5	Max.	319	1706	**2240**	**2147**	**2624**	**2467**	**2322**
	Min.	-169	-564	-715	-906	-1028	-1075	-1011
6	Max.	54	890	1067	940	1128	1134	1987
	Min.	-129	-123	-73	-112	-140	-173	-539
7	Max.	182	1179	3135	-1370	**-2258**	-1935	**N/A**
	Min.	-424	-1722	**-4664**	**-9100**	**-11107**	**-60916**	**N/A**
8	Max.	999	**10874**	**22391**	**24789**	**24887**	**31833**	**N/A**
	Min.	-423	-544	**5367**	**10753**	**11701**	**11088**	**14376**
9	Max.	722	1898	**2605**	**2889**	**3874**	**4876**	**5919**
	Min.	-211	-500	-686	-825	-975	-1132	-935

Table 4-60 Measured Strain (Micro Strain) in Hinge Longitudinal Bars for THD-4 (Continued)

Strain Gauge No.		Motion (x Sylmar)						
		0.1	0.25	0.375	0.5	0.75	1	1.25
10	Max.	1229	6195	8643	16261	N/A	N/A	N/A
	Min.	-333	-939	-408	2325	2949	N/A	N/A
11	Max.	1158	12657	14506	12423	N/A	N/A	N/A
	Min.	-334	-697	4786	5682	-27497	-23278	N/A
12	Max.	464	4112	11054	12214	15764	35969	N/A
	Min.	-127	-115	1671	8190	8549	9953	12168
13	Max.	1197	6309	40300	89817	N/A	N/A	N/A
	Min.	-706	-809	N/A	-201759	-201759	76120	-201759
14	Max.	406	1211	1576	1906	12442	16849	N/A
	Min.	-578	-879	-984	-1198	-2154	-642	511
15	Max.	276	764	2611	3459	4551	N/A	N/A
	Min.	-682	-1060	-1426	-1763	-4010	-27289	-39306
16	Max.	551	1042	1711	1319	892	903	N/A
	Min.	-199	-285	-1151	-389	-66	-106	90

Table 4-61 Measured Strain (Micro Strain) in Hinge Longitudinal Bars for THD-4 (Continued)

Strain Gauge No.		Motion (x Sylmar)						
		0.1	0.25	0.375	0.5	0.75	1	1.25
17	Max.	98	754	1026	1015	1200	1160	N/A
	Min.	-6	-6	93	58	35	-47	-139
18	Max.	137	588	905	1040	1116	1216	N/A
	Min.	-104	-315	-638	-802	-931	-1013	N/A
19	Max.	66	229	305	346	358	428	N/A
	Min.	-28	-45	-151	-180	-268	-291	N/A
20	Max.	87	419	414	361	612	804	N/A
	Min.	-35	-187	-309	-326	-525	-909	-6561
21	Max.	19	89	183	207	219	248	N/A
	Min.	-16	-10	31	84	66	60	-21079
22	Max.	34	69	69	81	115	202	N/A
	Min.	-6	-18	-18	-12	-64	-151	-180
23	Max.	24	47	168	353	324	364	1242
	Min.	-23	-40	-23	18	-52	-138	-231

Table 4-62 Measured Strain (Micro Strain) in Hinge Spiral for THD-4

Strain Gauge No.		Motion (x Sylmar)						
		0.1	**0.25**	**0.375**	**0.5**	**0.75**	**1**	**1.25**
24	**Max.**	36	42	54	54	89	83	89
	Min.	-10	2	7	7	36	36	31
25	**Max.**	38	79	125	119	177	177	189
	Min.	3	9	26	32	73	73	79
26	**Max.**	29	29	40	58	58	69	75
	Min.	-41	-76	-129	-141	-193	-234	-228
27	**Max.**	99	257	415	321	309	303	391
	Min.	-12	-6	64	134	128	99	105
28	**Max.**	24	187	181	158	187	176	158
	Min.	-17	-17	-11	-17	-11	-17	-17
29	**Max.**	38	114	337	530	583	654	**52160**
	Min.	-149	-319	-683	-864	-1040	**-4744**	**N/A**
30	**Max.**	13	18	-28	70	134	464	643
	Min.	-40	-867	-693	-213	-254	-265	1
31	**Max.**	42	118	281	217	264	895	**N/A**
	Min.	6	-17	-64	-128	-99	-99	47
32	**Max.**	23	57	57	57	249	127	**N/A**
	Min.	-12	-12	5	17	5	-70	-70
33	**Max.**	13	144	144	151	144	144	**N/A**
	Min.	-21	-21	-21	-15	-21	-21	**-48181**

133

Table 4-63 Measured Strain (Micro Strain) in Hinge Spiral for THD-4 (Continued)

Strain Gauge No.		Motion (x Sylmar)						
		0.1	0.25	0.375	0.5	0.75	1	1.25
34	Max.	37	43	61	49	37	14	N/A
	Min.	-3	-3	8	2	-21	-56	-18197
35	Max.	14	19	37	43	19	25	N/A
	Min.	-16	-10	2	2	-27	-21	-42968
36	Max.	70	70	107	107	101	107	N/A
	Min.	-22	-22	-22	-22	-22	-22	-46523
37	Max.	26	32	43	66	95	72	N/A
	Min.	-9	-3	8	14	-9	-3	-1035
38	Max.	23	29	35	41	35	35	N/A
	Min.	-12	-6	0	6	6	0	12
39	Max.	N/A	N/A	N/A	N/A	N/A	N/A	N/A
	Min.	N/A	N/A	N/A	N/A	N/A	N/A	N/A
40	Max.	16	28	34	45	16	16	N/A
	Min.	-19	-7	-1	10	-19	-13	-7
41	Max.	32	38	44	50	38	N/A	N/A
	Min.	-2	3	3	3	3	-34718	-36242
42	Max.	-6	46	64	157	630	373	N/A
	Min.	-41	-65	-82	-105	41	-35	-40708
43	Max.	25	31	43	48	37	43	N/A
	Min.	-15	-4	2	8	2	8	-39726

134

Table 4-64 Measured Strain (Micro Strain) in Column Longitudinal Bars for THD-5

Strain Gauge No.		Motion (x Sylmar)													
		0.10	0.25	0.50	0.75	1.00	1.25	1.50	1.75	2.00	2.25	2.50	2.75	3.00	3.00
44	Max.	125	125	125	125	131	137	258	265	265	258	258	131	137	125
	Min.	-2	-8	-8	-8	58	-39	-51	-57	-87	-87	-87	-385	-591	-718
45	Max.	3	14	32	26	43	101	72	136	136	90	67	-96	-44	-67
	Min.	-38	-44	-55	-84	-90	-49	-67	-55	-55	-96	-310	-478	-258	-194
46	Max.	33	33	43	157	198	353	353	358	363	379	482	363	353	203
	Min.	-76	-86	-117	-122	-86	-76	-143	-117	-122	-127	-86	-24	-137	-406
47	Max.	-107	-78	-2	39	254	400	423	417	376	225	-43	-206	-136	-95
	Min.	-165	-200	-200	-165	-183	-148	-90	-305	-323	-532	-655	-602	-567	-416
48	Max.	315	1326	**2536**	**2675**	**2850**	**3320**	**10250**	**10889**	**12912**	**14674**	**17511**	**19476**	**20708**	**20830**
	Min.	-237	-592	-970	-1104	-1365	-1464	-1563	-406	100	286	937	2071	**3367**	**3628**
49	Max.	-97	494	1296	1425	1970	**2175**	**2192**	**2175**	**2315**	**2573**	**2725**	**2807**	**3165**	**3317**
	Min.	-595	-999	-1421	-1579	-1802	-1995	**-2141**	**-2282**	**-2586**	**-3008**	**-3617**	**-4050**	**-4320**	**-4536**
50	Max.	318	1144	2011	2086	**3470**	**8251**	**11333**	**11467**	**14224**	**16789**	**17743**	**15951**	**12532**	**10926**
	Min.	-333	-735	-1206	-1415	-1950	**-2247**	-1927	-1200	-857	-426	539	**2999**	**4599**	**3959**
51	Max.	-26	595	1419	1601	**2186**	**3046**	**3736**	**3958**	**4227**	**4666**	**4754**	**4572**	**5994**	**7105**
	Min.	-552	-973	-1465	-1599	-1722	**-2319**	**-3003**	**-3219**	**-3886**	**-4495**	**-5162**	**-5466**	**-5770**	**-6431**
52	Max.	636	1852	**4312**	**10138**	**14159**	**19161**	**25256**	**25788**	**31965**	**38691**	**48380**	**58267**	**68453**	**75383**
	Min.	-433	-982	-1579	-1894	-1859	-1339	-480	1413	**2670**	**4347**	**8105**	**14766**	**23316**	**30615**
53	Max.	386	1143	2017	**4657**	**7874**	**10945**	**14511**	**14802**	**18293**	**22366**	**28793**	**34644**	**40681**	**44987**
	Min.	-302	-640	-1048	-1164	-1077	-558	-185	596	1085	1895	**4010**	**7885**	**12337**	**16113**

135

Table 4-65 Measured Strain (Micro Strain) in Column Longitudinal Bars for THD-5 (Continued)

Strain Gauge No.		Motion (x Sylmar)													
		0.10	0.25	0.50	0.75	1.00	1.25	1.50	1.75	2.00	2.25	2.50	2.75	3.00	3.00
54	Max.	18	245	571	664	822	717	717	717	758	804	839	903	N/A	N/A
	Min.	-197	-360	-581	-698	-477	-552	-686	-721	-762	-832	-843	-710	-30011	-155542
55	Max.	55	900	2083	2491	6070	9590	10371	9852	10173	10936	9981	7498	N/A	N/A
	Min.	-616	-1070	-1688	-1886	-3081	-4783	-6689	-6654	-7586	-9160	-13170	-17221	-57805	-42004
56	Max.	247	1045	8639	9983	12284	14144	18217	18247	27267	N/A	N/A	N/A	N/A	N/A
	Min.	-340	-487	-651	1414	N/A	N/A	N/A	N/A	N/A	N/A	N/A	N/A	N/A	N/A
57	Max.	401	1447	6497	8323	11854	16691	22498	36945	42429	N/A	N/A	N/A	N/A	N/A
	Min.	-541	-952	-1304	-171	-749	-928	N/A	N/A	N/A	N/A	N/A	N/A	N/A	N/A
58	Max.	-1115	-640	1147	1535	3206	3809	3554	2985	3026	3426	3554	10270	3357	38094
	Min.	-1539	-1666	-1394	-1463	-2565	-3290	-4218	-3963	-5448	-4810	-5042	-5970	-10866	-194152
59	Max.	112	1000	2051	2337	5567	8826	8546	7827	8365	9726	18130	12529	13393	13621
	Min.	-565	-1126	-2066	-2463	-7235	-9116	-11072	-11580	-13145	-15400	-19984	-25667	-31957	-37739
60	Max.	261	459	383	138	91	63001	57045	50961	58311	68029	50326	56100	80704	105401
	Min.	-399	-1186	-2423	-2143	-1874	N/A	N/A	N/A	N/A	N/A	N/A	N/A	N/A	N/A
61	Max.	19	536	1192	1389	1894	1993	4001	1494	1006	873	530	257	228	159
	Min.	-486	-909	-1629	-1937	-2146	-2413	-2448	-2564	-2976	-3719	-3382	-3545	-3945	-3469
76	Max.	130	748	1645	1709	1901	2280	2530	2664	4027	2641	1569	1587	1505	1388
	Min.	-231	-446	-685	-738	-947	-843	-895	-971	-1157	-1017	-10	-773	-1227	-1058
77	Max.	-7	150	360	458	813	1046	1261	1296	1319	1400	1418	1551	1772	2354
	Min.	-222	-414	-710	-844	-978	-1286	-1245	-1187	-1082	-931	-954	-972	-966	-1024

Table 4-66 Measured Strain (Micro Strain) in Column Spiral for THD-5

Strain Gauge No.		Motion (x Sylmar)													
		0.10	0.25	0.50	0.75	1.00	1.25	1.50	1.75	2.00	2.25	2.50	2.75	3.00	3.00
62	Max.	31	37	48	66	204	568	707	805	932	1065	1117	1169	1343	1637
	Min.	-4	-4	2	8	37	152	291	407	499	696	828	863	805	811
63	Max.	39	39	44	39	73	514	711	838	1470	**2582**	**2414**	**2286**	**2182**	**2252**
	Min.	4	4	10	4	10	68	259	346	479	1047	2055	2043	1823	1806
64	Max.	36	36	77	88	158	345	386	467	572	648	677	742	841	899
	Min.	1	1	1	7	30	123	193	217	257	327	397	421	368	374
65	Max.	76	76	99	99	185	642	856	931	1024	1162	1203	1151	1220	1290
	Min.	35	35	47	53	58	197	365	434	480	573	648	654	544	492
66	Max.	22	22	45	97	190	417	522	615	662	708	743	819	923	981
	Min.	-13	-19	-13	-2	22	97	173	249	324	400	435	446	452	464
67	Max.	30	36	47	47	152	461	496	519	548	630	682	682	699	758
	Min.	-5	-5	1	7	24	100	263	321	309	315	333	344	356	362
68	Max.	14	66	305	410	486	754	888	999	1104	1186	1256	1337	1489	1559
	Min.	-27	-56	-80	-51	-27	54	142	194	235	288	317	346	375	434

Table 4-67 Measured Strain (Micro Strain) in Column Spiral for THD-5 (Continued)

Strain Gauge No.		Motion (x Sylmar)													
		0.10	0.25	0.50	0.75	1.00	1.25	1.50	1.75	2.00	2.25	2.50	2.75	3.00	3.00
69	Max.	49	49	72	90	252	837	1156	1266	1260	1324	1451	1434	1370	1306
	Min.	14	14	20	14	20	101	310	432	489	455	420	455	443	501
70	Max.	23	40	115	173	324	555	752	763	1012	1249	1504	1811	2082	**2453**
	Min.	-18	-41	-70	-81	-29	87	156	179	173	220	301	416	532	682
71	Max.	18	53	175	228	443	938	1578	1549	1916	**2673**	**4018**	**5258**	**6842**	**7913**
	Min.	-29	-29	6	47	82	134	204	408	455	676	1159	**2155**	**3244**	**4647**
72	Max.	30	59	105	128	326	593	738	744	918	1058	1185	1435	1720	2091
	Min.	-11	-23	-17	-23	6	70	128	151	157	181	233	297	221	-476
73	Max.	17	23	256	384	605	907	1210	1402	1524	1856	**2263**	**2688**	**3741**	**3997**
	Min.	-35	-41	-12	64	93	209	267	442	430	477	605	680	948	1571
74	Max.	80	254	329	323	329	358	352	277	265	237	213	208	242	532
	Min.	-59	-100	-140	-169	-198	-181	-204	-163	-111	-181	-239	-279	-129	86
75	Max.	-25	33	61	-25	61	314	240	337	251	165	837	590	50	-226
	Min.	-65	-151	-134	-174	-226	-186	-94	-278	-473	-450	-519	-898	-1318	-1473

Table 4-68 Measured Strain (Micro Strain) in Hinge Longitudinal Bars for THD-5

Strain Gauge No.		Motion (x Sylmar)													
		0.10	**0.25**	**0.50**	**0.75**	**1.00**	**1.25**	**1.50**	**1.75**	**2.00**	**2.25**	**2.50**	**2.75**	**3.00**	**3.00**
1	**Max.**	-8	44	50	56	236	363	421	427	421	601	543	601	555	369
	Min.	-153	-199	-442	-512	-570	-692	-709	-744	-674	-709	-674	-756	-703	-385
2	**Max.**	-162	-97	26	50	155	249	414	461	502	560	637	695	654	302
	Min.	-215	-238	-261	-279	-285	-308	-297	-314	-291	-285	-303	-279	-238	-15
3	**Max.**	-658	-90	293	334	462	578	583	578	467	409	375	311	3	-844
	Min.	-1023	-1319	-1841	**-2143**	**-2503**	**-2688**	**-2746**	**-2694**	**-2305**	**-2294**	**-2416**	**-2340**	**-2149**	-1470
4	**Max.**	-370	-67	334	409	619	584	595	770	1165	1427	1078	1258	**2136**	**6257**
	Min.	-695	-1021	-1276	-1398	-1555	-1712	-1660	-1590	-1334	-1090	-1509	-1358	-1055	194
5	**Max.**	-483	-231	425	706	1485	1907	**2235**	**2200**	**2212**	**2323**	**2487**	**2540**	**2218**	859
	Min.	-694	-870	-1045	-1081	-1174	-1315	-1245	-1245	-1163	-1092	-1127	-688	-430	431
6	**Max.**	-764	-688	-257	92	1197	**2152**	**2466**	**2204**	1000	-426	-4388	1151	**7988**	**12555**
	Min.	-816	-874	-979	-1060	-1188	-1340	-1310	-1444	-1863	**-10358**	**-11278**	**-9649**	**-5273**	-7
7	**Max.**	-1977	-662	**3661**	**4847**	**8197**	**7402**	**4148**	**N/A**	**N/A**	**N/A**	**N/A**	**N/A**	**N/A**	**N/A**
	Min.	**-3087**	**-5266**	**-7527**	**-7465**	**-8747**	**-13666**	**-23834**	**-76968**	**N/A**	**N/A**	**N/A**	**N/A**	**N/A**	**N/A**
8	**Max.**	-910	-220	**3549**	**5506**	**7583**	**7716**	**7636**	**7139**	**8857**	**11027**	**9355**	**9574**	**N/A**	**N/A**
	Min.	-1567	**-2190**	-2051	138	988	1618	1678	-1348	1193	**5075**	1837	**2481**	**4252**	**N/A**

139

Table 4-69 Measured Strain (Micro Strain) in Hinge Longitudinal Bars for THD-5 (Continued)

Strain Gauge No.		Motion (x Sylmar)													
		0.10	0.25	0.50	0.75	1.00	1.25	1.50	1.75	2.00	2.25	2.50	2.75	3.00	3.00
9	Max.	-702	-535	275	1189	**16235**	**19450**	**25915**	**24782**	**60859**	**49207**	-1304	**N/A**	**N/A**	**N/A**
	Min.	-835	-910	-986	-997	**-111023**	**-89529**	**-166564**	**N/A**	**N/A**	**N/A**	**N/A**	**N/A**	**N/A**	**N/A**
10	Max.	-479	-5	1131	**2683**	**11735**	**23650**	**44628**	**58610**	**47298**	**N/A**	**N/A**	**N/A**	**N/A**	**N/A**
	Min.	-994	-1685	**-2247**	**-2311**	**-2534**	**-2944**	**-2224**	**-194033**	**7525**	**N/A**	**N/A**	**N/A**	**N/A**	**N/A**
11	Max.	-1757	-1509	-715	-298	970	**6840**	**9399**	**N/A**	**N/A**	**N/A**	**N/A**	**N/A**	**N/A**	**N/A**
	Min.	-1914	-1995	-2099	**-2192**	**-2724**	**-6106**	**-7582**	**-8804**	**N/A**	**N/A**	**N/A**	**N/A**	**N/A**	**N/A**
12	Max.	**N/A**	**N/A**	**N/A**	**N/A**	**N/A**	**N/A**	**N/A**	**N/A**	**N/A**	**N/A**	**N/A**	**N/A**	**N/A**	**N/A**
	Min.	**N/A**	**N/A**	**N/A**	**N/A**	**N/A**	**N/A**	**N/A**	**N/A**	**N/A**	**N/A**	**N/A**	**N/A**	**N/A**	**N/A**
14	Max.	-237	-150	24	-80	-376	-428	-909	-1060	-1037	**N/A**	**N/A**	**N/A**	**N/A**	**N/A**
	Min.	-793	-1617	-2099	**-2853**	**-3270**	**-4546**	**-4593**	**-5555**	**-5793**	**-6304**	**-19290**	**N/A**	**N/A**	**N/A**
15	Max.	-654	-75	431	-648	-1531	-1868	-1787	-1787	-850	**N/A**	**N/A**	**N/A**	**N/A**	**N/A**
	Min.	-1153	-1517	-1726	**-5757**	**-2609**	**-3519**	**-3944**	**-4105**	**-3600**	**-3303**	**N/A**	**N/A**	**N/A**	**N/A**
16	Max.	-501	-216	466	1031	1445	1235	**4802**	**3374**	**N/A**	**N/A**	**N/A**	**N/A**	**N/A**	**N/A**
	Min.	-711	-810	-874	-909	-1055	-991	**-4185**	**-6219**	-1550	**N/A**	**N/A**	**N/A**	**N/A**	**N/A**

140

Table 4-70 Measured Strain (Micro Strain) in Hinge Longitudinal Bars for THD-5 (Continued)

Strain Gauge No.		Motion (x Sylmar)													
		0.10	0.25	0.50	0.75	1.00	1.25	1.50	1.75	2.00	2.25	2.50	2.75	3.00	3.00
17	Max.	-1010	-912	-360	-17	337	75	-29	-75	-81	N/A	N/A	N/A	N/A	N/A
	Min.	-1057	-1098	-1179	-1185	-1249	-889	-767	-1028	-1405	-1283	N/A	N/A	N/A	N/A
18	Max.	37	135	176	158	100	-131	-525	-577	-531	-548	N/A	N/A	N/A	N/A
	Min.	-386	-779	-1017	-1063	-1179	-1659	-1578	-1549	-1457	-1399	-1254	N/A	N/A	N/A
19	Max.	-140	-140	-2	-140	-146	38	181	348	767	1140	1129	N/A	N/A	N/A
	Min.	-272	-376	-525	-525	-738	-755	-990	-1220	-749	-686	-893	-939	N/A	N/A
20	Max.	-502	-455	32	238	913	1647	1988	2000	**2111**	N/A	N/A	N/A	N/A	N/A
	Min.	-549	-614	-702	-760	-907	-1101	-1166	-1201	-1342	-1166	N/A	N/A	N/A	N/A
21	Max.	-510	-516	-434	-347	56	913	1158	1047	N/A	N/A	N/A	N/A	N/A	N/A
	Min.	-545	-586	-673	-755	-1064	-1338	-1443	-1495	-1495	N/A	N/A	N/A	N/A	N/A
22	Max.	311	416	509	550	667	830	737	754	743	743	783	N/A	N/A	N/A
	Min.	-80	-191	-360	-471	-641	-1300	-1557	-1814	-2006	**-2158**	**-2537**	**-2642**	N/A	N/A
23	Max.	-424	-424	-261	-174	187	2842	1416	1381	N/A	N/A	N/A	N/A	N/A	N/A
	Min.	-471	-517	-569	-593	-703	-721	670	636	566	N/A	N/A	N/A	N/A	N/A

Table 4-71 Measured Strain (Micro Strain) in Hinge Spiral for THD-5

Strain Gauge No.		Motion (x Sylmar)													
		0.10	0.25	0.50	0.75	1.00	1.25	1.50	1.75	2.00	2.25	2.50	2.75	3.00	3.00
24	Max.	56	56	56	56	56	56	68	68	178	184	189	189	184	184
	Min.	-8	-8	-8	-8	-8	39	39	39	39	39	44	44	44	39
25	Max.	10	10	10	10	54	176	187	214	214	214	225	231	225	225
	Min.	-7	-7	-7	-7	-7	37	37	43	48	48	48	37	54	70
26	Max.	98	116	122	248	308	494	686	680	452	482	518	644	524	494
	Min.	50	50	50	62	68	170	170	128	98	50	-22	-88	-58	50
27	Max.	18	47	244	267	302	319	342	336	319	331	331	325	348	365
	Min.	-34	-28	-17	-11	1	58	116	134	163	151	180	180	192	209
28	Max.	60	83	124	130	153	211	240	269	298	292	269	246	252	275
	Min.	19	25	31	37	13	-33	-16	13	165	130	112	106	83	147
29	Max.	10	51	63	228	375	834	**6393**	**N/A**	**N/A**	**N/A**	**N/A**	**N/A**	**N/A**	**N/A**
	Min.	-125	-125	-178	-196	-266	-7	181	**-20696**	**N/A**	**N/A**	**N/A**	**N/A**	**N/A**	**N/A**
30	Max.	1	89	77	-144	19	-202	-237	**5623**	**15798**	**17354**	**19816**	**21628**	**23156**	**N/A**
	Min.	-103	-196	-527	-695	-742	-1148	-1480	-1689	**2992**	**12795**	**14032**	**17482**	**18539**	**17360**
31	Max.	178	311	433	467	827	792	722	**N/A**	**N/A**	**N/A**	**N/A**	**N/A**	**N/A**	**N/A**
	Min.	33	-42	-100	-152	-54	16	-66	**-40361**	-1734	**N/A**	**N/A**	**N/A**	**N/A**	**N/A**
32	Max.	33	33	51	57	196	841	1108	1131	1160	980	1207	**N/A**	**N/A**	**N/A**
	Min.	-2	-2	10	10	22	103	225	318	254	271	295	-1599	**N/A**	**N/A**
33	Max.	81	81	112	81	112	124	-72	-114	**N/A**	**N/A**	**N/A**	**N/A**	**N/A**	**N/A**
	Min.	-10	-59	-72	-84	-194	-267	-475	-389	-328	**N/A**	**N/A**	**N/A**	**N/A**	**N/A**
34	Max.	17	35	29	23	87	23	-64	613	2316	**N/A**	**N/A**	**N/A**	**N/A**	**N/A**
	Min.	-41	-53	-59	-82	-59	-298	-519	-578	-502	280	**N/A**	**N/A**	**N/A**	**N/A**

Table 4-72 Measured Strain (Micro Strain) in Hinge Spiral for THD-5 (Continued)

Strain Gauge No.		Motion (x Sylmar)													
		0.10	0.25	0.50	0.75	1.00	1.25	1.50	1.75	2.00	2.25	2.50	2.75	3.00	3.00
35	Max.	113	113	113	113	113	306	724	911	N/A	N/A	N/A	N/A	N/A	N/A
	Min.	-24	-24	-30	-74	-143	-136	63	294	-6212	-45565	N/A	N/A	N/A	N/A
36	Max.	106	106	112	112	118	258	112	-58	-76	N/A	N/A	N/A	N/A	N/A
	Min.	-22	-22	-22	-22	-10	-143	-338	-399	-283	-5328	-39085	-95499	N/A	N/A
37	Max.	57	63	74	74	150	666	932	793	526	N/A	N/A	N/A	N/A	N/A
	Min.	22	22	28	22	39	39	22	161	132	-210	N/A	N/A	N/A	N/A
38	Max.	161	161	161	161	211	211	211	211	224	355	405	548	N/A	N/A
	Min.	30	30	37	30	68	74	86	143	143	143	143	68	-37180	N/A
39	Max.	49	55	55	55	61	190	190	196	196	237	N/A	N/A	N/A	N/A
	Min.	-4	-10	-10	-10	-10	37	37	37	37	43	67	N/A	N/A	N/A
40	Max.	51	51	74	74	127	494	802	N/A	N/A	N/A	N/A	N/A	N/A	N/A
	Min.	16	16	28	5	-65	-269	-368	-6089	-240	N/A	N/A	N/A	N/A	N/A
41	Max.	38	44	55	49	67	131	125	142	136	177	206	N/A	N/A	N/A
	Min.	3	9	15	15	15	49	61	73	73	67	73	38	N/A	N/A
42	Max.	13	13	13	7	25	89	94	106	94	164	N/A	N/A	N/A	N/A
	Min.	-22	-22	-22	-28	-22	25	36	42	48	48	-34319	-41412	N/A	N/A
43	Max.	17	17	28	28	40	75	93	104	N/A	N/A	N/A	N/A	N/A	N/A
	Min.	-19	-13	-7	-13	-7	28	40	46	57	N/A	N/A	N/A	N/A	N/A

143

Table 5-1 Relative Increase in Steel Yield & Ultimate Strength due to Strain Rate Effect

Specimen	Location	Rebar Diameter		Steel Yield Stress		Steel Ultimate Stress		Increase Due to Strain Rate	
		(inch)	(mm)	(Ksi)	(MPa)	(Ksi)	(MPa)	R_{yield}	$R_{ultimate}$
THD-1	Column	0.875	22.23	61.75	425.8	100	689.5	1.08	1.06
	Hinge	0.375	9.53	74	510.2	109	751.6	1.07	1.05
THD-2	Column	0.875	22.23	61.75	425.8	100	689.5	1.09	1.06
	Hinge	0.375	9.53	81	558.5	114.5	789.5	1.07	1.05
THD-3	Column	0.5	12.70	62.6	431.6	99	682.6	1.07	1.05
	Hinge	0.375	9.53	82	565.4	112	772.2	1.09	1.06
THD-4	Column	0.625	15.88	65.9	454.4	101	696.4	1.10	1.06
	Hinge	0.375	9.53	82	565.4	112	772.2	1.07	1.05
THD-5	Column	0.875	22.23	62.7	432.3	104.2	718.5	1.13	1.08
	Hinge	0.375	9.53	82	565.4	112	772.2	1.07	1.05

Table 5-2 Relative Increase in Concrete Compression Strength due to Strain Rate Effect

Specimen	Location	Concrete Compressive Stength		Increase Due to SRI
		(Ksi)	(MPa)	$R_{con.}$
THD-1	Column	5.16	35.6	1.088
	Hinge	7.72	53.2	1.031
THD-2	Column	5.1	35.2	1.074
	Hinge	5.91	40.7	1.066
THD-3	Column	7.49	51.6	1.115
	Hinge	5.66	39.0	1.103
THD-4	Column	7.32	50.5	1.067
	Hinge	5.64	38.9	1.108
THD-5	Column	7.42	51.2	1.072
	Hinge	5.31	36.6	1.096

Table 5-3 Comparison of the Hinge Confinement Concrete Properties Using Different Methods

Specimen	Location	f'_c		Proposed Method				Griezic's			Hawkins'	
				f'_{cc}		e'_{cc}	e'_{cu}	f'_{cc}		e'_{cc}	f'_{cc}	
		(Ksi)	(MPa)	(Ksi)	(MPa)			(Ksi)	(MPa)		(Ksi)	(MPa)
THD-1	Clear Cover	7.72	53.23	11.3	77.91	0.0066	0.0252	11.99	82.69	0.0052	10.36	71.40
	Core			12.45	85.84	0.008	0.0231					
THD-2	Clear Cover	5.91	40.75	9.346	64.44	0.0078	0.0297	9.18	63.30	0.0052	8.22	56.65
	Core			10.48	72.26	0.0097	0.0288					
THD-3	Clear Cover	5.66	39.03	9.07	62.54	0.008	0.0304	8.79	60.62	0.0052	7.92	54.59
	Core			10.15	69.98	0.0099	0.0355					
THD-4	Clear Cover	5.64	38.89	9.04	62.33	0.008	0.0305	8.76	60.41	0.0052	7.89	54.42
	Core			10.13	69.85	0.01	0.0355					
THD-5	Clear Cover	5.31	36.61	8.68	59.85	0.0083	0.0316	10.11	69.74	0.0071	8.95	61.73
	Core			9.74	67.16	0.01	0.0368					

Table 5-4 Comparison of the Calculated Two-Way Hinge Shear Strength Using Shear Friction Method

Specimens	THD-1			THD-2			THD-4			THD-5			Range of	Average	Standard
	V			V			V			V					
items	(Kips)	(KN)	V / V_{test}	(Kips)	(KN)	V / V_{test}	(Kips)	(KN)	V / V_{test}	(Kips)	(KN)	V / V_{test}	Ratio	Ratio	Deviation
Measured Shear force (V_{test})	84.3	375.2	1.0	53.0	235.9	1.0	38.1	169.5	1.0	67.7	301.3	1.0	100%	1.00	0.00
Shear Friction with ACI Limit	62.83	279.6	0.75	62.83	279.6	1.19	31.85	141.8	0.84	40.19	178.9	0.59	59% to 119%	0.84	0.25
Shear Friction without ACI Limit	99.83	444.2	1.18	79.61	354.3	1.50	42.02	187.0	1.10	100.93	449.1	1.49	110% to 149%	1.32	0.21

Table 5-5 Comparison of the Calculated Two-Way Hinge Shear Strength Using Different Methods

Specimens	THD-1			THD-2			THD-4			THD-5			Range of	Average	Standard
	V			V			V			V					
items	(Kips)	(KN)	V / V_{test}	(Kips)	(KN)	V / V_{test}	(Kips)	(KN)	V / V_{test}	(Kips)	(KN)	V / V_{test}	Ratio	Ratio	Deviation
Measured Shear Force (V_{test})	84.3	375.2	1.0	53.0	235.9	1.0	38.1	169.5	1.0	67.7	301.3	1.0	100%	1.00	0.00
ACI 318 Shear Friction	62.83	279.6	0.75	62.83	279.6	1.19	31.9	141.8	0.84	40.19	178.9	0.59	59% to 119%	0.84	0.25
ACI 318 Diagonal Shear	45.74	203.5	0.54	39.32	175.0	0.74	33.7	150.1	0.89	31.78	141.4	0.47	47% to 89%	0.66	0.19
AASHTO LRFD (2nd Ed)	62.83	279.6	0.75	62.83	279.6	1.19	47.9	213.4	1.26	40.19	178.9	0.59	59% to 165%	0.95	0.33
AASHTO Standard (17th Ed) (Load factor design)	62.83	279.6	0.75	62.83	279.6	1.19	42.0	187.0	1.10	40.19	178.9	0.59	59% to 165%	0.91	0.28
Proposed Method	72.12	320.9	0.86	57.85	257.4	1.09	33.0	146.6	0.86	63.83	284.1	0.94	86% to 109%	0.94	0.11

147

Table 5-6 μ Factor Calculation Based on Experimental Data

	Units	THD-1	THD-2	THD-4	THD-5
Lateral Force (V)	(Kips)	84.3	53.0	38.1	67.7
	(KN)	375.2	235.9	169.5	301.3
Axial load	(Kips)	108.5	68.5	8.5	108.5
	(KN)	482.8	304.8	37.8	482.8
Compression in Steel (Cs)	(Kips)	18.3	20.1	9.7	29.7
	(KN)	81.5	89.5	43.1	132.4
Tension in Steel (T)	(Kips)	51.8	60.1	64.7	33.4
	(KN)	230.3	267.3	288.0	148.4
Compression in Concrete (Cc)	(Kips)	141.9	108.4	63.5	112.1
	(KN)	631.6	482.6	282.7	498.9
Compression in Steel & Concrete (Cc+Cs)	(Kips)	160.3	128.6	73.2	141.9
	(KN)	713.1	572.1	325.9	631.2
μ for Cc+Cs		**0.53**	**0.41**	**0.52**	**0.48**
Average μ value (THD1,THD2,THD4,THD5):					**0.48**
Standard deviation: (THD1, THD2, THD4, THD5):					**0.053**

Table 5-7 Properties of Two-Way Hinge at Two Column Bent Specimen

Study	Specimen	Column Aspect Ratio	Hinge Type	Hinge Area		Hinge Steel Ratio	Total Axial Load		$P/A_{hinge}f'c$
				(in^2)	(mm^2)		(kips)	(KN)	
Pulido et al.	B2RC	3.4	Mini Column	126	81270	1.05%	63	280	3.7%
Nada et al.	LFCD1	5.3	Cluster	50.4	32523	1.59%	102	454	16.9%
	LFCD2	5.3	Cluster	50.4	32523	1.59%	102	454	16.9%
	SFCD2	3.25	Cluster	50.4	32523	1.59%	102	454	15.4%
Moustafa et al.	B2CS	6.64	Cluster	78.8	50818	1.02%	75	334	11.6%
	B2CM	4.5	Cluster	78.8	50818	1.02%	75	334	11.6%
	B2CT	2.5	Cluster	78.8	50818	1.02%	75	334	11.6%
Chandane et al.	SFCD3	3.25	Cluster	50.4	32523	1.59%	90	401	13.4%
Sureshkumar et al.	B2DA	3.75	Cluster	44.3	28585	0.99%	65.5	291	11.4%
	B2DC	3.75	Cluster	44.3	28585	0.99%	65.5	291	11.4%

Table 5-8 Hinge Shear Strength Comparison for Two Column Bent Specimen

Study	Specimen	Hinge Failure	Measured Peak Load (V_{test})		Proposed Design Method				V_{cal} / V_{test}
					C_c+C_s		$V_{cal} = \phi (C_c+C_s)$		
		(Yes / No)	(Kips)	(KN)	(Kips)	(KN)	(Kips)	(KN)	
Pulido et al.	**B2RC**	**Yes**	72.9	324	164.5	732	74.0	329	**102%**
Nada et al.	**LFCD1**	No	64.0	285	190.5	848	85.7	381	134%
	LFCD2	No	60.4	269	190.4	847	85.7	381	142%
	SFCD2	**Yes**	97.4	433	190.7	849	85.8	382	**88%**
Moustafa et al.	**B2CS**	**Yes**	92.0	409	164.9	734	74.2	330	**81%**
	B2CM	No	50.2	223	162.4	723	73.1	325	146%
	B2CT	No	33.0	147	161	716	72.5	322	220%
Chandane et al.	**SFCD3**	**Yes**	96.8	431	184	819	82.8	368	**86%**
Sureshkumar et al.	**B2DA**	No	49.3	219	120.1	534	54.0	241	110%
	B2DC	No	49.7	221	120	534	54.0	240	109%

Table 5-9 Two-Way Hinge Shear Model Data Calibration

Specimen	Slippage (d)		Lateral Force (V)		DV/Dd		F = Kd, (d=**0.25"**)		F / V
	in	mm	Kips	KN	Kip/in	KN/mm	Kips	KN	
THD-1	0.109	2.8	81.4	362.2					
	0.09	2.3	82.8	368.5	-73.68	-12.91	-18.42	-81.97	22.2%
THD-2	0.346	8.8	49.2	218.9					
	0.169	4.3	53.7	239.0	-25.42	-4.45	-6.36	-28.28	11.8%
THD-4	0.72	18.3	24.8	110.4					
	0.54	13.7	37.9	168.7	-72.78	-12.75	-18.19	-80.97	48.0%
THD-5	0.432	11.0	65.6	291.9					
	0.312	7.9	74.4	331.1	-73.33	-12.85	-18.33	-81.58	24.6%
							Average Ratio:		**26.7%**

Table 5-10 Hinge Rotation Calculation Using Classic Method

Specimen			THD-1	THD-2	THD-3	THD-4	THD-5
Calculated	Yield	$\theta_{flexure(y)}$	0.0006	0.0006	0.0006	0.0005	0.0010
		$\theta_{bond\text{-}slip(y)}$	0.0046	0.0056	0.0059	0.0044	0.0087
		θ_{yield}	0.0052	0.0062	0.0065	0.0049	0.0097
	Ult.	$\theta_{flexure(u)}$	0.0110	0.0143	0.0131	0.0143	0.0129
		$\theta_{bond\text{-}slip(u)}$	0.0350	0.0601	0.0366	0.0609	0.0276
		$\theta_{ultimate}$	0.0460	0.0744	0.0497	0.0752	0.0406
Test		Yield	0.0049	0.0056	0.0063	0.0054	0.0093
		Ultimate	0.0722	0.0550	0.0658	0.0500	0.0630
$\theta_{cal}/\theta_{test}$		Yield	105.7%	110.6%	103.4%	90.9%	103.7%
		Ultimate	63.8%	135.2%	75.6%	150.5%	64.4%

Table 5-11 Development of Two-Way Hinge Plastic Length Using Test Data

Specimen	$\theta_{measure}$ (rad)	Gap (g) (in)	(mm)	f_{ult} (rad/in)	(rad/mm)	f_y (rad/in)	(rad/mm)	$\theta_y = f_y g$ (rad)	$L_p = (\theta_{measure}-\theta_y)/(f_u - f_y)$ (in)	(mm)	$X = (L_p - g)/ f_y d_b$
THD-1	0.0722	1.20	30.48	0.0110	0.0004	0.0007	0.0000	0.0008	6.9	175.2	**0.19**
THD-2	0.0550	1.00	25.40	0.0143	0.0006	0.0008	0.0000	0.0008	4.0	101.9	**0.09**
THD-3	0.0658	0.90	22.86	0.0131	0.0005	0.0008	0.0000	0.0007	5.3	134.2	**0.13**
THD-4	0.0500	0.90	22.86	0.0143	0.0006	0.0007	0.0000	0.0006	3.6	92.1	**0.08**
THD-5	0.0630	0.90	22.86	0.0129	0.0005	0.0012	0.0000	0.0010	5.3	133.8	**0.13**
									Average x :		**0.13**
									Standard Devation:		**0.04**

Table 5-12 Hinge Rotation Calculation Using Proposed Plastic Length Method

Item	Unit	THD-1	THD-2	THD-3	THD-4	THD-5
L_p	(in)	5.6	5.9	5.9	5.8	5.9
	(mm)	143.3	149.8	151.0	148.3	148.8
f_y	(rad/in)	0.0007	0.0008	0.0008	0.0007	0.0012
	(rad/m)	0.0277	0.0299	0.0318	0.0274	0.0457
f_{ult}	(rad/in)	0.0110	0.0143	0.0131	0.0143	0.0129
	(rad/m)	0.4348	0.5623	0.5165	0.5638	0.5089
q_p	(rad)	0.0583	0.0797	0.0732	0.0795	0.0689
q_{ult}	(rad)	0.0590	0.0805	0.0740	0.0802	0.0701
q_{test}	(rad)	0.0722	0.0550	0.0658	0.0500	0.0630
q_{ult} / q_{test}	----	81.8%	146.4%	112.5%	160.5%	111.2%

Table 5-13 Two-Way Hinge Closure Analysis Using Test Data

Specimen	Hinge Gap		Clear Thickness (g)		D/2		Rotation at Gap Closure (rad)		q_{cal} / q_{test}
	(in)	(mm)	(in)	(mm)	(in)	(mm)	Calculated	Measured	
THD-1	1.2	30.5	0.80	20.3	8.0	203.2	0.10	0.075	134%
THD-2	1	25.4	0.60	15.2	8.0	203.2	0.08	0.055	136%
THD-3	0.9	22.9	0.50	12.7	8.0	203.2	0.06	0.071	88%
THD-4	0.9	22.9	0.50	12.7	8.0	203.2	0.06	0.050	125%
THD-5	0.9	22.9	0.50	12.7	8.0	203.2	0.06	0.050	125%
							Average:		**1.22**
							Standard Deviation:		**0.19**

Note:
Clear Thickness = Hinge Gap - Diameter of All-Thread-Rod.

Table 5-14 Input Parameter for Column M-f Analysis

Column Input	Unit	THD-1	THD-2	THD-3	THD-4	THD-5
Axial Load	(Kips)	111.85	72.97	111.85	11.85	111.85
	(KN)	497.7	324.7	497.7	52.7	497.7
f'_c	(Ksi)	5.70	5.72	8.20	8.38	8.68
	(Mpa)	39.3	39.5	56.5	57.8	59.8
f'_{cc}	(Ksi)	9.11	9.14	11.82	12.01	12.32
	(Mpa)	62.8	63.0	81.5	82.8	85.0
e'_{cc}	---	0.0080	0.0080	0.0064	0.0063	0.0062
e_{cu}	---	0.0303	0.0302	0.0243	0.0240	0.0235
$f_{y\ long.}$	(Ksi)	66.7	67.4	66.8	72.3	71.0
	(Mpa)	459.9	464.8	460.6	498.7	489.4
$f_{u\ long.}$	(Ksi)	105.8	106.3	104.2	107.4	112.3
	(Mpa)	729.6	732.7	718.6	740.6	774.0
e_{sh}	---	0.01	0.01	0.009	0.01	0.008
e_{ult}	---	0.15	0.15	0.16	0.14	0.14

Table 5-15 Input Parameter for Hinge M-f Analysis

Hinge Input		Unit	THD-1	THD-2	THD-3	THD-4	THD-5
Axial Load		(Kips)	108.50	68.50	108.50	8.50	108.50
		(KN)	482.8	304.8	482.8	37.8	482.8
Clear	f'_{cc}	(Ksi)	12.25	10.26	10.15	9.89	9.51
		(Mpa)	84.5	70.8	70.0	68.2	65.6
	e'_{cc}	---	0.0062	0.0072	0.0073	0.0074	0.0077
Cover	e_{cu}	---	0.0236	0.0274	0.0276	0.0282	0.0292
Core	f'_{cc}	(Ksi)	13.43	11.46	11.30	11.03	10.62
		(Mpa)	92.6	79.0	77.9	76.0	73.2
	e'_{cc}	---	0.0076	0.0090	0.0090	0.0092	0.0095
	e_{cu}	---	0.0217	0.0267	0.0323	0.0330	0.0341
$f_{y\ long.}$		(Ksi)	78.9	87.1	89.7	87.8	88.1
		(Mpa)	544.3	600.3	618.5	605.3	607.5
$f_{u\ long.}$		(Ksi)	114.4	120.0	118.2	117.2	117.9
		(Mpa)	788.6	827.1	815.2	807.9	812.6
e_{sh}		---	0.0027	0.0064	0.012	0.012	0.012
e_{ult}		---	0.15	0.1	0.12	0.12	0.12

Table 5-16 Comparison of the Column M-f Analysis Result (RCMC) with or Without the Increase Due to Stress Rate Effect

Result for Column		Unit	THD-1	THD-2	THD-3	THD-4	THD-5
With SRI Effect	M_{yield}	(Kip-in)	3433	3144	1769	1513	2997
		(KN-m)	387.9	355.3	199.9	171.0	338.7
	f_{yield}	(rad/in)	0.0004	0.0004	0.0003	0.0003	0.0004
		(rad/m)	0.0143	0.0144	0.0128	0.0138	0.0144
	$M_{ult.}$	(Kip-in)	4098	3897	2048	1941	3508
		(KN-m)	463.1	440.4	231.4	219.3	396.4
	f_{ult}	(rad/in)	0.0068	0.0066	0.0079	0.0088	0.0066
		(rad/m)	0.2685	0.2595	0.3103	0.3456	0.2610
W/O SRI Effect	M_{yield}	(Kip-in)	3204	2906	1692	1403	2702
		(KN-m)	362.1	328.4	191.2	158.5	305.3
	f_{yield}	(rad/in)	0.0003	0.0003	0.0003	0.0003	0.0003
		(rad/m)	0.0132	0.0132	0.0118	0.0126	0.0129
	$M_{ult.}$	(Kip-in)	3880	3678	1972	1827	3254
		(KN-m)	438.4	415.6	222.8	206.5	367.7
	f_{ult}	(rad/in)	0.0072	0.0070	0.0083	0.0095	0.0072
		(rad/m)	0.2828	0.2760	0.3251	0.3737	0.2844
$(M_y)_{SRE} / M_y$		---	107.1%	108.2%	104.6%	107.8%	110.9%
$(f_y)_{SRE} / f_y$		---	108.3%	109.2%	108.1%	108.8%	111.0%
$(M_u)_{SRE} / M_u$		---	105.6%	106.0%	103.9%	106.2%	107.8%
$(f_u)_{SRE} / f_u$		---	94.9%	94.0%	95.4%	92.5%	91.8%

Table 5-17 Comparison of the Hinge M-f Analysis Result with and Without the Increase Due to Stress Rate Effect

Result for Hinge		Unit	THD-1	THD-2	THD-3	THD-4	THD-5
With SRI Effect	M_{yield}	(Kip-in)	620	512.5	617.6	315.7	398
		(KN-m)	70.1	57.9	69.8	35.7	45.0
	f_{yield}	(rad/in)	0.0007	0.0008	0.0008	0.0007	0.0012
		(rad/m)	0.0277	0.0299	0.0318	0.0274	0.0457
	$M_{ult.}$	(Kip-in)	654.9	570.8	651.4	380.5	407.9
		(KN-m)	74.0	64.5	73.6	43.0	46.1
	f_{ult}	(rad/in)	0.0110	0.0143	0.0131	0.0143	0.0129
		(rad/m)	0.4348	0.5623	0.5165	0.5638	0.5089
W/O SRI Effect	M_{yield}	(Kip-in)	601.1	490.5	580.7	293.7	375.7
		(KN-m)	67.9	55.4	65.6	33.2	42.5
	f_{yield}	(rad/in)	0.0007	0.0007	0.0007	0.0006	0.0010
		(rad/m)	0.0272	0.0270	0.0286	0.0250	0.0409
	$M_{ult.}$	(Kip-in)	630	549	619.3	364.4	389.2
		(KN-m)	71.2	62.0	70.0	41.2	44.0
	f_{ult}	(rad/in)	0.0113	0.0149	0.0136	0.0163	0.0131
		(rad/m)	0.4443	0.5856	0.5349	0.6421	0.5171
$(M_y)_{SRE} / M_y$		---	103.1%	104.5%	106.4%	107.5%	105.9%
$(f_y)_{SRE} / f_y$		---	102.0%	110.9%	110.9%	109.9%	111.7%
$(M_u)_{SRE} / M_u$		---	104.0%	104.0%	105.2%	104.4%	104.8%
$(f_u)_{SRE} / f_u$		---	97.9%	96.0%	96.6%	87.8%	98.4%

Table 5-18 Experimental Average Bond Stress

Location	Before 1st Yielding		After Yielding		$u_{before(y)} / u_{after(y)}$
	Avg. Bond Strength (u) (f'c^1/2)	Standard Deviation	Avg. Bond Strength (u) (f'c^1/2)	Standard Deviation	
Loading Header	9.25	6.45	11.2	7.65	0.83
Column	7.5	5.35	9.7	6.23	0.77
u_{Head} / u_{Column}	123.3%	-----	115.5%	-----	-----

Table 5-19 Comparison of Average Bond Stress Based on Experimental Results and Classical Values

Location	Before 1st Yielding	After Yielding	Leet's Equation (f'c^1/2)	$u_{Leet's} / u_{test(avg.)}$
	Avg. Bond Strength (f'c^1/2)	Avg. Bond Strength (f'c^1/2)		
Loading Header	9.25	11.2	9.68	0.95
Column	7.5	9.7	9.47	1.10
Average	8.38	10.45	9.57	1.02

Table 5-20 Yield Deflections Using Existing Calculations

	Unit	THD-1	THD-2	THD-3	THD-4	THD-5
D_{flex}	(in)	0.213	0.387	0.154	0.196	0.232
	(mm)	5.42	9.83	3.92	4.98	5.90
$D_{bond-slip}$	(in)	0.186	0.259	0.169	0.161	0.222
	(mm)	4.73	6.59	4.30	4.08	5.64
D_{shear}	(in)	0.012	0.011	0.006	0.005	0.009
	(mm)	0.30	0.27	0.15	0.12	0.22
D_y	(in)	0.412	0.657	0.329	0.361	0.463
	(mm)	10.46	16.69	8.37	9.17	11.76

Table 5-21 Ultimate Deflections Using Existing Calculations

	Unit	THD-1	THD-2	THD-3	THD-4	THD-5
$D_{flex(y)}$	(in)	0.213	0.387	0.154	0.196	0.232
	(mm)	5.42	9.83	3.92	4.98	5.90
$D_{shear(ult)}$	(in)	0.092	0.085	0.048	0.042	0.072
	(mm)	2.33	2.15	1.23	1.07	1.83
D_p	(in)	3.021	4.623	2.908	3.453	2.994
	(mm)	76.73	117.43	73.86	87.71	76.05
D_{ult}	(in)	3.326	5.095	3.111	3.691	3.298
	(mm)	84.48	129.41	79.01	93.75	83.77

Table 5-22 Rotation Hinge Properties Used in SAP2000 Push-over Analysis

Input		Unit	THD-1	THD-2	THD-3	THD-4	THD-5
Column Base Hinge	$M_{y\ 1st}$	(Kip-in)	1957	1913	1356	1039	1921
		(KN-m)	221.1	216.2	153.2	117.4	217.1
	θ_{y1st}	----	0.0054	0.0066	0.0043	0.0049	0.0060
	M_{ye}	(Kip-in)	3433	3144	1769	1513	2997
		(KN-m)	387.9	355.3	199.9	171.0	338.7
	θ_{ye}	----	0.0087	0.0099	0.0056	0.0072	0.0085
	M_{ult}	(Kip-in)	4098	3897	2048	1941	3508
		(KN-m)	463.1	440.4	231.4	219.3	396.4
	θ_{ult}	----	0.0716	0.0798	0.0572	0.0788	0.0735
Top Hinge	$M_{y\ 1st}$	(Kip-in)	488.8	385.4	495.6	217.1	329.3
		(KN-m)	55.2	43.6	56.0	24.5	37.2
	θ_{y1st}	----	0.0056	0.0061	0.0072	0.0052	0.0099
	M_{ye}	(Kip-in)	620	512.5	617.6	315.7	398
		(KN-m)	70.1	57.9	69.8	35.7	45.0
	θ_{ye}	----	0.0071	0.0081	0.0089	0.0075	0.0120
	M_{ult}	(Kip-in)	654.9	570.8	651.4	380.5	407.9
		(KN-m)	74.0	64.5	73.6	43.0	46.1
	θ_{ult}	----	0.0348	0.0601	0.0776	0.0538	0.0083

Table 5-23 Shear Spring Properties Used in SAP2000 Push-over Analysis

		Unit	THD-1	THD-2	THD-3	THD-4	THD-5
Control Point 1	V_1	(Kips)	80.1	64.3	82.2	36.6	70.9
		(KN)	356.6	286.0	365.8	162.9	315.6
	Δ_1	(in)	0.054	0.036	0.042	0.019	0.045
		(mm)	1.37	0.92	1.06	0.47	1.13
Control Point 2	V_2	(Kips)	80.1	64.3	82.2	36.6	70.9
		(KN)	356.6	286.0	365.8	162.9	315.6
	Δ_2	(in)	0.25	0.25	0.25	0.25	0.25
		(mm)	6.35	6.35	6.35	6.35	6.35
Control Point 3	V_3	(Kips)	71.4	55.5	73.5	27.9	62.2
		(KN)	317.6	247.1	326.9	124.0	276.7
	Δ_3	(in)	0.5	0.44	0.51	0.47	0.48
		(mm)	12.70	11.18	12.95	11.94	12.19
Control Point 4	V_4	(Kips)	97.0	83.3	98.2	57.7	90.5
		(KN)	431.8	370.8	437.2	256.8	402.5
	Δ_4	(in)	1.45	1.44	1.44	1.42	1.44
		(mm)	36.93	36.48	36.62	36.03	36.69

Table 5-24 Comparison of SAP2000 Push-Over Analysis Results with Measured Data

Result for Column		Unit	THD-1	THD-2	THD-3	THD-4	THD-5
Push-Over Result	V_{yield}	(Kip)	86.398	61.31	49.345	38.12	68.31
		(KN)	384.5	272.8	219.6	169.6	304.0
	D_{yield}	(in)	0.8	1.4	0.7	0.8	1.1
		(mm)	21.4	35.3	18.3	20.8	28.0
	D_{Ult}	(in)	4.4	7.0	5.2	4.1	7.0
		(mm)	112.8	178.3	132.1	104.0	177.8
Measured Result	V_{yield}	(Kip)	83.3	52.6	51.6	33.2	72.8
		(KN)	370.7	234.1	229.6	147.8	324.1
	D_{yield}	(in)	0.7	0.9	0.6	0.5	0.8
		(mm)	17.1	23.5	14.0	13.0	21.0
	D_{Ult}	(in)	4.8	7.4	4.7	2.8	8.6
		(mm)	120.7	187.6	120.0	71.0	218.3
$(V_y)_{cal} / (V_y)_{test}$		---	103.7%	116.5%	95.7%	114.7%	93.8%
$(D_y)_{cal} / (D_y)_{test}$		---	125.2%	150.4%	130.8%	160.8%	133.4%
$(D_{ult})_{cal} / (D_{ult})_{test}$		---	93.4%	95.0%	110.1%	146.5%	81.4%

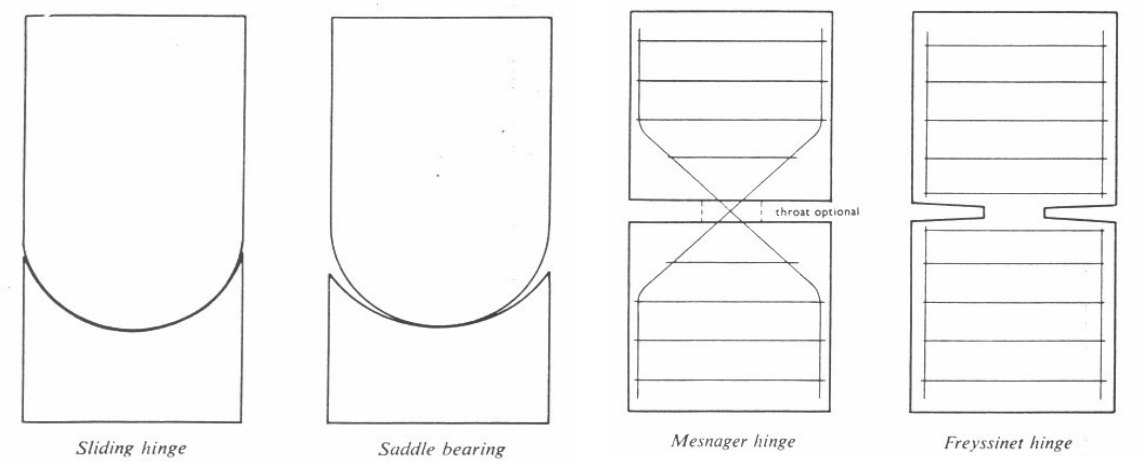

Figure 1-1 Four Types of Traditional Concrete Hinges

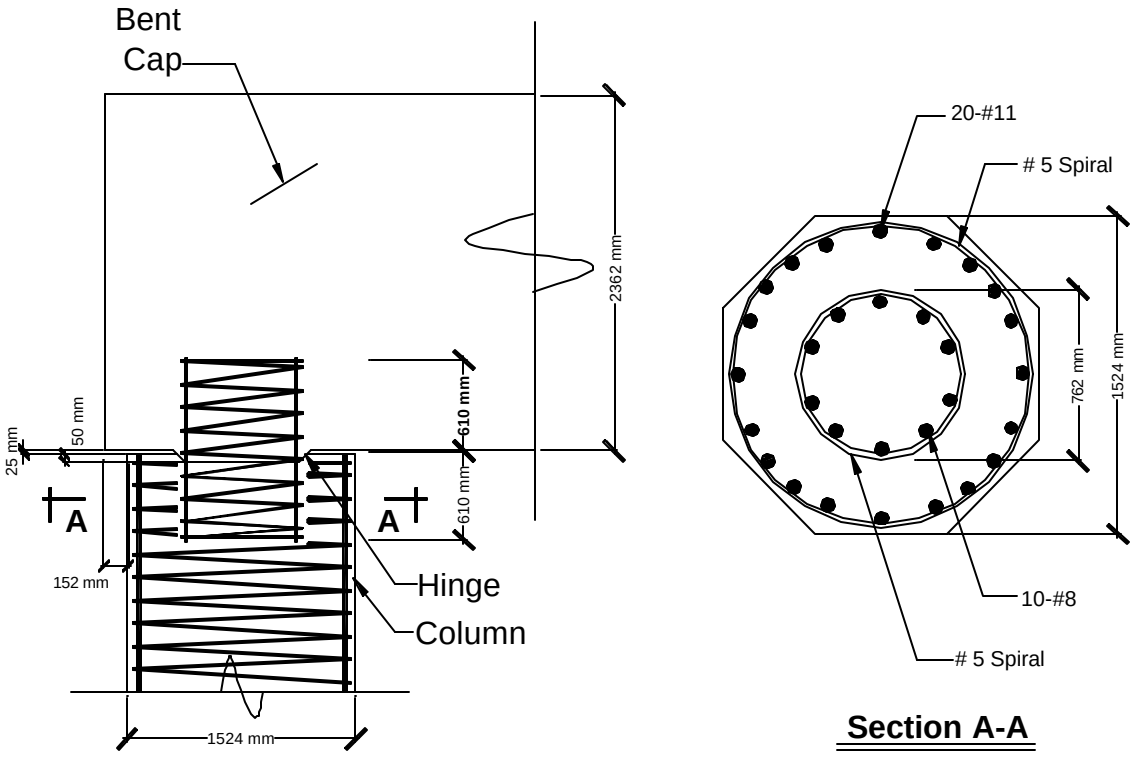

Figure 1-2 NDOT Top Hinge Detail

Figure 1-3 NDOT Bridge Column with Top Hinge

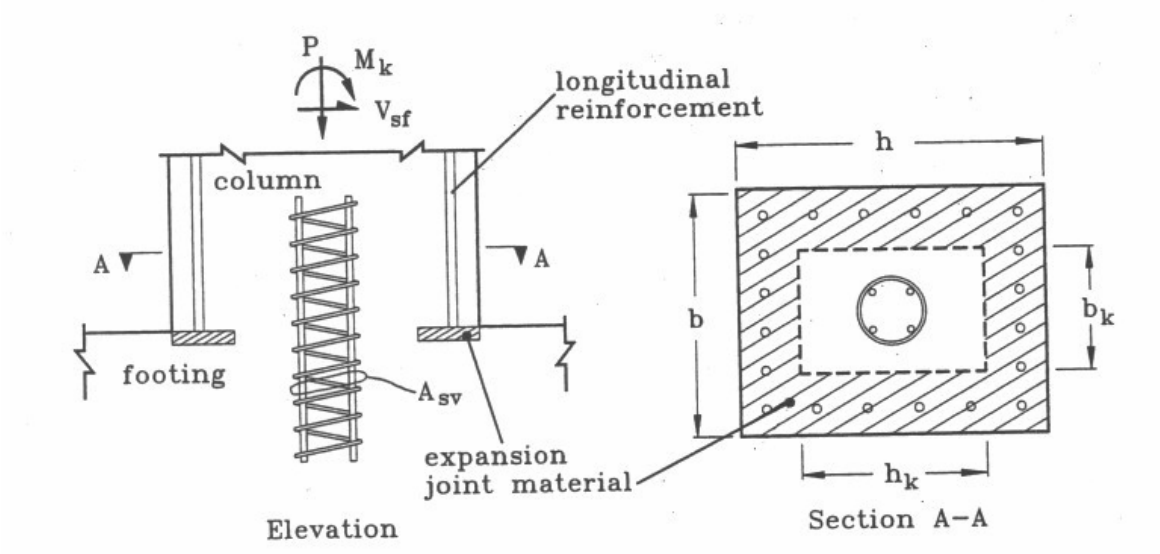

Figure 1-4 Typical Two-Way Hinge

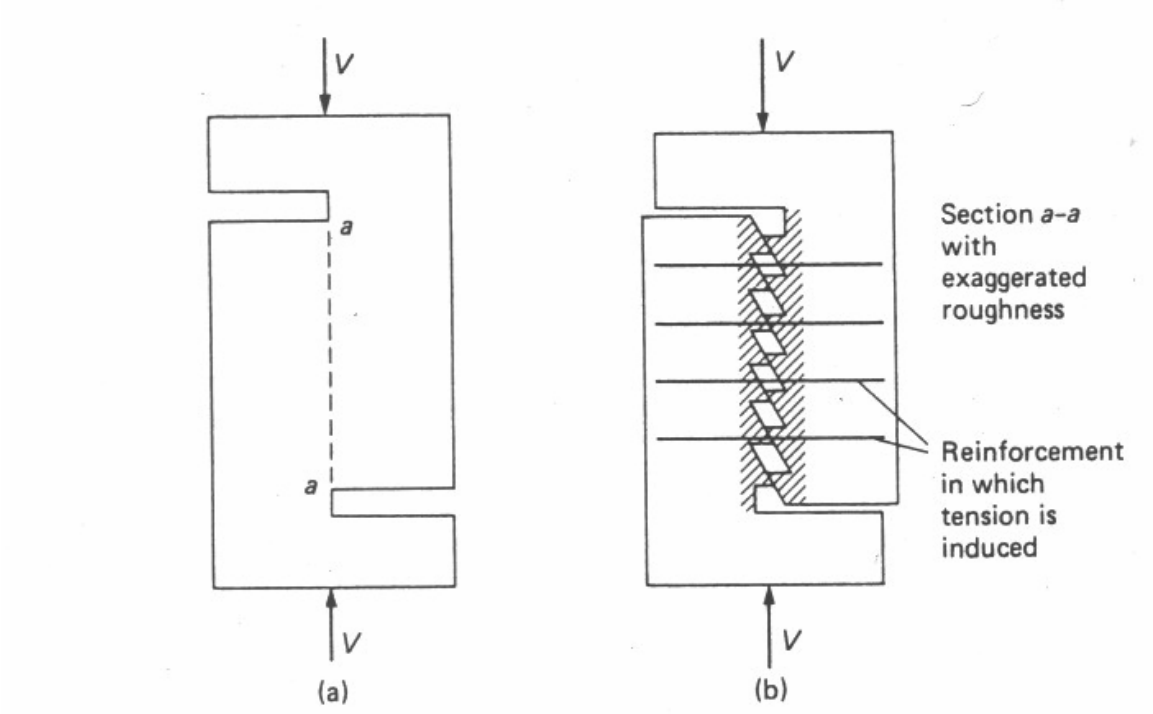

Figure 2-1 Idealization of the Shear-Friction Concept

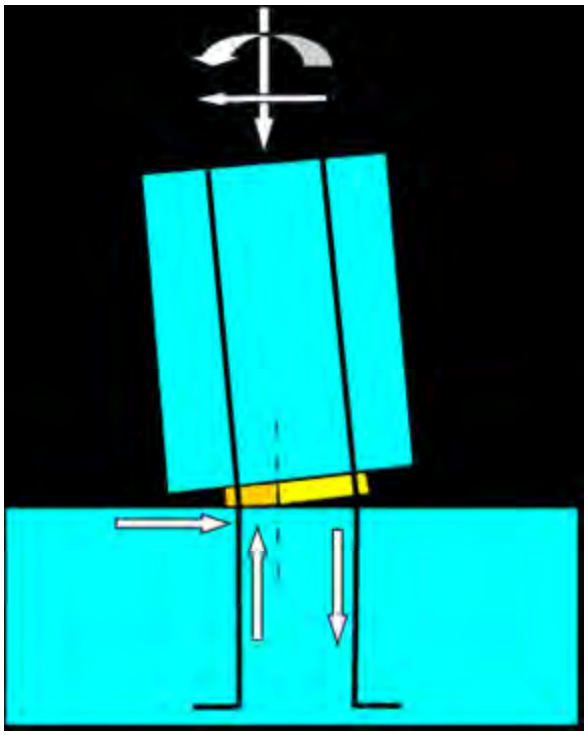

Figure 2-2 Two-way Hinge Mechanism

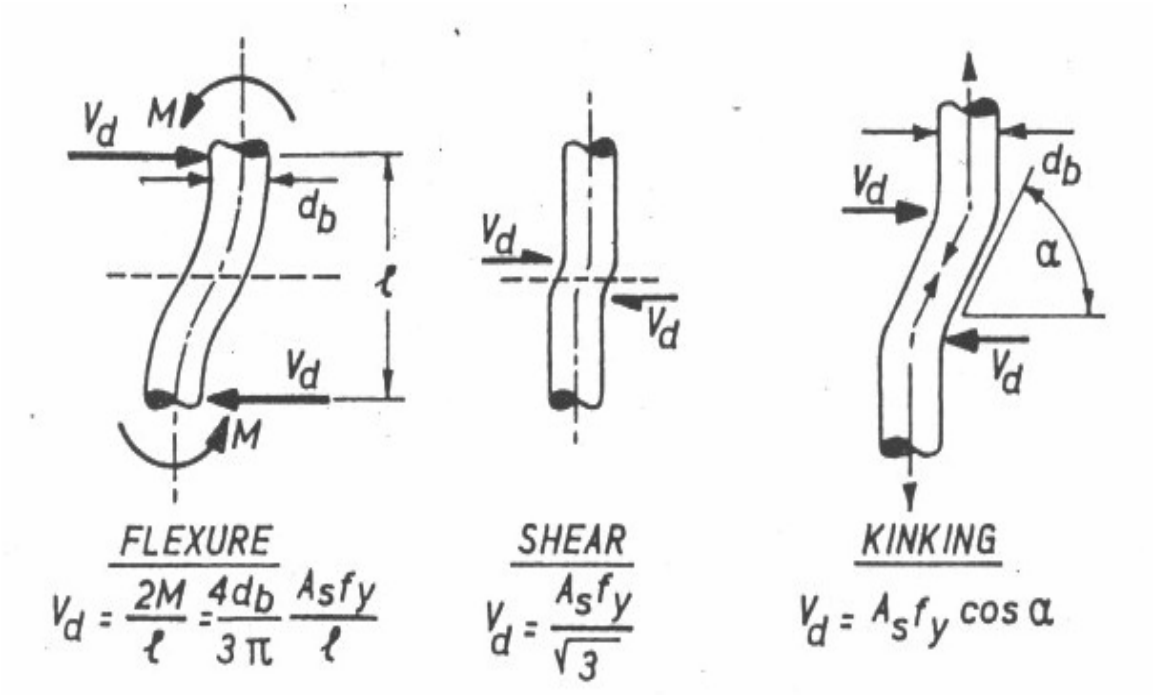

Figure 2-3 Mechanism of Dowel Action Across a Shear Interface

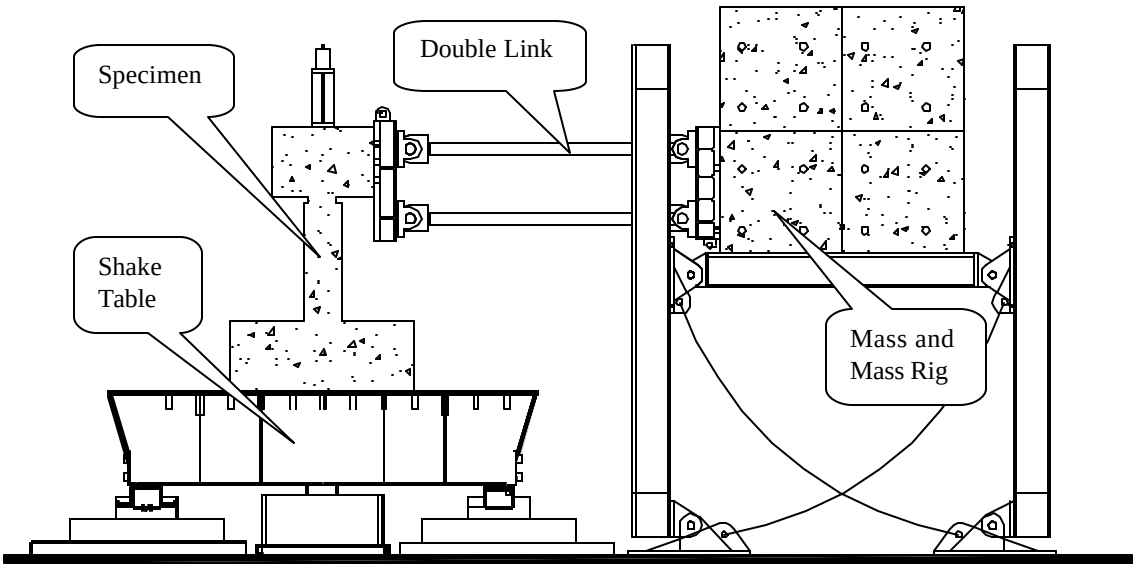

Figure 2-4 UNR Shaking Table System

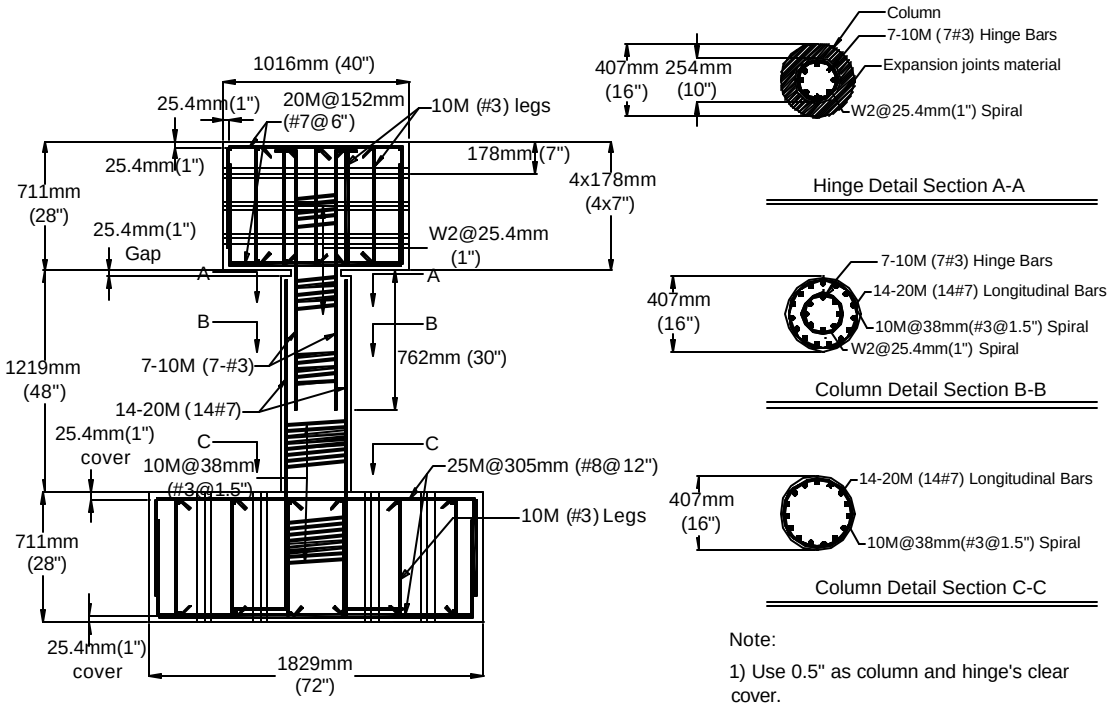

Figure 2-5 THD-1 Detail

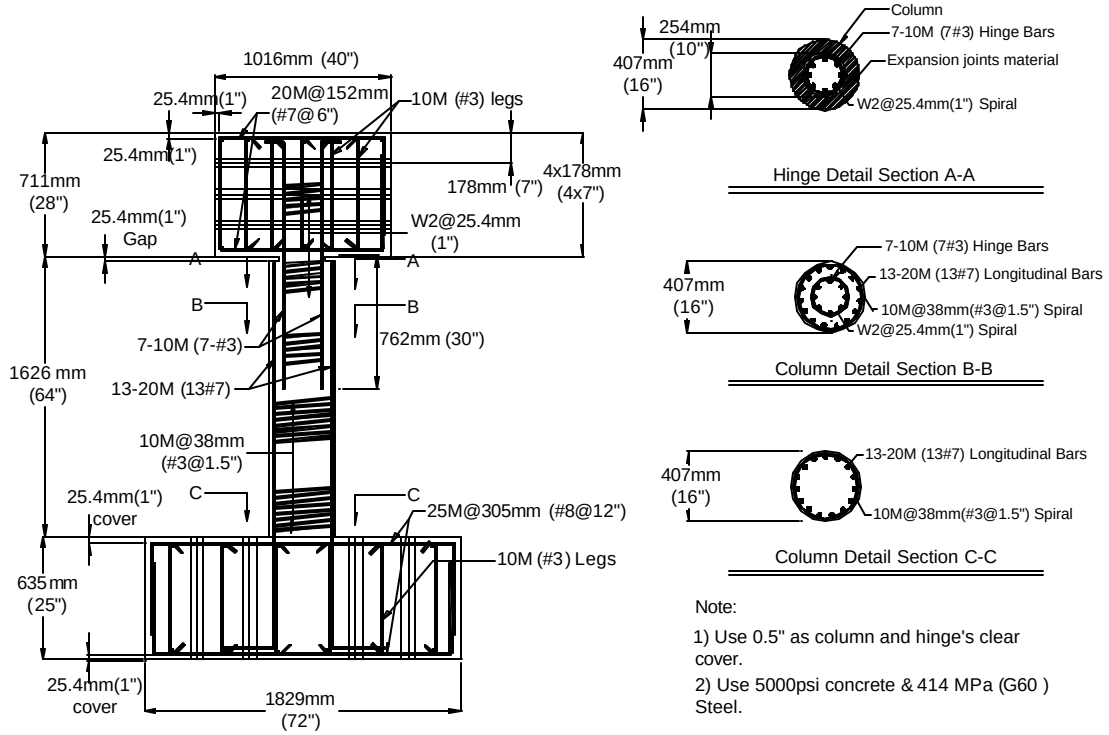

Figure 2-6 THD-2 Detail

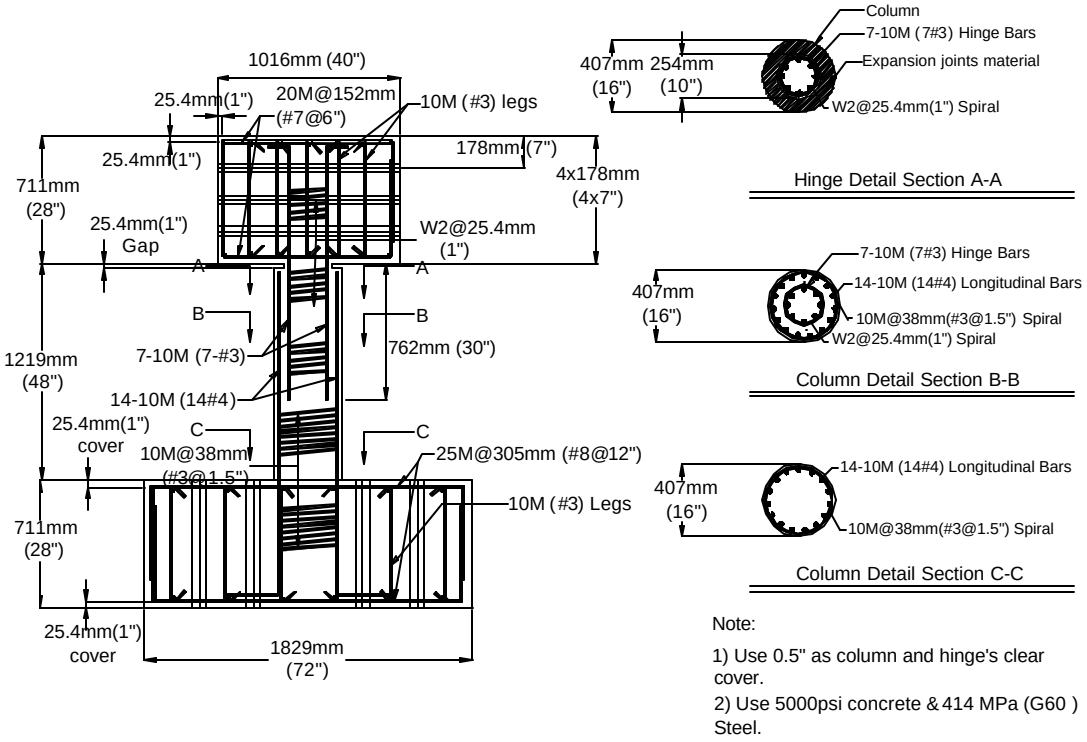

Note:

1) Use 0.5" as column and hinge's clear cover.

2) Use 5000psi concrete & 414 MPa (G60) Steel.

Figure 2-7 THD-3 Detail

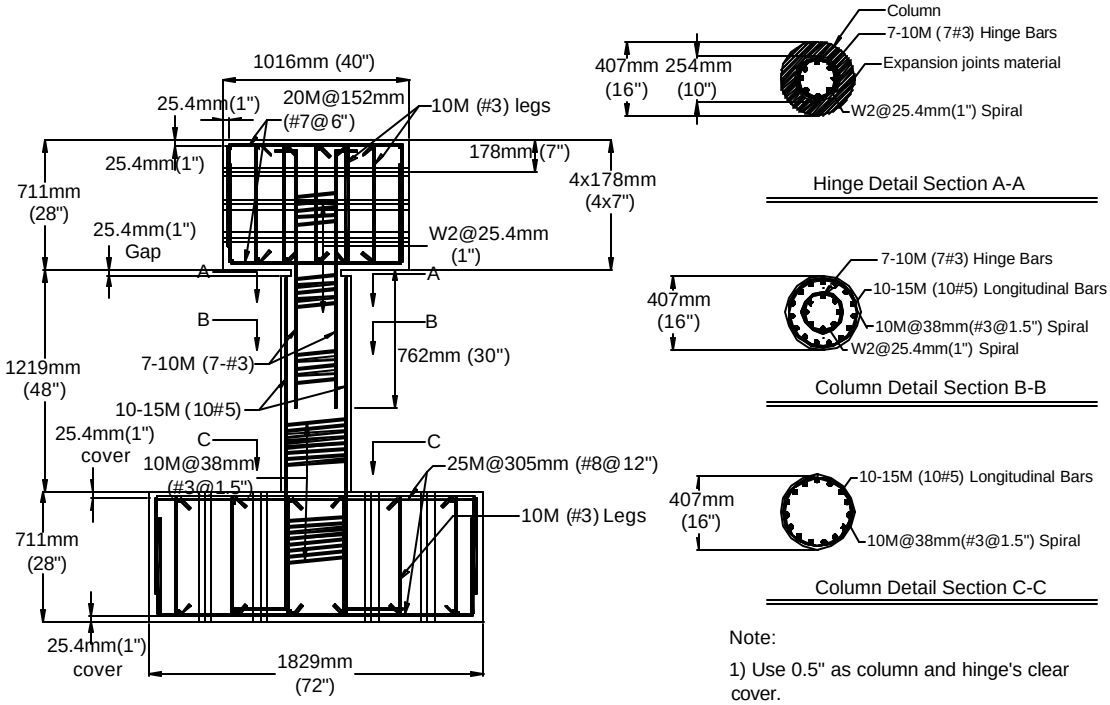

Note:

1) Use 0.5" as column and hinge's clear cover.

2) Use 5000psi concrete & 414 MPa (G60) Steel.

Figure 2-8 THD-4 Detail

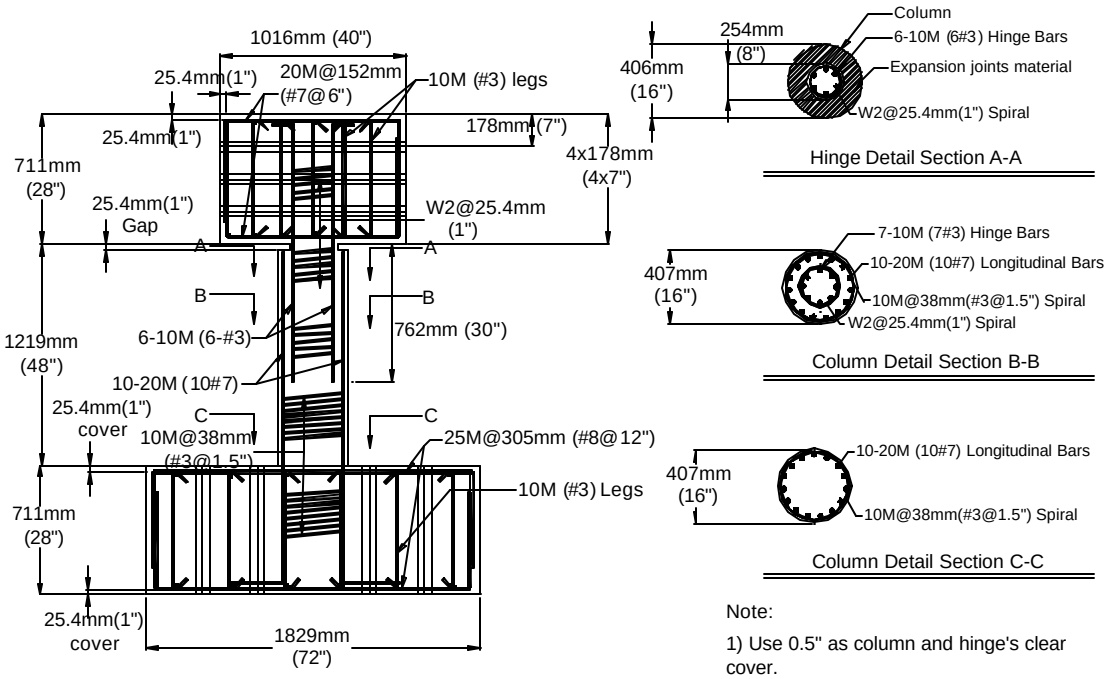

Figure 2-9 THD-5 Detail

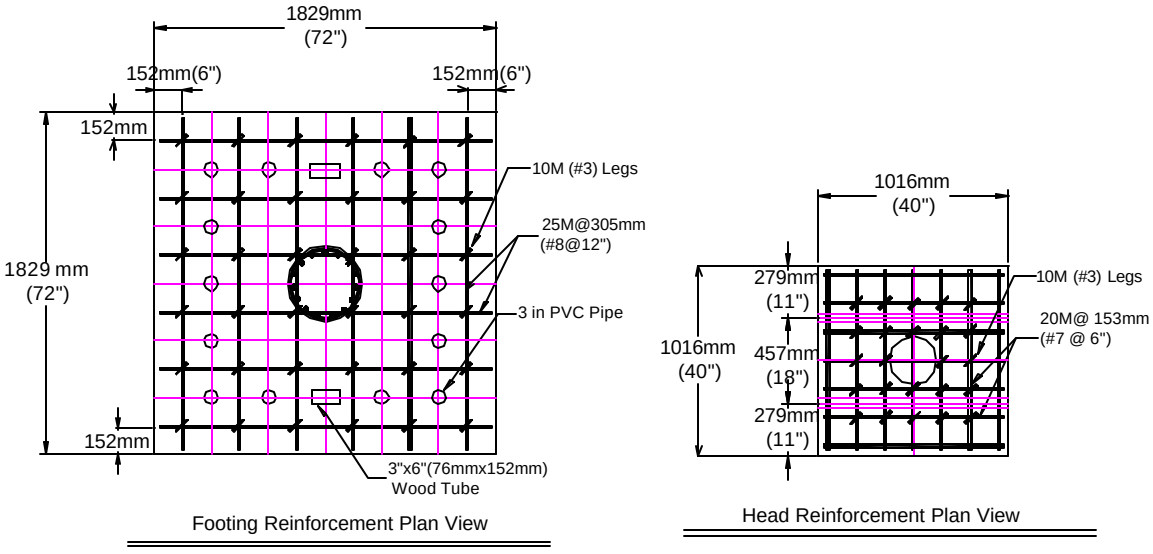

Figure 2-10 Footing and Head Detail

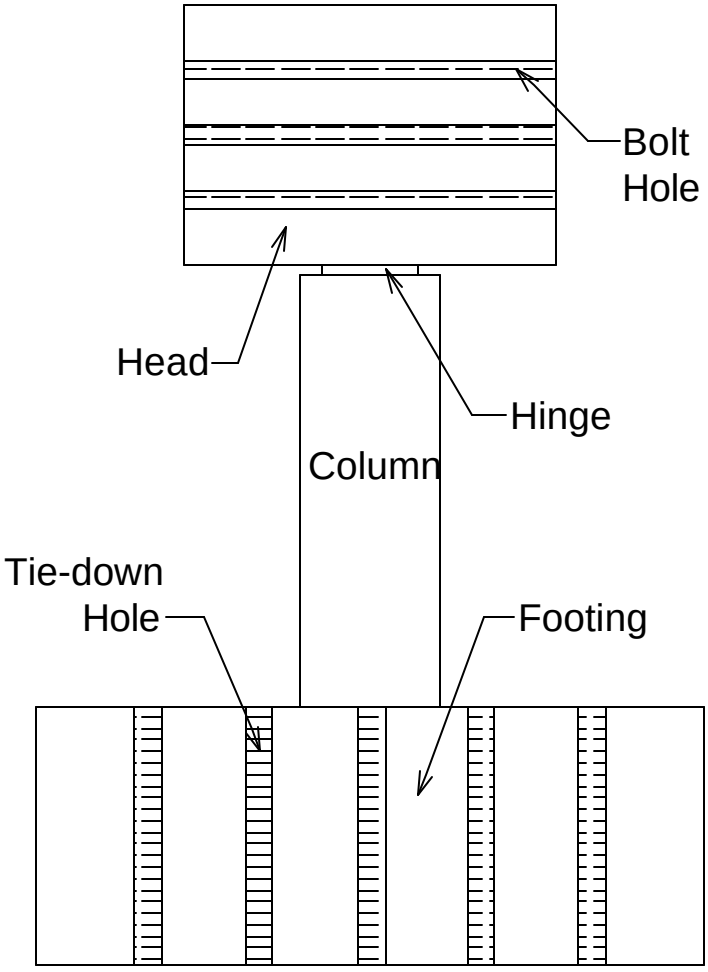

Figure 2-11 Specimen Outline

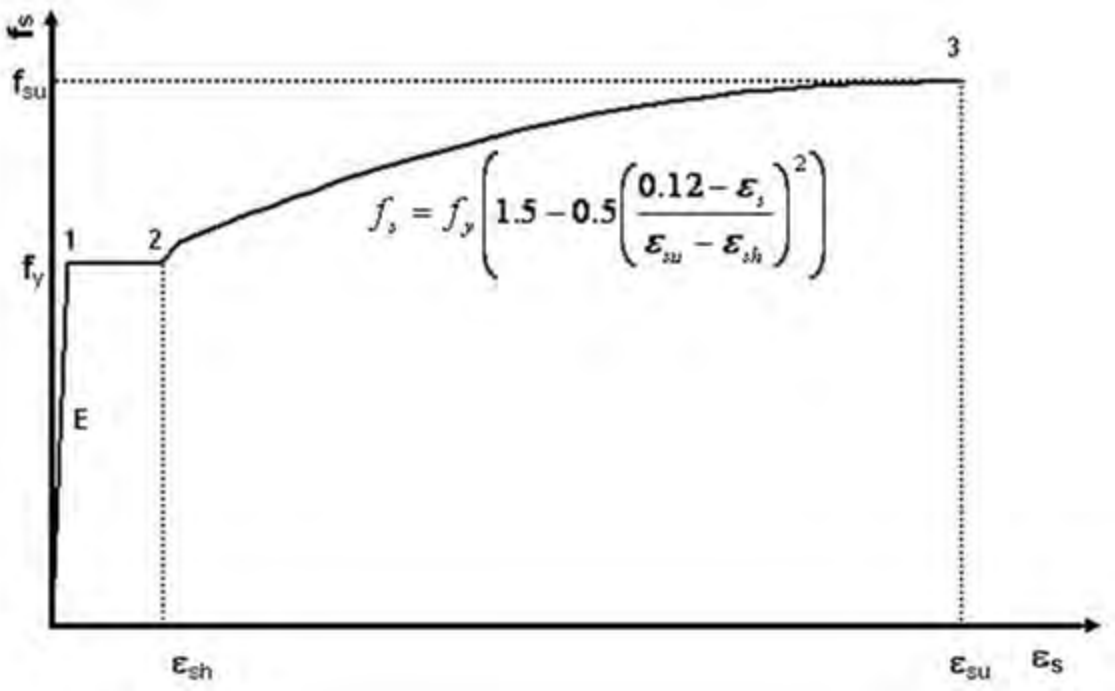

Figure 2-12 The Parabolic Strain Hardening Steel Model

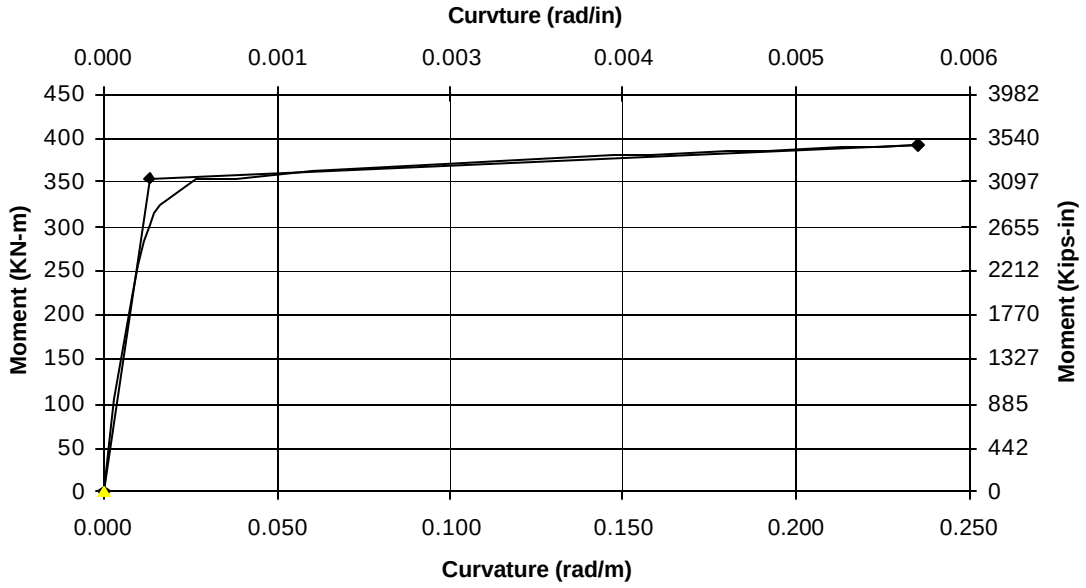

Figure 2-13 M-f Curve for Specimen THD-1 Column

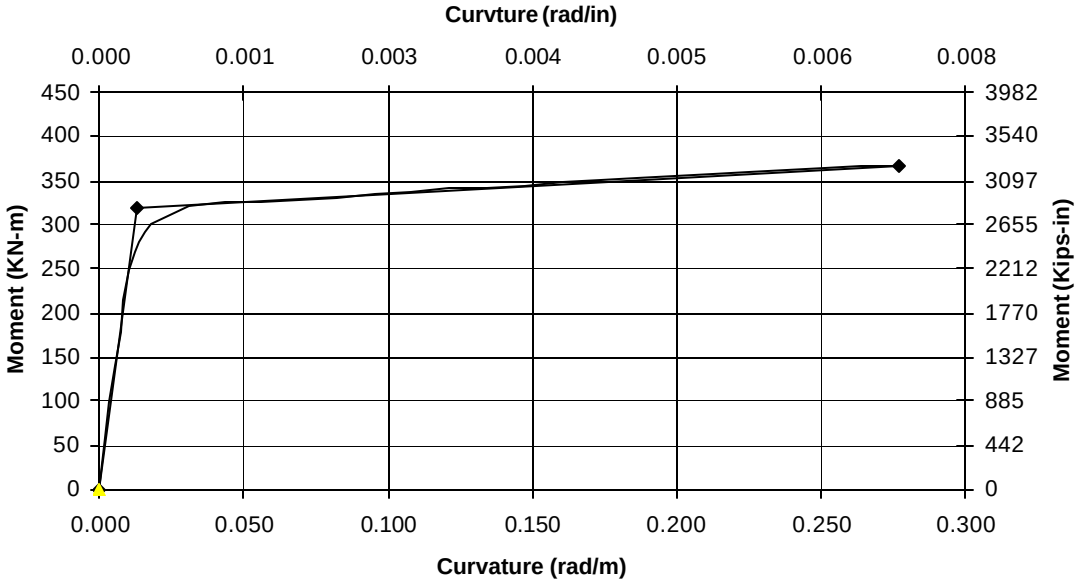

Figure 2-14 M-f Curve for Specimen THD-2 Column

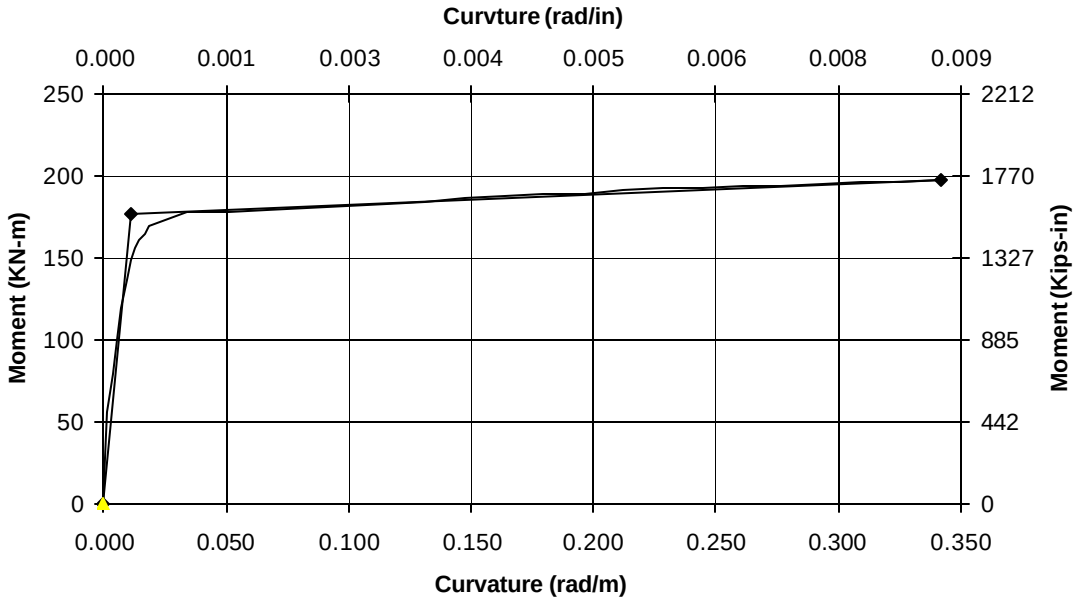

Figure 2-15 M-f Curve for Specimen THD-3 Column

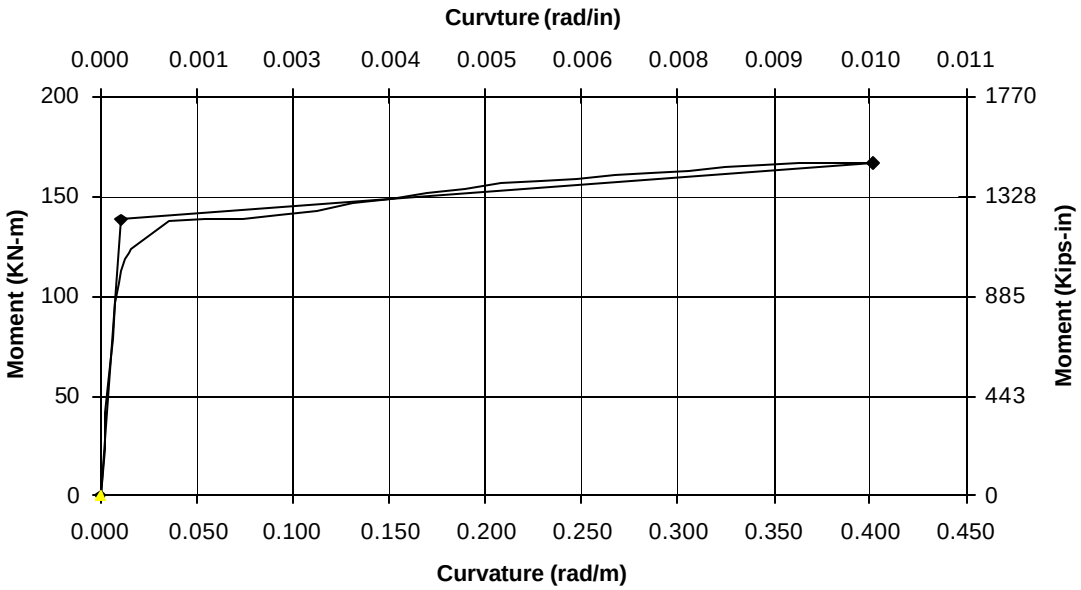

Figure 2-16 M-f Curve for Specimen THD-4 Column

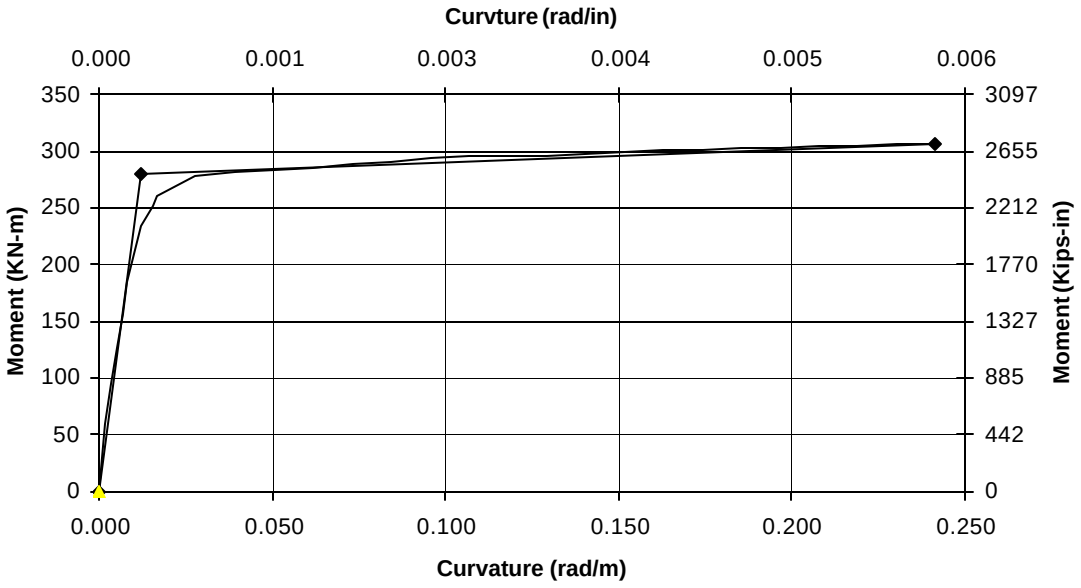

Figure 2-17 M-f Curve for Specimen THD-5 Column

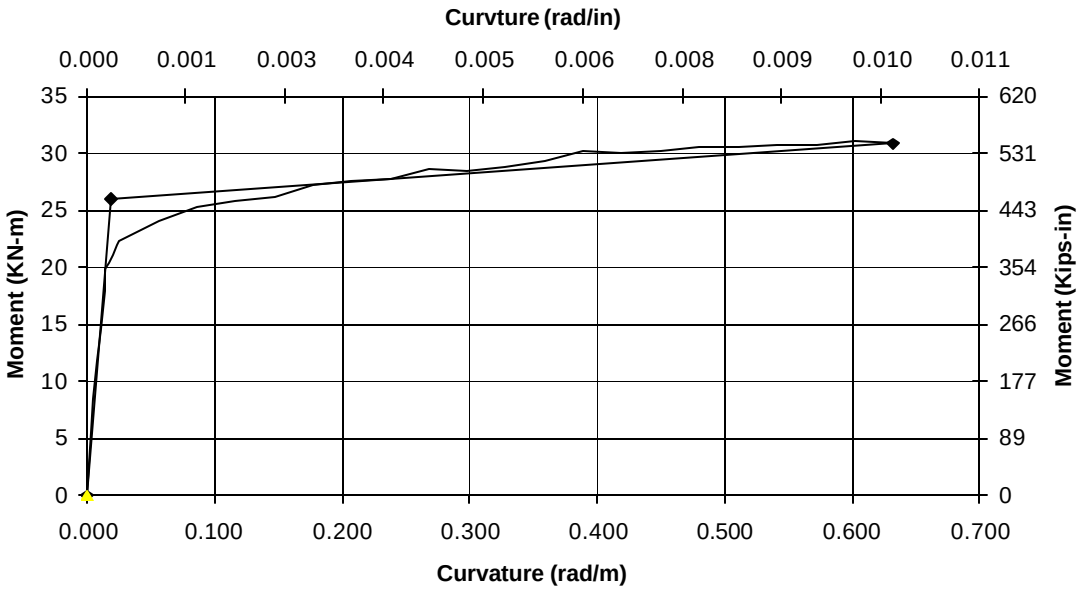

Figure 2-18 M-f Curve for Specimen THD-1 and THD-3 Hinge

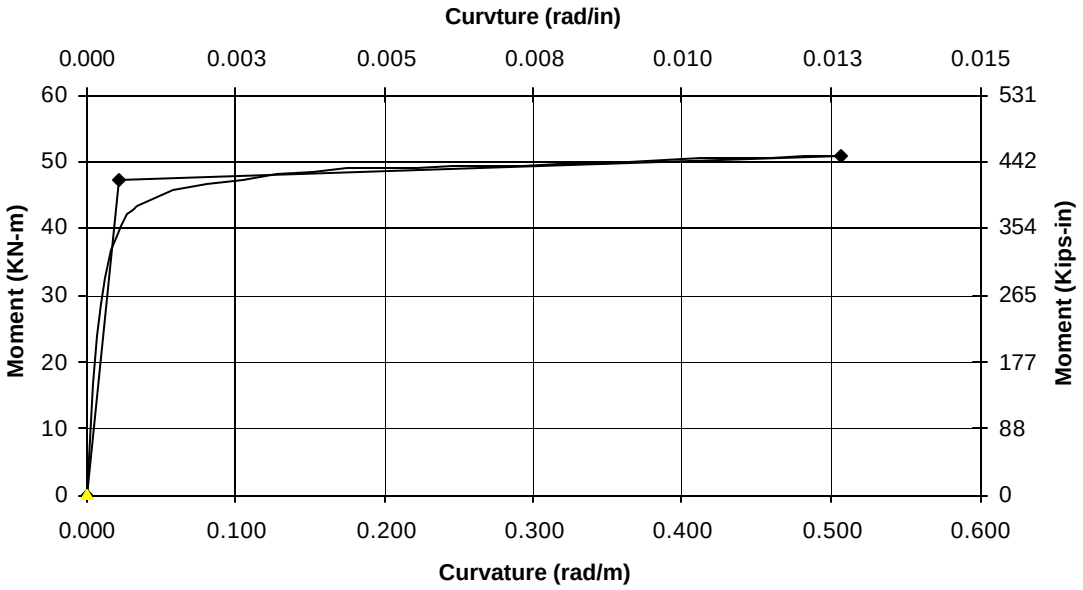

Figure 2-19 M-f Curve for Specimen THD-2 Hinge

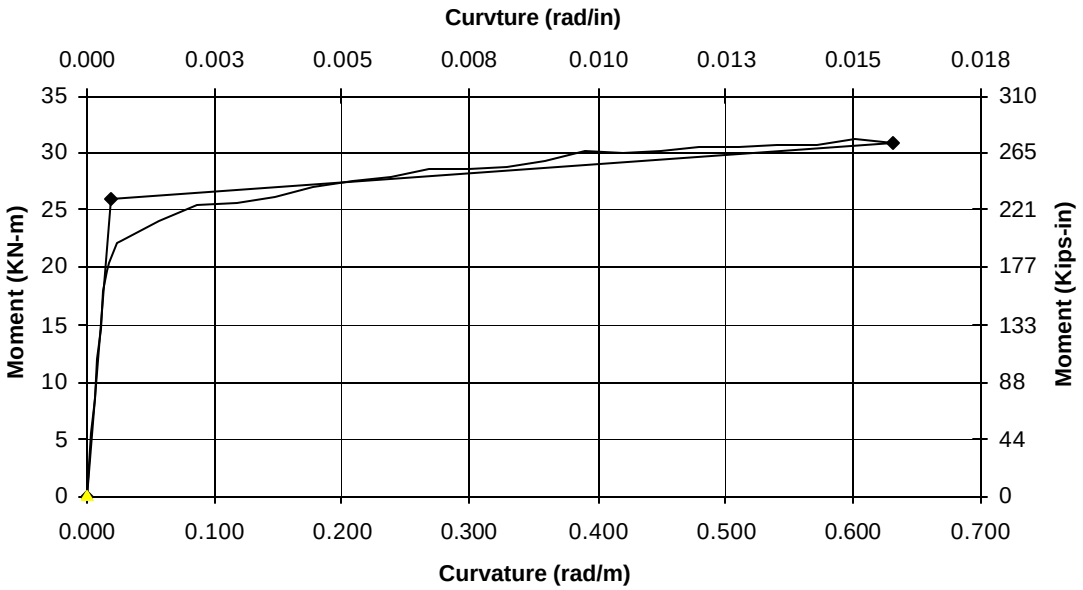

Figure 2-20 M-f Curve for Specimen THD-4 Hinge

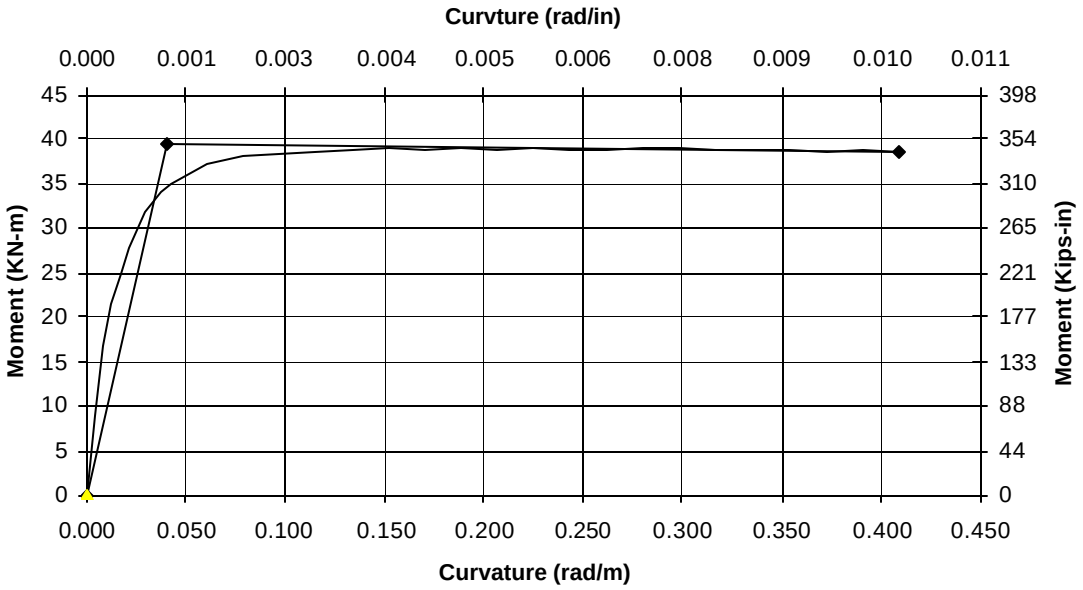

Figure 2-21 M-f Curve for Specimen THD-5 Hinge

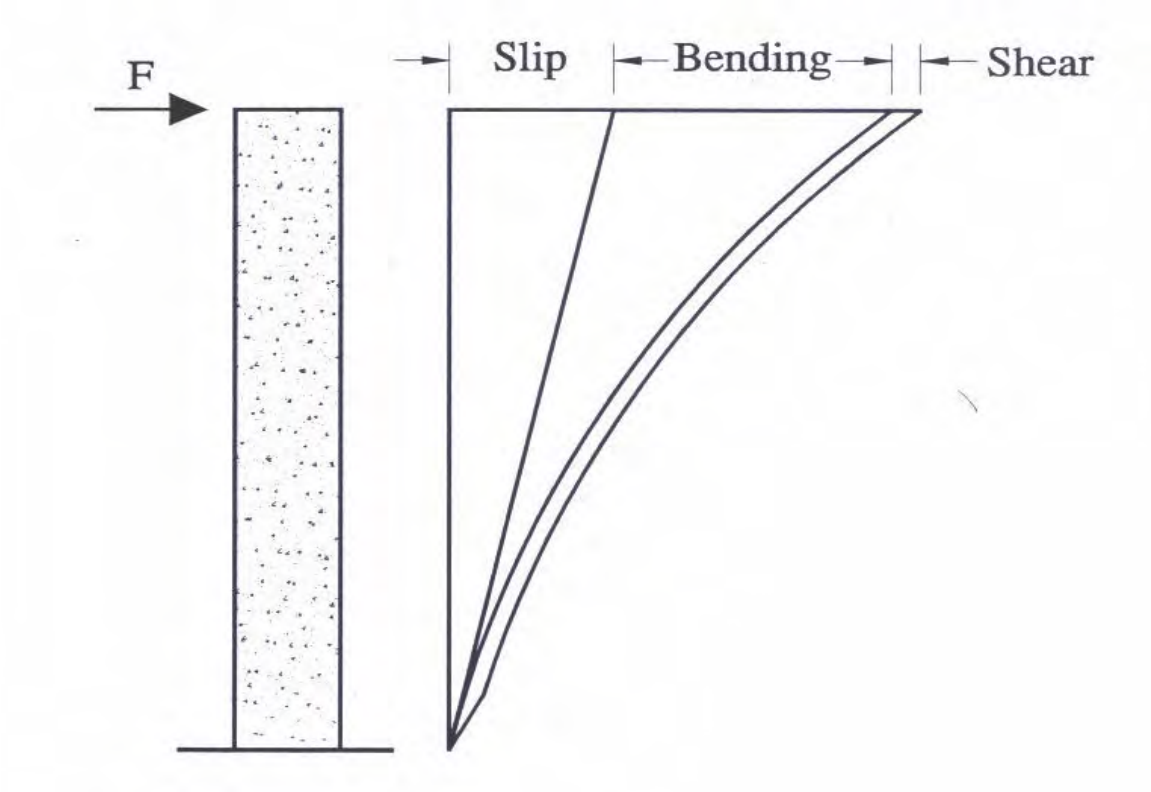

Figure 2-22 Displacement Components for a Cantilever Column

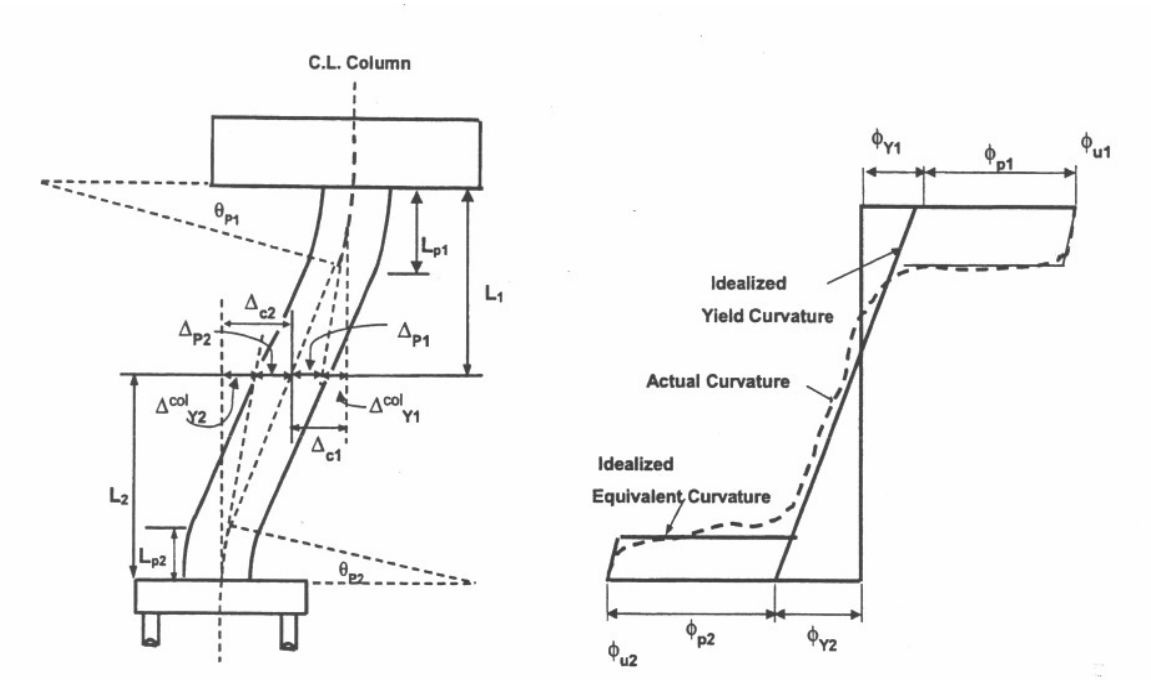

Figure 2-23 Double Curvature Column Tip Displacement

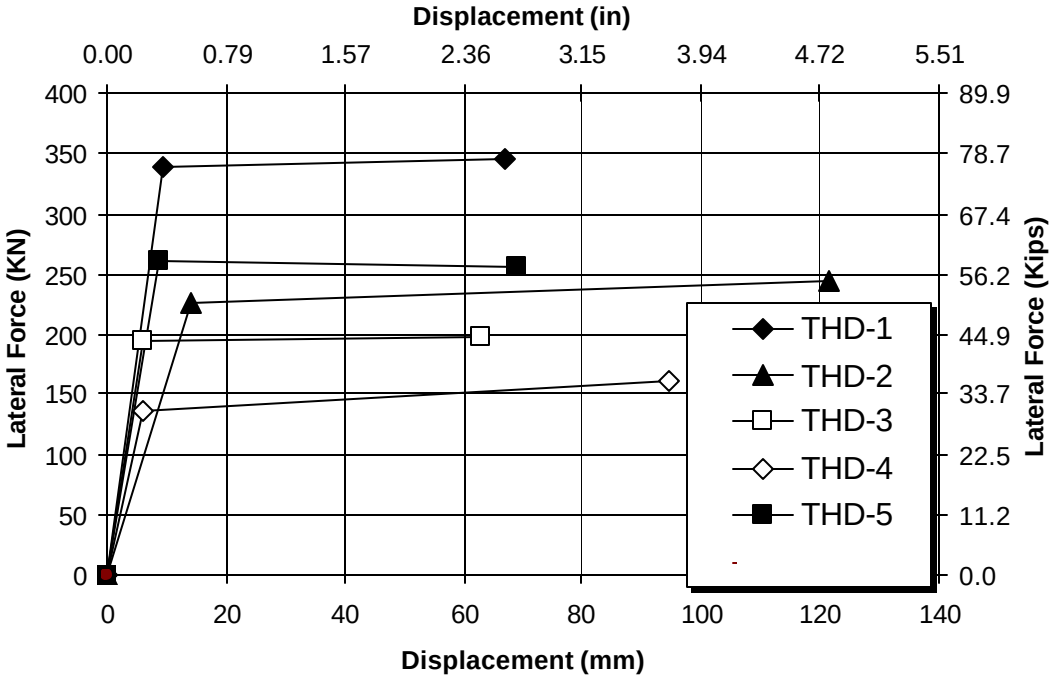

Figure 2-24 Predicted Later Force-Displacement Relation (THD-1 to THD-5)

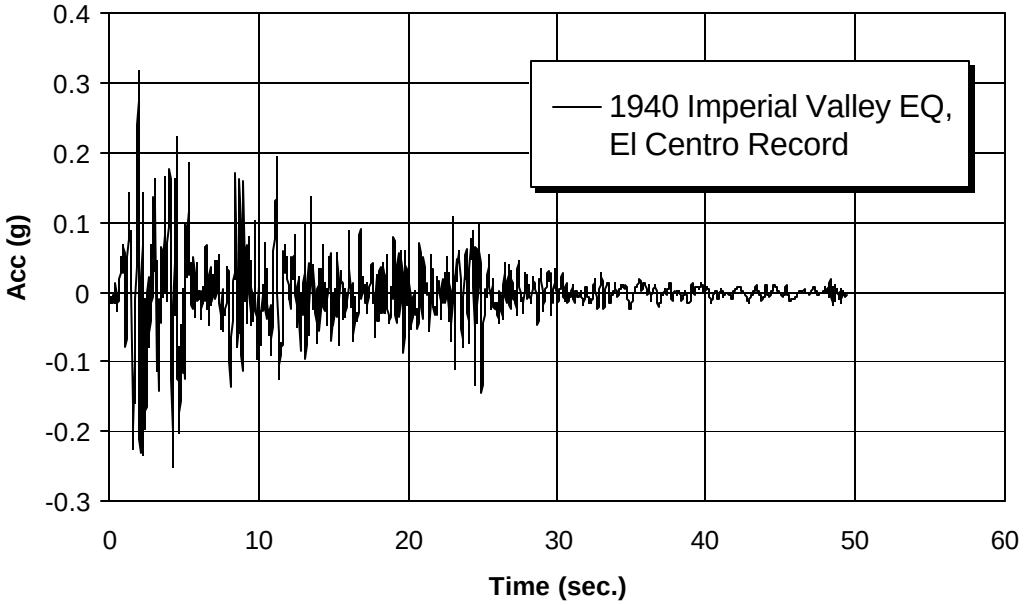

Figure 2-25 El Centro Record

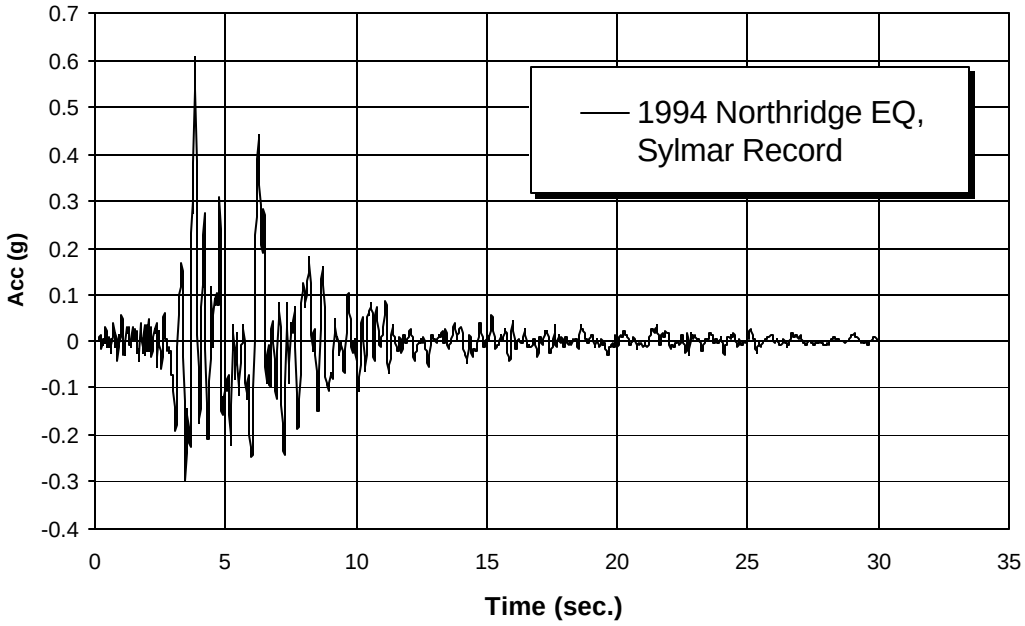

Figure 2-26 Sylmar Record

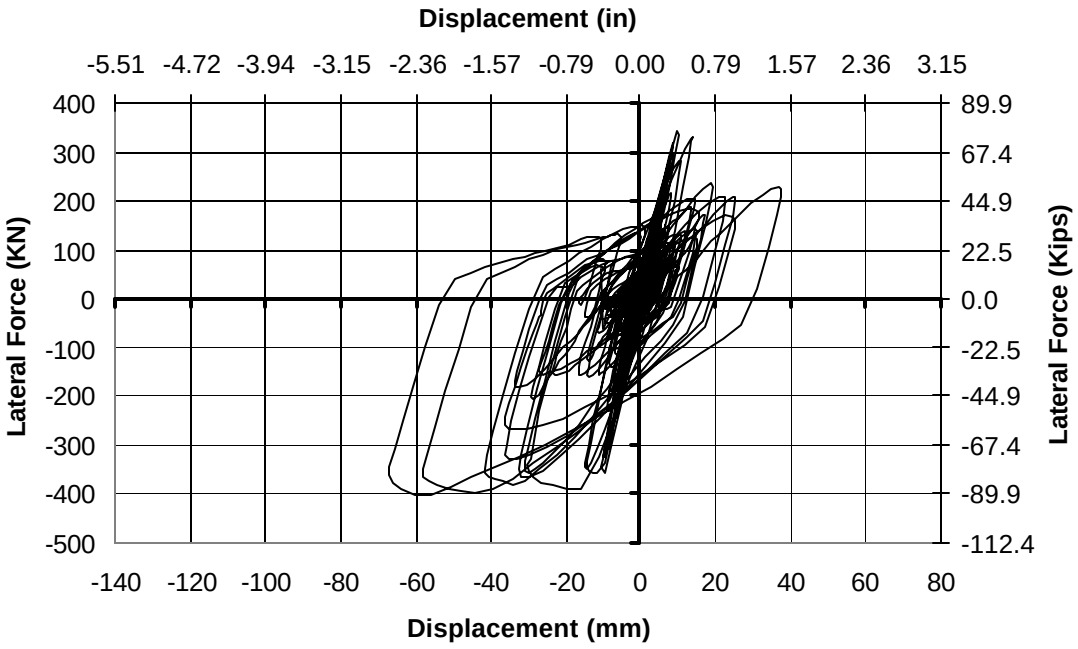

Figure 2-27 RC-Shake Force Displacement Hysteresis for THD-1 under Sylmar Motion

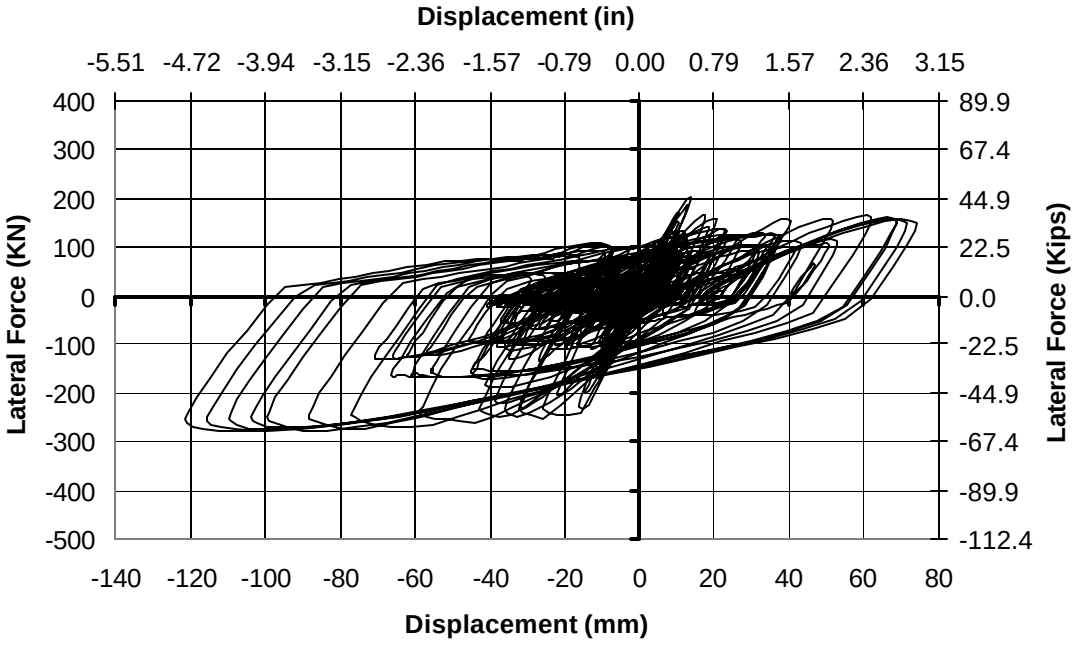

Figure 2-28 RC-Shake Force Displacement Hysteresis for THD-2 under Sylmar Motion

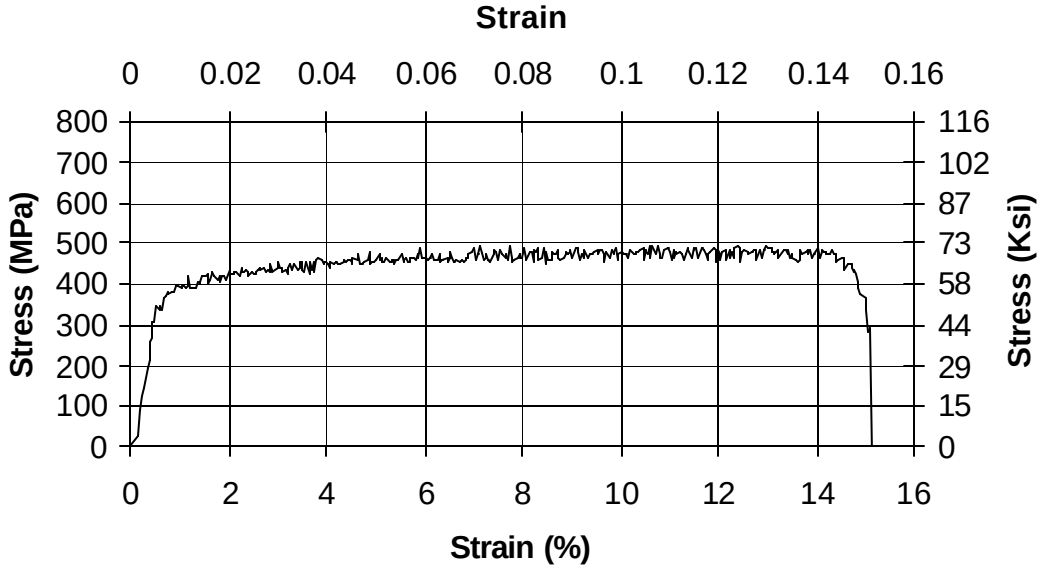

Figure 2-29 Stress-Strains for Sample Test W2.1 Smooth Wire

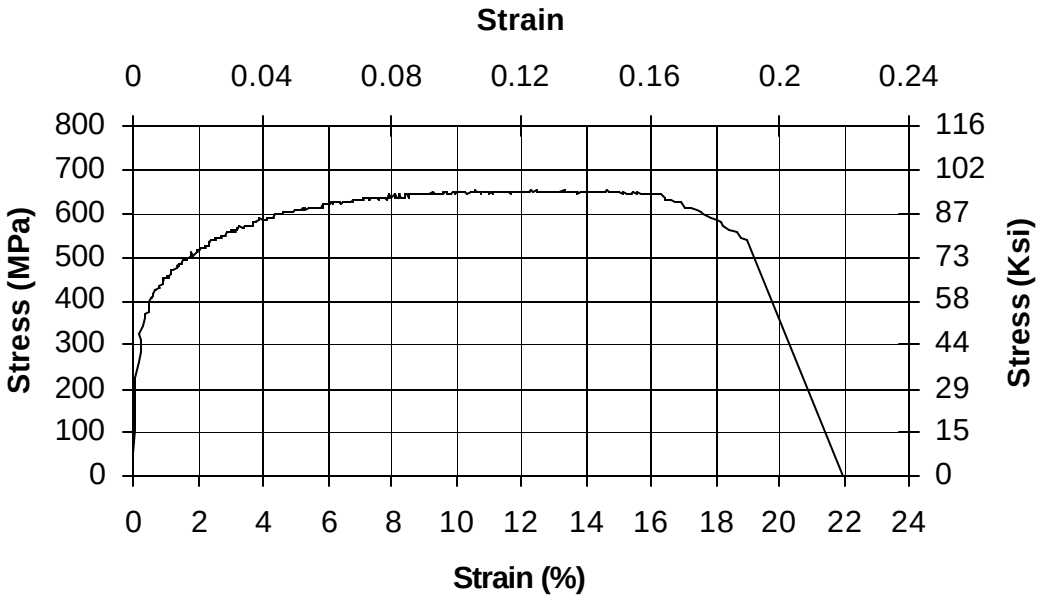

Figure 2-30 Stress-Strains for Sample Test No.3 Spiral Rebar

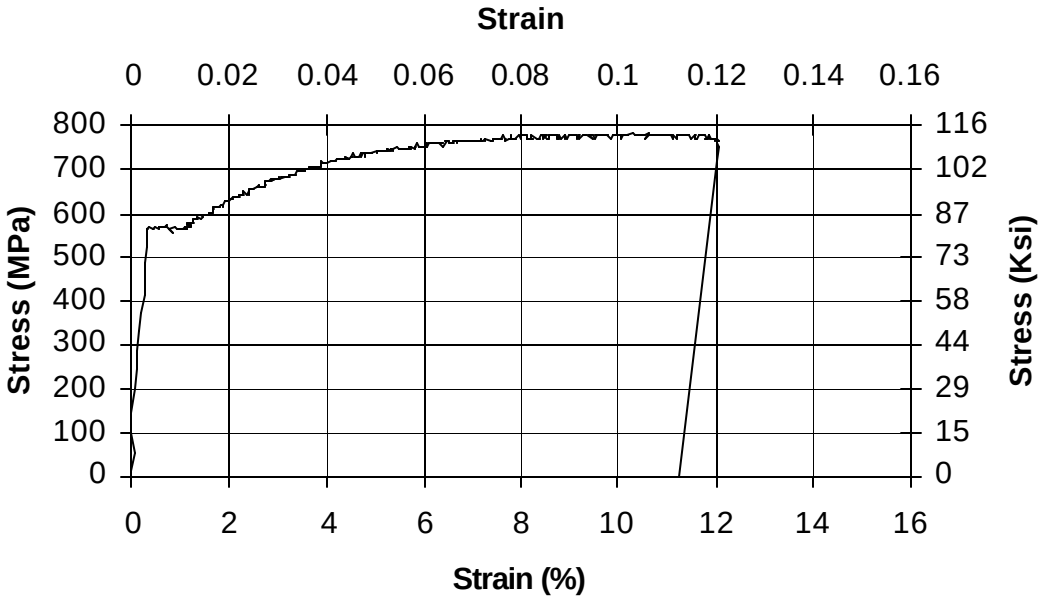

Figure 2-31 Stress-Strains for Sample Test No.3 Longitudinal Rebar

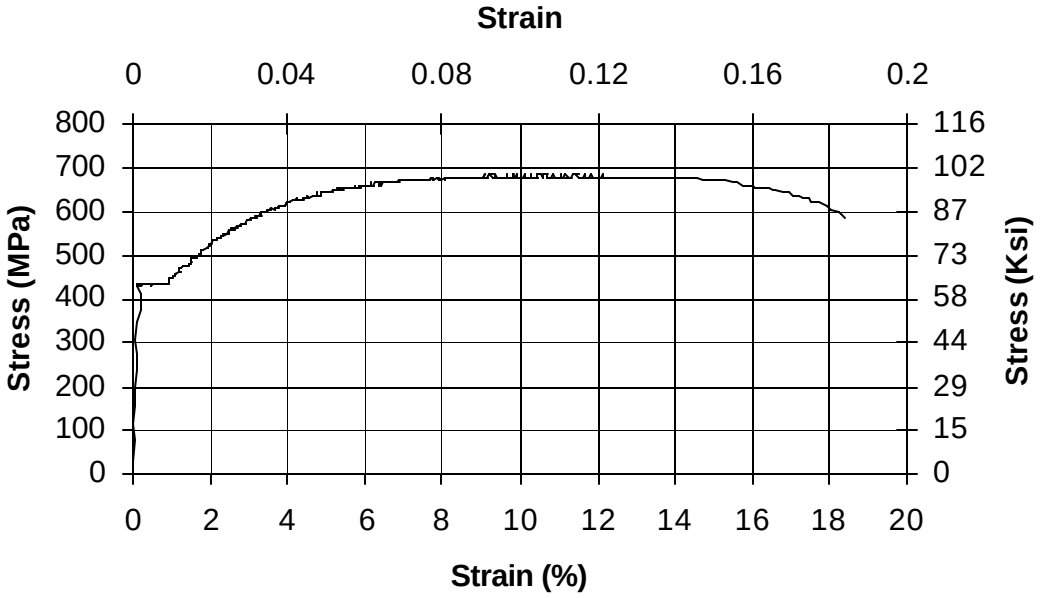

Figure 2-32 Stress-Strains for Sample Test No.4 Longitudinal Rebar

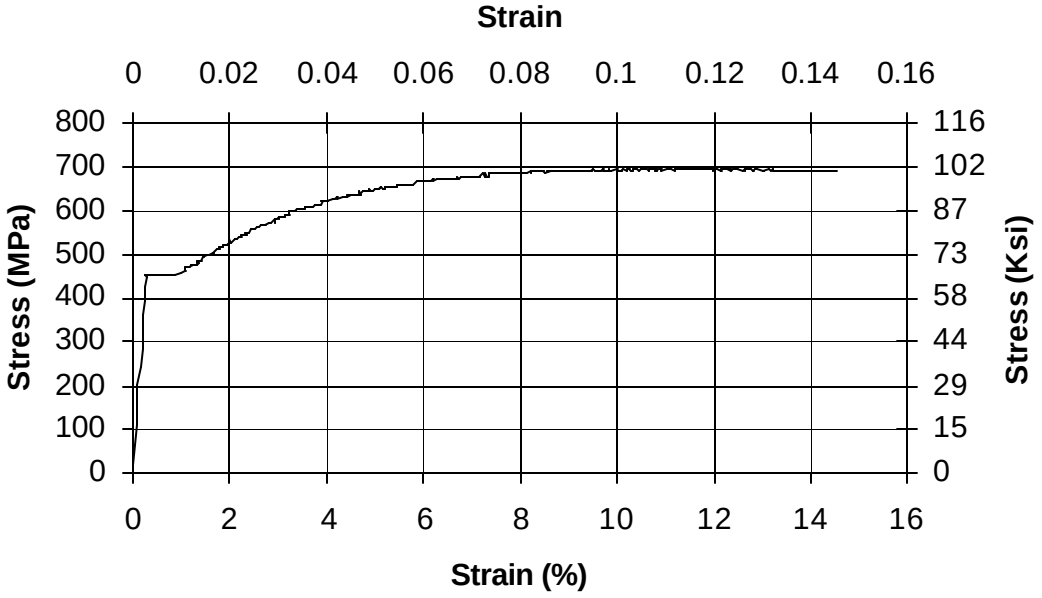

Figure 2-33 Stress-Strains for Sample Test No.5 Longitudinal Rebar

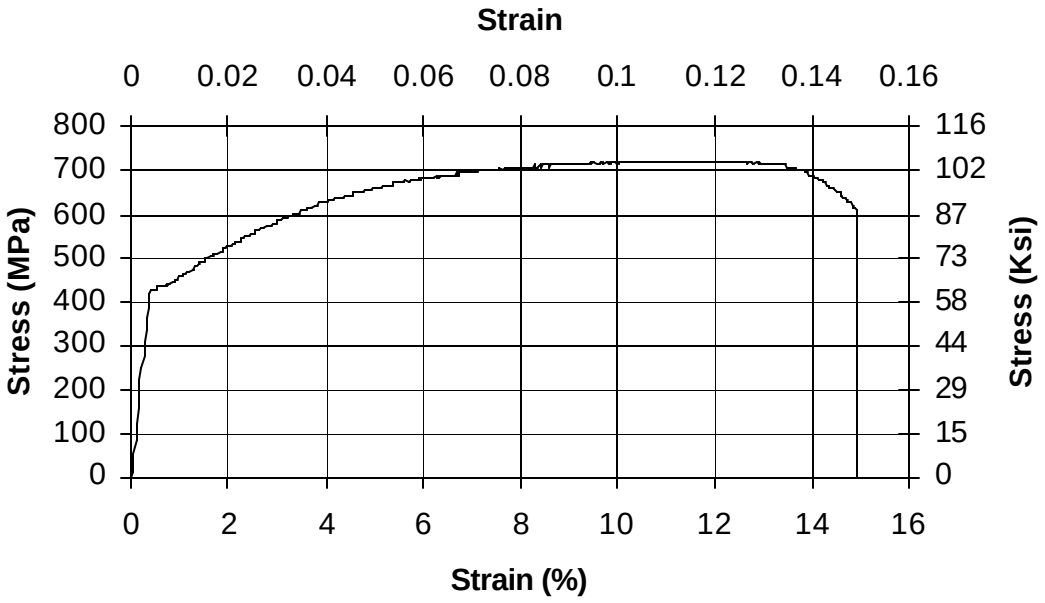

Figure 2-34 Stress-Strains for Sample Test No.7 Longitudinal Rebar

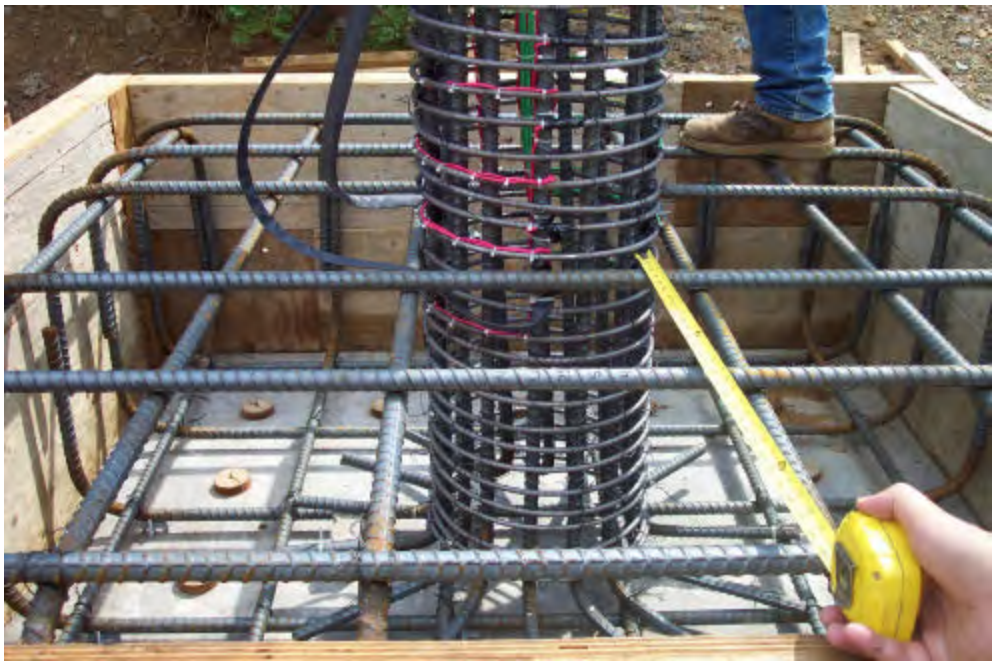

Figure 3-1 Footing Reinforcement Mats

Figure 3-2 Footing Ready for Casting

Figure 3-3 Column Form

Figure 3-4 Hinge Reinforcement

Figure 3-5 Specimen Head and Hinge Form

Figure 3-6 Specimen Form Removed

Figure 3-7 Side View of Setup

Figure 3-8 Test Setup of Specimen THD-1, THD-3, THD-5

Figure 3-9 Test Setup of Specimen THD-2

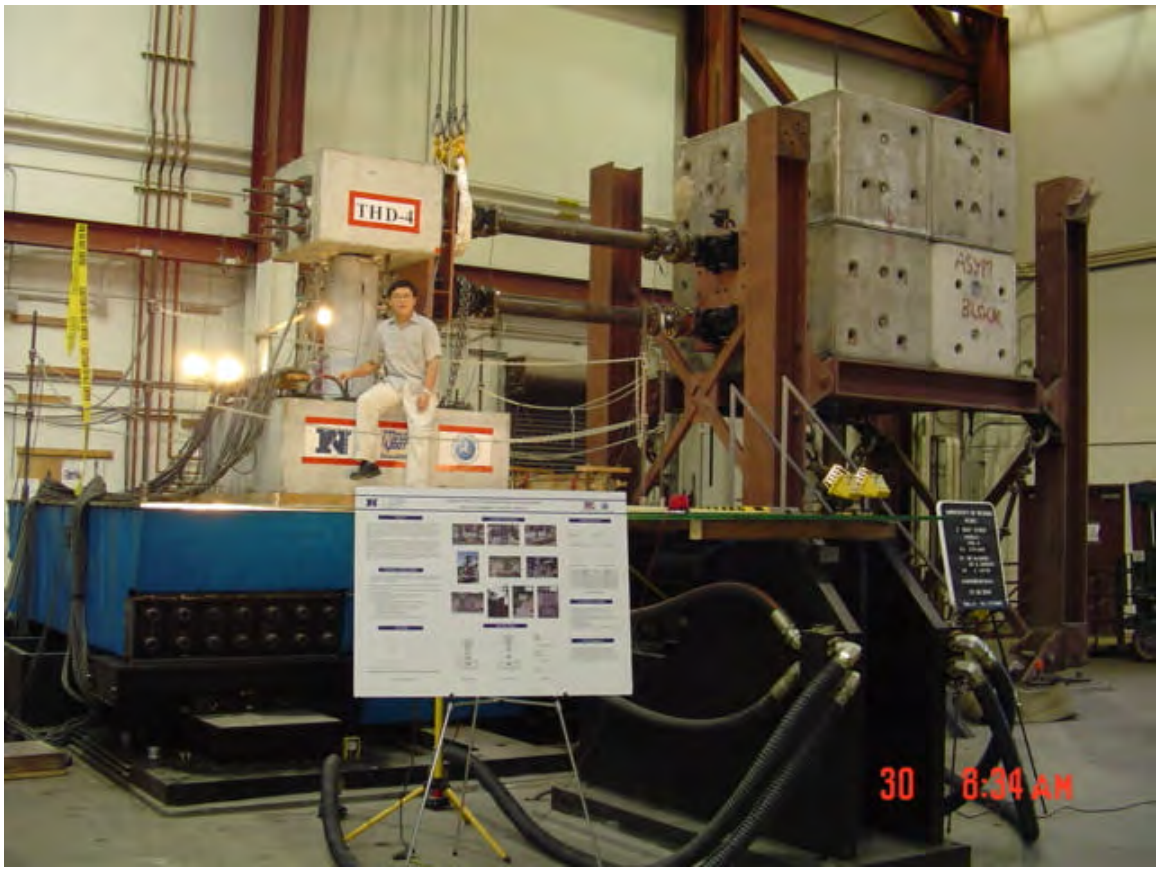

Figure 3-10 Test Setup of Specimen THD-4

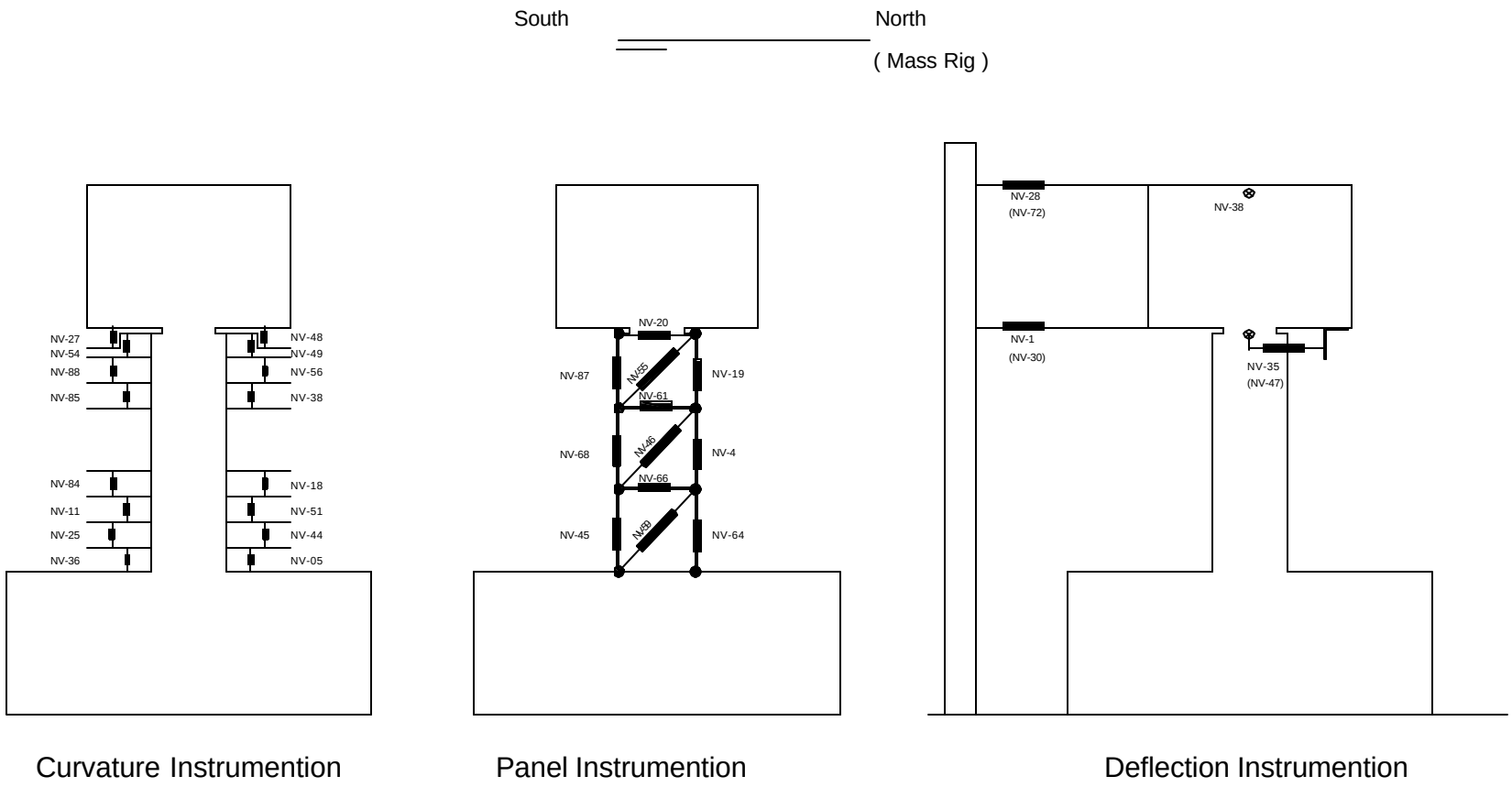

Figure 3-11 Transducer Instrumentation for Specimen THD-1

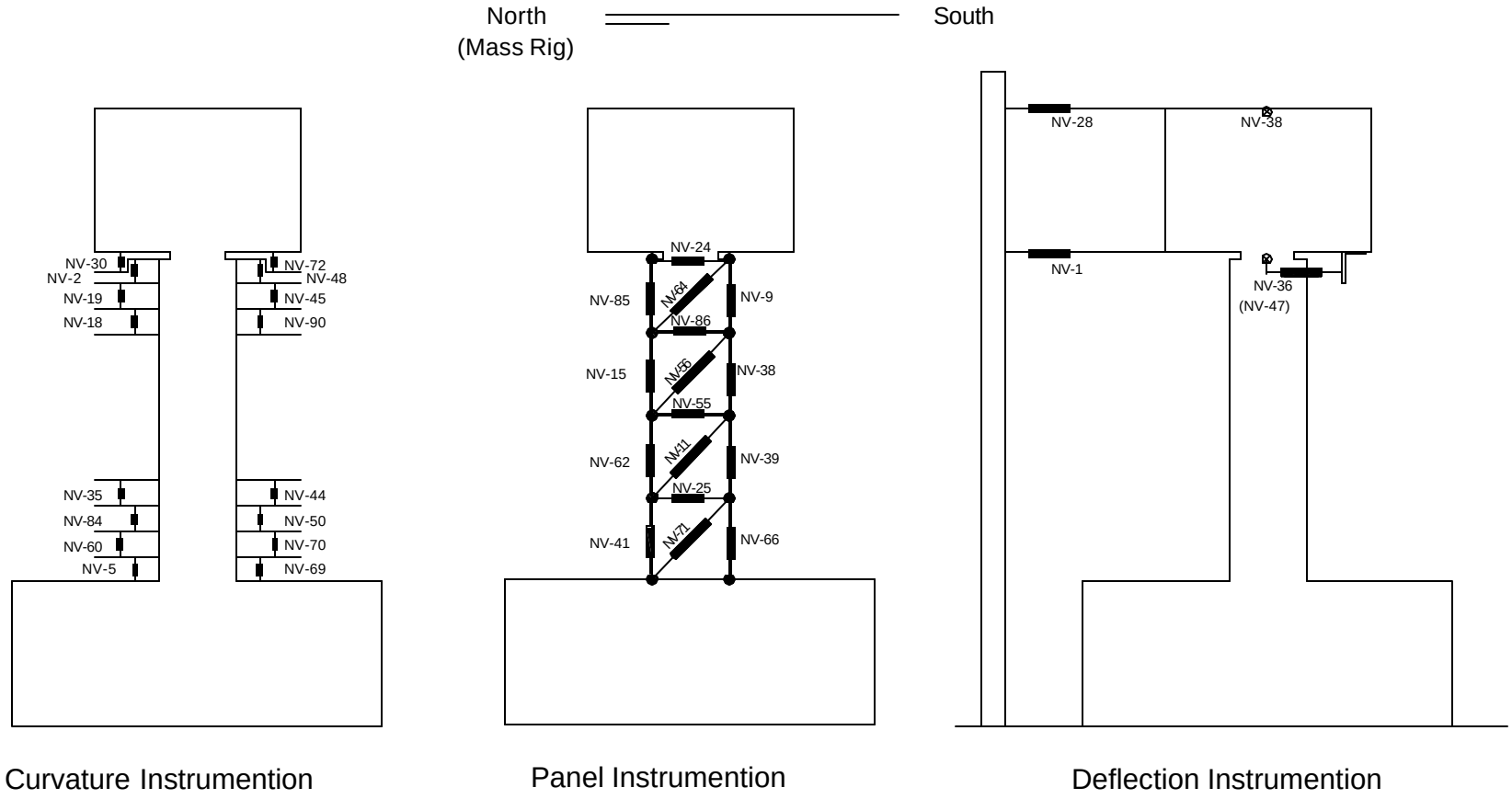

Figure 3-12 Transducer Instrumentation for Specimen THD-2

187

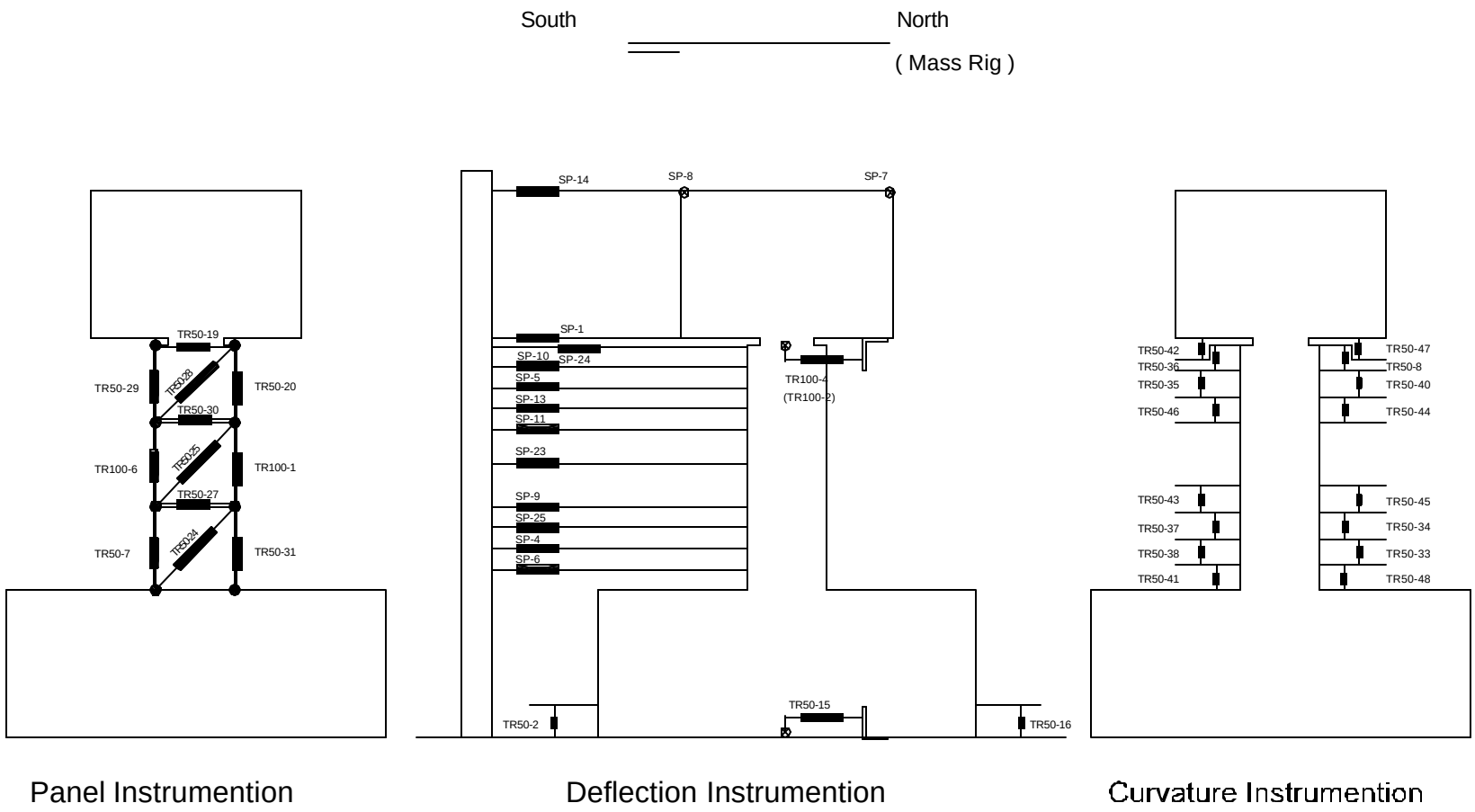

Figure 3-13 Transducer Instrumentation for Specimen THD-3

Figure 3-14 Transducer Instrumentation for Specimen THD-4

189

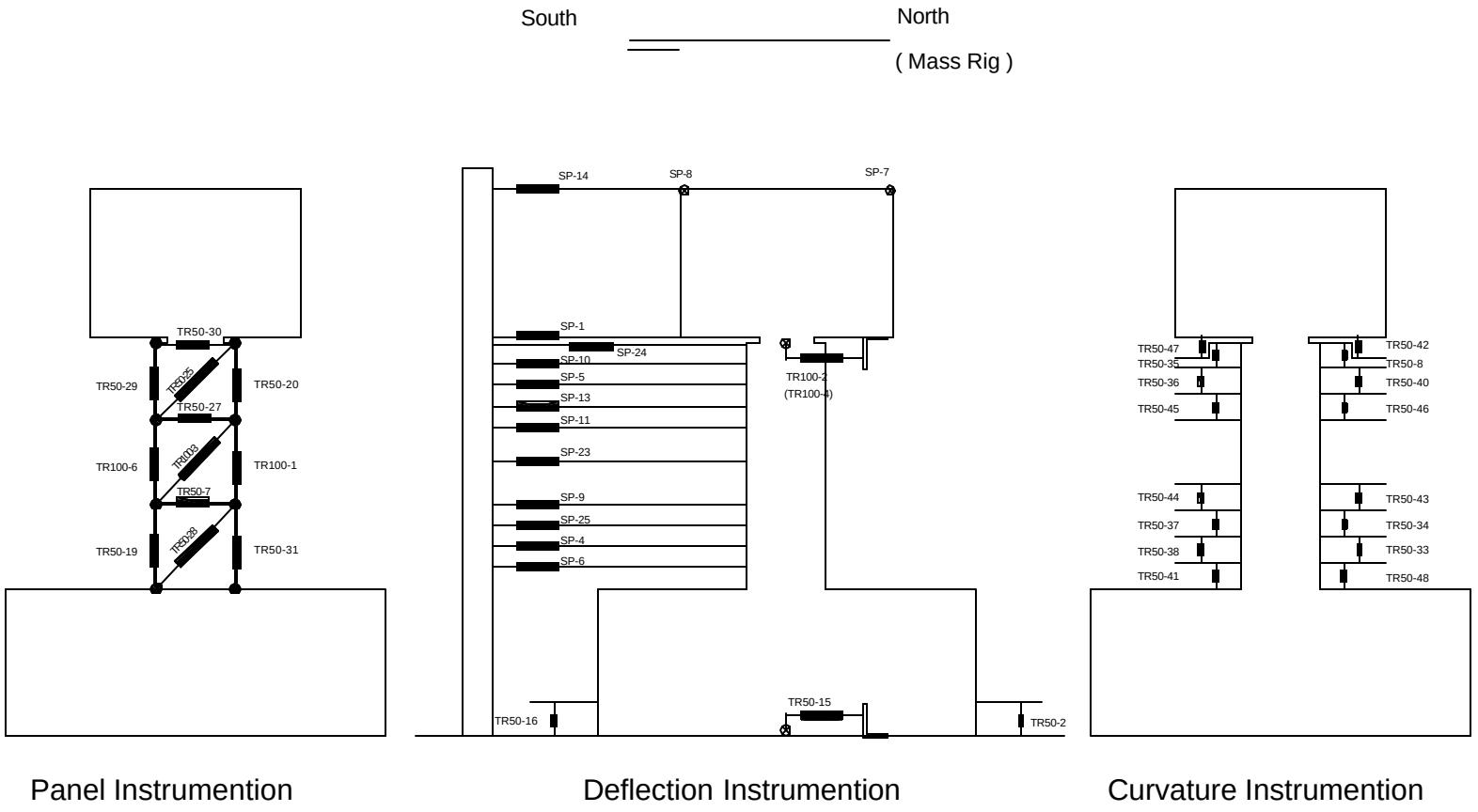

Figure 3-15 Transducer Instrumentation for Specimen THD-5

190

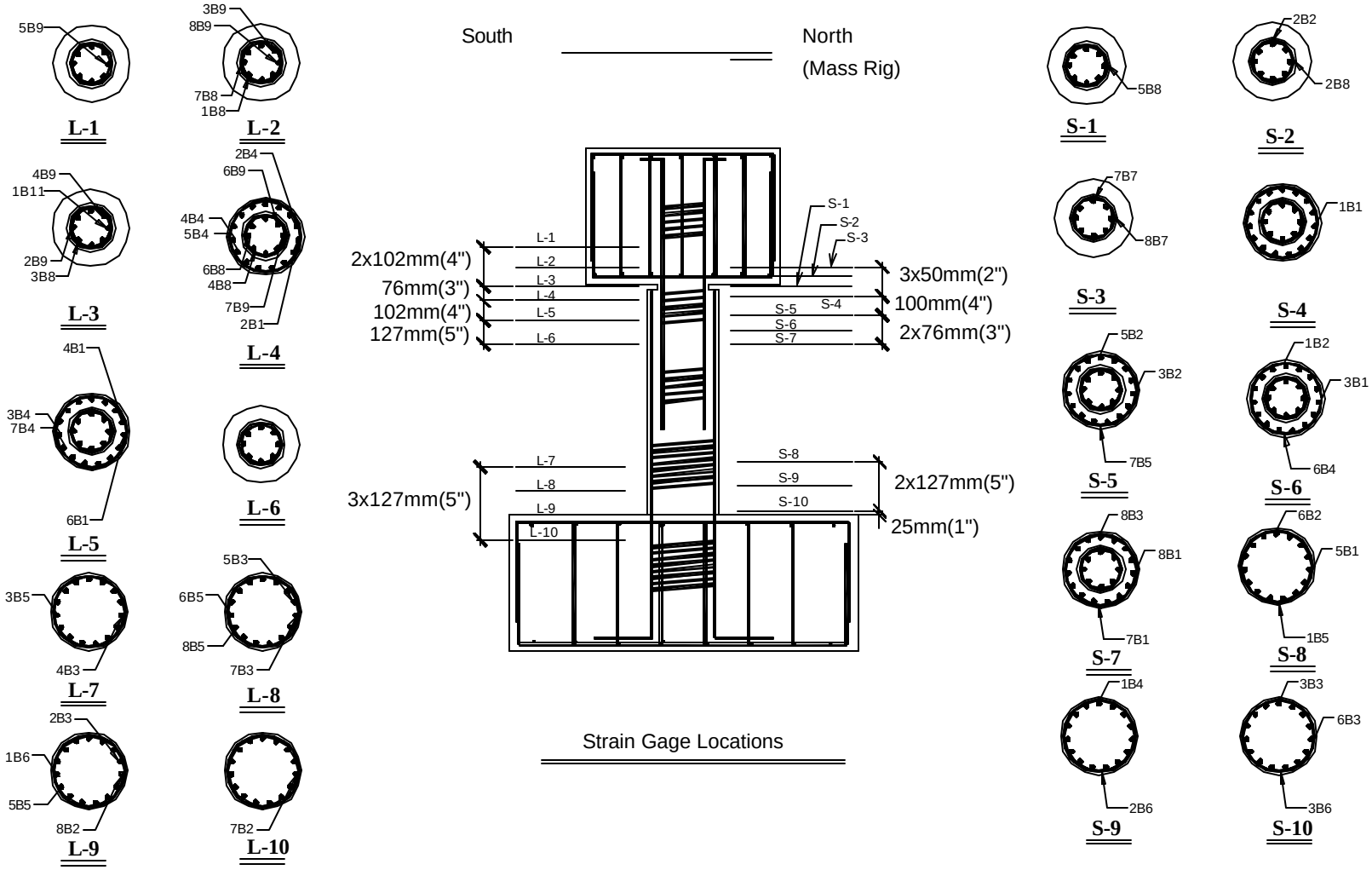

Figure 3-16 Strain Gauge Detail for Specimen THD-1

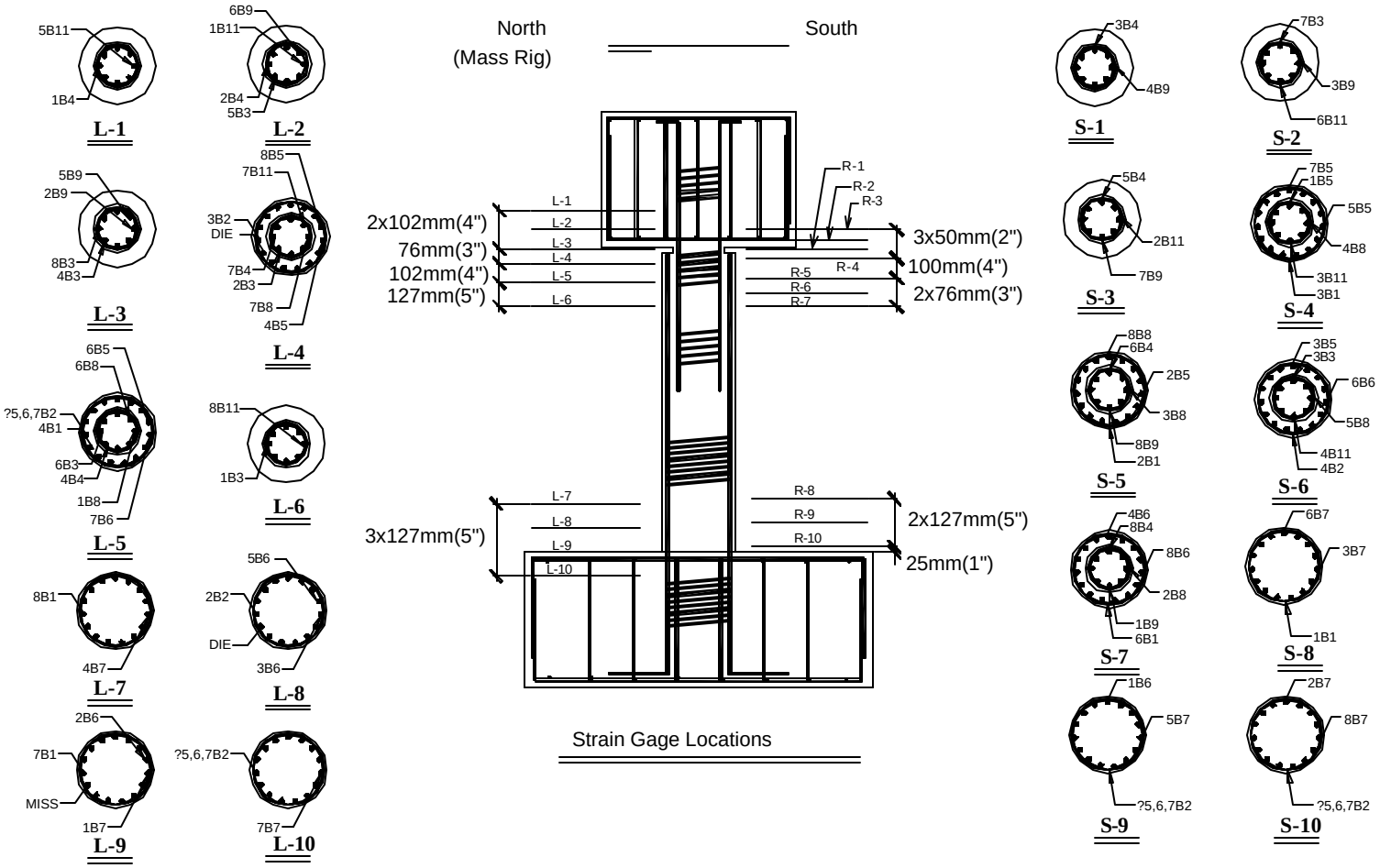

Figure 3-17 Strain Gauge Detail for Specimen THD-2

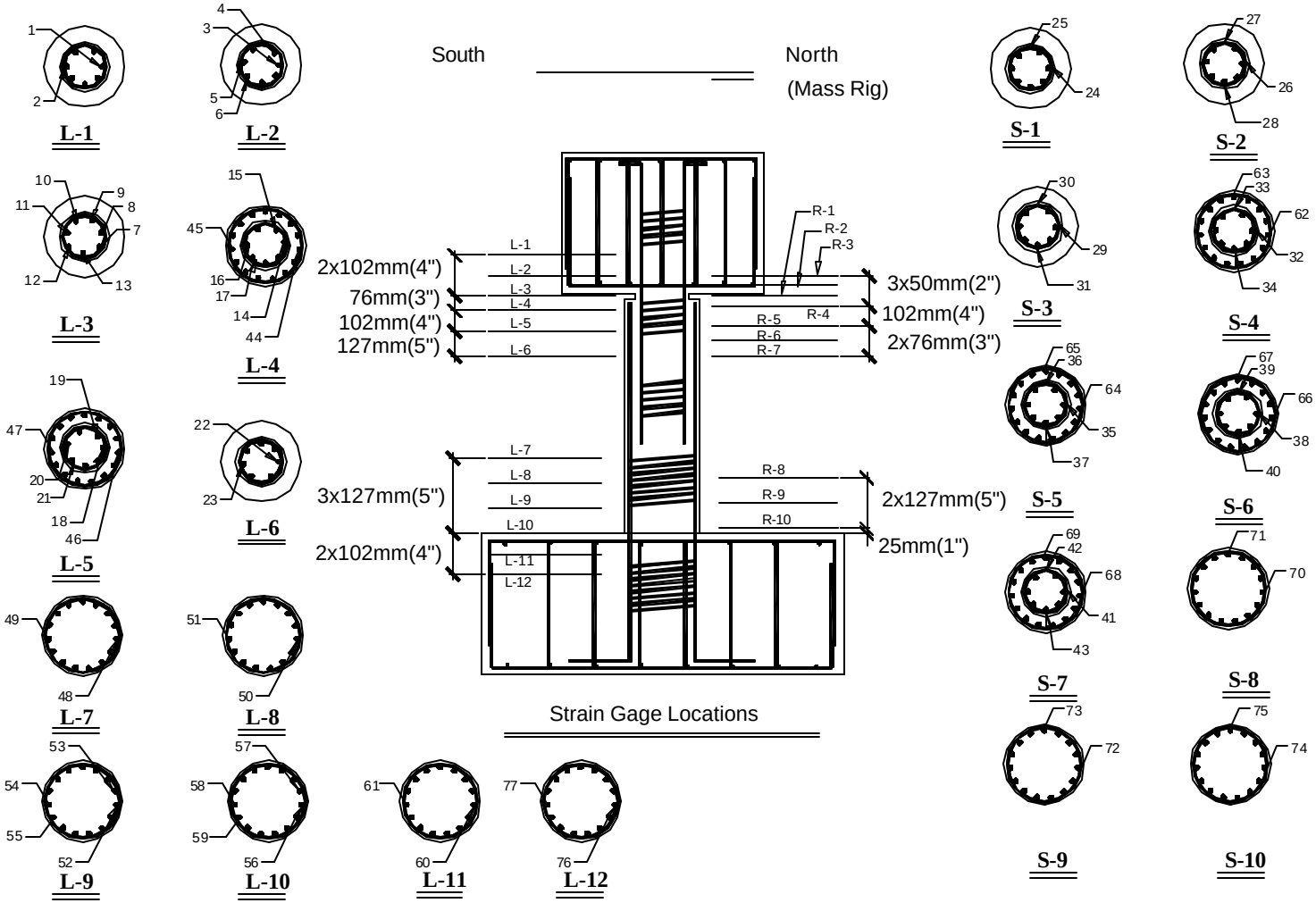

Figure 3-18 Strain Gauge Detail for Specimen THD-3

193

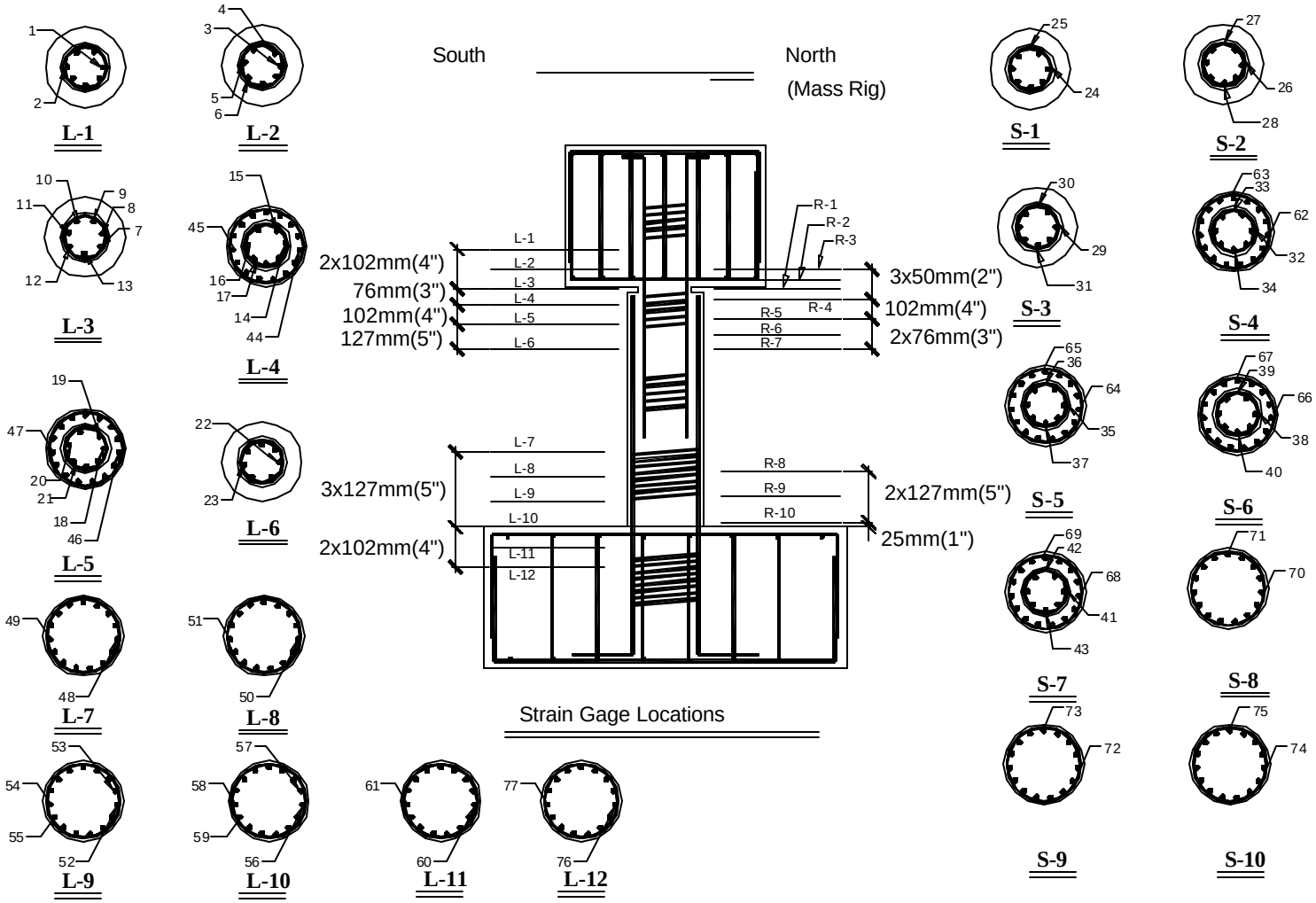

Figure 3-19 Strain Gauge Detail for Specimen THD-4

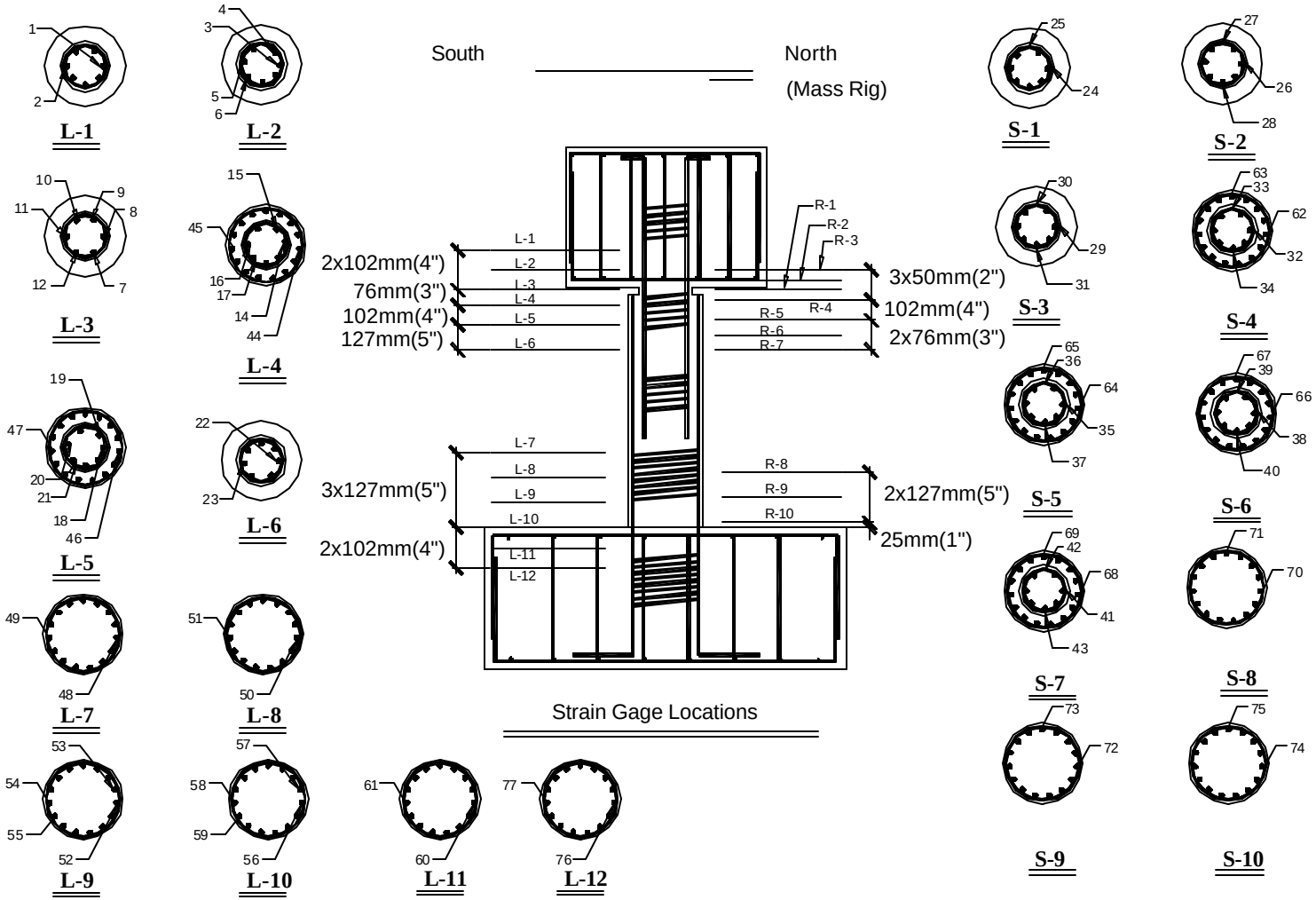

Figure 3-20 Strain Gauge Detail for Specimen THD-5

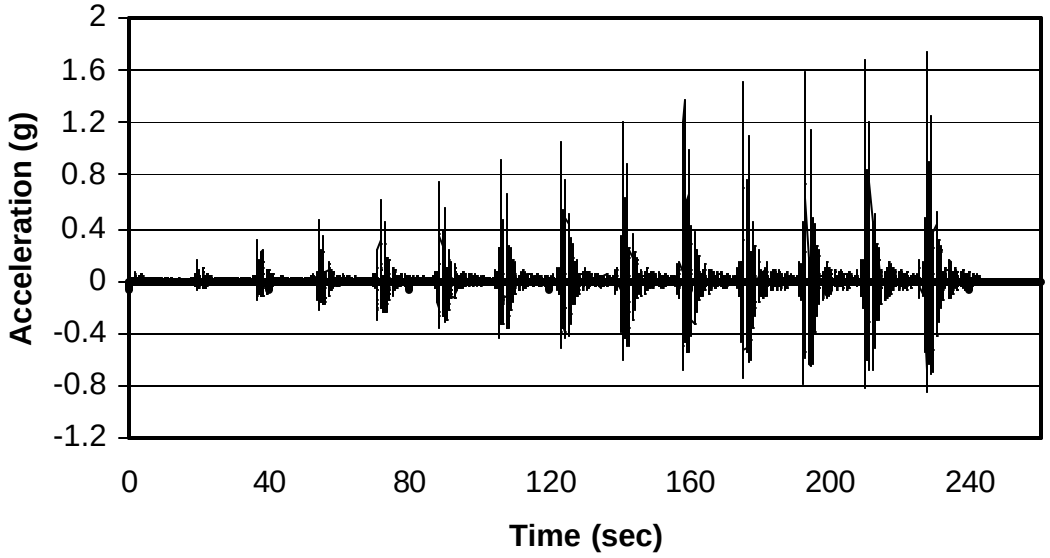

Figure 3-21 Typical Table Input Motion

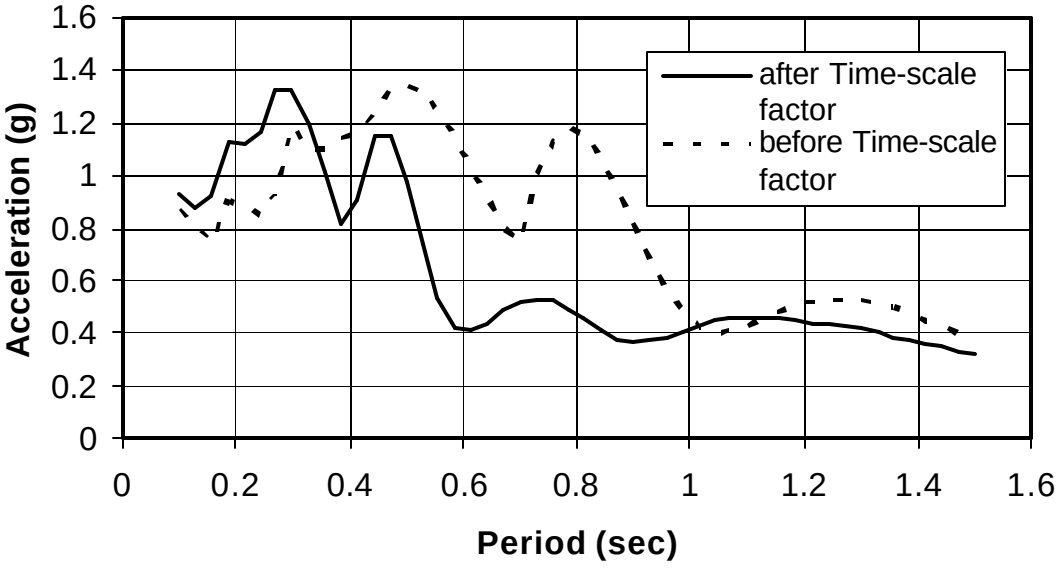

Figure 3-22 Sylmar Record Response Spectral Comparison

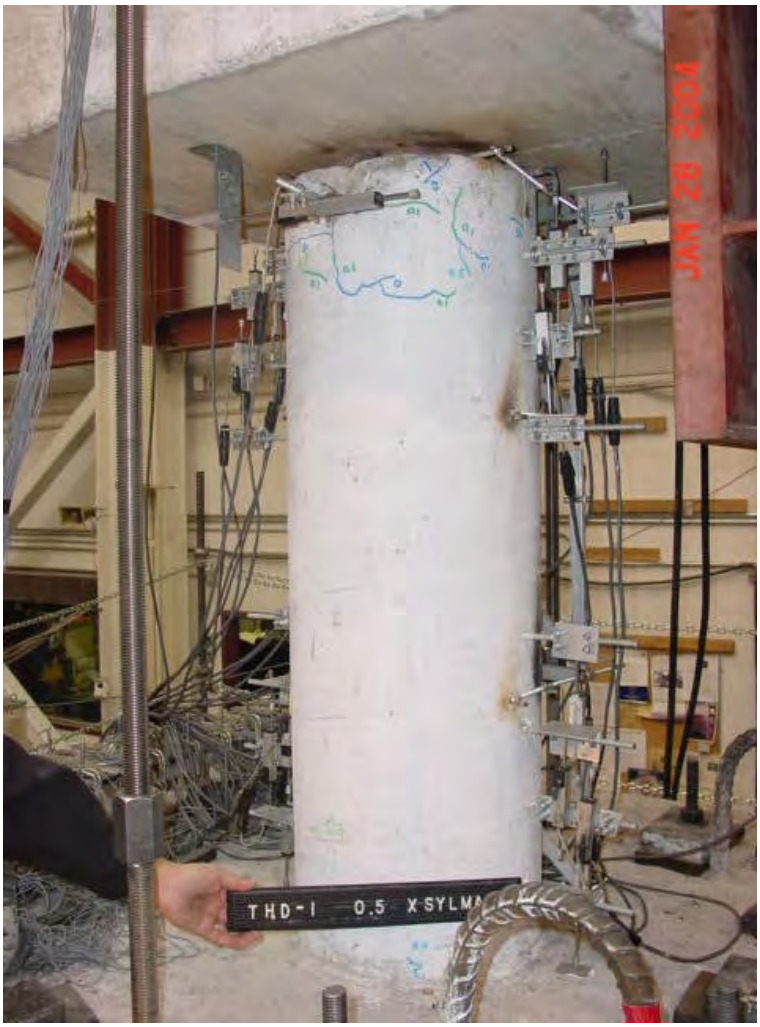

Figure 4-1 THD-1 at 0.5 x Sylmar

(a) Column Base

(b) Hinge Region

Figure 4-2 THD-1 at 1.25 x Sylmar

Figure 4-3 THD-1 at 1.5 x Sylmar

Figure 4-4 THD-1 at 2.25 x Sylmar

Figure 4-5 THD-1 at 2.875 x Sylmar (Final Run)

Figure 4-6 THD-2 at 0.75 x Sylmar

(a) Hinge Region

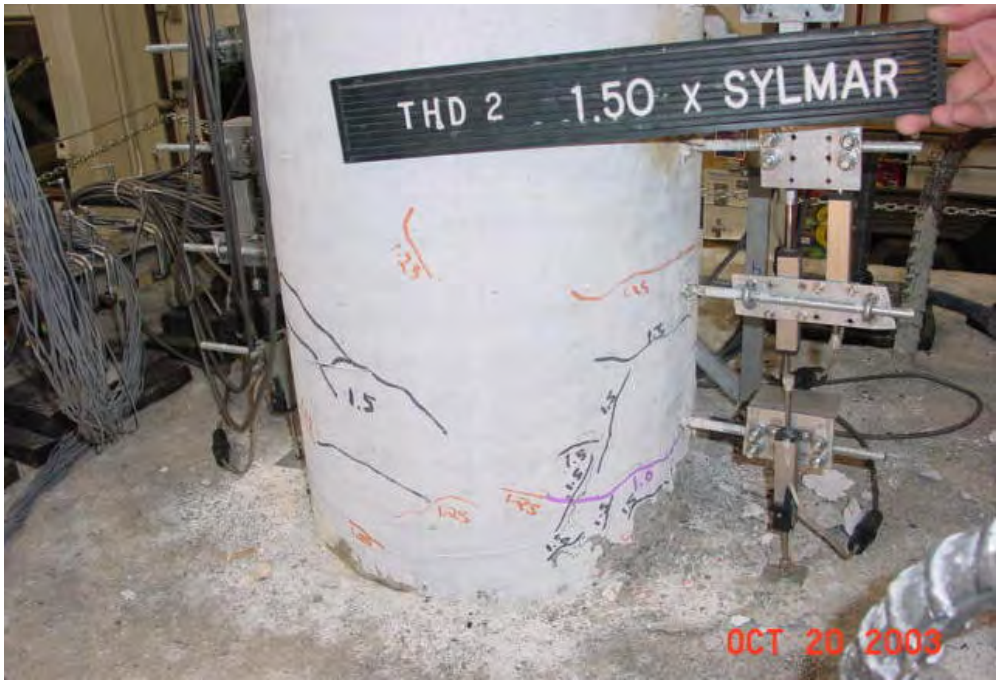

(b) Column Base

Figure 4-7 THD-2 at 1.5 x Sylmar

(a) Hinge Region

(b) Column Base

Figure 4-8 THD-2 at 2.0 x Sylmar

Figure 4-9 THD-2 at 2.25 x Sylmar

Figure 4-10 THD-2 at 2.5 x Sylmar

Figure 4-11 THD-2 at 2.625 x Sylmar

Figure 4-12 THD-3 at 0.75 x Sylmar

(a) Hinge Region

(b) Column Base

Figure 4-13 THD-3 at 1.25 x Sylmar

Figure 4-14 THD-3 at 1.75 x Sylmar

Figure 4-15 THD-3 at 2.25 x Sylmar

(a) Hinge Region

(b) Column Base

Figure 4-16 THD-3 at 2.5 x Sylmar (Final Run)

Figure 4-17 THD-4 at 0.5 x Sylmar

Figure 4-18 THD-4 at 0.75 x Sylmar

Figure 4-19 THD-4 at 1.25 x Sylmar (Final Run)

(a) Hinge Region

(b) Column Base

Figure 4-20 THD-5 at 0.5 x Sylmar

Figure 4-21 THD-5 at 1.5 x Sylmar

Figure 4-22 THD-5 at 1.75 x Sylmar

Figure 4-23 THD-5 at 2.0 x Sylmar

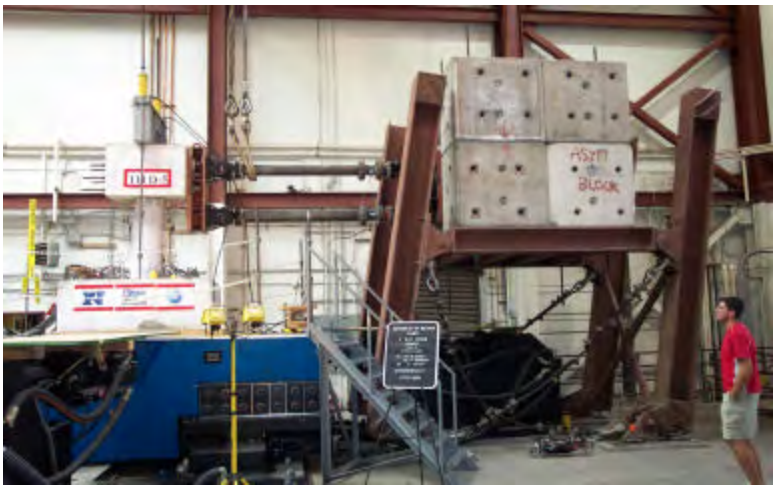

(a) Over View

(b) Hinge Region

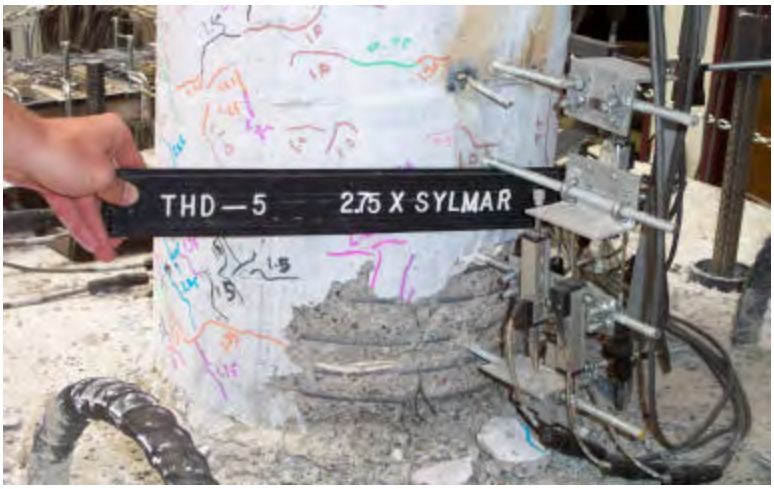

(c) Column Base

Figure 4-24 THD-5 at 2.75 x Sylmar

(a) Hinge Region

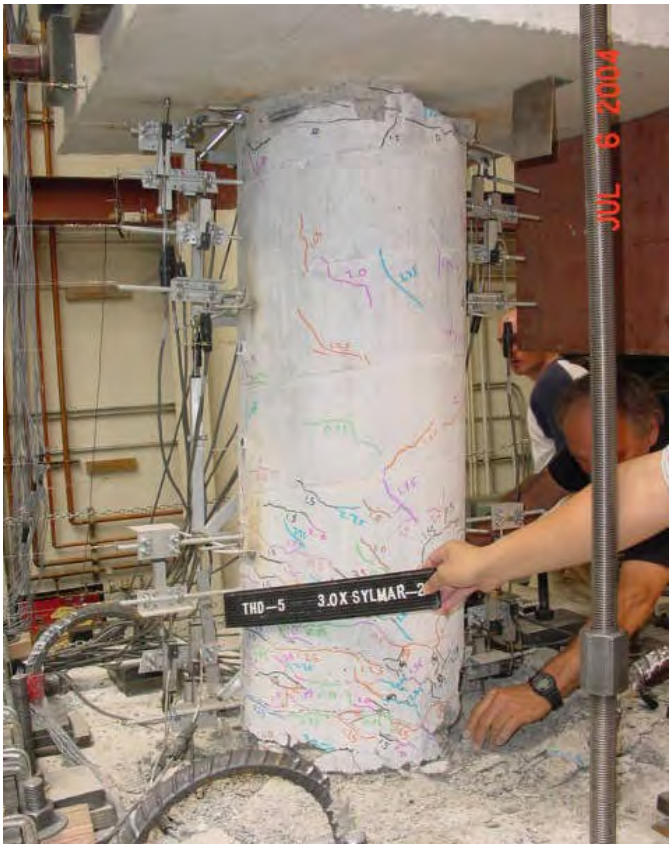

(a) Column Base

Figure 4-25 THD-5 at 3.0 x Sylmar (Final Run)

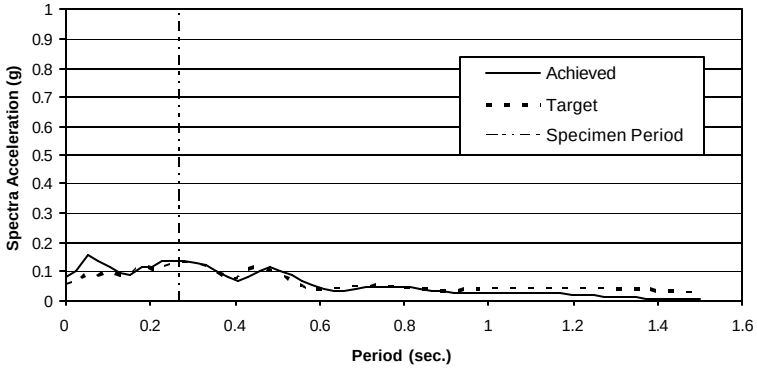

Figure 4-26 Response Spectra of THD-1 at 0.1 x Sylmar

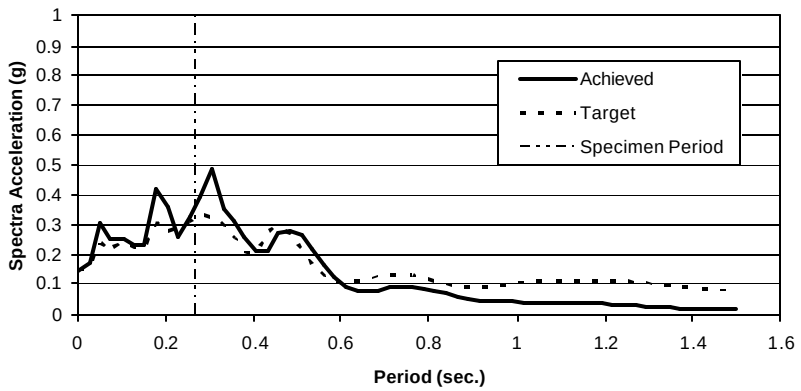

Figure 4-27 Response Spectra of THD-1 at 0.25 x Sylmar

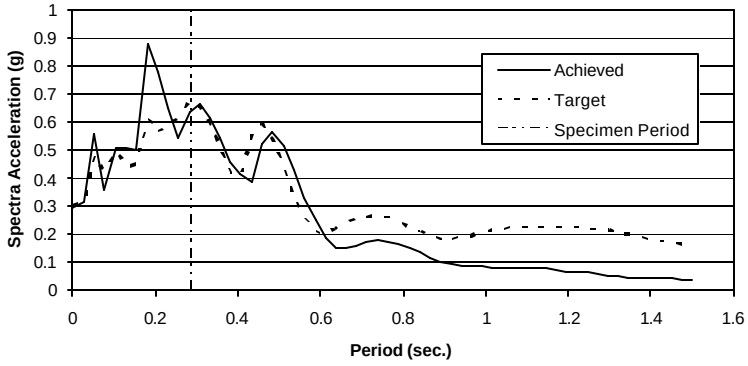

Figure 4-28 Response Spectra of THD-1 at 0.5 x Sylmar

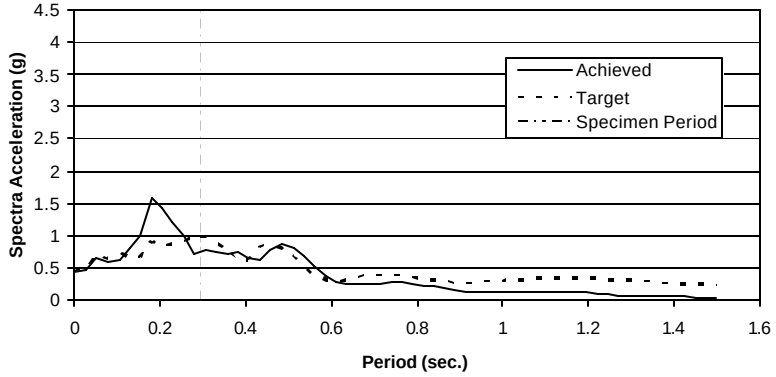

Figure 4-29 Response Spectra of THD-1 at 0.75 x Sylmar

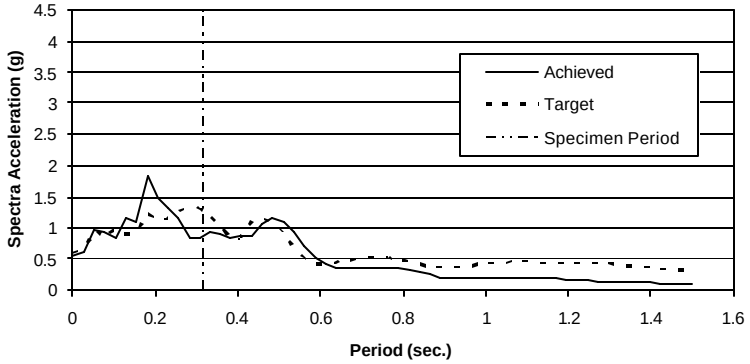

Figure 4-30 Response Spectra of THD-1 at 1.0 x Sylmar

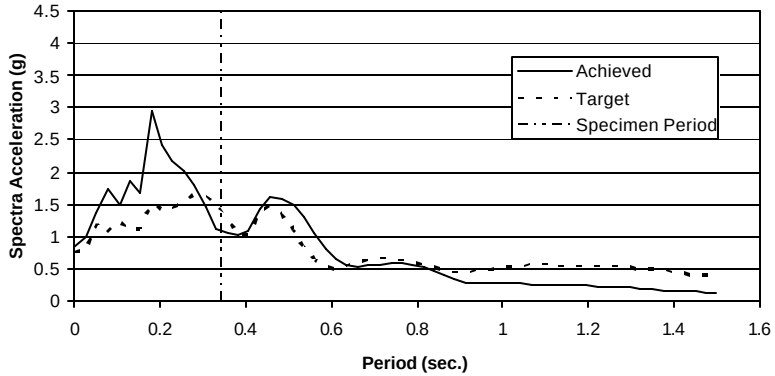

Figure 4-31 Response Spectra of THD-1 at 1.25 x Sylmar

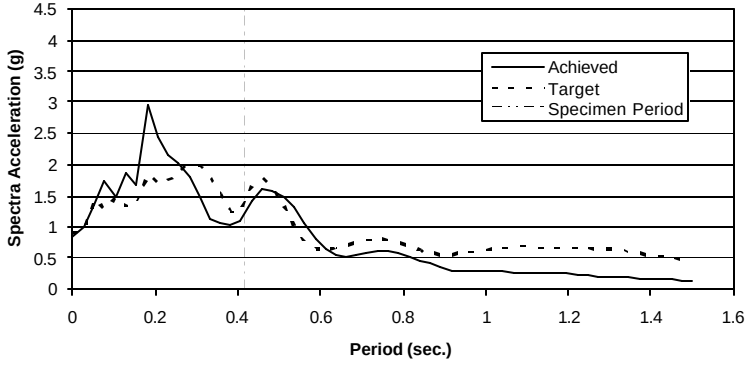

Figure 4-32 Response Spectra of THD-1 at 1.5 x Sylmar

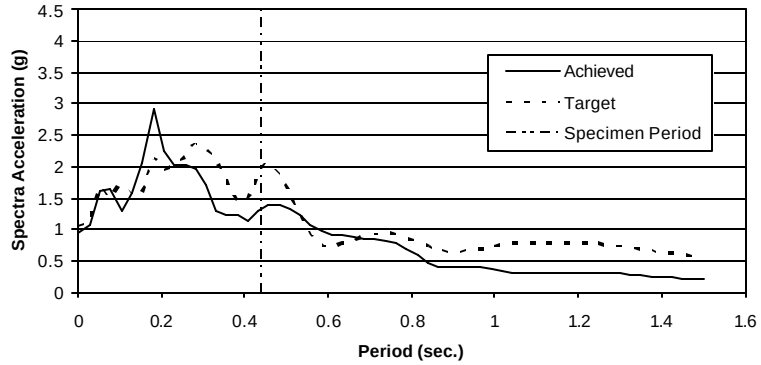

Figure 4-33 Response Spectra of THD-1 at 1.75 x Sylmar

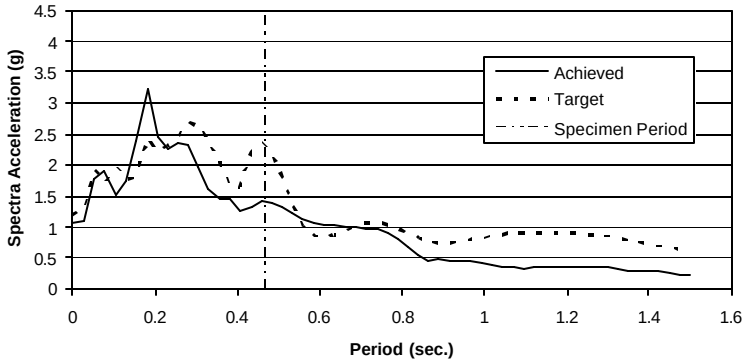

Figure 4-34 Response Spectra of THD-1 at 2.0 x Sylmar

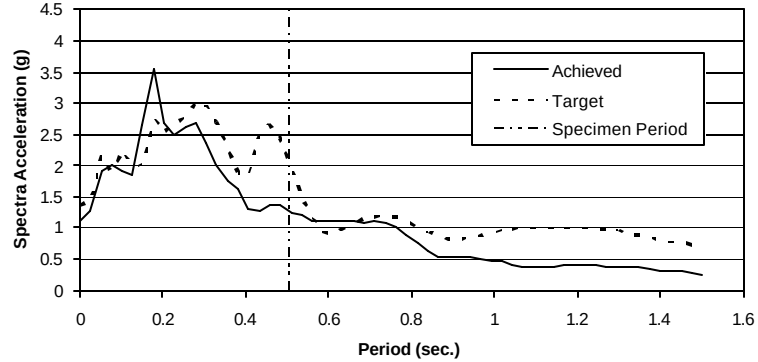

Figure 4-35 Response Spectra of THD-1 at 2.25 x Sylmar

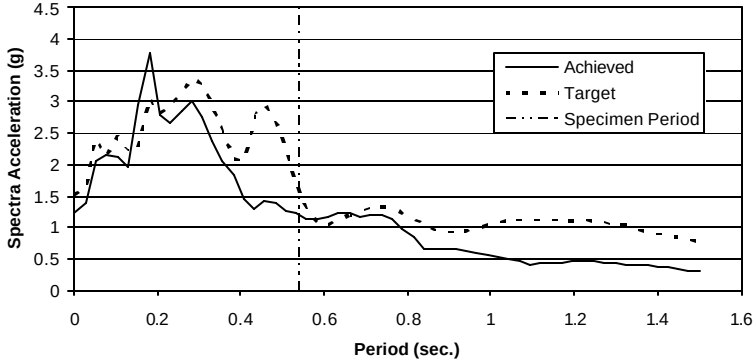

Figure 4-36 Response Spectra of THD-1 at 2.5 x Sylmar

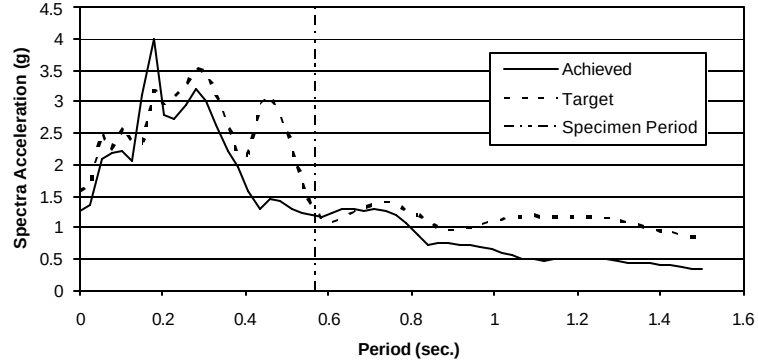

Figure 4-37 Response Spectra of THD-1 at 2.625 x Sylmar

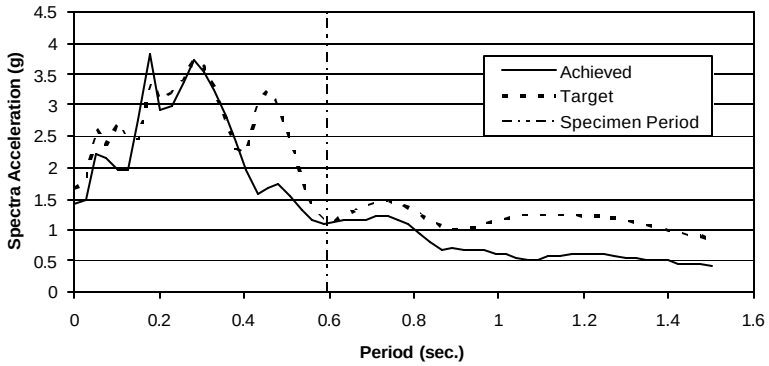

Figure 4-38 Response Spectra of THD-1 at 2.75 x Sylmar

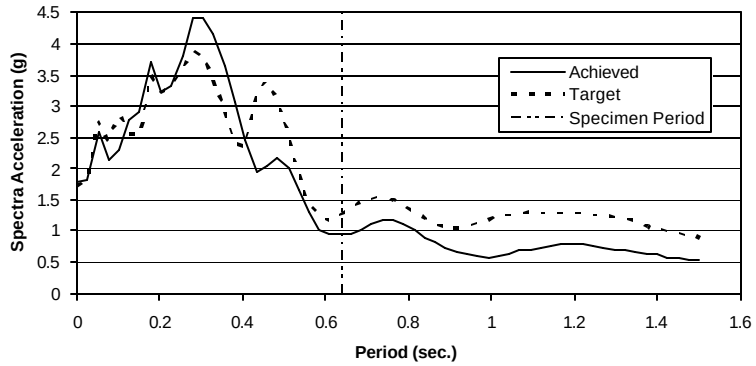

Figure 4-39 Response Spectra of THD-1 at 2.875 x Sylmar

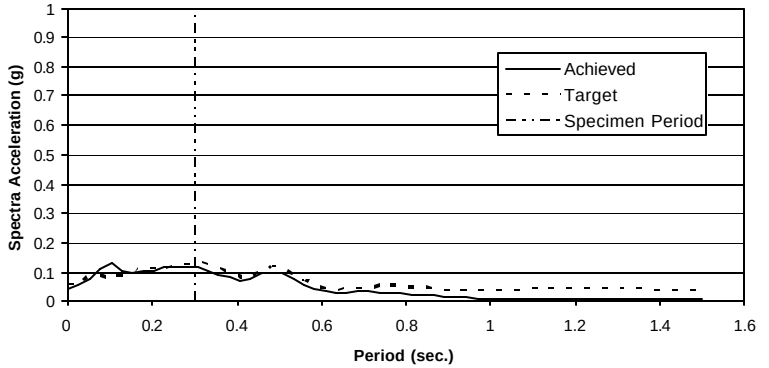

Figure 4-40 Response Spectra of THD-2 at 0.1 x Sylmar

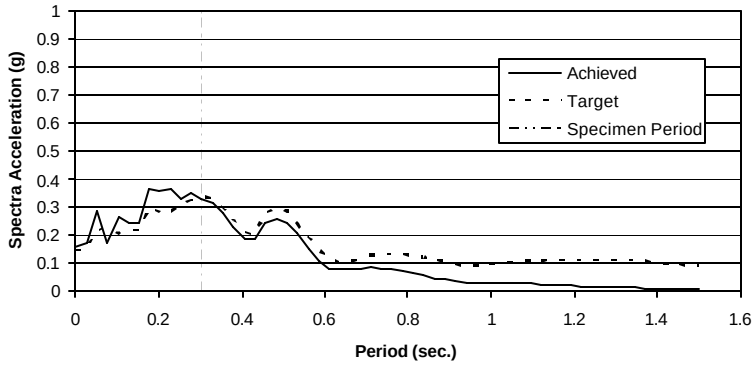

Figure 4-41 Response Spectra of THD-2 at 0.25 x Sylmar

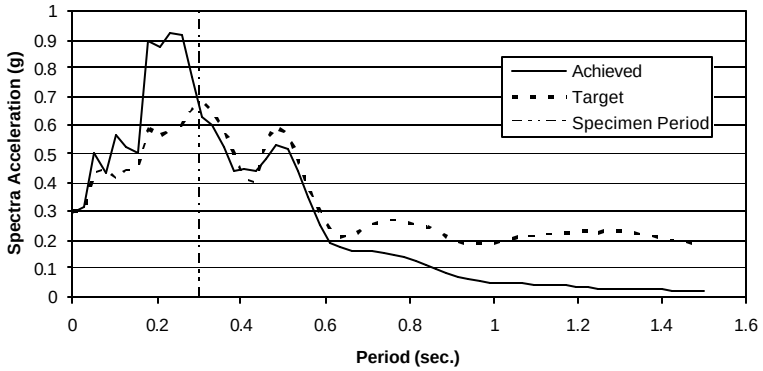

Figure 4-42 Response Spectra of THD-2 at 0.5 x Sylmar

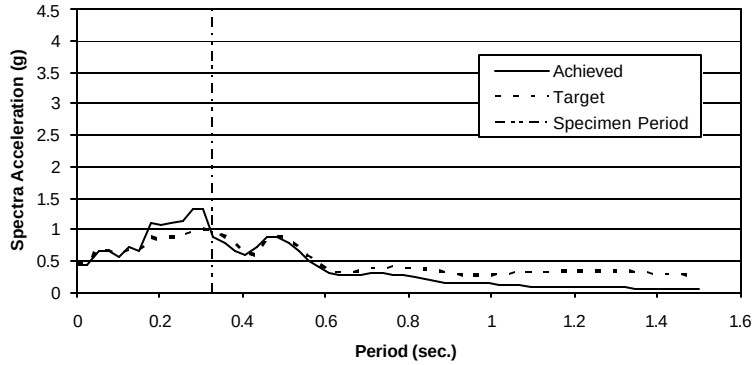

Figure 4-43 Response Spectra of THD-2 at 0.75 x Sylmar

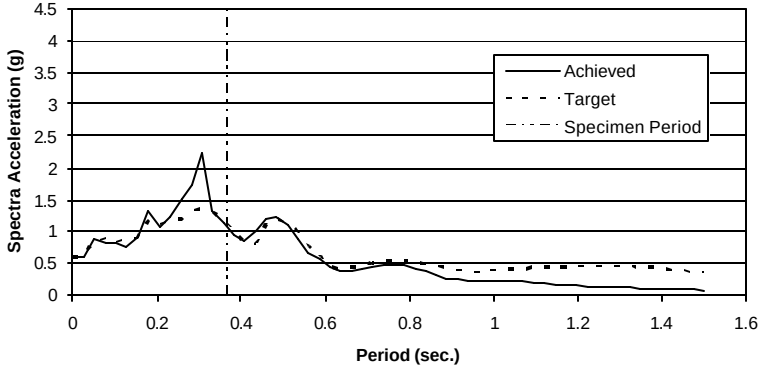

Figure 4-44 Response Spectra of THD-2 at 1.0 x Sylmar

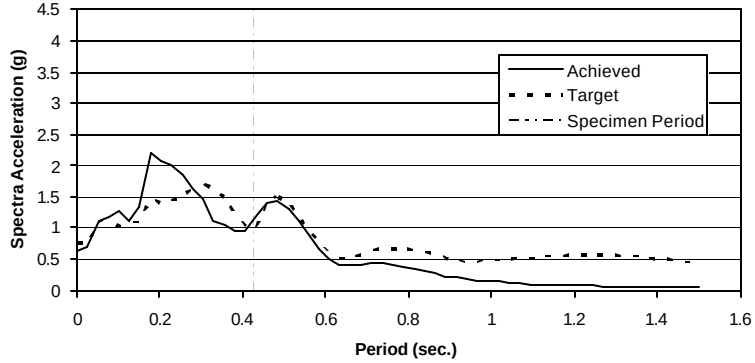

Figure 4-45 Response Spectra of THD-2 at 1.25 x Sylmar

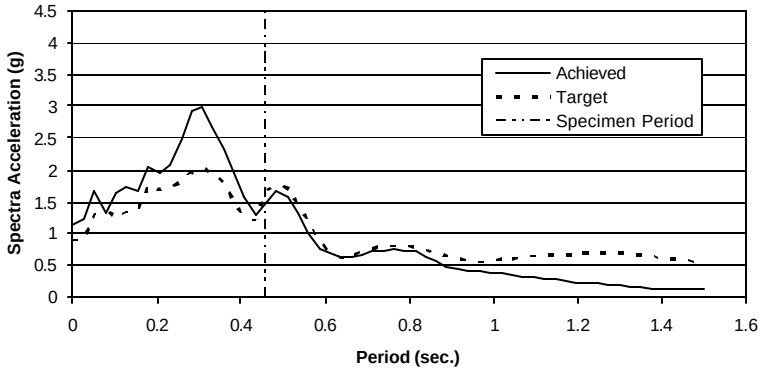

Figure 4-46 Response Spectra of THD-2 at 1.5 x Sylmar

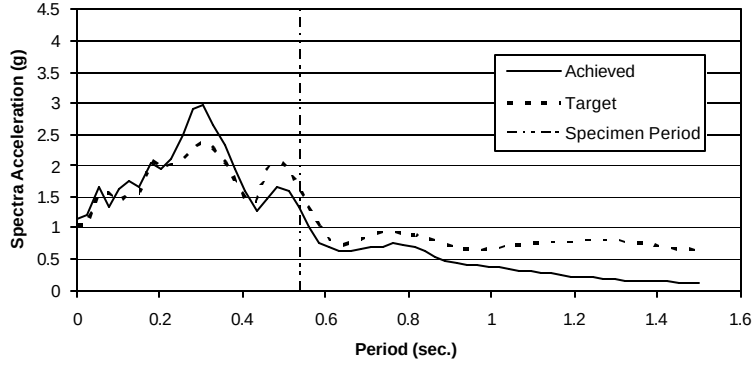

Figure 4-47 Response Spectra of THD-2 at 1.75 x Sylmar

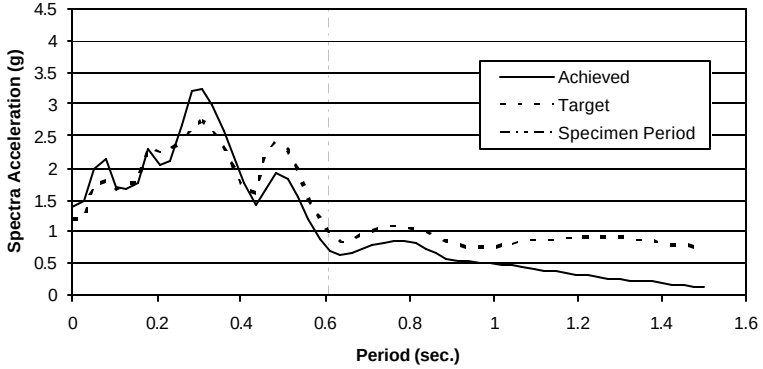

Figure 4-48 Response Spectra of THD-2 at 2.0 x Sylmar

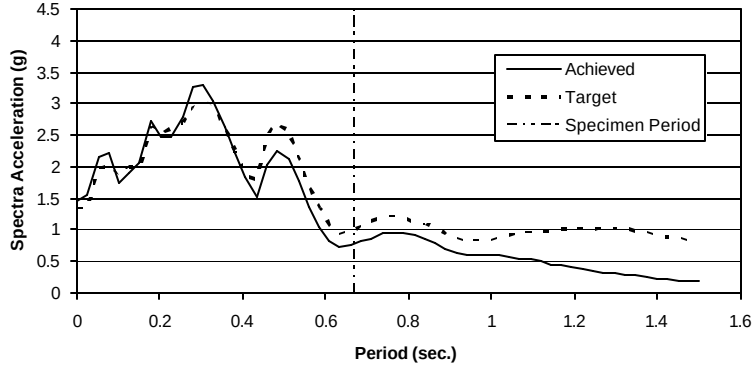

Figure 4-49 Response Spectra of THD-2 at 2.25 x Sylmar

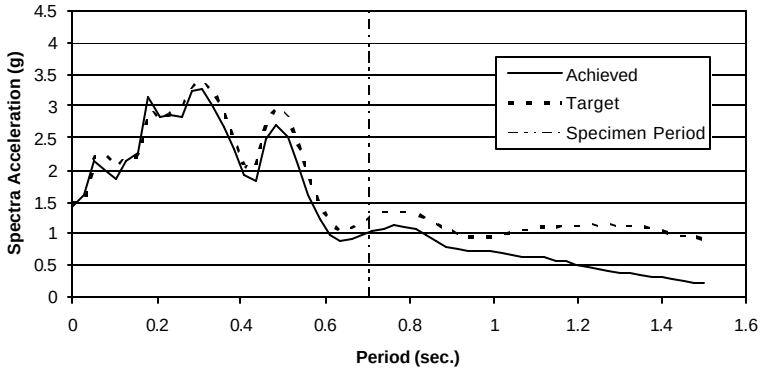

Figure 4-50 Response Spectra of THD-2 at 2.5 x Sylmar

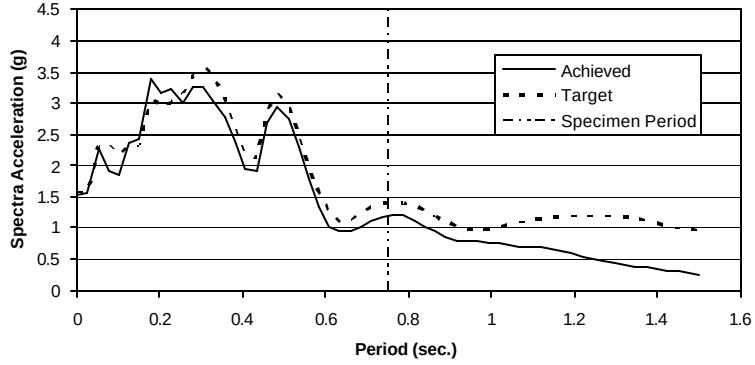

Figure 4-51 Response Spectra of THD-2 at 2.625 x Sylmar

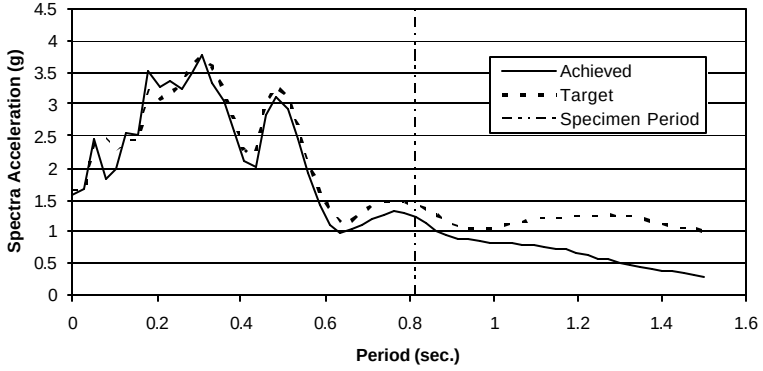

Figure 4-52 Response Spectra of THD-2 at 2.75 x Sylmar

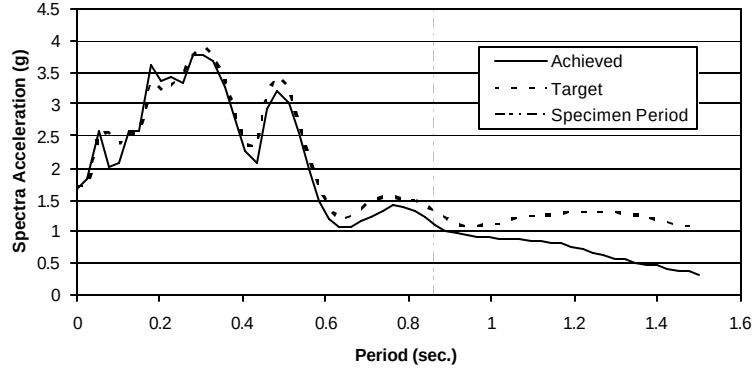

Figure 4-53 Response Spectra of THD-2 at 2.875 x Sylmar

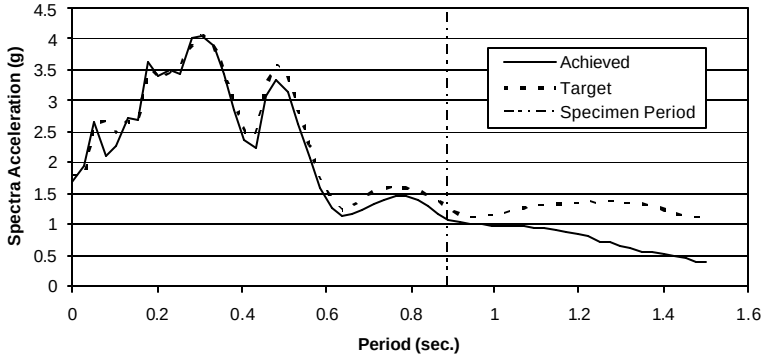

Figure 4-54 Response Spectra of THD-2 at 3.0 x Sylmar

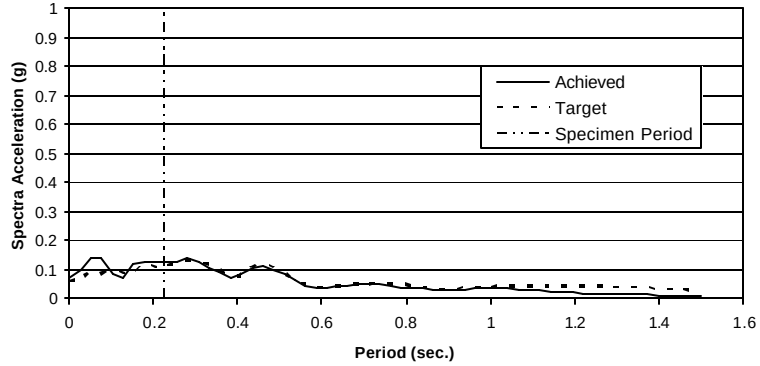

Figure 4-55 Response Spectra of THD-3 at 0.1 x Sylmar

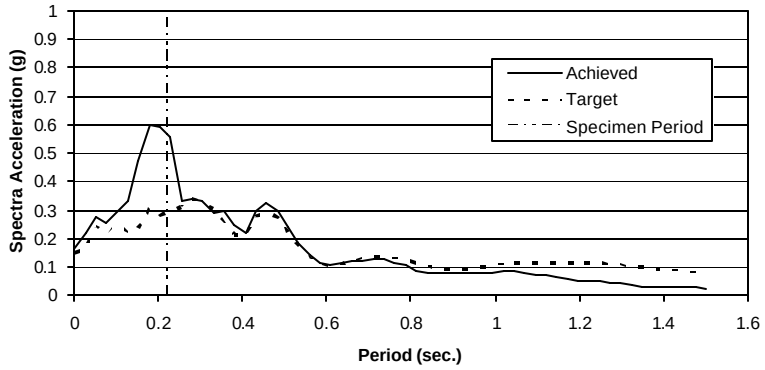

Figure 4-56 Response Spectra of THD-3 at 0.25 x Sylmar

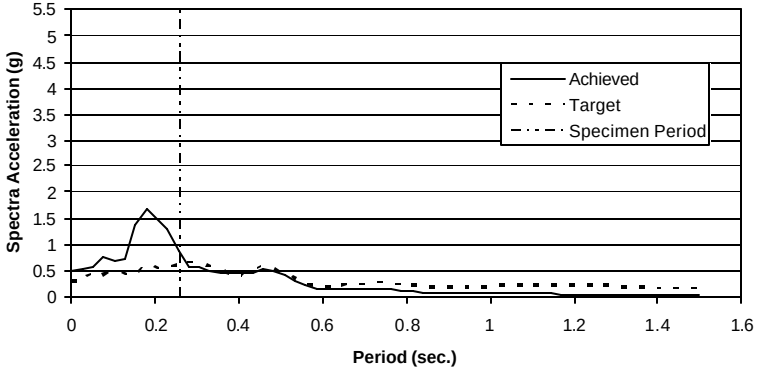

Figure 4-57 Response Spectra of THD-3 at 0.5 x Sylmar

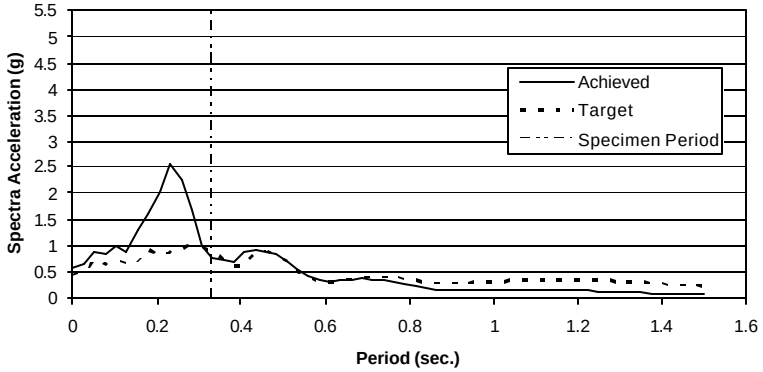

Figure 4-58 Response Spectra of THD-3 at 0.75 x Sylmar

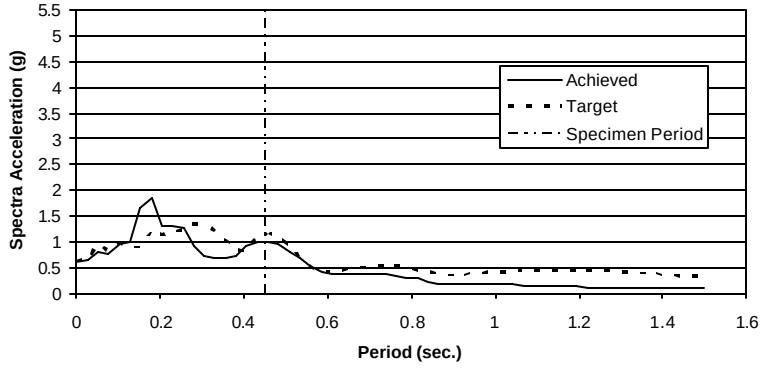

Figure 4-59 Response Spectra of THD-3 at 1.0 x Sylmar

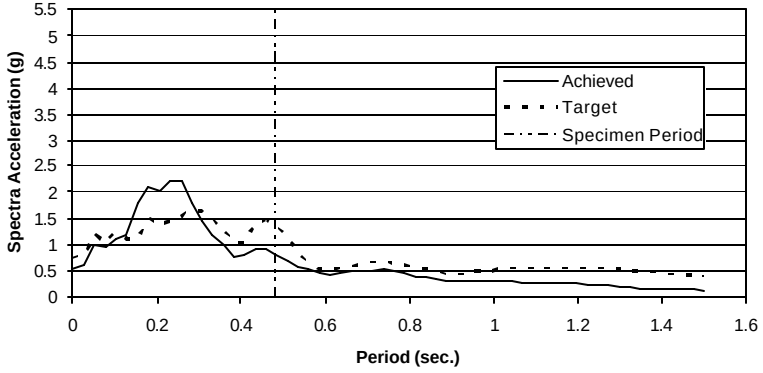

Figure 4-60 Response Spectra of THD-3 at 1.25 x Sylmar

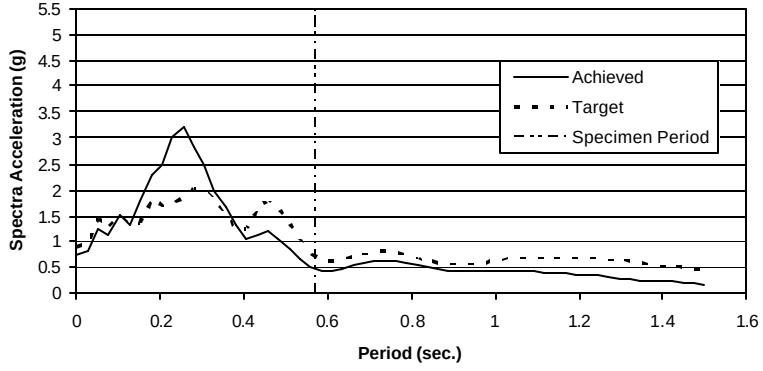

Figure 4-61 Response Spectra of THD-3 at 1.5 x Sylmar

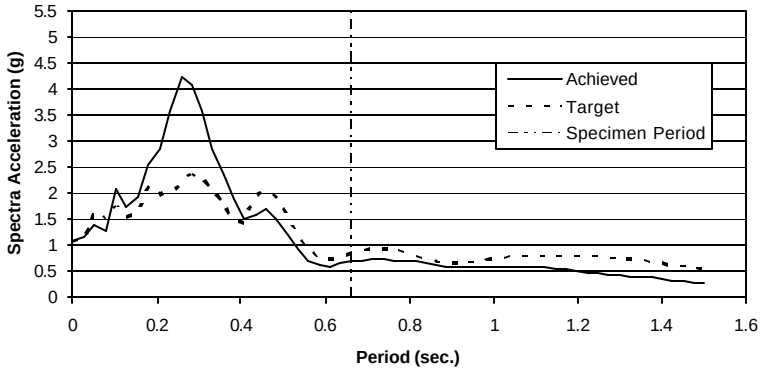

Figure 4-62 Response Spectra of THD-3 at 1.75 x Sylmar

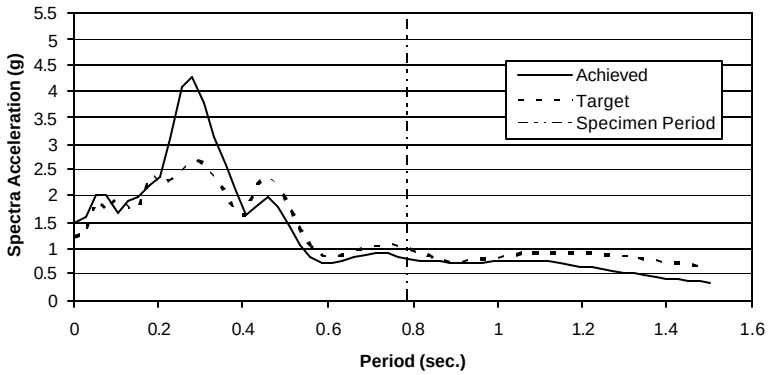

Figure 4-63 Response Spectra of THD-3 at 2.0 x Sylmar

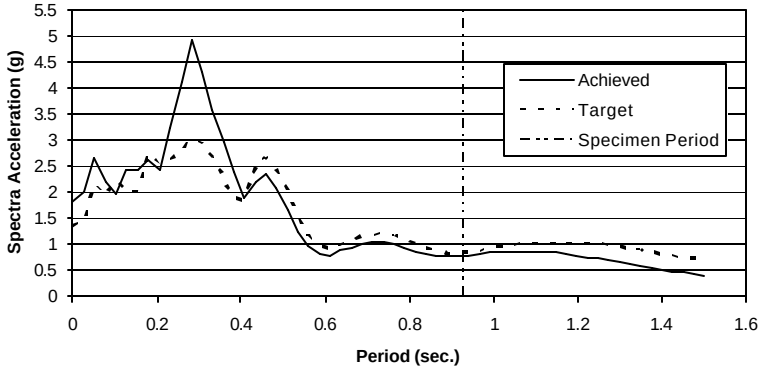

Figure 4-64 Response Spectra of THD-3 at 2.25 x Sylmar

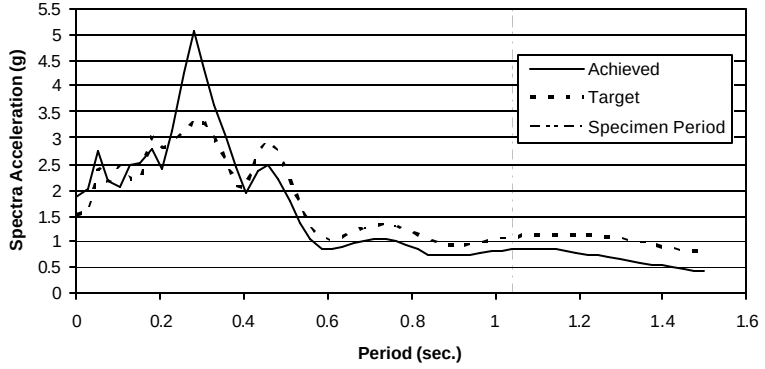

Figure 4-65 Response Spectra of THD-3 at 2.5 x Sylmar

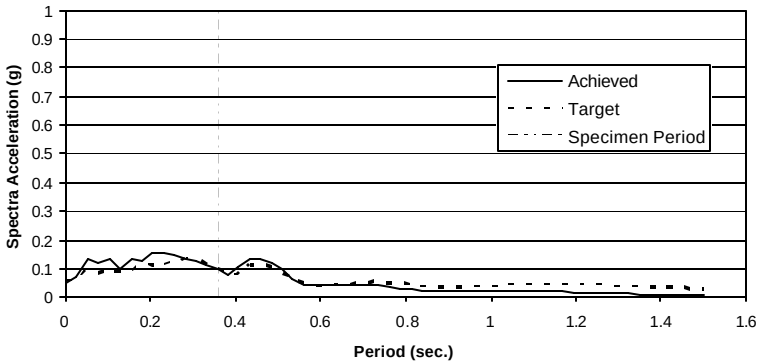

Figure 4-66 Response Spectra of THD-4 at 0.1 x Sylmar

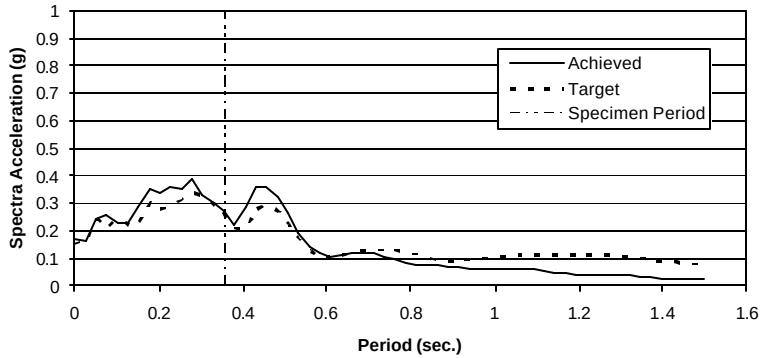

Figure 4-67 Response Spectra of THD-4 at 0.25 x Sylmar

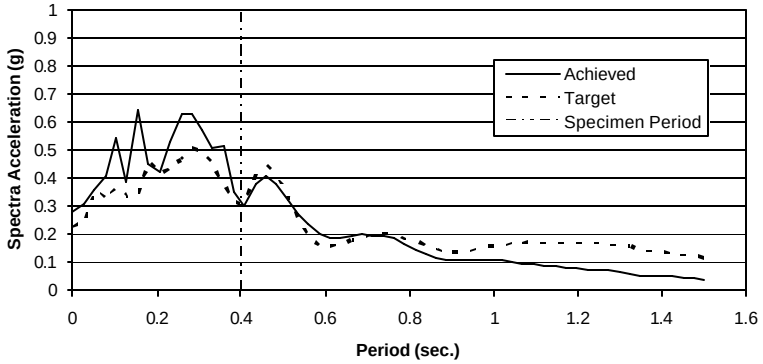

Figure 4-68 Response Spectra of THD-4 at 0.375 x Sylmar

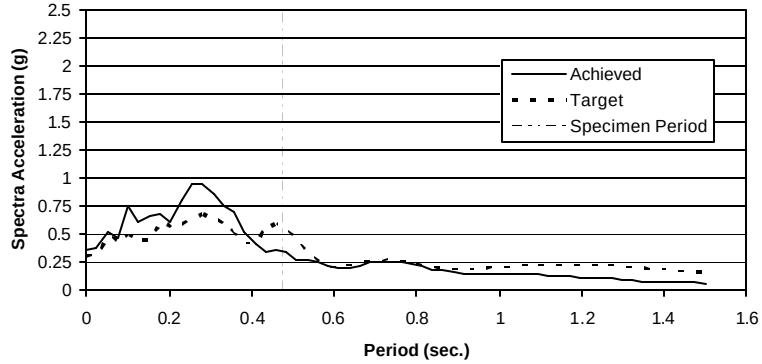

Figure 4-69 Response Spectra of THD-4 at 0.5 x Sylmar

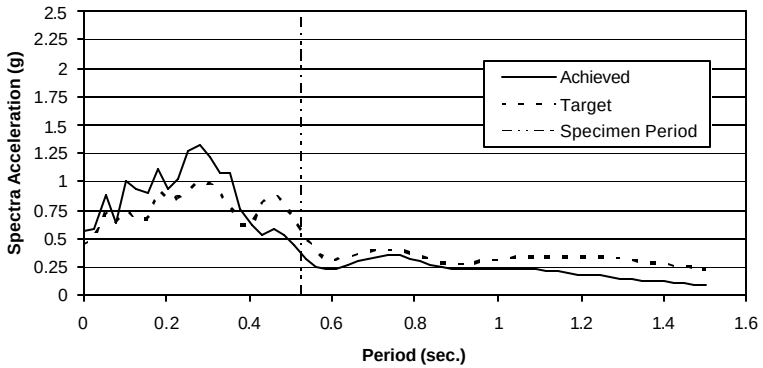

Figure 4-70 Response Spectra of THD-4 at 0.75 x Sylmar

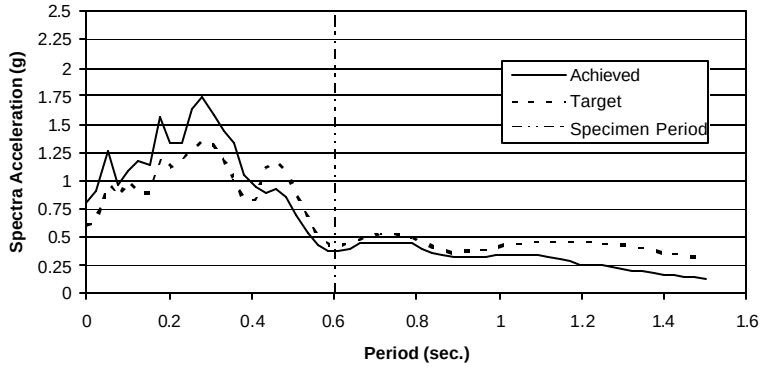

Figure 4-71 Response Spectra of THD-4 at 1.0 x Sylmar

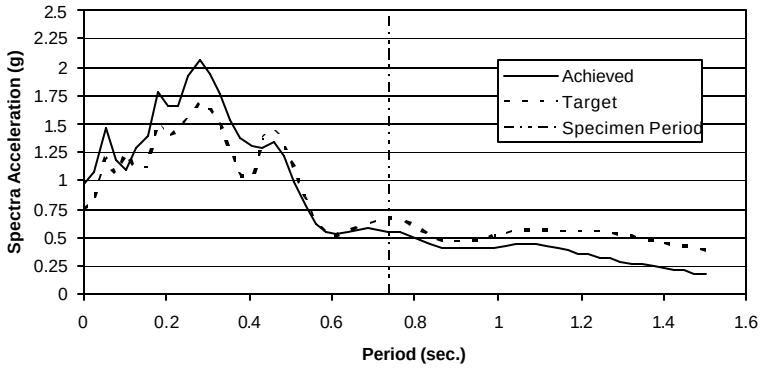

Figure 4-72 Response Spectra of THD-4 at 1.25 x Sylmar

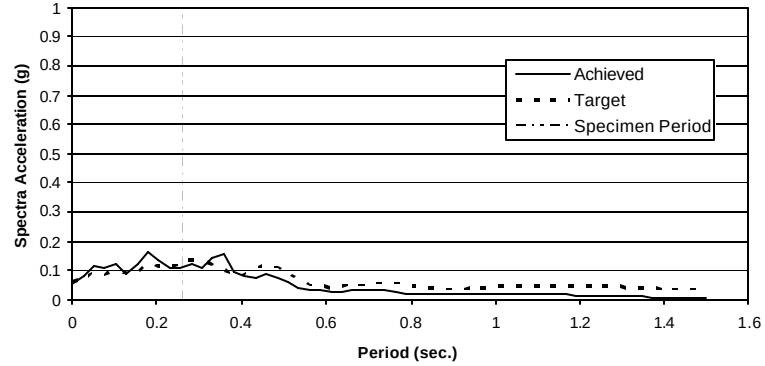

Figure 4-73 Response Spectra of THD-5 at 0.1 x Sylmar

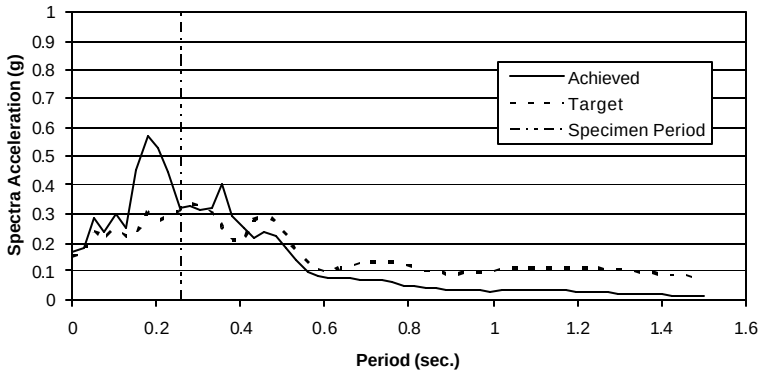

Figure 4-74 Response Spectra of THD-5 at 0.25 x Sylmar

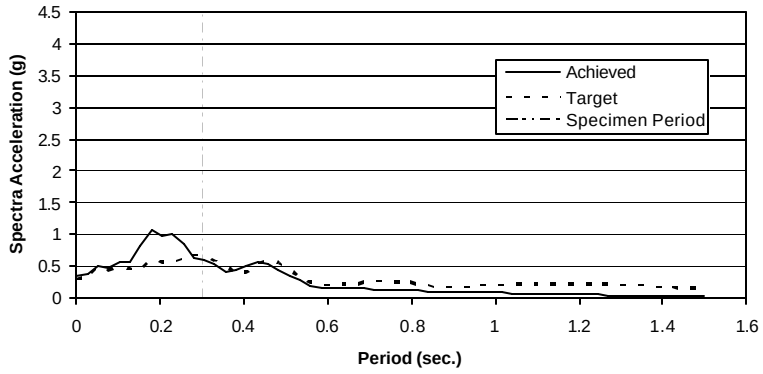

Figure 4-75 Response Spectra of THD-5 at 0.5 x Sylmar

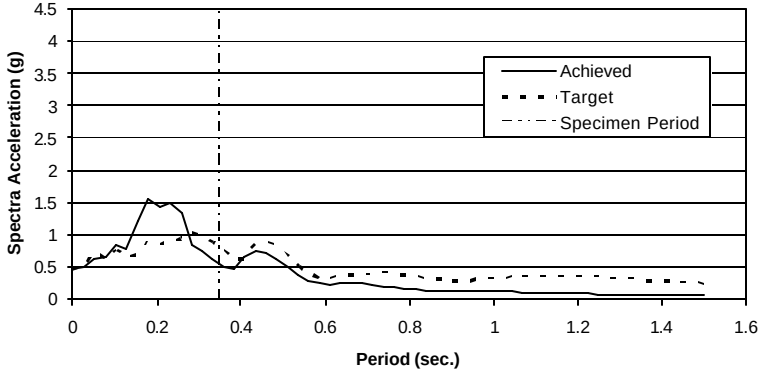

Figure 4-76 Response Spectra of THD-5 at 0.75 x Sylmar

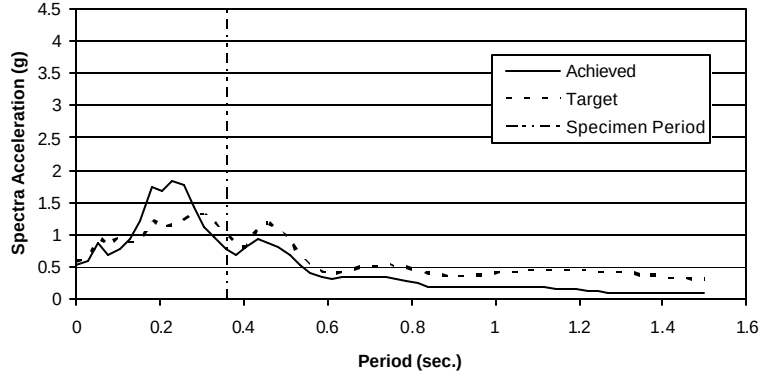

Figure 4-77 Response Spectra of THD-5 at 1.0 x Sylmar

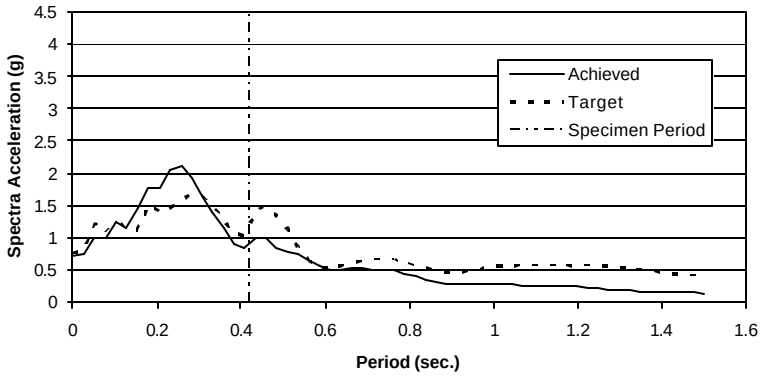

Figure 4-78 Response Spectra of THD-5 at 1.25 x Sylmar

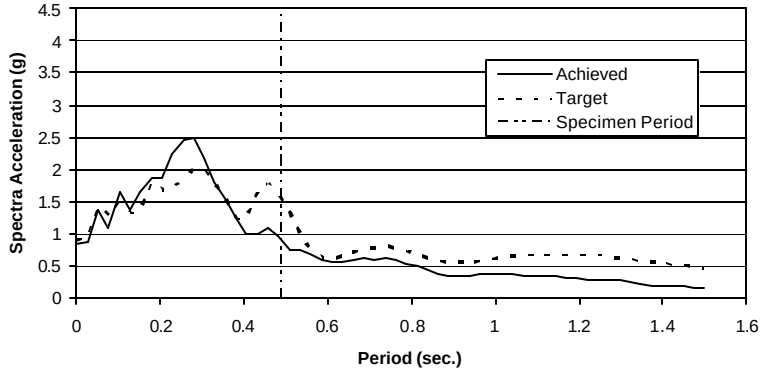

Figure 4-79 Response Spectra of THD-5 at 1.5 x Sylmar

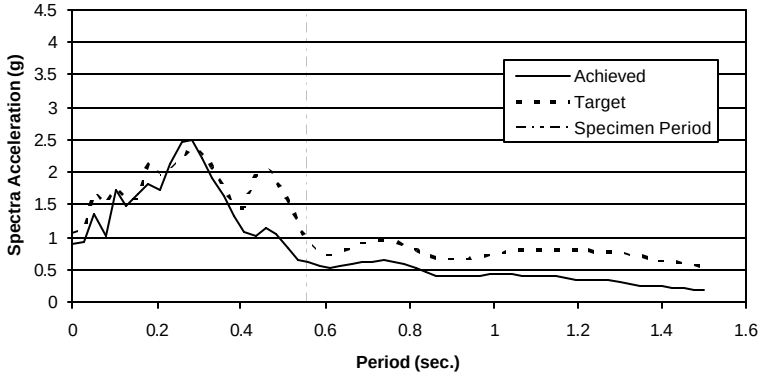

Figure 4-80 Response Spectra of THD-5 at 1.75 x Sylmar

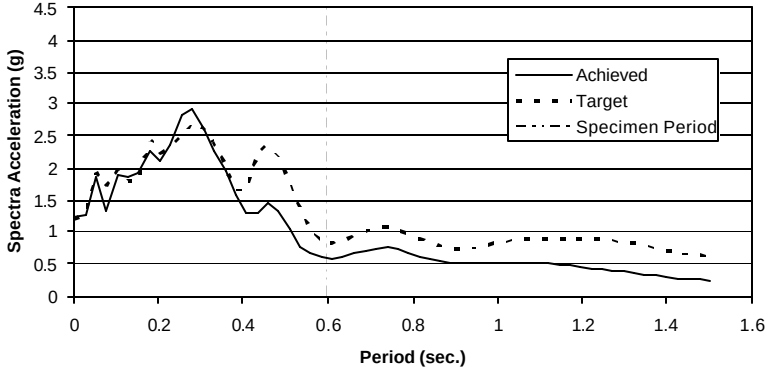

Figure 4-81 Response Spectra of THD-5 at 2.0 x Sylmar

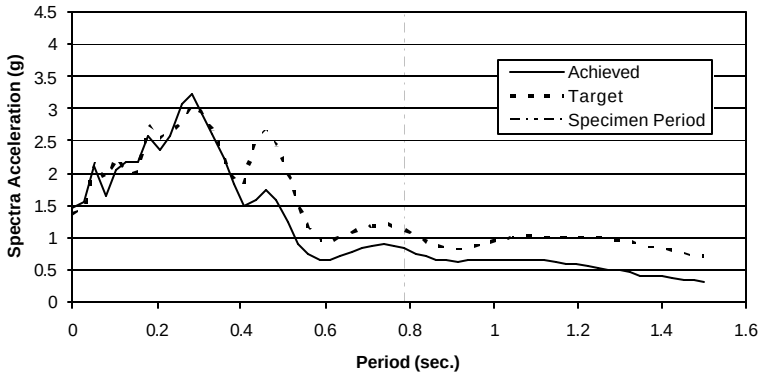

Figure 4-82 Response Spectra of THD-5 at 2.25 x Sylmar

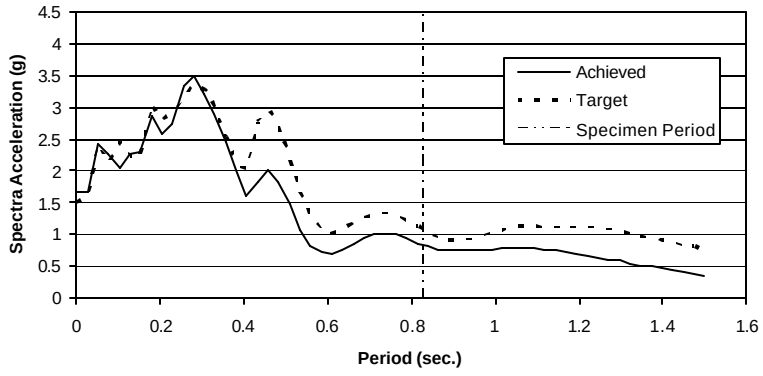

Figure 4-83 Response Spectra of THD-5 at 2.5 x Sylmar

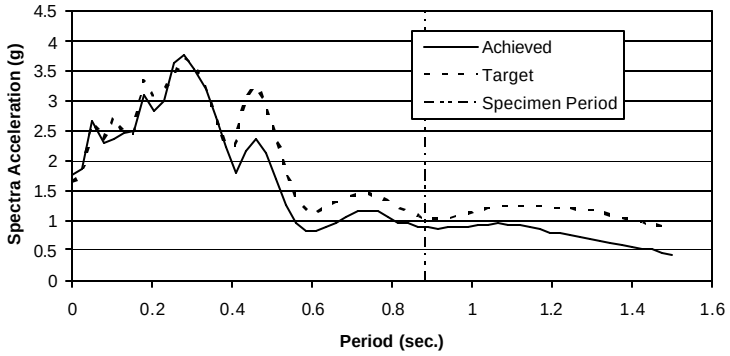

Figure 4-84 Response Spectra of THD-5 at 2.75 x Sylmar

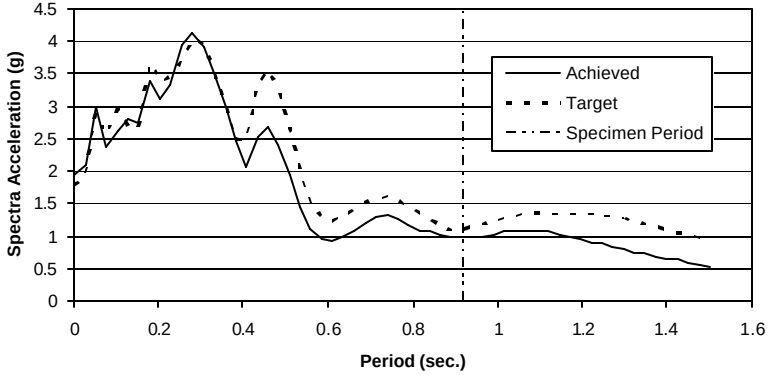

Figure 4-85 Response Spectra of THD-5 at 3.0 x Sylmar

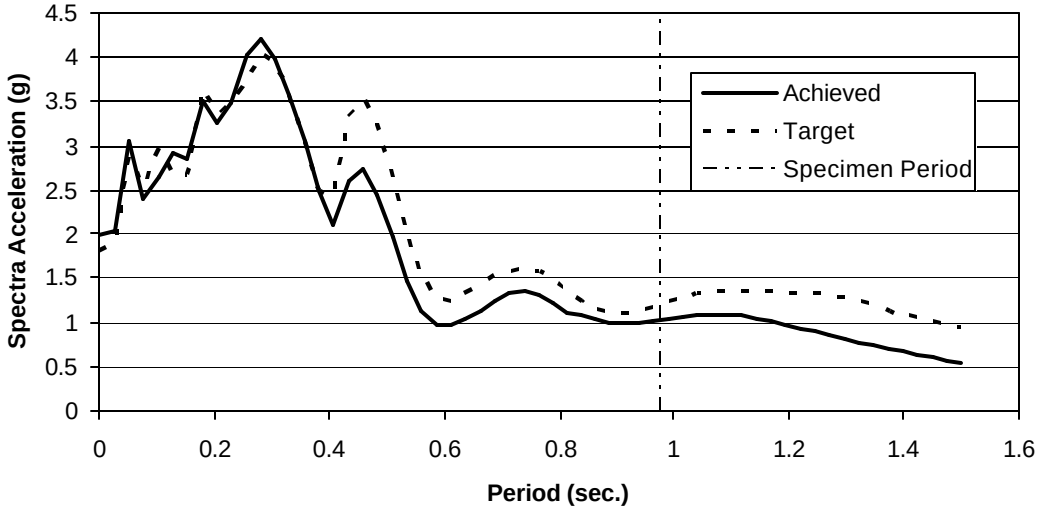

Figure 4-86 Response Spectra of THD-5 at 3.0 x Sylmar (2nd time)

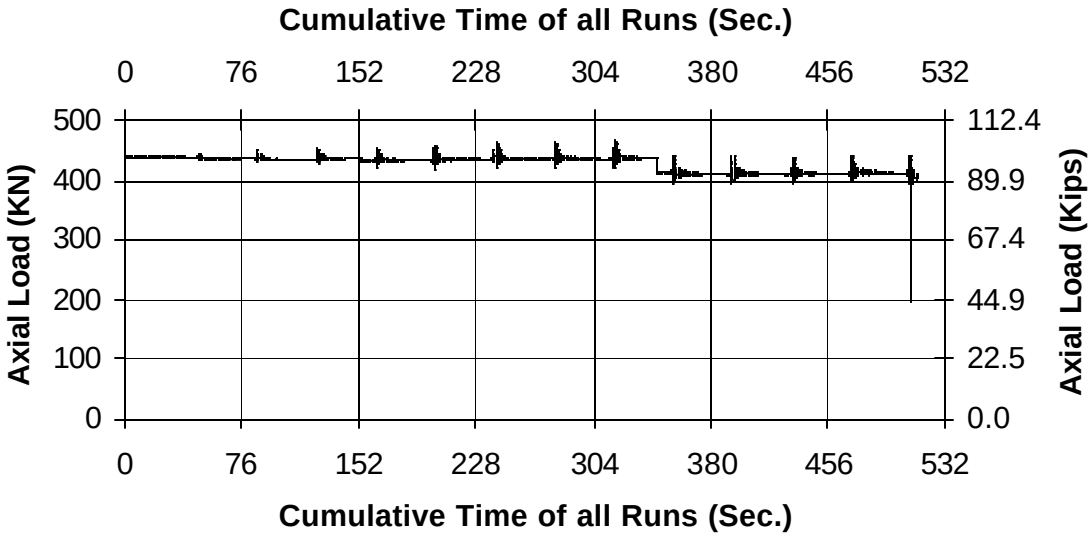

Figure 4-87 Axial Load Variation History for THD-1

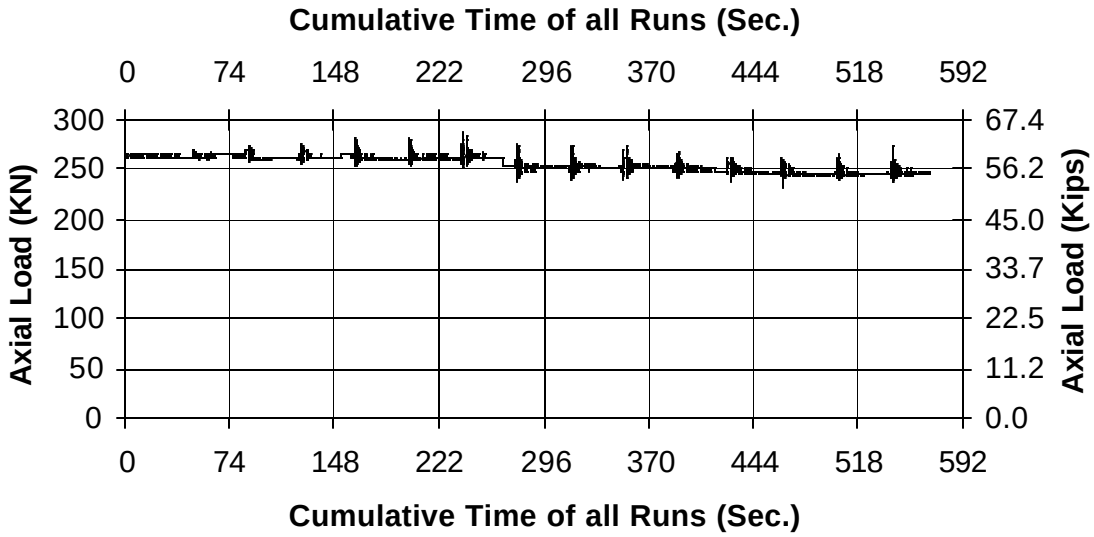

Figure 4-88 Axial Load Variation History for THD-2

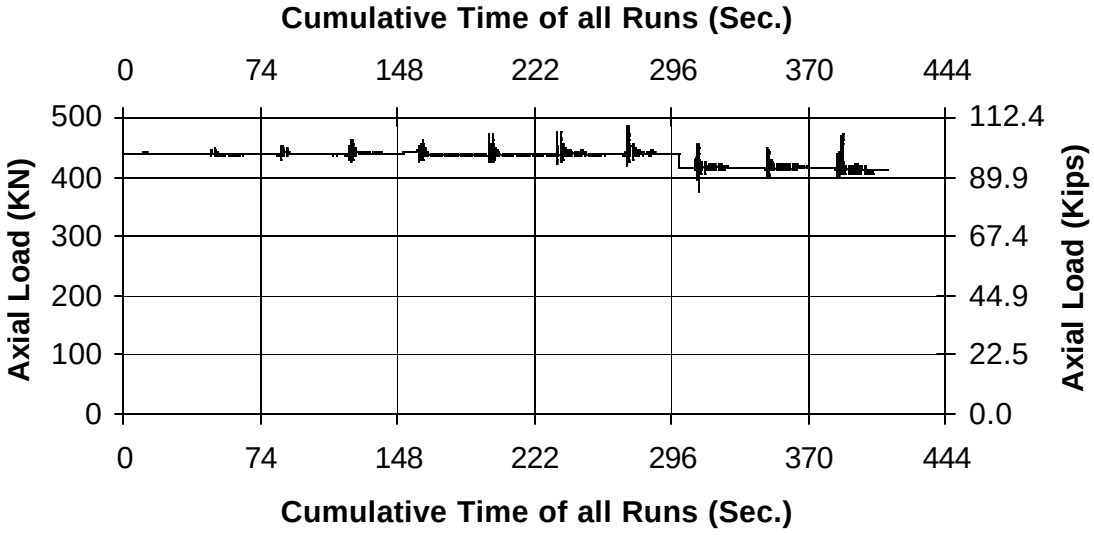

Figure 4-89 Axial Load Variation History for THD-3

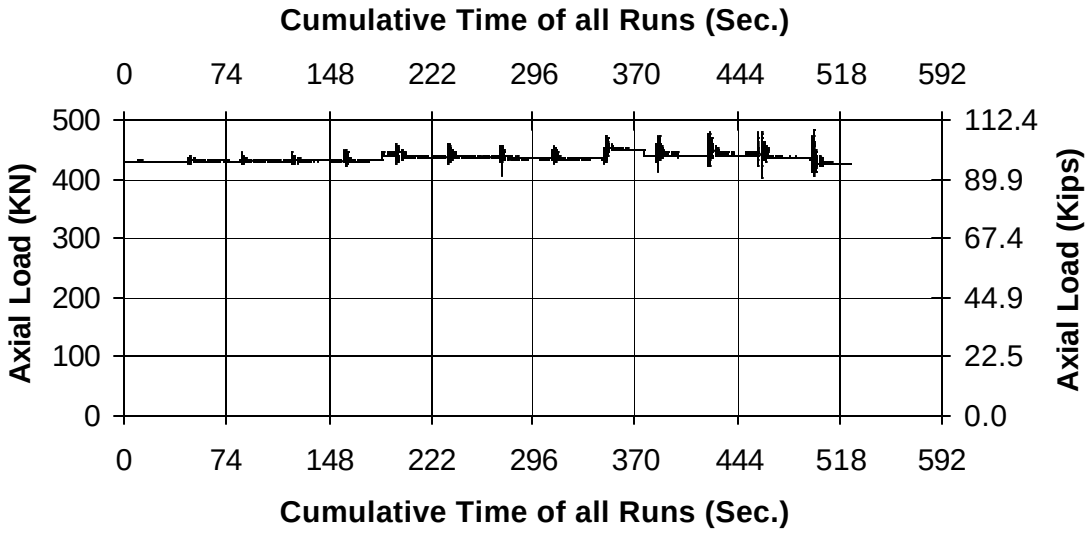

Figure 4-90 Axial Load Variation History for THD-5

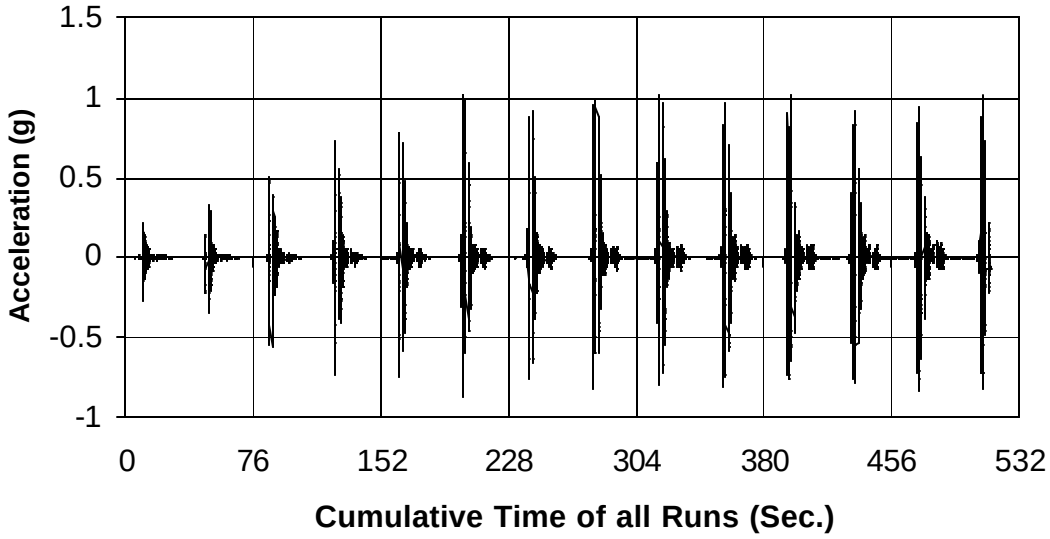

Figure 4-91 Acceleration History Recorded at Top of Specimen THD-1

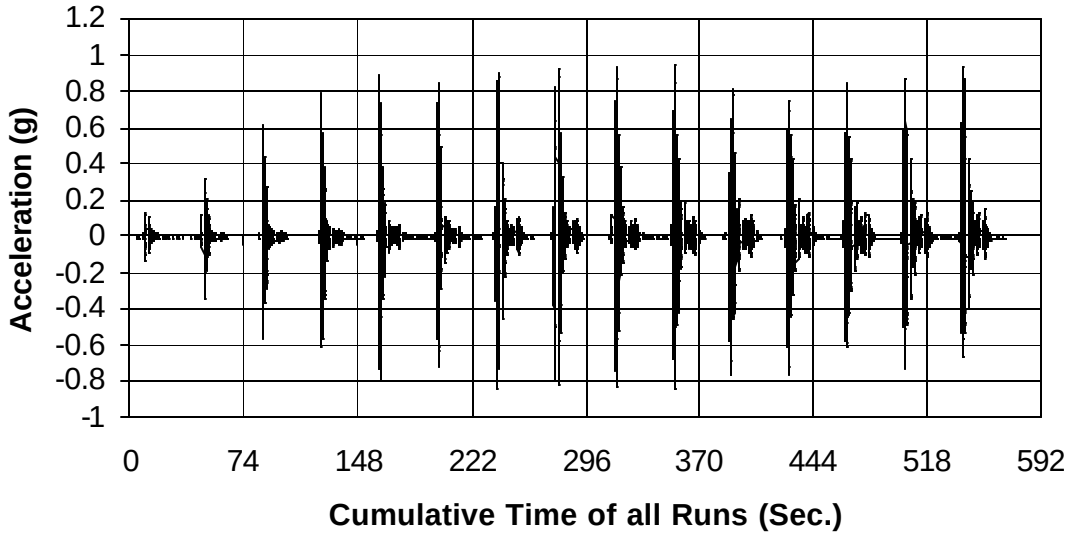

Figure 4-92 Acceleration History Recorded at Top of Specimen THD-2

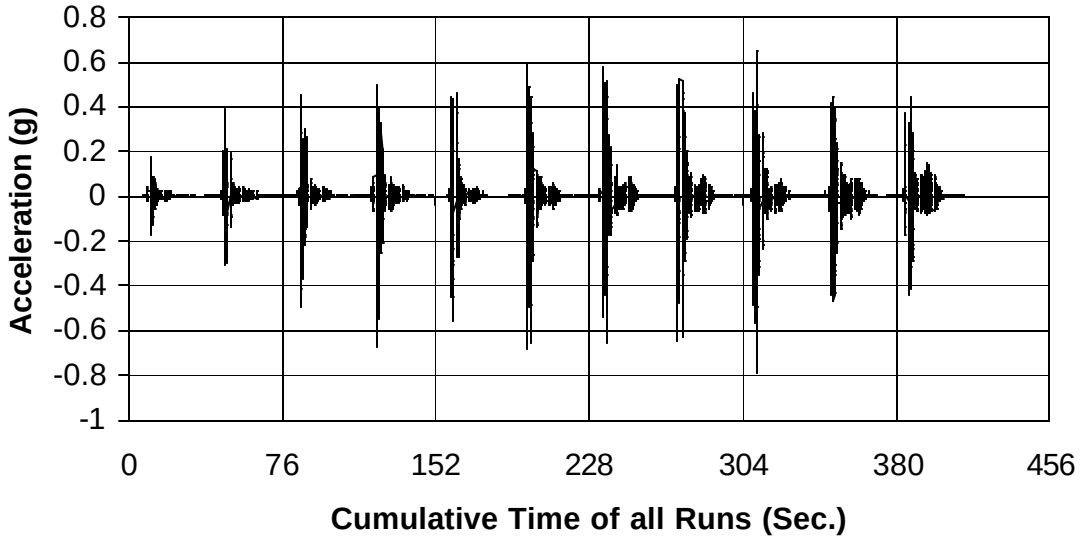

Figure 4-93 Acceleration History Recorded at Top of Specimen THD-3

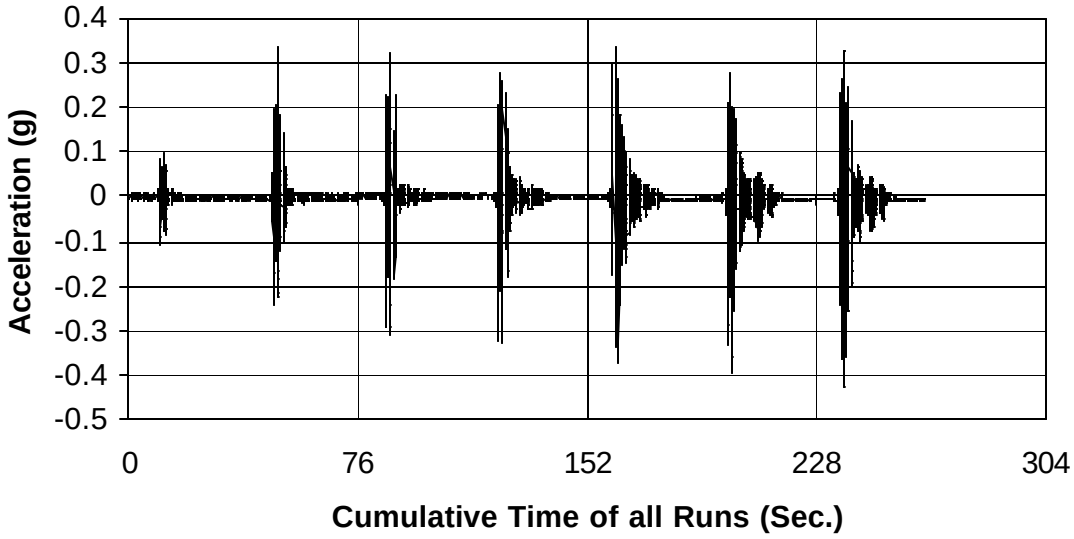

Figure 4-94 Acceleration History Recorded at Top of Specimen THD-4

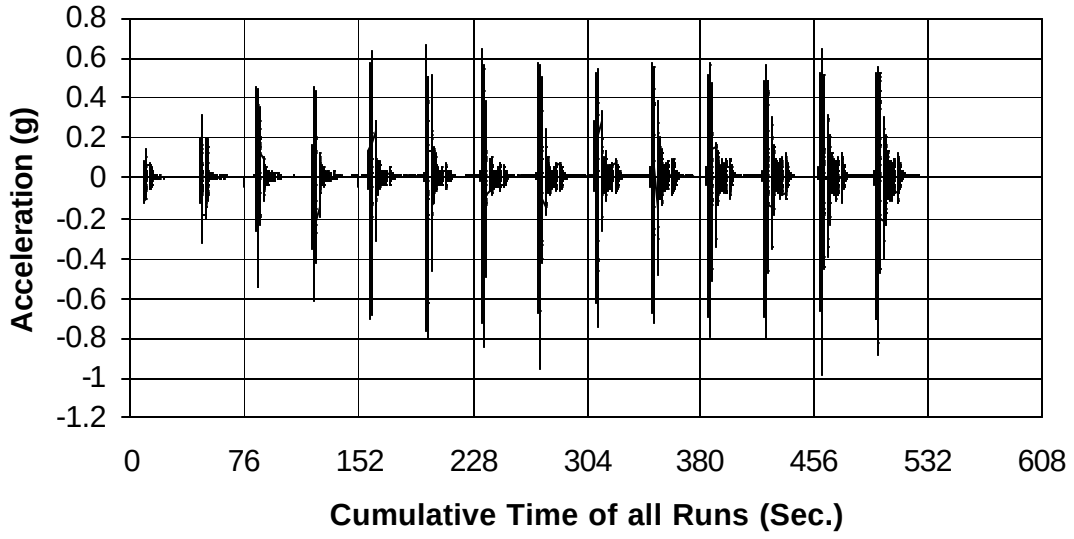

Figure 4-95 Acceleration History Recorded at Top of Specimen THD-5

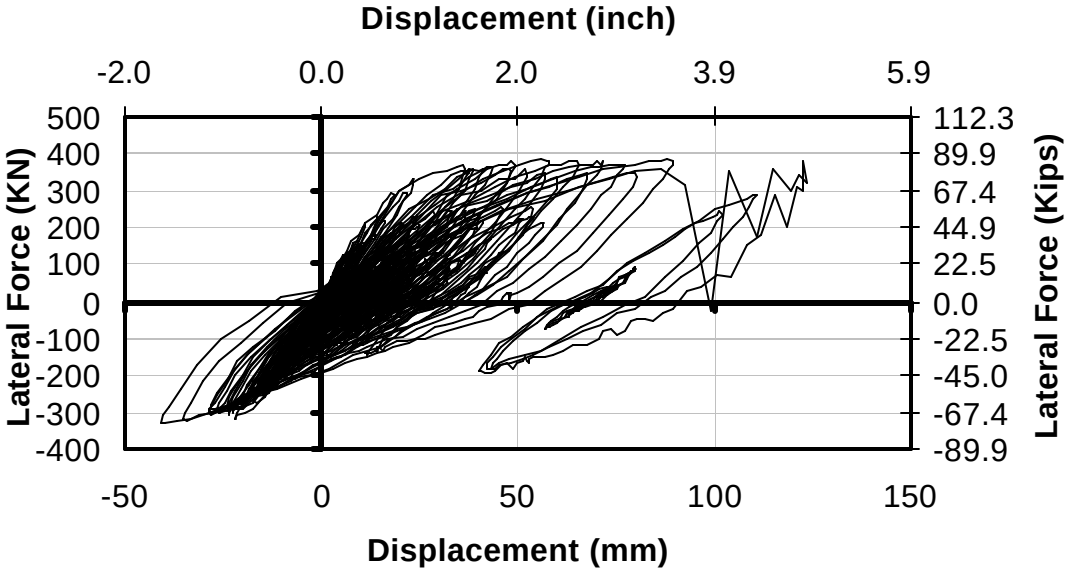

Figure 4-96 Accumulated Force Displacement Hysteresis for THD-1

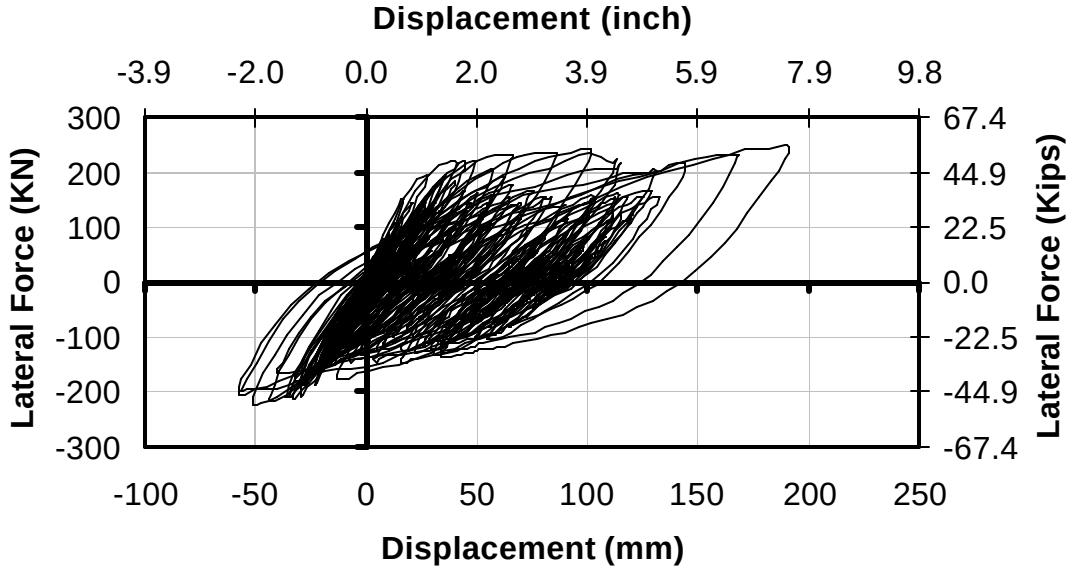

Figure 4-97 Accumulated Force Displacement Hysteresis for THD-2

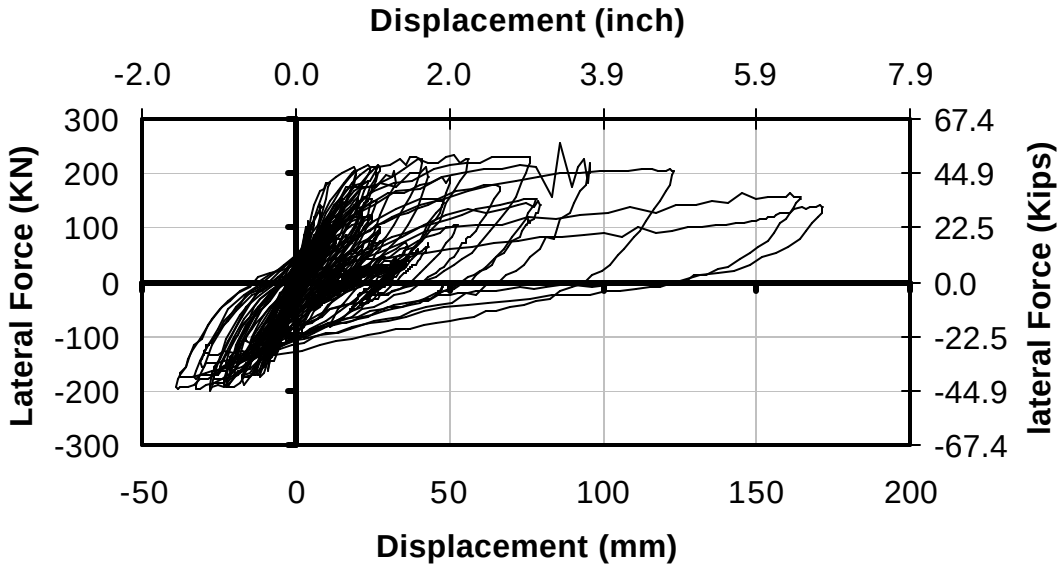

Figure 4-98 Accumulated Force Displacement Hysteresis for THD-3

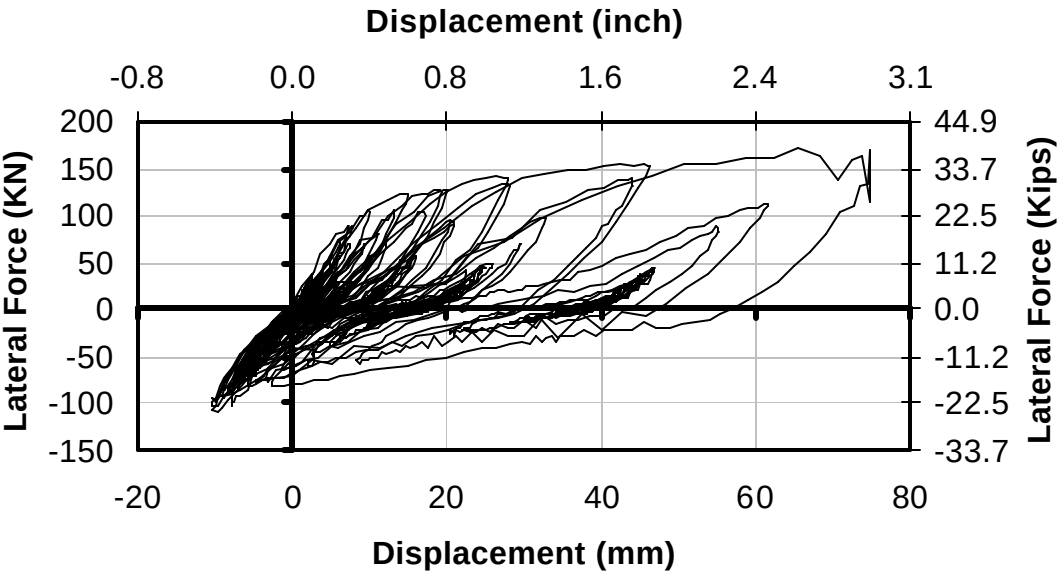

Figure 4-99 Accumulated Force Displacement Hysteresis for THD-4

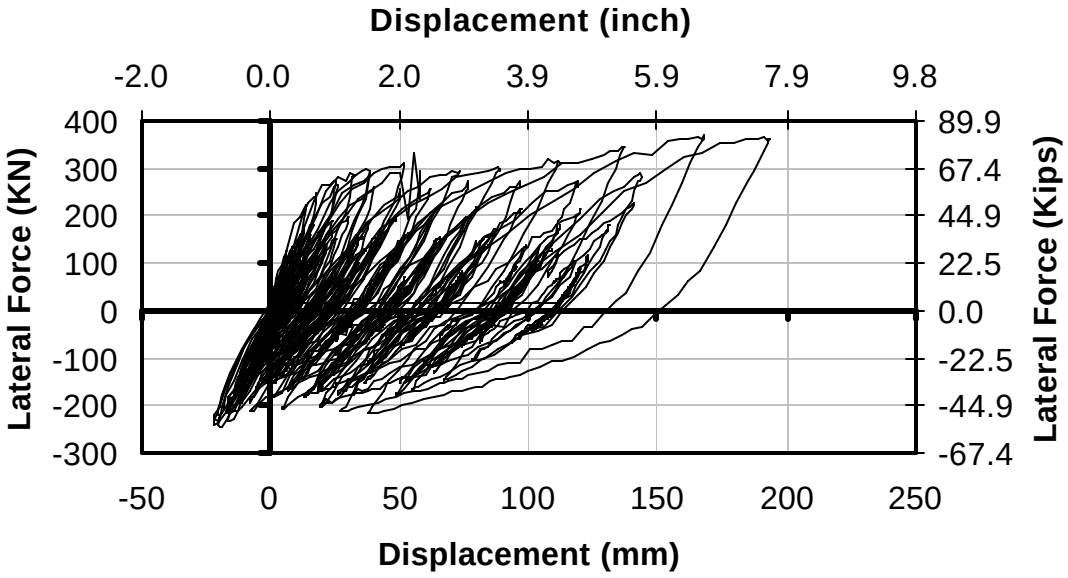

Figure 4-100 Accumulated Force Displacement Hysteresis for THD-5

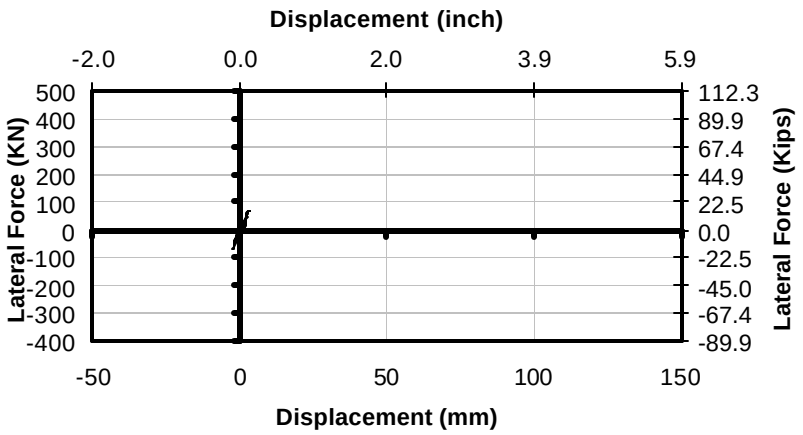

Figure 4-101 F-D Hysteresis for THD-1 at 0.1 x Sylmar

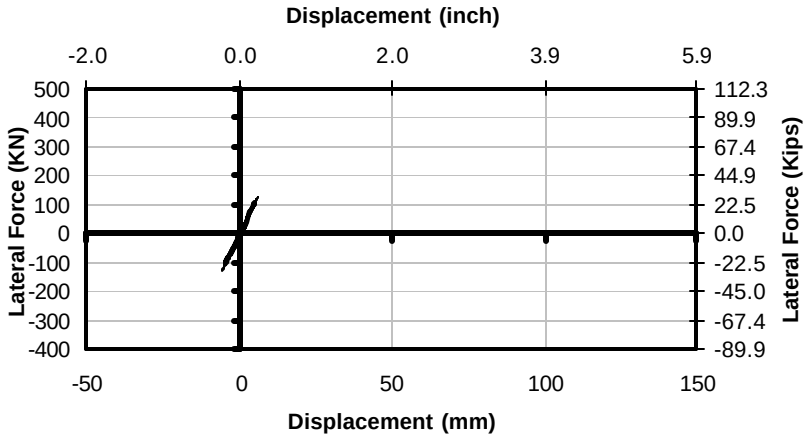

Figure 4-102 F-D Hysteresis for THD-1 at 0.25 x Sylmar

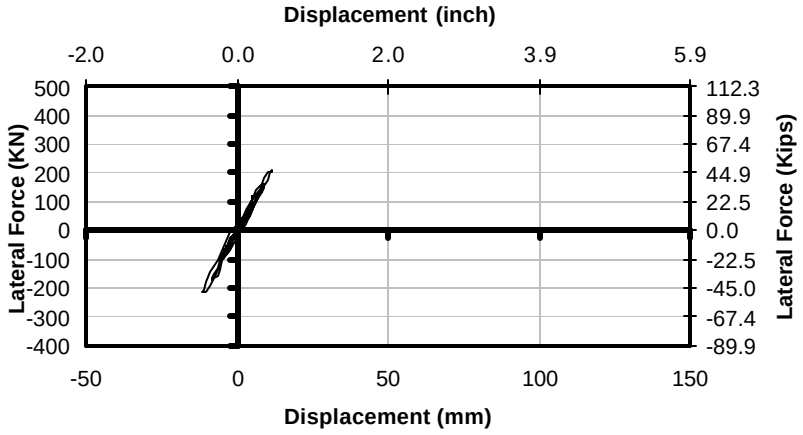

Figure 4-103 F-D Hysteresis for THD-1 at 0.5 x Sylmar

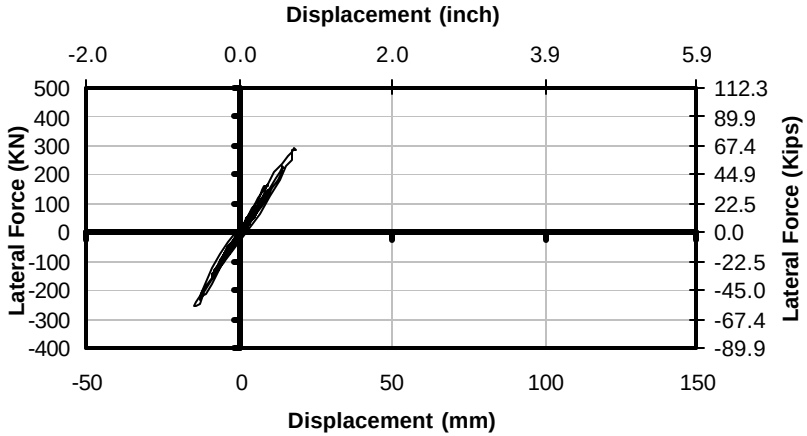

Figure 4-104 F-D Hysteresis for THD-1 at 0.75 x Sylmar

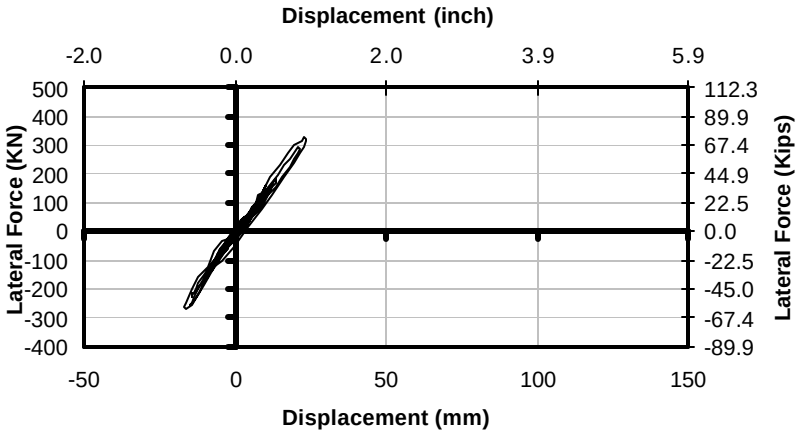

Figure 4-105 F-D Hysteresis for THD-1 at 1.0 x Sylmar

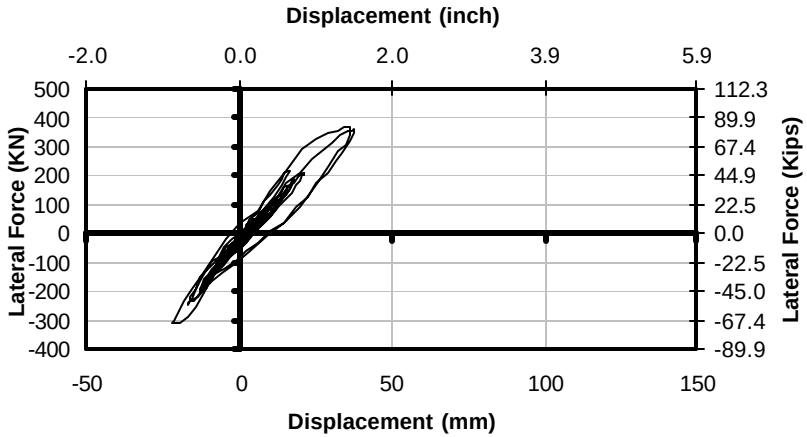

Figure 4-106 F-D Hysteresis for THD-1 at 1.25 x Sylmar

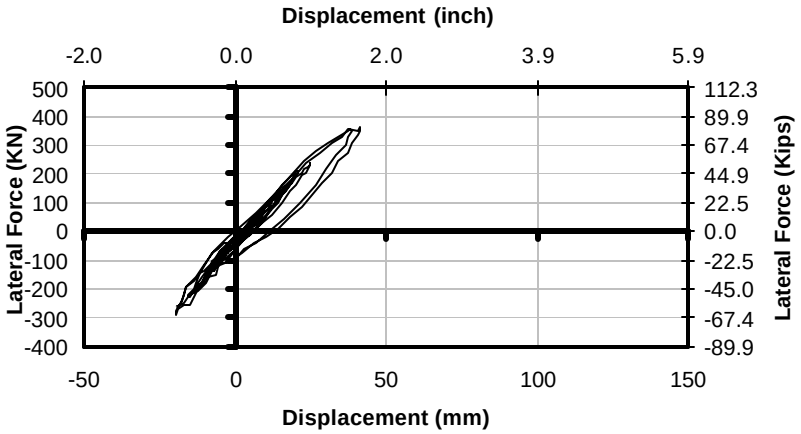

Figure 4-107 F-D Hysteresis for THD-1 at 1.5 x Sylmar

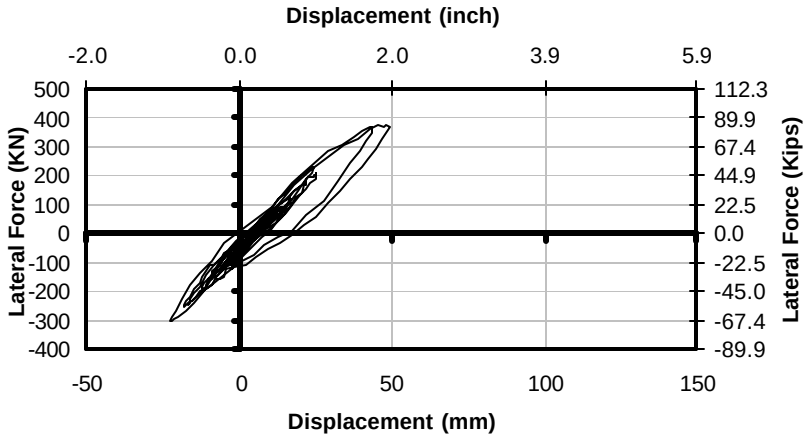

Figure 4-108 F-D Hysteresis for THD-1 at 1.75 x Sylmar

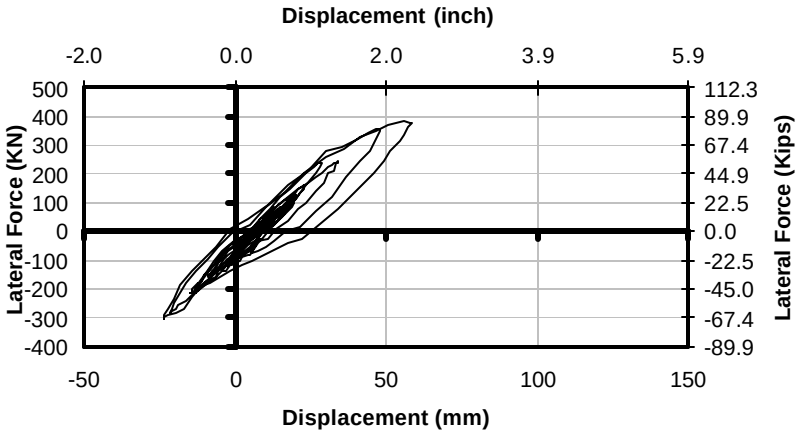

Figure 4-109 F-D Hysteresis for THD-1 at 2.0 x Sylmar

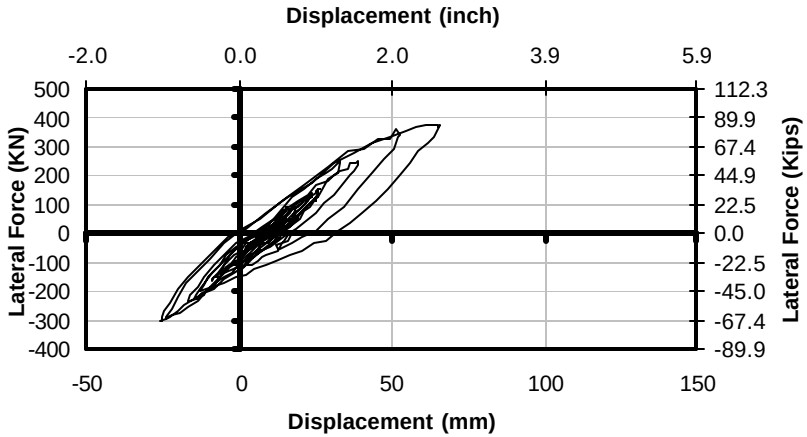

Figure 4-110 F-D Hysteresis for THD-1 at 2.25 x Sylmar

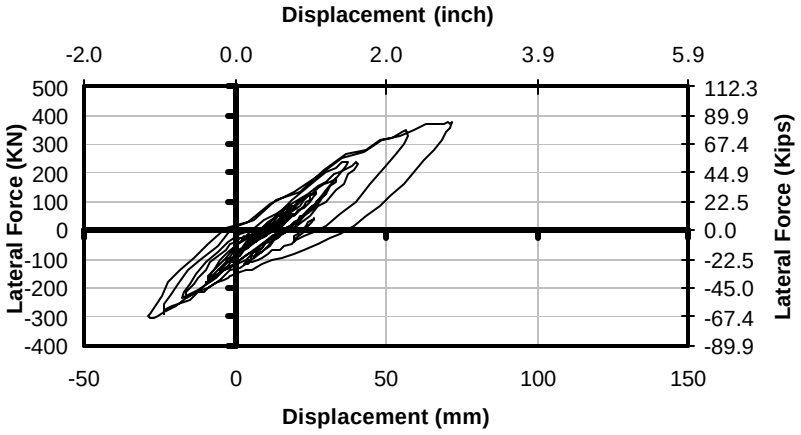

Figure 4-111 F-D Hysteresis for THD-1 at 2.5 x Sylmar

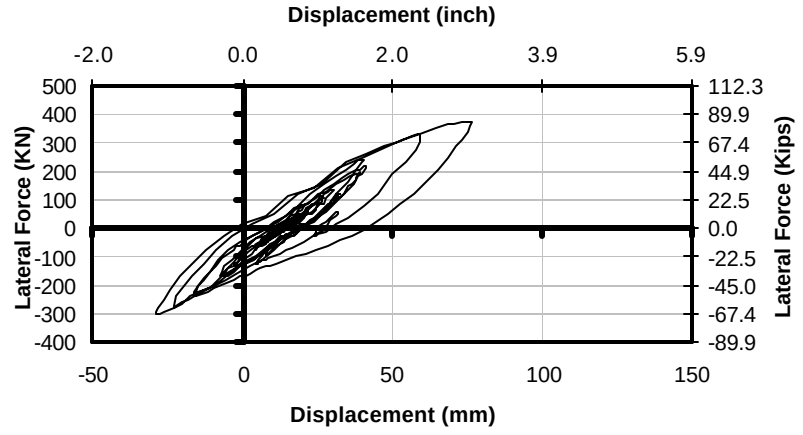

Figure 4-112 F-D Hysteresis for THD-1 at 2.625 x Sylmar

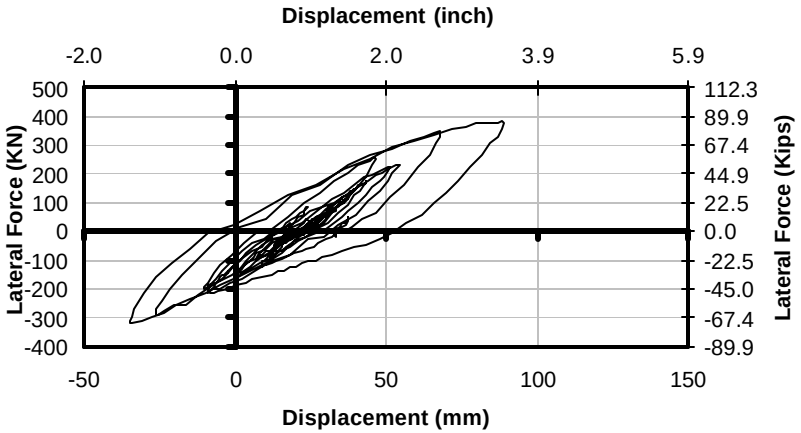

Figure 4-113 F-D Hysteresis for THD-1 at 2.75 x Sylmar

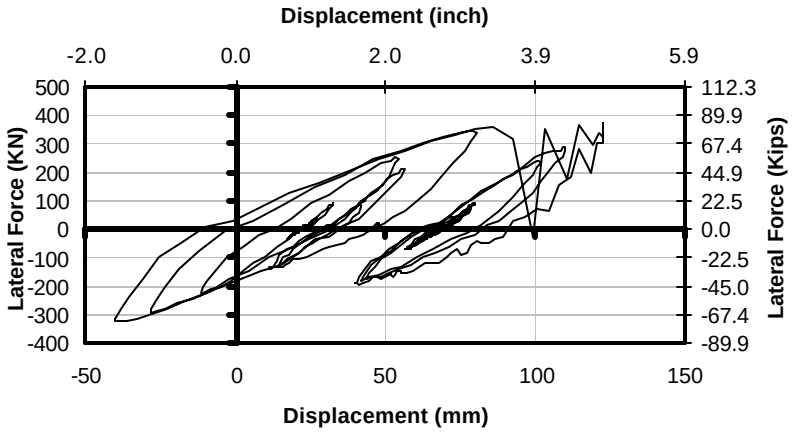

Figure 4-114 F-D Hysteresis for THD-1 at 2.875 x Sylmar

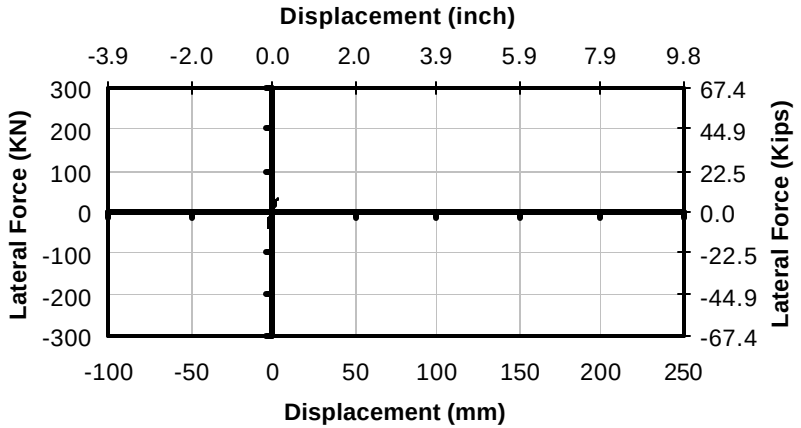

Figure 4-115 F-D Hysteresis for THD-2 at 0.1 x Sylmar

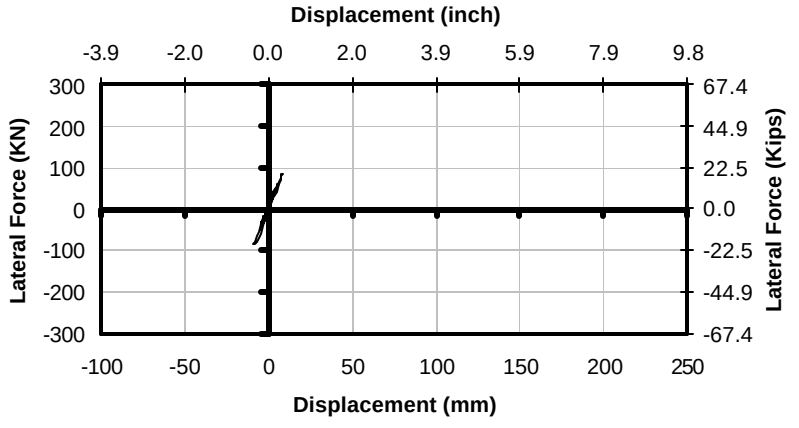

Figure 4-116 F-D Hysteresis for THD-2 at 0.25 x Sylmar

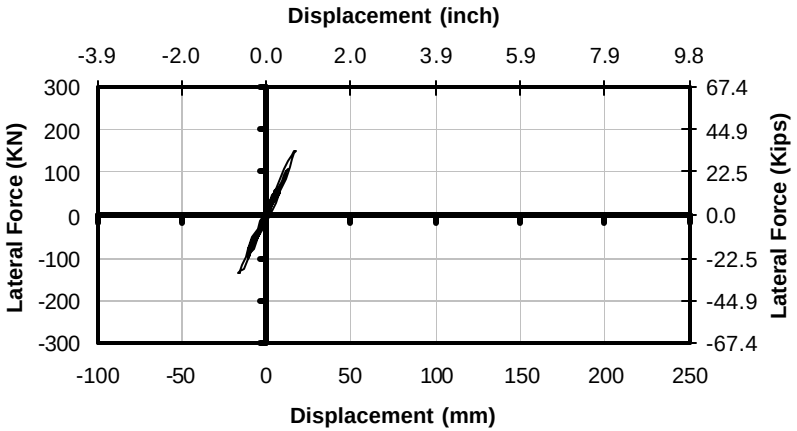

Figure 4-117 F-D Hysteresis for THD-2 at 0.5 x Sylmar

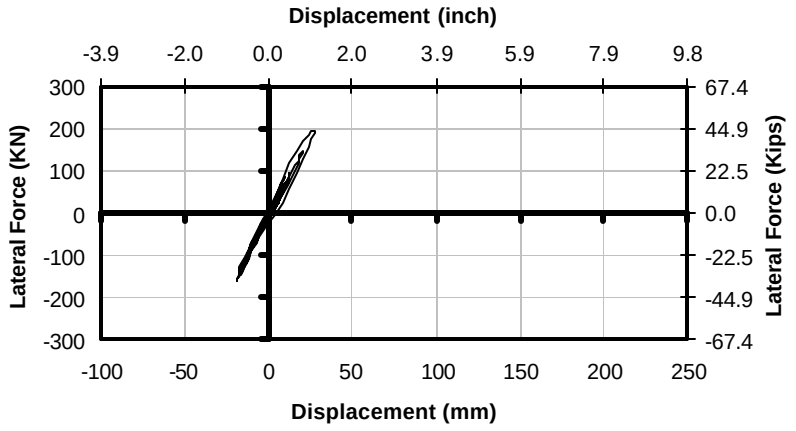

Figure 4-118 F-D Hysteresis for THD-2 at 0.75 x Sylmar

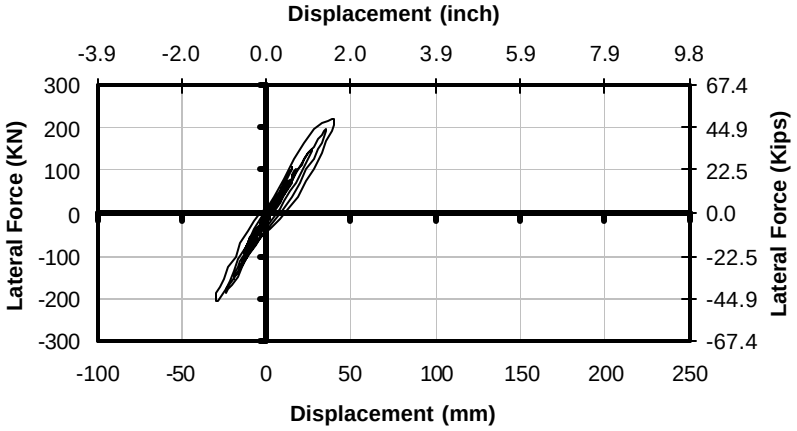

Figure 4-119 F-D Hysteresis for THD-2 at 1.0 x Sylmar

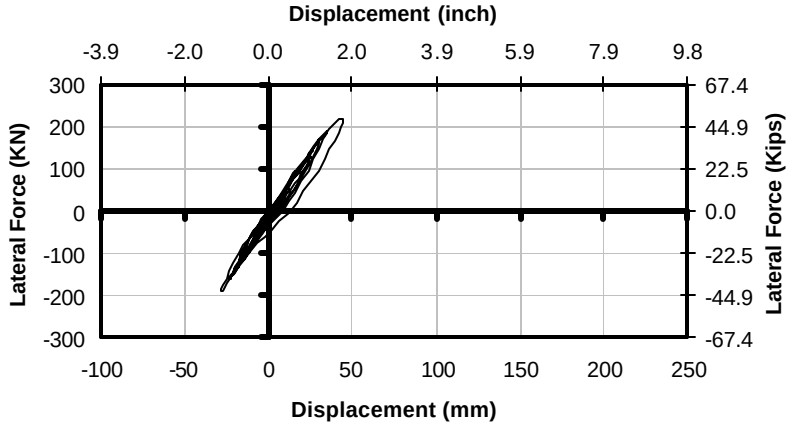

Figure 4-120 F-D Hysteresis for THD-2 at 1.25 x Sylmar

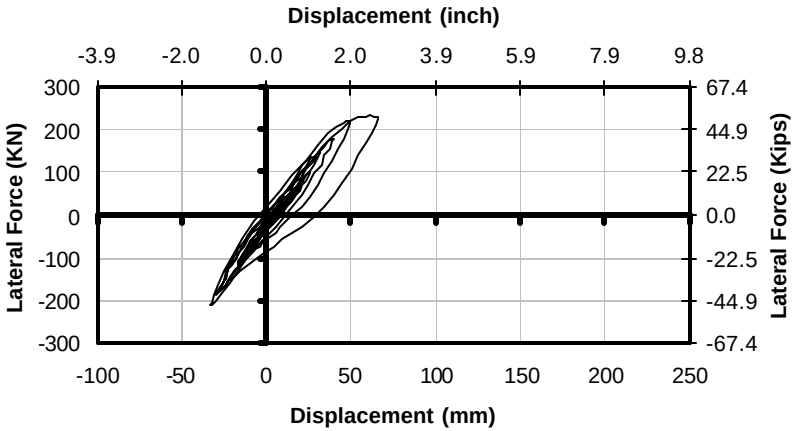

Figure 4-121 F-D Hysteresis for THD-2 at 1.5 x Sylmar

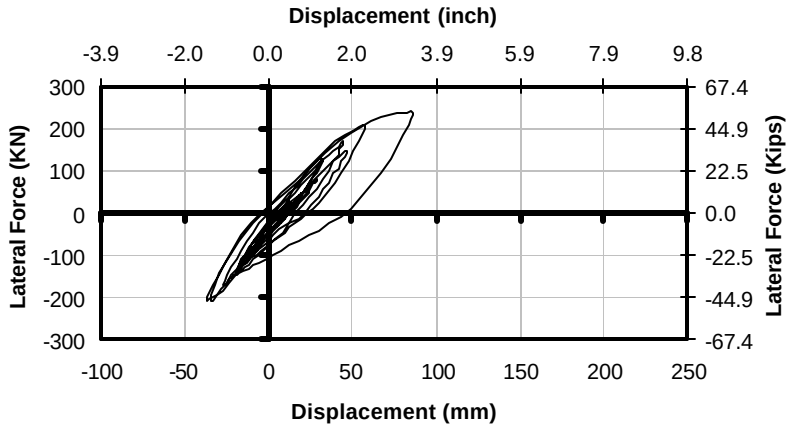

Figure 4-122 F-D Hysteresis for THD-2 at 1.75 x Sylmar

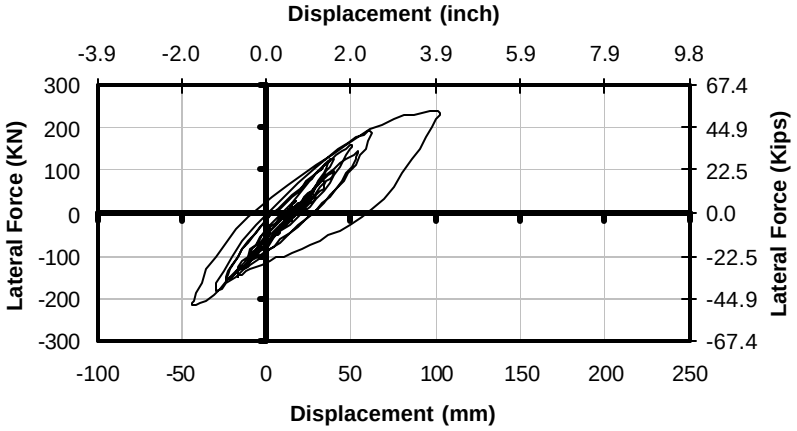

Figure 4-123 F-D Hysteresis for THD-2 at 2.0 x Sylmar

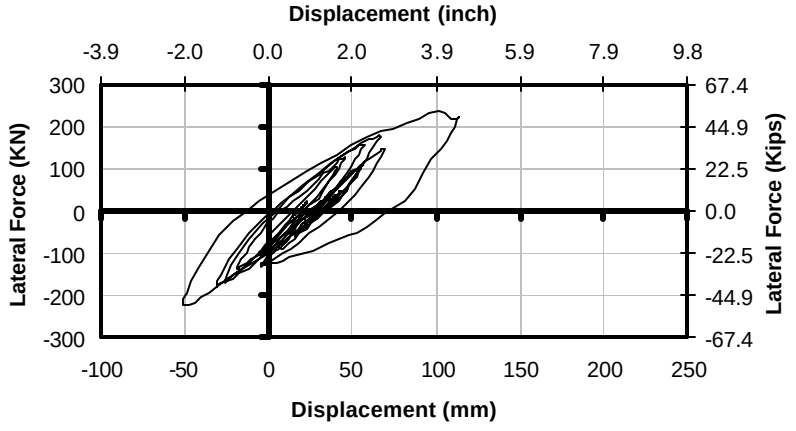

Figure 4-124 F-D Hysteresis for THD-2 at 2.25 x Sylmar

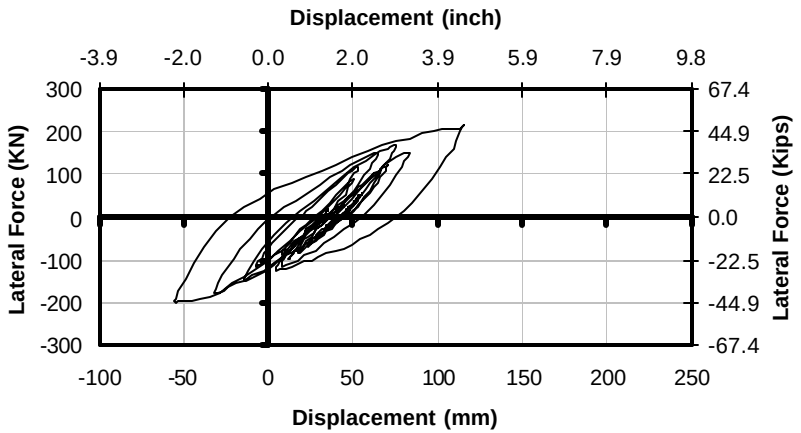

Figure 4-125 F-D Hysteresis for THD-2 at 2.5 x Sylmar

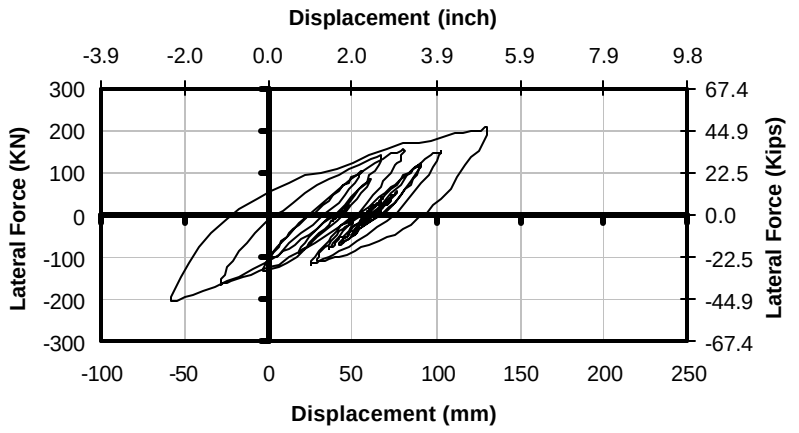

Figure 4-126 F-D Hysteresis for THD-2 at 2.625 x Sylmar

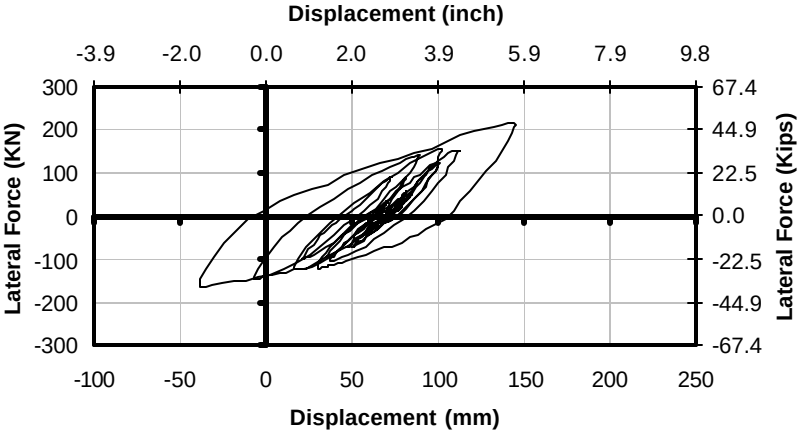

Figure 4-127 F-D Hysteresis for THD-2 at 2.75 x Sylmar

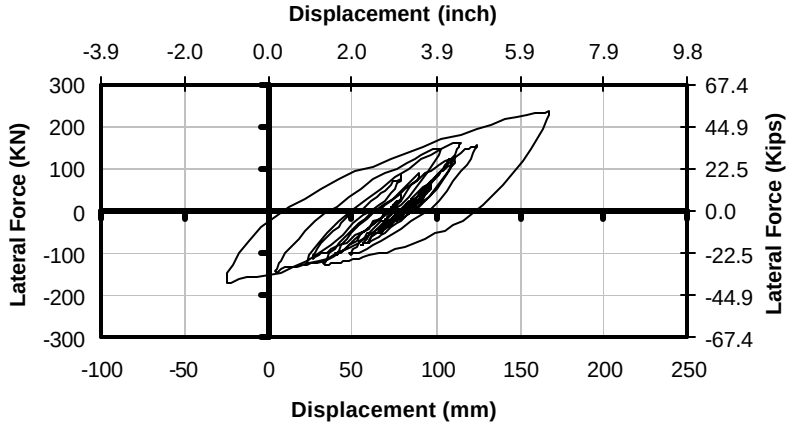

Figure 4-128 F-D Hysteresis for THD-2 at 2.875 x Sylmar

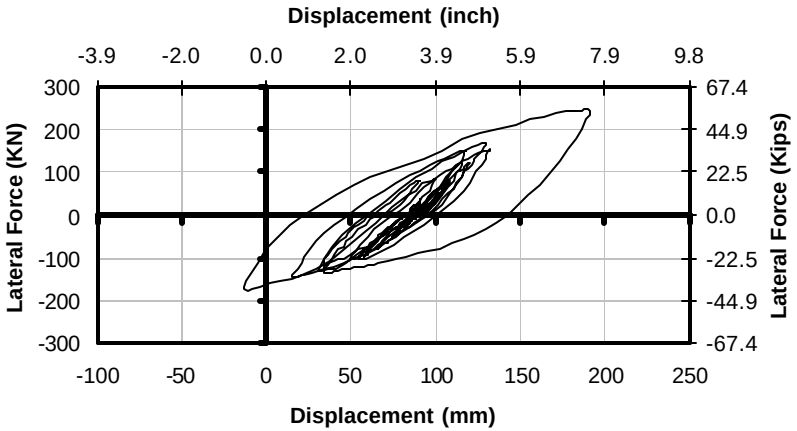

Figure 4-129 F-D Hysteresis for THD-2 at 3.0 x Sylmar

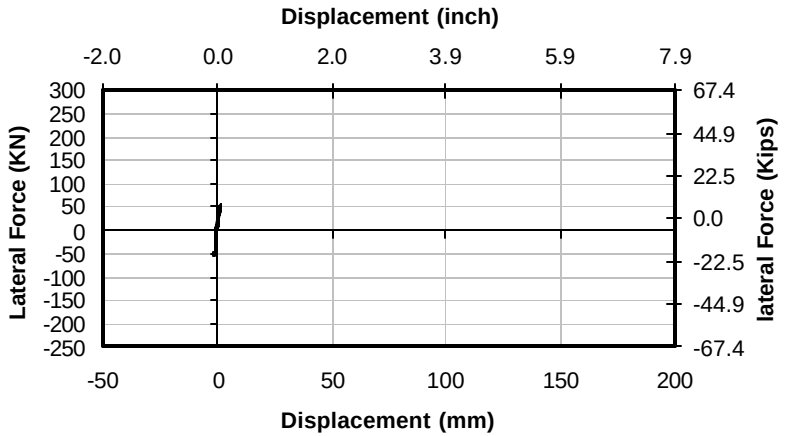

Figure 4-130 F-D Hysteresis for THD-3 at 0.1 x Sylmar

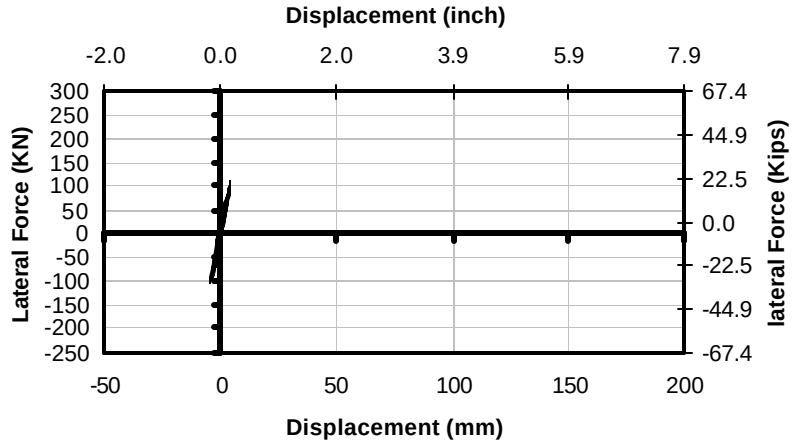

Figure 4-131 F-D Hysteresis for THD-3 at 0.25 x Sylmar

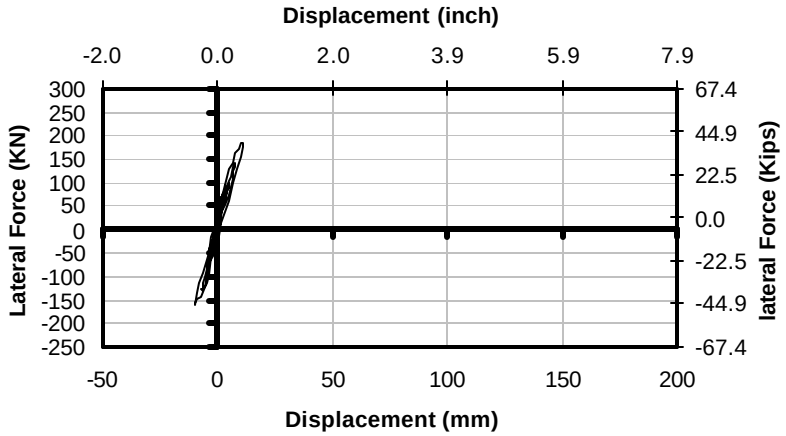

Figure 4-132 F-D Hysteresis for THD-3 at 0.5 x Sylmar

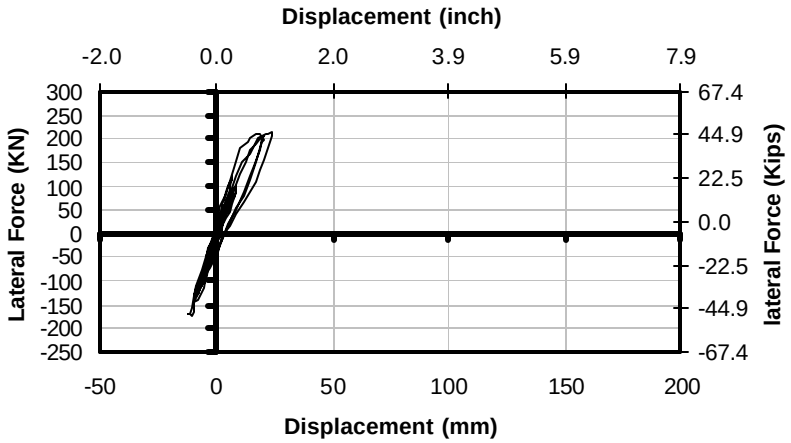

Figure 4-133 F-D Hysteresis for THD-3 at 0.75 x Sylmar

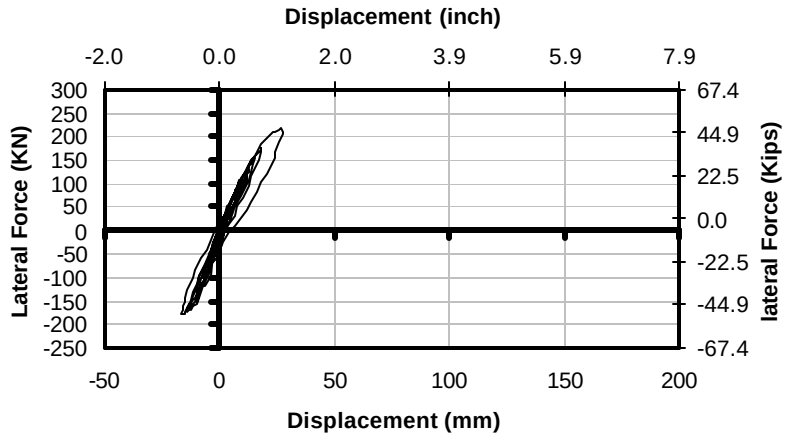

Figure 4-134 F-D Hysteresis for THD-3 at 1.0 x Sylmar

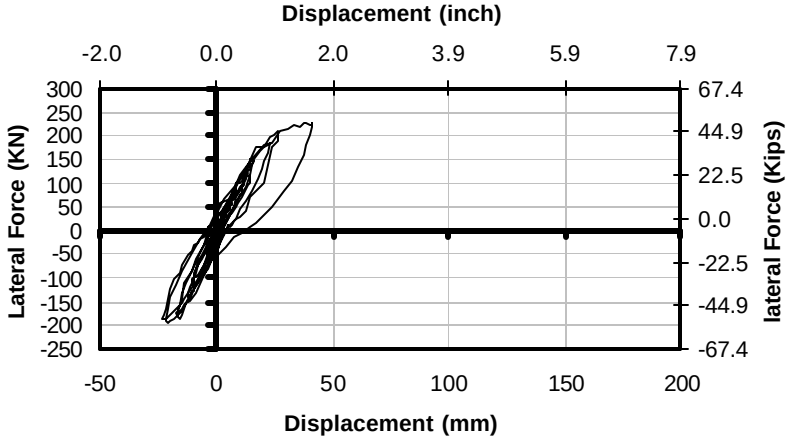

Figure 4-135 F-D Hysteresis for THD-3 at 1.25 x Sylmar

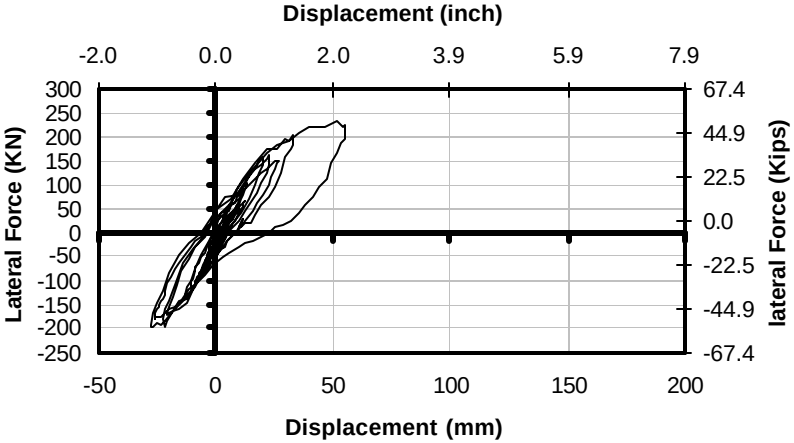

Figure 4-136 F-D Hysteresis for THD-3 at 1.5 x Sylmar

246

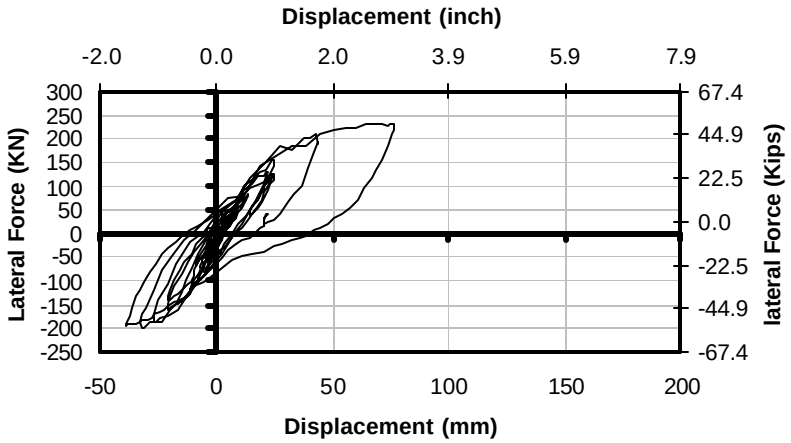

Figure 4-137 F-D Hysteresis for THD-3 at 1.75 x Sylmar

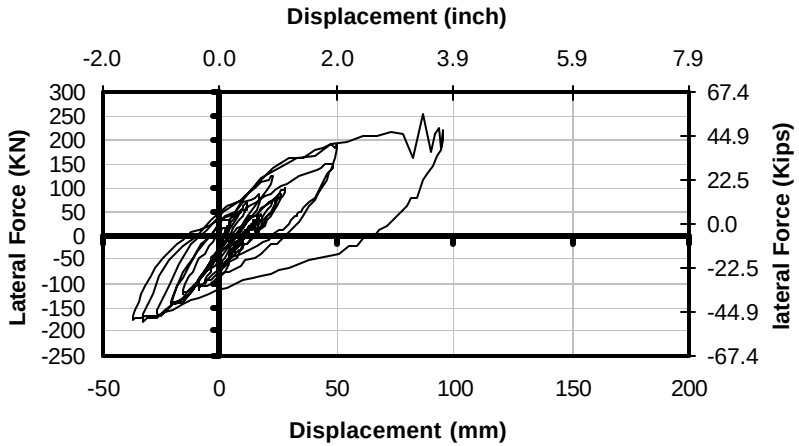

Figure 4-138 F-D Hysteresis for THD-3 at 2.0 x Sylmar

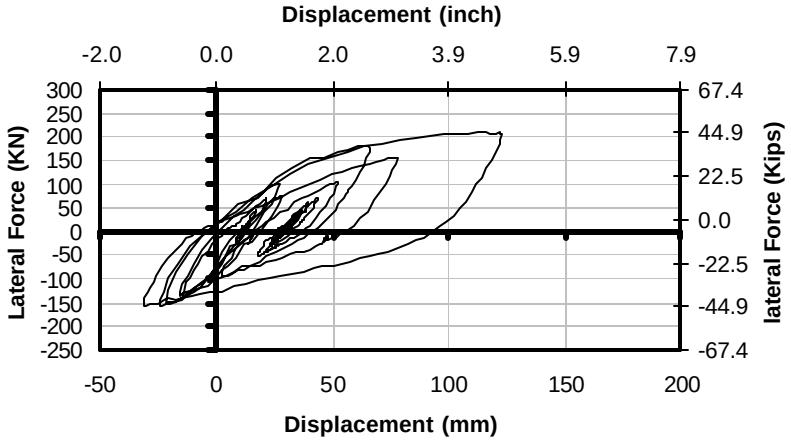

Figure 4-139 F-D Hysteresis for THD-3 at 2.25 x Sylmar

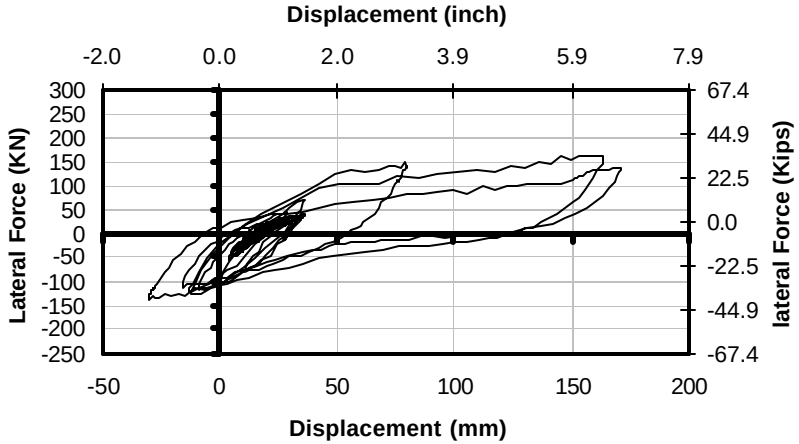

Figure 4-140 F-D Hysteresis for THD-3 at 2.5 x Sylmar

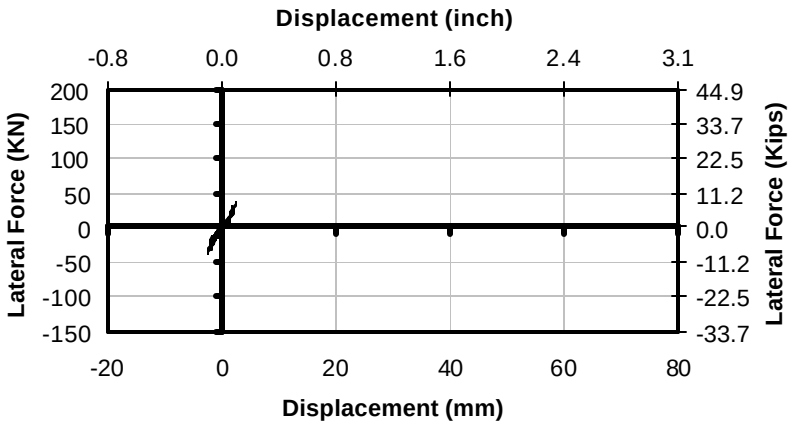

Figure 4-141 F-D Hysteresis for THD-4 at 0.1 x Sylmar

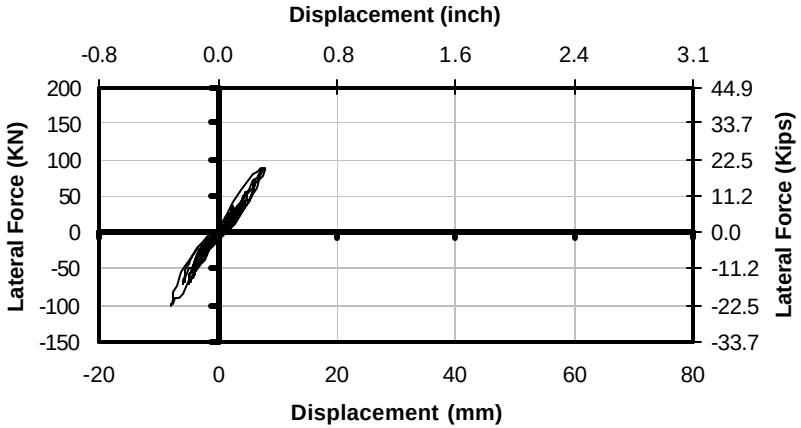

Figure 4-142 F-D Hysteresis for THD-4 at 0.25 x Sylmar

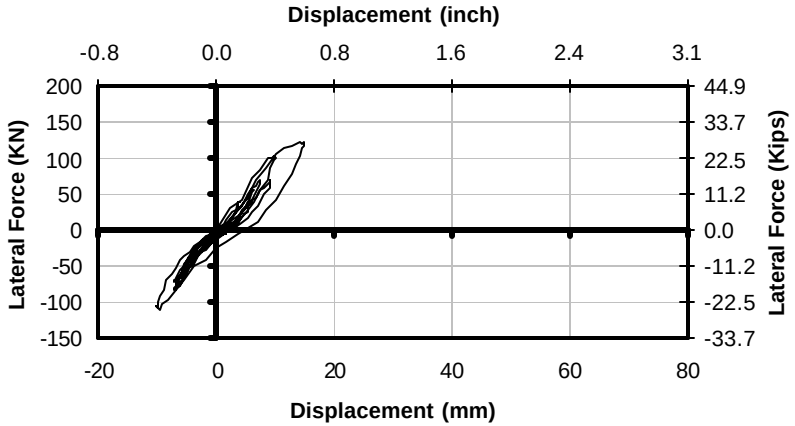

Figure 4-143 F-D Hysteresis for THD-4 at 0.375 x Sylmar

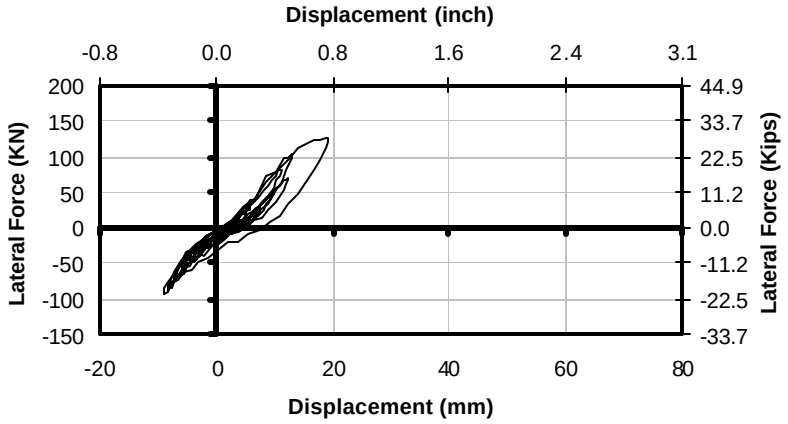

Figure 4-144 F-D Hysteresis for THD-4 at 0.5 x Sylmar

248

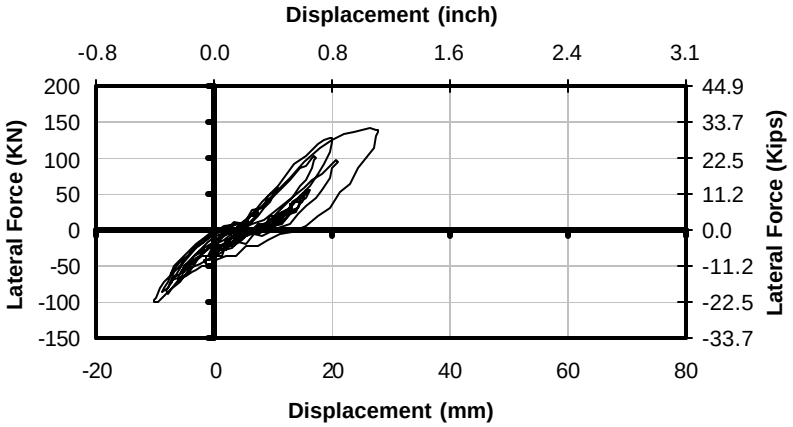

Figure 4-145 F-D Hysteresis for THD-4 at 0.75 x Sylmar

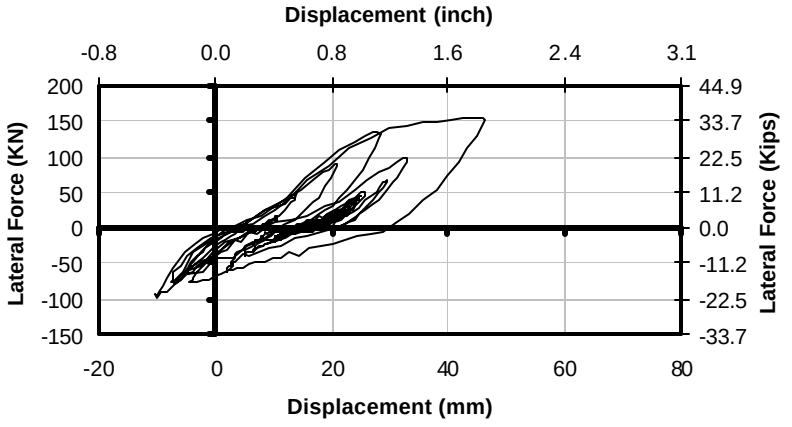

Figure 4-146 F-D Hysteresis for THD-4 at 1.0 x Sylmar

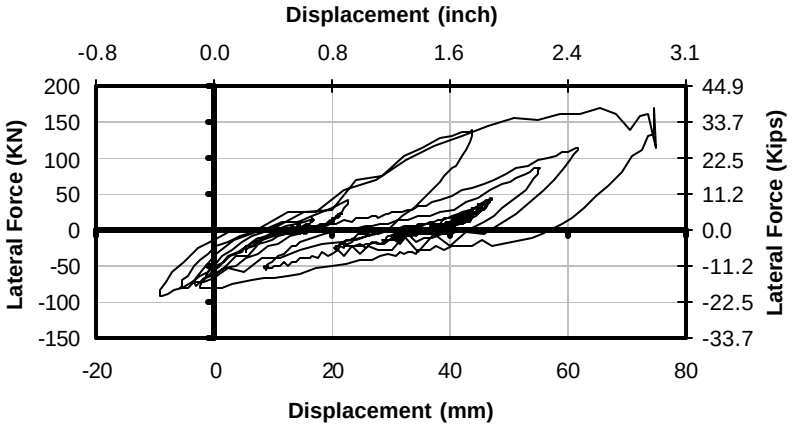

Figure 4-147 F-D Hysteresis for THD-4 at 1.25 x Sylmar

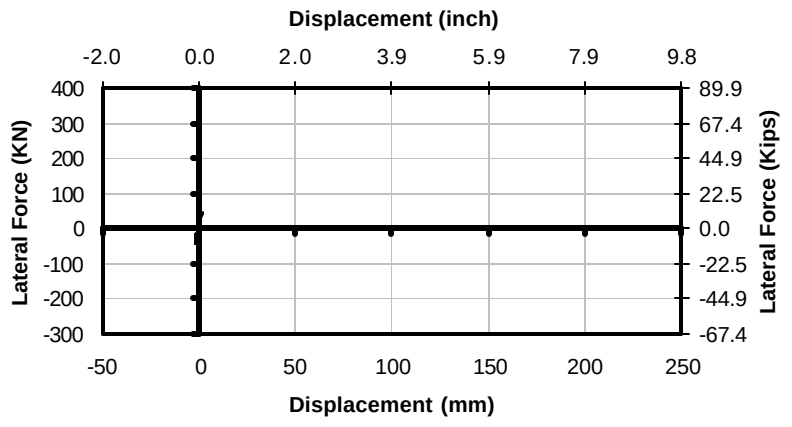

Figure 4-148 F-D Hysteresis for THD-5 at 0.1 x Sylmar

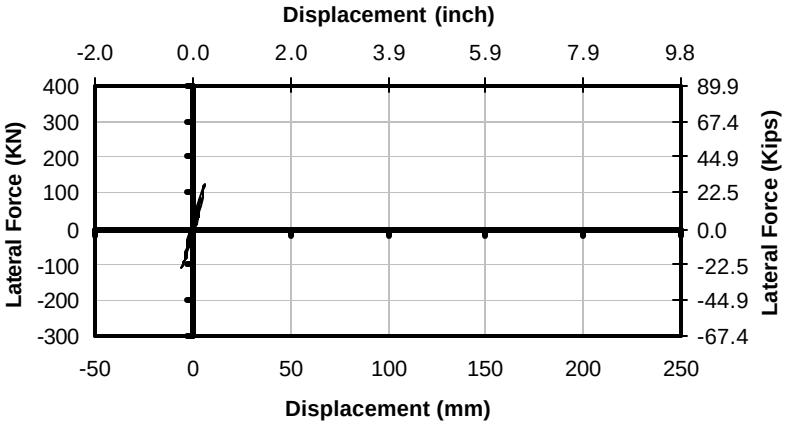

Figure 4-149 F-D Hysteresis for THD-5 at 0.25 x Sylmar

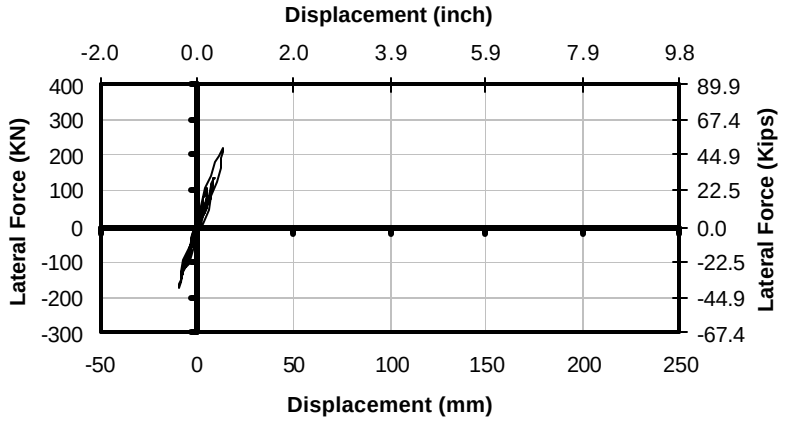

Figure 4-150 F-D Hysteresis for THD-5 at 0.5 x Sylmar

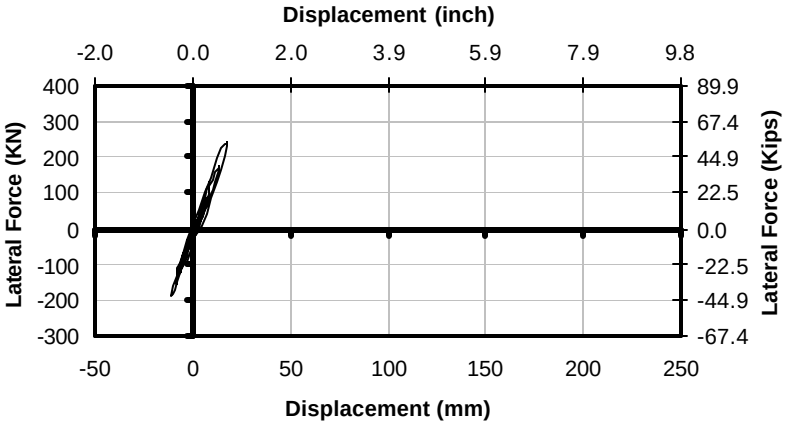

Figure 4-151 F-D Hysteresis for THD-5 at 0.75 x Sylmar

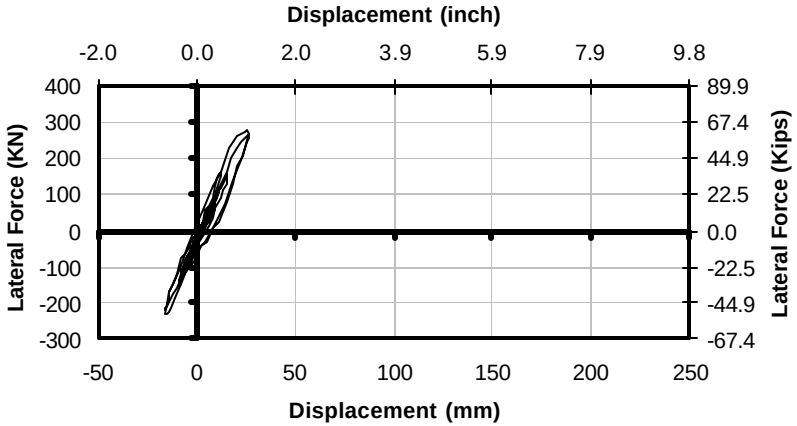

Figure 4-152 F-D Hysteresis for THD-5 at 1.0 x Sylmar

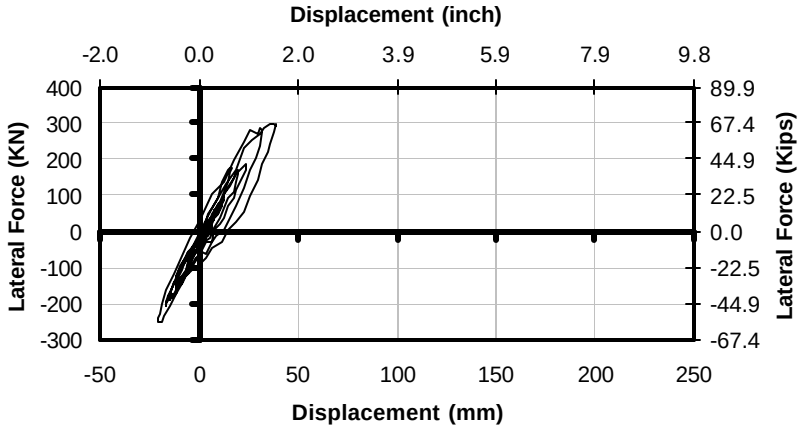

Figure 4-153 F-D Hysteresis for THD-5 at 1.25 x Sylmar

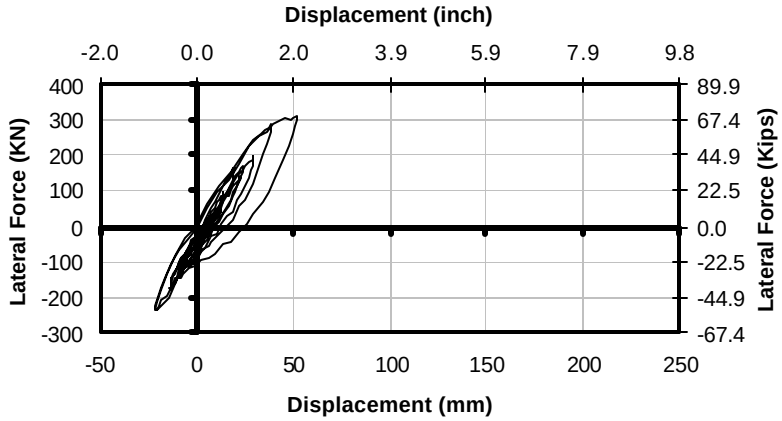

Figure 4-154 F-D Hysteresis for THD-5 at 1.5 x Sylmar

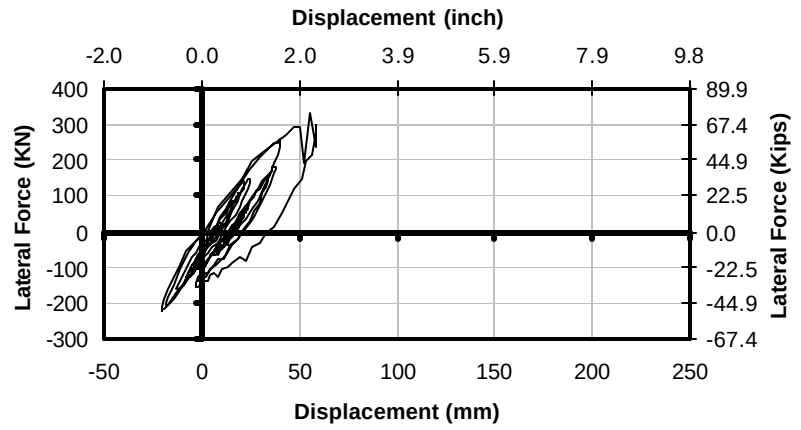

Figure 4-155 F-D Hysteresis for THD-5 at 1.75 x Sylmar

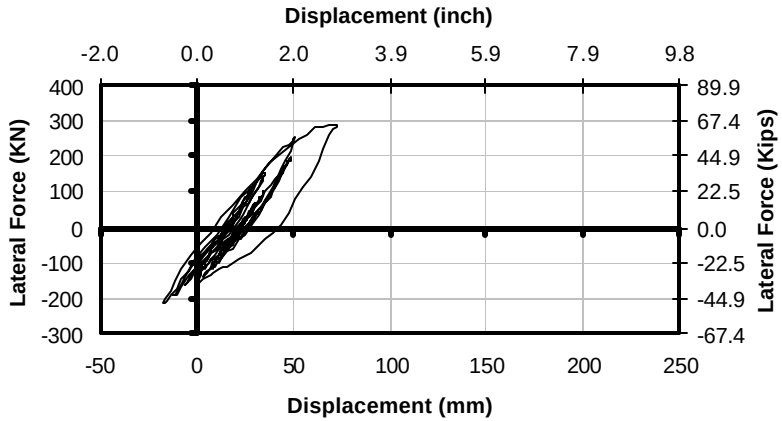

Figure 4-156 F-D Hysteresis for THD-5 at 2.0 x Sylmar

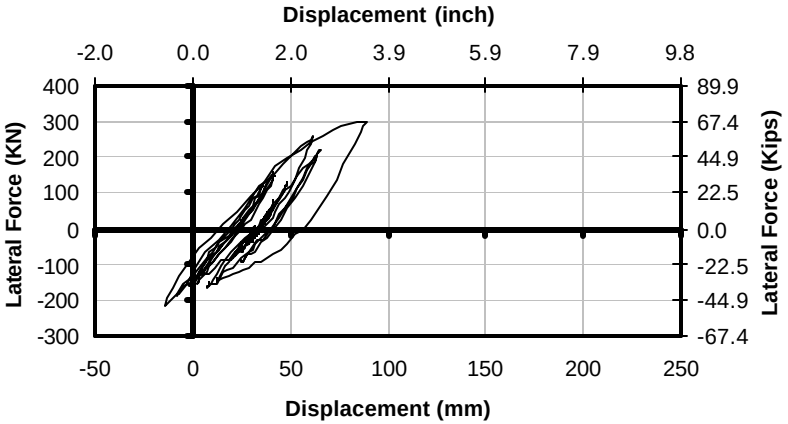

Figure 4-157 F-D Hysteresis for THD-5 at 2.25 x Sylmar

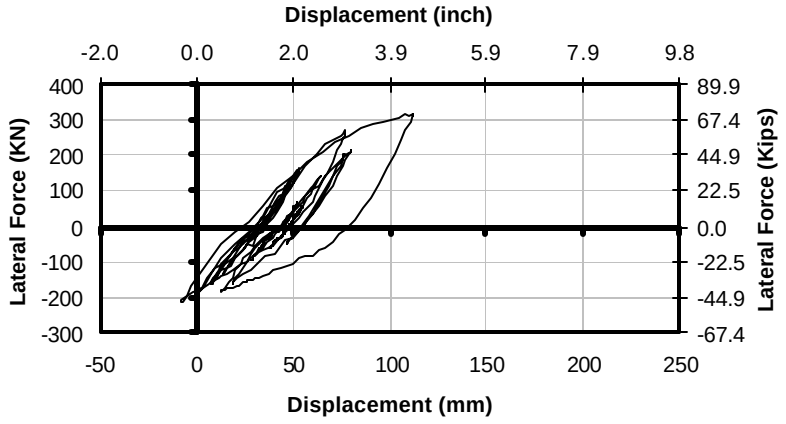

Figure 4-158 F-D Hysteresis for THD-5 at 2.5 x Sylmar

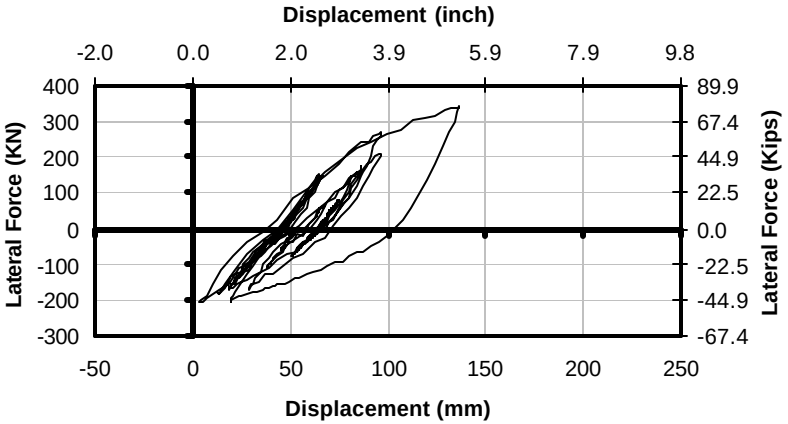

Figure 4-159 F-D Hysteresis for THD-5 at 2.75 x Sylmar

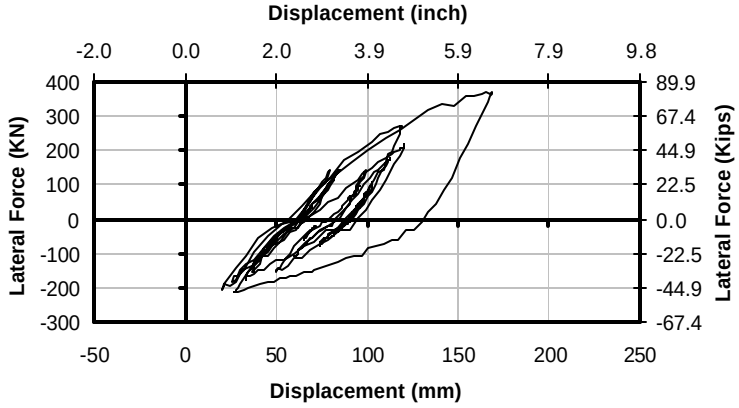

Figure 4-160 F-D Hysteresis for THD-5 at 3.0 x Sylmar

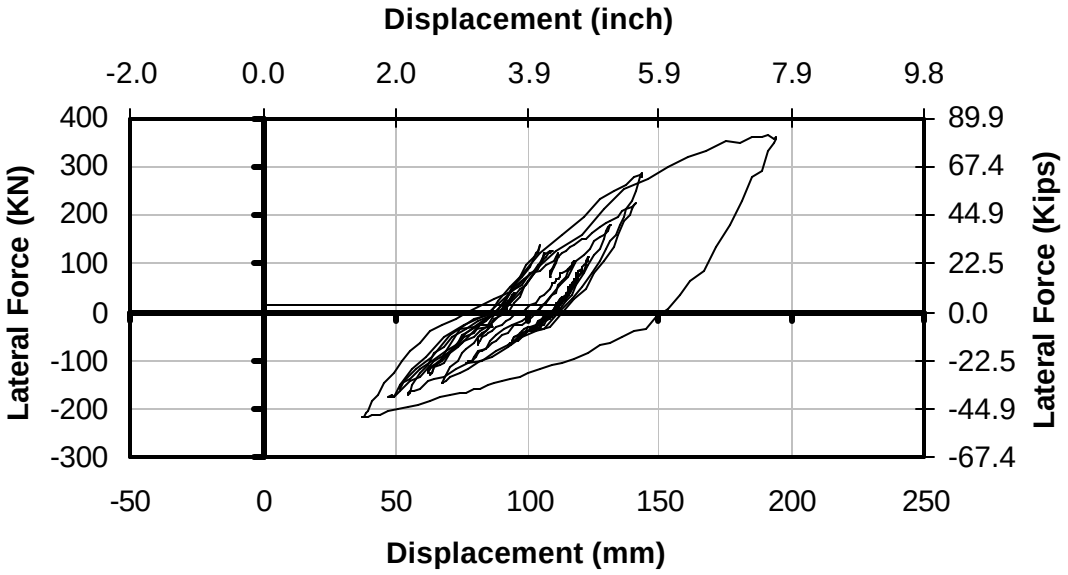

Figure 4-161 F-D Hysteresis for THD-5 at 3.0 x Sylmar (2nd Time)

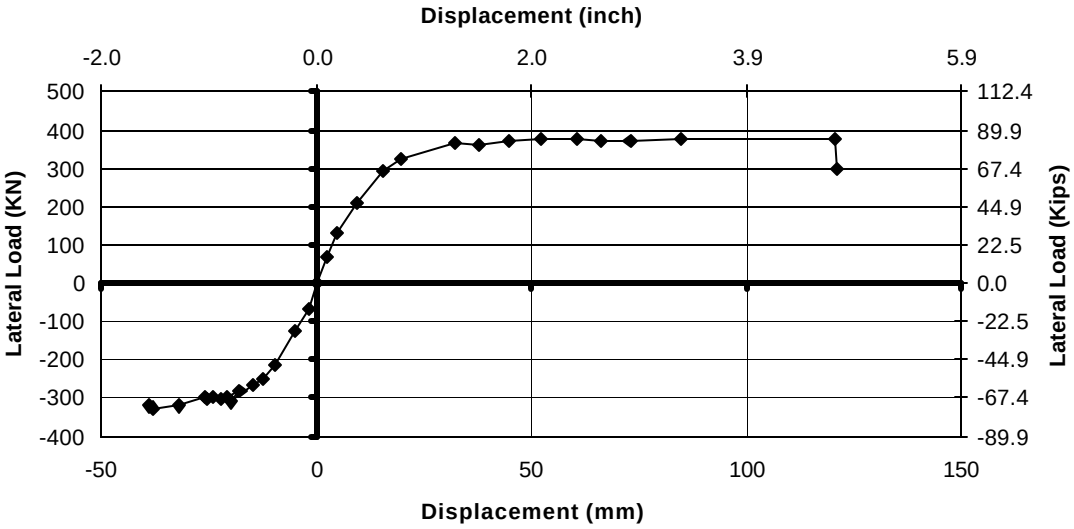

Figure 4-162 Envelope of Accumulated Force Displacement Hysteresis for THD-1

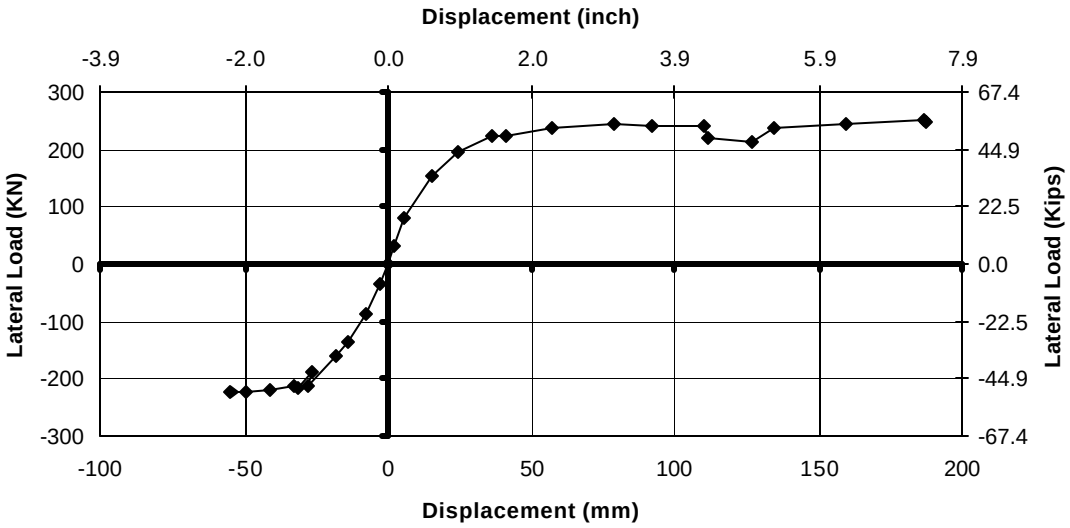

Figure 4-163 Envelope of Accumulated Force Displacement Hysteresis for THD-2

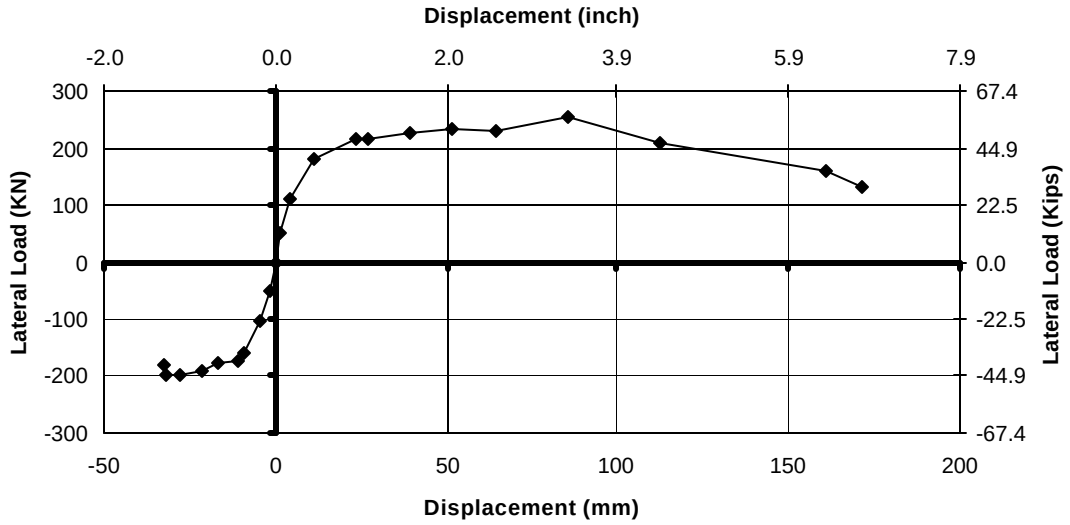

Figure 4-164 Envelope of Accumulated Force Displacement Hysteresis for THD-3

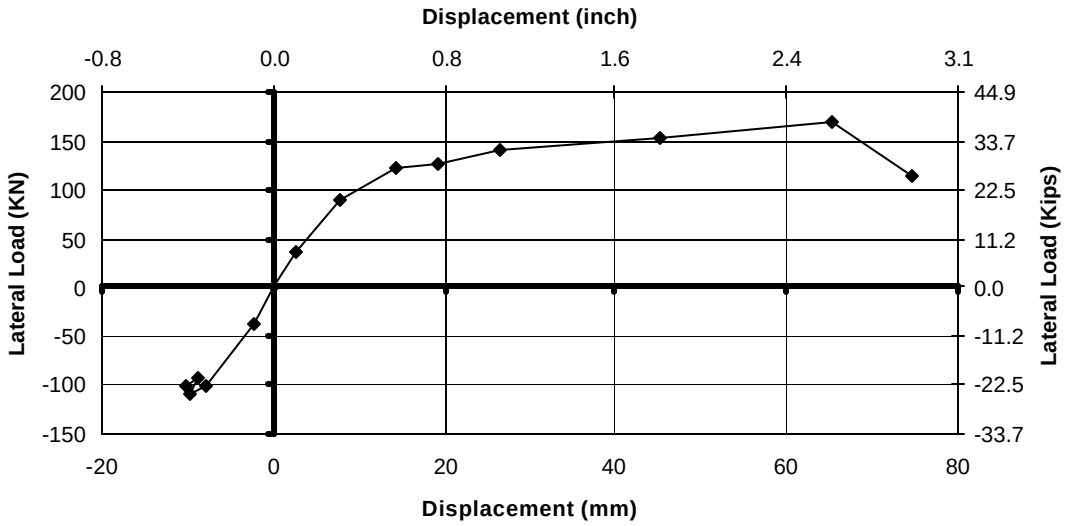

Figure 4-165 Envelope of Accumulated Force Displacement Hysteresis for THD-4

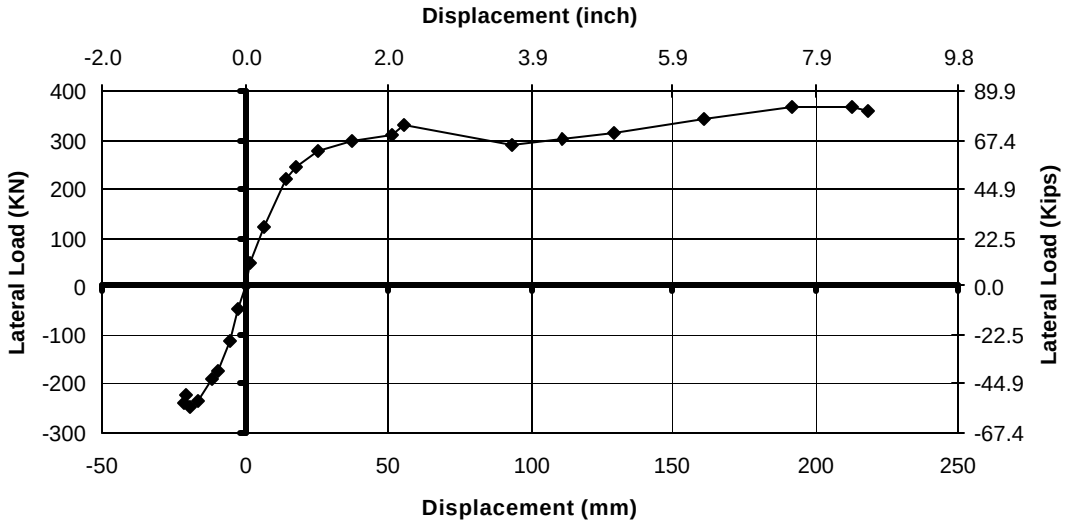

Figure 4-166 Envelope of Accumulated Force Displacement Hysteresis for THD-5

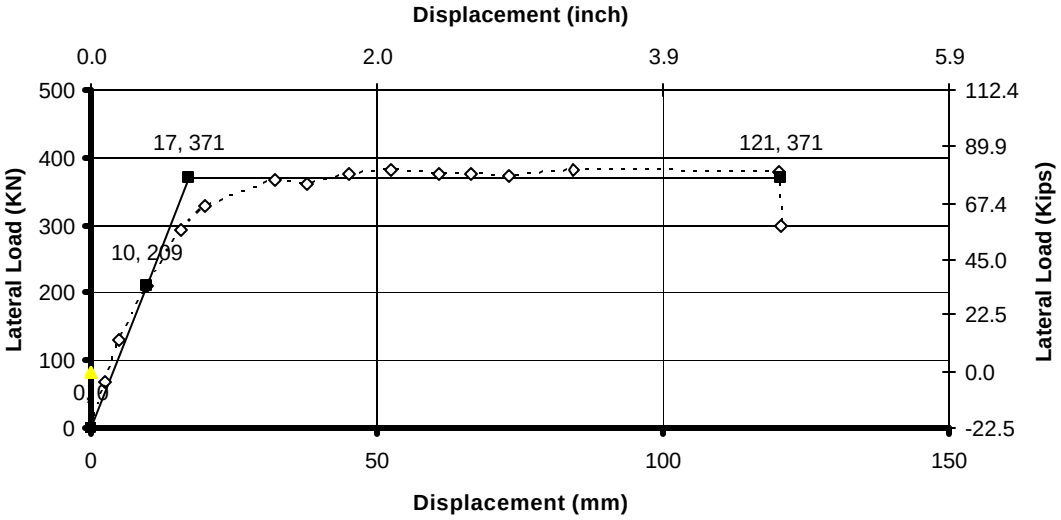

Figure 4-167 Elasto-Plastic Idealized Force Displacement Curve for THD-1

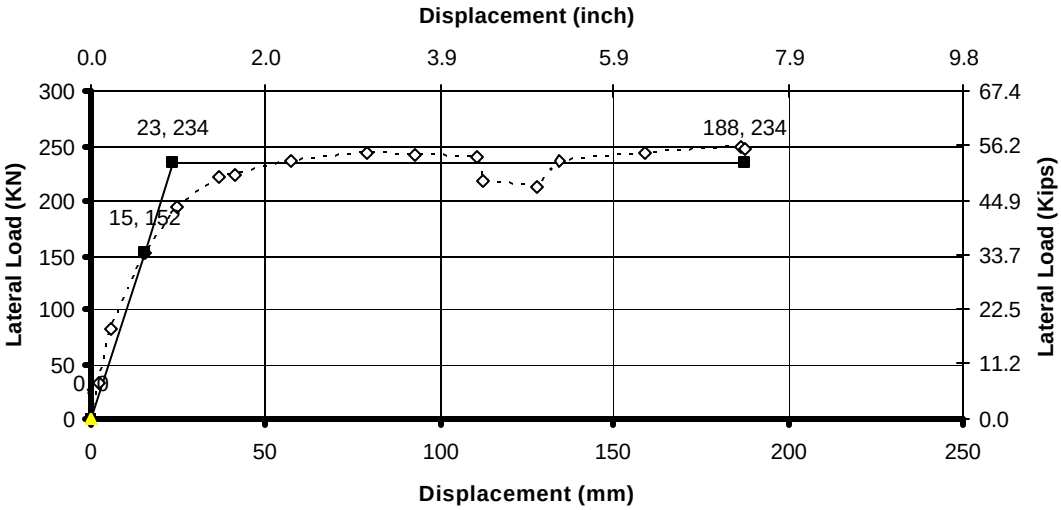

Figure 4-168 Elasto-Plastic Idealized Force Displacement Curve for THD-2

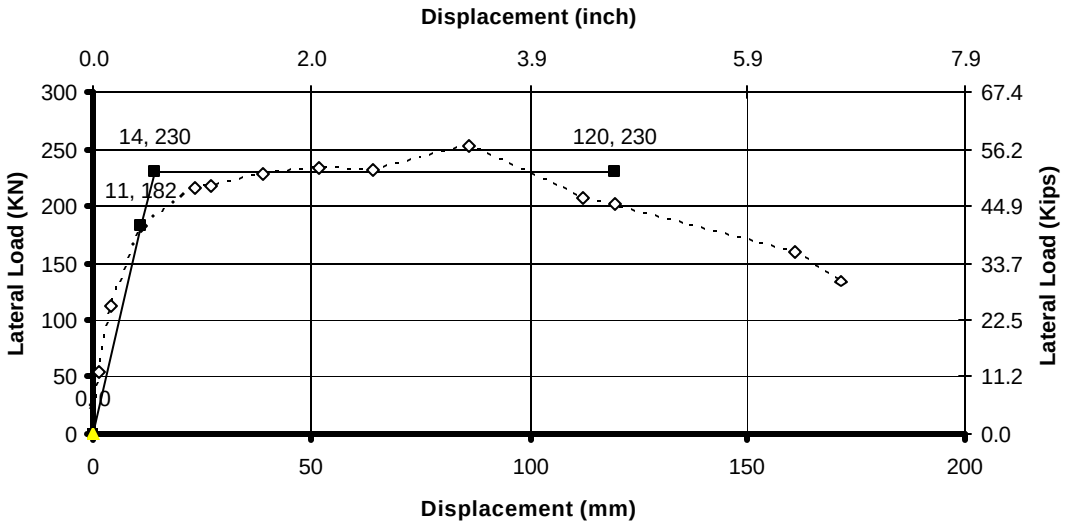

Figure 4-169 Elasto-Plastic Idealized Force Displacement Curve for THD-3

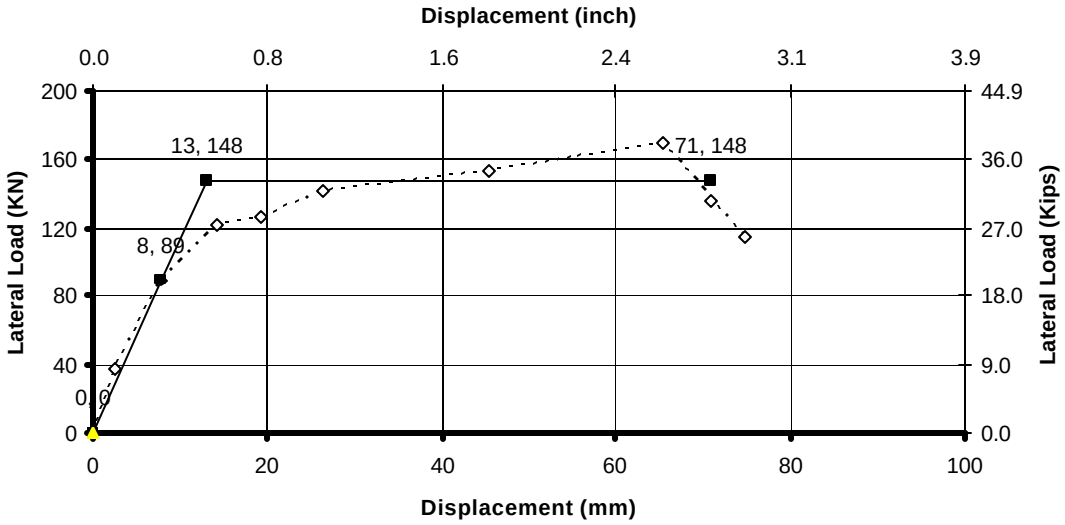

Figure 4-170 Elasto-Plastic Idealized Force Displacement Curve for THD-4

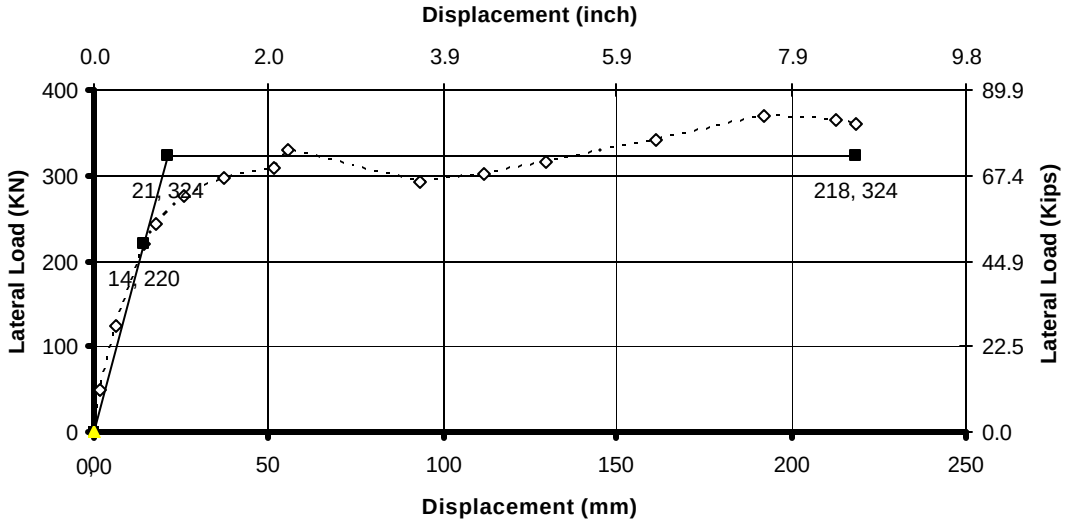

Figure 4-171 Elasto-Plastic Idealized Force Displacement Curve for THD-5

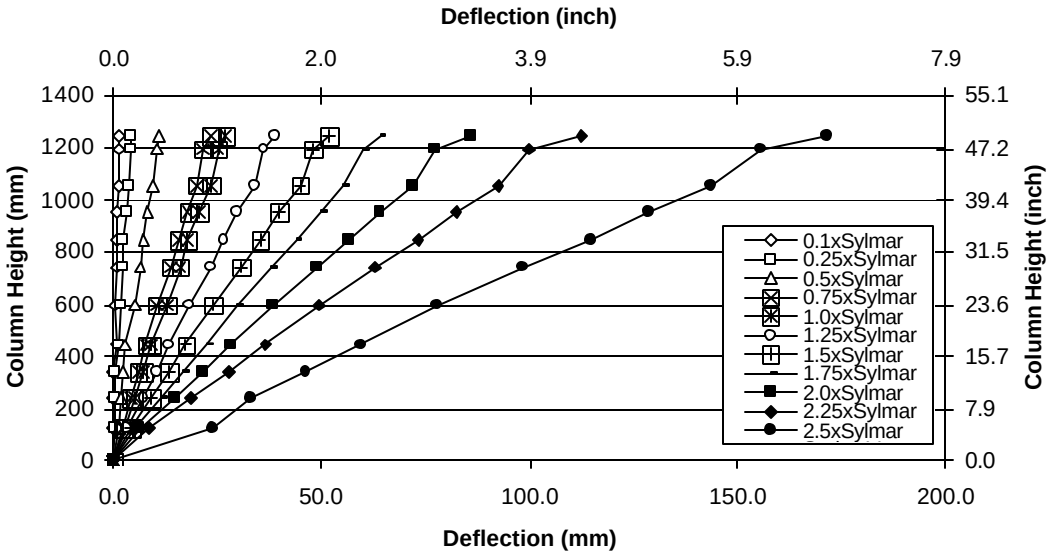

Figure 4-172 Specimen Deflection Profile for THD-3

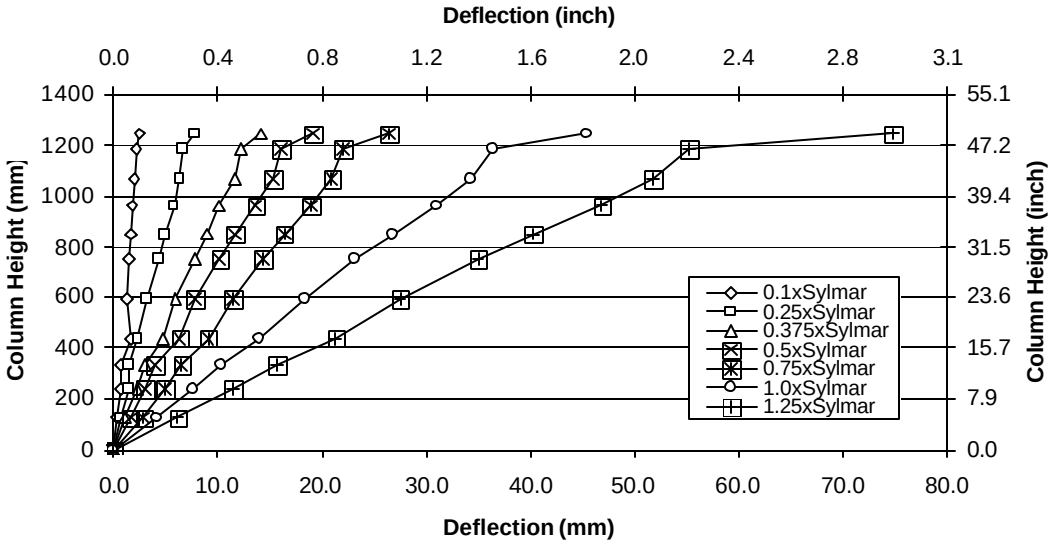

Figure 4-173 Specimen Deflection Profile for THD-4

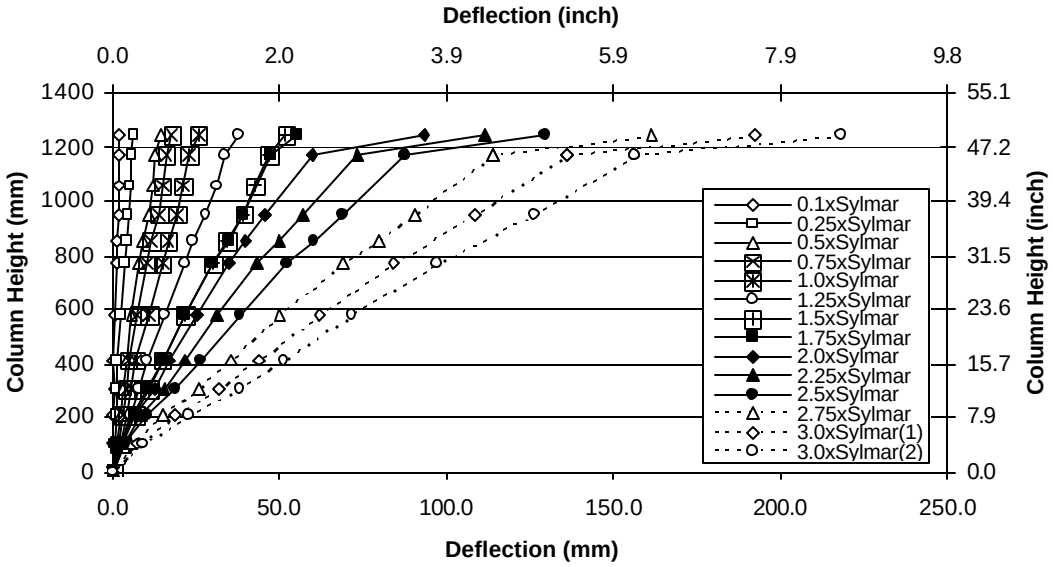

Figure 4-174 Specimen Deflection Profile for THD-5

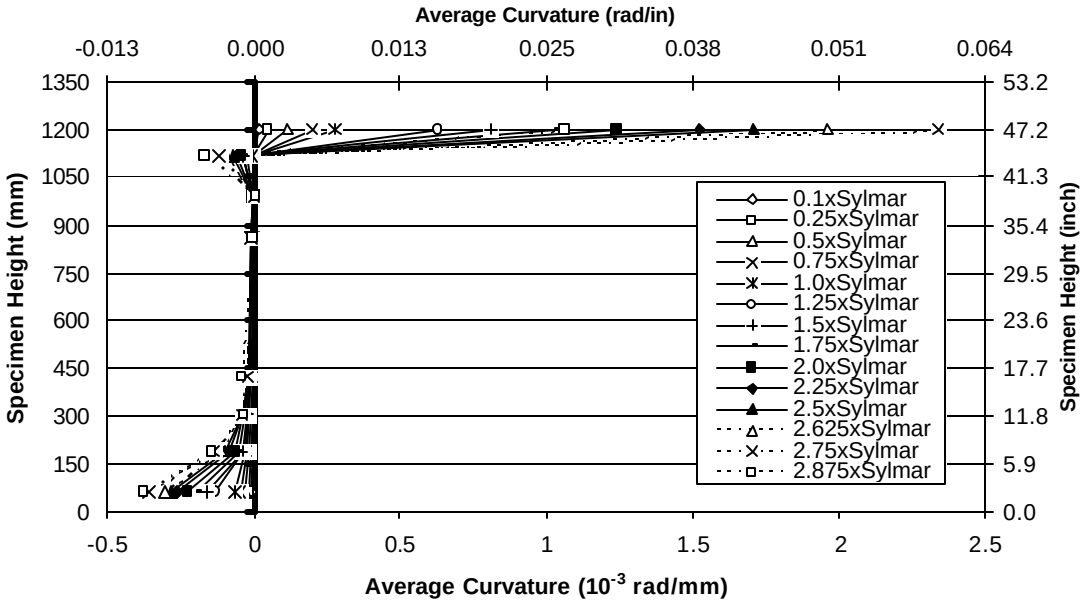

Figure 4-175 Curvature Profile at Max. Peak Force for THD-1

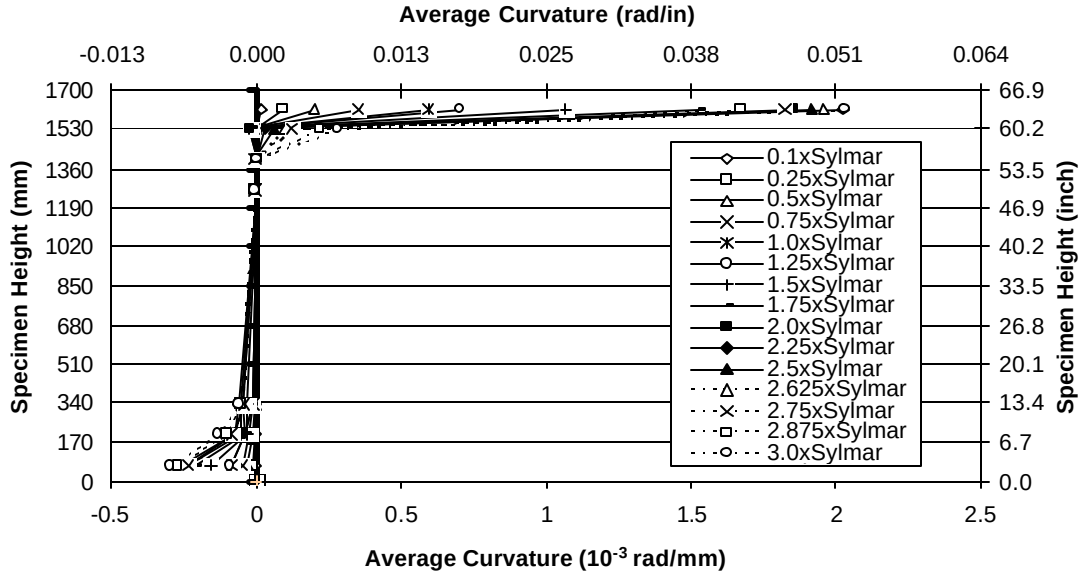

Figure 4-176 Curvature Profile at Max. Peak Force for THD-2

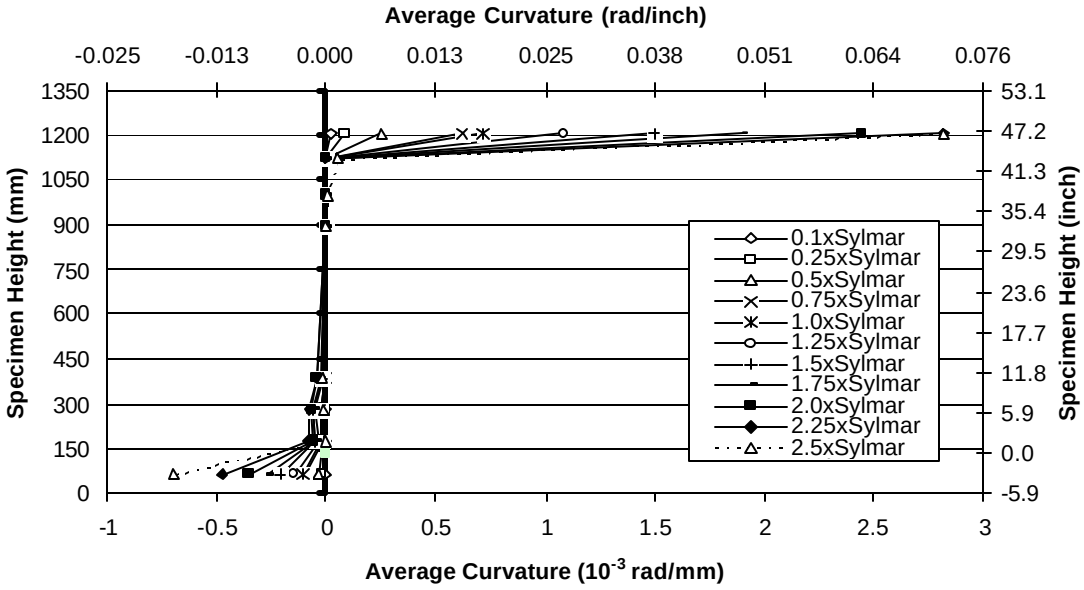

Figure 4-177 Curvature Profile at Max. Peak Force for THD-3

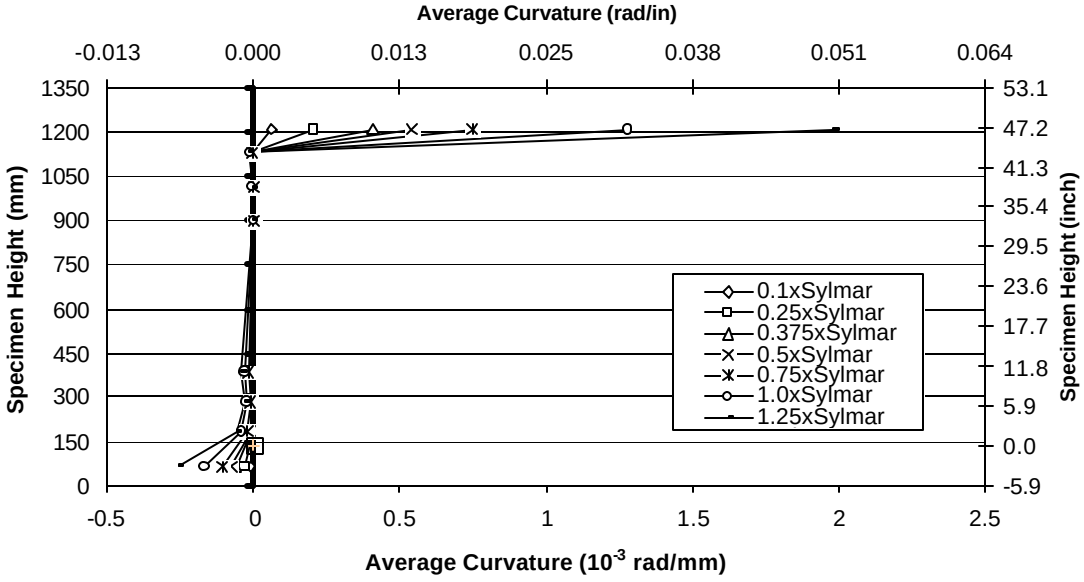

Figure 4-178 Curvature Profile at Max. Peak Force for THD-4

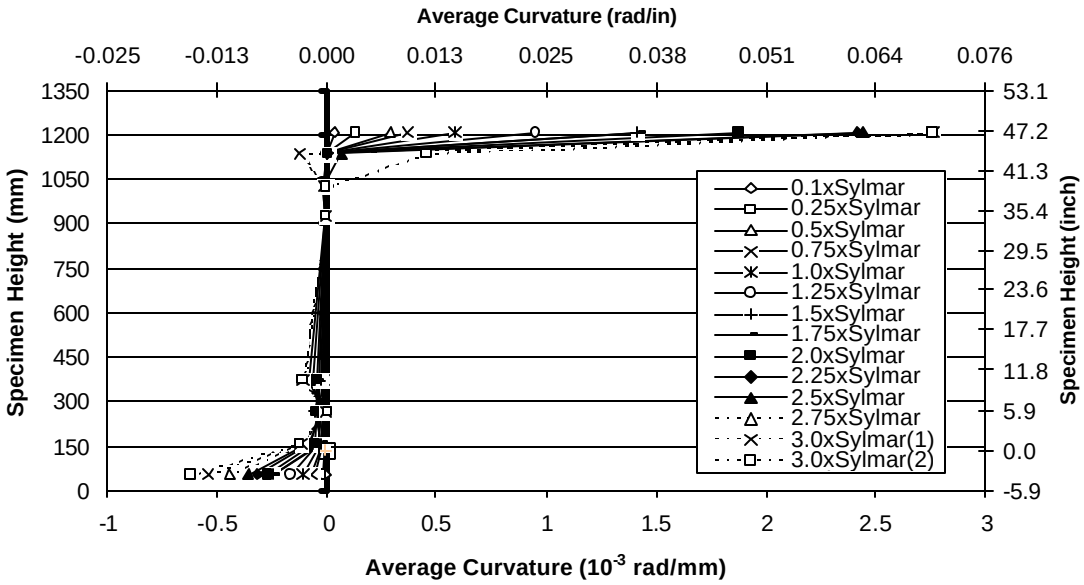

Figure 4-179 Curvature Profile at Max. Peak Force for THD-5

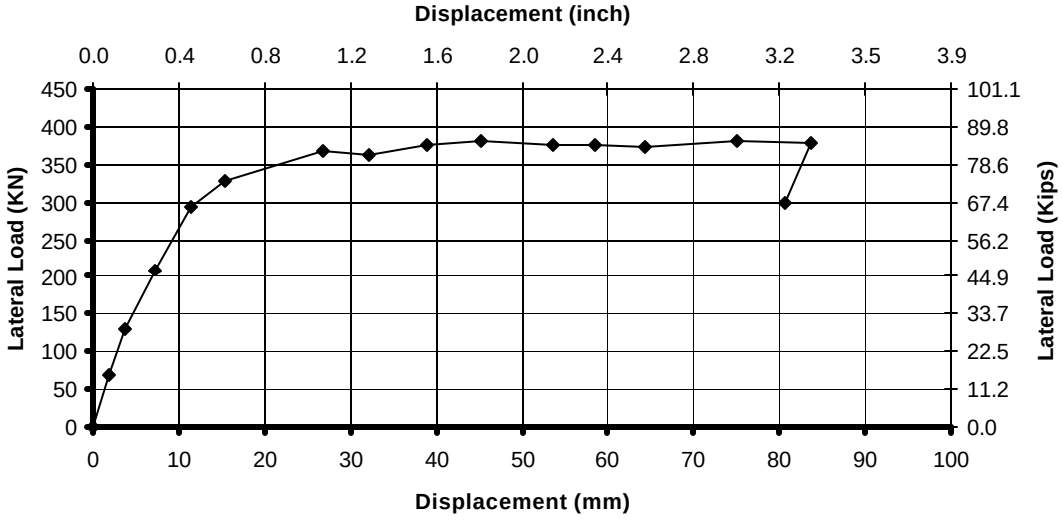

Figure 4-180 Lateral Force versus Flexural Deformation for THD-1

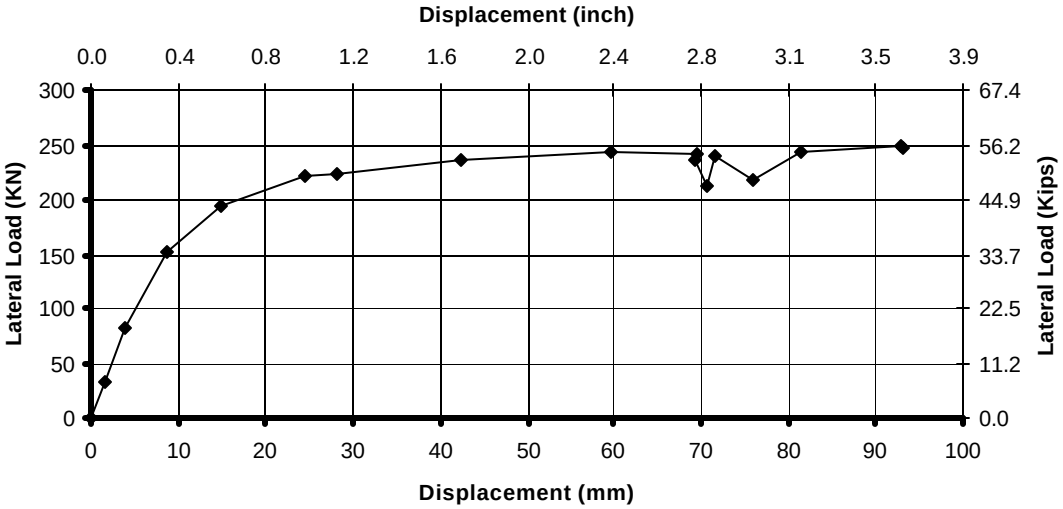

Figure 4-181 Lateral Force versus Flexural Deformation for THD-2

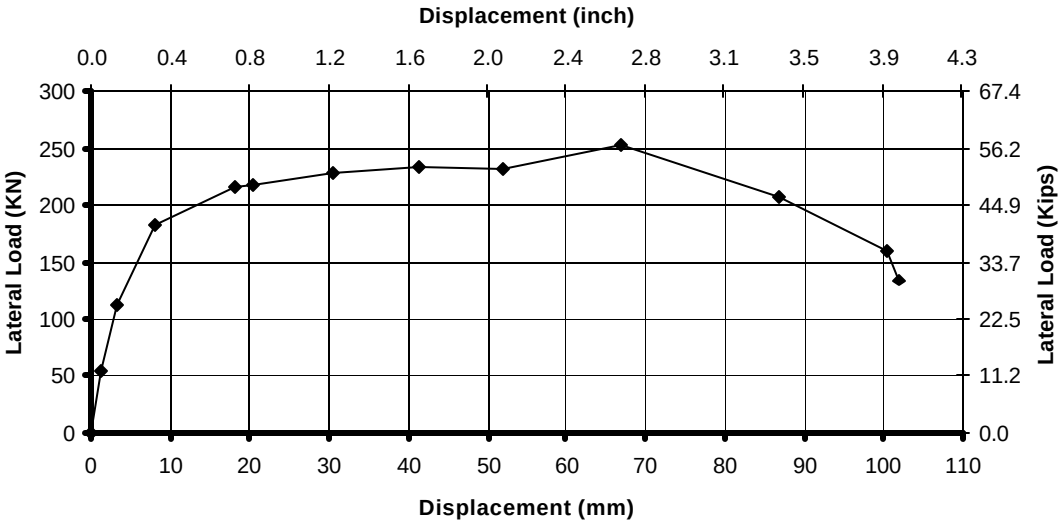

Figure 4-182 Lateral Force versus Flexural Deformation for THD-3

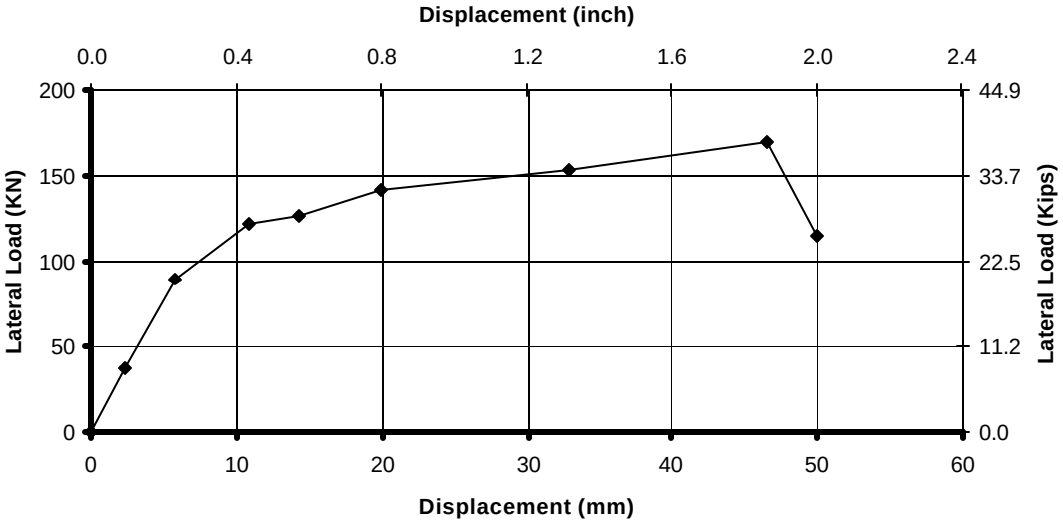

Figure 4-183 Lateral Force versus Flexural Deformation for THD-4

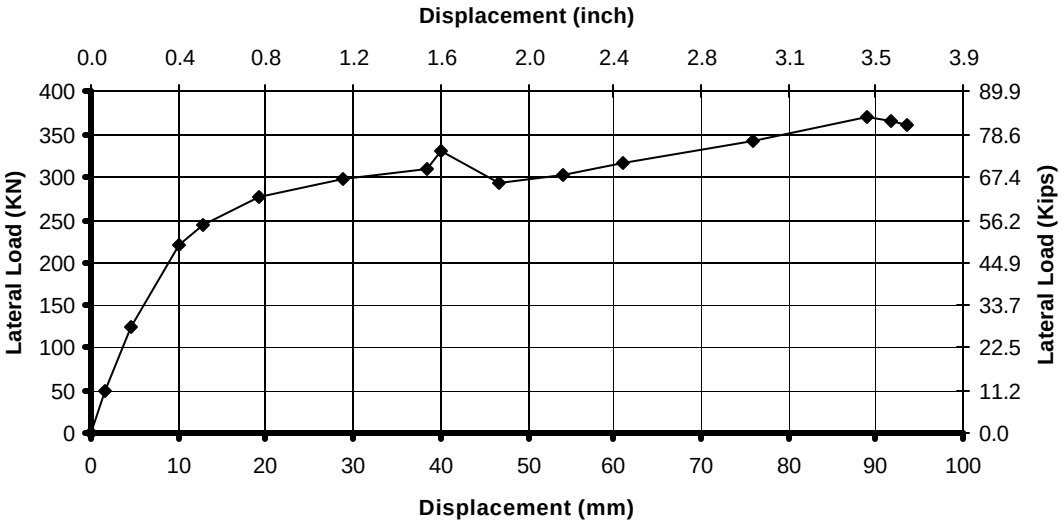

Figure 4-184 Lateral Force versus Flexural Deformation for THD-5

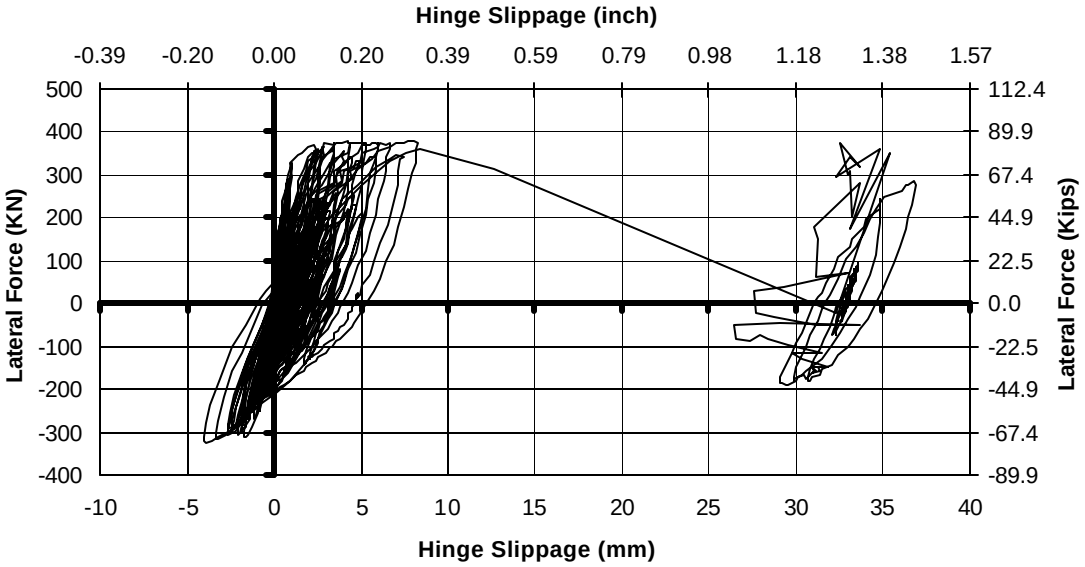

Figure 4-185 Lateral Force vs. Hinge Slippage Hysteresis for THD-1

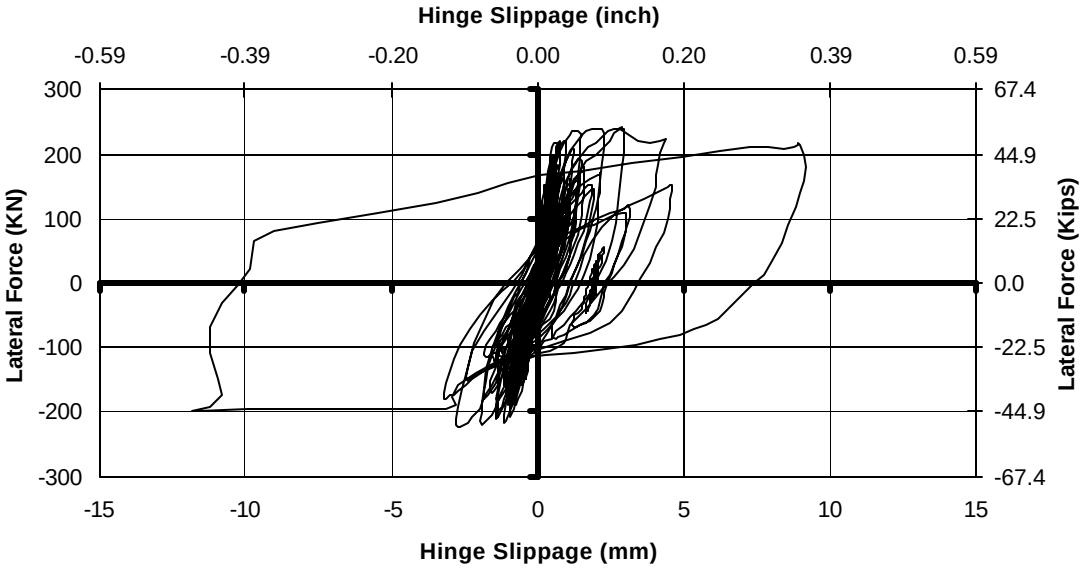

Figure 4-186 Lateral Force vs. Hinge Slippage Hysteresis for THD-2 (0.1xSylmar to 2.25 Sylmar)

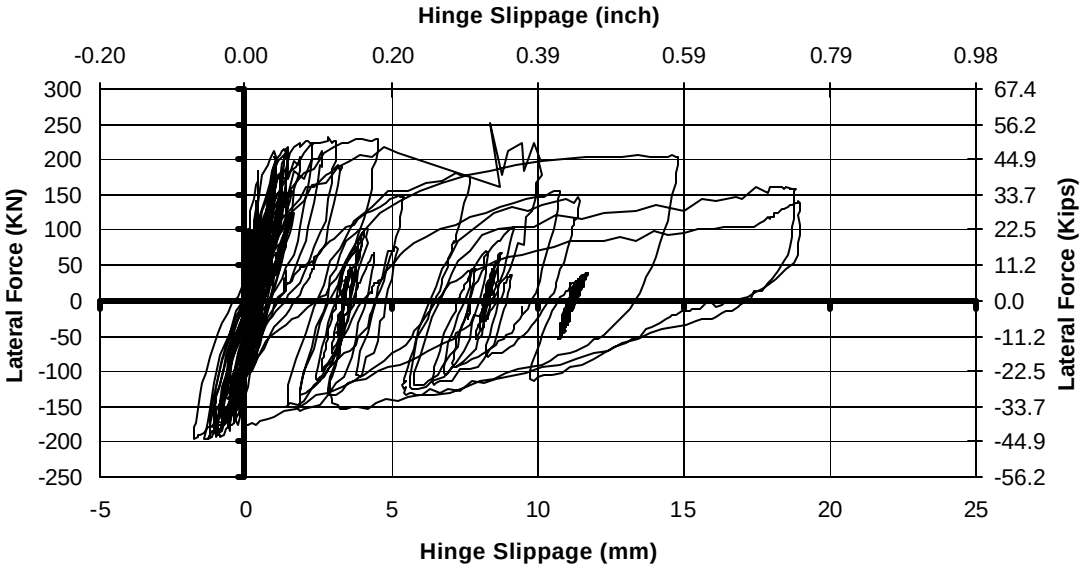

Figure 4-187 Lateral Force vs. Hinge Slippage Hysteresis for THD-3

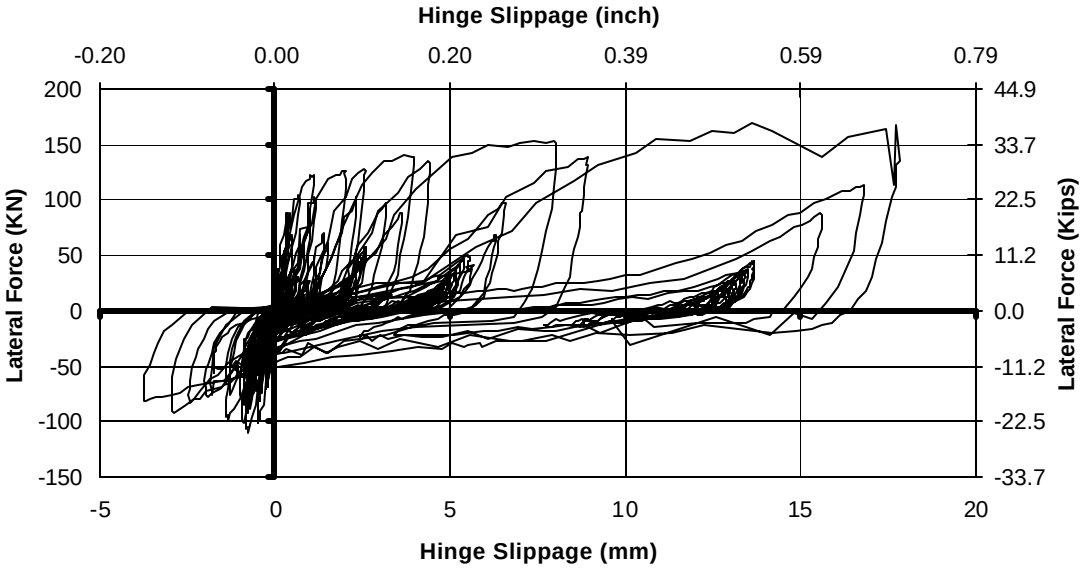

Figure 4-188 Lateral Force vs. Hinge Slippage Hysteresis for THD-4

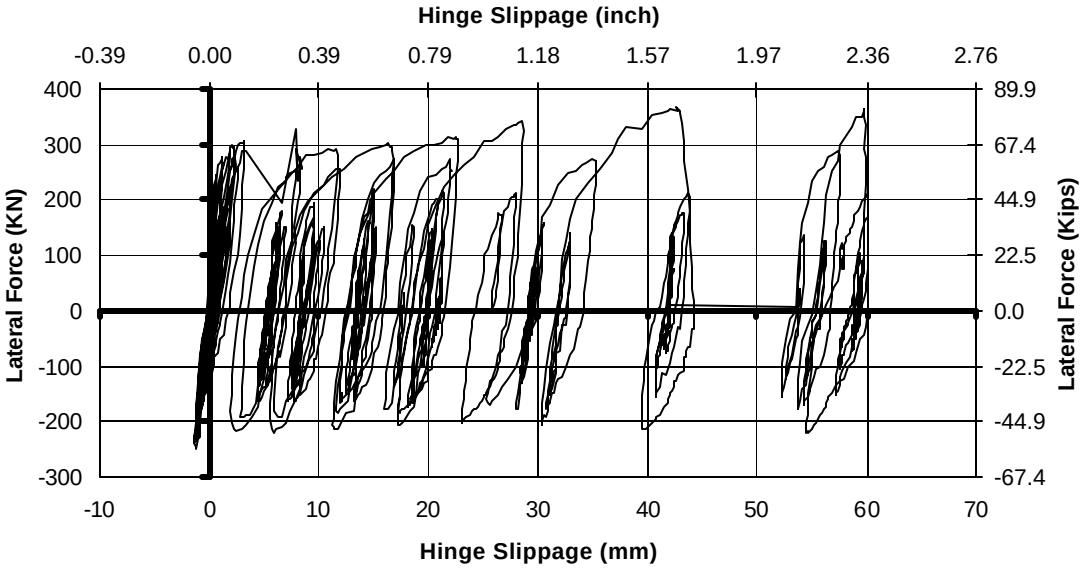

Figure 4-189 Lateral Force vs. Hinge Slippage Hysteresis for THD-5

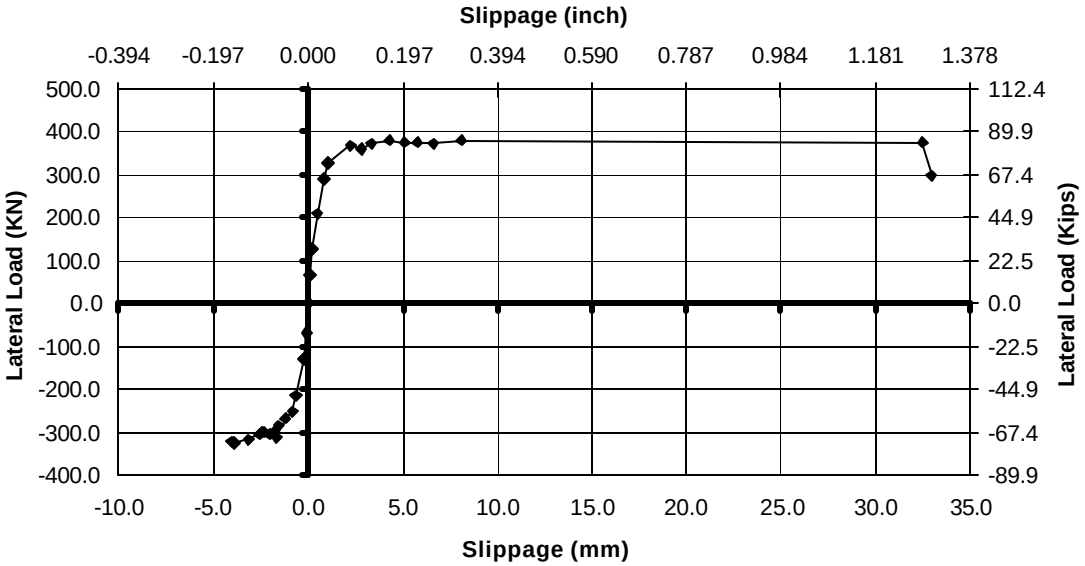

Figure 4-190 Envelope of Force vs. Hinge Slippage Hysteresis for THD-1

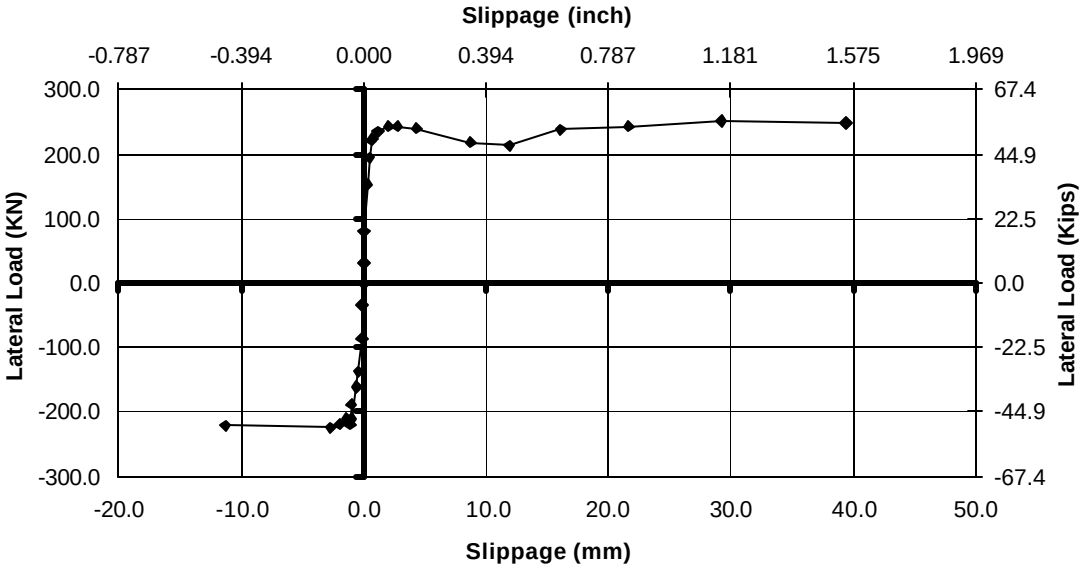

Figure 4-191 Envelope of Force vs. Hinge Slippage Hysteresis for THD-2

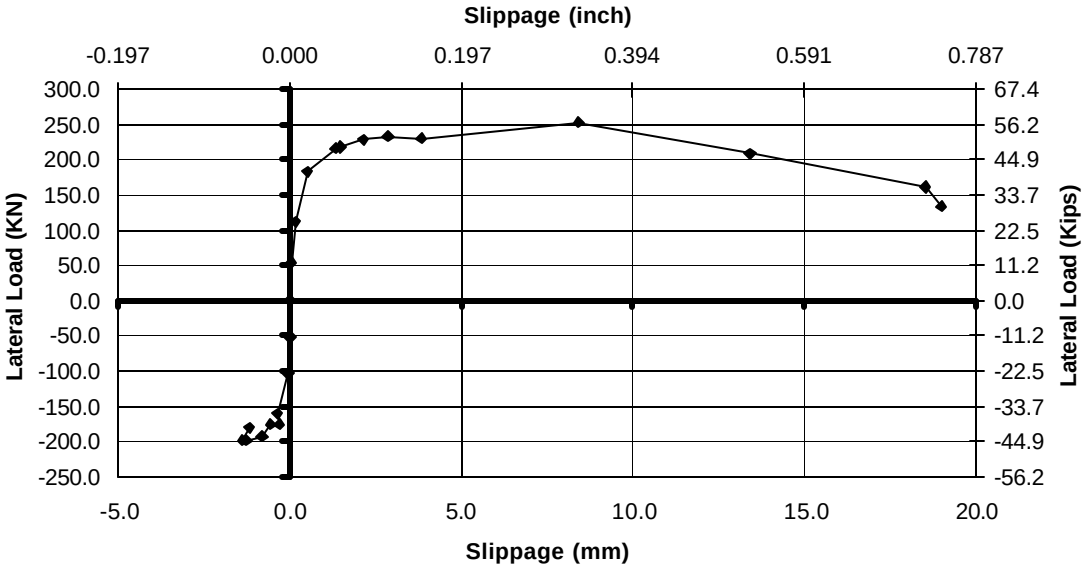

Figure 4-192 Envelope of Force vs. Hinge Slippage Hysteresis for THD-3

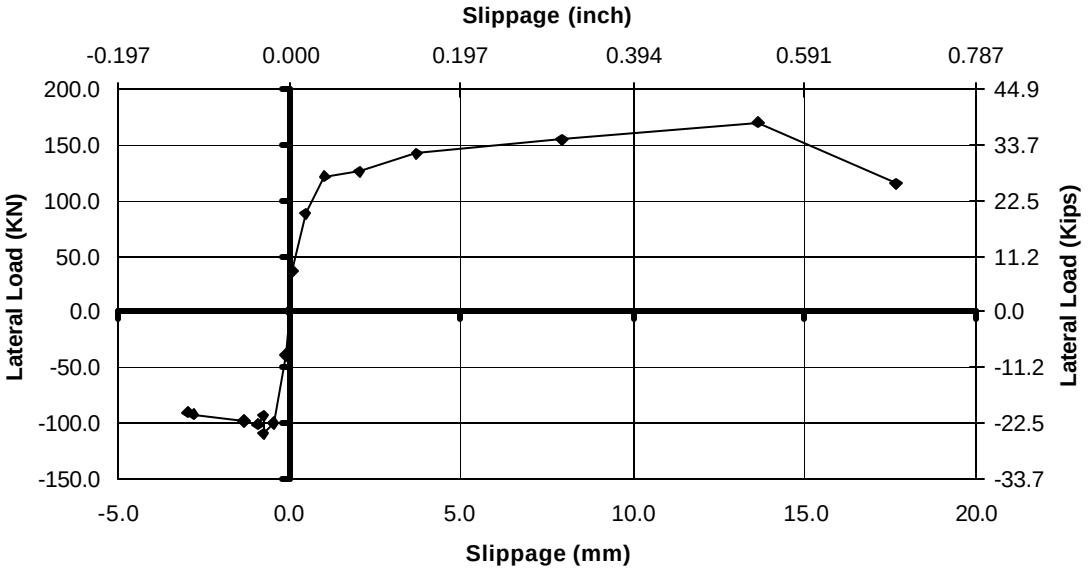

Figure 4-193 Envelope of Force vs. Hinge Slippage Hysteresis for THD-4

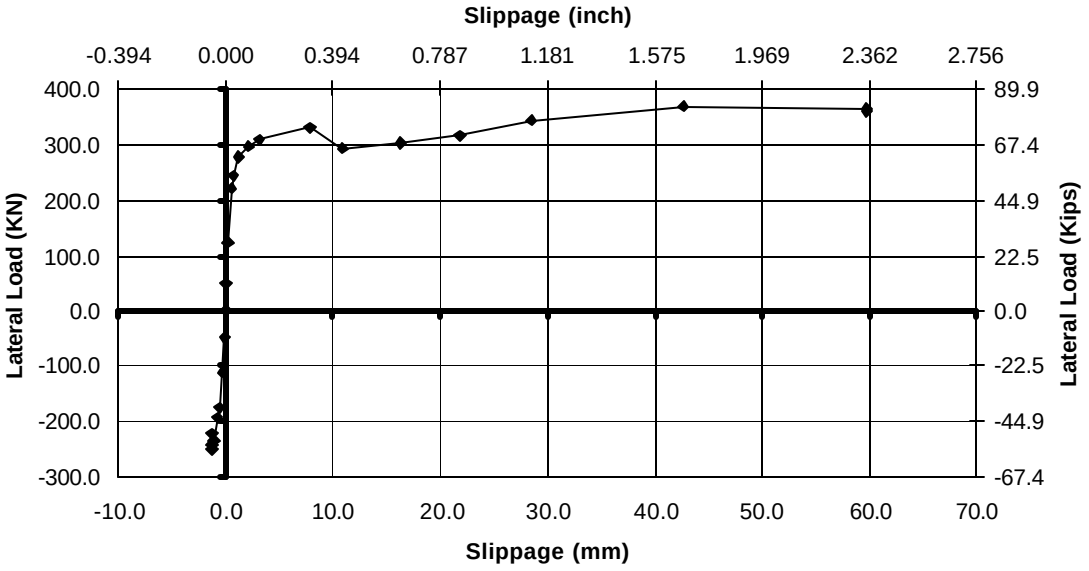

Figure 4-194 Envelope of Force vs. Hinge Slippage Hysteresis for THD-5

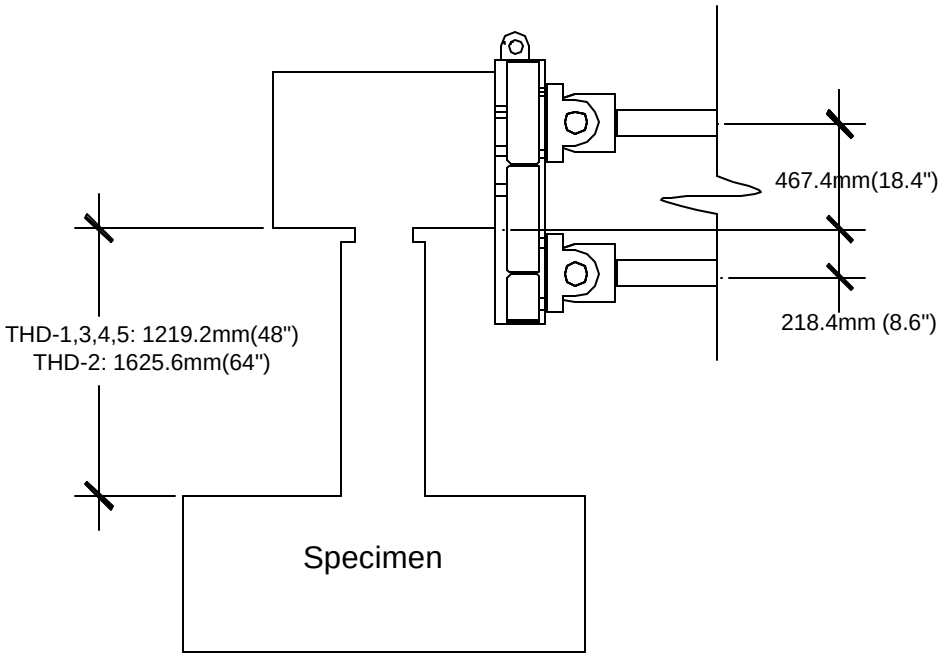

Figure 4-195 Link Location & Moment Arms to Calculate Moment Demand at the Top and Bottom of the Column

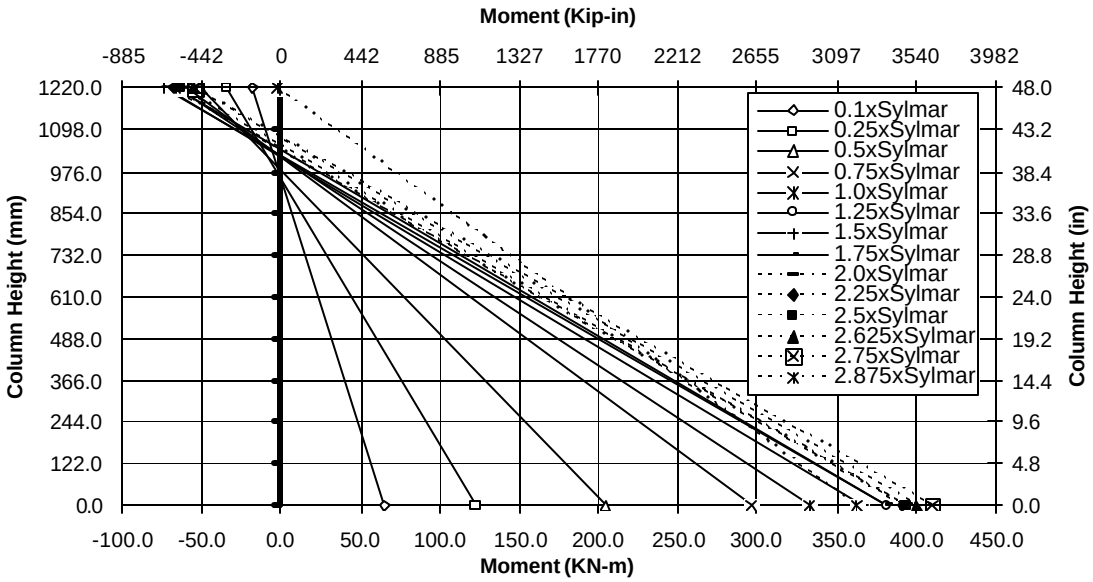

Figure 4-196 Moment Distribution at Max. Peak Force for THD-1

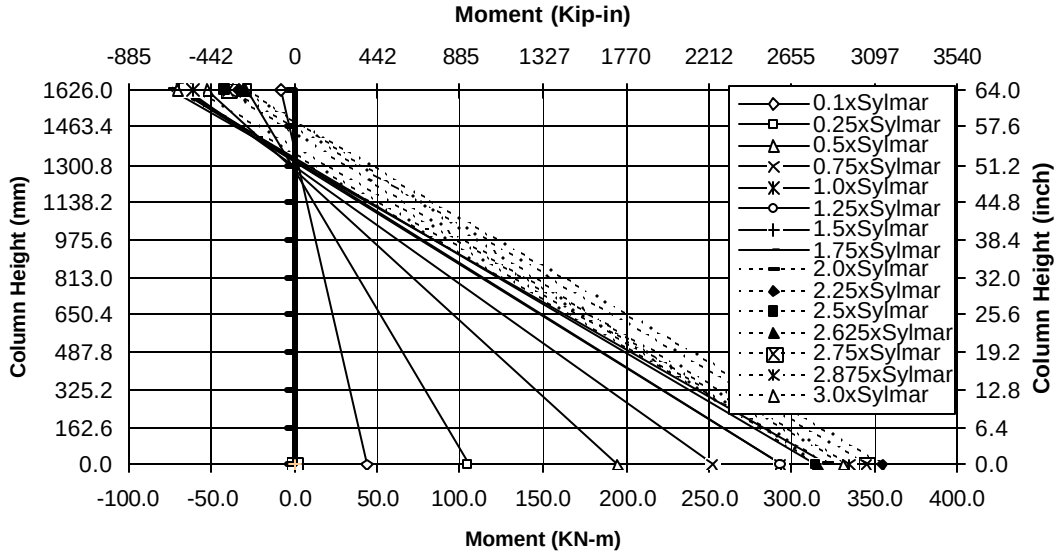

Figure 4-197 Moment Distribution at Max. Peak Force for THD-2

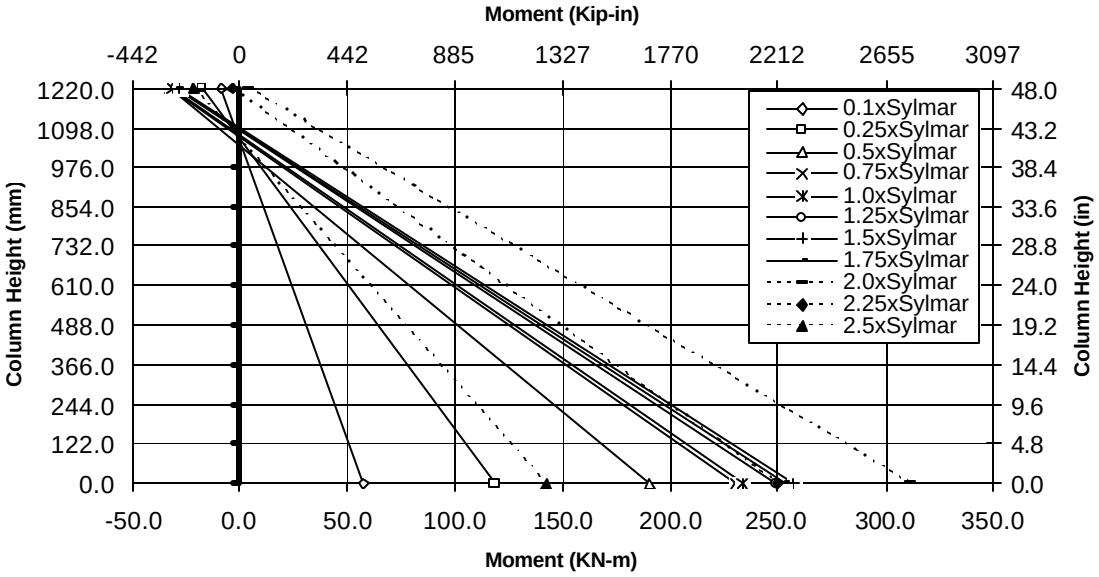

Figure 4-198 Moment Distribution at Max. Peak Force for THD-3

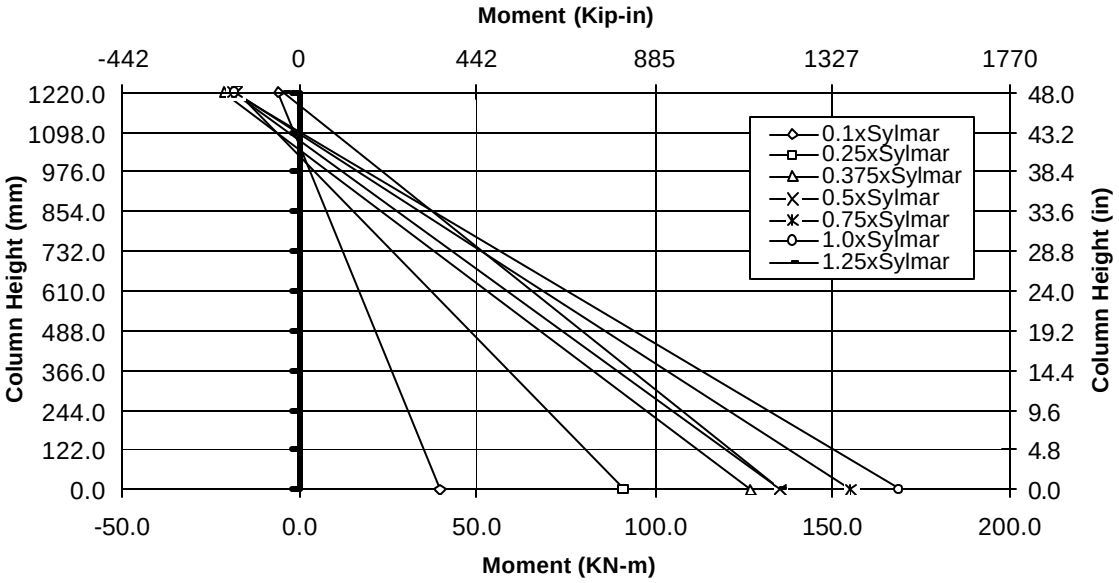

Figure 4-199 Moment Distribution at Max. Peak Force for THD-4

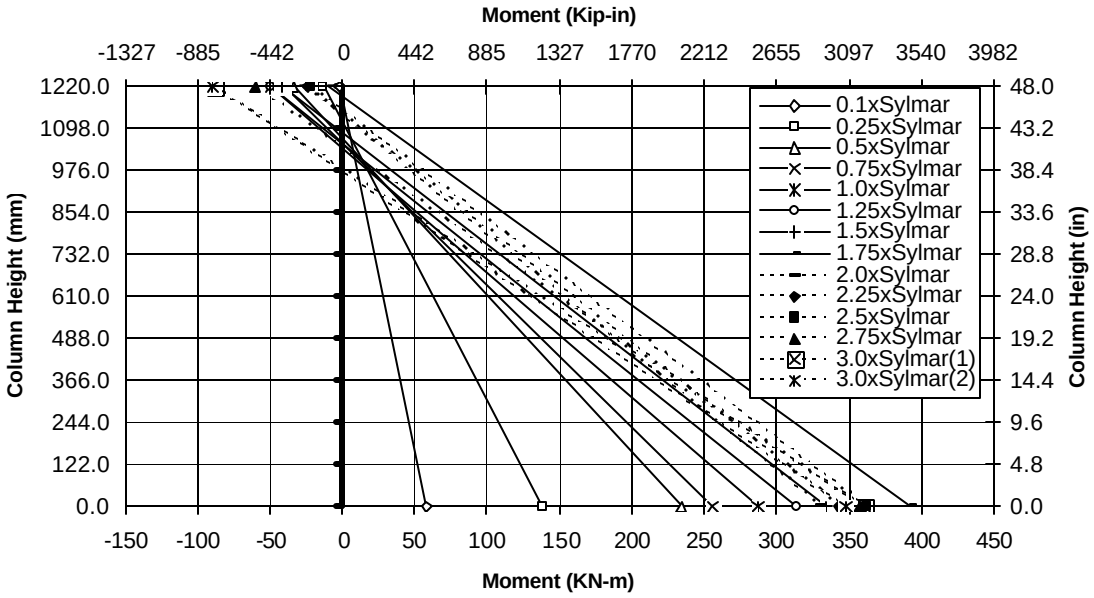

Figure 4-200 Moment Distribution at Max. Peak Force for THD-5

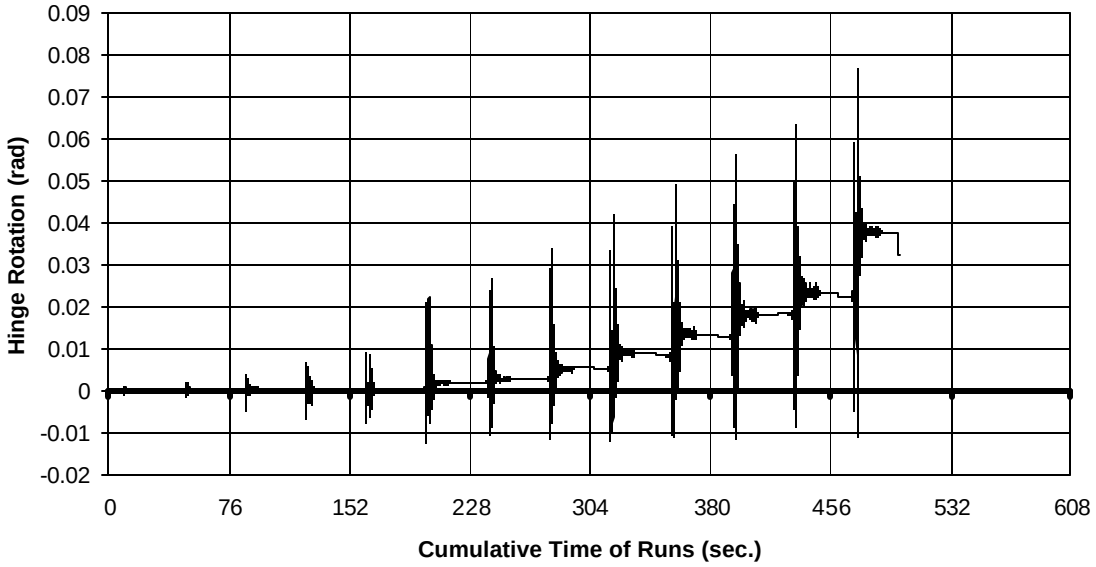

Figure 4-201 Hinge Rotation History of THD-1 (0.1xSylmar to 2.75xSylmar)

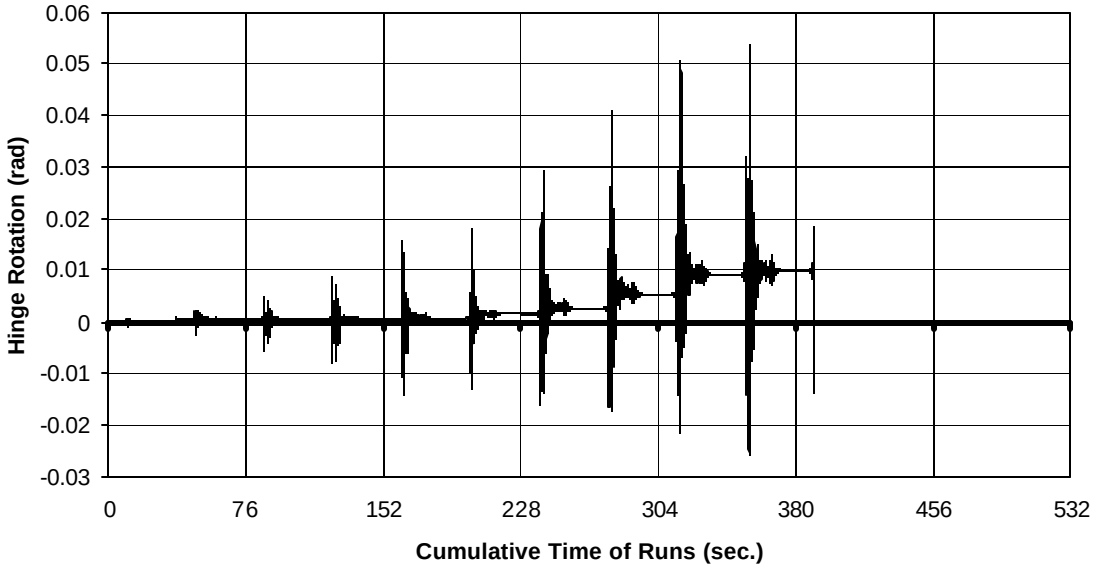

Figure 4-202 Hinge Rotation History of THD-2 (0.1xSylmar to 2.25xSylmar)

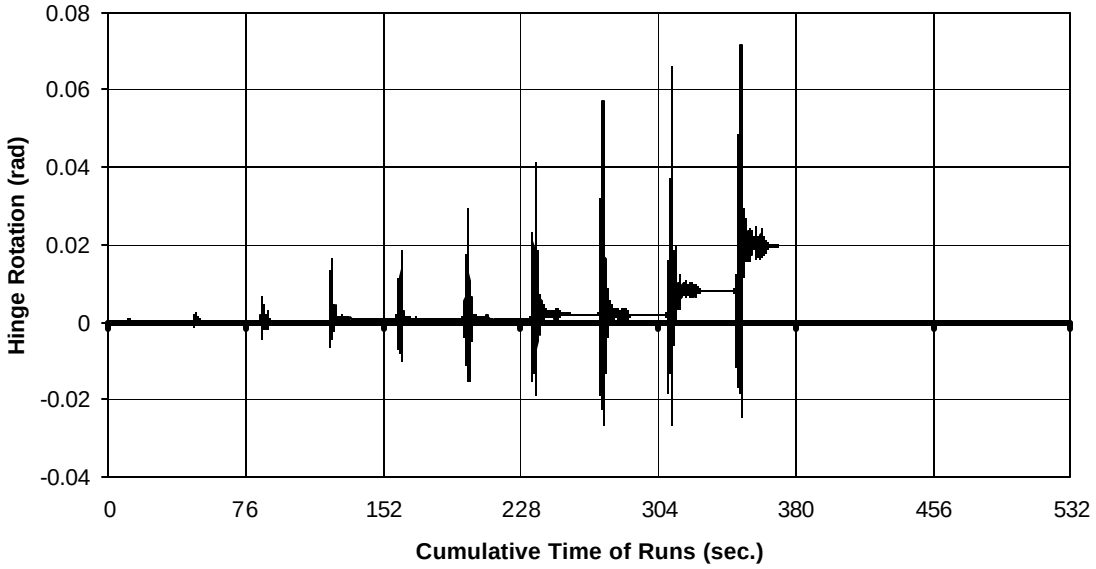

Figure 4-203 Hinge Rotation History of THD-3 (0.1xSylmar to 2.25xSylmar)

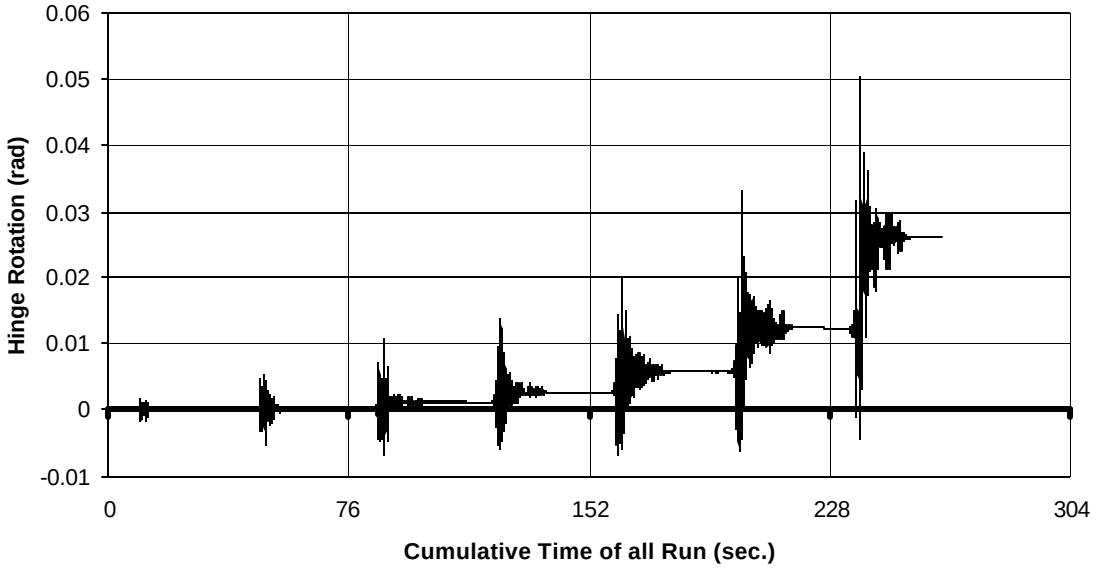

Figure 4-204 Hinge Rotation History of THD-4

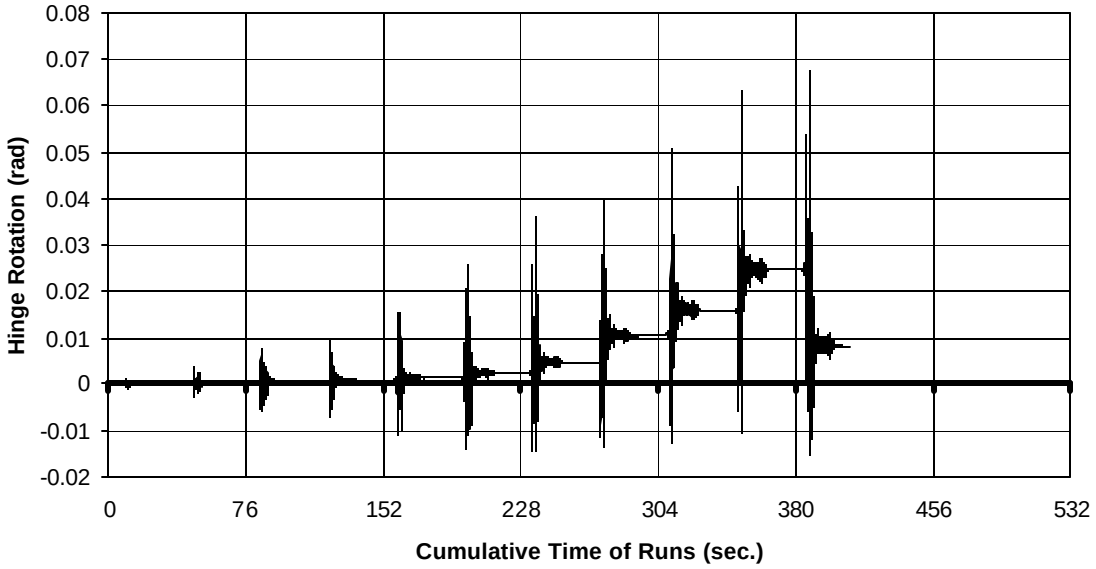

Figure 4-205 Hinge Rotation History of THD-5 (0.1xSylmar to 2.5xSylmar)

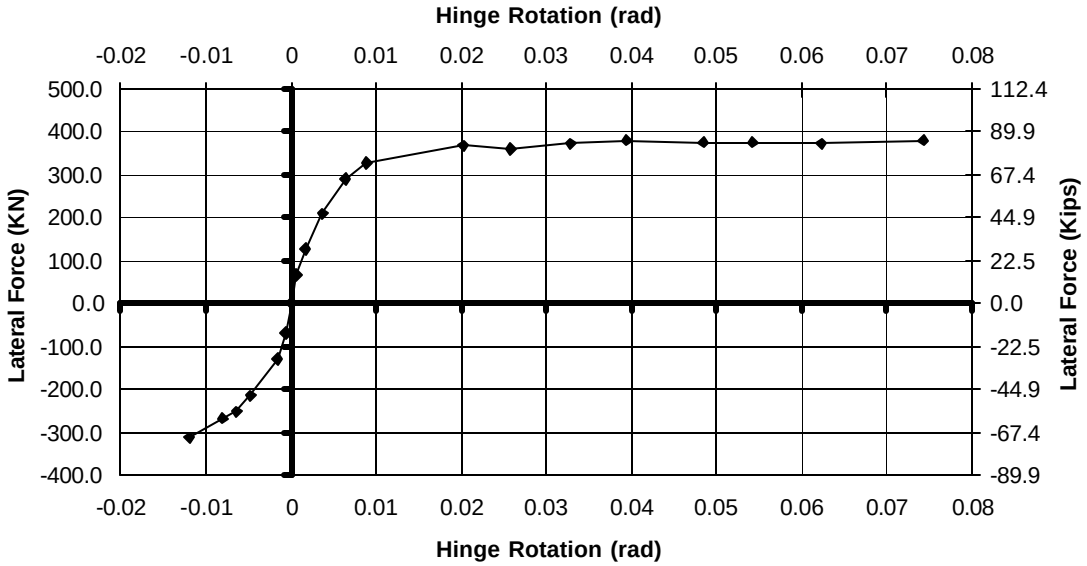

Figure 4-206 Envelope of Force vs. Hinge Rotation Hysteresis for THD-1 (0.1xSylmar to 2.75xSylmar)

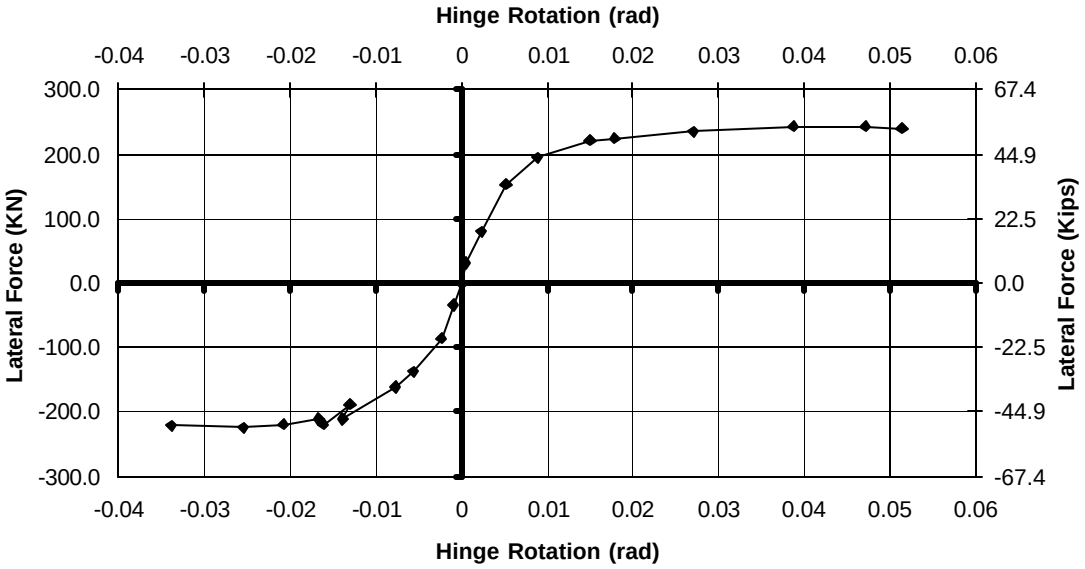

Figure 4-207 Envelope of Force vs. Hinge Rotation Hysteresis for THD-2 (0.1xSylmar to 2.25xSylmar)

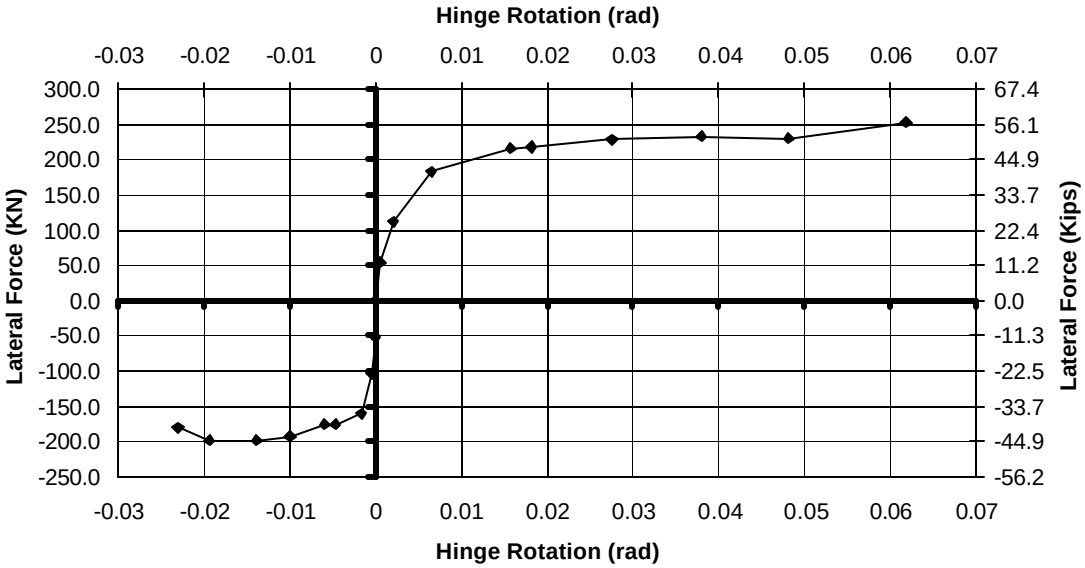

Figure 4-208 Envelope of Force vs. Hinge Rotation Hysteresis for THD-3 (0.1xSylmar to2.25xSylmar)

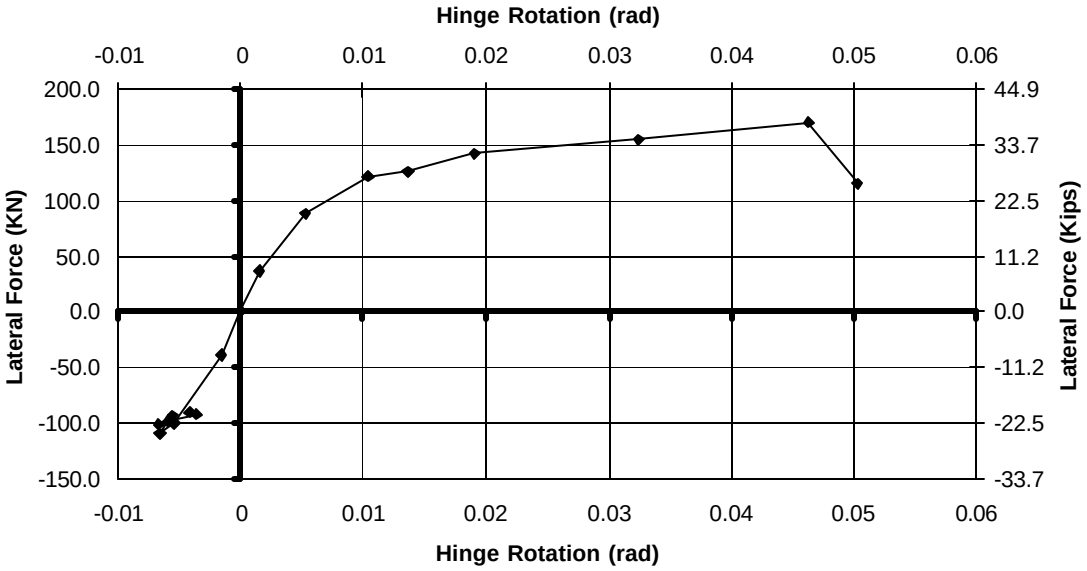

Figure 4-209 Envelope of Force vs. Hinge Rotation Hysteresis for THD-4

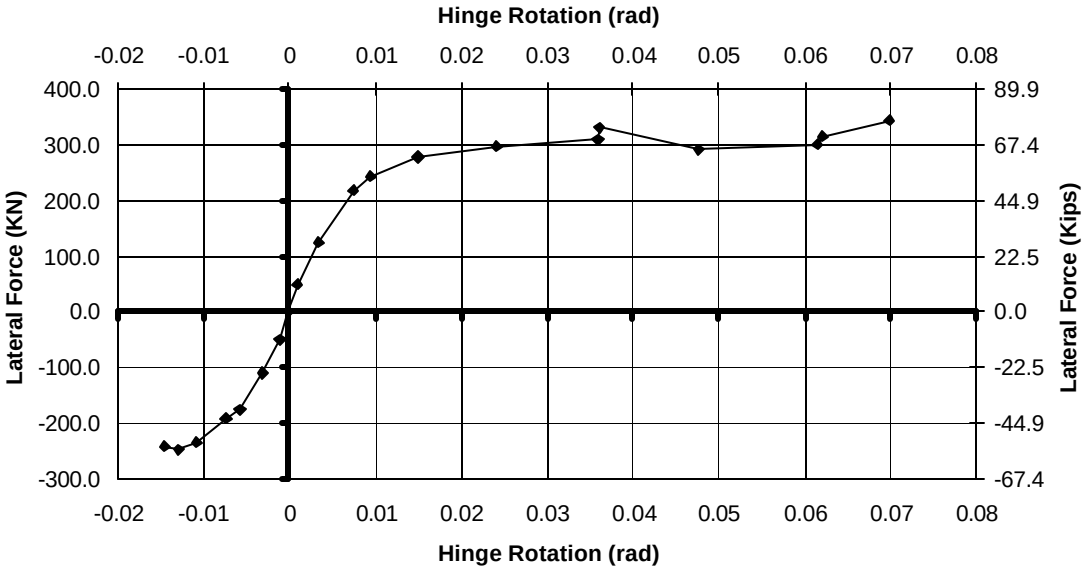

Figure 4-210 Envelope of Force vs. Hinge Rotation Hysteresis for THD-5 (0.1xSylmar to 2.5xSylmar)

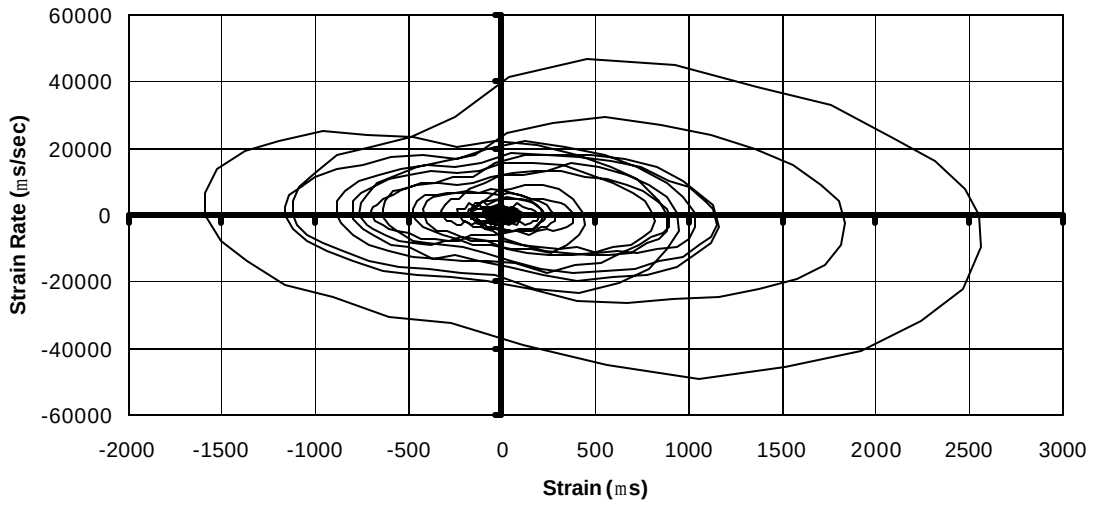

Figure 5-1 Typical Measured Strain Rate Versus Strain for Steel

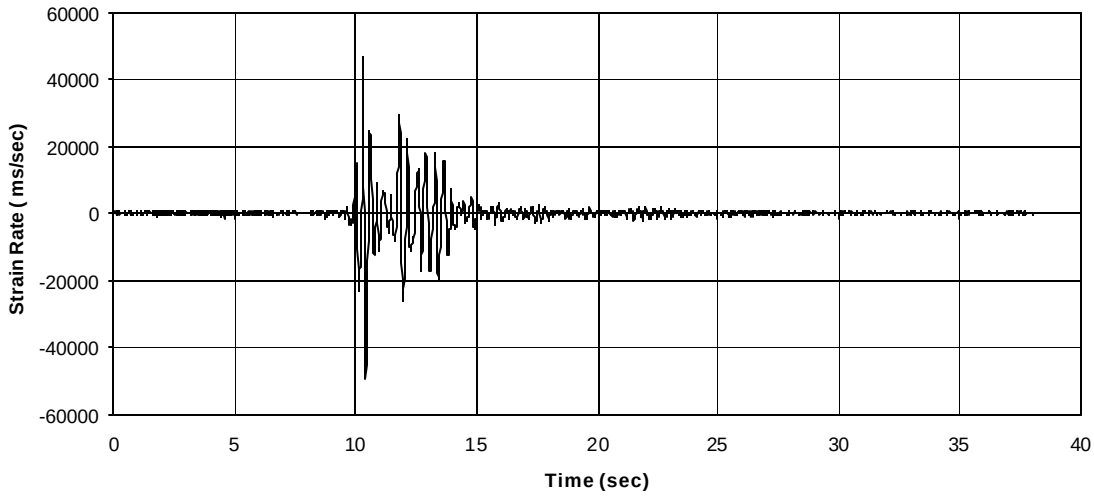

Figure 5-2 Typical Measured Strain Rate History for Steel

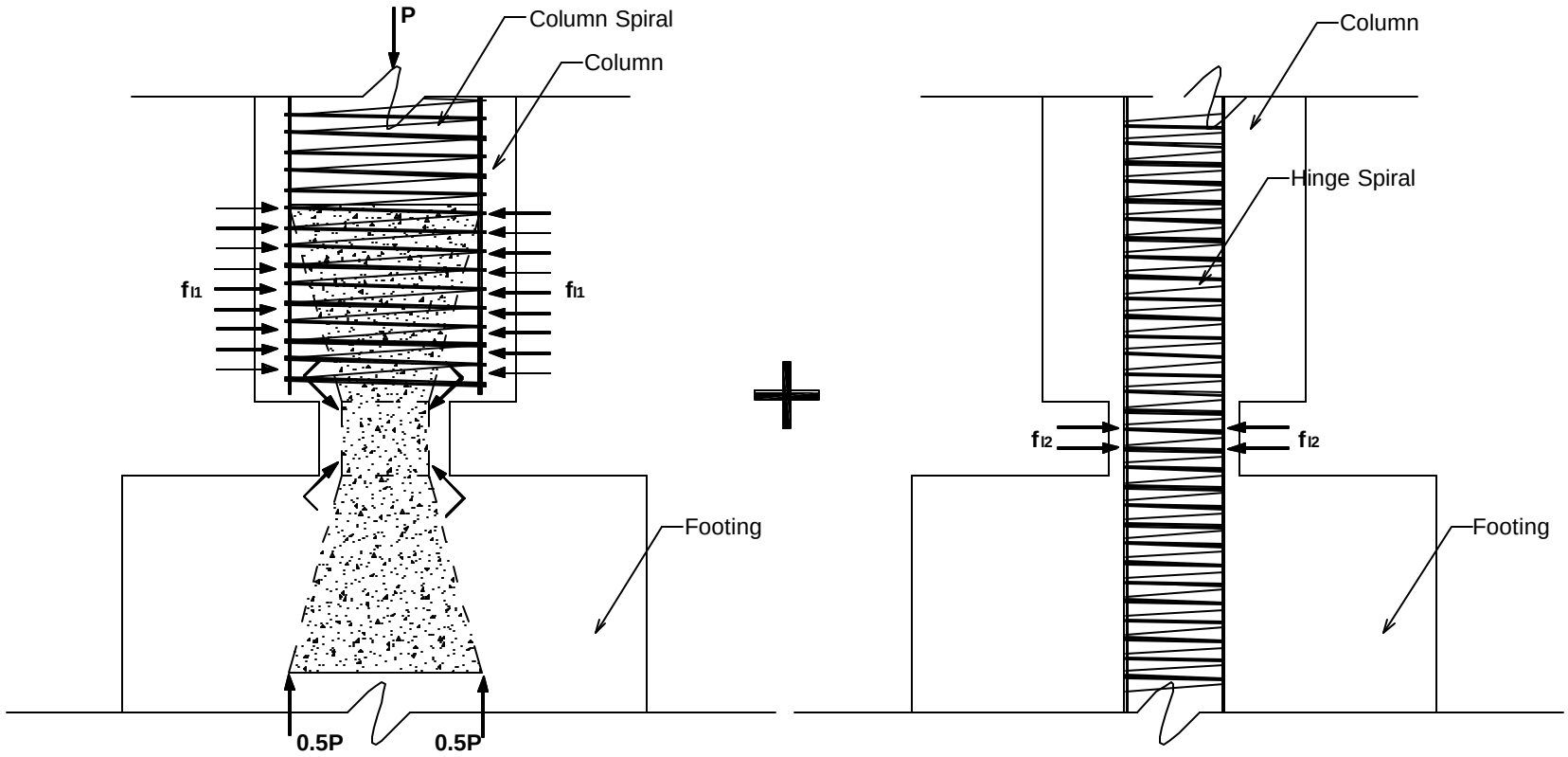

Figure 5-3 Two-Way Hinge Confinement Mechanism

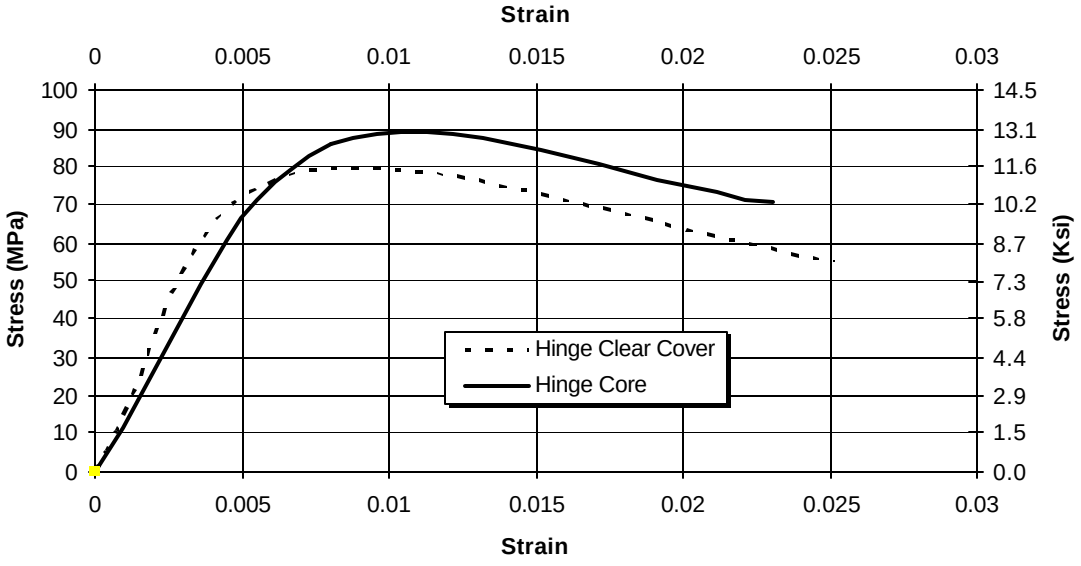

Figure 5-4 THD-1 Two-Way Hinge Concrete Stress-Strain Relationship

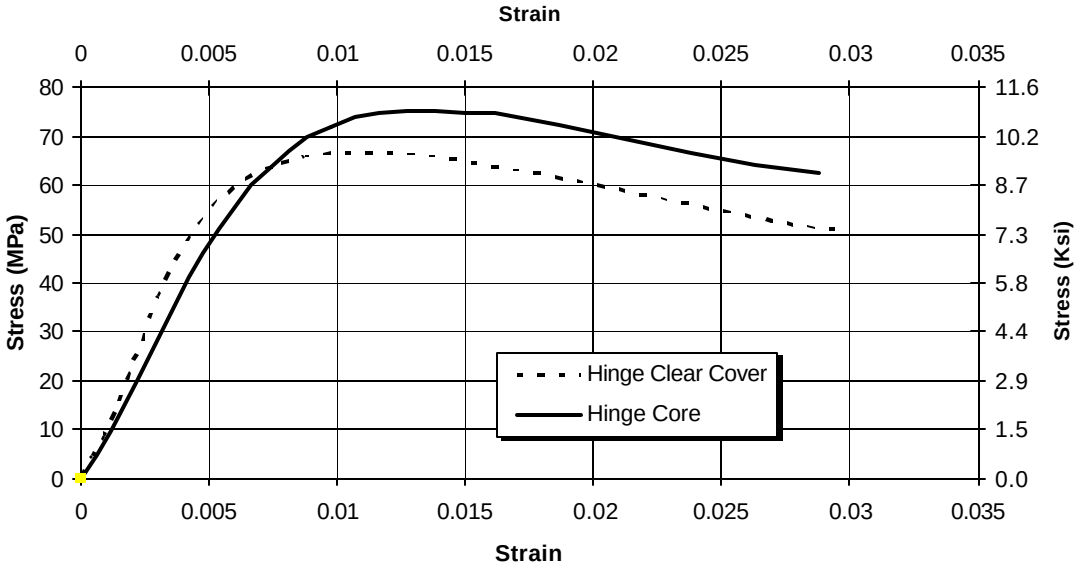

Figure 5-5 THD-2 Two-Way Hinge Concrete Stress-Strain Relationship

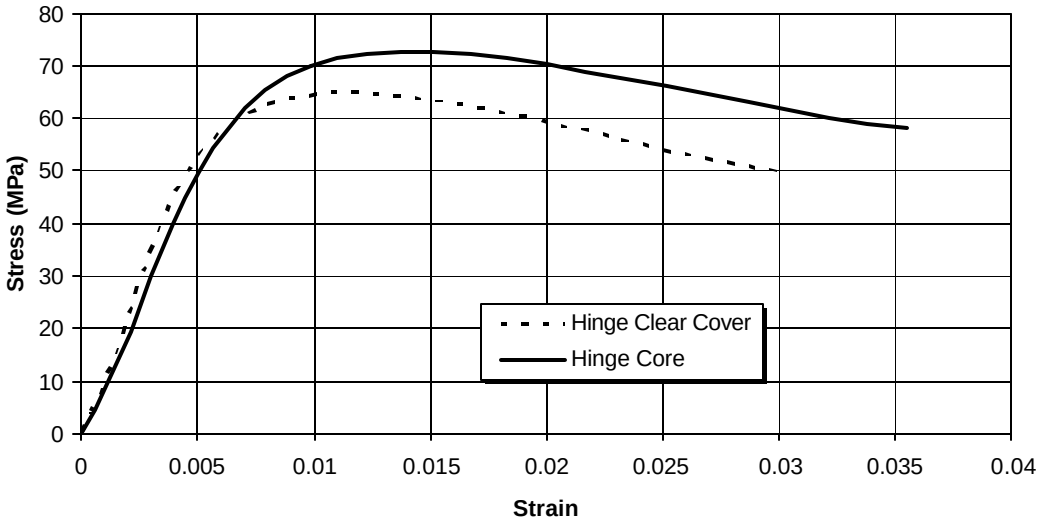

Figure 5-6 THD-3 Two-Way Hinge Concrete Stress-Strain Relationship

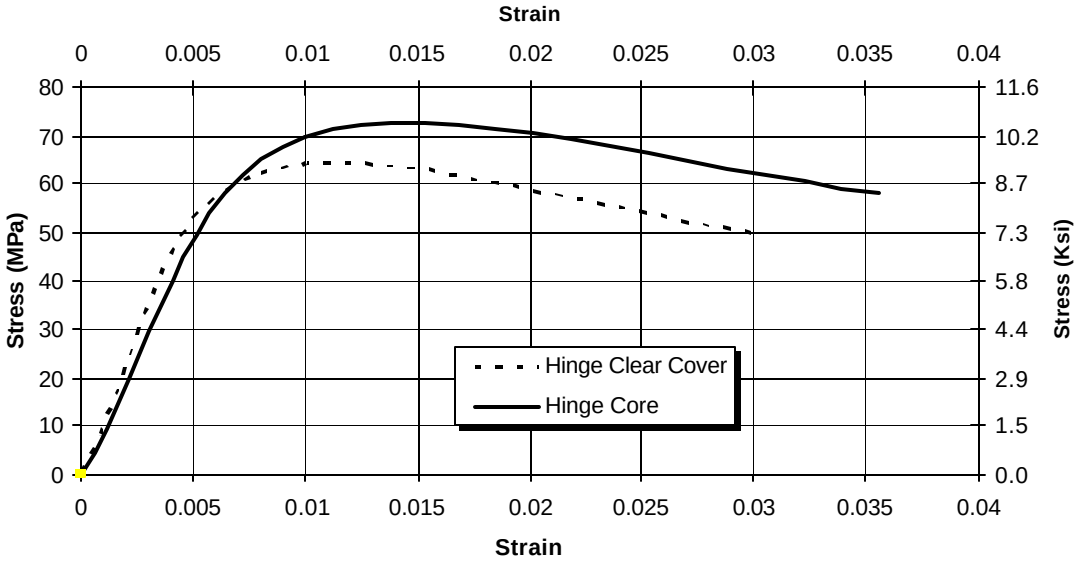

Figure 5-7 THD-4 Two-Way Hinge Concrete Stress-Strain Relationship

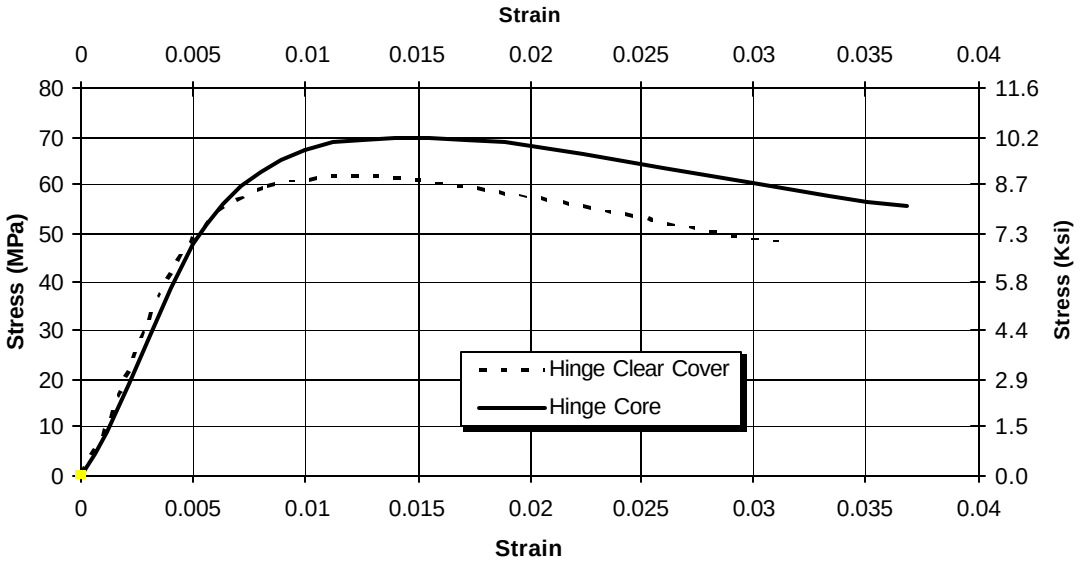

Figure 5-8 THD-5 Two-Way Hinge Concrete Stress-Strain Relationship

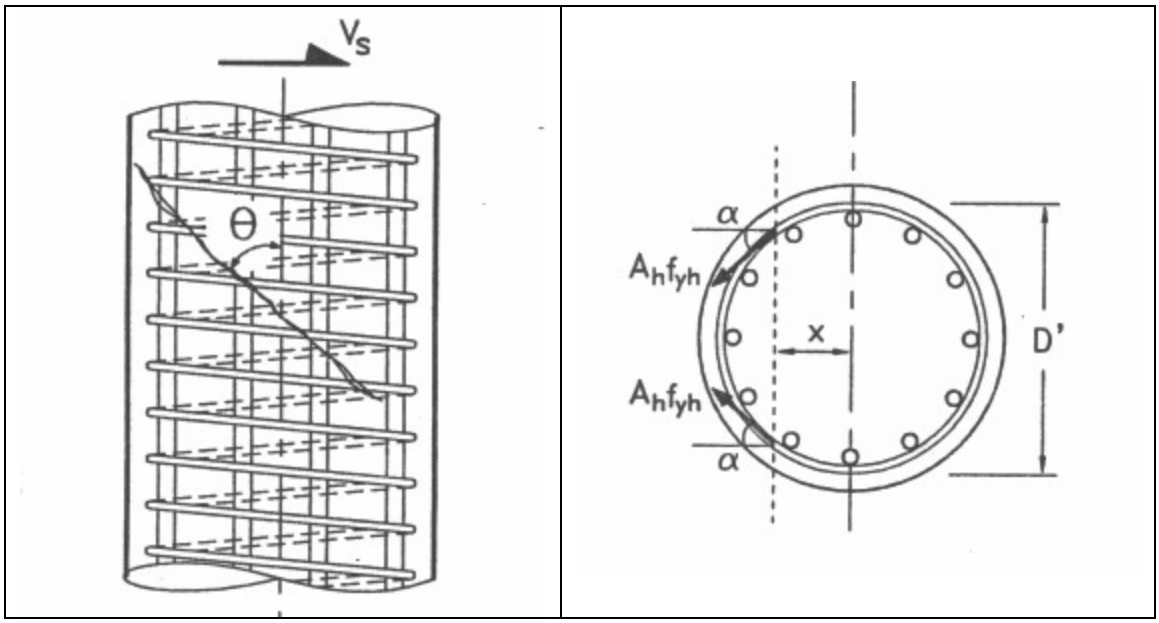

Figure 5-9 Diagonal Shear Mechanism

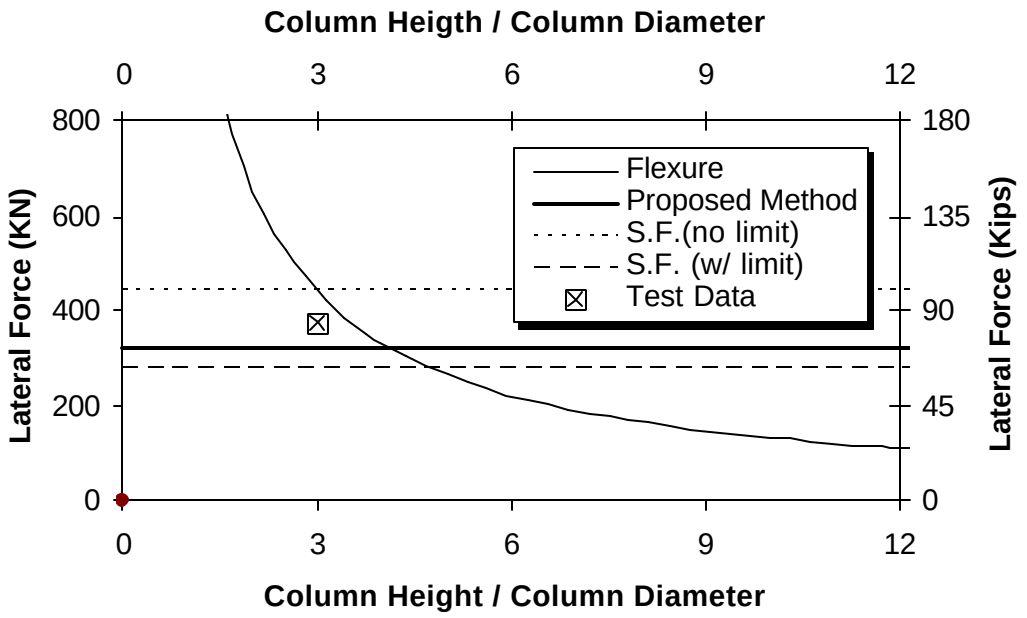

Figure 5-10 THD-1 Variation of Ultimate Shear with Column Aspect Ratio

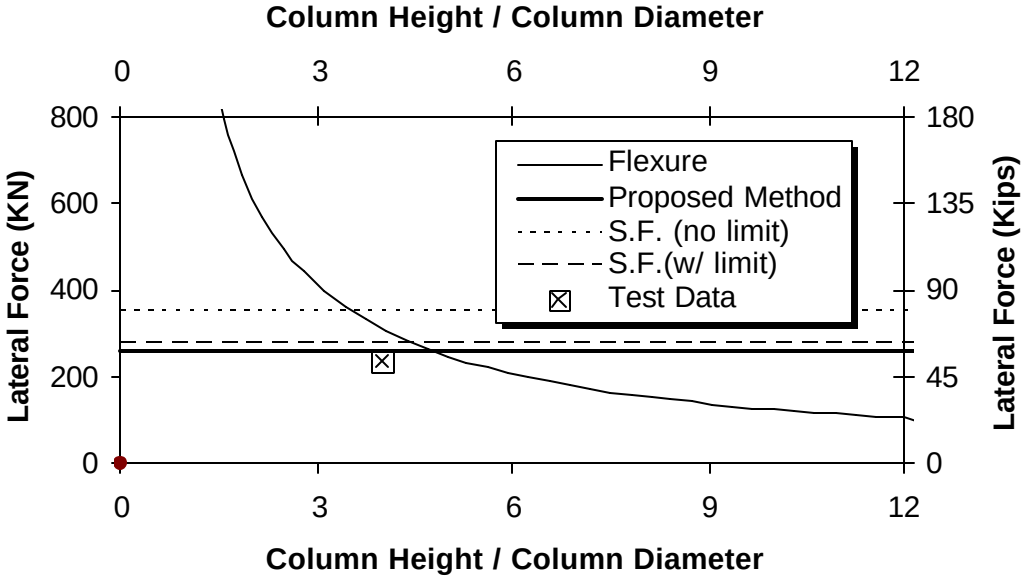

Figure 5-11 THD-2 Variation of Ultimate Shear with Column Aspect Ratio

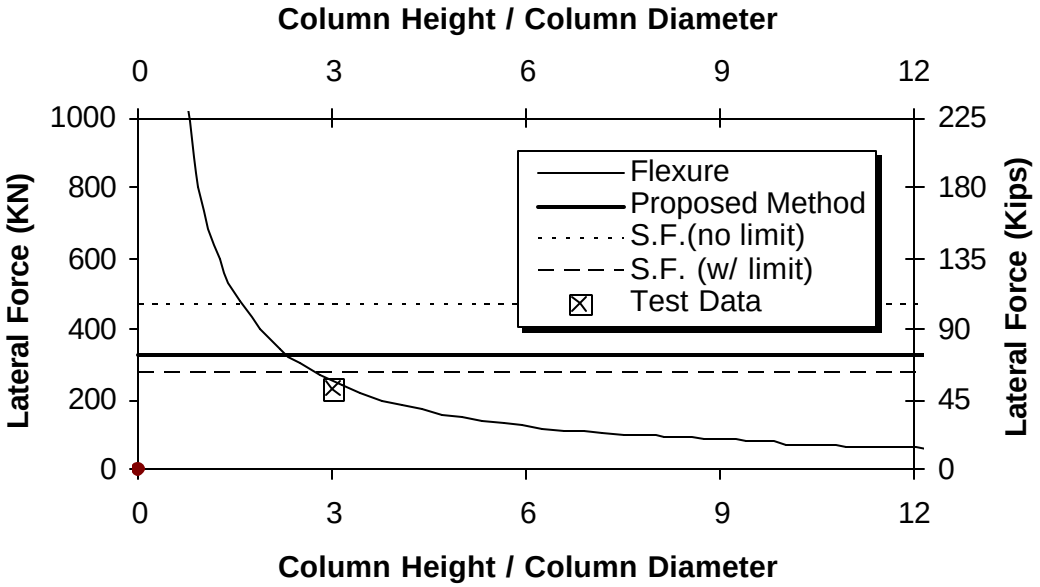

Figure 5-12 THD-3 Variation of Ultimate Shear with Column Aspect Ratio

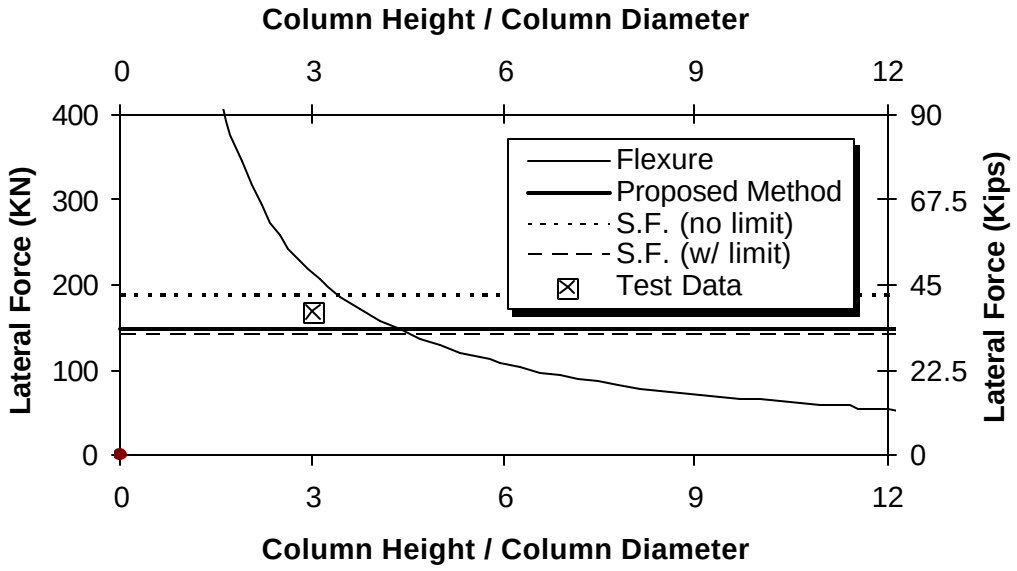

Figure 5-13 THD-4 Variation of Ultimate Shear with Column Aspect Ratio

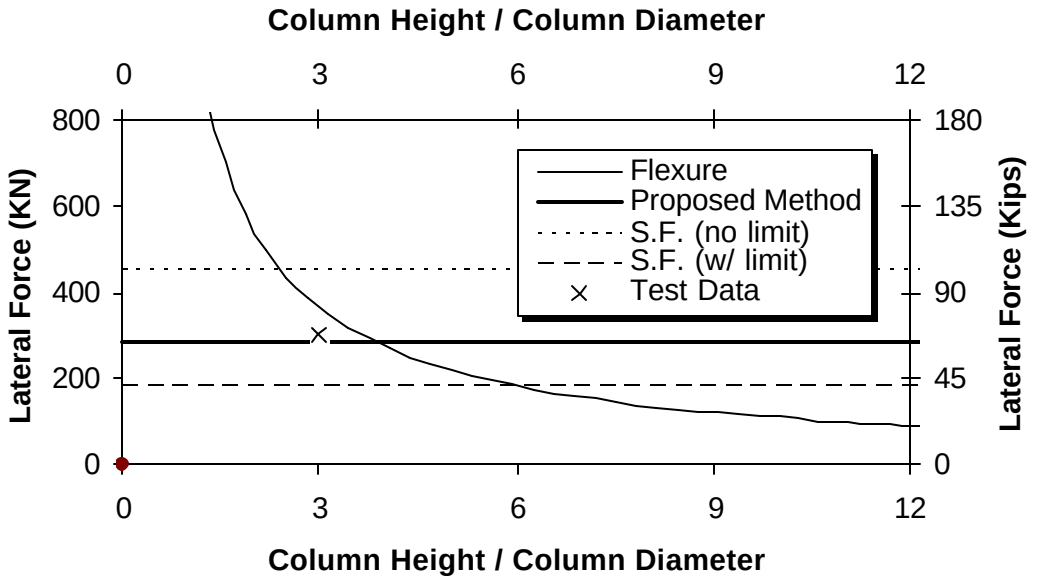

Figure 5-14 THD-5 Variation of Ultimate Shear with Column Aspect Ratio

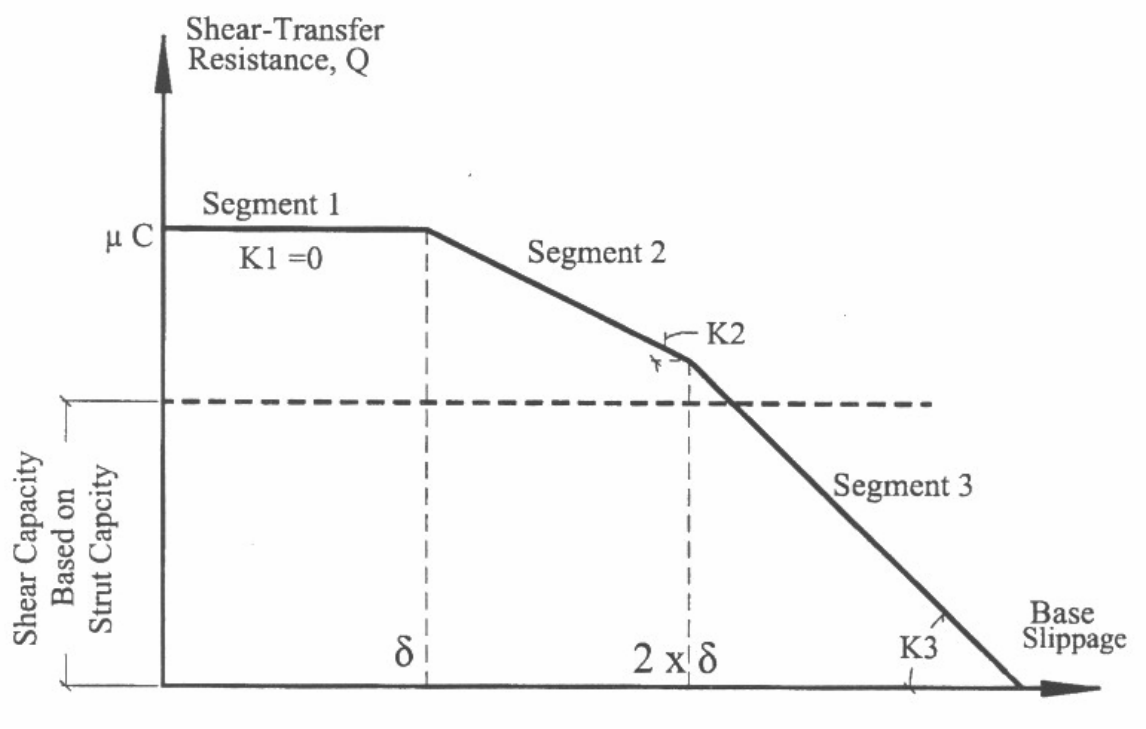

Figure 5-15 Base Hinge Shear-Slippage Model from Moustafa's

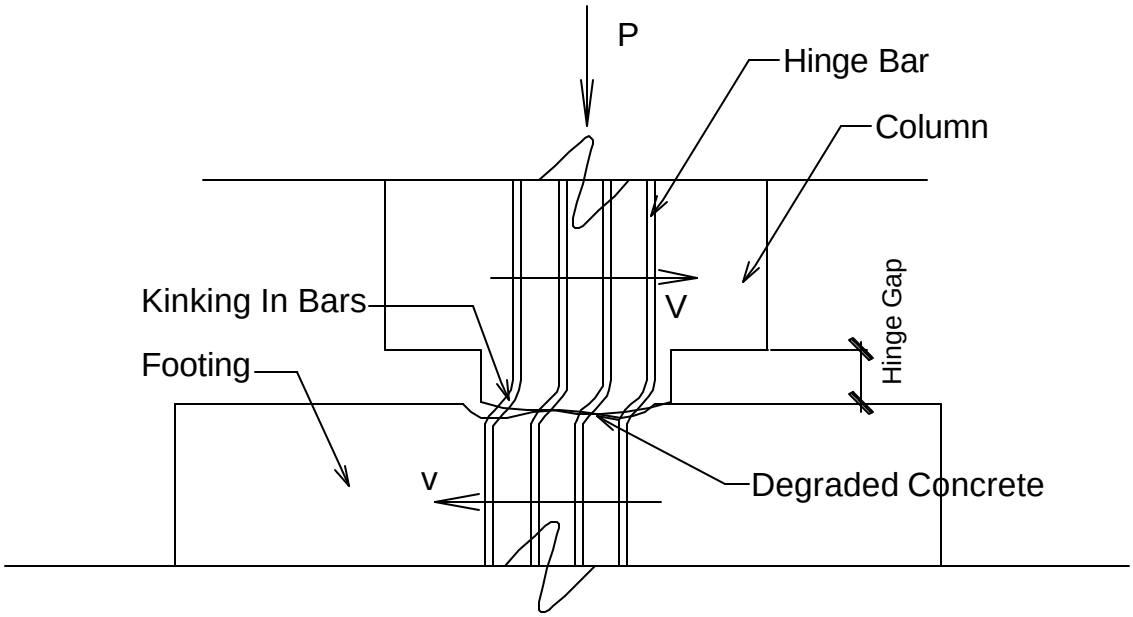

Figure 5-16 Two-Way Hinge Dowel Action Kinking Mechanism

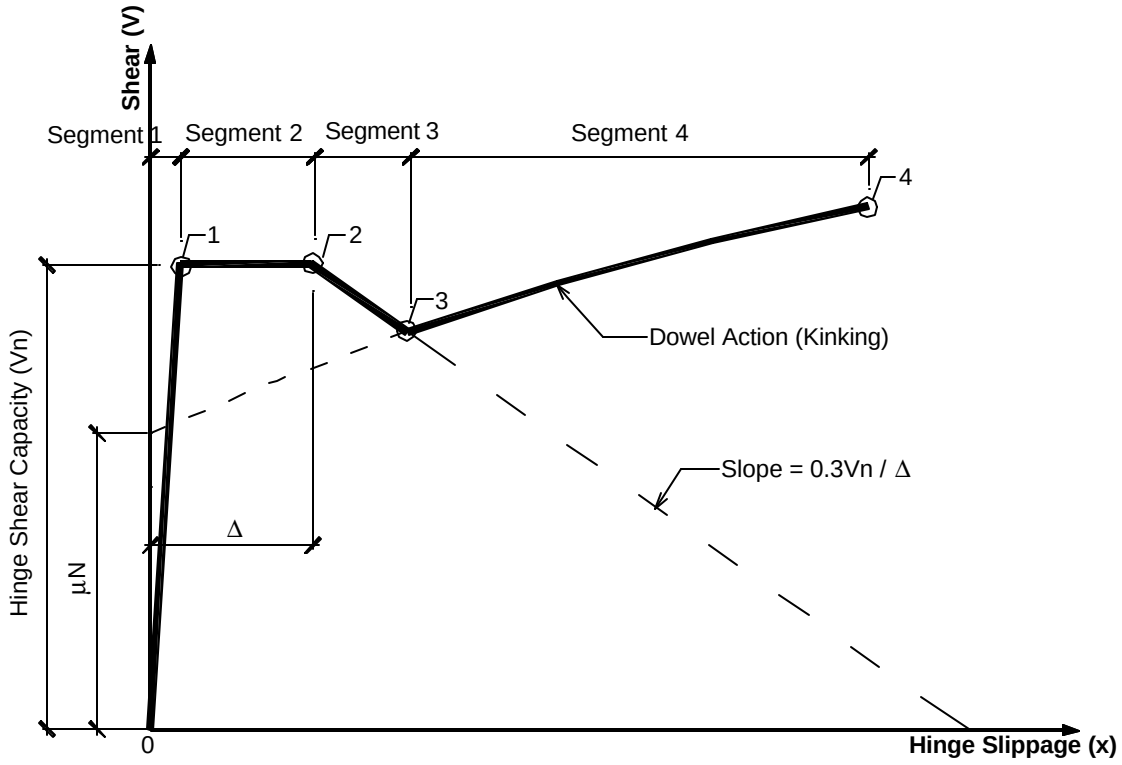

Figure 5-17 Proposed Two-Way Hinge Shear-Slippage Model

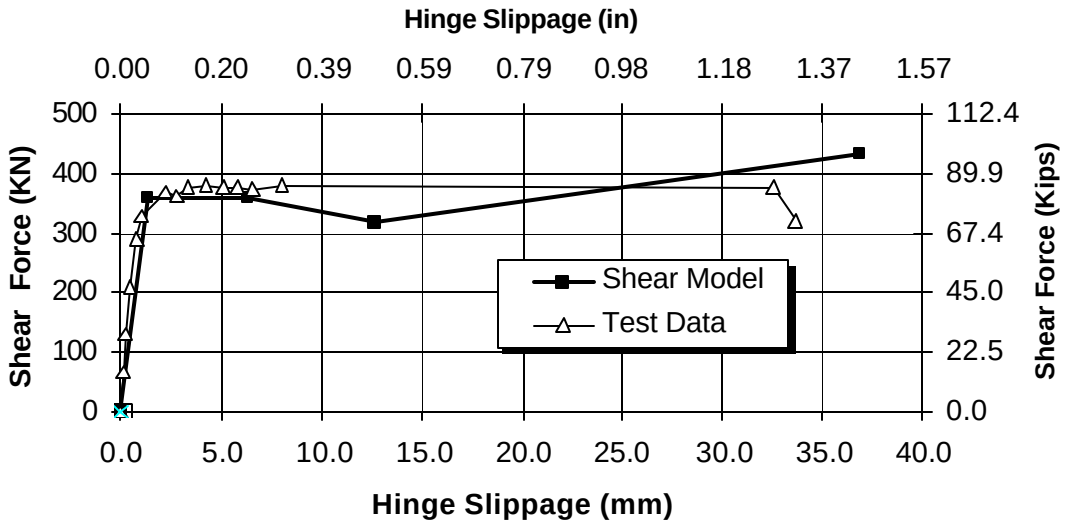

Figure 5-18 Comparison of Shear-Slippage Relationship Using Proposed Shear Model Versus Experimental Results For THD-1

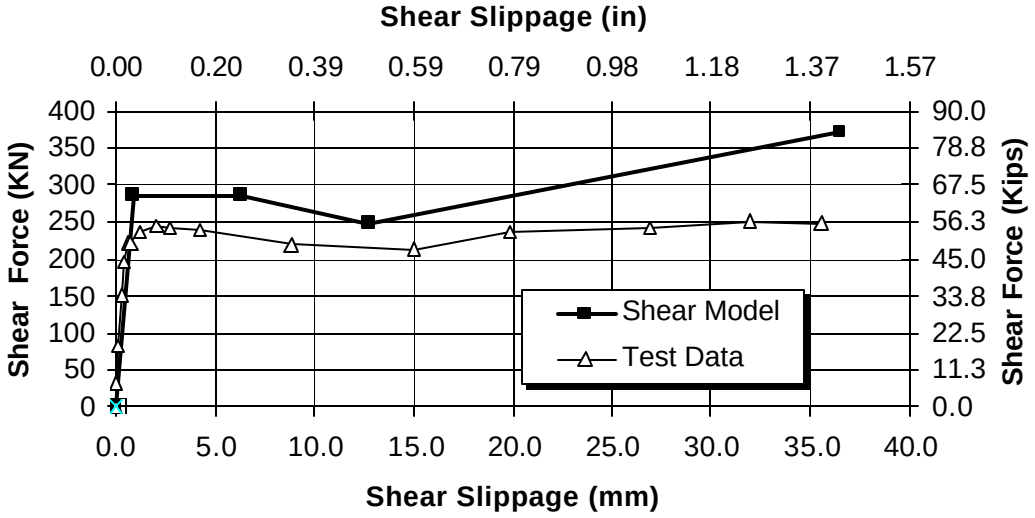

Figure 5-19 Comparison of Shear-Slippage Relationship Using Proposed Shear Model Versus Experimental Results For THD-2

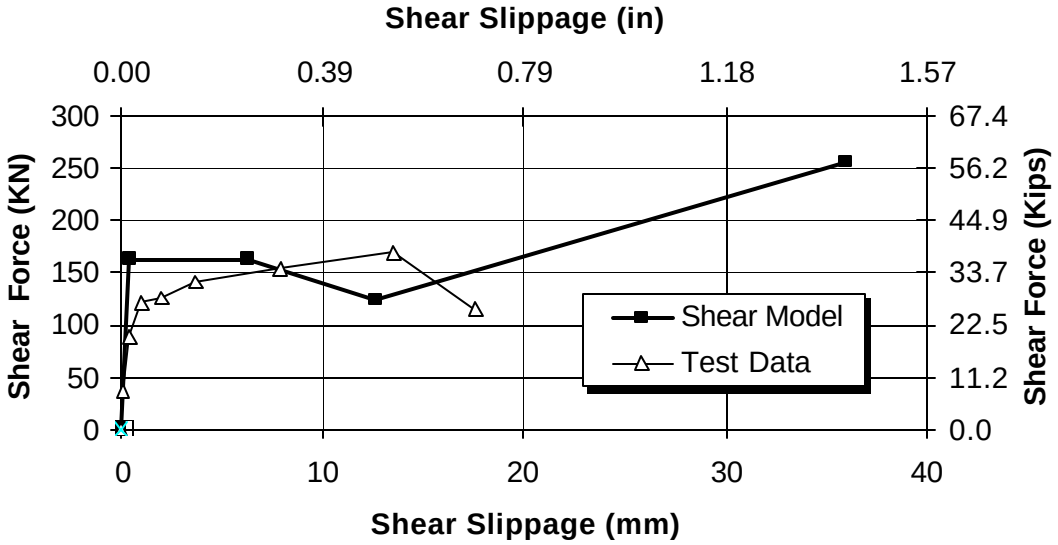

Figure 5-20 Comparison of Shear-Slippage Relationship Using Proposed Shear Model Versus Experimental Results For THD-4

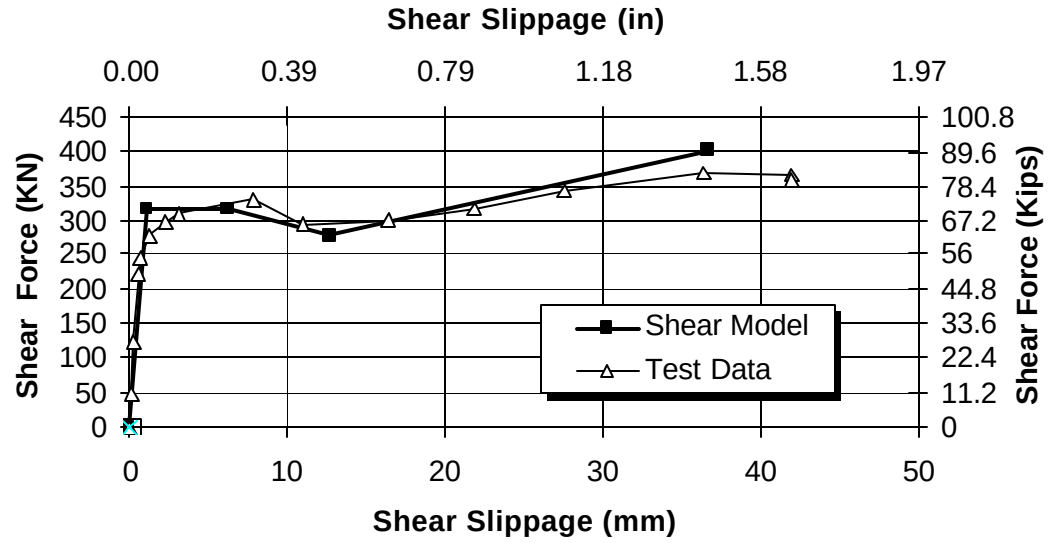

Figure 5-21 Comparison of Shear-Slippage Relationship Using Proposed Shear Model Versus Experimental Results For THD-5

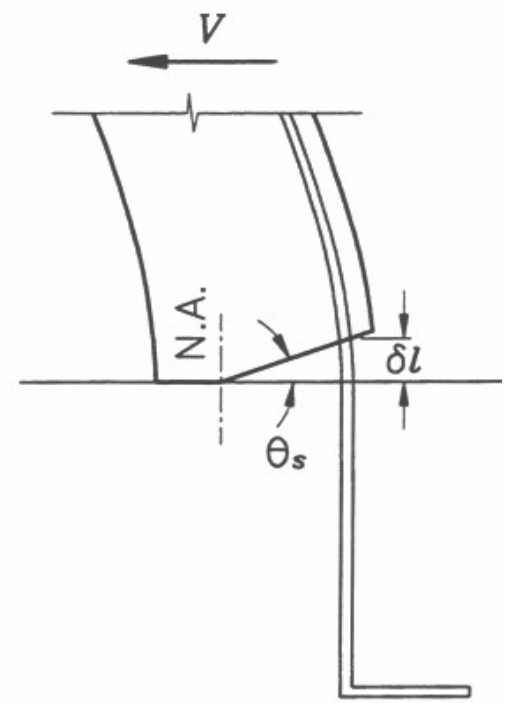

Figure 5-22 Ordinary Bond-Slip Mechanism

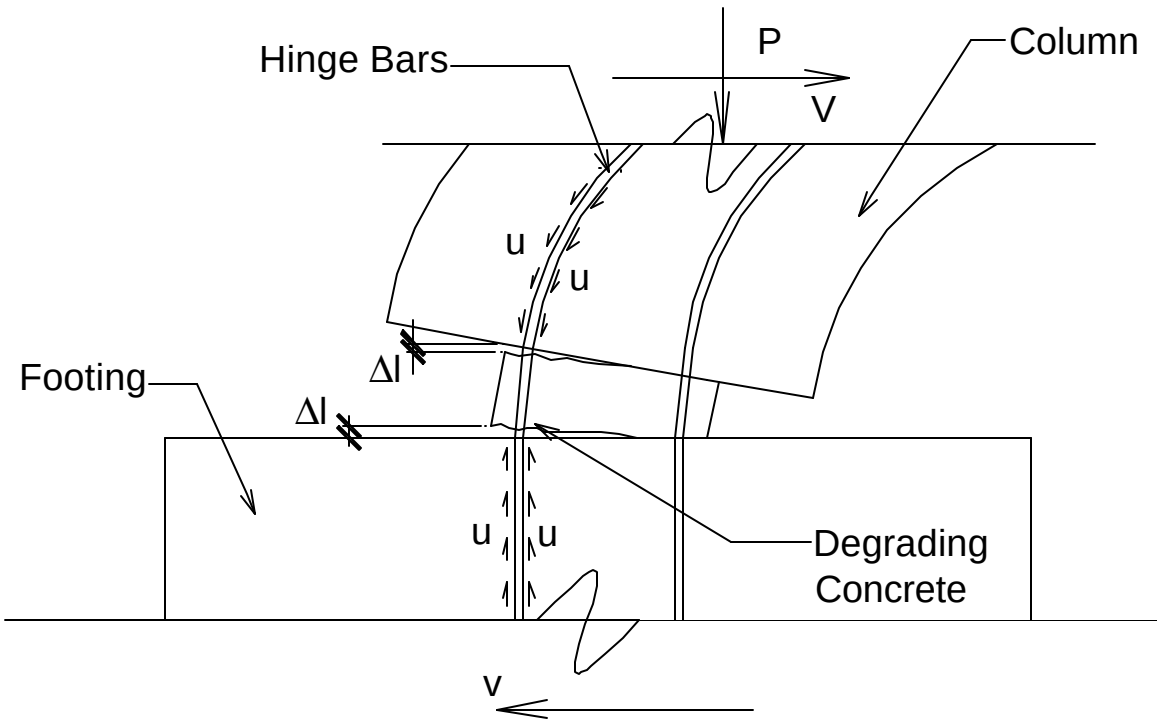

Figure 5-23 Two-Way Hinge Bond-Slip Mechanism

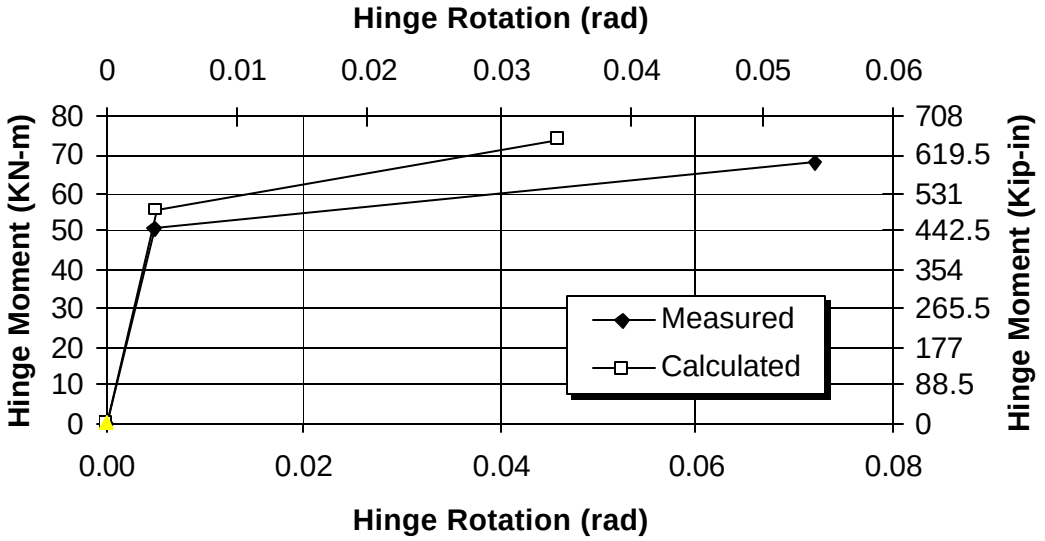

Figure 5-24 Comparison of Hinge Rotation Using Existing Calculation Versus Experimental Results For THD-1

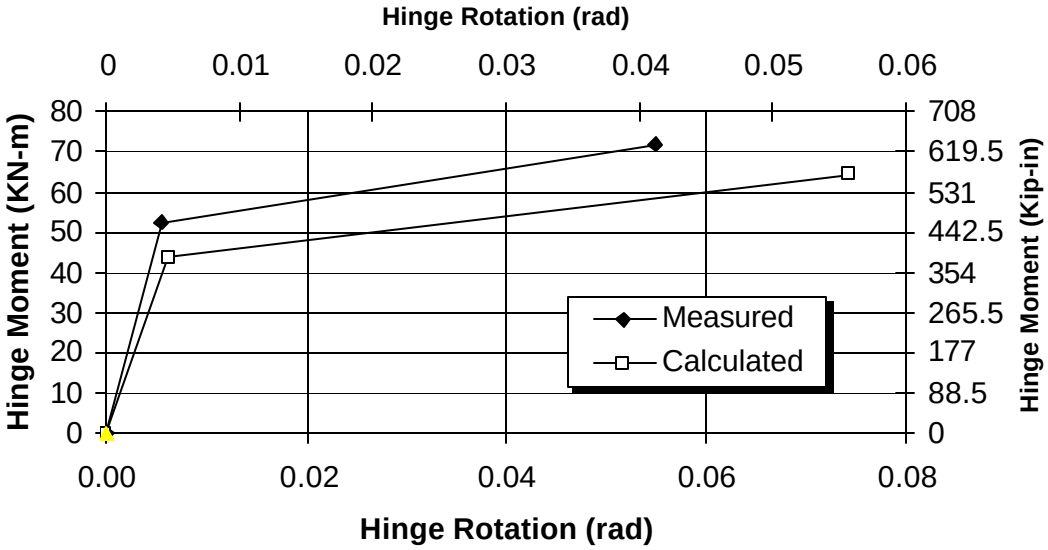

Figure 5-25 Comparison of Hinge Rotation Using Existing Calculation Versus Experimental Results For THD-2

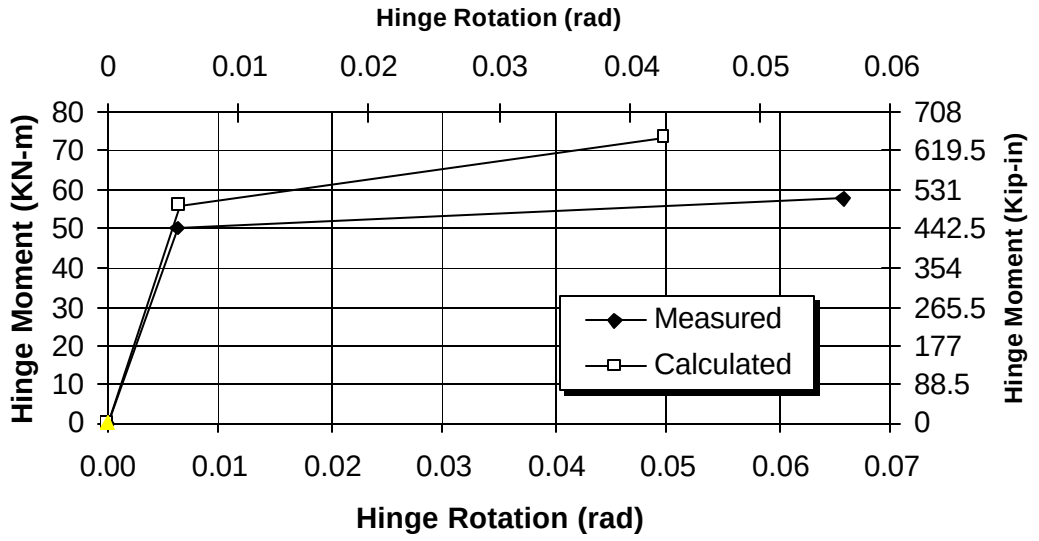

Figure 5-26 Comparison of Hinge Rotation Using Existing Calculation Versus Experimental Results For THD-3

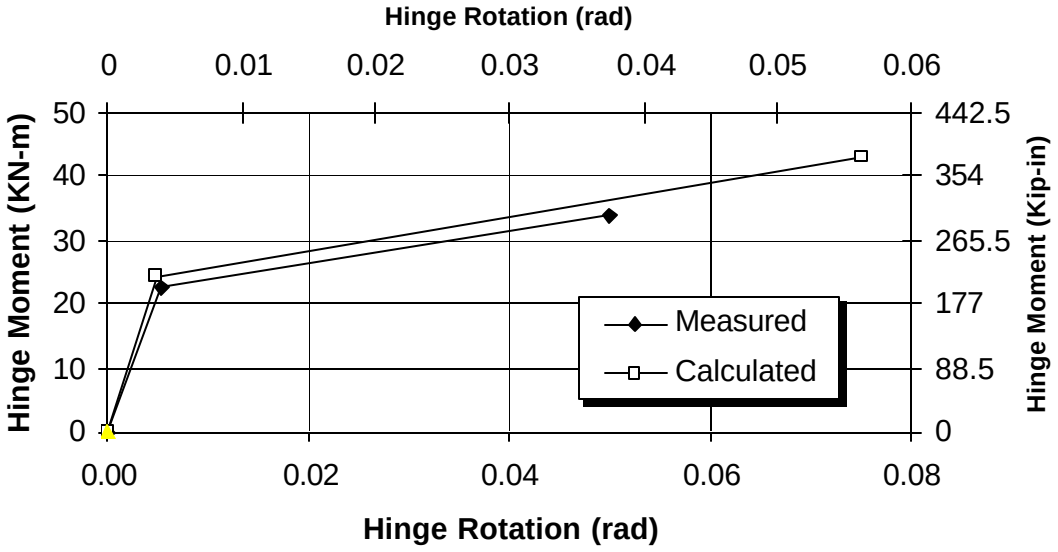

Figure 5-27 Comparison of Hinge Rotation Using Existing Calculation Versus Experimental Results For THD-4

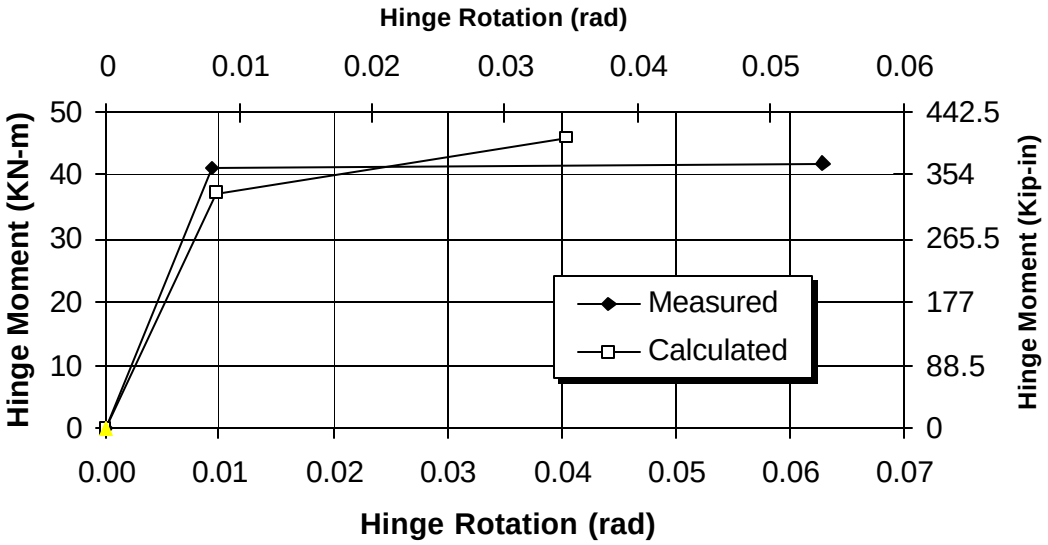

Figure 5-28 Comparison of Hinge Rotation Using Existing Calculation Versus Experimental Results For THD-5

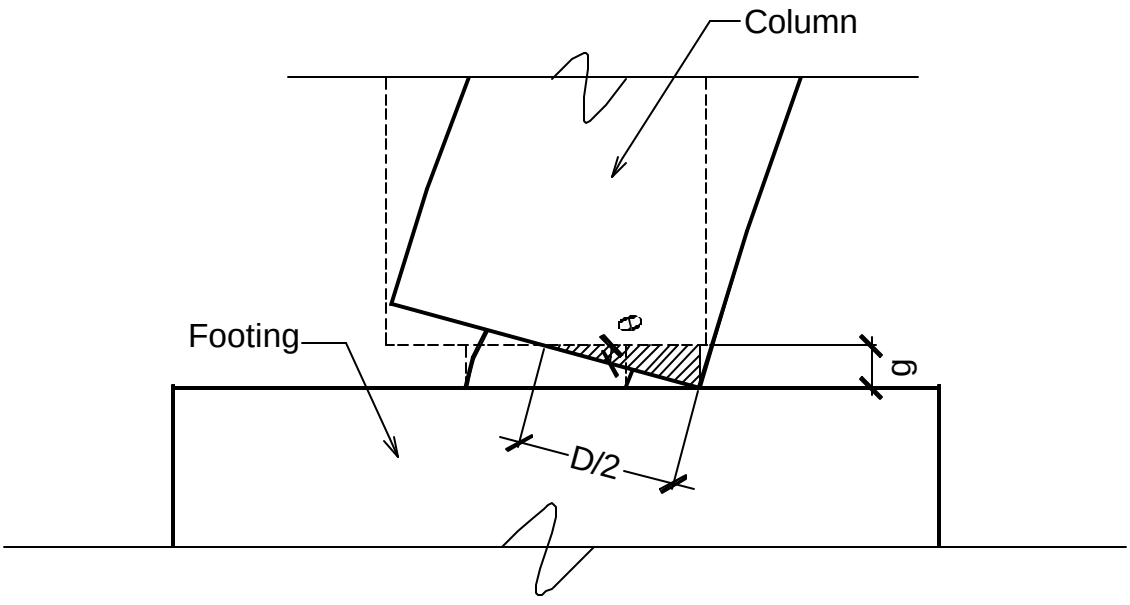

Figure 5-29 Two-Way Hinge Closure

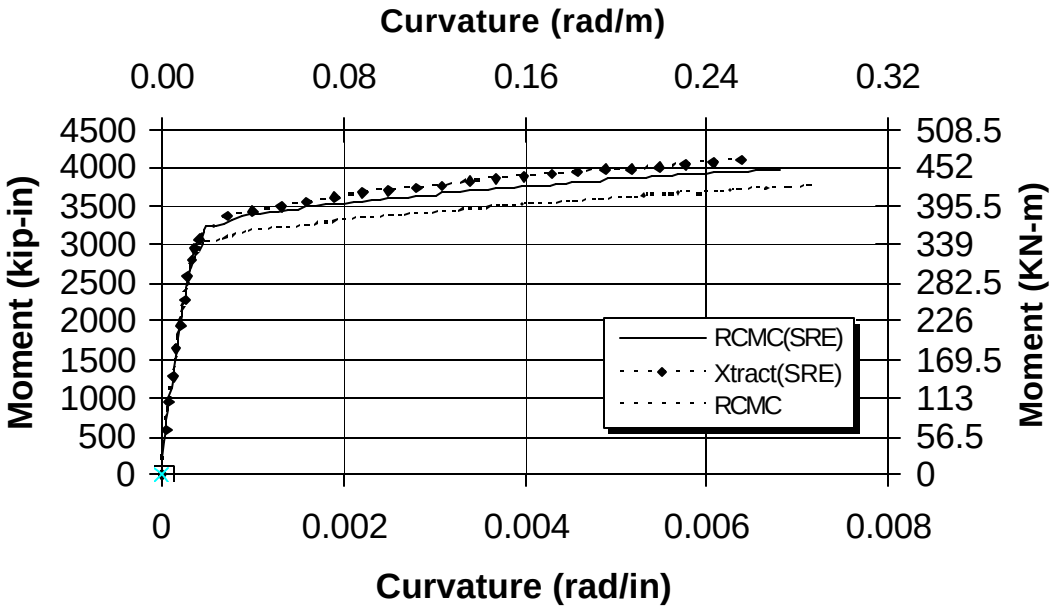

Figure 5-30 M-f Analysis for THD-1 Column Section

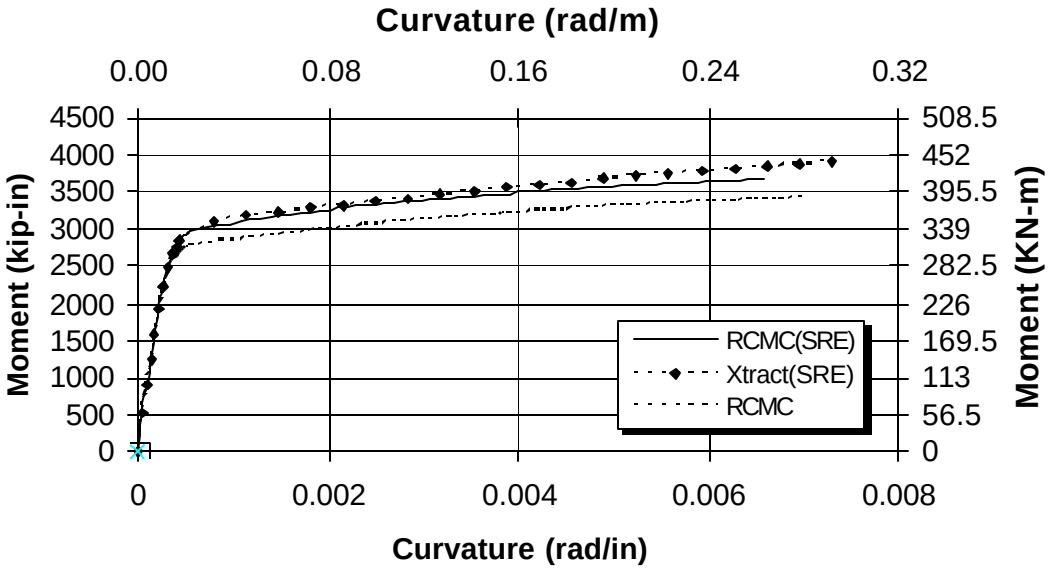

Figure 5-31 M-f Analysis for THD-2 Column Section

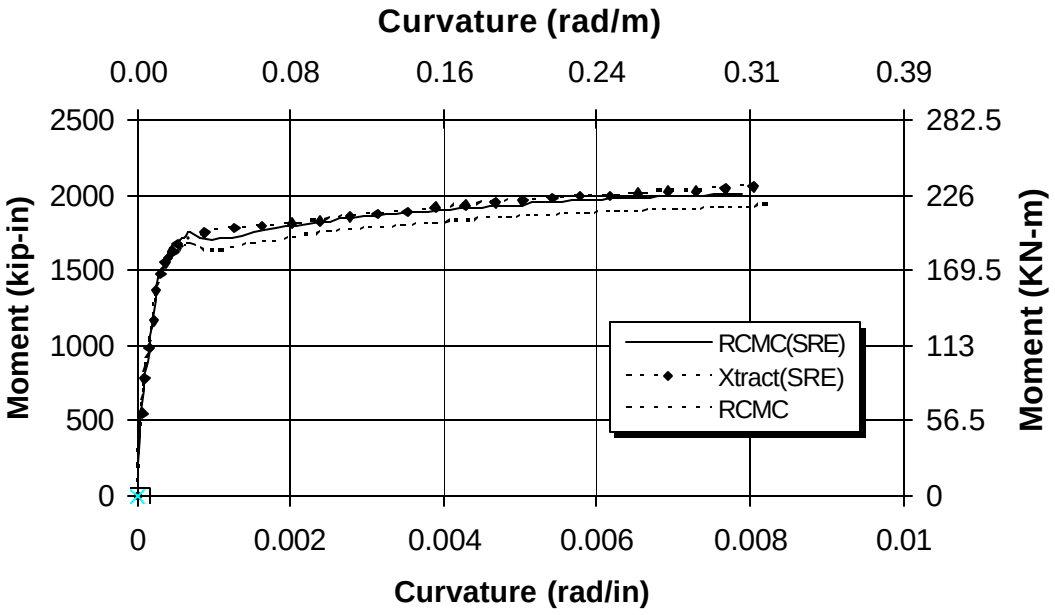

Figure 5-32 M-f Analysis for THD-3 Column Section

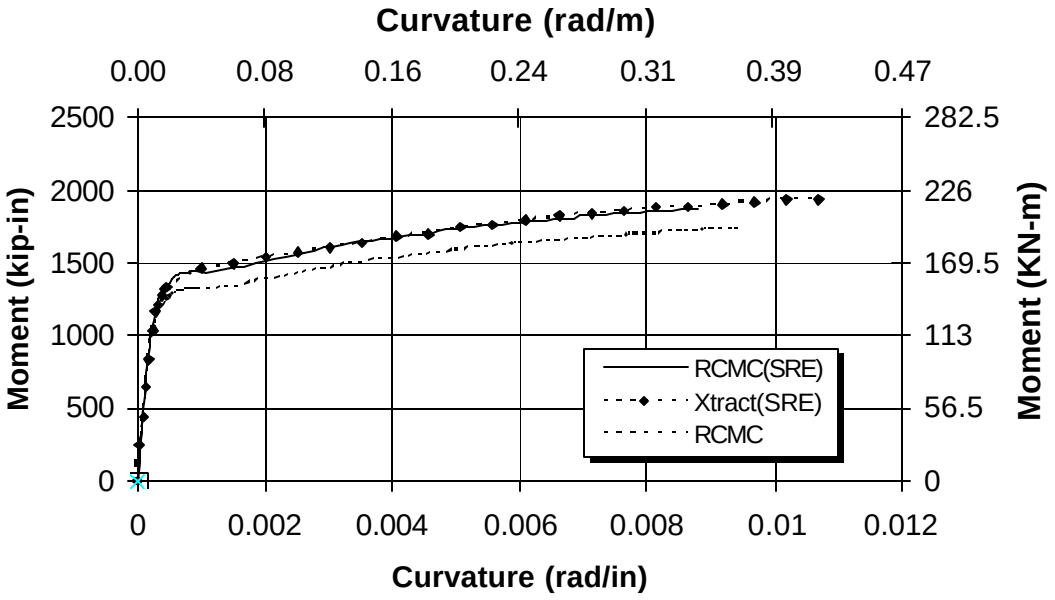

Figure 5-33 M-f Analysis for THD-4 Column Section

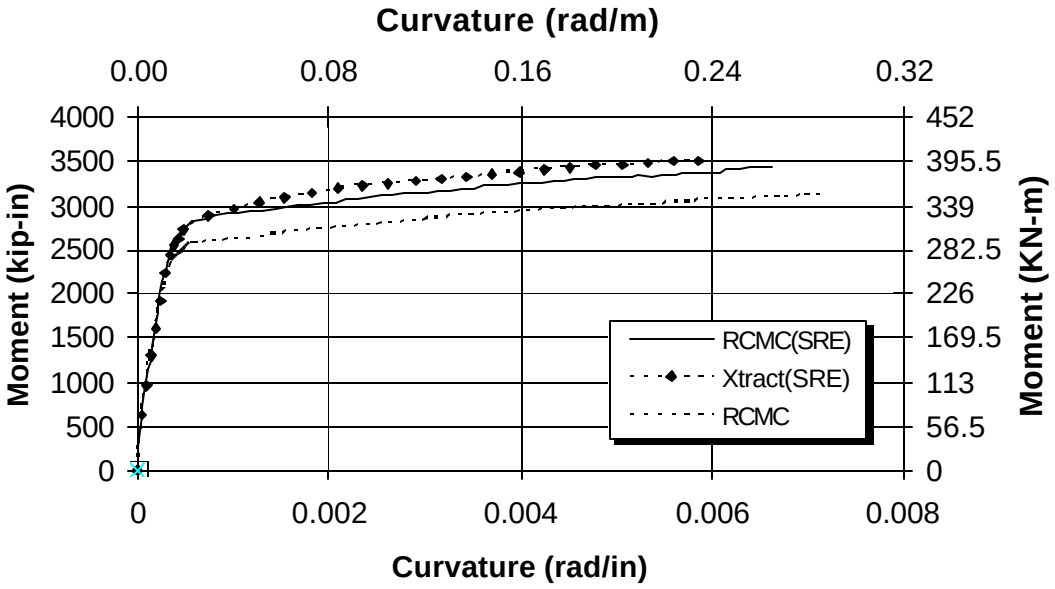

Figure 5-34 M-f Analysis for THD-5 Column Section

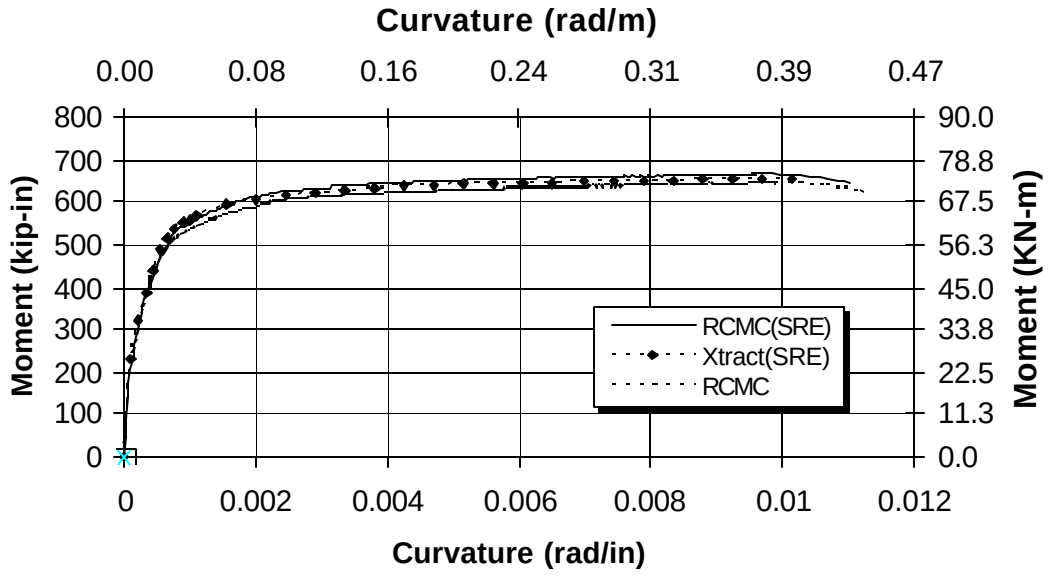

Figure 5-35 M-f Analysis for THD-1 Hinge Section

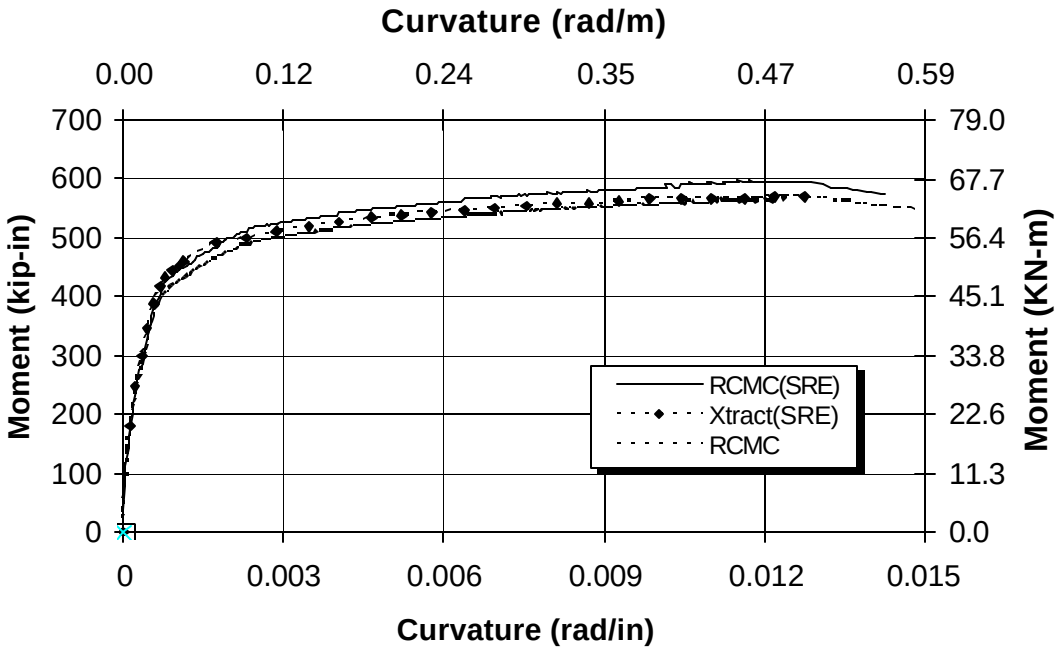

Figure 5-36 M-f Analysis for THD-2 Hinge Section

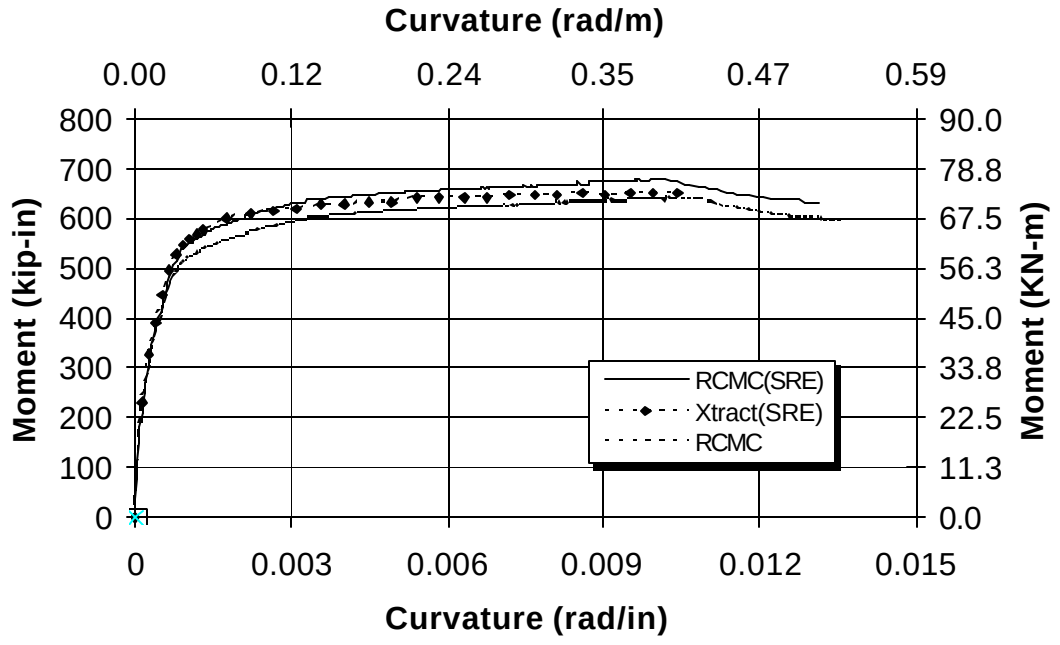

Figure 5-37 M-f Analysis for THD-3 Hinge Section

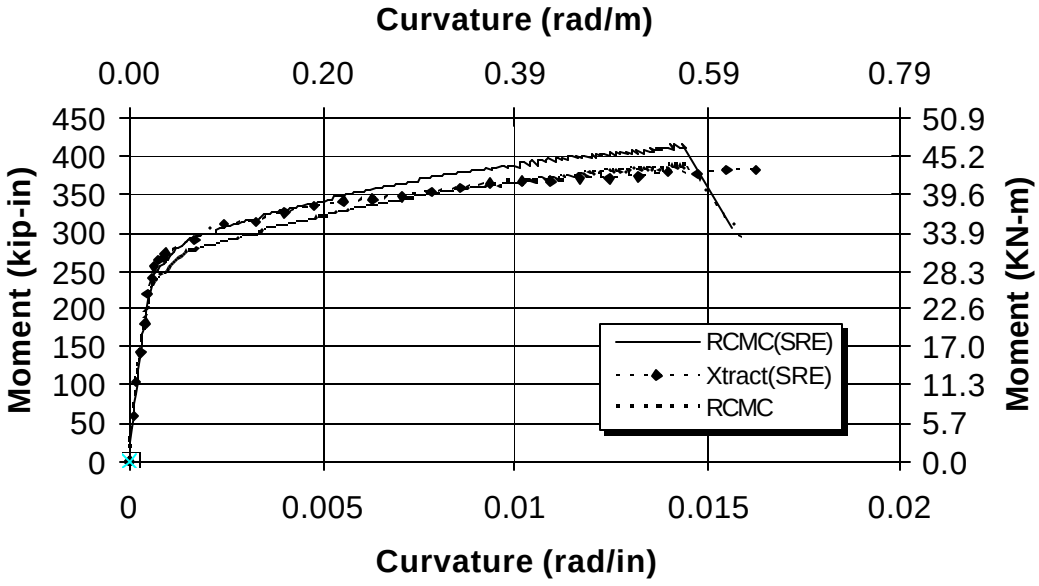

Figure 5-38 M-f Analysis for THD-4 Hinge Section

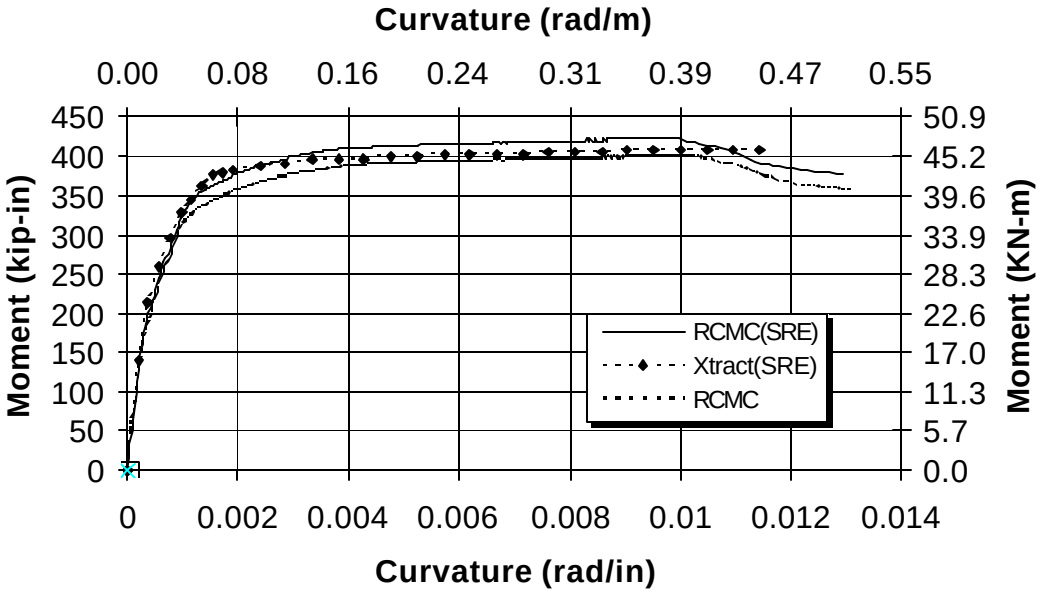

Figure 5-39 M-f Analysis for THD-5 Hinge Section

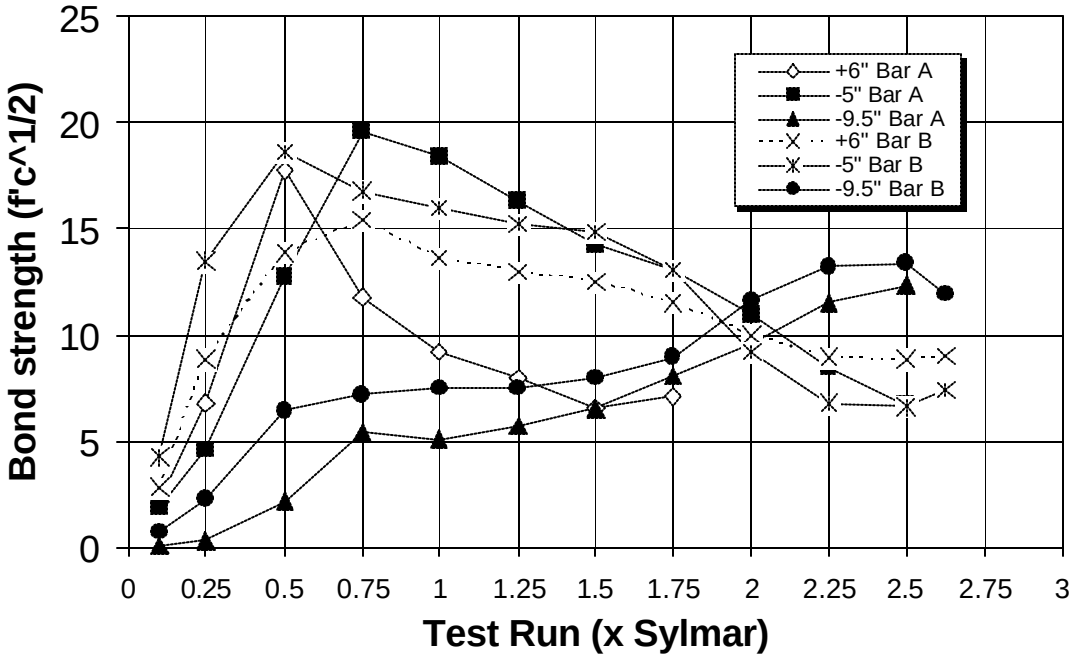

Figure 5-40 Typical Average Bond Stress Profile for Hinge Steel (Specimen THD-2)

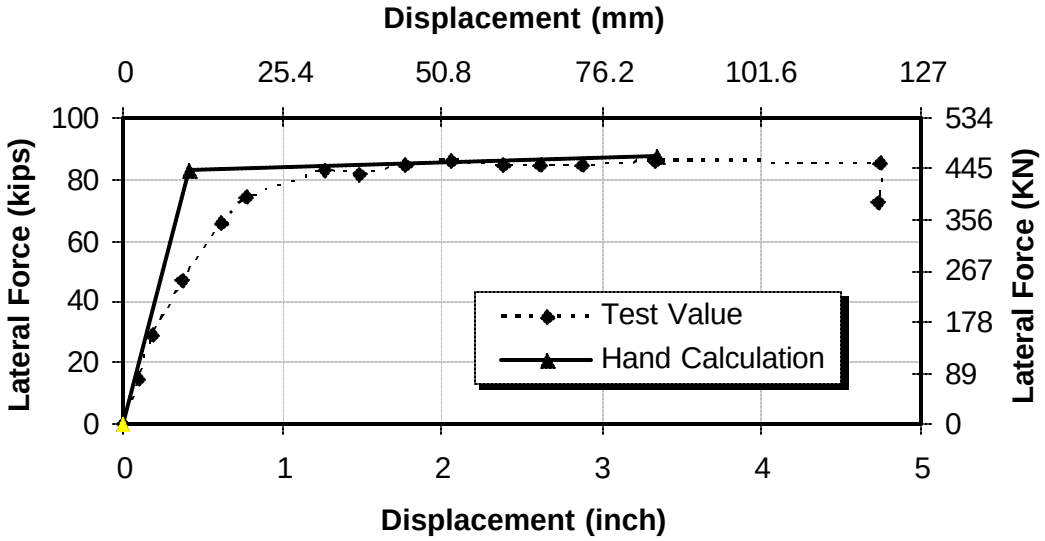

Figure 5-41 Comparison of Force-Deflection Curve Using Hand Calculation Versus Experimental Results for THD-1

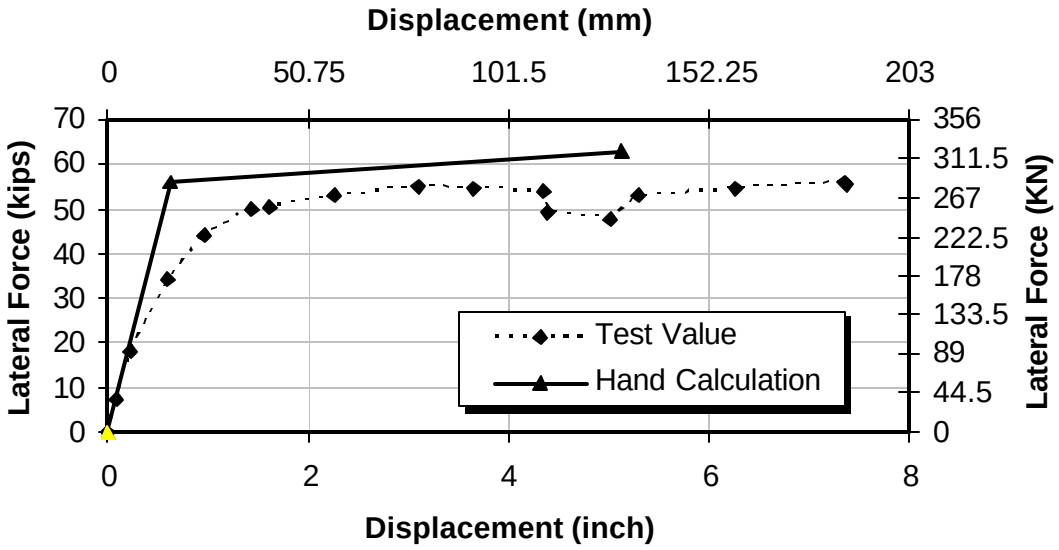

Figure 5-42 Comparison of Force-Deflection Curve Using Hand Calculation Versus Experimental Results for THD-2

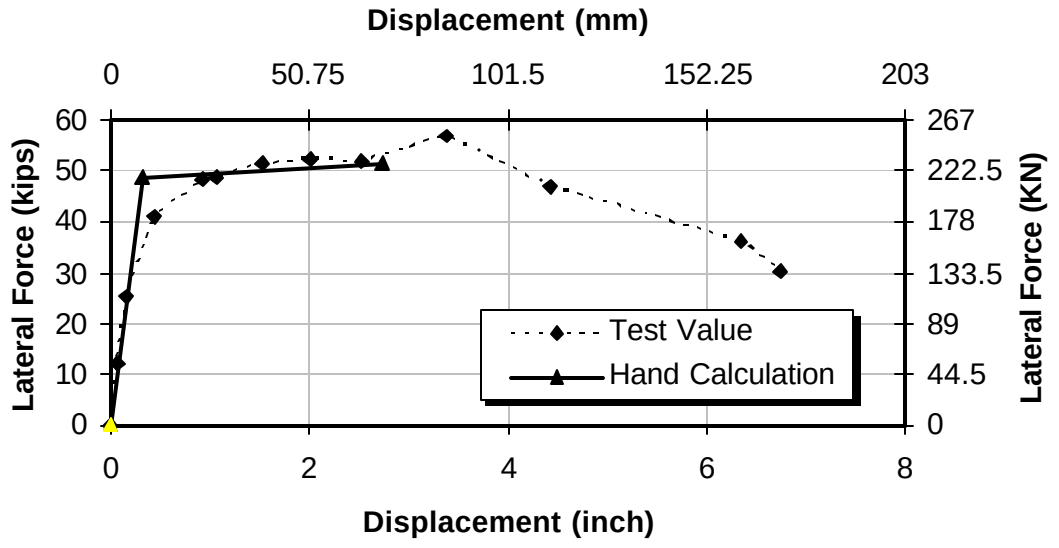

Figure 5-43 Comparison of Force-Deflection Curve Using Hand Calculation Versus Experimental Results for THD-3

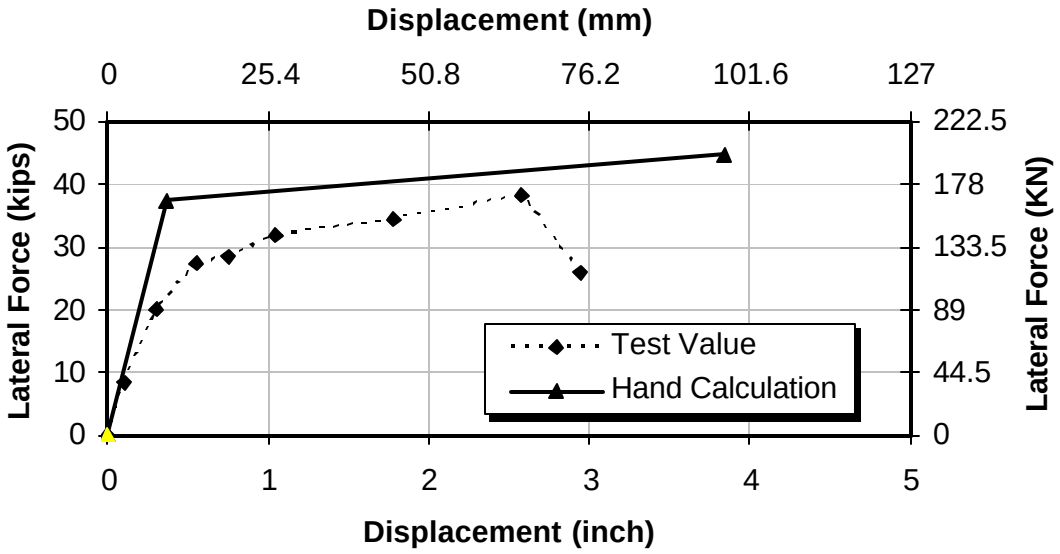

Figure 5-44 Comparison of Force-Deflection Curve Using Hand Calculation Versus Experimental Results for THD-4

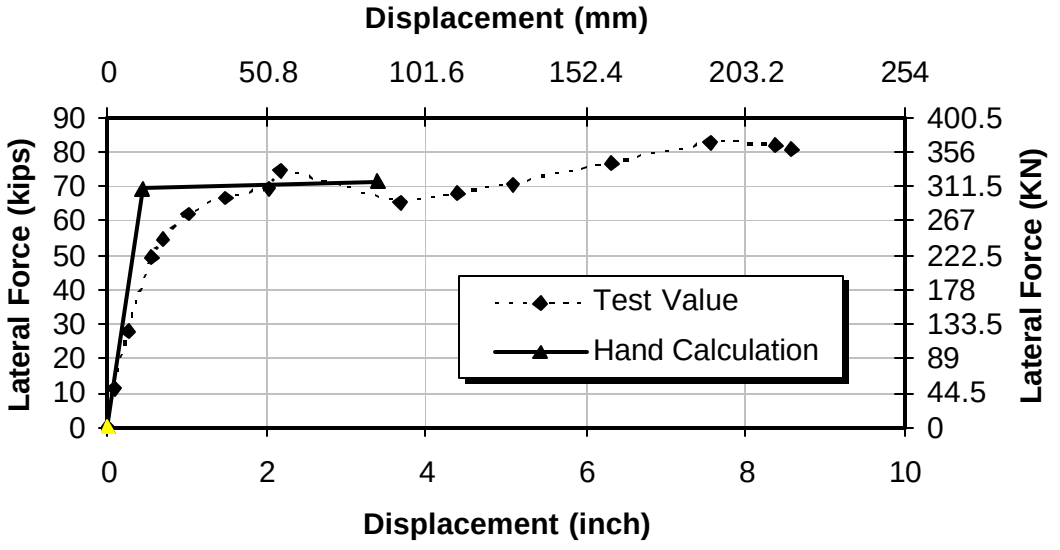

Figure 5-45 Comparison of Force-Deflection Curve Using Hand Calculation versus Experimental Results for THD-5

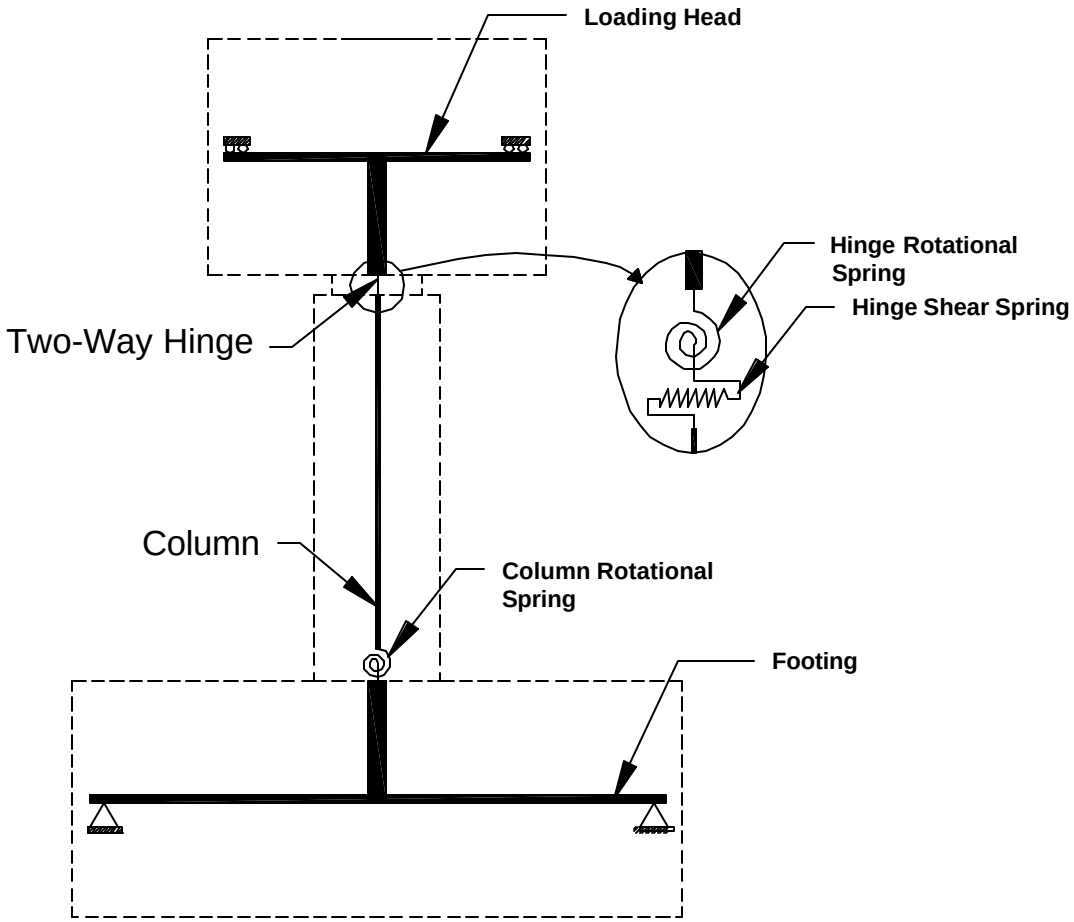

Figure 5-46 Push-Over Model for Two-Way Hinge Specimen

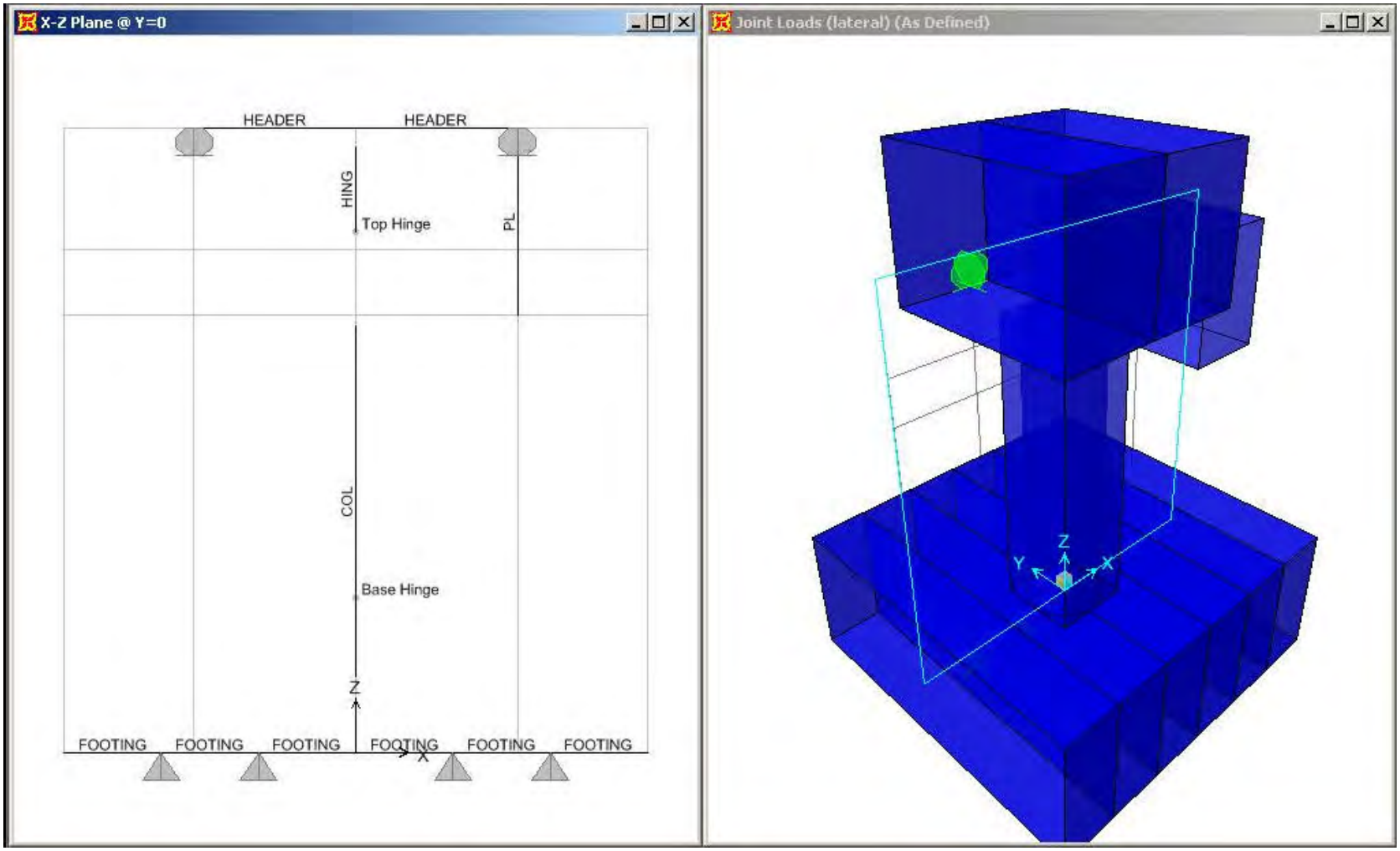

Figure 5-47 SAP2000 Push-Over Analysis for Two-Way Hinge Specimen

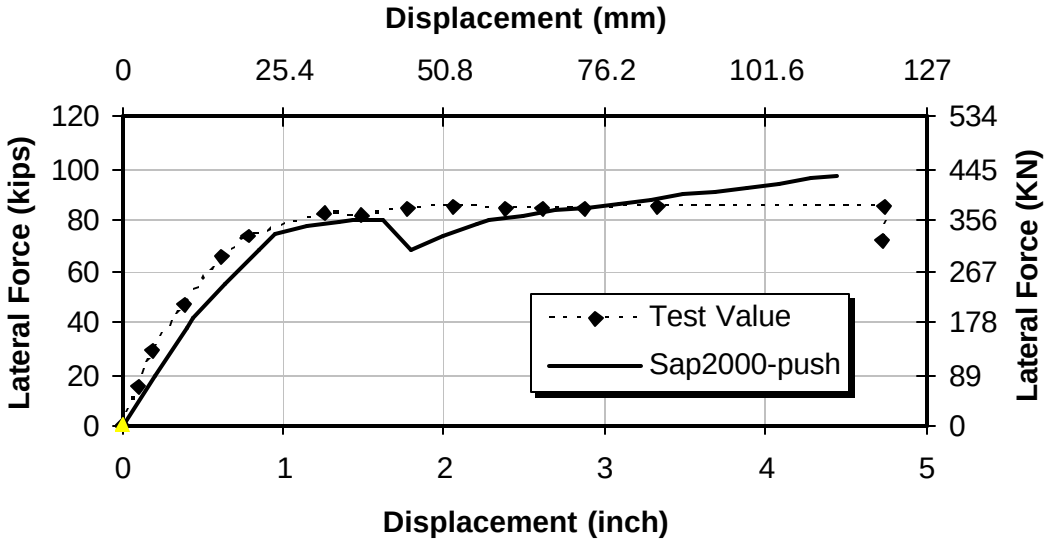

Figure 5-48 Comparison of Force-Deflection Curve Using SAP2000 Push-Over Analysis versus Experimental Results for THD-1

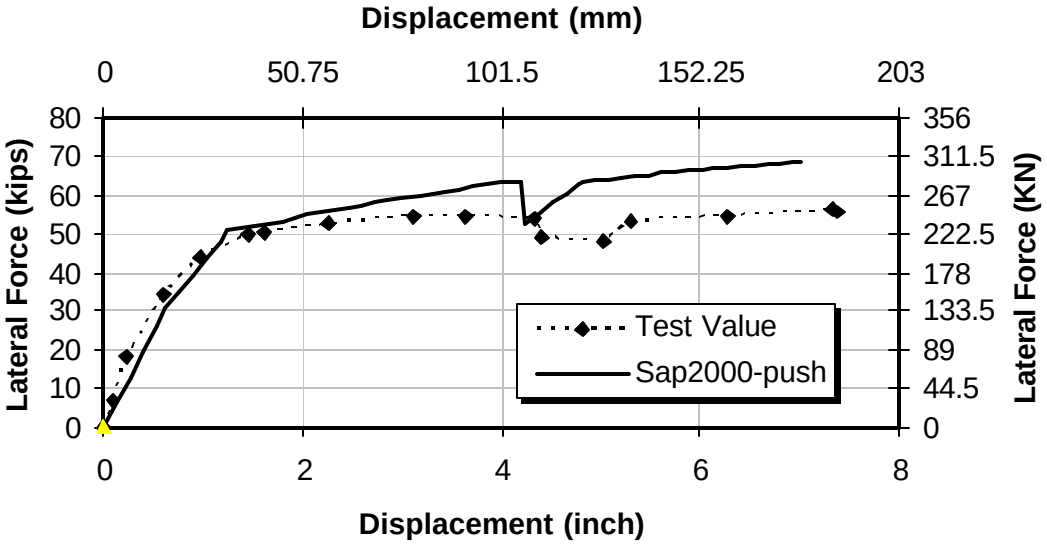

Figure 5-49 Comparison of Force-Deflection Curve Using SAP2000 Push-Over Analysis versus Experimental Results for THD-2

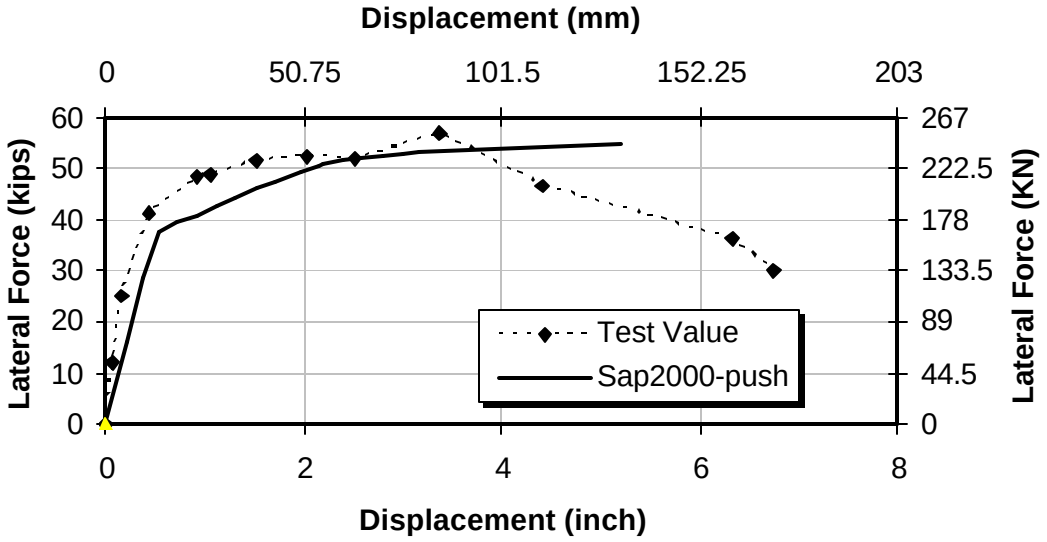

Figure 5-50 Comparison of Force-Deflection Curve Using SAP2000 Push-Over Analysis versus Experimental Results for THD-3

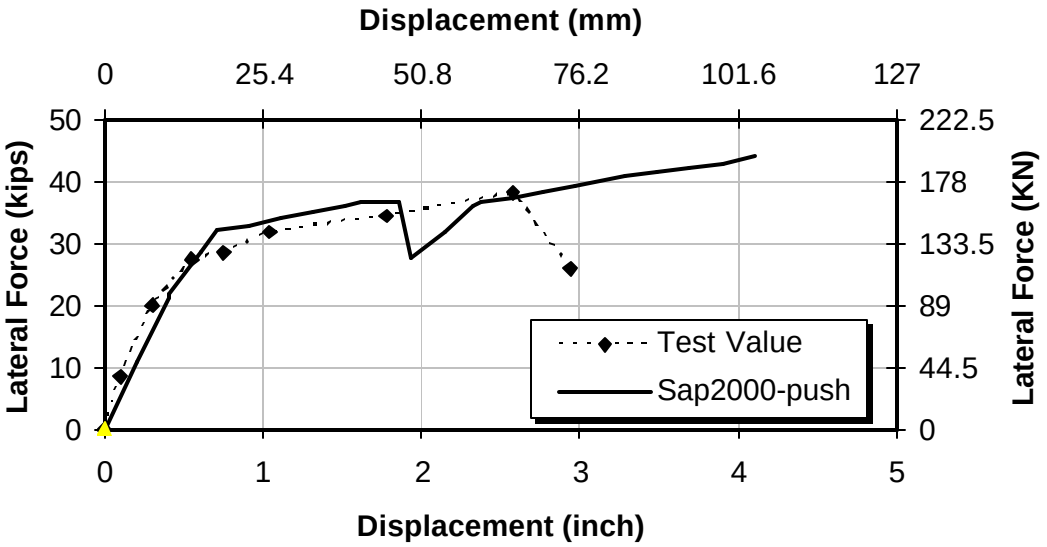

Figure 5-51 Comparison of Force-Deflection Curve Using SAP2000 Push-Over Analysis versus Experimental Results for THD-4

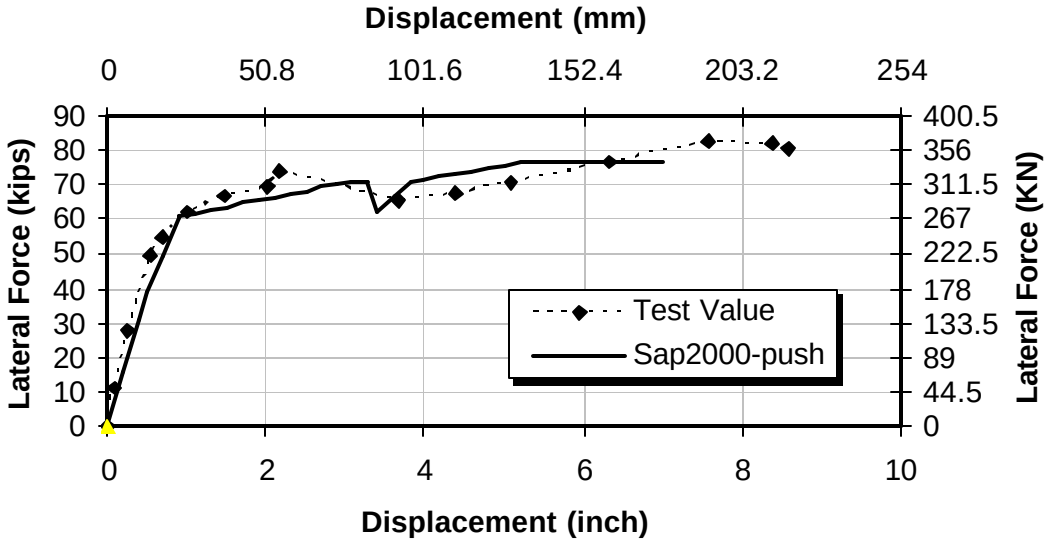

Figure 5-52 Comparison of Force-Deflection Curve Using SAP2000 Push-Over Analysis versus Experimental Results for THD-5

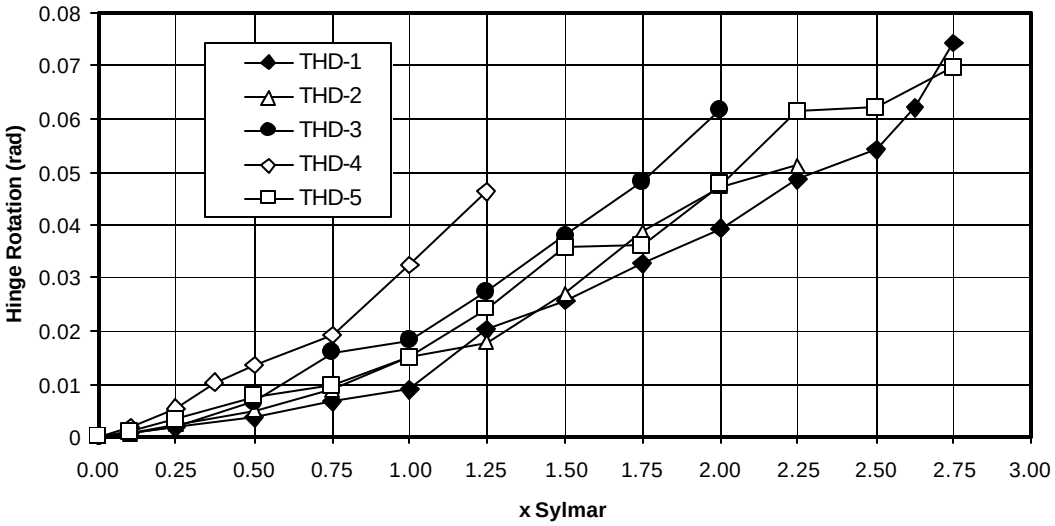

Figure 5-53 Two-Way Hinge Rotation vs. Test Runs

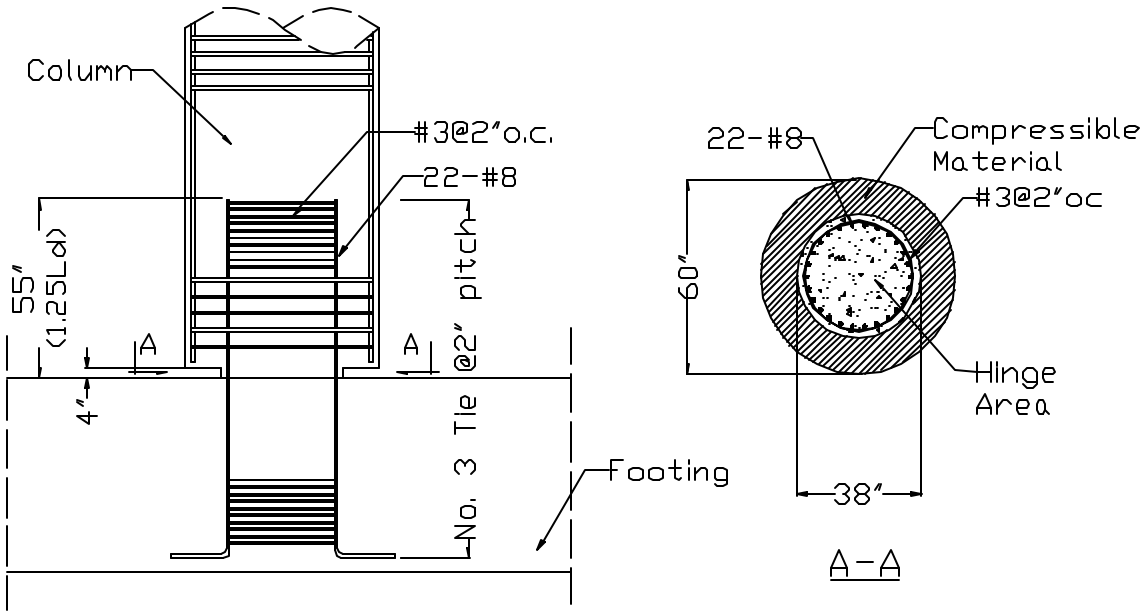

Figure 6-1 Two-Way Hinge Structural Drawing for Example Problem (US Customary Units)

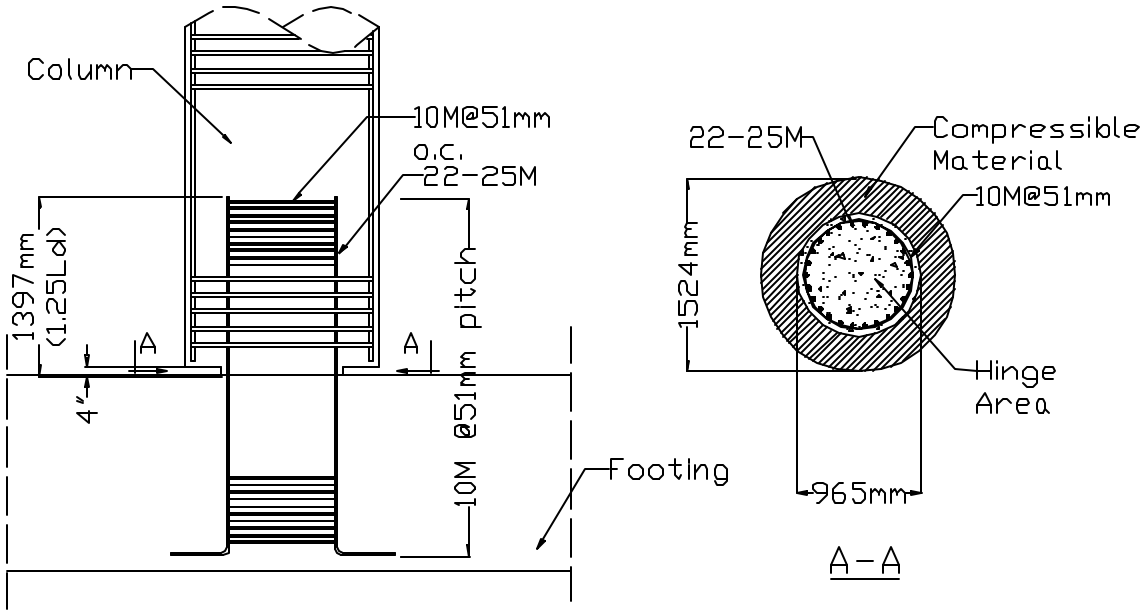

Figure 6-2 Two-Way Hinge Structural Drawing for Example Problem (SI Units)

APPENDIX

Strain Gauge Time History

For all Five Specimens

(See Figs. 3-16 to 3-20 for the locations of each gauge)

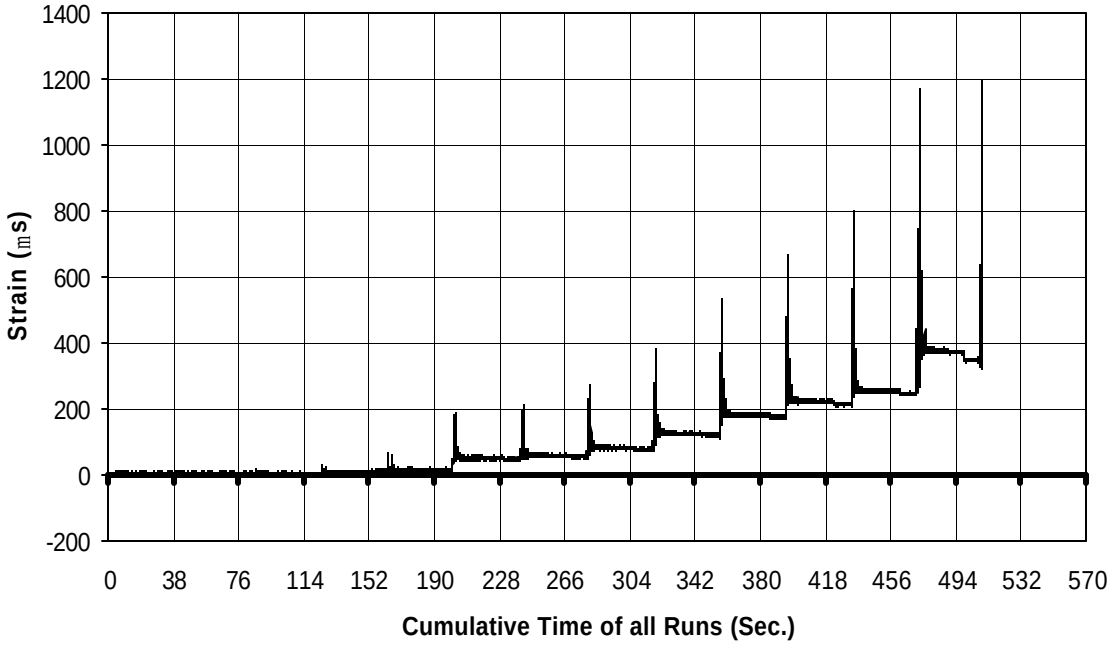

Fig. A-1 THD -1 Measured Strain in Gauge SG1B1

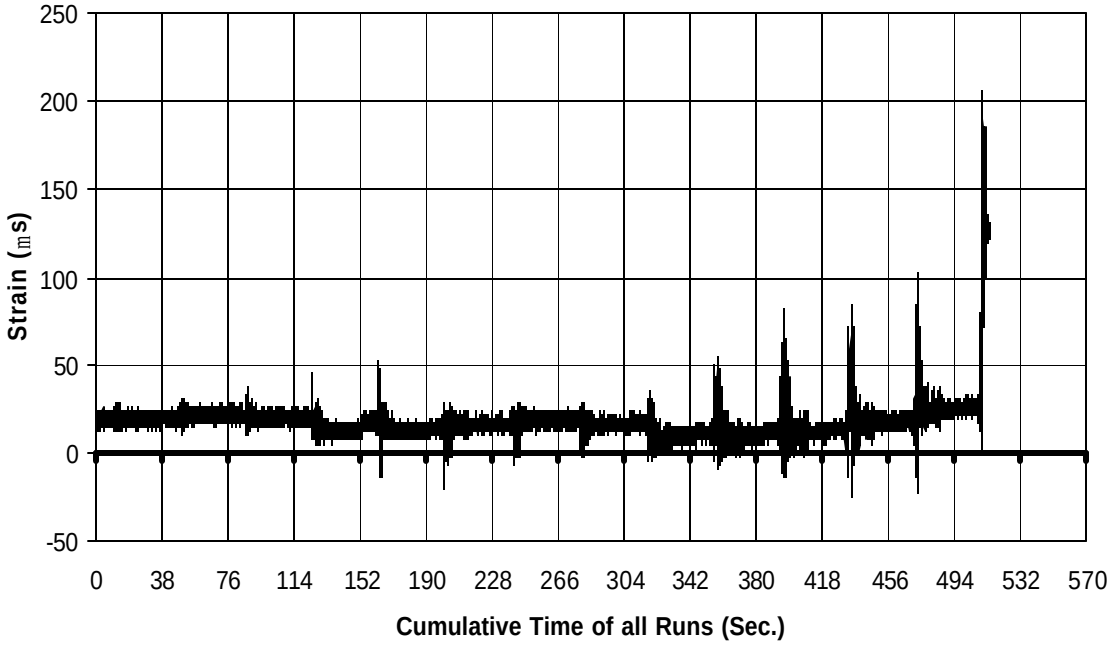

Fig. A-2 THD -1 Measured Strain in Gauge SG2B1

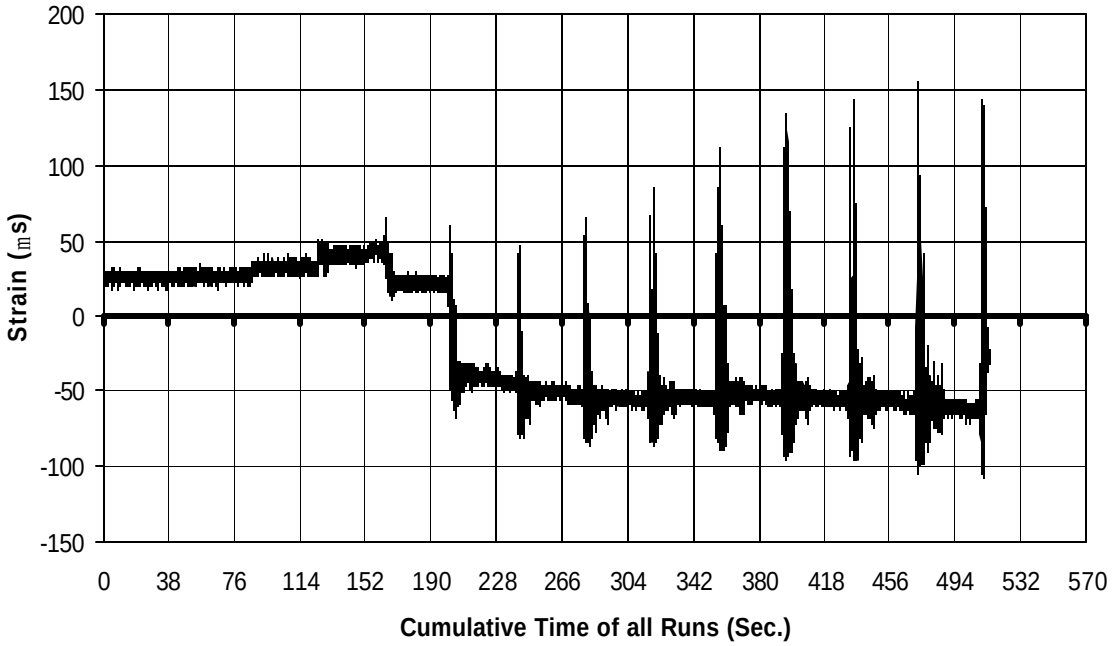

Fig. A-3 THD -1 Measured Strain in Gauge SG3B1

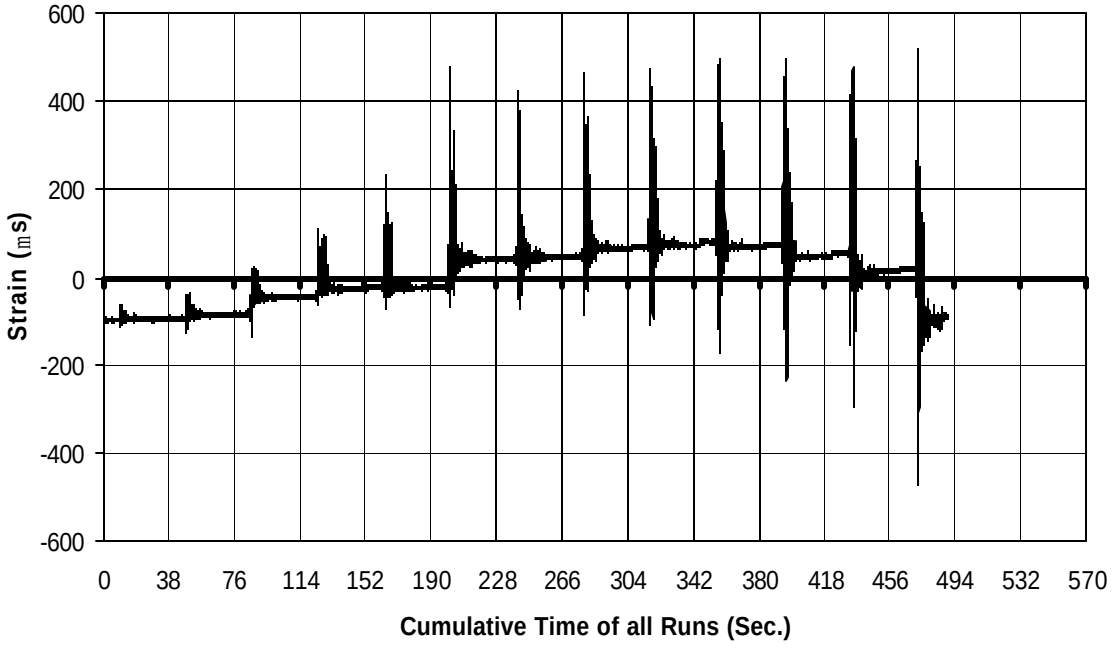

Fig. A-4 THD -1 Measured Strain in Gauge SG4B1

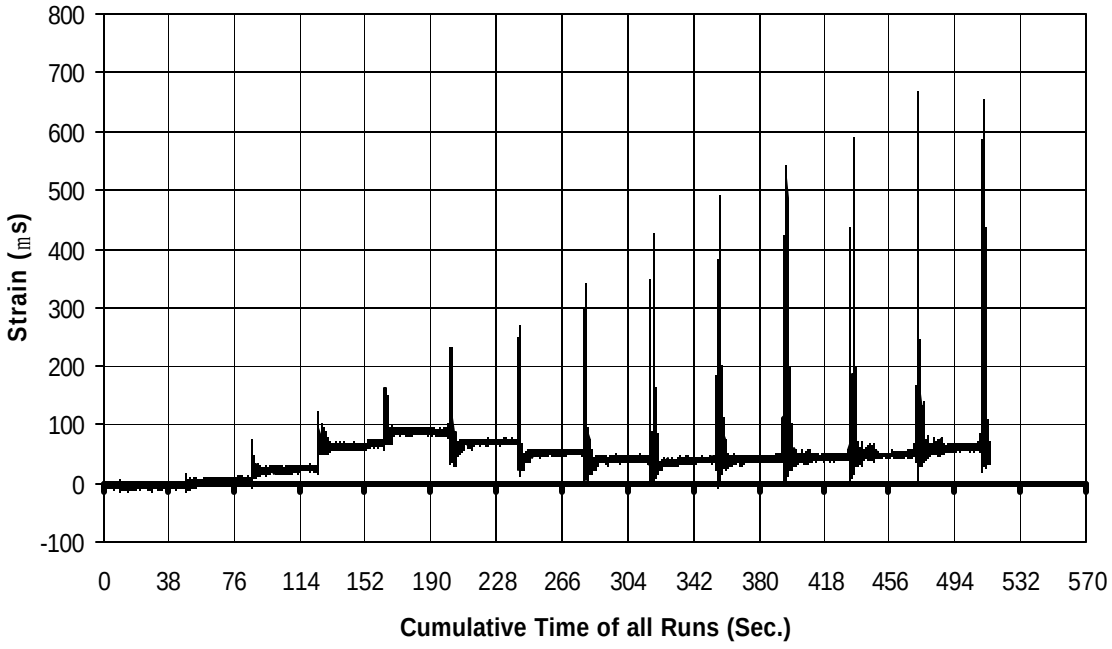

Fig. A-5 THD -1 Measured Strain in Gauge SG5B1

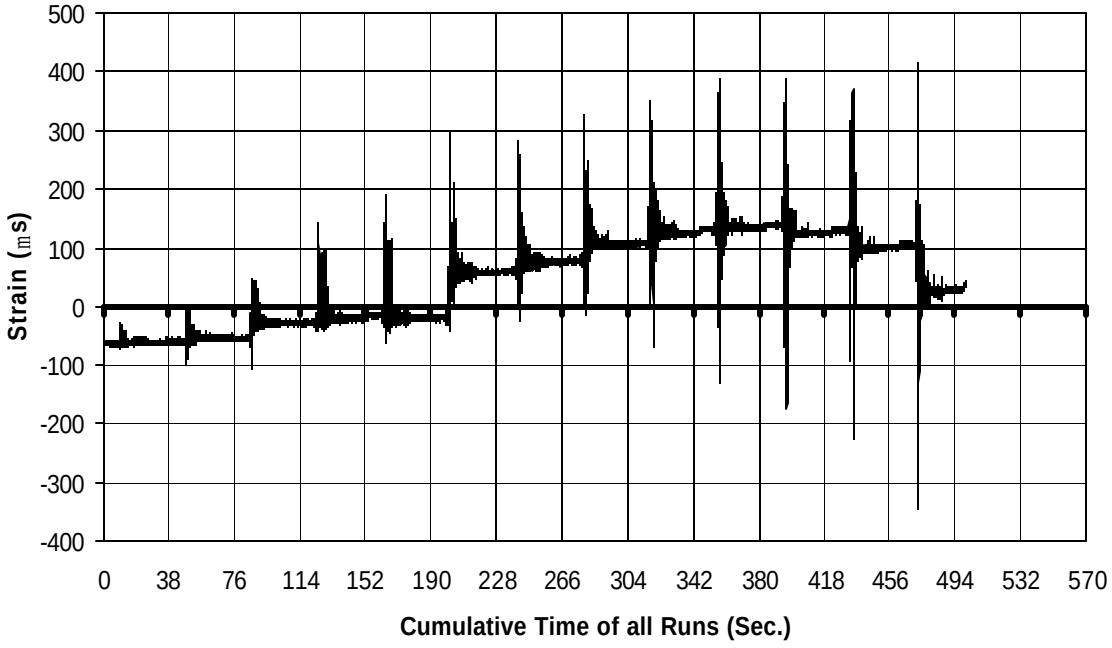

Fig. A-6 THD -1 Measured Strain in Gauge SG6B1

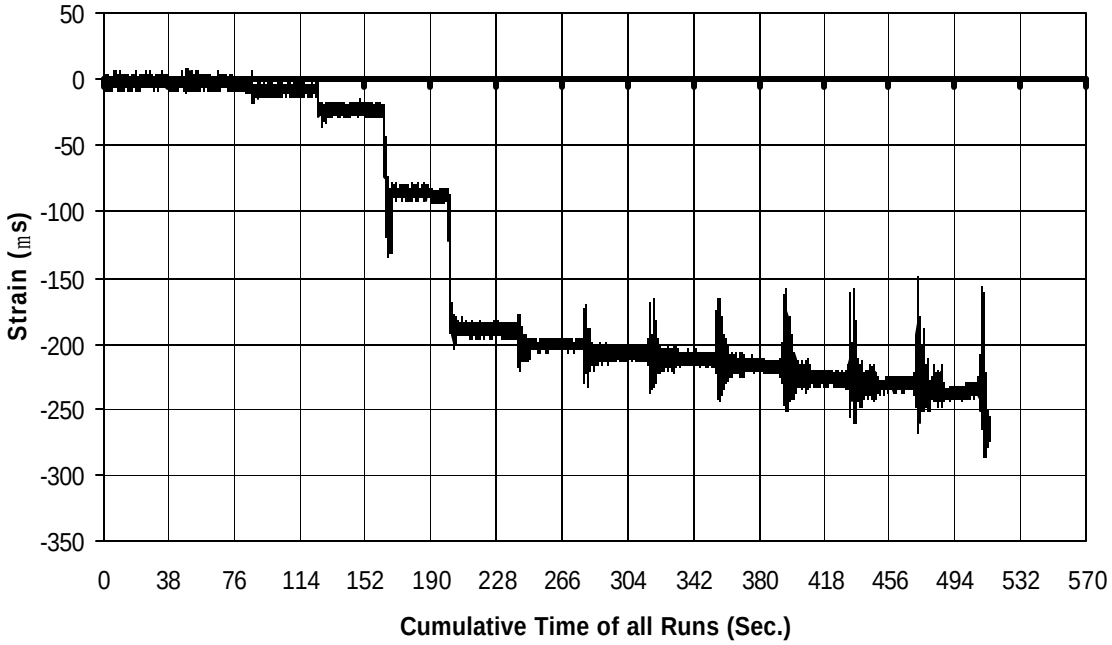

Fig. A-7 THD -1 Measured Strain in Gauge SG8B1

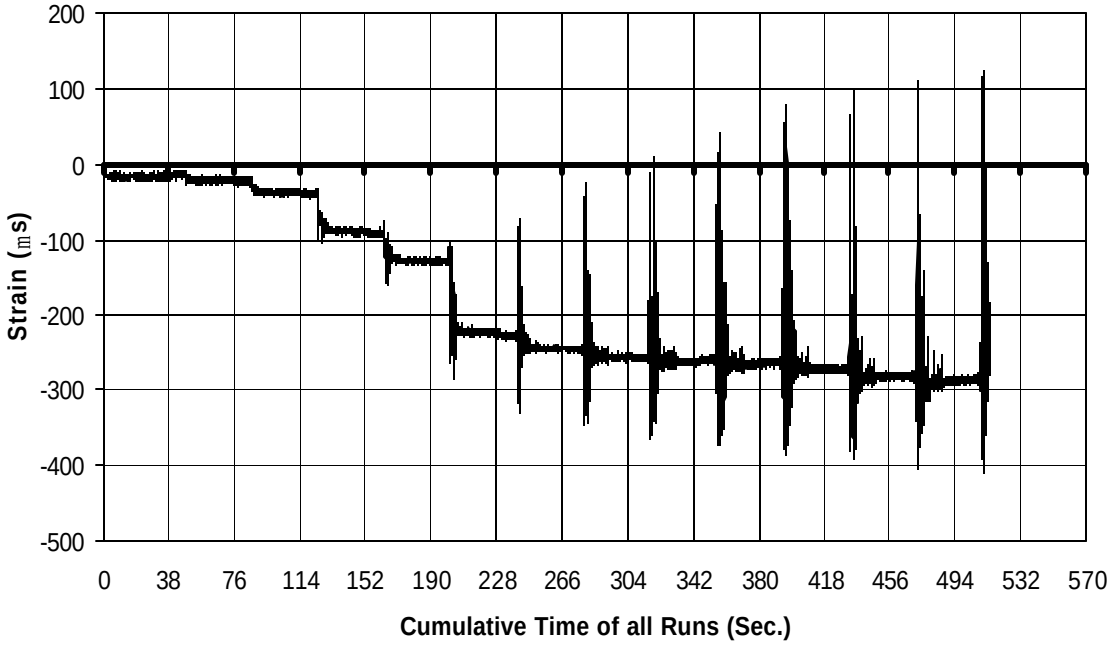

Fig. A-8 THD -1 Measured Strain in Gauge SG1B2

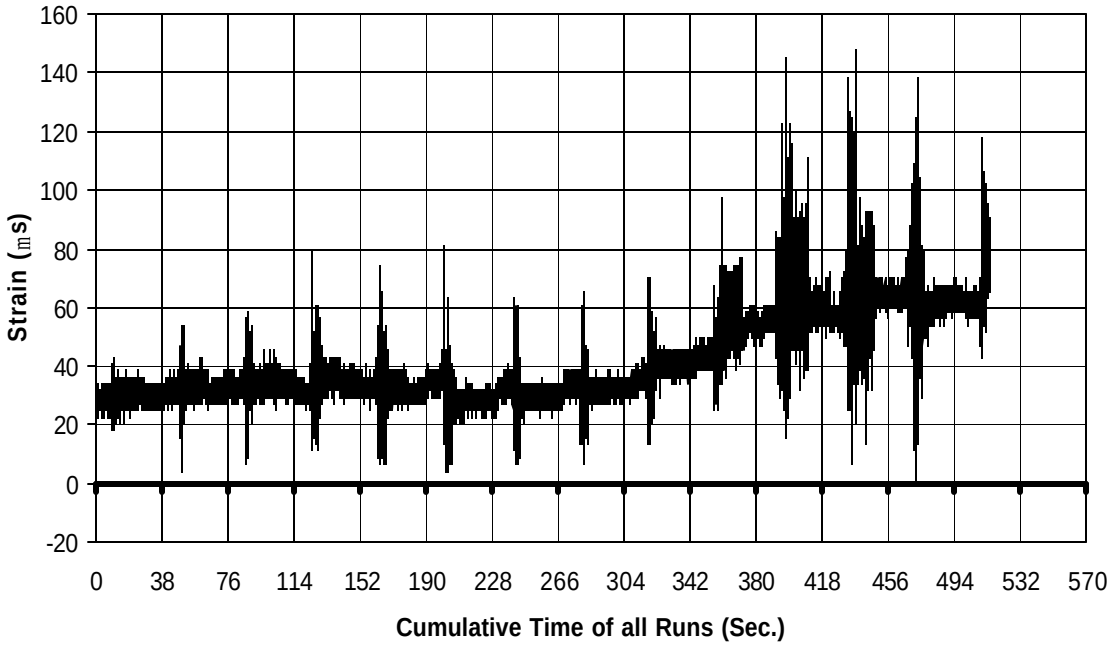

Fig. A-9 THD -1 Measured Strain in Gauge SG2B2

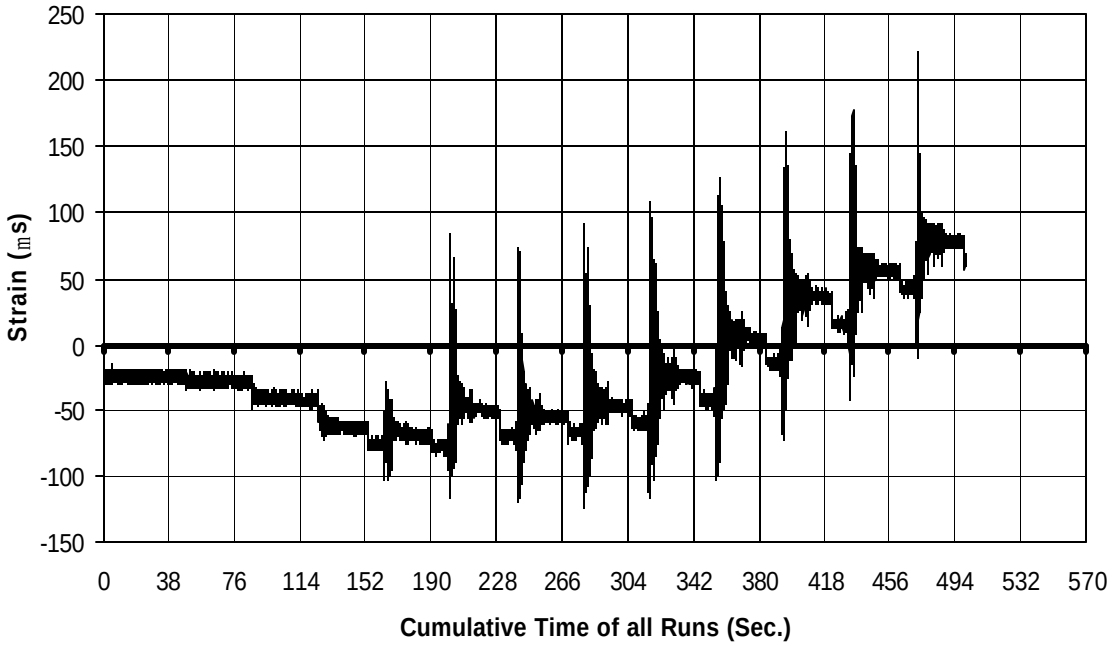

Fig. A-10 THD -1 Measured Strain in Gauge SG3B2

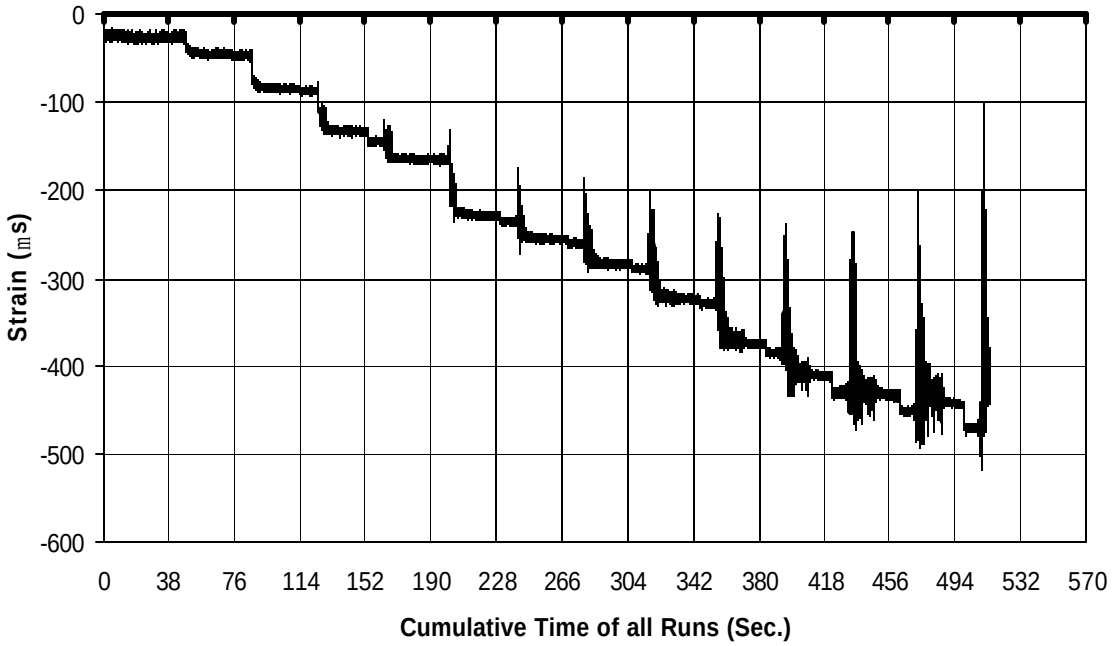

Fig. A-11 THD -1 Measured Strain in Gauge SG5B2

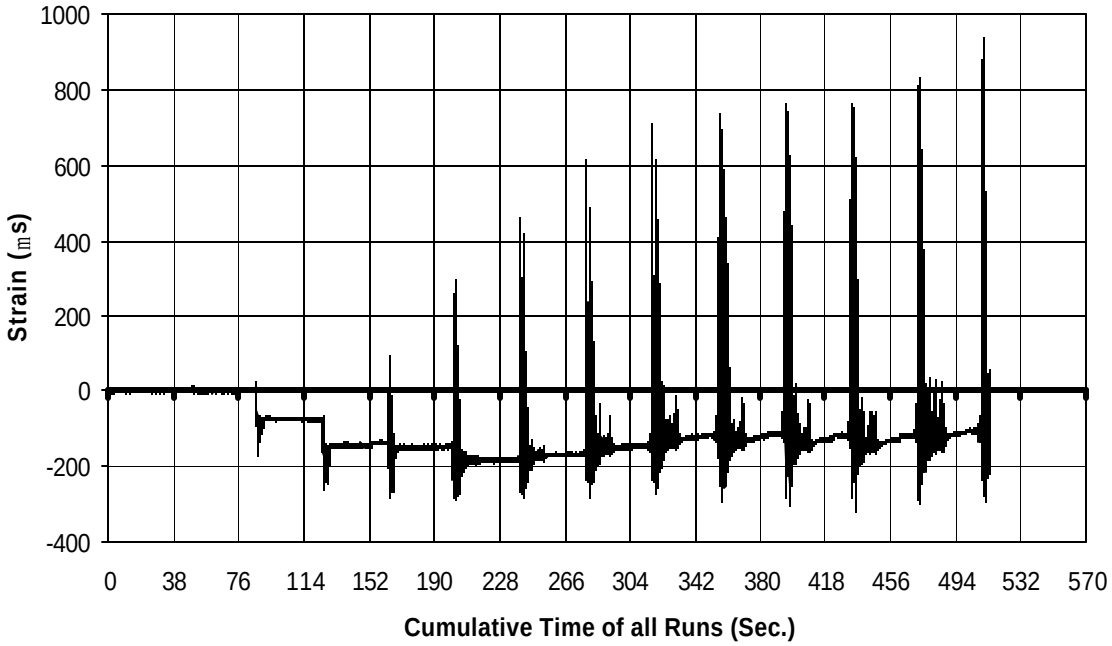

Fig. A-12 THD -1 Measured Strain in Gauge SG6B2

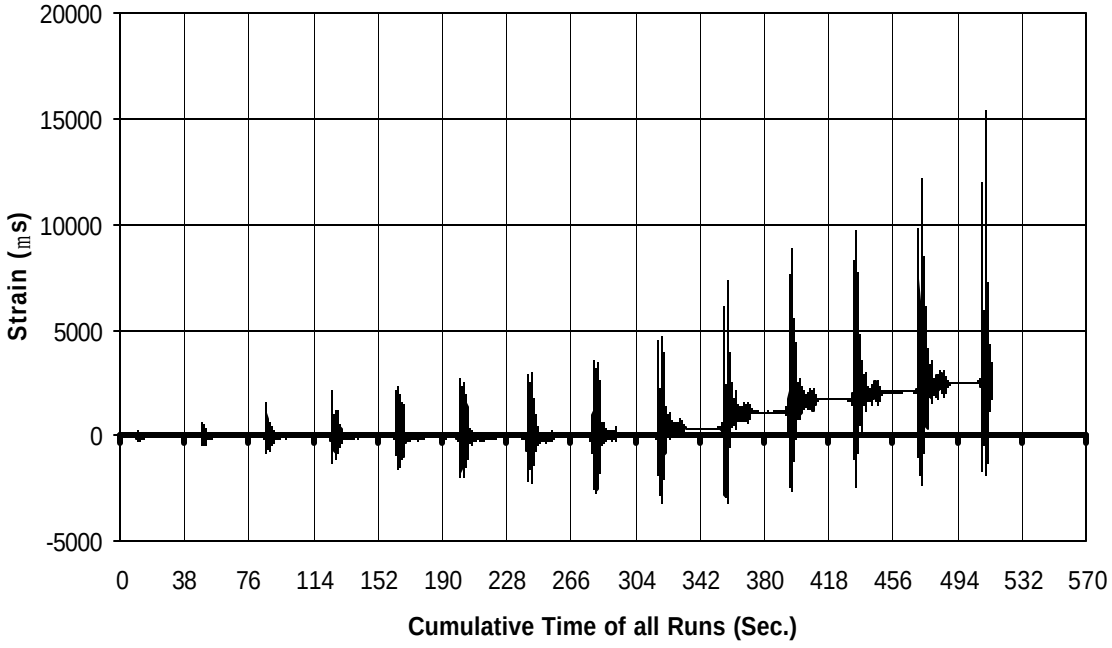

Fig. A-13 THD -1 Measured Strain in Gauge SG7B2

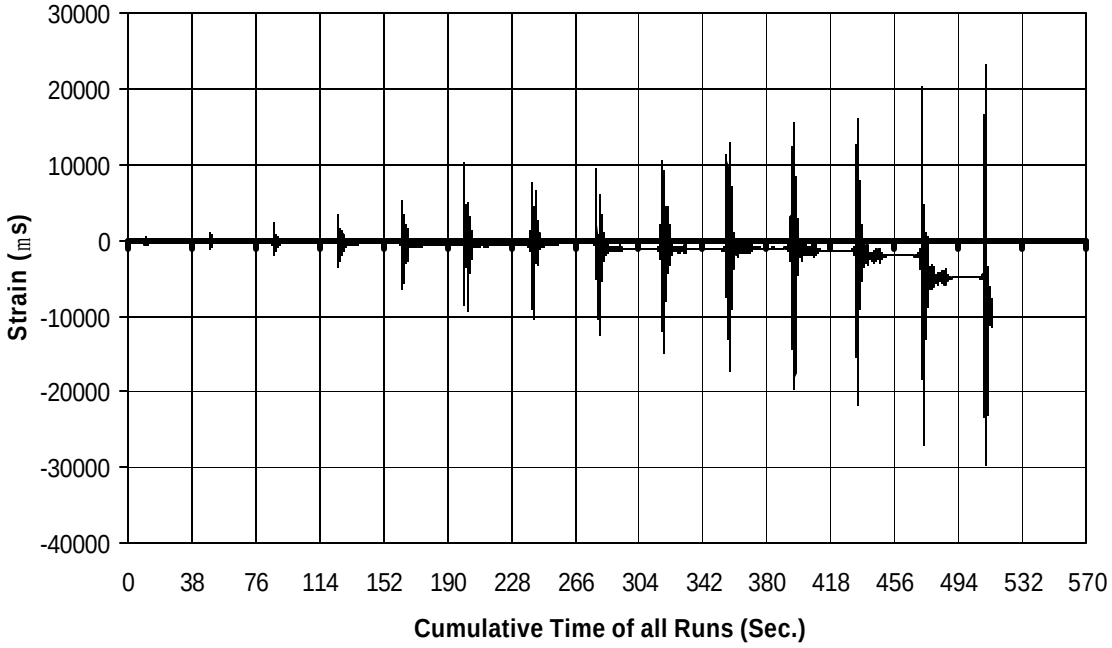

Fig. A-14 THD -1 Measured Strain in Gauge SG8B2

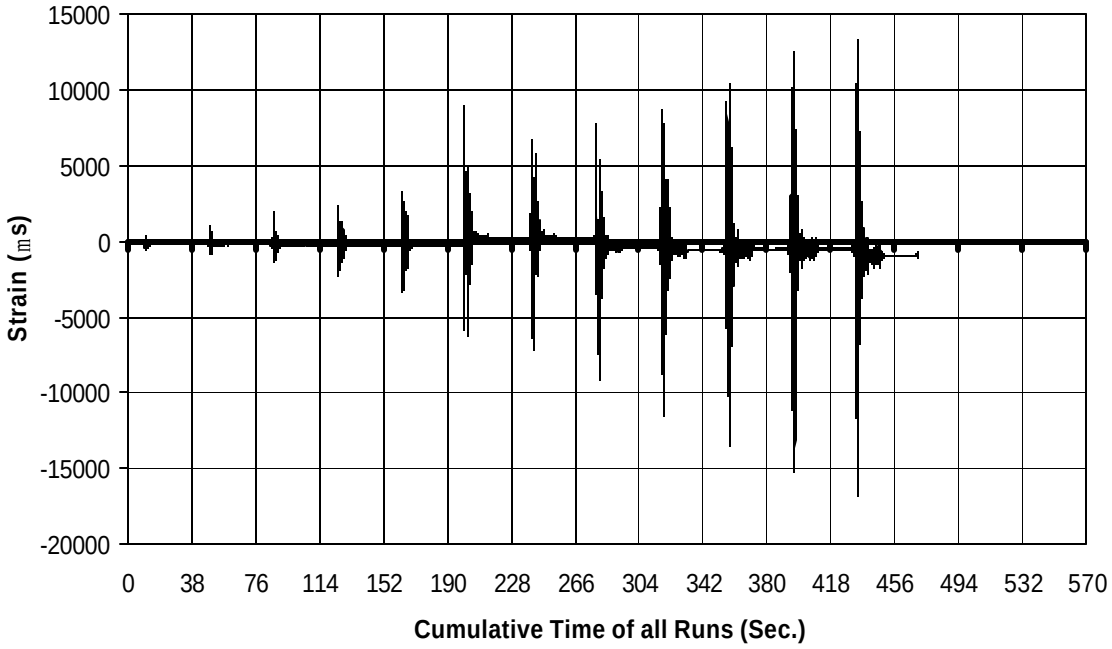

Fig. A-15 THD -1 Measured Strain in Gauge SG2B3

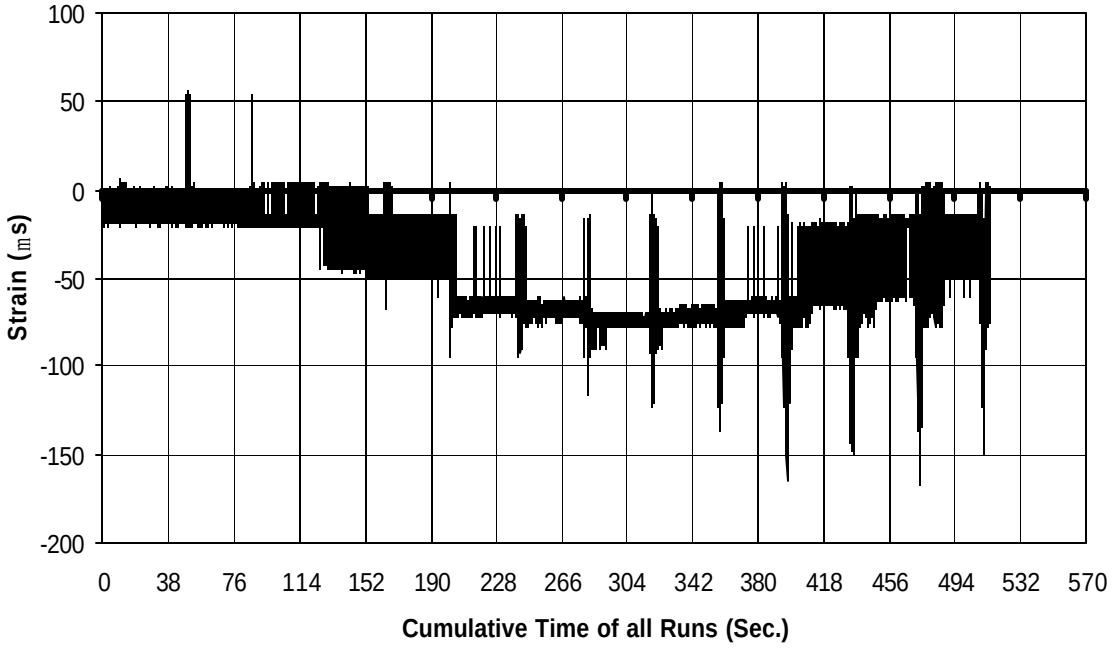

Fig. A-16 THD -1 Measured Strain in Gauge SG3B3

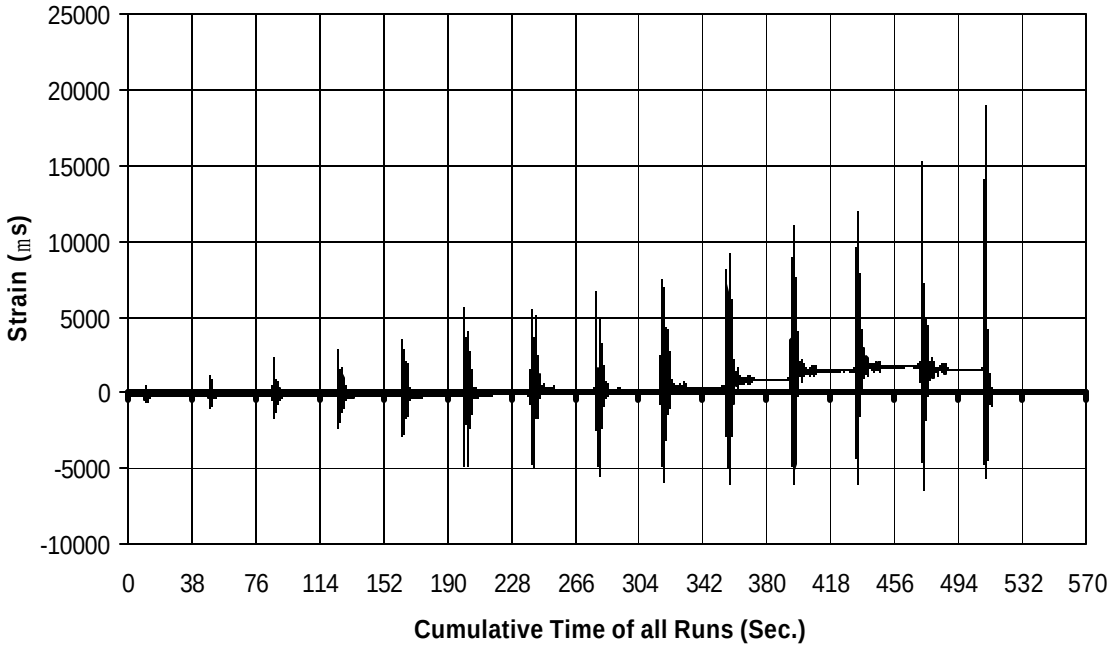

Fig. A-17 THD -1 Measured Strain in Gauge SG4B3

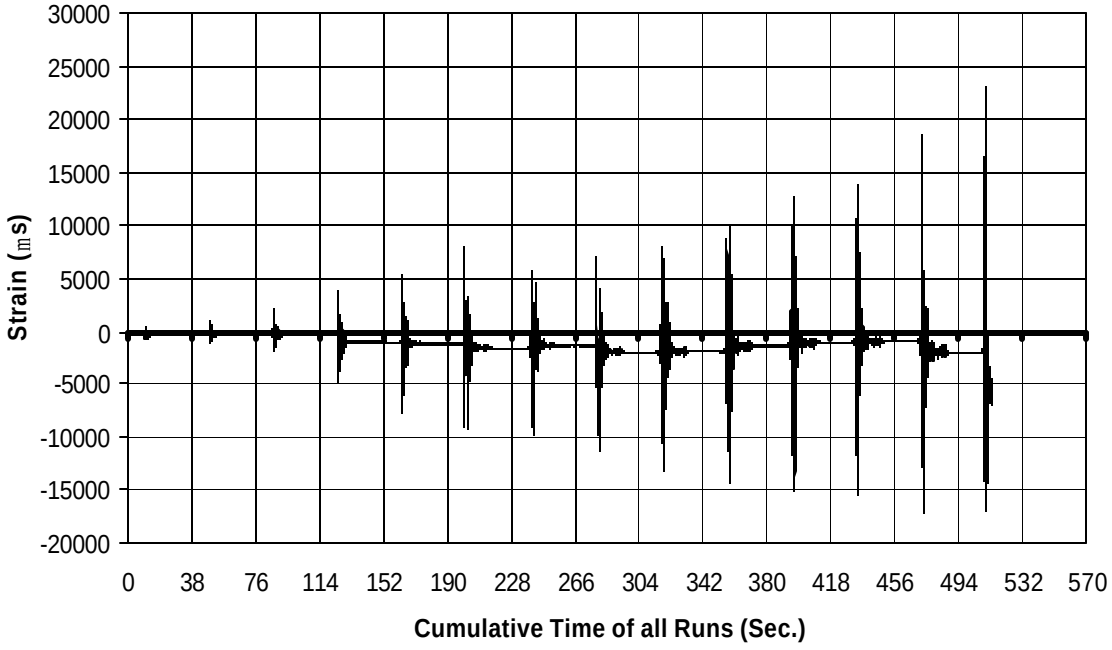

Fig. A-18 THD -1 Measured Strain in Gauge SG5B3

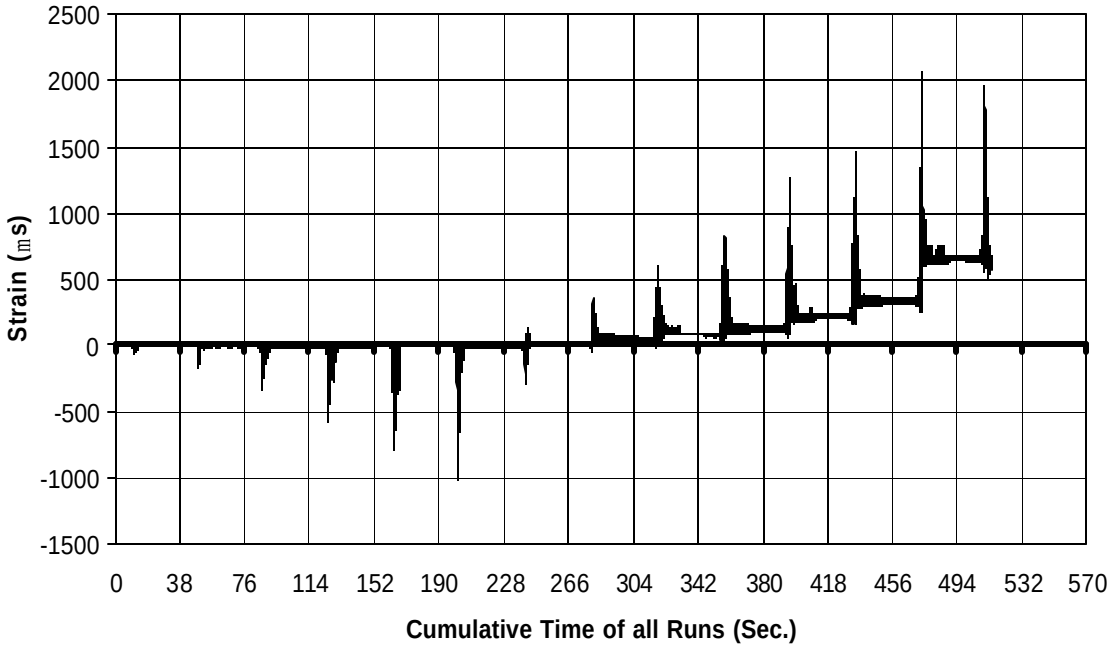

Fig. A-19 THD -1 Measured Strain in Gauge SG6B3

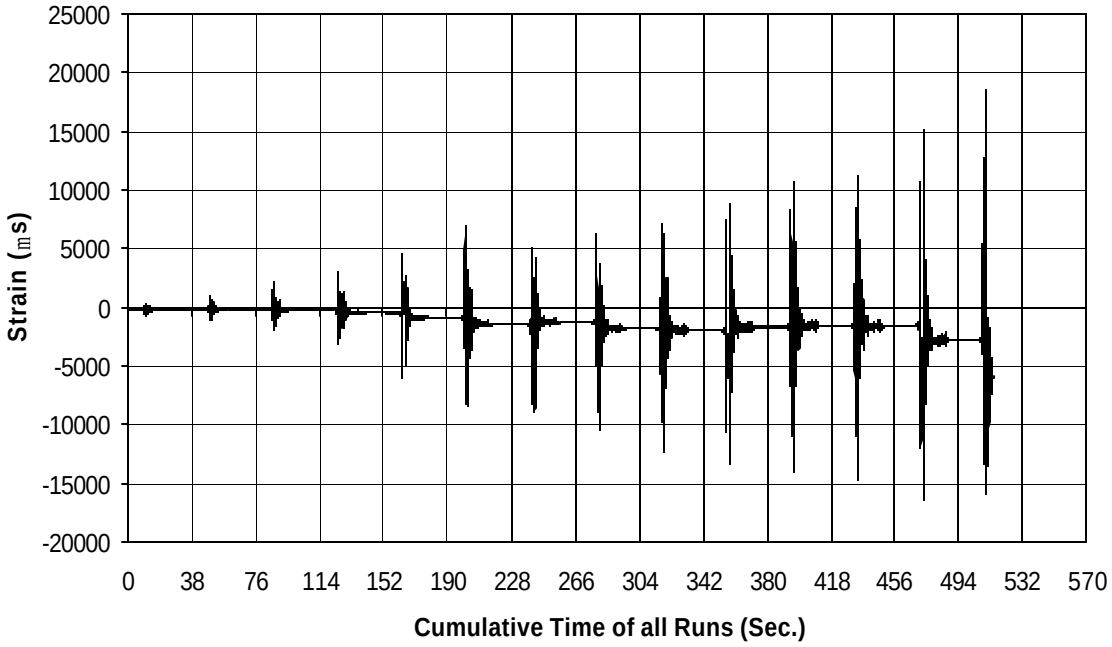

Fig. A-21 THD -1 Measured Strain in Gauge SG7B3

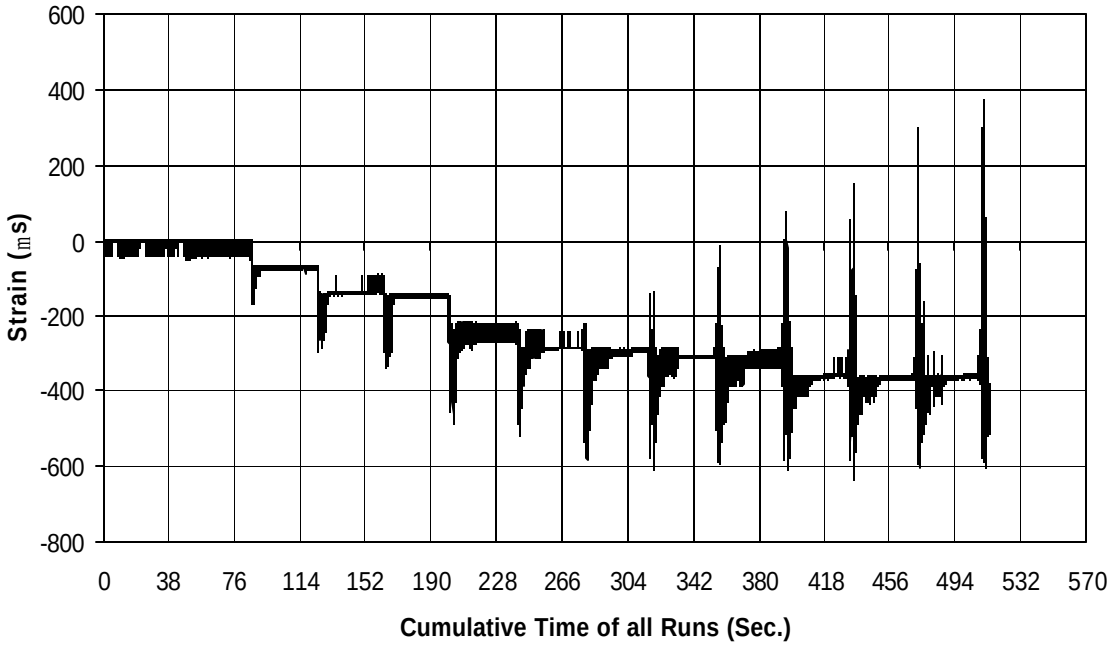

Fig. A-22 THD -1 Measured Strain in Gauge SG1B4

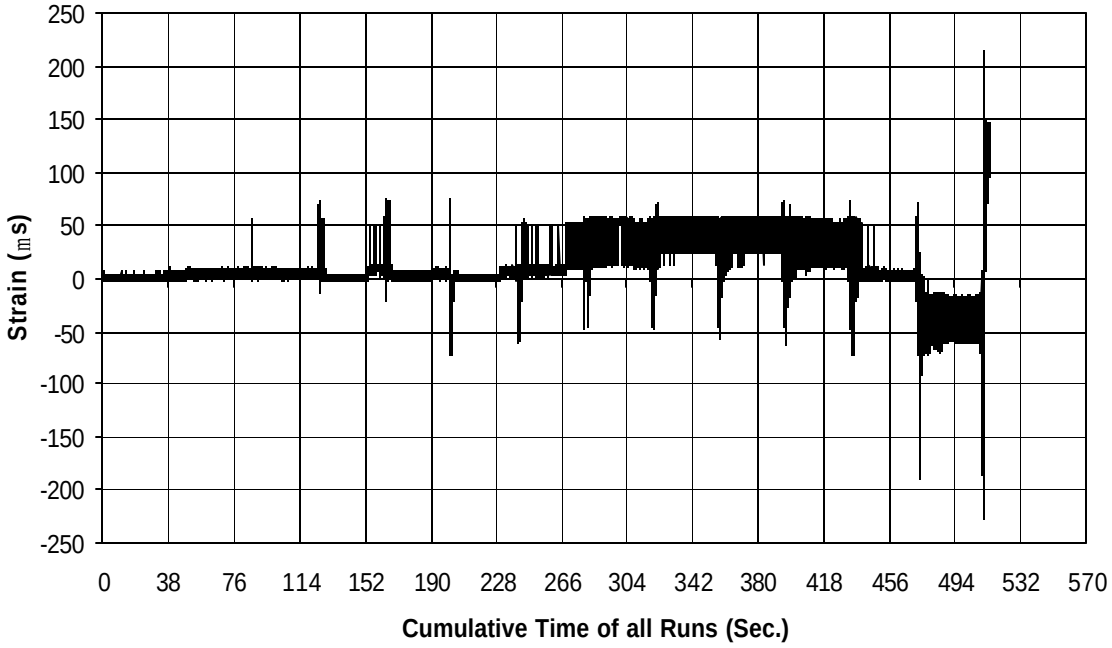

Fig. A-23 THD -1 Measured Strain in Gauge SG2B4

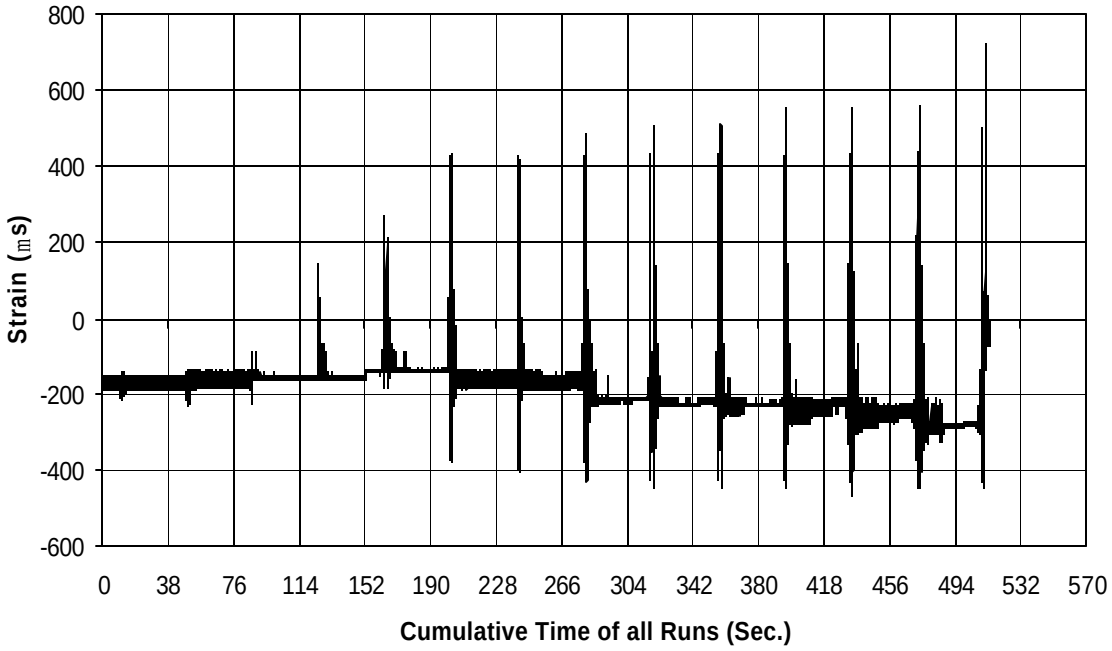

Fig. A-24 THD -1 Measured Strain in Gauge SG3B4

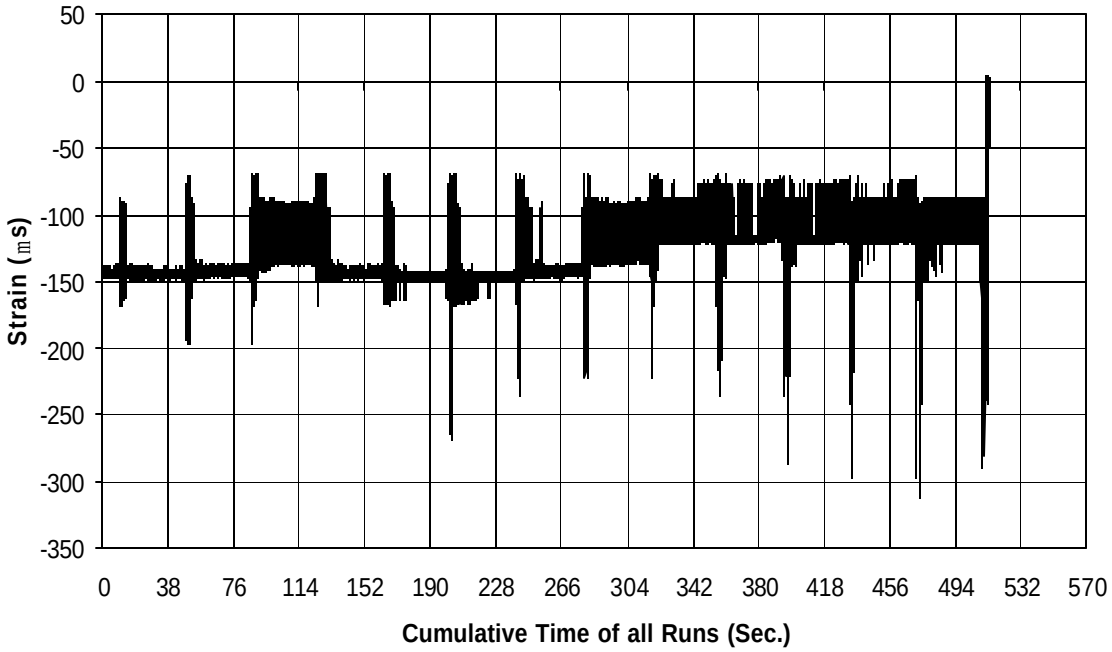

Fig. A-25 THD -1 Measured Strain in Gauge SG4B4

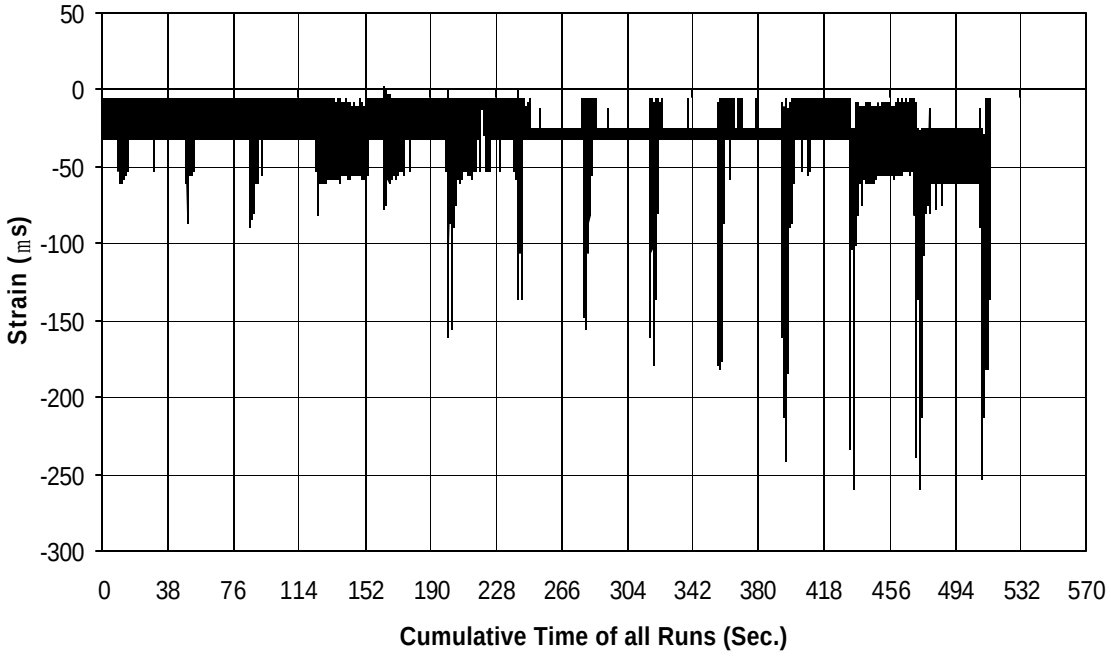

Fig. A-26 THD -1 Measured Strain in Gauge SG5B4

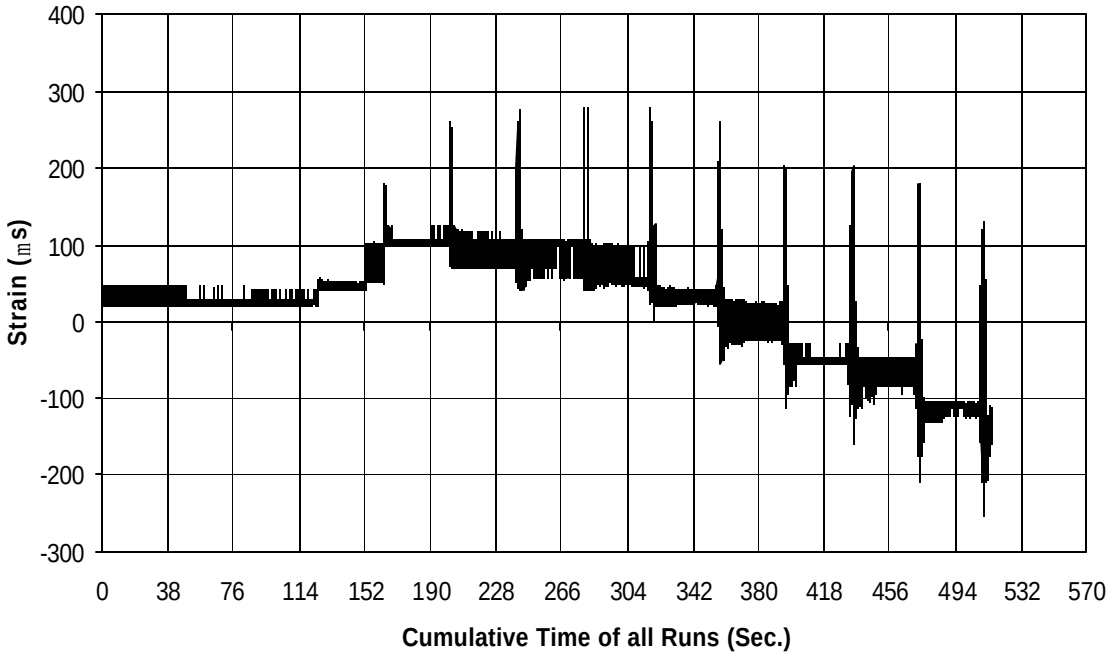

Fig. A-27 THD -1 Measured Strain in Gauge SG6B4

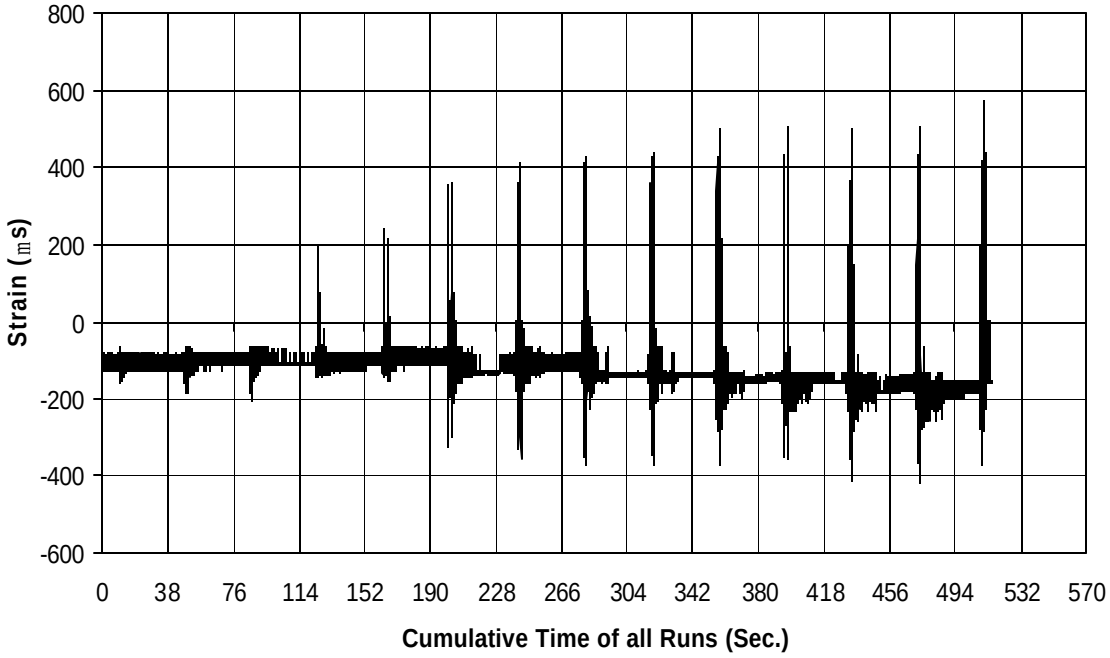

Fig. A-28 THD -1 Measured Strain in Gauge SG7B4

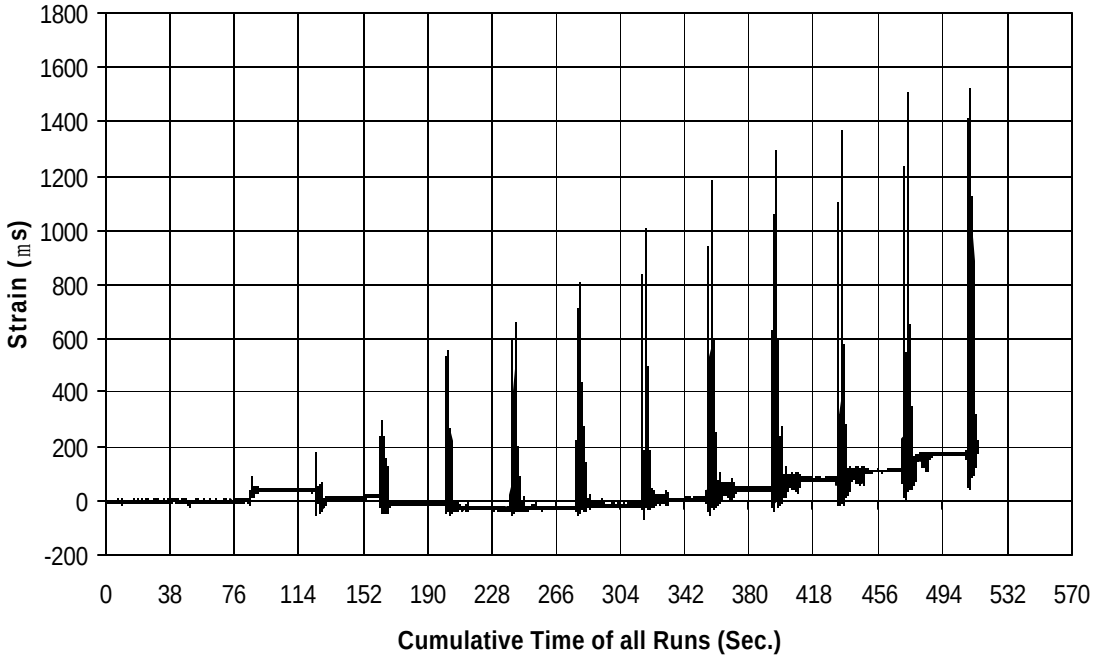

Fig. A-29 THD -1 Measured Strain in Gauge SG1B5

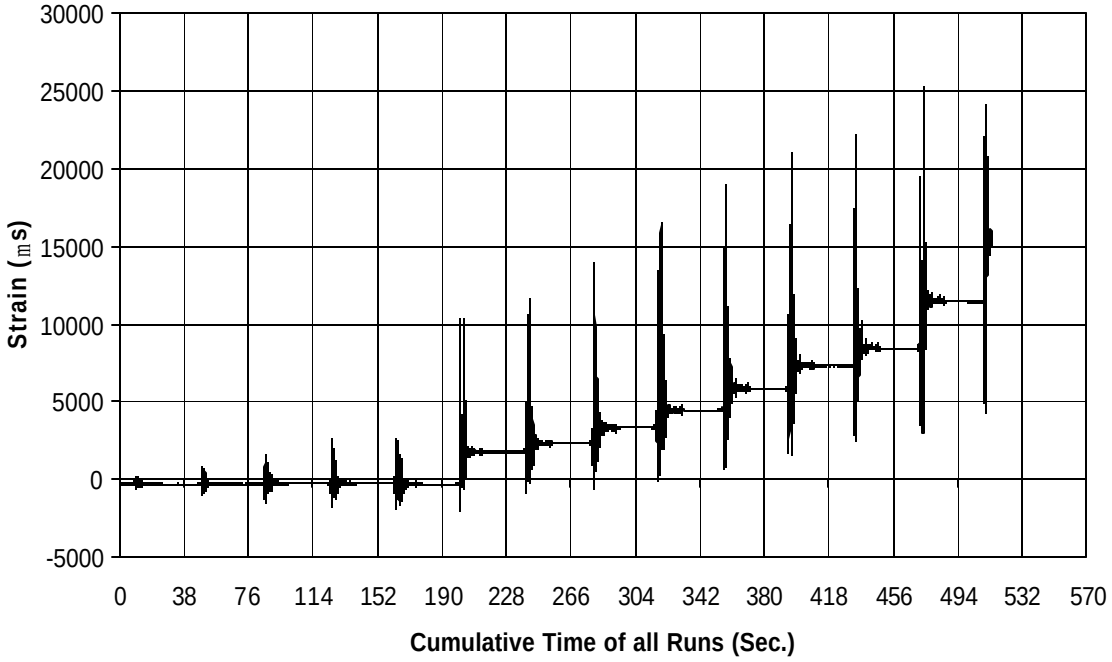

Fig. A-30 THD -1 Measured Strain in Gauge SG3B5

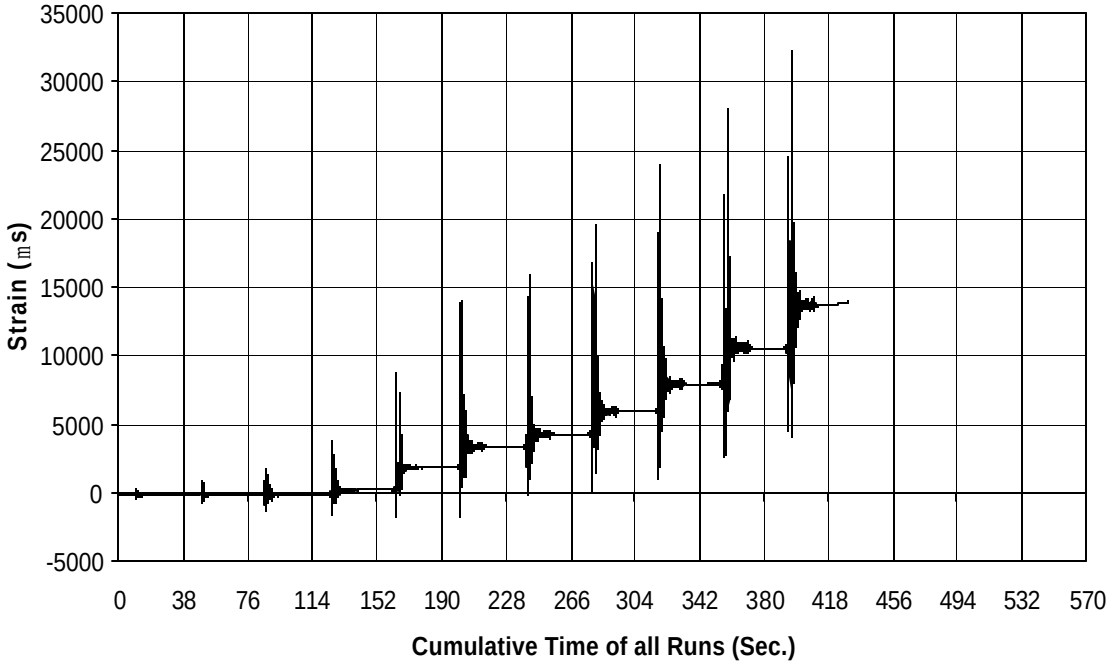

Fig. A-31 THD -1 Measured Strain in Gauge SG5B5

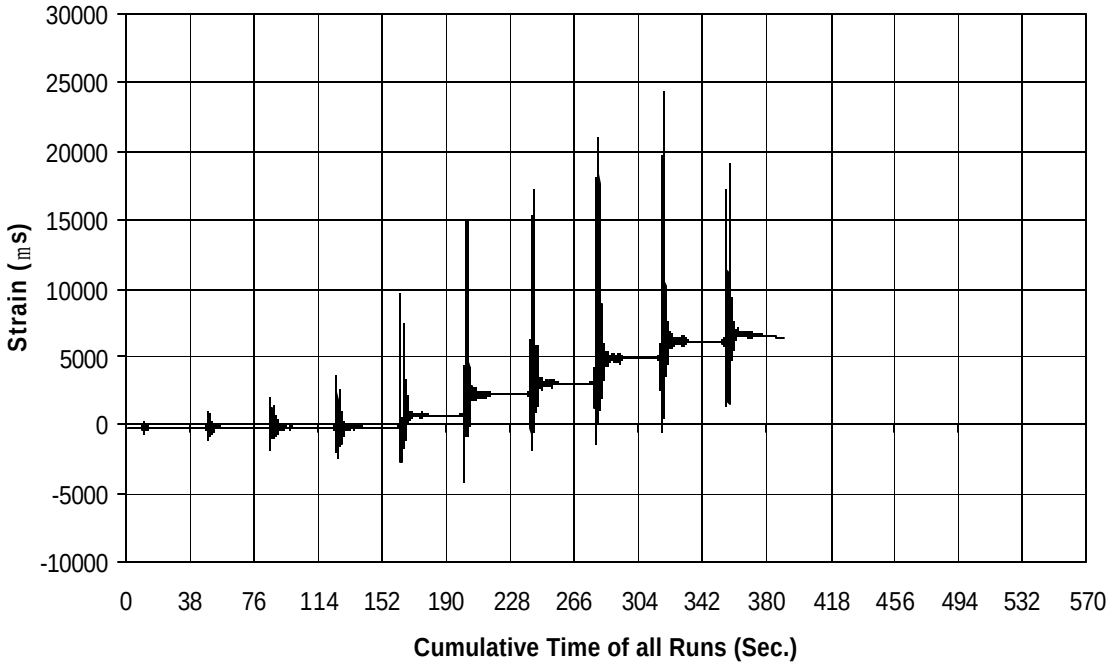

Fig. A-32 THD -1 Measured Strain in Gauge SG6B5

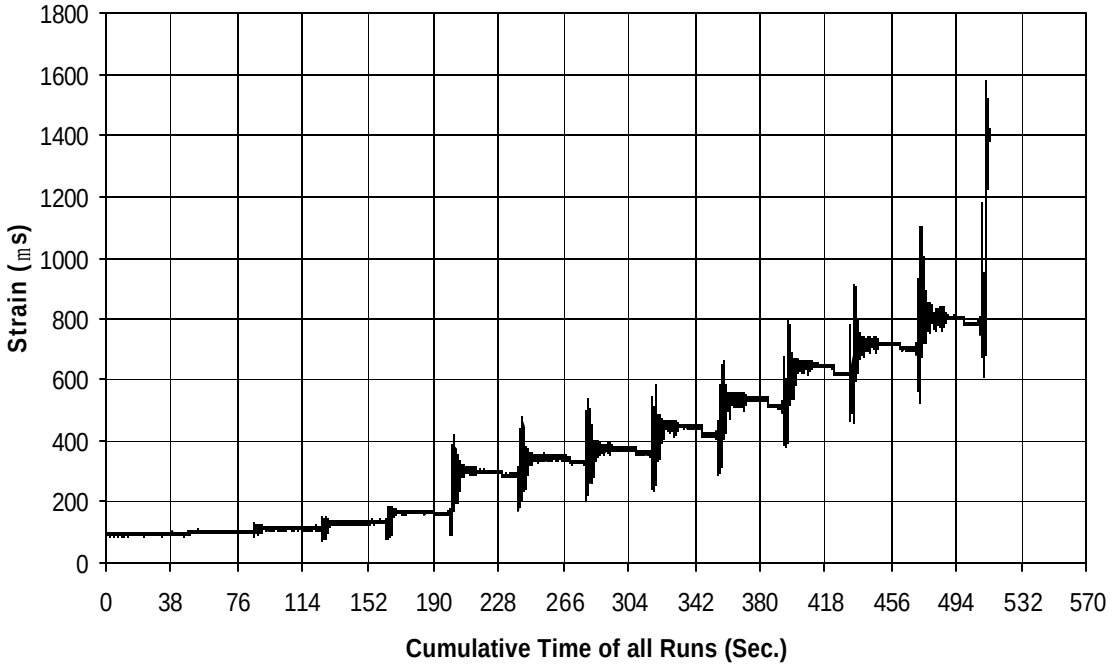

Fig. A-33 THD -1 Measured Strain in Gauge SG7B5

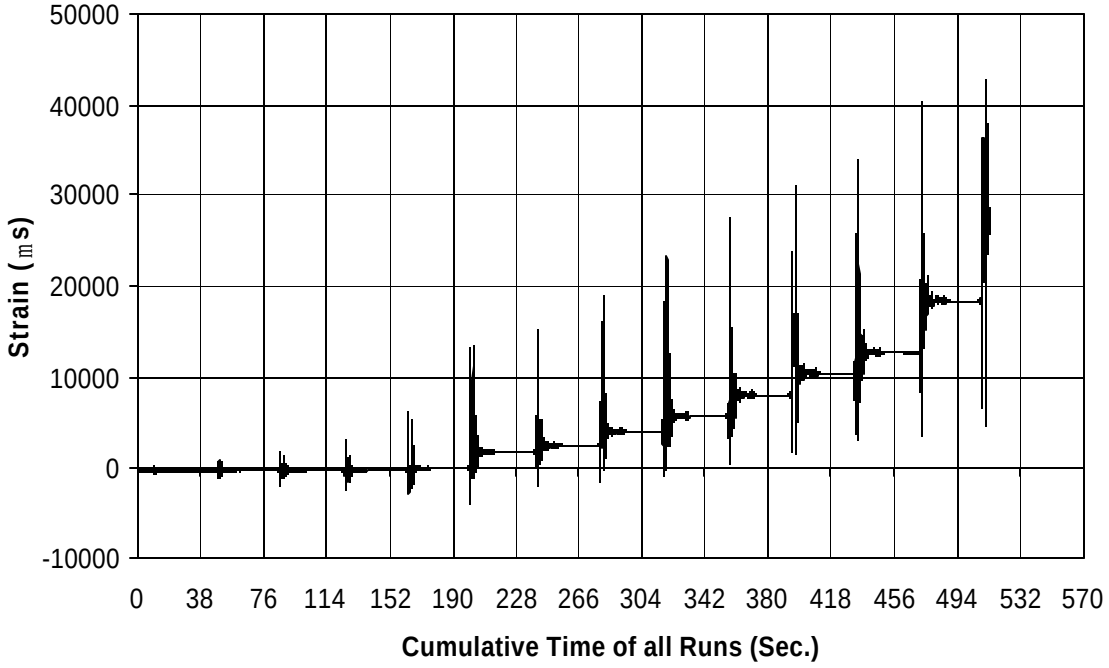

Fig. A-34 THD -1 Measured Strain in Gauge SG8B5

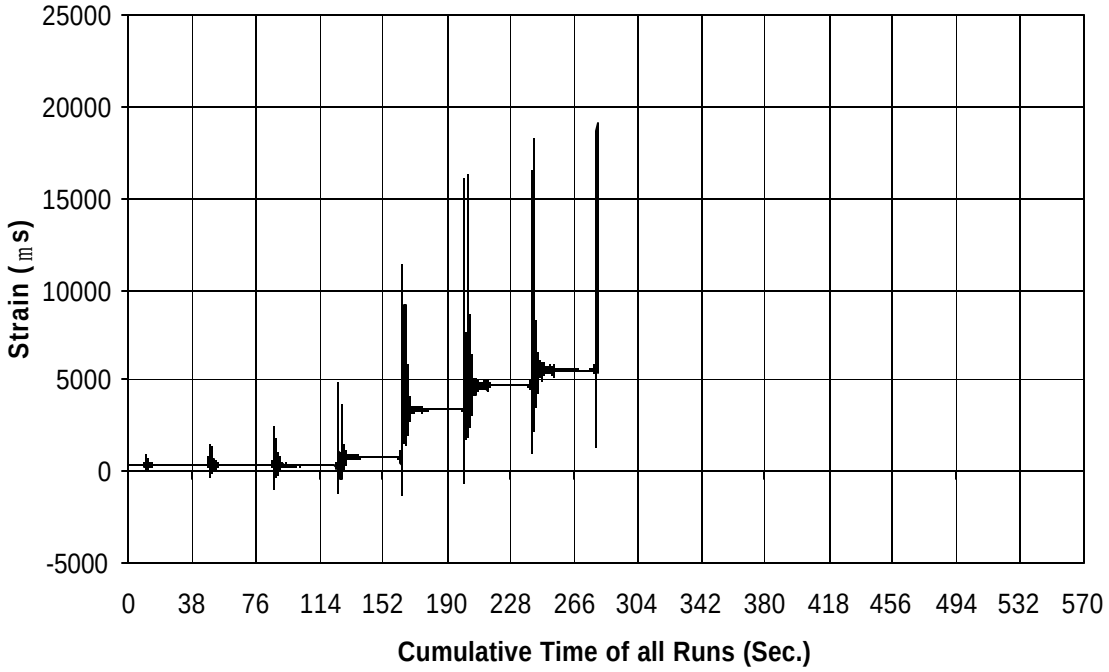

Fig. A-35 THD -1 Measured Strain in Gauge SG1B6

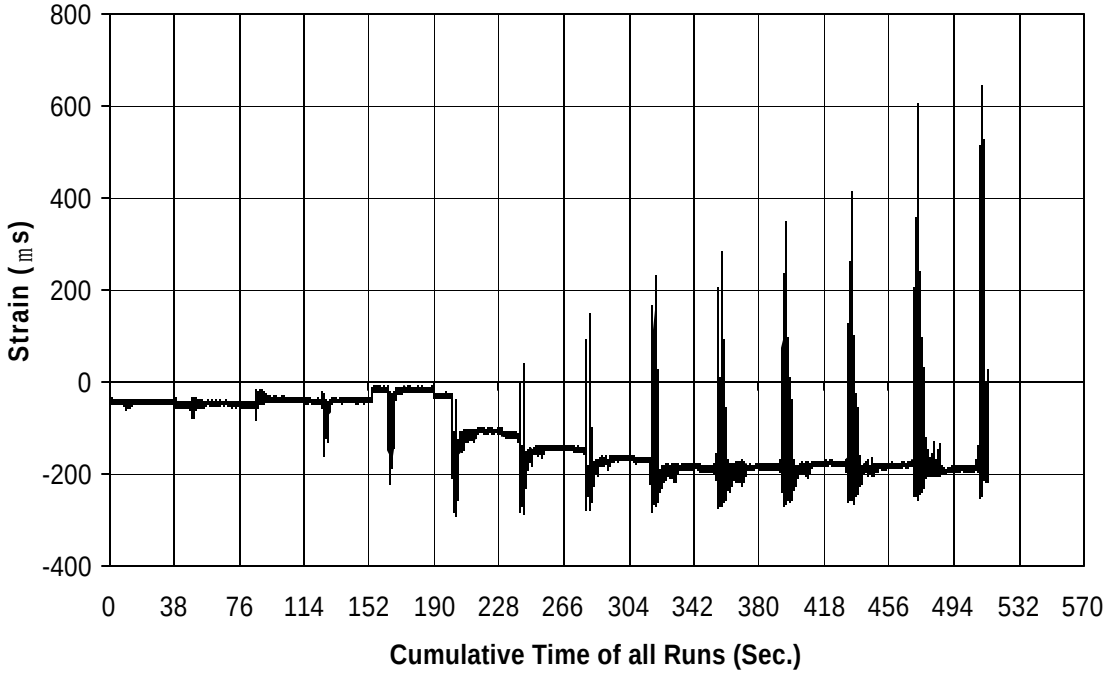

Fig. A-36 THD -1 Measured Strain in Gauge SG2B6

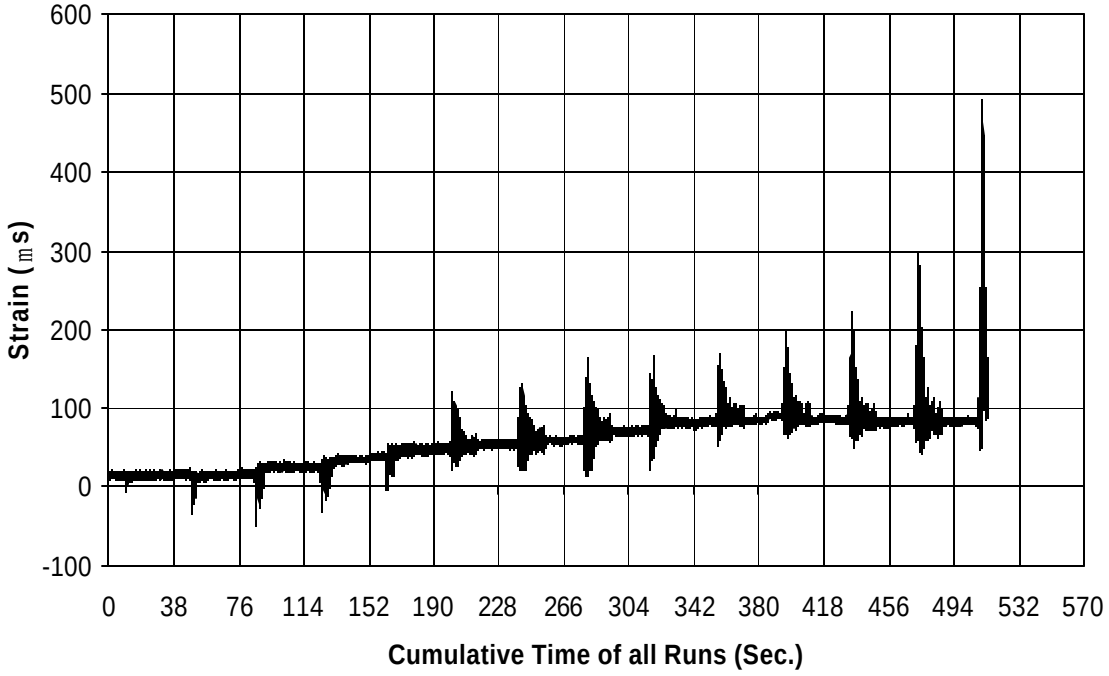

Fig. A-37 THD -1 Measured Strain in Gauge SG3B6

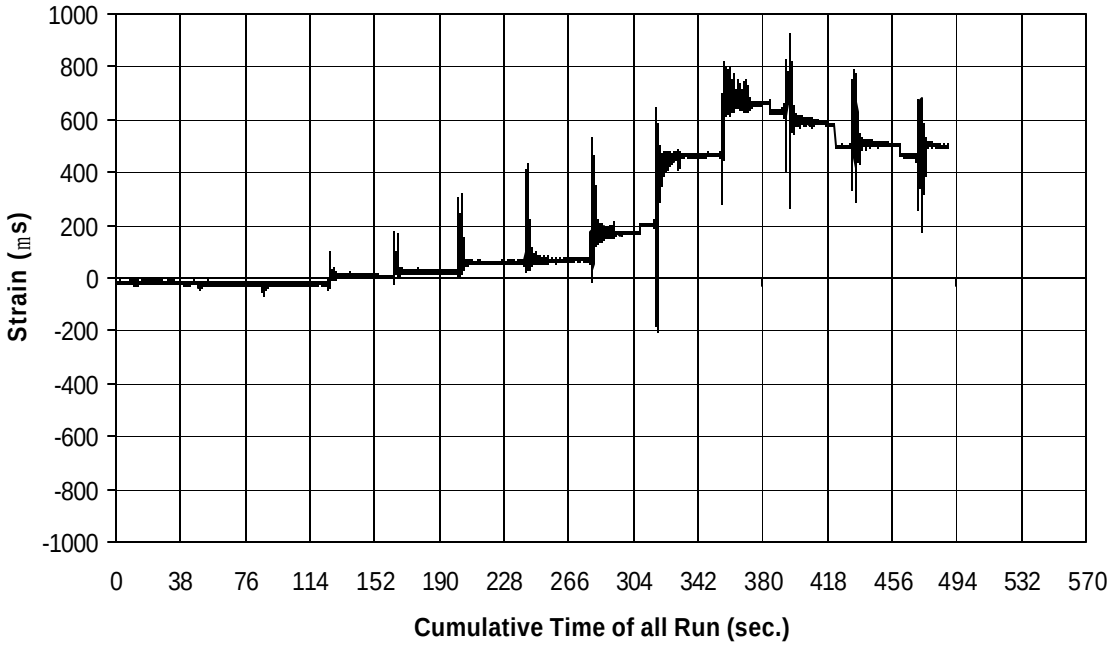

Fig. A-38 THD -1 Measured Strain in Gauge SG8B7

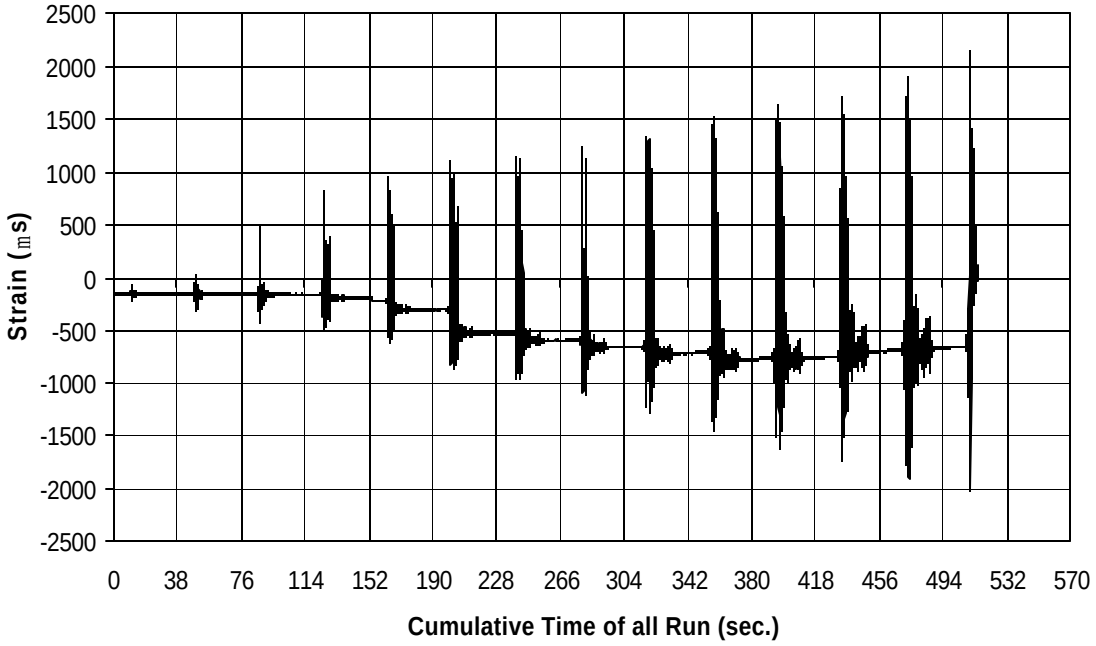

Fig. A-39 THD -1 Measured Strain in Gauge SG1B8

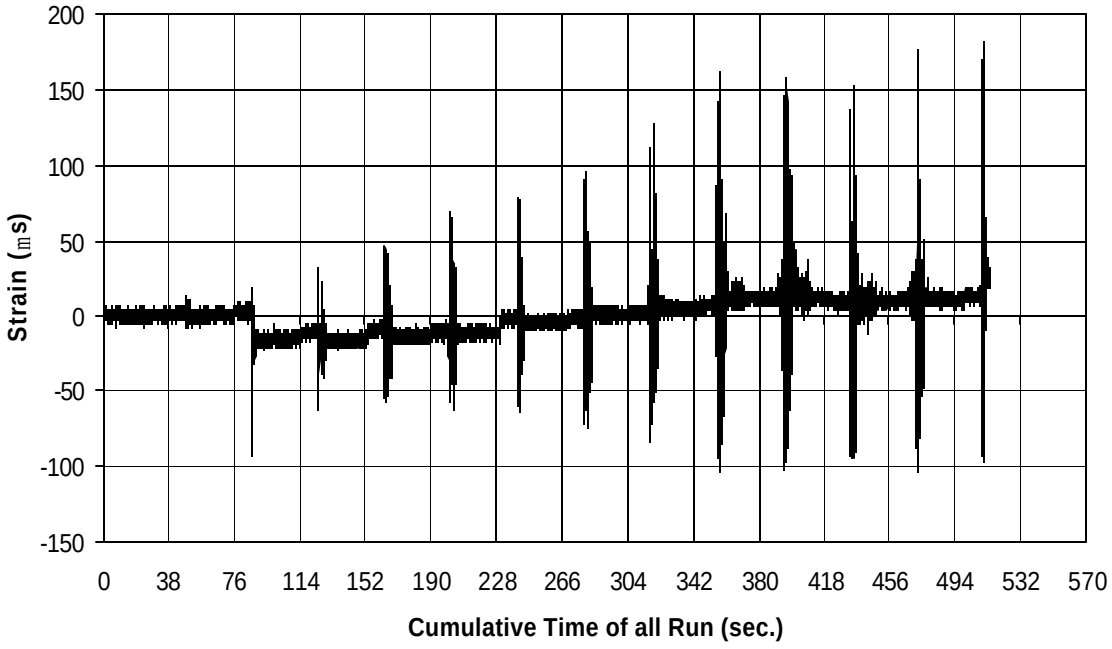

Fig. A-40 THD -1 Measured Strain in Gauge SG2B8

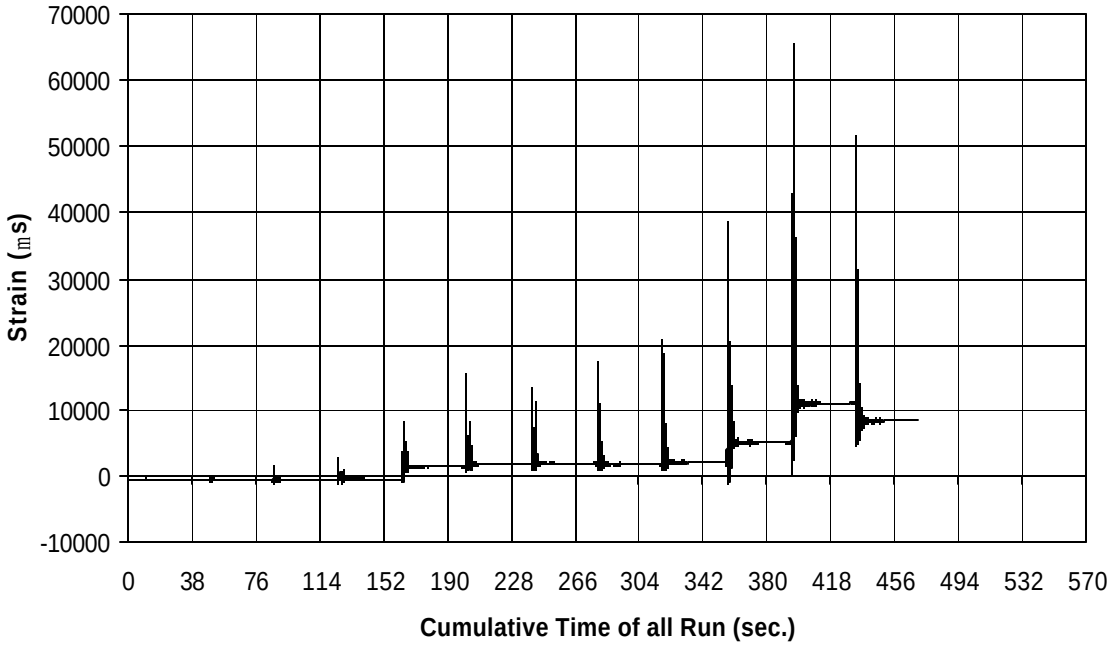

Fig. A-41 THD -1 Measured Strain in Gauge SG3B8

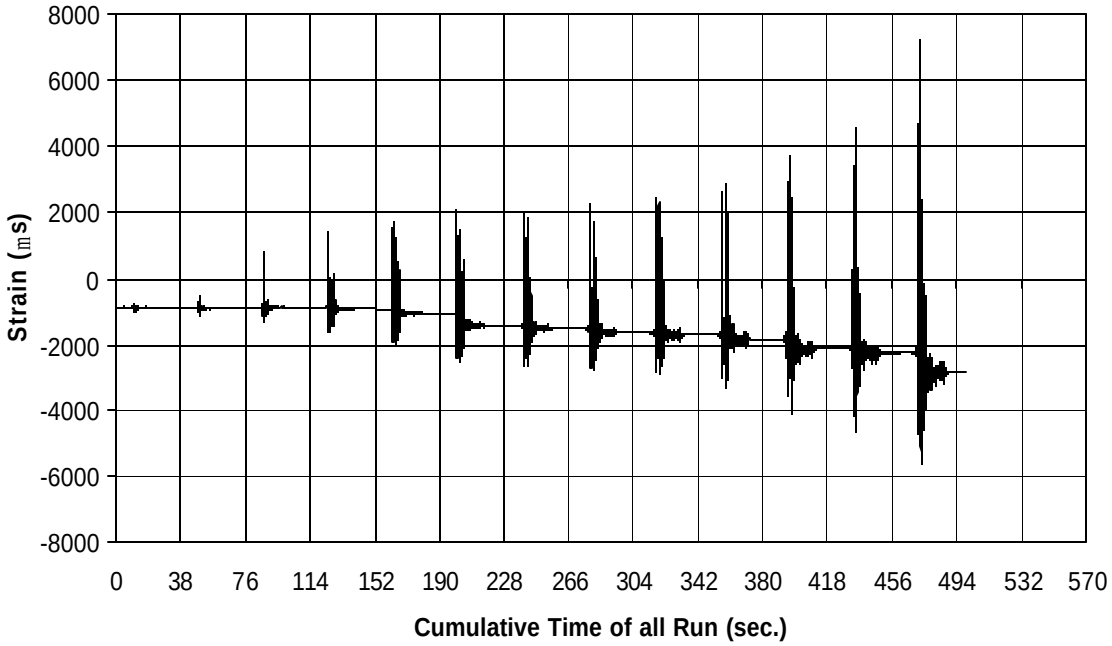

Fig. A-42 THD -1 Measured Strain in Gauge SG4B8

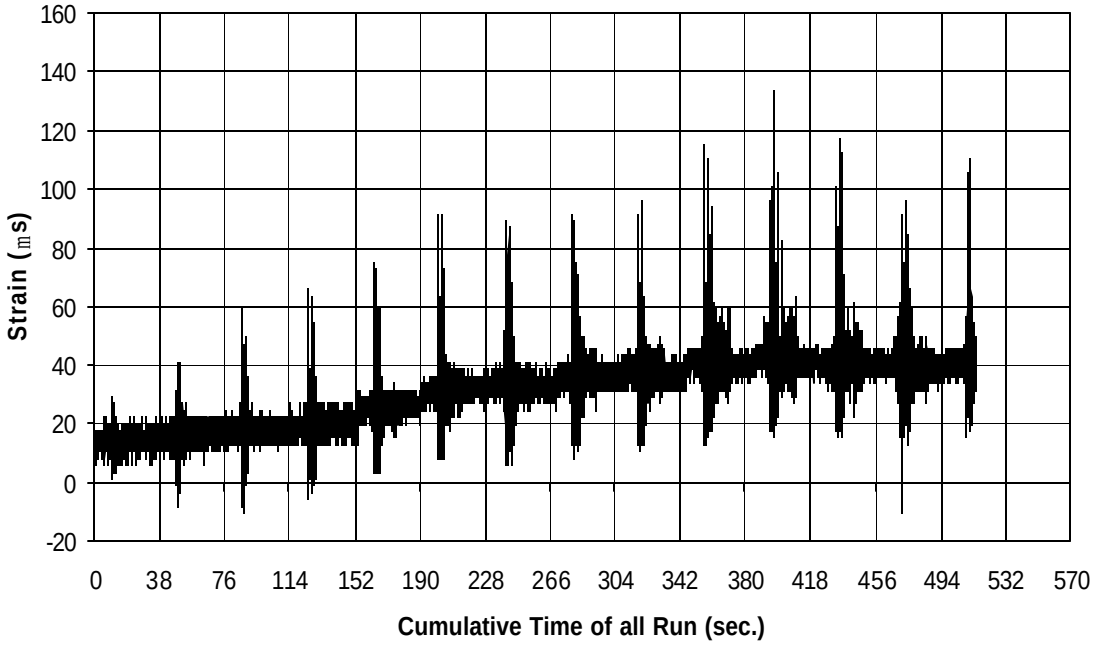

Fig. A-43 THD -1 Measured Strain in Gauge SG5B8

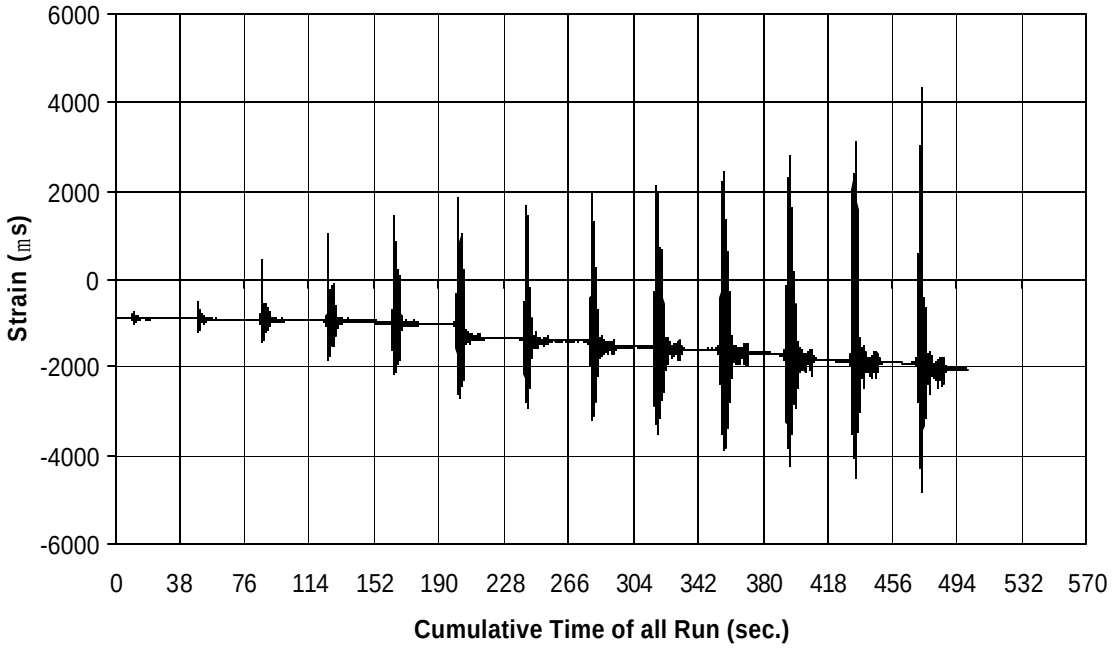

Fig. A-44 THD -1 Measured Strain in Gauge SG6B8

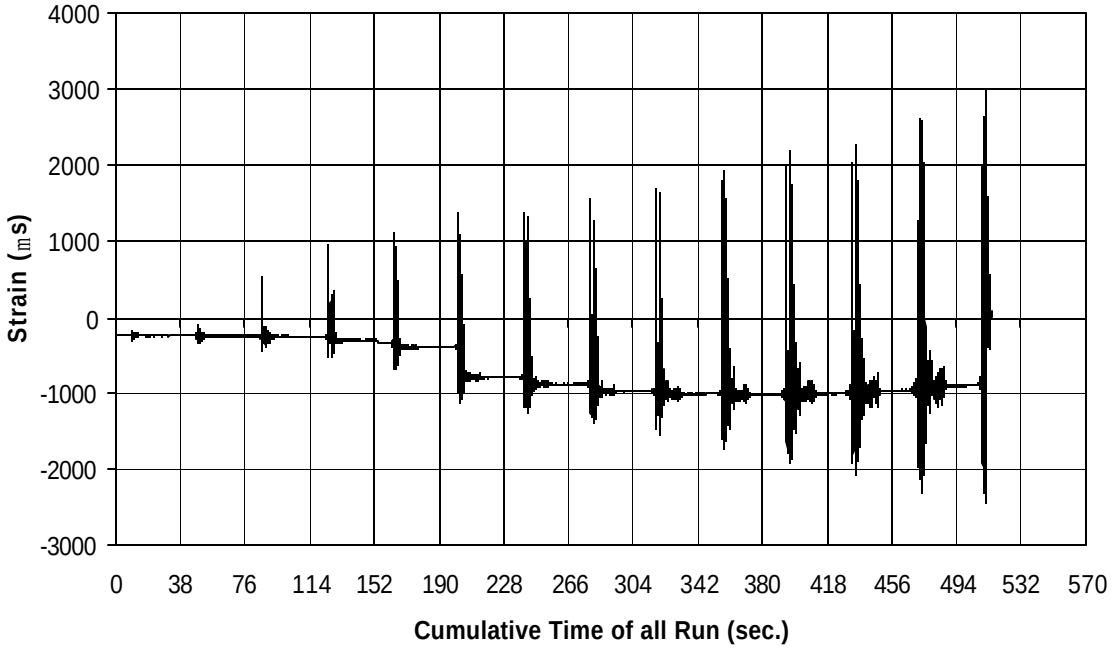

Fig. A-45 THD -1 Measured Strain in Gauge SG7B8

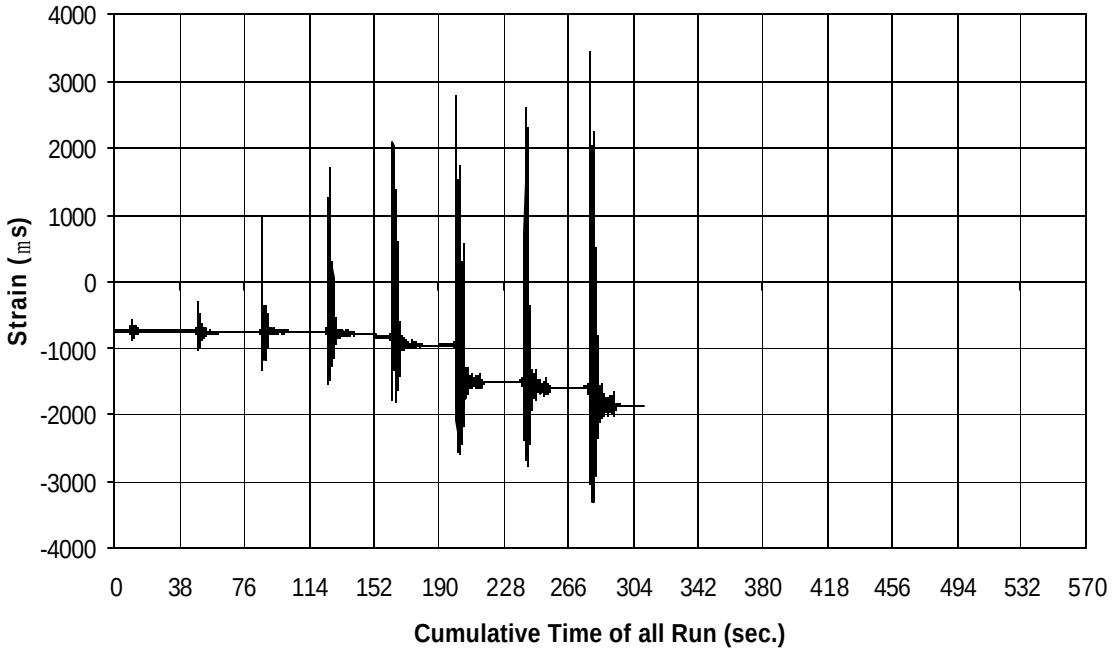

Fig. A-46 THD -1 Measured Strain in Gauge SG2B9

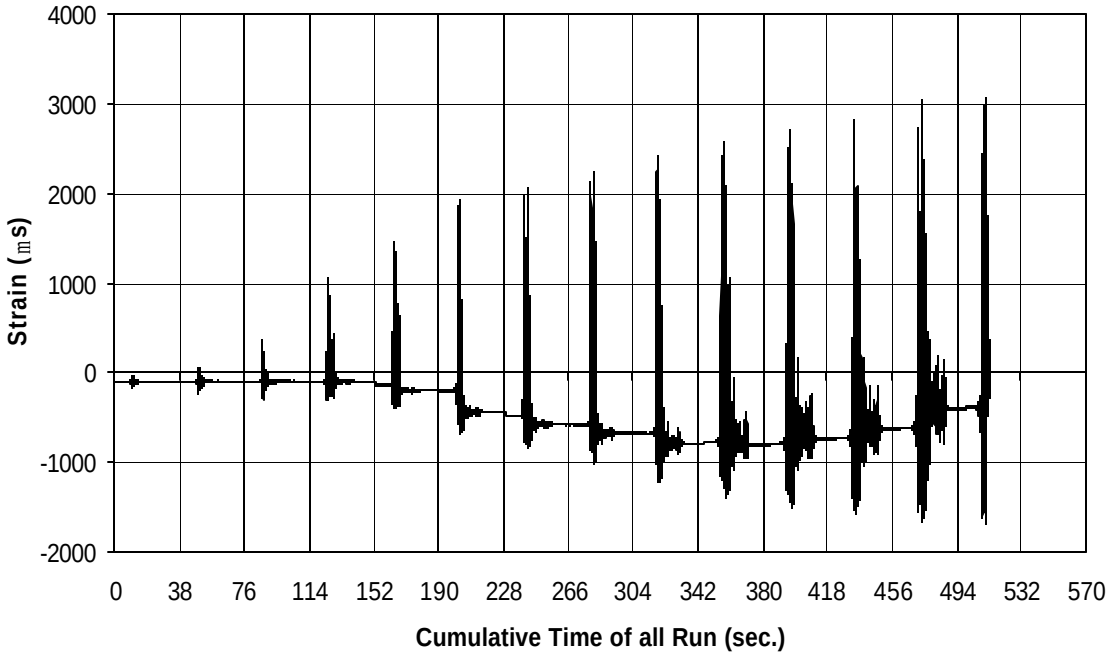

Fig. A-47 THD -1 Measured Strain in Gauge SG3B9

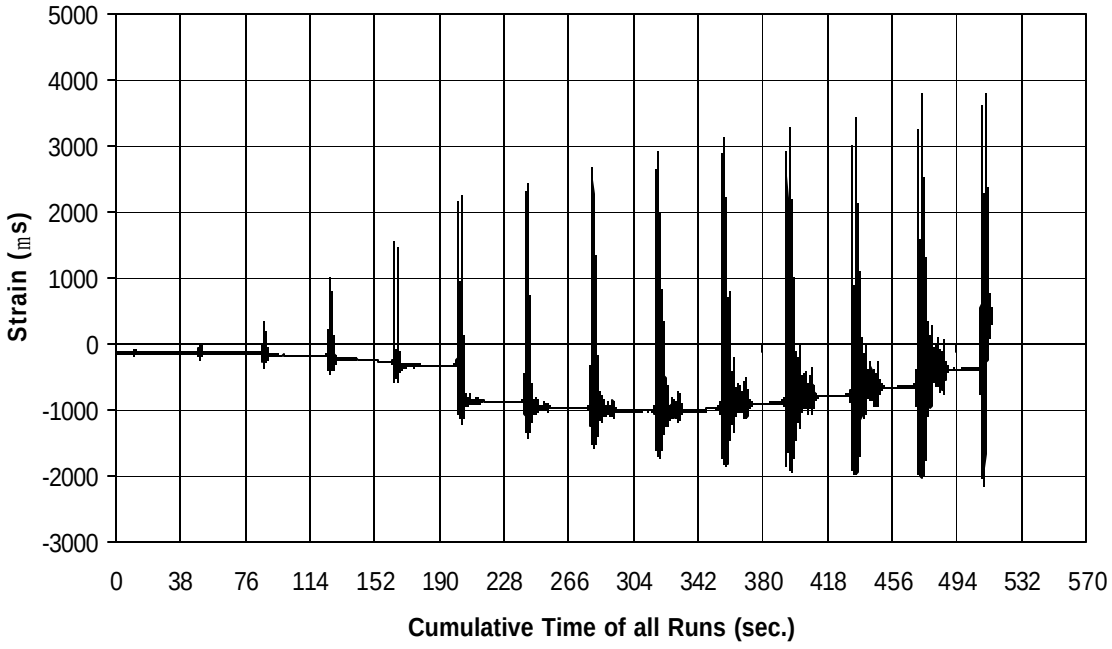

Fig. A-48 THD -1 Measured Strain in Gauge SG5B9

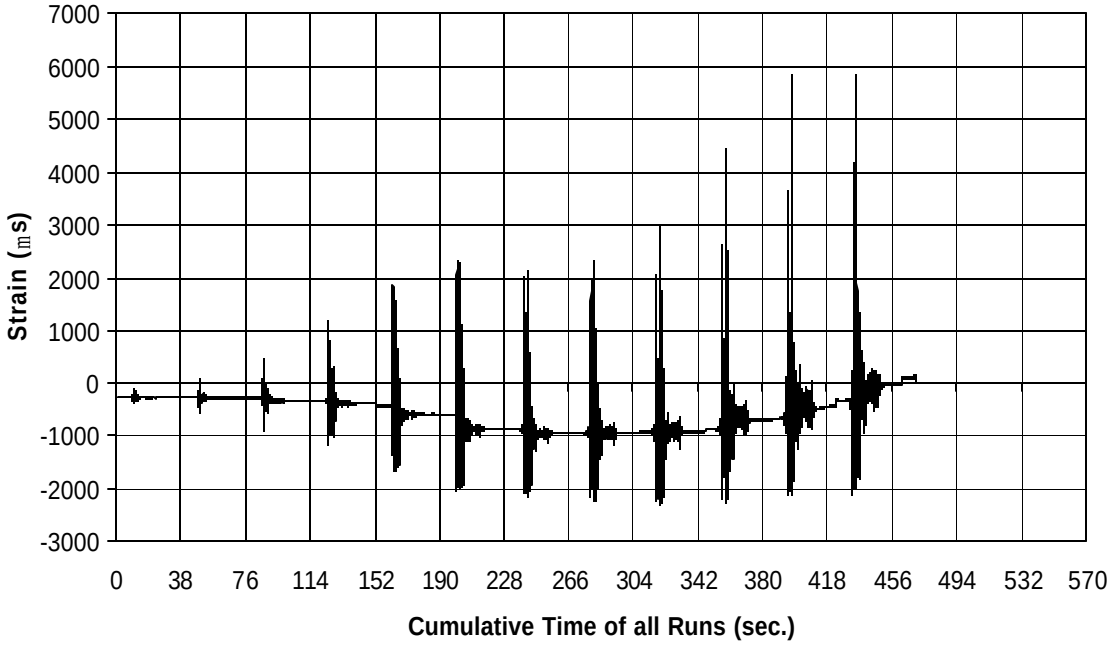

Fig. A-49 THD -1 Measured Strain in Gauge SG6B9

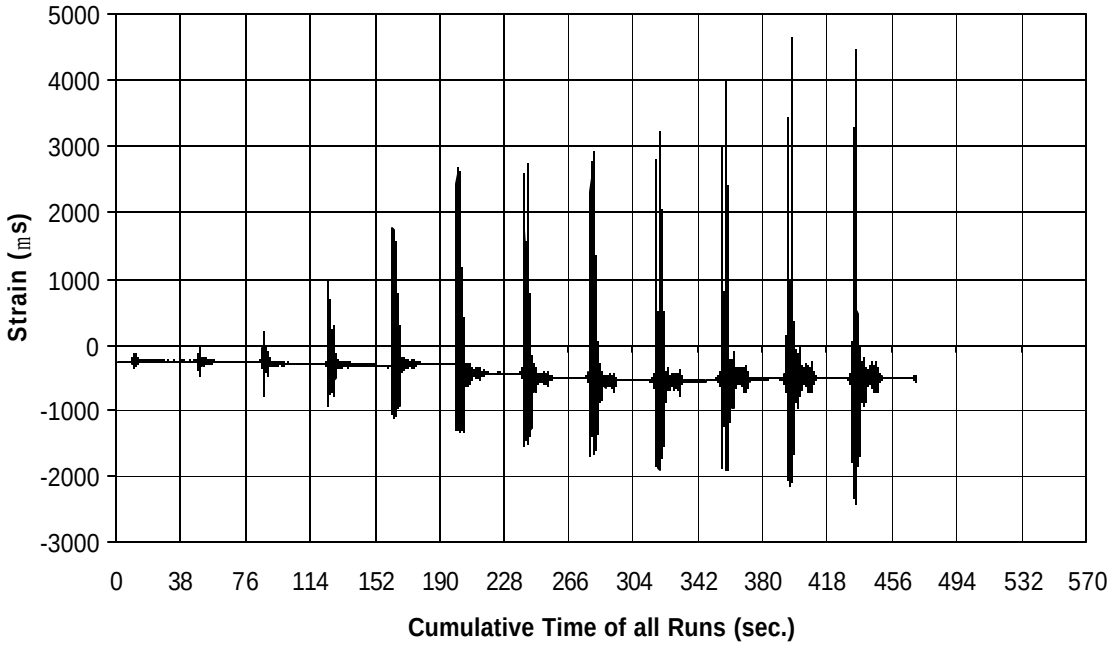

Fig. A-50 THD-1 Measured Strain in Gauge SG7B9

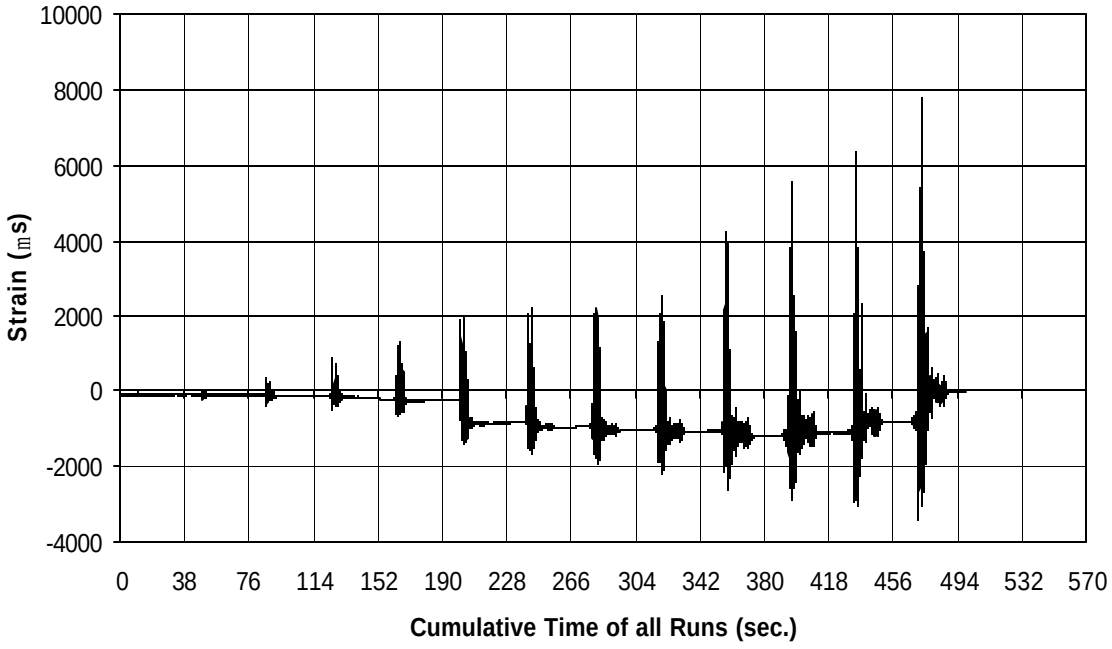

Fig. A-51 THD-1 Measured Strain in Gauge SG8B9

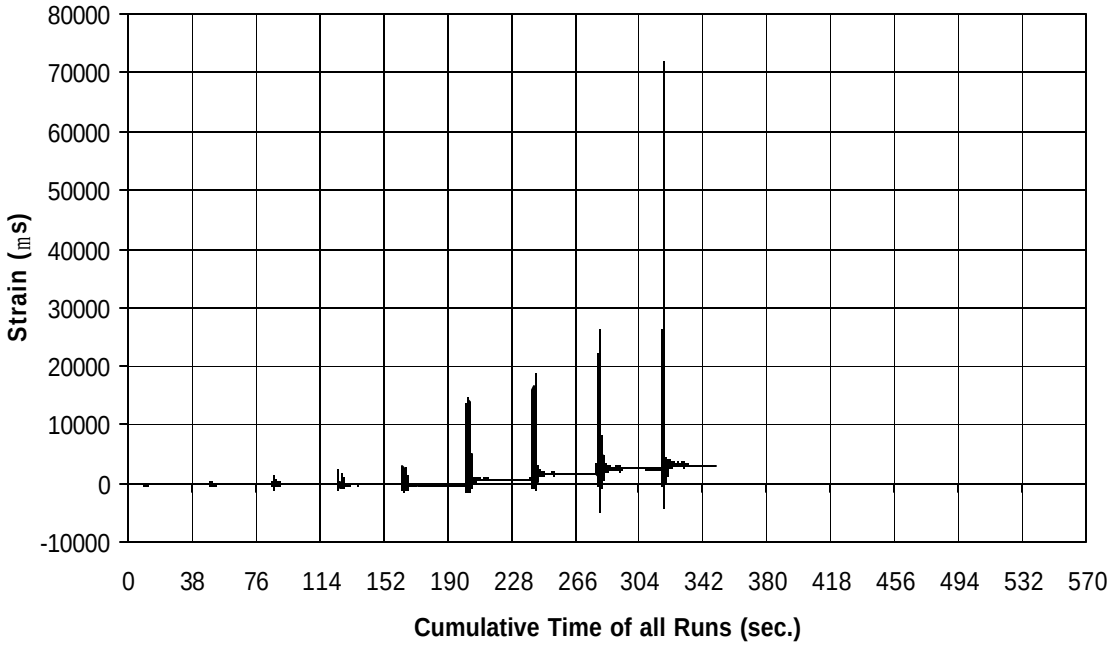

Fig. A-52 THD-1 Measured Strain in Gauge SG1B11

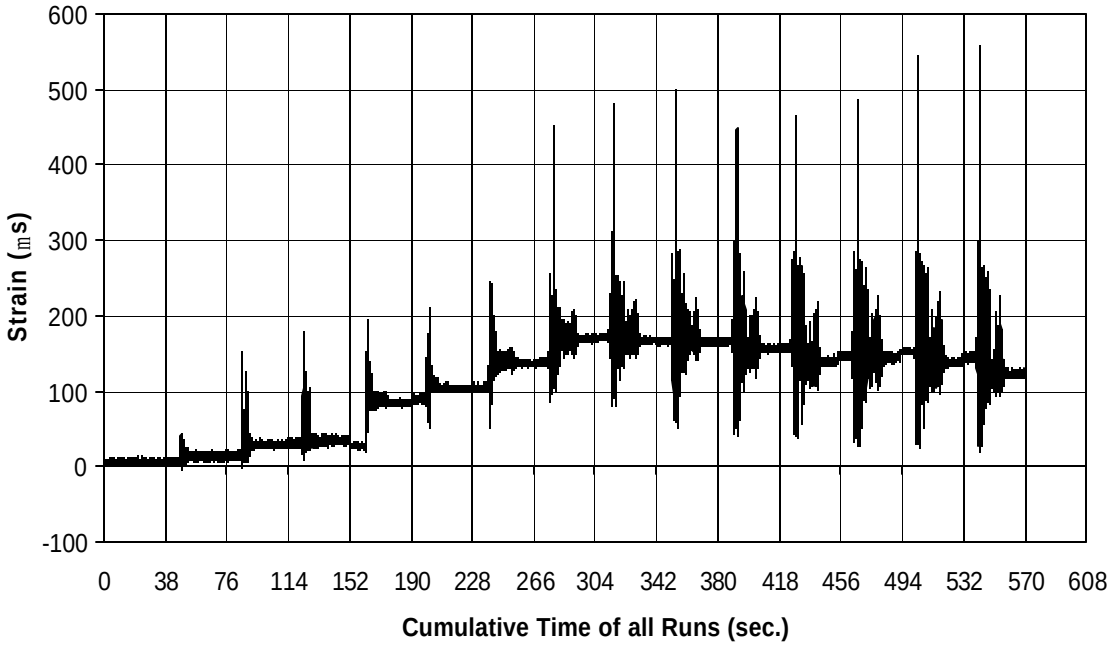

Fig. A-53 THD -2 Measured Strain in Gauge SG1B1

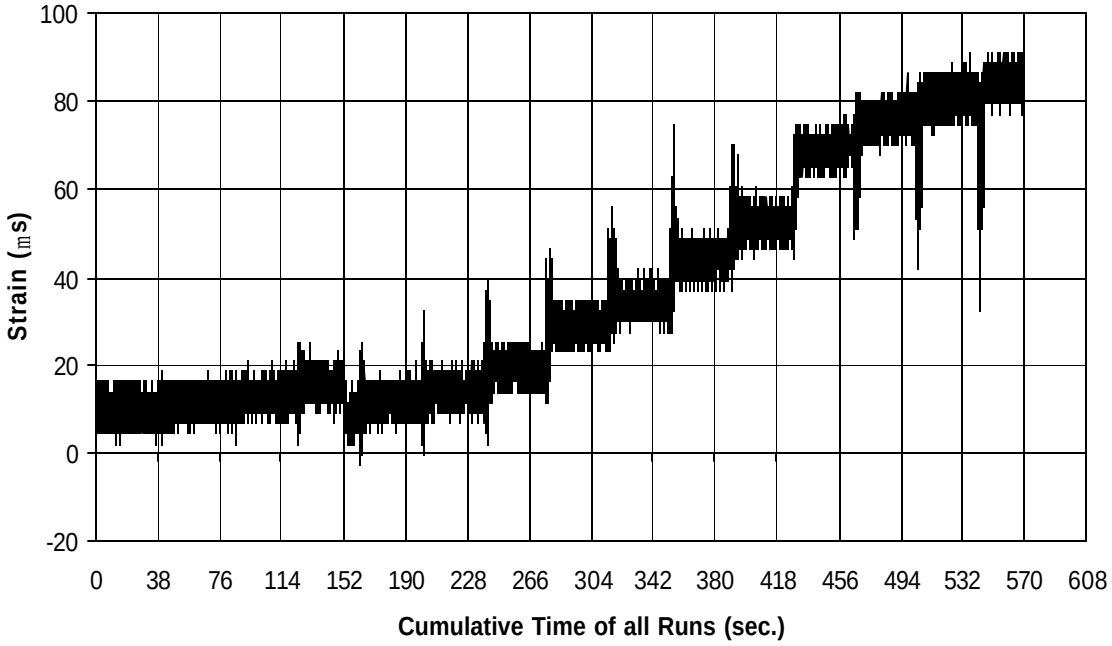

Fig. A-54 THD -2 Measured Strain in Gauge SG2B1

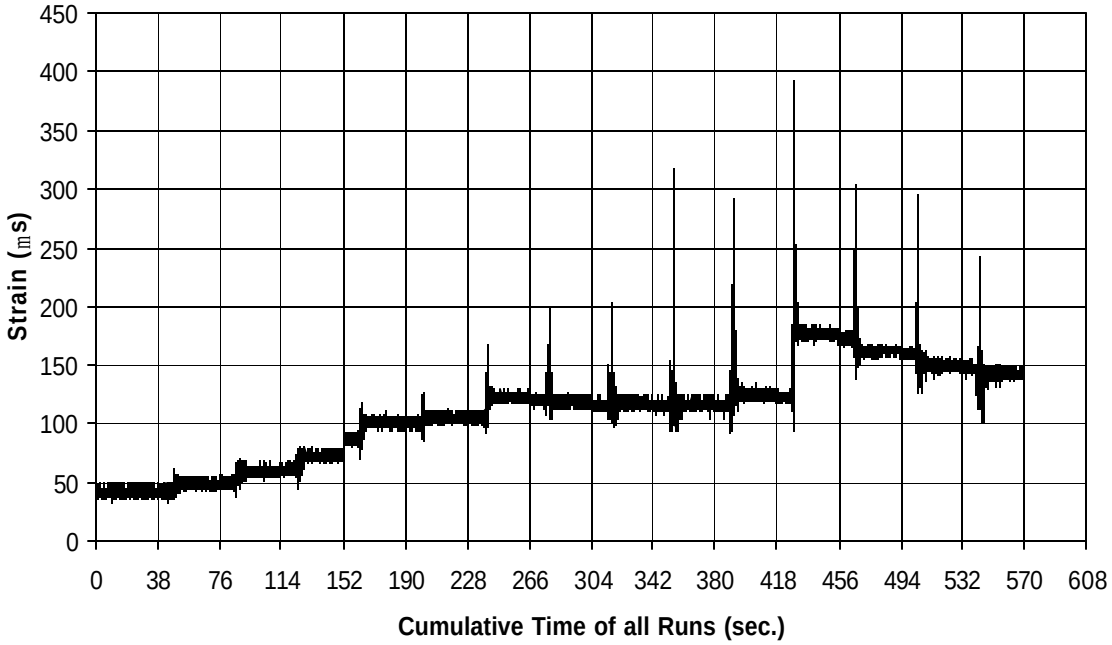

Fig. A-55 THD -2 Measured Strain in Gauge SG3B1

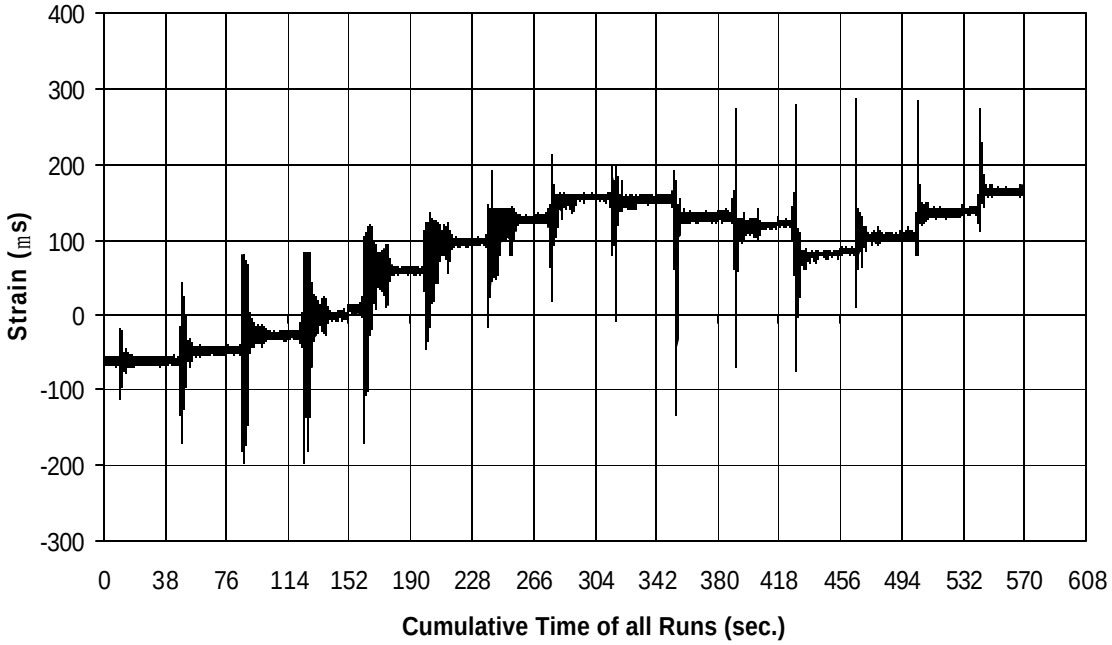

Fig. A-56 THD -2 Measured Strain in Gauge SG4B1

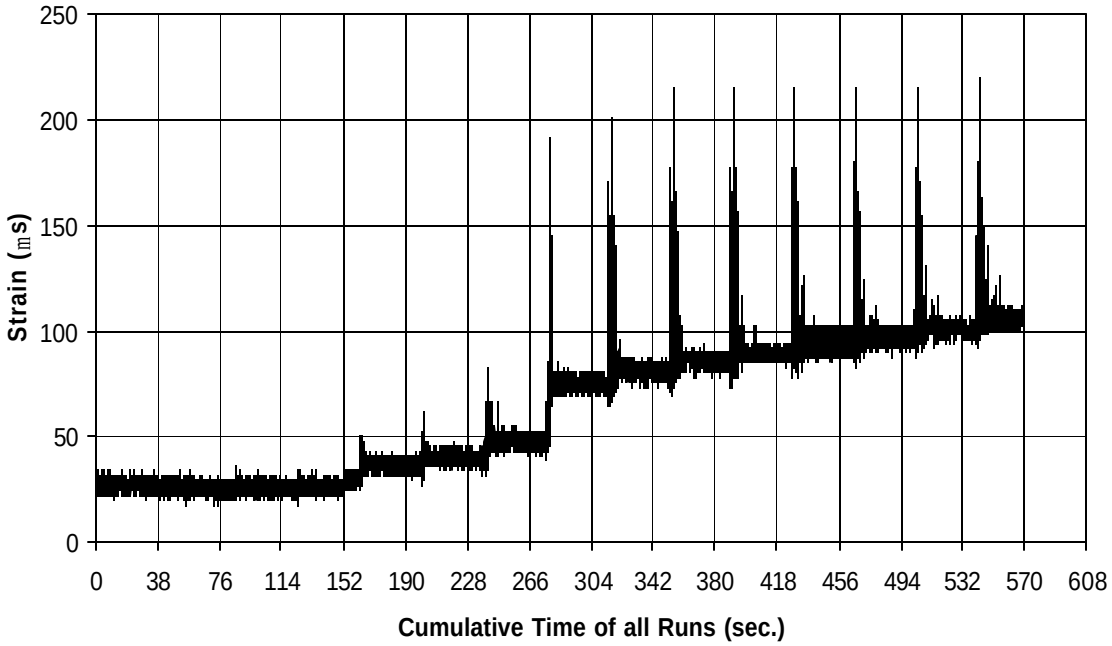

Fig. A-57 THD -2 Measured Strain in Gauge SG6B1

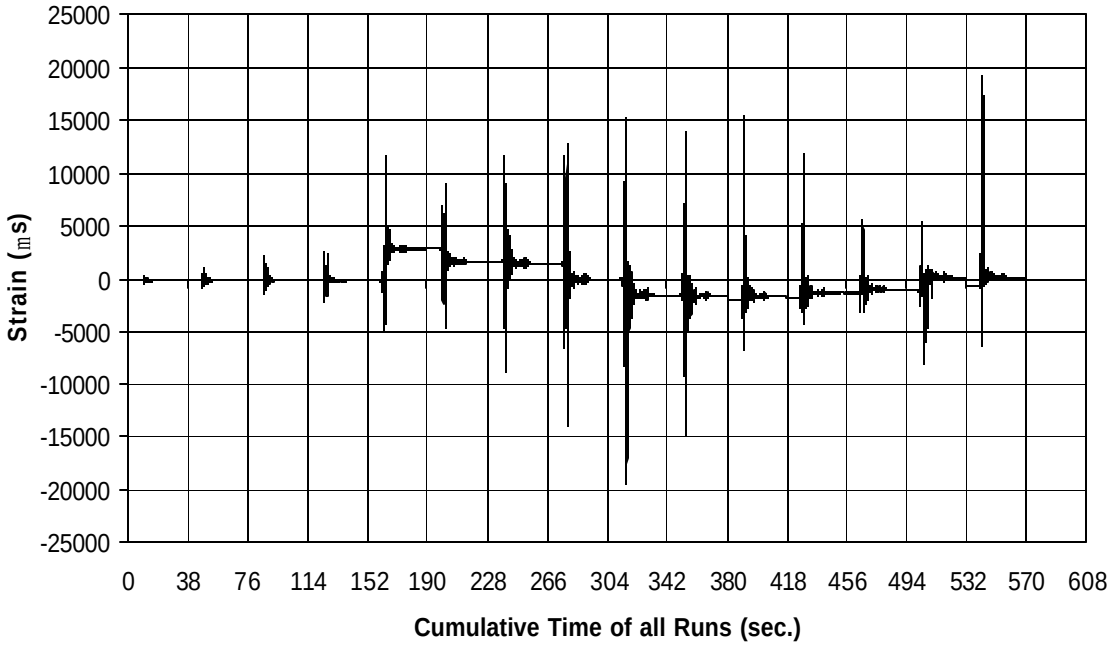

Fig. A-58 THD -2 Measured Strain in Gauge SG7B1

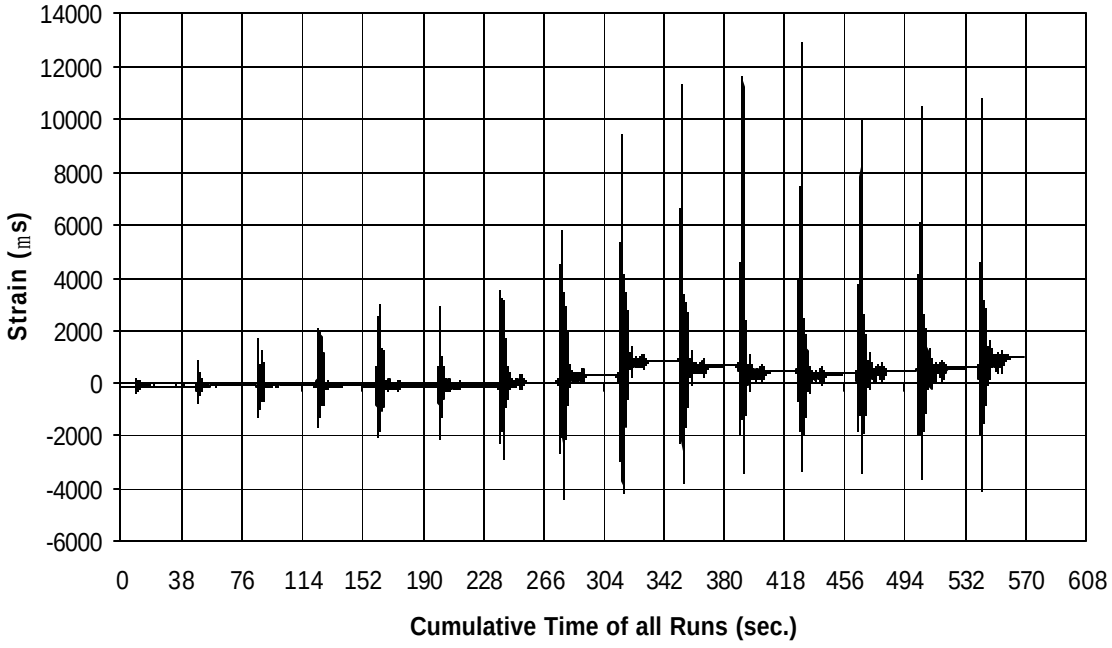

Fig. A-59 THD -2 Measured Strain in Gauge SG8B1

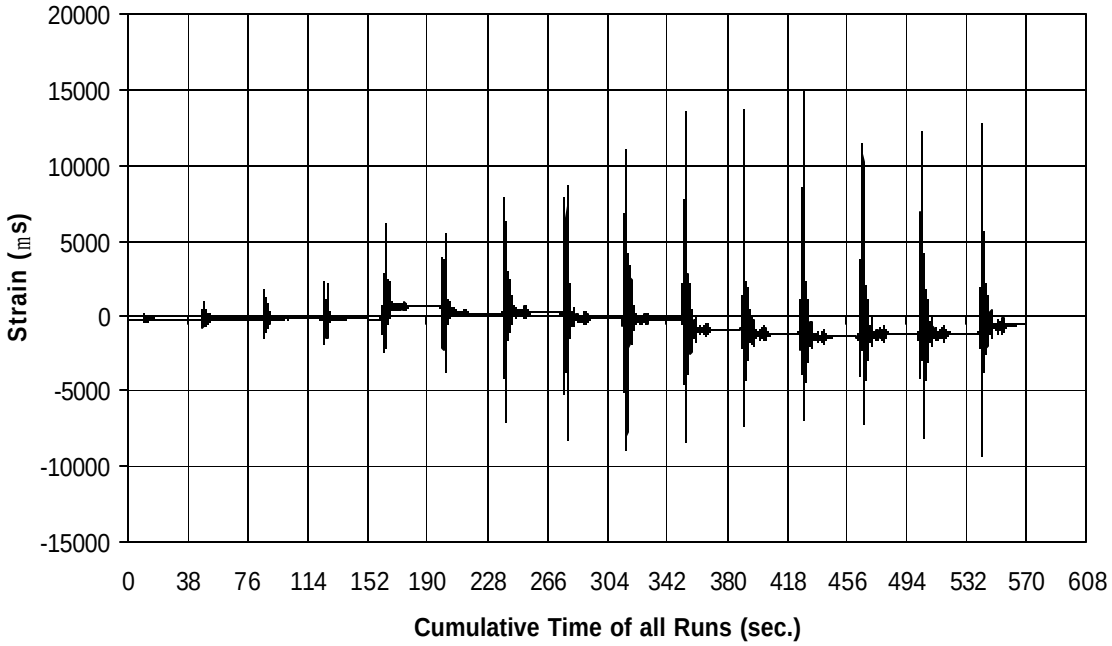

Fig. A-60 THD -2 Measured Strain in Gauge SG2B2

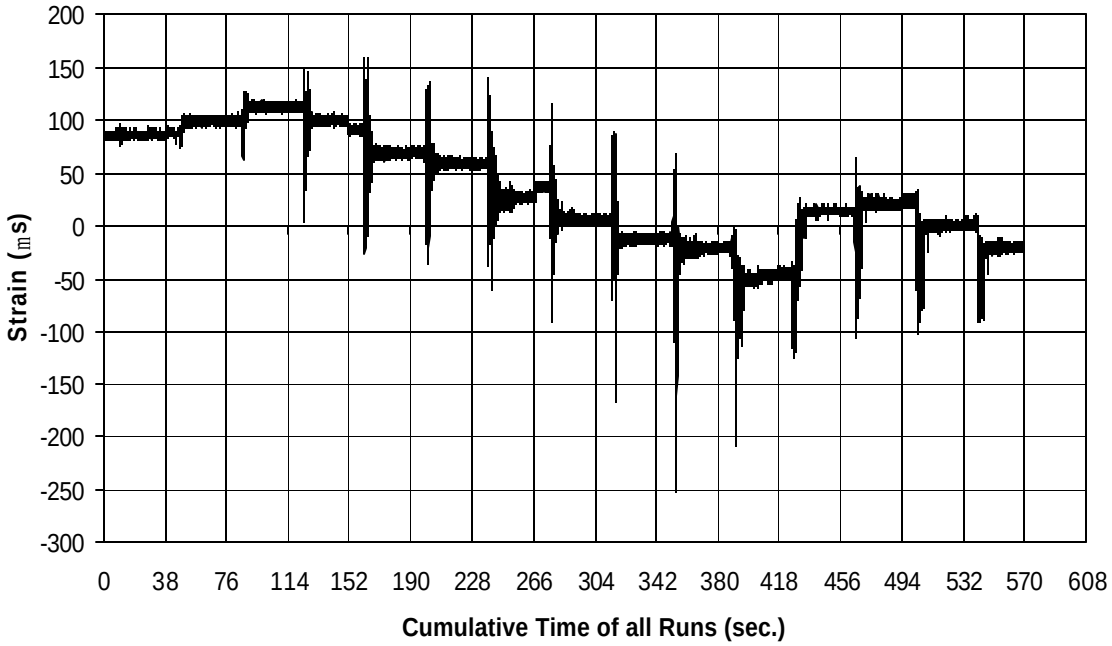

Fig. A-61 THD -2 Measured Strain in Gauge SG3B2

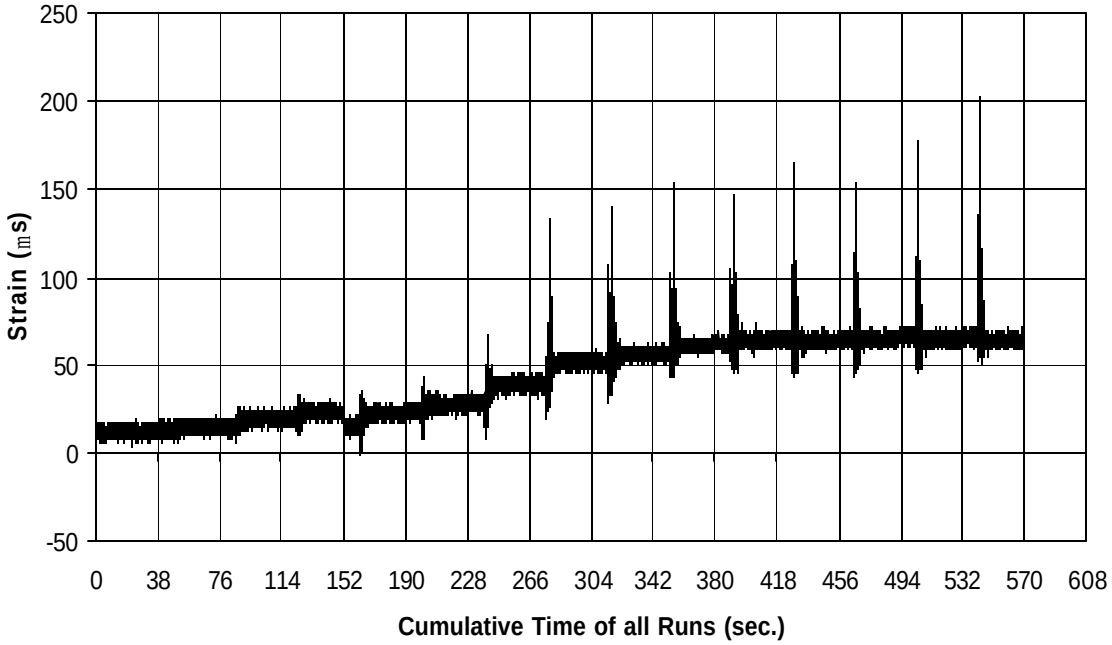

Fig. A-62 THD -2 Measured Strain in Gauge SG4B2

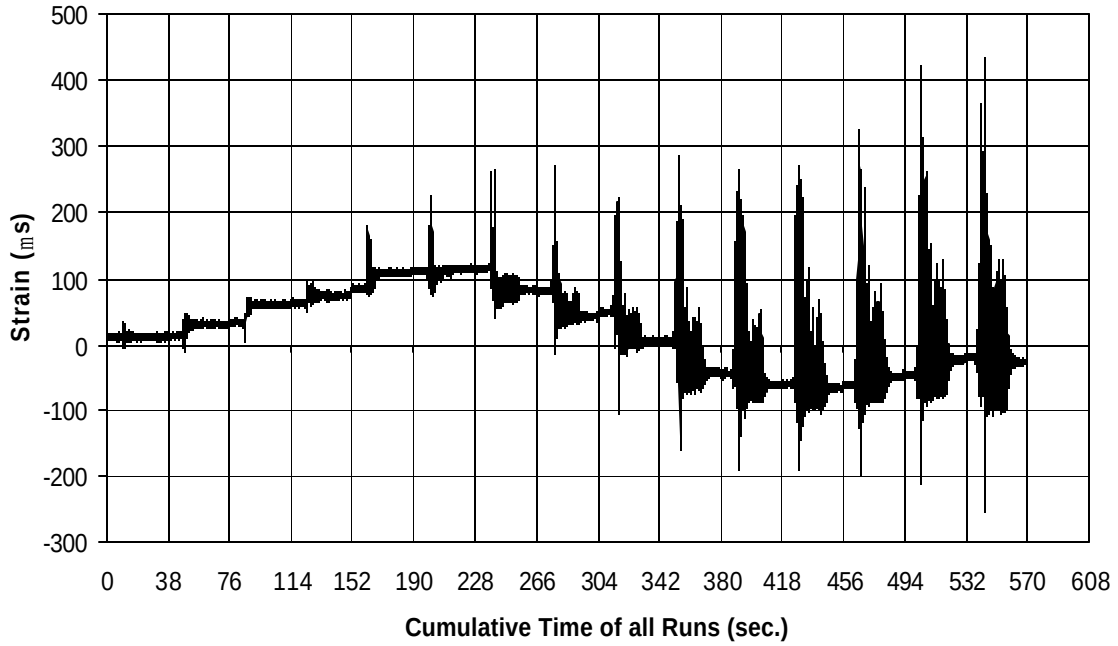

Fig. A-63 THD -2 Measured Strain in Gauge SG5B2

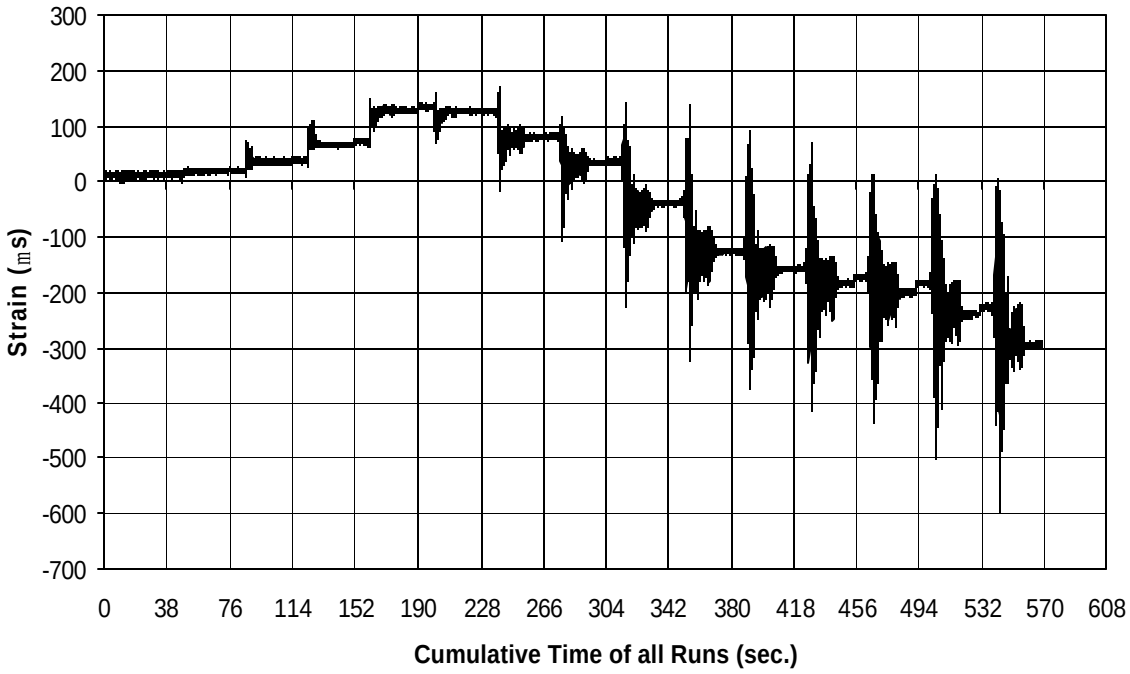

Fig. A-64 THD -2 Measured Strain in Gauge SG6B2

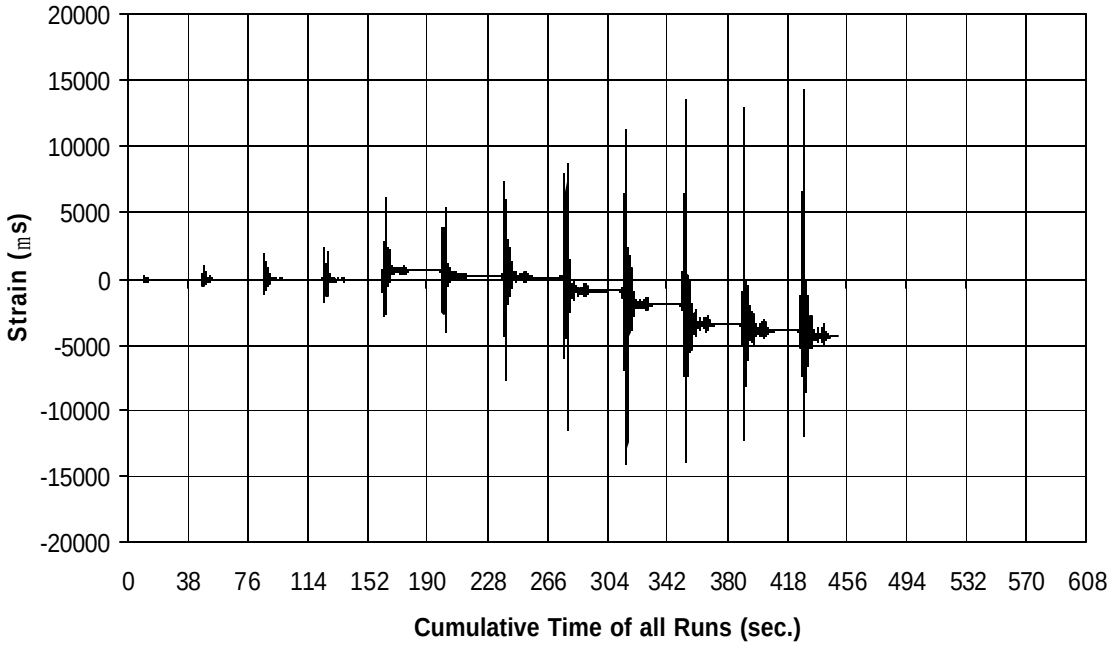

Fig. A-65 THD -2 Measured Strain in Gauge SG7B2

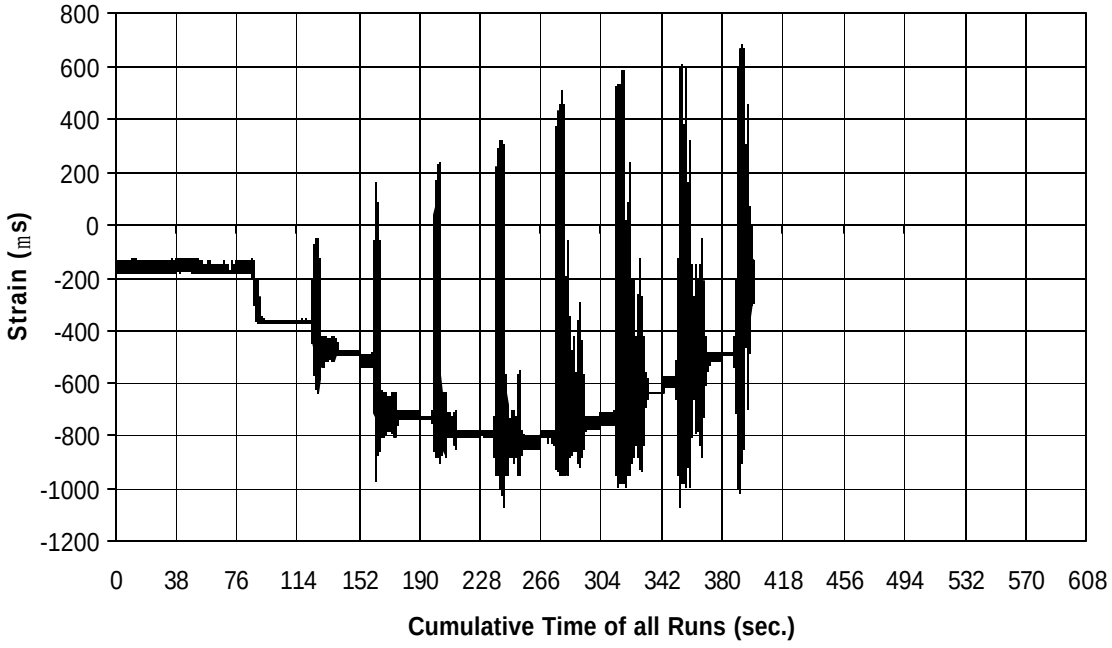

Fig. A-66 THD -2 Measured Strain in Gauge SG1B3

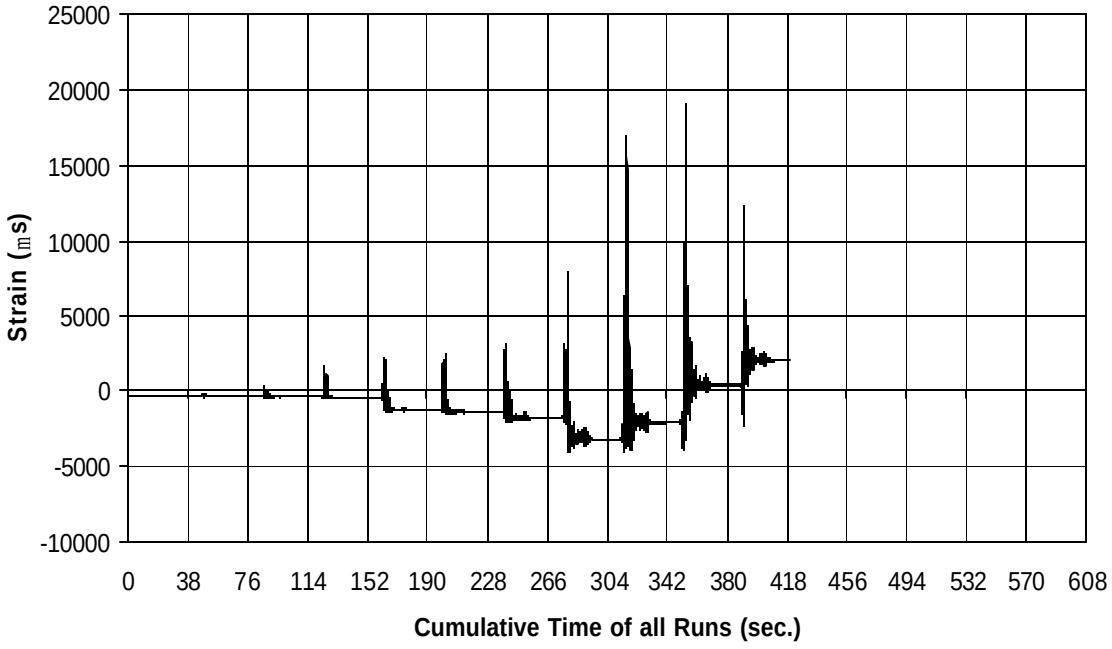

Fig. A-67 THD -2 Measured Strain in Gauge SG2B3

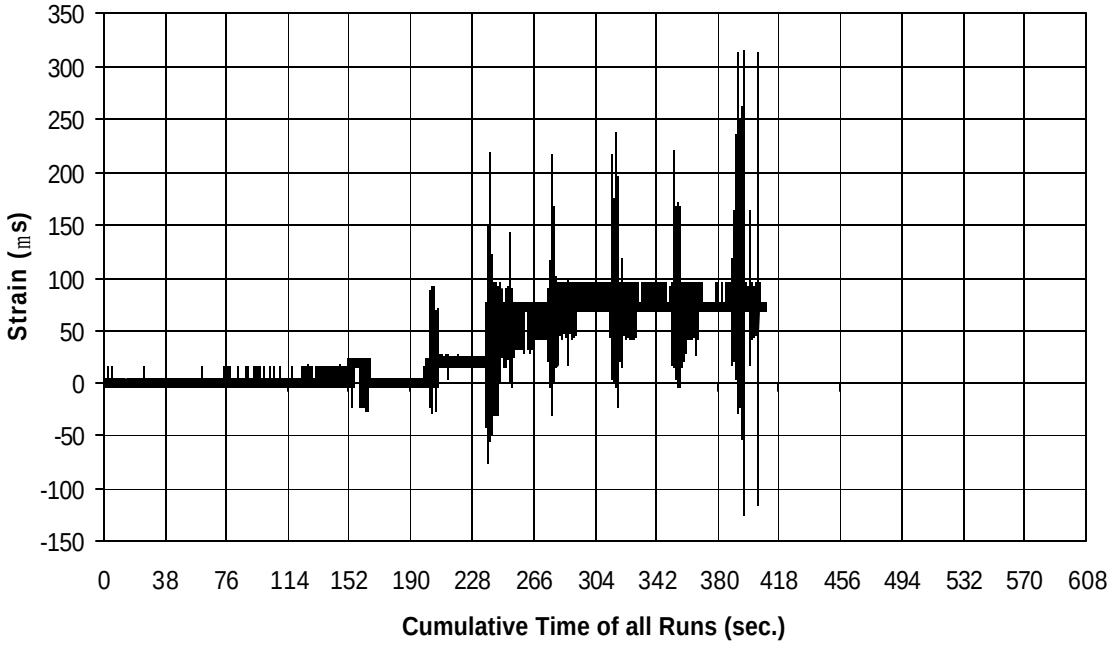

Fig. A-68 THD -2 Measured Strain in Gauge SG3B3

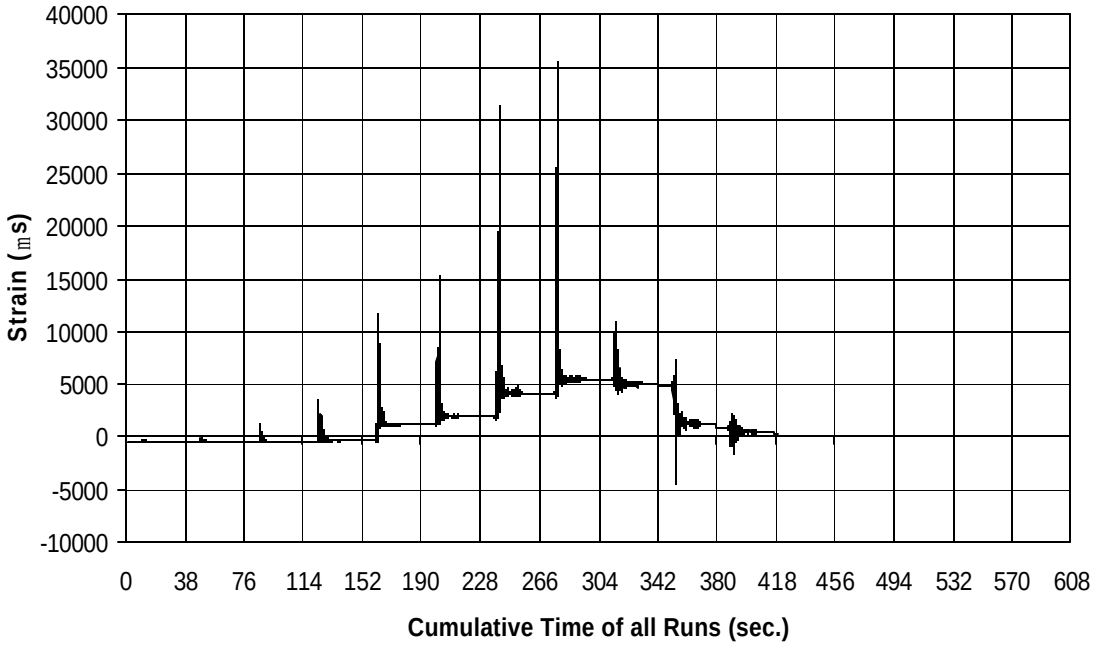

Fig. A-69 THD -2 Measured Strain in Gauge SG4B3

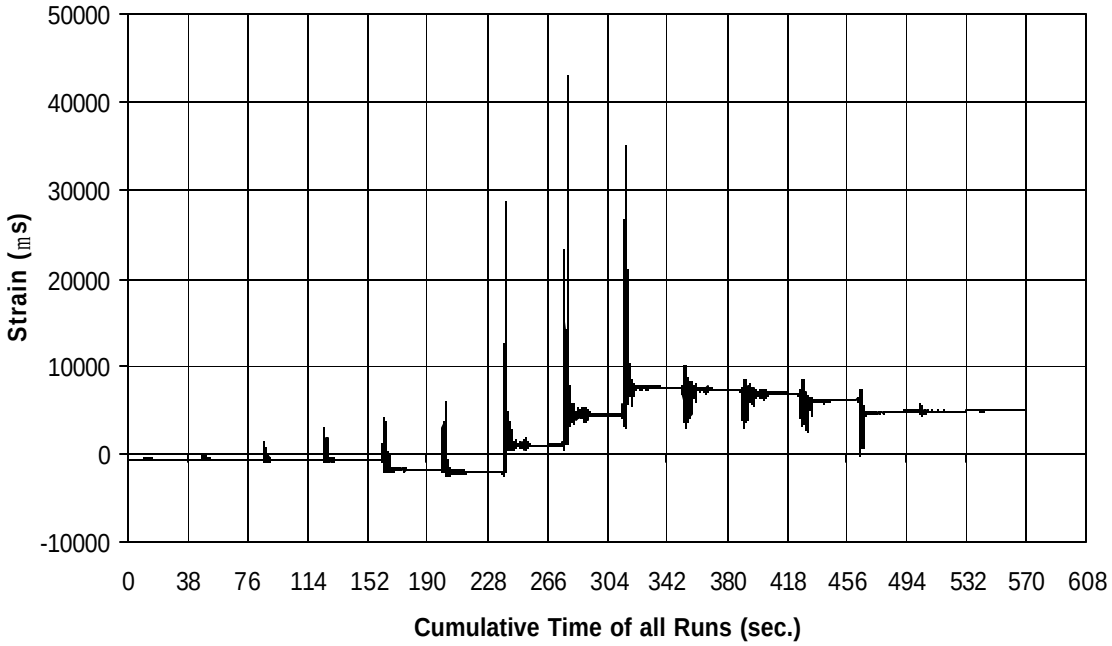

Fig. A-70 THD -2 Measured Strain in Gauge SG5B3

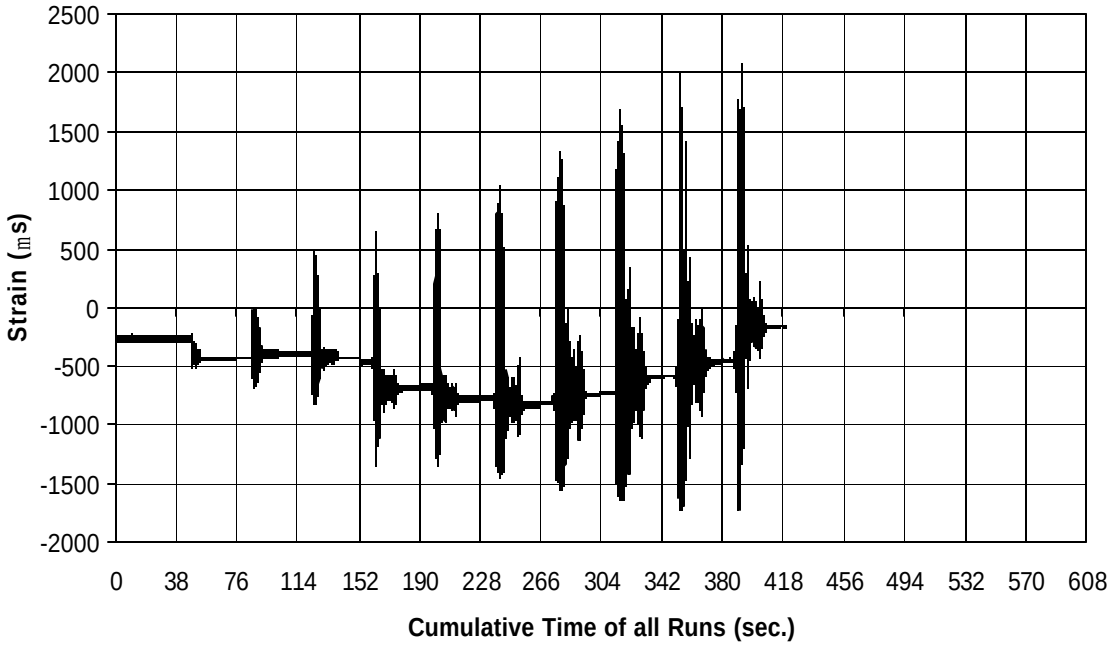

Fig. A-71 THD -2 Measured Strain in Gauge SG6B3

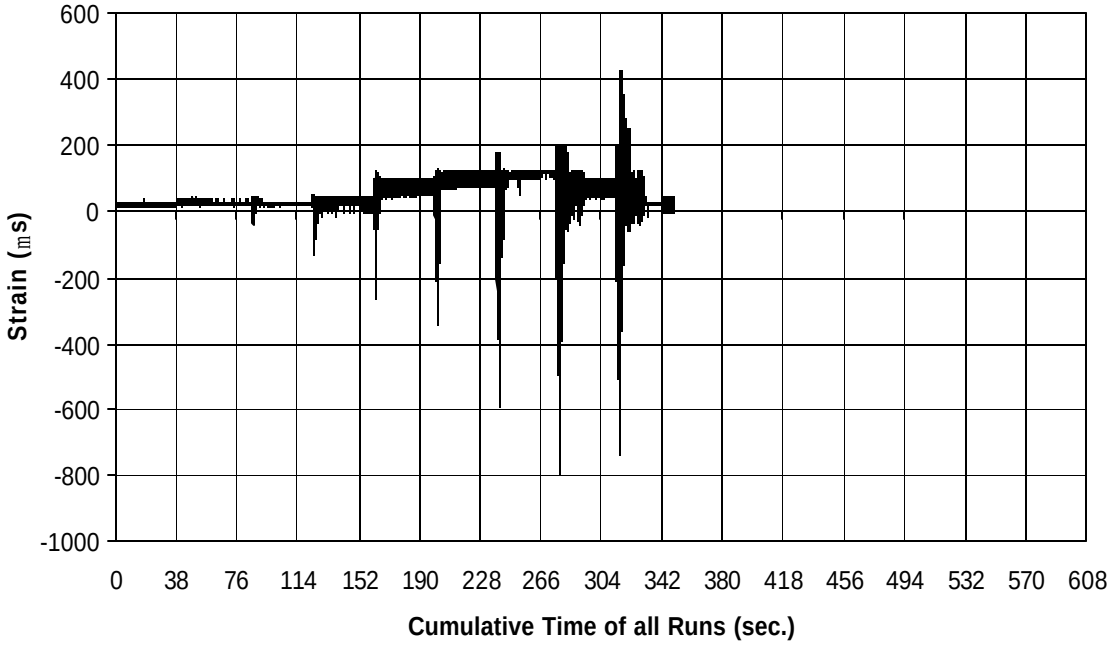

Fig. A-72 THD -2 Measured Strain in Gauge SG7B3

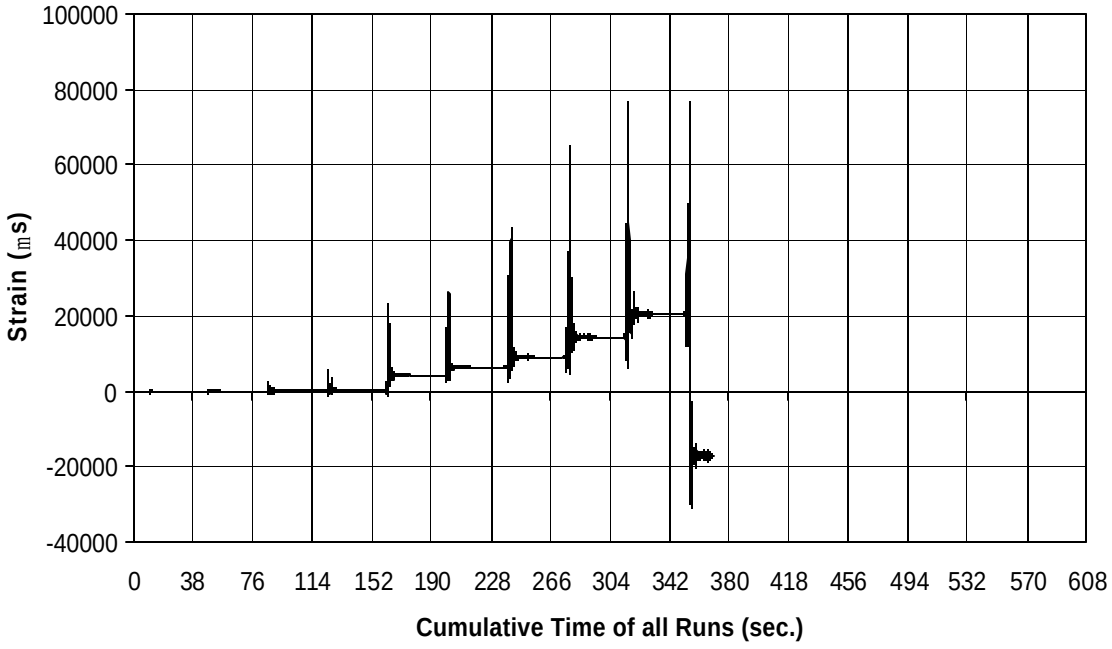

Fig. A-73 THD -2 Measured Strain in Gauge SG8B3

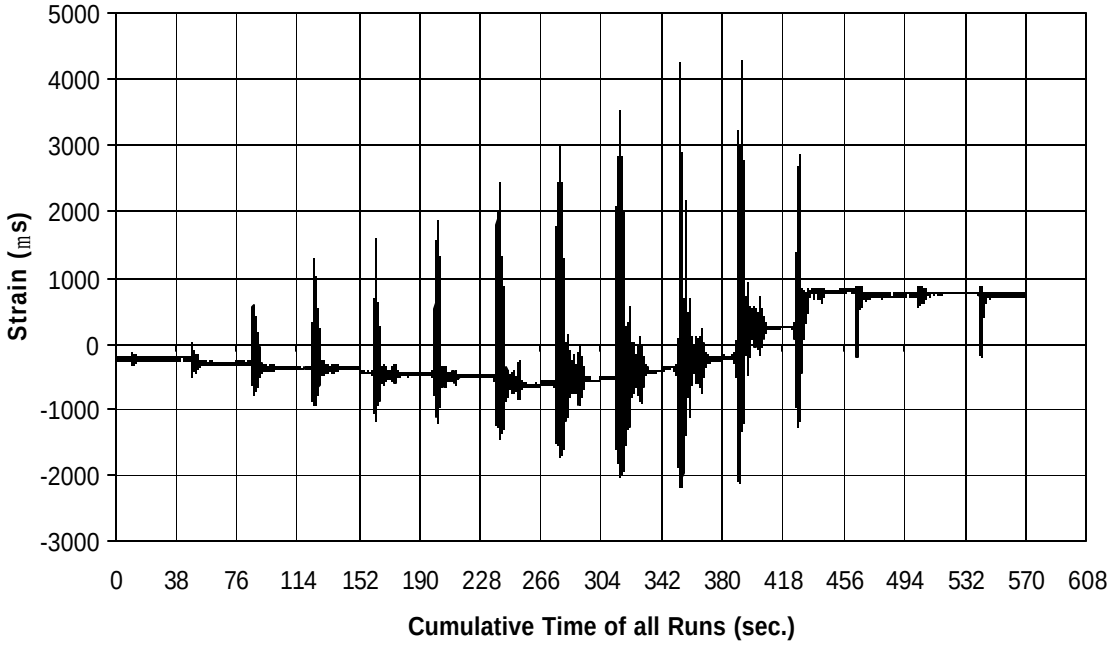

Fig. A-74 THD -2 Measured Strain in Gauge SG1B4

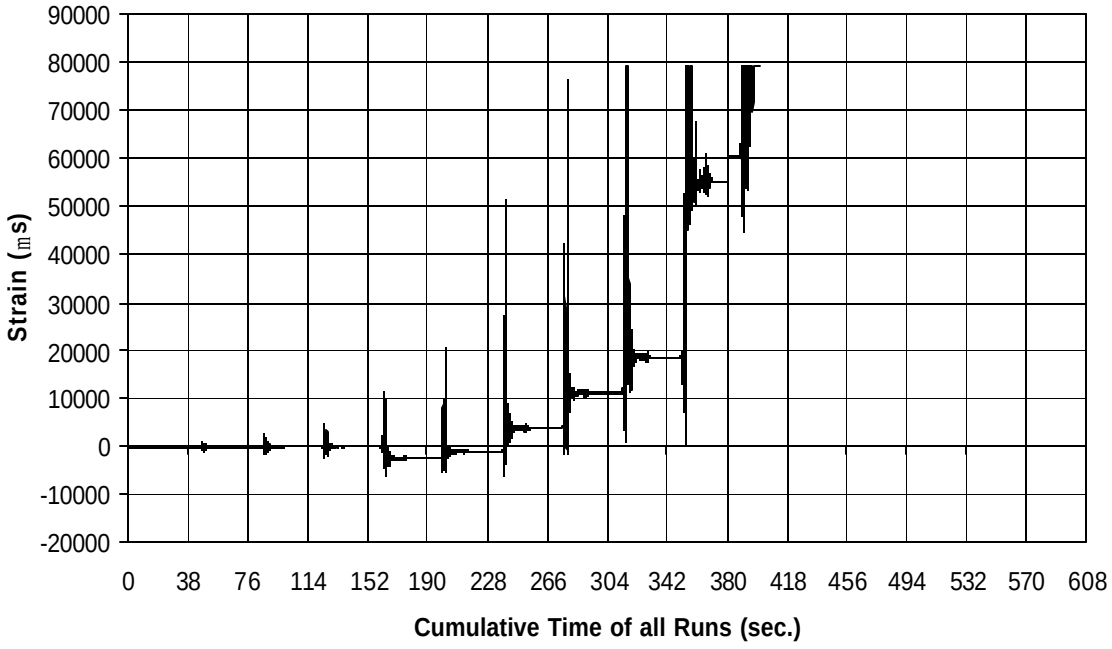

Fig. A-75 THD -2 Measured Strain in Gauge SG2B4

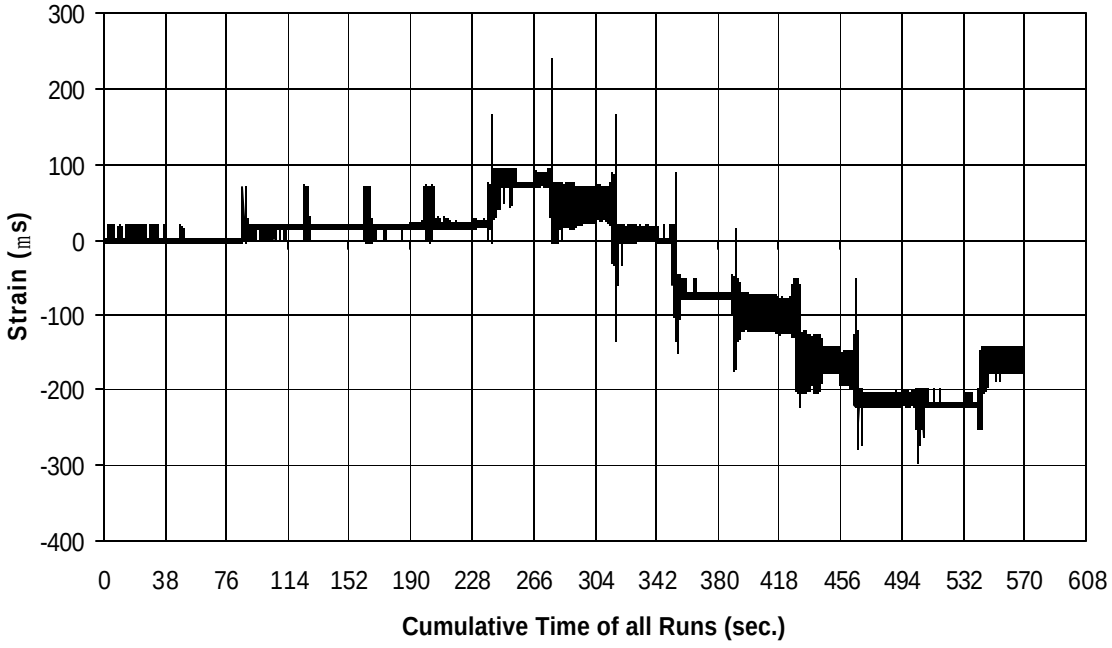

Fig. A-76 THD -2 Measured Strain in Gauge SG3B4

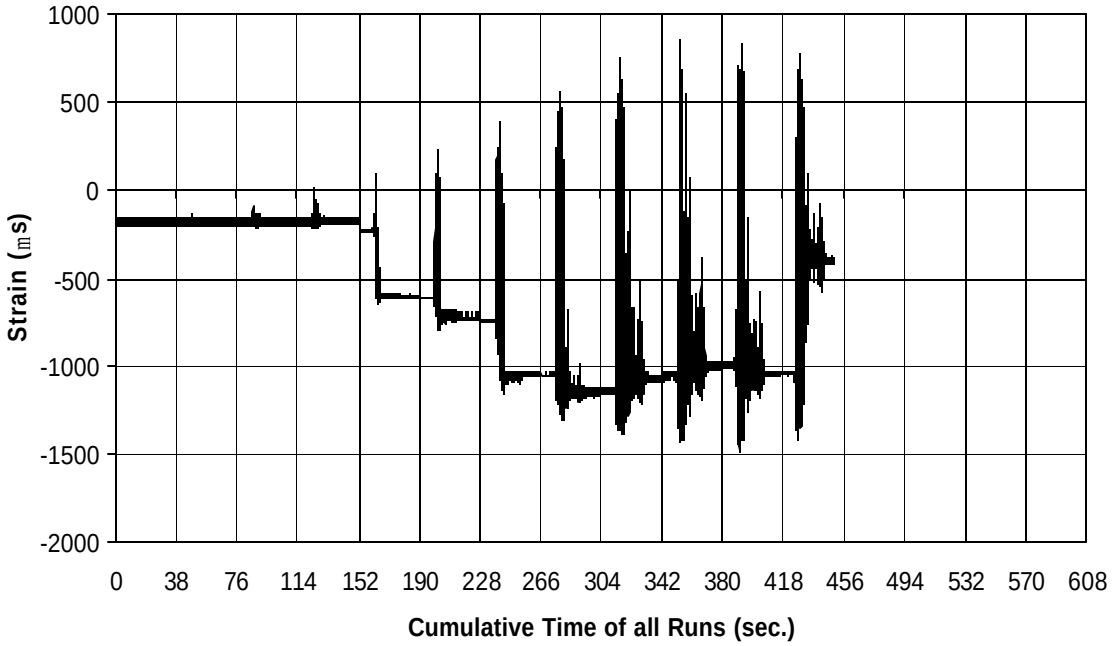

Fig. A-77 THD -2 Measured Strain in Gauge SG4B4

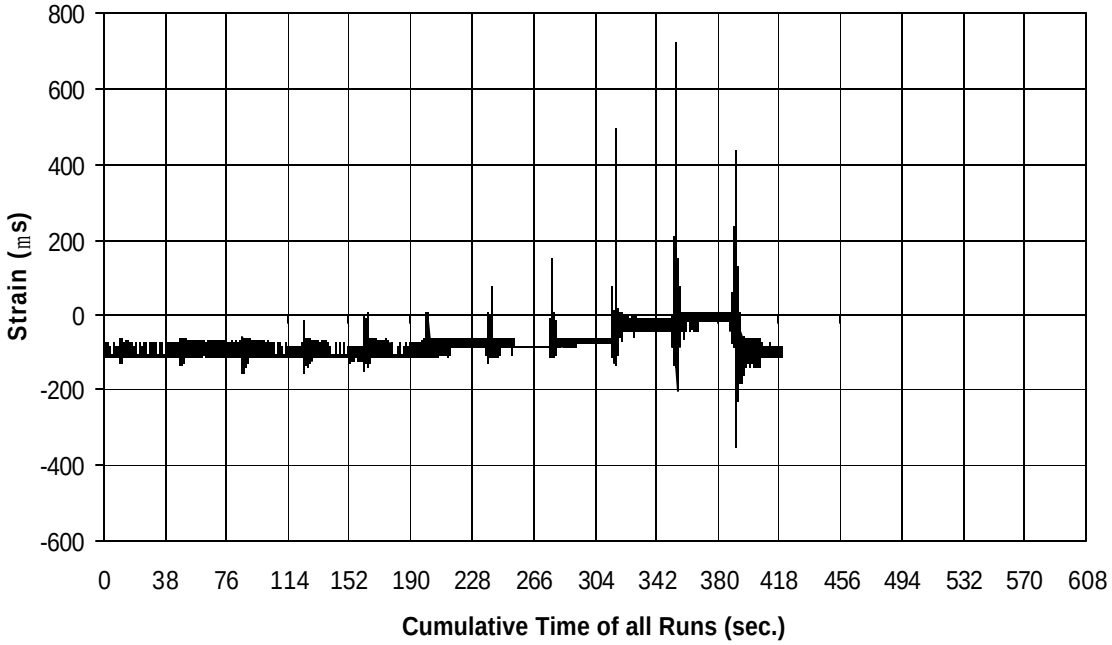

Fig. A-78 THD -2 Measured Strain in Gauge SG5B4

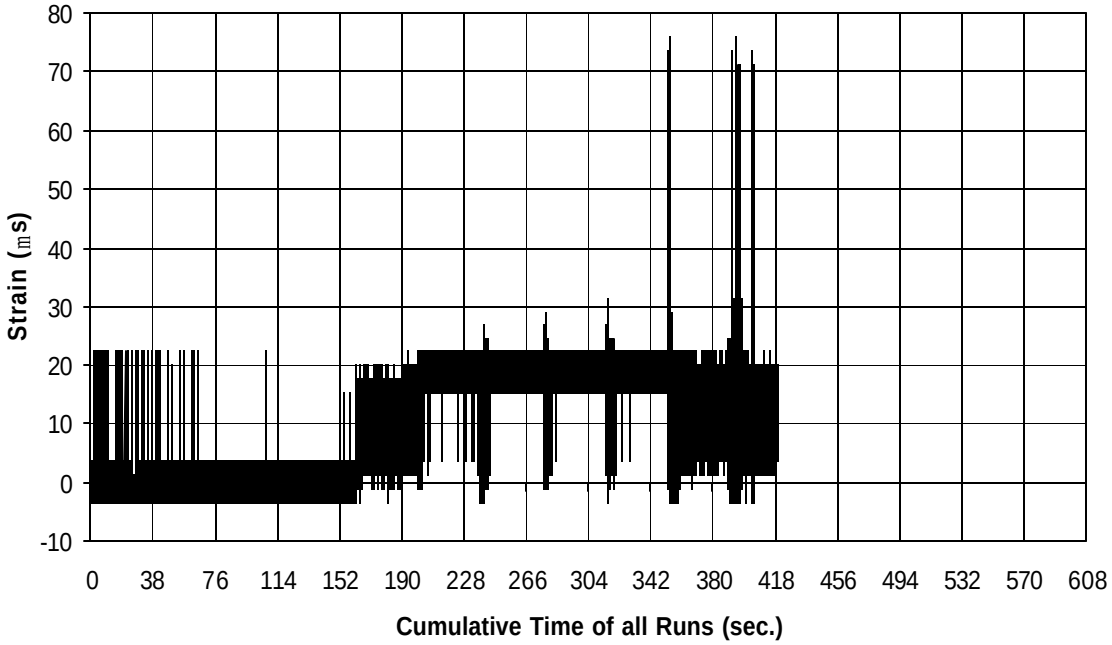

Fig. A-79 THD -2 Measured Strain in Gauge SG6B4

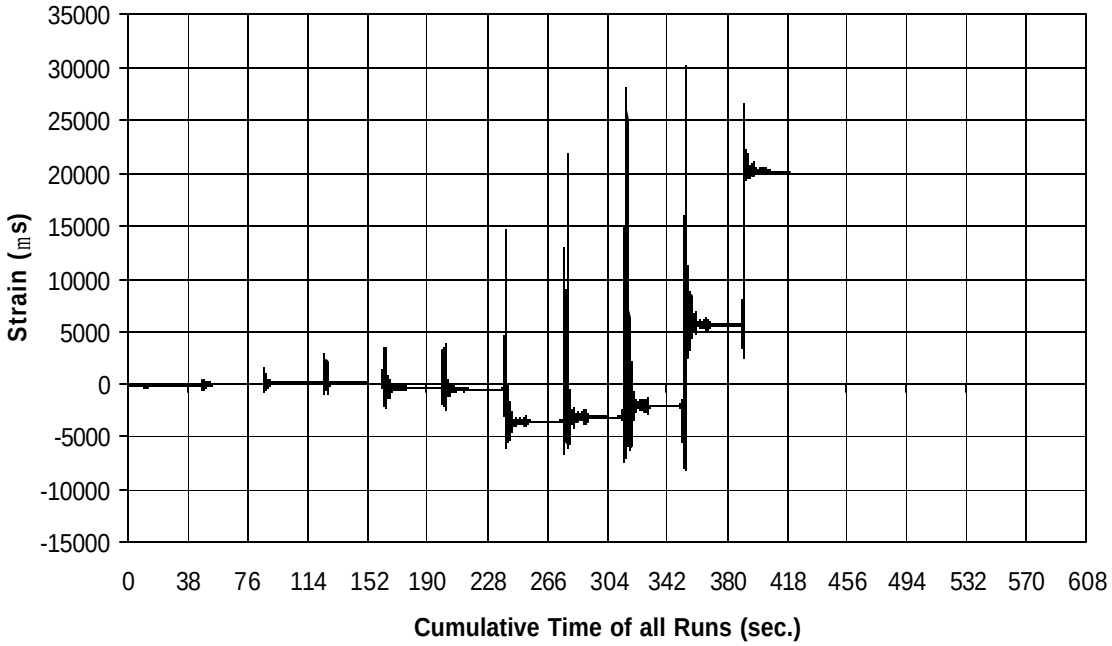

Fig. A-80 THD -2 Measured Strain in Gauge SG7B4

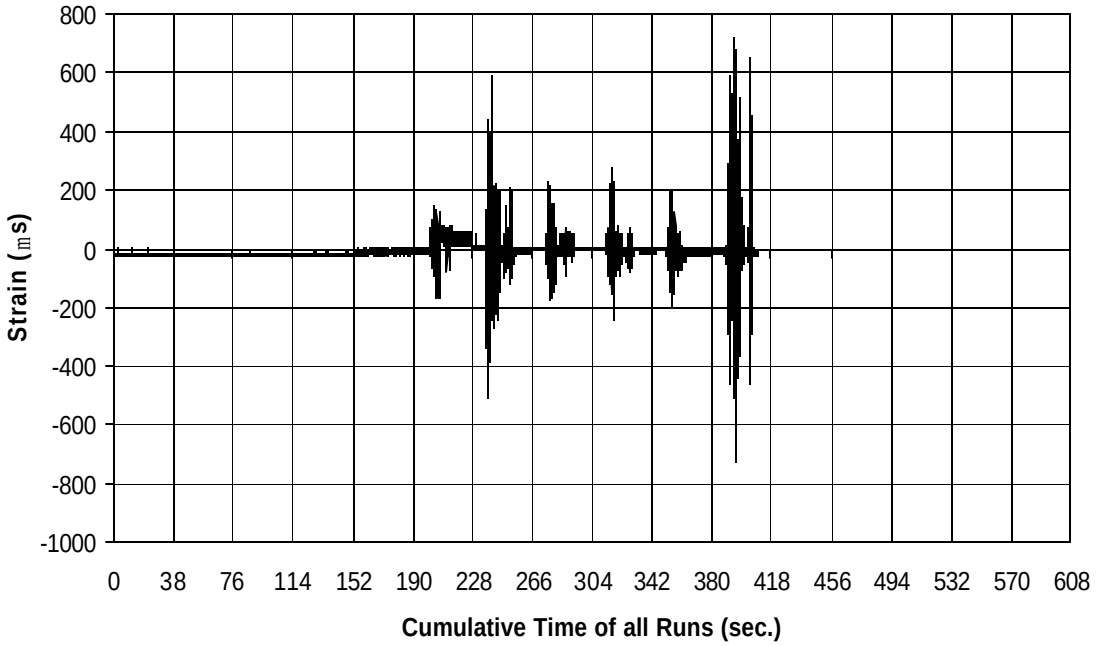

Fig. A-81 THD -2 Measured Strain in Gauge SG8B4

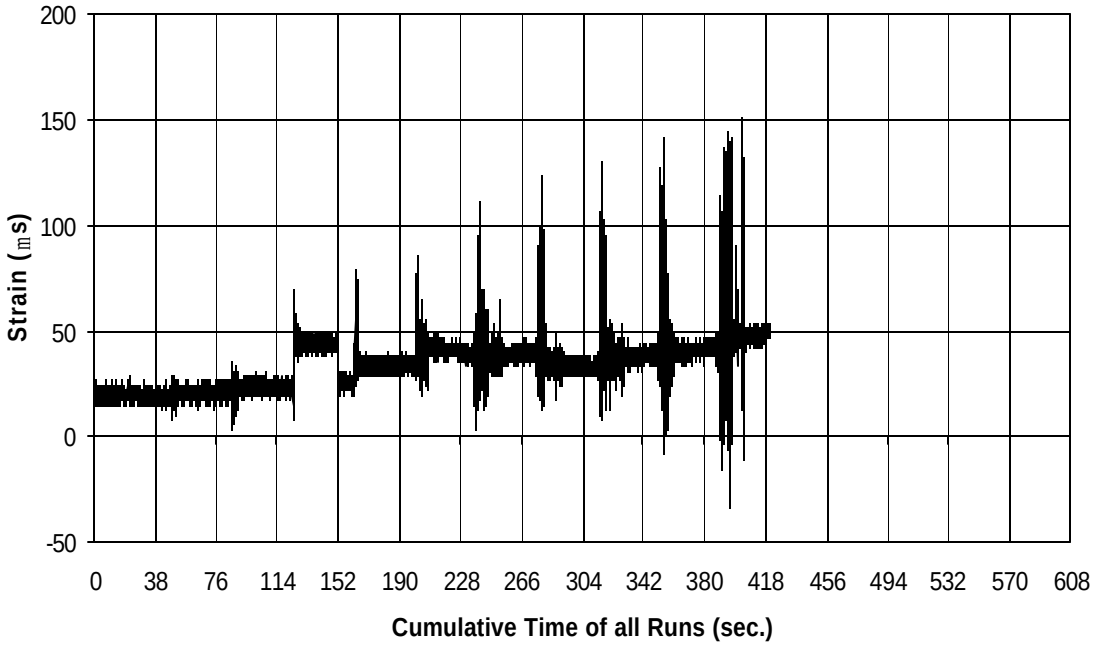

Fig. A-82 THD -2 Measured Strain in Gauge SG1B5

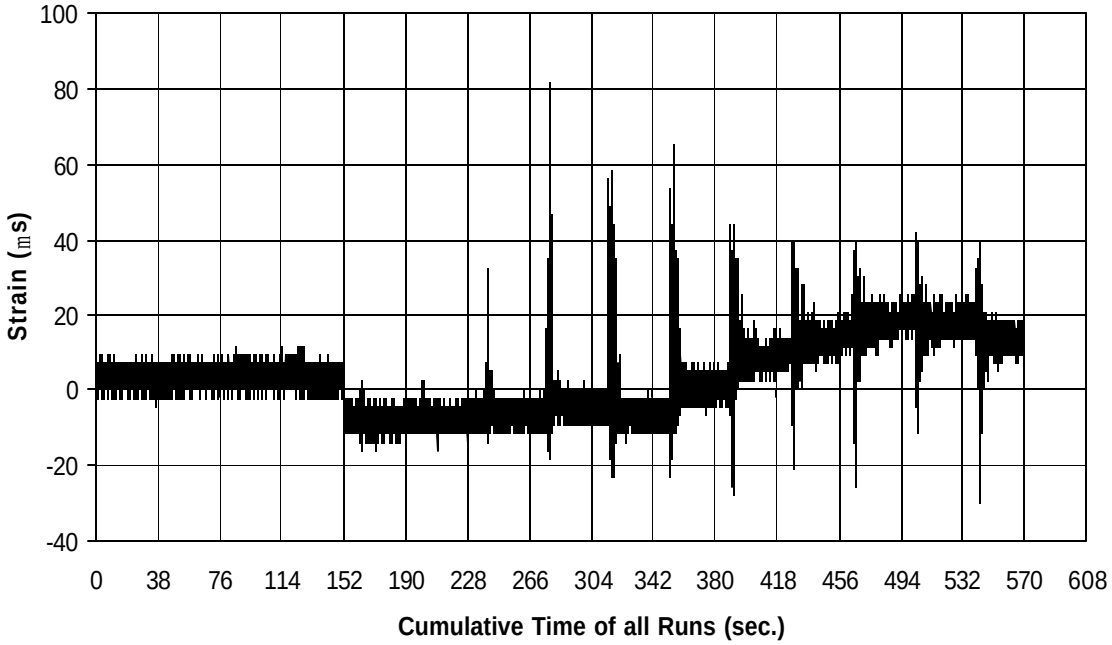

Fig. A-83 THD -2 Measured Strain in Gauge SG2B5

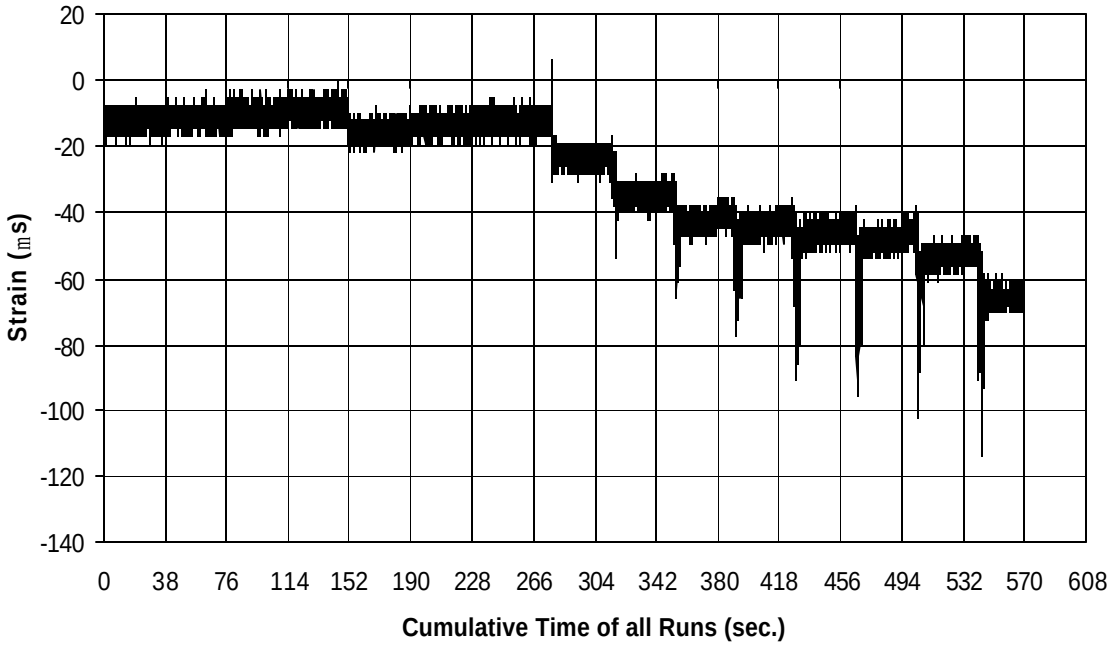

Fig. A-84 THD -2 Measured Strain in Gauge SG3B5

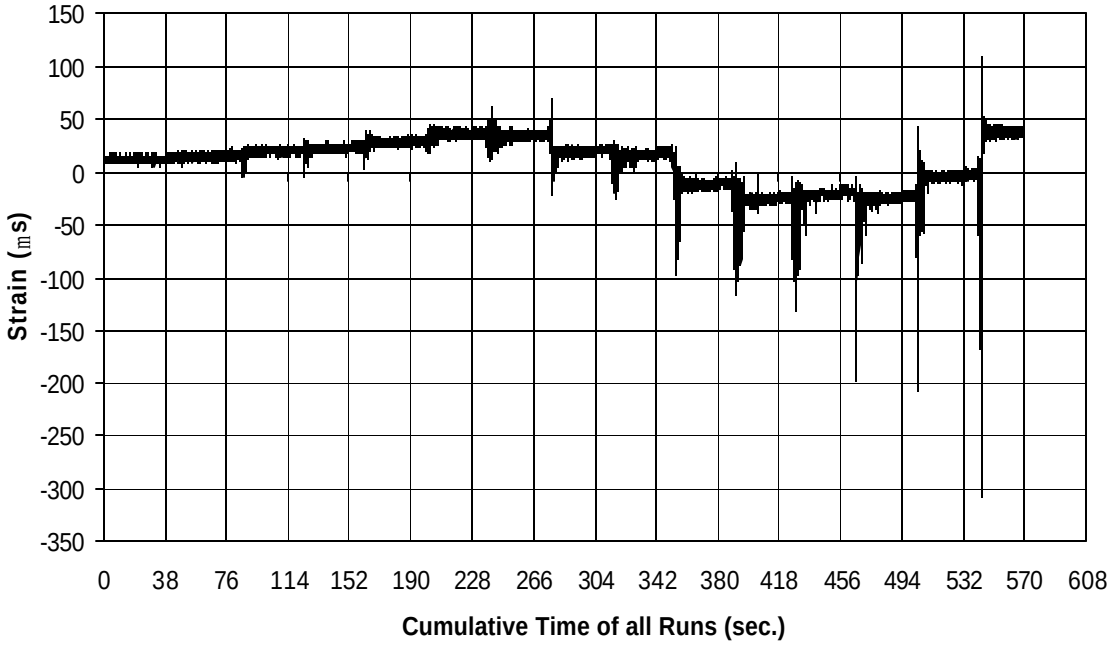

Fig. A-85 THD -2 Measured Strain in Gauge SG4B5

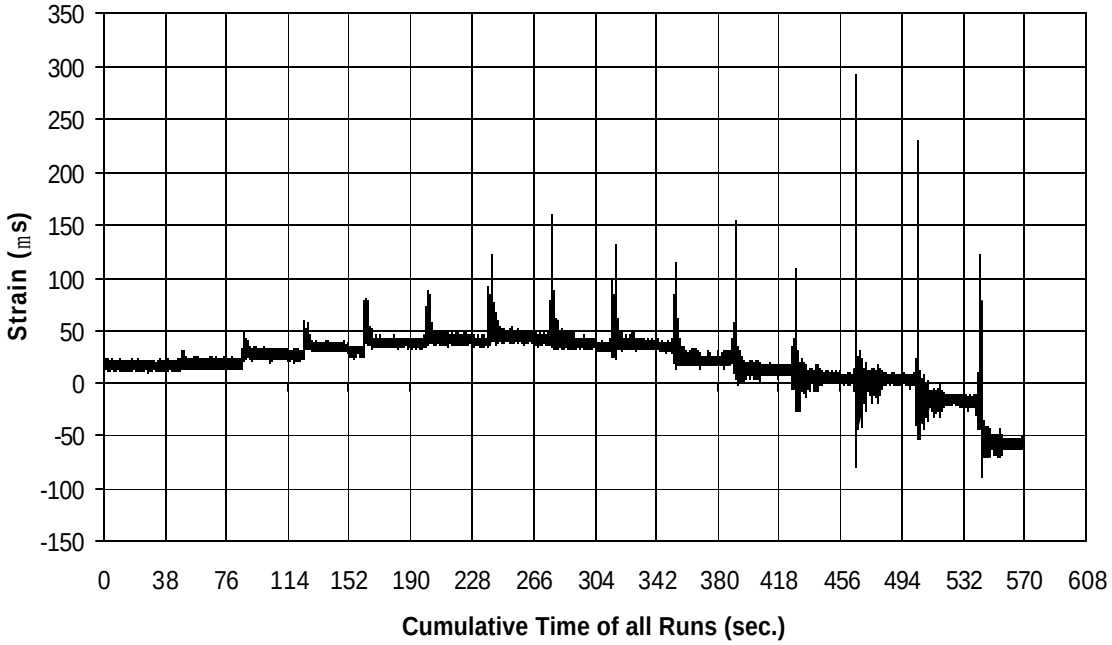

Fig. A-86 THD -2 Measured Strain in Gauge SG5B5

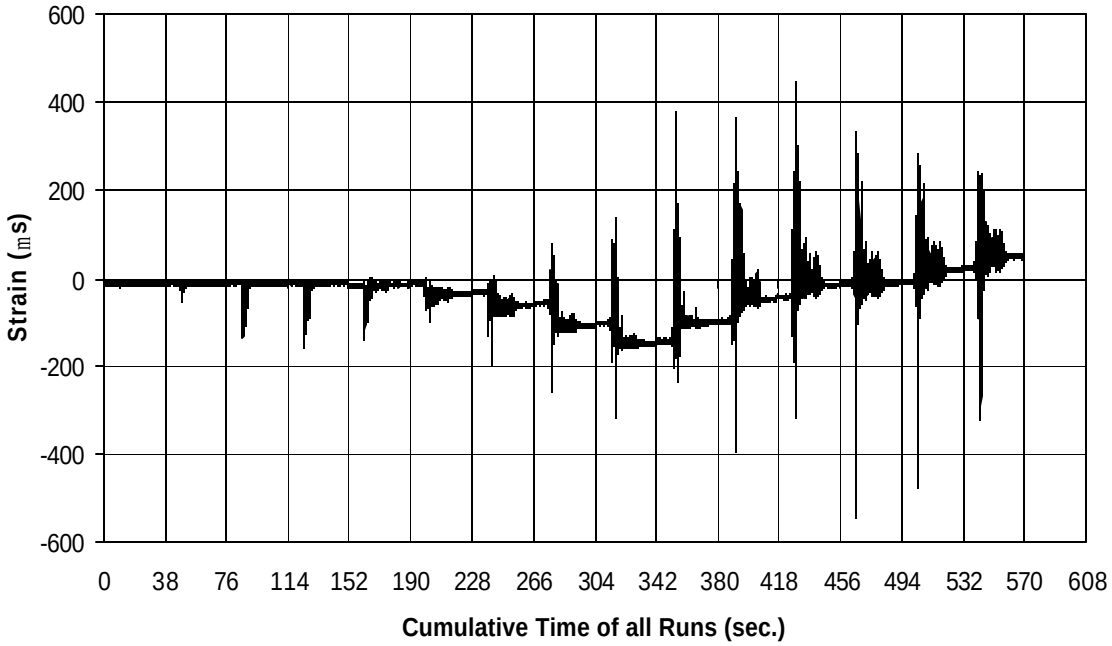

Fig. A-87 THD -2 Measured Strain in Gauge SG6B5

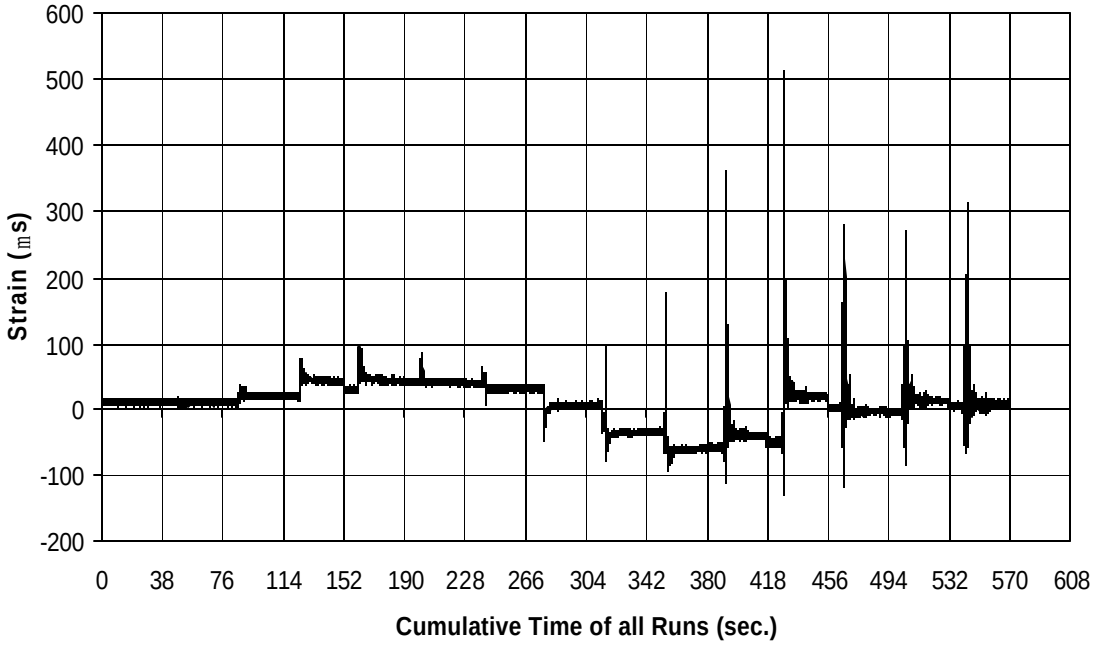

Fig. A-88 THD -2 Measured Strain in Gauge SG7B5

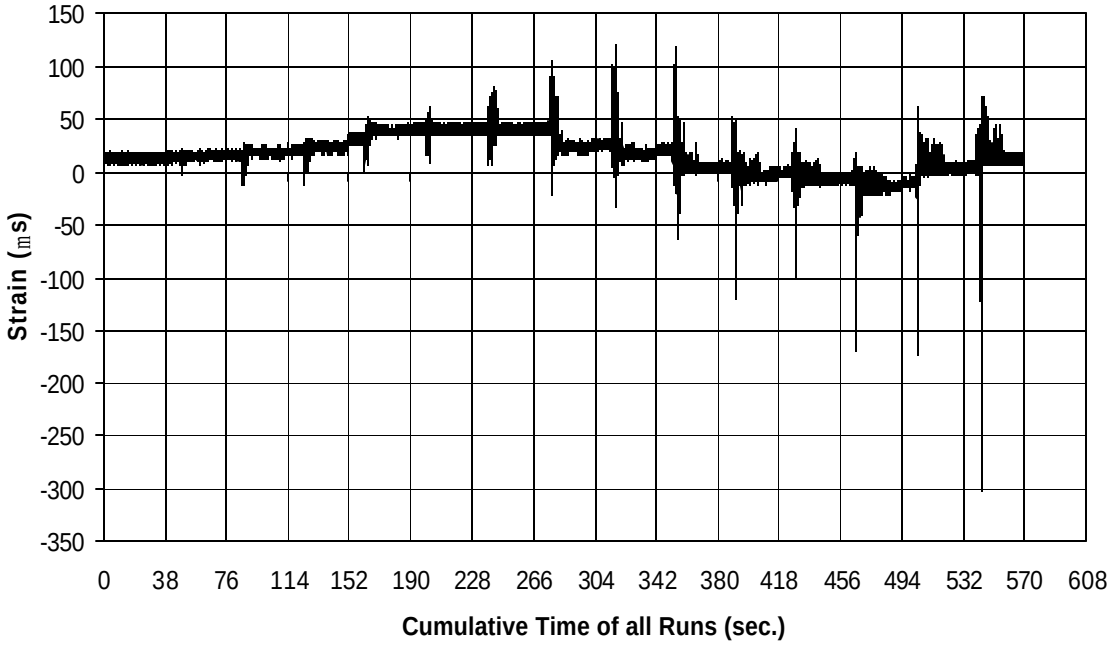

Fig. A-89 THD -2 Measured Strain in Gauge SG8B5

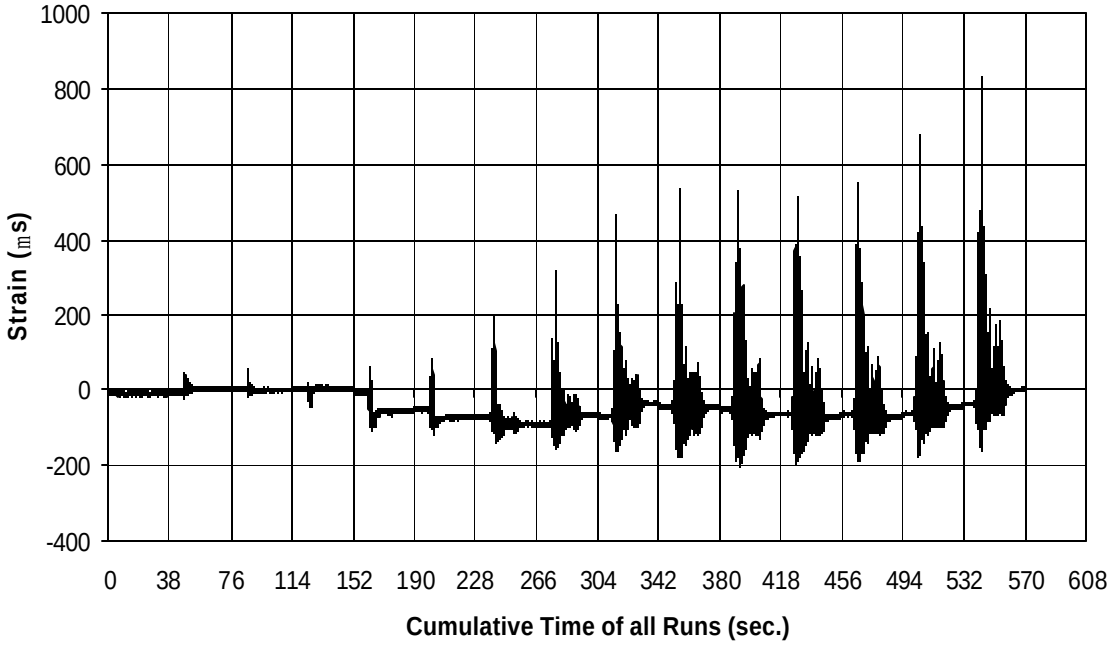

Fig. A-90 THD -2 Measured Strain in Gauge SG1B6

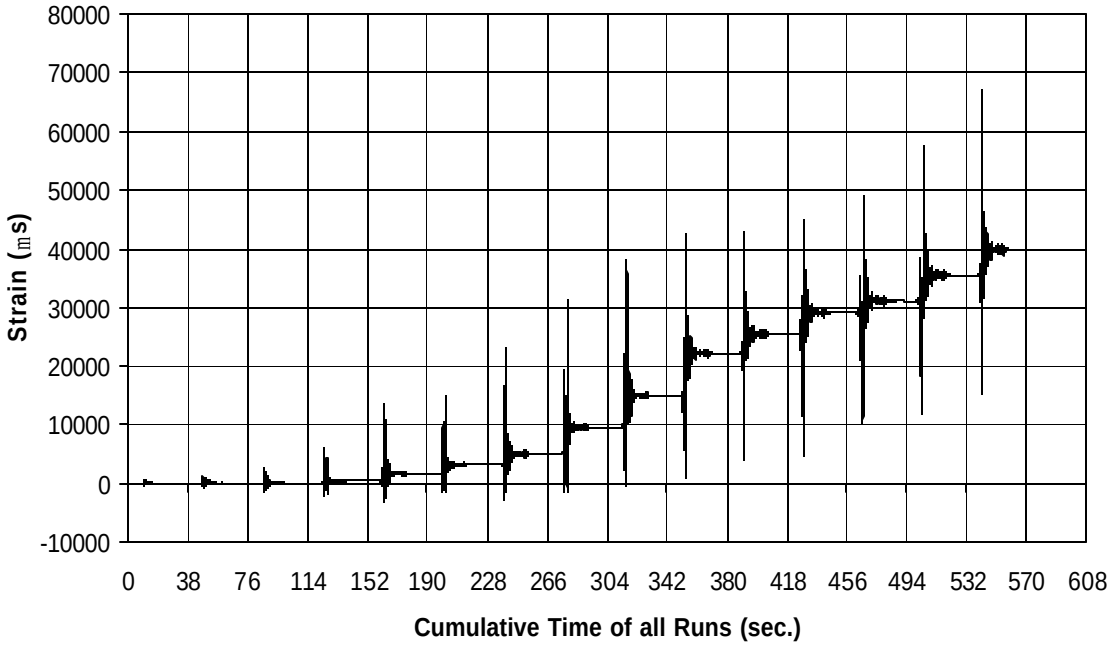

Fig. A-91 THD -2 Measured Strain in Gauge SG2B6

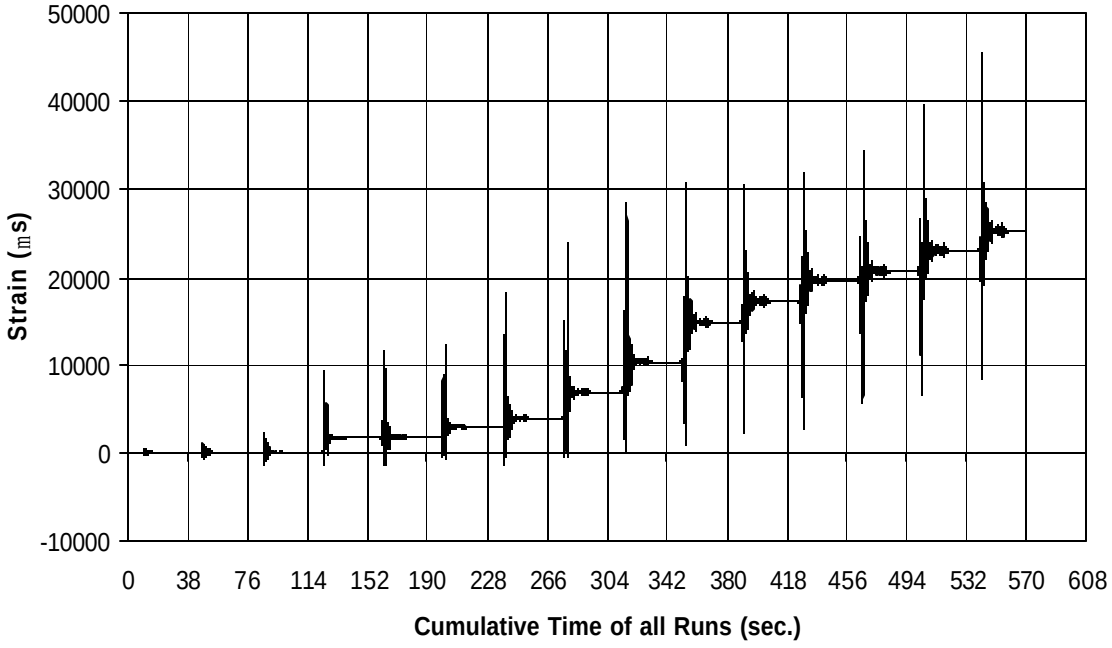

Fig. A-92 THD -2 Measured Strain in Gauge SG3B6

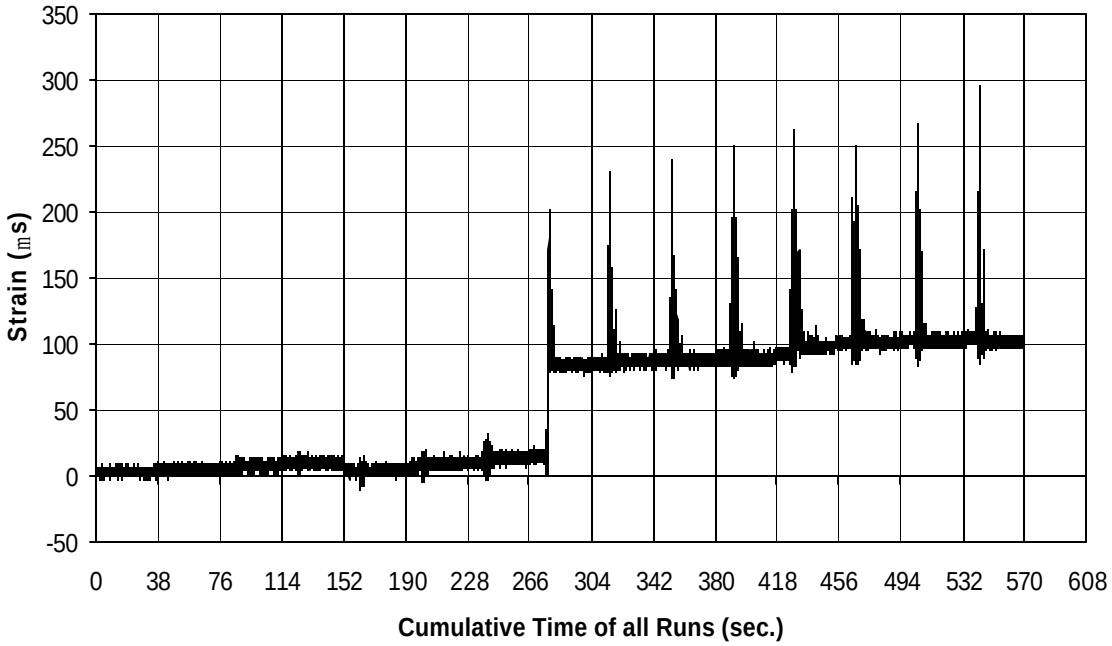

Fig. A-93 THD -2 Measured Strain in Gauge SG4B6

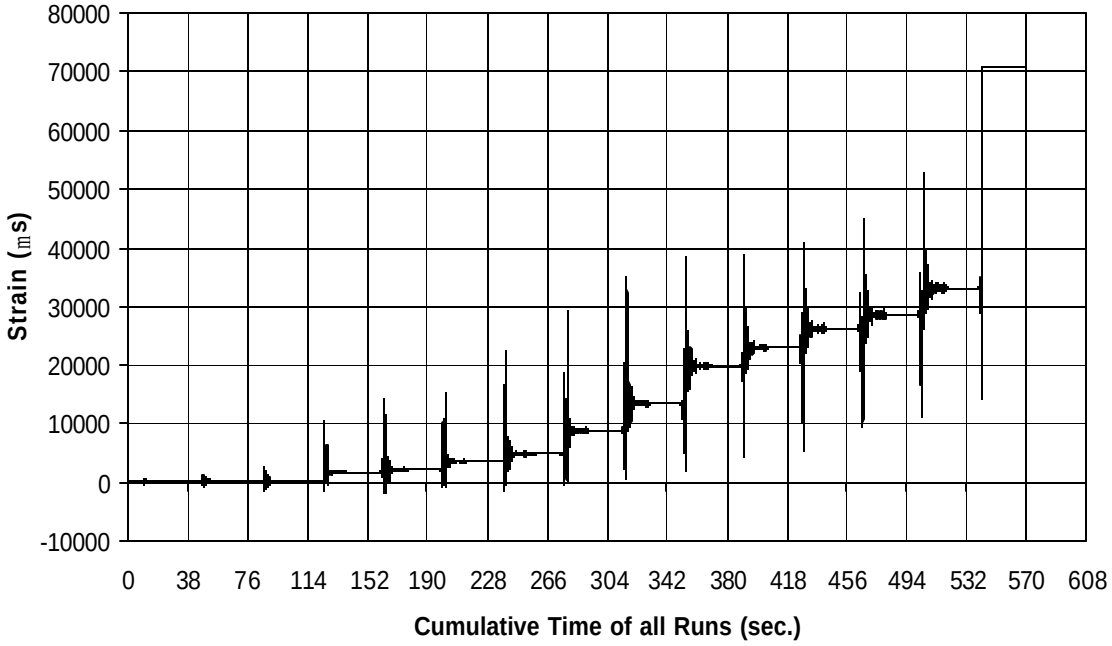

Fig. A-94 THD -2 Measured Strain in Gauge SG5B6

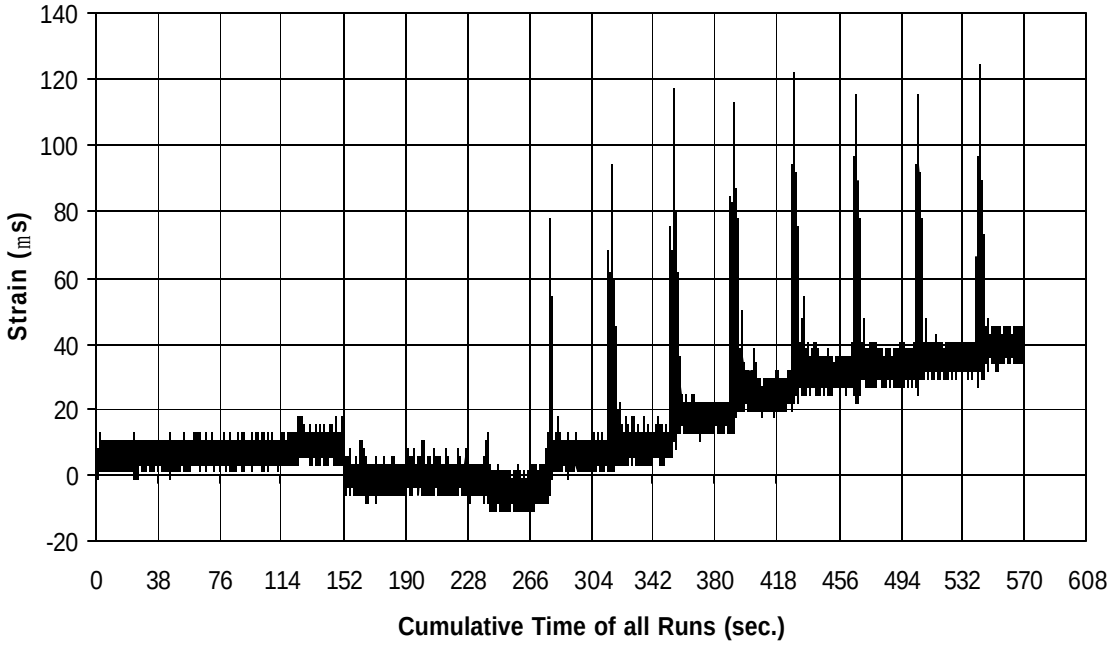

Fig. A-95 THD -2 Measured Strain in Gauge SG6B6

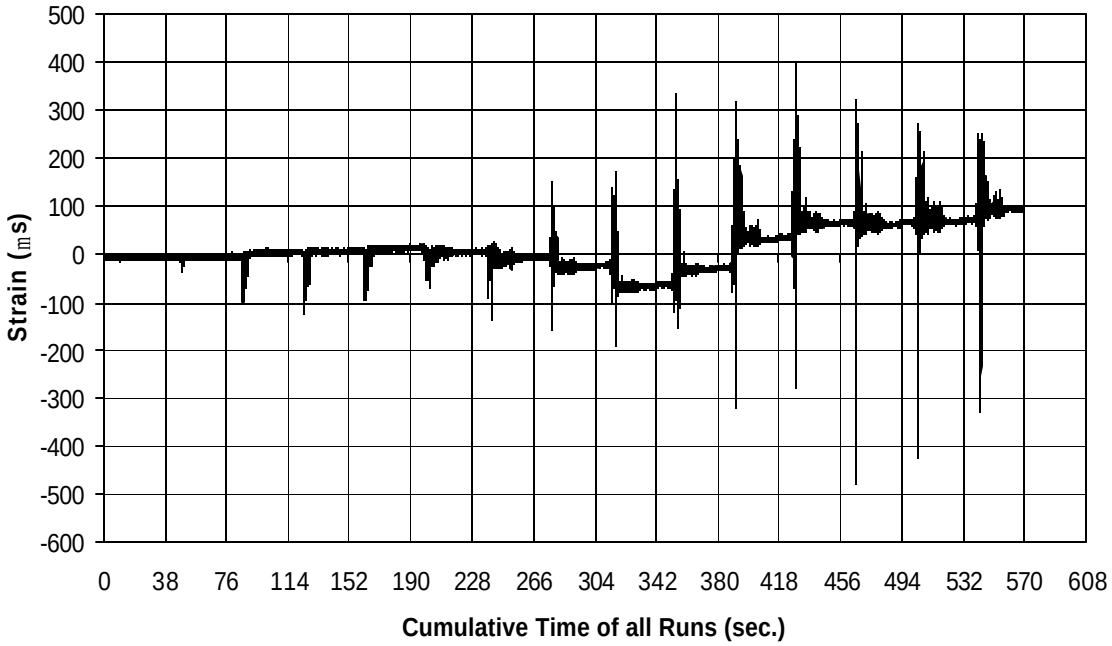

Fig. A-96 THD -2 Measured Strain in Gauge SG7B6

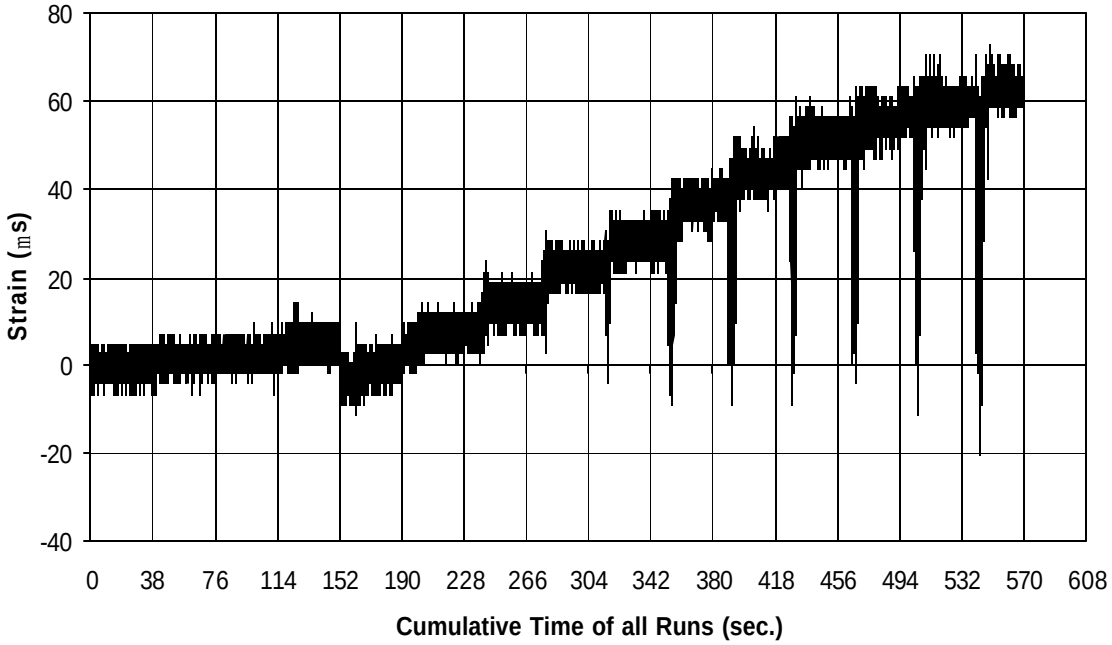

Fig. A-97 THD -2 Measured Strain in Gauge SG8B6

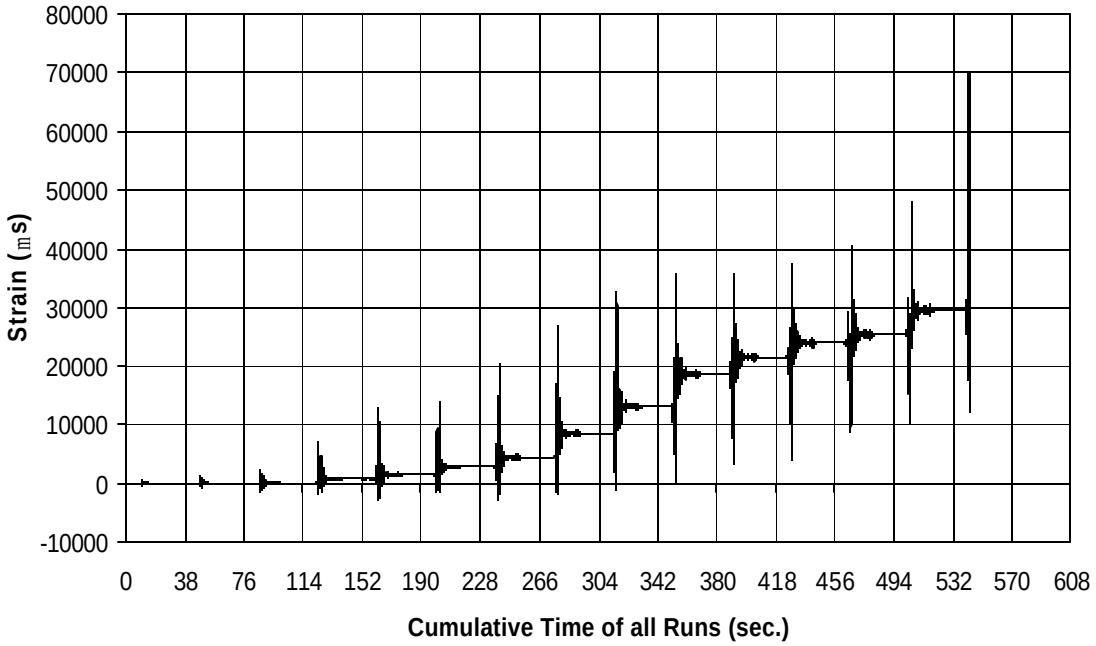

Fig. A-98 THD -2 Measured Strain in Gauge SG1B7

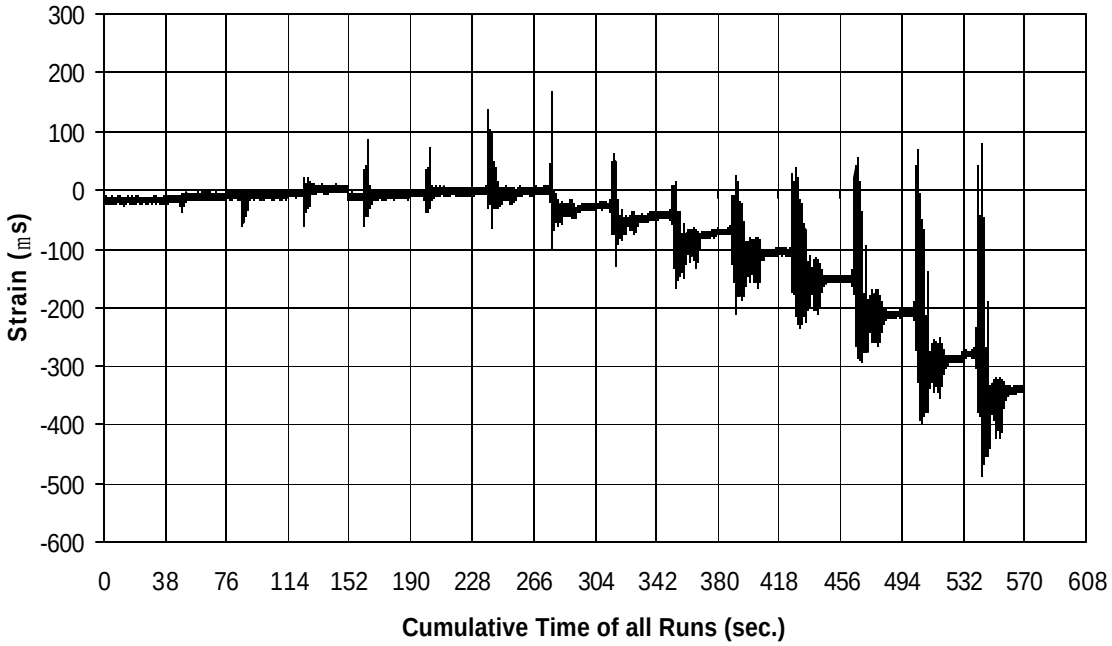

Fig. A-99 THD -2 Measured Strain in Gauge SG2B7

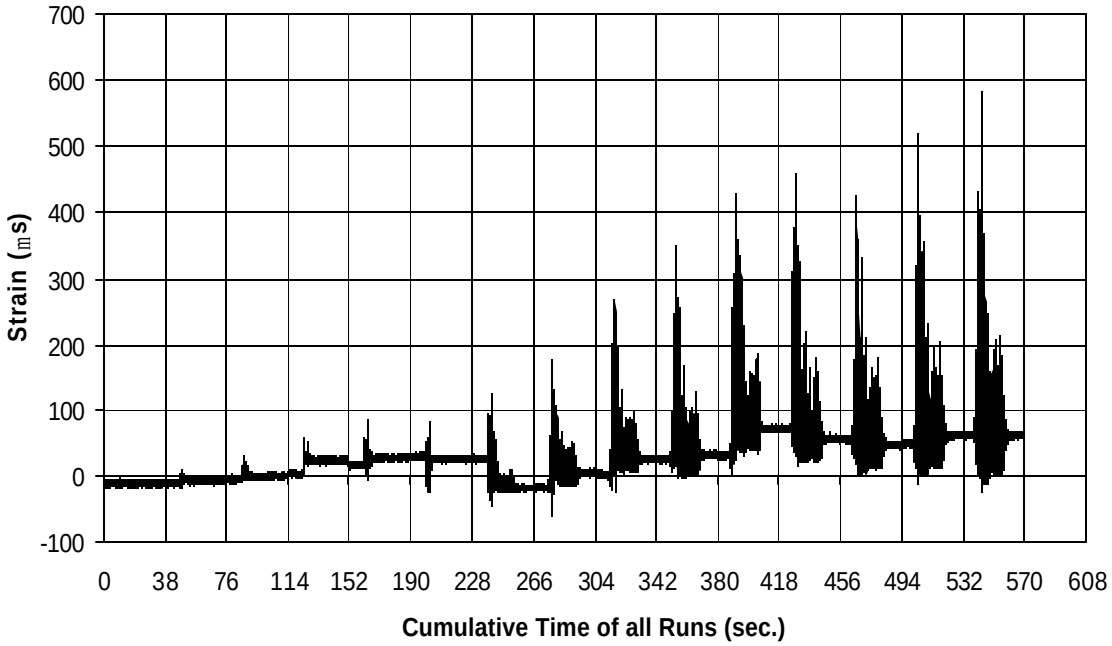

Fig. A-100 THD -2 Measured Strain in Gauge SG3B7

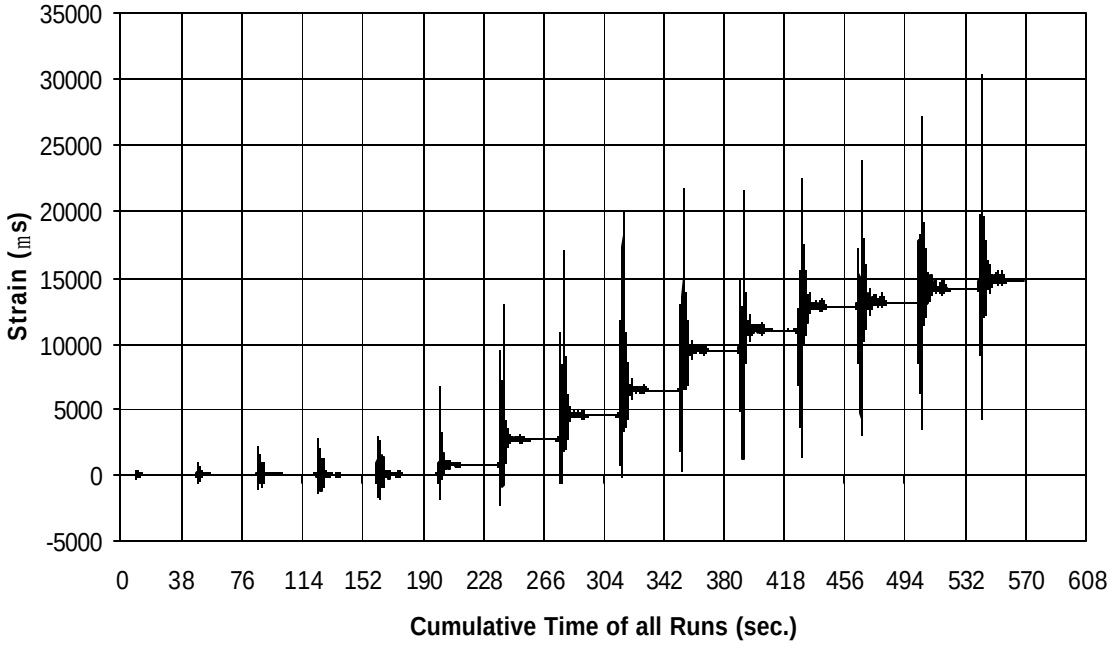

Fig. A-101 THD -2 Measured Strain in Gauge SG4B7

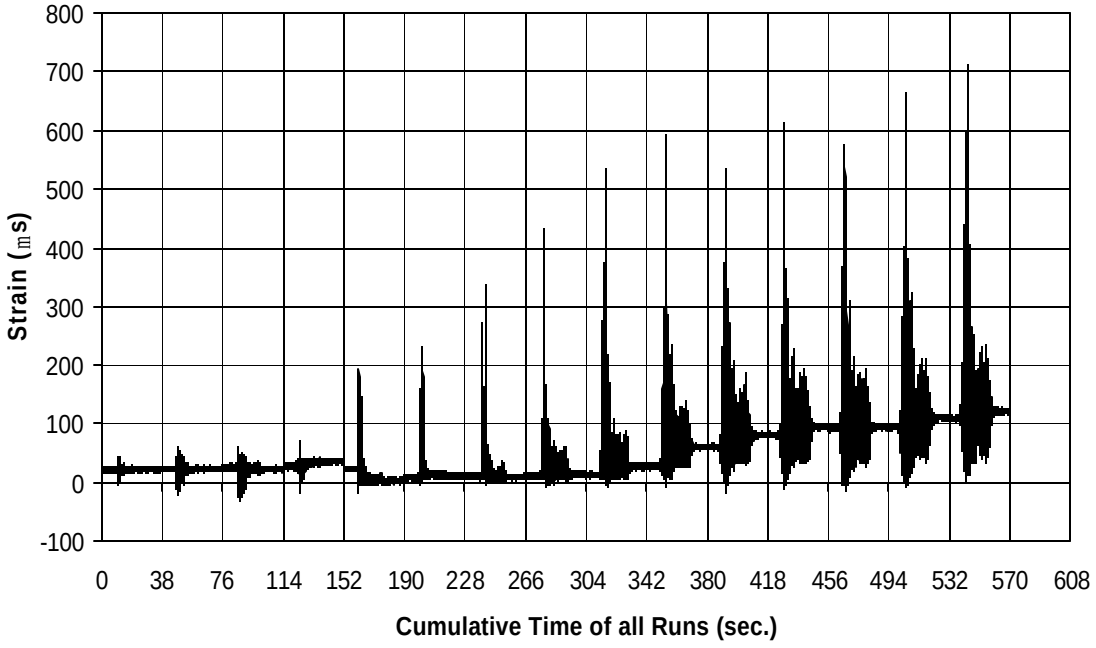

Fig. A-102 THD -2 Measured Strain in Gauge SG5B7

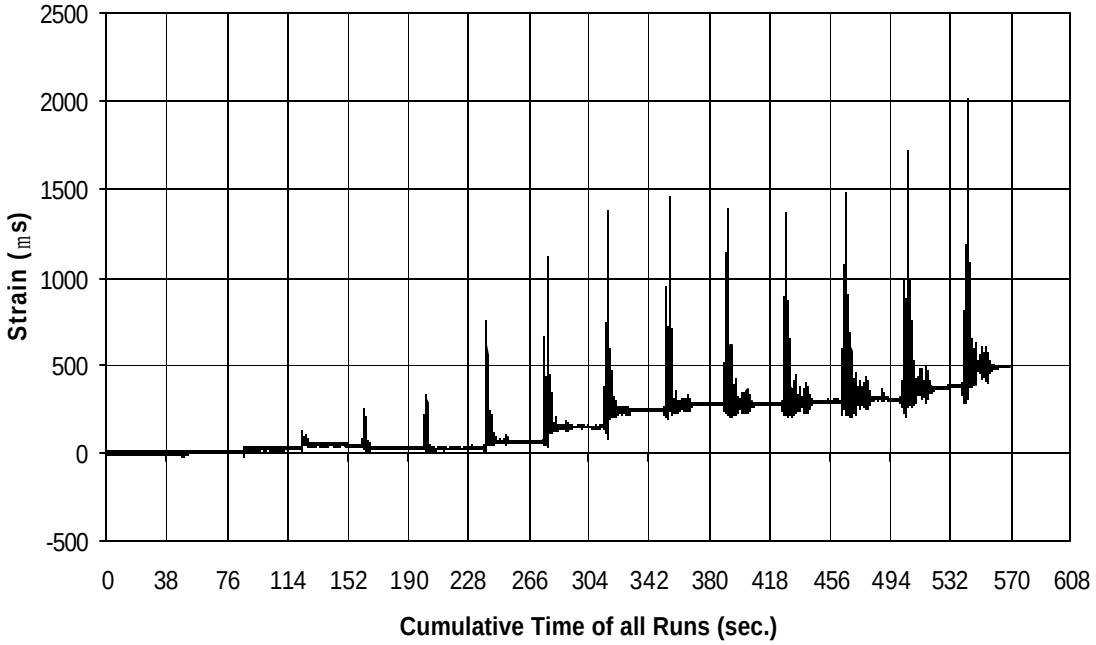

Fig. A-103 THD -2 Measured Strain in Gauge SG6B7

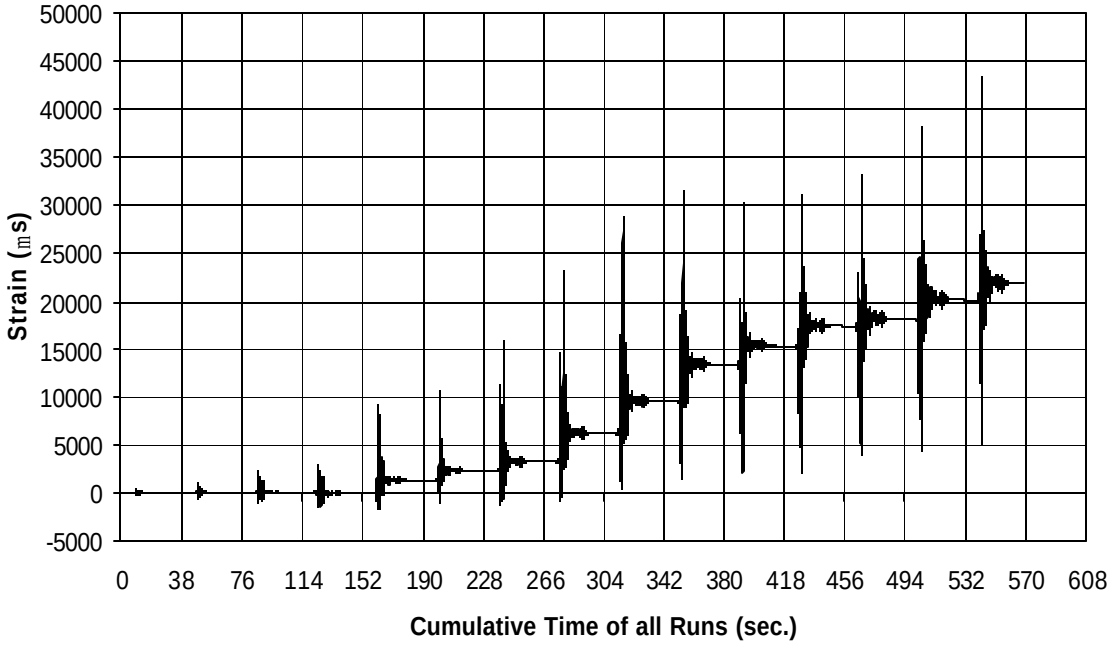

Fig. A-104 THD -2 Measured Strain in Gauge SG7B7

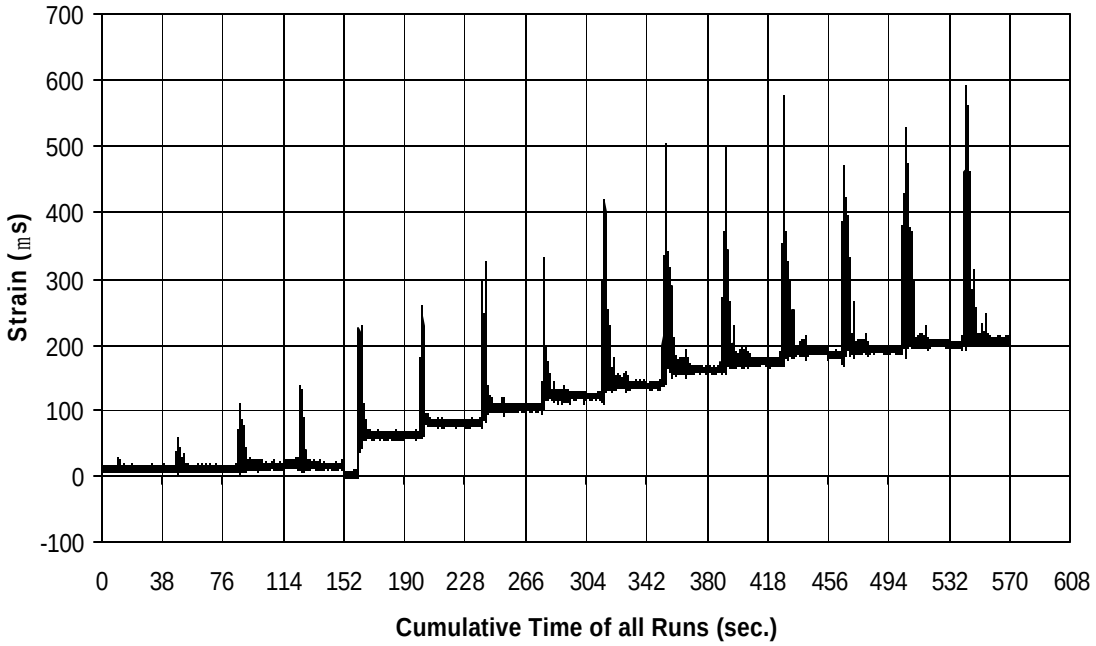

Fig. A-105 THD -2 Measured Strain in Gauge SG8B7

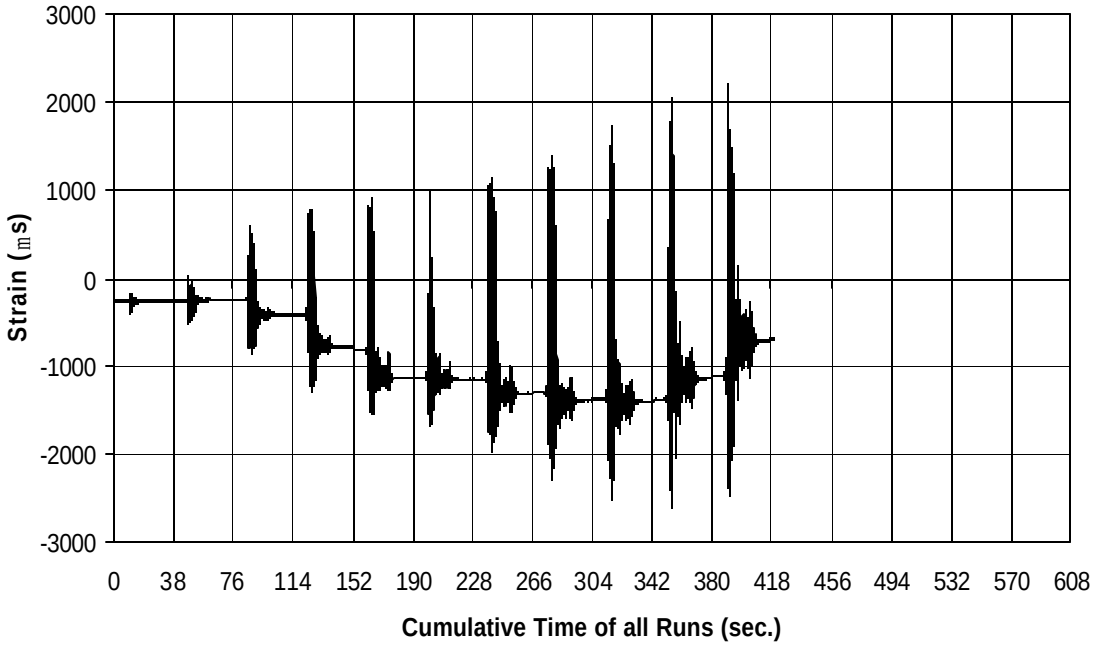

Fig. A-106 THD -2 Measured Strain in Gauge SG1B8

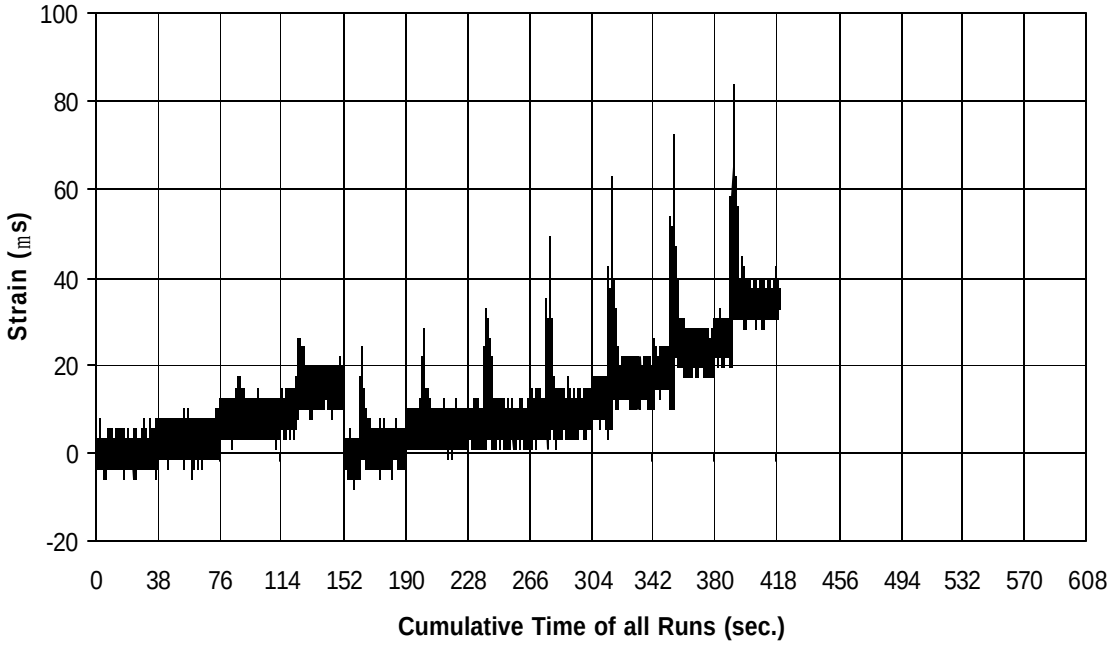

Fig. A-107 THD -2 Measured Strain in Gauge SG2B8

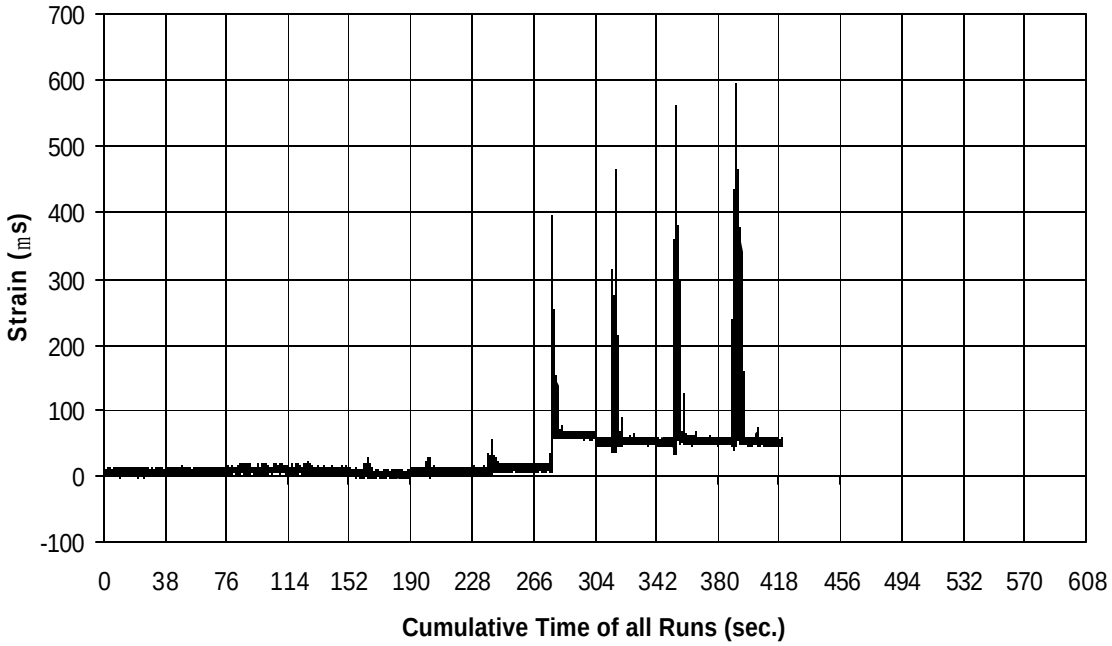

Fig. A-108 THD -2 Measured Strain in Gauge SG3B8

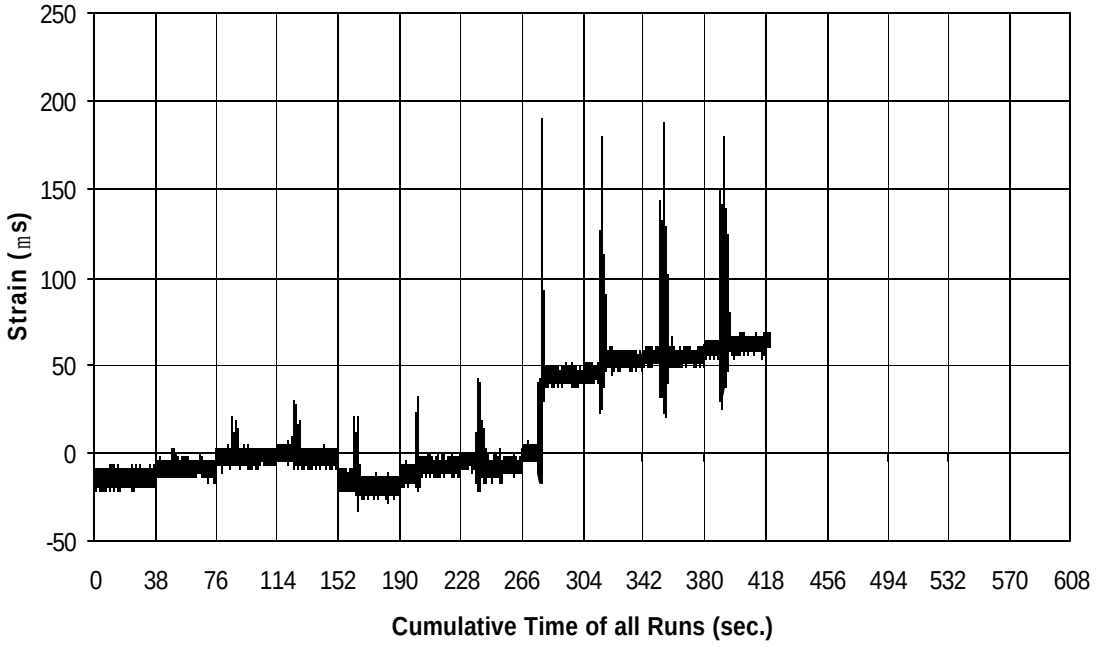

Fig. A-109 THD -2 Measured Strain in Gauge SG4B8

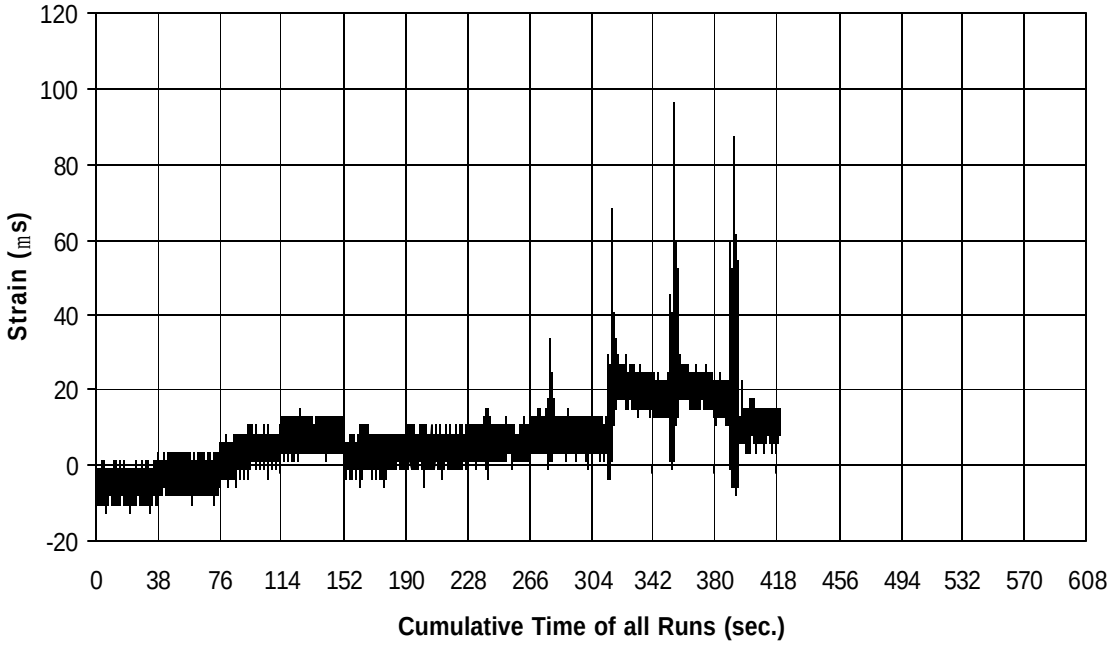

Fig. A-110 THD -2 Measured Strain in Gauge SG5B8

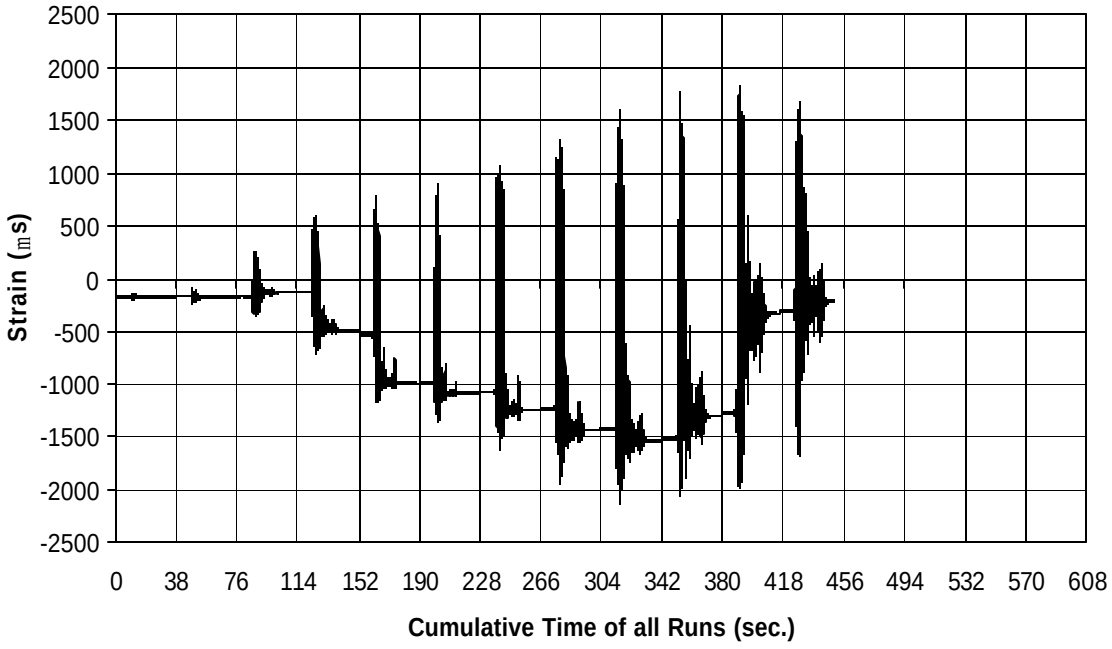

Fig. A-111 THD -2 Measured Strain in Gauge SG6B8

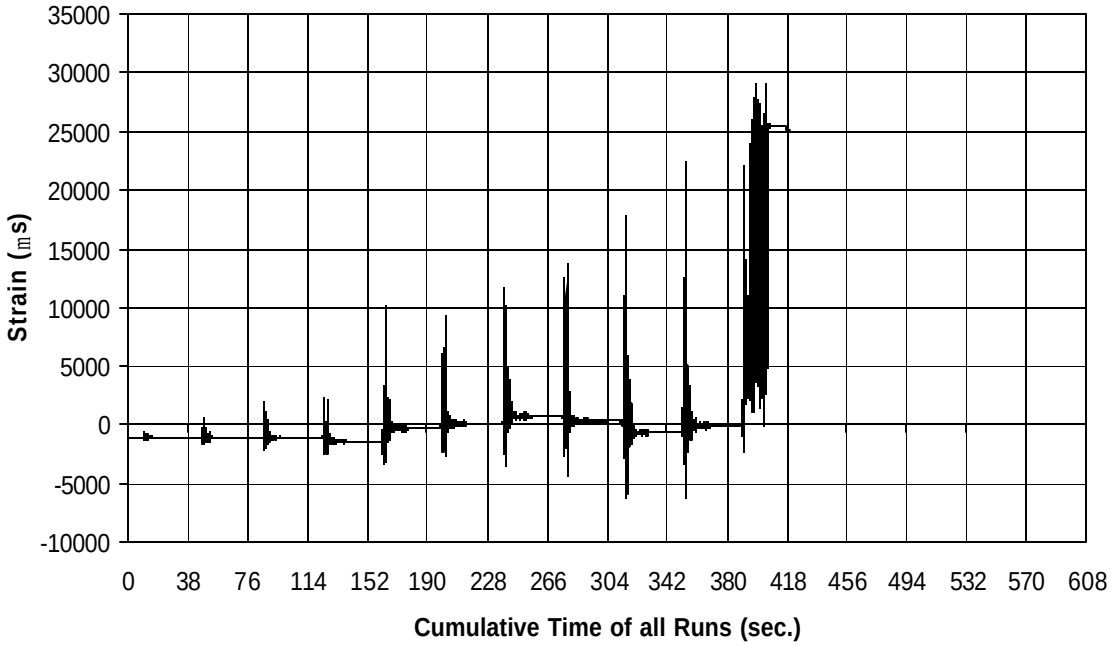

Fig. A-112 THD -2 Measured Strain in Gauge SG7B8

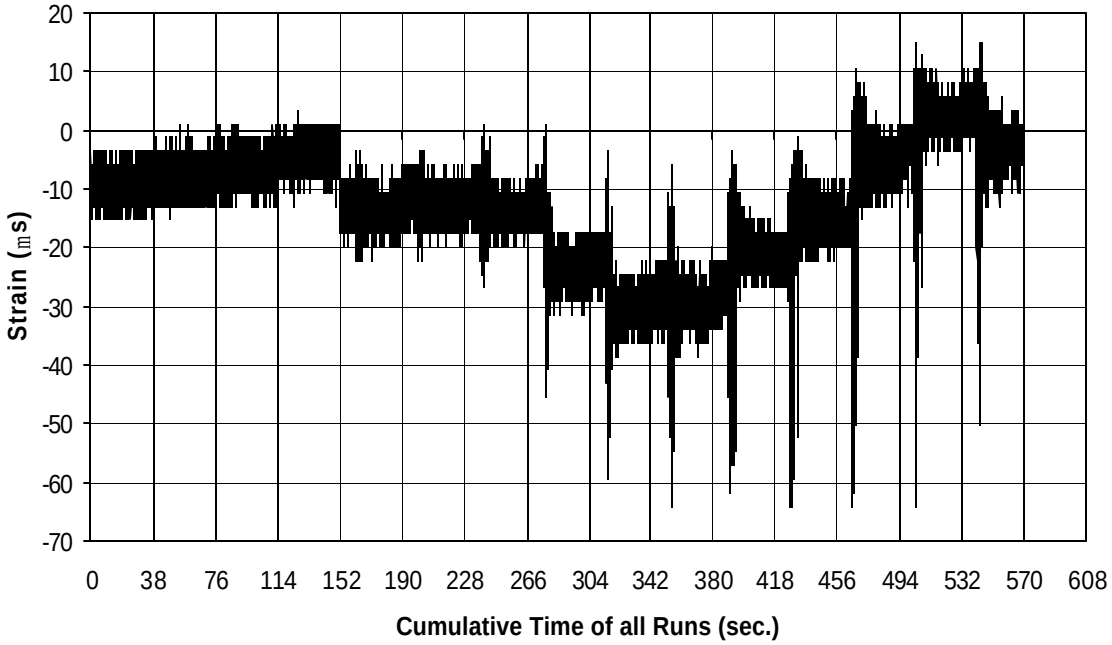

Fig. A-113 THD -2 Measured Strain in Gauge SG8B8

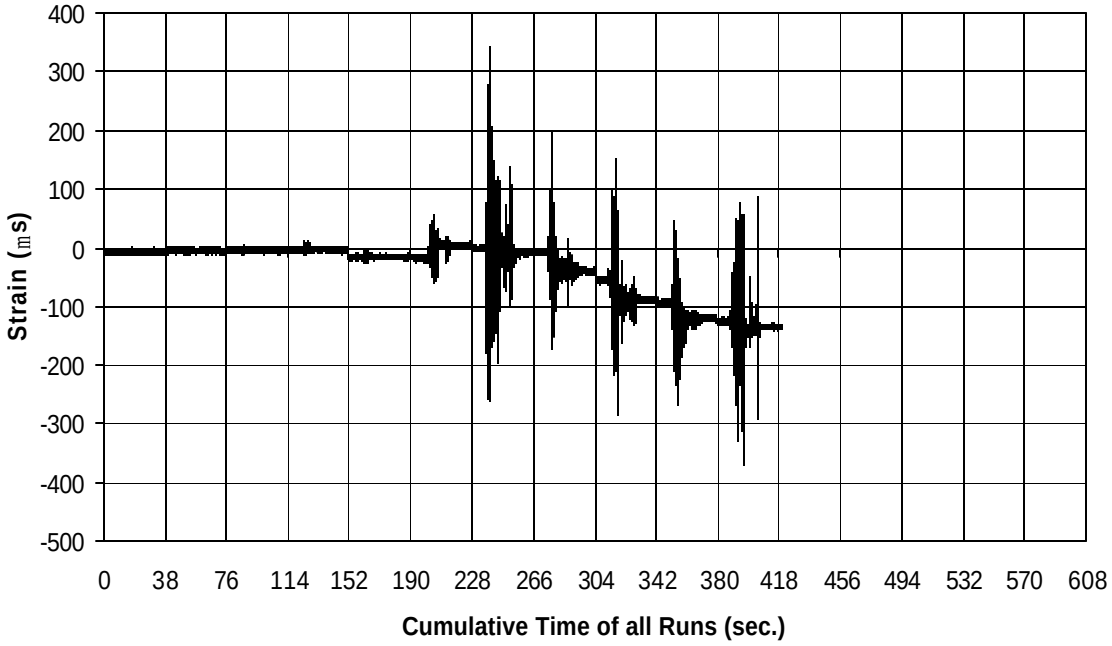

Fig. A-114 THD -2 Measured Strain in Gauge SG1B9

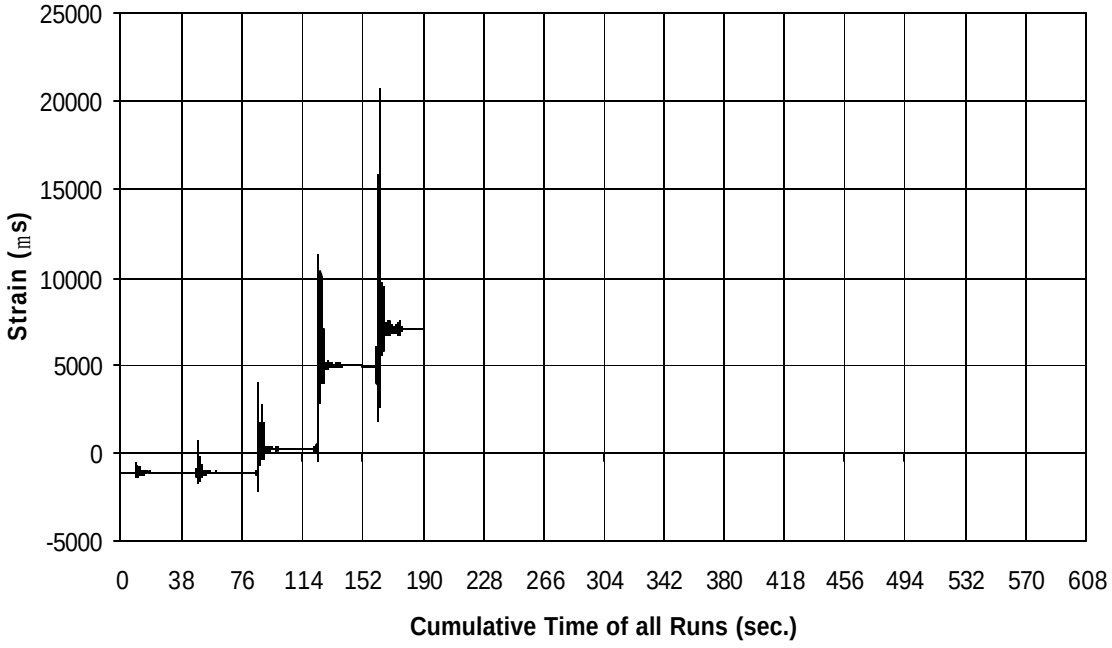

Fig. A-115 THD -2 Measured Strain in Gauge SG2B9

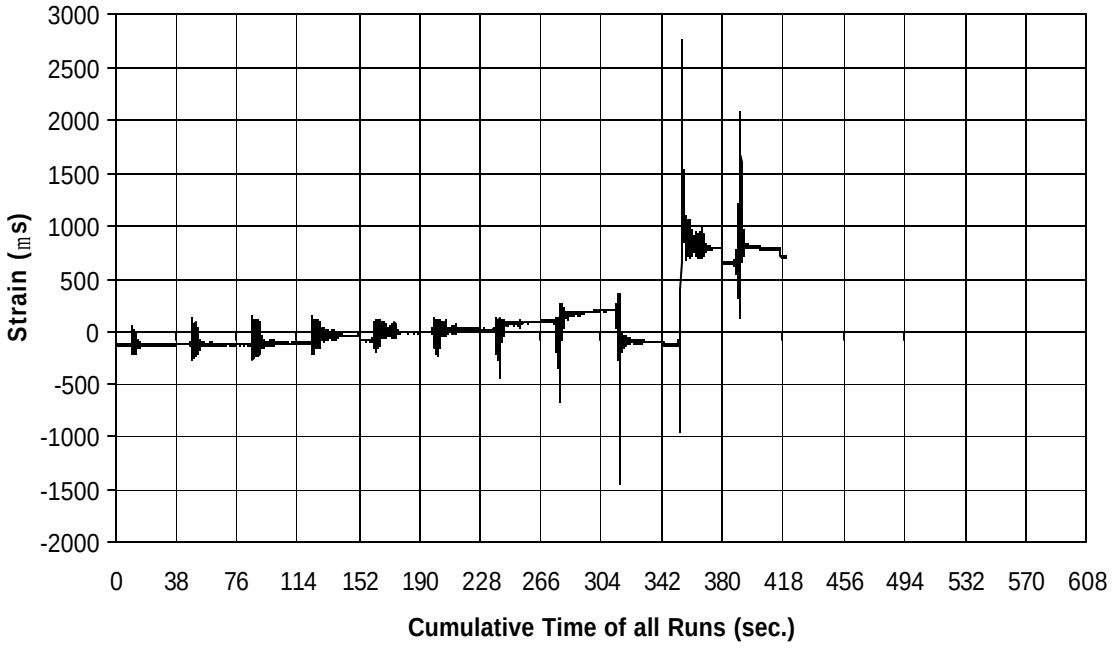

Fig. A-116 THD -2 Measured Strain in Gauge SG3B9

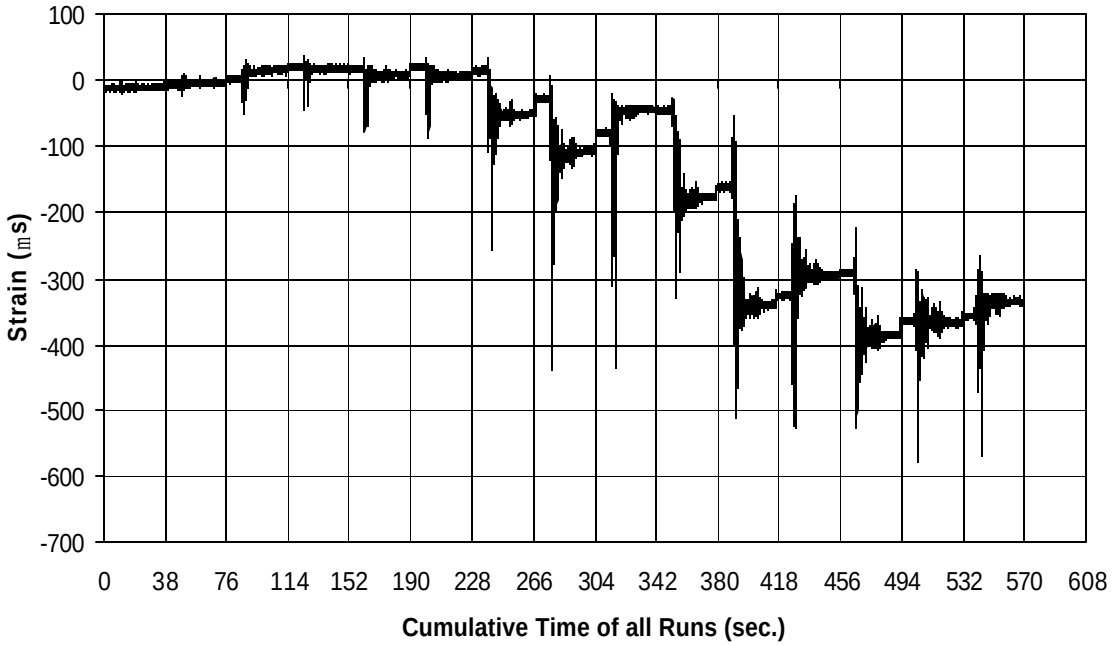

Fig. A-117 THD -2 Measured Strain in Gauge SG4B9

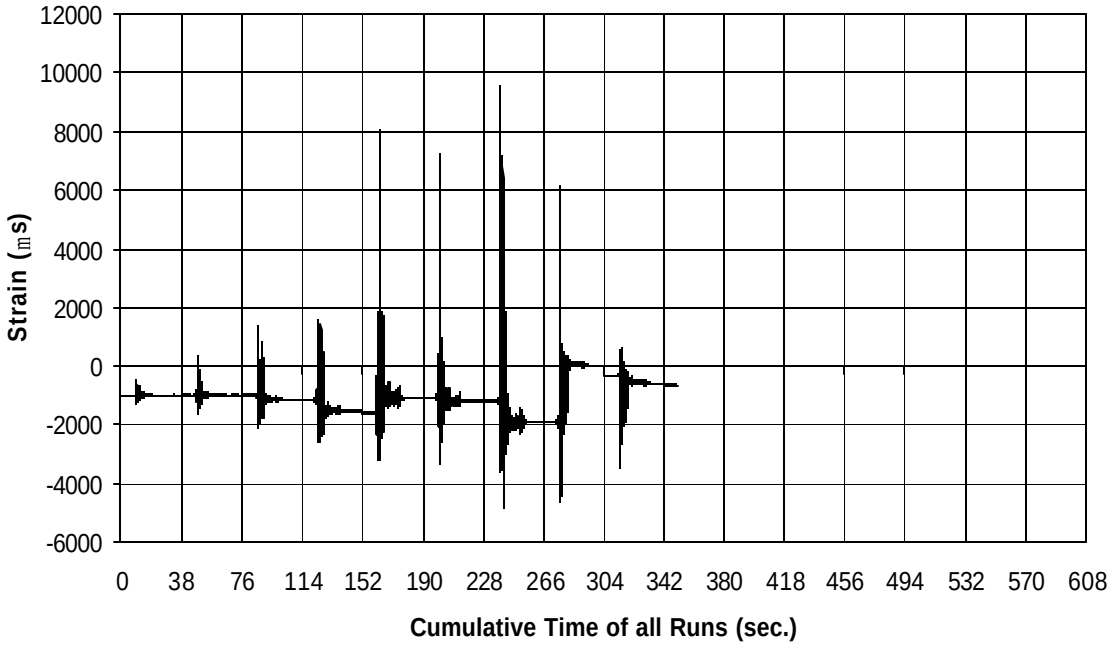

Fig. A-118 THD -2 Measured Strain in Gauge SG5B9

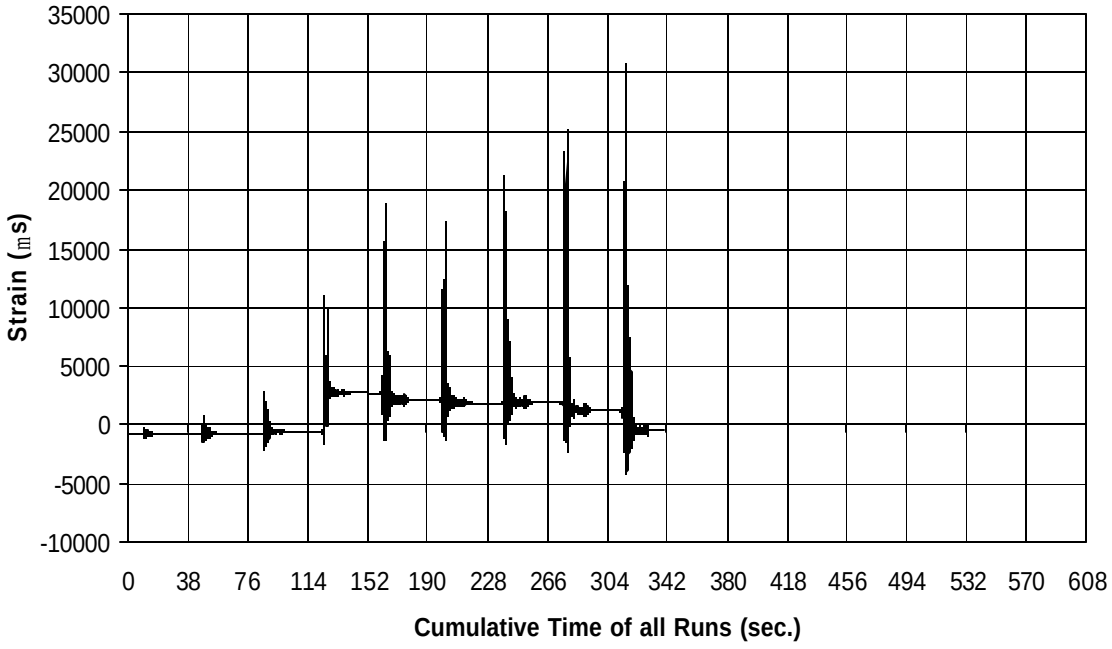

Fig. A-119 THD -2 Measured Strain in Gauge SG6B9

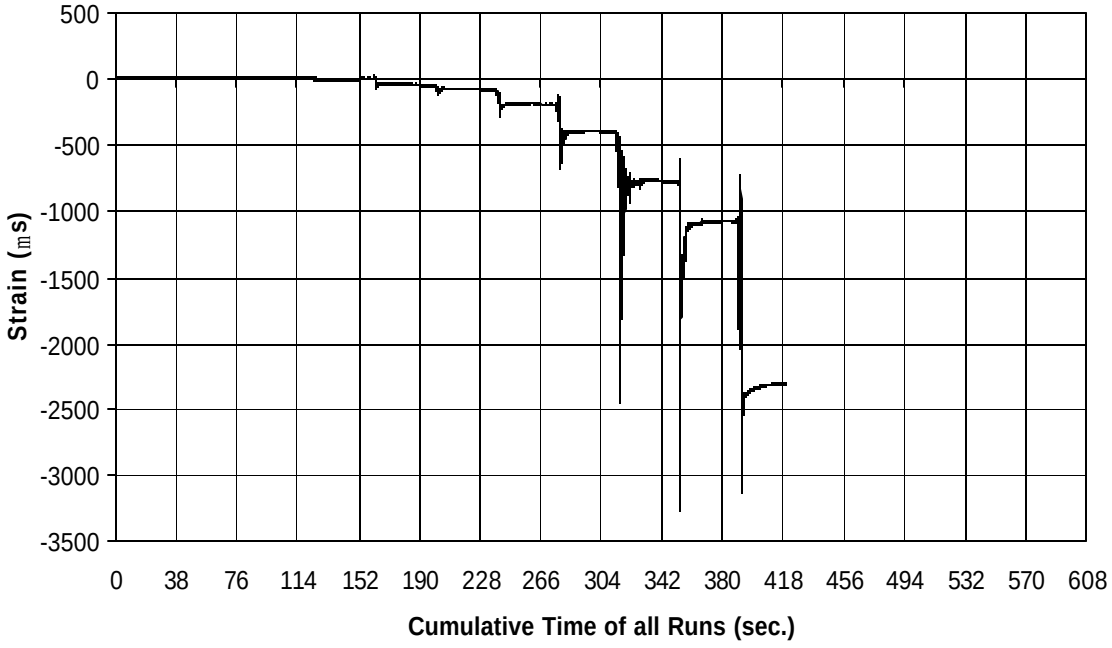

Fig. A-120 THD -2 Measured Strain in Gauge SG7B9

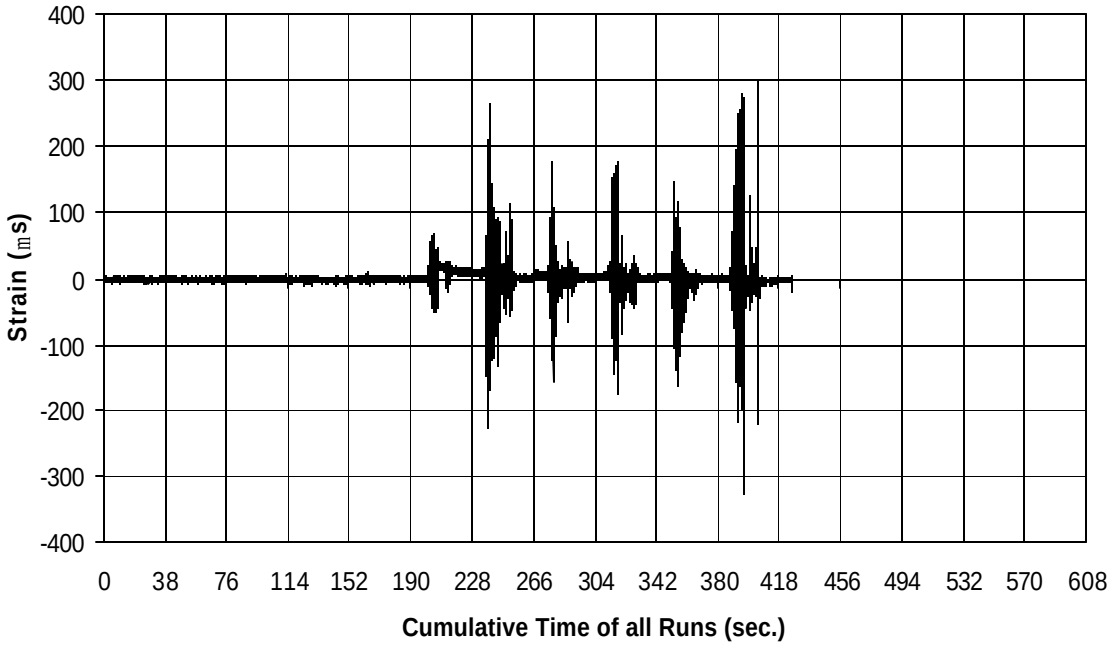

Fig. A-121 THD -2 Measured Strain in Gauge SG8B9

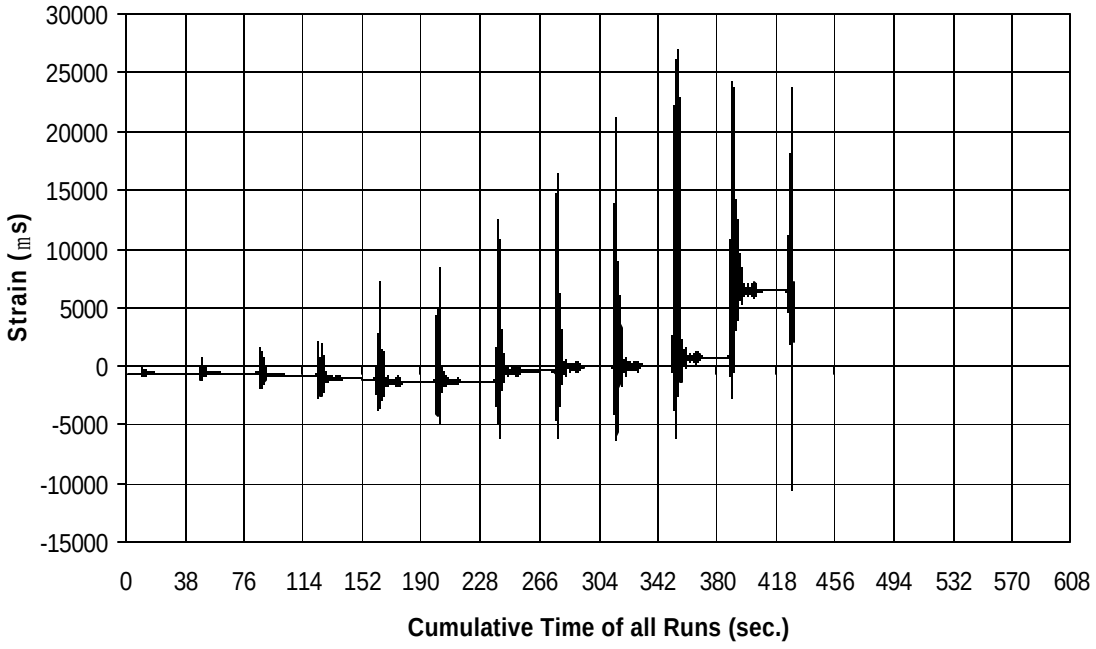

Fig. A-122 THD -2 Measured Strain in Gauge SG1B11

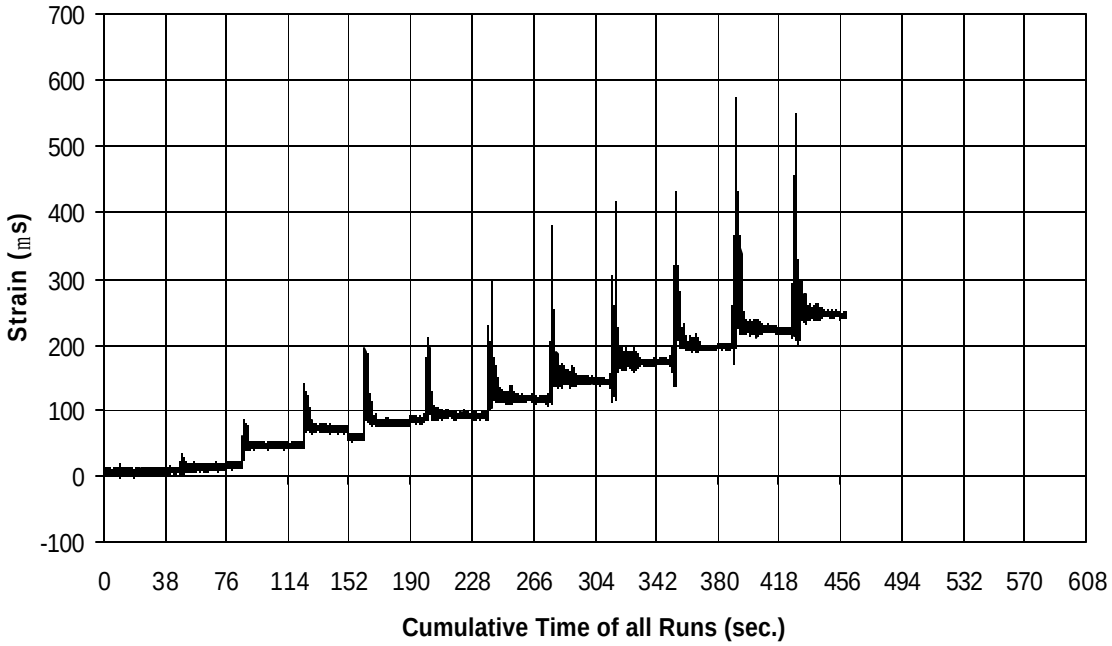

Fig. A-123 THD -2 Measured Strain in Gauge SG2B11

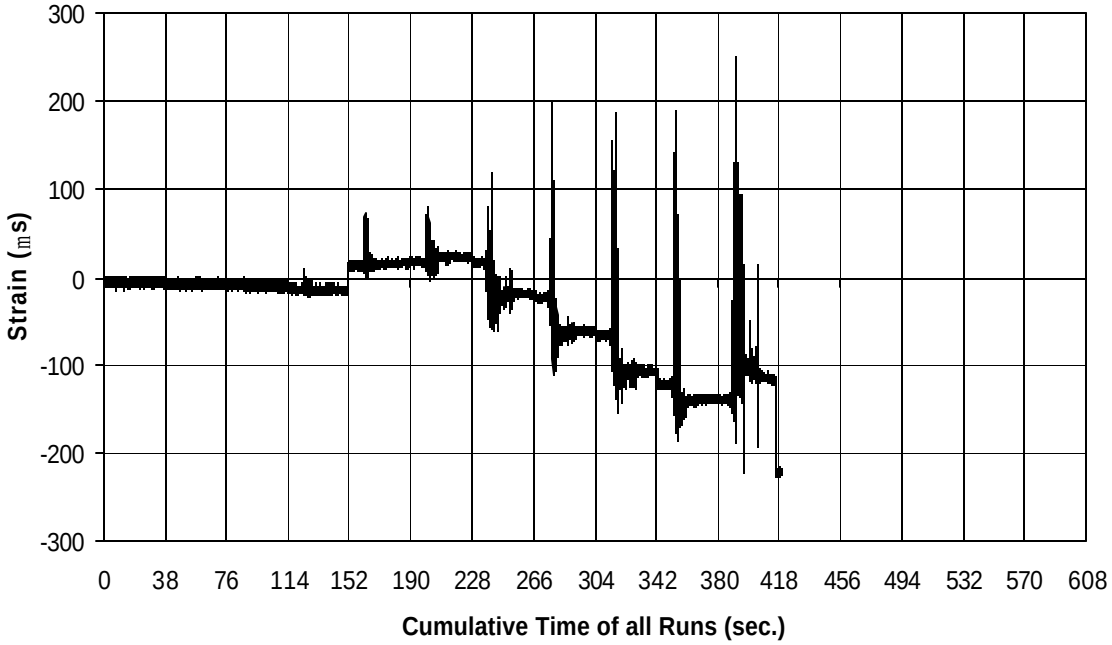

Fig. A-124 THD -2 Measured Strain in Gauge SG3B11

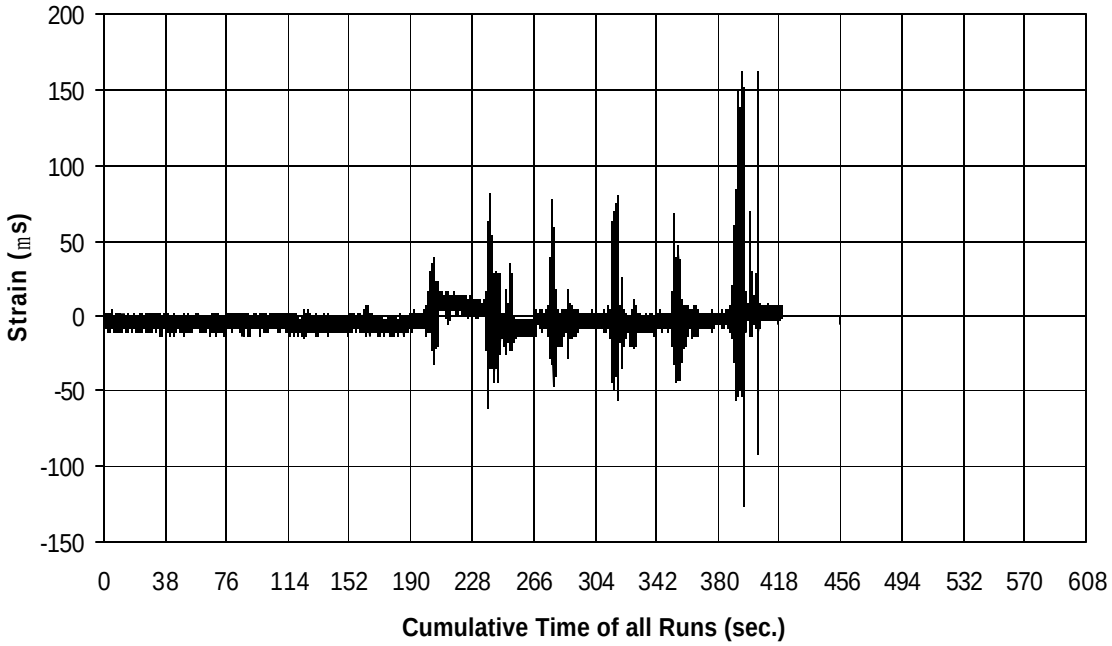

Fig. A-125 THD -2 Measured Strain in Gauge SG4B11

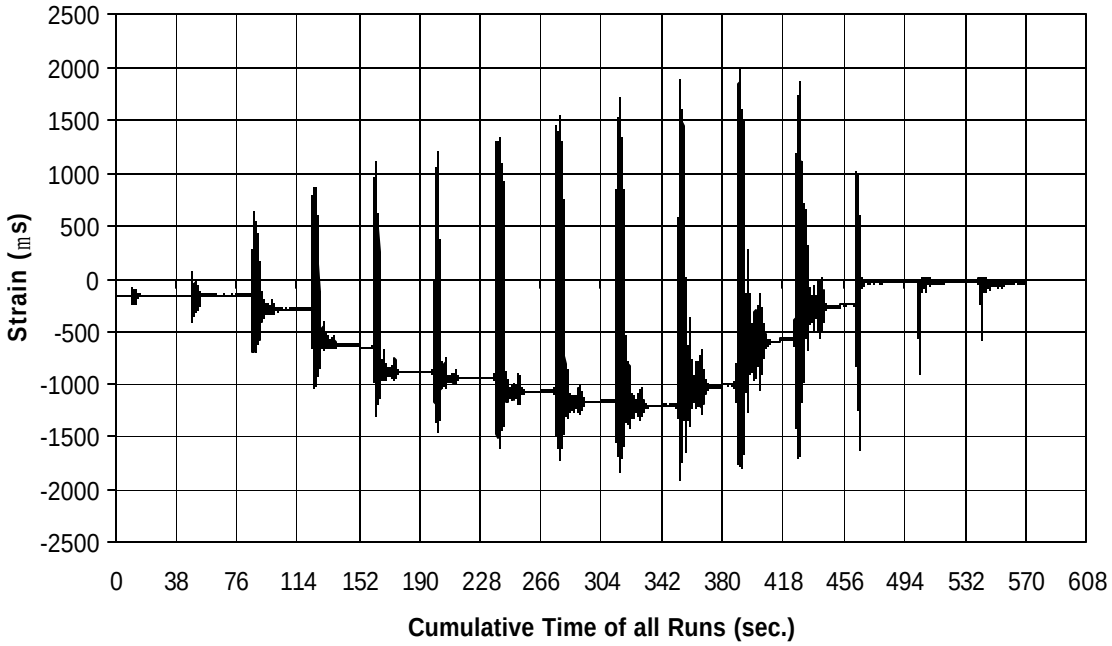

Fig. A-126 THD -2 Measured Strain in Gauge SG5B11

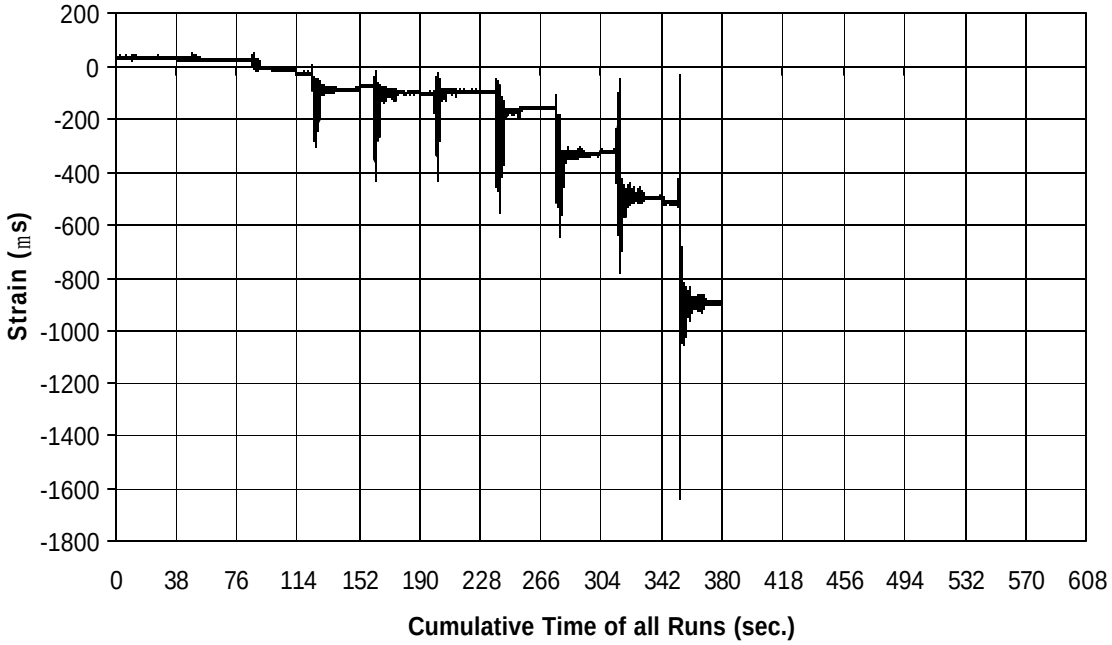

Fig. A-127 THD -2 Measured Strain in Gauge SG6B11

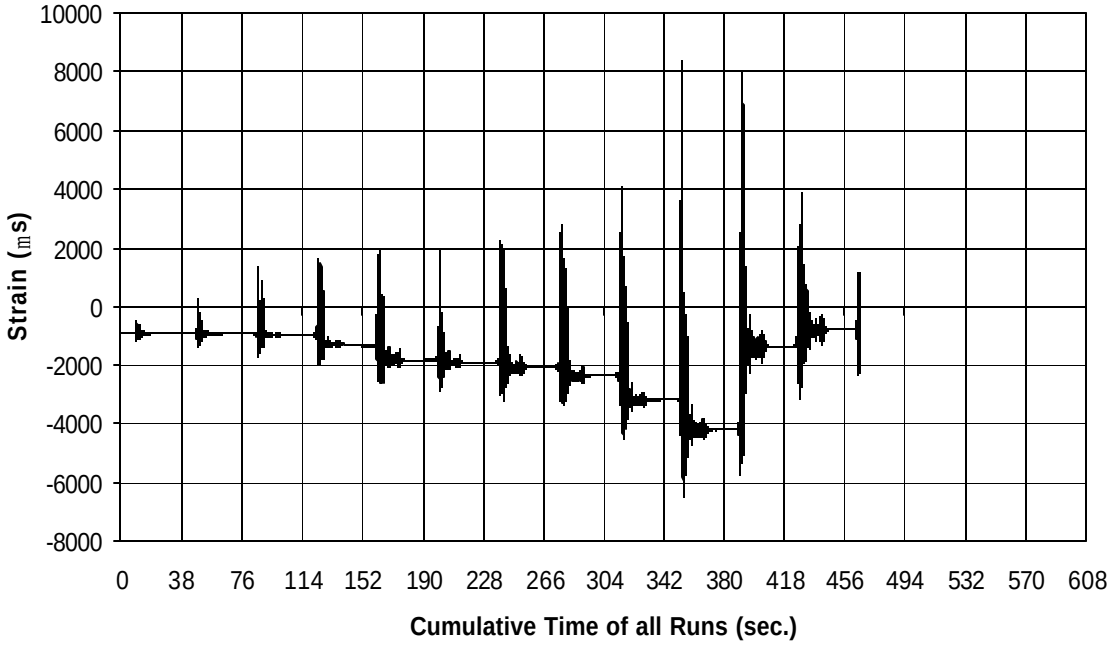

Fig. A-128 THD -2 Measured Strain in Gauge SG7B11

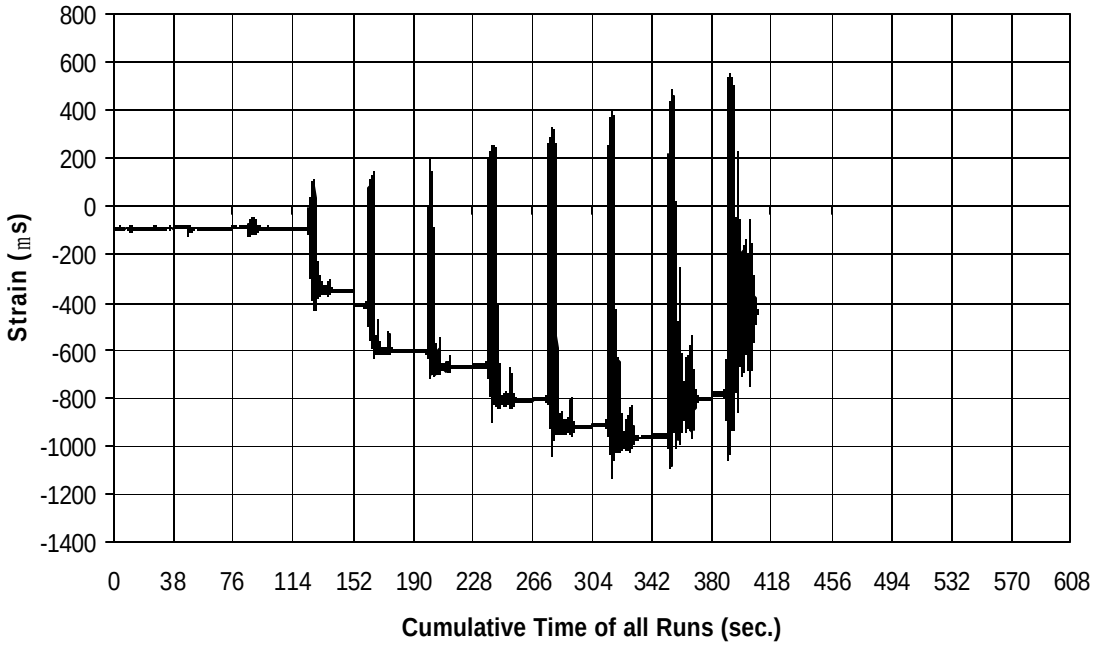

Fig. A-129 THD -2 Measured Strain in Gauge SG8B11

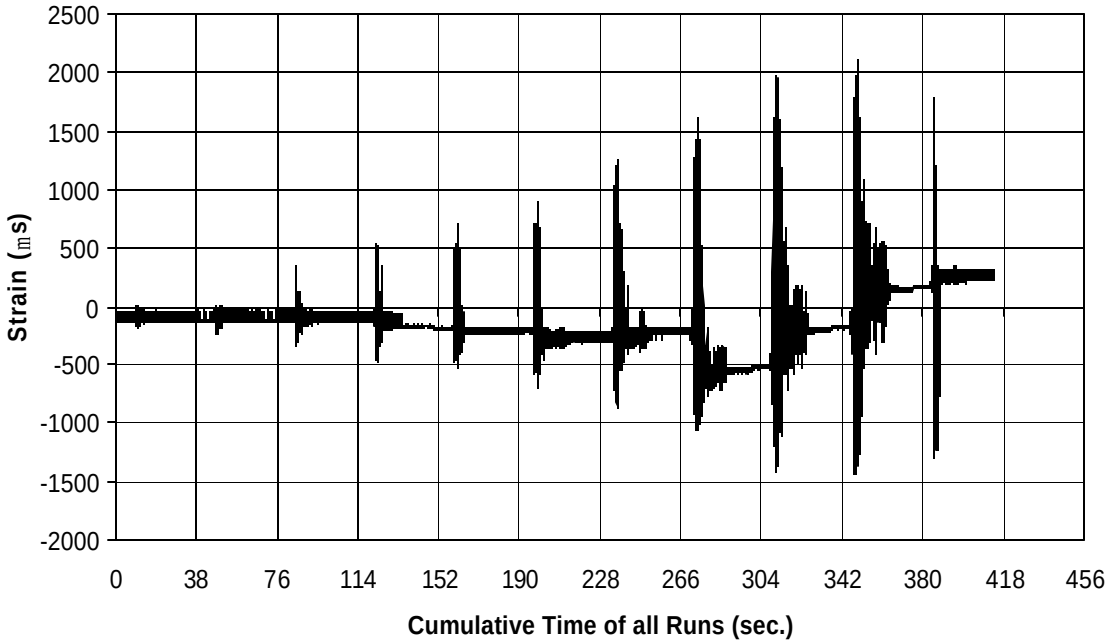

Fig. A-130 THD -3 Measured Strain in Gauge SG1

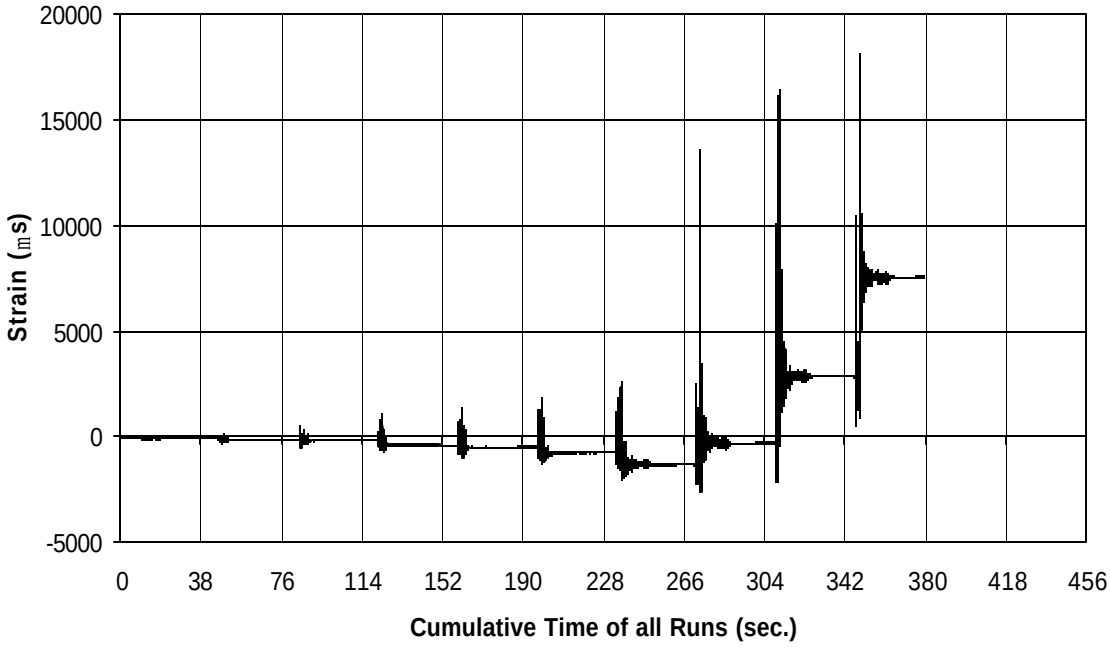

Fig. A-131 THD -3 Measured Strain in Gauge SG2

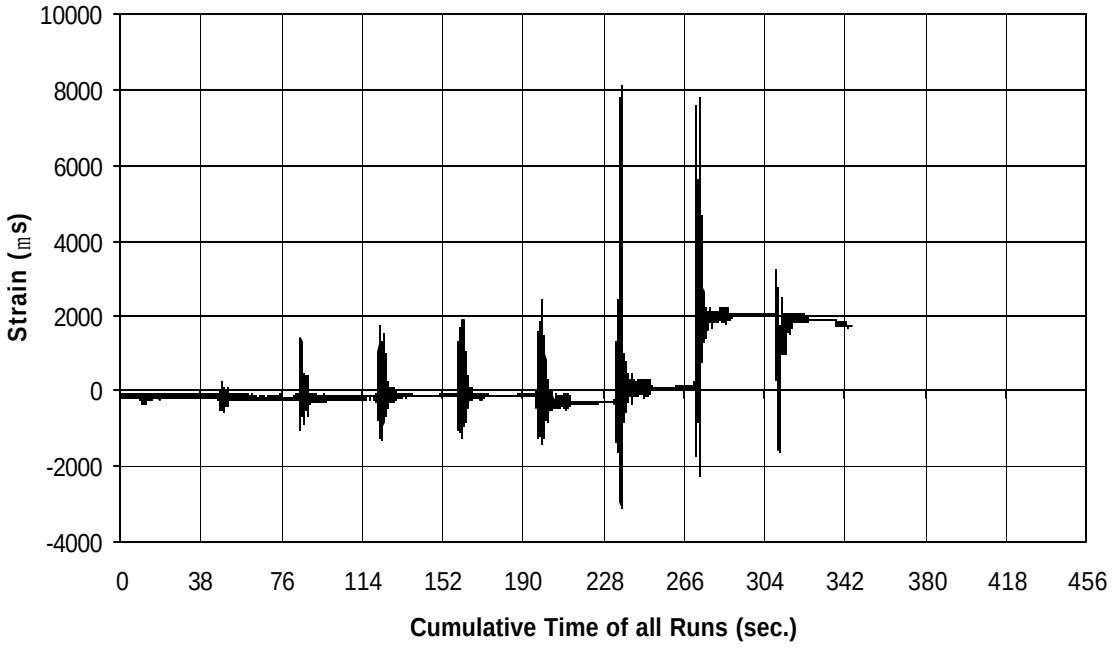

Fig. A-132 THD -3 Measured Strain in Gauge SG3

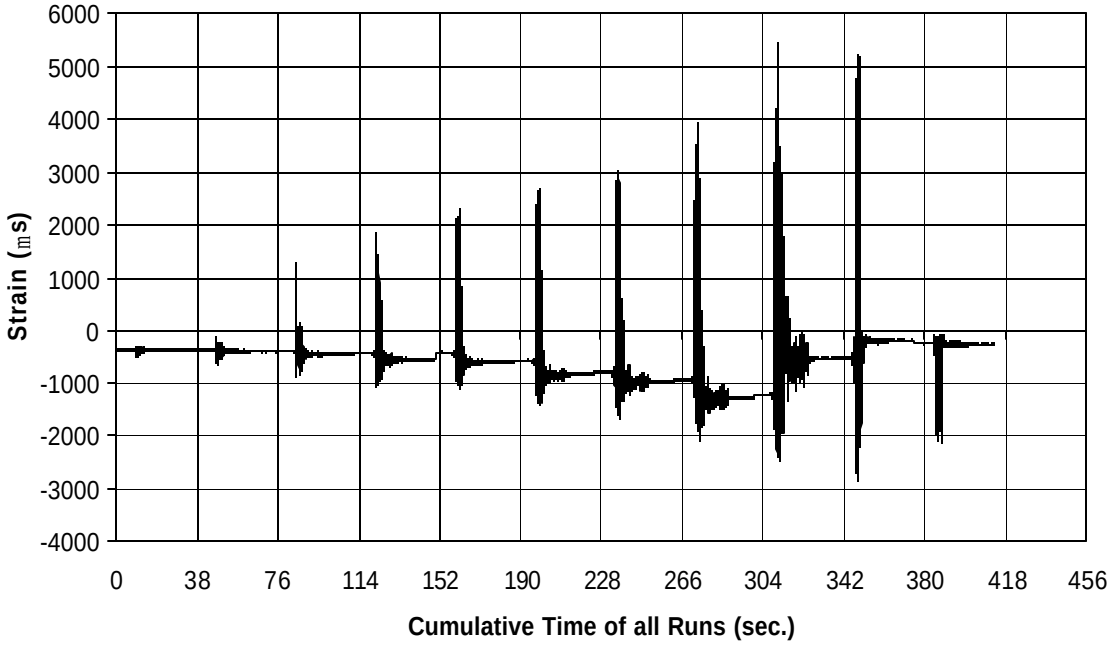

Fig. A-133 THD -3 Measured Strain in Gauge SG4

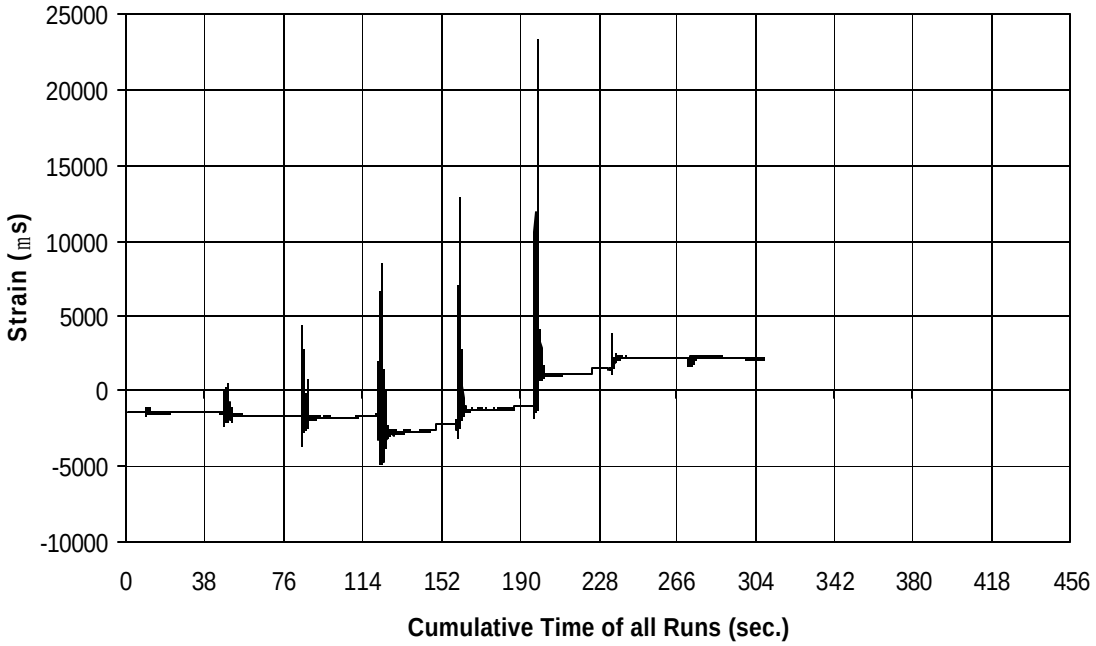

Fig. A-134 THD -3 Measured Strain in Gauge SG5

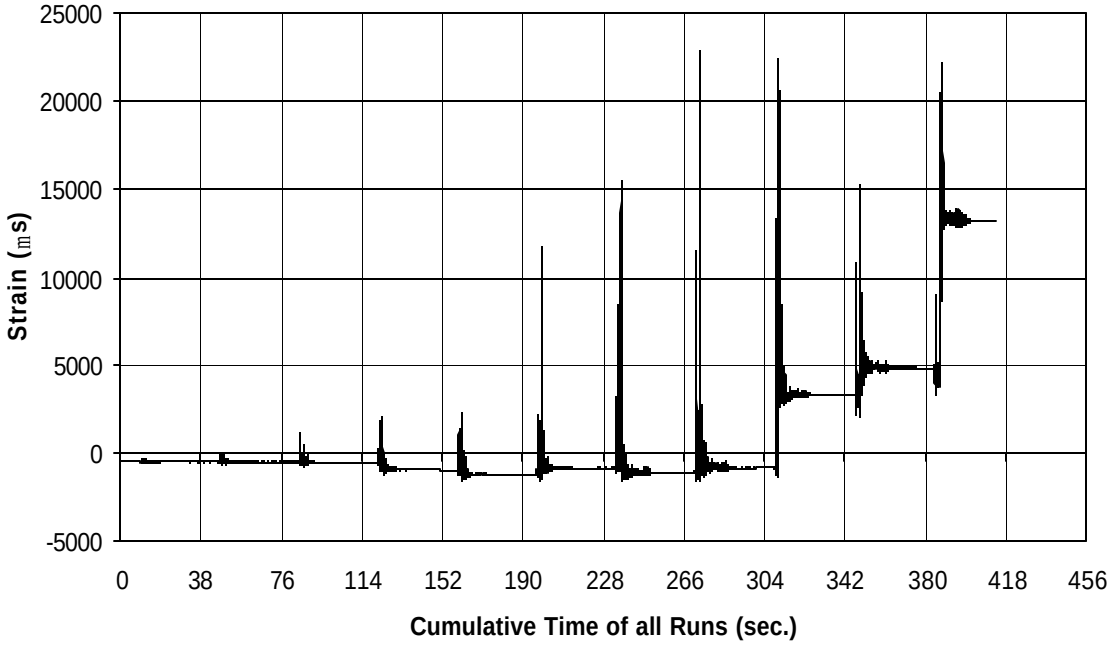

Fig. A-135 THD -3 Measured Strain in Gauge SG6

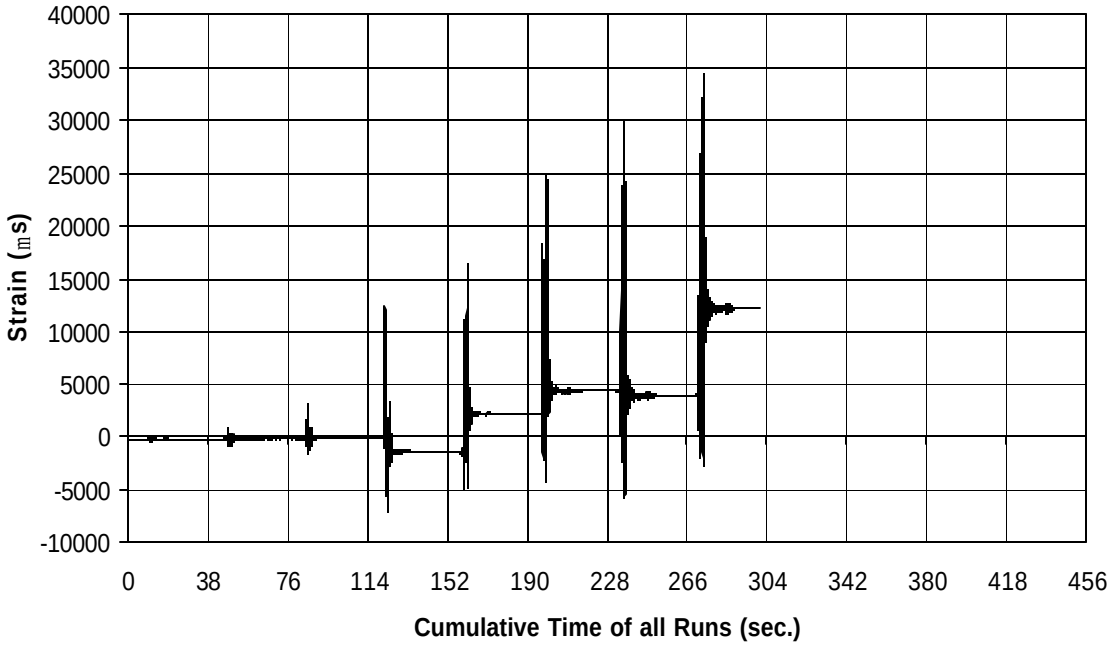

Fig. A-136 THD -3 Measured Strain in Gauge SG7

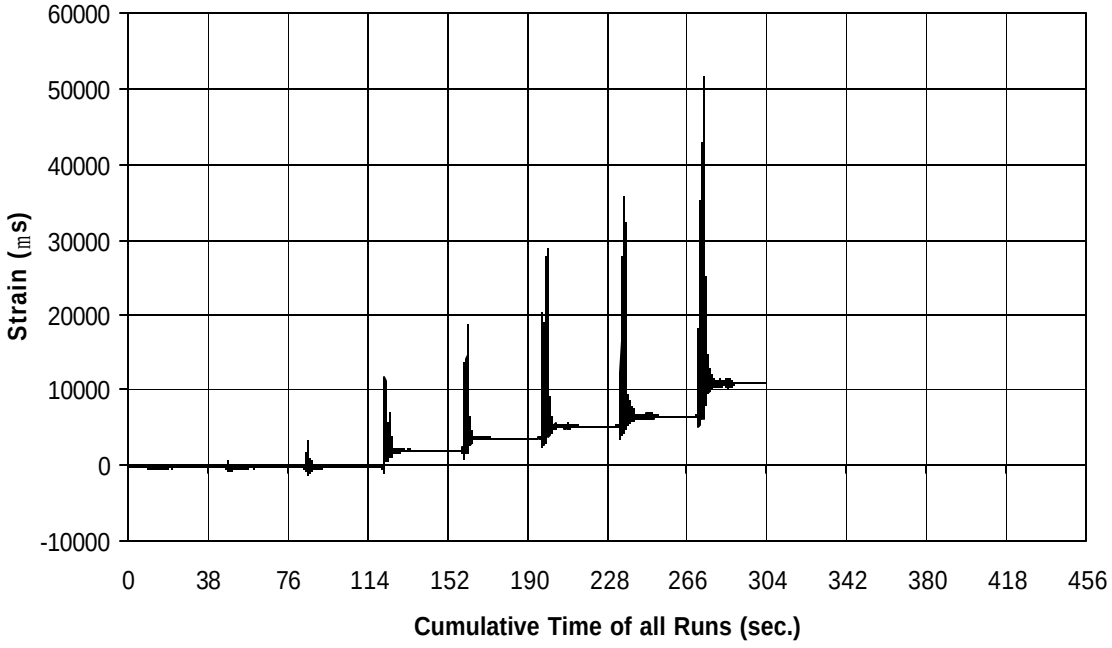

Fig. A-137 THD -3 Measured Strain in Gauge SG8

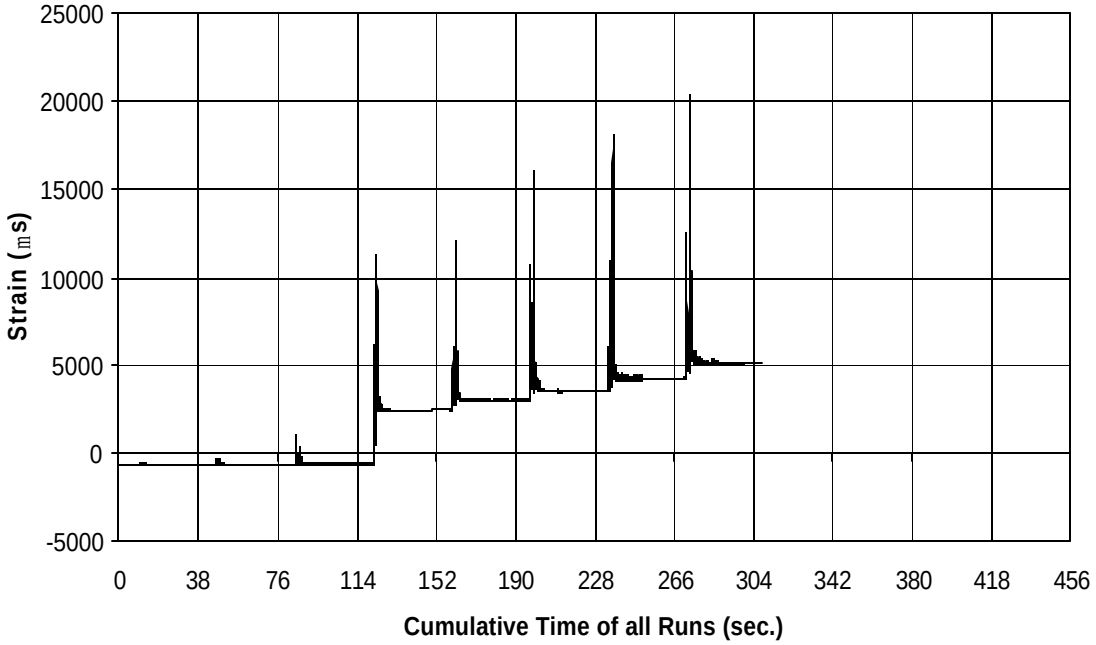

Fig. A-138 THD -3 Measured Strain in Gauge SG9

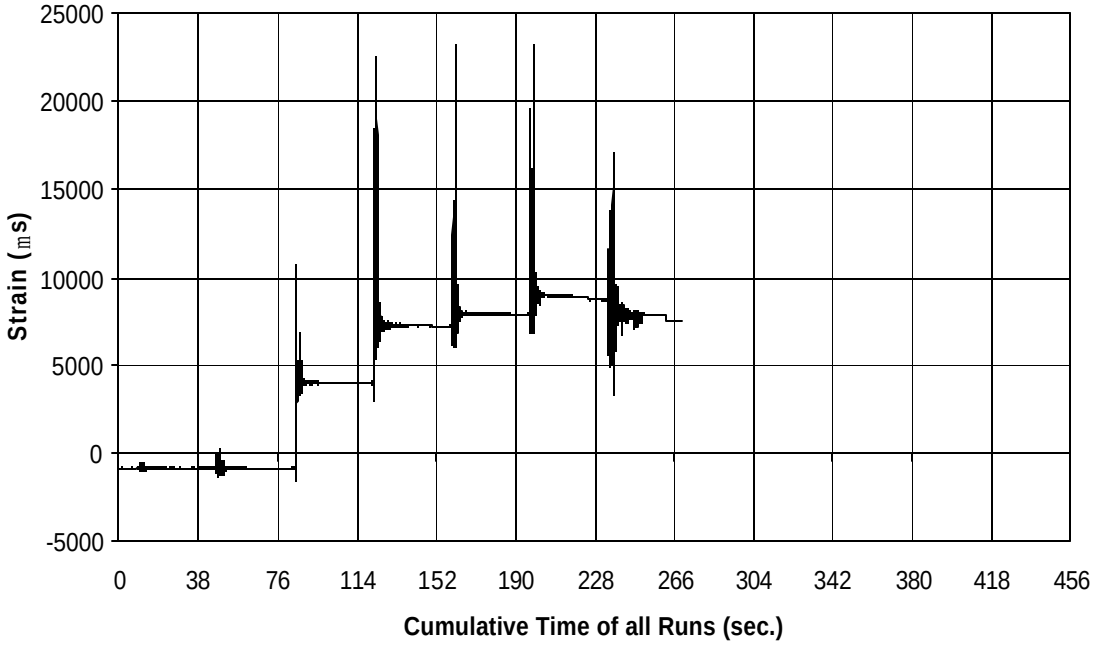

Fig. A-139 THD -3 Measured Strain in Gauge SG10

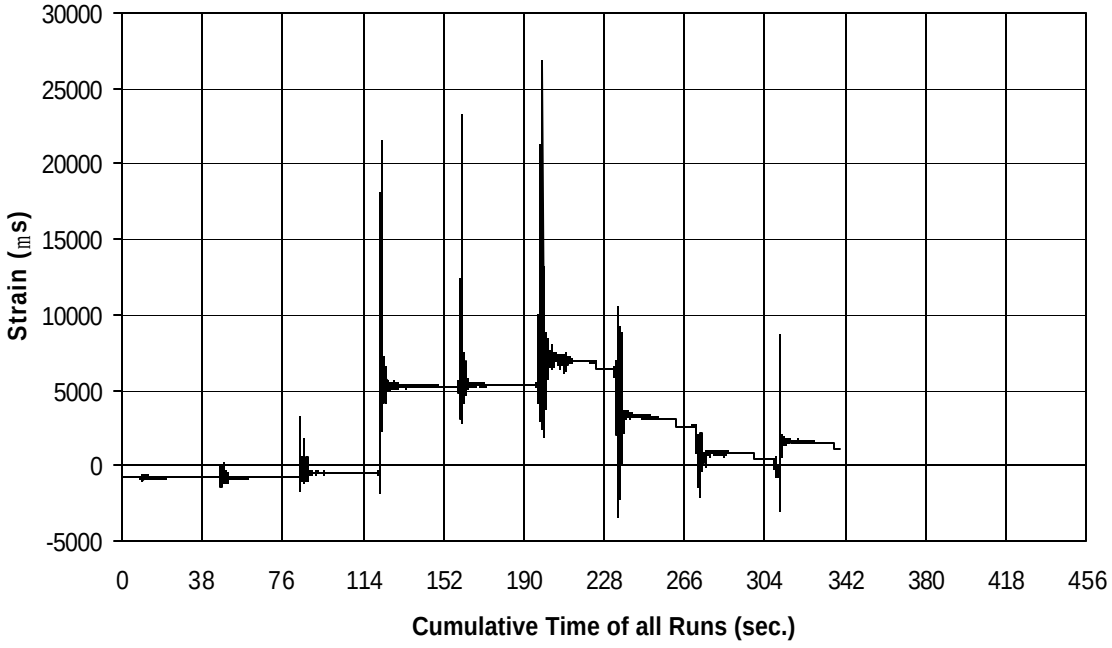

Fig. A-140 THD -3 Measured Strain in Gauge SG11

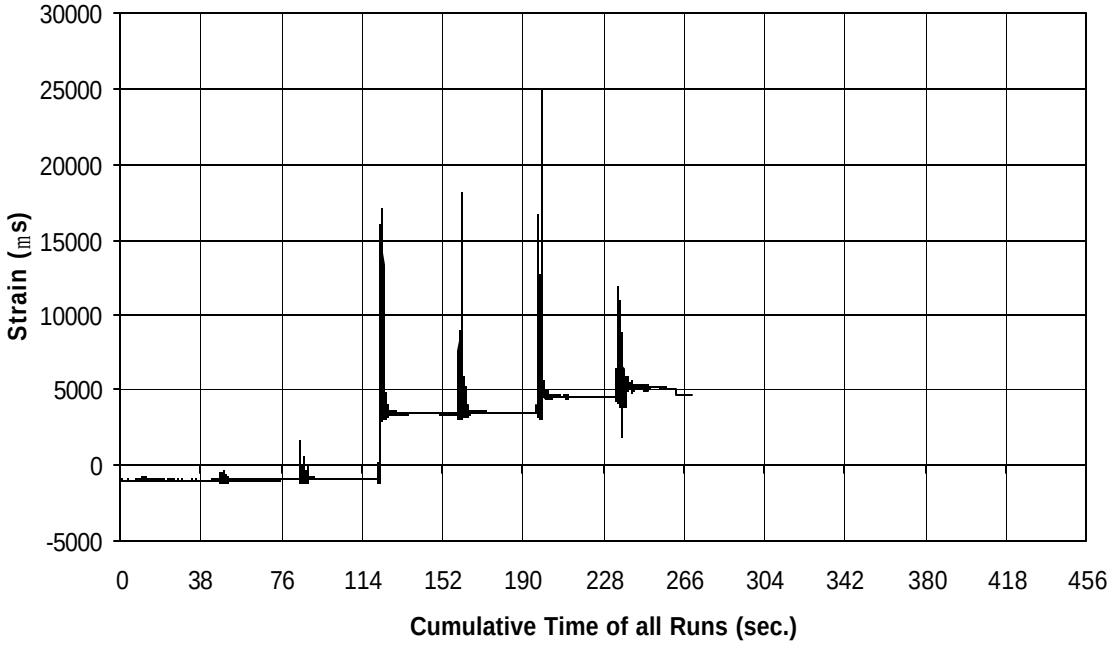

Fig. A-141 THD -3 Measured Strain in Gauge SG12

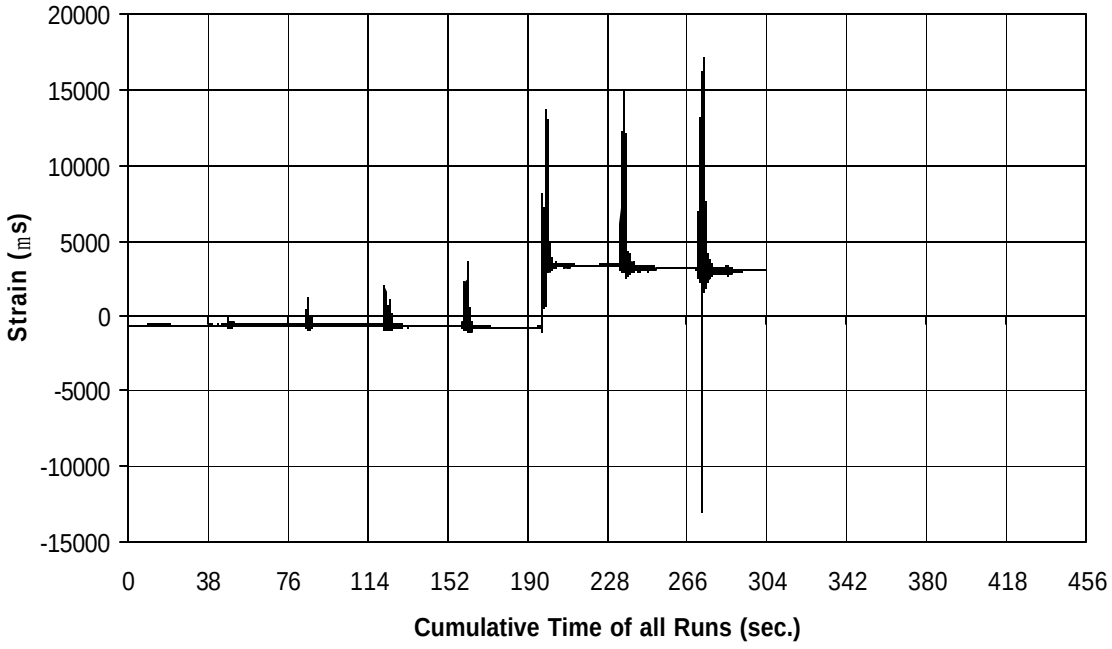

Fig. A-142 THD -3 Measured Strain in Gauge SG13

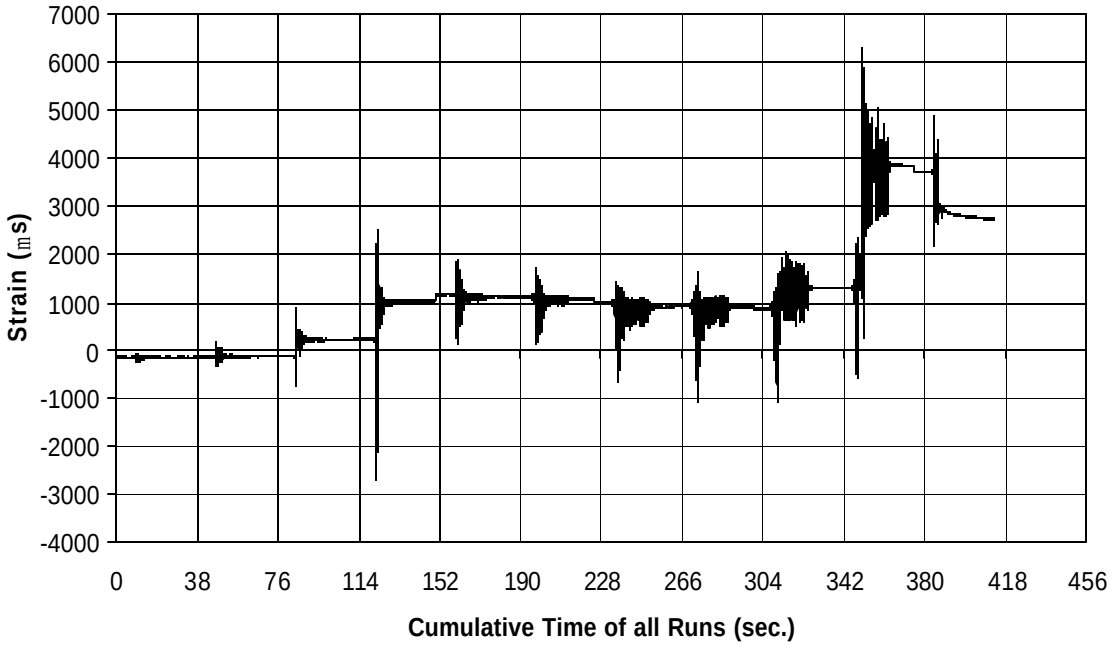

Fig. A-143 THD -3 Measured Strain in Gauge SG14

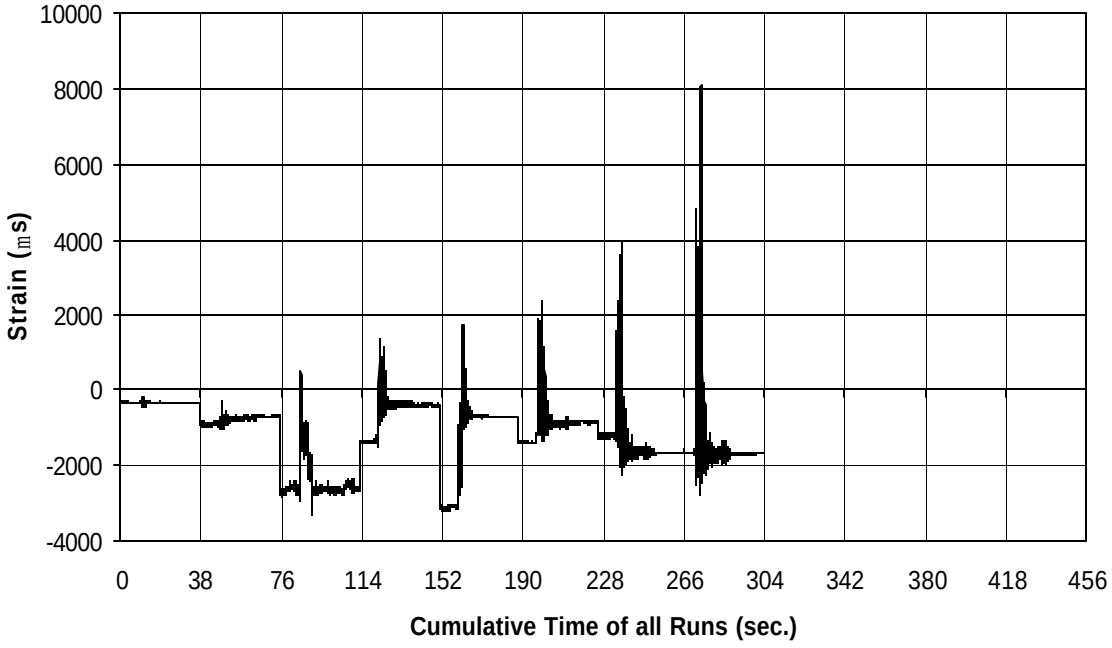

Fig. A-144 THD -3 Measured Strain in Gauge SG15

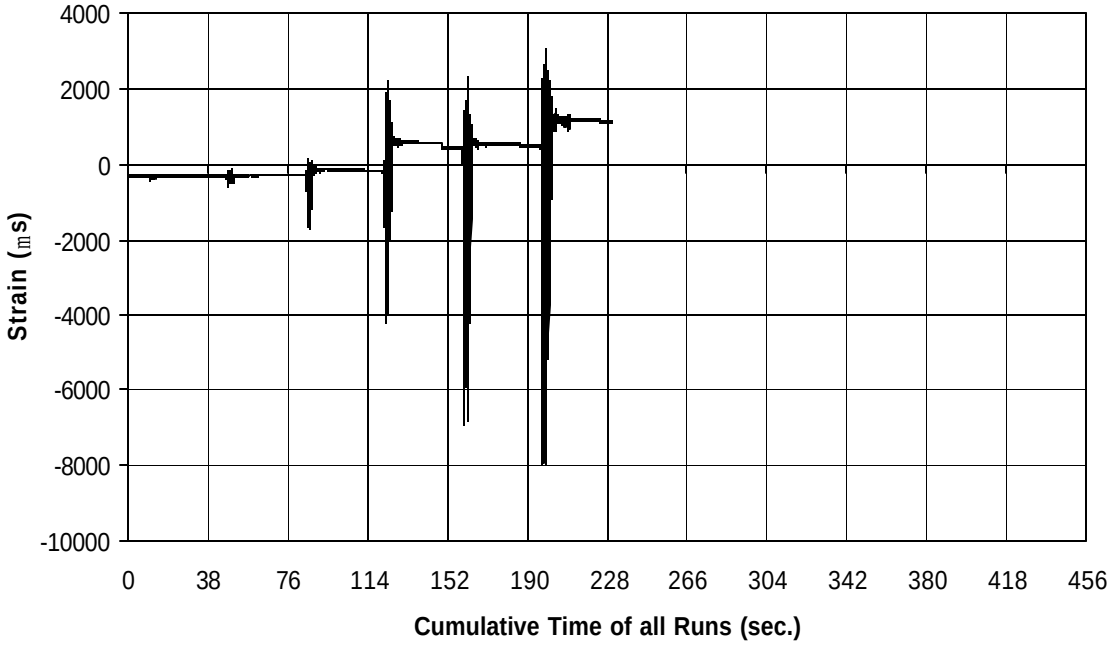

Fig. A-145 THD -3 Measured Strain in Gauge SG16

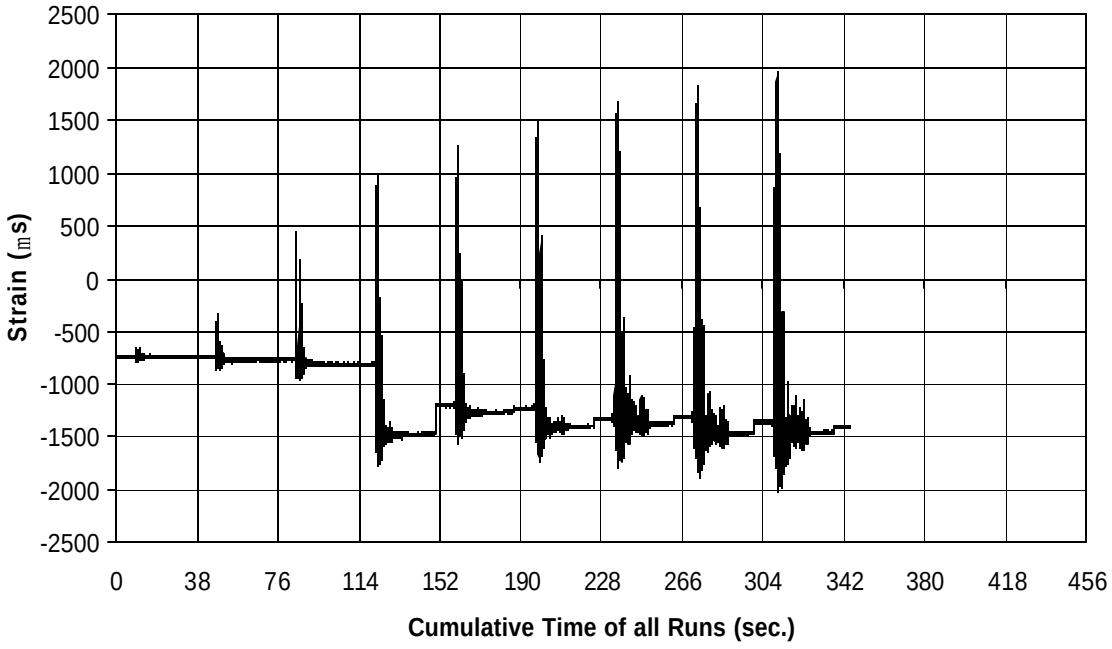

Fig. A-146 THD -3 Measured Strain in Gauge SG17

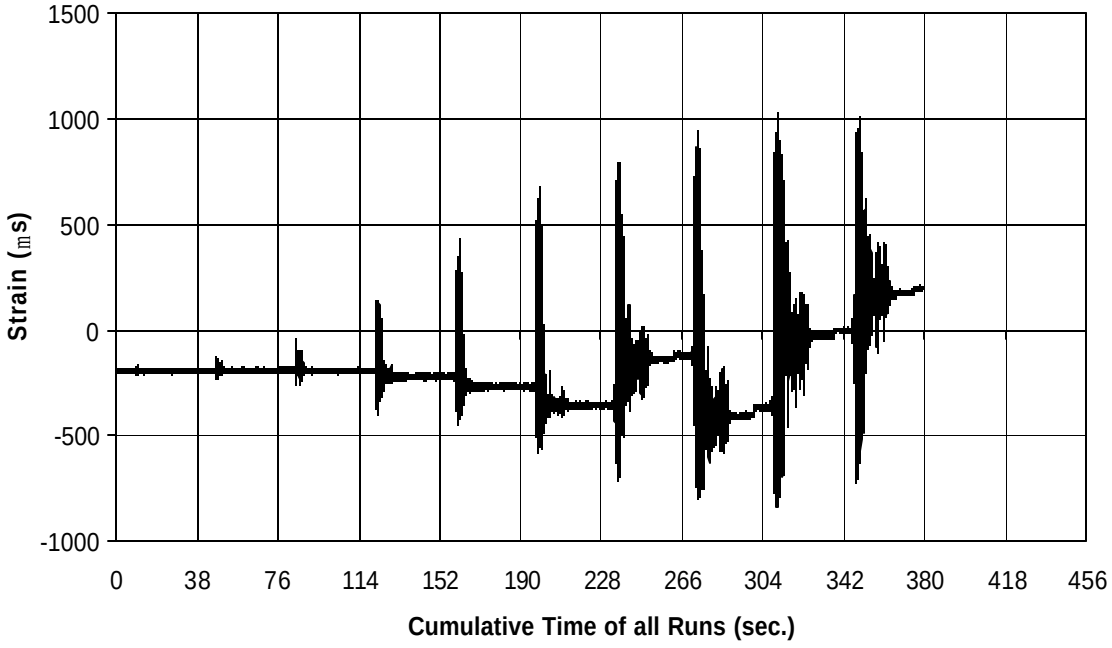

Fig. A-147 THD -3 Measured Strain in Gauge SG18

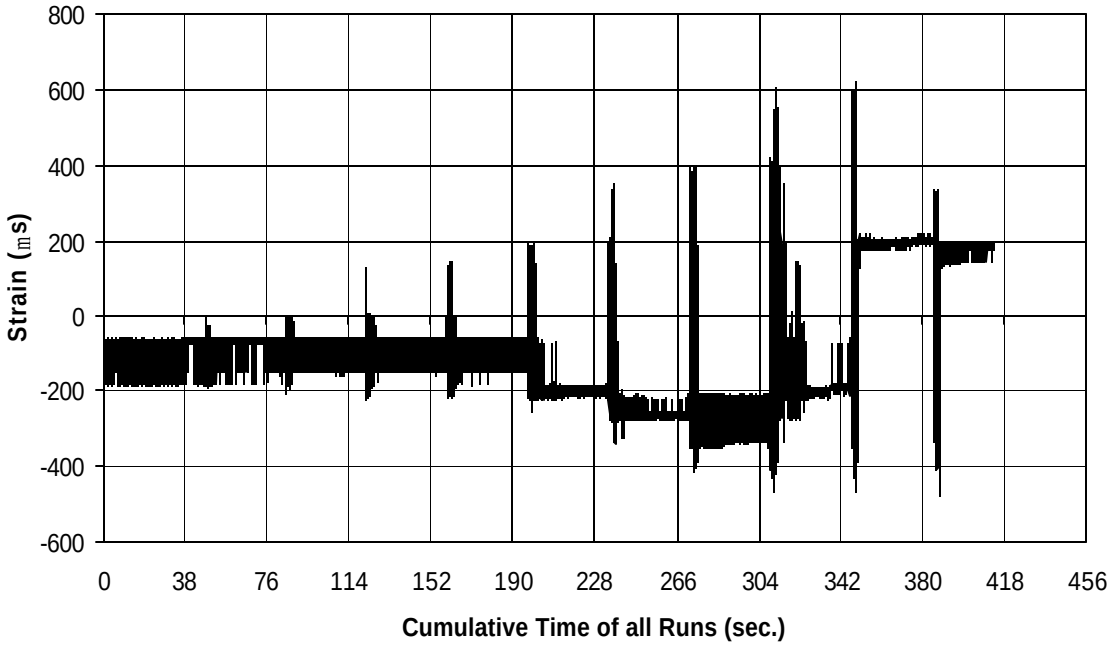

Fig. A-148 THD -3 Measured Strain in Gauge SG19

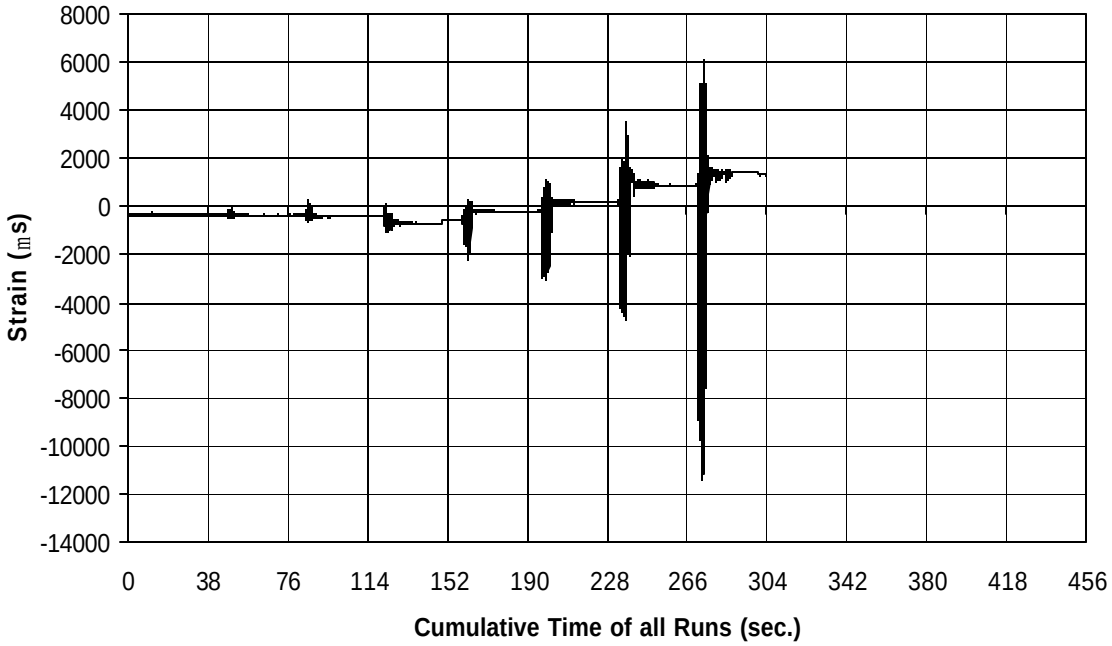

Fig. A-149 THD -3 Measured Strain in Gauge SG20

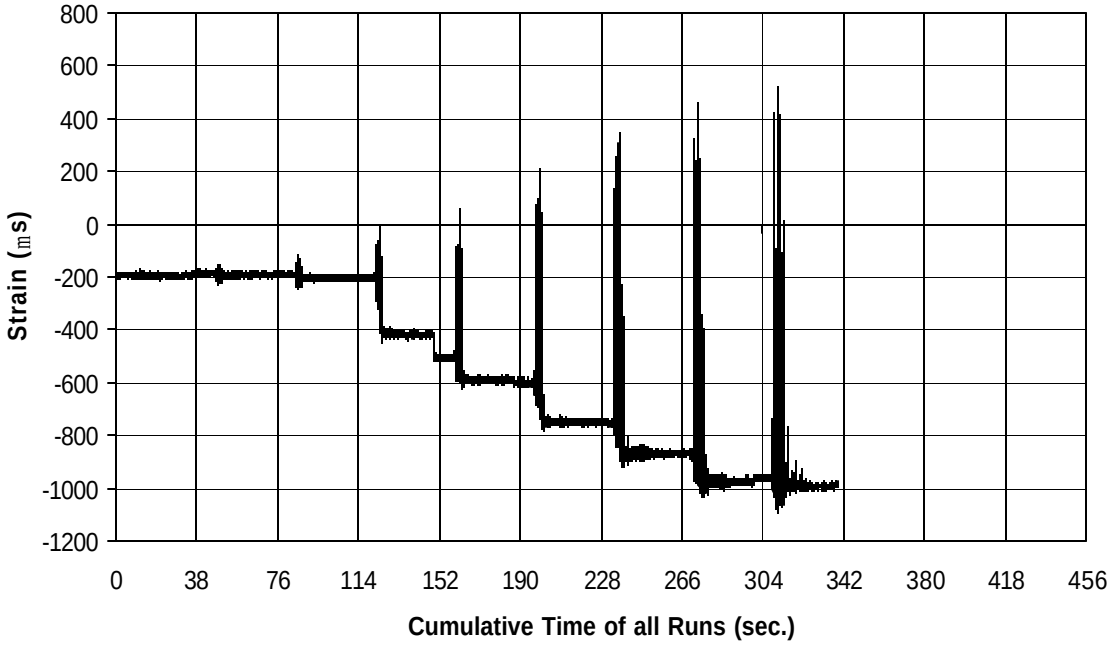

Fig. A-150 THD -3 Measured Strain in Gauge SG21

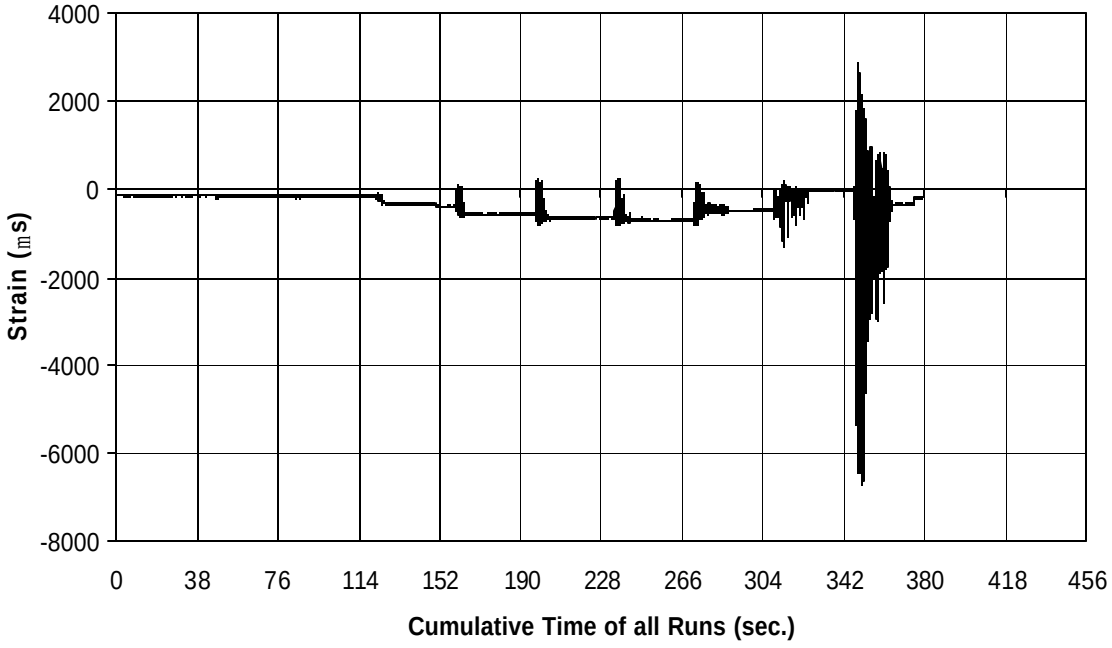

Fig. A-151 THD -3 Measured Strain in Gauge SG22

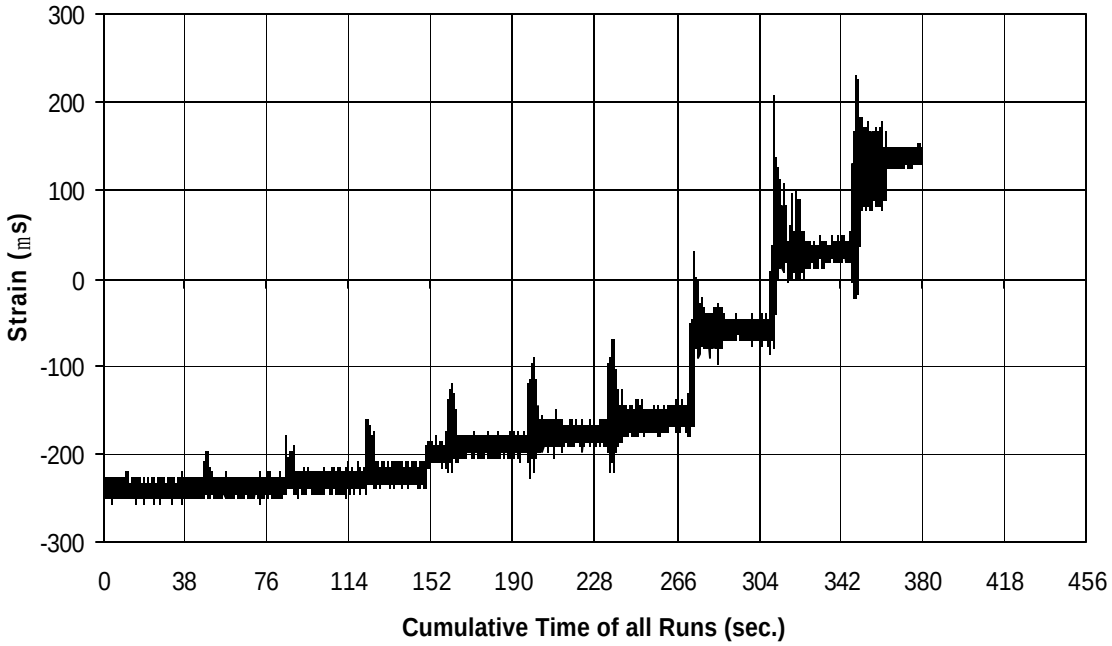

Fig. A-152 THD -3 Measured Strain in Gauge SG23

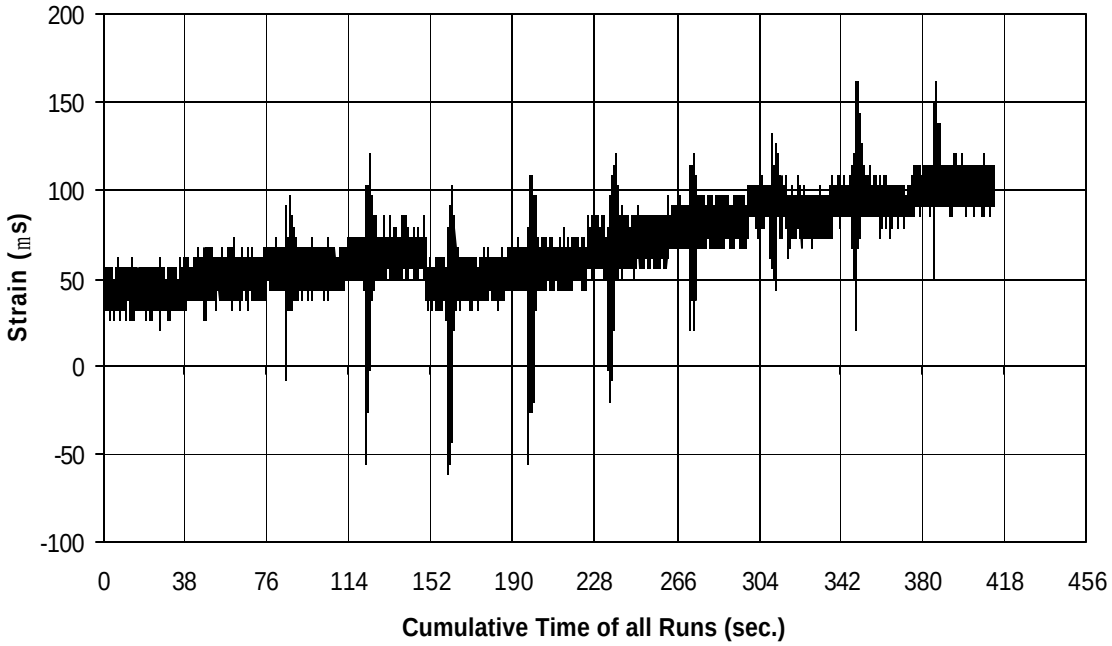

Fig. A-153 THD -3 Measured Strain in Gauge SG24

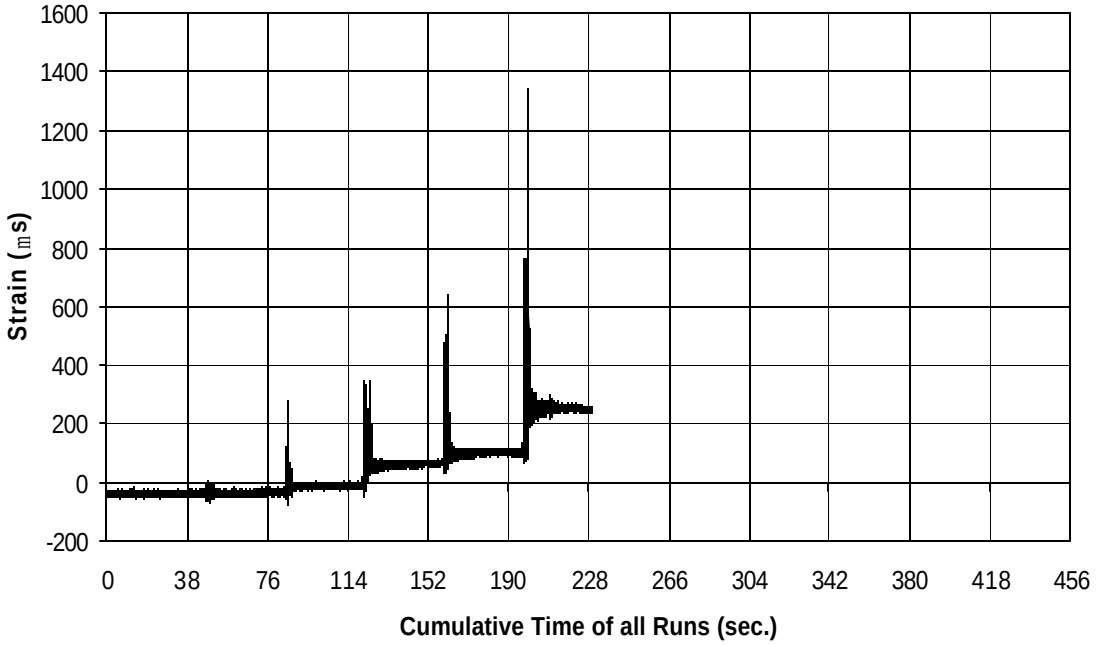

Fig. A-154 THD -3 Measured Strain in Gauge SG26

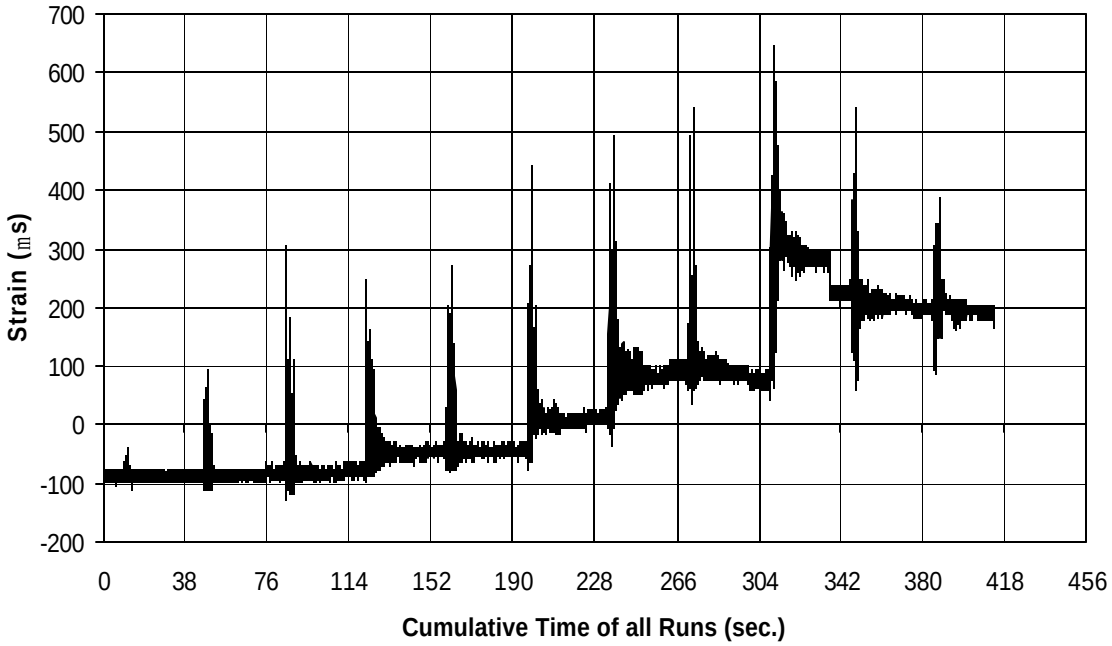

Fig. A-155 THD -3 Measured Strain in Gauge SG27

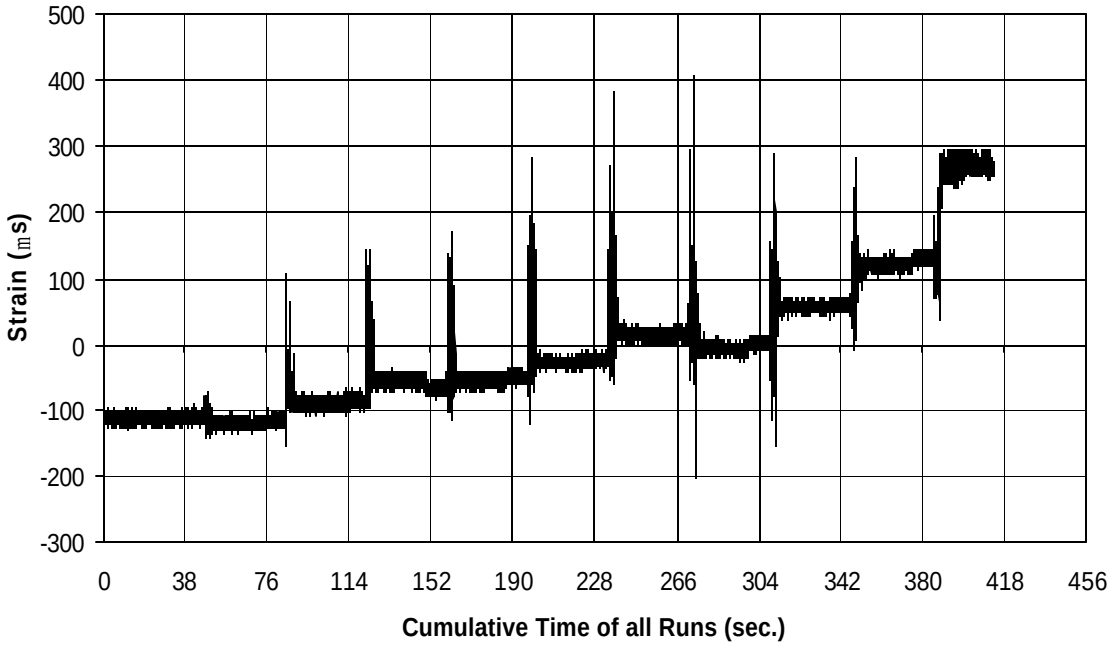

Fig. A-156 THD -3 Measured Strain in Gauge SG28

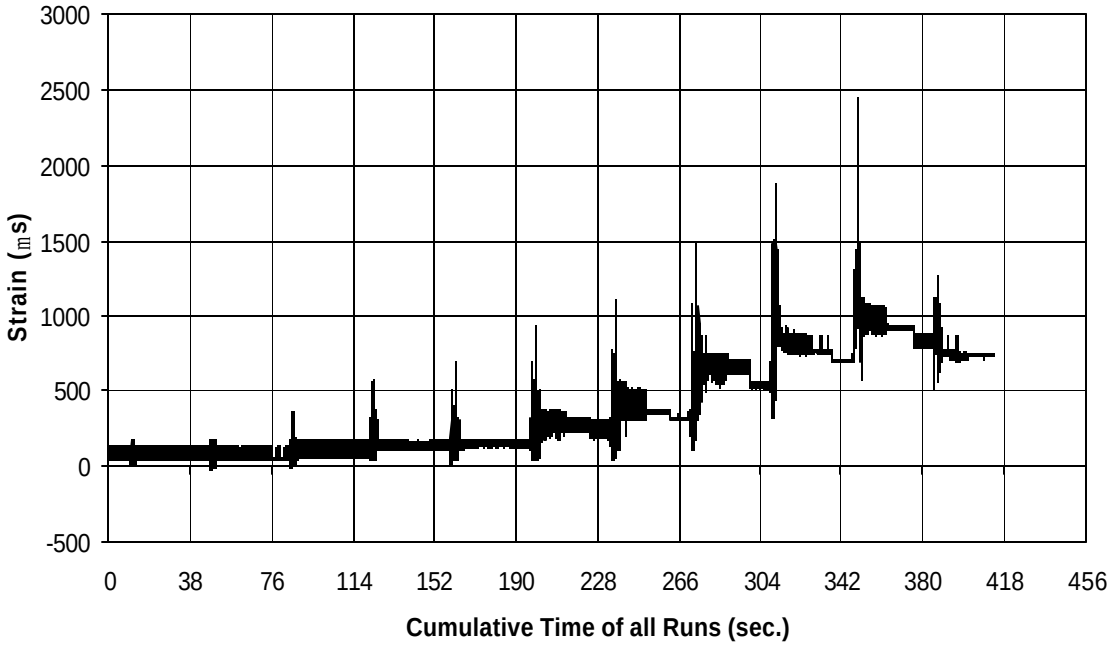

Fig. A-157 THD -3 Measured Strain in Gauge SG29

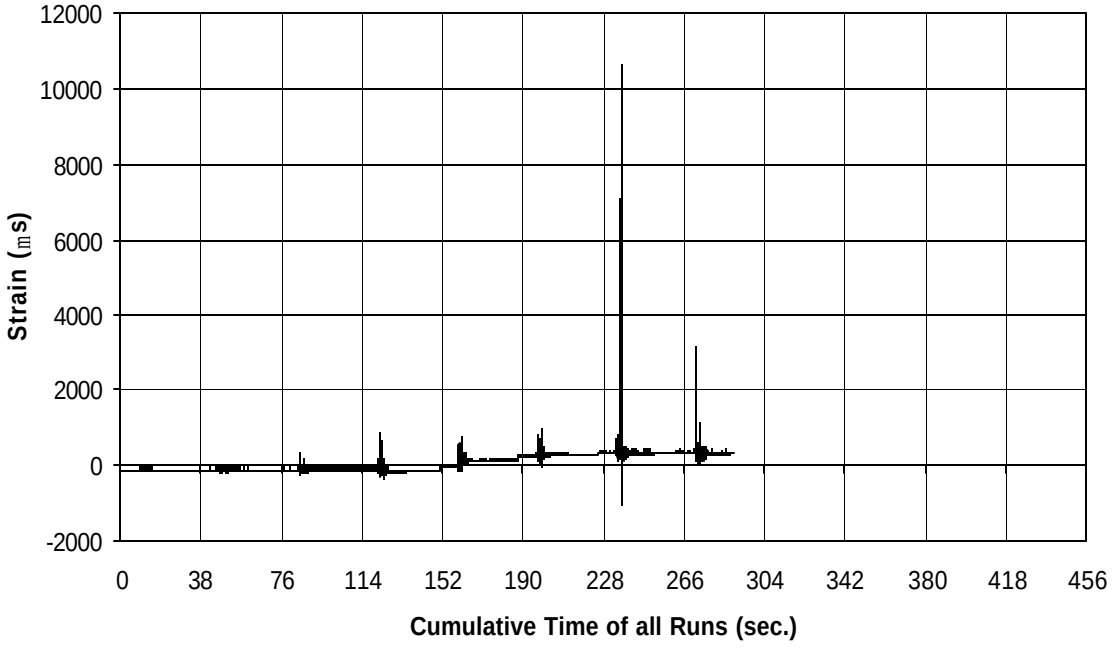

Fig. A-158 THD -3 Measured Strain in Gauge SG30

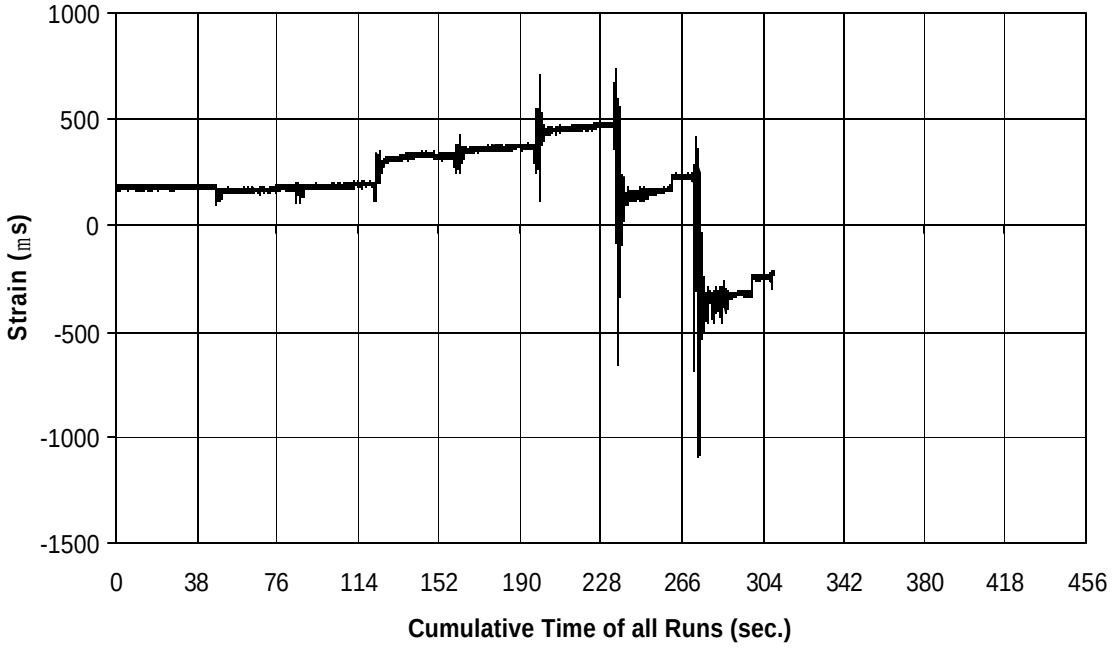

Fig. A-159 THD -3 Measured Strain in Gauge SG31

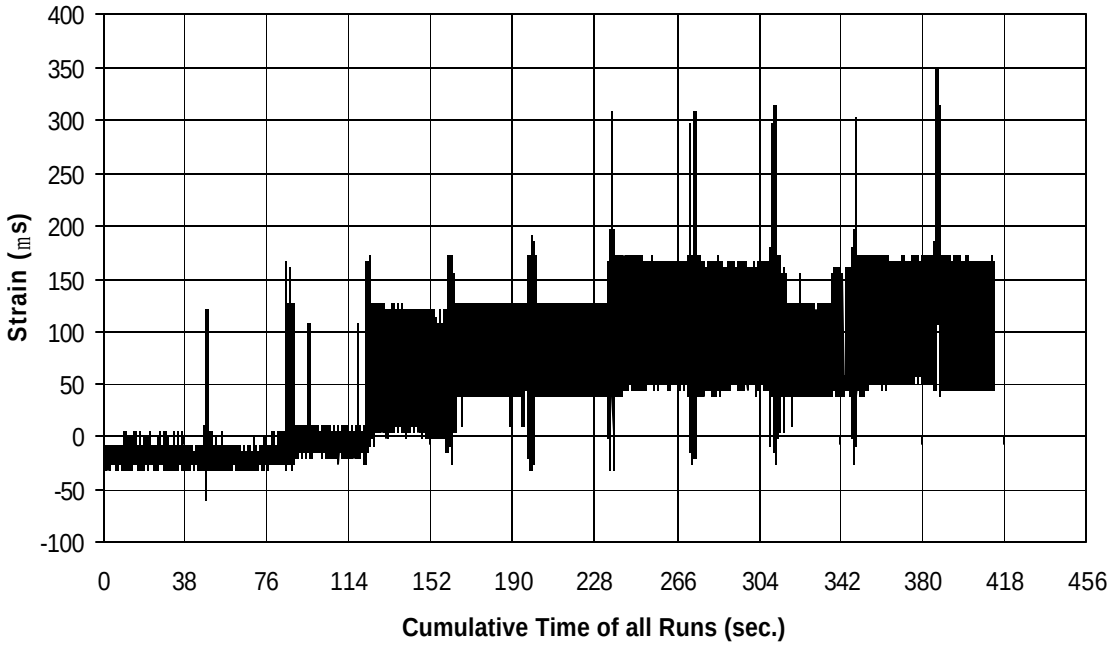

Fig. A-160 THD -3 Measured Strain in Gauge SG32

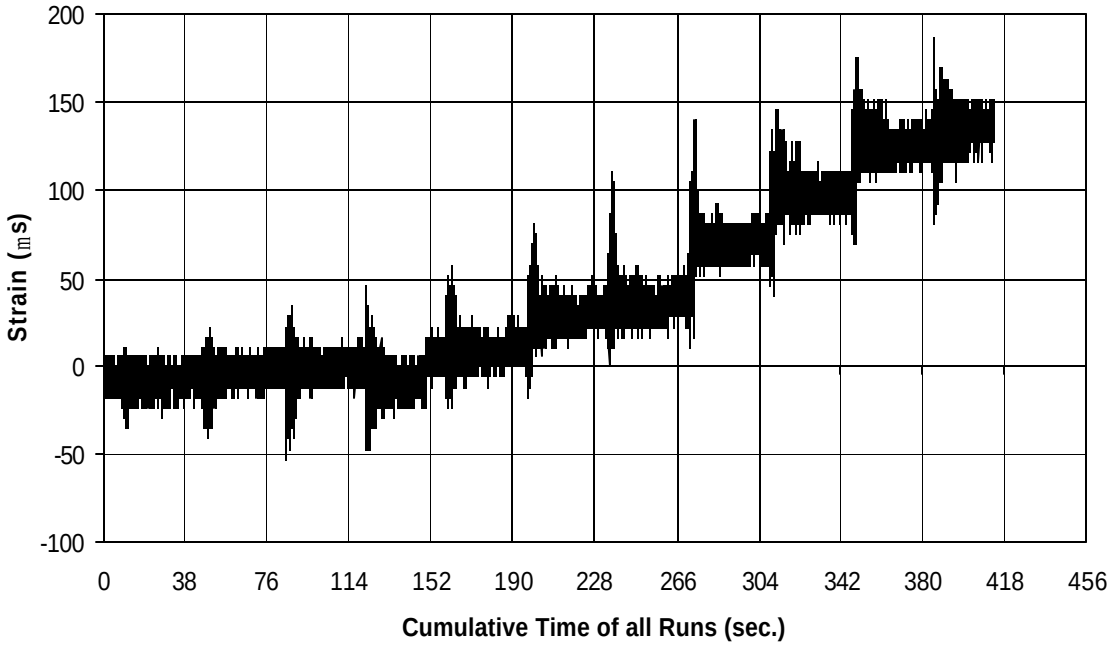

Fig. A-161 THD -3 Measured Strain in Gauge SG33

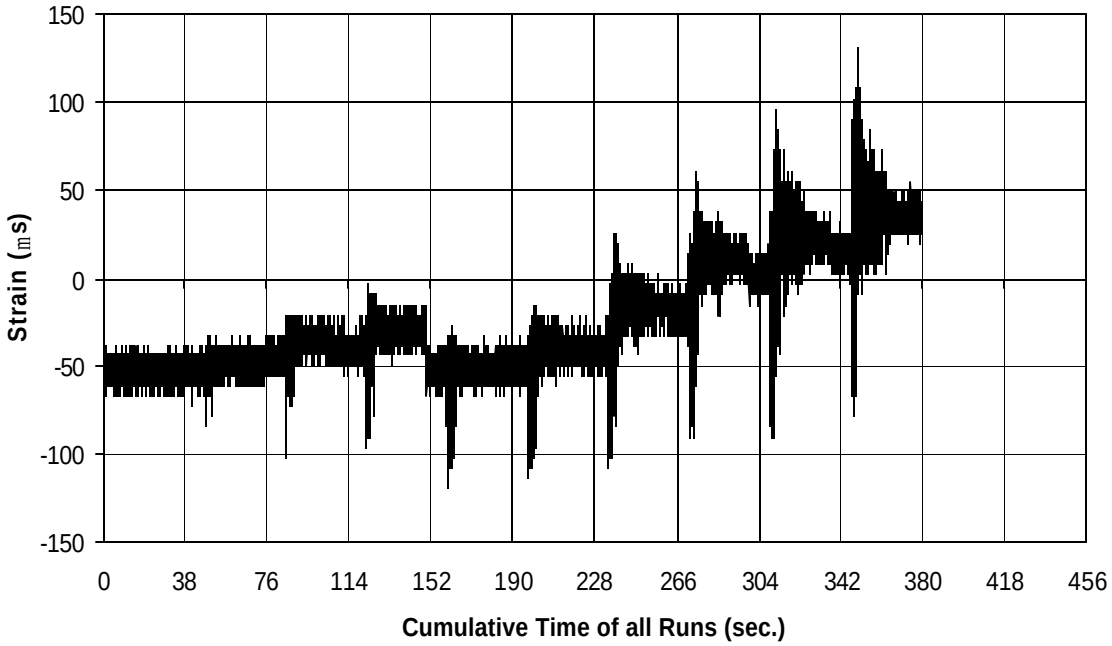

Fig. A-162 THD -3 Measured Strain in Gauge SG34

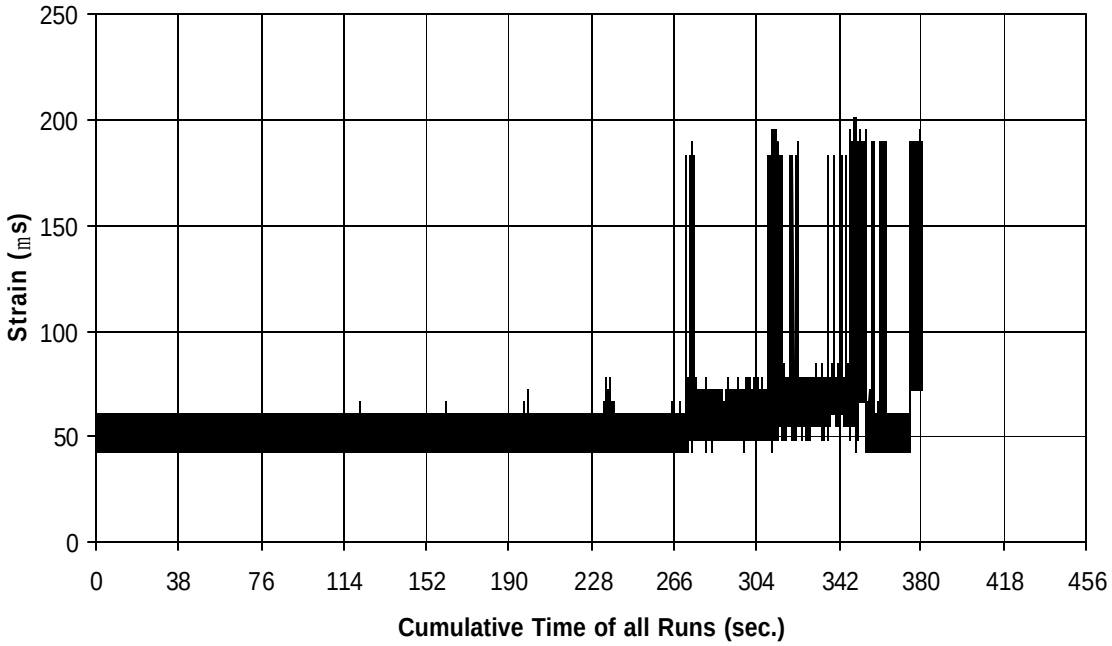

Fig. A-163 THD -3 Measured Strain in Gauge SG35

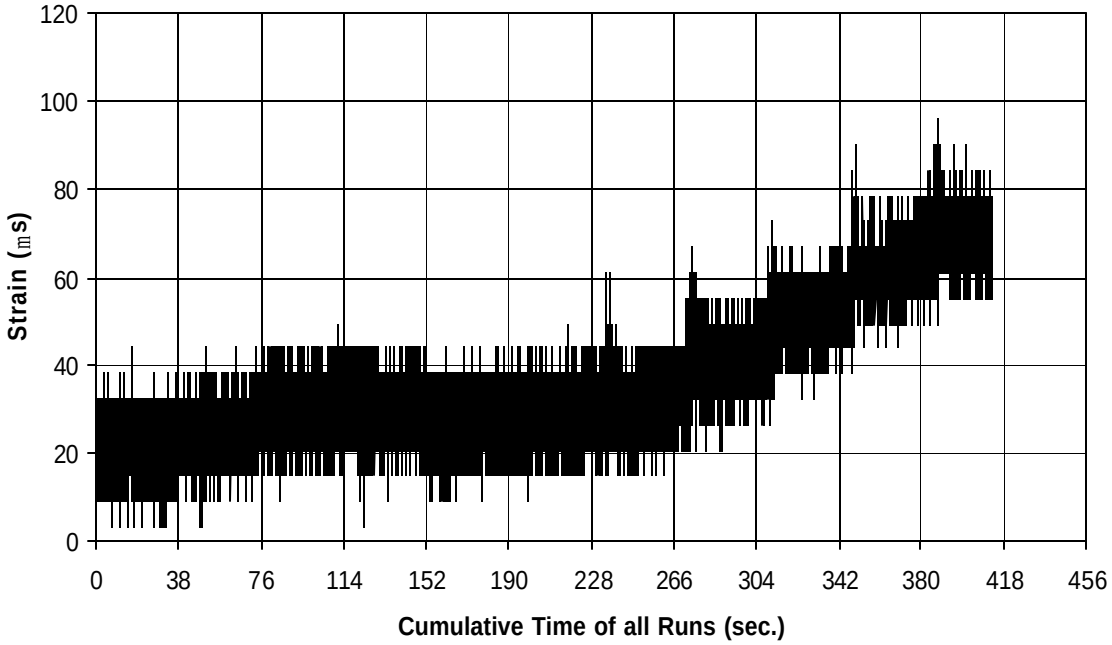

Fig. A-164 THD -3 Measured Strain in Gauge SG36

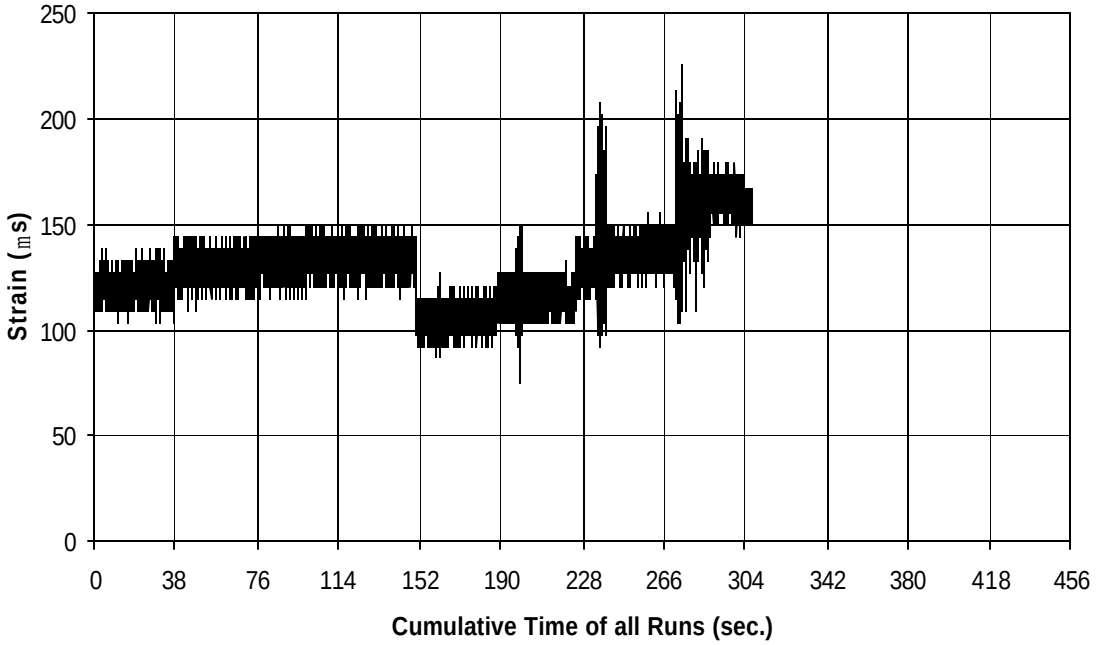

Fig. A-165 THD -3 Measured Strain in Gauge SG37

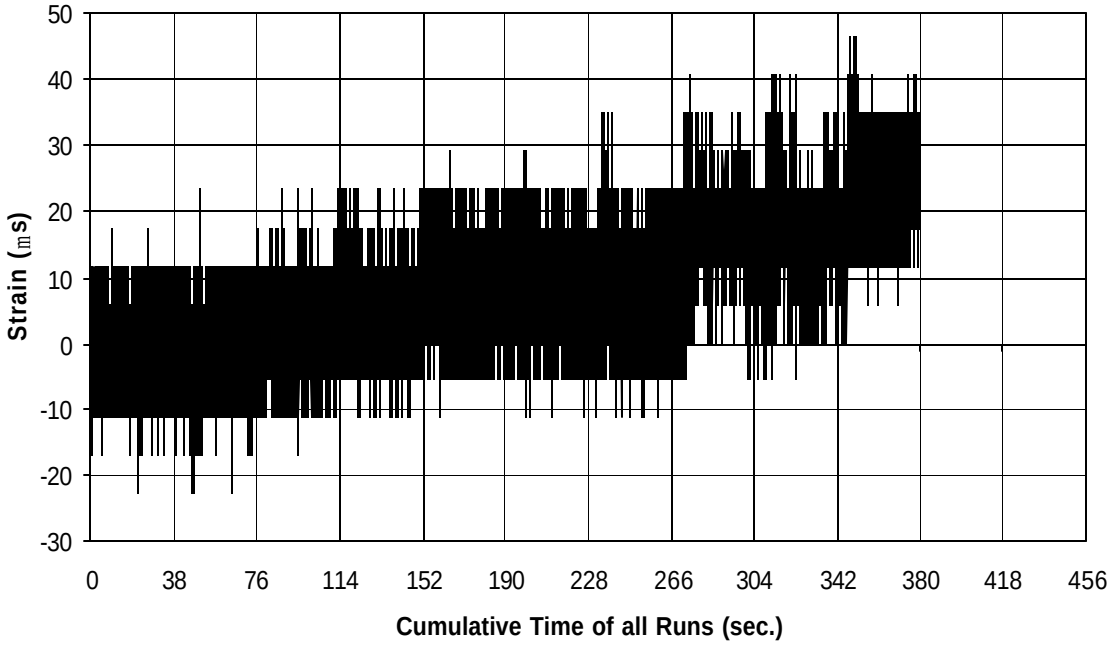

Fig. A-166 THD -3 Measured Strain in Gauge SG38

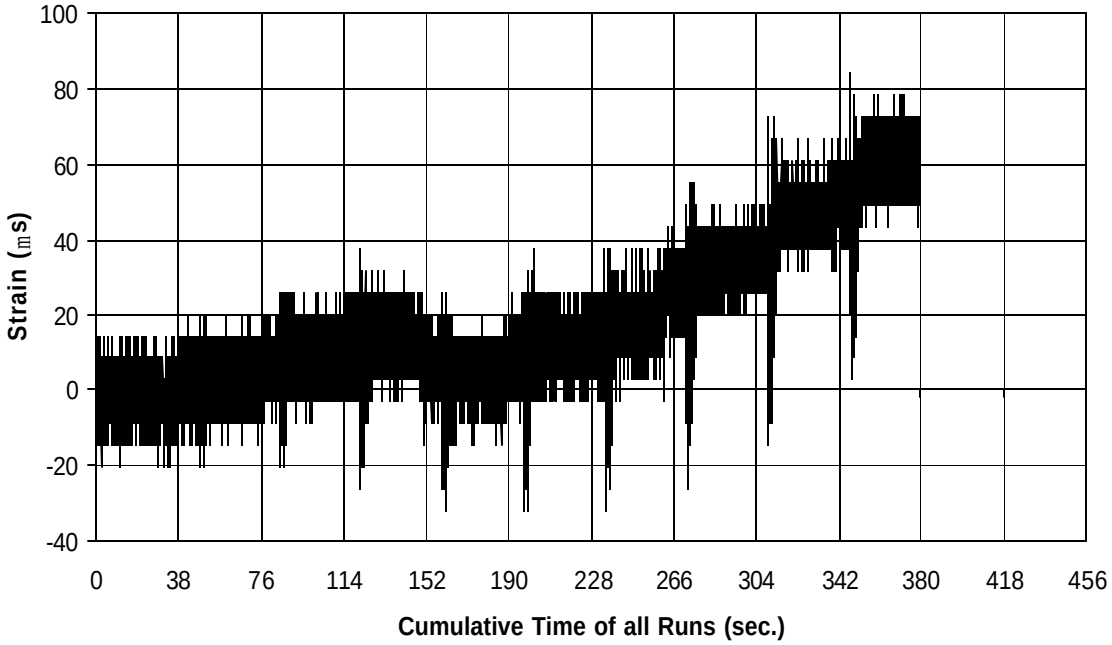

Fig. A-167 THD -3 Measured Strain in Gauge SG39

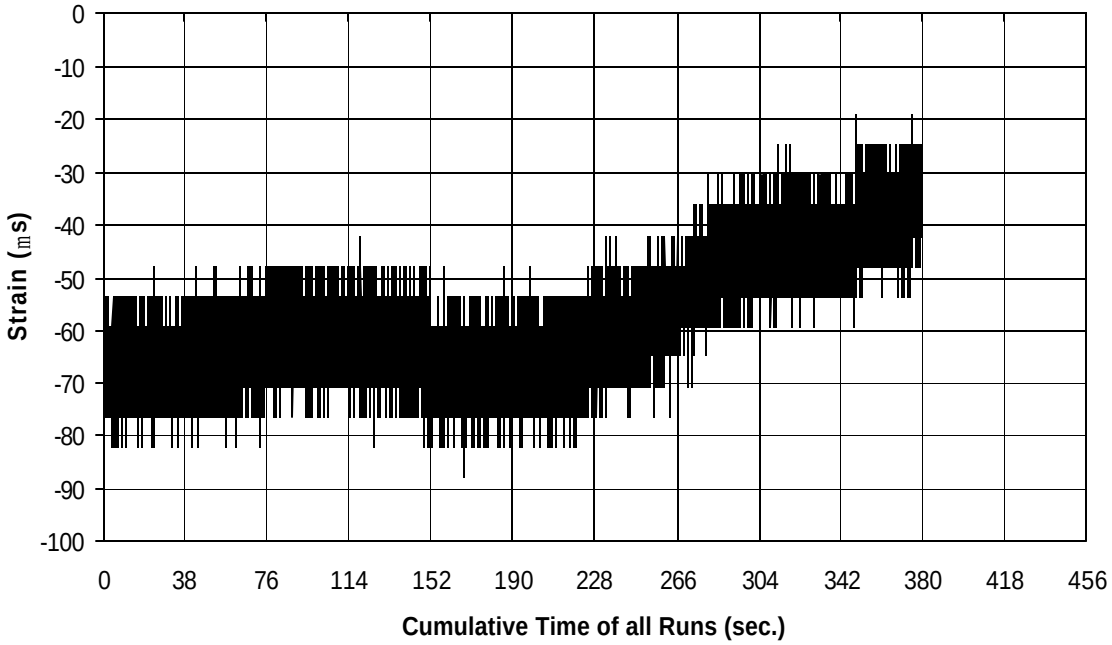

Fig. A-168 THD -3 Measured Strain in Gauge SG40

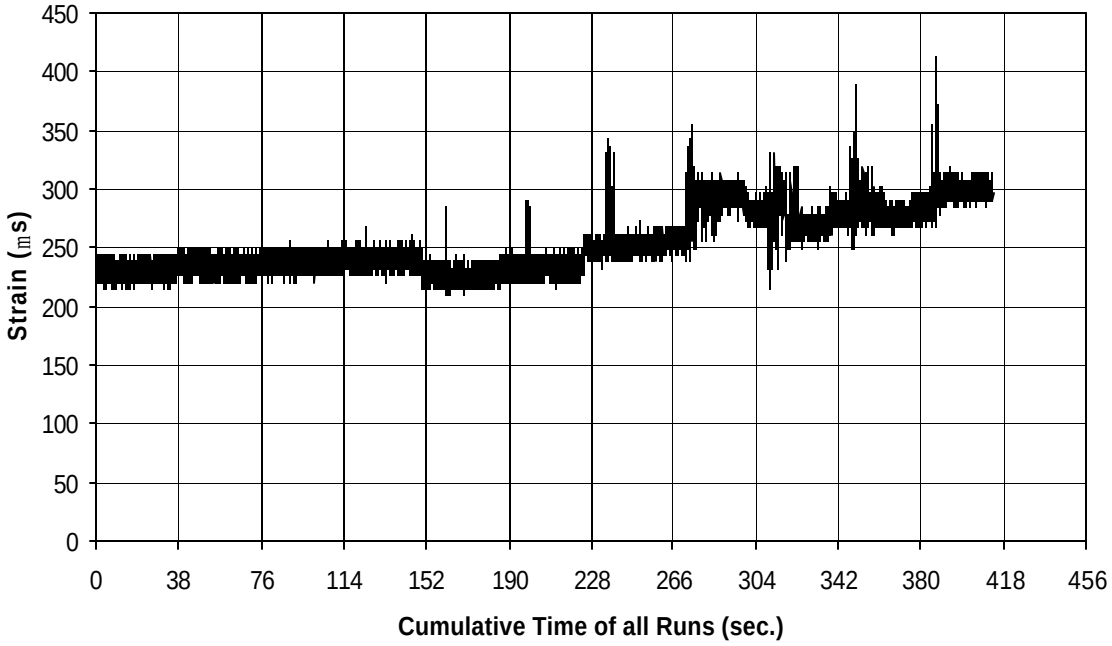

Fig. A-169 THD -3 Measured Strain in Gauge SG41

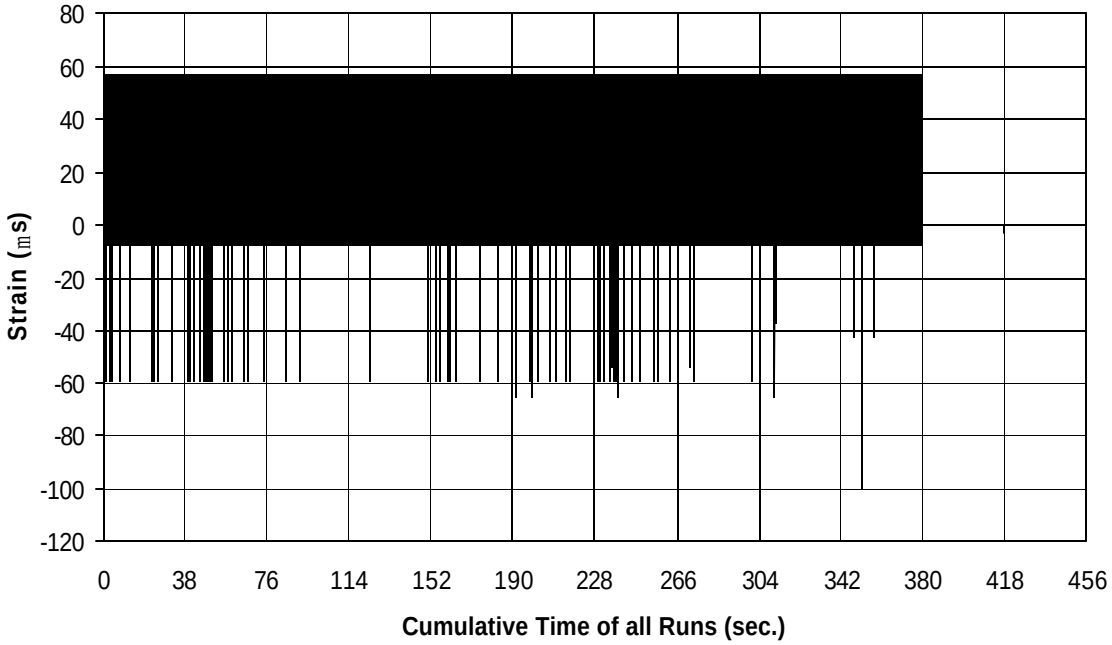

Fig. A-170 THD -3 Measured Strain in Gauge SG42

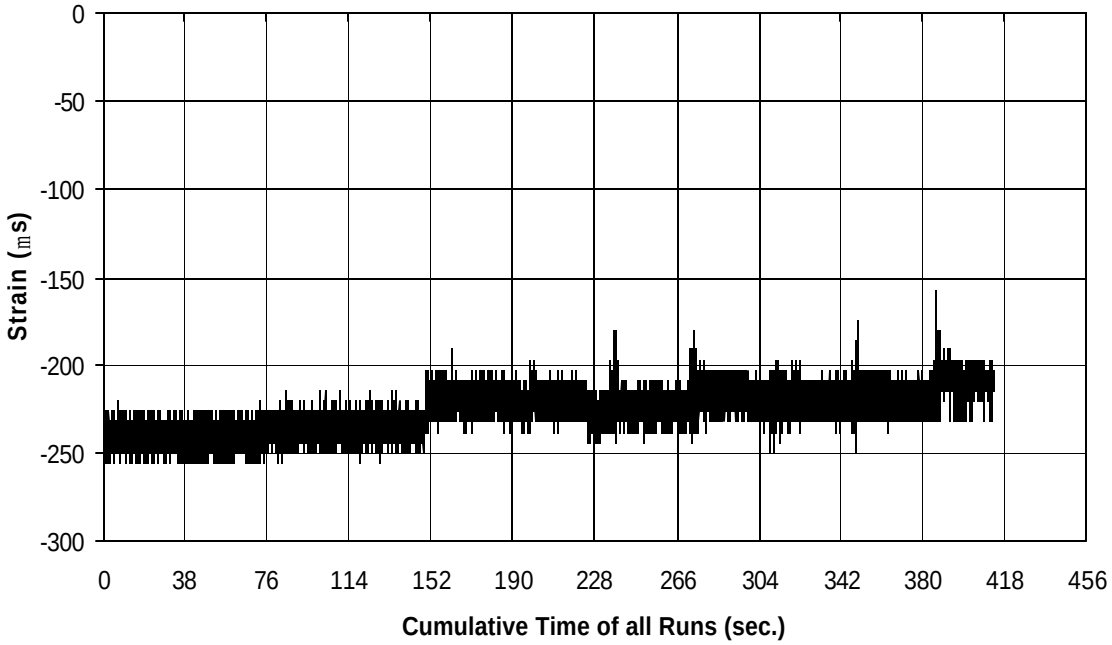

Fig. A-171 THD -3 Measured Strain in Gauge SG43

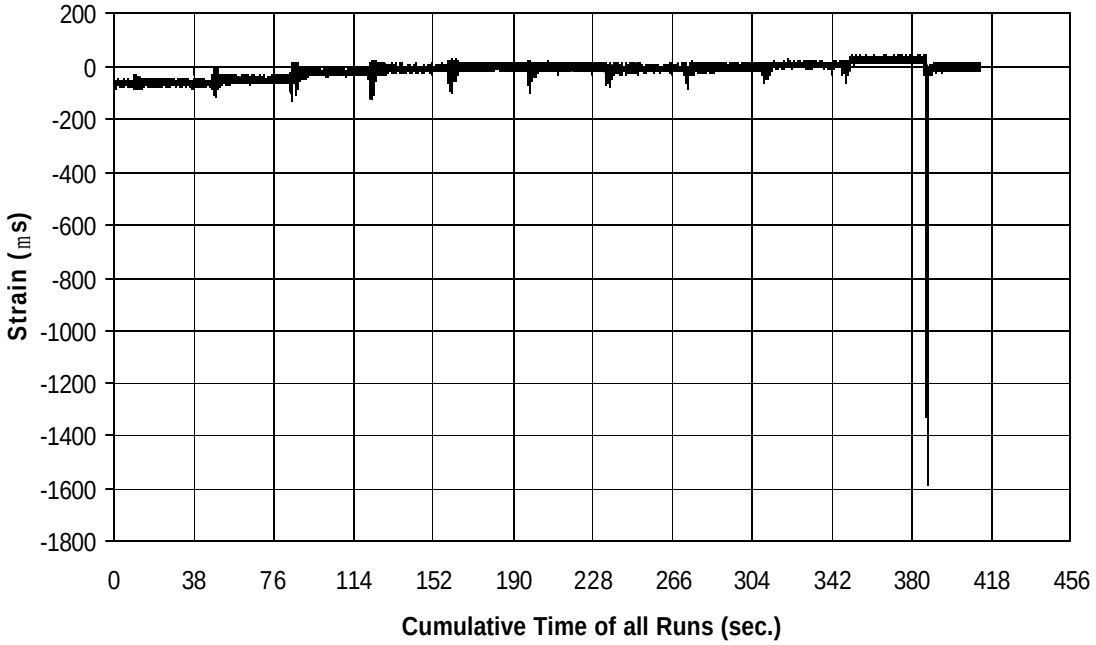

Fig. A-172 THD -3 Measured Strain in Gauge SG44

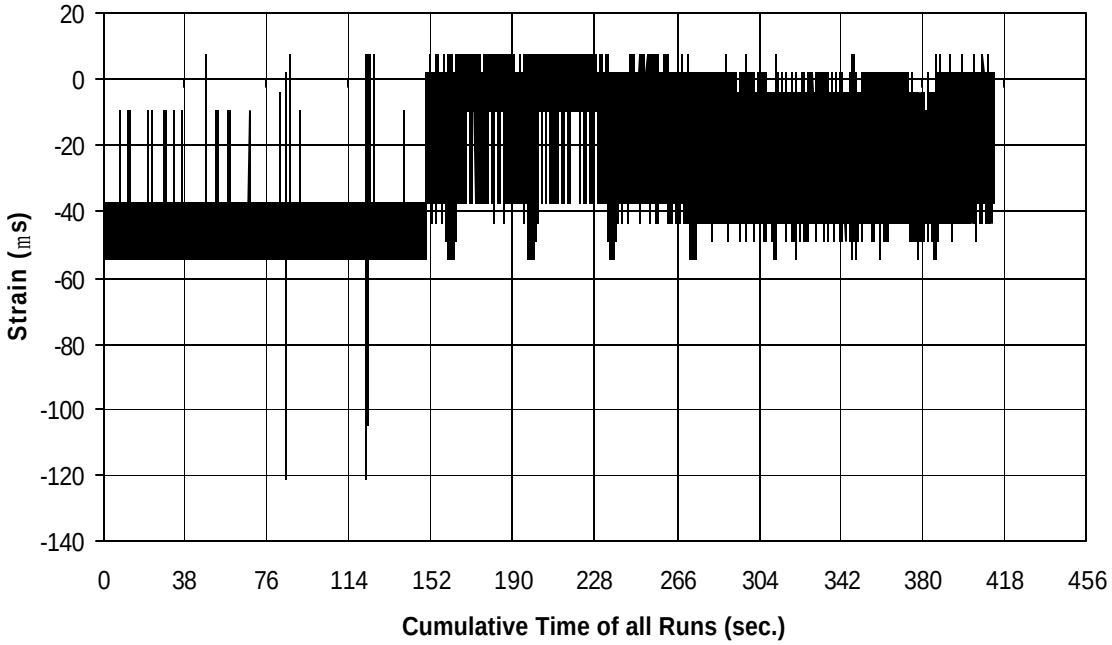

Fig. A-173 THD -3 Measured Strain in Gauge SG45

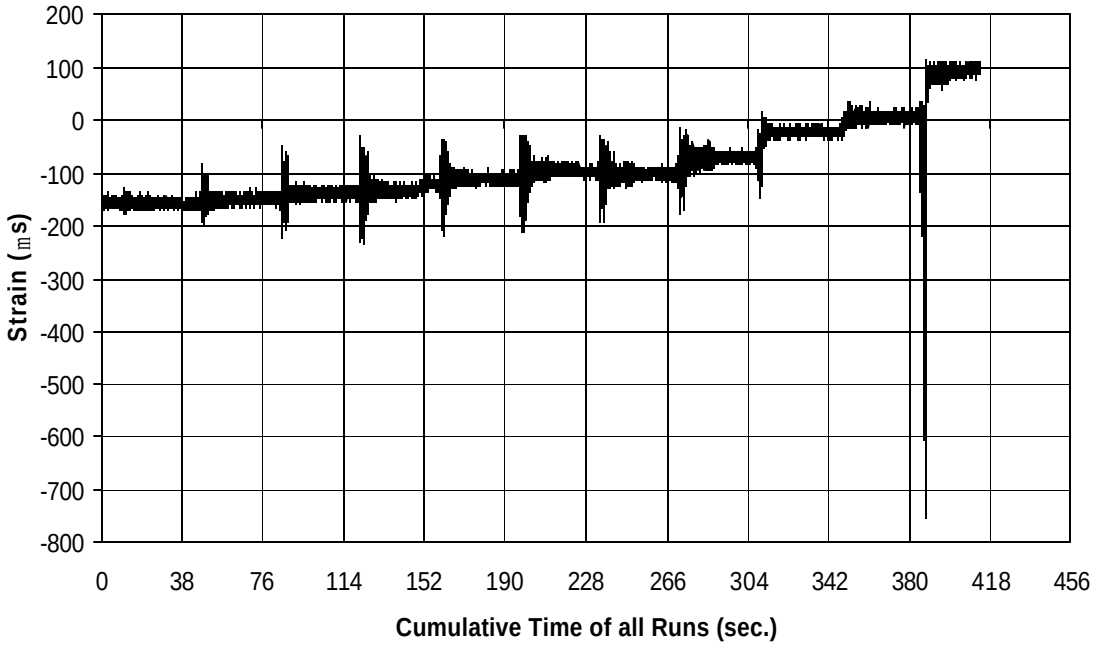

Fig. A-174 THD -3 Measured Strain in Gauge SG46

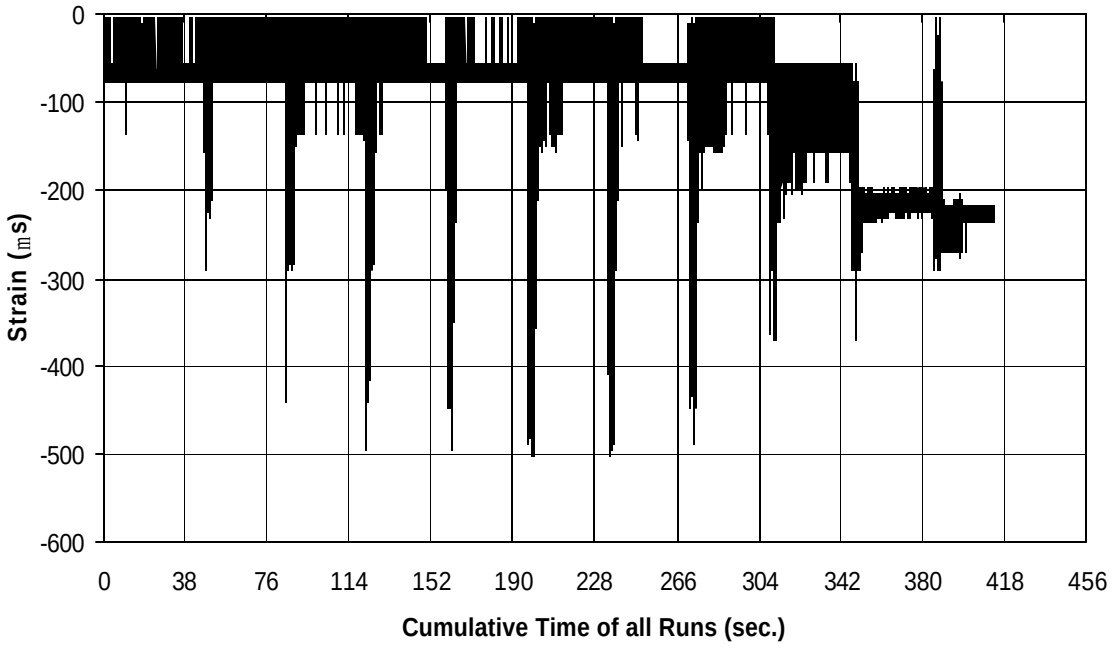

Fig. A-175 THD -3 Measured Strain in Gauge SG47

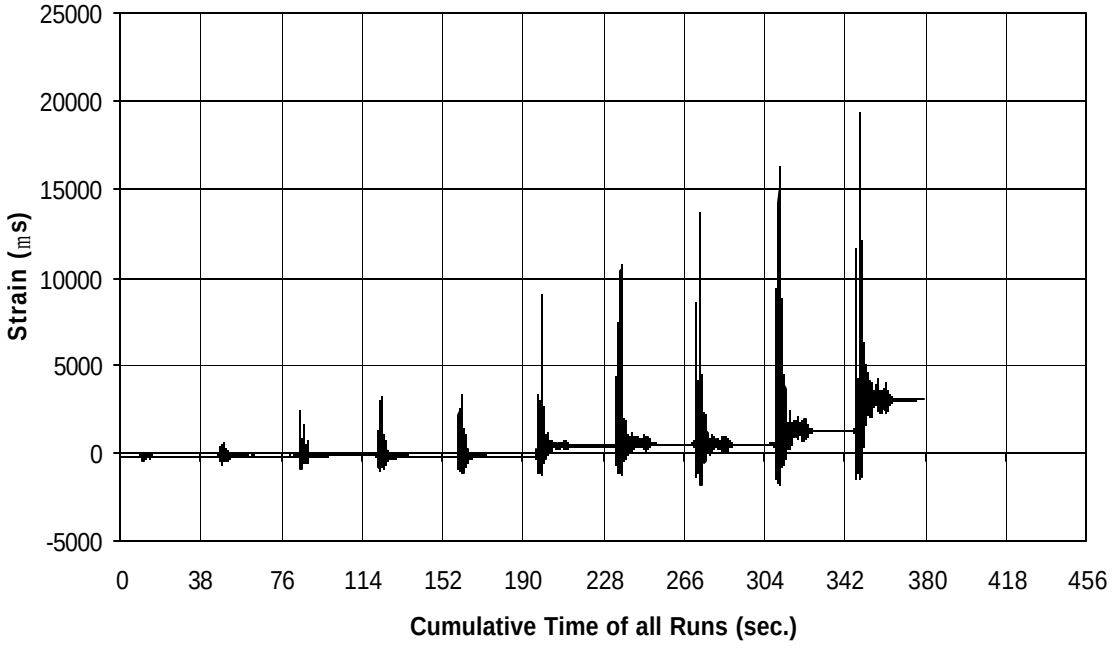

Fig. A-176 THD -3 Measured Strain in Gauge SG48

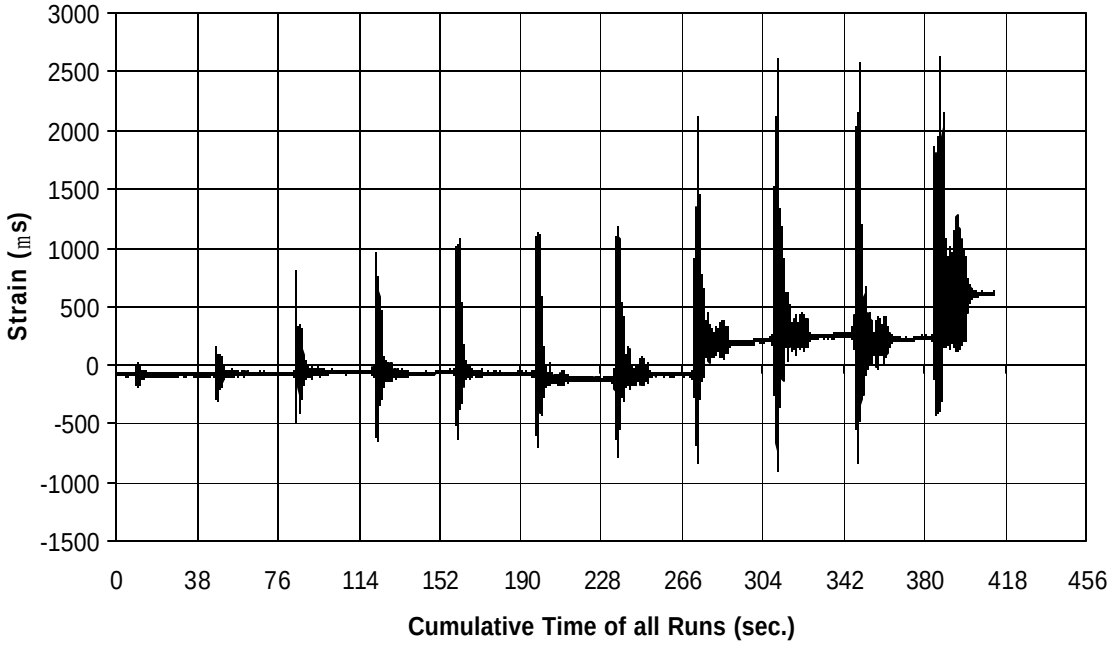

Fig. A-177 THD -3 Measured Strain in Gauge SG49

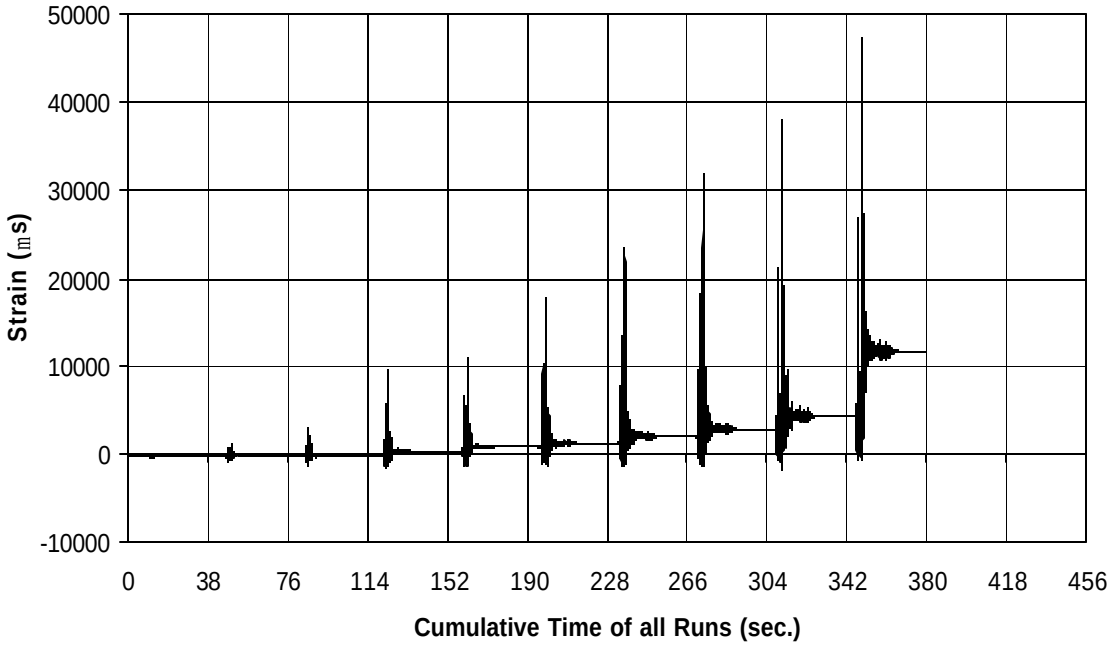

Fig. A-178 THD -3 Measured Strain in Gauge SG50

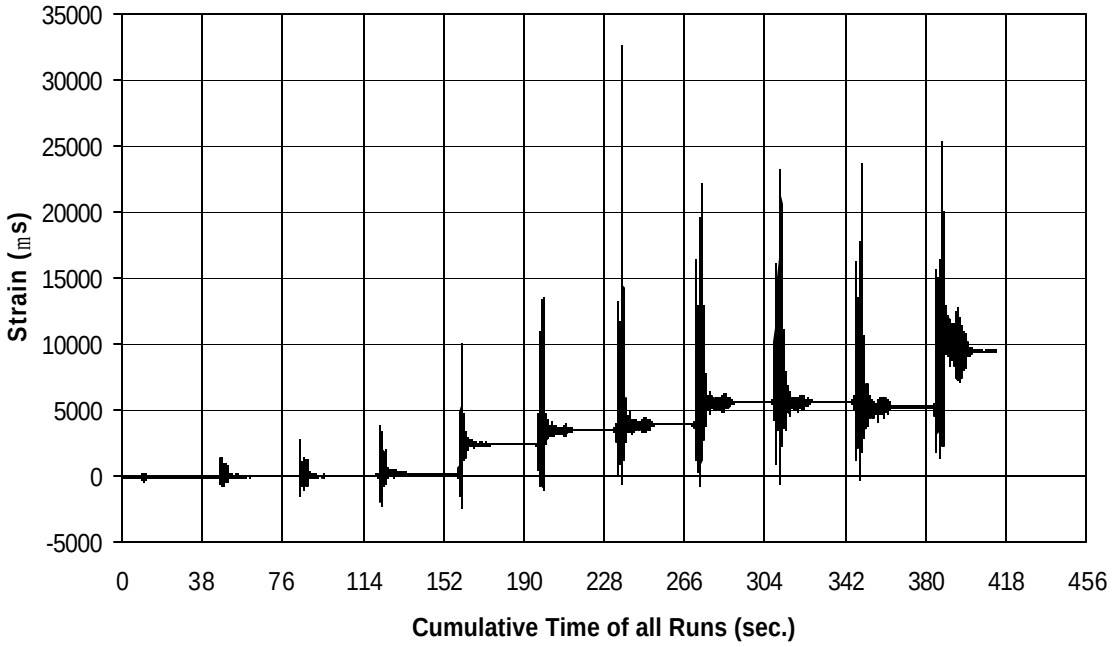

Fig. A-179 THD -3 Measured Strain in Gauge SG51

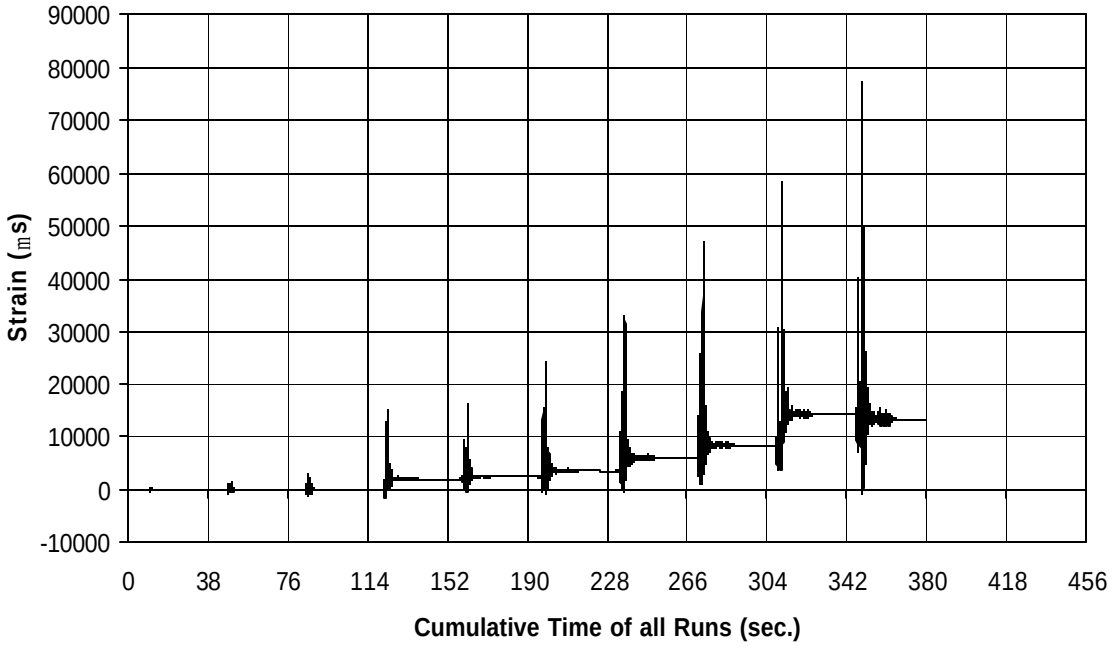

Fig. A-180 THD -3 Measured Strain in Gauge SG52

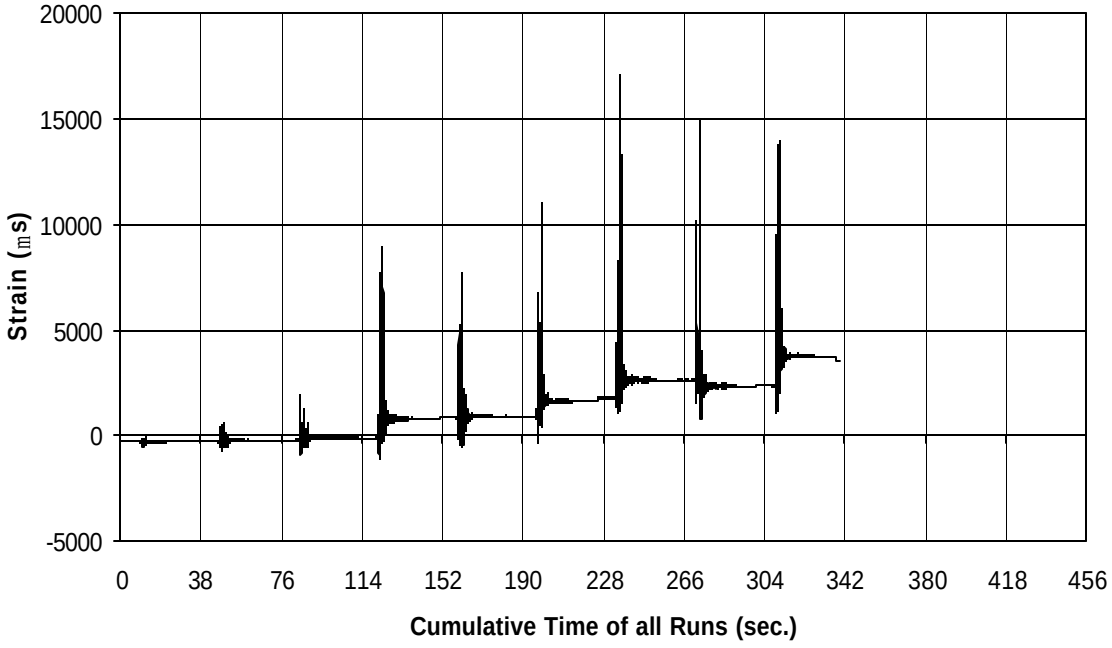

Fig. A-181 THD -3 Measured Strain in Gauge SG53

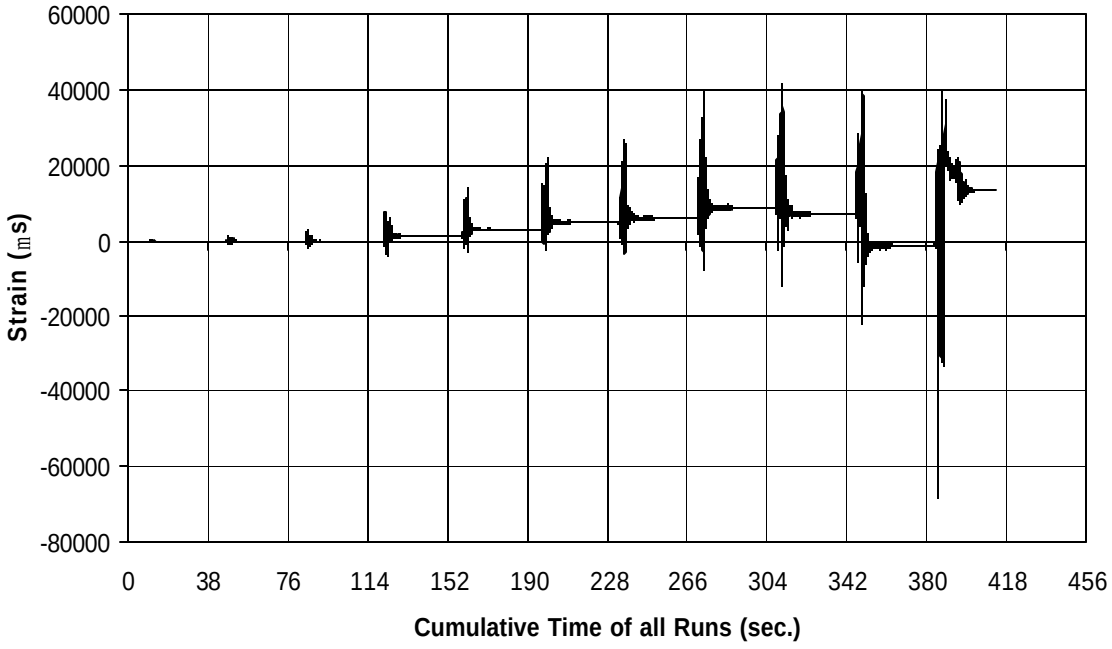

Fig. A-182 THD -3 Measured Strain in Gauge SG54

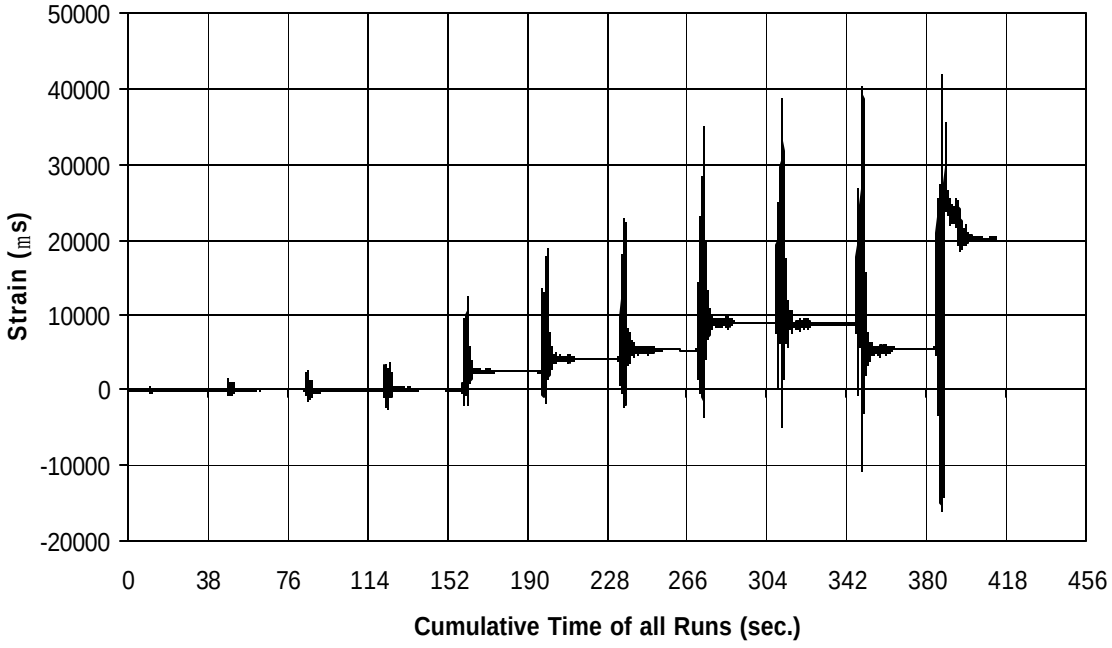

Fig. A-183 THD -3 Measured Strain in Gauge SG55

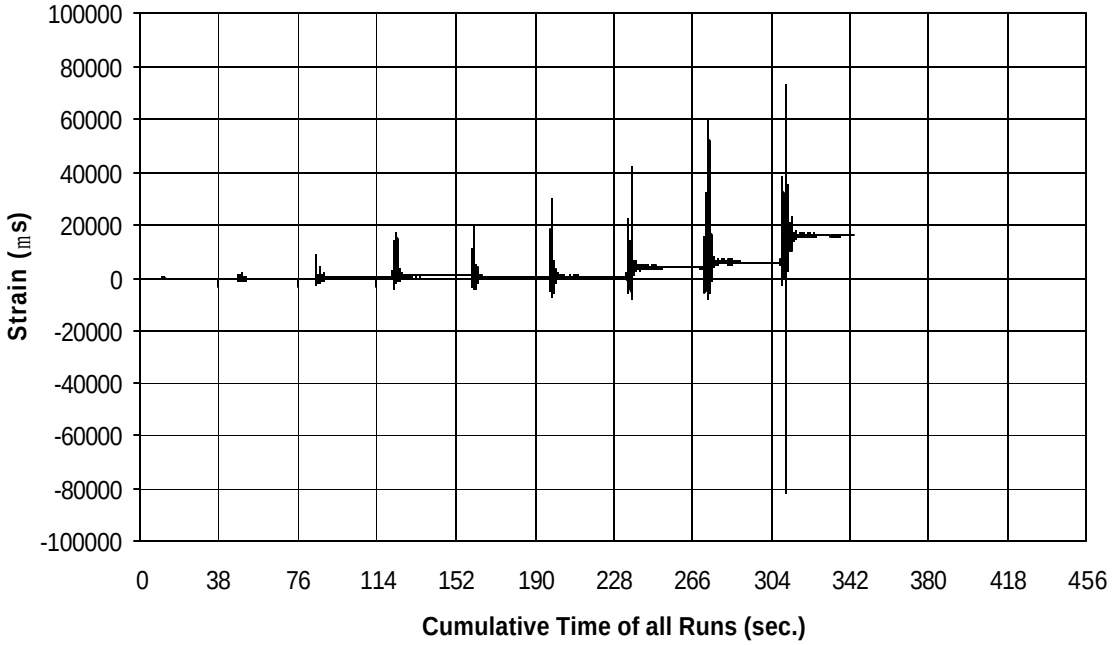

Fig. A-184 THD -3 Measured Strain in Gauge SG56

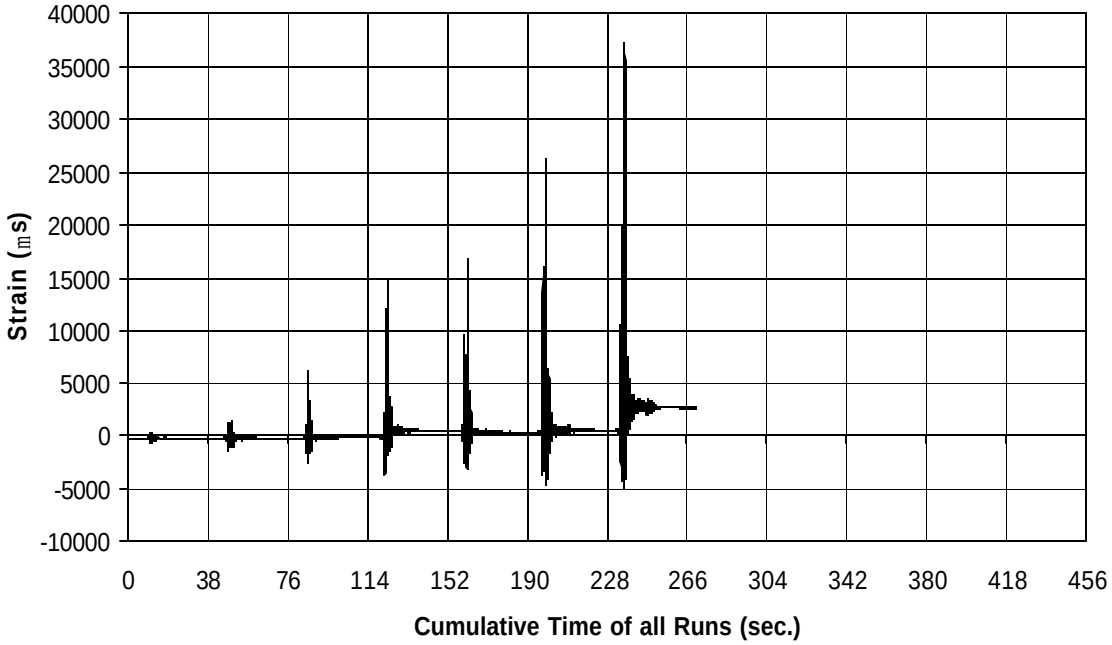

Fig. A-185 THD -3 Measured Strain in Gauge SG57

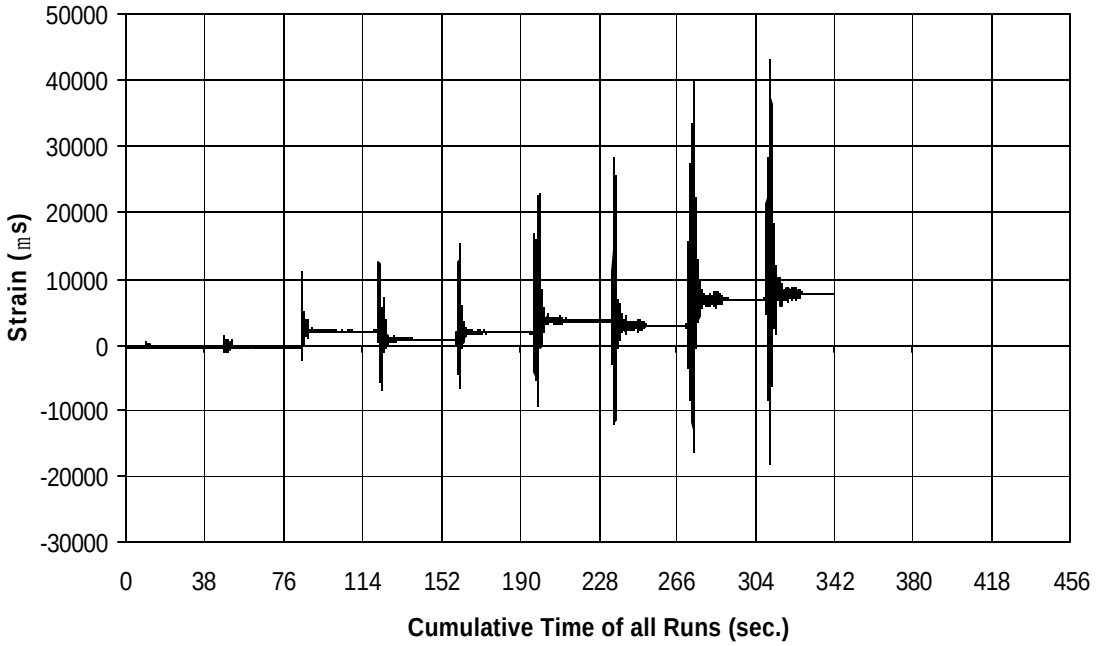

Fig. A-186 THD -3 Measured Strain in Gauge SG58

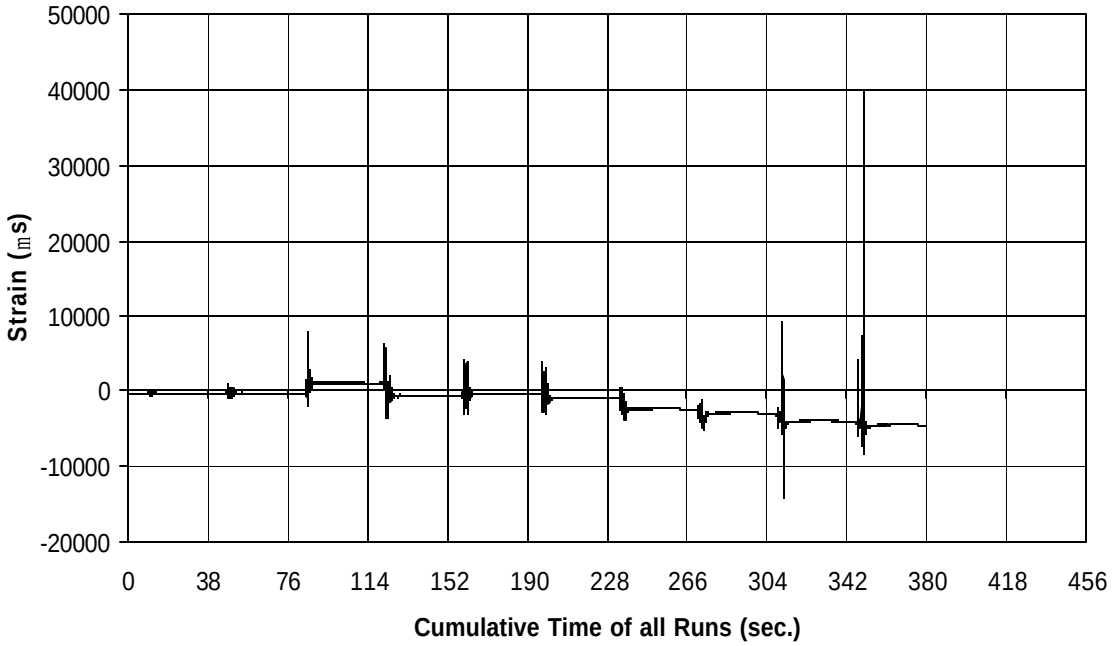

Fig. A-187 THD -3 Measured Strain in Gauge SG59

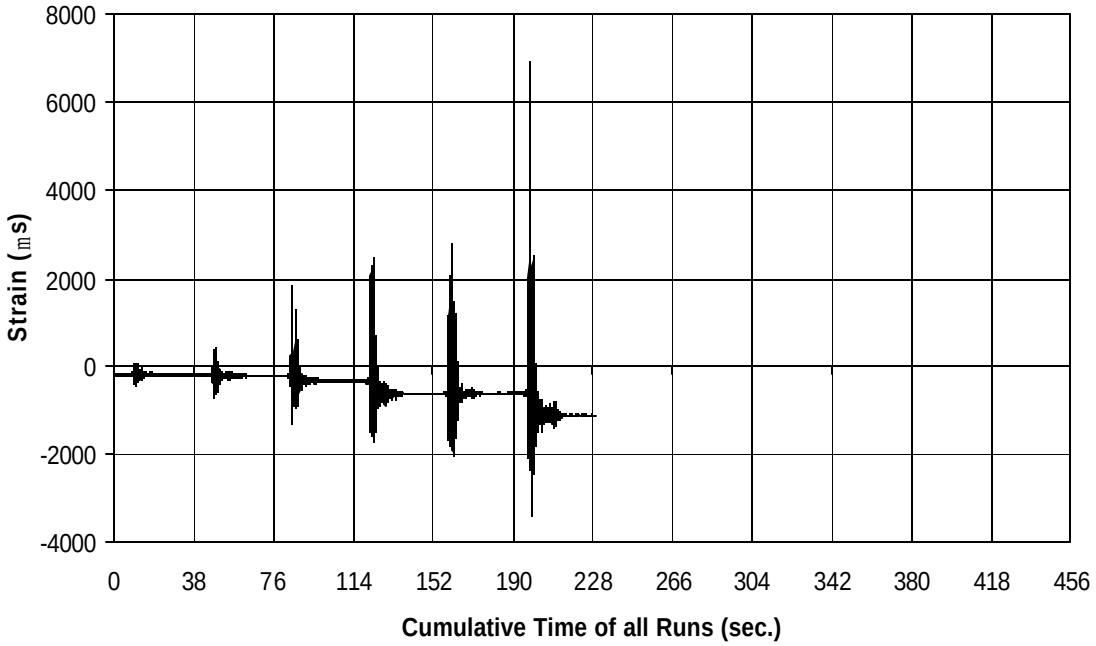

Fig. A-188 THD -3 Measured Strain in Gauge SG60

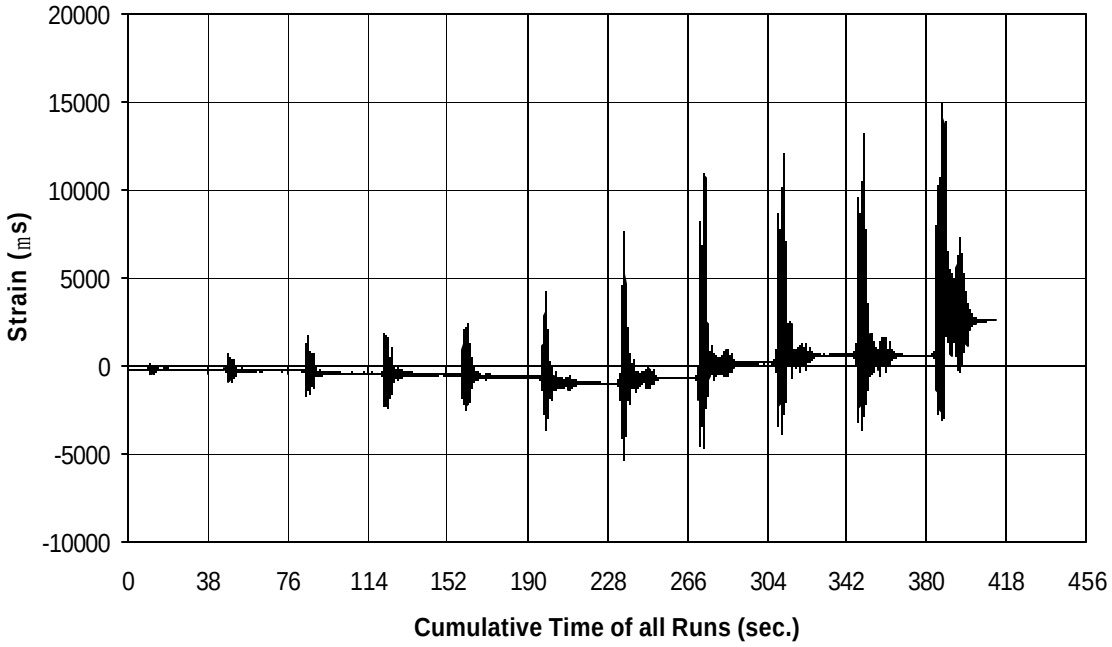

Fig. A-189 THD -3 Measured Strain in Gauge SG61

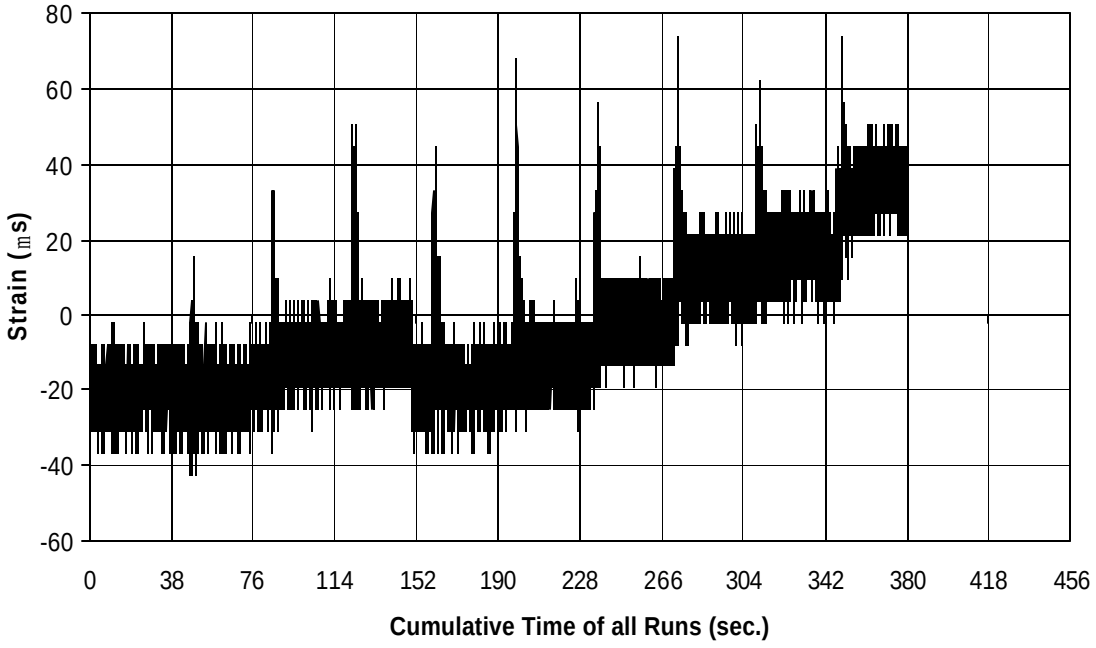

Fig. A-190 THD -3 Measured Strain in Gauge SG62

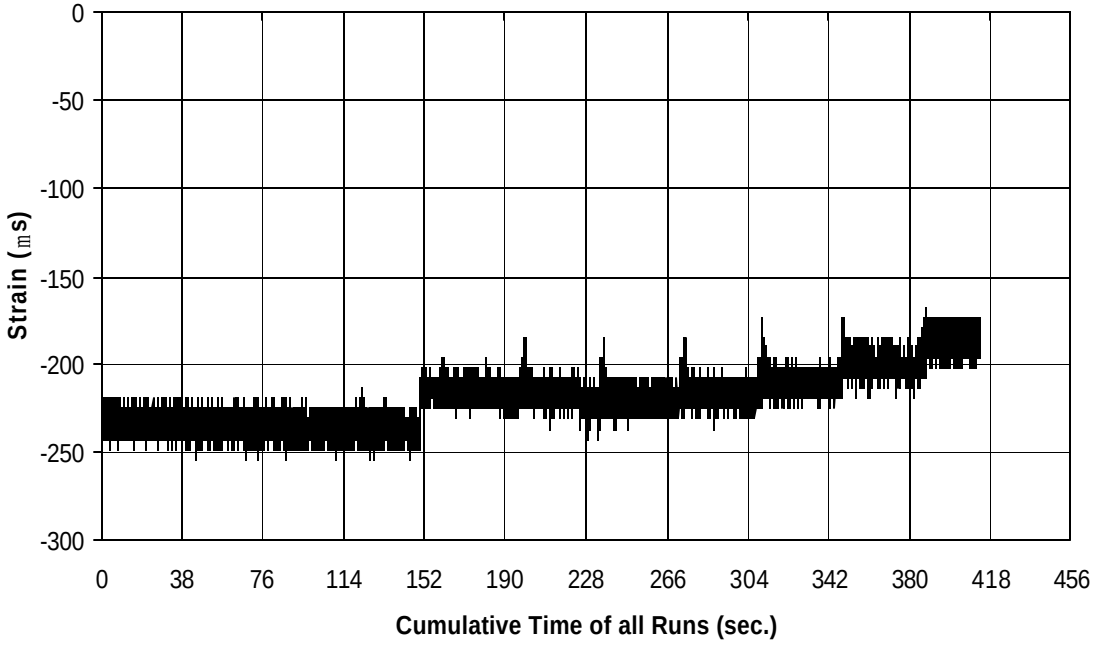

Fig. A-191 THD -3 Measured Strain in Gauge SG63

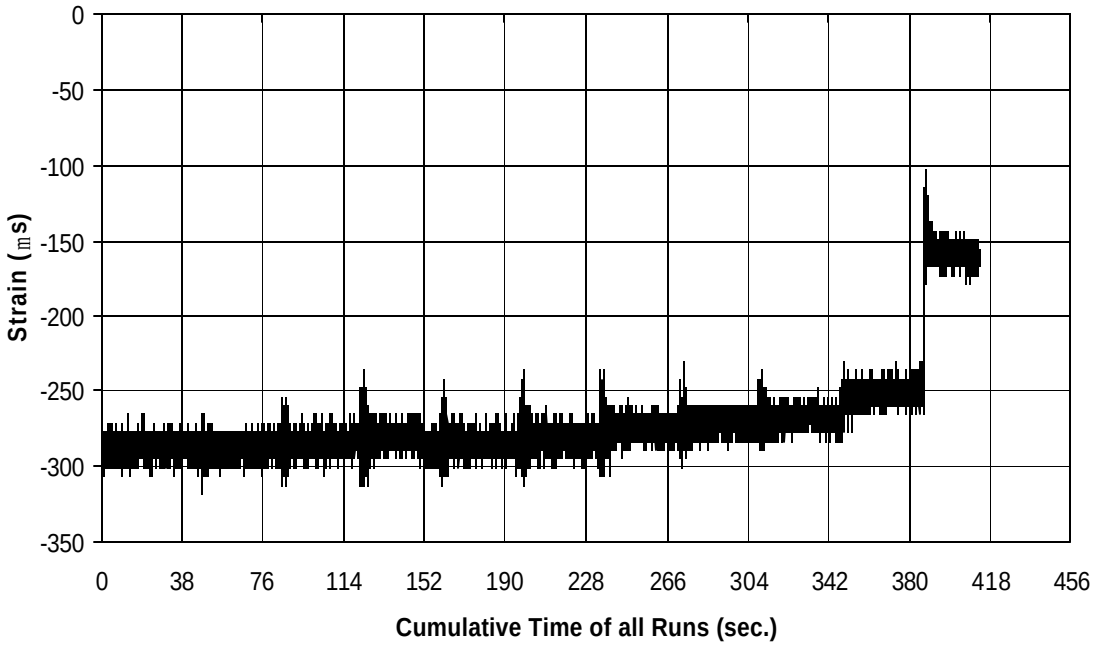

Fig. A-192 THD -3 Measured Strain in Gauge SG64

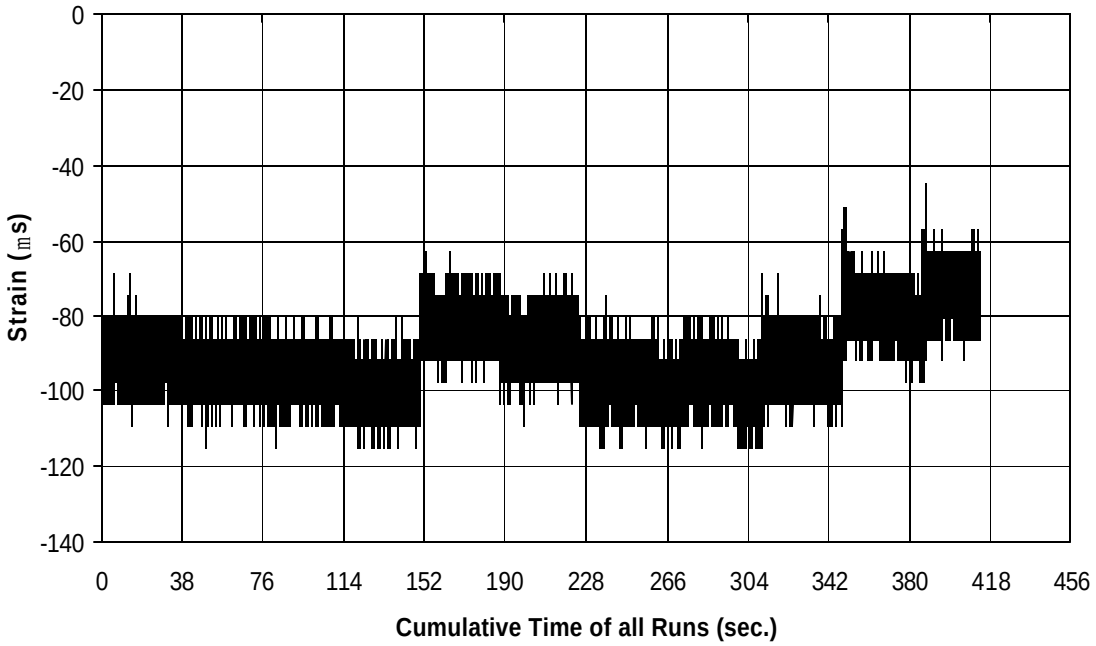

Fig. A-193 THD -3 Measured Strain in Gauge SG65

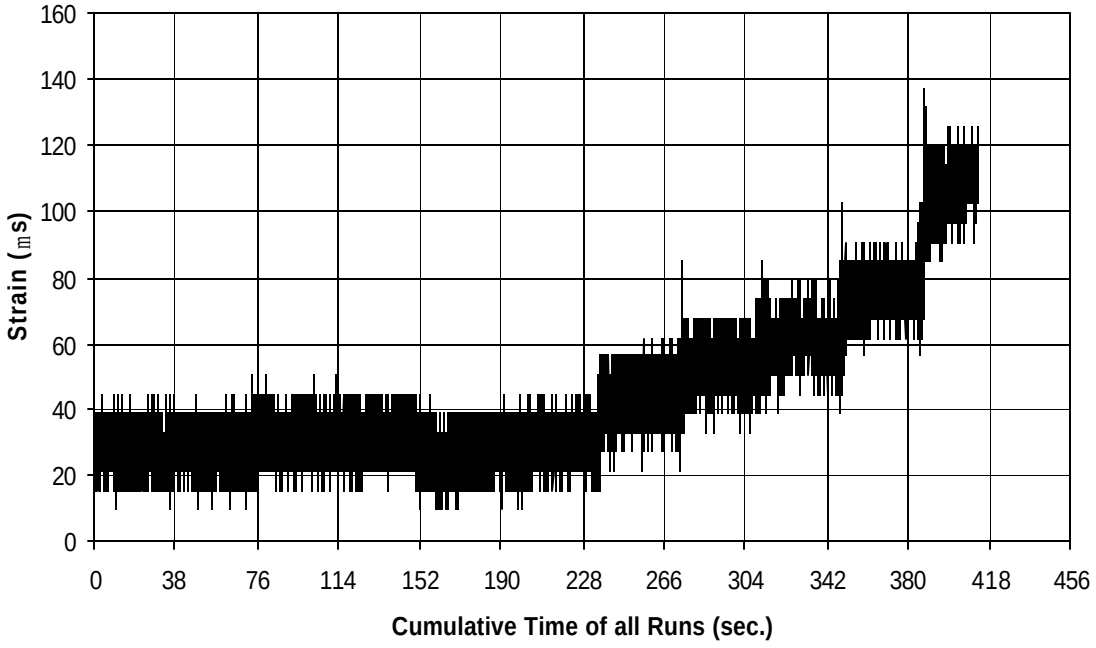

Fig. A-194 THD -3 Measured Strain in Gauge SG66

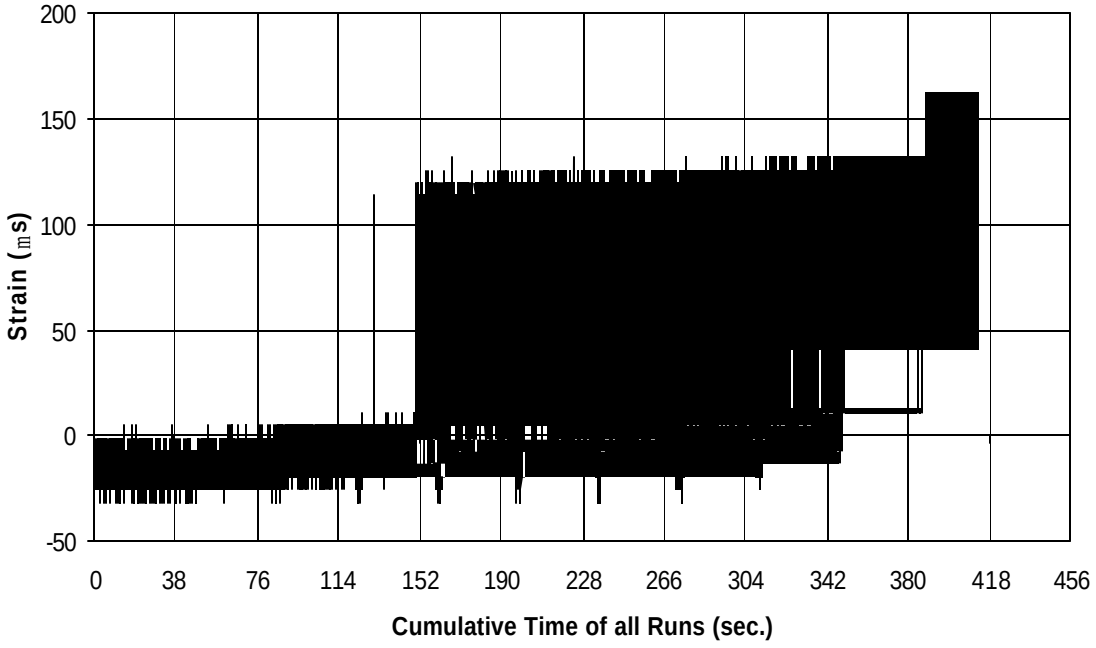

Fig. A-195 THD -3 Measured Strain in Gauge SG67

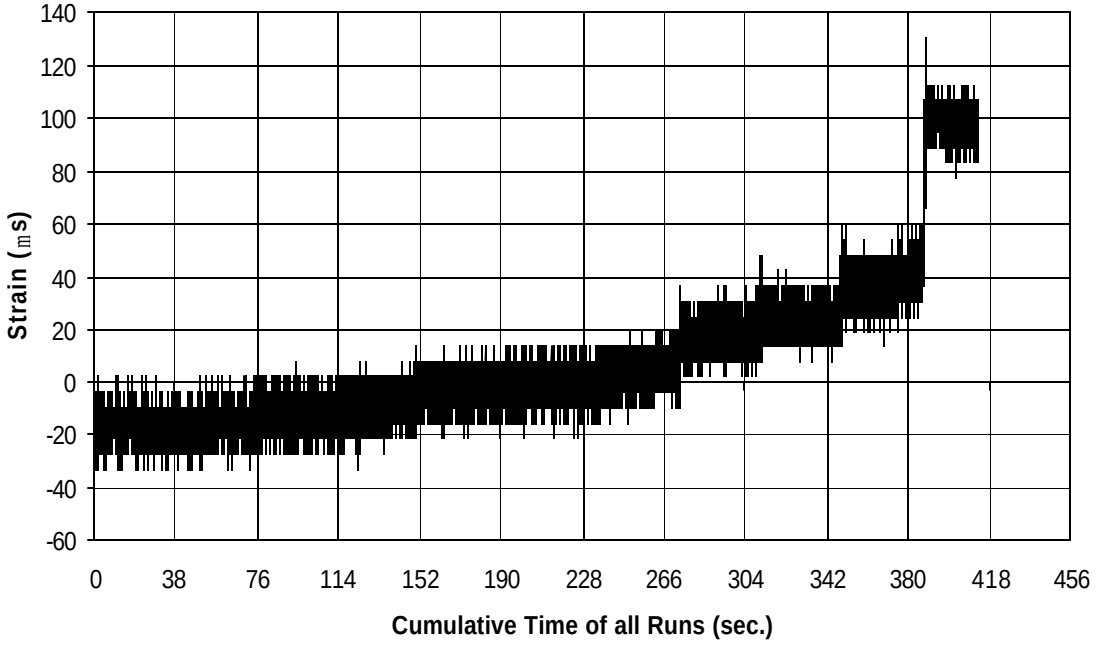

Fig. A-196 THD -3 Measured Strain in Gauge SG68

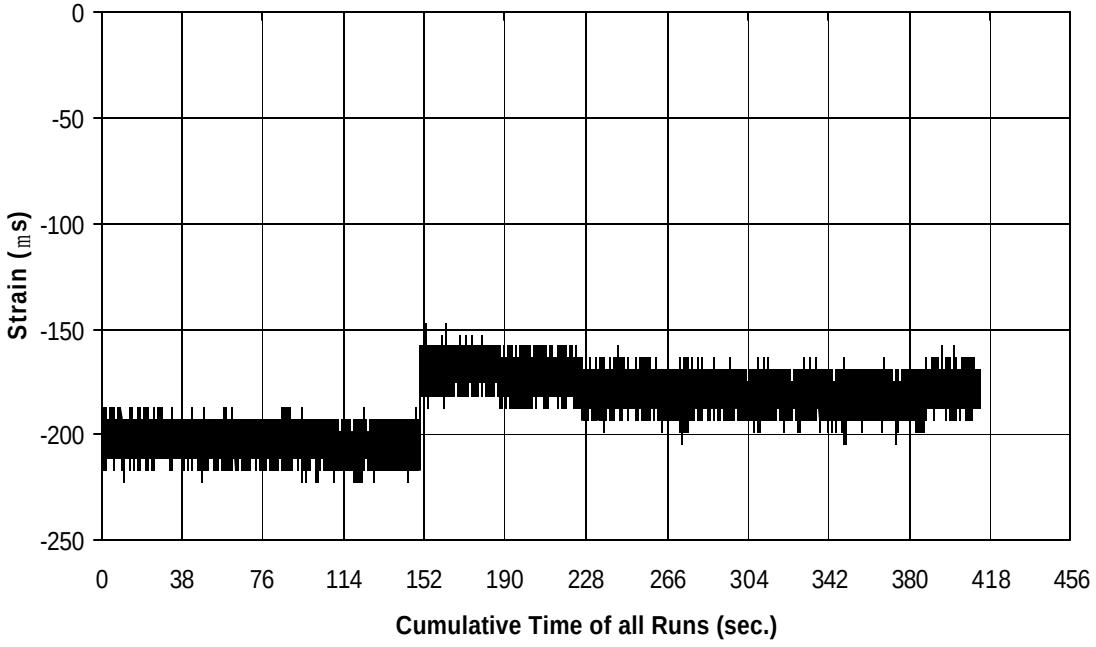

Fig. A-197 THD -3 Measured Strain in Gauge SG69

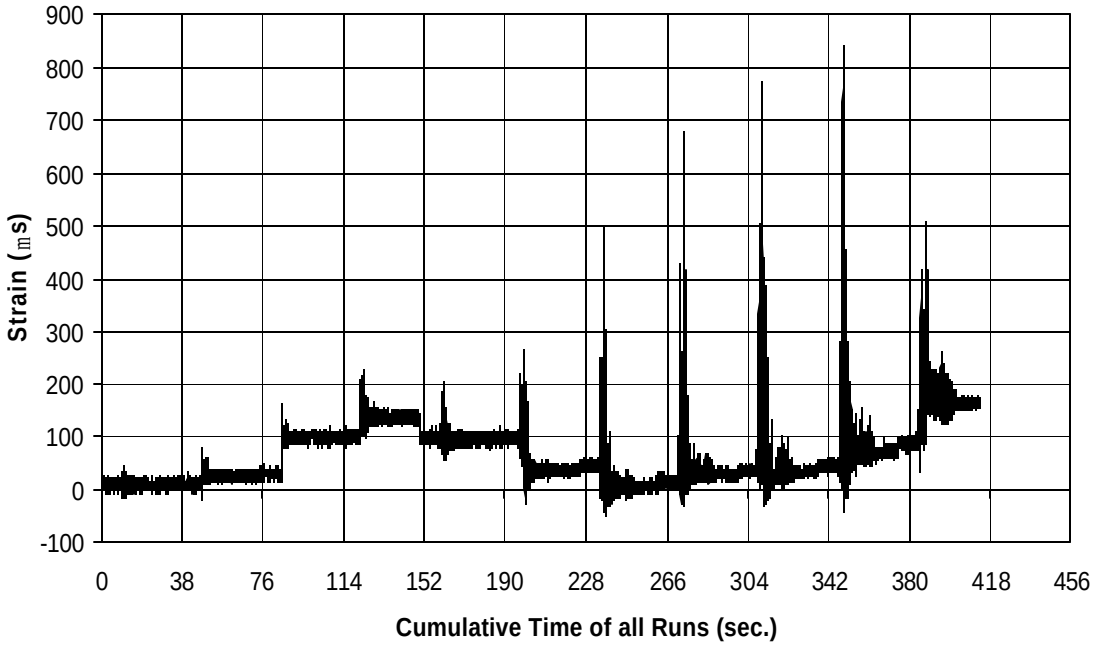

Fig. A-198 THD -3 Measured Strain in Gauge SG70

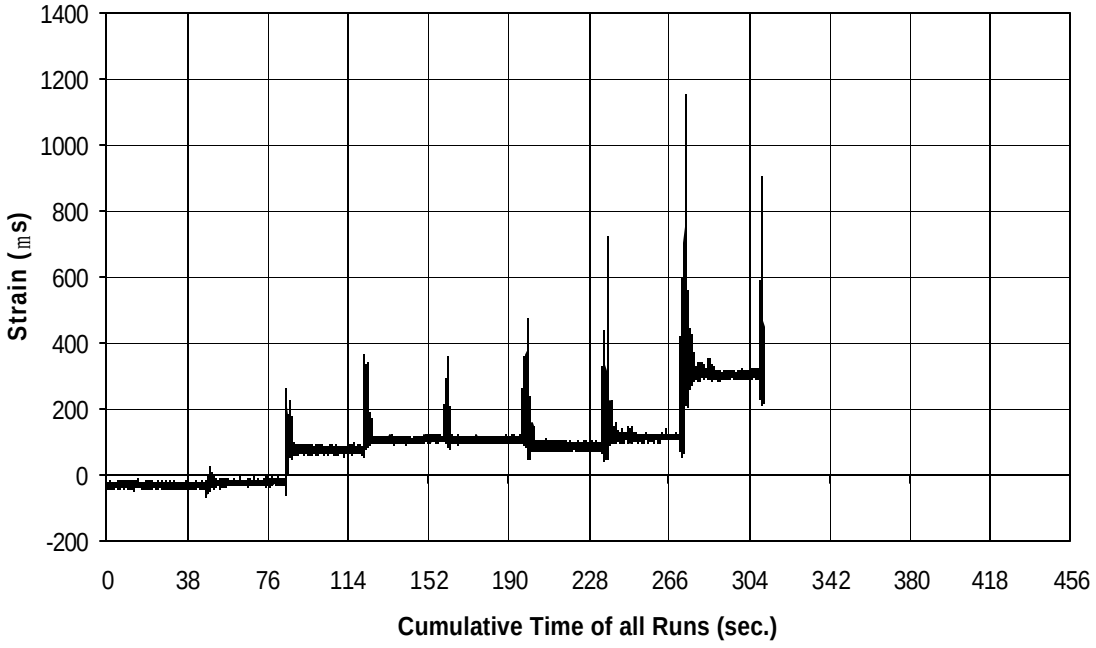

Fig. A-199 THD -3 Measured Strain in Gauge SG71

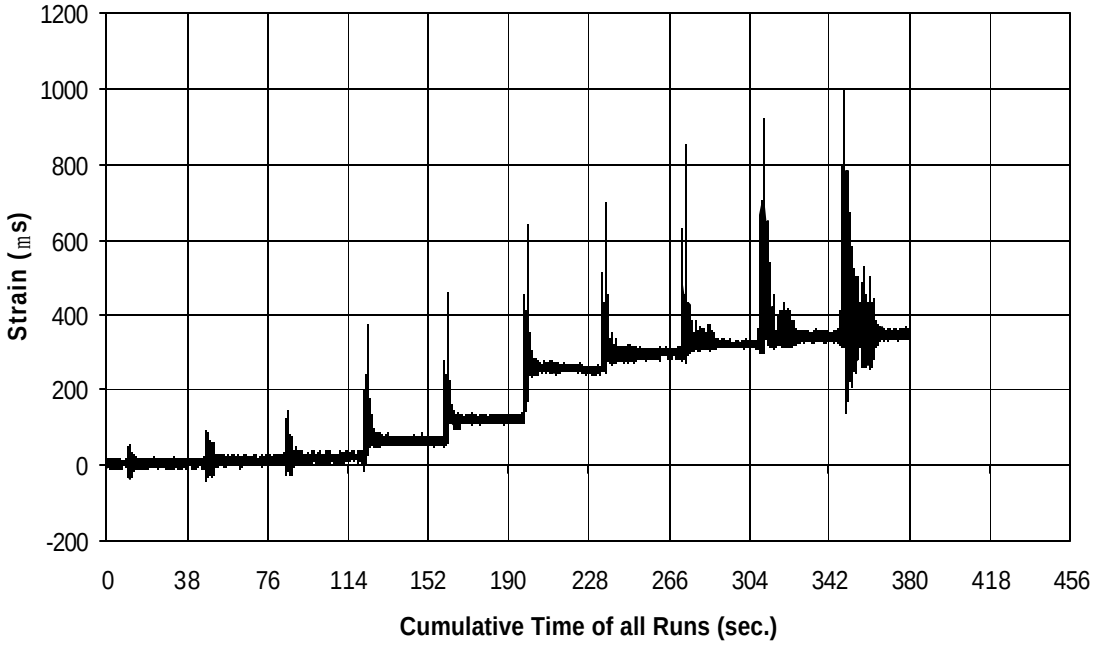

Fig. A-200 THD -3 Measured Strain in Gauge SG72

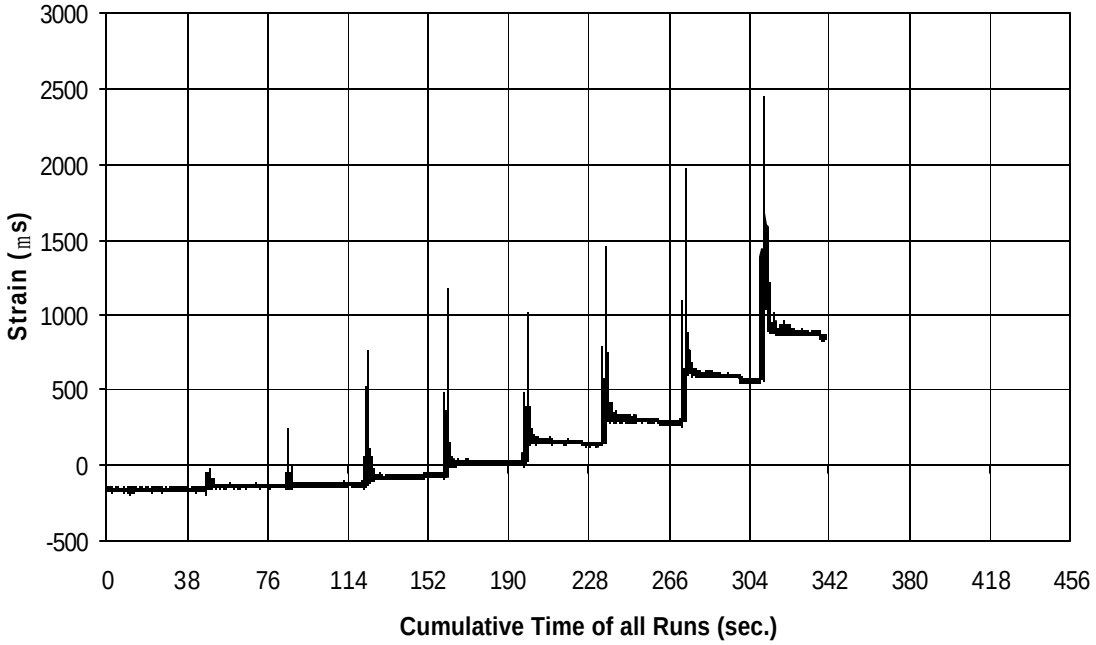

Fig. A-201 THD -3 Measured Strain in Gauge SG73

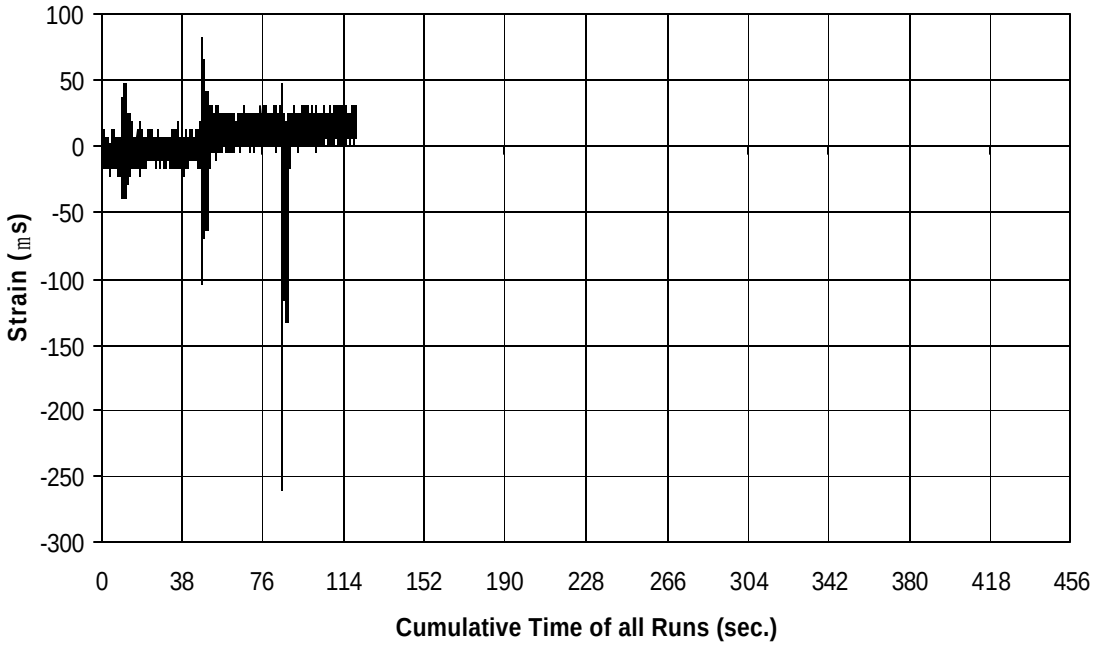

Fig. A-202 THD -3 Measured Strain in Gauge SG74

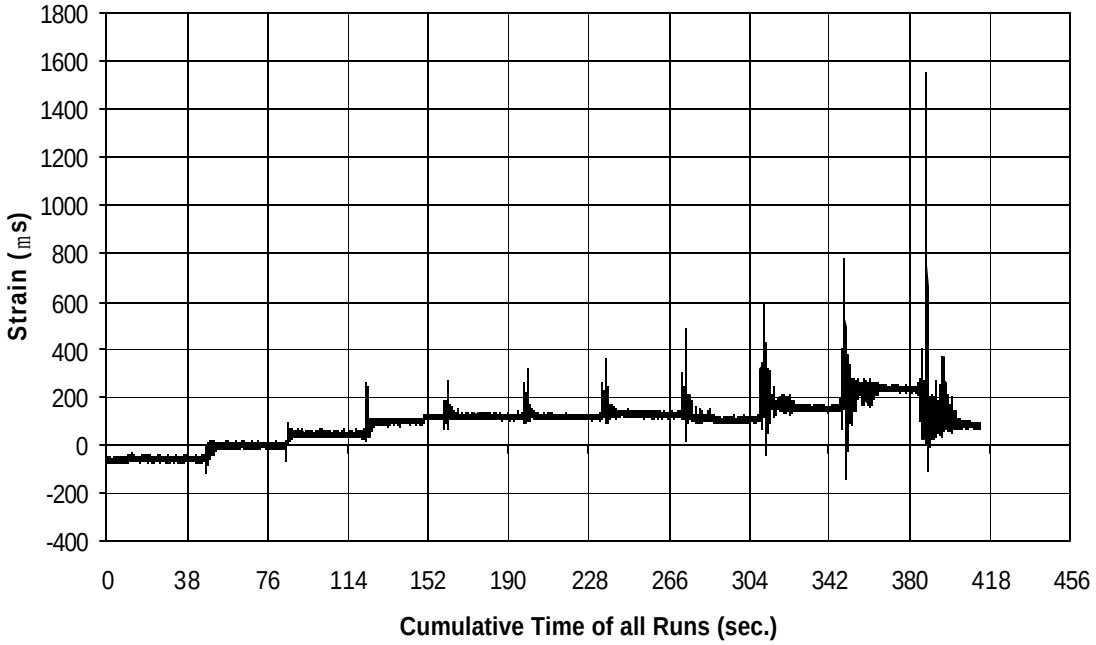

Fig. A-203 THD -3 Measured Strain in Gauge SG75

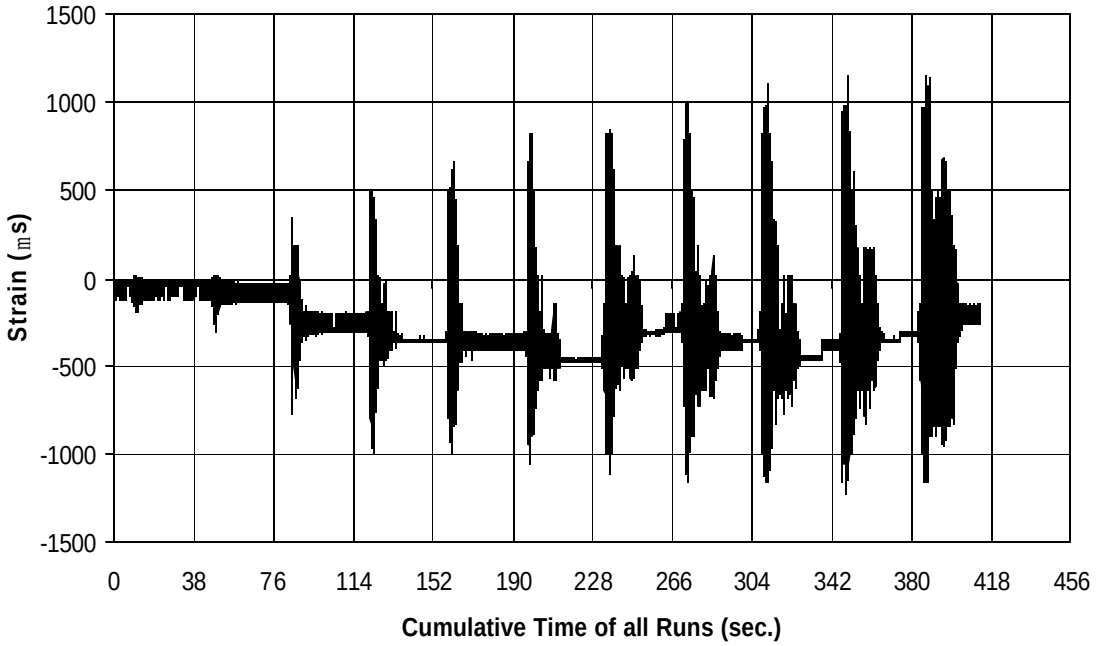

Fig. A-204 THD -3 Measured Strain in Gauge SG77

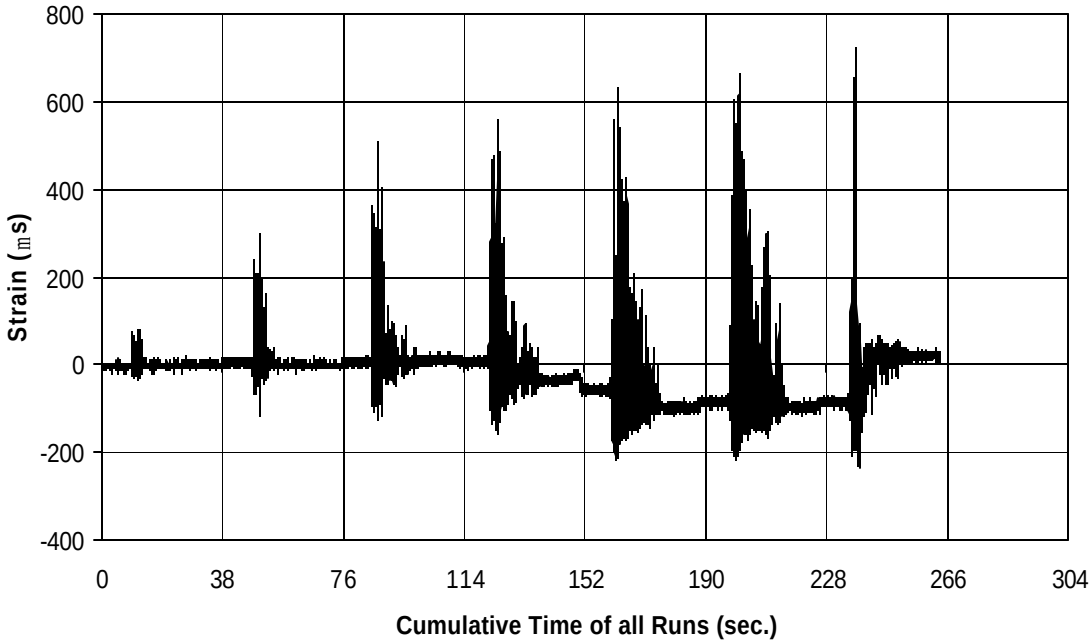

Fig. A-205 THD -4 Measured Strain in Gauge SG1

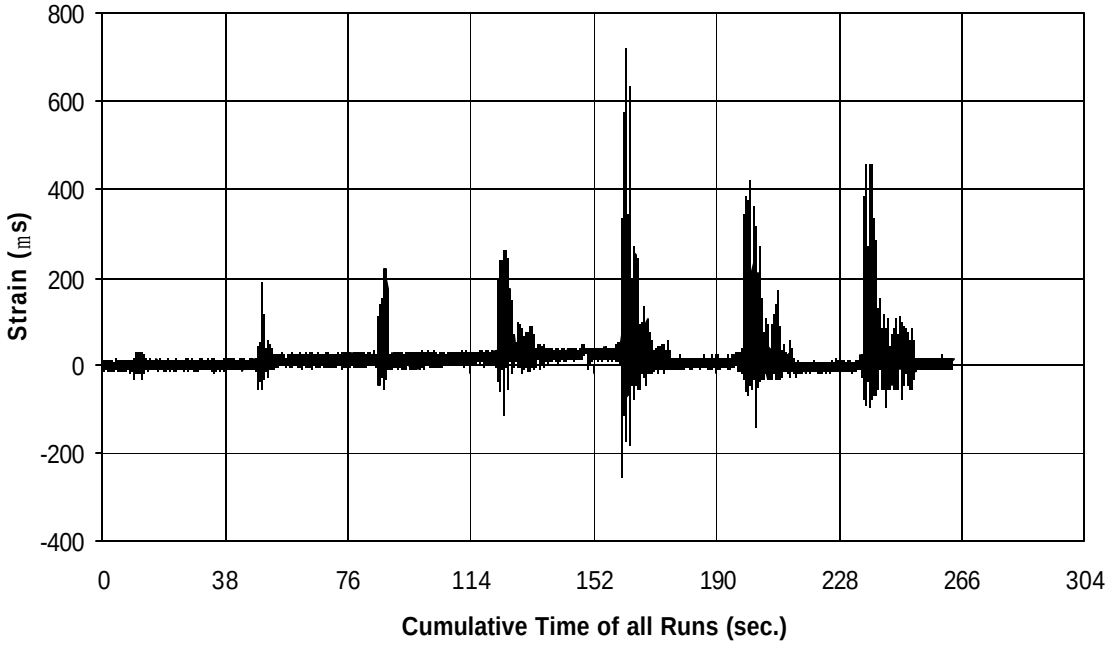

Fig. A-206 THD -4 Measured Strain in Gauge SG2

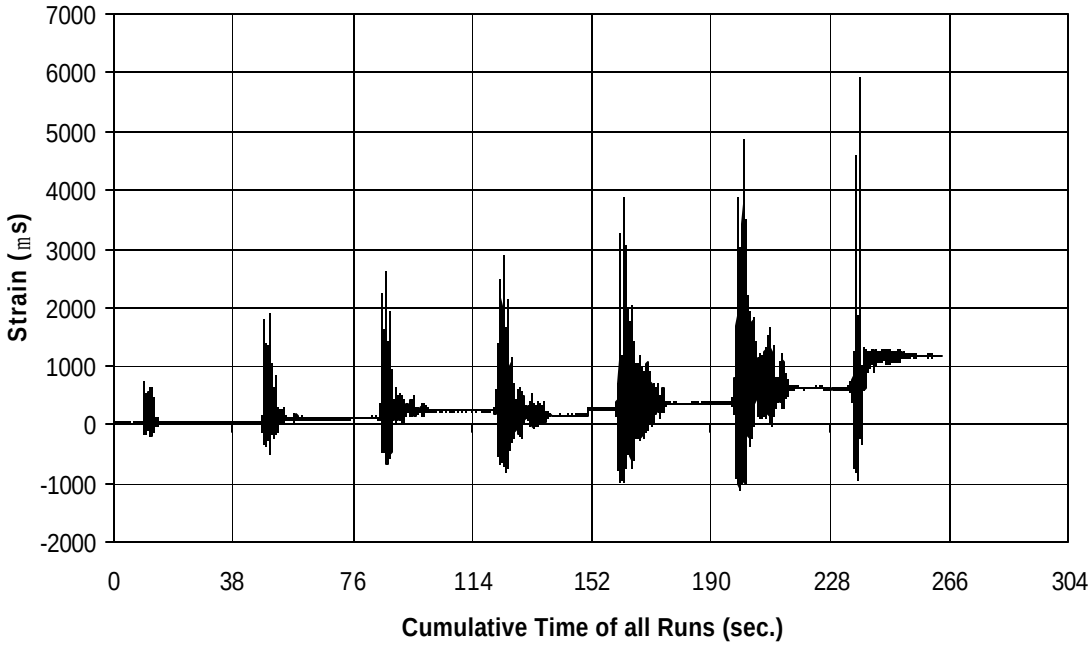

Fig. A-207 THD -4 Measured Strain in Gauge SG3

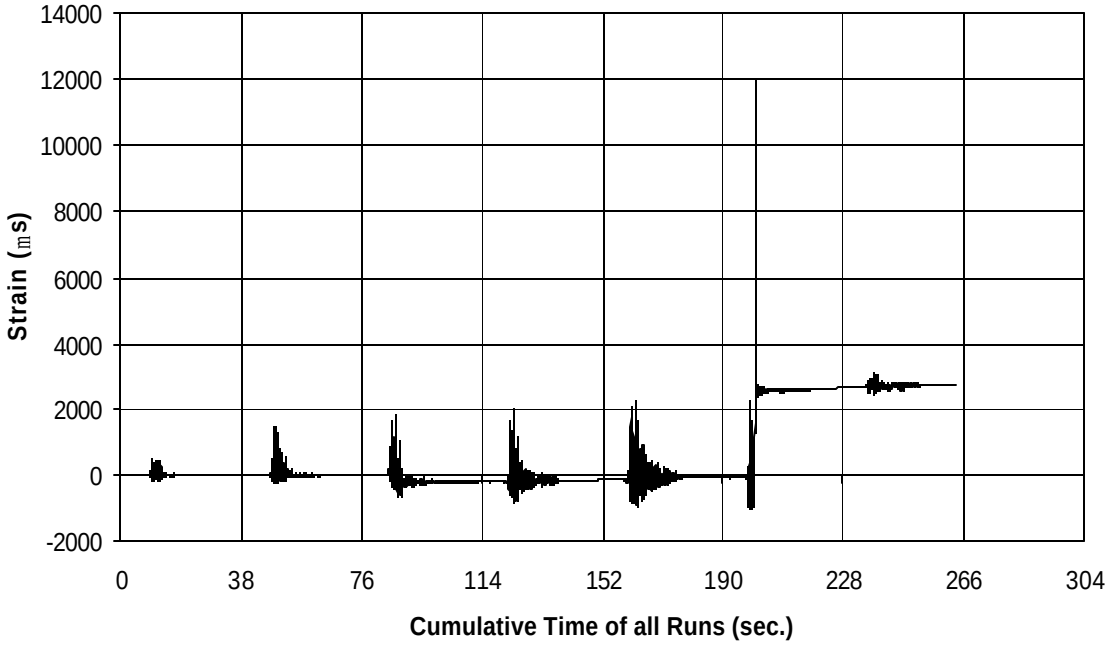

Fig. A-208 THD -4 Measured Strain in Gauge SG4

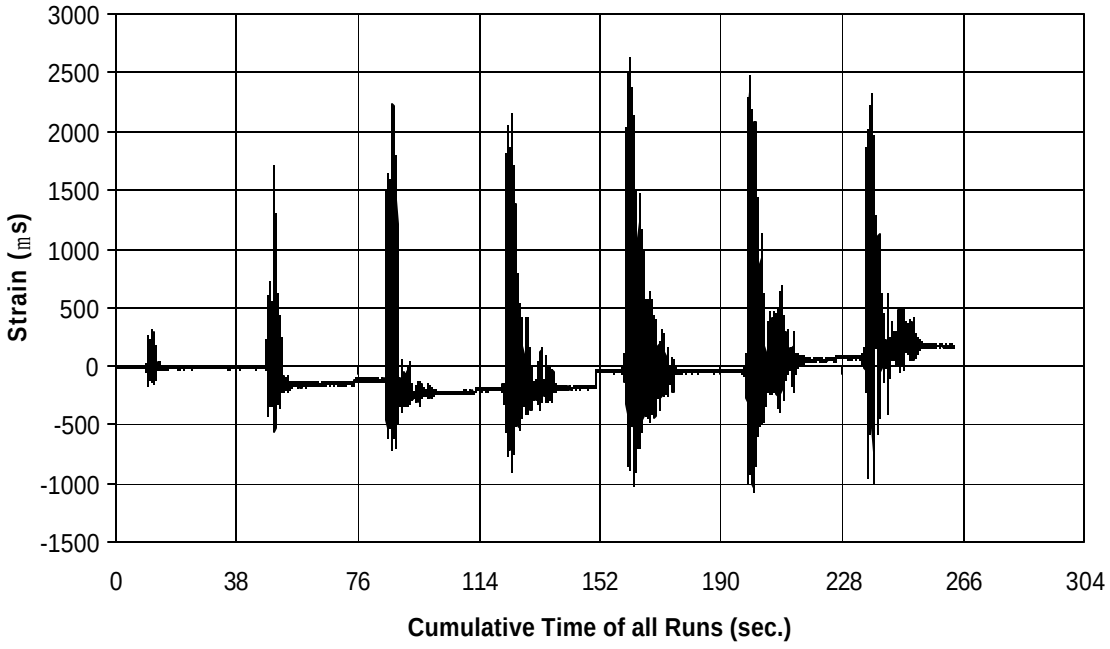

Fig. A-209 THD -4 Measured Strain in Gauge SG5

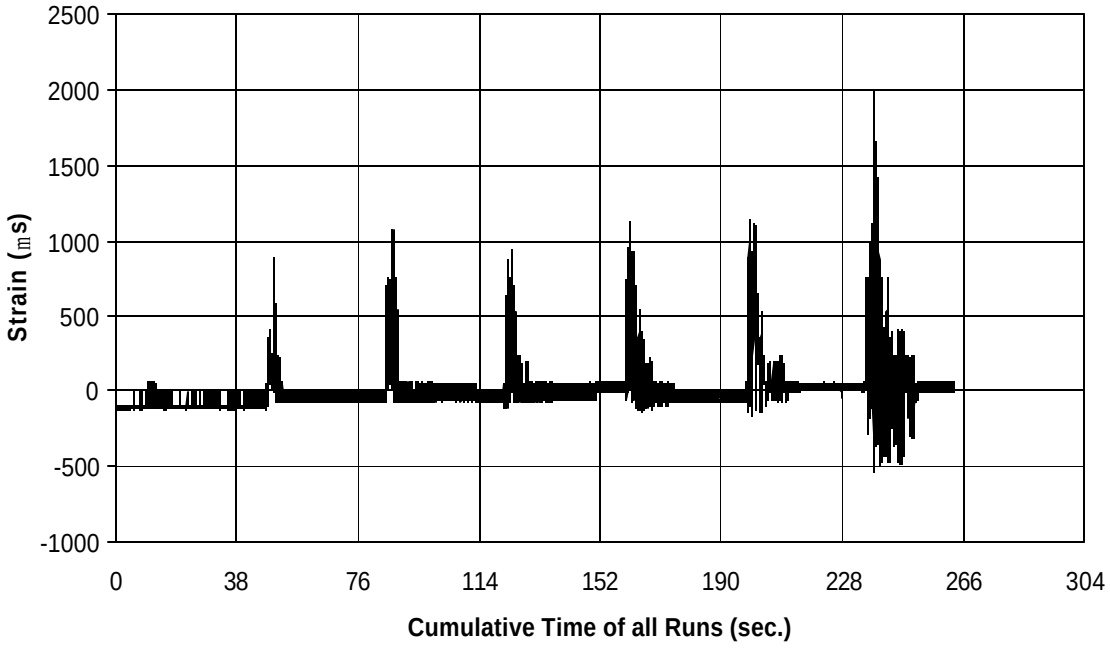

Fig. A-210 THD -4 Measured Strain in Gauge SG6

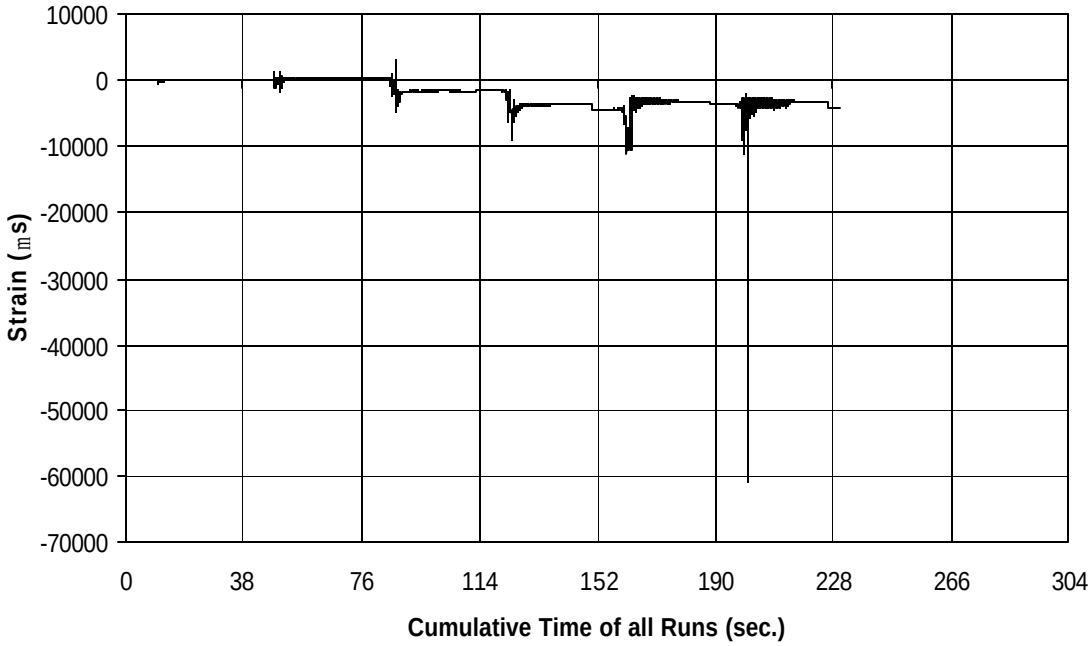

Fig. A-211 THD -4 Measured Strain in Gauge SG7

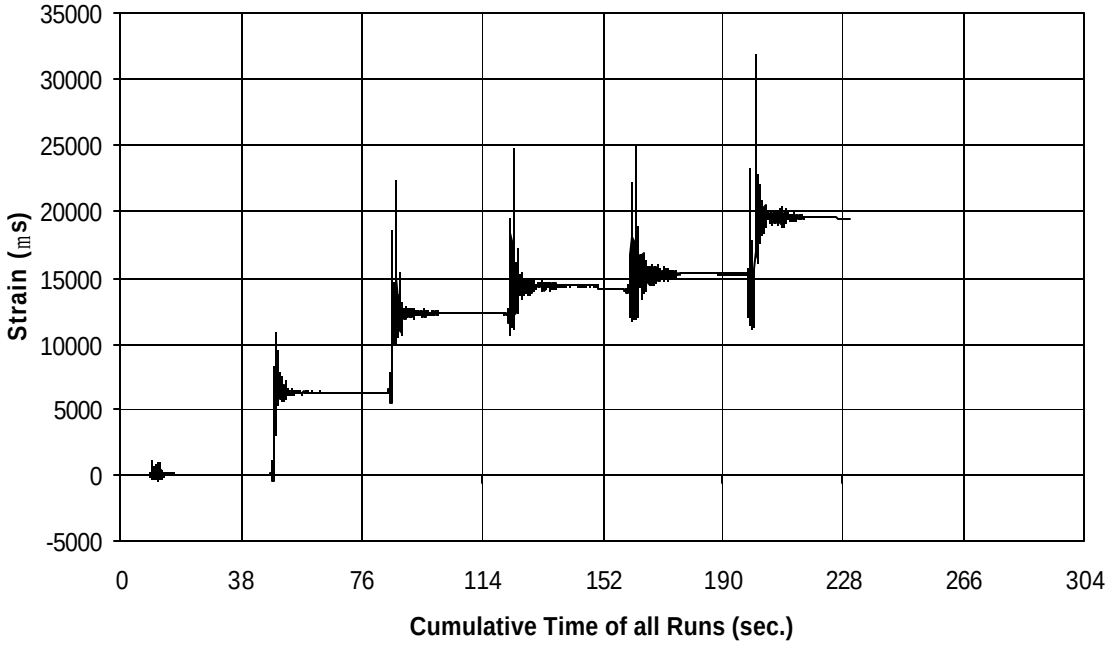

Fig. A-212 THD -4 Measured Strain in Gauge SG8

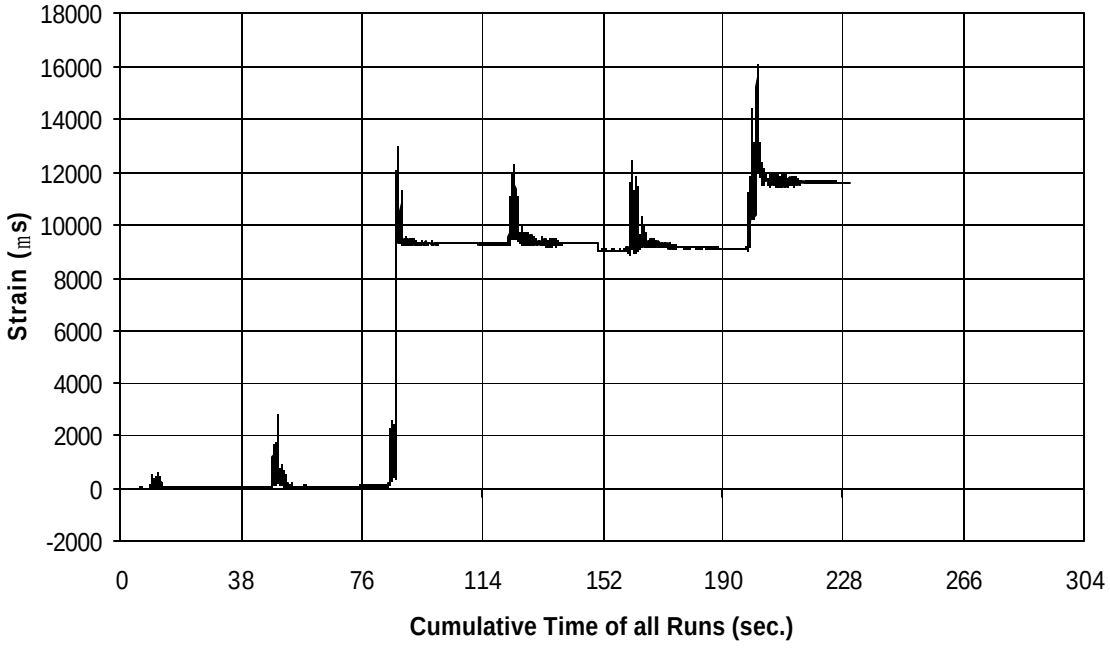

Fig. A-213 THD -4 Measured Strain in Gauge SG9

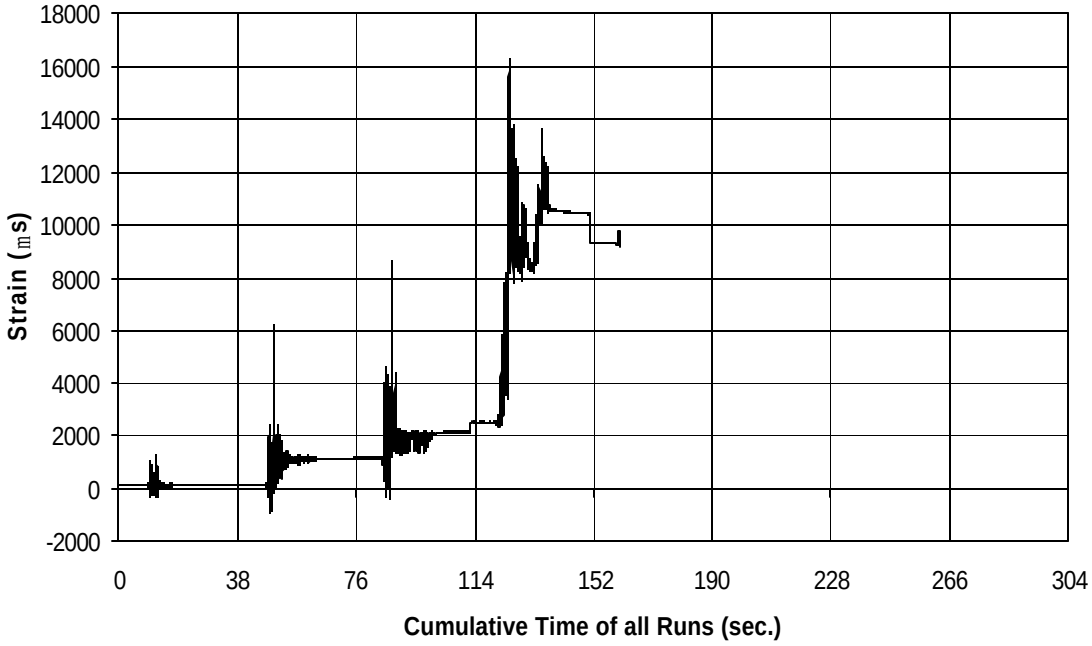

Fig. A-214 THD -4 Measured Strain in Gauge SG10

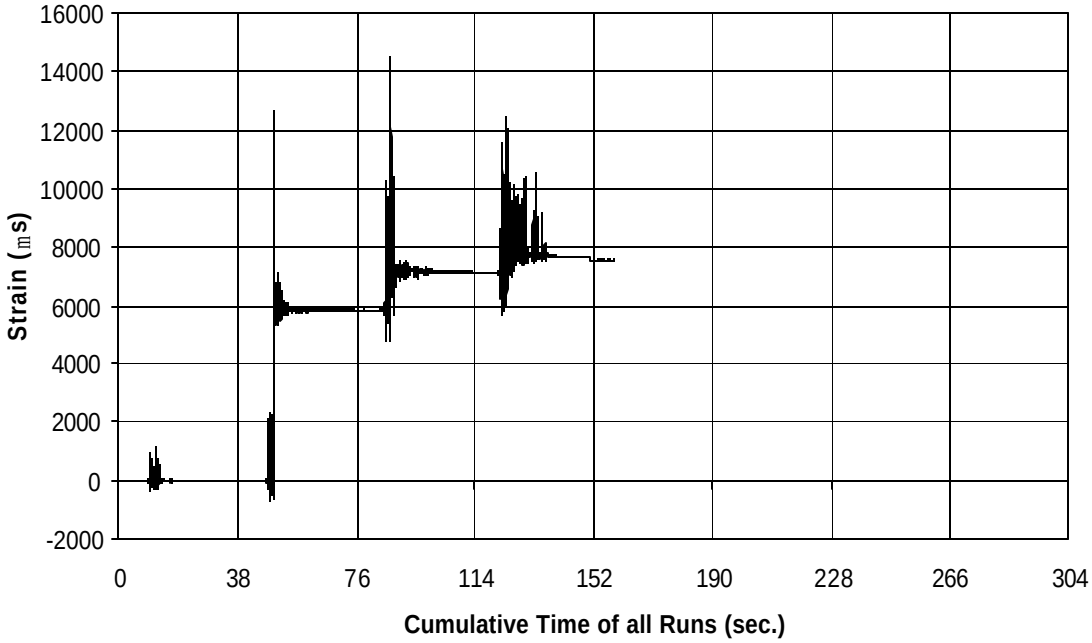

Fig. A-215 THD -4 Measured Strain in Gauge SG11

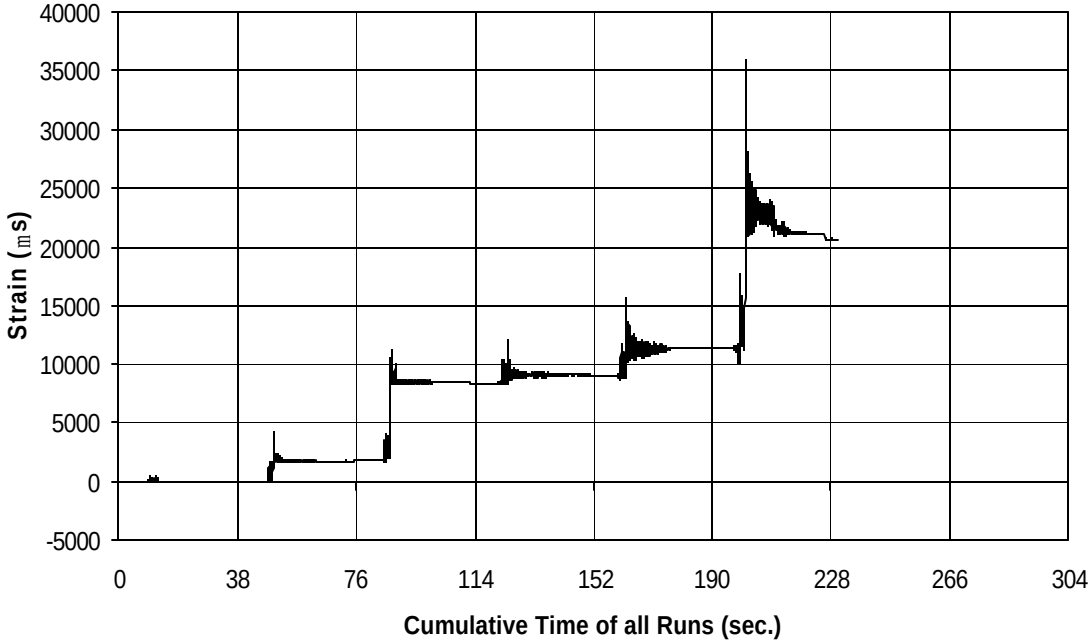

Fig. A-216 THD -4 Measured Strain in Gauge SG12

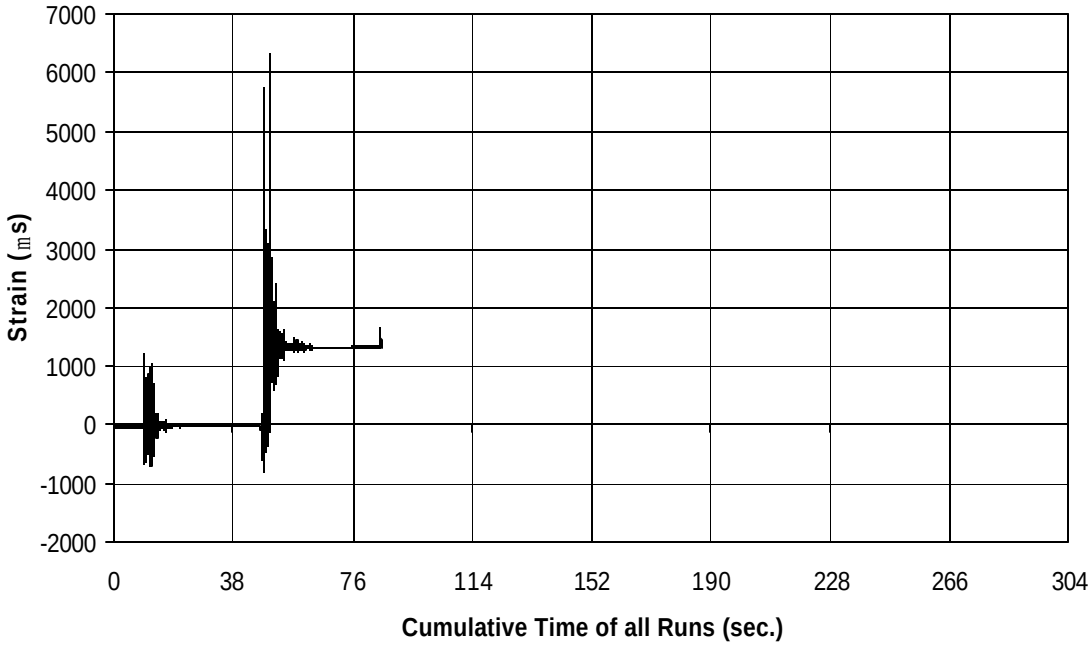

Fig. A-217 THD -4 Measured Strain in Gauge SG13

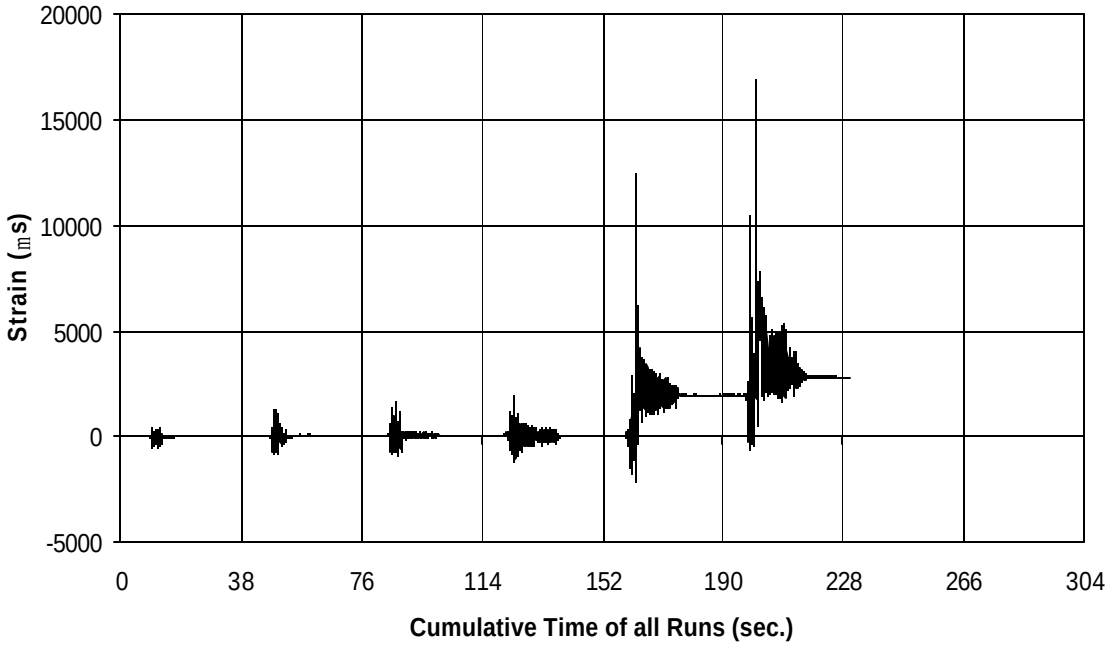

Fig. A-218 THD -4 Measured Strain in Gauge SG14

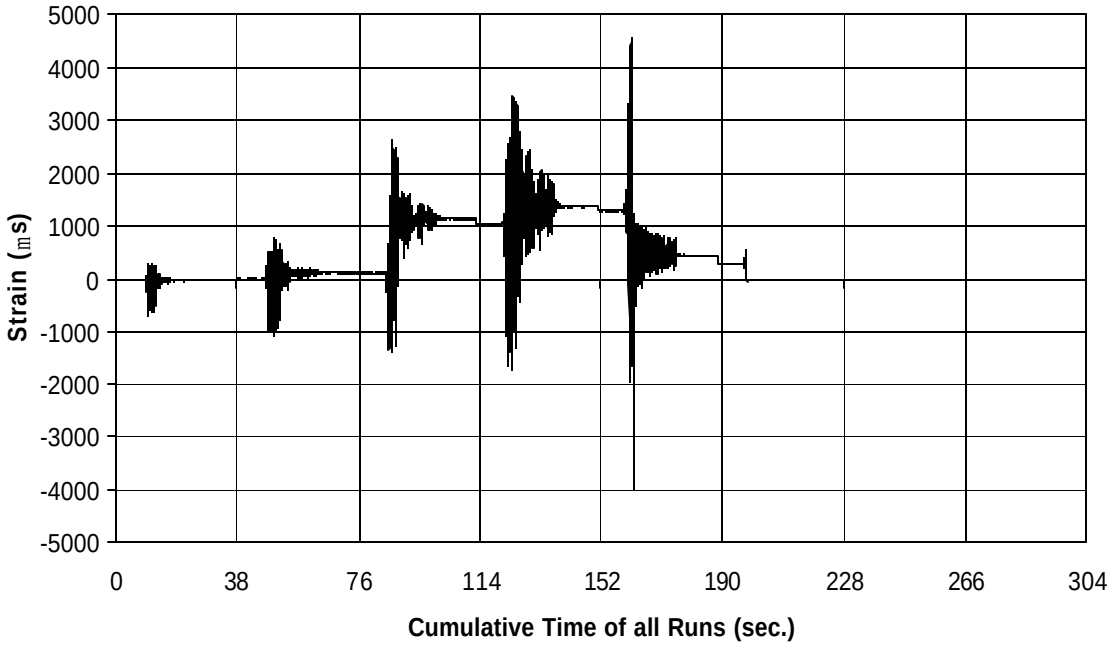

Fig. A-219 THD -4 Measured Strain in Gauge SG15

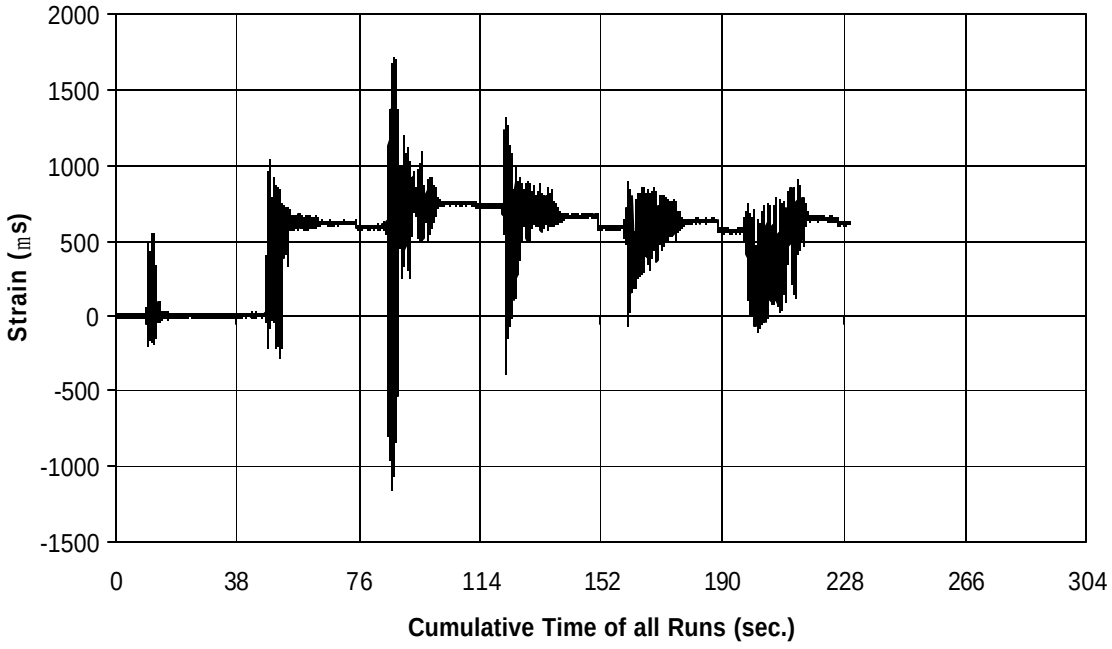

Fig. A-220 THD -4 Measured Strain in Gauge SG16

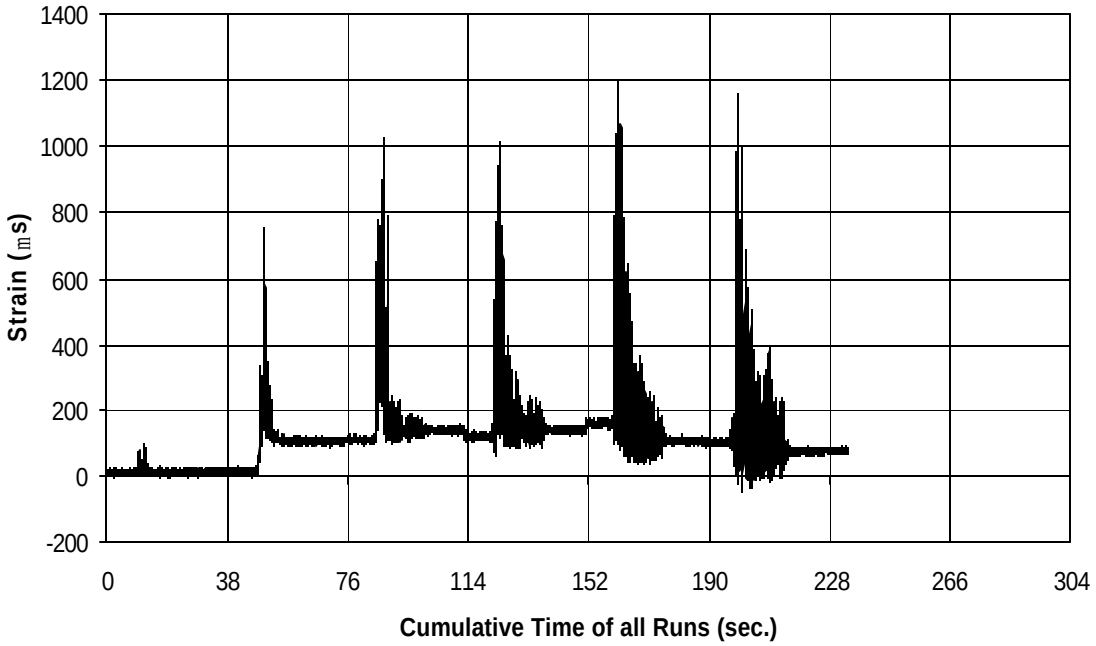

Fig. A-221 THD -4 Measured Strain in Gauge SG17

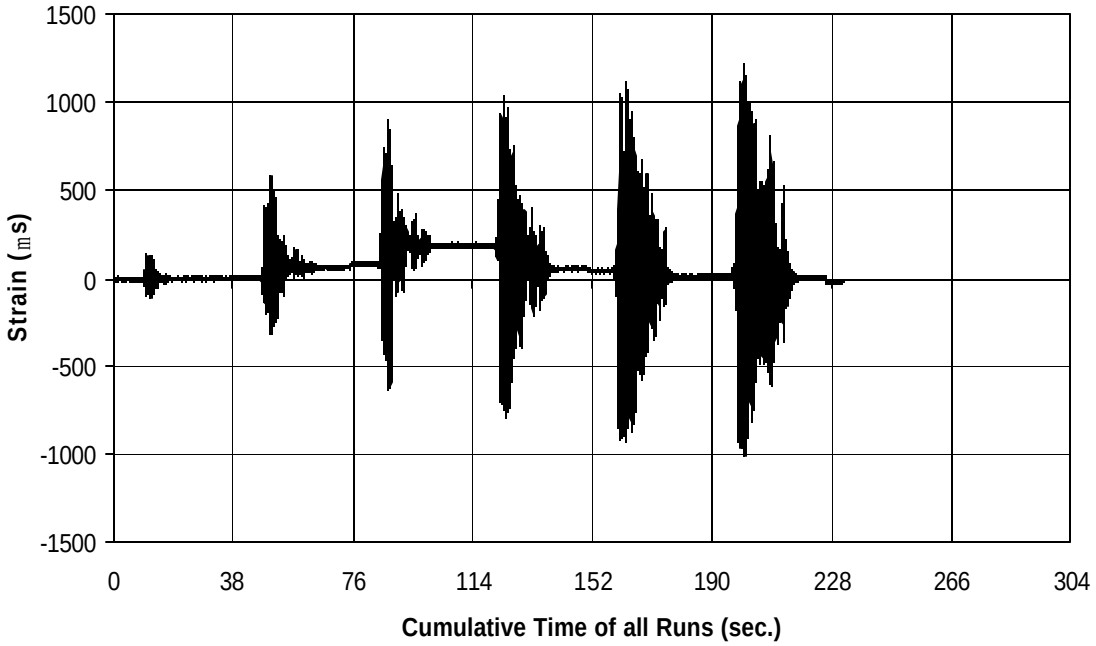

Fig. A-222 THD -4 Measured Strain in Gauge SG18

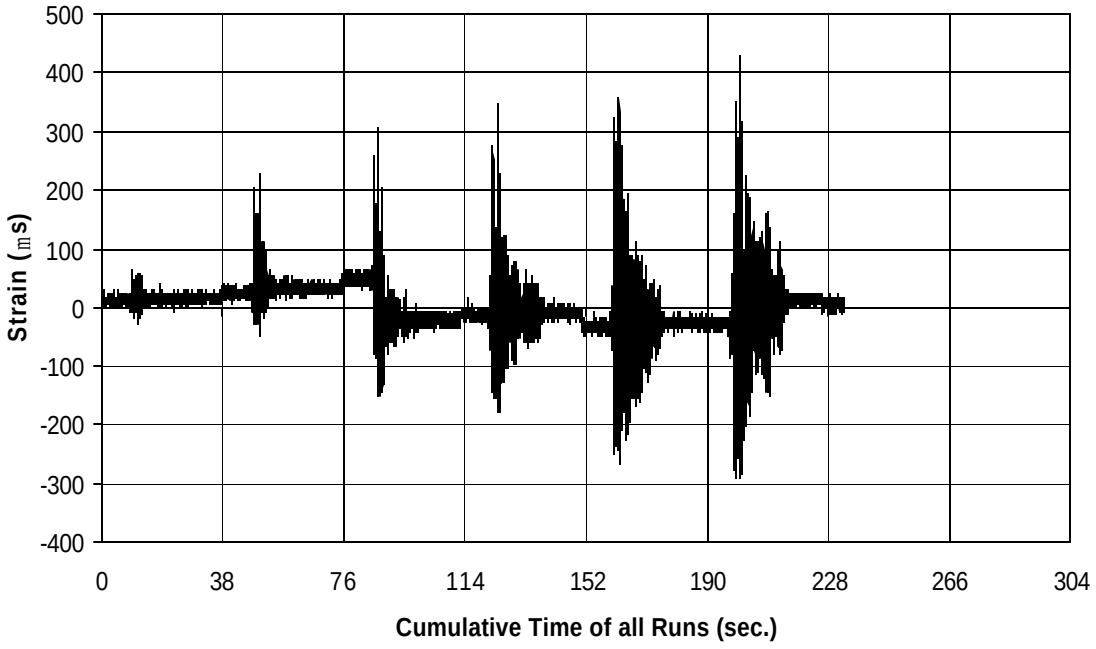

Fig. A-223 THD -4 Measured Strain in Gauge SG19

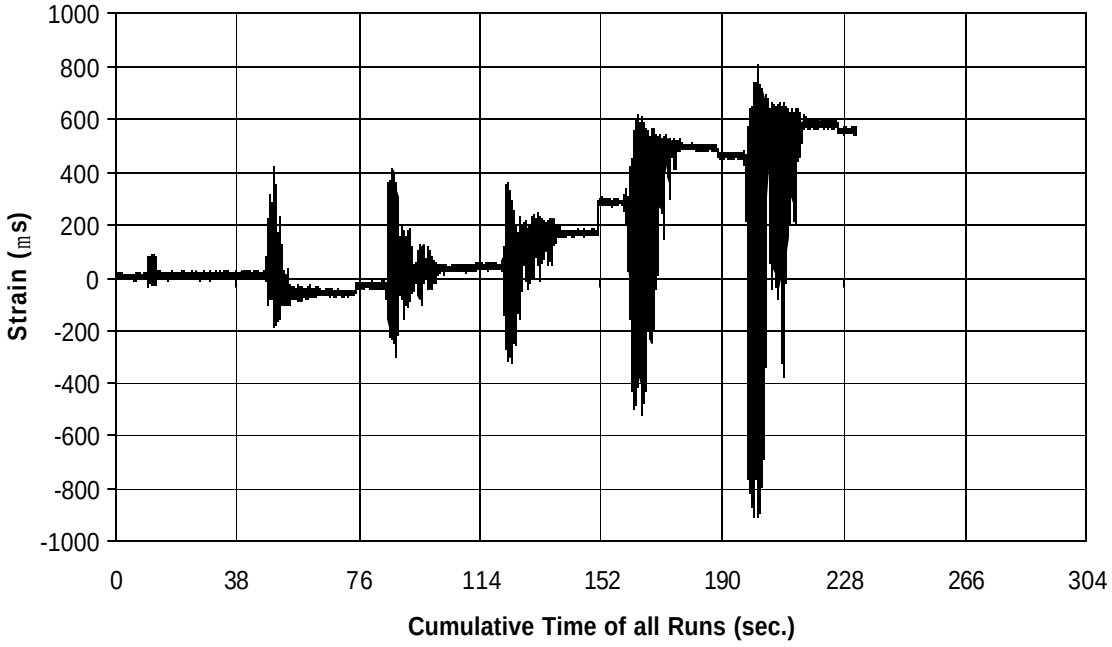

Fig. A-224 THD -4 Measured Strain in Gauge SG20

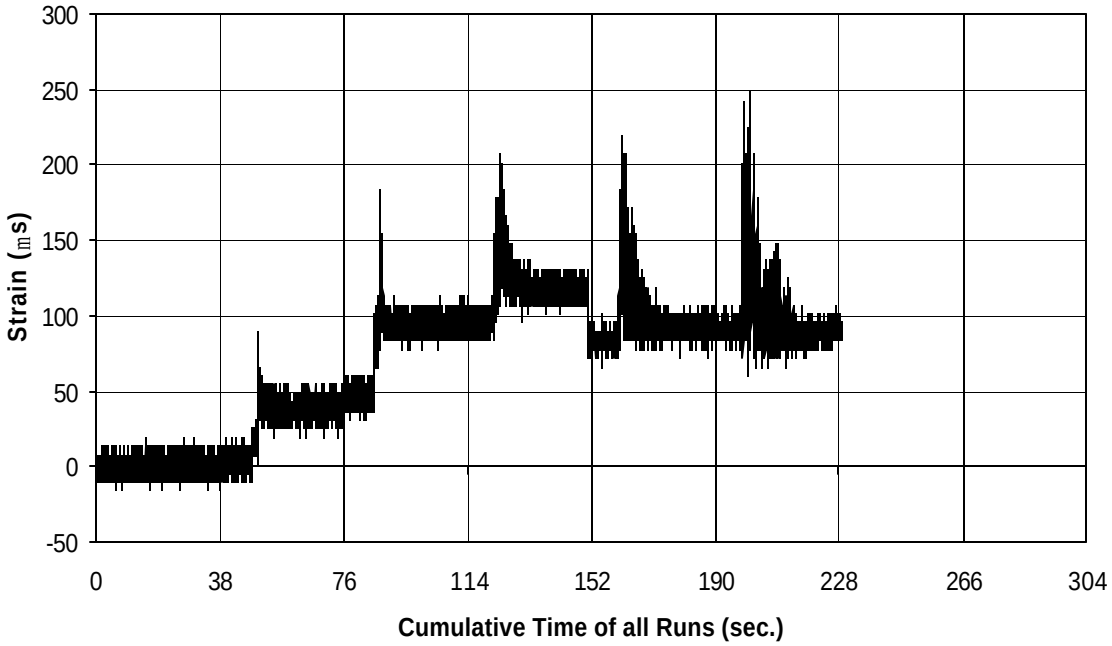

Fig. A-225 THD -4 Measured Strain in Gauge SG21

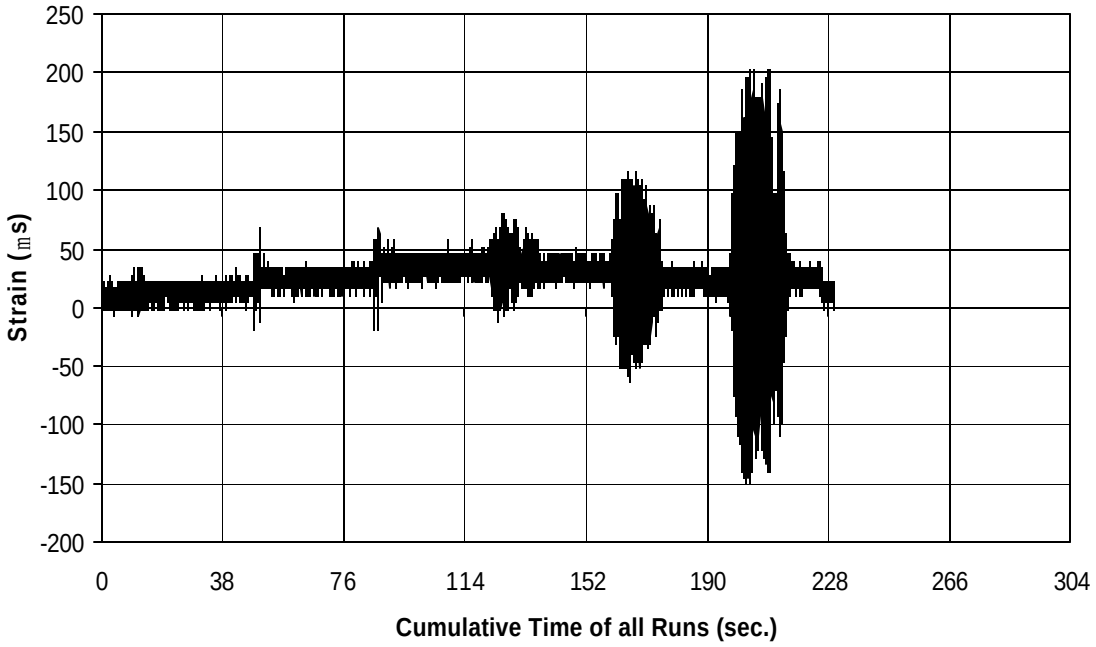

Fig. A-226 THD -4 Measured Strain in Gauge SG22

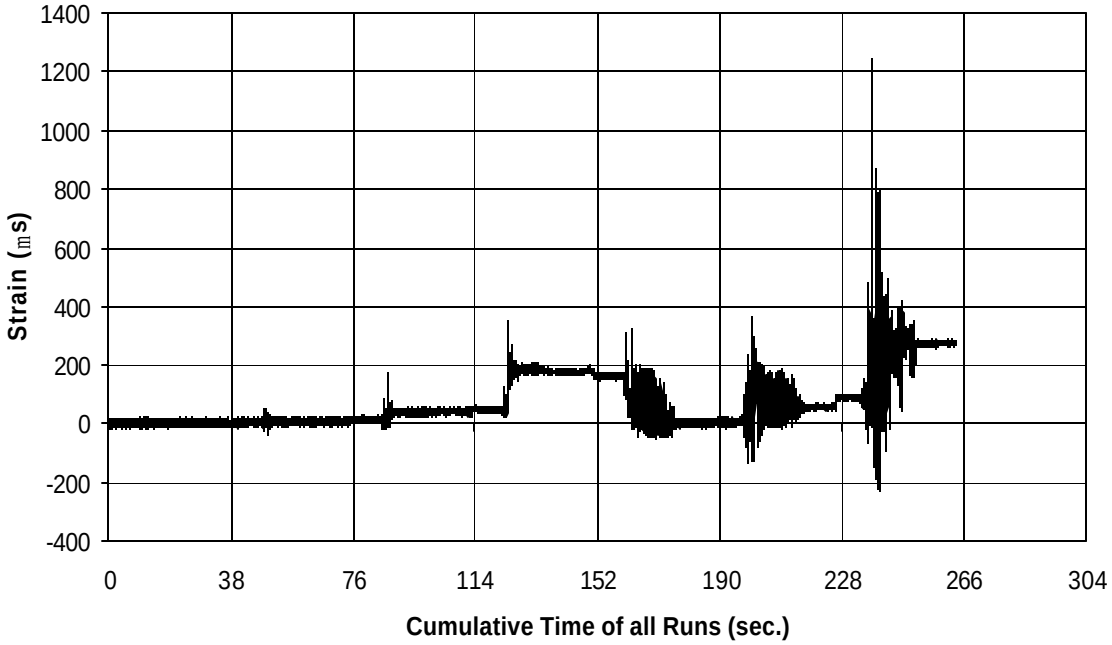

Fig. A-227 THD -4 Measured Strain in Gauge SG23

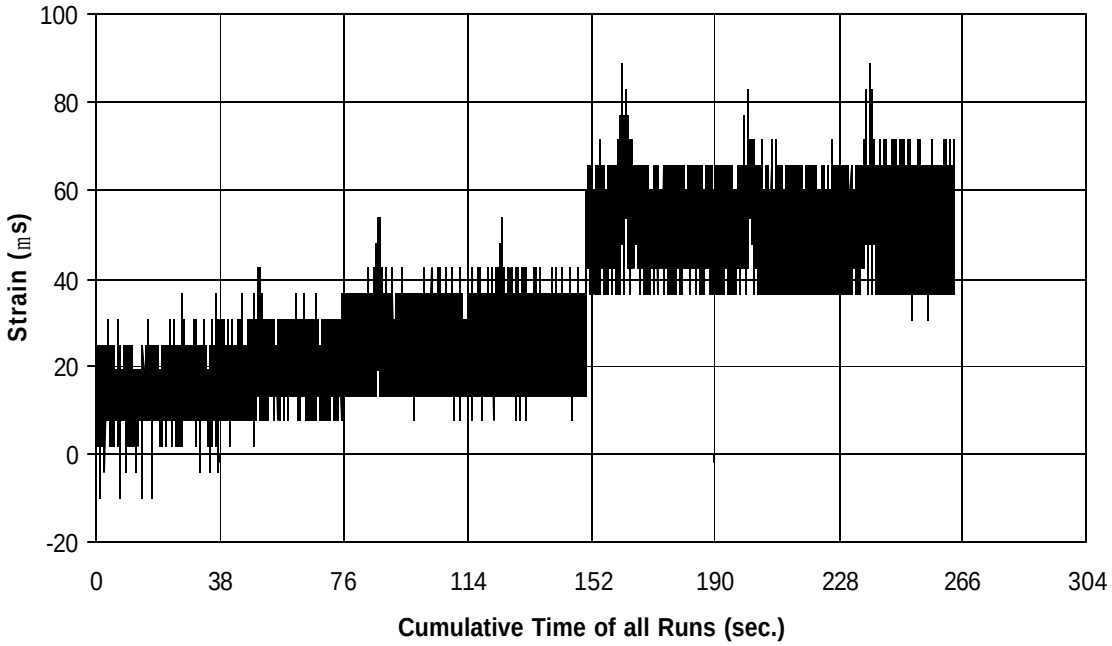

Fig. A-228 THD -4 Measured Strain in Gauge SG24

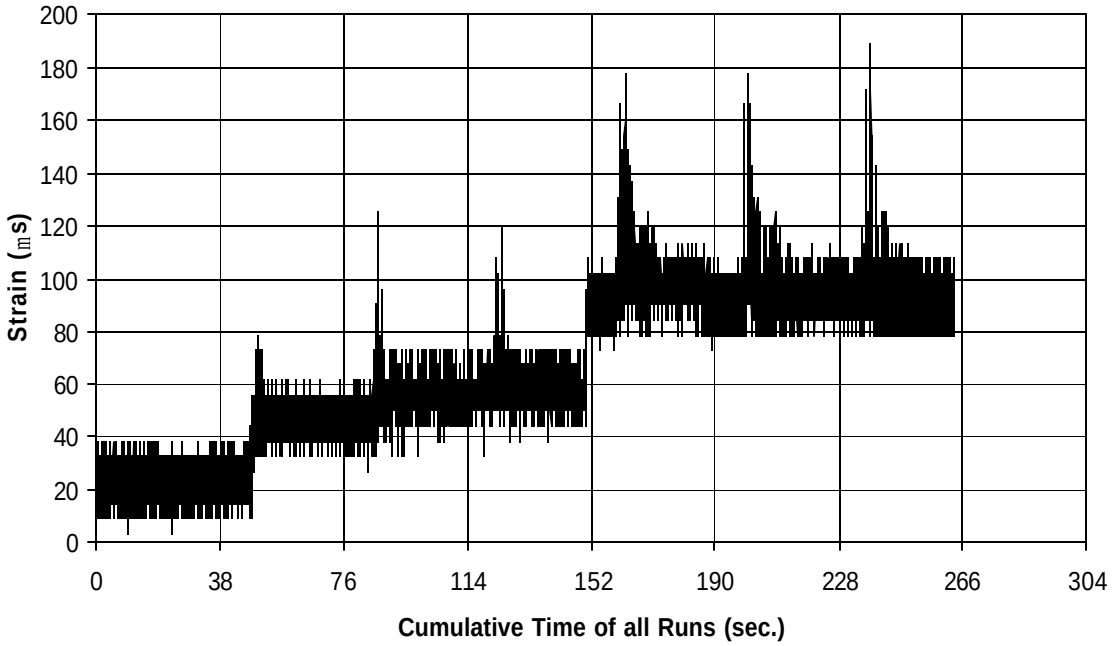

Fig. A-229 THD -4 Measured Strain in Gauge SG25

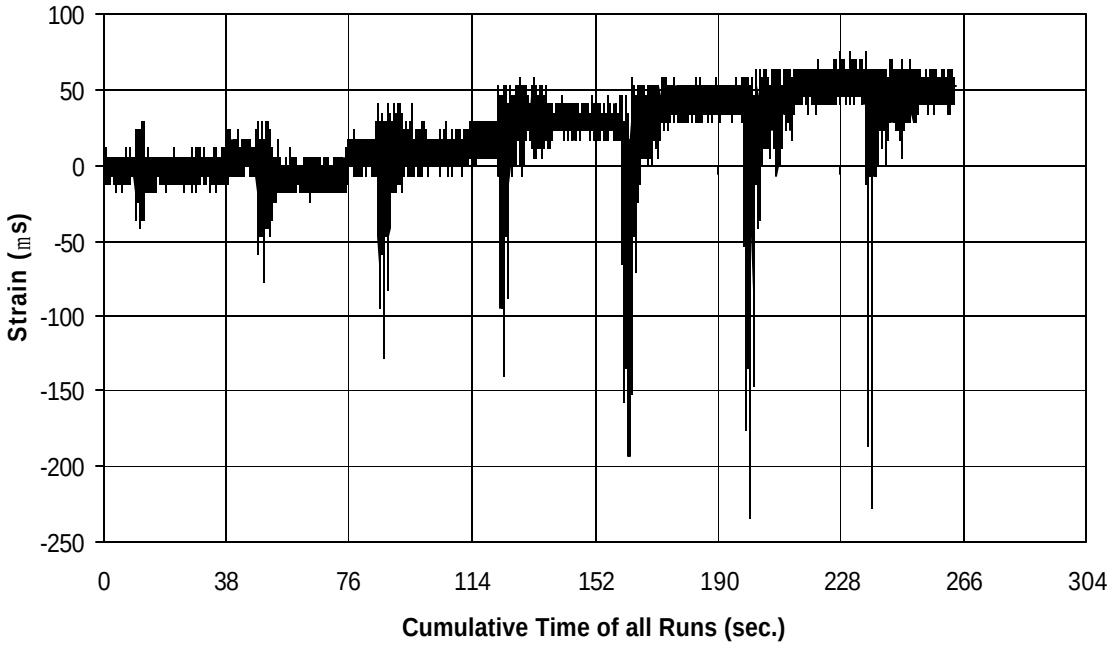

Fig. A-230 THD -4 Measured Strain in Gauge SG26

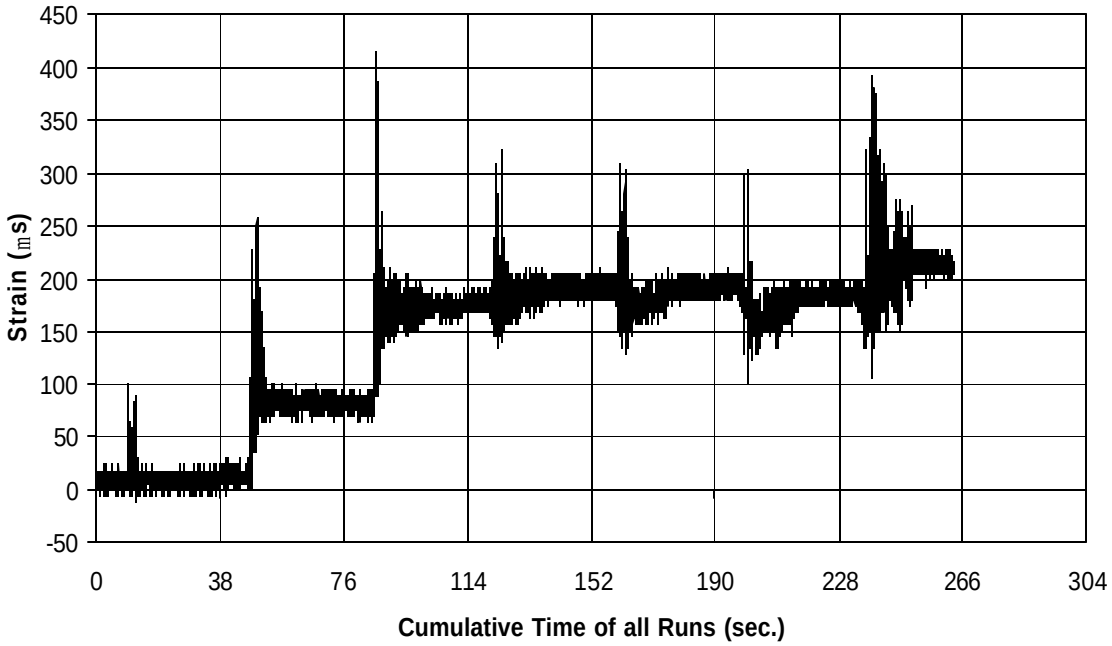

Fig. A-231 THD -4 Measured Strain in Gauge SG27

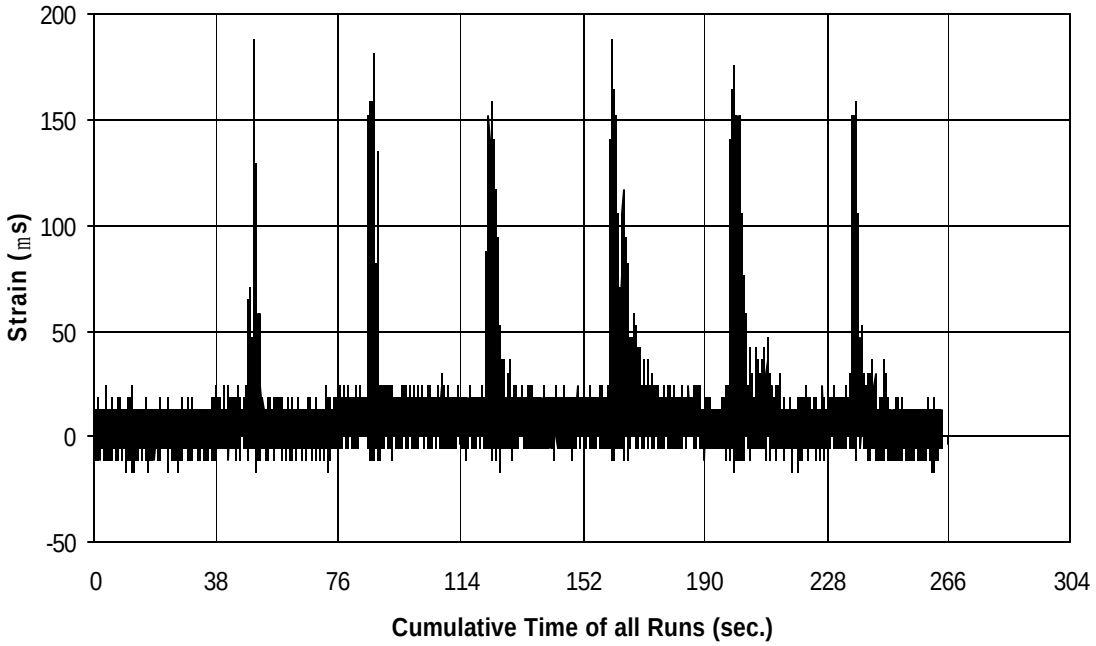

Fig. A-232 THD -4 Measured Strain in Gauge SG28

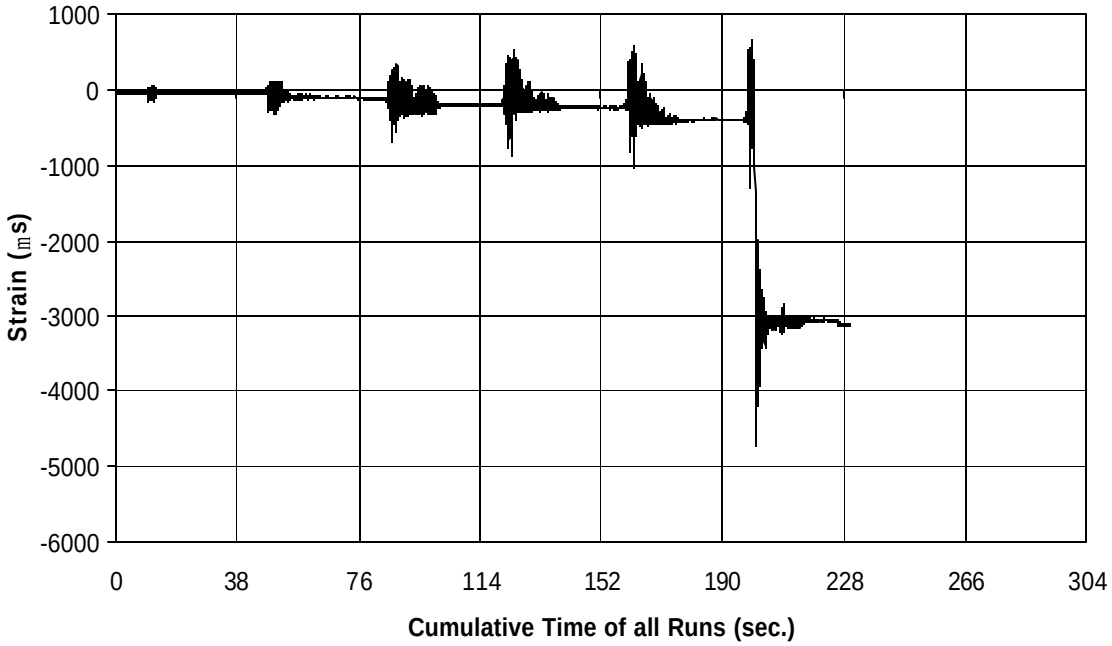

Fig. A-233 THD -4 Measured Strain in Gauge SG29

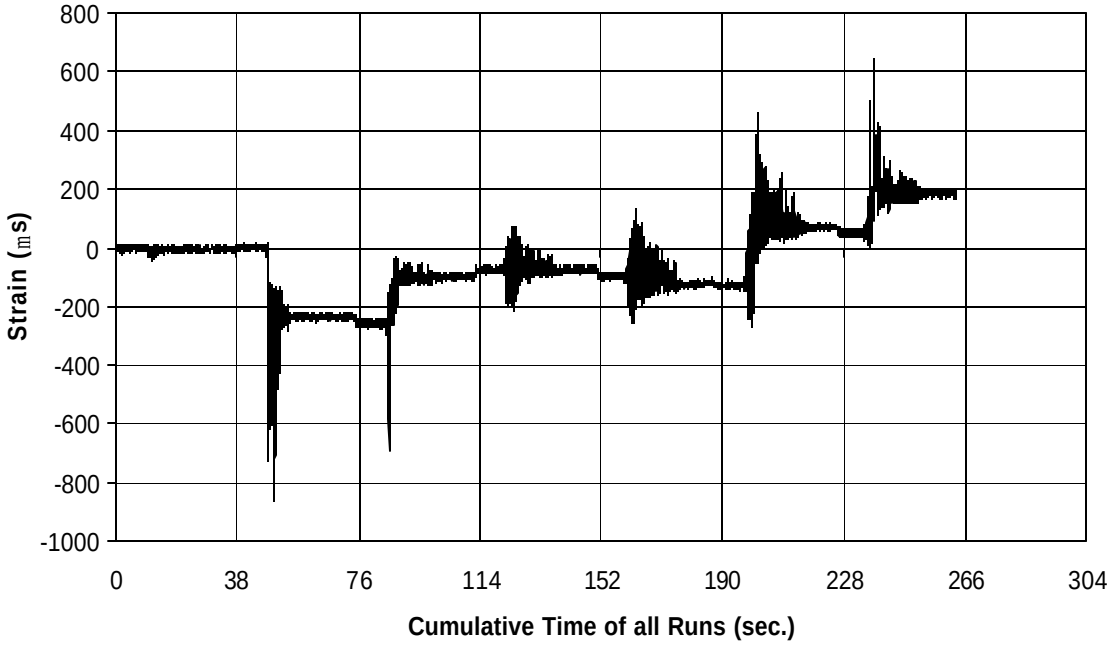

Fig. A-234 THD -4 Measured Strain in Gauge SG30

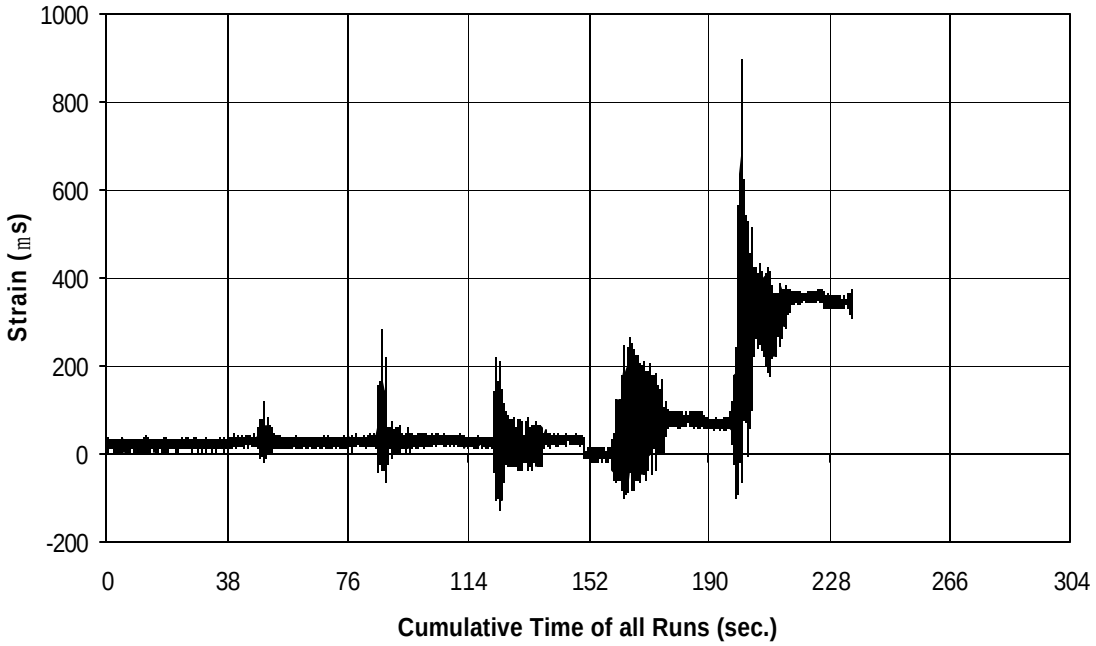

Fig. A-235 THD -4 Measured Strain in Gauge SG31

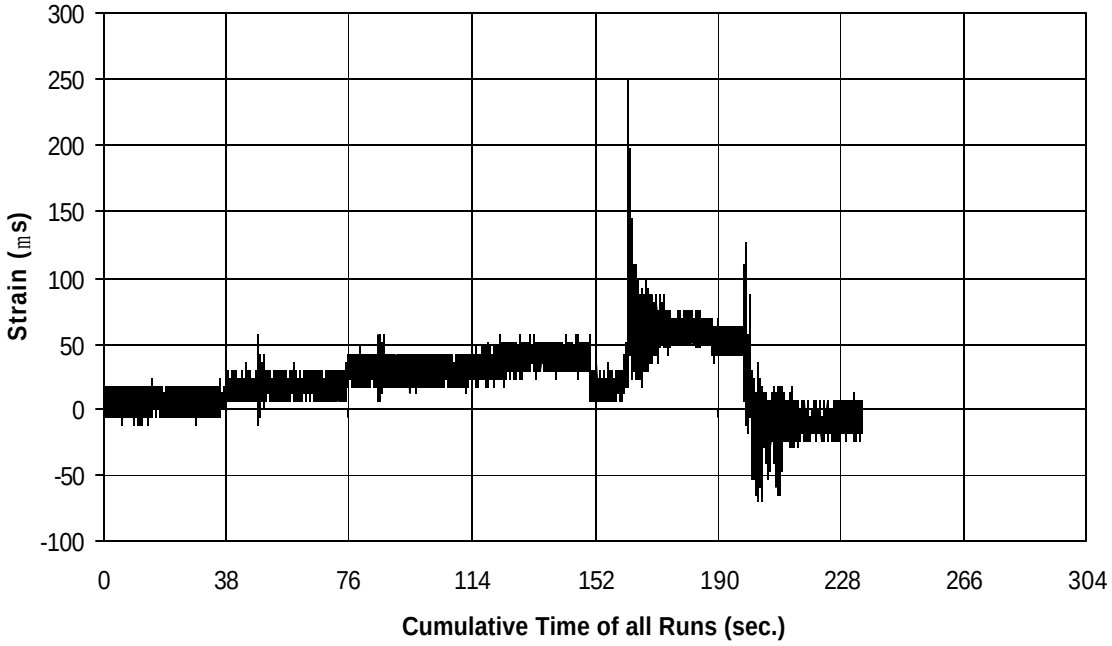

Fig. A-236 THD -4 Measured Strain in Gauge SG32

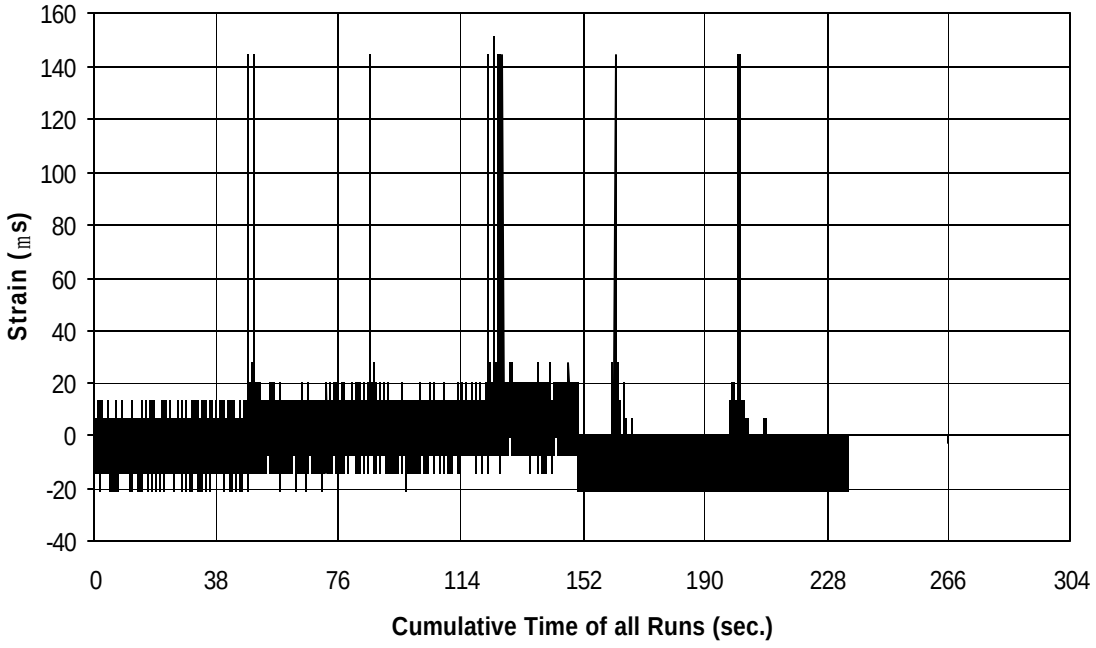

Fig. A-237 THD -4 Measured Strain in Gauge SG33

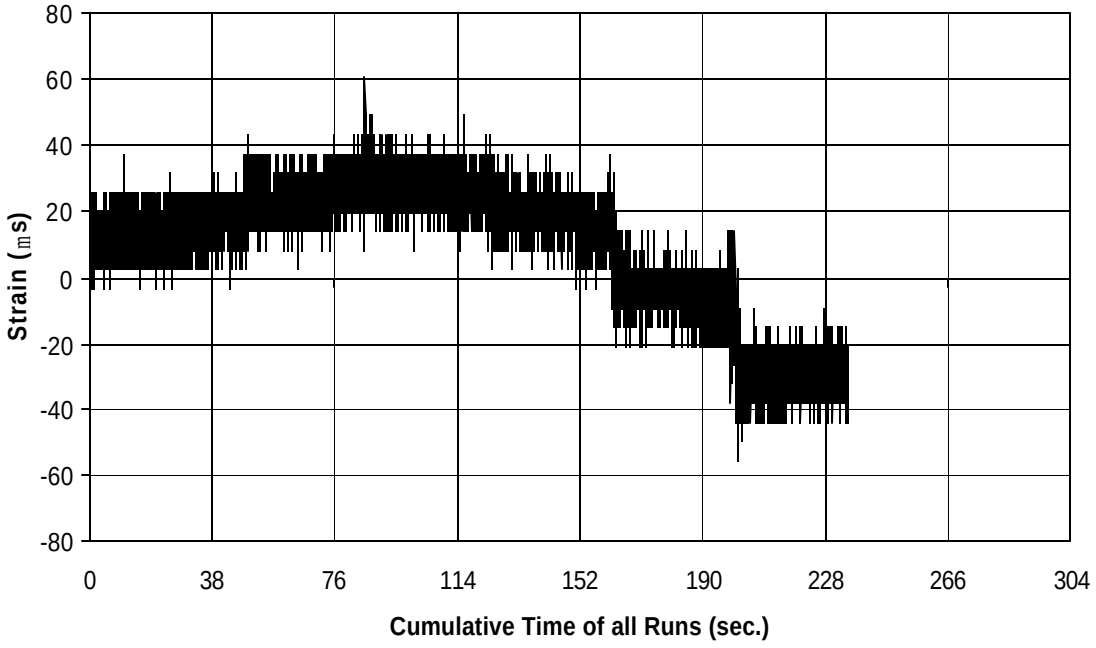

Fig. A-238 THD -4 Measured Strain in Gauge SG34

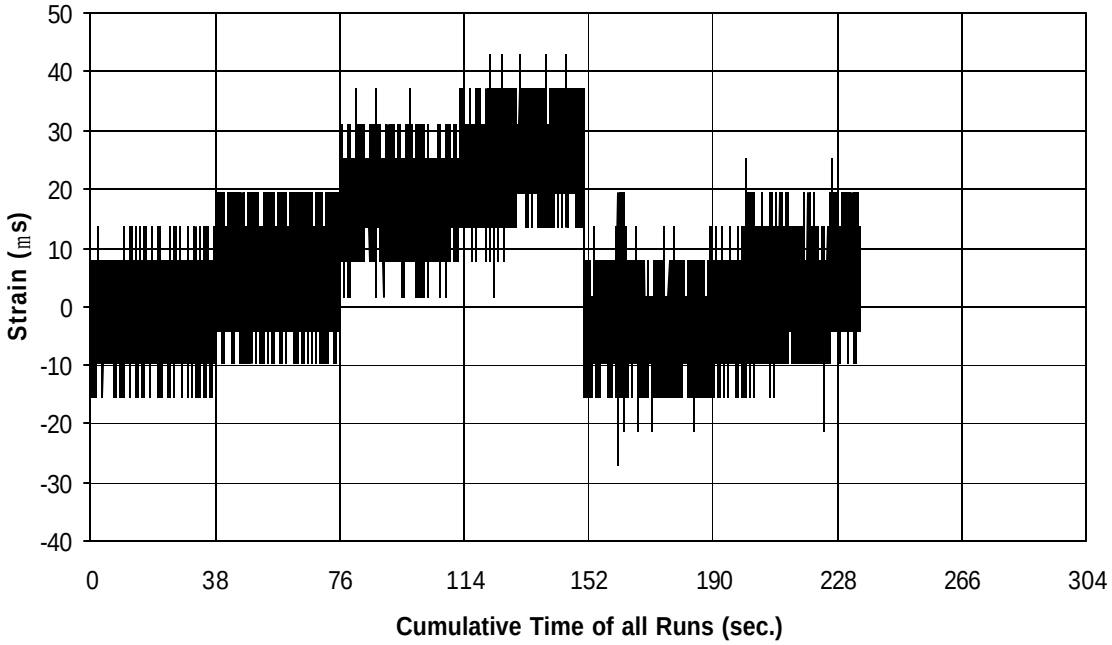

Fig. A-239 THD -4 Measured Strain in Gauge SG35

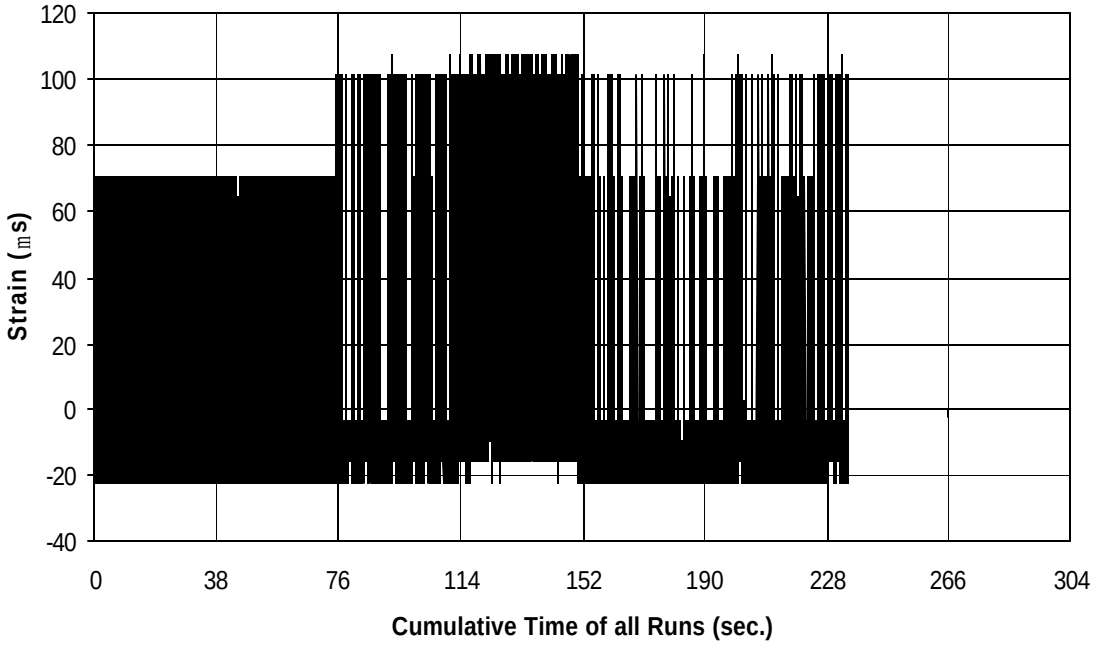

Fig. A-240 THD -4 Measured Strain in Gauge SG36

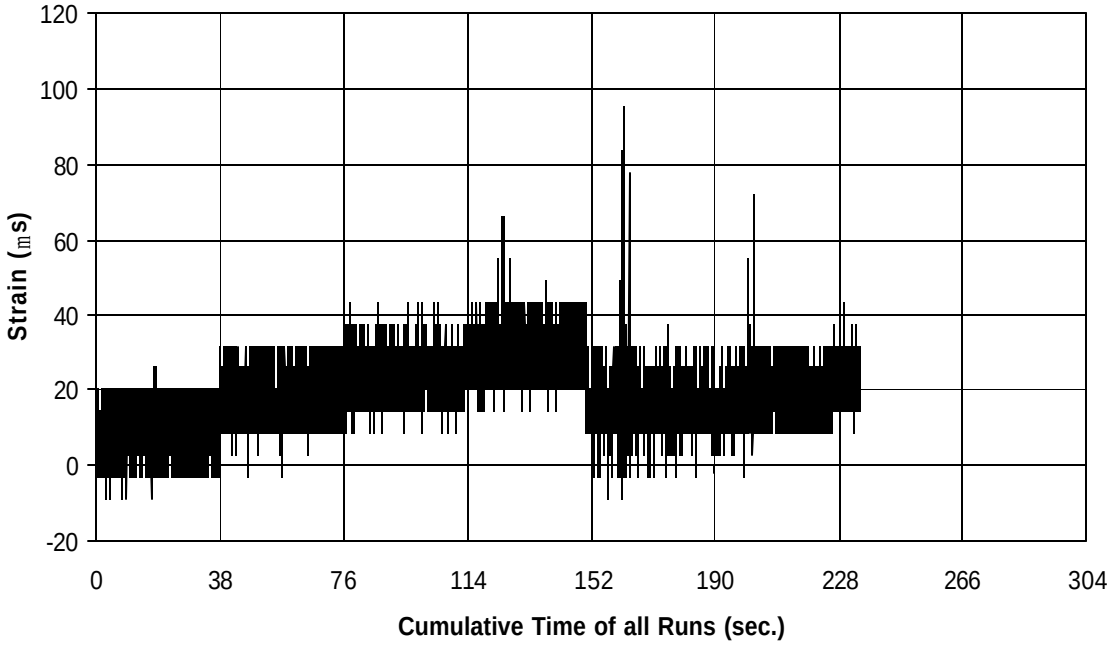

Fig. A-241 THD -4 Measured Strain in Gauge SG37

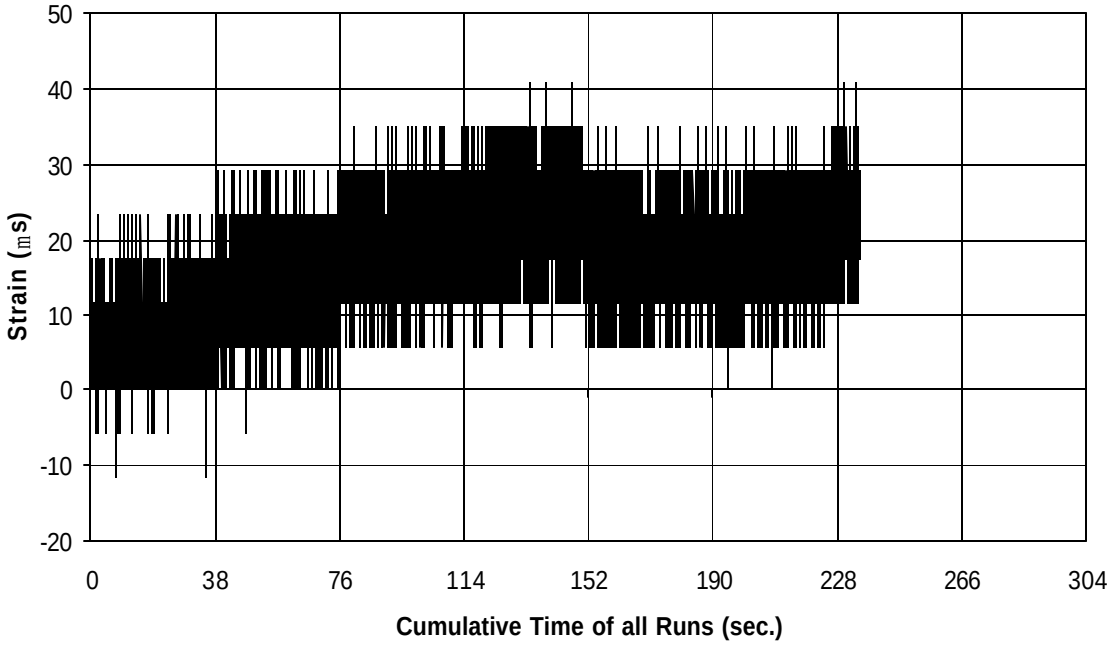

Fig. A-242 THD -4 Measured Strain in Gauge SG38

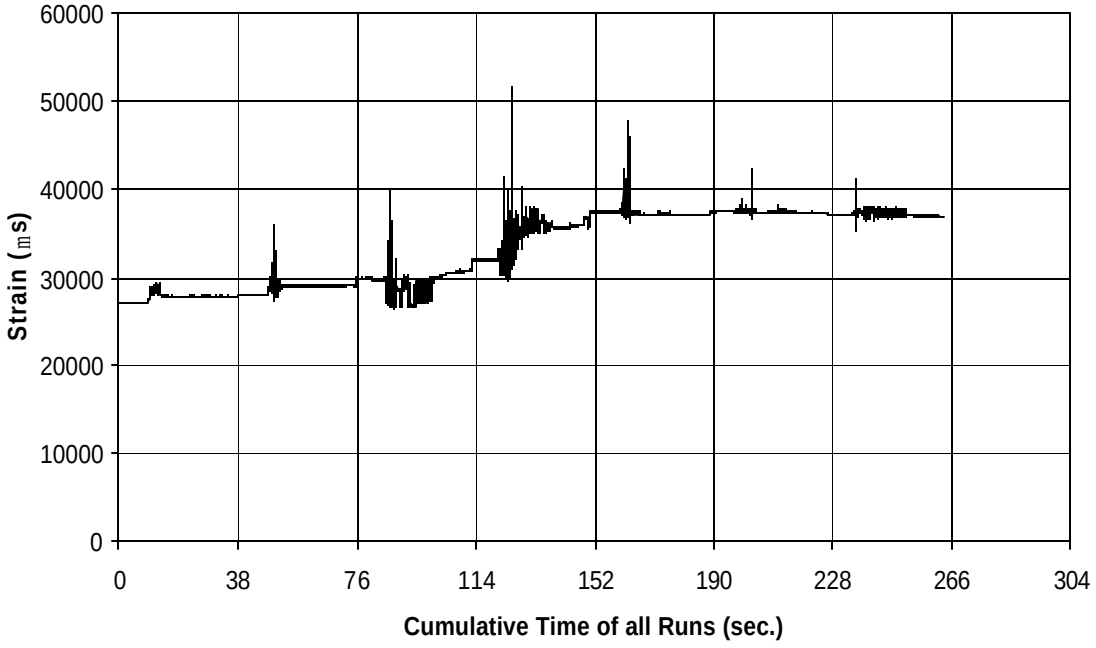

Fig. A-243 THD -4 Measured Strain in Gauge SG39

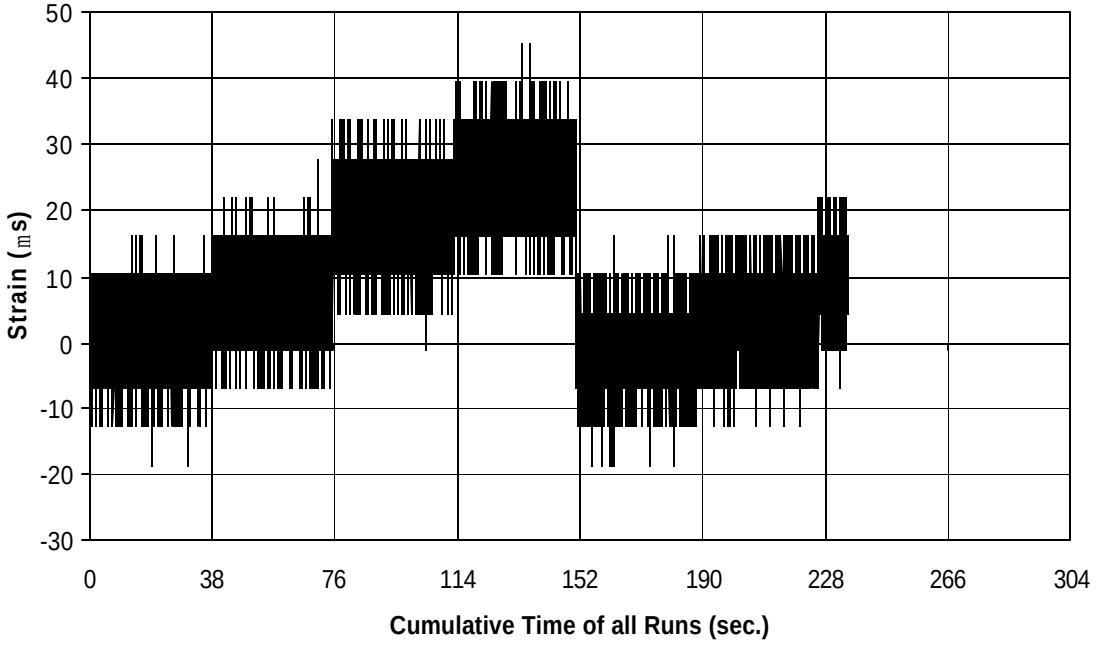

Fig. A-244 THD -4 Measured Strain in Gauge SG40

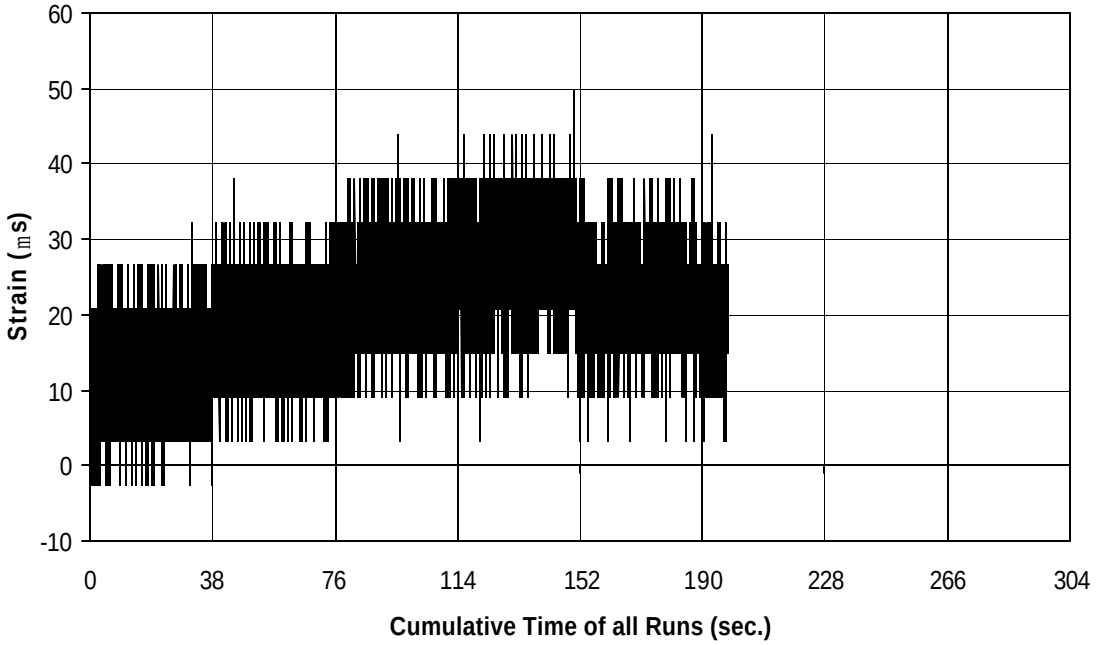

Fig. A-245 THD -4 Measured Strain in Gauge SG41

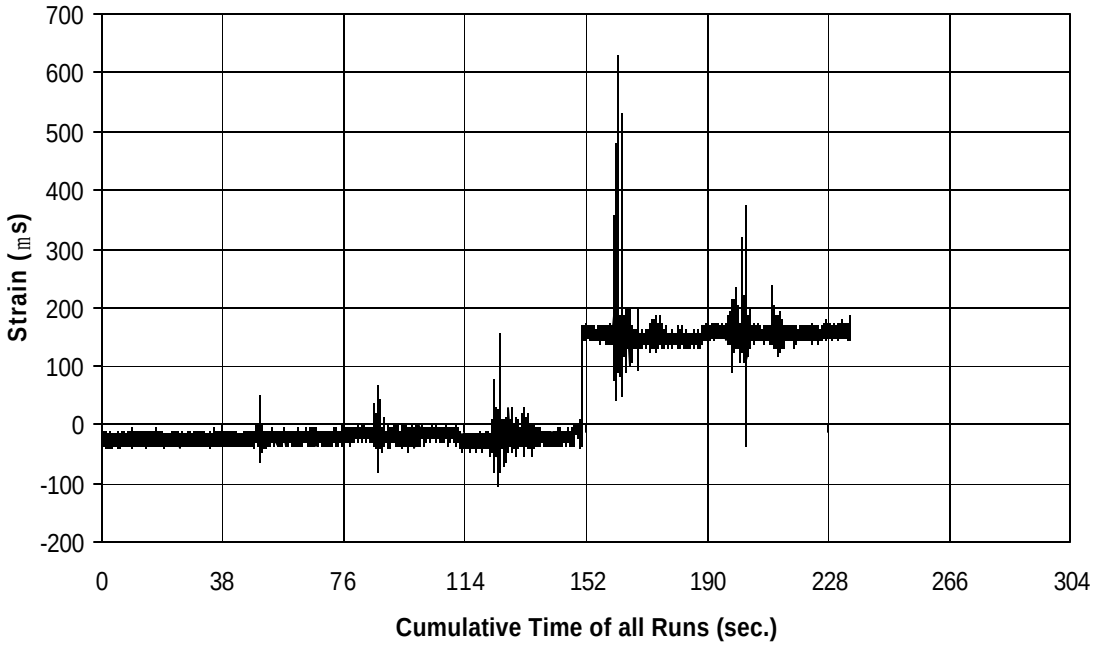

Fig. A-246 THD -4 Measured Strain in Gauge SG42

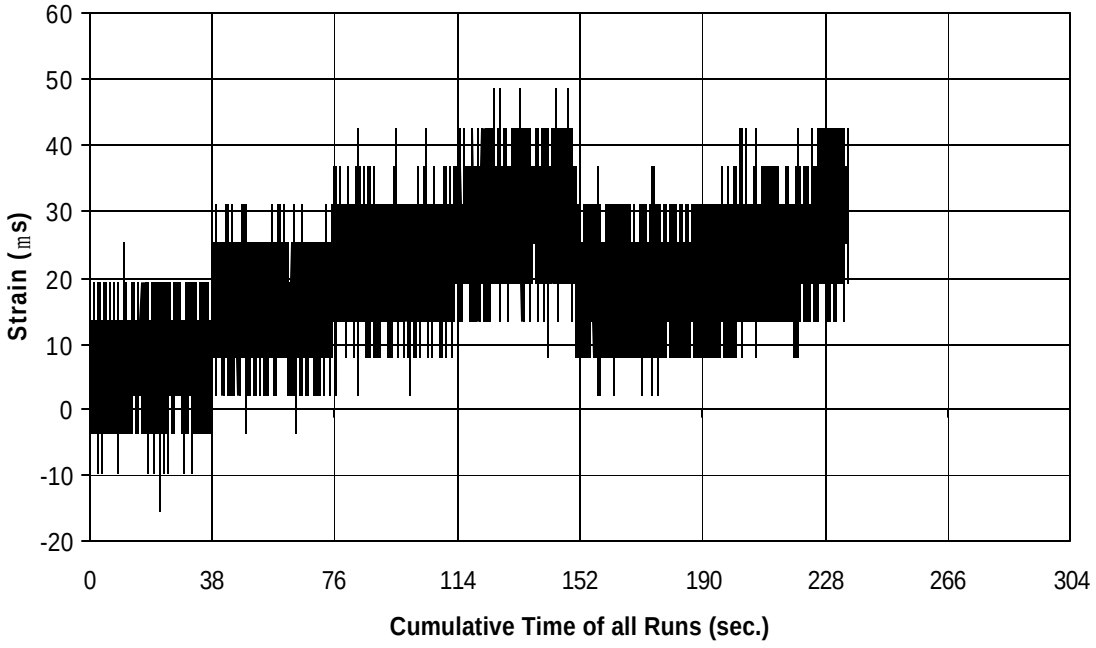

Fig. A-247 THD -4 Measured Strain in Gauge SG43

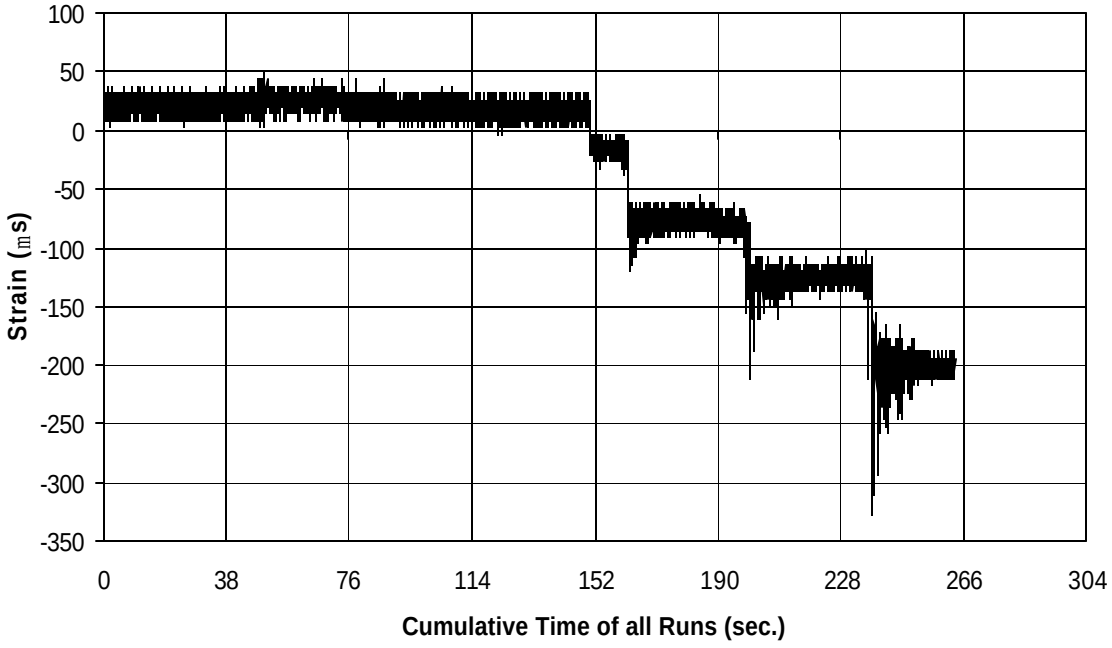

Fig. A-248 THD -4 Measured Strain in Gauge SG44

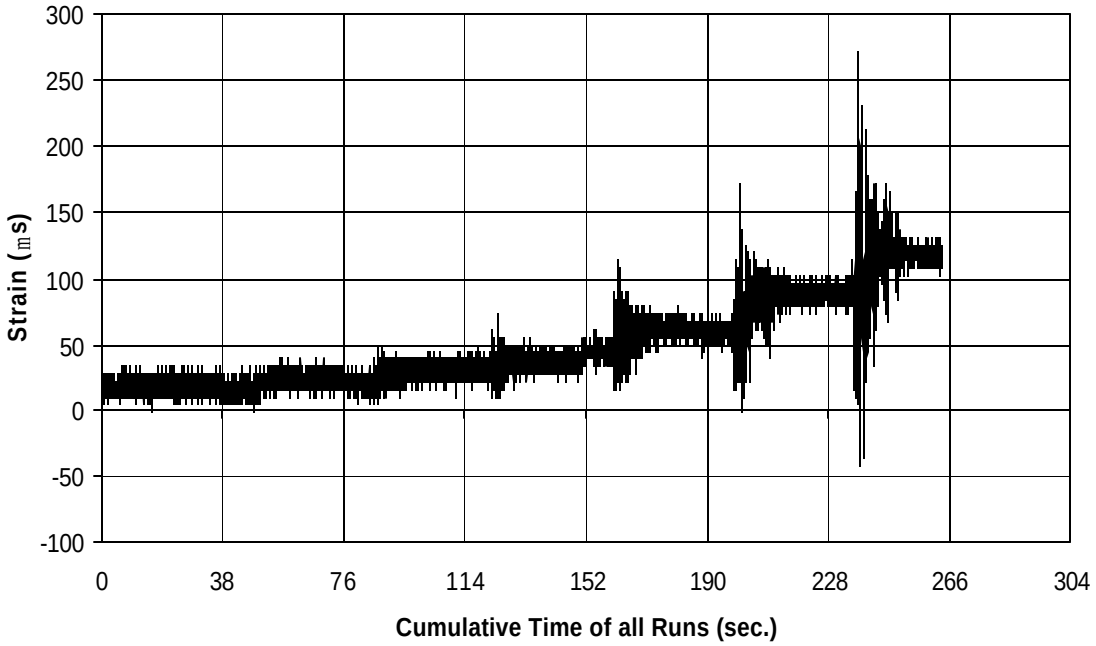

Fig. A-249 THD -4 Measured Strain in Gauge SG45

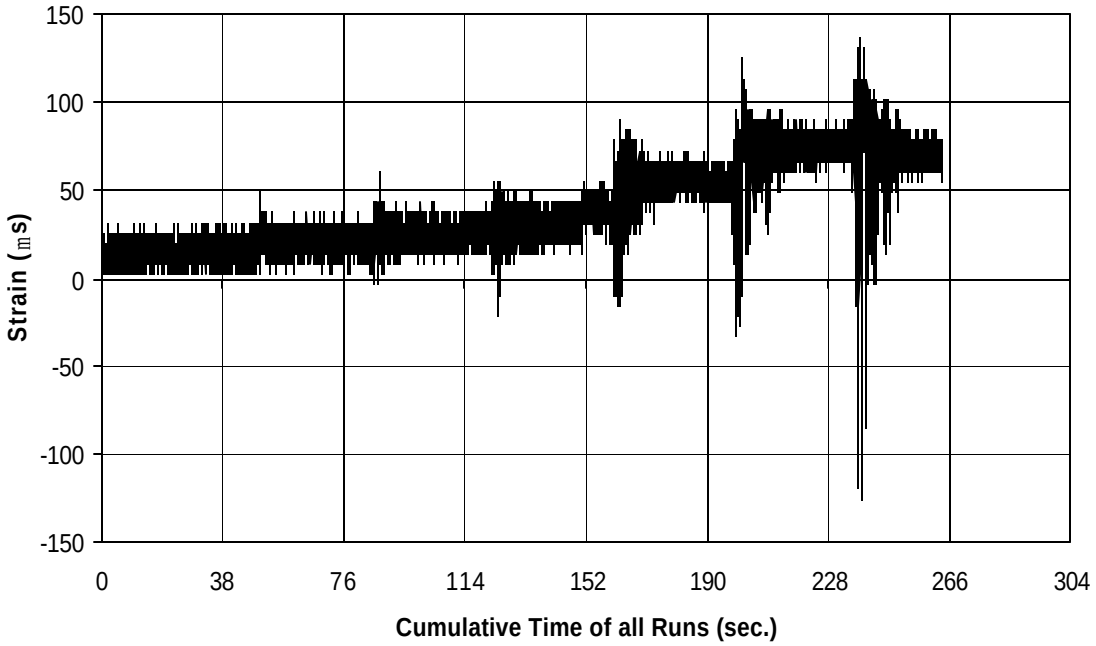

Fig. A-250 THD -4 Measured Strain in Gauge SG46

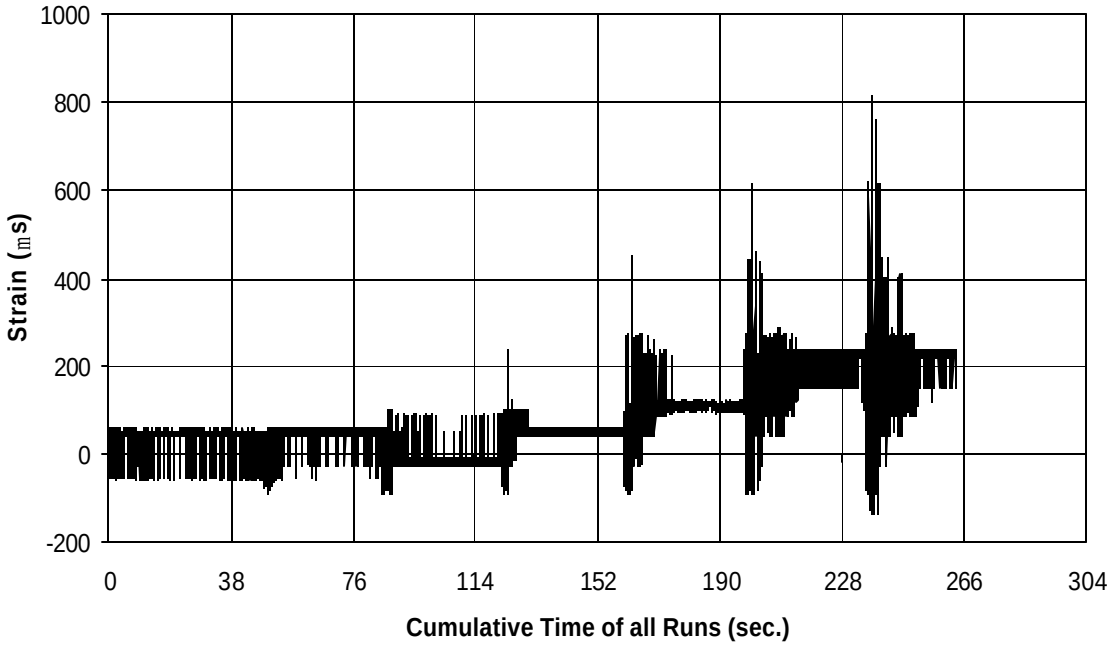

Fig. A-251 THD -4 Measured Strain in Gauge SG47

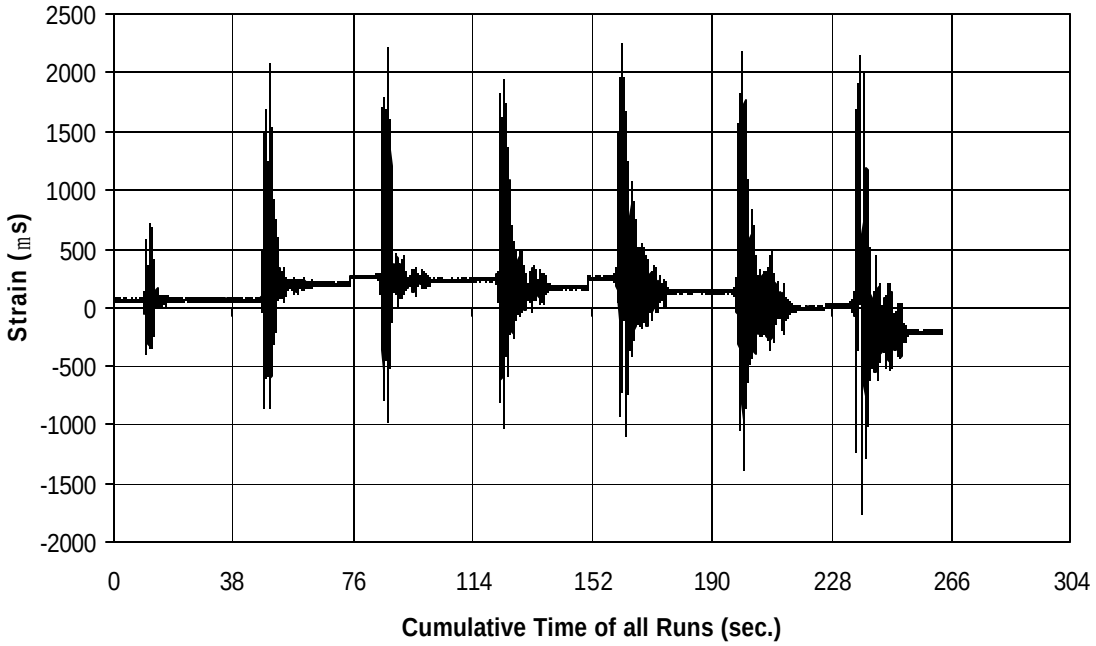

Fig. A-252 THD -4 Measured Strain in Gauge SG48

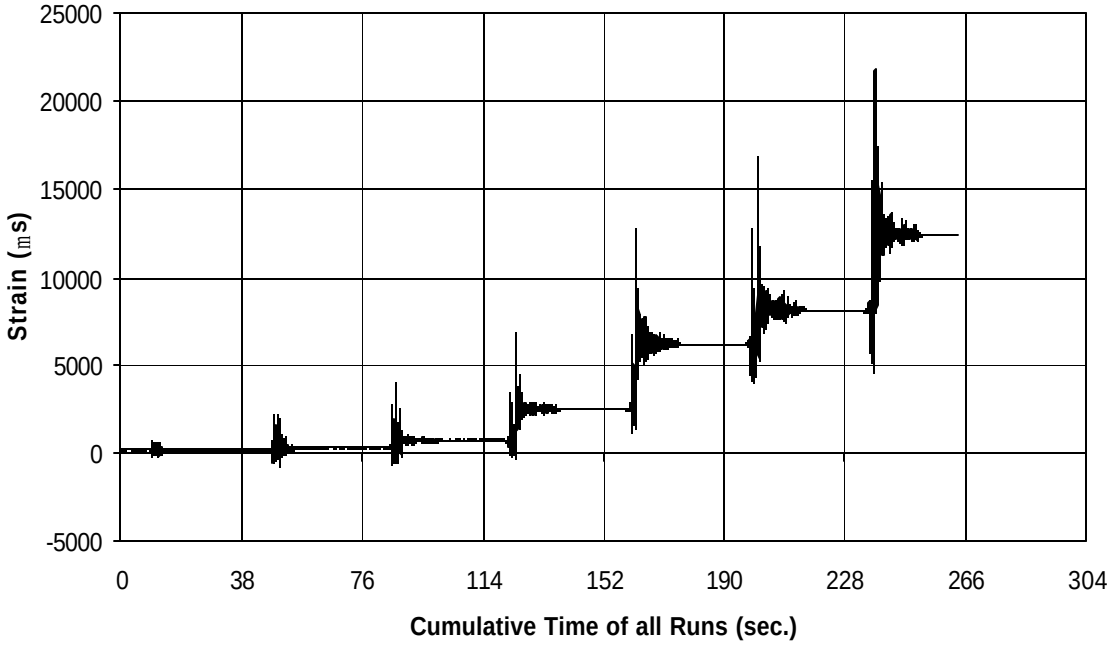

Fig. A-253 THD -4 Measured Strain in Gauge SG49

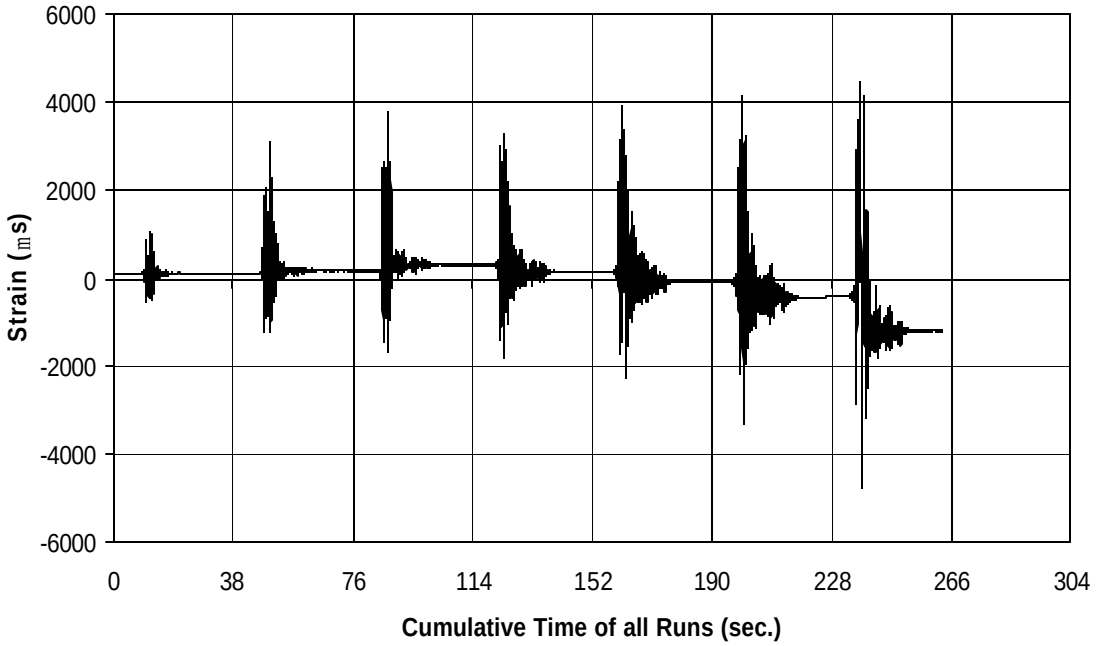

Fig. A-254 THD -4 Measured Strain in Gauge SG50

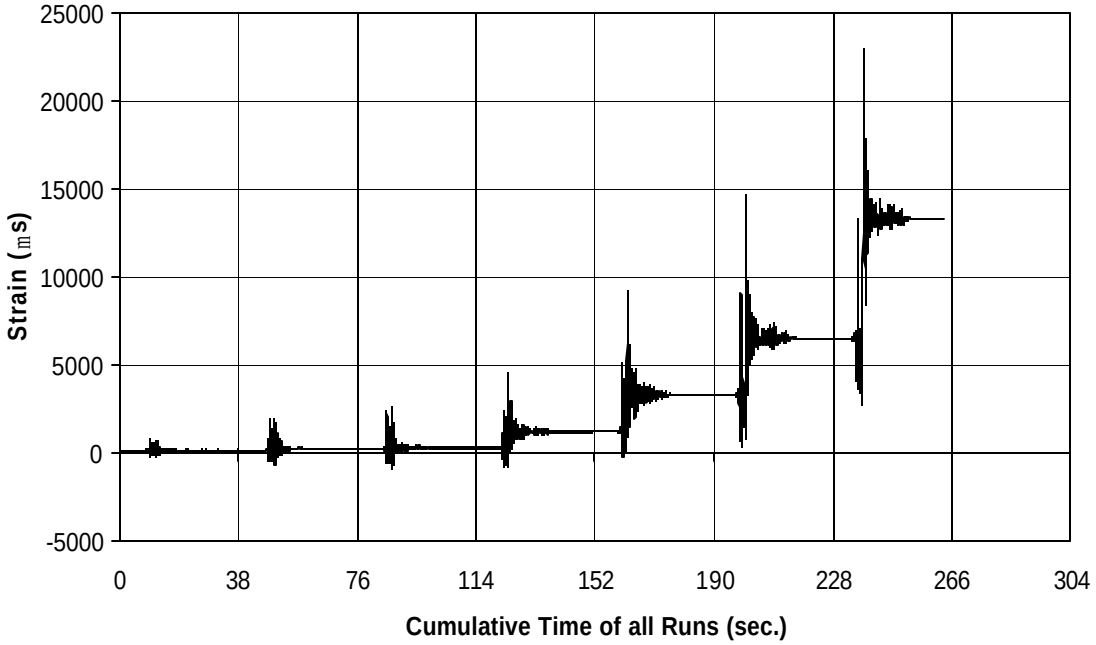

Fig. A-255 THD -4 Measured Strain in Gauge SG51

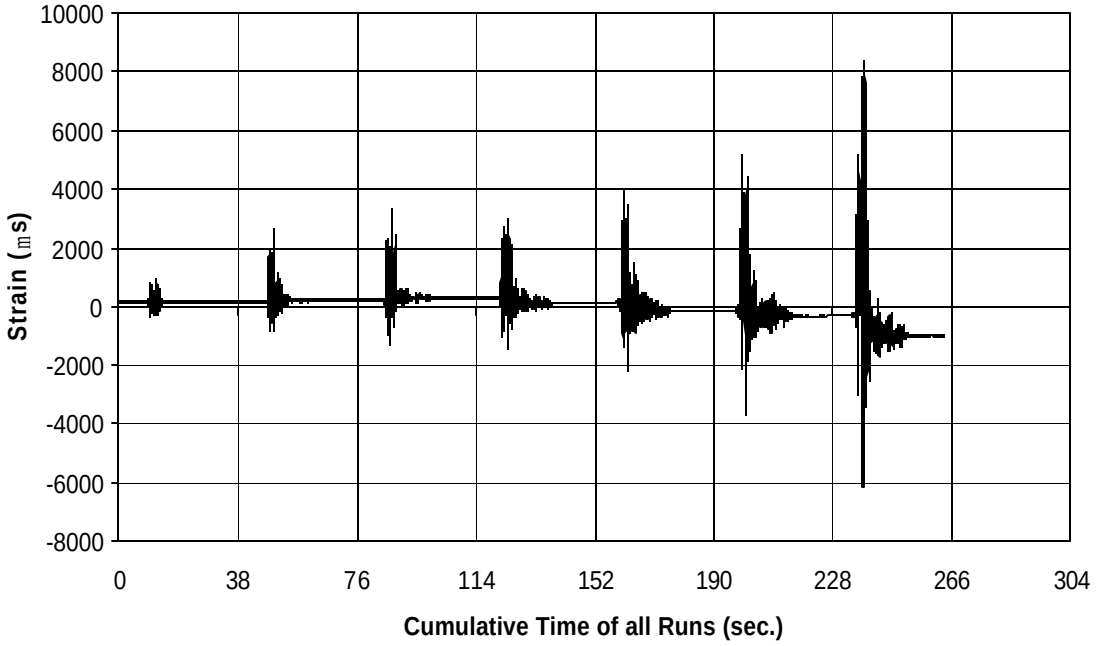

Fig. A-256 THD -4 Measured Strain in Gauge SG52

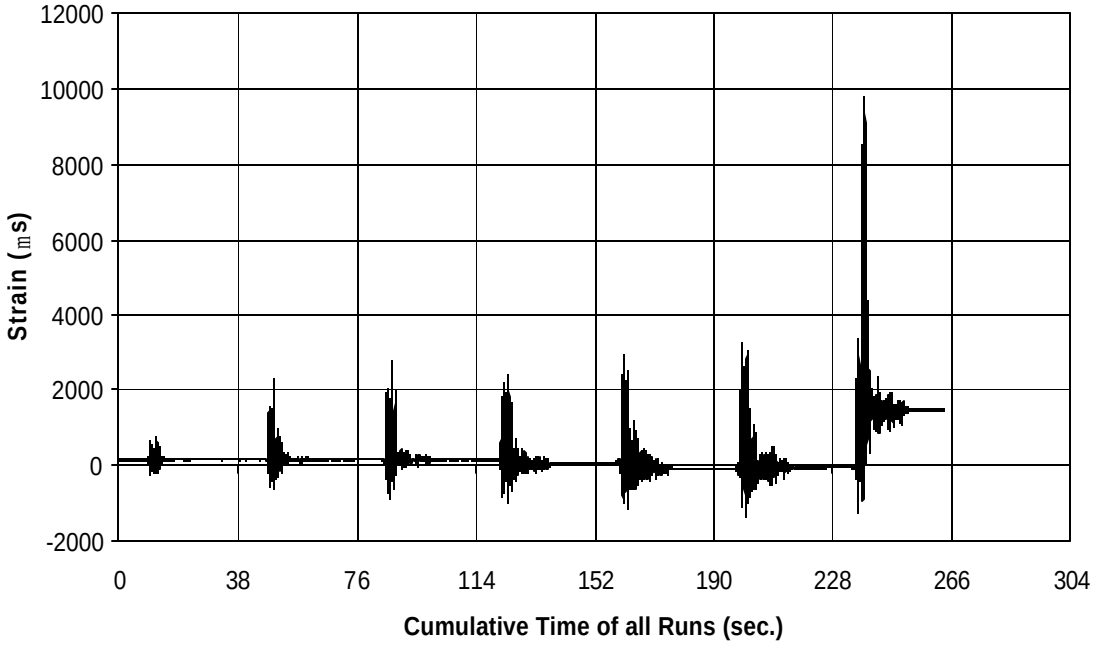

Fig. A-257 THD -4 Measured Strain in Gauge SG53

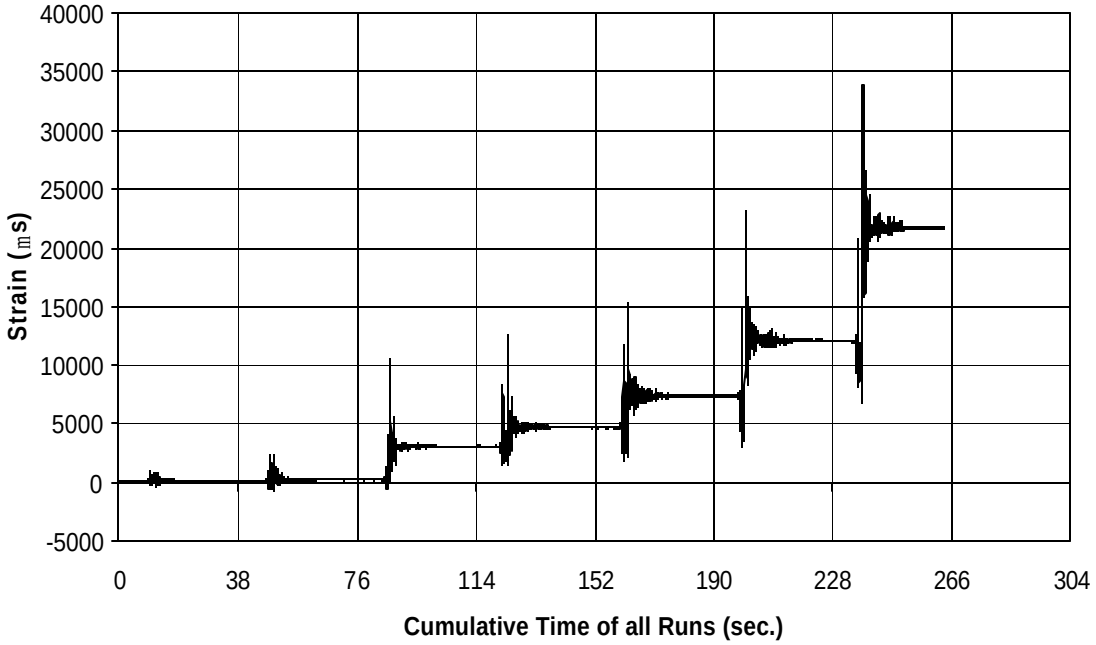

Fig. A-258 THD -4 Measured Strain in Gauge SG54

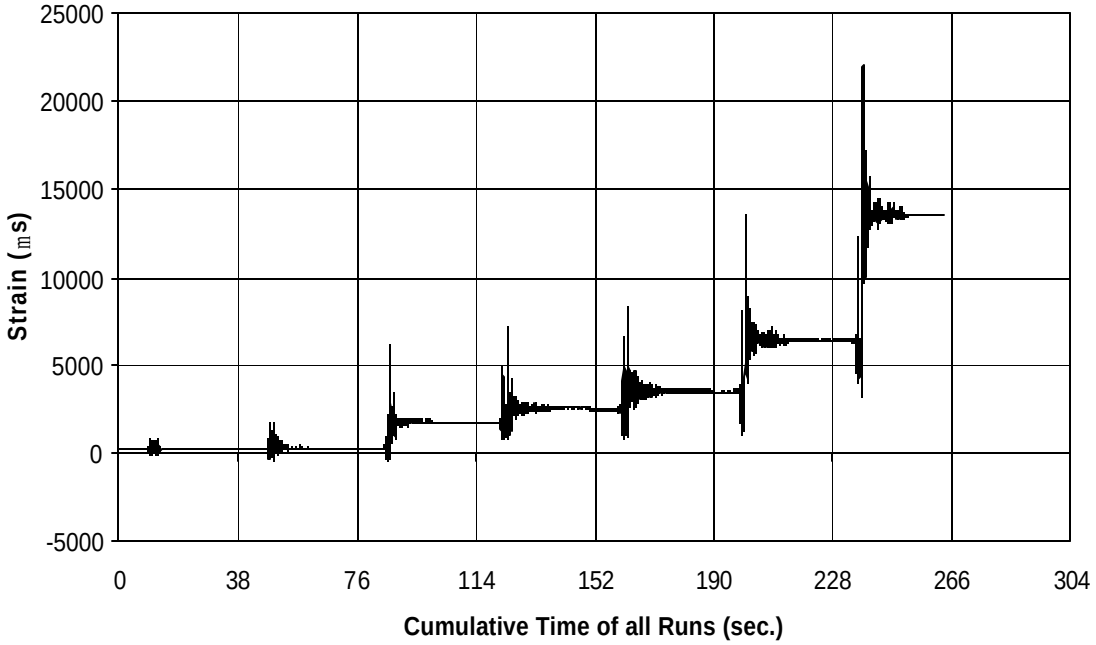

Fig. A-259 THD -4 Measured Strain in Gauge SG55

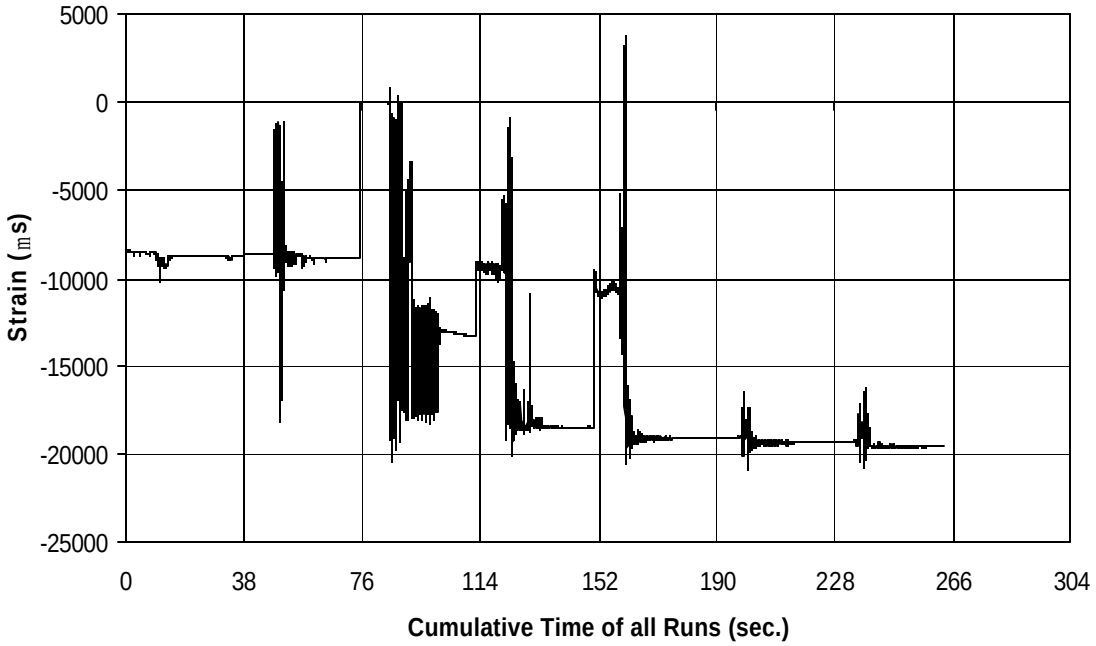

Fig. A-260 THD -4 Measured Strain in Gauge SG56

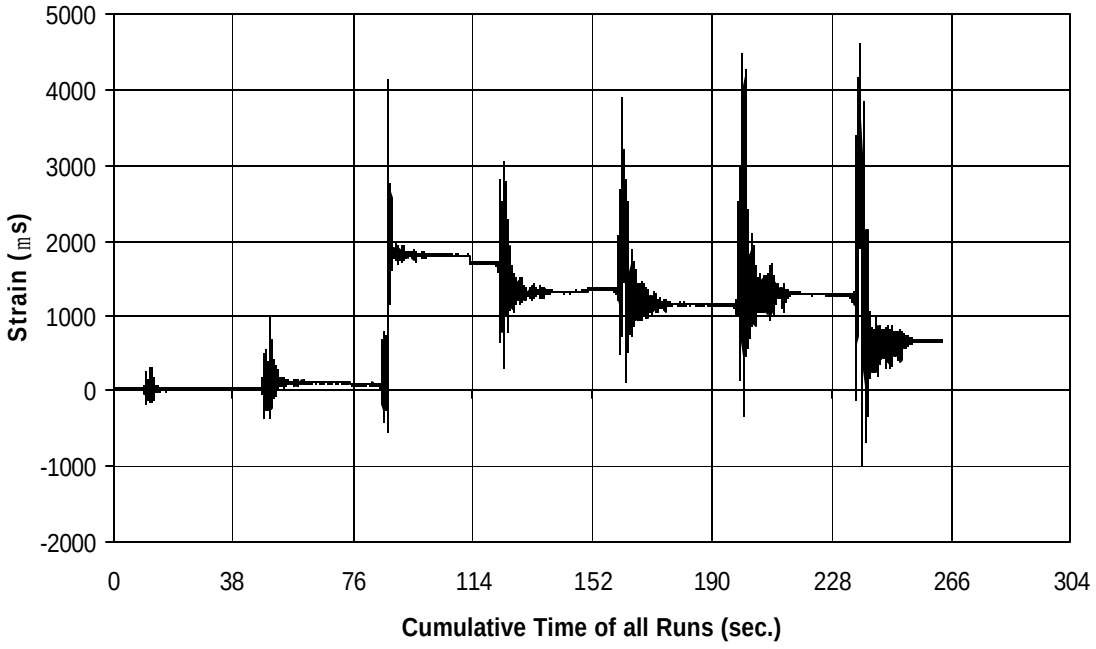

Fig. A-261 THD -4 Measured Strain in Gauge SG57

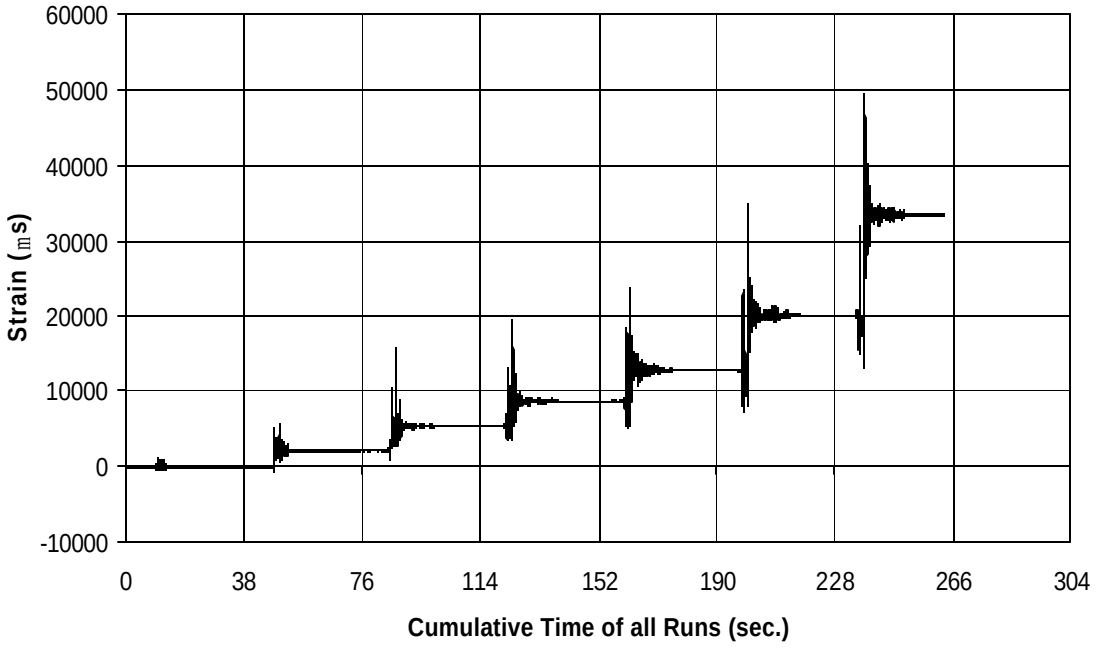

Fig. A-262 THD -4 Measured Strain in Gauge SG58

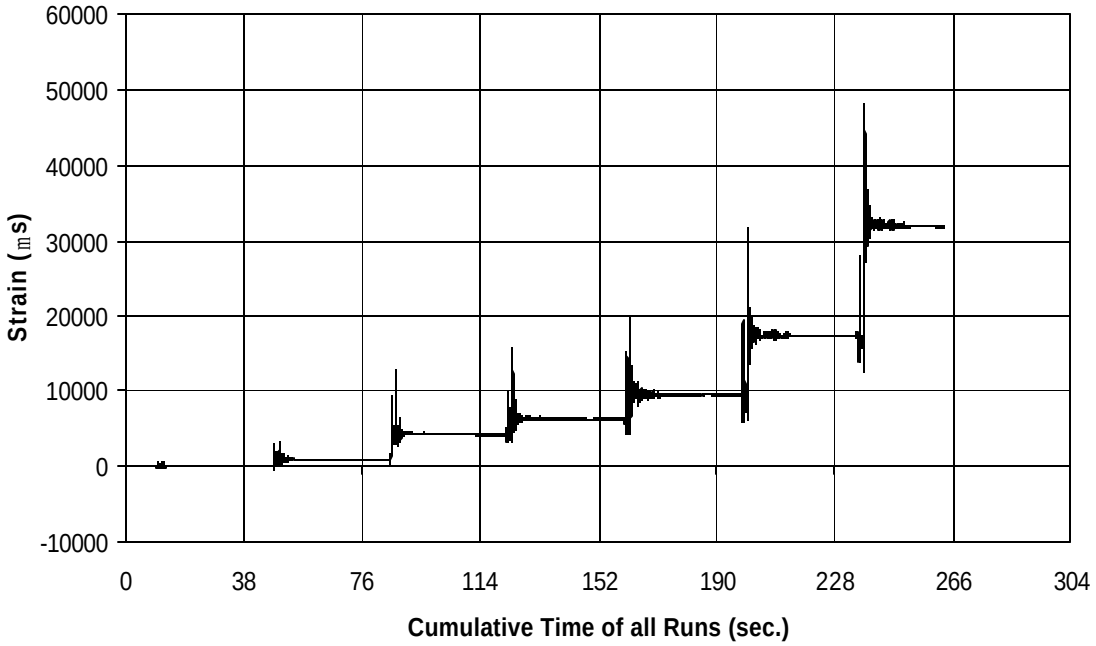

Fig. A-263 THD -4 Measured Strain in Gauge SG59

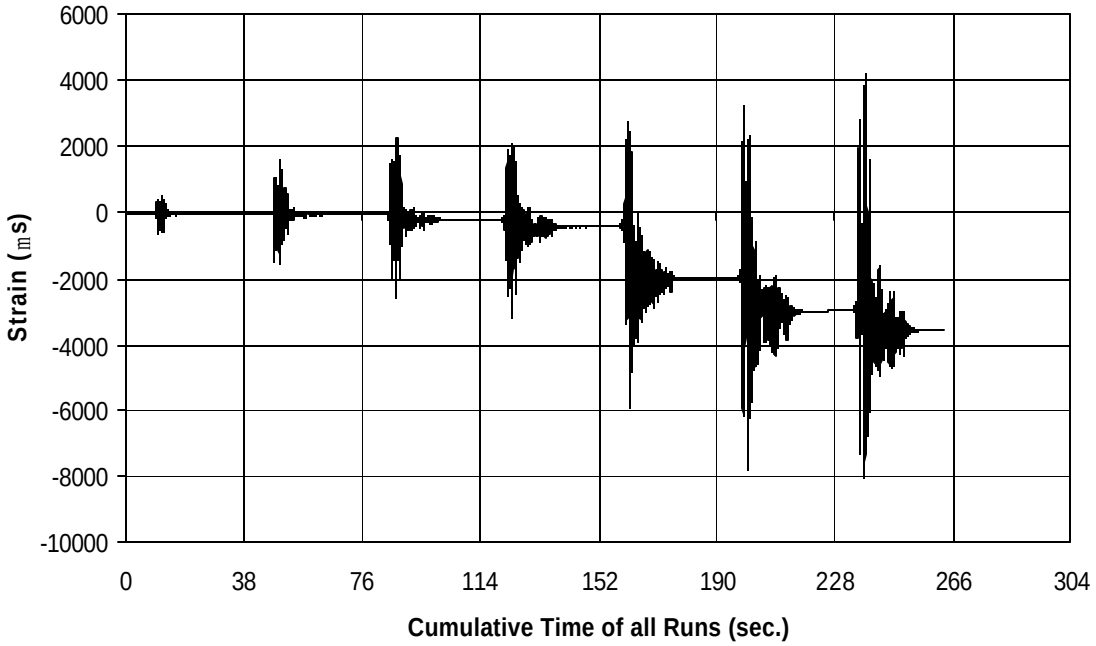

Fig. A-264 THD -4 Measured Strain in Gauge SG60

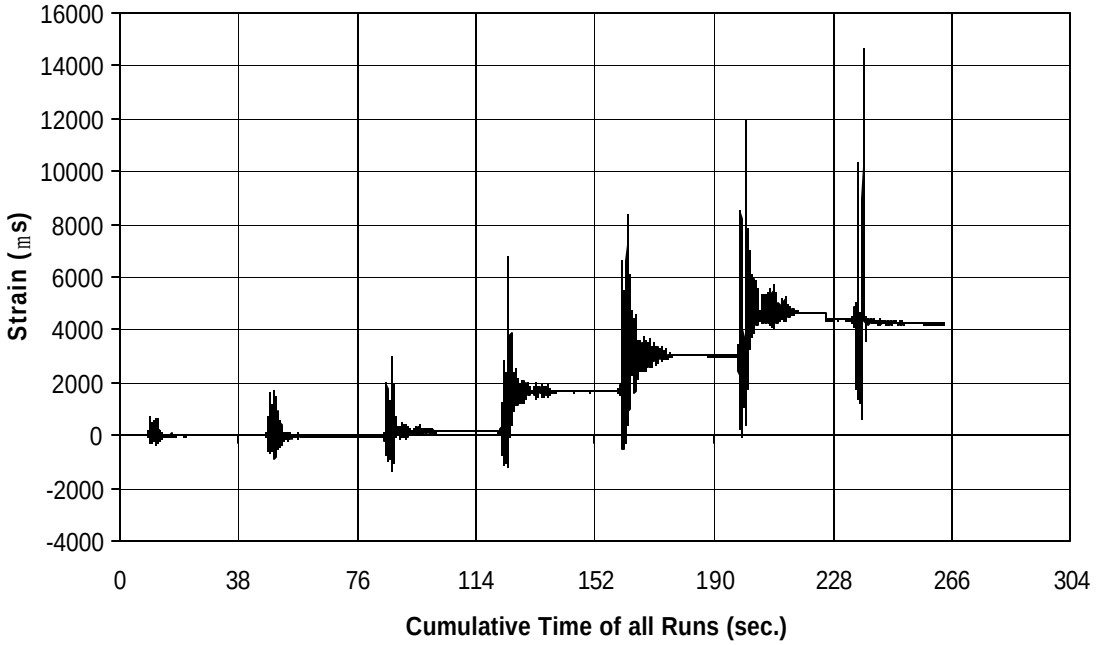

Fig. A-265 THD -4 Measured Strain in Gauge SG61

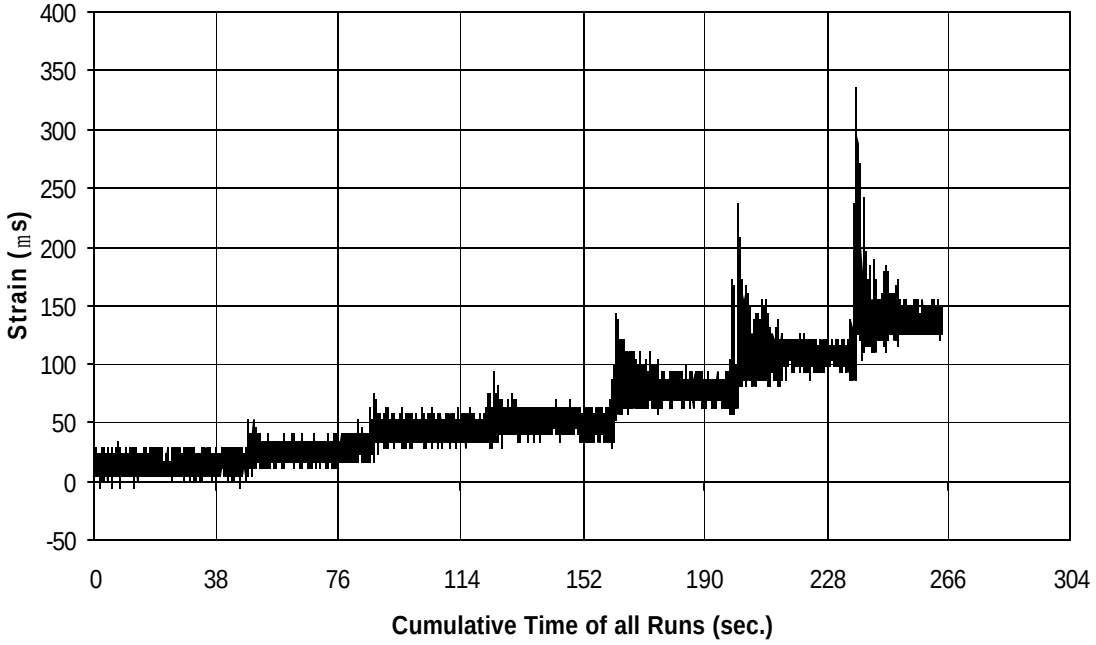

Fig. A-266 THD -4 Measured Strain in Gauge SG62

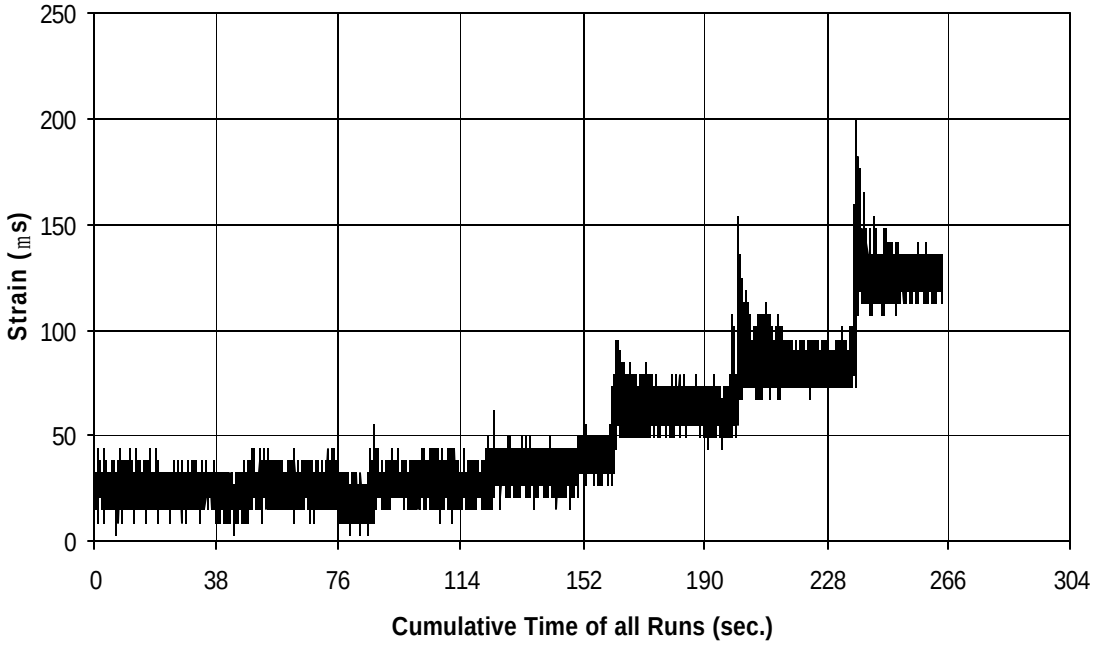

Fig. A-267 THD -4 Measured Strain in Gauge SG63

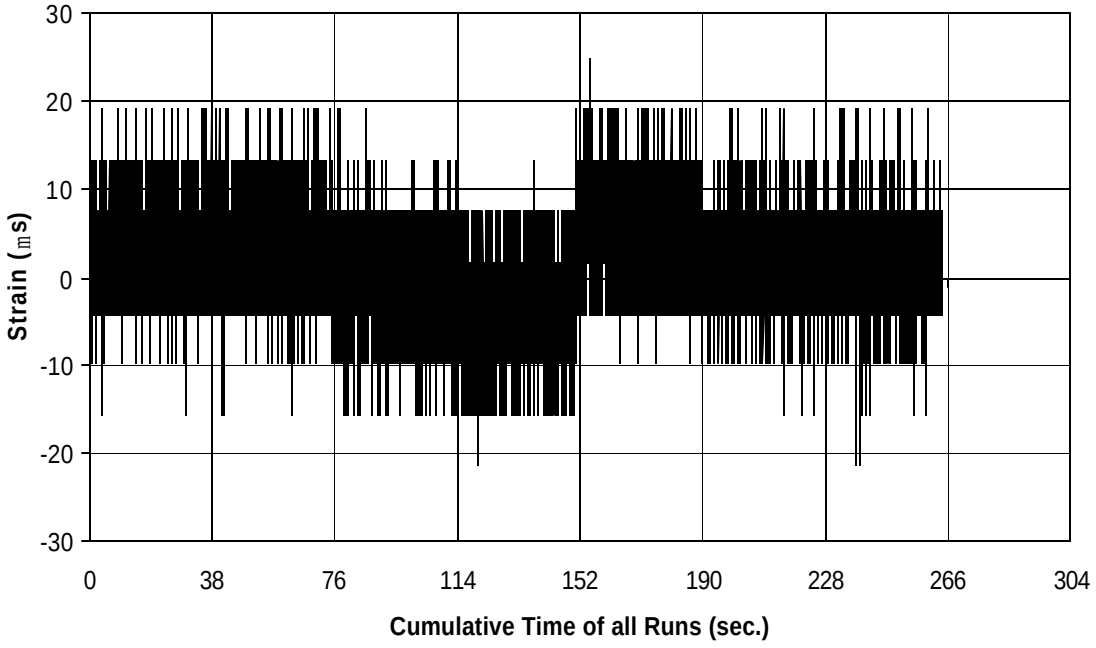

Fig. A-268 THD -4 Measured Strain in Gauge SG64

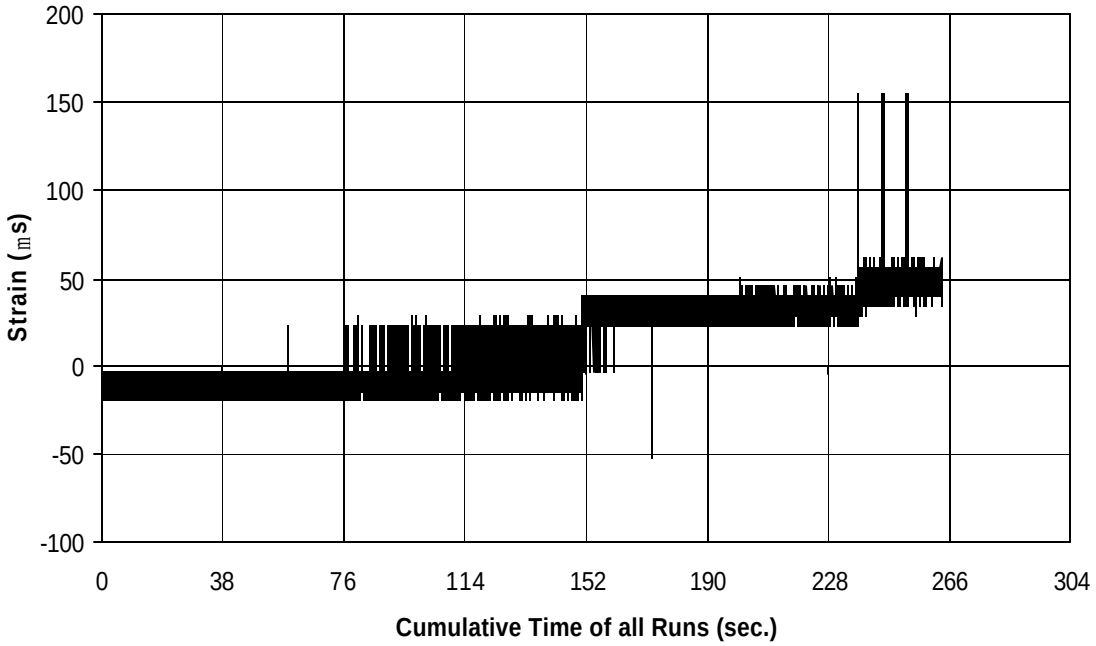

Fig. A-269 THD -4 Measured Strain in Gauge SG65

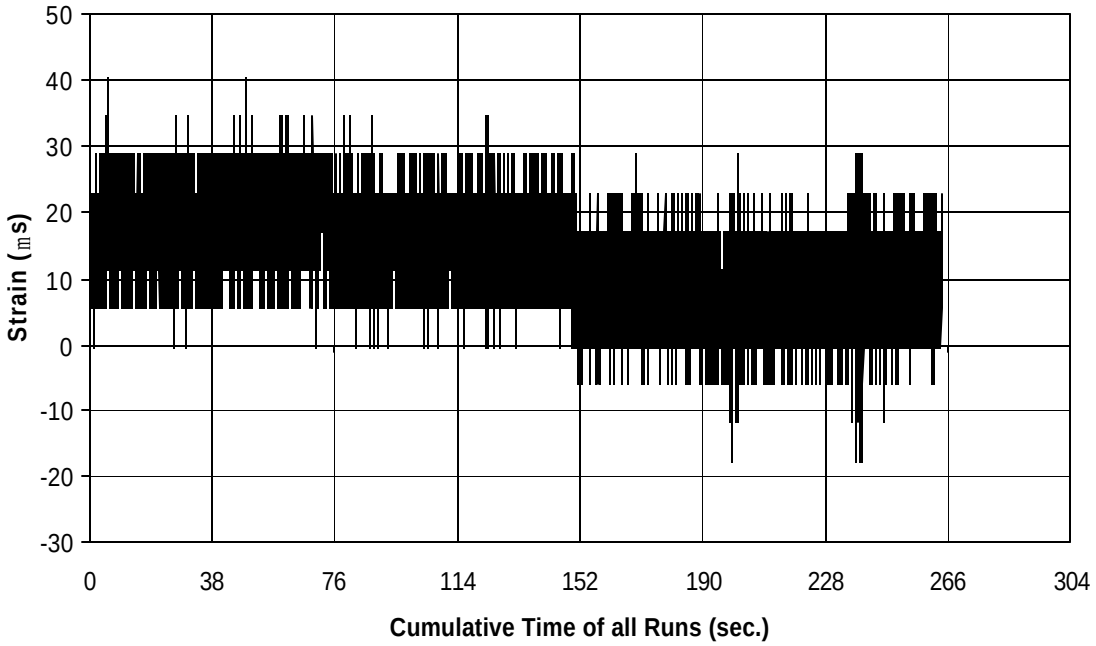

Fig. A-270 THD -4 Measured Strain in Gauge SG66

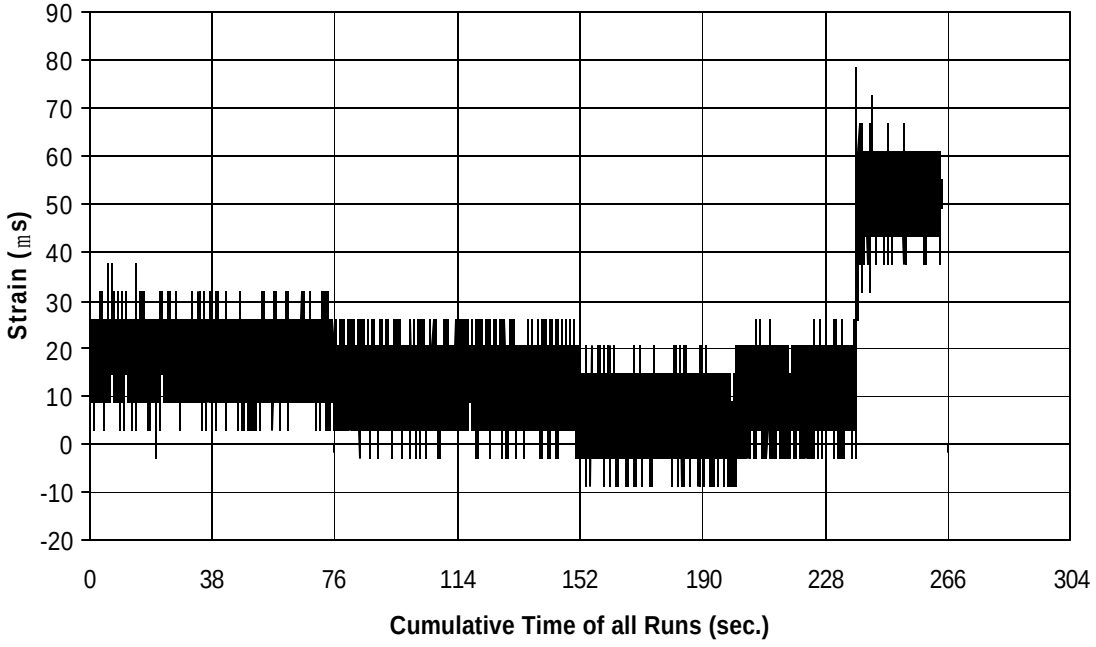

Fig. A-271 THD -4 Measured Strain in Gauge SG67

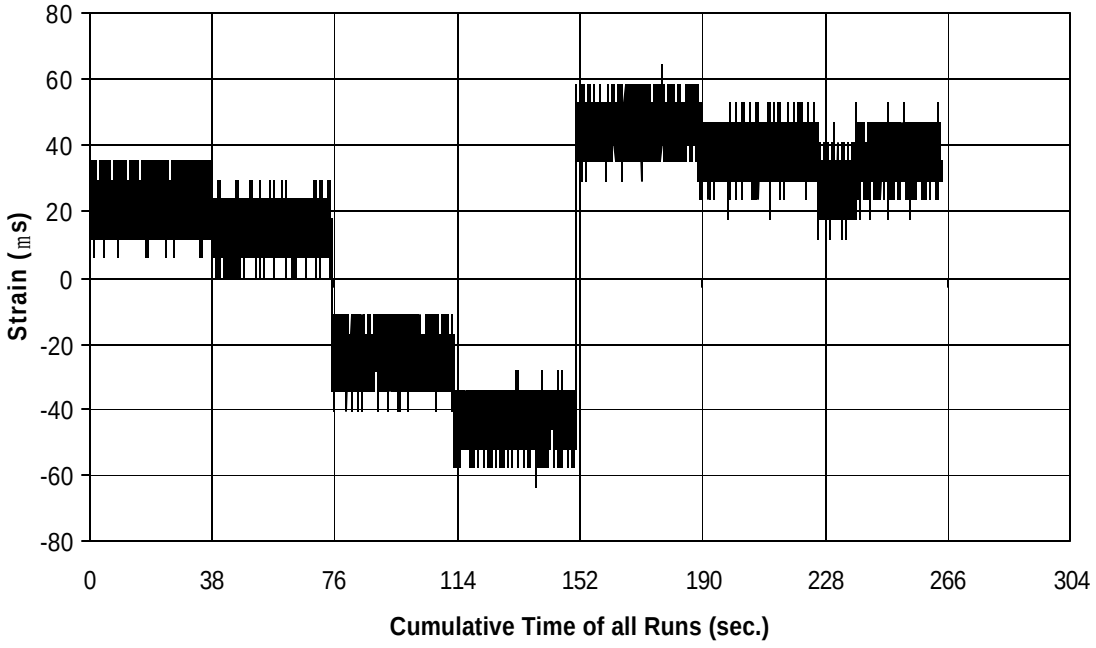

Fig. A-272 THD -4 Measured Strain in Gauge SG68

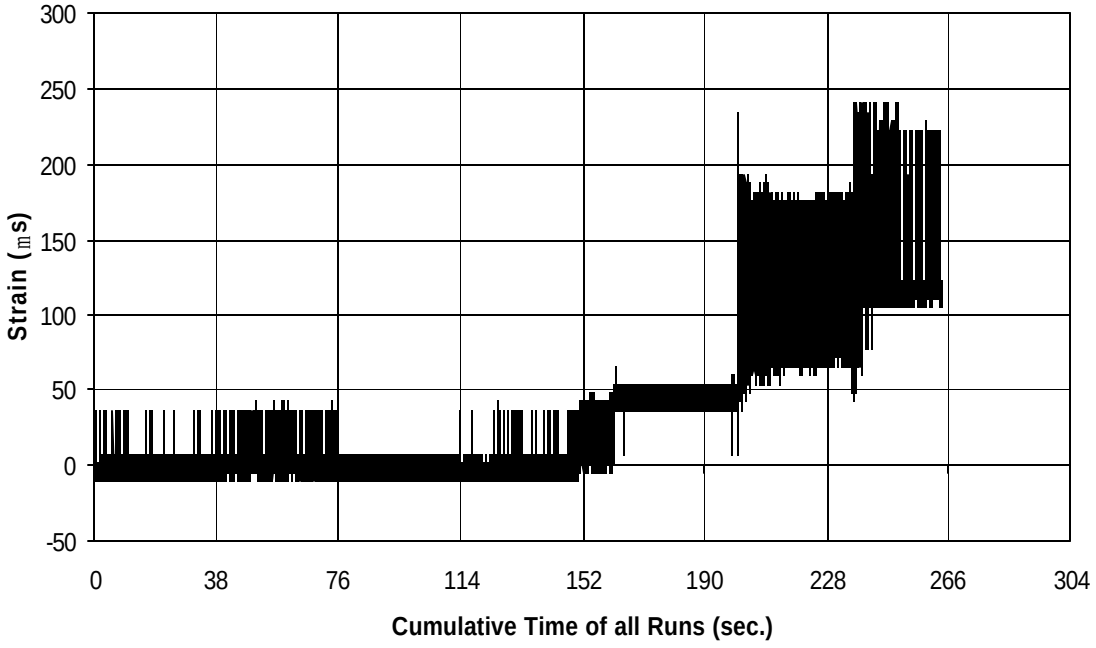

Fig. A-273 THD -4 Measured Strain in Gauge SG69

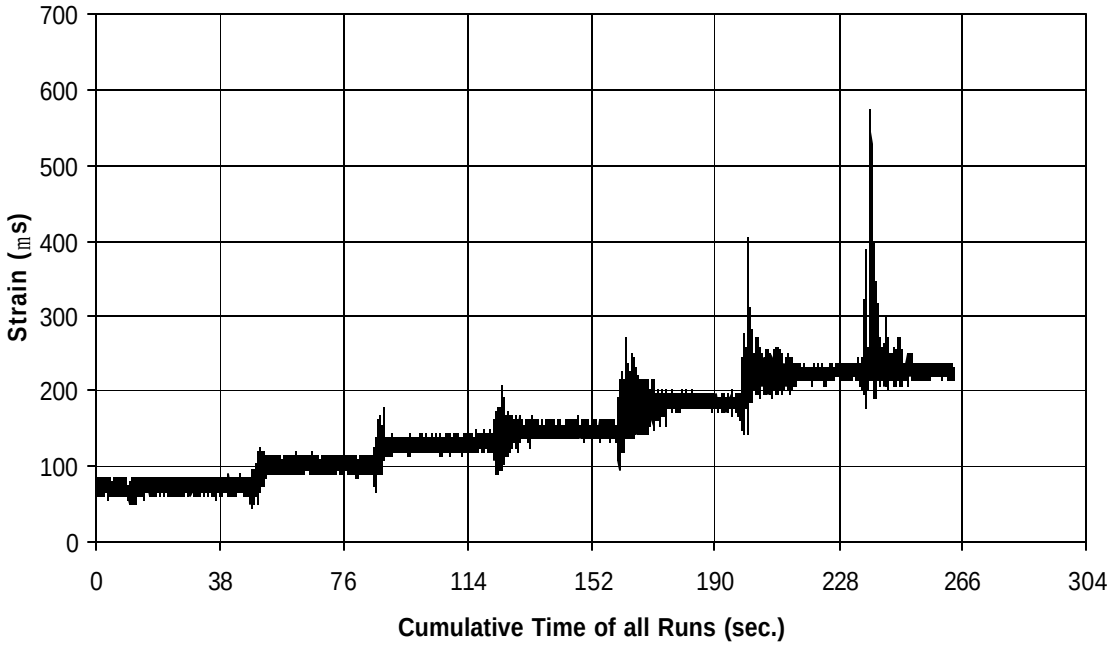

Fig. A-274 THD -4 Measured Strain in Gauge SG70

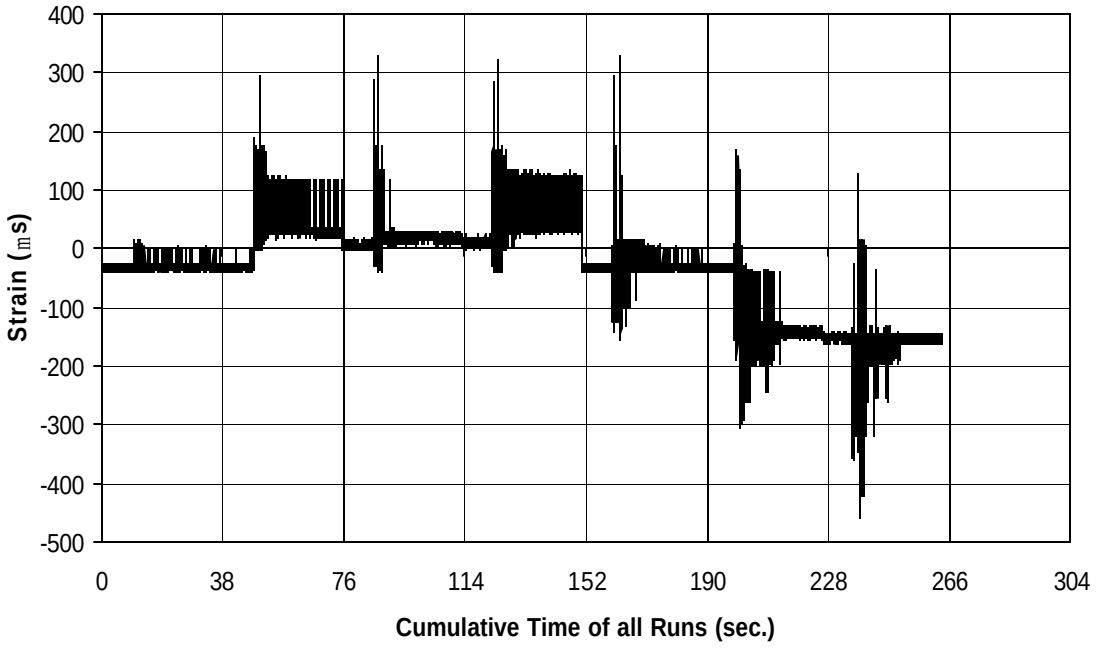

Fig. A-275 THD -4 Measured Strain in Gauge SG71

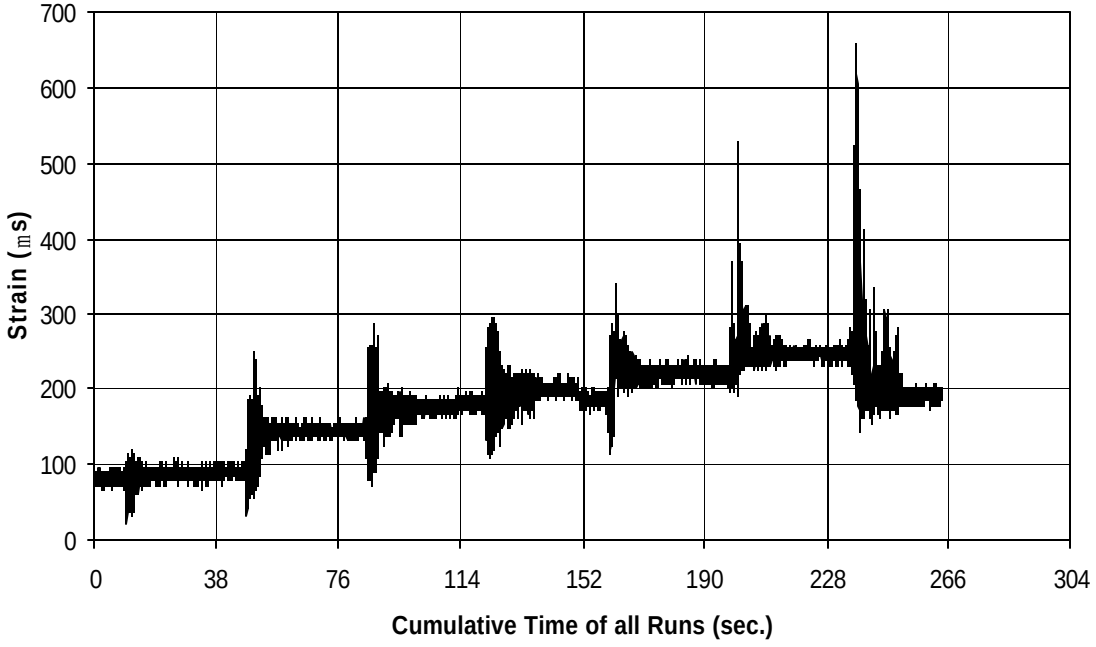

Fig. A-276 THD -4 Measured Strain in Gauge SG72

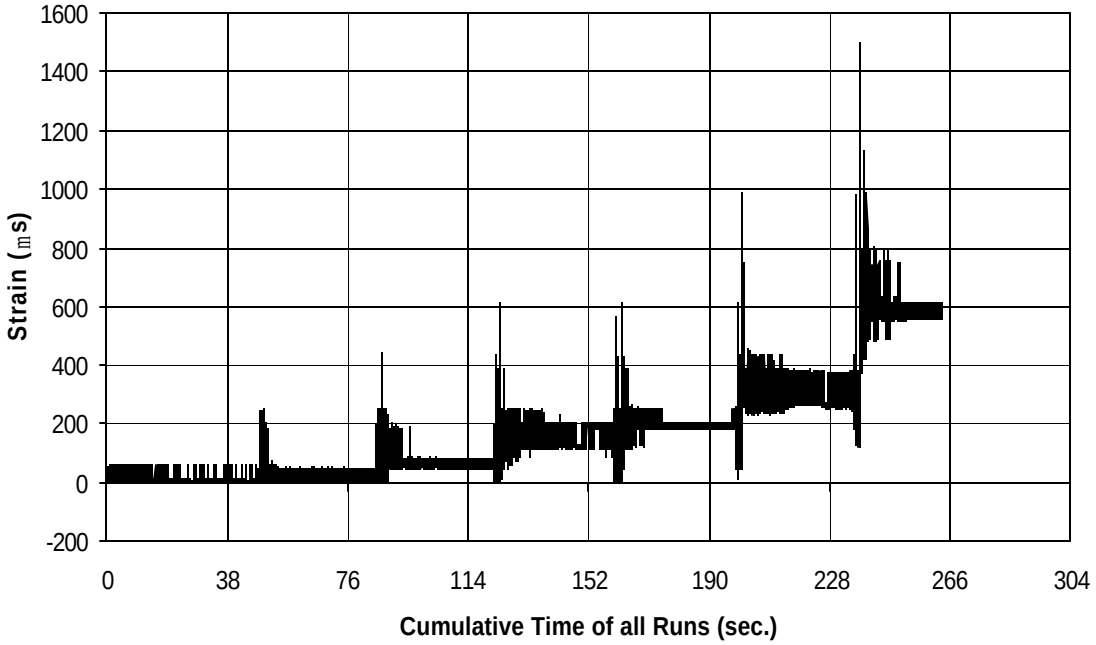

Fig. A-277 THD -4 Measured Strain in Gauge SG73

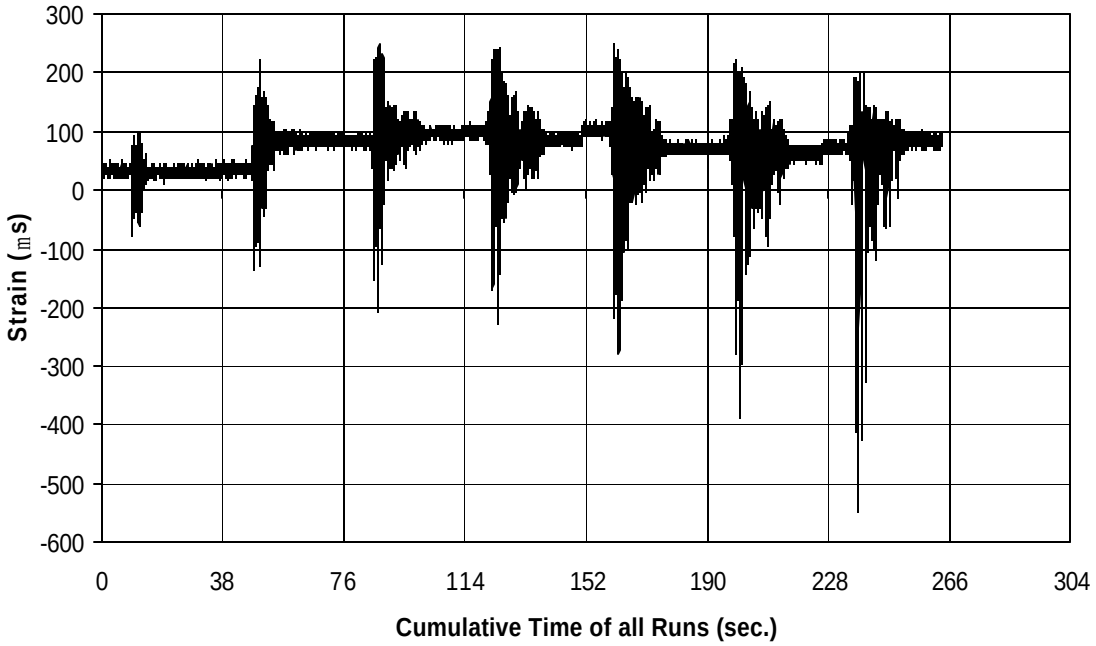

Fig. A-278 THD -4 Measured Strain in Gauge SG74

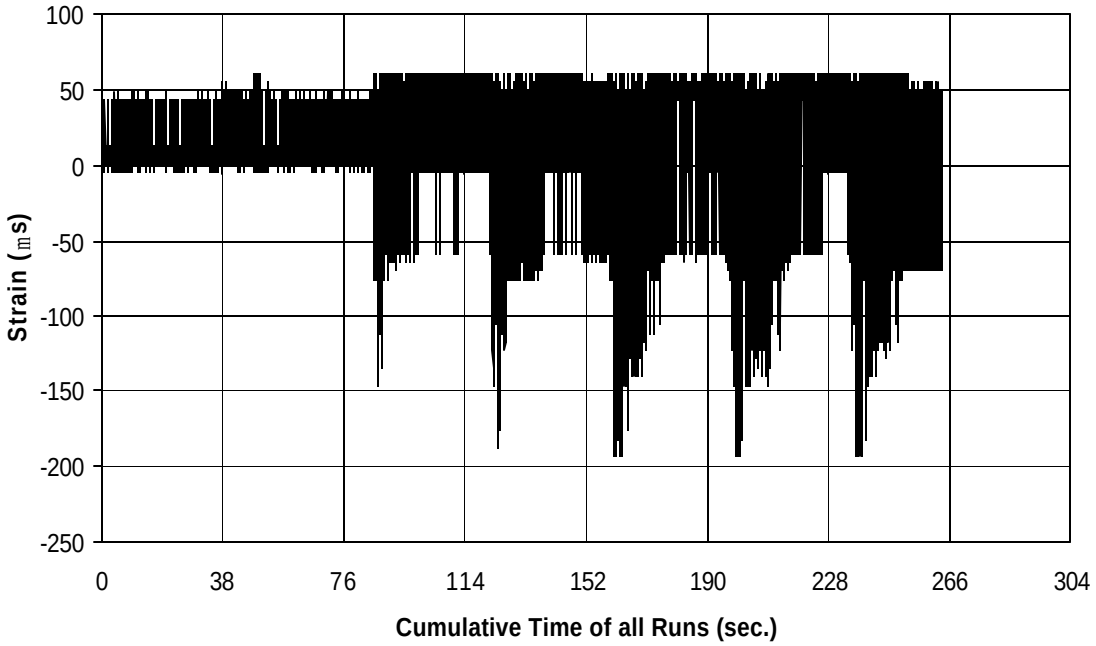

Fig. A-279 THD -4 Measured Strain in Gauge SG75

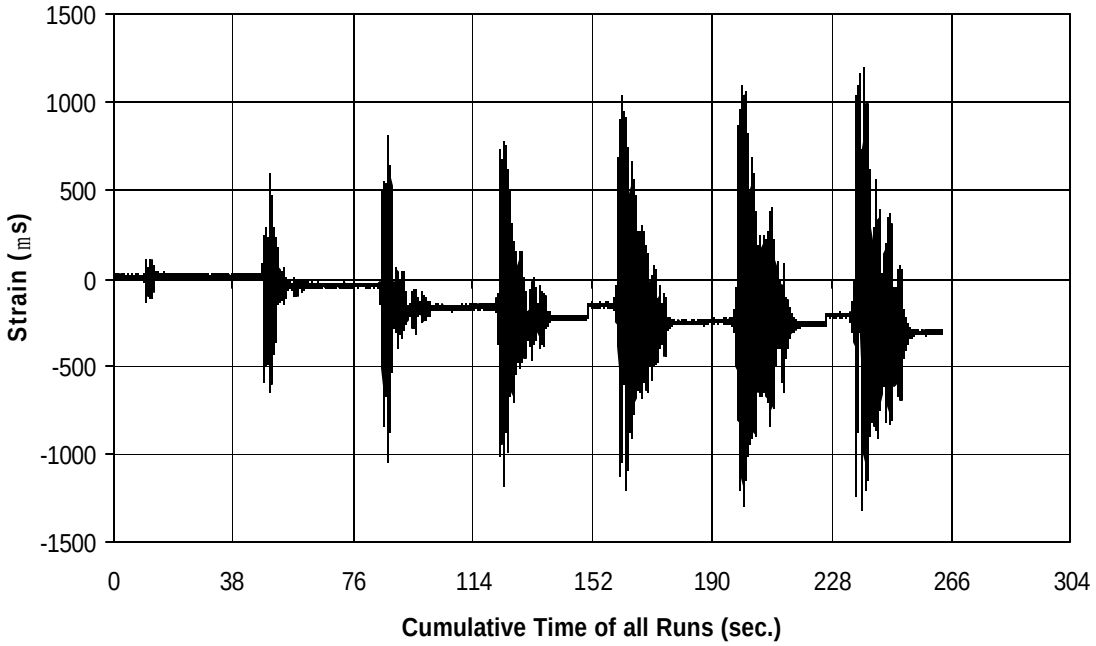

Fig. A-280 THD -4 Measured Strain in Gauge SG76

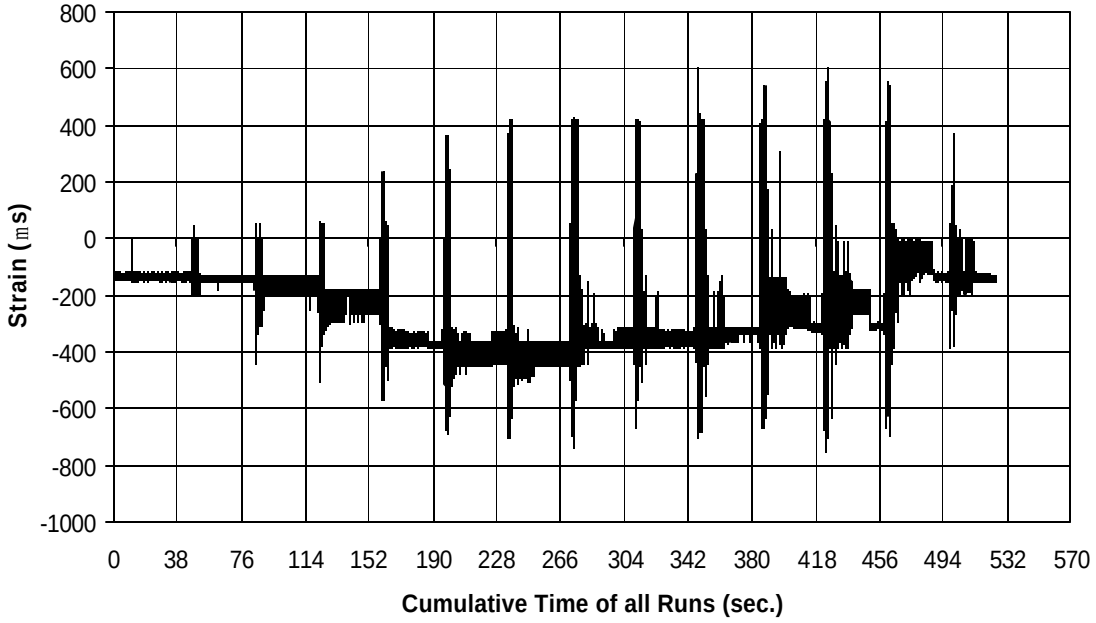

Fig. A-281 THD -5 Measured Strain in Gauge SG1

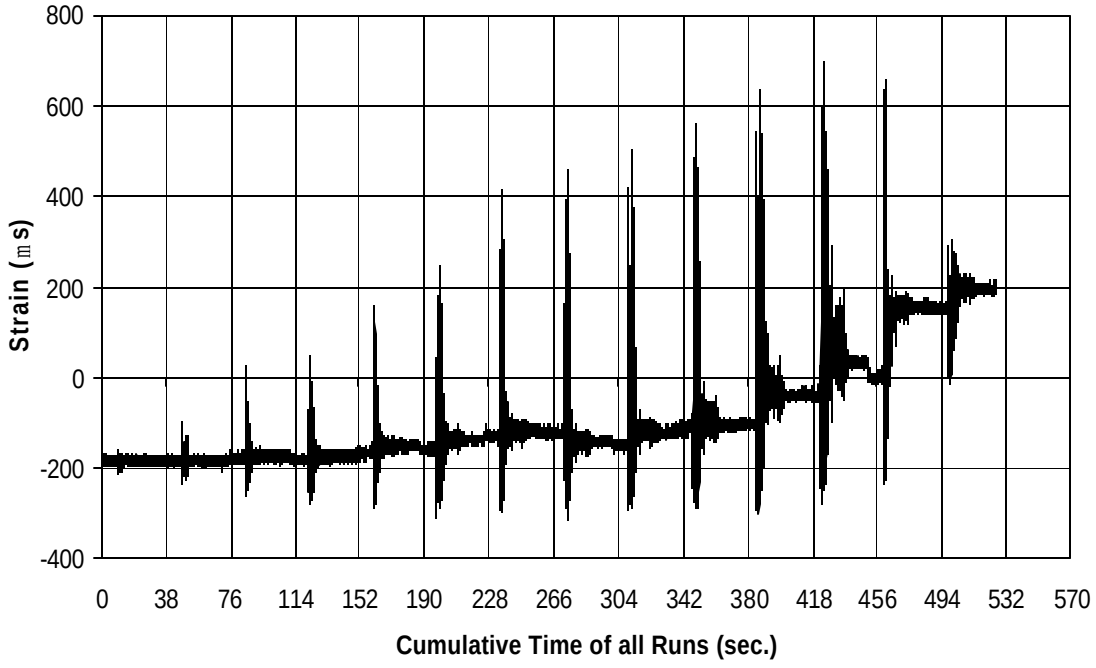

Fig. A-282 THD -5 Measured Strain in Gauge SG2

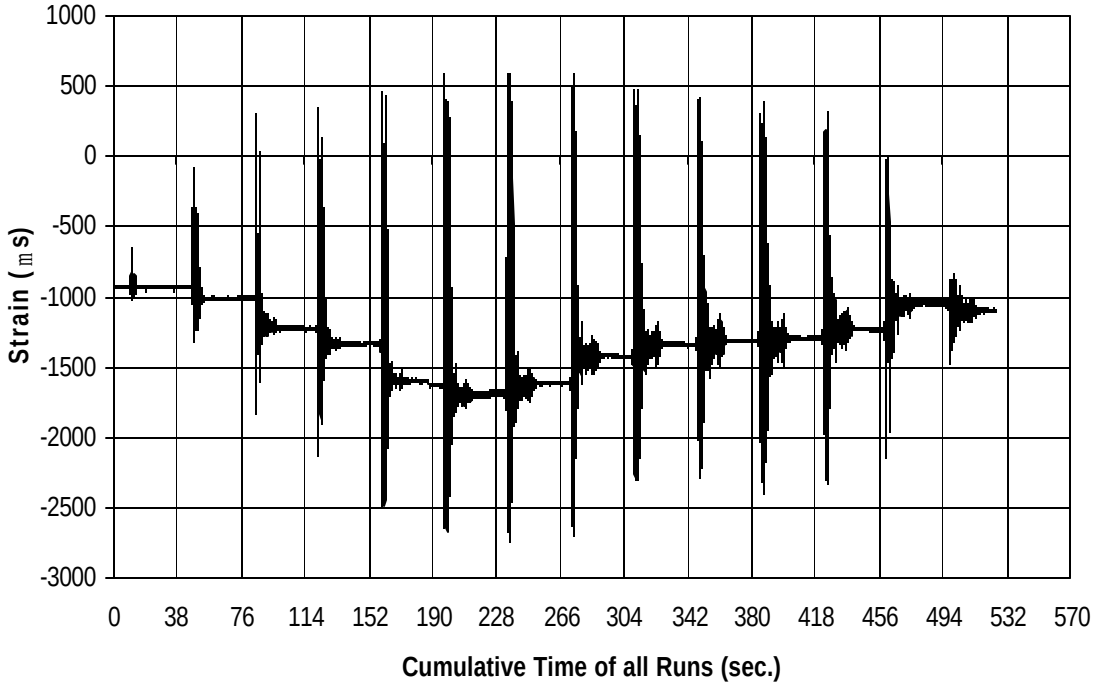

Fig. A-283 THD -5 Measured Strain in Gauge SG3

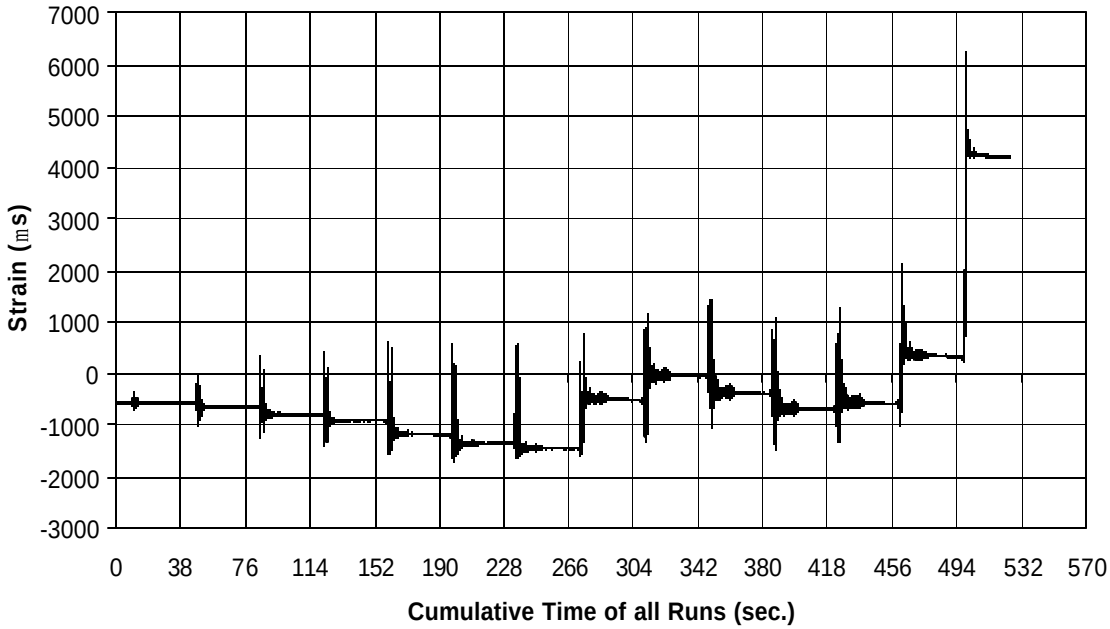

Fig. A-284 THD -5 Measured Strain in Gauge SG4

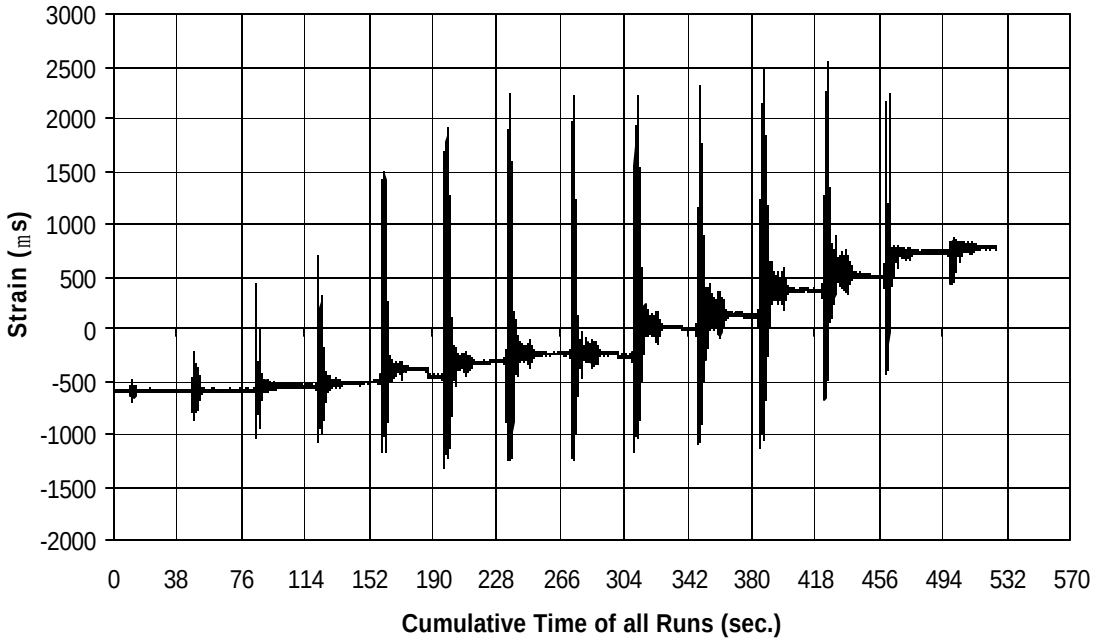

Fig. A-285 THD -5 Measured Strain in Gauge SG5

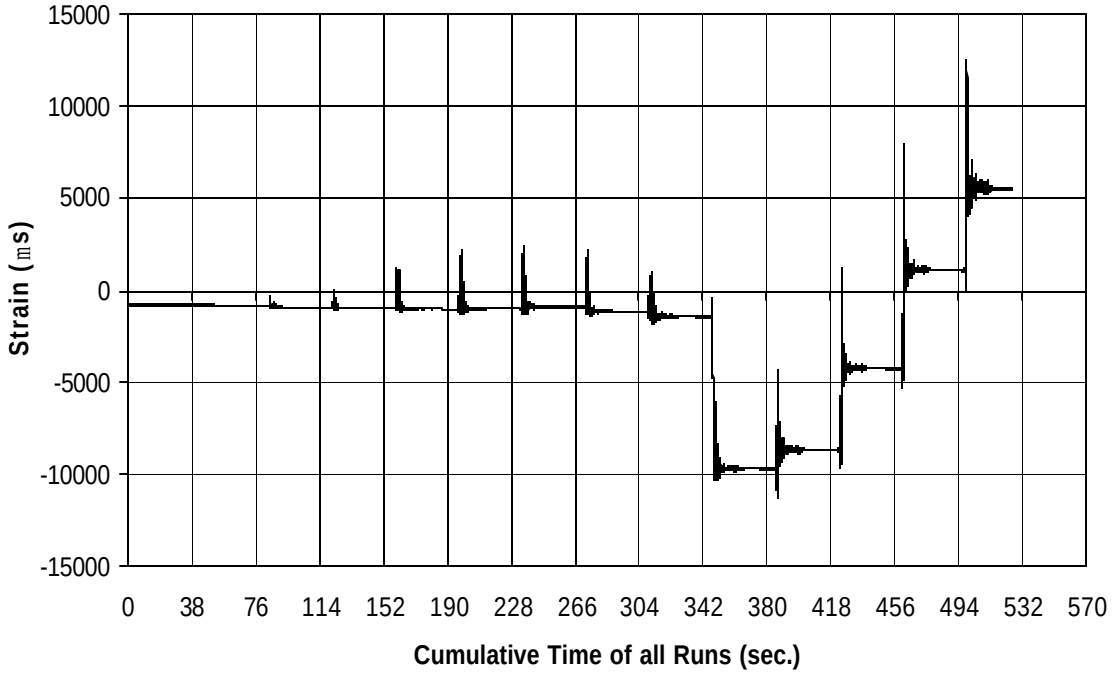

Fig. A-286 THD -5 Measured Strain in Gauge SG6

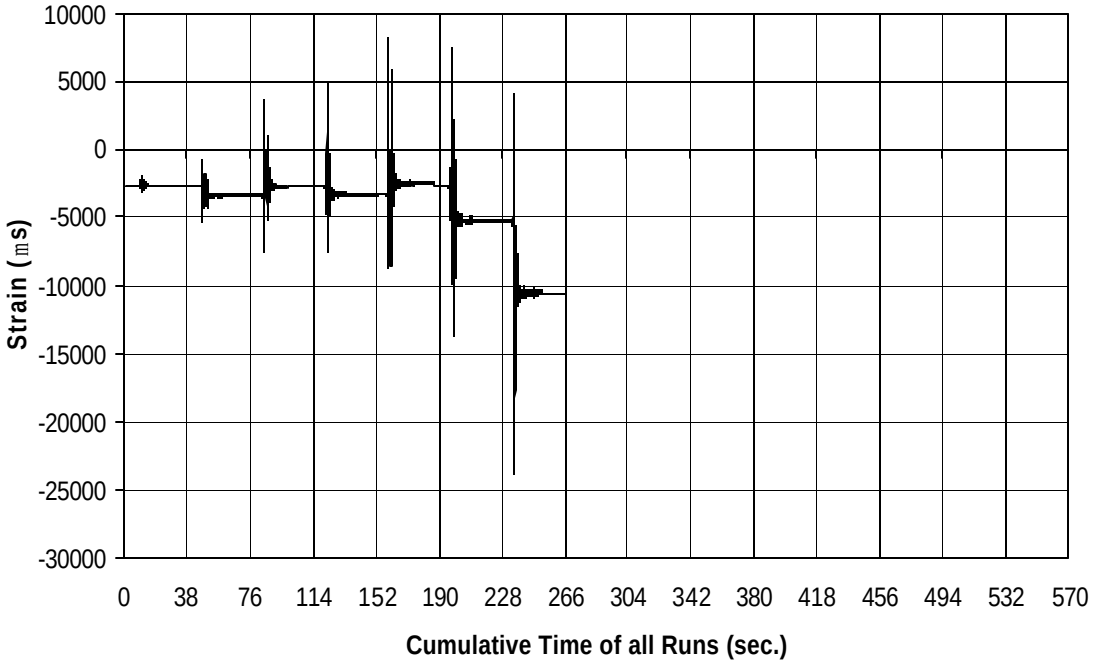

Fig. A-287 THD -5 Measured Strain in Gauge SG7

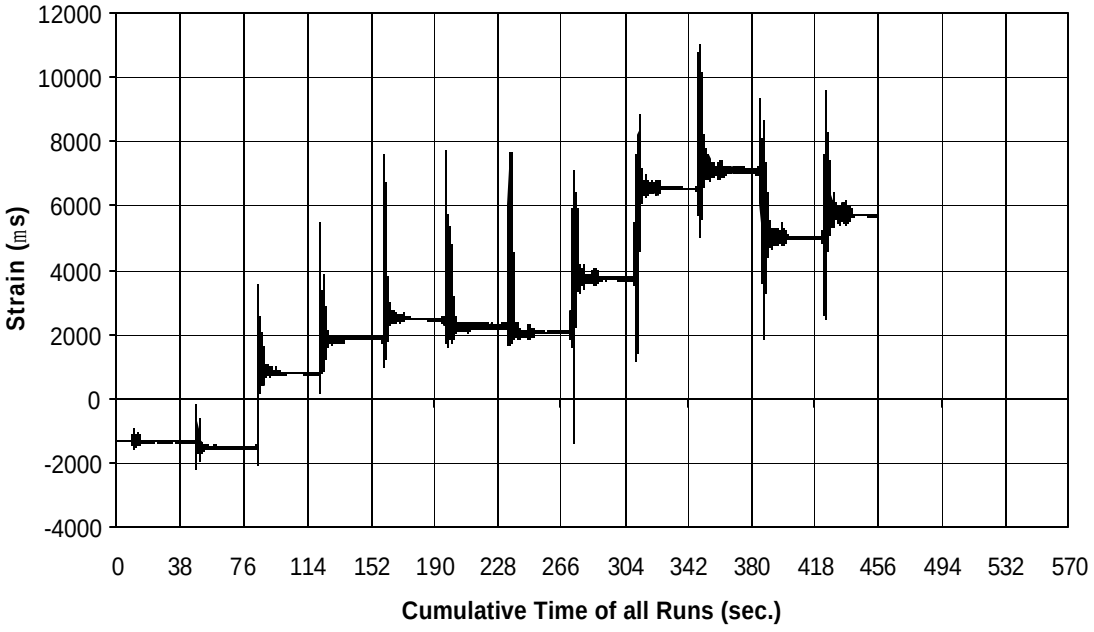

Fig. A-288 THD -5 Measured Strain in Gauge SG8

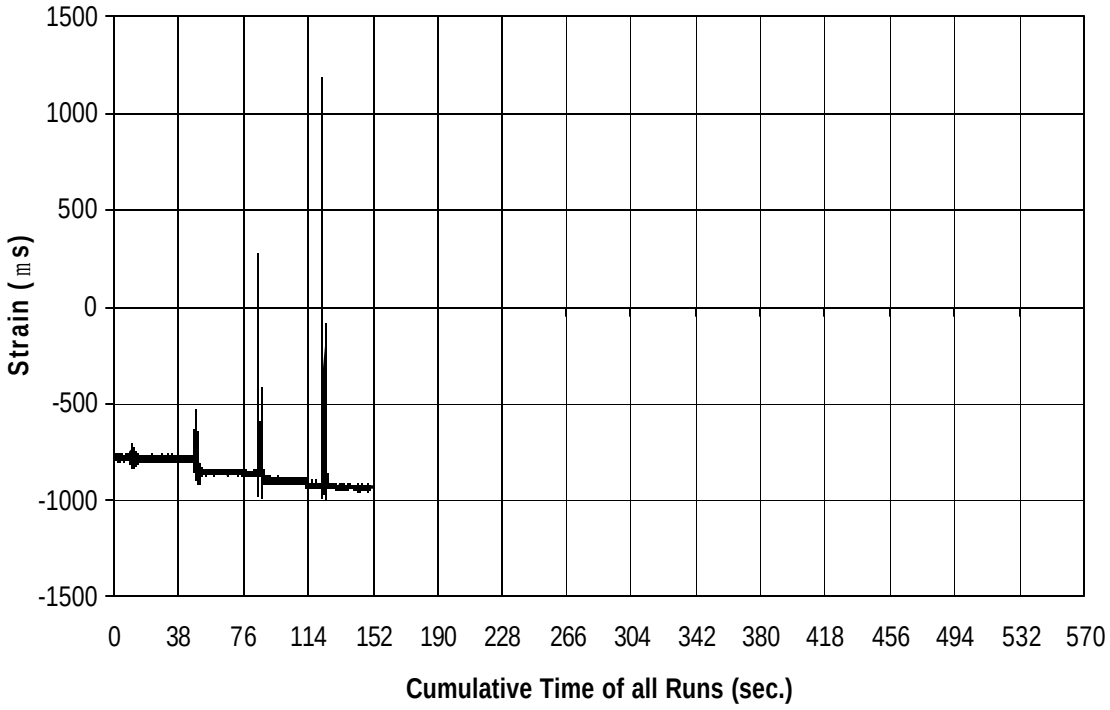

Fig. A-289 THD -5 Measured Strain in Gauge SG9

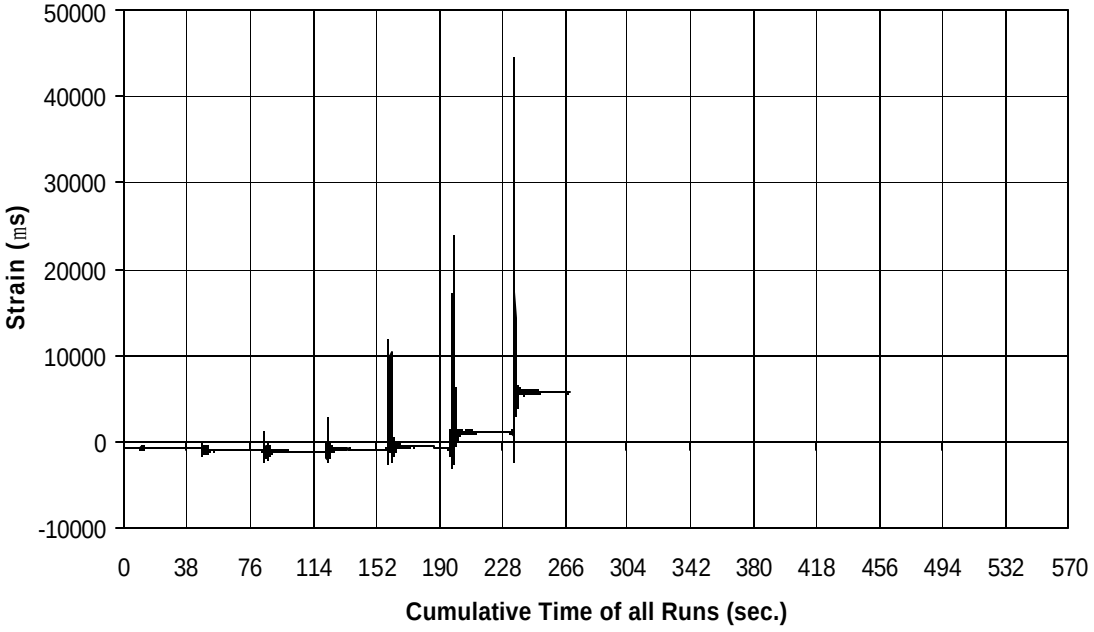

Fig. A-290 THD -5 Measured Strain in Gauge SG10

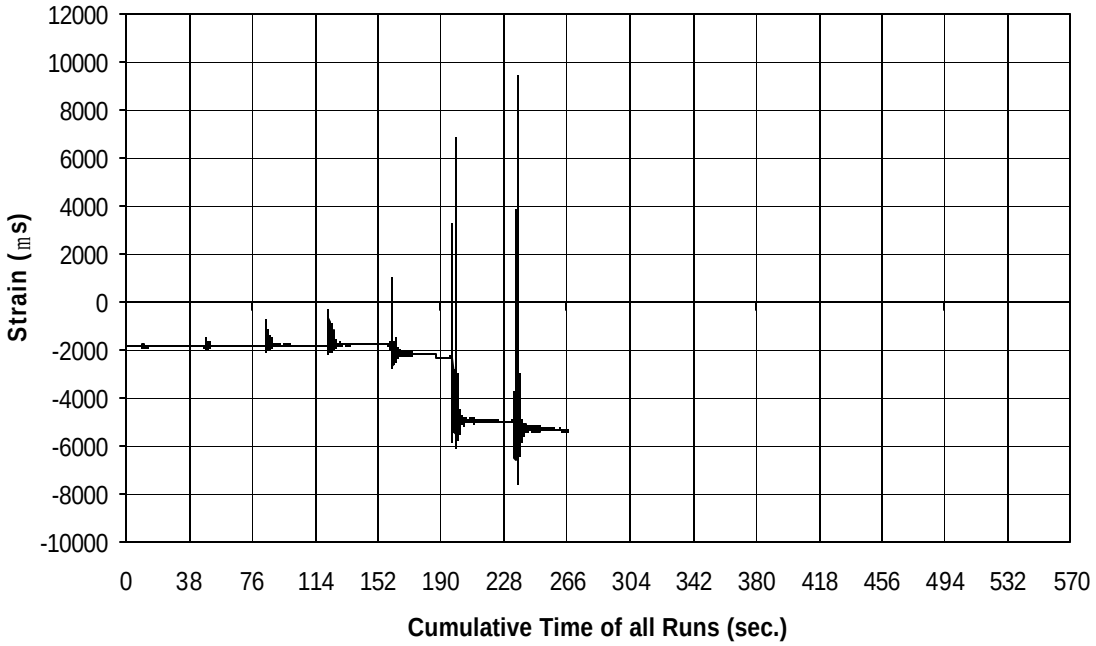

Fig. A-291 THD -5 Measured Strain in Gauge SG11

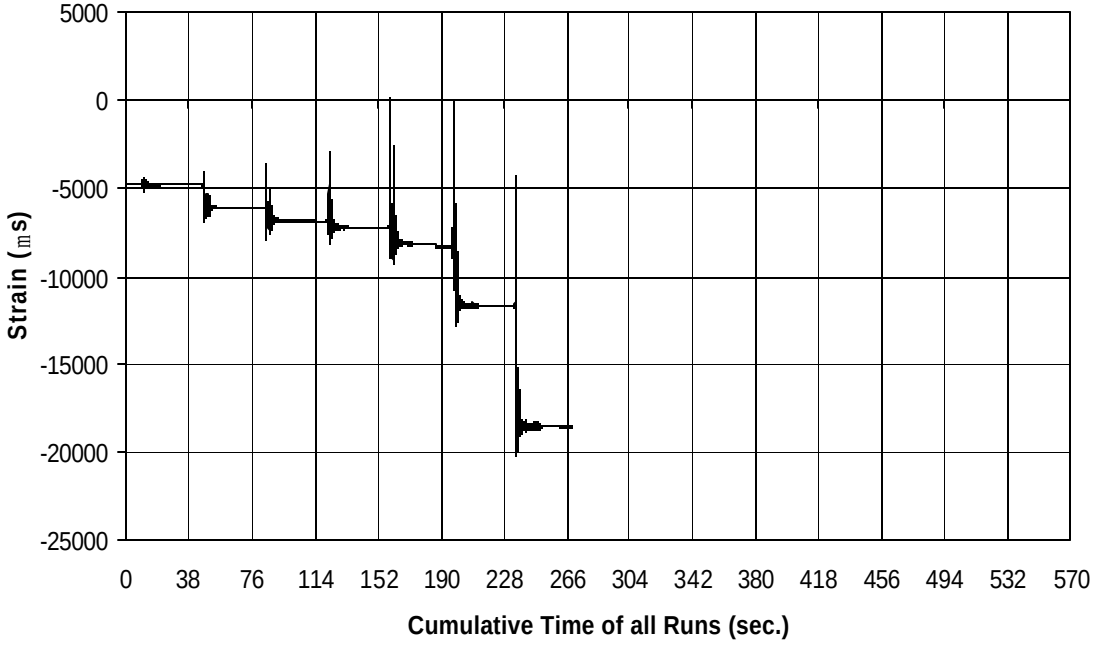

Fig. A-292 THD -5 Measured Strain in Gauge SG12

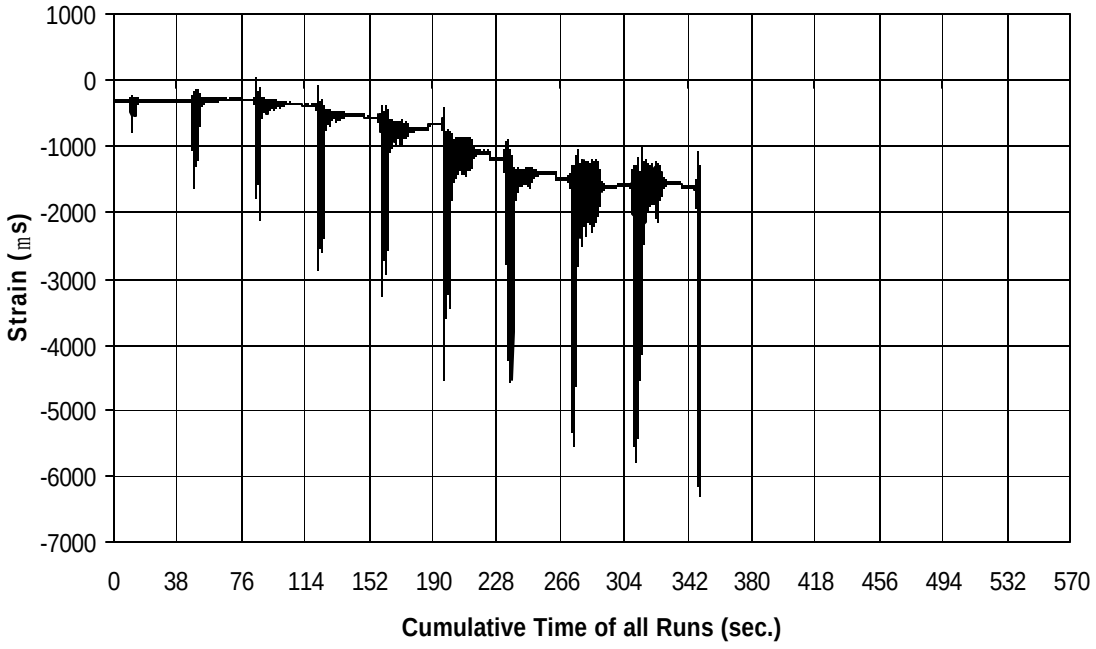

Fig. A-293 THD -5 Measured Strain in Gauge SG14

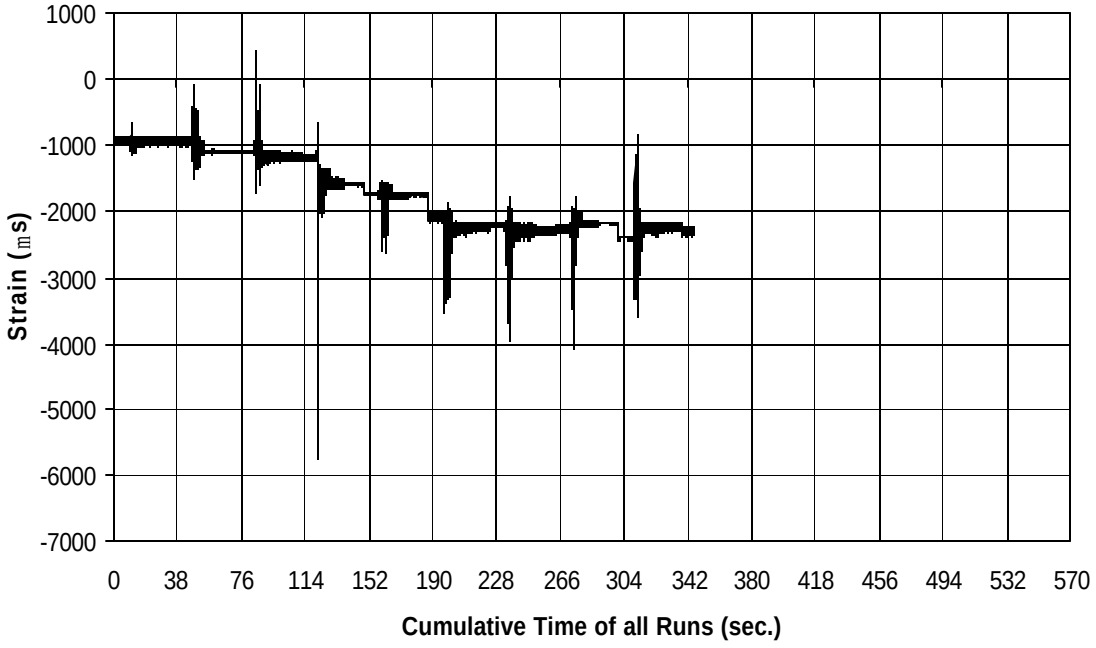

Fig. A-294 THD -5 Measured Strain in Gauge SG15

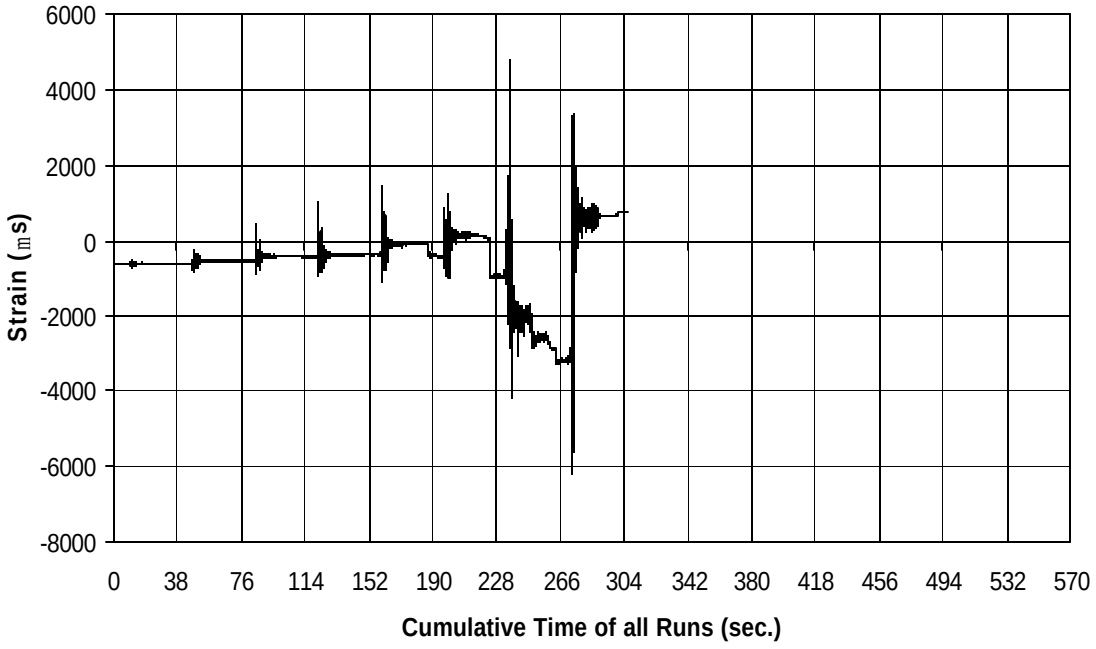

Fig. A-295 THD -5 Measured Strain in Gauge SG16

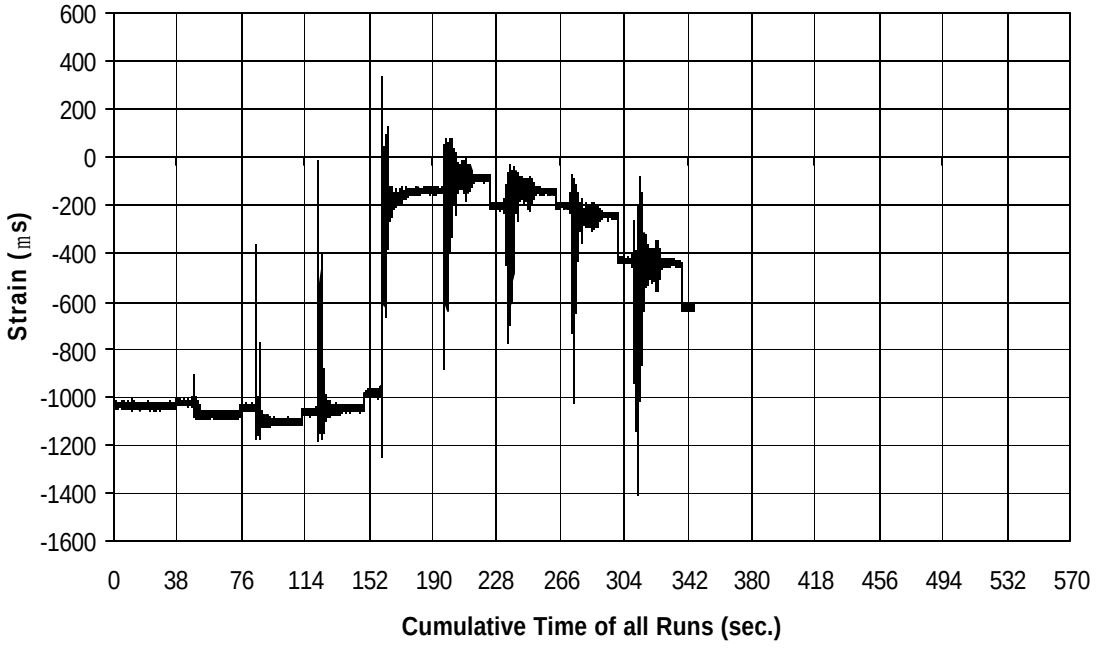

Fig. A-296 THD -5 Measured Strain in Gauge SG17

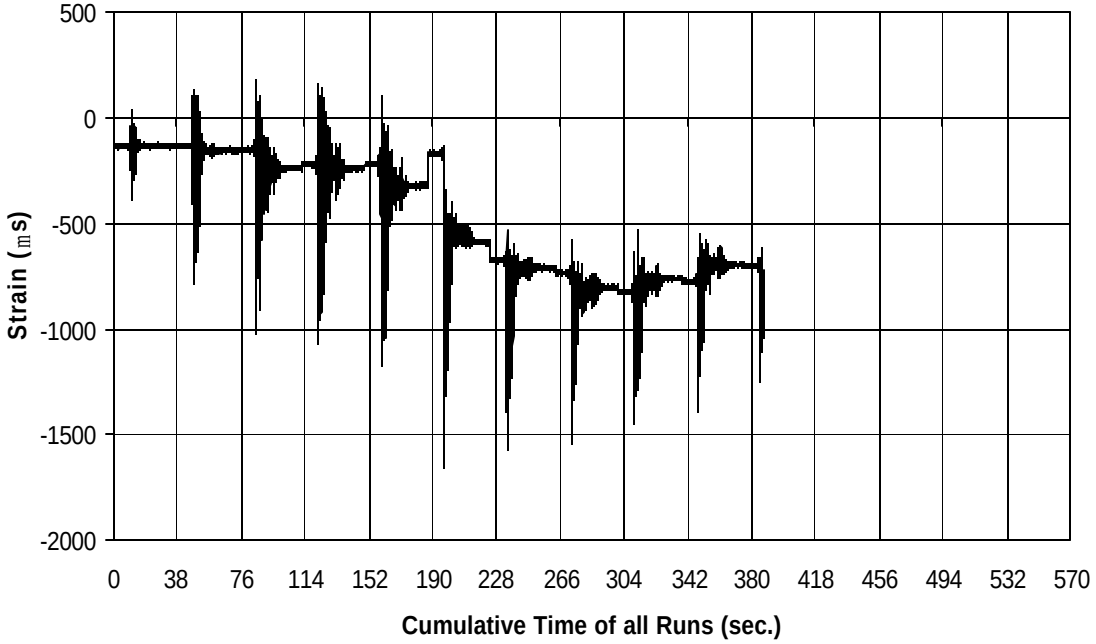

Fig. A-297 THD -5 Measured Strain in Gauge SG18

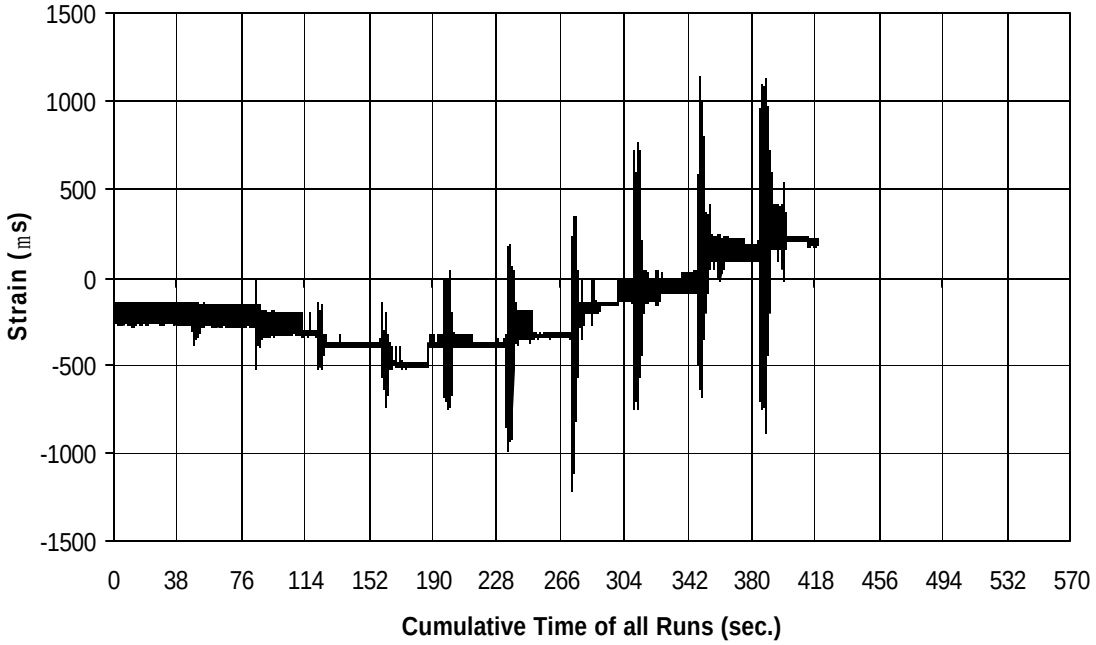

Fig. A-298 THD -5 Measured Strain in Gauge SG19

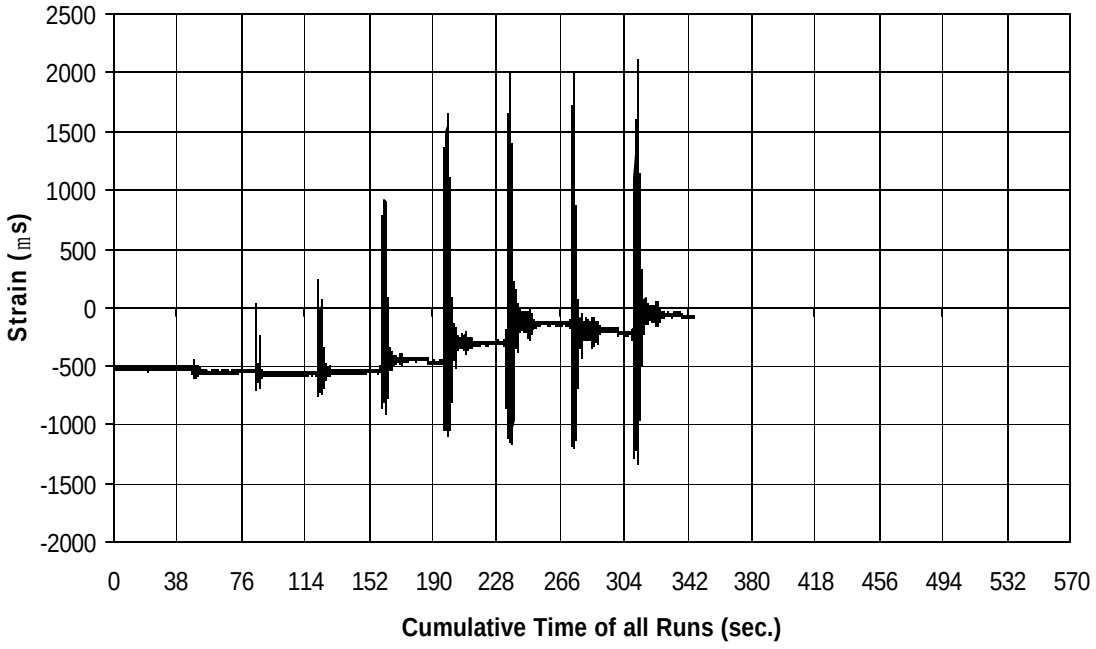

Fig. A-299 THD -5 Measured Strain in Gauge SG20

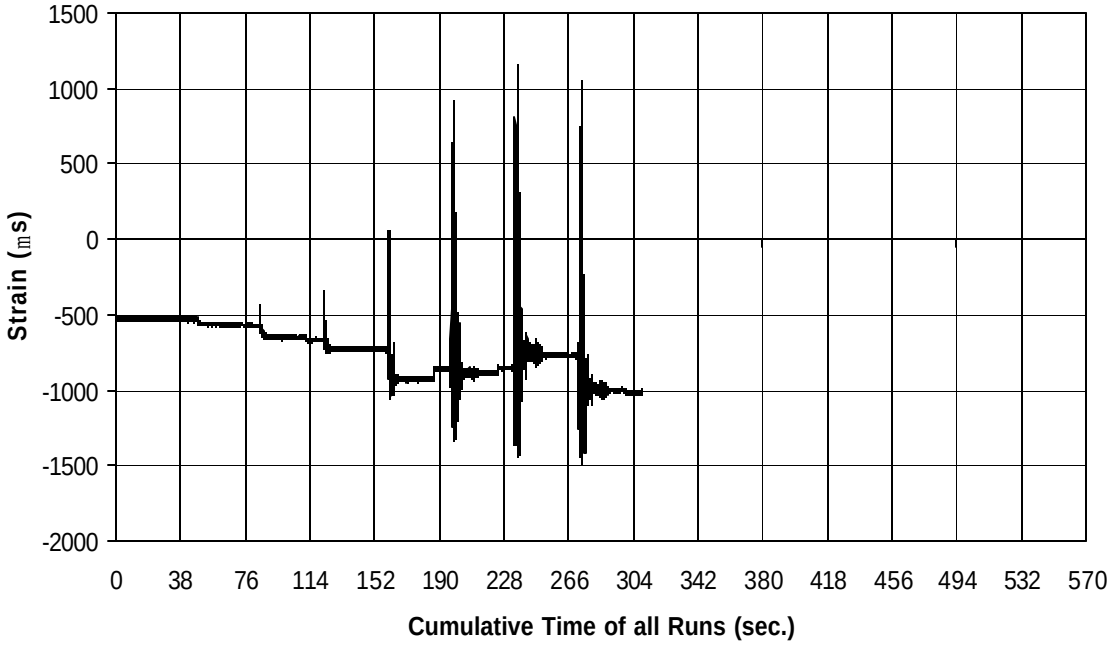

Fig. A-300 THD -5 Measured Strain in Gauge SG21

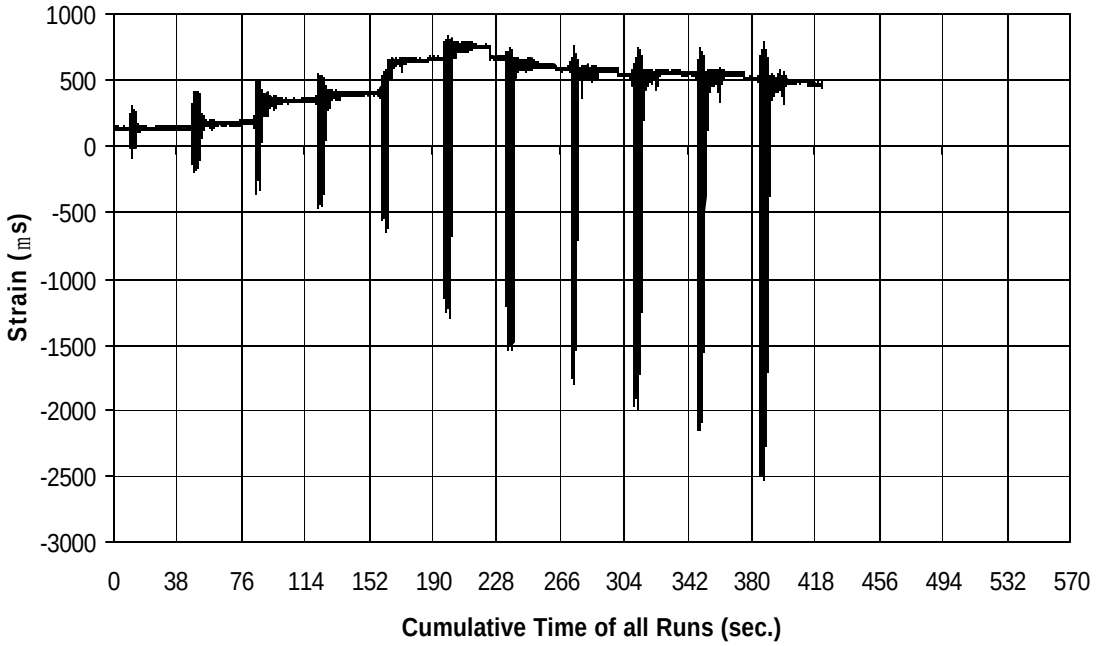

Fig. A-301 THD -5 Measured Strain in Gauge SG22

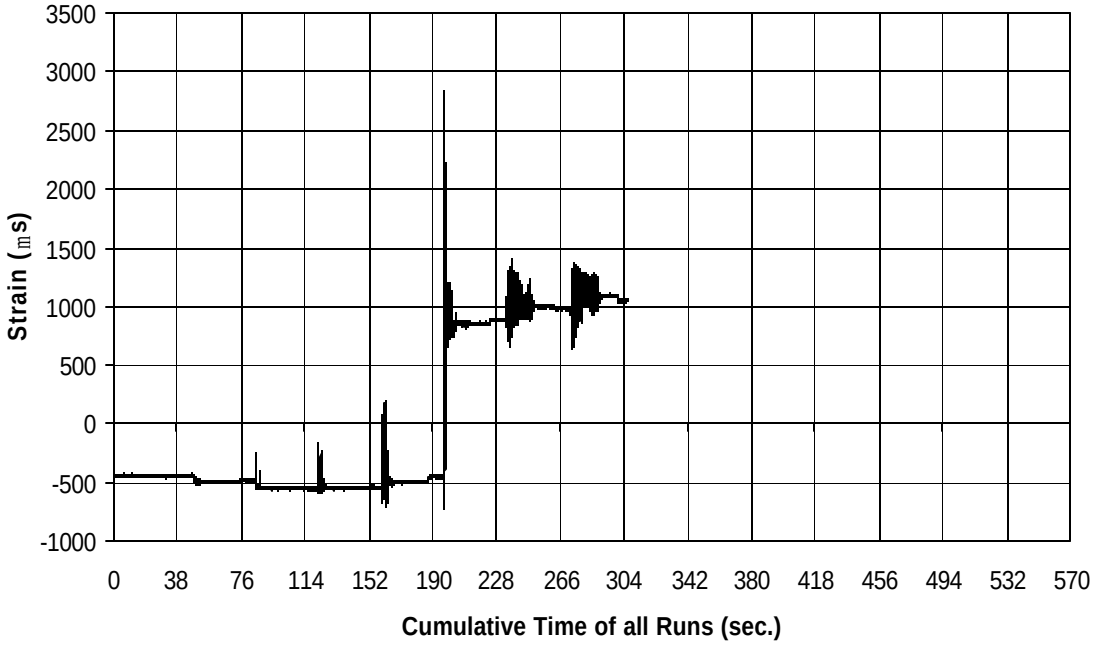

Fig. A-302 THD -5 Measured Strain in Gauge SG23

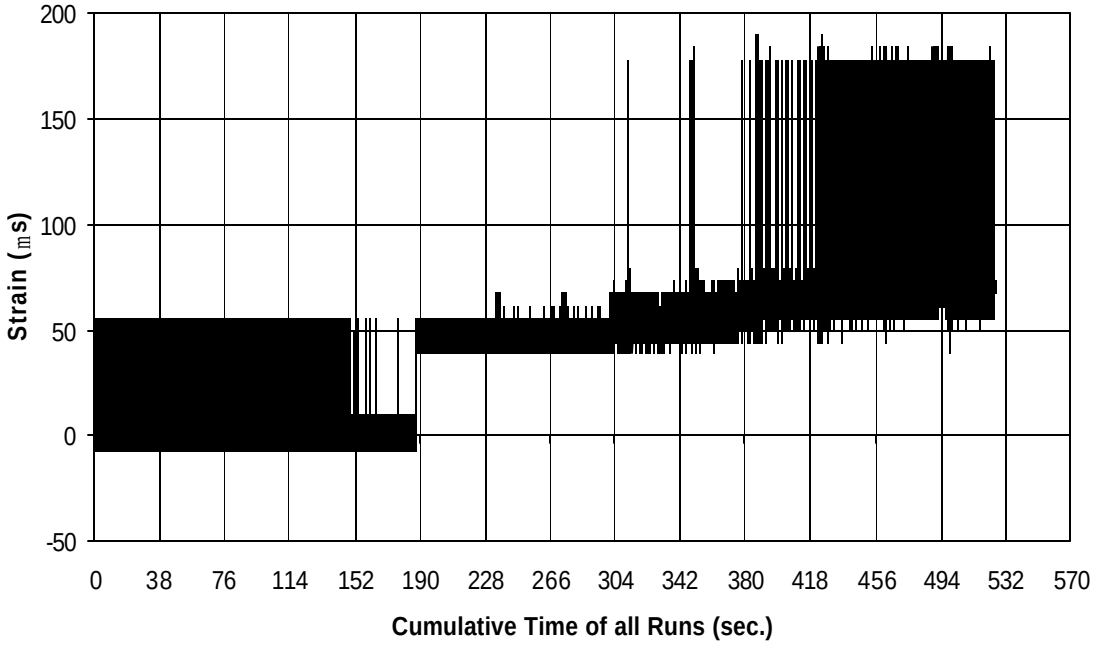

Fig. A-303 THD -5 Measured Strain in Gauge SG24

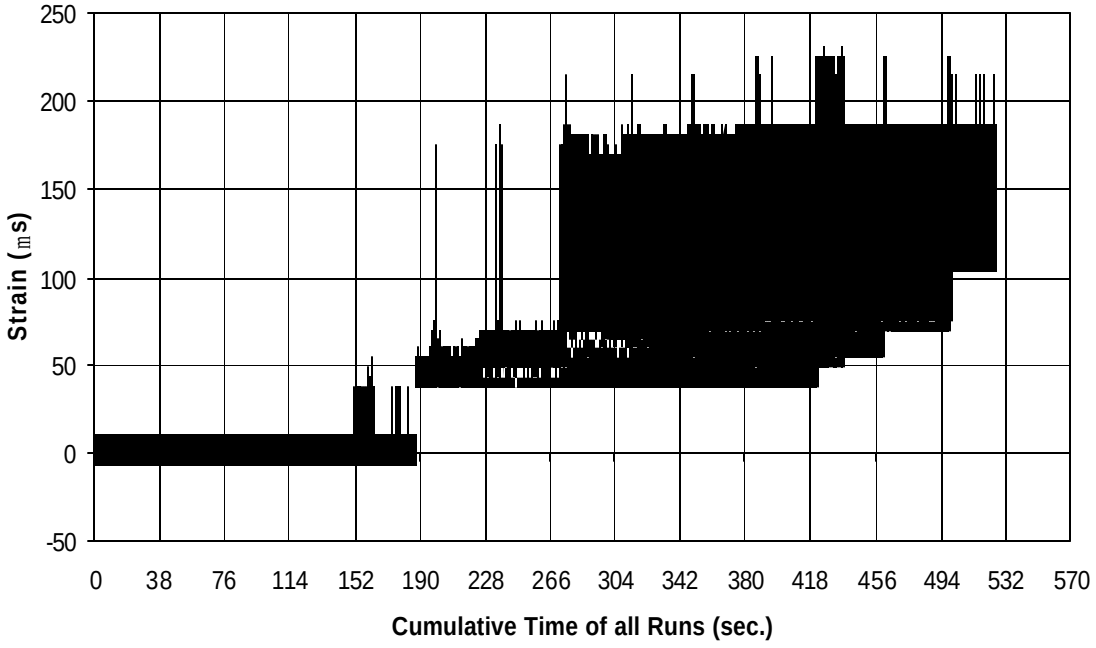

Fig. A-304 THD -5 Measured Strain in Gauge SG25

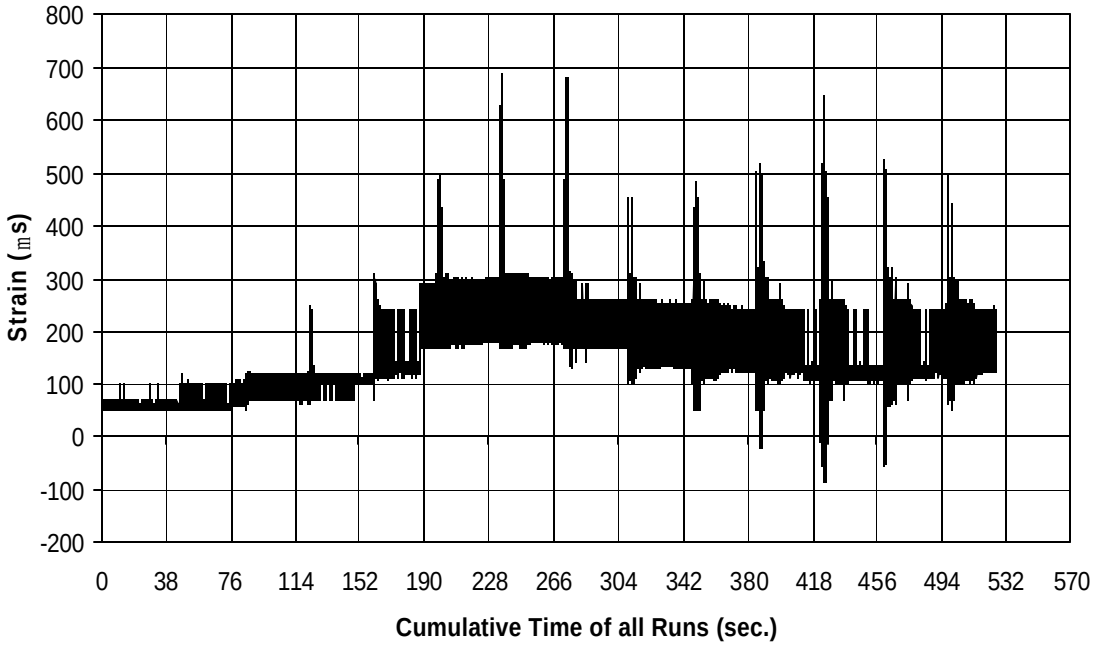

Fig. A-305 THD -5 Measured Strain in Gauge SG26

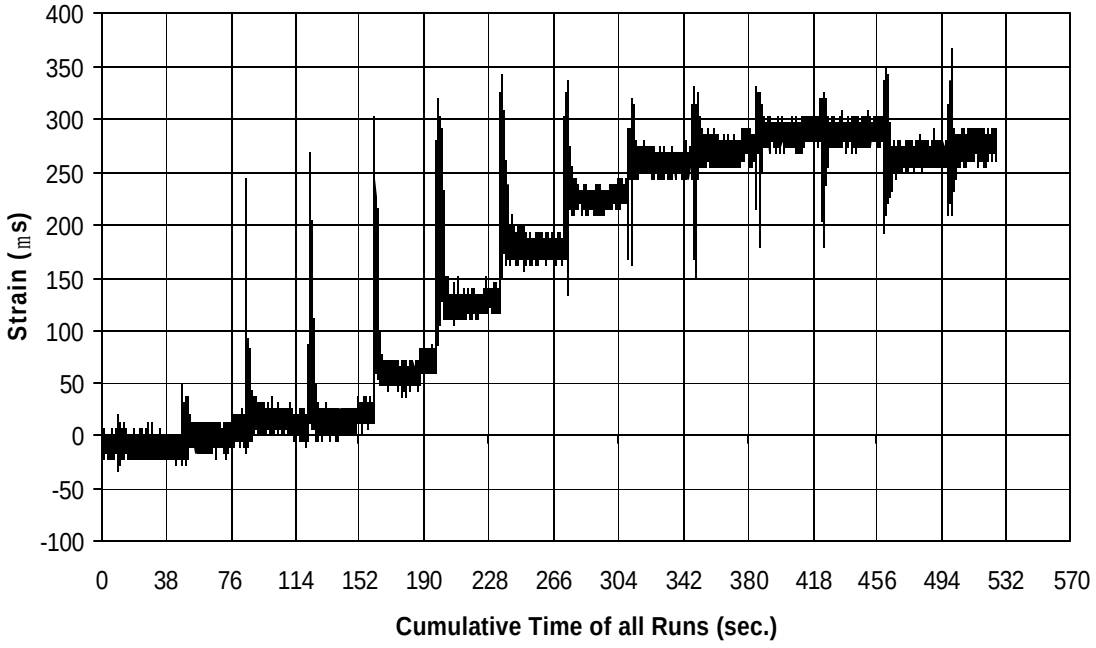

Fig. A-306 THD -5 Measured Strain in Gauge SG27

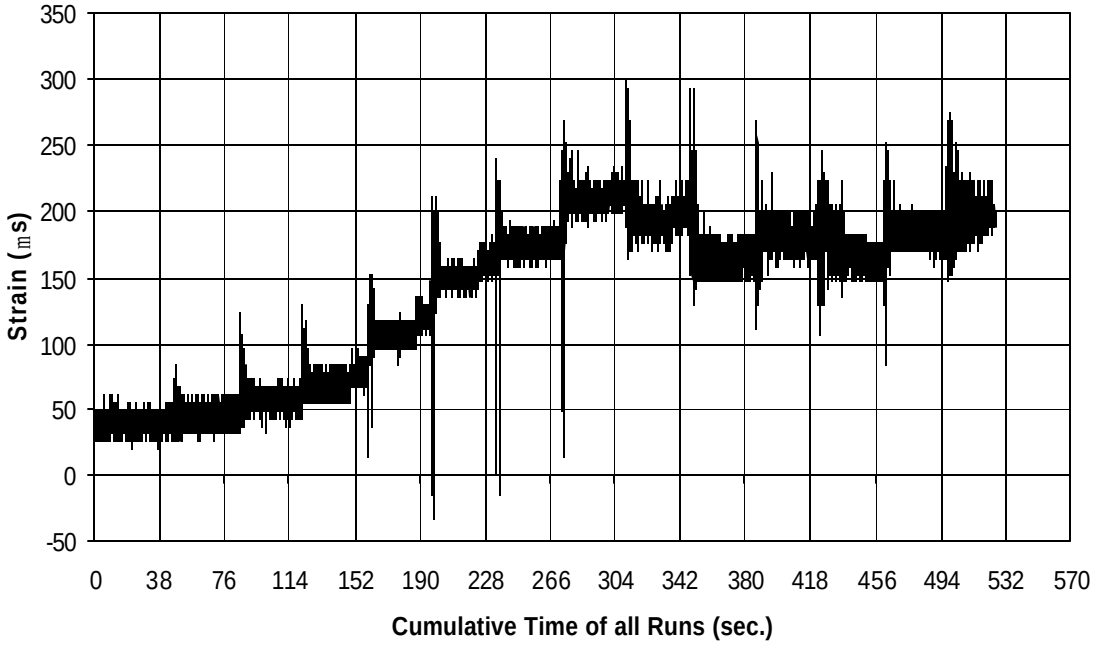

Fig. A-307 THD -5 Measured Strain in Gauge SG28

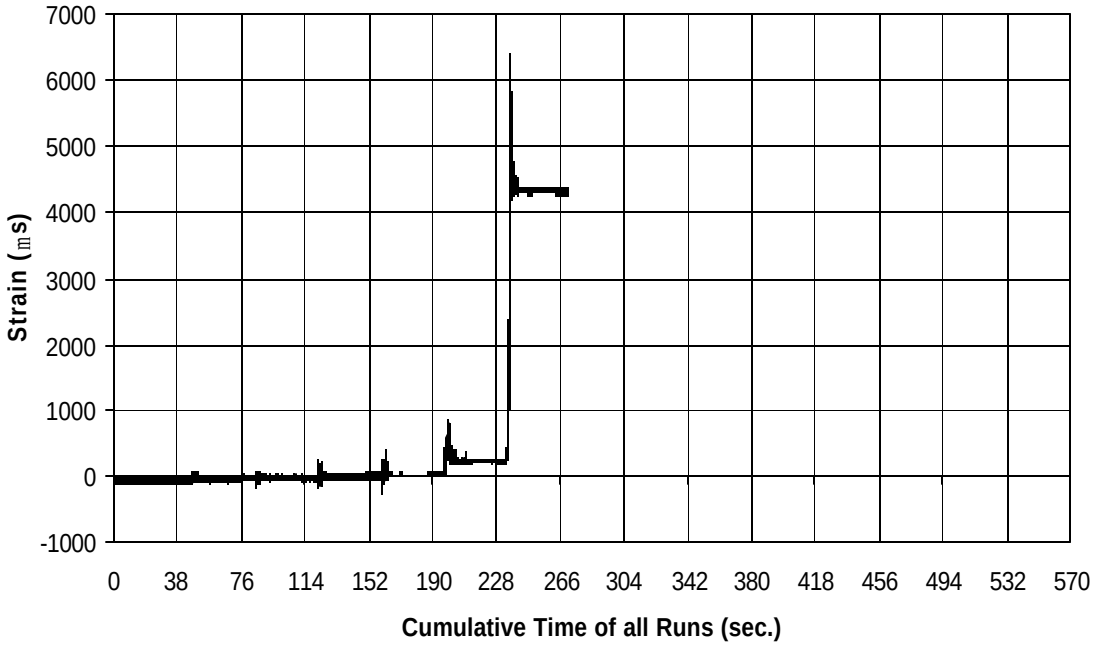

Fig. A-308 THD -5 Measured Strain in Gauge SG29

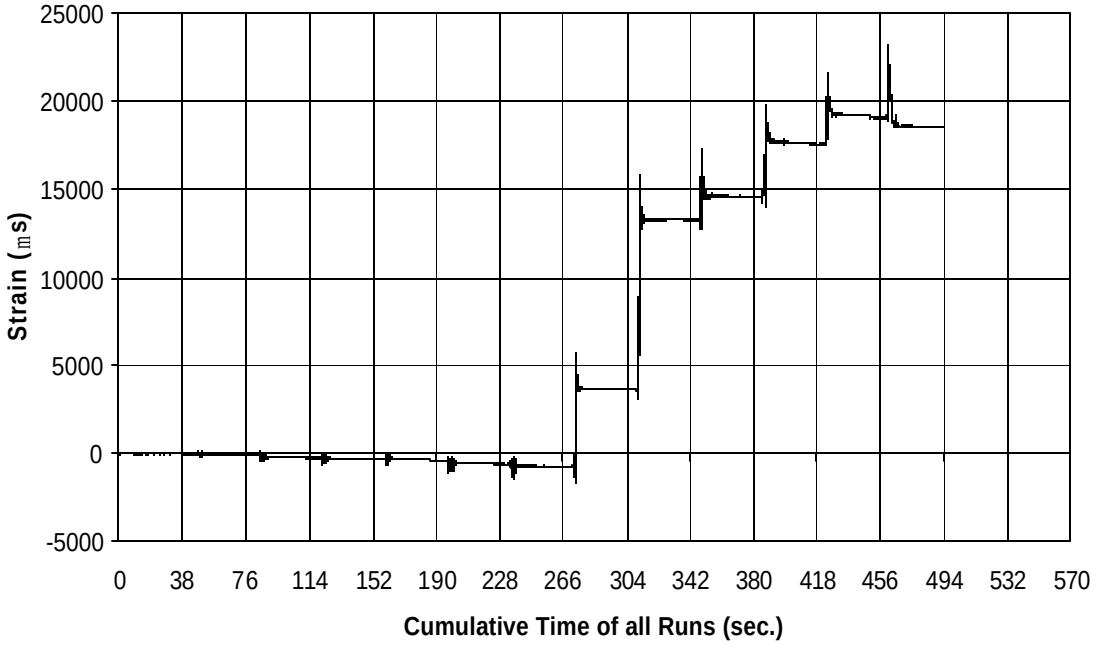

Fig. A-309 THD -5 Measured Strain in Gauge SG30

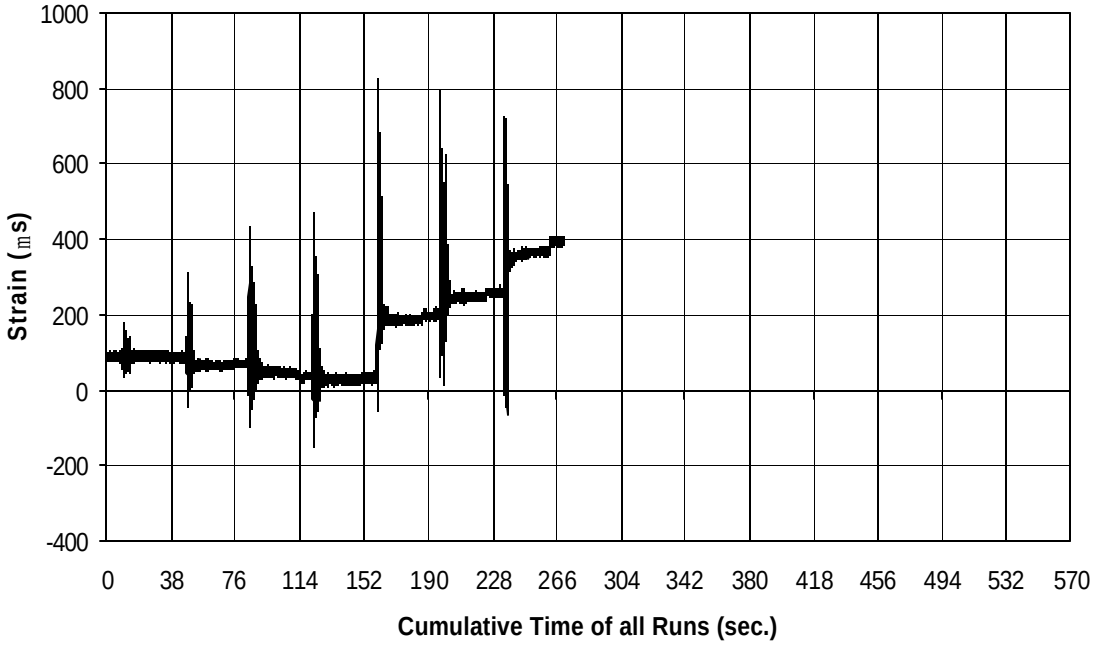

Fig. A-310 THD -5 Measured Strain in Gauge SG31

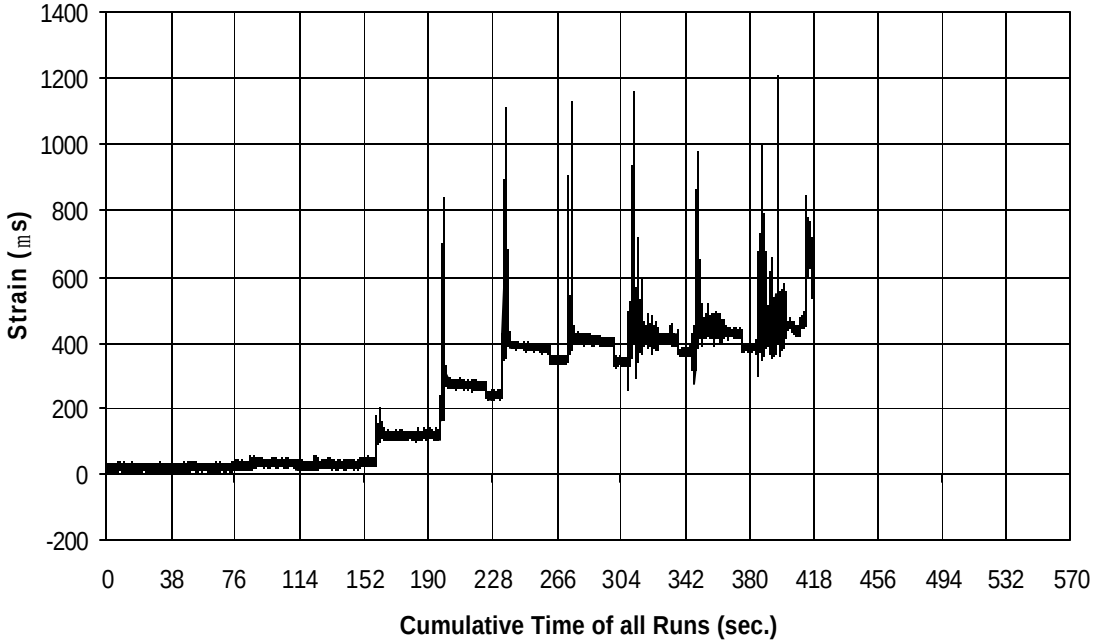

Fig. A-311 THD -5 Measured Strain in Gauge SG32

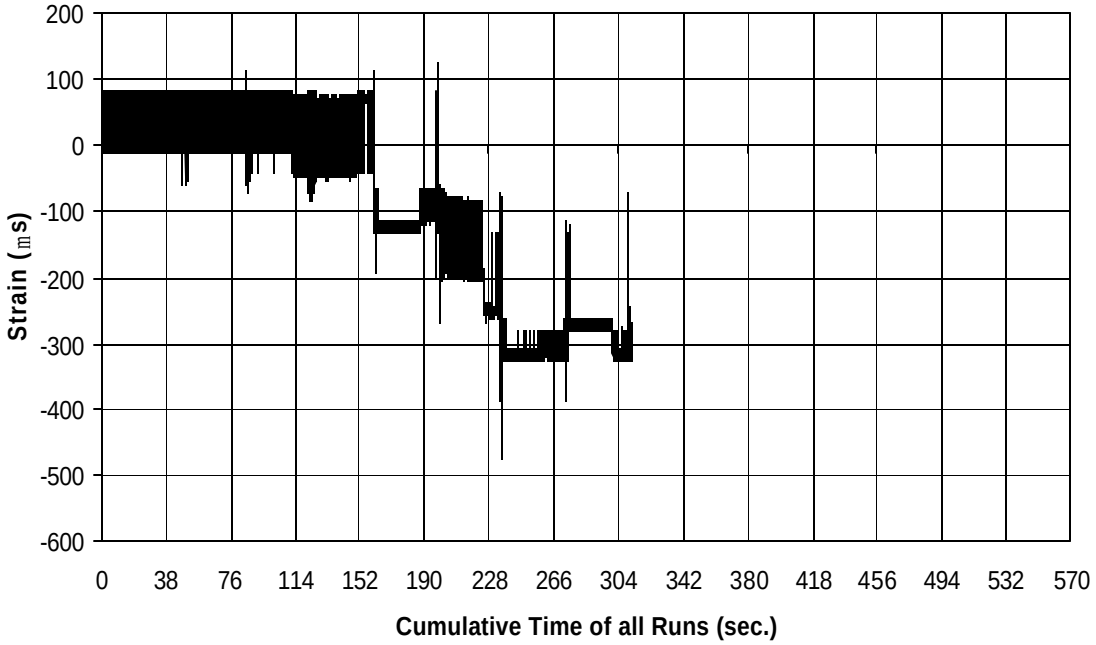

Fig. A-312 THD -5 Measured Strain in Gauge SG33

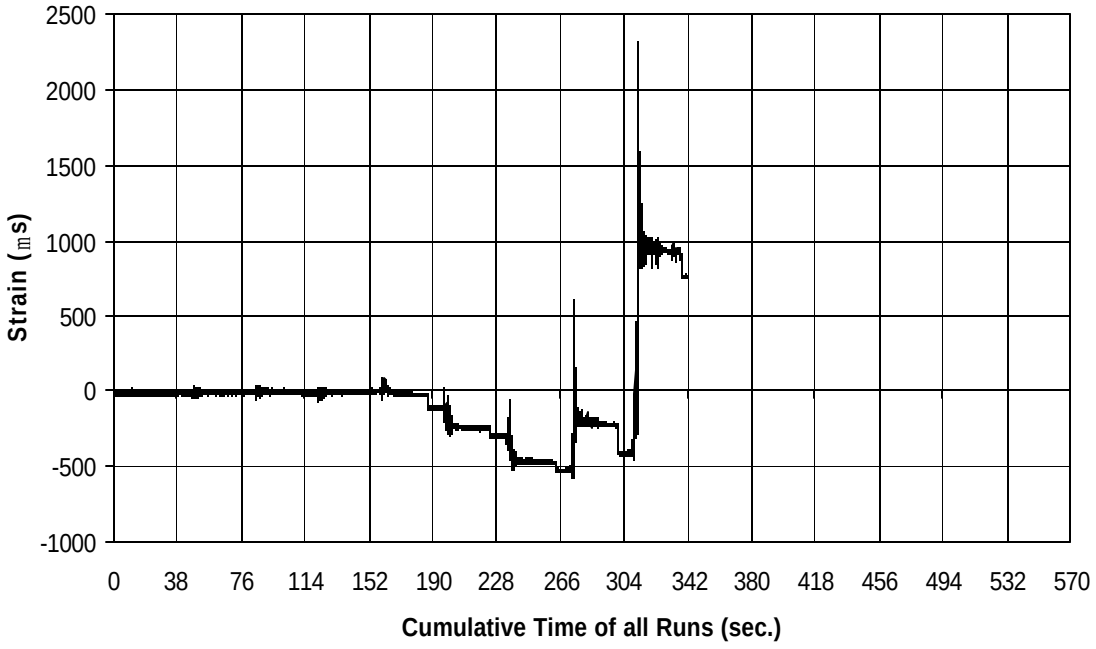

Fig. A-313 THD -5 Measured Strain in Gauge SG34

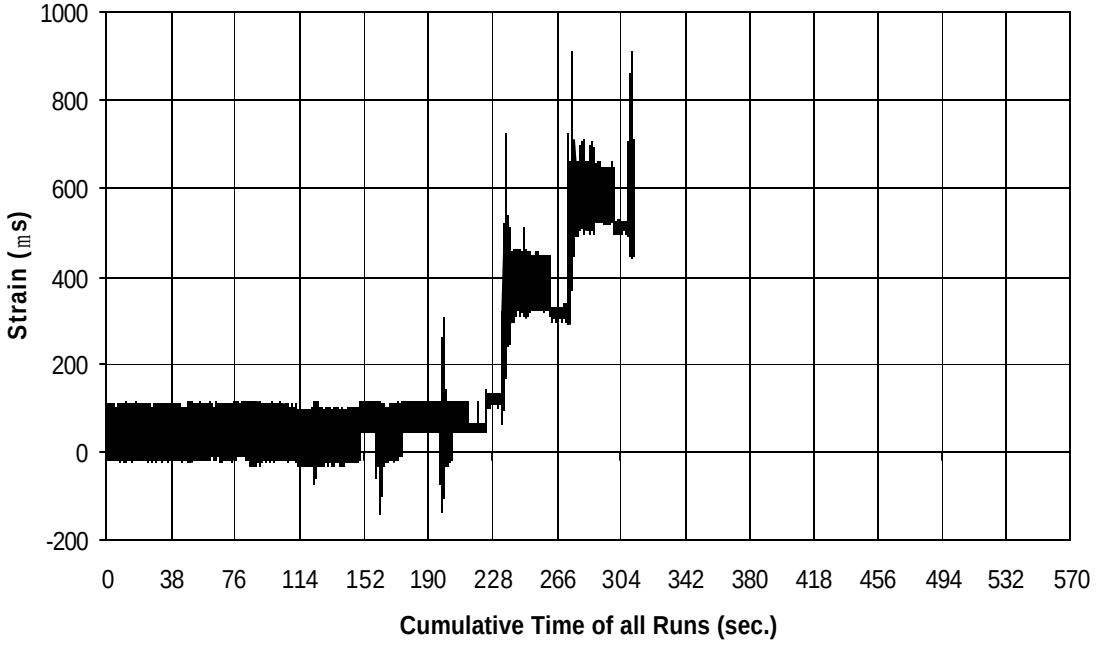

Fig. A-314 THD -5 Measured Strain in Gauge SG35

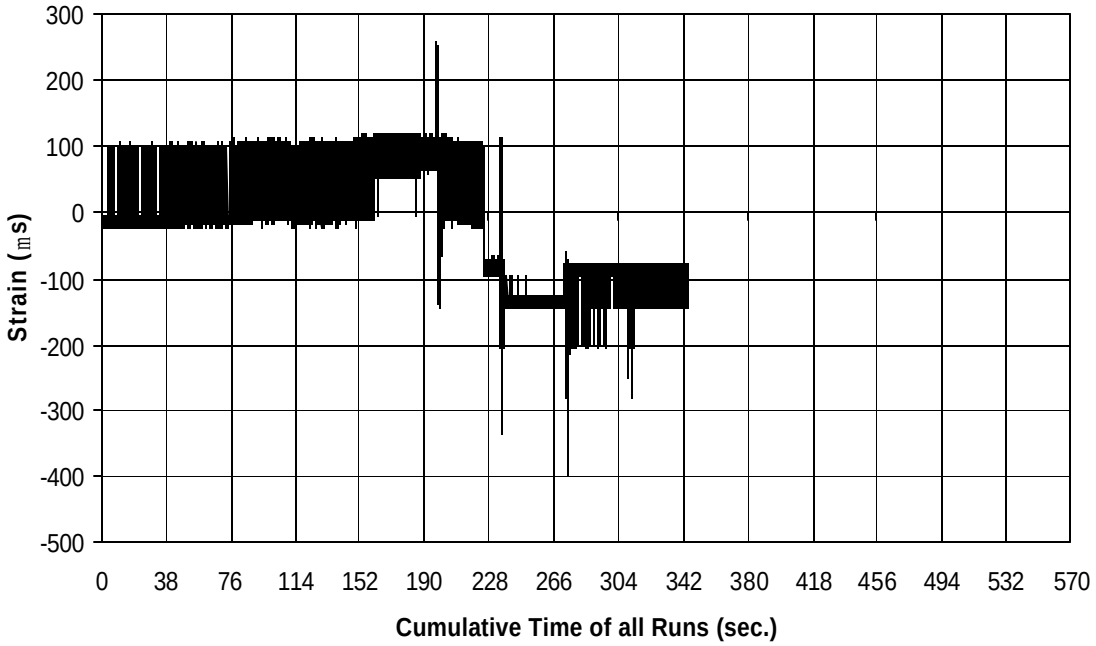

Fig. A-315 THD -5 Measured Strain in Gauge SG36

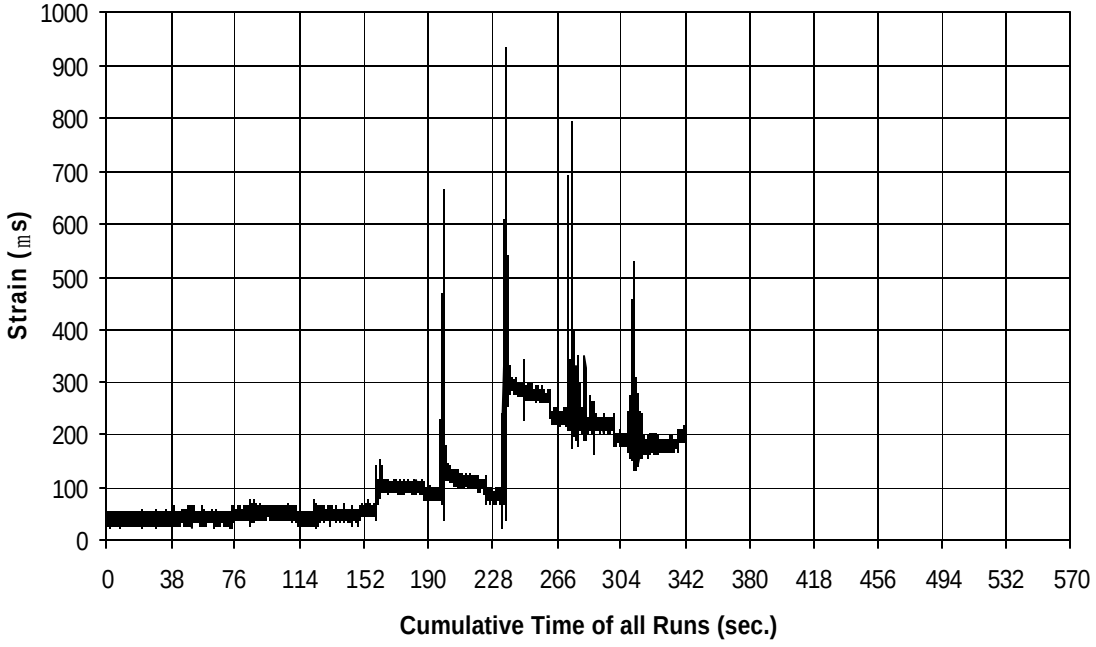

Fig. A-316 THD -5 Measured Strain in Gauge SG37

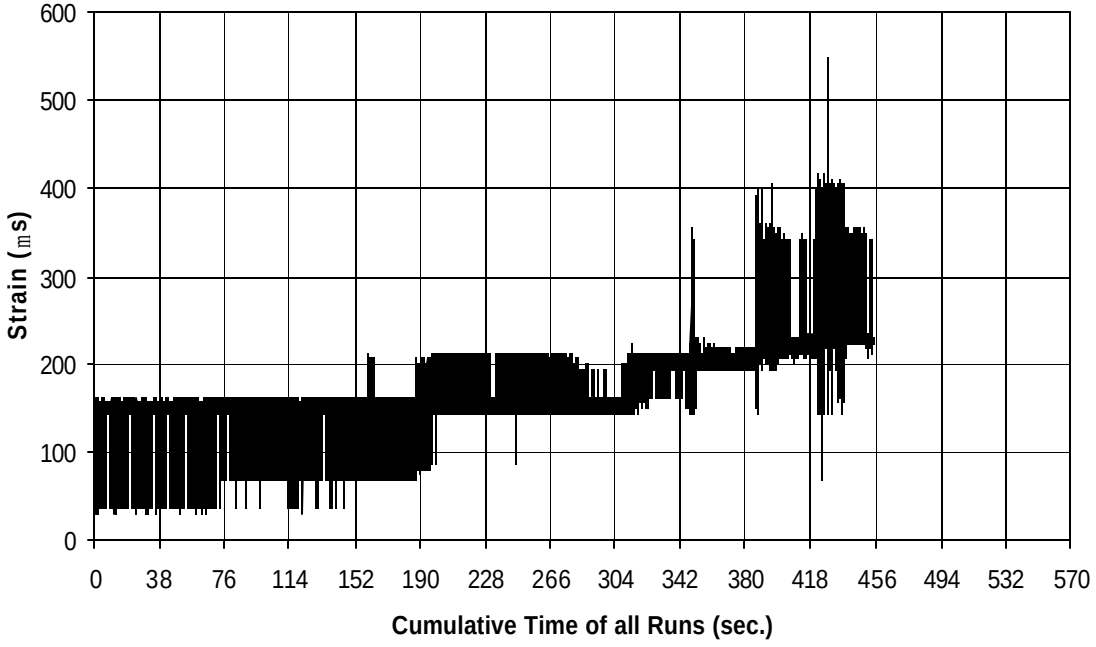

Fig. A-317 THD -5 Measured Strain in Gauge SG38

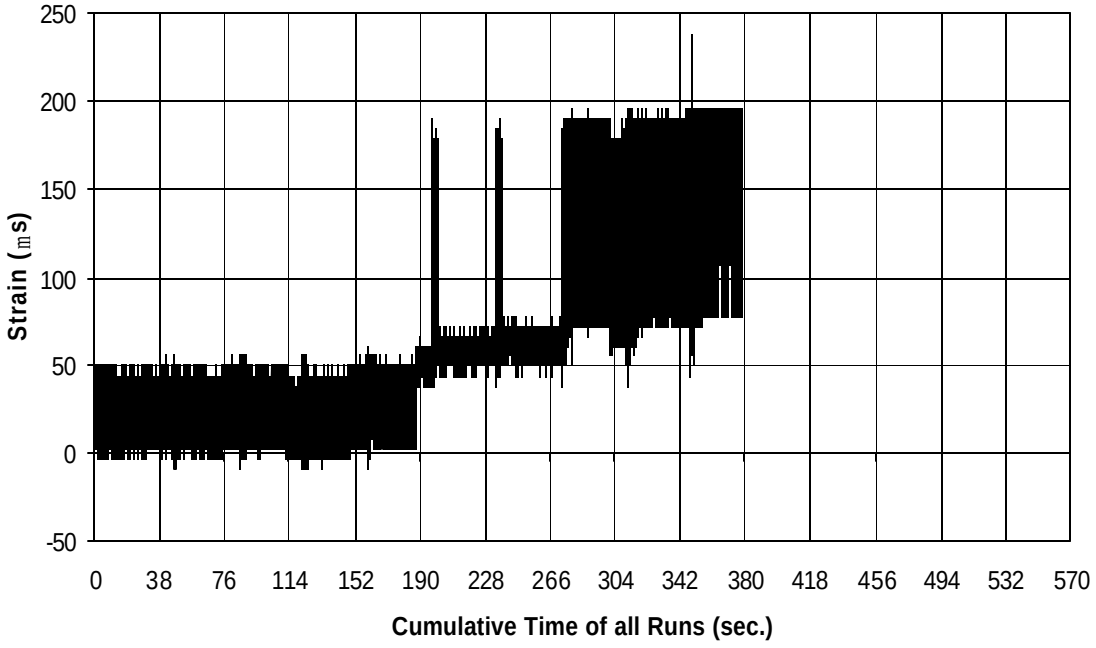

Fig. A-318 THD -5 Measured Strain in Gauge SG39

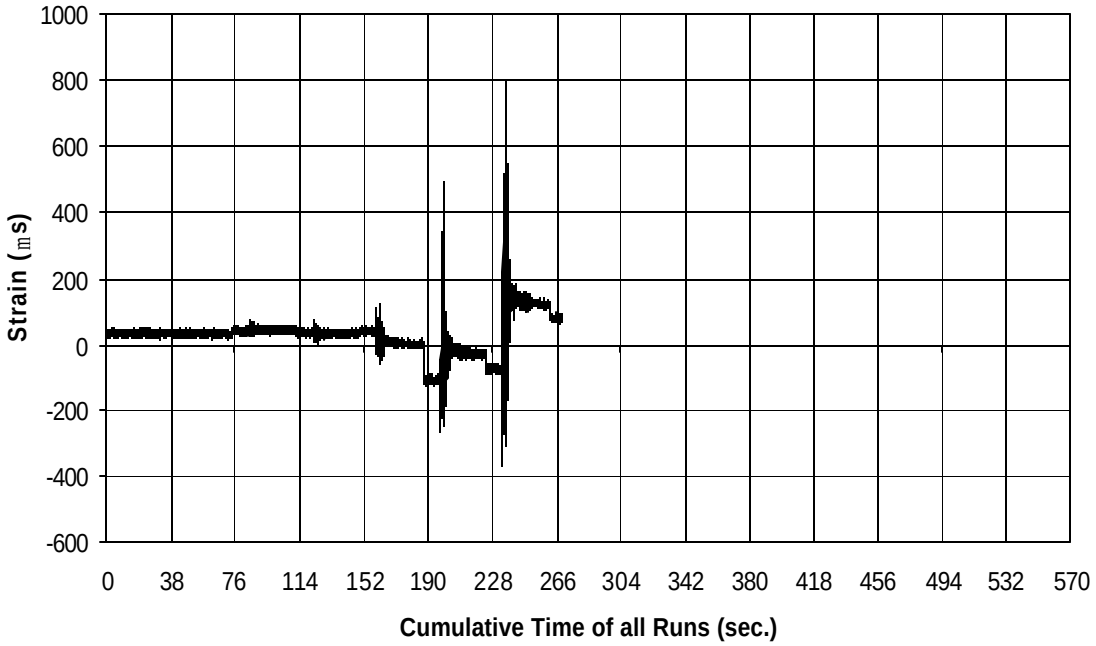

Fig. A-319 THD -5 Measured Strain in Gauge SG40

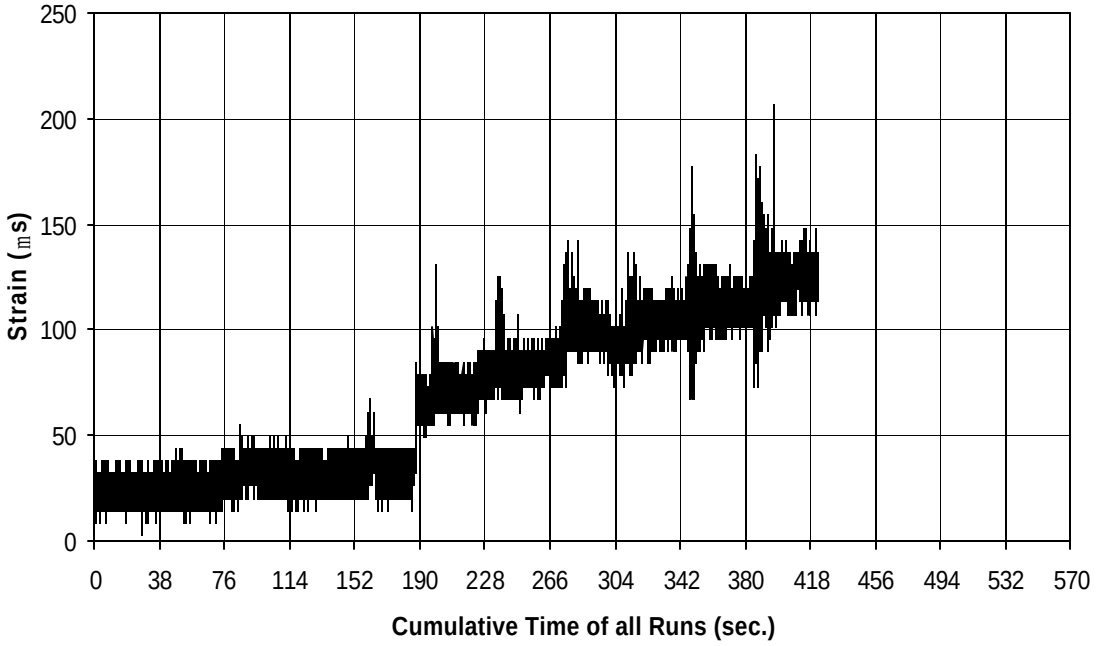

Fig. A-320 THD -5 Measured Strain in Gauge SG41

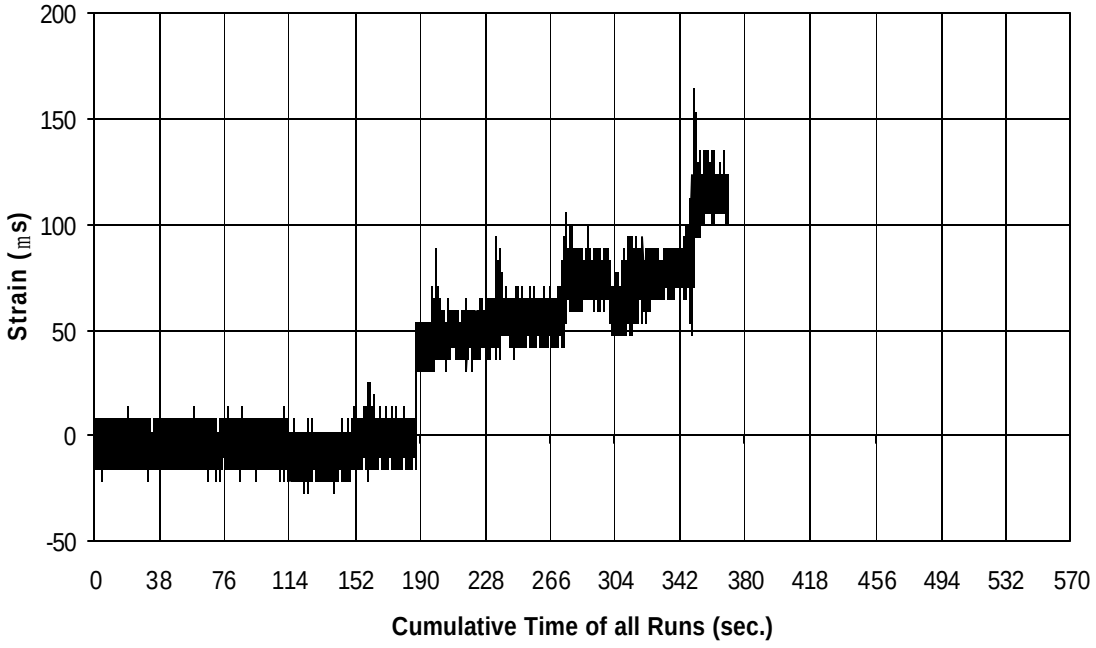

Fig. A-321 THD -5 Measured Strain in Gauge SG42

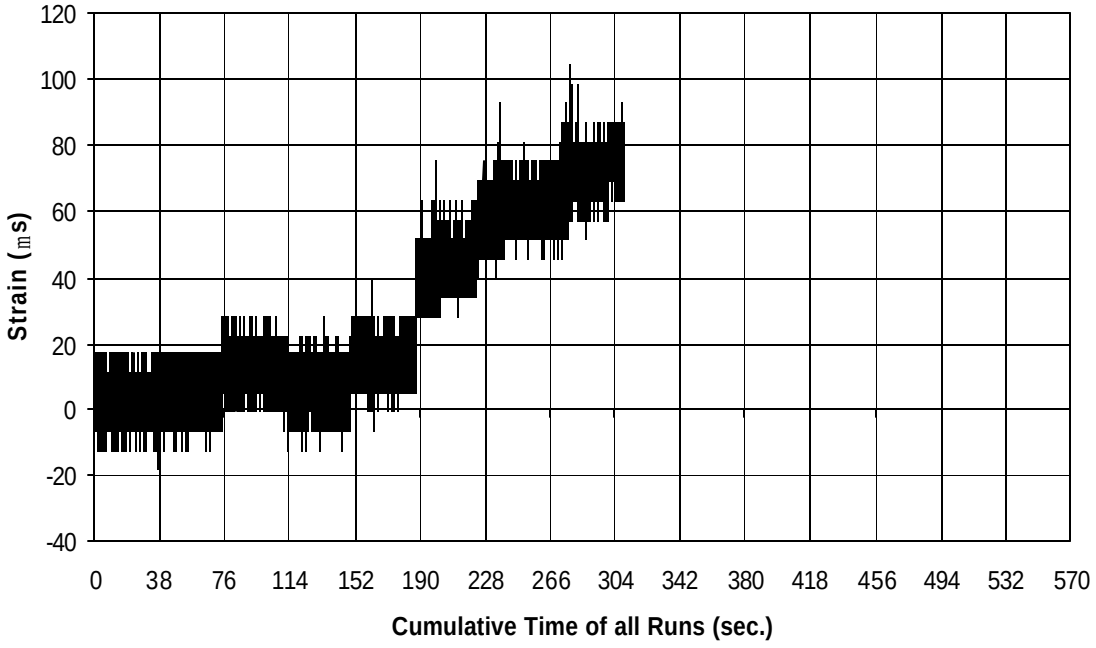

Fig. A-322 THD -5 Measured Strain in Gauge SG43

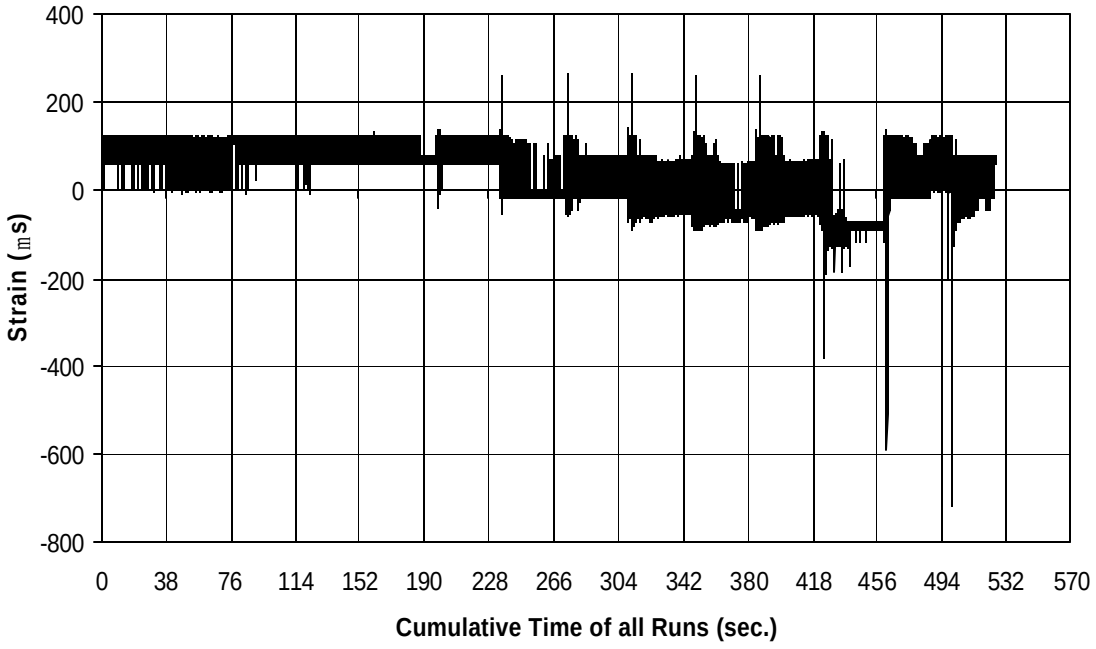

Fig. A-323 THD -5 Measured Strain in Gauge SG44

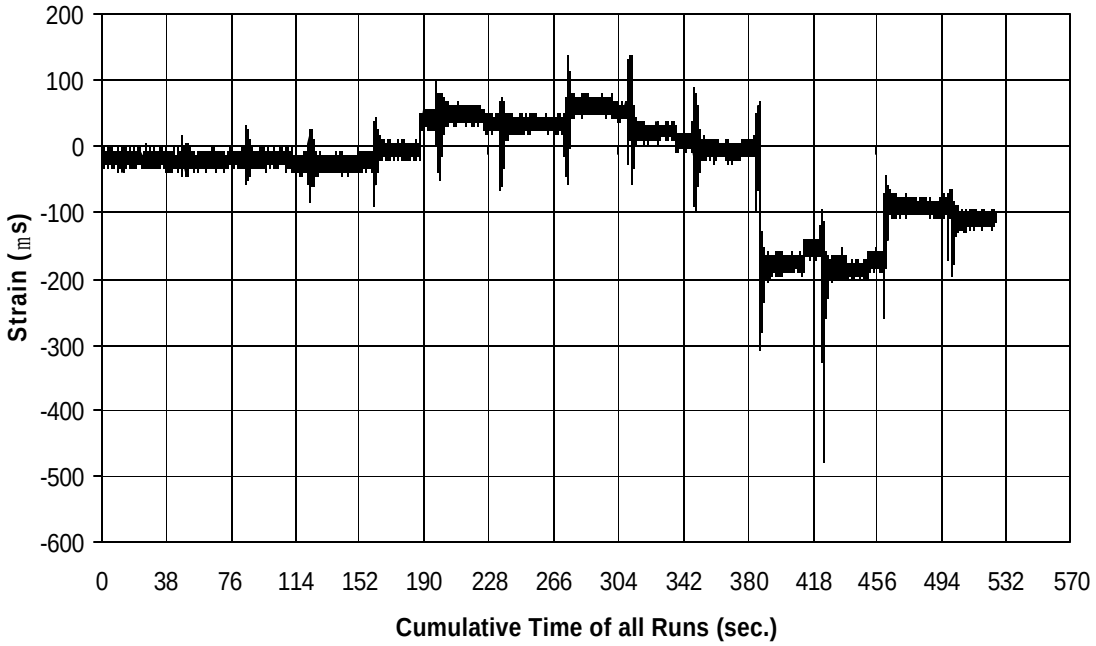

Fig. A-324 THD -5 Measured Strain in Gauge SG45

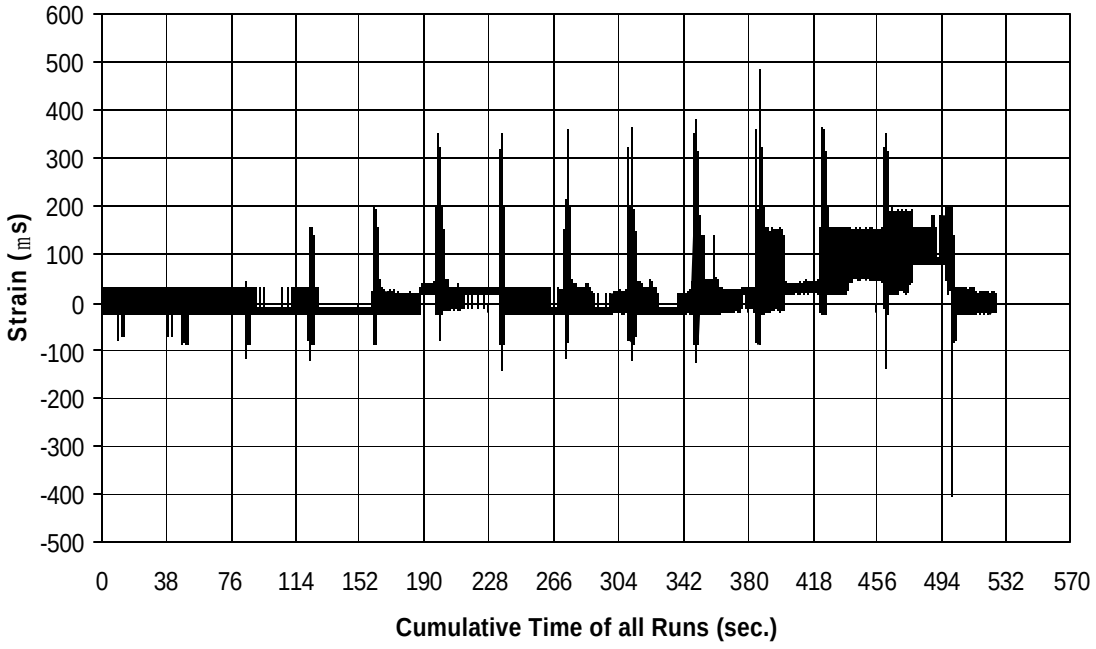

Fig. A-325 THD -5 Measured Strain in Gauge SG46

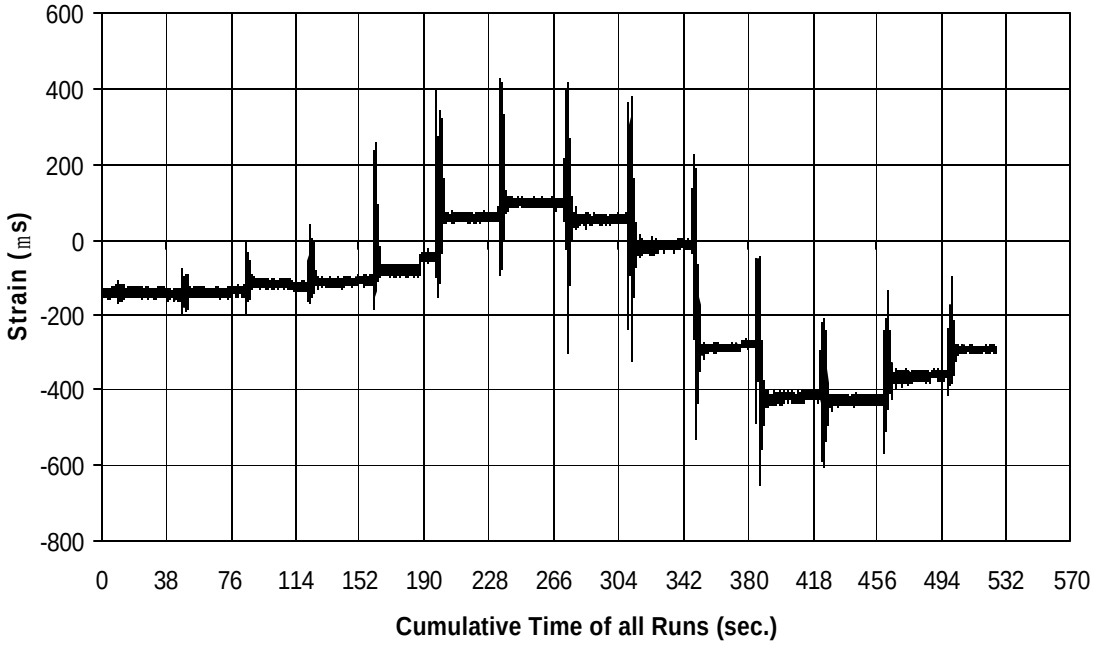

Fig. A-326 THD -5 Measured Strain in Gauge SG47

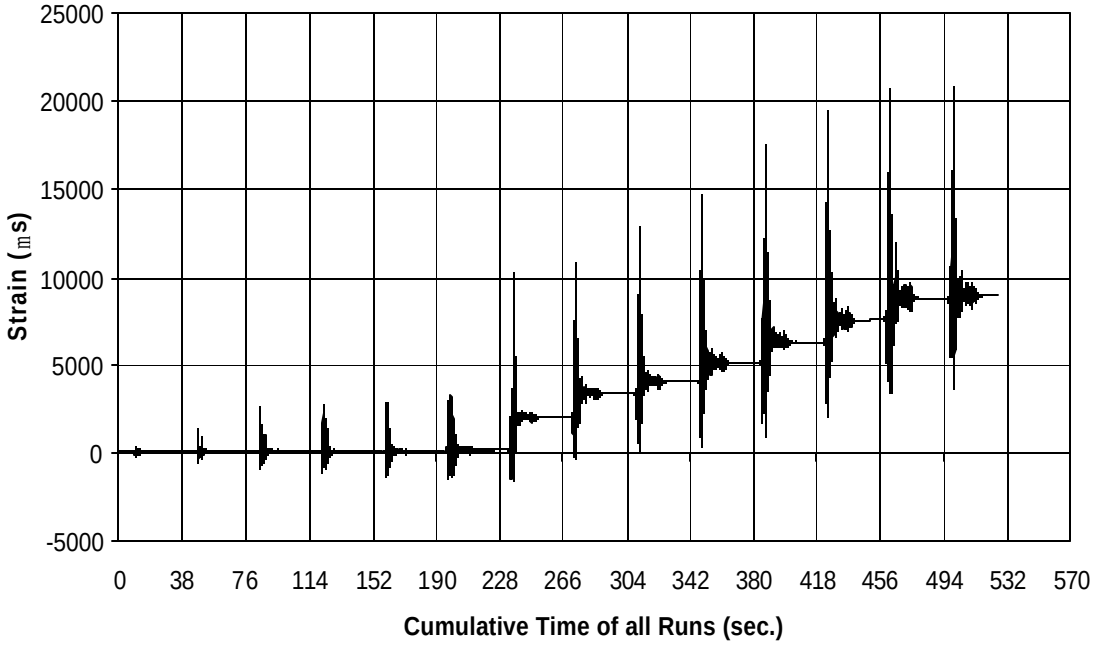

Fig. A-327 THD -5 Measured Strain in Gauge SG48

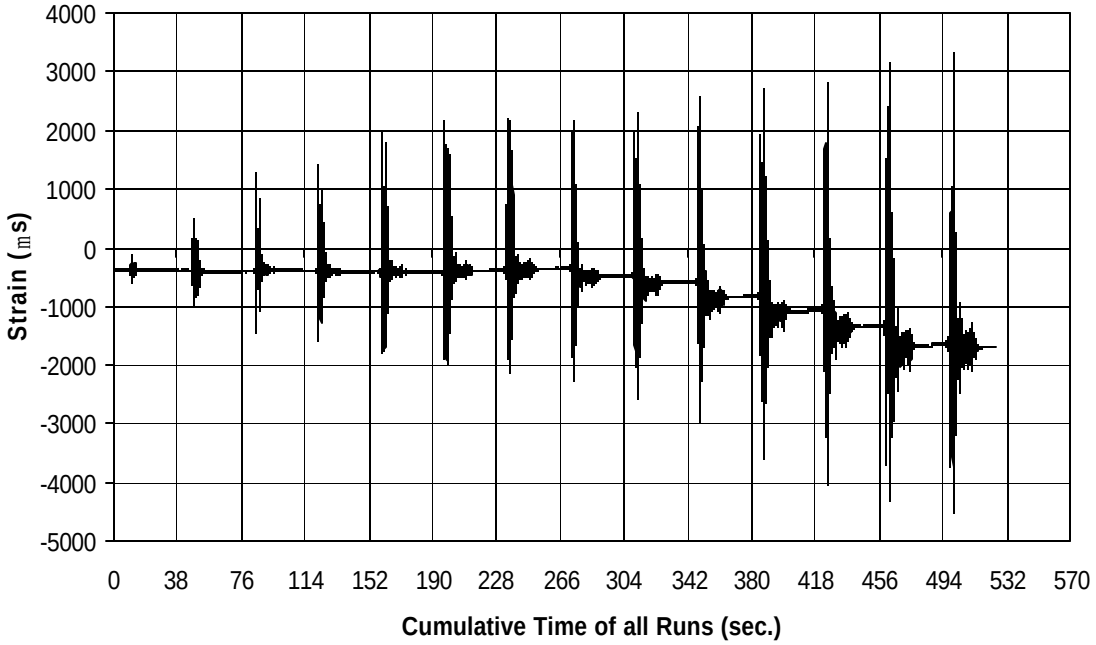

Fig. A-328 THD -5 Measured Strain in Gauge SG49

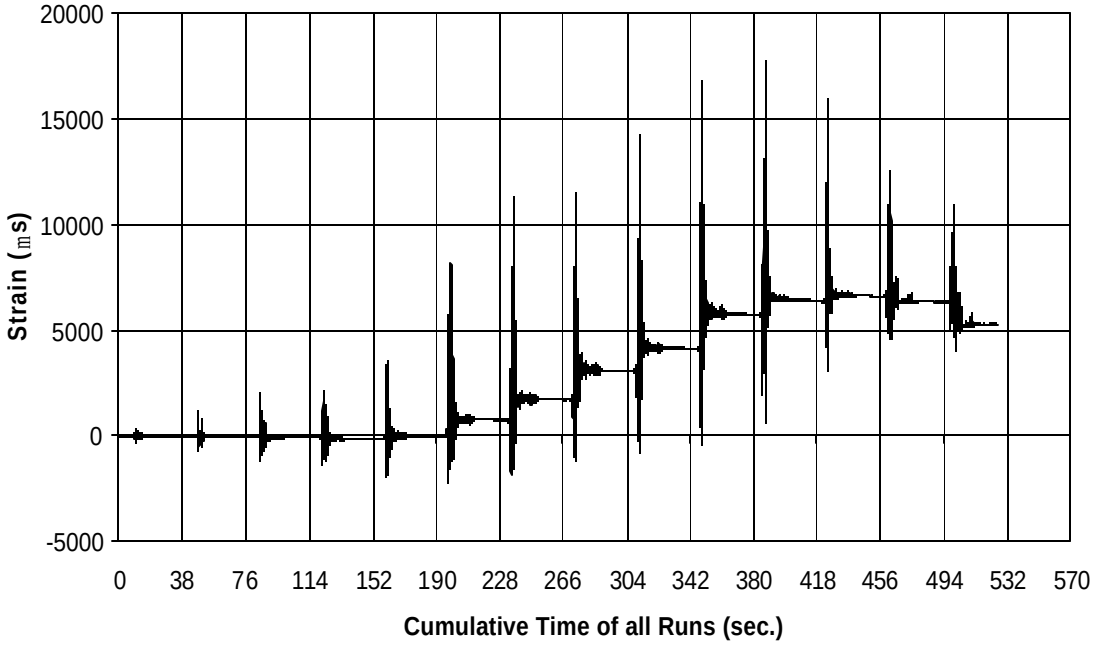

Fig. A-329 THD -5 Measured Strain in Gauge SG50

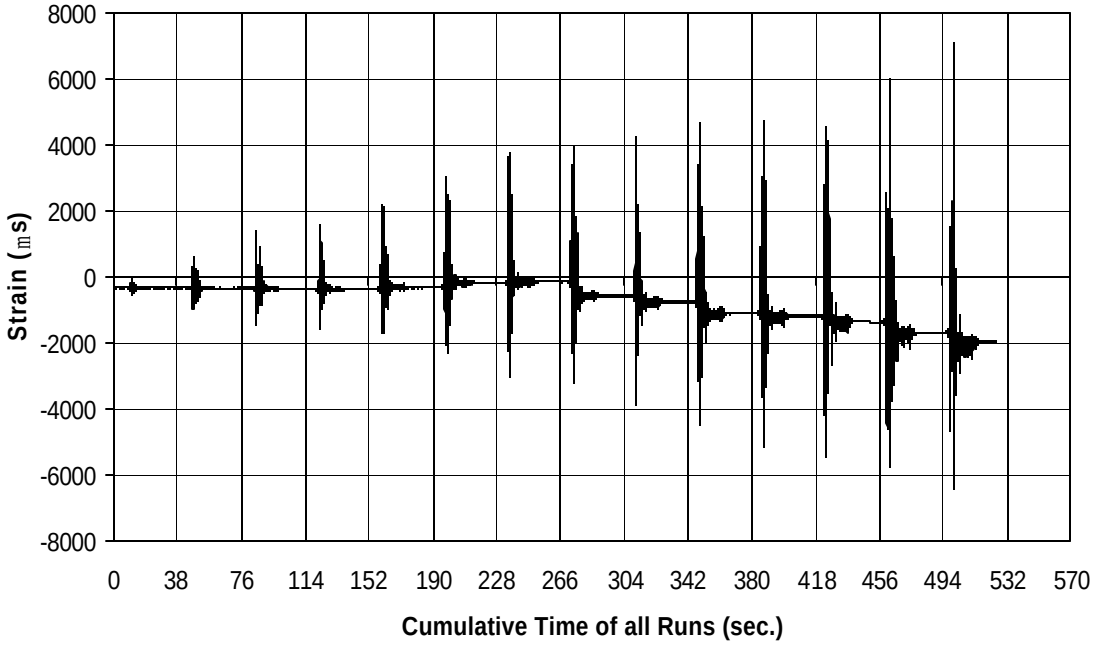

Fig. A-330 THD -5 Measured Strain in Gauge SG51

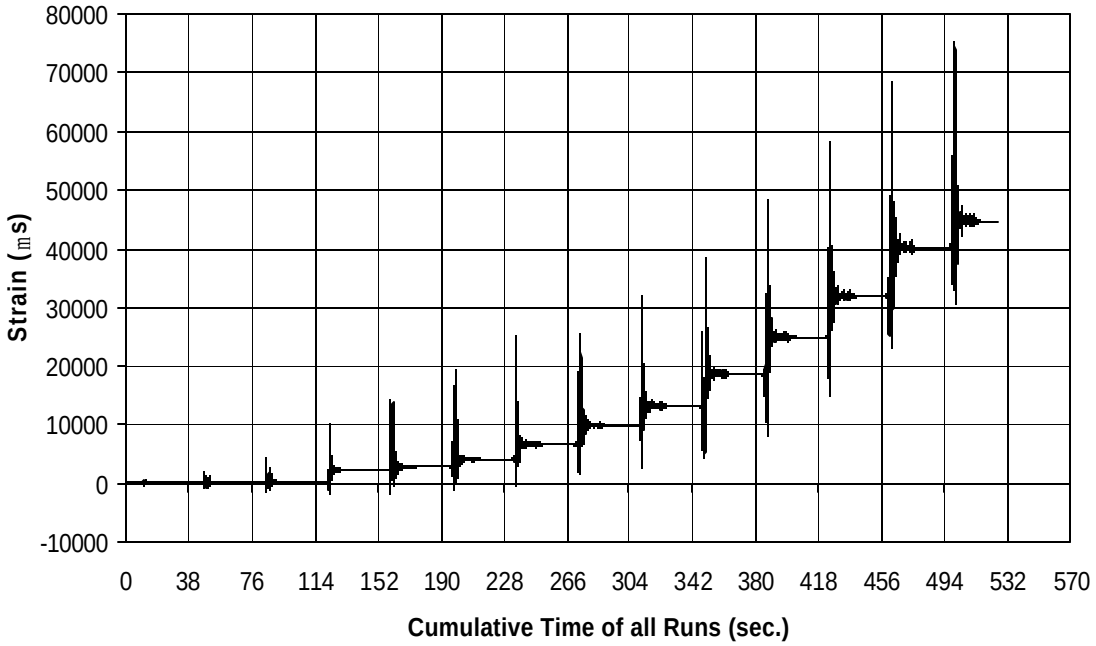

Fig. A-331 THD -5 Measured Strain in Gauge SG52

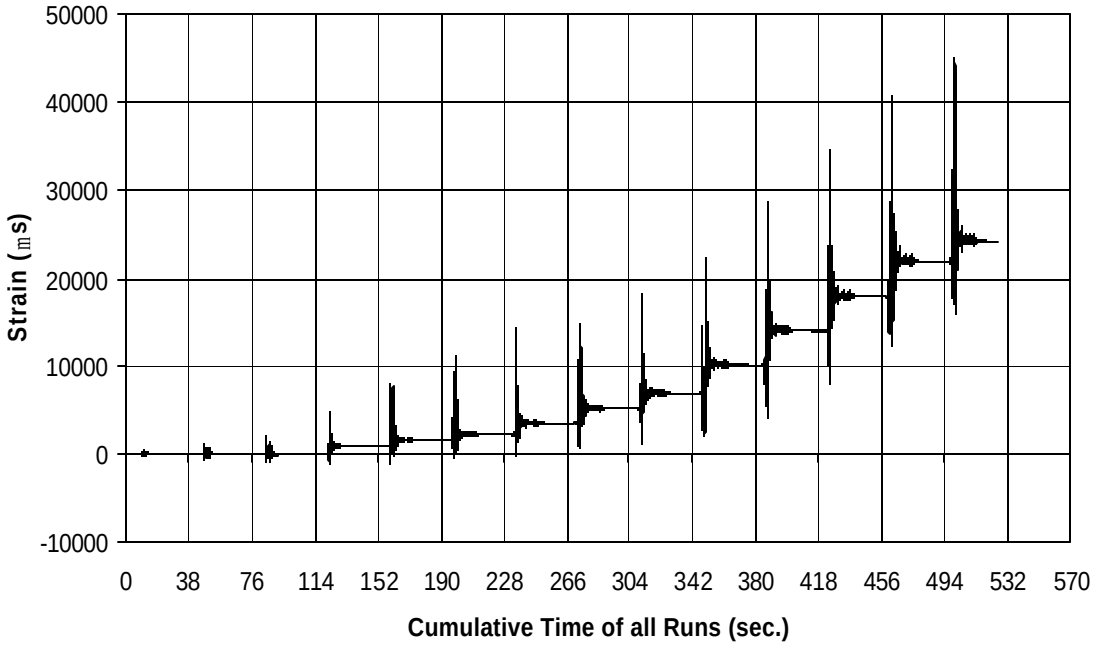

Fig. A-332 THD -5 Measured Strain in Gauge SG53

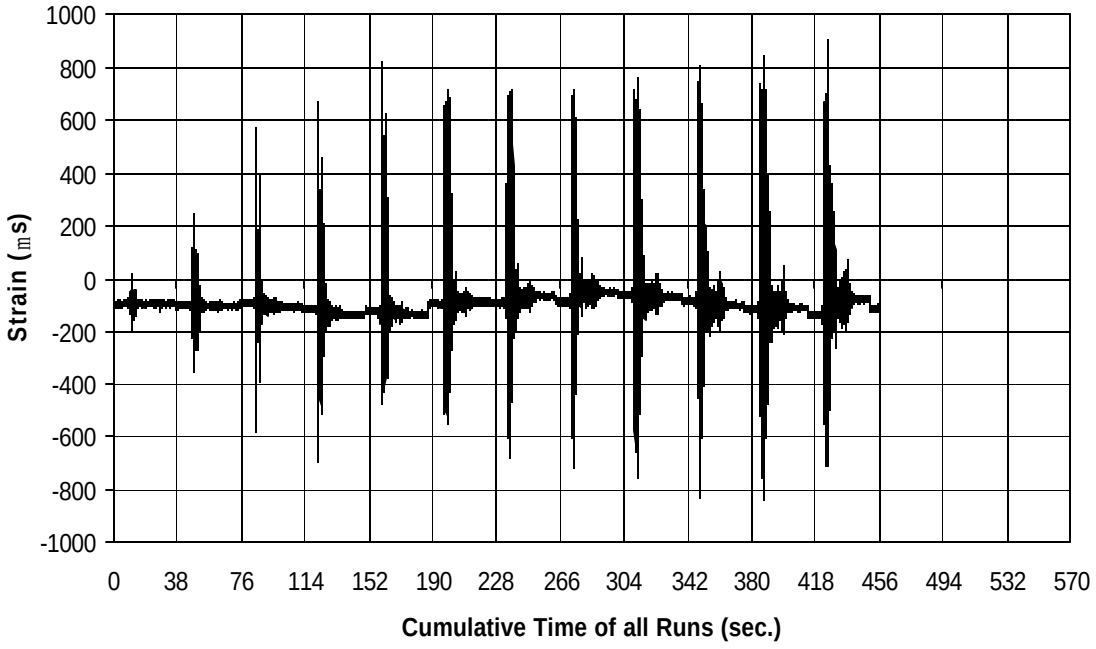

Fig. A-333 THD -5 Measured Strain in Gauge SG54

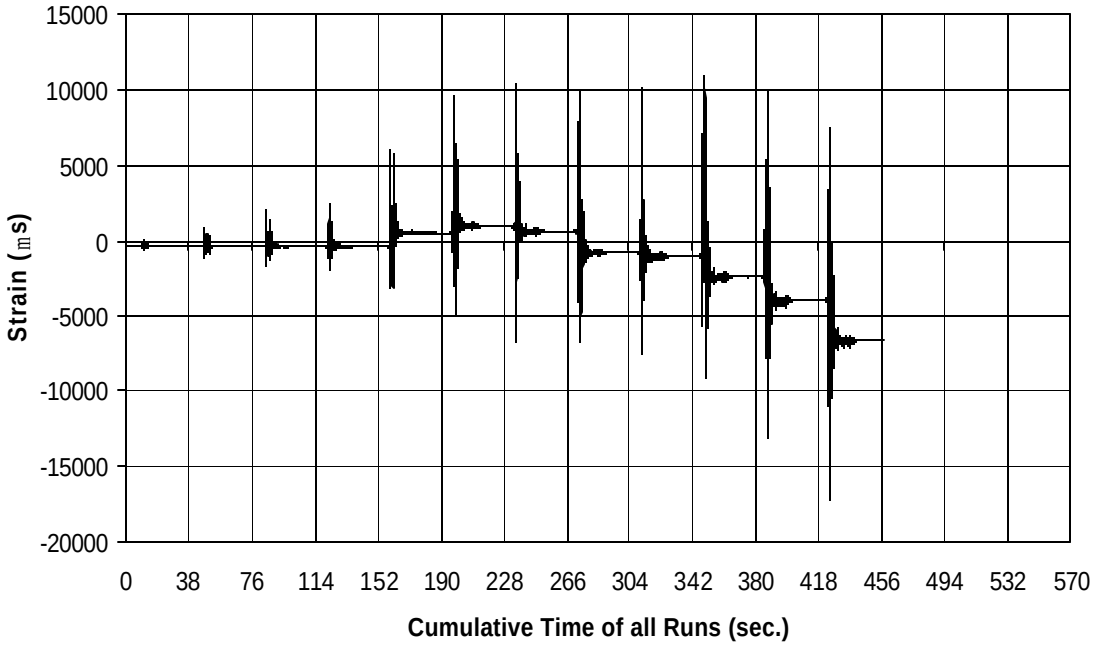

Fig. A-334 THD -5 Measured Strain in Gauge SG55

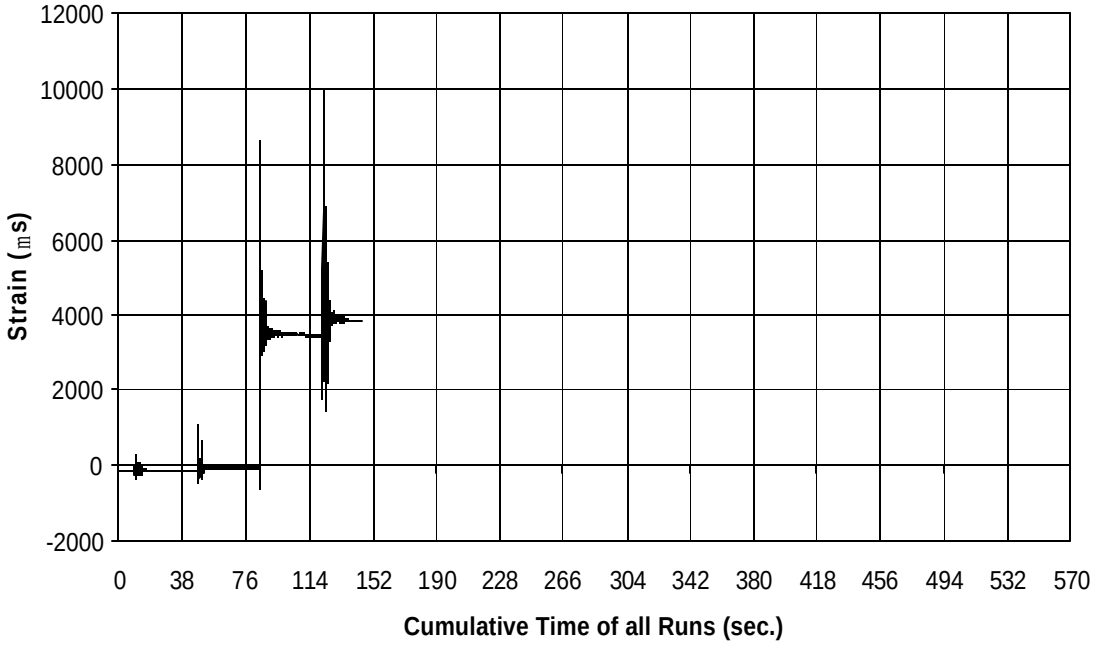

Fig. A-335 THD -5 Measured Strain in Gauge SG56

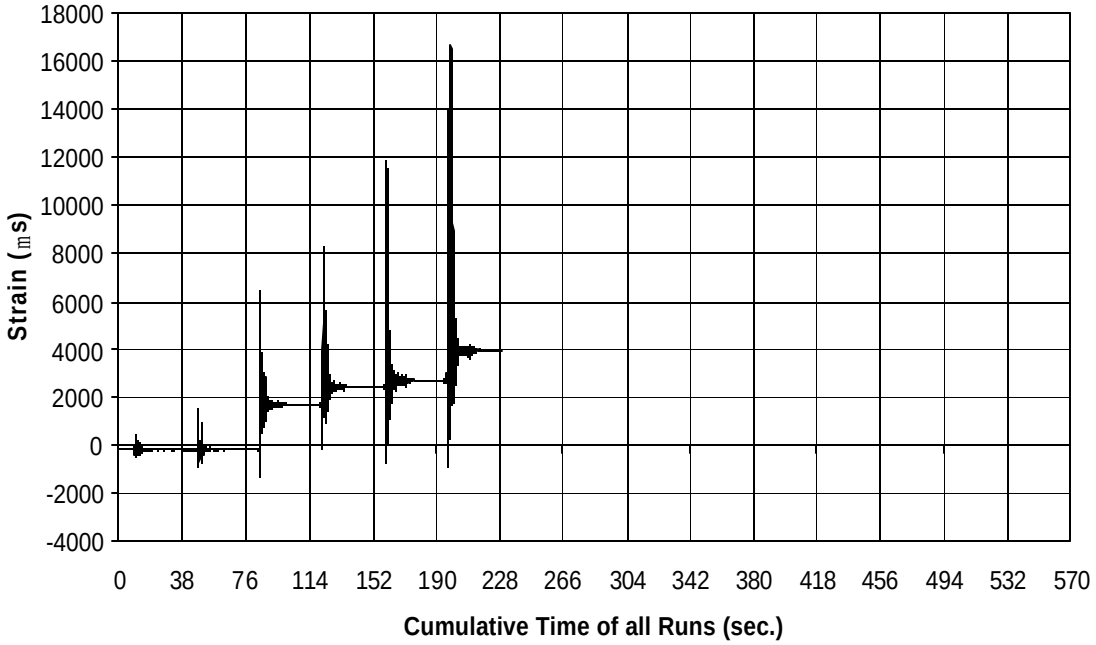

Fig. A-336 THD -5 Measured Strain in Gauge SG57

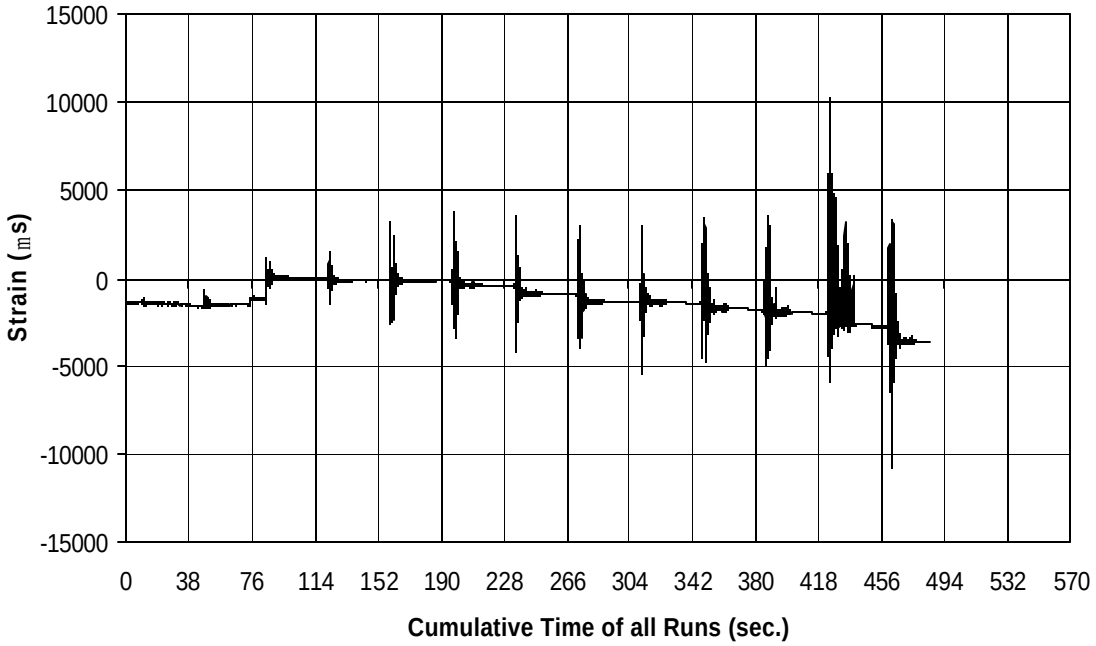

Fig. A-337 THD -5 Measured Strain in Gauge SG58

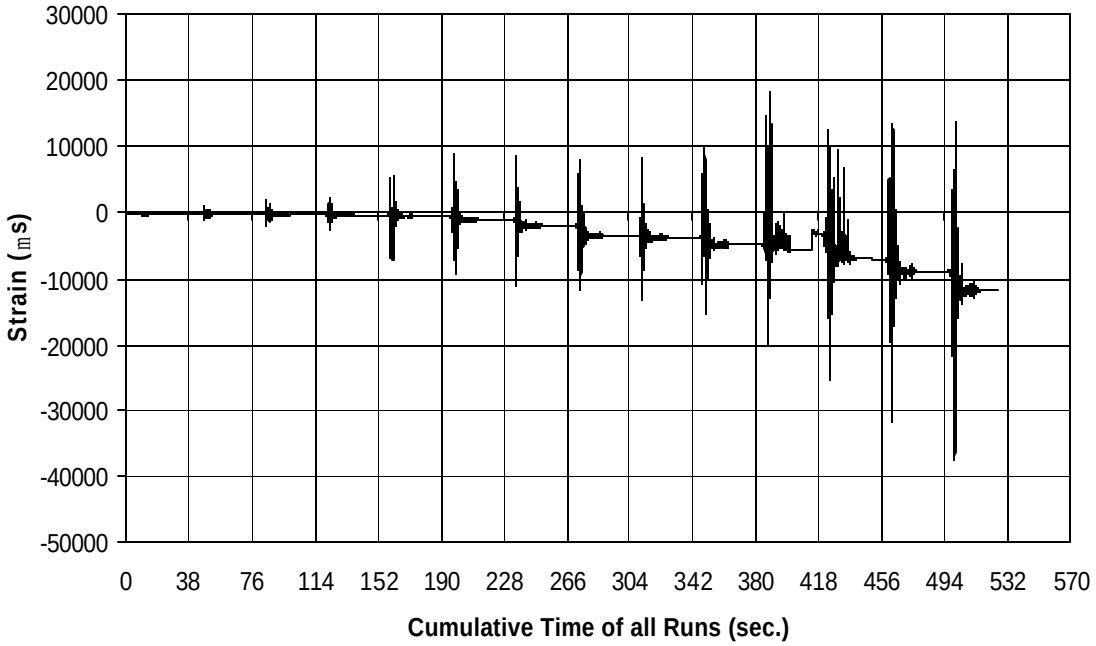

Fig. A-338 THD -5 Measured Strain in Gauge SG59

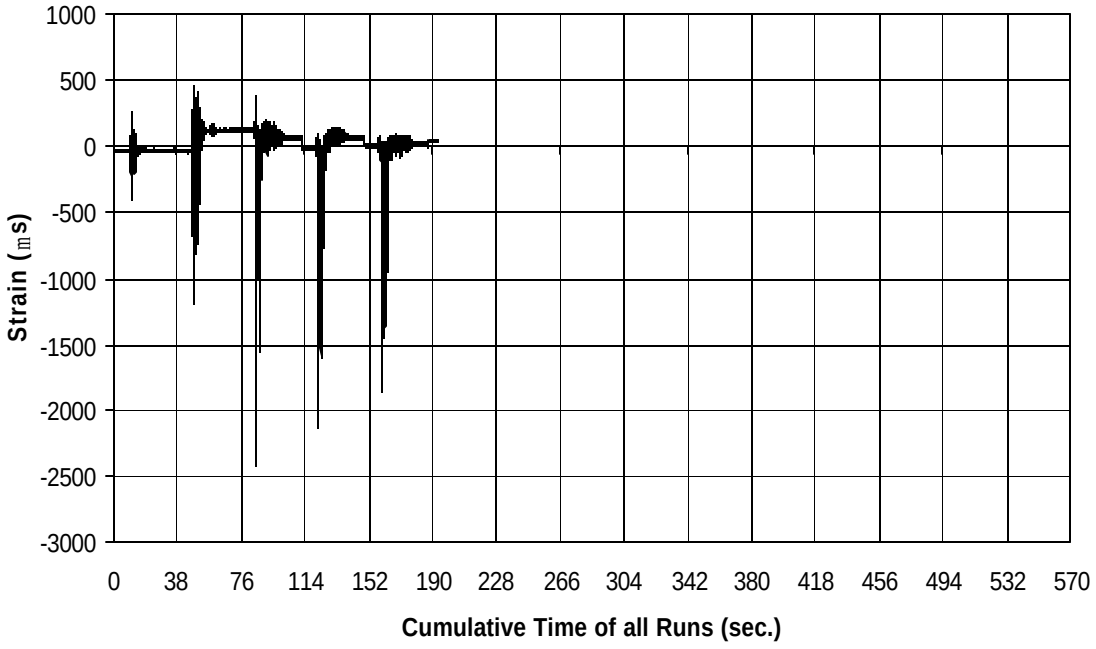

Fig. A-339 THD -5 Measured Strain in Gauge SG60

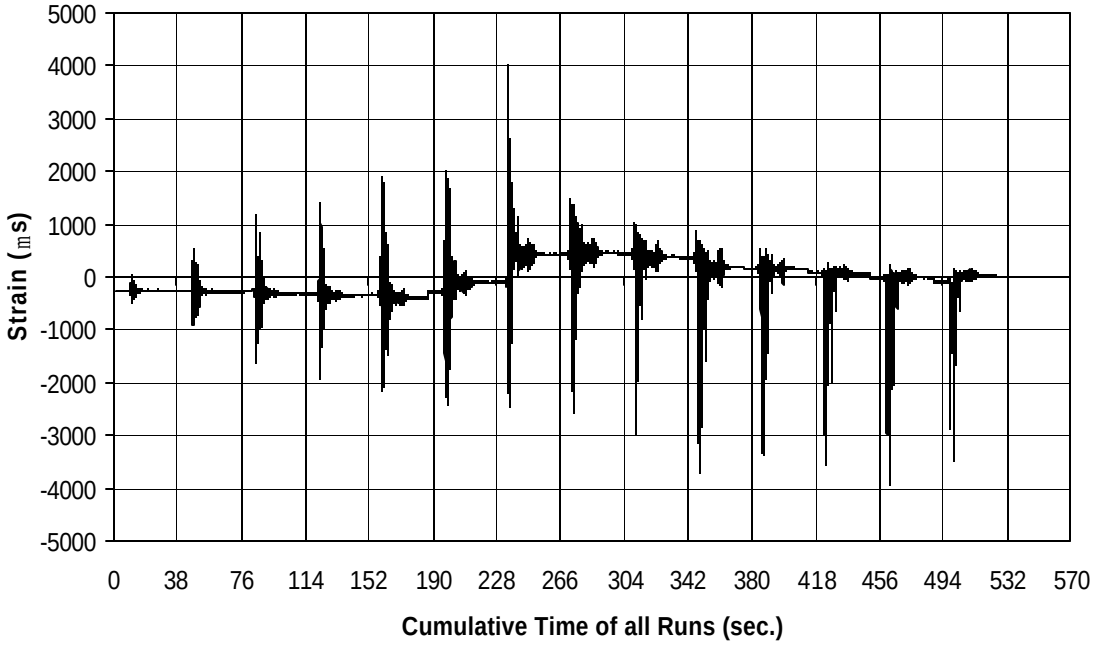

Fig. A-340 THD -5 Measured Strain in Gauge SG61

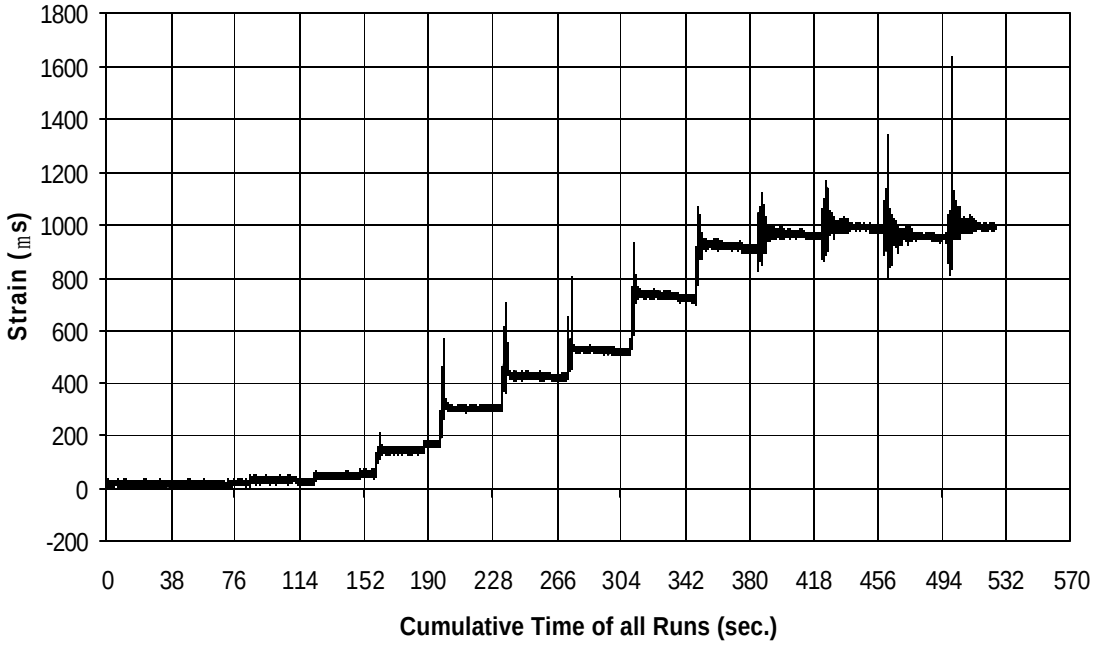

Fig. A-341 THD -5 Measured Strain in Gauge SG62

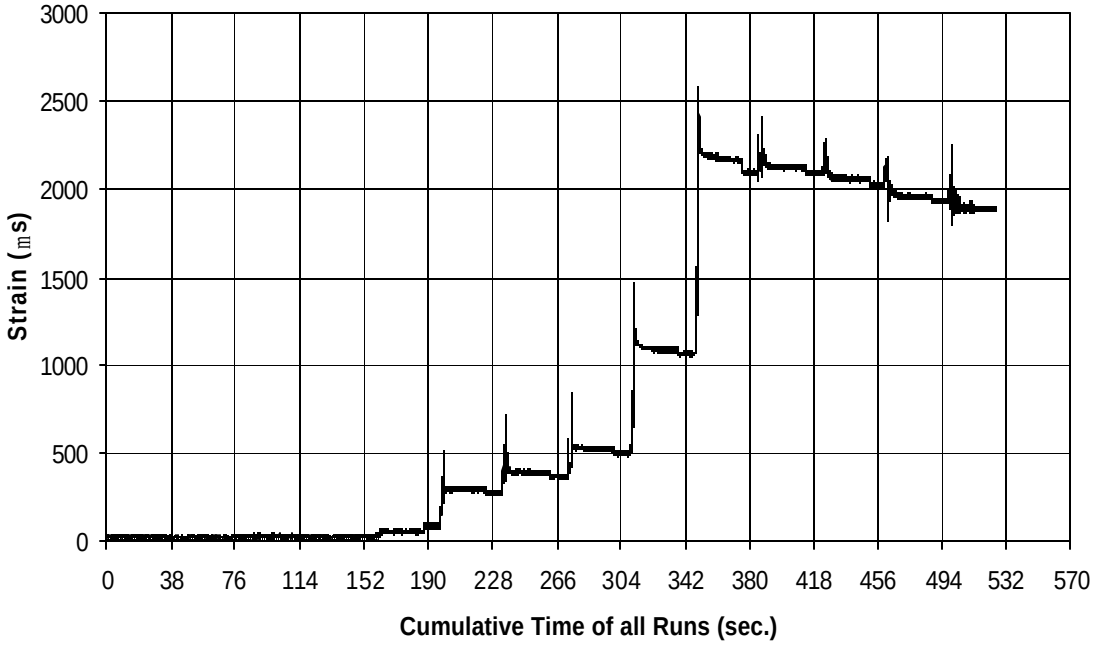

Fig. A-342 THD -5 Measured Strain in Gauge SG63

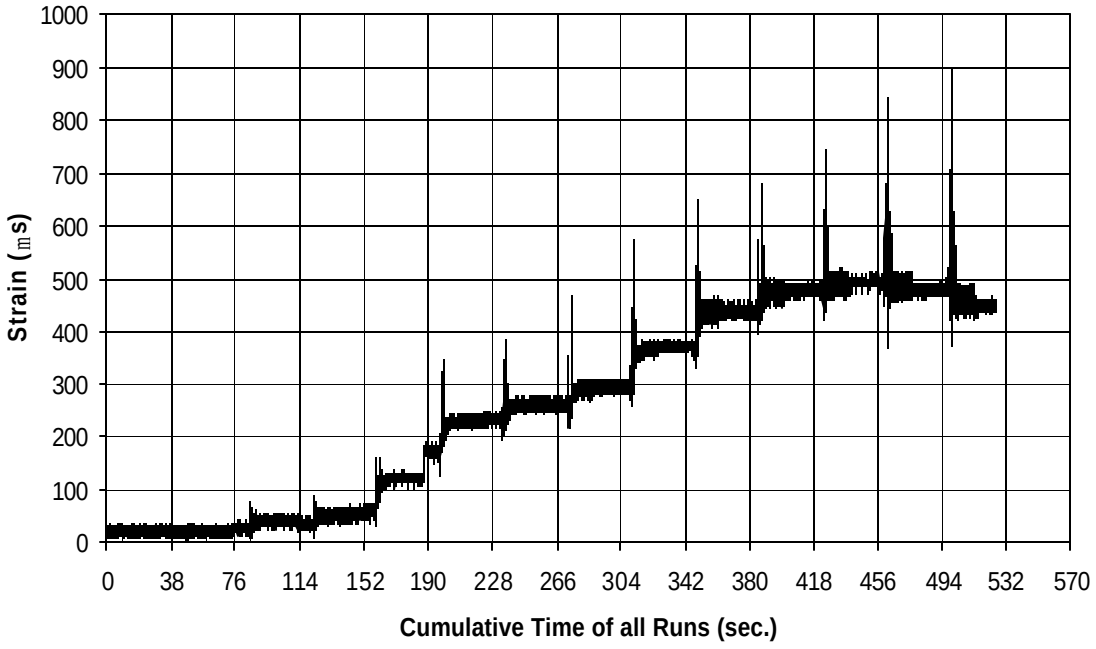

Fig. A-343 THD -5 Measured Strain in Gauge SG64

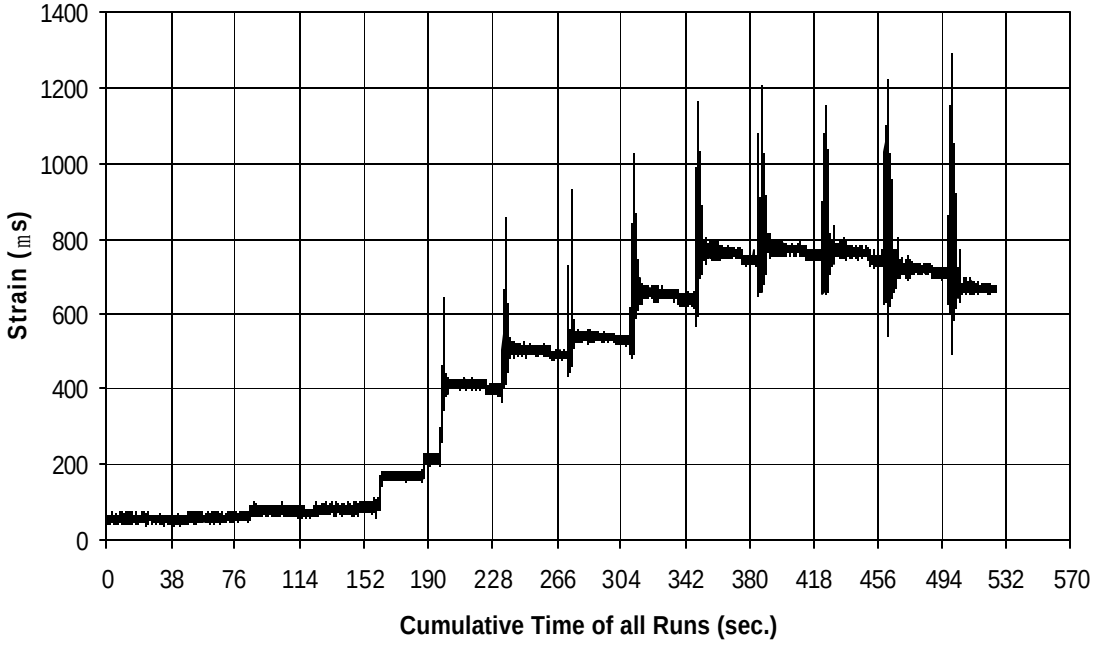

Fig. A-344 THD -5 Measured Strain in Gauge SG65

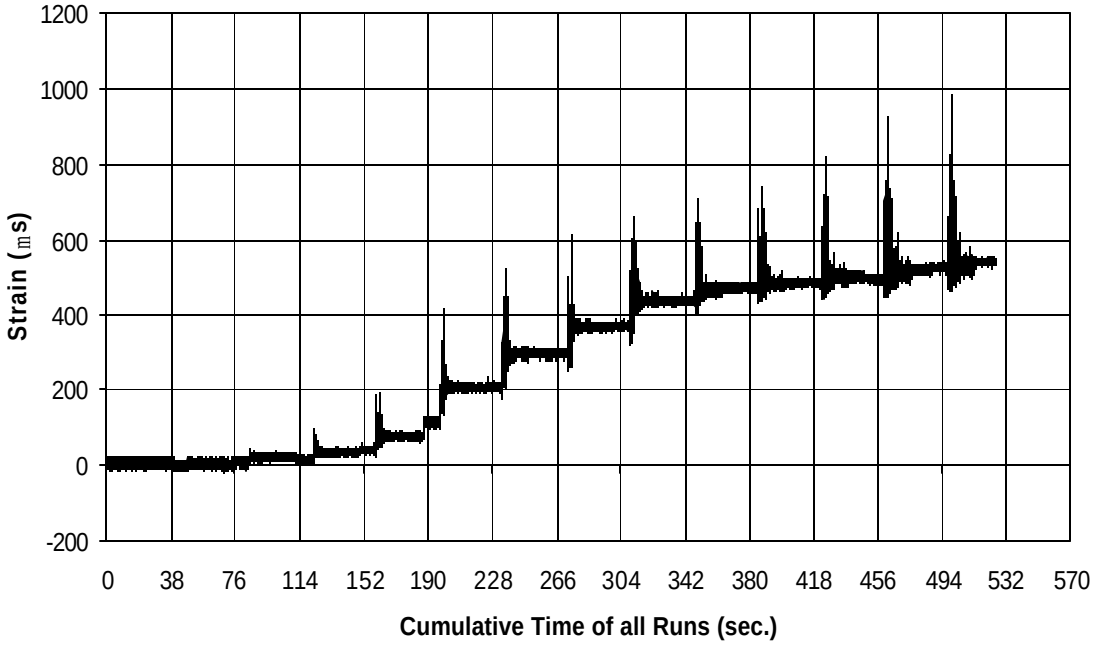

Fig. A-345 THD -5 Measured Strain in Gauge SG66

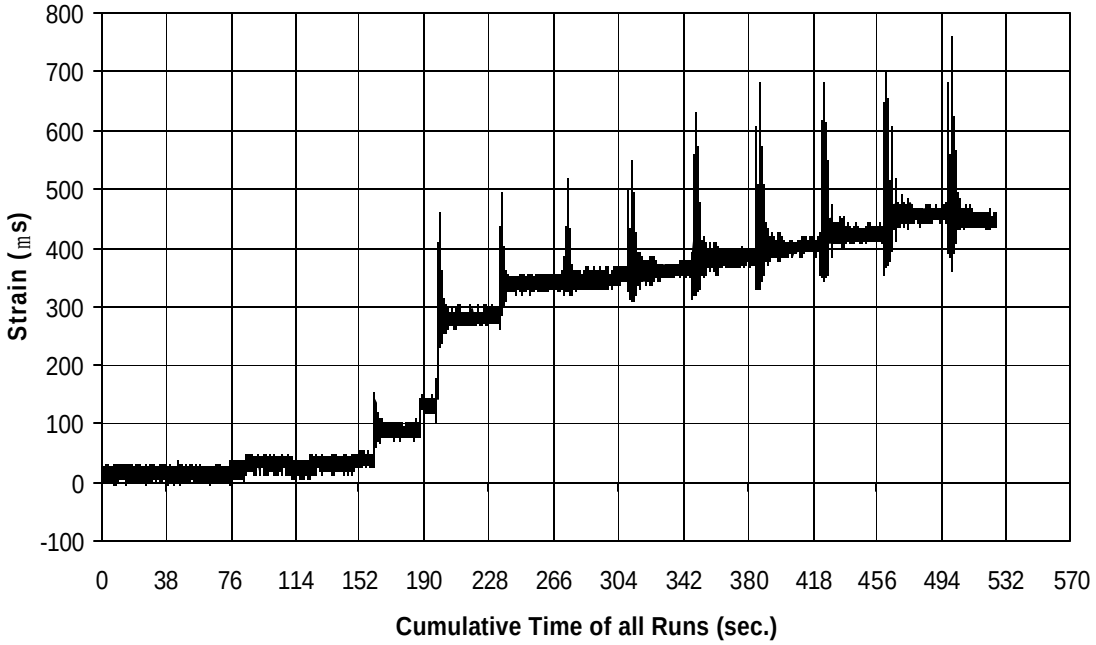

Fig. A-346 THD -5 Measured Strain in Gauge SG67

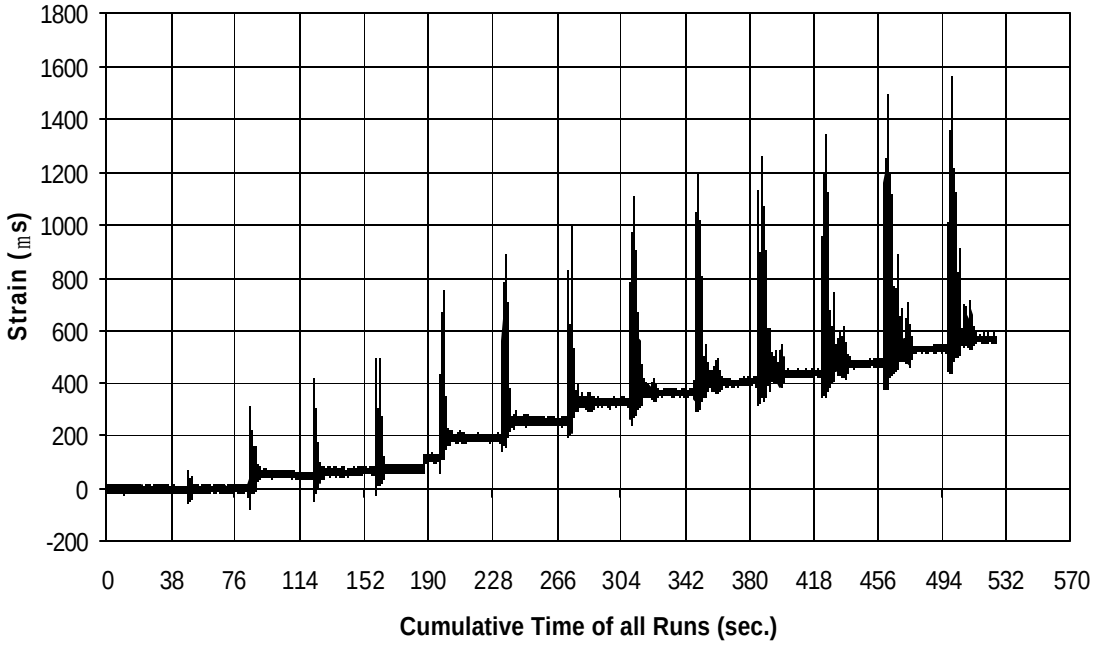

Fig. A-347 THD -5 Measured Strain in Gauge SG68

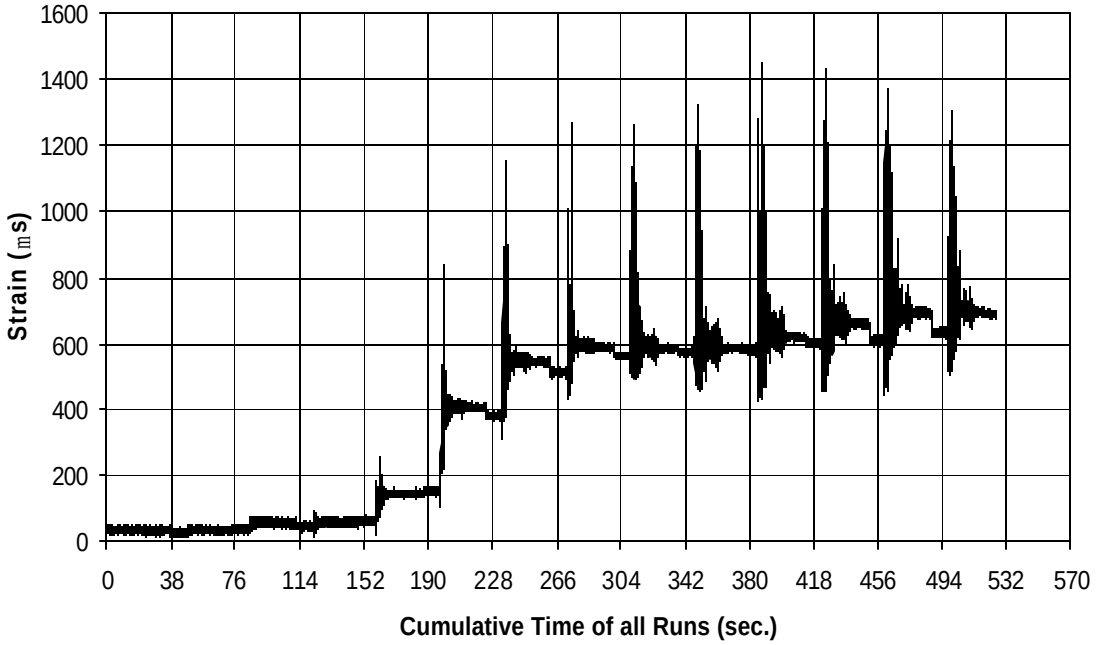

Fig. A-348 THD -5 Measured Strain in Gauge SG69

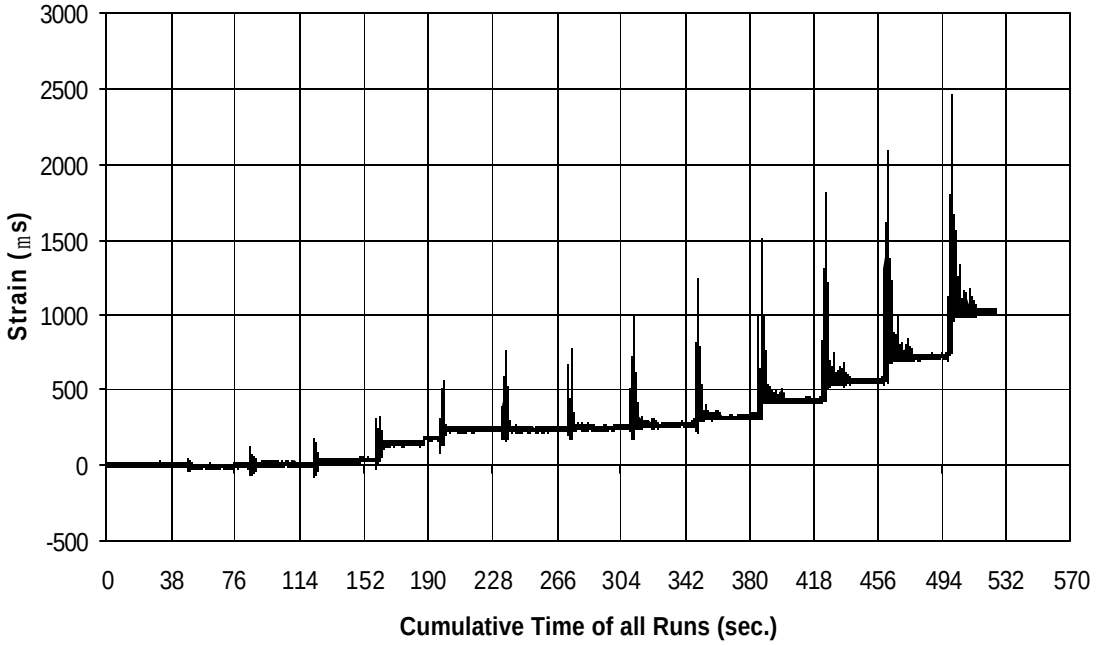

Fig. A-349 THD -5 Measured Strain in Gauge SG70

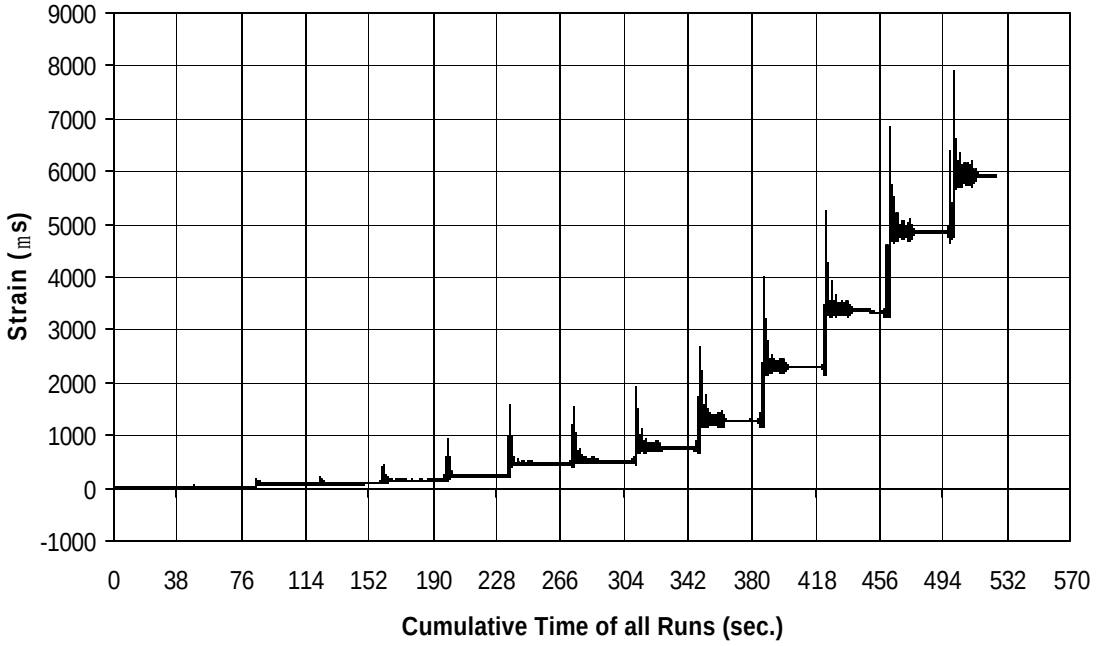

Fig. A-350 THD -5 Measured Strain in Gauge SG71

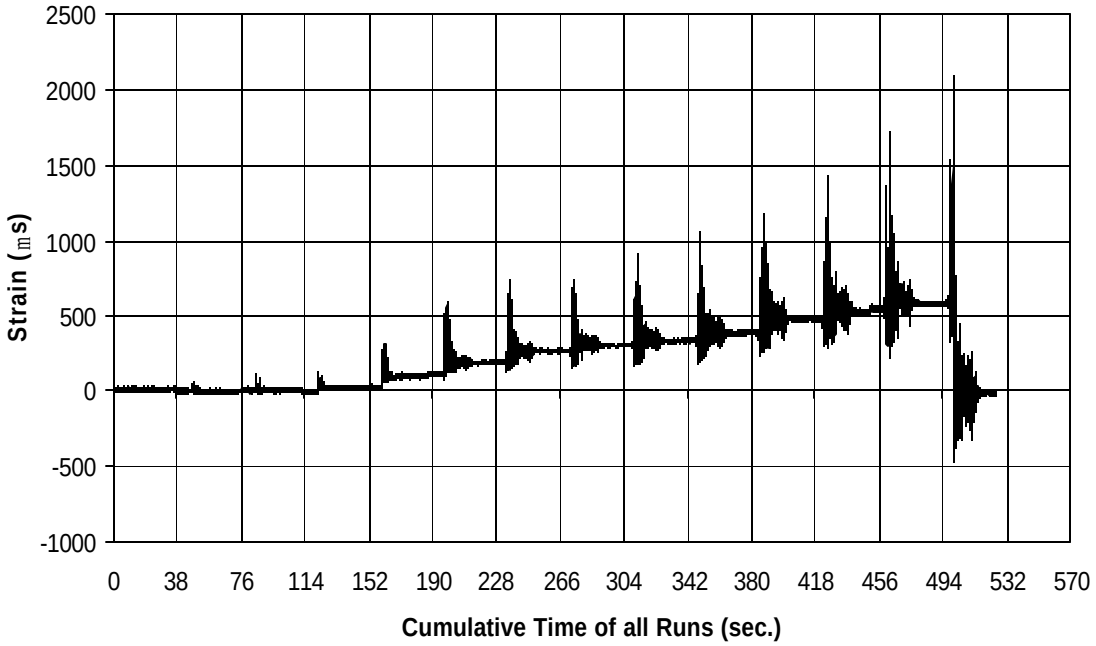

Fig. A-351 THD -5 Measured Strain in Gauge SG72

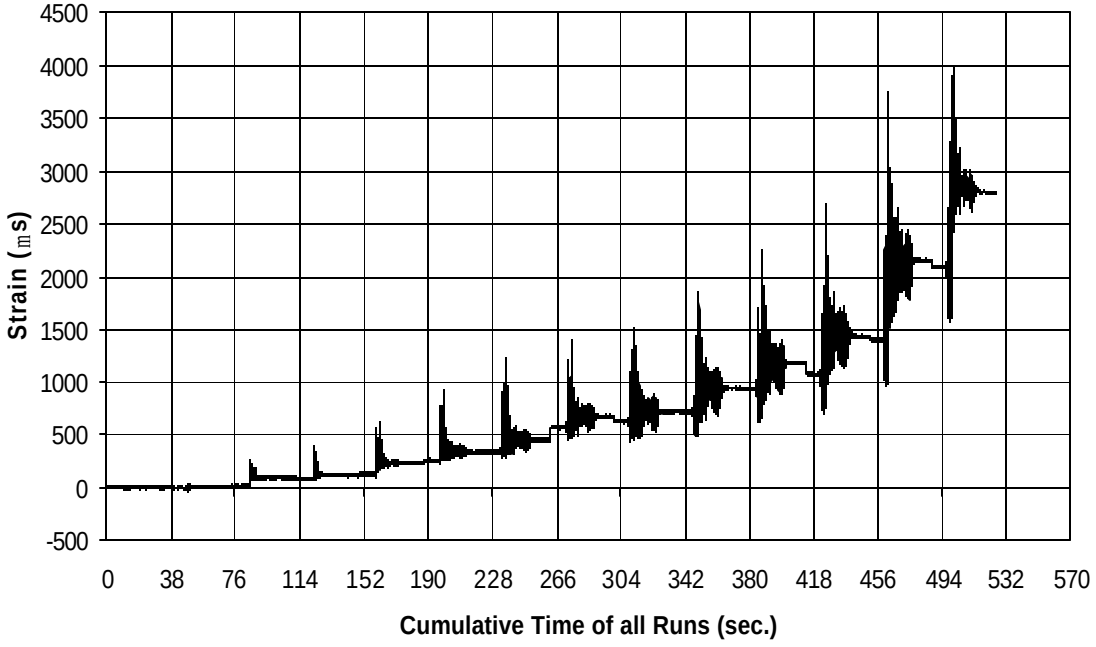

Fig. A-352 THD -5 Measured Strain in Gauge SG73

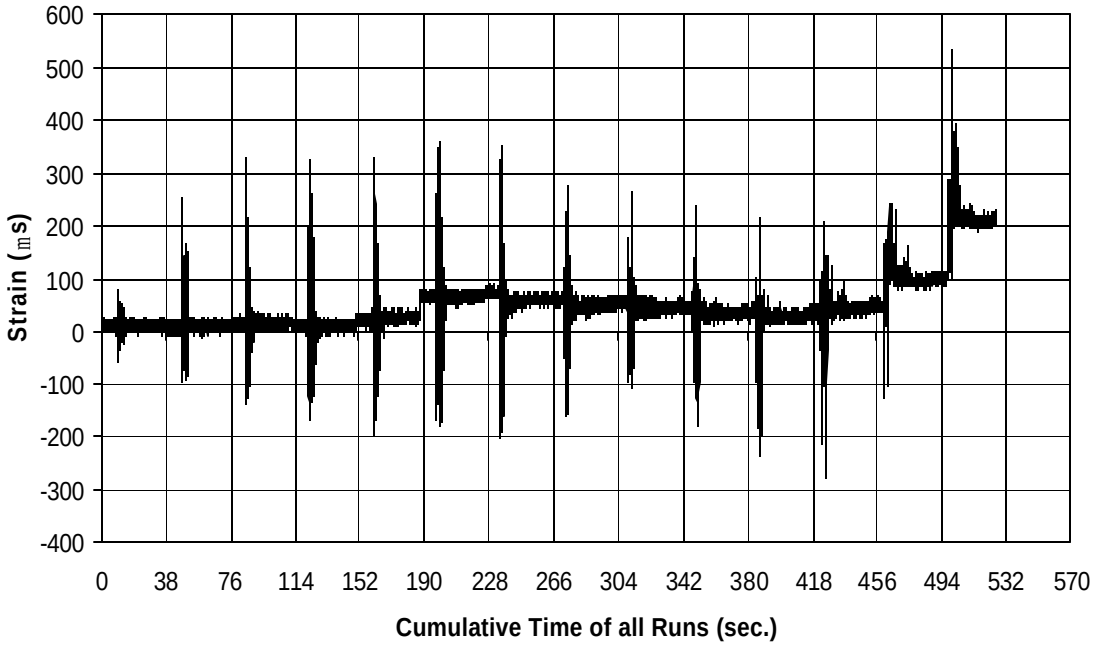

Fig. A-353 THD -5 Measured Strain in Gauge SG74

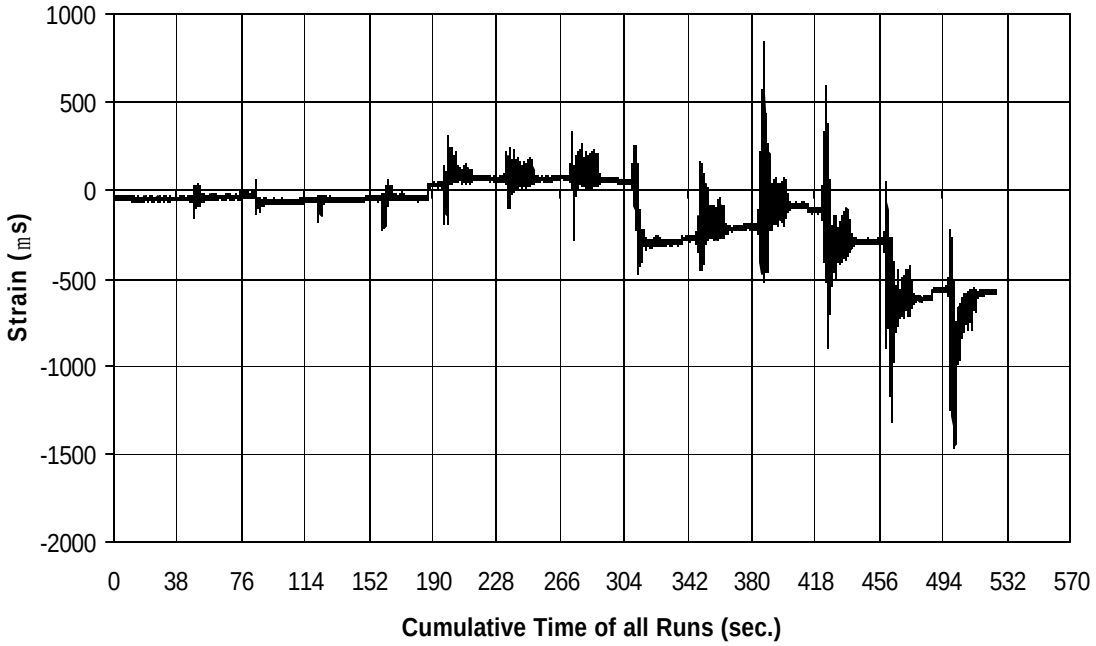

Fig. A-354 THD -5 Measured Strain in Gauge SG75

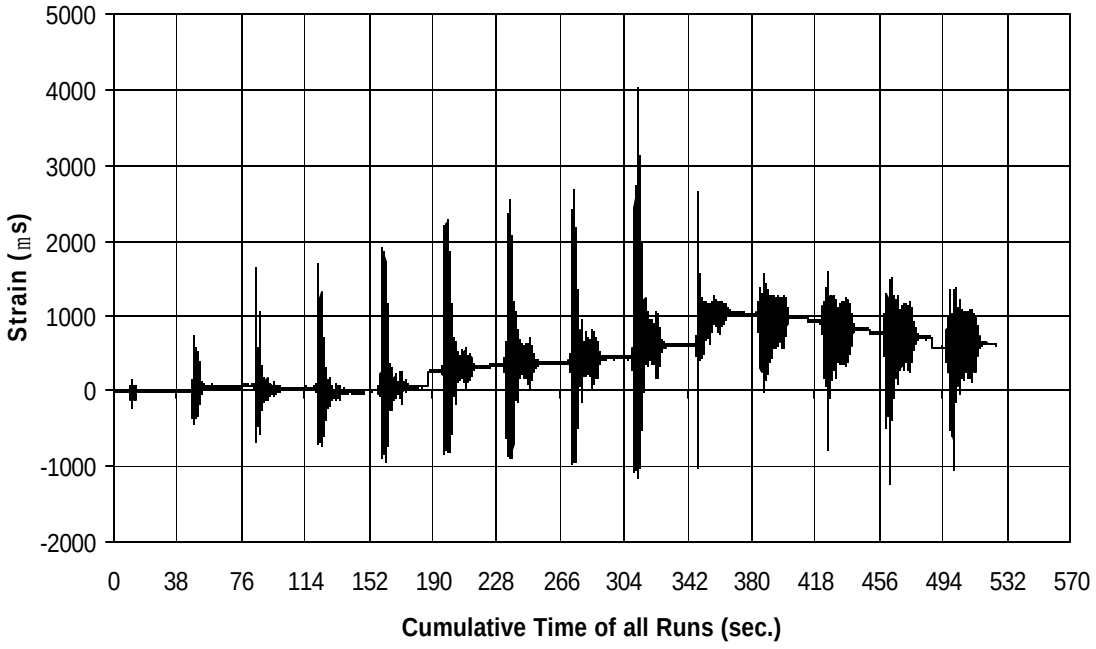

Fig. A-355 THD -5 Measured Strain in Gauge SG76

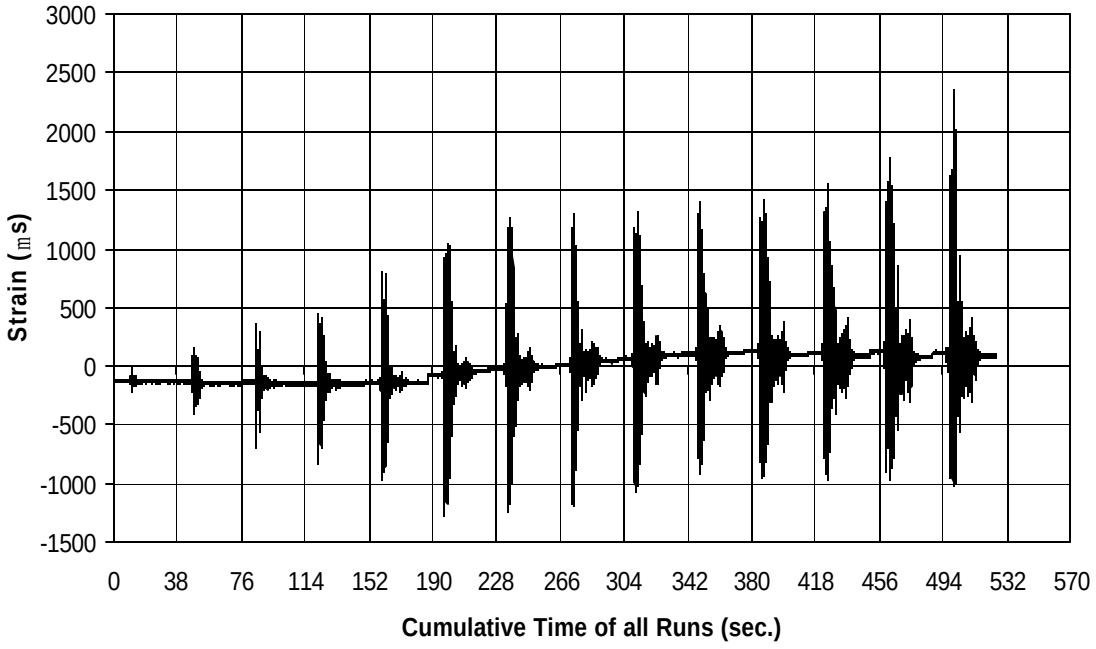

Fig. A-356 THD -5 Measured Strain in Gauge SG77

LIST OF CCEER PUBLICATIONS

Report No.	Publication
CCEER-84-1	Saiidi, M., and R. Lawver, "User's Manual for LZAK-C64, A Computer Program to Implement the Q-Model on Commodore 64," Civil Engineering Department, Report No. CCEER-84-1, University of Nevada, Reno, January 1984.
CCEER-84-2	Douglas, B. and T. Iwasaki, "Proceedings of the First USA-Japan Bridge Engineering Workshop," held at the Public Works Research Institute, Tsukuba, Japan, Civil Engineering Department, Report No. CCEER-84-2, University of Nevada, Reno, April 1984.
CCEER-84-3	Saiidi, M., J. Hart, and B. Douglas, "Inelastic Static and Dynamic Analysis of Short R/C Bridges Subjected to Lateral Loads," Civil Engineering Department, Report No. CCEER-84-3, University of Nevada, Reno, July 1984.
CCEER-84-4	Douglas, B., "A Proposed Plan for a National Bridge Engineering Laboratory," Civil Engineering Department, Report No. CCEER-84-4, University of Nevada, Reno, December 1984.
CCEER-85-1	Norris, G. and P. Abdollaholiaee, "Laterally Loaded Pile Response: Studies with the Strain Wedge Model," Civil Engineering Department, Report No. CCEER-85-1, University of Nevada, Reno, April 1985.
CCEER-86-1	Ghusn, G. and M. Saiidi, "A Simple Hysteretic Element for Biaxial Bending of R/C in NEABS-86," Civil Engineering Department, Report No. CCEER-86-1, University of Nevada, Reno, July 1986.
CCEER-86-2	Saiidi, M., R. Lawver, and J. Hart, "User's Manual of ISADAB and SIBA, Computer Programs for Nonlinear Transverse Analysis of Highway Bridges Subjected to Static and Dynamic Lateral Loads," Civil Engineering Department, Report No. CCEER-86-2, University of Nevada, Reno, September 1986.
CCEER-87-1	Siddharthan, R., "Dynamic Effective Stress Response of Surface and Embedded Footings in Sand," Civil engineering Department, Report No. CCEER-86-2, University of Nevada, Reno, June 1987.
CCEER-87-2	Norris, G. and R. Sack, "Lateral and Rotational Stiffness of Pile Groups for Seismic Analysis of Highway Bridges," Civil Engineering Department, Report No. CCEER-87-2, University of Nevada, Reno, June 1987.
CCEER-88-1	Orie, J. and M. Saiidi, "A Preliminary Study of One-Way Reinforced Concrete Pier Hinges Subjected to Shear and Flexure," Civil Engineering Department, Report No. CCEER-88-1, University of Nevada, Reno, January 1988.
CCEER-88-2	Orie, D., M. Saiidi, and B. Douglas, "A Micro-CAD System for Seismic Design of Regular Highway Bridges," Civil Engineering Department, Report No. CCEER-88-2, University of Nevada, Reno, June 1988.
CCEER-88-3	Orie, D. and M. Saiidi, "User's Manual for Micro-SARB, a Microcomputer Program for Seismic Analysis of Regular Highway Bridges," Civil Engineering Department, Report No. CCEER-88-3, University of Nevada, Reno, October 1988.
CCEER-89-1	Douglas, B., M. Saiidi, R. Hayes, and G. Holcomb, "A Comprehensive Study of the Loads and Pressures Exerted on Wall Forms by the Placement of Concrete," Civil Engineering Department, Report No. CCEER-89-1, University of Nevada, Reno, February 1989.

CCEER-89-2 Richardson, J. and B. Douglas, "Dynamic Response Analysis of the Dominion Road Bridge Test Data," Civil Engineering Department, Report No. CCEER-89-2, University of Nevada, Reno, March 1989.

CCEER-89-2 Vrontinos, S., M. Saiidi, and B. Douglas, "A Simple Model to Predict the Ultimate Response of R/C Beams with Concrete Overlays," Civil Engineering Department, Report NO. CCEER-89-2, University of Nevada, Reno, June 1989.

CCEER-89-3 Ebrahimpour, A. and P. Jagadish, "Statistical Modeling of Bridge Traffic Loads - A Case Study," Civil Engineering Department, Report No. CCEER-89-3, University of Nevada, Reno, December 1989.

CCEER-89-4 Shields, J. and M. Saiidi, "Direct Field Measurement of Prestress Losses in Box Girder Bridges," Civil Engineering Department, Report No. CCEER-89-4, University of Nevada, Reno, December 1989.

CCEER-90-1 Saiidi, M., E. Maragakis, G. Ghusn, Y. Jiang, and D. Schwartz, "Survey and Evaluation of Nevada's Transportation Infrastructure, Task 7.2 - Highway Bridges, Final Report," Civil Engineering Department, Report No. CCEER 90-1, University of Nevada, Reno, October 1990.

CCEER-90-2 Abdel-Ghaffar, S., E. Maragakis, and M. Saiidi, "Analysis of the Response of Reinforced Concrete Structures During the Whittier Earthquake 1987," Civil Engineering Department, Report No. CCEER 90-2, University of Nevada, Reno, October 1990.

CCEER-91-1 Saiidi, M., E. Hwang, E. Maragakis, and B. Douglas, "Dynamic Testing and the Analysis of the Flamingo Road Interchange," Civil Engineering Department, Report No. CCEER-91-1, University of Nevada, Reno, February 1991.

CCEER-91-2 Norris, G., R. Siddharthan, Z. Zafir, S. Abdel-Ghaffar, and P. Gowda, "Soil-Foundation-Structure Behavior at the Oakland Outer Harbor Wharf," Civil Engineering Department, Report No. CCEER-91-2, University of Nevada, Reno, July 1991.

CCEER-91-3 Norris, G., "Seismic Lateral and Rotational Pile Foundation Stiffnesses at Cypress," Civil Engineering Department, Report No. CCEER-91-3, University of Nevada, Reno, August 1991.

CCEER-91-4 O'Connor, D. and M. Saiidi, "A Study of Protective Overlays for Highway Bridge Decks in Nevada, with Emphasis on Polyester-Styrene Polymer Concrete," Civil Engineering Department, Report No. CCEER-91-4, University of Nevada, Reno, October 1991.

CCEER-91-5 O'Connor, D.N. and M. Saiidi, "Laboratory Studies of Polyester-Styrene Polymer Concrete Engineering Properties," Civil Engineering Department, Report No. CCEER-91-5, University of Nevada, Reno, November 1991.

CCEER-92-1 Straw, D.L. and M. Saiidi, "Scale Model Testing of One-Way Reinforced Concrete Pier Hinges Subject to Combined Axial Force, Shear and Flexure," edited by D.N. O'Connor, Civil Engineering Department, Report No. CCEER-92-1, University of Nevada, Reno, March 1992.

CCEER-92-2 Wehbe, N., M. Saiidi, and F. Gordaninejad, "Basic Behavior of Composite Sections Made of Concrete Slabs and Graphite Epoxy Beams," Civil Engineering Department, Report No. CCEER-92-2, University of Nevada, Reno, August 1992.

CCEER-92-3 Saiidi, M. and E. Hutchens, "A Study of Prestress Changes in A Post-Tensioned Bridge During the First 30 Months," Civil Engineering Department, Report No. CCEER-92-3, University of Nevada, Reno, April 1992.

CCEER-92-4 Saiidi, M., B. Douglas, S. Feng, E. Hwang, and E. Maragakis, "Effects of Axial Force on Frequency of Prestressed Concrete Bridges," Civil Engineering Department, Report No. CCEER-92-4, University of Nevada, Reno, August 1992.

CCEER-92-5 Siddharthan, R., and Z. Zafir, "Response of Layered Deposits to Traveling Surface Pressure Waves," Civil Engineering Department, Report No. CCEER-92-5, University of Nevada, Reno, September 1992.

CCEER-92-6 Norris, G., and Z. Zafir, "Liquefaction and Residual Strength of Loose Sands from Drained Triaxial Tests," Civil Engineering Department, Report No. CCEER-92-6, University of Nevada, Reno, September 1992.

CCEER-92-7 Douglas, B., "Some Thoughts Regarding the Improvement of the University of Nevada, Reno's National Academic Standing," Civil Engineering Department, Report No. CCEER-92-7, University of Nevada, Reno, September 1992.

CCEER-92-8 Saiidi, M., E. Maragakis, and S. Feng, "An Evaluation of the Current Caltrans Seismic Restrainer Design Method," Civil Engineering Department, Report No. CCEER-92-8, University of Nevada, Reno, October 1992.

CCEER-92-9 O'Connor, D., M. Saiidi, and E. Maragakis, "Effect of Hinge Restrainers on the Response of the Madrone Drive Undercrossing During the Loma Prieta Earthquake," Civil Engineering Department, Report No. CCEER-92-9, University of Nevada, Reno, February 1993.

CCEER-92-10 O'Connor, D., and M. Saiidi, "Laboratory Studies of Polyester Concrete: Compressive Strength at Elevated Temperatures and Following Temperature Cycling, Bond Strength to Portland Cement Concrete, and Modulus of Elasticity," Civil Engineering Department, Report No. CCEER-92-10, University of Nevada, Reno, February 1993.

CCEER-92-11 Wehbe, N., M. Saiidi, and D. O'Connor, "Economic Impact of Passage of Spent Fuel Traffic on Two Bridges in Northeast Nevada," Civil Engineering Department, Report No. CCEER-92-11, University of Nevada, Reno, December 1992.

CCEER-93-1 Jiang, Y., and M. Saiidi, "Behavior, Design, and Retrofit of Reinforced Concrete One-way Bridge Column Hinges," edited by D. O'Connor, Civil Engineering Department, Report No. CCEER-93-1, University of Nevada, Reno, March 1993.

CCEER-93-2 Abdel-Ghaffar, S., E. Maragakis, and M. Saiidi, "Evaluation of the Response of the Aptos Creek Bridge During the 1989 Loma Prieta Earthquake," Civil Engineering Department, Report No. CCEER-93-2, University of Nevada, Reno, June 1993.

CCEER-93-3 Sanders, D.H., B.M. Douglas, and T.L. Martin, "Seismic Retrofit Prioritization of Nevada Bridges," Civil Engineering Department, Report No. CCEER-93-3, University of Nevada, Reno, July 1993.

CCEER-93-4 Abdel-Ghaffar, S., E. Maragakis, and M. Saiidi, "Performance of Hinge Restrainers in the Huntington Avenue Overhead During the 1989 Loma Prieta Earthquake," Civil Engineering Department, Report No. CCEER-93-4, University of Nevada, Reno, June 1993 (in final preparation).

CCEER-93-5 Maragakis, E., M. Saiidi, S. Feng, and L. Flournoy, "Effects of Hinge Restrainers on the Response of the San Gregorio Bridge During the Loma Prieta Earthquake," (in final preparation) Civil Engineering Department, Report No. CCEER-93-5, University of Nevada, Reno.

CCEER-93-6 Saiidi, M., E. Maragakis, S. Abdel-Ghaffar, S. Feng, and D. O'Connor, "Response of

Bridge Hinge Restrainers During Earthquakes -Field Performance, Analysis, and Design," Civil Engineering Department, Report No. CCEER-93-6, University of Nevada, Reno, May 1993.

CCEER-93-7 Wehbe, N., Saiidi, M., Maragakis, E., and Sanders, D., "Adequacy of Three Highway Structures in Southern Nevada for Spent Fuel Transportion, Civil Engineering Department, Report No. CCEER-93-7, University of Nevada, Reno, August 1993.

CCEER-93-8 Roybal, J., Sanders, D.H., and Maragakis, E., "Vulnerability Assessment of Masonry in the Reno-Carson City Urban Corridor," Civil Engineering Department, Report No. CCEER-93-8, University of Nevada, Reno, May 1993.

CCEER-93-9 Zafir, Z. and Siddharthan, R., "MOVLOAD: A Program to Determine the Behavior of Nonlinear Horizontally Layered Medium Under Moving Load," Civil Engineering Department, Report No. CCEER-93-9, University of Nevada, Reno, August 1993.

CCEER-93-10 O'Connor, D.N., Saiidi, M., and Maragakis, E.A., "A Study of Bridge Column Seismic Damage Susceptibility at the Interstate 80/U.S. 395 Interchange in Reno, Nevada," Civil Engineering Department, Report No. CCEER-93-10, University of Nevada, Reno, October 1993.

CCEER-94-1 Maragakis, E., B. Douglas, and E. Abdelwahed, "Preliminary Dynamic Analysis of a Railroad Bridge," Report CCEER-94-1, January 1994.

CCEER-94-2 Douglas, B.M., Maragakis, E.A., and Feng, S., "Stiffness Evaluation of Pile Foundation of Cazenovia Creek Overpass," Civil Engineering Department, Report No. CCEER-94-2, University of Nevada, Reno, March 1994.

CCEER-94-3 Douglas, B.M., Maragakis, E.A., and Feng, S., "Summary of Pretest Analysis of Cazenovia Creek Bridge," Civil Engineering Department, Report No. CCEER-94-3, University of Nevada, Reno, April 1994.

CCEER-94-4 Norris, G.M. and Madhu, R., "Liquefaction and Residual Strength of Sands from Drained Triaxial Tests, Report 2," Civil Engineering Department, CCEER-94-4, University of Nevada, Reno, August 1994.

CCEER-94-5 Saiidi, M., Hutchens, E., and Gardella, D., "Prestress Losses in a Post-Tensioned R/C Box Girder Bridge in Southern Nevada," Civil Engineering Department, CCEER-94-5, University of Nevada, Reno, August 1994.

CCEER-95-1 Siddharthan, R., El-Gamal, M., and Maragakis, E.A., "Nonlinear Bridge Abutment , Verification, and Design Curves," Civil Engineering Department, CCEER-95-1, University of Nevada, Reno, January 1995.

CCEER-95-2 Norris, G.M., Madhu, R., Valceschini, R., and Ashour, M., "Liquefaction and Residual Strength of Loose Sands from Drained Triaxial Tests," Report 2, Civil Engineering Department, Report No. CCEER-95-2, University of Nevada, Reno, February 1995.

CCEER-95-3 Wehbe, N., Saiidi, M., Sanders, D., and Douglas, B., "Ductility of Rectangular Reinforced Concrete Bridge Columns with Moderate Confinement,"Civil Engineering Department, Report No. CCEER-95-3, University of Nevada, Reno, July 1995.

CCEER-95-4 Martin, T., Saiidi, M., and Sanders, D., “Seismic Retrofit of Column-Pier Cap Connections in Bridges in Northern Nevada,” Civil Engineering Department, Report No. CCEER-95-4, University of Nevada, Reno, August 1995.

CCEER-95-5 Darwish, I., Saiidi, M., and Sanders, D., “Experimental Study of Seismic Susceptibility

Column-Footing Connections," Civil Engineering Department, Report No. CCEER-95-5, University of Nevada, Reno, September 1995.

CCEER-95-6 Griffin, G., Saiidi, M., and Maragakis, E., "Nonlinear Seismic Response of Isolated Bridges and Effects of Pier Ductility Demand," Civil Engineering Department, Report No. CCEER-95-6, University of Nevada, Reno, November 1995.

CCEER-95-7 Acharya, S., Saiidi, M., and Sanders, D., "Seismic Retrofit of Bridge Footings and Column-Footing Connections," Report for the Nevada Department of Transportation, Civil Engineering Department, Report No. CCEER-95-7, University of Nevada, Reno, November 1995.

CCEER-95-8 Maragakis, E., Douglas, B., and Sandirasegaram, U., "Full-Scale Field Resonance Tests of a Railway Bridge," A Report to the Association of American Railroads, Civil Engineering Department, Report No. CCEER-95-8, University of Nevada, Reno, December 1995.

CCEER-95-9 Douglas, B., Maragakis, E., and Feng, S., "System Identification Studies on Cazenovia Creek Overpass," Report for the National Center for Earthquake Engineering Research, Civil Engineering Department, Report No. CCEER-95-9, University of Nevada, Reno, October 1995.

CCEER-96-1 El-Gamal, M.E. and Siddharthan, R.V., "Programs to Computer Translational Stiffness of Seat-Type Bridge Abutment," Civil Engineering Department, Report No. CCEER-96-1, University of Nevada, Reno, March 1996.

CCEER-96-2 Labia, Y., Saiidi, M., and Douglas, B., "Evaluation and Repair of Full-Scale Prestressed Concrete Box Girders," A Report to the National Science Foundation, Research Grant CMS-9201908, Civil Engineering Department, Report No. CCEER-96-2, University of Nevada, Reno, May 1996.

CCEER-96-3 Darwish, I., Saiidi, M., and Sanders, D., "Seismic Retrofit of R/C Oblong Tapered Bridge Columns with Inadequate Bar Anchorage in Columns and Footings," A Report to the Nevada Department of Transportation, Civil Engineering Department, Report No. CCEER-96-3, University of Nevada, Reno, May 1996.

CCEER-96-4 Ashour, M., Pilling, P., Norris, G., and Perez, H., "The Prediction of Lateral Load Behavior of Single Piles and Pile Groups Using the Strain Wedge Model," A Report to the California Department of Transportation, Civil Engineering Department, Report No. CCEER-96-4, University of Nevada, Reno, June, 1996.

CCEER-97-1-A Rimal, P. and Itani, A. "Sensitivity Analysis of Fatigue Evaluations of Steel Bridges", Center for Earthquake Research, Department of Civil Engineering, University of Nevada, Reno, Nevada Report No. CCEER-97-1-A, September, 1997.

CCEER-97-1-B Maragakis, E., Douglas, B., and Sandirasegaram, U. "Full-Scale Field Resonance Tests of a Railway Bridge," A Report to the Association of American Railroads, Civil Engineering Department, University of Nevada, Reno, May, 1996.

CCEER-97-2 Wehbe, N., Saiidi, M., and D. Sanders, "Effect of Confinement and Flares on the Seismic Performance of Reinforced Concrete Bridge Columns," Civil Engineering Department, Report No. CCEER-97-2, University of Nevada, Reno, September 1997.

CCEER-97-3 Darwish, I., M. Saiidi, G. Norris, and E. Maragakis, "Determination of In-Situ Footing Stiffness Using Full-Scale Dynamic Field Testing," A Report to the Nevada Department of Transportation, Structural Design Division, Carson City, Nevada, Report No. CCEER-97-3, University of Nevada, Reno, October 1997.

CCEER-97-4 Wehbe, N., and M. Saiidi, “User’s manual for RCMC v. 1.2 : A Computer Program for Moment-Curvature Analysis of Confined and Unconfined Reinforced Concrete Sections,” Center for Civil Engineering Earthquake Research, Department of Civil Engineering, University of Nevada, Reno, Nevada, Report No. CCEER-97-4, November, 1997.

CCEER-97-5 Isakovic, T., M. Saiidi, and A. Itani, “Influence of new Bridge Configurations on Seismic Performance,” Department of Civil Engineering, University of Nevada, Reno, Report No. CCEER-97-5, September, 1997.

CCEER-98-1 Itani, A., Vesco, T. and Dietrich, A., “Cyclic Behavior of “as Built” Laced Members With End Gusset Plates on the San Francisco Bay Bridge” Center for Civil Engineering Earthquake Research, Department of Civil Engineering, University of Nevada, Reno, Nevada Report No. CCEER-98-1, March, 1998.

CCEER-98-2 G. Norris and M. Ashour, “Liqueficiation and Undraned response evaluation of Sands from Drained Formulation.” Center for Civil Engineering Earthquake Research, Department of Civil Engineering, University of Nevada, Reno, Nevada, Report No. CCEER-98-2, May, 1998.

CCEER-98-3 Qingbin, Chen, B. M. Douglas, E. Maragakis, and I. G. Buckle, "Extraction of Nonlinear Hysteretic Properties of Seismically Isolated Bridges from Quick-Release Field Tests", Center for Civil Engineering Earthquake Research, Department of Civil Engineering, University of Nevada, Reno, Nevada, Report No. CCEER-98-3, June, 1998.

CCEER-98-4 Maragakis, E., B. M. Douglas, and C. Qingbin, "Full-Scale Field Capacity Tests of a Railway Bridge", Center for Civil Engineering Earthquake Research, Department of Civil Engineering, University of Nevada, Reno, Nevada, Report No. CCEER-98-4, June, 1998.

CCEER-98-5 Itani, A., Douglas, B., and Woodgate, J., “Cyclic Behavior of Richmond-San Rafael Retrofitted Tower Leg”. Center for Civil Engineering Earthquake Research, Department of Civil Engineering, University of Nevada, Reno. Report No. CCEER-98-5, June 1998

CCEER-98-6 Moore, R., Saiidi, M., and Itani, A., “Seismic Behavior of New Bridges with Skew and Curvature”. Center for Civil Engineering Earthquake Research, Department of Civil Engineering, University of Nevada, Reno. Report No. CCEER-98-6, October, 1998.

CCEER-98-7 Itani, A and Dietrich, A, “Cyclic Behavior of Double Gusset Plate Connections”, Center for Civil Engineering Earthquake Research, Department of Civil Engineering, University of Nevada, Reno, Nevada, Report No. CCEER-98-5, December, 1998.

CCEER-99-1 Caywood, C., M. Saiidi, and D. Sanders, “ Seismic Retrofit of Flared Bridge Columns With Steel Jackets,” Civil Engineering Department, University of Nevada, Reno, Report No. CCEER-99-1, February 1999.

CCEER-99-2 Mangoba, N., M. Mayberry, and M. Saiidi, “Prestress Loss in Four Box Girder Bridges in Northern Nevada,” Civil Engineering Department, University of Nevada, Reno, Report No. CCEER-99-2, March 1999.

CCEER-99-3 Abo-Shadi, N., M. Saiidi, and D. Sanders, "Seismic Response of Bridge Pier Walls in the Weak Direction", Civil Engineering Department, University of Nevada, Reno, Report No. CCEER-99-3, April 1999.

CCEER-99-4 Buzick, A., and M. Saiidi, "Shear Strength and Shear Fatigue Behavior of Full-Scale Prestressed Concrete Box Girders", Civil Engineering Department, University of Nevada, Reno, Report No. CCEER-99-4, April 1999.

CCEER-99-5 Randall, M., M. Saiidi, E. Maragakis and T. Isakovic, "Restrainer Design Procedures For Multi-Span Simply-Supported Bridges", Civil Engineering Department, University of Nevada, Reno, Report No. CCEER-99-5, April 1999.

CCEER-99-6 Wehbe, N. and M. Saiidi, "User's Manual for RCMC v. 1.2, A Computer Program for Moment-Curvature Analysis of Confined and Unconfined Reinforced Concrete Sections", Civil Engineering Department, University of Nevada, Reno, Report No. CCEER-99-6, May 1999.

CCEER-99-7 Burda, J. and A. Itani, "Studies of Seismic Behavior of Steel Base Plates," Civil Engineering Department, University of Nevada, Reno, Report No. CCEER-99-7, May 1999.

CCEER-99-8 Ashour, M., and G. Norris, "Refinement of the Strain Wedge Model Program," Civil Engineering Department, University of Nevada, Reno, Report No. CCEER-99-8, March 1999.

CCEER-99-9 Dietrich, A., and A. Itani, "Cyclic Behavior of Laced and Perforated Steel Members on the San Francisco-Oakland Bay Bridge," Civil Engineering Department, University, Reno. December 1999.

CCEER 99-10 Itani, A., A. Dietrich, "Cyclic Behavior of Built Up Steel Members and their Connections," Civil Engineering Department, University of Nevada, Reno. December 1999.

CCEER 99-11 Itani, A., J. Woodgate, "Axial and Rotational Ductility of BuiltUp Structural Steel Members," Civil Engineering Department, University of Nevada, Reno December 1999.

CCEER-99-12 Sgambelluri, M., Sanders, D.H., and Saiidi, M.S., Behavior of One-Way Reinforced Concrete Bridge Column Hinges in the Weak Direction, Report No. Department of Civil Engineering, University of Nevada, Reno, December 1999.

CCEER-99-13 Laplace, P., Sanders, D.H., Douglas, B, and Saiidi, M, Shake Table Testing of Flexure Dominated Reinforced Concrete Bridge Columns, Report No. Department of Civil Engineering, University of Nevada, Reno, December 1999.

CCEER-99-14 Ahmad M. Itani, Jose A. Zepeda, and Elizabeth A. Ware "Cyclic Behavior of Steel Moment Frame Connections for the Moscone Center Expansion," December 1999.

CCEER 00-1 Ashour, M., and Norris, G. "Undrained Lateral Pile and Pile Group Response in Saturated Sand", Civil Engineering Department, University of Nevada, Reno, Report No. CCEER-00-1, May 1999. January 2000.

CCEER 00-2 Saiidi, M. and Wehbe, N., "A Comparison of Confinement Requirements in Different Codes for Rectangular, Circular, and Double-Spiral RC Bridge Columns," Civil Engineering Department, University of Nevada, Reno, Report No. CCEER-00-2, January 2000.

CCEER 00-3 McElhaney, B., M. Saiidi, and D. Sanders, "Shake Table Testing of Flared Bridge Columns With Steel Jacket Retrofit," Civil Engineering Department, University of Nevada, Reno, Report No. CCEER-00-3, January 2000.

CCEER 00-4 Martinovic, F., M. Saiidi, D. Sanders, and F. Gordaninejad, "Dynamic Testing of Non-Prismatic Reinforced Concrete Bridge Columns Retrofitted with FRP Jackets," Civil Engineering Department, University of Nevada, Reno, Report No. CCEER-00-4, January 2000.

CCEER 00-5 Itani, A., and M. Saiidi, "Seismic Evaluation of Steel Joints for UCLA Center for Health Science Westwood Replacement Hospital," Civil Engineering Department, University of Nevada, Reno, Report No. CCEER-00-5, February 2000.

CCEER 00-6 Will, J. and D. Sanders, "High Performance Concrete Using Nevada Aggregates," Civil Engineering Department, University of Nevada, Reno, Report No. CCEER-00-6, May 2000.

CCEER 00-7 French, C., and M. Saiidi, "A Comparison of Static and Dynamic Performance of Models of Flared Bridge Columns ," Civil Engineering Department, University of Nevada, Reno, Report No. CCEER-00-7, October 2000.

CCEER 00-8 Itani, A., H. Sedarat, "Seismic Analysis of the AISI LRFD Design Example of Steel Highway Bridges," Civil Engineering Department, University of Nevada, Reno, Report No. CCEER 00-08, November 2000.

CCEER 00-9 Moore, J., D. Sanders, and M. Saiidi, "Shake Table Testing of 1960's Two Column Bent with Hinges Bases," Civil Engineering Department, University of Nevada, Reno, Report No. CCEER 00-09, December 2000.

CCEER 00-10 Asthana, M., D. Sanders, and M. Saiidi, "One-Way Reinforced Concrete Bridge Column Hinges in the Weak Direction," Civil Engineering Department, University of Nevada, Reno, Report No. CCEER 00-10, April 2001.

CCEER 01-1 Ah Sha, H., D. Sanders, M. Saiidi, "Early Age Shrinkage and Cracking of Nevada Concrete Bridge Decks, "Civil Engineering Department, University of Nevada, Reno, Report No. CCEER 01-01, May 2001.

CCEER 01-2 Ashour, M. and G. Norris, "Pile Group program for Full Material Modeling an Progressive Failure." Civil Engineering Department, University of Nevada, Reno, Report No. CCEER 01-02, July 2001.

CCEER 01-3 Itani, A., C. Lanaud, and P. Dusicka, "Non-Linear Finite Element Analysis of Built-Up Shear Links." Civil Engineering Department, University of Nevada, Reno, Report No. CCEER 01-03, July 2001.

CCEER 01-4 Saiidi, M., J. Mortensen, and F. Martinovic, "Analysis and Retrofit of Fixed Flared Columns with Glass Fiber-Reinforced Plastic Jacketing," Civil Engineering Department, University of Nevada, Reno, Report No. CCEER 01-4, August 2001

CCEER 01-5 Saiidi, M., A. Itani, I. Buckle, and Z. Cheng," Performance of A Full-Scale Two-Story Wood Frame Structure Supported on Ever-Level Isolators," Civil Engineering Department, University of Nevada, Reno, Report No. CCEER 01-5, October 2001

CCEER 01-6 Laplace, P., D. Sanders, and M. Saiidi, "Experimental Study and Analysis of Retrofitted Flexure and Shear Dominated Circular Reinforced Concrete Bridge Columns Subjected to Shake Table Excitation, "Civil Engineering Department, University of Nevada, Reno, Report No. CCEER 01-6, June 2001.

CCEER 01-7 Reppi, F., and D. Sanders, "Removal and Replacement of Cast-in-Place, Post-tensioned, Box Girder Bridge," Civil Engineering Department, University of Nevada, Reno, Report No. CCEER 01-7, December 2001.

CCEER 02-1 Pulido, C., M. Saiidi, D. Sanders, and A. Itani, "Seismic Performance and Retrofitting of Reinforced Concrete Bridge Bents," Civil Engineering Department, University of Nevada, Reno, Report No. CCEER 02-1, January 2002.

CCEER 02-2 Yang, Q., M. Saiidi, H. Wang, and A. Itani, "Influence of Ground Motion Incoherency on Earthquake Response of Multi-Support Structures," Civil Engineering Department, University of Nevada, Reno, Report No. CCEER 02-2, May 2002.

CCEER 02-3 M. Saiidi, B. Gopalakrishnan, E. Reinhardt, and R. Siddharthan, A Preliminary Study of Shake Table Response of A Two-Column Bridge Bent on Flexible Footings Civil Engineering Department, University of Nevada, Reno, Report No. CCEER 02-03, June 2002.

CCEER 02-4 Not Published

CCEER 02-5 Banghart, A., Sanders, D., Saiidi, M., "Evaluation of Concrete Mixes for Filling the Steel Arches in the Galena Creek Bridge," Civil Engineering Department, University of Nevada, Reno, Report No. CCEER 02-05, June 2002.

CCEER 02-6 Dusicka, P., Itani, A., Buckle, I. G., "Cyclic Behavior of Shear Links and Tower Shaft Assembley of San Francisco – Oakland Bay Bridge Tower" Civil Engineering Department, University of Nevada, Reno, Report No. CCEER 02-06, July 2002.

CCEER 02-7 Mortensen, J., and M. Saiidi, " A Performance-Based Design Method for Confinement in Circular Columns," Civil Engineering Department, University of Nevada, Reno, Report No. CCEER 02-07, November 2002.

CCEER 03-1 Wehbe, N., and M. Saiidi, "User's manual for SPMC v. 1.0 : A Computer Program for Moment-Curvature Analysis of Reinforced Concrete Sections with Interlocking Spirals," Center for Civil Engineering Earthquake Research, Department of Civil Engineering, University of Nevada, Reno, Nevada, Report No. CCEER-03-1, May, 2003.

CCEER 03-2 Wehbe, N., and M. Saiidi, "User's manual for RCMC v. 2.0 : A Computer Program for Moment-Curvature Analysis of Confined and Unconfined Reinforced Concrete Sections," Center for Civil Engineering Earthquake Research, Department of Civil Engineering, University of Nevada, Reno, Nevada, Report No. CCEER-03-2, June, 2003.

CCEER 03-3 Nada, H., D. Sanders, and M. Saiidi, " Seismic Performance of RC Bridge Frames with Architectural-Flared Columns," Civil Engineering Department, University of Nevada, Reno, Report No. CCEER 03-3, January 2003.

CCEER 03-4 Reinhardt, E., M. Saiidi, and R. Siddharthan, " Seismic Performance of a CFRP/ Concrete Bridge Bent on Flexible Footings." Civil Engineering Department, University of Nevada, Reno. Report No. CCEER 03-4, August 2003.

CCEER 03-5 Johnson, N., M. Saiidi, A. Itani, and S. Ladkany, "Seismic Retrofit of Octagonal Columns with Pedestal and One-Way Hinge at the Base," Center for Civil Engineering Earthquake Research, Department of Civil Engineering, University of Nevada, Reno, Nevada, Report No. CCEER-03-5, August 2003.

CCEER 03-6 Mortensen, C., M. Saiidi, and S. Ladkany, "Creep and Shrinkage Losses in Highly Variable Climates," Center for Civil Engineering Earthquake Research, Department of Civil Engineering, University of Nevada, Reno, Nevada, Report No. CCEER-03-6, September 2003.

CCEER 03- 7 Ayoub, C., M. Saiidi, and A. Itani, "A Study of Shape-Memory-Alloy-Reinforced Beams and Cubes," Center for Civil Engineering Earthquake Research, Department of Civil Engineering, University of Nevada, Reno, Nevada, Report No. CCEER-03-7, October 2003.

CCEER 03-8 Chandane, S., D. Sanders, and M. Saiidi, "Static and Dynamic Performance of RC Bridge Bents with Architectural-Flared Columns," Center for Civil Engineering Earthquake Research, Department of Civil Engineering, University of Nevada, Reno, Nevada, Report No. CCEER-03-8, November 2003.

CCEER 04-1 Olaegbe, C., and Saiidi, M., "Effect of Loading History on Shake Table Performance of A Two-Column Bent with Infill Wall," Center for Civil Engineering Earthquake Research, Department of Civil Engineering, University of Nevada, Reno, Nevada, Report No. CCEER-04-1, January 2004.

CCEER 04-2 Johnson, R., Maragakis, E., Saiidi, M., and DesRoches, R., "Experimental Evaluation of Seismic Performance of SMA Bridge Restrainers," Center for Civil Engineering Earthquake Research, Department of Civil Engineering, University of Nevada, Reno, Nevada, Report No. CCEER-04-2, February 2004.

CCEER 04-3 Moustafa, K., Sanders, D., and Saiidi, M., "Impact of Aspect Ratio on Two-Column Bent Seismic Performance," Center for Civil Engineering Earthquake Research, Department of Civil Engineering, University of Nevada, Reno, Nevada, Report No. CCEER-04-3, February 2004.

CCEER 04-4 Maragakis, E., Saiidi, M., Sanchez-Camargo, F., and Elfass, S., "Seismic Performance of Bridge Restrainers At In-Span Hinges," Center for Civil Engineering Earthquake Research, Department of Civil Engineering, University of Nevada, Reno, Nevada, Report No. CCEER-04-4, March 2004.

CCEER 04-5 Ashour, M., Norris, G. and Elfass, S., "Analysis of Laterally Loaded Long or Intermediate Drilled Shafts of Small or Large Diameter in Layered Soil," Center for Civil Engineering Earthquake Research, Department of Civil Engineering, University of Nevada, Reno, Nevada, Report No. CCEER-04-5, June 2004.

CCEER 04-6 Correal, J., Saiidi, M. and Sanders, D., "Seismic Performance of RC Bridge Columns Reinforced with Two Interlocking Spirals," Center for Civil Engineering Earthquake Research, Department of Civil Engineering, University of Nevada, Reno, Nevada, Report No. CCEER-04-6, August 2004.

CCEER 04-7 Dusicka, P., Itani, A. and Buckle, I., "Cyclic Response and Low Cycle Fatigue Characteristics of Plate Steels," Center for Civil Engineering Earthquake Research, Department of Civil Engineering, University of Nevada, Reno, Nevada, Report No. CCEER-04-7, November 2004.

CCEER 04-8 Dusicka, P., Itani, A. and Buckle, I., " Built-up Shear Links as Energy Dissipaters for Seismic Protection of Bridges," Center for Civil Engineering Earthquake Research, Department of Civil Engineering, University of Nevada, Reno, Nevada, Report No. CCEER-04-8, November 2004.

CCEER 04-9 Sureshkumar, K., Saiidi, S., Itani, A. and Ladkany, S., "Seismic Retrofit of Two-Column Bents with Diamond Shape Columns," Center for Civil Engineering Earthquake Research, Department of Civil Engineering, University of Nevada, Reno, Nevada, Report No. CCEER-04-9, November 2004.

CCEER 05-1 Wang, H. and Saiidi, S., "A Study of RC Columns with Shape Memory Alloy and Engineered Cementitious Composites," Center for Civil Engineering Earthquake Research, Department of Civil Engineering, University of Nevada, Reno, Nevada, Report No. CCEER-05-1, January 2005.

CCEER 05-2 Johnson, R., Saiidi, S. and Maragakis, E., "A Study of Fiber Reinforced Plastics for Seismic Bridge Restrainers," Center for Civil Engineering Earthquake Research, Department of Civil Engineering, University of Nevada, Reno, Nevada, Report No. CCEER-05-2, January 2005.

CCEER 05-3 Carden, L.P., Itani, A.M., Buckle, I.G, "Seismic Load Path in Steel Girder Bridge Superstructures," Center for Civil Engineering Earthquake Research, Department of Civil Engineering, University of Nevada, Reno, Nevada, Report No. CCEER-05-3, January 2005.

CCEER 05-4 Carden, L.P., Itani, A.M., Buckle, I.G, "Seismic Performance of Steel Girder Bridge Superstructures with Ductile End Cross Frames and Seismic Isolation," Center for Civil Engineering Earthquake Research, Department of Civil Engineering, University of Nevada, Reno, Nevada, Report No. CCEER-05-4, January 2005.

CCEER 05-5 Goodwin, E., Maragakis, M., Itani, A. and Luo, S., "Experimental Evaluation of the Seismic Performance of Hospital Piping Subassemblies," Center for Civil Engineering Earthquake Research, Department of Civil Engineering, University of Nevada, Reno, Nevada, Report No. CCEER-05-5, February 2005.

CCEER 05-6 Zadeh M. S., Saiidi, S, Itani, A. and Ladkany, S., "Seismic Vulnerability Evaluation and Retrofit Design of Las Vegas Downtown Viaduct," Center for Civil Engineering Earthquake Research, Department of Civil Engineering, University of Nevada, Reno, Nevada, Report No. CCEER-05-6, February 2005.

CCEER 05-7 Phan, V., Saiidi, S. and Anderson, J., "Near Fault (Near Field) Ground Motion Effects on Reinforced Concrete Bridge Columns" Center for Civil Engineering Earthquake Research, Department of Civil Engineering, University of Nevada, Reno, Nevada, Report No. CCEER-05-7, August 2005.

CCEER 05-8 Carden, L., Itani, A. and Laplace, P., "Performance of Steel Props at the UNR Fire Science Academy subjected to Repeated Fire" Center for Civil Engineering Earthquake Research, Department of Civil Engineering, University of Nevada, Reno, Nevada, Report No. CCEER-05-8, August 2005.

CCEER 05-9 Yamashita, R. and Sanders, D., "Shake Table Testing and an Analytical Study of Unbonded Prestressed Hollow Concrete Column Constructed with Precast Segments" Center for Civil Engineering Earthquake Research, Department of Civil Engineering, University of Nevada, Reno, Nevada, Report No. CCEER-05-9, August 2005.

CCEER 05-10 Moustafa, K. D. Sanders, and M. Saïidi, "Seismic Behavior of R/C Bridge Bents with Architectural-Flared Columns Including both Horizontal and Vertical Gaps," Center for Civil Engineering Earthquake Research, Department of Civil Engineering, University of Nevada, Reno, Nevada, Report No. CCEER-05-10, February 2005.

CCEER 05-11 Carden, L., Itani., A., and Peckan, G., "Recommendations for the Design of Beams and Posts in Bridge Falsework," Center for Civil Engineering Earthquake Research, Department of Civil Engineering, University of Nevada, Reno, Nevada, Report No. CCEER-05-11, October 2005.

CCEER 06-01 Cheng, Z., Saiidi, S., and Sanders, D., "Development of a Seismic Design Method for Reinforced Concrete Two-Way Bridge Column Hinges," Center for Civil Engineering Earthquake Research, Department of Civil Engineering, University of Nevada, Reno, Nevada, Report No. CCEER-06-01, February 2006.

Kenny C. Guinn, Governor

Jeff Fontaine, P.E. Director
Prepared by Research Division
Tie He, Research Division Chief
(775) 888-7803
the@dot.state.nv.us
1263 South Stewart Street
Carson City, Nevada 89712